Annex(es)

WORK PLAN MSC THESIS

II

LITERATURE STUDY – PART I



Literature Study – Part I

Redesign of bridges Twentekanaal in Ultra-High Performance Concrete

MSc Thesis

14 June 2020

Company	Witteveen+Bos
MSc thesis project	Redesign of bridges Twentekanaal in Ultra-High Performance Concrete
Document	Literature Study – Part I
Status	Final version
Version	D1.0
Date	14 June 2020

Author	ing. M. Dorland
Student id	4719980
Degree programme	MSc Civil Engineering
Track	Structural Engineering – Concrete Structures

Company Supervisors	ing. T. Petersen RC ir. A. ten Voorde
Supervisors TU Delft	Dr. ir. Y. Yang Dr. ir. M.A.N. Hendriks Dr. ir. S. Grünewald

TABLE OF CONTENT

PREFACE 1

DEFINITIONS 2

1 BASICS OF CONVENTIONAL CONCRETE 3

1.1 Introduction to concrete 3

1.2 Properties of concrete 4

1.2.1 Fresh concrete 4
1.2.2 Hardening concrete 8
1.2.3 Hardened concrete 10

1.3 Concrete Technology: Concrete mix and constituents 15

1.3.1 Cement 15
1.3.2 Aggregate 20
1.3.3 Mixing water 25
1.3.4 Admixtures and additives 25
1.3.5 Fillers 27

1.4 Concrete Technology: Strength of hardened concrete 27

1.4.1 Importance of concrete compressive strength 27
1.4.2 Strength of hardened concrete – Porosity 31
1.4.3 Strength of hardened concrete – Pore size and microcracking 33
1.4.4 Practical factors influencing the strength of hardened concrete 36

1.5 Concrete and sustainability 37

1.5.1 Durability versus sustainability 37
1.5.2 Sustainability of concrete 37
1.5.3 Circular economy and raw materials 38
1.5.4 Conventional concrete versus UHPC 40

1.6 Summary first chapter 40

1.7 Bibliography 42

2 INTRODUCTION TO SPECIAL CONCRETES 43

2.1 Introduction to special concretes 43

2.2 Basics of Ultra-High Performance Concrete 43

2.2.1 Introduction to Ultra-High Performance Concrete 43
2.2.2 The principles of UHPC 47
2.2.3 Mix design of UHPC 49

2.2.4 Properties of UHPC: Fresh and hardening concrete 52
2.2.5 Properties of UHPC: Hardened concrete 53
2.3 Basics of conventional fibre-reinforced concrete 57
2.3.1 Introduction to conventional fibre-reinforced concrete 57
2.3.2 Mix design of conventional fibre-reinforced concrete 58
2.3.3 Plastic fibre-reinforced concrete (Polypropylene) 59
2.3.4 Steel fibre-reinforced concrete 60
2.4 Steel fibres in UHPC 63
2.5 Types of UHPC 66
2.6 Practical considerations UHPC 67
2.6.1 Mixing UHPC 67
2.6.2 Placing and fibre orientation 68
2.6.3 Curing UHPC 69
2.7 Summary second chapter 70
2.8 Bibliography 72
3 DESIGNING IN ULTRA-HIGH PERFORMANCE CONCRETE 73
3.1 Introduction to designing in UHPC 73
3.2 Considerations for designing in UHPC 73
3.2.1 Challenges of designing in UHPC 73
3.2.2 Development of codes 75
3.2.3 Overview of available codes 76
3.3 Description of the codes 77
3.3.1 Design Guidelines for Ductal Prestressed Concrete Beams (2000) 77
3.3.2 AFGC-SETRA recommendations (2002) 78
3.3.3 Recommendations for Design and Construction of UHSFRC structures (2006) 78
3.3.4 AFGC-SETRA recommendations (2013) 79
3.3.5 SIA 2052 (2016) 80
3.3.6 NF P18-470, NF P18-710 and NF P18-451 (2016-2018) 80
3.3.7 Selecting a code for redesign 81
3.4 Summary third chapter 82
3.5 Bibliography 83
4 CONCLUSIONS 84
Final page 84
Annex(es) Number of pages

PREFACE

This document comprises part I of the literature study as a part of the thesis 'Redesign of bridges Twentekanaal in Ultra-High Performance Concrete'. The goal of this part of the literature study is to collect information regarding UHPC. This will be done from two different 'perspectives':

- Concrete science & technology, to become familiar to the material behaviour and the more fundamental concepts behind it;
- Design & execution, to understand how to apply the material in calculations and in practice.

Achieving these goals means that an answer can be formulated to the following two research questions:

- What are the basic concepts of UHPC from a concrete science & technology point of view?
- What are the basic concepts of design in UHPC in accordance with state-of-the-art standards?

Answering these two research questions are essential in order to be able to start with the subsequent parts of the project. To provide an overview, the literature study in relation to the total thesis project is given in the following figure.

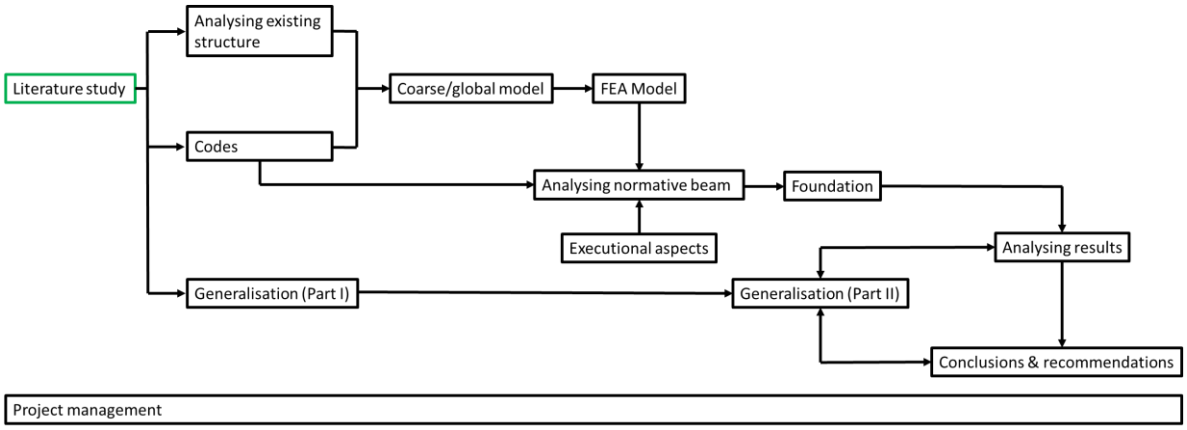


Figure 1 Literature in relation to the project

Reading guide

The literature study presented in this report consists of the following chapters:

- Chapter 1: The literature study starts in the first chapter with a discussion of the basics of conventional concrete that are deemed to be essential for further successful elaboration of the literature study and project;
- Chapter 2: In the second chapter UHPC is introduced from a concrete science & technology point of view. It's key characteristics and properties are described and explained. Moreover, fibre-reinforced concrete and the effect of adding fibres to UHPC is also briefly discussed;
- Chapter 3: Designing in UHPC is discussed by looking at particular challenges, identifying current codes and guidelines and discussing the main design rules in the most relevant guidelines;
- Chapter 4: The literature study is concluded in the fourth chapter with the formulation of the answers to the aforementioned research questions.

DEFINITIONS

Workability:	The amount of useful internal work that is required to produce full compaction of the concrete (or in more practical terms: how easy it can be processed).
Consistency:	The firmness of form of the fresh concrete and therefore the ease with which the material will flow.
Segregation:	The separation of the constituents of the heterogeneous concrete mixture in such a way that their distribution is no longer uniform.
Setting/stiffening:	The change of the material from fluid state into rigid state.
Creep:	The increase of the deformation of a material under a constant load.
Relaxation:	The gradual decrease of stresses in a material under a constant displacement.
Permeability:	A property of the material that describes how liquids and/or gasses may pass through the material.
Porosity:	The relative volume of pores and voids in the cement paste.
Hydraulic material:	A material that reacts with water into a hardened paste (a process known as 'hydration') and that does not dissolve in water after the material has hardened.
Latent hydraulic:	A hydraulic material of which the hydration reaction has to be initiated by an activator.
Pozzolans:	Siliceous materials that react with lime and water (not only water) to form compounds that process cementitious (i.e. binding) properties.
Heat of hydration:	The heat that evolves during the hydration at a given temperature.
Toughness:	The work required to cause failure of a specimen and therefore a measure of the resistance against impact loads.
Curing:	Preventing the evaporation of water from fresh concrete.
Durability:	The concept of a structure functioning for a long period of time (service life) under expected external influences (loads, environmental influences) without requiring excessive maintenance.
Sustainability:	The concept of characterizing a structure or object based on its impact on the environment.

1

BASICS OF CONVENTIONAL CONCRETE

The first chapter of this part of the literature study is dedicated to the (re)collection of relevant knowledge about conventional concrete, i.e. concrete of normal strength. The goal is to gain an overview of the main properties of the material and some more in-depth knowledge regarding concrete technology (constituents of concrete and factors determining concrete strength).

All topics selected to be discussed in this chapter were chosen because it is expected that good understanding of the basics of concrete will help in the subsequent parts of this literature study and the remainder of the project, i.e. to help with design and/or to help with the understanding later topics. The outline of this chapter is as follows:

- The chapter starts with an introduction in which some main points of reinforced concrete are mentioned;
- After that, the more in-depth discussion of the material starts by reviewing the main properties of concrete in fresh, hardening and hardened state;
- Subsequently the concrete mix itself will be discussed and different constituents and their properties are described;
- In the next paragraph it is discussed what the different parameters are that determine the strength of hardened concrete;
- Thereafter, sustainability related aspects of concrete are discussed;
- The chapter is concluded with a summary of the main points.

Throughout this chapter the reader should be aware that, unless specifically stated otherwise, this chapter refers to normal strength concrete.

1.1 Introduction to concrete

A very broad definition of concrete is that it is a product made by the use of a cementing medium. A more practical definition is to define concrete as a mixture of roughly 1 volume of cement, 2 volumes of sand (fine aggregate) and 3 volumes of gravel (coarse aggregate), mixed with an amount of water of about half the weight of the cement.

Later in this chapter however, it will become clear that there are many different constituents. The many different available constituents enable modification of the concrete mixture in order to obtain 'good concrete': concrete that has satisfactory properties in all its states: fresh concrete, hardening concrete and hardened concrete. In each of these states, different properties are of particular importance.

Concrete is a construction material that offers many options and benefits:

- Freedom of shape: Concrete structures can be made in pretty much any desired shape;

- Durability: Concrete structures are durable and provide high load bearing capacity, even in demanding environment, e.g. hydraulic structures;
- Possibilities of mix design: The properties can be modified in order to obtain a concrete mixture that optimally matches the intended application;
- Costs: Conventional concrete is a relatively cheap material.

Most concrete structures are actually reinforced concrete structures. The reasons why concrete and reinforcement go together very well are:

- The concrete protects the reinforcement bars encased in it against corrosion;
- Concrete and reinforcing steel have approximately the same coefficient of thermal expansion (which is $10 * 10^{-6}$ per °C);
- The materials complement one another: the concrete provides compressive strength while the reinforcement steel provides tensile strength;
- The materials allow for good bond at the interface between the rebar and the concrete.

Reinforcement itself will not be discussed in the remainder of the chapter, but the previous points are still worth mentioning. However, reference will be made to the reinforcement on different occasions. For example, when studying different deterioration mechanisms.

1.2 Properties of concrete

As mentioned in the introduction, concrete can be described in three different 'states':

- Fresh concrete: After the constituents are mixed, the obtained mixture is called 'fresh concrete'.
- Hardening concrete: In this stage the concrete hardens, thus developing its properties such as strength.
- Hardened concrete: In its hardened state, the concrete fulfils the function it was designed for.

The goal is to obtain a mixture that has satisfactory properties in all these states. In each state different properties are of relevance:

- Fresh concrete: Requirements with respect to consistency and workability are most important.
- Hardening concrete: During this stage properties related to strength development are important.
- Hardening concrete: Properties relevant for the functioning of the structure are most important.

The main properties for each of these phases will be discussed.

1.2.1 Fresh concrete

Fresh concrete is the material that is obtained after mixing the different constituents. The fresh concrete is transported to the construction site, casted, compacted and curing takes place. Because of these activities, requirements with respect to consistency and workability are most important. As soon as the concrete is in its final place in the formwork, it starts developing its properties, which takes place in the following stage.

Importance of workability and compaction

Many long-term properties of hardened concrete are affected by the compaction of the fresh concrete after casting, think of properties such as strength and durability. In order to optimally develop these properties, good compaction should be achieved.

Two definitions to describe the state of fresh concrete are workability and consistency:

- Workability may be defined as the amount of useful internal work that is required to produce full compaction (or in more practical terms: how easy it can be processed).

- Consistency may be defined as the firmness of form of the fresh concrete and therefore the ease with which the material will flow.

Workability: In practice it is not possible to measure the workability of concrete as it is defined in the definition but it is possible to determine the workability related to a certain method used for compacting the concrete.

In practice, the workability of concrete is classified using consistency classes ranging from 'dry' to 'very flowable'. Which consistency class is required for a certain project depends on the way in which the concrete will be applied and compacted.

The presence of voids reduces the density of concrete and as a result the strength of the hardened concrete (as well as other properties) is reduced. That means that in order to achieve a strength value as high as possible, it is essential to achieve the maximum possible density. Achieving high density requires good workability.

Consistency: The consistency of the concrete determines the plastic behaviour of the material as well as its susceptibility to deformation (stability) and segregation.

To allow for achieving good compaction, consistency and the workability of the fresh concrete should be as such that compacting is possible. Moreover, segregation should be prevented during transportation, casting and finishing because segregation negatively contributes to the compaction as well.

Factors affecting the workability

Workability depends on a number of factors:

- Water content
- Aggregate type
- Grading of the aggregate
- Porosity/absorption by the aggregate
- Aggregate/cement ratio
- Admixtures (plasticizers)
- Fineness of cement

To make matters more complicated these factors interact with one another. For example: finer particles require more water because they have a larger specific surface and rounded aggregate particles require less water than more angular aggregate particles.

Water content: One way of increasing workability straight away is by increasing the water content because water acts as a lubricant between the particles in the mixture, but other factors are also to be considered if you want to achieve a concrete with minimum voids and maximum density. Note however that a high water/cement ratio will not be profitable to the porosity of the material in the end.

Aggregate type: Certain types of aggregates are known lower workability.

Grading of the aggregate: The ratio of coarse versus fine aggregate has to be balanced out. High volume of coarse aggregate vs fine aggregate may result in lower workability and segregation. High volume of fine aggregate results in higher workability but less durable concrete.

Porosity/absorption by the aggregate: If aggregates absorb mixing water, this amount of water is removed from the mix. Because water acts as lubricant between the particles the workability might be influenced negatively.

Aggregate/cement ratio: Suppose that the water/cement ratio is kept equal. The workability increases if the aggregate/cement ratio is reduced. This is because the amount of water relative to the surface of the solids increases.

Admixtures (plasticizers): Adding air into the concrete may improve the properties of the fresh concrete because the consistency and workability are improved (a certain air content may also prove to be helpful for hardened concrete in increasing the resistance against freeze/thaw). Note however that the amount of air has to be within precise limits, both too much and too little are not beneficial. Plasticizers increase workability without having to add more water.

Fineness of cement: Finer cement means greater water demand. However, finer cement particles do not increase the workability that much.

Two additional ''external factors'' also play a role in the workability:

- **Time**: Freshly mixed concrete both stiffens and sets as time passes. Stiffening means that mixing water is used up (evaporation, absorbed by aggregates or used for chemical reaction) and as a result there is a loss of workability (this loss of workability is known a 'slump loss').

- **Temperature**: A higher temperature results in a reduction of the workability.

Segregation and bleeding

An important aspect of the workability of fresh concrete is that the concrete should be cohesive (which means that it should not segregate) in order to be able to achieve good compaction. The following definition may be formulated:

Segregation: Segregation may be defined as the separation of the constituents of the heterogeneous concrete mixture in such a way that their distribution is no longer uniform.

Concrete contains particles of different sizes, this is the main cause of segregation. This implies that sufficient attention for grading and handling the concrete is important. One can distinguish two distinct forms of segregation:

- **Separation of coarse particles**: The separation of the coarser particles out of the mix (which is a typical risk for a dry mix) is caused by the fact that the coarser particles settle more than fine particles.

- **Separation of the grout**: The separation of grout, i.e. cement and water from the mix, typically occurs in wet mixes.

The risk of segregation can be greatly reduced by using correct ways of transporting, placing and handling the fresh concrete. For example: casting concrete from a height into the formwork or continuing vibration for too long increases the risk of segregation.

Bleeding: Bleeding is a distinct form of segregation, after casting the concrete, a layer of water may form at the top of the concrete. This is caused by the solids in the concrete mix being unable to hold all the mixing water while the solid parts are settling down. The bleeding stops as soon as the cement paste has achieved sufficient stiffness to prevent further settlement of the solid parts.

Bleeding does not have to be harmful. In limited amounts it may even prevent the drying of the concrete surface. However, it may become harmful if the rising water carries finer cement particles with it, creating a porous surface layer. Moreover, if water evaporation from the surface of the fresh concrete is faster than the bleeding rate, plastic shrinkage may occur.

Bleeding is dependent on the water content and the bleeding is lower with finer cements. If the amount of bleeding water becomes very large it means that the fresh concrete is unstable.

Testing workability

As mentioned in at the beginning of the section, workability as defined cannot be tested. To somewhat quantify the workability of fresh concrete, a number of workability tests can be performed. There is no ideal test for workability: each test is suitable for distinct mixtures and situations. Some examples are given below.

- **Slump test**: A cone shaped mould is filled with concrete in three layers, each layer is tamped. This is all done following prescribed procedures. After filling the cone is lifted after which the concrete will slump. The slump is measured. The measured slump can subsequently be related to the degree of workability. The method is very useful for application on the construction site, is unreliable for lean mixes. Figure 2 shows the principle of the slump test.

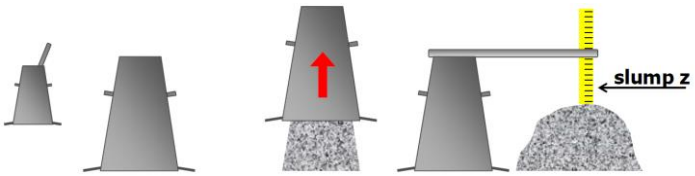


Figure 2 Slump test - (Ye & Schlangen et al., 2018)

- **Compactability test**: This method determines the degree of compaction that is achieved by a standard amount of work. The test is performed using an apparatus consisting of two hoppers and a cylinder, the apparatus is shown in Figure 3.

  The upper hopper is filled with concrete and the bottom door is opened. The concrete falls into the second hopper. The bottom door of the second hopper is released and the concrete falls into the cylinder. The net mass of the concrete in the cylinder (a known volume) is determined after which the density of the concrete is calculated as well as the compacting factor. The compacting factor can subsequently be related to workability. This test is more sensitive for concretes with low workability and provides a good measure of it. However, it is not a practical test for the construction site because of the size of the apparatus.

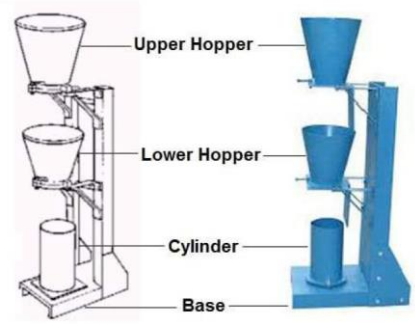


Figure 3 Compactability test - (Ye & Schlangen et al., 2018)

- **Vebe test**: A slump cone is filled and compacted following a standard manner and using a vibrating table. The point at which full compaction may be assumed to be achieved is prescribed as well. The required time to achieve this compacted state is measured (''Vebe seconds'') and this can be related to the workability. It is a good laboratory test, especially for dry mixes.

- **Flow table test**: A cone filled with concrete is placed on the flow table, see Figure 7 for the test setup. After lifting the mould and the table top is lifted and dropped following a prescribed procedure. The concrete spreads and, following the prescribed procedures, the flow is determined, which is related to the workability. The test is very suitable for 'flowing concrete' and also offers an indication of cohesiveness of the concrete mix.

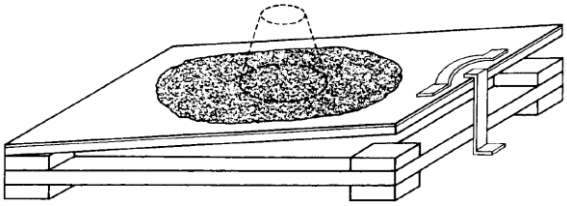


Figure 4 Flow table test - (Neville & Brooks, 2010), p.88

1.2.2 Hardening concrete

In the second stage the concrete hardens, i.e. it is developing its properties such as strength. During this phase the concrete is also called 'young concrete' or 'early-age concrete'. During this stage properties related to strength development are important:

- Development of the strength
- Heat development
- Shrinkage

Development of strength

The development of strength of concrete depends on a number of factors:

- Temperature
- Cement
- Water/cement ratio

The influence of the temperature on the development of strength can be quantified by determining the 'maturity' of the concrete. Note that higher temperature curing leads to a higher strength at early age but to a lower strength at later stage. This can be seen in Figure 5.

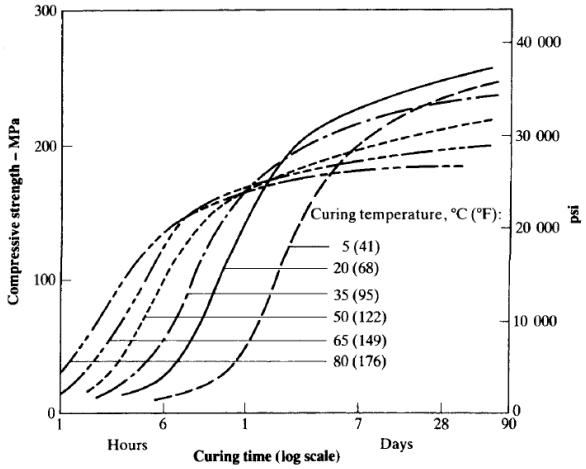


Figure 5 Relation between compressive strength and curing time at different curing temperatures – (Neville & Brooks, 2010), p.181

After the products of hydration are formed, they diffuse away from the cement particles and precipitate in the space in between the particles. If there is a high initial temperature, these products of hydration don't have the time to diffuse away. As a result, the formed precipitation is not uniform, most of it takes place around the hydrating cement particles. This results in the cement gel being non-uniform and having a more porous structure.

Heat development

Because hydration of cement is an exothermic chemical process, heat is produced and released. There are different methods to determine the heat of hydration. The heat of hydration, and the corresponding temperature, influence the development of strength.

The development of heat may result in the risk of cracking due to temperature shrinkage, this is especially relevant for mass concrete and may result in having to select other cement types (low heat cement) or provide cooling measures.

Shrinkage

Shrinkage is related to the loss of moisture (water) in the concrete and is one of the main causes of cracking of concrete. One may distinguish the following types of shrinkage related to moisture:

- Plastic shrinkage
- Chemical shrinkage
- Autogenous shrinkage
- Drying shrinkage

Shrinkage may already occur in the plastic stage (plastic shrinkage). After that it may occur in the remaining phases of the hardening process (chemical and autogenous shrinkage) or even after hardening (drying shrinkage). NOTE: Other types of shrinkage exist as well, for example due to temperature.

Plastic shrinkage: The phenomenon 'plastic shrinkage' can be summarized as the premature drying of the fresh (and still plastic, i.e. before setting) concrete, it takes place in the plastic stage (i.e. before setting). If the rate of evaporation of water at the surface of the fresh (and still plastic) concrete is larger than the rate of the water supply in the form of bleeding, the fresh concrete shrinks. This may lead to irregular crack patterns at the top surface of the fresh concrete.

The causes liable to this form of shrinkage are often external factors: the air humidity, and temperature difference between the concrete and air for example. It may be prevented by taking measures to provide good curing conditions, i.e. to prevent this premature drying. Moreover, one should pay attention to the mix design. Stable mixtures (for example high strength concrete) are more susceptible to plastic shrinkage because there is only very little internal transport of water possible due to the mixture composition.

Chemical shrinkage: The hardening of cement is a chemical process, the total volume of the cement and water is larger than the total volume of the reaction products. Chemical shrinkage cannot be seen from the outside because it results in microcracking and internal pore space within the hardened cement paste.

Autogenous shrinkage: Autogenous shrinkage is a distinct form of chemical shrinkage which is especially important for mixtures with a lower water/cement ratio.

During the hydration of these mixtures, all water is used up for the chemical reactions. This results in internal drying of the hardening concrete which causes volume change of the cement paste and shrinkage of the concrete.

Drying shrinkage: Drying shrinkage is caused by change moisture content due to difference in relative humidity between the concrete and the surrounding air. Free water may be present in the capillary pores within the hardened concrete. If this free water evaporates, the pores contract which causes drying shrinkage. In practice, this is an important cause of cracking in structures where deformations are restrained, this is one of the reasons why dilation is important. The opposite may happen as well, which is a phenomenon called 'swelling'.

1.2.3 Hardened concrete

In the hardened state, properties relevant for the functioning of the structure are most important. Categories of properties one might think of are:

- Mechanical properties of hardened concrete
- Physical properties of concrete
- Properties related to durability

Mechanical properties of hardened concrete

Compressive strength: The compressive strength is an important, if not the most important, property of hardened concrete. In the codes, concrete is characterised using its 28-day compressive strength. This is done using compressive strength classes. In the Eurocode, this is a notation of the form:

CX/Y

Where:
X: Characteristic value of the cylinder compressive strength
Y: Characteristic value of the cube compressive strength

The characteristic value is the value above which 95% of the results of the tested samples will be. Many mechanical properties of the concrete are related to the compressive strength value, this is reflected in the codes where formulas are given in which the compressive strength is used to directly obtain other values and properties. This is convenient, but this does not have to be completely true. Some quantities may be a function not only of the compressive strength, but also of other properties as well.

A second remark should be made as well. When designing concrete structures, the value of the compressive strength as obtained by selecting a strength class is the value that is to be used. But that does not mean that this will be the 'real' concrete compressive strength value that could be measured by, for example, drilling out and testing a cylinder from the structure. There are a few reasons for this:

- The 'real' strength of concrete depends on the constituents of the concrete mix, the conditions under which the material hardens, etc. The exact numerical value of the strength therefore is difficult to determine beforehand;

- The 'real' compressive strength is in practice often higher than the 'prescribed' strength using the strength class because:

    - Creating margin during design
    - Ongoing hydration process value

The strength values of the strength classes are the values after 28 days of hardening. Therefore, in practice sometimes a higher strength class than strictly required is chosen (for example to have some margin). Moreover, hydration is a continuous process that does not stop after 28 days. Depending on the concrete, an appreciable strength increase after 28 days may be observed, especially if the concrete mix contains latent hydraulic (e.g. blast furnace slag) or pozzolanic (e.g. fly ash) materials as binder or filler.

Tensile strength: The tensile strength is, roughly speaking, about 10% of the compressive strength and can be determined in a number of ways, resulting in the following values:

- Axial tensile strength
- Splitting tensile strength
- Flexural tensile strength

The tensile strength is influenced by the composition of the concrete mix, for example:

- Suppose that the compressive strength is kept constant but the maximum size of the aggregate particles is reduced. In this caste the tensile strength would increase;

- Some aggregates give a higher tensile strength. The shape and texture also influence the tensile strength: a more angular particle results in higher tensile strength.

Modulus of elasticity: The modulus of elasticity gives the relation between the stress due to the load and the corresponding elastic deformation. Under the assumption that the material behaviour may be described using Hooke's law:

$$E = \frac{\sigma}{\varepsilon}$$

Where:
E: Modulus of elasticity
σ: Stress
ε: Strain

This equation suggests that the material is homogeneous. In reality, this is not the case: concrete is heterogeneous and therefore the modulus of elasticity is determined by the composition of the concrete mixture, the aggregate plays a dominant role in this.

To further complicate matters, the modulus of elasticity as determined above only holds for short term. Phenomenon such as cracking, creep, etc may result in deformations larger than one would expect based on the modulus of elasticity.

Shrinkage: As described in the previous chapter, shrinkage plays an important role and this is not limited to the hardening stage: plastic shrinkage is related to the plastic stage of the fresh concrete, chemical shrinkage and autogenous shrinkage are related to the hydration process but drying shrinkage however, is related to relative humidity and remains a 'risk' even in hardened state.

Creep: An additional cause of deformation of concrete is creep, a phenomenon which may be defined as an increase of the deformation under a constant load. A portion of this increased deformation is permanent.

The cause of creep is the deformation of the gel structure of the hardened concrete, i.e. the hardened cement paste. The gel structure may deform due to capillary stresses caused by the water present in the pores. The magnitude of the creep is influenced by a number of factors:

- Relative humidity
- The age of the concrete
- The strength class of the cement and concrete
- The geometry of the concrete cross section
- The duration of the loading

Relaxation: Relaxation may be defined as the gradual decrease of stresses under a constant displacement. It is related to/caused by creep, the mechanism causing creep is the same mechanism that causes relaxation. In practical terms, relaxation means that the actual stresses decrease gradually and are therefore lower than one would expect based on the modulus of elasticity alone.

Creep and relaxation can influence the force distribution within the structure. Some typical examples of this are as follows:

- Examples creep:
  - Increase of deformation of a structure, for example a concrete beam;
  - Redistribution of forces (e.g. due to settlements) within the structure.

- Examples relaxation:
  - Decrease of stresses in the structure caused by imposed deformation, for example due to settlement of a support of a statically indeterminate structure;
  - Decrease of the prestressing force in a prestressed concrete beam.

Physical properties of concrete

Among the physical properties of concrete, some important features can be summarised as:

- Volumetric mass
- Thermal properties
- Hygric properties

Volumetric mass: The high volumetric mass is a typical characteristic of concrete and can be used to make a distinction between three classes of concrete, for example:

- Lightweight concrete: Up to about 2000 kg/m^3
- Normal weight concrete: About 2400 kg/m^3
- Heavyweight concrete: Heavier than about 2600 kg/m^3

Thermal properties: Concrete has many different thermal properties, but when it comes to engineering practice, the following two properties are often of particular relevance:

- Heat of hydration: Hydration of concrete is an exothermic chemical reaction, that means that heat is released and this has many different implications. The release of heat results in a change of temperature which affects the development of strength.

  Moreover, in the case of mass concrete a temperature gradient may be observed between the inner part and outer part of the structure. Due to the increase in temperature, the concrete expands but at a certain point the temperature starts to decrease and the concrete contracts to take more or less its original dimensions. At this point, the concrete has developed a certain stiffness and strength, causing stresses due to the shortening. This may lead to cracking.

- Coefficient of thermal expansion: The coefficient of thermal expansion describes the amount of expansion or shrinkage of a material caused by change in temperature. In the case of concrete, the coefficient of thermal expansion of the aggregate plays a dominant role in determining the coefficient for the concrete as a whole. Although the exact value depends on the constituents of the material, a typical value for concrete is $10 * 10^{-6}$ per °C.

Hygric properties: Concrete is a porous material and there is a whole range of pores of different sizes present. If many pores are linked, the concrete is not only porous but also permeable. Due to the pores, transport of moisture and water vapor is possible.

Properties related to durability

Depending on the surroundings, there are many mechanisms that may cause deterioration of the concrete. In the case of many of these mechanisms, permeability of concrete plays an important role.

Permeability & porosity: The permeability of concrete describes how liquids and/or gasses may pass through the material. In other words, this also determines the susceptibility to harmful substances. Permeability of concrete is related to the porosity of the concrete.

Concrete is a porous material, it contains a whole range of pores of different sizes. If pores are interconnected, the material becomes permeable. Note however that this does not have to be the case. A permeable material is not the same as a porous material.

Capillary pores are the dominant factor when it comes to determining the permeability of the concrete because these pores are large enough for water particles to pass through. As will be studied later on, the

most important factor determining the volume of the capillary pores within the concrete is the water/cement ratio.

Environmental classes: If a durable structure is to be designed, the mix design, execution and design of the structure should be appropriate for the conditions in which the structure will have to function. Codes provide a practical way of describing the environment of a structure using environmental classes, these classes are related to different deterioration mechanisms that may occur in practice.

During the design phase, it is decided which environmental classes are relevant for a structure of a part of a structure. The selected environmental classes are subsequently used to determine requirements such as requirements for the mix design, the allowable crack width in the structure and the required concrete cover.

Deterioration mechanisms of reinforced concrete: There are many different deterioration mechanisms that can affect the durability of (reinforced) concrete. If one wishes to make a distinction between risk for the reinforcement and the concrete, the following distinction can be made:

- Corrosion of reinforcement due to:
  - Carbonation-induced corrosion
  - Chloride-induced corrosion
- Deterioration of concrete due to:
  - Sulphate attack
  - Alkali-silica reaction
  - Acids
  - Freeze/thaw
- Other ''mechanisms'': Fire

These mechanisms will subsequently be described in more detail.

Corrosion of the reinforcement: One of the 'strengths' of reinforced concrete is that the concrete protects the reinforcement against corrosion, this is achieved via the alkalinity of the pore water present. If the pH is sufficiently high, a protective layer is formed at the surface of the reinforcement bars. This protective layer protects the reinforcement from further corrosion. However, the protective layer may be broken down due to two different causes:

- Reduction of pH due to carbonation
- Increase in chloride content

These two causes eventually result in carbonation-induced and chloride-induced corrosion of the reinforcement respectively.

- Carbonation-induced corrosion: Carbonation means that CO_2 from the air dissolves into the pore water, causing it to become more acidic and de pH to become lower. As a result of this, the protection due to the protective layer is reduced.

  In humid environment, the corrosion of the rebar can now occur as the rebar is no longer sufficiently protected. In dry environment, carbonation is not a risk for the durability and in a permanently wet environment carbonation will not occur.

- Chloride-induced corrosion: Chloride ions may react with iron ions in the protective layer. As a result, a chemical reaction takes place, the reaction product (hydrochloric acid) of which causes the pH to decrease.

This process accelerates itself, the iron ions dissolve more rapidly, the pH drops faster etc. This results in very local corrosion of the reinforcement: pitting corrosion. This process is related to the ''chloride diffusion coefficient'', a measure for the speed with which the chloride ions can penetrate and diffuse through the concrete. Factors determining this quantity are:

- Type of cement
- Fineness of cement
- Water/cement ratio
- Density of concrete

For example: Blast furnace slag cement has a very low value for the chloride diffusion coefficient, making it very suitable for application in marine environments (a situation in which there is a considerable source of chlorides…). Moreover, a denser concrete means a decrease of the coefficient, which can be understood quite intuitively. The importance of the latter point will become clear in the second chapter of this report.

Sulphate attack: Sulphates may result in deterioration of concrete because they may cause a mechanism that results in the formation of expansive ettringite. This formation in turn causes stresses and, eventually, this may result in cracking. Sources of sulphate are, for example, sea water and fertilizers from the agriculture.

Alkali-silica reaction: Alkali-silica reaction is the reaction of alkalis (Na_2O and K_2O, i.e. sodium oxide and potassium oxide respectively, these are present in the pore water of the concrete) with reactive silica which comes from the aggregate.

Due to this reaction, reaction products are formed that bind with water and as a result increase in volume. This may eventually result in cracking due to the increase of stress due to internal swelling. The reaction develops slowly and damage becomes only apparent after a long time (years). The susceptibility to ASR can be limited by using appropriate cement and aggregate without reactive silica.

Acids: Acids may cause deterioration of concrete via leaching (concentration of calcium and hydroxide ions is reduced) and dissolving (solid matter is dissolved) of material.

Freeze and thaw: Freezing may cause damage to concrete if pore water freezes and expands. De-icing salts may result in developing temperature differences between the surface and the concrete underneath. The top layer may be damaged due to formation of ice between the top layer. Entrained air may help increase the resistance against freeze and thaw because it creates space for the freezing water to expand to without creating internal stresses.

Fire: Concrete is a non-combustible material, however, under sustained extremely high temperatures damage may still occur, for example due to:

- Expansion of the material: Due to the increase in temperature the material expands which may give rise to stresses and therefore result in cracking;

- Spalling: If there is a large but sudden increase in heat spalling may occur. Moist present within the pores of the concrete becomes vapour. Vapour has a larger volume than moisture but it cannot escape, this results in a build-up of pressure and eventually this may result in spalling of the outer layer;

  More dense concrete, for example high strength concrete, is more susceptible to spalling. The risk of spalling in case of fire can be decreased by adding polypropylene fibres to the mixture;

- Loss of strength of concrete: An increase in temperature eventually results in a decrease of the strength of the material, this may be observed starting at a temperature of about 200 °C;

- Loss of strength of reinforcement: Although the reinforcement is protected by a concrete cover, its temperature will increase as well. At a temperature of about 300 °C the strength decreases.

  A larger concrete cover implies a better protection and therefore a slower increase of temperature of the reinforcement.

1.3 Concrete Technology: Concrete mix and constituents

As written in the introduction of this chapter, one could think of concrete as a mix of about 1 volume of cement, 2 volumes of sand and 3 volumes of gravel, mixed with an amount of water of about half the weight of the cement. In practice however, it is not this straight forward. There are many more constituents and of each component (e.g. cement or aggregate), many types are available. Each with its own properties and fields of application.

A basic concrete mixture at least contains the following constituents:

- Cement (binder)
- Aggregate (fine and coarse)
- Water

Cement, fine aggregate & water is known as 'mortar.' Additionally, one could add:

- Admixtures and additives
- Fillers

The many different available constituents, this enables modification of the properties of the concrete. In practice, the concrete mix is altered as such that it optimally meets the requirements that are set based on the intended execution of the project and use of the structure. As written before, 'good concrete' has satisfactory properties in all its states (each state different properties being of particular relevance).

1.3.1 Cement

Although other binders are also available, cement is the most common one and will be explored in this paragraph. All cements described in this paragraph are based on Portland cement clinker unless stated otherwise. Although the amount of cement in concrete is limited in a typical mix, many properties of the concrete are determined by it, as will be seen in the remainder of the sub paragraph.

Prescribed cement types

Types of cement that are used in the Netherlands are described in NEN-EN 197-1 and the Dutch addition NEN 3550. The type of cement is denoted using a 'code', an example is used to describe this notation:

$CEM\ II/B\ -V\ 42{,}5\ N$

Where:
$CEMII$: Denotes the main type of cement:

- $CEM\ I$: Portland cement
- $CEM\ II$: Portland-composite cement
- $CEM\ III$: Blast furnace slag cement
- $CEM\ IV$: Pozzolanic cement
- $CEM\ V$: Composite cement

B: Denotes the ratio of the main components. The clinker component is denoted with A, B and C where A is the largest clinker content and C the smallest.

V: Denotes the type of second main component, some examples are:

- S: Slag
- P: Natural pozzolan
- V: Fly ash

$42{,}5$: Denotes the strength class. Distinction can be made between three strength classes: $32{,}5; 42{,}5$ and $52{,}5$.

N: Denotes the rate of the hydration process:

- L: Low rate
- N: Normal rate
- R: Rapid hydration

The strength class and rate of hydration are generally achieved by the fineness of the cement. The hydration starts at the surface of the cement particles, finer cement implies a larger surface area. That means that more material is available for hydration and the rate of hydration is therefore increased (and therefore the heat liberated as well). Note that larger cement particles may never hydrate completely.

The main type of cement that is to be selected depends on the situation. Some typical cement types that are commonly used (in the Netherlands) are:

- CEM I – Portland cement: A general cement and therefore widely used, although to a lesser extent in the Netherlands, where blast furnace slag cement is very common. A point of attention is the amount of heat liberated;

- CEM II/B-V – Portland-composite cement: Widely used in the Netherlands. The fly ash has pozzolanic properties and therefore contributes to the development of strength. This development is slower than in the case of Portland cement. This results in a reduced liberation of heat, which can be profitable for mass concrete. Moreover, in the long-term fly ash contributes to a higher density.

- CEM III/A and B – Blast furnace slag cement: Blast furnace slag cement is commonly used in the Netherlands. As mentioned before, it is very suitable for marine environment due to its high resistance to chloride ingress. The development of strength is slower than that of Portland cement, and therefore the liberation of heat is lower as well.

- Mixing types of cements: The main types of cement I up to V can be mixed, this is common practice in the Netherlands. The mixing influences the properties of the concrete and can therefore be done for different reasons.

Portland Cement

As Portland cement is widely used cement type and the main component for many other cement types, some details on Portland cement are covered in this paragraph.

Portland cement is a hydraulic binder: it reacts with water into a hardened paste (a process known as 'hydration') and does not dissolve in water after the material has hardened.

Definition of Portland cement: Portland cement is obtained by mixing silica-, alumina-, and iron oxide-bearing materials, these are burned at a very high temperature. This causes chemical reactions, eventually resulting in Portland clinker. Subsequently the clinker is ground into cement powder. Gypsum may be added to control the rate of the hardening process, but no other materials.

Production of Portland cement: The raw materials of Portland cement are:

- Marl, limestone and/or chalk (calcareous material, i.e. lime)
- Sand, clay and shale (source of silica and alumina)
- Source of iron oxide

The raw materials are ground into a fine powder and subsequently mixed. The mixture is fed into a large rotary kiln and burned at high temperature, up to 1400 degrees. Under the influence of the high temperature, chemical reactions take place.

At the lower end of the kiln, the materials recombine: they partially fuse into more complex reaction products. These reaction products form Portland clinker. After cooling of the clinker, it is ground into powder and mixed with gypsum, which is added to control the speed of hydration (it prevents flash-set of the cement). The result is Portland cement.

Chemistry of cement: The raw materials used for cement production consist sources of lime, silica, alumina and iron oxide. In the kiln, these compounds form a series of reaction products and these products together form Portland clinker. Under the assumption that chemical equilibrium is reached, also after cooling the clinker, the compound composition of Portland cement can be studied. This is required to study the hydration process later on.

The exact compound composition of the Portland cement may be determined from the quantities of the different oxides present in the clinker, this may be done using 'Bogue's equations. Note that in practice, shorthand notation is often used. That way each oxide can be described by one letter:

Table 1 Shorthand notations

Name	Notation	Shorthand notation
Lime (calcium oxide)	CaO	C
Silica (silicon dioxide)	SiO_2	S
Alumina (aluminic oxide)	Al_2O_3	A
Ferric oxide	Fe_2O_3	F
Water in hydrated cement	H_2O	H

The following four compounds are the major constituents of Portland cement, note the right-most column with the shorthand notation:

Table 2 Main compounds in Portland cement - (Neville & Brooks, 2010), p.10

Name of compound	Oxide composition	Abbreviation
Tricalcium silicate	$3CaO.SiO_2$	C_3S
Dicalcium silicate	$2CaO.SiO_2$	C_2S
Tricalcium aluminate	$3CaO.Al_2O_3$	C_3A
Tetracalcium aluminoferrite	$4CaO.Al_2O_3.Fe_2O_3$	C_4AF

An amount of gypsum is present to control the rate of the hydration. In addition, a number of minor compounds may be present, such as MgO, TiO_2, Mn_2O_3, K_2O and Na_2O.

All these different compounds considered, the following table presents the approximate composition limits of Portland cement:

Table 3 Approximate composition limits of PC - (Neville & Brooks, 2010), p.11

Oxide	Content, per cent
CaO	60–67
SiO_2	17–25
Al_2O_3	3–8
Fe_2O_3	0.5–6.0
MgO	0.1–4.0
Alkalis	0.2–1.3
SO_3	1–3

All compounds fulfil their own role in the cement:

- C_3S and C_2S: These compounds are mainly responsible for the strength of the hydrated cement paste, therefore they are the most important compounds;
- C_3A: Facilitates the combination of lime and silica, therefore it is beneficial in the manufacturing stage of cement. In cement itself, however, it does not contribute to the strength of the cement except for the early age. Moreover, if the hardened cement is attacked by sulphates it may contribute to the ettringite formation, causing damage. Therefore, its presence in cement is not desirable;
- C_4AF: Does not really affect the behaviour of cement. However, it reacts with gypsum and it may accelerate the hydration of the silicates (C_2S and C_3S);
- Gypsum: Gypsum aids in guiding the hydration process, the amount of gypsum should be as such that a desirable rate of hydration is achieved, this ensures that only a small amount of C_3A remains after all gypsum has reacted. Note that too small amount means that C_3A remains available while too much means expansion of the cement paste;
- Na_2O and K_2O: Are of importance because they may react with certain types of aggregate (alkali-aggregate reaction, which is unwanted) and affect the rate of strength development. These two compounds are often denoted as the 'alkalis.'

Hydration of Portland cement: In the presence of water, the silicates and aluminates in the cement form hydration products (hydrates). This eventually results in hardened cement paste. The reactions are:

$$2C_2S + 4H \rightarrow C_3S_2H_3 + Ca(OH)_2$$

$$2C_3S + 6H \rightarrow C_3S_2H_3 + 3Ca(OH)_2$$

$$C_3A + 6H \rightarrow C_3AH_6$$

- The silicates (C_3S and C_2S) react with water, two hydration products are formed: calcium silicate hydrates (abbreviated as CSH) and lime in crystalline form, i.e.: calcium hydroxide $Ca(OH)_2$;
- Both silicates behave pretty much in the same way, the difference being that the reaction products of C_2S contain less lime (C_3S produces almost twice as much) and C_3S reacts more rapidly than C_2S;
- C_3S contributes most to the strength development during the first four weeks while C_2S influences the strength increase after this phase. After a certain period of time the contribution of both components is about equal;
- Note that C_3S and C_2S contain impurities that have a strong effect on the properties of the hydrates. Impure C_3S and C_2S are denoted as 'alite' and 'belite' respectively;
- C_3A reacts very rapidly with water, this is called flash set. In order to prevent this, gypsum is added to the cement to react with it. But even despite this, the reaction of C_3A is still more rapid than C_3S and C_2S.

The whole process from components of raw materials to the hydration of Portland cement is summarized in Figure 6.

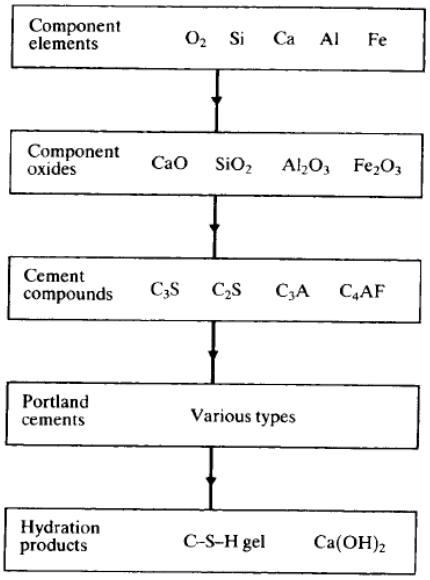


Figure 6 Formation and hydration of PC - (Neville & Brooks, 2010), p.14

Heat of hydration: Hydration of cement is an exothermic reaction. The heat of hydration may be defined as the heat that evolves during the hydration at a given temperature. The temperature at which hydration occurs affects the rate of the heat development, this is important in practice.

The heat of hydration depends on the composition of the cement and it is approximately equal to the sum of the heat of hydration of the individual components (the two silicates and the two aluminates). Note that the fineness of cement affects the rate of the heat development, but it does not affect the total amount of heat that will be produced.

Setting of cement: The setting of cement means that it changes from a fluid state into a rigid state, in other words: the stiffening of the cement paste. The setting is mainly caused by the hydration of C_3A and C_3S and it is accompanied by a rise in temperature in the cement paste as the hydration process continues.

Different cement types: In practice Portland cement is not a generic material, different cement types based on Portland cement have been mentioned before. Cements of different chemical compositions may exhibit different properties during hardening and in hardening state. That means that one may select raw materials as such that the most desirable properties are achieved for a particular case. Cement has a large contribution to the properties of concrete, but it is not the only factor though. Other cement types will be discussed in more detail in the next section.

Other cements

Blast furnace slag cement: Blast furnace slag contains lime, silica and alumina. It is a waste product and therefore its composition can vary.

Blast furnace slag is a latent hydraulic material, that means that the hydration of slag has to be initiated by an activator. Otherwise the hydration would hardly start. Portland cement is generally used as an activator. When the hydration of the Portland cement starts, the lime that is formed provides the correct alkalinity within the mixture to start the hydration of the slag.

Because of this reason, early strength of blast furnace slag cement is generally lower that of Portland cement, but later on the strength is similar. Blast furnace slag cement is regarded as a cement for general use. Typical use is for mass concrete (because it has lower heat of hydration) and structures in marine environment because of the good sulphate resistance (because of the lower C_3A content).

Pozzolans: Pozzolans are siliceous materials that react with lime and water to form compounds that process cementitious (i.e. binding) properties. Pozzolans do not react with water only (hence they are not a hydraulic

material), but they react if both water and lime are provided. In practice, lime (calcium hydroxide) is provided by the hydrating Portland cement.

Pozzolans can be both of natural or artificial origin, examples of pozzolans are:

- Vulcanic ash (original pozzolan)
- Rice husk ash
- Fly ash
- Silica fume

Two well-known examples are fly ash and silica fume, which are industrial by-products. These two will be covered in more detail.

- Fly ash: Fly ash is a by-product from coal combustion. It is a fine powder that consists of sphere-shaped glass like particles of at least the same size a cement particle. It has an amorphous structure, that means that it is non-crystalline.

  Applying fly ash results in improved workability (''ball bearing effect''). Its reaction starts relatively late, hence the hydration process is slower. Fly ash contributes to long term strength development) and therefore lower heat of hydration and results in a denser concrete (and therefore a higher strength in the end) due to its pozzolanic reaction.

- Silica fume: Silica fume is a by-product from the silicon production. It consists of small spherical shaped particles of amorphous (i.e. glass-like) silica (SiO_2). It is reactive in combination with water and the calcium hydroxide (lime) from the hydration of Portland cement.

  The reaction of silica fume starts relatively late (just like fly ash). Adding silica fume results in a very dense concrete because it fills the empty space between the cement particles, thus improving packing. This results in a denser structure and reduces bleeding. A denser structure means a stronger and less permeable concrete.

High-alumina cement: Alumina cement is not based on Portland clinker, but it is produced from bauxite and limestone or chalk. Crushing these raw materials and heating them results in a clinker with high hardness. Alumina cement is a cement type that hardens very rapidly, which is accompanied by a high rate of heat development.

Geopolymer concrete: Geopolymer concrete is a form of concrete in which no Portland cement is used. Binders such as blast furnace slag or fly ash are activated using an alkali solution.

1.3.2 Aggregate

The aggregate can be regarded as the 'skeleton' of the hardened concrete and it comprises about 75% of the concrete volume, therefore it is of great importance for the quality of the concrete. The properties of the aggregate affect for example:

- Concrete strength
- Durability
- Structural performance

Different properties are relevant at different stages:

- Fresh concrete: Grading and particle size are important for the workability
- Hardened concrete: Bond and strength of the particles are important for the strength

Origin of aggregate

Aggregate may originate from various sources, the type of aggregate and its properties depend on the source.

- **Natural sources**: Mining from quarries or material obtained from river or sea are the main sources of natural aggregate. Natural aggregates are formed by weathering and abrasion (or by crushing, which is artificial) and that means that many properties of the aggregate depend on the type of rock from which it is, e.g. hardness, pore structure and colour. Other properties depend on for example the processing and weathering (particle shape and size, texture of the aggregate…). All these properties may influence the quality of both the fresh and hardened concrete.

- **Heavy materials**: Heavy aggregate (this can be both natural materials like basalt and by-products from industry) can be used for structures where high mass is needed, e.g. for shielding.

- **Lightweight material**: Lightweight aggregate can be both artificial- or natural material (e.g. expanded clay or pumice) and can be used if a light weight structure is to be constructed.

- **Recycled material**: Demolition waste can be used as a source of aggregate for new concrete: recycled aggregate. To produce this, the old concrete is crushed to obtain particles of right size. Shape and texture are also to be taken into consideration.

  When using recycled concrete aggregate for new concrete, there are some specific points that should be taken into consideration. The material contains hardened cement paste, which affects porosity, absorption and density. Moreover, the strength of the old concrete partially controls the strength of the new material, as well as other properties, e.g. freeze/thaw due to the void system of the old concrete. In addition to this, the recycled aggregate might be unsuitable if it contains harmful substances or if it has been subjected to for certain deterioration mechanisms during the surface life of the old structure.

The remainder of this subparagraph focusses on natural aggregates.

Classification of aggregate

It is difficult to state when aggregate is suitable for concrete. Aggregate with good properties means that it will result in good quality concrete, but aggregate with a property that might not be optimal does not mean that the concrete will be of bad quality. However, aggregate with multiple bad properties cannot be expected to result in good quality concrete.

This illustrates the importance of testing and classifying aggregates. Aggregate can be classified according to a number of classifications, which helps in obtaining a number of its properties. Moreover, to test for the suitability of the material, different types of tests can be performed.

Size classification: Concrete is made with particles of a whole range of different sizes. Typically, the maximum particle size is 10-50 mm, depending on the concrete type. Distinction is often made between fine aggregate and coarse aggregate.

Petrographic classification: Aggregate may be classified based on petrography, see Figure 7. Many properties can already be deduced by looking at the parent rock: aggregates can be divided into distinct groups of rocks, each group having common characteristics.



Figure 7 Petrographic classification – (Ye & Schlangen et al., 2018)

Classification shape and texture: The shape and texture are important parameters as they influence properties of both the fresh and hardened concrete.

- Classification based on shape is possible by using the notions notion 'roundness' and 'sphericity'. Roundness is a measure for the angularity of the edges of a piece of aggregate, an example of such a classification is given in Table 4.

Table 4 Particle shape classification - (Neville & Brooks, 2010), p.43

Classification	Description	Examples
Rounded	Fully water-worn or completely shaped by attrition	River or seashore gravel; desert, seashore and wind-blown sand
Irregular	Naturally irregular, or partly shaped by attrition and having rounded edges	Other gravels; land or dug flint
Flaky	Material of which the thickness is small relative to the other two dimensions	Laminated rock
Angular	Possessing well-defined edges formed at the intersection of roughly planar faces	Crushed rocks of all types; talus; crushed slag
Elongated	Material, usually angular, in which the length is considerably larger than the other two dimensions	—
Flaky and Elongated	Material having the length considerably larger than the width, and the width considerably larger than the thickness	—

- The influence of the shape on the workability and end product is illustrated in Figure 8. Elongated and flaky particles are known to lower the workability of the concrete mix. Moreover, flaky particles may affect the durability in a negative way, as voids may form underneath these particles. Shape and texture influence the water requirement of the concrete mix, especially fine aggregate.

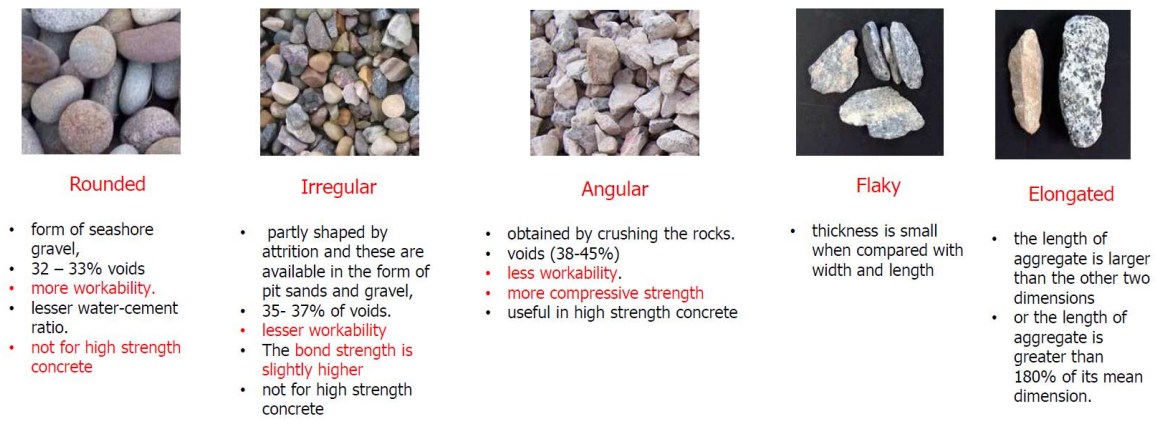


Figure 8 Properties of particles with certain shape classification – (Ye & Schlangen et al., 2018)

- Next to 'roundness' another aspect of the shape of aggregate is called 'sphericity', which may be defined as the ratio of surface area of a particle versus its volume.

- Classification based on surface texture is performed by studying the texture and subsequently describing the roughness of the particles, an example of a classification based on the surface texture is given in Table 5.

Table 5 Surface texture classification - (Neville & Brooks, 2010), p.45

Group	Surface Texture	Characteristics	Examples
1	Glassy	Conchoidal fracture	Black flint, vitreous slag
2	Smooth	Water-worn, or smooth due to fracture of laminated or fine-grained rock	Gravels, chert, slate, marble, some rhyolites
3	Granular	Fracture showing more or less uniform rounded grains	Sandstone, oolite
4	Rough	Rough fracture of fine- or medium-grained rock containing no easily visible crystalline constituents	Basalt, felsite, porphyry, limestone
5	Crystalline	Containing easily visible crystalline constituents	Granite, gabbro, gneiss
6	Honeycombed	With visible pores and cavities	Brick, pumice, foamed slag, clinker, expanded clay

It must be noted that, for example, the classification of the roundness or surface texture tell about many properties of the parent rock and abrasion of the aggregate. For example: The roundness of a particle depends on the strength of the parent rock, the resistance to abrasion and the wear imposed upon the piece of aggregate. Surface texture depends on factors such as hardness and pore characteristic of the parent rock, etc. Therefore, relatively 'simple' ways of classifying result in a lot of usable information.

Mechanical properties of aggregate

Important mechanical properties of aggregate are:

- Bond
- Strength
- Toughness
- Hardness

Bond: The bond between the aggregate and hardened cement paste is essential for the strength of the hardened concrete: better bond means stronger concrete. Rougher texture and surface that permits penetration of the aggregate particles by the cement paste means better bonding between particles and cement.

Strength: The strength of the aggregate particles is an important factor in determining the compressive strength of the concrete. Information about the strength may be obtained by determining the crushing strength, however, this is a difficult parameter to determine.

The required aggregate strength for concrete is higher than the strength of the hardened concrete because local stresses at contact points between the aggregate particles may exceed the nominal compressive stress in the hardened concrete.

Toughness: The toughness of aggregate may be defined as the resistance of aggregate to impact loads. The toughness is related to the crushing strength.

Hardness: The hardness of aggregate may be defined as the resistance to wear. It is especially important for aggregate used in concrete that will be subjected to traffic load, for example concrete road surfaces.

Physical properties of aggregate

Specific gravity: The most general definition of specific gravity is the ratio of the density of a certain material to the density of a reference material. In the case of concrete, many definitions are used:

- Absolute specific gravity and particle density: Refer to volume of the solid material excluding all pores;

- Apparent specific gravity and apparent particle density: Refer to volume of solid material including the impermeable pores but does not include the capillary pores. Most natural aggregates have an apparent specific gravity of 2,6-2,7.

In practice the bulk specific gravity and bulk particle density are values that are often used for calculating the yield of concrete or the amount of aggregate required to produce a certain volume of concrete.

Bulk density: Because aggregate consists of particles, there are always voids present. That means that when working with volumes of aggregate, bulk density is to be used (instead of absolute density, which refers to individual particle). Bulk density depends on the size distribution, particle shape and compaction. The higher the bulk density, the smaller is the remaining volume of the voids and, therefore, the smaller is the required amount of cement paste to fill these voids.

Porosity and absorption: Porosity, permeability and absorption are notions that are related to one another and they influence a number of factors:

- Bond of aggregate and cement paste
- Resistance of concrete to freeze and thaw cycles
- Chemical stability
- Resistance to abrasion
- Specific gravity

The pores in aggregate have different sizes (although even the smallest pores in aggregate are larger than the gel pores in the aggregate) and the amount of these pores opening onto the surface of the aggregate particles determines the permeability and absorption of the aggregate.

Depending on how the water penetrates into the particles and the subsequent amount of water in the pores, one may distinguish between moist (pores are filled with water and free moisture is present on the surface), saturated and surface dry (SSD, all pores in the aggregate are filled with water), air dry (aggregate is left in dry air so moisture will evaporate) or oven dry aggregates (after drying in an oven to remove moisture completely).

Moisture content: A term related to the porosity and absorption of moisture is the notion of 'moisture content', which is defined as the water in excess of the saturated and surface-dry aggregate.

A reason of why the moisture content is important, is because of the composition of the concrete mix. Stored aggregate may collect moisture, e.g. due to rain, and keep this over a long time. If this is not considered, this may result in a significant increase of the amount of water added to the concrete mix.

Thermal properties: From the thermal properties of aggregate, the coefficient of thermal expansion is generally of large significance because it is the dominant factor in determining the coefficient of thermal expansion of concrete, though the magnitude of its influence depends on the composition of the concrete mix. Typical values for the coefficient of thermal expansion of natural aggregate is between $5 * 10^{-6}$ and $13 * 10^{-6}$ per °C

Sieve analysis

As mentioned in the introduction to aggregates, grading and particle size of the aggregate are important for the workability of the concrete mixture. The goal is to achieve a practical grading that provides a mix with good workability and minimum segregation.

Sieve analysis can be performed to determine the grading or size distribution of the aggregate. It means that the aggregate sample is divided into fractions of the same particle size. The results may be presented in a grading curve, which presents the cumulative percentage of particles passing the sieve of particular size.

Strength is independent of grading, its importance is because of the workability. However, there is a relation between strength and grading. High strength requires good compaction and good compaction can only be achieved if a workable concrete mix is applied.

Harmful particles and substances

It is to be avoided that certain harmful substances are added to the concrete via the aggregate, some typical examples are:

- Impurities that negatively affect the hydration process of the cement, e.g. organic matter;
- Surface coatings preventing the bond between the cement paste and aggregate, e.g. clay;
- Weak particles in the aggregate, e.g. shells;
- Salts causing corrosion of reinforcement, e.g. in aggregate from the sea.

1.3.3 Mixing water

The mixing water should be suitable for use, that means that it should not contain substances that might interfere with the hydration process or may influence the durability of the hardened concrete, such as:

- Substances interfering with the setting or affecting the strength of the material;
- Substances causing staining of the concrete or corrosion of the reinforcement.

A practical example of when to be careful is seawater, which may cause efflorescence and increase the risk of corrosion of the reinforcement because of the chloride content. A rule of thumb is that water fit for drinking is also fit for mixing, although this is not always the case.

Note:

- Surface moisture in the aggregate is also added to the concrete mix if this aggregate is used, which can make up considerable portion of the total water within the concrete mix (25-30% of the total water content of the concrete mix assuming average values for the water moisture content of aggregate);

- This water might contain impurities and might result in having to correct the values of the water content in the mix design;

- In addition to water for mixing, water for curing might be required as well. Generally speaking, water suitable for mixing is also suitable for curing.

1.3.4 Admixtures and additives

Admixtures and additives can be used to change the properties of cement or the concrete mix. A property of admixtures is that they already result in significant change of the property of the fresh concrete or hardened concrete if they are added in small quantities (equal to or less than 5% of the mass of the cement).
Distinction can be made between:

- Additives: Substances added at the cement manufacturing stage;
- Admixtures: Substances added at the mixing stage.

There is a wide variety of admixtures and additives available. Distinction can be made between different 'categories' of admixtures, admixtures can be categorized to the effect that they have. Each admixture has its own field of application and purposes, for example:

- Plasticizers
- Super plasticizers
- Set-retarders
- Accelerators
- Air-entrainer

Plasticizers

Plasticizers can be used for multiple purposes:

- Achieving a higher compressive strength by decreasing the water/cement ratio whilst keeping the same workability;
- Decreasing the cement content in order to reduce the heat of hydration (for mass concrete) whilst achieving the same workability;
- Increase the workability for casting and processing concrete at inaccessible locations.

The effect of plasticizers is based on surface-active agents that are absorbed on the cement particles, and that give these particles a negative charge. As a result, repulsion occurs between the different cement particles. This way the cement particles have greater mobility and water becomes available to lubricate the particles in the concrete mix. The result is an increase in workability.

A potential side effect of this admixture is that the early age strength increases compared to plasticizer free mixture with the same water/cement ratio. This effect is contributed to the dispersing ability of these admixtures, as a result of this a larger surface of the cement particles becomes available for hydration. Long term properties are not really changed but if they are, durability might improve due to these admixtures. Possible negative side effects are entraining too much air within the concrete or an increase of bleeding.

Superplasticizers

Superplasticizers are more effective plasticizers, there are a few typical situations in which the application of superplasticizers can be beneficial:

- In the case concrete has to be flowable, e.g. for inaccessible locations due to large amounts of reinforcement;
- For very-high strength concrete, superplasticizers allow for achieving normal workability while the water/cement ratio is very low.

In the next chapter it will become clear that the development of superplasticizers has been essential for the development of UHPC mixtures.

Set-retarders

Set-retarders delay the setting (i.e. the stiffening) of concrete. This is useful if the normal setting is affected (accelerated) by for example higher ambient temperature.

Generally speaking, a delay in hardening also occurs if set-retarders are used. Retarders reduce the early age strength, but the long-term strength is not really different compared to set-retarder free mixture.

Accelerators

Accelerators are used to accelerate the hardening/development of early strength of the concrete. Although the setting of the concrete might be increased as well, accelerators meant to accelerate hardening of the concrete are not specifically meant for this. Distinct set-accelerating admixtures are also available, these are specifically developed to reduce the setting time.

Air entrainer

Air entrainers are used to add a certain amount of air into the concrete mix. Empty space is created within the concrete, this helps in increasing the freeze/thaw resistance as ice being formed within the concrete may expand into the air bubbles. Moreover, cohesion is improved using air entrainer and bleeding is reduced.

General remark

As described in this paragraph, there are many different admixtures available. Each one has its own field of application and its own effects. Apart from the effect the admixture is used for, side effects may occur as well. Moreover, if multiple admixtures are used within a single mix, admixtures might influence one another.

These two remarks might raise questions in practice. Therefore, when in doubt, trial mixes should be made using the admixture or combination of admixtures with the actual concrete mix that is to be used.

1.3.5 Fillers

Fillers are finely-ground materials that have beneficial effects on the properties of the concrete, for example of the density. The contribution of fillers is usually physical, as most fillers are chemically inert, but not all of them are because certain materials can also act as a binder. The following distinction can roughly be made:

- Inert fillers and pigments
- Fillers acting as binder

Inert fillers: These fillers are added to give the concrete more consistency and stability or to increase the density. An important property for fillers is that they should have uniform properties, e.g. with respect to fineness and particle size.

Pigments: Pigments are used to give colour to the concrete, but except for this they do not contribute in another way. Therefore, they may be regarded as inert filler.

Fillers acting as binder: A number of fillers is available that can be used as a binder. Examples of this are blast furnace slag, fly ash and silica fume. In this context they are often denoted as 'mineral admixtures.' These materials contribute to a higher density but because they are also latent hydraulic or pozzolanic materials, they may be used to replace a part of the Portland cement within the mixture.

1.4 Concrete Technology: Strength of hardened concrete

In the case of concrete in its hardened state, the material is often described and classified using its 28 days compressive strength, this is done because the compressive strength is relatively easy to determine and provides a way of measuring the concrete quality because many properties are related to the compressive strength, for example:

- Tensile strength
- Density
- Durability
- Permeability and resistance to chlorides

This is reflected in the codes, where many quantities can be calculated immediately from the values for the compressive strength, although in reality it is not true that the aforementioned quantities are only a function of the concrete compressive strength. The concrete compressive strength is often regarded as the most important property of hardened concrete (even though other properties such as durability might be more important in practical applications) because it is directly related to the microstructure of the hardened cement paste. Because it is also relatively easy to determine, this makes the compressive strength into a practical way of determining the overall quality of the material.

Because of its importance in practice and its importance for this thesis (as (ultra) high strength concrete will be discussed later), the concrete compressive strength and the concrete tensile strength will be further analysed from a concrete technology point of view in this chapter, to find out what factors determine these quantities and in order to be able to understand later how high strength concrete 'works' from a concrete technology point of view.

1.4.1 Importance of concrete compressive strength

''Sources of weakness'' in hardened concrete

The strength of hardened concrete depends for a large part on the structure of the hydration products of the cement. If this is analysed, discontinuities and pores can be seen. These are sources of weakness in the

structure of the hardened cement paste, influencing the strength in a negative way. A notion related to this is porosity, which may be defined as the relative volume of pores and voids in the cement paste.

There is another source of weakness, which comes from the aggregate particles. These particles may contain flaws and give rise to microcracking at the interface between the particles and the hardened cement paste.

A practical problem is that it is difficult to quantify the porosity of cement paste or microcracking. Therefore, empirical studies have to be performed to study the effects of different factors on the strength of hardened concrete. From this, two conclusions can be drawn:

- The water/cement ratio is the most important factor in determining the concrete strength
- There are other factors that influence strength, but their influence is less significant

In the subsequent sections, tensile failure, compressive failure and influencing factors regarding the strength of concrete will be covered.

Tensile strength

The discussion is started by only looking at the cement paste. Aggregate particles are omitted until further notice. The actual strength of the hardened cement paste is limited due to the presence of 'weak points' in the structure such as cracks. It should be noted that these weaknesses are already present before load is applied to the material.

When loaded, cracks result in stress concentrations at their tips, and this can result in growth of the crack (localized fracture near the crack tip) even if the nominal stresses on the material are low. The 'worst case scenario' is the situation where the crack is perpendicular to the direction of the load and a crack which is long and sharp. In this case the stress concentration will be at its largest. If the load acting upon the material increases, the stress at the crack tip also increases until it reaches the stress at which the material fails (the brittle fracture strength). If this happens, the crack grows.

According to the fracture theory, energy is stored in the material and it is released if the crack grows. Moreover, the largest crack normal to the load initiates failure. In a brittle material, the energy that is released at the onset of the propagation of the crack is sufficiently large to result in failure of the whole cross section (a so called 'brittle failure') because the maximum stress value at the tip increases if the crack length increases.

In reality however, this 'truly brittle behaviour' may not occur. Certain 'obstacles' could put the propagation of the crack to a hold, for example an unhydrated cement particle or a piece of more ductile material that requires more energy to cause fracture.

In reality, concrete does not only consist of cement paste, but also aggregate is present and the situation is more complicated than explained so far:

- There are cracks from various sources. The presence of aggregate for example is also liable to initial microcracking. In the end, the concrete is therefore not as strong as only the cement paste.

- All different cracks with their different sizes, lengths and orientation are distributed in the concrete in a random manner.

- The stress distribution does not have to be uniform, and the propagation of a crack might be stopped by surrounding material that is subjected to lower stress. This implies that the load has to be increased up to the point where a different crack also starts to propagate etc. Eventually, multiple cracks will grow together, resulting in the failure of the cross section.

In short: Microcracks are already present in the material from the start, both due to weak points in the matrix and due to the aggregate. If the structure is loaded, even by a low nominal stress, stress concentrations

occur due to these cracks. If the load becomes sufficiently high, these cracks will start to propagate. The loading is probably non-uniform in practice, and the microstructure is complex (random distribution of all the cracks) and as a result multiple cracks propagate if the load is continuously increased. Eventually, these cracks link together and will result in the failure of the cross section.

When failure occurs, the failure path typically goes through the cement paste, following the interfaces of the larger aggregate particles. A typical failure path of concrete under tension is depicted in Figure 9.

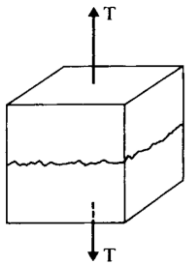


Figure 9 Failure pattern tensile failure - (Neville & Brooks, 2010), p.98

Compressive stress

Even if the specimen is loaded in compression by the external load, tensile stresses occur within the material and in combination with the already present microcracks and other flaws within the structure this results in propagation and eventually failure of the specimen. This principle is depicted in Figure 10.

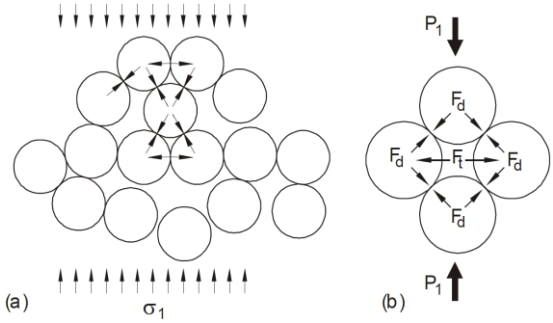


Figure 10 Failure of concrete loaded in 1D compression - (Ye & Schlangen et al., 2018)

The failure is caused by splitting forces (these tensile forces are the driving forces for the failure) between the stacked particles resulting in failure of the material. The microcracks (and other weak points in the material) are the locations where failure is initiated. If the load is increased, the cracks grow, eventually grow together into macrocracks and this results in failure. Depending on the loading (uniaxial or biaxial) typical crack patterns are formed. Note that triaxial loading works differently: crushing occurs.

- **Uniaxial compression**: Cracks are formed parallel to the load (caused by local tensile stress in the direction normal to the compression) and some inclined (development of shear plane). The failure is explained by Figure 10 and a typical failure pattern is depicted in Figure 11.

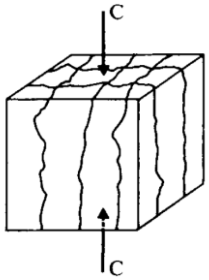


Figure 11 Failure in uniaxial compression – (Neville & Brooks, 2010), p.98

- **Biaxial compression**: If the specimen is subjected to biaxial compression, failure occurs in one plane parallel to the load, see Figure 12.

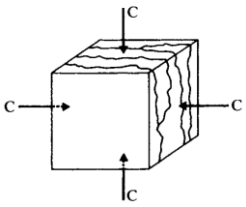


Figure 12 Failure in biaxial compression – (Neville & Brooks, 2010), p.98

The stress state resulting in failure is clarified by Figure 13.

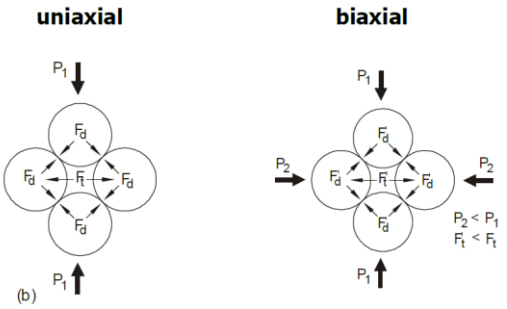


Figure 13 Uniaxial vs biaxial failure – (Ye & Schlangen et al., 2018)

- **Triaxial compression**: In the case of triaxial compression, a completely different failure mechanism occurs. Failure no longer takes place due to brittle fracture, but due to crushing of the material instead.

Limiting strain: The previous discussion is based on the assumption that the strength of concrete is limited by a maximum stress value, but in reality this might not be the case and the real real failure criterion might be the limiting strain. The higher the strength of the concrete, the lower the strain at failure and a practical value for normal strength concrete is 3,5 promille compressive strain at failure (a value typically used in design with normal strength concrete).

Failure criterion: As can be seen from the previous discussion, strength is also a funciton of the system of stresses that acts at the concrete specimen. Different values may be measured if different possible stress combinations act at the specimen, each combination has its own distinct failure criterion.

Setup of the compressive test

One should note that the previous figures are made under the assumption that there is no restraint acting upon the specimen during a compressive test. In reality however, such a restraint is usually present and this affects the test results. This can be seen in Figure 14.

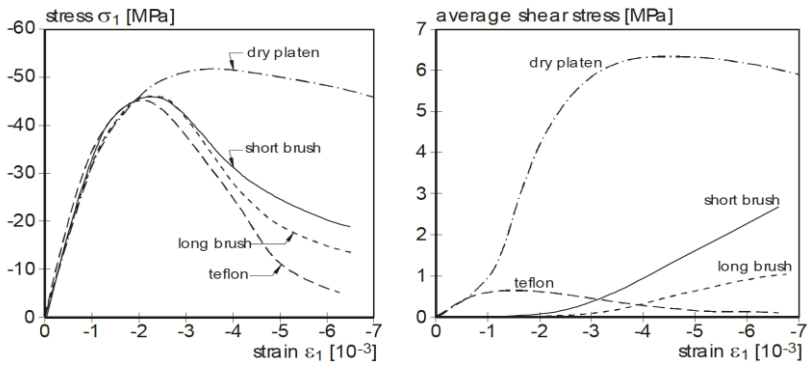


Figure 14 Effect of boundary friction in uniaxial compression - (Ye & Schlangen et al., 2018)

One may observe that the larger the friction (thus the larger the restraint), the larger the measured load on the specimen. This is explained as follows: When the cube is loaded in compression, it wants to expand sideways (Poisson ratio). Due to the restraint however, stresses develop that ''support'' the concrete: tensile cracks will develop at a higher load.

This effect can be mitigated by either selecting a material to reduce friction or by using a specimen with length to width ratio larger than two (this way the middle of the specimen is not affected by the 'restraining effect').

1.4.2 Strength of hardened concrete – Porosity

Effect of porosity on hardened cement paste

As mentioned in the introduction, the strength of concrete is influenced by a number of factors. These factors are difficult to quantify, let alone to combine them into an equation that can be used to determine the strength of the material. It was concluded that empirical studies have to be performed to study the effects of different factors on the strength of concrete. That means that these factors have to be identified first, the most important factor will be elaborated on in this sub paragraph:

- As it turns out, the water/cement ratio is the most important factor because it determines the porosity (the volume of pores and voids in the cement paste) of the hardened cement paste.

First the cement paste only is assessed. Before hardening, the fresh cement paste is a mixture of cement particles and water. The paste starts to set and its gross volume remains about constant after this. Products of hydration are formed that make up the structure of the hardened cement paste: the hydrates of the cement and $Ca(OH)_2$. The volume which is available for these hydration products is the sum of the initial volumes of the cement and water.

The hydrated cement is also called 'cement gel' and it consists of:

- Solid hydration products
- Gel water

Due to the hydration process, the mix water is present in the hardened cement paste in one of the following three forms:

- Combined water: Combined water is the water combined with the hydration products. it is held very firmly and does not evaporate.

- Gel water: Gel water is the water held or absorbed by the surface of the hydrates and is located in the gel pores (the area between the solid hydration products).

- Capillary pore water: Capillary pore water is the water present in the residual space (the capillary pores).

The pores within the structure of the hardened paste can be divided into two types:

- Gel pores: Very small and impermeable pores located between the hydration products

- Capillary pores: Larger and permeable pores, this is the residual space because the products of hydration occupy a smaller volume than the original cement and water. These pores may be full or empty with water, depending on the amount of mix water.

Some residual space will always be formed because of the difference of volume between the products of hydration and the initial volume of cement and water and typically this residual space is about 18,5% of the initial volume of the dry cement. However, if more water is added to the mix than required for full hydration

of the cement, additional capillary pores will be formed. A diagram presenting the volumetric proportions before and during the hydration process is given in Figure 15.

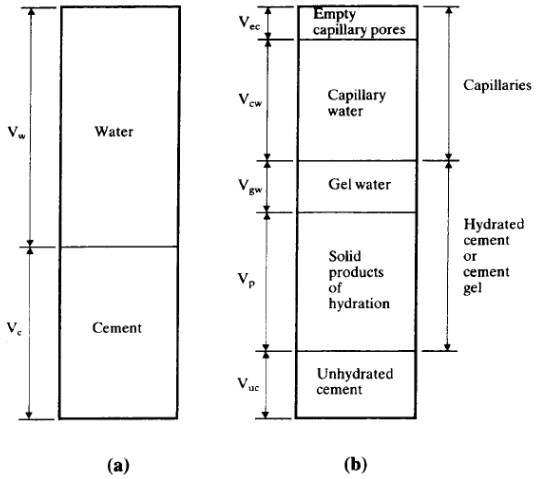


Figure 15 Volumetric proportions before (a) and during (b) hydration - (Neville & Brooks, 2010), p.101

It should be noted that a certain minimum water/cement ratio is required to be able to achieve full hydration of the cement. This is because sufficient space is required to accommodate the hydration products and the pores should contain enough water required for the reactions and to obtain sufficiently high relative internal humidity, to allow for these reactions to take place.

From the considerations up to now it is clear that the water/cement ratio is an important factor because it determines the porosity. However, it is not the only factor that influences the porosity because it actually depends on two factors:

- The water/cement ratio: Higher water/cement ratios than required for full hydration result in higher porosity;
- The degree of hydration: A higher degree of hydration means that more reaction products have been formed, the smaller the volume of pores.

Note that in practice air might be entrapped as well into the material if it is not fully compacted, this results in higher porosity.

The water/cement ratio has now been related to the porosity of the hardened cement paste and there is a corresponding relation between the porosity and the strength of the material. Figure 16 shows the relation between porosity and strength of hardened cement paste. One may observe that very high strength values have been obtained. This was made possible by special treatment which was applied to the material to obtain good compaction at a very low water/cement ratio.

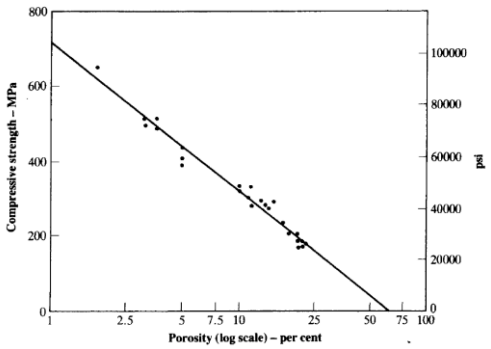


Figure 16 Relation of compressive strength and porosity - (Neville & Brooks, 2010), p.106

Effect of porosity on hardened concrete

The effect of the volume of voids on the strength of hardened cement paste has now been discussed and the step can be made to look at the effect of the volume of voids on the strength of hardened concrete. To give an indication of the volumetric proportions, Figure 17 presents the proportions of a concrete mix before and during hydration.

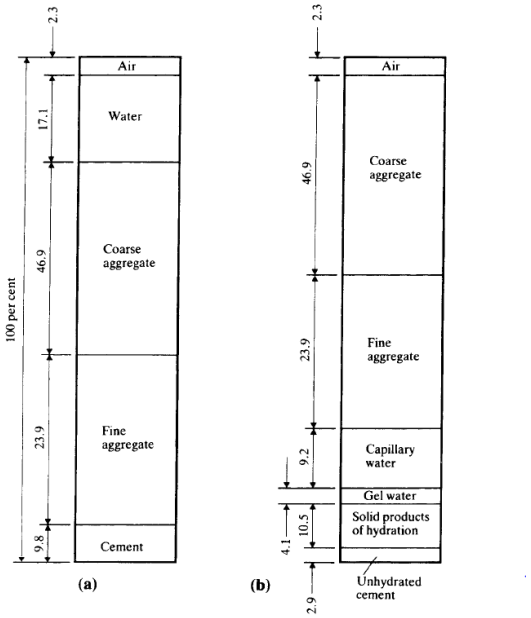


Figure 17 Proportions concrete mix before (a) and during (b) hydration - (Neville & Brooks, 2010), p.110

From this discussion one may conclude that if the porosity of the total concrete mixture is decreased, the strength of the concrete mixture will increase as well.

1.4.3 Strength of hardened concrete – Pore size and microcracking

In the previous sub paragraph, the influence of the water/cement ratio has been discussed extensively, because it is the main influencing factor of concrete strength: it controls the underlying parameter of porosity. However, it is not just the total volume of the pores that is relevant. The features of the pores are also influencing factors of the concrete strength:

- Pore size distribution
- Microcracking and stress-strain relation

Pore size distribution

Hardened cement paste contains pores of many different sizes but a rough distinction can be made between capillary pores and gel pores, also see Figure 18:

- Gel pores: Very small, impermeable pores
- Capillary pores: Much larger than gel pores and therefore permeable

If the capillary pores form a system of interlinked pores, this results in a lower strength and a reduced durability, this typically happens at a lower degree of hydration. If the degree of hydration is sufficiently high, the capillary pore system is divided due to newly formed hydration products that are blocking the way and the capillary pores are only interconnected by the smaller impermeable gel pores.

Designation	Diameter	Description	Affected
Capillary pores	50 nm to 0.5 µm	Large capillaries	Strength, permeability
	10 to 50 nm	Medium capillary	Strength, permeability, shrinkage at high humidity
Gel pores	2.5 to 10 nm	Small capillaries	Shrinkage to 50% RH
	0.5 to 2.5 nm	Micropores	Shrinkage, creep
	<0.5 nm	Micropores (interlayer)	Shrinkage, creep

Figure 18 Classification of pores in hydrated cement paste - (Ye & Schlangen et al., 2018)

Microcracking and stress-strain relation

Up until now the focus was on the hardened cement paste and the volume of voids in it, and therefore the volume of voids in the concrete.

In reality, this is not the full story because aggregate particles also contribute via microcracks (bond cracks) at the interface between the aggregate particles and the hardened cement paste. These cracks occur even before the load is applied, they are the result of difference in properties of the aggregate and cement paste, e.g. differences in stress-strain relation of the aggregate particle and the cement paste. These cracks are initially stable and only start to propagate if the load becomes sufficiently high (approximately 30% of the ultimate strength). In the following sections, the effects of these microcracks will be elaborated on.

Stress-strain curve uniaxial compression – constant increase of stress

Suppose that cement paste, aggregate and concrete specimen are loaded in compression and the stress is gradually increased. A stress-strain diagram is plotted, see Figure 19.

The effect of the microcracks is clearly noticeable in Figure 19, which shows the stress-strain relationship for the cement paste, aggregate particles and the concrete. The first two are characterised by a linear curve while the third is not. This is explained by the propagation of the microcracks which is initiated at a load of about 30% of the ultimate strength.

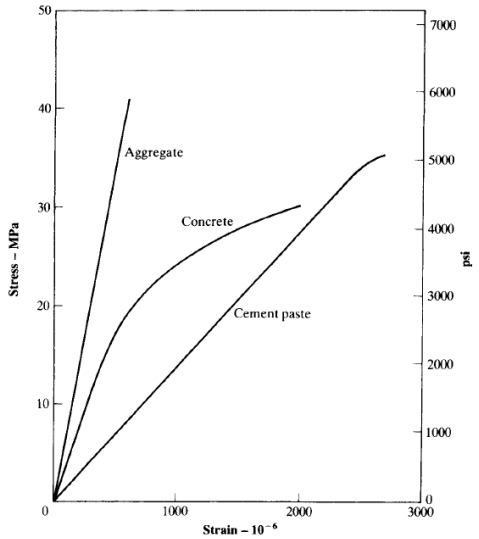


Figure 19 Stress-strain relations for cement paste, aggregate and concrete - (Neville & Brooks, 2010), p.113

One may study the effect of these microcracks by looking at a loaded specimen and distinguishing two phases until eventually failure occurs:

- Slow propagation: As soon as the 30% threshold is reached, the microcracks propagate, become wider and increase in number and as a result the strain increases faster than the stress; the curve flattens. Note that under a sustained load, the cracks are stable until creep starts to play a role. The propagation of microcracks allows concrete to redistribute high local stresses.

- Fast propagation: At a certain point (70-90% of ultimate strength) the cracks open up and grow together through the mortar.

- Failure: If the load is sustained long enough (static fatigue) or if the load is increased further, the specimen will fail.

Note: The previous graph shows the axial compressive strain under a load that is increased until failure. If the lateral strain is measured, one may observe extension of the specimen in lateral direction. Up to about 30% of the ultimate load, the Poisson's ratio is constant. If the load is increased further, the Poisson ratio increases (and so does the volume) and it increases slowly up to 70-90% of the ultimate strength is reached, when it suddenly increases rapidly. This behaviour can all be explained by the formation and growth of the microcracks. See also Figure 20

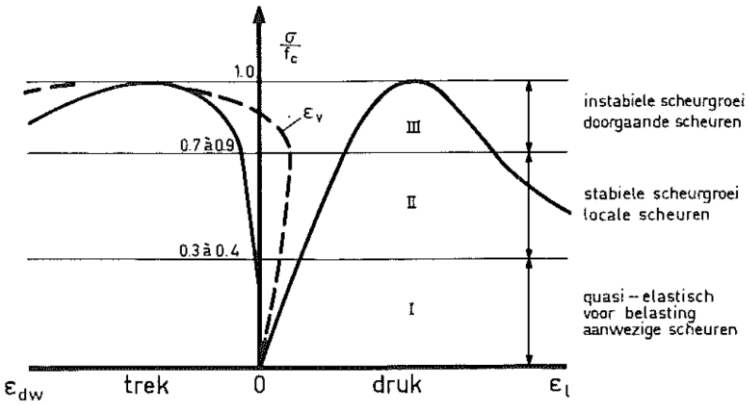


Figure 20 Stages of crack growth - (Ye & Schlangen et al., 2018)

Stress-strain curve uniaxial compression – constant increase of strain

Suppose that a concrete specimen is loaded in compression, but this time it is loaded at a constant strain rate instead of constant stress rate (see Figure 19, which is done for standard compression tests). A different graph is obtained, see Figure 21.

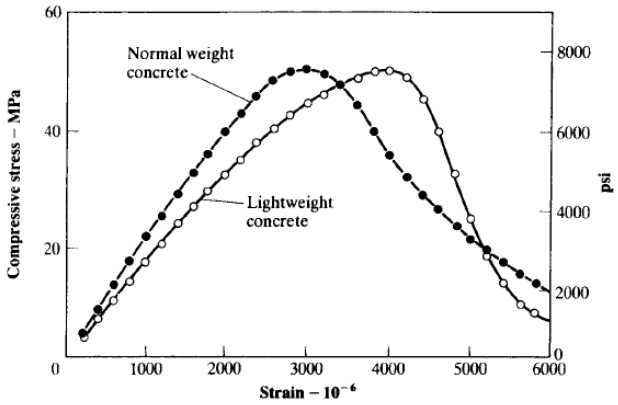


Figure 21 Stress-strain diagram – (Neville & Brooks, 2010), p.115

Important observations can be made:

- The descending branch after the peak implies that the concrete is still able to withstand a certain load after the maximum load was passed. This can again be explained by the microcracks: the linking of these cracks is delayed before complete failure.

- Note that a steeper curve implies more brittle behaviour of the material. Therefore, one may expect high strength concrete to have a steeper curve (both the ascending and descending branch).

The area enclosed by the curve is the fracture toughness, which is the work required to cause failure of the specimen.

1.4.4 Practical factors influencing the strength of hardened concrete

So far it has become clear that the primary underlying factor for strength is porosity, while other factors such as pore size distribution and microcracking contribute as well, albeit to a lesser extent. It was also stated that these properties are difficult to quantify and thus difficult to work with. Therefore, more practical factors are used in practice. These 'practical factors' influence the 'underlying factors' of porosity, pore size distribution and microcracking.

The primary 'practical' influencing factors on the strength are:

- Water/cement ratio
- Degree of compaction
- Age
- Temperature

Other 'practical' influencing factors of lesser importance:

- Aggregate/cement ratio
- Properties of the aggregate (shape, texture, strength, stiffness, particle sizes and grading)
- Transition zone (interface aggregate and cement paste)

In the remainder of this paragraph these different factors will be discussed in more detail.

Water/cement ratio, degree of compaction, age and temperature

The 'practical' factors of water/cement ratio, degree of compaction and age & temperature influence the underlying factor of porosity. The lower the porosity, the stronger the concrete. The influence of the water/cement has already been discussed.

Better compaction means more dense concrete and hence higher strength. In practice however, some entrapped air will almost always be present. Assuming full compaction and keeping age and normal temperature equal, the strength of the concrete is inversely proportional to the water/cement ratio, this is known as 'Abrams' law'. Figure 22 presents the relation between compressive strength, water/cement ratio and the influence of compaction.

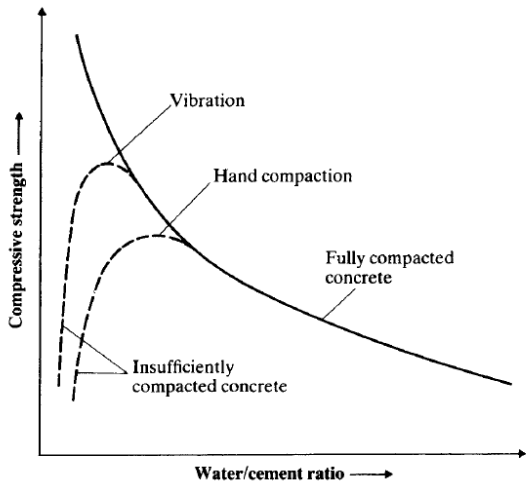


Figure 22 Relation strength and water/cement ratio - (Neville & Brooks, 2010), p.117

The water/cement ratio and degree of hydration determine the porosity of the cement paste. A lower water cement ratio and a higher age (thus increase in degree of hydration) therefore implies an increase in

strength. Note: Aggregate uses some water to reach SSD condition at time of mixing. The strength depends on the effective water/cement ratio, which is the mix water minus the water used up by the aggregate.

Aggregate/cement ratio

Keeping the water/cement ratio constant, a higher aggregate/cement ratio (a ''leaner mix'') results in higher strength. This is because the cement paste is a smaller portion of the total concrete volume: the total void volume in the concrete is lower and therefore the strength is higher.

Aggregate properties

More rough and angular aggregate provides better bonding and less microcracking. This results in the observation that cracking occurs at higher stresses than in the case of more smooth and rounded aggregate.

Transition zone

The transition zone is the interface between the aggregate particles and the hydrated cement paste. The transition zone generally has higher porosity than the hydrated paste further away from the aggregate. As a result, the transition zone is of lower strength. Some aggregates produce a more dense (thus stronger) interface than others. Pozzolanic materials such as silica fume can contribute to an increase in strength of this zone over time because these materials react with $Ca(OH)_2$ released by the hydration of Portland cement.

1.5 Concrete and sustainability

1.5.1 Durability versus sustainability

When studying concrete and its impact on and relation to the environment, a distinction can be made between durability and sustainability. A somewhat ''loose'' definition for these two notions in relation to concrete structures is given below:

- **Durability:** The concept of a structure functioning for a long period of time (service life) under expected external influences (loads, environmental influences) without requiring excessive maintenance.

- **Sustainability**: The concept of characterizing a structure or object based on its impact on the environment.

A well-designed concrete structure is durable, that means that it fulfils its function for a long period of time (at least the intended service life) with only limited (periodical) maintenance. To achieve such a well-designed structure, the situation under which the structure will have to function as well as possible deterioration mechanisms that may occur as a result of this should be kept in mind. This can be taken into consideration via the environmental classes, to specify the ways the direct environment affects the structure. Apart from durability, sustainability is also to be considered. This will be done in the remainder of this paragraph.

1.5.2 Sustainability of concrete

As mentioned in (Braam, Lagendijk, Soen, & Linssen, 2015), the annual concrete production in the Netherlands is 14 to 15 million m^3 of concrete. Given the importance and the quantity of the material, it is clear that the sustainability of concrete is an important factor. The sustainability is commonly expressed using CO_2 or equivalent CO_2 values. Some important notions are:

- **CO_2 emission**: The amount of CO_2 released due to certain activities;

- **Environmental impact**: In addition to CO_2, there are other gasses harmful to the environment that can be released as well. The term environmental impact describes the extend of the combined total damage to the environment due to all these gasses;

- **CO_2 footprint**: A term used to denote an equivalent CO_2 value. All harmful gasses accounted for in the analysis are converted to an equivalent amount of CO_2.

There are many possibilities to improve on the sustainability of concrete. These different possibilities occur due to the different life cycle stages or phases of the material. A number of examples is given:

- **Design phase**: By formulating a more optimized design, it might be possible to save material. Saving material means a lower CO_2 footprint. Moreover, using different materials (e.g. UHSB instead of conventional concrete), it might be possible to reduce the CO_2 footprint even more.

- **Raw materials and transportation**: The raw materials of the concrete mix are a major contributor to the CO_2 footprint of concrete, especially Portland cement because of emissions. Aggregates make up the majority of the volume of concrete, re-use of the aggregate is therefore also very beneficial in terms of sustainability. Careful selection of raw materials is a large influencing factor. An additional factor is transport (which occurs in all steps), and limiting transportation distances and number of movements is also beneficial.

- **Execution**: The strength development of concrete is influenced or manipulated as such that the desired speed of construction can be optimised as much as possible. However, concrete develops its strength over time. This development does not stop after construction. By giving the material more time to harden, the mixture can be modified as such that a lower CO_2 footprint is achieved (less cement is needed) and thus a more sustainable solution is achieved.

- **Re-use/demolition**: Concrete structures generally have a long service life. Therefore, existing structures provide many opportunities. For example, using more refined calculation methods it can often be proven that a structure has sufficient capacity to function in a safe manner even if the service life the structure originally was designed for has been exceeded. This can save structures from unnecessary demolition.

1.5.3 Circular economy and raw materials

In this subparagraph, two important categories of raw materials of concrete are covered. To increase sustainability, it is important to select the raw materials as such that the CO_2 footprint per amount of volume is kept low. A notion that is also related to this is the concept of circular economy, which will also be introduced. In addition to that, it is briefly illustrated that very sustainable solutions can often be found in structures that already exist.

Cement

The production of Portland cement clinker is a relatively CO_2 intensive process. According to (Ye & Schlangen et al., 2018), This is partly because of the calcination process (approximately 50% of the CO_2 emission at cement production) and fuel, electricity and transport (these are accountable for the remaining 50%). The estimation is that this results in about 1 ton of CO_2 for each ton of cement produced, the cement production being responsible for about 5% of the CO_2 emission worldwide, see Figure 23.

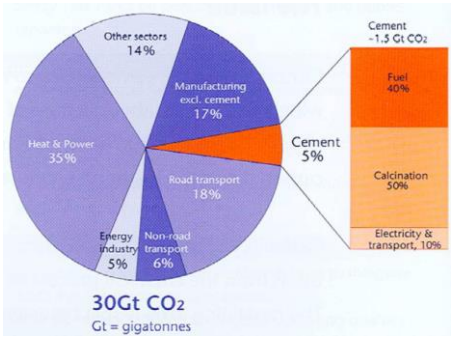


Figure 23 Contribution of cement production to CO_2 emissions - (Ye & Schlangen et al., 2018)

Therefore, reducing the amount of clinker while at the same time being able to produce cement types with good properties is an important and positive way to reduce the amount of CO_2 emission due to cements.

A practical way of achieving this is by using by-products from other industries. Examples are, as mentioned in 1.3.1, blast furnace slag, silica fume and fly ash. This can result in very significant reduction of CO_2 emission, as is illustrated in Figure 24 . However, it must be noted that not every type of cement is suitable for every application. Therefore, looking at CO_2 emission only does not result in the most sustainable and durable solution. Another possibility is the development of cement types that do not contain Portland cement at all. An example of this is geopolymer concrete.

Table 3: CO_2e of combinations with ggbfs produced at the concrete plant [141]

Combination (CEM I + ggbfs)	Content of the addition	CO_2e * (without transport of constituents to the concrete plant)
	wt.-%	kg CO_2e / t (addition content low – high)
CIIB-S	21 – 35 (ggbfs)	735 – 617
CIIIA	36 – 65 (ggbfs)	608 – 363
CIIIB	66 – 80 (ggbfs)	354 – 236

* CO_2e can be interpolated for proportions of addition between the minimum and maximum, noting that the minimum CO_2e is associated with the highest proportion of addition.

Figure 24 Reduction of equivalent CO2 emission by adding blast furnace slag - (Ye & Schlangen et al., 2018)

Aggregate

Because of its sheer volume alone, it can be very profitable if aggregate can be recycled. In (Ye & Schlangen et al., 2018) it is mentioned that the production of aggregate is about 40 billion tons per year. If done efficiently, aggregate can be regained from demolition waste, which can be used for new concrete structures. The way it can be applied, as well as the amount of it, depends on the desired use of the new concrete element.

Circular economy

A notion related to sustainability is 'circular economy'. This is a system in which it is strived for to optimise the reusability of products and raw materials. This minimises the loss of potentially valuable materials and is therefore contrary to the 'linear economy' in which products after use are simply considered as waste and are disposed of.

The examples given before illustrate that concrete offers many possibilities with respect to the circular economy. For best effect it is important to make it possible to regain the raw materials as easy as possible after the use of the structure and that the reused material does not negatively influence the quality of the new concrete. However, using different materials with their own properties, the properties of the concrete are influenced as well. It is important to keep this in mind. Some examples in the context of circular economy are use of by-products such as blast furnace slag and recycled aggregate.

Service life and reuse of elements

In the Netherlands, many structures in the infrastructure are about to reach the end of the service life these structures were initially designed for. Many structures were constructed around the 1970's. In addition to the service life, the traffic loads and number of vehicles has increased since construction. If it can be proven that these structures still have sufficient capacity to function in a safe way, this is the most sustainable option. Using refined calculation methods and investigating the real material strength, e.g. contribution of ongoing hydration of cement after 28 days, may result in the conclusion that a structure can remain to function in a safe way for an appreciable period of time.

Other sustainable solutions are to reuse for example the foundation or substructure of a bridge or viaduct, even when the deck does no longer satisfy the requirements. Another solution can be found in the prefabrication industry. If designed for this, it can be made possible to demount a structure and reuse the full prefabricated elements.

1.5.4 Conventional concrete versus UHPC

In the next chapter, Ultra-High Performance Concrete (UHPC) will extensively be discussed. It will be illustrated that these types of concrete have excellent properties with respect to durability due to a dense structure and low porosity. But ahead of the next chapter, the sustainability related aspects of UHPC and a comparison with conventional concrete is already discussed in this subparagraph.

It was illustrated in this paragraph that a design with less material means a more sustainable solution. UHPC results in more slender structures compared to conventional concrete. However, UHPC also contains significantly more Portland cement than conventional concrete. The question now is what would result in the lowest CO_2 footprint. If only a single m^3 of concrete is considered, conventional concrete scores better than UHPC in terms of the CO_2 footprint. However, if a comparison is made over a longer period of time in which aspects such as transportation, the reinforcement needed, the service life, etc., the conclusion might be different and UHPC may turn out to be much more promising sustainability wise than the comparison based on only a single m^3 of concrete suggests. Another example where UHPC may turn out to be more promising sustainability wise is if its application results in the possibility to reuse the existing foundation of a structure with only limited modifications, because this saves emission related to demolishing the existing substructure and replacing it by a new one.

As it turns out, UHPC is a more sustainable material compared to conventional concrete. This is shown in the article (Ng, Voo, & Foster, 2011). This article describes the so-called ''sustainability design approach'', which is a design approach that considers environmental impact (sustainability), durability and limit state design of a structure.

Two structures are presented (a 40 m span concrete traffic bridge and a 1,5 m high retaining wall). For both structures, a solution is given in conventional concrete using Portland cement, a solution in UHPC (Reactive Powder Concrete) and geopolymer concrete. An environmental impact calculation is performed for both structures. It was concluded that the UHPC and geopolymer resulted in lower material consumption, embodied energy, CO_2 emissions and global warming potential. When it comes to durability, UHPC and geopolymer concrete also scored much better than conventional concrete, resulting in a significantly longer potential service life. It was concluded that UHPC (RPC) and geopolymer concrete were greener construction materials than conventional Portland Cement concrete, and therefore can contribute to a sustainable future in construction.

1.6 Summary first chapter

Concrete is a material obtained by the use of a cementing medium; in this chapter it was assumed that the concrete contained cements based on Portland clinker although other cement types are available as well. A concrete mixture contains at least the following constituents:

- Cement (binder)
- Aggregate (fine and coarse)
- Water

One may also add admixtures and additives and/or fillers.
The many different available constituents enable modification of the concrete mixture to optimally match the requirements to the concrete with regard to execution and use of the structure. This way, one can obtain 'good concrete', which means that it has satisfactory properties in all its three states: fresh concrete, hardening concrete and hardened concrete. In each of these states, different properties are developed and different properties are of relevance:

- **Fresh state**: The concrete obtained after mixing. After mixing the concrete is transported, casted, compacted, etc. Therefore, workability and consistency are the most important properties during its fresh state.

- **Hardening concrete**: During hardening the concrete develops its properties and it is also known as young concrete. Important for this stage are properties such as heat development and shrinkage.

- **Hardened state**: In the hardened state the concrete structure fulfils its intended role. Therefore, properties related to the functioning of the structure are important. For example: strength and durability. Many properties in the hardened state are expressed in or related to the compressive strength.

Moreover, properties in one state may also affect properties in later stages. For example, a concrete mix with low workability or low consistency may result in suboptimal compaction and hence in lower strength and high heat development due to substantial liberation of hydration heat might result in cracking and thus lower durability in the hardened state.

The different constituents and their effects on the behaviour and properties of the concrete have been discussed. Cement is the binder and determines many properties such as strength of the material, durability (due to the pH in the pore water or resistance to chloride ingress), heat of hydration, etc. The aggregate may be regarded as the 'skeleton' of the concrete. Because it comprises the majority of the volume of the material it plays an important (e.g. strength) or even dominant (e.g. coefficient of thermal expansion) role in properties of the material. Admixtures and fillers provide even more possibilities to alter the mix to optimally meet the requirements.

The strength of a construction material is one of its most important properties in design. In the case of concrete in its hardened state, the material is often described and classified using its 28 days compressive strength. Moreover, many properties are related to it.

The concrete compressive strength is often regarded as the most important property of hardened concrete (even though in practice other properties might be more important). This is because the strength is directly related to the microstructure of the hardened cement paste. Because the compressive strength is also relatively easy to determine, the compressive strength is a practical way of determining the overall quality of the material.

The strength of concrete is determined by (or perhaps better: limited by) factors such as porosity, pore size distribution and microcracking, porosity being the primary factor. These factors are difficult to work with in practice, therefore, 'practical' factors are often used that determine these 'underlying' factors. The primary 'practical' influencing factors on the strength are:

- Water/cement ratio
- Degree of compaction
- Age
- Temperature

Other 'practical' influencing factors of lesser importance:

- Aggregate/cement ratio
- Properties of the aggregate
- Transition zone (interface)

These 'practical' factors each influence one or more of the 'underlying' factors: the porosity, pore size distribution and microcracking.

Concluding from the discussions in this chapter one may conclude that in general a concrete with higher strength has better properties and that concrete with lower porosity and stronger interface means a higher strength.

The chapter was concluded by a discussion of sustainability related topics of concrete. It is illustrated that there are many possibilities in which the sustainability of concrete can be improved throughout the service life. In addition, it is illustrated that applying UHPC in the right situations instead of normal strength concrete can also contribute to achieving more sustainable solutions.

1.7 Bibliography

Braam, R., Lagendijk, P., Soen, H., & Linssen, J. (2015). *Basiskennis beton.* Aeneas Media.

Neville, A., & Brooks, J. (2010). *Concrete Technology* (second edition ed.). Harlow: Pearson.

Ng, T. S., Voo, Y. L., & Foster, S. J. (2011). Sustainability with Ultra-High Performance and Geopolymer Concrete Construction. In M. N. Fardis, *Innovative Materials and Techniques in Concrete Construction* (pp. 81-98). Springer.

Soen, H. (2007). *Praktische Betonkennis.* 's-Hertogenbosch: Cement&BetonCentrum.

Ye, G., & Schlangen et al., E. (2018). Lecture Notes Concrete Science and Technology CIE5110. Delft.

2

INTRODUCTION TO SPECIAL CONCRETES

2.1 Introduction to special concretes

Up to a certain extent all concrete can be regarded as 'special' because the concrete mix can be designed as such that the material meets the requirements in the most optimal way. However, over time certain types of concrete have been developed that have properties that are significantly different from 'conventional' concrete and these concrete types offered new possibilities. In this chapter an introduction to these special concretes is given, but the scope is limited to the types of concrete that are relevant for the project.

- This chapter starts with perhaps the most important development of all: the increase of the maximum concrete compressive strength, and it is defined what UHPC actually is;
- The chapter continuous with introducing UHPC from a ''concrete technology point of view'' to become familiar with its most important characteristics and to be able to explain where these characteristics come from;
- To aid in the understanding, a brief discussion of conventional fibre-reinforced concrete follows;
- After that the contribution of fibres to UHPC is discussed, different UHPC types and products are discussed and practical considerations (e.g. casting and the importance of fibre orientation) regarding UHPC are covered;
- The chapter is concluded with a summary.

2.2 Basics of Ultra-High Performance Concrete

2.2.1 Introduction to Ultra-High Performance Concrete

History of high strength concrete

The increase of the compressive strength of concrete has been a continuous field of research. In the 1950's, concrete with a strength up to 70 N/mm^2 was produced. Developments continued: it became clear that the use of silica fume in concrete could be beneficial, and superplasticizers were developed as well. These developments contributed to pushing the boundary of the maximum concrete strength that could be achieved, and in the 1980's it became possible to produce concrete of strength beyond what is now known as ''normal strength concrete'': a compressive strength up to 100 N/mm^2 became the new limit, enabling new possibilities in construction using this material.

For a long time, it was deemed to be unlikely that the strength of concrete could surpass 120 N/mm^2, because of the structure of the material: a large volume of aggregate is present in concrete (see chapter 1), which would become the weakest link in the material. However, developments still continued. An important name in this is H.H. Bache, a Danish researcher who published his findings in 1981.

Bache was the first to develop and apply new concepts regarding the composition of concrete, resulting in the development of Ultra-High Strength Concrete. Thanks to these concepts, the maximum of 100 N/mm^2

was shifted all the way up to values in the range of 150 to 200 N/mm^2. In addition to this, fibres could be added to the material. These developments opened up new possibilities and opportunities.

The concepts developed by Bache were picked up by others as well. Different companies used these concepts as a starting point to further develop and produce new products. Different commercial UHSC mixtures and products were developed, for example, this led to the development of Reactive Powder Concrete.

The first practical application of UHSC on a larger scale was a bicycle and pedestrian bridge in Sherbrooke (Quebec, Canada) which was constructed in 1997. In 2002 the first pre-standard (AFGC-SETRA) was published in France. As will be illustrated in the third chapter, this document has been used as a reference all over the world as there were no other guidelines available. Since then, many different initiatives for the development of guidelines have been initiated. In Figure 25 the development of the concrete compressive strength is depicted. The relation to the water cement ratio can be seen as well.

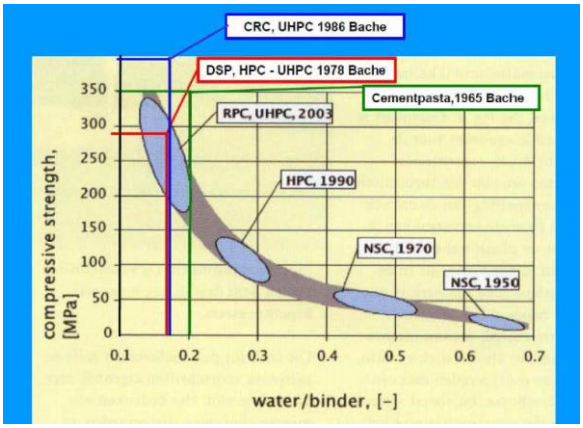


Figure 25 Development compressive strength - (Ye & Schlangen et al., 2018)

Definitions

The first point to consider is perhaps the definition of (Ultra-)High Strength Concrete. As mentioned in the first chapter concrete is categorised by looking at 28-day concrete compressive strength. In literature different limit values and ways of denoting concrete of 'higher strength' can be identified, for example:

- Eurocode 2 starts to give other properties for strength classes higher than C50/60, which already implies that the stronger the concrete becomes, properties change and the more brittle its behaviour. No explicit limit is given for normal strength concrete though. The code supports strength classes up to and including C90/105.

- In the old CUR-97 ''Hogesterktebeton'', high strength concrete (HSC) was defined as concrete with a cube compressive strength higher than 65 N/mm^2 up to 105 N/mm^2.

- Next to high strength concrete is the range of concrete materials called very-high strength concrete (VHSC), of 105-150 N/mm^2. Ultra-High Strength Concrete (UHSC) typically starts at a concrete compressive strength of 150 N/mm^2.

A typical classification in accordance with different sources of literature is given in Table 6.

Table 6 Classification of concrete based on compressive strength

Nederlands	**English**	**Compressive strength**
[-]	[-]	[N/mm^2]
Normaal beton (NB)	Normal Strength Concrete (NSC)	≤ 65
Hogesterktebeton (HSB)	High Strength Concrete (HSC)	$65 - 105$
Zeer-hogesterktebeton (ZHSB)	Very-High Strength Concrete (VHSC)	$105 - 150$
Ultra-hogesterktebeton (UHSB)	Ultra-High Strength Concrete (UHSC)	> 150

In the construction practice, commercial products with a compressive strength in the range of 150 – 200 N/mm^2 are available. These materials can be produced and processed in practice without requiring special treatment, as illustrated in (Hunger & Spiesz, 2016). Much higher strength values are reported, even up to 800 N/mm^2. However, special treatment is required to achieve these high strengths involving increased temperature and/or increased pressure and can therefore only be achieved under controlled conditions in a factory or laboratory.

In the first chapter of this report, it was explained that the concrete compressive strength is related to other properties. An increase in strength up to the range of UHSC is accompanied by, for example, higher tensile strength, higher modulus of elasticity and a much higher density and lower porosity (thus increase in durability).

UHSC does not only have a very high strength, but also other properties are far superior to conventional concrete. The decision can be made to apply USHC because of these other properties, and not because of its strength. For this reason the international term of Ultra-High Performance Concrete is often used instead of UHSC to underline that there can be different reasons to choose for this material than its compressive strength alone, even though the material is still classified by its 28-day compressive strength.

UHPC is a broader term than UHSC, it is a class of materials that can be selected for multiple reasons although these materials typically have a high compressive strength in common. But this in turn raises the question what UHPC actually is, and what an appropriate definition would be. Depending on the source, one may find different definitions for (Ultra-)High Performance Concrete. For example:

- *"High performance concrete, formerly named high strength concrete, can mean concrete having a high durability (low permeability) as well as high strength."* (Neville & Brooks, 2010);

- *"UHPC-class materials: Cementitious-based composite materials with discontinuous fibre reinforcement, compressive strength above 150 MPA, pre- and post-cracking tensile strengths above 5 MPa, and enhanced durability via their discontinuous pore structure."* (Russell & Graybeal, 2013);

- *"High Performance Concrete: Concrete mixtures that possess the following three properties: high-workability, high-strength, and high durability."* (Mehta & Monteiro, 2006).

Based on the previous discussion and examples, one could also formulate a more 'loose' and practical definition. For this thesis project the material is defined as follows:

- *UHPC is a concrete with a concrete compressive strength higher than 150 N/mm^2 and accompanied by higher tensile strength, E-modulus and a denser structure (and thus improved durability) compared to normal strength concrete.*

This is just a practical definition for the sake of understanding and to create a starting point for the further elaboration of the project. This definition underlines what is important for the project (high compressive strength to allow the design of a structure and eventually the re-use of the existing foundation) as well as accounting for some of the key characteristics of the material (this will be clarified in the subsequent sections).

Typical characteristics of UHPC

A definition for UHPC has now been formulated. The next step is to identify some of the typical characteristics that these materials have in common, and that are important for the application. These characteristics will be elaborated on in the subsequent subparagraphs.

- **High mechanical properties**: The most obvious mechanical property is the high compressive strength; it is accompanied by a higher tensile strength and modulus of elasticity compared to normal strength concrete. This allows for more slender design and lighter structures. Moreover, the material has high resistance against wear and with the addition of fibres the material shows

more ductile behaviour and reinforcement can be reduced (or is not required at all). Table 7 gives an overview of typical values for UHPC, as well as other classes of concrete;

Table 7 Mechanical properties at different concrete strength classes - (Betoniek, 2017)

Property	**Unit**	**NSC**	**HSC**	**UHPC**
Compressive strength	[N/mm^2]	20-65	65-105	150-200
Tensile strength	[N/mm^2]	2,3-4,3	4,5-5,0	6,0-10,0
Modulus of elasticity	[N/mm^2]	28.000-38.000	38.000-41.000	50.000-60.000
Volumetric mass	[kg/m^3]	2400	2450	2525
Drying shrinkage	[magnitude]	+++	++	+
Autogenous shrinkage	[magnitude]	+	++	+++
Creep coefficient φ	[-]	Approx. 2,0	Approx.1,0	Approx.0,8

- **Good durability**: The high mechanical properties are accompanied by good durability. In subsequent sections it will become clear that the high mechanical properties and durability can be attributed to the dense structure and low porosity of the material. For the sake of comparison, Table 8 presents a number of properties related to durability;

Table 8 Durability related properties at different concrete strength classes - (Betoniek, 2017)

Property	**Unit**	**NSC**	**HSC**	**UHPC**
Porosity	[% v/v]	14-20	10-13	1,5-5
Air permeability	[m^2]	10^{-16}	10^{-17}	10^{-19}
Chloride diffusion factor	[m^2/s]	$2*10^{-16}$	$2*10^{-17}$	$2*10^{-19}$
Freeze/thaw resistance	[-]	Moderate/Good	Excellent	Excellent
Carbonation after 3 years	[mm]	Approx. 7	Approx. 4	Approx. 0,2

- **Good workability**: As will become clear in the subsequent parts of the paragraph, typically a large dosage of superplasticizer is used for the production of UHPC. Along with the other constituents of the mix, this results in good workability (fresh UHPC is often a stable and flowable concrete with good consistency and often even with self-compacting properties). This is very profitable for, for example, prefabrication.

The benefits of using material of high strength are obvious, it allows for more slender designs compared to conventional concrete because the required cross-sectional dimensions can be smaller. Moreover, the strength is accompanied by higher stiffness, which is also a useful property in design and determining cross-sectional dimensions. However, the material also has some characteristics that are to be kept in mind when designing:

- **Brittleness (without fibres)**: Although the material has high strength values, it is also very brittle unless precautions are taken: the addition of fibres. For this reason, a typical UHPC mix contains fibres to increase the ductility of the material.

- **Long term behaviour**: Long term behaviour is also a point of attention, especially because of autogenous shrinkage, which is very predominant in the case of UHPC. The creep coefficient is rather low.

These points of attention show that one should be familiar with the material properties and that concrete with high strength is not necessarily the same as durable concrete: high shrinkage and creep might result in cracking for example, if cracking occurs at the beginning of the service life of the structure that cannot be regarded as durable behaviour.

- **Initial costs & optimization**: Another ''characteristic'' is the price of the material. The initial costs of UHPC are significantly higher than that of conventional concrete. According to (Fehling, Schmidt, Walraven, Leutbecher, & Fröhlich, 2014), UHPC has a price 4 to 5 times that of conventional concrete per cubic meter. This illustrates the importance of optimizing the use

of the material. To make a 'fair' comparison between UHPC and conventional concrete, and to take full account of all benefits of UHPC (e.g. also good durability and low maintenance), a comparison should be made by looking at the whole project. When designed properly, UHPC solutions can be more cost-effective in the long run than the comparable solution in conventional concrete.

Considerations for selecting a strength class

As mentioned in the introduction of this paragraph the concrete strength developed quite rapidly from about 100 N/mm^2 to 200 N/mm^2 (more or less the maximum strength that can be achieved under practical conditions, i.e. no special treatment) in the nineties of the previous century. The range of strength classes in between was more or less neglected for some time. One should ask however if neglecting all these intermediate strength classes would always yield the best result, as mentioned in (Walraven, Ultra-hogesterktebeton: een materiaal in ontwikkeling, 2006), because a 'traditional' concrete structure in normal strength concrete has the benefits that it is robust and durable while it is also relatively affordable.

UHPC mixtures have considerably higher initial costs compared to normal strength concrete. It was explained that UHPC therefore requires the design to be as optimal as possible, to save on material. One should consider if the highest strength classes are required in the first place.

One might select UHPC for different reasons than for strength, e.g. durability (high density and low porosity) or because of workability (UHPC is often flowable and self-compacting). If this is the case, one might consider optimising the material from the cost point of view (e.g. by saving on the amount or type of fibres or aggregate), as mentioned in (Kaptijn, 2002).

Examples of considerations are given in (Walraven, UHSB op weg naar regelgeving, 2012), it illustrates that in practice one should consider multiple aspects, such as mass, durability and costs. Suppose that one would strengthen an existing steel bridge with a thin layer of UHPC. Although UHPC allows for optimizing as such that only a thin layer of it is used, this is not the most beneficial for the steel: due to the thin layer the stress variation in the steel (cause of fatigue damage) would not be reduced sufficiently. As mentioned in the article, a concrete overlay within the range of the strength lasses of 120-140 N/mm^2 would be the most optimal if one considers the aforementioned aspects.

2.2.2 The principles of UHPC

In this paragraph the main principles of UHPC are discussed to be able to explain where the characteristic properties of UHPC come from. As mentioned before, new concepts about the composition of concrete were introduced that enabled the production of concrete with a compressive strength in the range of 150-200 N/mm^2. To achieve this, a number of principles has to be followed, namely:

- Low water/cement ratio (about 0,20) to bind all water, made possible by using superplasticizer;
- Optimize the packing density of the particles;
- Limiting the maximum aggregate particle size (more homogeneous material);
- Addition of fibres.

A mixture with these properties results in a high-performance material characterised by high mechanical properties and a very dense structure with low porosity. Therefore, the material is also durable. These four principles are explored in greater detail below to answer the question why following these four principles results in a strong and durable material.

Low water/cement ratio to bind all the water

If more water is added to a concrete mix than required for hydration, the mixing water will result in capillary pores filled with capillary water, as mentioned in 1.4. This was found not to be profitable for the strength and density of the material.

Therefore, the water/cement ratio is kept very low, a typical value is about 0,2. To achieve a water/cement ratio this low a large amount of cement is added to the mix. All the water will be bound. Due to the large amount of cement compared to the amount of water, an amount of unhydrated cement remains, which acts as a filler. Essential is the use of superplasticizer, which makes it possible to design a mix with an optimal packing but still flowable, even at such a low water/cement ratio.

Optimizing packing density (grading)

An optimized packing density is important because this results in the reduction of stresses on the contact surface of the different particles. If these stresses are limited, microcracks will start to form only at high stress levels. This gives the concrete higher strength. In addition, a very dense microstructure also gives high durability.

The goal is to select all the constituents as such that a very dense packing (i.e. optimal packing density) of particles is obtained:

- Typically, a large amount of cement is used as well as aggregate particles of smaller size than in NSC;
- Silica fume is added, which acts as a 'microfiller' to fill up the space between the cement particles;
- Fillers are added (such as fly ash and mineral fines) to improve the packing between the aggregate and cement.

This way, particles with a whole range of different sizes (from smallest to largest: silica fume – cement – fillers – aggregate) are used to obtain a packing as dense as possible. The grading of the particles is depicted in the following graph, it can be seen that the different types of particles complement one another in terms of particle size.

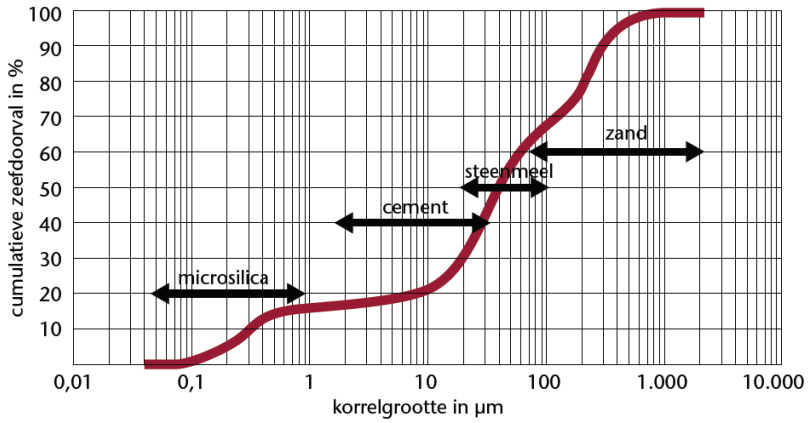


Figure 26 Grading of a UHPC mix – (Betoniek, 2017)

The grading curve is 'discontinuous', one can see that the different materials are each within a certain range of particle size. Due to this difference in particle size, the free space between the particles of each material (and thus each range of particle size) are optimally packed by a material with even smaller particle size. This principle is also depicted in the following figure.

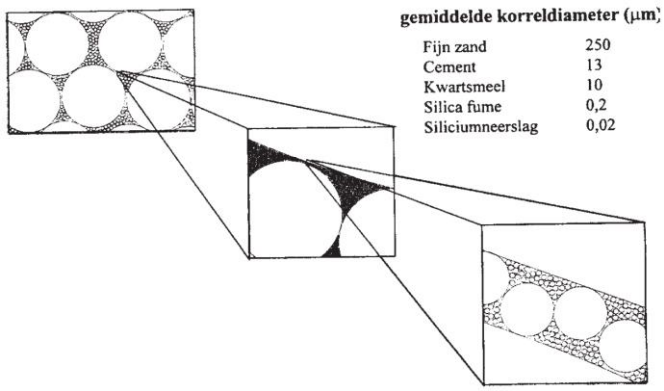


Figure 27 Optimal packing due to different particle sizes - (Kaptijn, 2002)

Limiting the maximum aggregate particle size

Large aggregate particles result in larger stress concentrations in the material as well as a larger porous interface between the aggregate particle and the hardened paste. This limits the strength of the material. By limiting the aggregate particle size (smaller size than conventional concrete), this effect is reduced and the material becomes more homogenized and these stress concentrations are limited.

Addition of fibres

The higher the strength of concrete, the more brittle its behaviour becomes. This also holds true for UHPC. Therefore, fibres are added to increase the ductility. In addition, the fibres contribute to the tensile capacity of the material and provide post cracking strength. UHPC structures are often executed using steel fibres and prestressing without additional passive reinforcement. Details with regard to the fibres are given in 2.3 and 2.4.

2.2.3 Mix design of UHPC

In the previous paragraph the principles behind the composition of an Ultra-High Performance Concrete mix were explained. From this discussion it was clear that a 'typical' UHPC mix is different from a concrete mix within the range of normal strength concretes. The following table provides some numbers:

Table 9 Global mix composition (in kg/m^3) – Edited, after: (Ye & Schlangen et al., 2018) & (Kaptijn, 2002)

	B45	**B85**	**B200**	**B800**
Cement	360	475	950	980
Silica fume	-	25	235	225
Quartz powder	-	-	-	380
Sand	790	785	995	490
Gravel	1110	960	-	-
Steel fibres 13 mm	-	-	145	-
Steel fibres 3 mm	-	-	-	615
Superplasticizer	0,5	4,6	17	18
Water	145	150	180	185
Specific mass	2405	2400	2525	2895
Water/binder ratio	0,4	0,3	0,15	0,14

The following graph gives a number of mixtures for conventional concrete, high strength concrete and a number of UHPC mixtures. It can again be seen that the mix composition is vastly different.

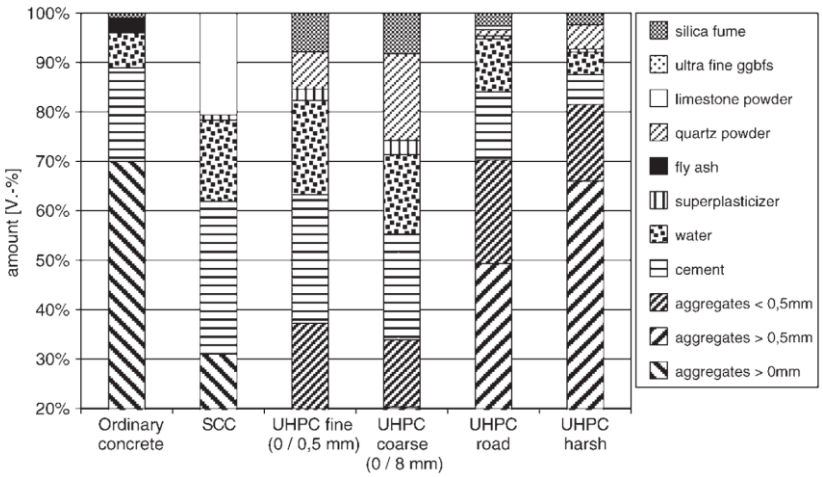


Figure 28 Comparison of mixture composition - (Fehling, Schmidt, Walraven, Leutbecher, & Fröhlich, 2014), p.7

In this paragraph the different constituents of a 'typical' UHPC mix are discussed in greater detail, as well as some of the requirements to these constituents and the underlying principles. This way, the requirements in terms of mixture composition as mentioned in the previous subparagraph can be met.

Cement

A typical UHPC mix has a large cement content. Portland cement is generally used in large quantities but, depending on the requirements of the mix and the availability, other cement types can be used as well, e.g. Portland cement in combination with fly ash or blast furnace slag. Cement using blast furnace slag can be used if the structure is susceptible to effects due to temperature, and thus the heat of hydration is to be reduced.

As mentioned before, a large amount of cement remains unhydrated, up to about 30%. For this reason, a part of the cement can be replaced by a filler (e.g. quartz powder). However, the presence of unhydrated cement also gives another benefit: the potential to close cracks.

Aggregate

For normal strength concrete, the influence of the type of aggregate and the grading of the particles did not have a large influence on the strength of the material, other factors were more important (see 1.3.2 and 1.4.4.). For concrete of higher strength, this no longer holds: both the aggregate type and the aggregate grading play a major role in determining the strength.

A typical UHPC mix has a very small maximum particle size compared to conventional concrete. The maximum value is often 5-7 mm, while mixtures with a maximum particle size of 1-2 mm are also used, i.e. fine aggregate with coarser grading. There are two reasons for limiting the particle size to these dimensions:

- **To decrease the size of the porous interface**: The interface between the hardened cement paste and aggregate particles is porous and therefore weaker than the paste further away from the interface. This is the zone where microcracks often occur due to the differences in the properties of the hydrated cement paste and the aggregate. Reducing the size of this zone is thus profitable;

- **To reduce peak stresses**: The hardened cement matrix and the aggregate have different properties, e.g. the modulus of elasticity. This results in peak stresses and therefore in a risk of microcracking. Reducing the size of the aggregate particles means that the peak stresses are reduced and therefore the risk of cracking reduces as well.

It is not only the size which is of importance: the aggregate has to be selected with great care; strong aggregate is required. The reason for this is as follows: the matrix has a high compressive strength due to the

low water/cement ratio, and therefore it should be prevented that the aggregate becomes the weaker part in the hardened concrete.

A particular type of high strength concrete is high strength concrete produced using lightweight aggregate, this creates a material that is both strong and very light and it is used for special structures, e.g. structures in the offshore industry. The quality of the aggregates (i.e. the strength and density of the aggregate) are the dominant factor in determining the strength and the density of the material. Note that the strength of this material is in the 'high strength concrete' range, but its unique properties made it worth mentioning.

Admixtures and additives

A typical UHPC mix contains a large dosage of superplasticizer, this admixture type has made it possible to create mixtures with high strength in the hardened state and high workability in the fresh state, despite the mix having a low water/cement ratio.

Just as for normal strength concrete, many types of admixtures in addition to superplasticizers are available. The addition of admixtures to the concrete depends on the intended use of the material.

Fillers

A typical UHPC mixture contains, in addition to a relatively large amount of cement, also a high dosage of fillers (which can partially replace the cement). As mentioned before, fillers are used to obtain optimal density packing, thus reducing porosity. Although the contribution is mostly physical (this is called the 'filler-effect' or 'microfiller-effect'), fillers can be reactive or inert.

Reactive fillers: Types of reactive fillers are silica fume, fly ash (both pozzolanic material) and blast furnace slag (latent hydraulic material).

- Silica fume: Acts in the first place as a filler through the physical ''filler-effect''. Especially if heat treatment is applied (80 – 90 °C) it starts to contribute through the formation of hydration products, thus increasing strength in this way as well. Silica fume is the main factor in determining the water and superplasticizer requirement as well as the rheological properties of the fresh UHPC. This is explained by the large specific surface and the high force between silica fume particles.

- Blast furnace slag: Can be used to replace a part of the Portland cement. This results in a lower water and superplasticizer demand.

- Fly ash: Fly ash can also be used as a reactive filler, thus partially replacing cement.

As mentioned before, the effect of fillers is predominantly physical, this is via the so-called ''filler-effect'', this means that the fillers fill up the empty space between the cement particles and strengthen the interface between the hardened cement paste and the aggregate particles, this results in better bonding between the two. To summarize, the ''filler-effect'' results in a denser structure and strength.

The contribution of reactive fillers is predominantly through this ''filler-effect'' and not via the pozzolanic or latent hydraulic reaction (if this occurs at all, e.g. because sufficient heat is required for silica fume). The hydration of the pozzolanic or latent hydraulic material can still contribute though. These materials react with the calcium hydroxide liberated form the hydration of the Portland cement, forming hydration products. This also results in a reduction of the size of the capillary pores.

Inert fillers: Inert fillers only contribute through the physical effect; they are used to optimize the packing of the different particles. To achieve this, it is essential that these fillers are graded carefully. Examples of inert fillers are quartz powder and limestone. Limestone has lower strength and gives more sticky UHPC. Quarts powder is a good filler because of its high strength.

Fibres

Contrary to normal strength concrete, a typical UHPC mixture contains fibres (typically steel fibres) to provide ductility. The Fibres are generally used in a high dosage of about 2% of the volume of the mix and are integrated into the microstructure of the material. The mechanical properties of UHPC with fibres is as such that in many applications passive reinforcement is not required. In practice, the use of fibres does not have to exclude the use of conventional steel reinforcement, these can be combined. This can result in very durable and cost-effective solutions. An example is CRC, which will be discussed in 2.5. Combinations of fibre reinforcement and prestressing (and, if required, traditional reinforcement) can also be applied.

Not only steel fibres are available, there are many different fibres of different materials, shapes and sizes. These can also be used in combination with one another. Principles of fibre-reinforced concrete and fibres in UHPC will be covered in 2.3 and 2.4 respectively.

2.2.4 Properties of UHPC: Fresh and hardening concrete

In this and the following subsections typical properties of UHPC are discussed for all three states (fresh, hardening and hardened UHPC).

Just as for normal concrete, the most important properties of fresh UHPC are related to consistency and workability. A typical UHPC mixture has good consistency, good workability and is often even self-compacting. The large amount of fine material results in high consistency and reduces bleeding and segregation

As described in (Fehling, Schmidt, Walraven, Leutbecher, & Fröhlich, 2014), UHPC is generally processed in a flowing consistency. In fresh state, UHPC is more similar to self-compacting concrete than to conventional concrete, due to the large number of smaller particles and the large dosage of superplasticizer. However, it is more viscous and cohesive (i.e. it flows slower) due to the composition of the mix, which is optimized for packing. Contrary to self-compacting concrete, it is not always self-deaerating. In such a case, this has to be done by adding sufficient vibration energy, which takes longer than for conventional concrete.

Development of strength

A high 28-day compressive strength implies that the early age strength of UHPC is also high, especially when compared to normal strength concrete. This makes higher strength concrete (not even necessarily UHPC) into a material suitable for situations where high construction speed is required. The strength development can be controlled using heat treatment.

Heat development & thermal shrinkage

Because UHPC contains a large amount of cement, the liberation of heat and subsequent rise in temperature during the hardening can substantial. Especially in the case of larger structures there is a risk of thermal shrinkage, which can result in cracking.

Shrinkage

Autogenous shrinkage: Autogenous shrinkage is caused by volume change of the cement paste due to water being used for the hydration process (it is therefore often denoted with ''self-desiccation''). Because UHPC contains a large amount of fine material, has a low water/cement ratio and because there is no coarse aggregate, high values for autogenous shrinkage can therefore be expected. Typically, autogenous shrinkage is the largest contribution to the total shrinkage value of UHPC.

Drying shrinkage: Drying shrinkage is caused by the change in moisture content due to difference in relative humidity between the concrete and the surrounding air. Drying shrinkage is related to higher water/cement ratios and capillary porosity. Because UHPC is a very dense material and because it is strived for to prevent capillary pores and achieve bonding all the water, the values for drying shrinkage are low compared to normal strength concrete. In addition, structures made of UHPC typically have smaller dimensions than normal strength concrete structures, therefore, one may argue that drying would occur more rapidly, but this is compensated for by the higher density.

In (Fehling, Schmidt, Walraven, Leutbecher, & Fröhlich, 2014), it is given that a total shrinkage strain of 0,6 – 0,9 mm/m can be assumed for the design of UHPC components made from non-heat treated and low capillary material. This latter point means a water/cement ratio smaller than or equal to 0,25. It is also mentioned that heat treatment can be applied to control shrinkage, after the treatment no further shrinkage occurs.

2.2.5 Properties of UHPC: Hardened concrete

This section gives an overview of the most important properties of hardened UHPC. Its high compressive strength is the most obvious characteristic, but other (mechanical) properties such as stiffness and durability related performance is also superior compared to normal strength and high strength concrete.

Mechanical properties of hardened concrete

Compressive strength: A key feature of UHPC is its high compressive strength, which is typically in the range of 150 – 200 N/mm^2 for mixes applied in practice. Even higher values, up to 800 N/mm^2 have also been reported, but this requires special treatment. The high compressive strength can be explained by looking at some of the features of the microstructure:

- Dense microstructure: The hardened matrix is very dense, which results in higher strength. The dense matrix is attributed to the low water/cement ratio (which also causes there are hardly capillary pores) and the optimized packing, this way a physical effect occurs that increases strength: the filler effect.

- Homogeneity of microstructure: UHPC is a mix with fine particles. As a result, the microstructure is more homogeneous. If external stresses are subsequently imposed upon the concrete, the stresses are more uniform.

Because of its microstructure, the failure mechanism of UHPC is also different than that of conventional concrete. If a crack is formed, it propagates straight through both the matrix and the aggregate, and UHPC fails abruptly and in a brittle manner. This is contrary to conventional concrete, which retains some of its capacity after reaching its strength and shows more ductile behaviour due to the change of the microstructure, see Figure 21.

In uniaxial compression the behaviour is approximately linear until the compressive strength is reached. The observed deviation from the linear curve is due to the formation of microcracks. Without fibres, brittle failure occurs. The following figure gives a stress-strain diagram for UHPC without fibres in a uniaxial compression test.

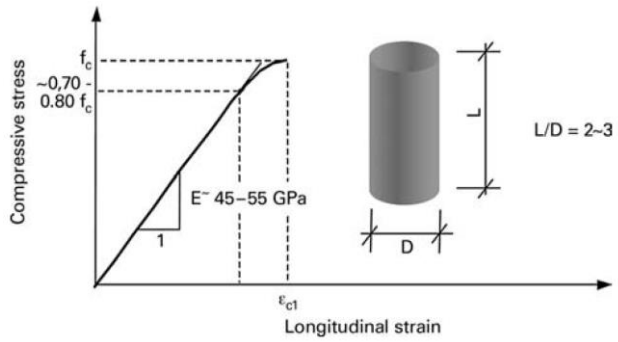


Figure 29 Stress-strain diagram UHPC without fibres in uniaxial compression (Fehling, Schmidt, Walraven, Leutbecher, & Fröhlich, 2014), p.24

Strain at maximum strength seems to depend on the grading of the aggregate. (Fehling, Schmidt, Walraven, Leutbecher, & Fröhlich, 2014) mentions that for fine-grained UHPC (up to 2 mm maximum) strain of 4,0 – 4,4, permille was reached while coarse-grained UHPC went towards 3,5 permille.

Adding fibres has little influence on the pre-peak part of the stress-strain diagram and the strength starts to increase only from about 2,5% fibres per volume. The post-peak behaviour however is more influenced and can be improved. The exact change of behaviour depends on a number of parameters, among which are fibre content, geometry, orientation and bond with the matrix. However, it is also mentioned that the exact course of the post-peak part of the stress-strain graph can hardly be predicted and should be established using laboratory studies. Moreover, these measured curves show more scatter than the ascending part due to the many fibre-related variables.

Another factor influencing the compressive strength is, for example, the curing temperature. Curing under higher temperatures can result in an increase of the material strength, as well as accelerate its development.

Tensile strength: It has been explained in the first chapter that the tensile stress is related to the compressive strength. From this one might intuitively expect that the tensile strength of UHPC is significantly higher than of normal strength concrete. The tensile strength of UHPC indeed is higher, however, the increase of tensile strength lags behind by the increase in compressive strength, this can be seen in Table 7.

The reason for this is as follows: The high strength of UHPC is partially contributed to the optimization of the packing density, fillers play an important role in this by filling the empty space between the cement particles. The contribution of these fillers to the increase of the compressive strength is therefore much more predominant than their contribution to the tensile strength.

- Typical axial tensile strength values for UHPC are 6 – 10 N/mm^2, according to (Fehling, Schmidt, Walraven, Leutbecher, & Fröhlich, 2014) there is little difference for fine and coarse grained UHPC without fibres and the main influencing factor in the addition of silica fume to the mix. Without fibres the failure in tension is very brittle. Because of the high strength of the matrix, cracks run through both the grains and the aggregate. Because of this the edges of the cracks are very smooth, interlocking effects that typically occur in conventional concrete are therefore absent.

  Moreover, it is mentioned that the results for UHPC justify the use of following formulas for deriving the axial tensile strength from the compressive strength:

$$f_{ctm} = 0{,}3 * f_{ck}^{\frac{2}{3}}$$

$$f_{ctk,0{,}05} = 0{,}7 * f_{ctm}$$

  These are the same equations as for normal strength concrete and these equations determine the tensile strength related to the matrix. The influence of fibres is not accounted for using these equations, if sufficient fibres are added, the actual tensile strength can be much higher.

- Adding fibres results in a higher axial tensile strength and forces can be transferred across wider cracks because the fibres bridge the cracks. Depending on the amount of fibres and their orientation, the fibres can transfer a part of the tensile strength of the matrix (softening) or even a higher stress (strain hardening). In the latter case an increase in strength is possible after the first crack in the UHPC matrix. The post cracking behaviour is determined by the same parameters that determine the post-peak behaviour in compression. The principle of adding fibres and the influence on the relation between the tensile stress and crack width is given in Figure 30.

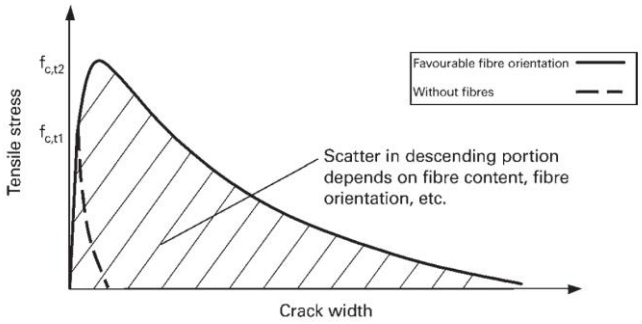


Figure 30 Stress-crack width behaviour of UHPC in tensile test (Fehling, Schmidt, Walraven, Leutbecher, & Fröhlich, 2014), p.29

- Flexural strength is another tensile strength quantity, which is easier to determine than axial tensile strength in tests. During these tests, a scale effect can be observed. Fibres result in less brittle behaviour and a more favourable distribution of flexural stresses. According to (Fehling, Schmidt, Walraven, Leutbecher, & Fröhlich, 2014) values are observed in the range of 15 – 40 N/mm^2, depending on the UHPC mixture.

Modulus of elasticity: Just as for tensile strength, a higher modulus of elasticity can be expected compared to normal strength concrete, because of the denser structure of UHPC. However, the increase of the modulus of elasticity is (just as the tensile strength) not proportional to the increase of the compressive strength (see Table 7). Because of this reason the equations in, for example, the Eurocode 2 should be used with care, UHPC is outside its range of validity.

According to (Fehling, Schmidt, Walraven, Leutbecher, & Fröhlich, 2014), the modulus of elasticity generally lies between 45.000 – 55.000 N/mm^2. Using bauxite, it can be increased to 70.000 N/mm^2. Just as for the compressive strength, fibres do not significantly increase the E-modulus up to about 2,5% per volume. Equations are given to determine the E-modulus, which is influenced by the aggregate size:

- Fine-grained UHPC:

$$E_c = 8800 * f_c^{\frac{1}{3}}$$

- Coarse-grained UHPC with basalt chippings:

$$E_c = 10200 * f_c^{\frac{1}{3}}$$

Where:

$f_c = f_{ck} + 8$ [N/mm²]

E_c: Modulus of elasticity [N/mm^2]
f_c: Cylinder compressive strength [N/mm^2]

Poisson ratio: The Poisson ratio is in the same order of magnitude as the Poisson ratio of conventional concrete, which has the typical value of 0,2. According to (Fehling, Schmidt, Walraven, Leutbecher, & Fröhlich, 2014), the Poisson ratio is found to be between 0,18 and 0,19 for fine-grained UHPC and about 0,21 for coarse-grained UHPC.

Creep and relaxation: Just as for normal strength concrete structures, creep is to be accounted for. The creep coefficient is related to the type of concrete. For concrete within the range of normal strength classes, the creep coefficient is about 2,0. For concrete within the range of high strength concrete the coefficient is about 1,0 and for UHPC the coefficient can go towards 0,8. Heat treatment can be applied to reduce creep.

In (Fehling, Schmidt, Walraven, Leutbecher, & Fröhlich, 2014) the following range of values is given for rough estimation:

- Final creep coefficient without heat treatment: $\varphi = 0{,}6 - 1{,}4$
- Final creep coefficient with heat treatment (70 – 90 °C): $\varphi = 0{,}2 - 0{,}4$

Moreover, the remark is made that for UHPC without heat treatment, a higher creep value was observed than what was predicted according to the creep theory. Nonetheless, from the given values it can be seen that a higher strength means lower creep coefficients, i.e. that UHPC structures creep less than normal strength concrete structures. However, a combination of low creep and high shrinkage makes higher strength concrete very susceptible to cracking.

Impact resistance: For concretes in general at high strain rates an increase in compressive strength and tensile strength is observed. In (Fehling, Schmidt, Walraven, Leutbecher, & Fröhlich, 2014) it is stated that the increase in compressive and tensile strength, which is expressed using the dynamic increase factors, are slightly below those of conventional concrete. Moreover, it is reported that fibre reinforcement is very effective in impact tests and that the compressive strength of UHPC is very important with regard to impact loads.

Fatigue: In (Fehling, Schmidt, Walraven, Leutbecher, & Fröhlich, 2014) reference is made to a number of research projects related to fatigue. The results of these projects were that there is no significant difference between conventional concrete and UHPC with regard to the admissible stress ranges. The similar conclusion was drawn for fibre reinforced UHPC, although the scatter was larger.

Properties related to durability

Many deterioration mechanisms are related to the presence of pores in the material (porosity) and its ability to take up and transport moisture. The increase in strength of UHPC is accompanied by a more dense structure and a decrease of porosity of the material. This implies that UHPC, with its denser structure and lower porosity, performs well with respect to durability. Especially when compared to normal strength concrete and high strength concrete. This is further illustrated by the following figure.

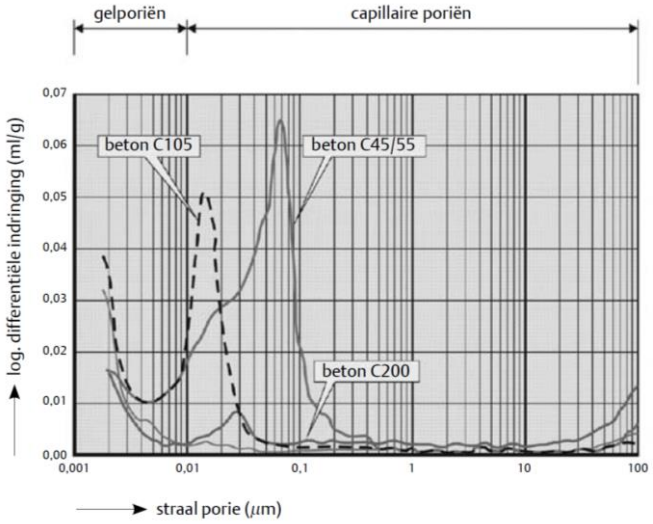


Figure 31 Comparison of pore size distribution of NSC C45/55, HSC C105 and UHPC C200 (Walraven, Ultra-hogesterktebeton: een materiaal in ontwikkeling, 2006)

Figure 31 shows the pore distribution in the concrete and is explained in (Walraven, Ultra-hogesterktebeton: een materiaal in ontwikkeling, 2006). The number of pores in normal strength concrete is larger than the number of pores in high strength concrete, moreover, its pores are larger as well. UHPC does not show a peak value at al. This is because of the combination of low water/cement ratio and the packing density. As a result of this, UHPC has practically no capillary pores, which in turn means that harmful substances can hardly permeate into the material. Note however that this is very delicate, if the water/cement ratio increases

only a little (in (Fehling, Schmidt, Walraven, Leutbecher, & Fröhlich, 2014) the number 0,22 is mentioned without heat treatment while for heat treated the water/cement ratio may be 0,25 due to a higher degree of hydration), then the material is no longer free from capillary pores.

Based on this information one may already expect good performance with respect to durability, because the moisture transport required for the occurrence of deterioration mechanisms will be largely absent. The main points of the findings as described in (Betoniek, 2017) and (Hunger & Spiesz, 2016) are given below, while some addition values for a comparison with normal strength concrete and high strength concrete are given in Table 8:

- **Carbonation**: According to measurements carbonation turns out to occur very slowly.

- **Chloride penetration**: UHPC shows a very high resistance against penetration of chlorides. This can be explained by the dense microstructure and low porosity of the material and hence the low value for the chloride diffusion coefficient. The same holds for other harmful substances: Because of the low porosity the material has high resistance against the penetration by harmful substances.

- **Alkali-silica reaction**: ASR is a chemical reaction that requires a certain supply of moisture. Because of the low permeability of the material this moisture supply is hardly possible and therefore there is a limited risk of ASR.

- **Acids**: When it comes to deterioration due to acids, the fact that there are hardly any capillary pores are present the deterioration will only take place very slowly. The material itself however is not more resistant to acids than normal strength concrete.

- **Freeze and thaw**: Because of the low porosity of the material there is hardly any water that may freeze due to low ambient temperatures. For this reason, UHPC performs significantly better than normal strength concrete under freeze thaw cycles, even without air entrainer.

Implications for design: The absence of capillary pores makes the material practically impermeable to harmful liquids and gasses on which the design codes are based. According to (Fehling, Schmidt, Walraven, Leutbecher, & Fröhlich, 2014), application rules can be revised as such that the capabilities of UHPC can be taken into account. it is stated that if there are no capillary pores, then the material is practically impermeable to liquids. The prerequisite for this is that the water/cement ratio is sufficiently low, so there are no capillary pores.

The durability related properties offer many opportunities for design. For example: a UHPC bridge deck does not require an additional layer to protect it from harmful substances as it is already practically impermeable to these harmful substances. For the same reason, the concrete cover can be reduced compared to conventional concrete structures. Another feature is that the unhydrated cement may allow for self-healing of cracks up to a certain crack width.

Fire: In the first chapter, see 1.2.3, it was already mentioned that the fire resistance of higher strength concretes requires special attention, so this especially holds true for UHPC. Spalling can occur due to the dense microstructure, this prevents the vapour from escaping. Polypropylene fibres (see next paragraph) can be helpful in mitigating the risk of spalling.

2.3 Basics of conventional fibre-reinforced concrete

2.3.1 Introduction to conventional fibre-reinforced concrete

In the previous paragraph it was explained that a typical UHPC mixture contains fibres to increase its ductility (UHPC is therefore often regarded as a 'special' type of fibre-reinforced concrete denoted as Ultra-High Performance Fibre-Reinforced Concrete, or UHPFRC). This chapter takes a step back and explains some of

the basics of conventional fibre-reinforced concrete, to help in the understanding of the contribution of the fibres to the conventional concrete. The contribution of fibres to UHPC is discussed in more detail in 2.4. Fibre-reinforced concrete may be defined as concrete containing discontinuous discrete fibres. There are multiple properties that can be improved by adding fibres:

- Tensile strength
- Toughness
- Impact strength
- Fatigue strength
- Fire resistance (spalling)

The fibres can be made of many different materials, natural materials and manufactured materials, e.g. steel or plastics such as polypropylene. In the following subsequent paragraphs different aspects of the material will be covered.

2.3.2 Mix design of conventional fibre-reinforced concrete

Different types of fibres

Fibres of many different materials are available, these can be divided in four categories:

- Steel (most commonly used for structural applications)
- Plastics (e.g. polypropylene)
- Glass
- Natural materials (e.g. wool)

Fibres of different materials and in all sorts of shapes and sizes are used, although typically one type of fibres is used in a particular fibre-reinforced concrete mix. Some properties are given in Table 10.

Table 10 Typical fibre properties – (Mehta & Monteiro, 2006), p.507

Type of fiber	Tensile strength (ksi)	Young's modulus (10^3 ksi)	Ultimate elongation (%)	Specific gravity
Acrylic	30–60	0.3	25–45	1.1
Asbestos	80–140	12–20	~0.6	3.2
Cotton	60–100	0.7	3–10	1.5
Glass	150–550	10	1.5–3.5	2.5
Nylon (high tenacity)	110–120	0.6	16–20	1.1
Polyester (high tenacity)	105–125	1.2	11–13	1.4
Polyethylene	~100	0.02–0.06	~10	0.95
Polypropylene	80–100	0.5	~25	0.90
Rayon (high tenacity)	60–90	1.0	10–25	1.5
Rock wool (Scandinavian)	70–110	10–17	~0.6	2.7
Steel	40–400	29	0.5–35	7.8

SOURCE: ACI Committee 544, Report 544.IR-82, *Concr. Int.*, Vol. 4, No. 5, p. 11, 1982.

The properties of the fibre influence the behaviour of the composite. The effect of the fibres is characterised in a stress-displacement (i.e. crack opening) diagram. Important properties of the fibre are:

- Material properties
- Length of the fibre
- Volume fraction
- Aspect ratio
- Bond with the matrix
- Shape, texture and structure

General remarks and considerations

The following overview provides some general remarks and considerations with respect to conventional fibre-reinforced concrete:

- To be able to use fibres effectively as reinforcement, their properties such as tensile strength, elongation at failure and modulus of elasticity have to be significantly higher than the corresponding values of the matrix the fibres are encased in.

- The fibres should exhibit low creep, otherwise stress relaxation occurs, which would lower their effect. Moreover, their Poisson ratio should be similar to the value of the matrix to avoid inducing lateral stresses if the fibres are loaded (this may affect the bond at the interface).

- The aspect ratio of the fibre is defined as the ratio of length to mean diameter, which is an influencing factor for the maximum stress the fibre can withstand.

- It is important to obtain good bond (large shear strength) to allow for the transfer of axial stress from the matrix to the fibres. Higher interfacial bond strength means a higher maximum stress in the fibre and it can be improved by using fibres with a deformed or roughened surface, larger or hooked ends, etc.

- For glass fibres ordinary glass cannot be used in concrete containing Portland cement because the material because of alkaline attack. Other glass types have better durability but still show deterioration over time. The same holds for natural fibres, most natural fibres are not resistant to the alkaline environment due to the Portland cement either.

- The mix design should be as such that the fibres can be processed and optimal result is obtained.

- There are many fibres available. It is important that they are undamaged before they are incorporated into the matrix, otherwise their effect might be reduced. Some fibres are very sensitive to damage while other are not. Steel or plastic fibres can be added using standard mixing technique.

  The mixing should provide a uniform distribution of the fibres. Segregation or balling of fibres is to be prevented. Fibre aspect ratio, particle size (fibres and aggregate), amount of fibres etc are all important when it comes to the mixing.

Two commonly use types of fibres are steel fibres and plastic fibres (Polypropylene), some details on these types of fibres will be discussed next.

Considerations with respect to mix design

Adding fibres and increasing the aspect ratio both result in a decrease of workability. As mentioned in (Grünewald, 2004), the mixture composition of fibre reinforced concrete often is a compromise between the requirements on the fresh and the hardened state. The shape of the fibres differs from that of the aggregates; due to the long-elongated shape and/or a higher surface area the workability of concrete is affected.

Due to the addition of steel fibres the concrete appears to be stiffer compared to concrete without the fibres and the aggregate particles are pushed apart by the stiff fibres. The effect of flexible fibres is different: because the fibres are flexible the fill the spaces between the aggregate particles.

2.3.3 Plastic fibre-reinforced concrete (Polypropylene)

A commonly used type of plastic fibre is polypropylene and has the following effect on the composite properties:

- In the fresh concrete state, the fibres improve the consistency of the material, making the fresh concrete less susceptible to plastic shrinkage;

- Polypropylene improves the resistance to spalling. In case of temperature increase due to fire the fibres melt and create space for the water vapour in the concrete to expand into;

- Resistance under impact load is increased by adding Polypropylene fibres. These fibres have a low modulus of elasticity under normal loading rate, but it significantly increases under impact loading.

Polypropylene fibres can used be in fibrillated or multifilament form. Typical dimensions are a diameter of 18-32 µm and a length of 12-20 mm. The dosage is typically 600 – 1000 gram per m^3 concrete.

2.3.4 Steel fibre-reinforced concrete

Fibre volume fraction

As mentioned in the introduction of the paragraph, fibres can be added to the material to achieve different effects:

- Improve ductility and cracking behaviour
- Improve toughness
- Improve tensile strength
- Improve impact resistance or fatigue strength

As mentioned in (Mehta & Monteiro, 2006), the change of properties of the concrete that will occur depends on the type of fibres and the volume fraction of fibres that is added to the concrete mix. Based on the volume fraction of fibres, the concrete can be classified as follows:

- <1% (low volume fraction): Fibres at this volume are added in order to reduce shrinkage cracking, e.g. pavement slabs;

- 1-2% (moderate volume fraction): Fibres at this volume are added to increase the fracture toughness, impact resistance and modulus of rupture;

- >2% (high volume fraction): Fibres at this volume are added to increase strain-hardening of the material.

The contribution of the fibres to the material behaviour is demonstrated in Figure 32. It represents a load-deflection curve for two specimens, a plain concrete one and a fibre-reinforced concrete specimen.

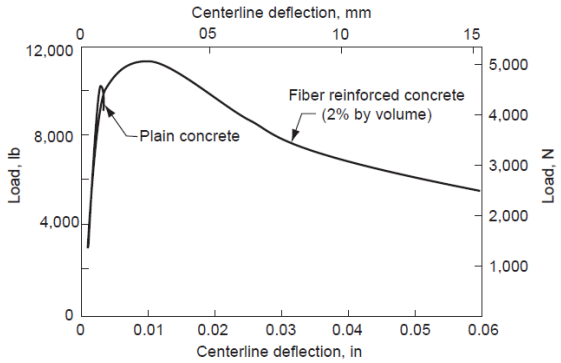


Figure 32 Load-deflection curve of plain concrete and FRC - (Mehta & Monteiro, 2006), p.504

One can observe that:

- The plain concrete specimen fails in a brittle manner as soon as the deflection that corresponds to the ultimate flexural strength has been exceeded. In the case of a plain concrete specimen, the plain specimen breaks;

- The fibre reinforced concrete specimen shows different behaviour: as soon as the deflection corresponding to the ultimate flexural strength has been exceeded the material cracks, however, it does not break and is still able to sustain load. Contrary to the plane specimen, the fibre reinforced specimen does not break after cracking. Failure of the fibre reinforced specimen is due to debonding or pull-out of the fibres, not due to the fracture of the concrete.

Toughening mechanism in fibre-reinforced concrete

The fibre-reinforced specimen does not break after the first crack is formed: the toughness (the area under the load-displacement curve) is increased. That means that the load has to do more work in order to let the specimen fail.

What happens is that as soon as a first crack occurs, the fibres act as a sort of micro-reinforcement (provided that their pull-out capacity is not exceeded and the fibres are not pulled out of the matrix). At the location of the first crack the matrix does not resist tension, the fibres carry the tensile load and transfer it to the matrix via bond. As long as the load on the fibres does not exceed the pull-out resistance or strength of the fibre, cracking may continue as the fibres continue to take over the tensile force at the location of the crack.

The increase in toughness that may be observed depends on two main aspects:

1. The fibre concentration: A higher fibre concentration means that a larger increase can be expected;
2. Pull-out resistance of the fibres.

The pull-out resistance of the fibres is a function of the parameters of the fibres, e.g. shape of the fibres or the surface texture. The pull-out resistance cannot be too weak or too strong:

- If the bond between the fibres and the matrix is too weak, the fibres slide out at a low load, this implies that the fracture toughness will be hardly increased;

- If the bond between the fibres and the matrix is too strong, they may not slide at all. This means that no energy will be dissipated. This is also an undesirable situation because the sliding action provides energy dissipation, this increases the toughness. Instead of dissipating energy by sliding out, the fibres will break before they can do so and the fibres only act as inclusions within the matrix.

Microcracking and macrocracking

In practice, one can distinguish between short fibres and long fibres. These fibres contribute in different ways to the increase of capacity of the material:

- Short fibres: Short fibres bridge the microcracks in the material. Their contribution results in an increase in strength.

- Long fibres: Long fibres cross the macrocracks that occur at higher load levels and increase the ductility.

Figure 33 illustrates the contribution of both fibre types in different stages of cracking of concrete in tension, the effect of short and long fibres is discussed in greater detail in section 2.3.

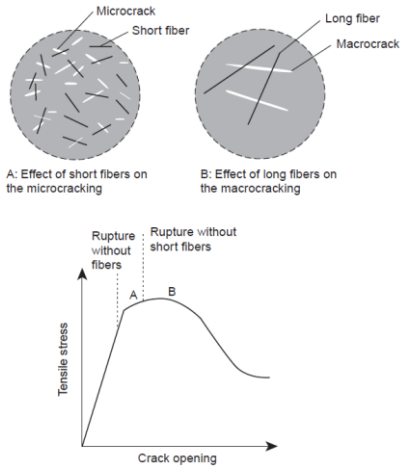


Figure 33 Influence of short and long fibres on cracking (Mehta & Monteiro, 2006), p.506

Properties of steel fibre-reinforced concrete

In this section a number of properties typical to conventional steel fibre-reinforced concrete are listed. To obtain an overview of the contribution to the change of mechanical properties, Figure 34 (Mehta & Monteiro, 2006) shows the relative improvement of a number of mechanical properties of plain concrete when straight fibres (length 25-38 mm) are incorporated into the material.

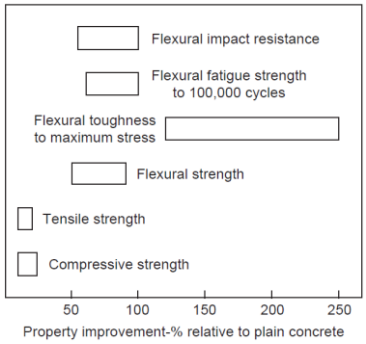


Figure 34 Relative improvement in various properties of concrete by fibre-reinforcement- (Mehta & Monteiro, 2006), p.517

Workability: Adding fibres results in a decrease of workability: As a general rule the loss of workability is proportional to the volume of fibres added, this holds for all types of fibres. An increase of aspect ratio also results in a reduction of workability. An optimum has to be found between the application of the fibres and the workability. Aggregate size, the use of admixtures, etc contribute to the workability as well. (Grünewald, 2004) distinguishes four causes why the fibres affect the workability:

1. The shape: The shape of the fibres is different compared to the aggregates, i.e. the fibres are elongated;

2. Change of structure: Steel fibres are stiff and as a result they push the larger aggregate particles apart, resulting in an increase of the porosity of the granular skeleton. The flexible fibres change the structure in the sense that they fill up the space between the particles;

3. Surface characteristics: The surface characteristics of the fibres are different than the surface characteristics of the cement and aggregate particles;

4. Friction due to deformation: Steel fibres are often deformed to improve anchorage, as a result the fiction between the deformed fibres and the aggregate particles are higher compared to fibres without these deformations (i.e. straight fibres).

As mentioned before, the mix design of fibre-reinforced concrete can be regarded as a compromise between the desired workability in the fresh state and the performance in the hardened state. Workability does not have to be a problem, it is simply an aspect that requires sufficient attention. In his dissertation, (Grünewald, 2004) demonstrated even that mixtures with fibres can be self-compacting by combining fibre-reinforced concrete and self-compacting concrete to self-compacting fibre-reinforced concrete, combining the best of both types of concrete.

Flexural toughness: For a low or moderate fibre content, the most significant change in properties is the flexural toughness of the material (not the strength).

Strength: When the amount of fibres is increased, the tensile strength also increases, albeit a smaller increase than the toughness. If the flexural strength is to be increased significantly, the solution is not to be sought for in the form of fibre reinforcement. In such a case providing traditional reinforcement is more effective for the same volume of steel.

Impact resistance: Related to the toughness is impact resistance, which is also increased by adding fibres. As described before Polypropylene fibres have been found to be very useful in these applications.

Fatigue resistance: The fatigue resistance is also related to flexural toughness, thus also increases when the amount of fibres is increased. Adding fibres to reinforced elements has shown to result in an increase in fatigue life and decrease in crack width.

Effect on E-modulus, creep and drying shrinkage: Adding steel fibres to the concrete has little effect on properties such as the modulus of elasticity, creep and drying shrinkage.

Durability: When it comes to durability, it seems that well compacted and well cured concrete with steel fibres result in durable structures, the prerequisite is that the fibres are protected by the cement paste. In most environments, some corrosion at the surface may be inevitable though.

2.4 Steel fibres in UHPC

In 2.2 the fundamentals of UHPC were covered, it was mentioned multiple times that a typical UHPC contains steel fibres to increase the ductility. In 2.3 the basics of conventional fibre-reinforced concrete were covered to aid in the understanding of the material. In this paragraph the focus will be specifically on the contribution of the fibres in UHPC.

For UHPC mixtures containing fibres, the term ''Ultra-High Performance Fibre-Reinforced Concrete'' (UHPFRC) is also often used. However, for the sake of simplicity, the term UHPC will be kept for the remainder of this report.

Effect of short and long fibres

In the previous paragraph the main principles of steel fibres were introduced. It was explained that one can distinguish between short fibres and long fibres. Both types of fibres contribute to the properties of the material in their own way, to illustrate this the fracture process is summarised first:

- Microcrack formation: Fine microcracks are formed at the weakest points in the concrete, i.e. the interface between the aggregate particles and the cement paste;
- Propagation: If the load increases the microcracks increase in number and propagate;
- Macrocracks: If the load continues to increase further the microcracks grow together and form macrocracks, eventually resulting in failure.

Both types of fibres contribute to the properties of the material in their own way, as described by (Markovic, 2006):

- Short fibres: Short fibres are activated by microcracking and bridge the microcracks in the material. Short fibres increase the tensile strength. See also Figure 35 a.
- Long fibres: Long fibres are activated by macrocracking, which will occur if the load becomes sufficiently high and the microcracks propagate and widen. The long fibres bridge the macrocracks in the material. Their primary contribution is to increase ductility. See also Figure 35 b.

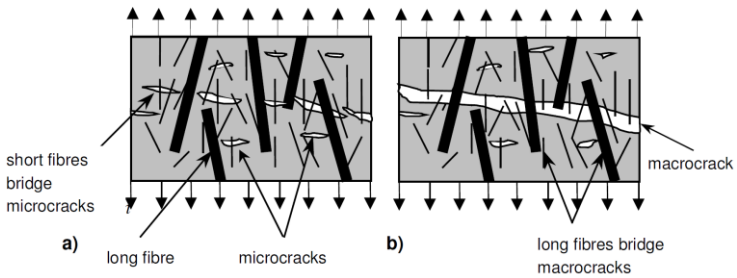


Figure 35 Main principle of hybrid-fibre concrete - (Markovic, 2006), p.8

Short fibres: The short fibres are relatively thin and for the same volume this will result in a larger number of fibres compared to longer fibres. Because of these points the short fibres can bridge the microcracks very well. The formation of the microcracks and the subsequent bridging of these cracks by the short fibres takes place in the initial stages of the tensile loading. This explains that the short fibres contribute to the tensile strength of the material, in other words: the material behaves elastic longer an there is an increase in pre-peak strength.

When the load is increased even further more and more microcracks appear and the cracks propagate and grow together into macrocracks. The longer fibres take over the role of the short fibres; the wider the cracks become the more the greater the reduction of the contribution of the short fibres because they are pulled out of the matrix, as described in 2.3.4.

Long fibres: As soon as the macrocracks appear, the longer fibres are activated and bridge these larger macrocracks, preventing these from becoming wider. The most important contribution of the long fibres is to the increase of ductility because of this effect (in other words: they affect the post-peak behaviour), but to a lesser extent they contribute to the tensile strength as well.

Hybrid fibre concrete

Instead of using just one type of fibres (approach of 'conventional' fibre-reinforced concrete), one could opt for using a combination of short fibres and long fibres to optimise the behaviour of the material, this type of fibre-reinforced concrete is also known as 'hybrid fibre concrete'. Combining these two fibres improves both the tensile strength (primary contribution of the short fibres) and the ductility (primary contribution of the long fibres).

Figure 36 shows experimental results from (Markovic, 2006), the flexural tensile strength of different types of (hybrid) fibre-reinforced concrete was tested. Combinations were used of short fibres (length of 13 mm) and long fibres (40 or 60 mm). One can see that the results are significantly influenced by varying the total volume of fibres and by combining different types of fibres.

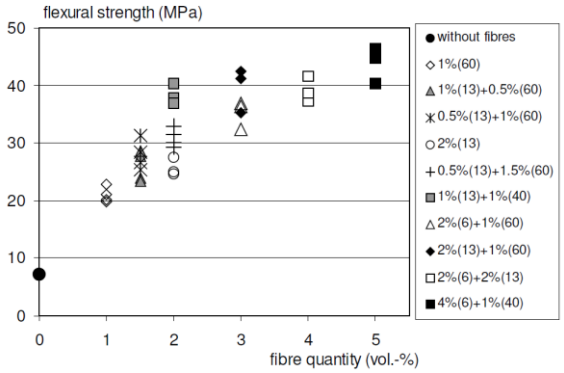


Figure 36 Flexural strengths of applied concretes with one and two types of steel fibres - (Markovic, 2006), p.76

Markovic performed both flexural tests (three-point bending tests) and uniaxial tensile tests. In both types of tests, it was found that the short fibres bridge the microcracks (these develop in the initial phases of the tensile loading, thus short fibres increase tensile strength) and the long fibres bridge the macrocracks (these develop later due to the propagation of the microcracks, thus these fibres increase ductility). A larger volume of short fibres turned out to increase the flexural strength.

It was also observed a phenomenon called 'strain hardening' in all his tested concretes, this means that the tensile load continued to increase after the formation of the first crack. The occurrence of strain hardening means that the material has a large deformation capacity after the occurrence of the first crack. A larger volume of long fibres resulted in more pronounce strain-hardening.

Another observation that was made was that during the initial phases of the tensile loading many small cracks occurred instead of the formation of a single large crack. This phenomenon is denoted as 'multiple cracking' and it can be an advantage related to durability.

From the experiments it turned out that better results were achieved in the flexural and tensile tests by using a combination of short and long fibres (hybrid fibre-reinforced concrete) than when only one type of fibres. This is attributed to the phenomenon of 'synergy', which means that the effect of the two combined is greater than the sum of the two contributions.

Markovic concluded that there are strong indications that the tensile strength and strain hardening behaviour (ductility) of hybrid-fibre concrete depends more on the applied combination of fibres than on the applied fibre volume content. The combination of the different fibre types offers possibilities for optimising the tensile behaviour.

Tensile properties of fibre-reinforced UHPC

As will be elaborated on in 2.5 there are different classes or types of UHPC available, each with their own mix composition (e.g. DSP or RPC, these materials are denoted as 'HPFRC' in the following graph). The uniaxial tensile response of these materials is rather similar though, as is explained in (Markovic, 2006), and also holds for hybrid-fibre reinforced concrete. For this reason, it will be covered in this section.

The following figure, shows the uniaxial tensile response of three types of concrete: plain concrete, conventional fibre-reinforced concrete and high-performance fibre-reinforced concrete.

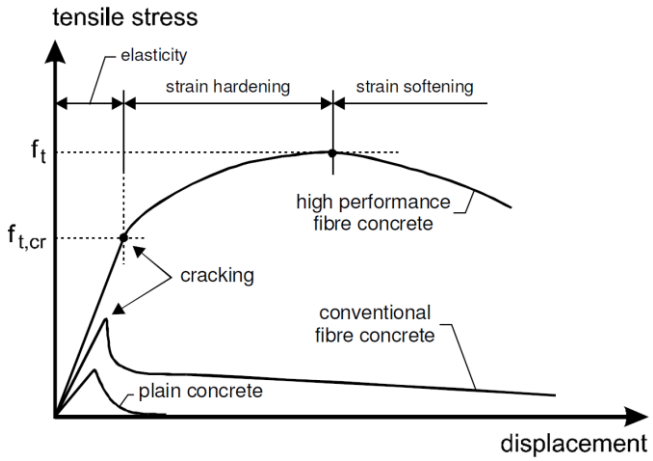


Figure 37 Uniaxial tensile behaviour of plain concrete, FRC and HPFRC - (Markovic, 2006), p.63

The load was increased until cracking occurred. As described before one can distinguish between two types of cracks: microcracks (develop in the early stages of the tensile loading, originating at the weaker zones) and macrocracks (a result of the microcracks propagating and growing together). From the figure, one can draw the following conclusions:

- **More pronounced microcracking**: Compared to conventional FRC, HPFR cracks at much higher tensile load levels. This can be contributed to the short fibres, especially if these are added in large quantities. Because of their presence, the effect of microcracking is more clearly present.

- **Occurrence of strain hardening**: Conventional FRC shows a decrease in the tensile capacity after the first large cracking (''softening''). HPFRC however shows the opposite: after the first large cracks have occurred the tensile load can be increased even further (''strain-hardening'').

- **Higher tensile strength**: Due to the strain-hardening, the tensile strength of the HPFRC is significantly higher than that of conventional FRC. After the tensile strength is reached one can observe that the tensile load is decreasing and softening will occur. This is explained by the fact that the crack opens further, which is resisted by the fibres. These fibres are pulled out of the matrix, as explained in 2.3.4. At a certain point there are no fibres (and thus no resistance) left and the tensile strength equals zero.

Hardening and softening behaviour

In the previous discussions the terms 'hardening' and 'softening' have been mentioned, these are important notions when describing the behaviour (force-displacement relation) of a material or structural element. Therefore, the findings are summarized and related to their importance for UHPC.

- Hardening: Tensile force increases after the tensile (cracking) strength is reached.
- Softening: Tensile force decreases after tensile/cracking strength is reached.

This has important consequences for the behaviour of the structure:

- Hardening: Due to the hardening, many smaller cracks develop.
- Softening: Due to softening a smaller number of wider cracks develops.

Hardening is typical behaviour of UHPC. According to Markovic it is a decisive difference between all conventional, and high-performance fibre concretes (Markovic, 2006). In (Walraven, Ultra-hogesterktebeton: een materiaal in ontwikkeling, 2006) it is mentioned that hardening behaviour is a typical feature of UHPC, it has to be visible for well-designed UHPC.

The importance of this behaviour is obvious: it provides the structure with deformation capacity, which would be impossible without the fibres because of the brittle behaviour. Moreover, it affects durability as a larger number of smaller cracks occurs instead of a smaller number of wider cracks.

This discussion does not mean that HPFRC does not show softening behaviour though, as can be seen in Figure 37 softening occurs after the tensile strength is reached.

2.5 Types of UHPC

Different types and commercial names: Denoting UHPC

In the introductory parts of this chapter, it was explained that UHPC is not just a single material, it is a very broad term covering many different mixtures, although they share a number of the same properties (high strength, durability, etc.) which means they can be designated as ''an Ultra-High Performance Concrete''. As a consequence, one may encounter many different terms or names to designate UHPC in daily practice.

Some of these designations are 'types' or 'classes' of UHPC (e.g. Reactive Powder Concrete) that have been developed in the recent decades, others are names of distinct commercial products or manufacturers (e.g. Ductal). In this paragraph a number of 'types' and commercial products is listed. The goal is to provide an overview by listing categories and names that are commonly encountered while going through the literature, but the reader should note that more types and products exist.

DSP (Densit)

H.H. Bache was the first to publish about UHPC, his invention became known under the name of 'Densified Systems containing homogeneously arranged ultrafine Particles (DSP). This first form of UHPC became commercially available under the name 'Densit' in 1983.

Compact Reinforced Composites (CRC)

Compact Reinforced Composite (CRC) is another invention made by H.H. Bache from 1986. It is a combination of fibre-reinforced concrete with a volume fraction of fibres and a large amount of conventional reinforcement. The fibres increase the tensile strength as well as the toughness of the material. The reinforcement is added to improve on the ductility of the material. The fibres control the cracks around the reinforcement bars. It is a material with high strength, ductility and durability but also expensive. Therefore, it is used if high mechanical properties or impact resistance is required.

Reactive powder concrete (RPC)

Reactive Powder Concrete (RPC) is an invention from France from 1993, made by the contractor Bouygues and cement manufacturer Lafarge, and it is a further development of the concepts devised by Bache. Mix proportions and conditions under which the material is cured were further optimized.

Optimizations made to the mix are that there is no coarse aggregate present, further optimization of the packing of the particles and the addition of steel fibres (2,5% of the volume, a larger volume is not possible because of workability for this type of mix).

The curing comprises of the application of pressure to the fresh concrete and heat treatment. The influence of the heat treatment is significant: it is reported that if the material is cured in hot water at 90 ^{o}C for three days, a compressive strength of 200 N/mm^2 can be reached. If it is cured at very high temperatures (i.e. 400 ^{o}C), compressive strength up to 800 N/mm^2 can be reached.

The material is commercially available (the commercial name of the Bouygues-Lafarge product is Ductal) and properties have been further improved, think of tensile strength, addition of other fibres or eliminating the need of the thermal treatment.

Commercial products of UHPC

Since the start of the development of UHPC, there have been different manufacturers who have developed UHPC products. These products (many, but not all, of French manufacturers) often fall within one of the aforementioned categories/types of UHPC. Some examples are:

- Densit (nowadays part of ITW)
- Ductal (by LafargeHolcim)
- BSI/Ceracem (by Eiffage)
- BCV (by Vicat)

Slurry-infiltrated-fibered concrete (SIFCON)

Slurry-infiltrated-fibered concrete follows a different approach compared to the previous materials, but is still commonly mentioned in the context of strong fibre-reinforced concrete materials. The production starts with placing steel fibres in a sort of formwork. After that, the fibres are infiltrated with a mortar slurry (a high water/cement ratio slurry is required) to infiltrate the fibres. As a result, large volumes of fibres can be processed.

The compressive strengths are up to 120 N/mm^2, the tensile strength up to 40 N/mm^2. Because of the fibre-directions the product is anisotropic and in the direction along the fibres the material shows ductile behaviour.

2.6 Practical considerations UHPC

2.6.1 Mixing UHPC

The mixing of UHPC has been summarised by Graybeal and has been included into (Russell & Graybeal, 2013). This summary provides a complete overview of the mixing process and has therefore been included into this report:

"Nearly any conventional concrete mixer will mix UHPC. However, it must be recognized that UHPC requires increased energy input compared to conventional concrete, so mixing time will be increased. This increased energy input, in combination with the reduced or eliminated coarse aggregate and low water content, necessitates the use of modified procedures to ensure that the UHPC does not overheat during mixing. This concern can be addressed through the use of a high-energy mixer or by lowering the temperatures of the constituents and partially or fully replacing the mix water with ice. These procedures have allowed UHPC to be mixed in conventional pan and drum mixers, including ready-mix trucks. (Russell & Graybeal, 2013), p.8

In (Fehling, Schmidt, Walraven, Leutbecher, & Fröhlich, 2014) more details are given on the mix procedure. As for conventional concrete, first the dry materials are put into the mixer and premixed. Water and superplasticizer are first mixed separately, and then added to the premixed dry materials. Mixing is continued until a stable and workable consistency is achieved. Fibres are then added and the mixing continuous until the fibres are properly mixed in.

The fact that UHPC can be mixed in conventional concrete plants was illustrated by a practical experiment performed in 2016, as described in (Hunger & Spiesz, 2016). This experiment was carried out to demonstrate the potential of UHPC produced in a 'normal' concrete mixing plant, transported by a truck mixer and casted on site.

The goal of this experiment was to produce an economically viable mix with a strength of about 200 N/mm^2 without requiring special treatment (e.g. heat treatment) and with using coarse aggregate (6 mm particle size was used as maximum) and readily available constituents. A concrete mix was composed that would not only have a high compressive strength, but also good self-compacting properties.

The result was a UHPC with excellent properties: The concrete compressive strength was about 195 N/mm^2, the modulus of elasticity was about 72.000 N/mm^2 and the resistance against carbonation and chloride penetration were also proven to be excellent. This experiment indeed demonstrated that UHPC with excellent properties can be produced in a 'normal' concrete plant without requiring special treatment or constituents. The remark should be made that good mix design is essential though.

2.6.2 Placing and fibre orientation

Casting operations

Typical properties of UHPC that should be kept in mind for the casting operations are:

- Presence of fibres and the effect of fibre-orientation on mechanical properties
- Well-designed UHPC mix is flowable and has self-compacting properties

The placement of UHPC has been summarised by Graybeal and has been included into (Russell & Graybeal, 2013). It has been included into this report because it proves a good overview of the casting operations:

''The placement of UHPC may immediately follow mixing or be delayed while additional mixes are completed. Although the dwell time prior to the initiation of the cement hydration reactions can be influenced by factors such as temperature and chemical accelerators, it frequently requires multiple hours before UHPC will begin to set. During extended dwell time, the UHPC should not be allowed to self-desiccate.

Casting of fibre-reinforced concretes requires special considerations in terms of placement operations. UHPCs tend to exhibit rheological behaviours similar to conventional self-consolidating concretes, thus possibly necessitating additional form preparation but also allowing for reduced during-cast efforts. Internal vibration of UHPC is not recommended due to fibre reinforcement, but limited external form vibration can be engaged as a means to facilitate the release of entrapped air.'' (Russell & Graybeal, 2013), p.9

Importance of fibre orientation

One aspect that should be kept in mind is the orientation of the fibres. UHPC with fibres is a composite which means that the fibre orientation is one of the factors determining the properties.

Single fibre: If the effect of fibre orientation is studied from the point of view from a single fibre it can be concluded that the reinforcing capacity of a fibre is affected by its orientation with respect to the crack. If a fibre is oriented in the direction of the tensile stress, its contribution is optimal. The contribution reduces if the fibre is not parallel to the crack but under an angle. Moreover, the distribution of the fibres through the material should be homogeneous.

Structural element: On a larger scale the effect of casting on the fibre orientation is of importance. If fibres are to bridge cracks, they should be distributed through the whole element. The fibre orientation can be affected by two factors:

- The dimensions of the structural element
- The way of casting the concrete

The flow of the concrete along the panels of the formwork can affect the orientation of the fibres which influences the mechanical properties of the hardened concrete. The orientation of the fibres can be accounted in calculations for using the ''orientation factor''. This is especially of importance because UHPC is very suitable for slender and thin structural elements. For this reason, a distinction is often made between thinner and thicker elements.

2.6.3 Curing UHPC

Relevant parameters

Just as for normal concrete, providing proper curing conditions are important to assure that the concrete can develop its properties. The curing conditions of UHPC are (just as for conventional concrete) governed by two parameters: temperature and moisture.

- **Temperature**: As mentioned in the first chapter, the temperature is important to control the rate of hydration. Higher temperature accelerates the process, resulting in faster development of the strength.

- **Moisture**: Another criterion is the moisture. UHPC is a dense material with low water/cement ratio. Because relatively little water is present in the first place, the loss of moisture has to be prevented.

Curing conditions influence the final properties of the material. As mentioned, compressive strengths up to about 200 N/mm^2 can be achieved without taking special measures (e.g. higher curing temperature). Taking additional measures can result in higher strengths. An example is RPC, which requires high pressure and temperature to reach a compressive strength up to 800 N/mm^2.

Moisture

A consequence of the low water content of the material is that its surface dries very quickly, to prevent a 'skin' forming on the surface if no measures are taken. For example:

- Cover the surface with plastic sheeting directly after concreting;
- Spray curing compound over the whole surface;
- Apply a thin water film on the surface.

Temperature and heat treatment

Heat treatment is often mentioned in relation to UHPC, it can increase the strength and speed of strength development. According to (Fehling, Schmidt, Walraven, Leutbecher, & Fröhlich, 2014), UHPC elements are typically produced in prefab factories, where it is common practice to apply this heat treatment. The procedure is described to be as follows: First the components are left in the mould for 24 hours and are covered up. The elements are then subsequently heated for 48 hours at 80 – 90 °C, heating for longer time has no effect. After the heat treatment, the elements should be given time to cool down slowly to prevent microcracking. It is mentioned that the compressive strength of heat treated UHPC is generally 20 – 30 N/mm^2 higher than identical components stored in water.

At higher temperature (80-90 °C), the silica fume reacts with the calcium hydroxide liberated by the hydration of Portland cement, and additional hydration products are formed. This results in a denser microstructure and higher compressive and flexural tensile strength than without heat treatment. Another benefit of heat treatment is that creep and shrinkage are reduced. After the treatment, no more shrinkage takes place.

Other temperature ranges can be found as well. Again, in (Fehling, Schmidt, Walraven, Leutbecher, & Fröhlich, 2014) it is stated that it is common practice to apply a temperature of 80 to 90 °C for one or two days. If heat treatment at 250 °C is applied, not only the rate of the reaction is influenced, but it also leads to a change in the microstructure due to the formation of other mineral phases, with much higher strengths as a result. In the context of Reactive Powder Concrete, even higher temperatures of 400 °C are mentioned, but the trend is clear: very high temperatures allow for very high strength.

2.7 Summary second chapter

In the 1980's, new developments pushed the limit of what could be achieved in terms of concrete compressive strength. H.H. Bache was the first to develop and apply new concepts regarding the composition of concrete, which made it possible to produce concrete with compressive strength in the range of 150 – 200 N/mm^2. To produce this ultra-high strength concrete, a number of principles has to be followed:

- **Low water/cement ratio**: The water/cement ratio is kept very low (typically about 0,2) to make sure that all the water is bound and the formation of capillary pores due to remaining water is prevented. The remaining cement acts as a filler. Superplasticizer is required to obtain a workable mix.

- **Optimize the packing density of the particles**: Optimizing the packing density result in limiting the stresses at the contact surfaces of the different particles, preventing the formation of microcracks until high stresses are reached. Moreover, a dense microstructure contributes to high durability.

- **Limiting the maximum aggregate particle size**: Limiting the maximum particle size results in a more homogeneous material with lower stress concentrations in and a reduction in size of the porous interface between the aggregate particles and the cement paste.

- **Addition of fibres**: Stronger concrete is also more brittle, adding fibres increases the ductility and contributes to the tensile strength as well.

Following these principles does not only result in concrete with a very high compressive strength, but this material has multiple characteristics that are far better than concretes with lower strength. Given these different properties, there may be other reasons to use this material than concrete compressive strength, therefore, the name Ultra-High Performance Concrete (UHPC) is generally used instead of UHSC. Typical characteristics of this material are:

- **Good mechanical properties**: The most important parameter is the high compressive strength, but the tensile strength and modulus of elasticity are also higher compared to normal strength concrete (although the development of tensile strength and modulus of elasticity lag behind the development of the compressive strength).

- **Good durability**: The high mechanical properties are accompanied by good durability due to the dense structure and low porosity. The larger pores are absent, making the material practically impermeable to harmful substances (liquids and gasses).

- **Good workability**: A typical UHPC mix has good workability and is often self-compacting (or can be optimised to obtain a self-compacting concrete).

The benefits of using material of high strength are obvious, it allows for more slender designs compared to conventional concrete because the required cross-sectional dimensions can be smaller. The higher stiffness and excellent properties regarding durability and workability can also be reasons to choose for UHPC. However, one should also keep other characteristics in mind while designing:

- **Brittleness (without fibres)**: One should keep in mind that UHPC is very brittle if no precautions are taken in the form of adding fibres to increase the ductility. Therefore, steel fibres are typically added.

- **Long term behaviour**: Long term behaviour is also a point of attention. Autogenous shrinkage is very predominant in the case of UHPC. Creep (lower creep coefficient compared to normal strength concrete) should also be accounted for. Applying heat treatment reduces the shrinkage and creep.

- **Initial costs & optimization**: The initial costs of UHPC are significantly higher than that of conventional concrete. However, when designed properly and compared in a 'fair' way with conventional concrete solutions over a longer period, UHPC solutions can be more cost-effective in the long run.

The new developments started by Bache were taken up by others as well. Nowadays, the term UHPC is therefore a very broad term that can be used to denote a whole 'class' of concretes that share a number of the same properties, typically the 28 days concrete compressive strength being the parameter used to classify the material. Because the term 'UHPC' comprehends many different mixtures, it is difficult to give a general definition or a general mixture composition. However, in the context of this project the following definition is used:

''UHPC is a concrete with a concrete compressive strength higher than 150 N/mm^2 and accompanied by higher tensile strength, E-modulus and density (and thus durability) compared to normal strength concrete.''

Fibres can be added to the material to change different properties, steel fibres are commonly used. One can distinguish between short fibres and long fibres. Short fibres bridge microcracks in the material, because these occur in the initial stages of loading short fibres contribute to an increase in tensile strength. Long fibres bridge macrocracks, preventing these from becoming wider and contributing primarily to the ductility of the material. Due to the addition of fibres, UHPC typically shows strain-hardening behaviour.

As mentioned before, UHPC is not a single material but it is a broad term for materials that share one or more of the same properties. In practice one can encounter different 'types' of UHPC (e.g. DSP, RPC) and moreover there are many different commercial UHPC products (e.g. Densit or Ductal).

Mixtures resulting in a compressive strength up to 200 N/mm^2 are commercially available or can be produced using normal mixing plants, readily available ingredients and without requiring special treatment. Good mix design is essential though. Higher strength values, values up to 800 N/mm^2 have been reported, can also be achieved, but this typically requires special treatment (high heat and/or pressure).

When it comes to the casting operation it is important to keep in mind that well-designed UHPC mixes have self-compacting properties (although it might not be self-deaerating and need compaction in some cases) and that the fibre orientation affects the mechanical properties of the hardened material. Fibres that are aligned with the direction of the tensile stress contribute in the most optimal way. Flow of concrete along the formwork can affect the direction of the fibres, by orienting them already in a certain direction.

When it comes to the curing of UHPC, two factors are very important: temperature and moisture. The temperature is important in controlling the rate of hydration. And because UHPC is a dense material with low water/cement ratio, a relatively small amount of water is present and the loss of moisture has to be prevented. In practice, this can be done in multiple ways. Heat treatment can be applied at different temperatures, heat treatment at 80 – 90 °C is common practice in the production of prefab UHPC elements. This results in a denser microstructure, a higher compressive strength and a reduction of shrinkage and creep compared to elements without the treatment. Applying even higher temperatures results in the formation of other mineral phases, resulting in even higher strengths.

2.8 Bibliography

Betoniek. (2017). Da's sterk! *Betoniek Standaard*, 1-12.

Buitelaar, P., & Quist Batista, C. (2019). Nieuwe generatie UHSB. *Cement*, 24-30.

Fehling, E., Schmidt, M., Walraven, J., Leutbecher, T., & Fröhlich, S. (2014). *Ultra-High Performance Concrete UHPC*. Berlin: Wilhelm Ernst & Sohn.

Grünewald, S. (2004). Performance-based design of self-compacting fibre reinforced concrete. *Proefschrift*. TU Delft.

Hunger, M., & Spiesz, P. (2016). Praktijkproef bewijst potentie UHSB. *Betoniek Vakblad*, 12-16.

Kaptijn, N. (2002). Toekomstige ontwikkelingen van zeer-hogesterktebeton. *Cement*, 56-63.

Markovic, I. (2006). High-Performance Hybrid-Fibre Concrete: Development and Utilisation. *Proefschrift*. TU Delft.

Mehta, P. K., & Monteiro, P. J. (2006). *Concrete: Microstructure, Properties, and Materials* (Third edition ed.). McGraw-Hill.

Neville, A., & Brooks, J. (2010). *Concrete Technology* (second edition ed.). Harlow: Pearson.

Russell, H. G., & Graybeal, B. A. (2013). *Ultra-High Performance Concrete: A State-of-the-Art Report for the Bridge Community*. Federal Highway Administration (FHWA), Office of Infrastructure Research and Development.

Soen, H. (2007). *Praktische Betonkennis*. 's-Hertogenbosch: Cement&BetonCentrum.

Walraven, J. (2006). Ultra-hogesterktebeton: een materiaal in ontwikkeling. *Cement*, 57-61.

Walraven, J. (2012). UHSB op weg naar regelgeving. *Cement*, 50-55.

Ye, G., & Schlangen et al., E. (2018). Lecture Notes Concrete Science and Technology CIE5110. Delft.

3

DESIGNING IN ULTRA-HIGH PERFORMANCE CONCRETE

3.1 Introduction to designing in UHPC

In the first chapter the essentials of conventional concrete were discussed to gain an overview of the main properties of the material and some more in-depth knowledge regarding concrete technology. This formed the basis of knowledge for the second chapter, in which UHPC was introduced. The main characteristics of concretes that can be denoted as UHPC were discussed and it was explained where the typical behaviour (high compressive strength and hardening due to the fibres) comes from. In this chapter the next step will be taken by looking at considerations and current recommendations for design in UHPC.

The start of this chapter is dedicated to identifying the challenges that one should keep in mind when designing in UHPC. The following part is dedicated to identifying the different guidelines that have been introduced since the introduction of UHPC, this will be used for deciding on which guideline to use in the design stage of the project. The chapter will be concluded with a summary.

3.2 Considerations for designing in UHPC

3.2.1 Challenges of designing in UHPC

Designing in UHPC is accompanied by additional challenges when compared to designing in normal strength concrete, multiple reasons for this were identified during the literature study. This sub paragraph gives an overview of these points of attention and is written mostly from the structural engineer's perspective, using sources such as (Van Nalta, 2015), (Hunger & Spiesz, 2016) and (Walraven, UHSB op weg naar regelgeving, 2012). The following discussion is mainly a summary from the relevant points found in these sources.

Validity of Eurocode 2 (use of codes)

The first point of attention is the use of codes. Standard practice for concrete structures is the use of Eurocode 2. Relying on this code is not possible in the case of UHPC. The first reason for this is that UHPC falls beyond the range of validity of Eurocode 2, it is only valid up to concrete strength class C90/105. From the previous chapter it is clear that UHPC behaves differently than lower strength concrete, thus one-to-one application of Eurocode 2 to UHPC structures is out of the question.

The second reason why UHPC could fall beyond the range of validity of Eurocode 2 is because of structural dimensions. UHPC allows for very slender designs, which is often required to make a UHPC solution (economically) attractive. The result however might be that the structure or structural element is so slender that it falls beyond the minimum dimensions as prescribed in Eurocode 2. If the design falls beyond the validity of the current codes, there are two options:

1. New codes & guidelines
2. Provide additional research & documentation

New codes & guidelines: As will be discussed in greater detail in 3.2.2., development of codes and guidelines is a continuous process. This process typically lags behind technological advancements. Generally

accepted codes and regulations regarding UHPC are lacking, although there are many different initiatives to formulate codes and guidelines for the use of UHPC.

Additional research & documentation: As mentioned in (Van Nalta, 2015), a practical approach to the lack of information regarding UHPC in the codes is by using Eurocode 2 as a starting point and supplement the code with extensive documentation of the used UHPC whenever deviation from Eurocode 2 is made. Using this extensive documentation, one can still prove that the design is safe, even when it is not compliant to the Eurocode.

For each deviation from the guidelines and standard methods of modelling and analysis, proper investigation and clarification is required to explain how the material behaves and which calculation methods and approaches from mechanics can be used to obtain a safe design. A practical example as given in the article is the reduction of the concrete compressive strength.

In Eurocode 2 a reduction is prescribed for all concrete strength classes above C50/60, this is done because of the brittleness of the material. Suppose one would extrapolate this rule to the values of UHPC, then this would result in very significant reduction of the strength because of the brittleness. Should one want to deviate from this rule, then again this should be justified using knowledge of the material properties, i.e. extensive documentation.

Mix composition

The second point of attention concerns the mix composition of UHPC and subsequently the properties in hardened state and the relation to the codes. The available UHPC mixtures are often used as premixes. Dry premixes are delivered to the construction site after which water is added to the mixture or by mixing the constituents following the instructions from the supplier. Anyhow, the composition of the UHPC is not always completely known, let alone its properties and the differences between different products. This means that in design one should often rely on the documentation belonging to a single commercial product.

A further complication is that the available guidelines are sometimes written for a specific commercial product. This means that care should be taken because knowledge on one type of UHPC or one guideline on UHPC is not always directly interchangeable with other UHPC mixtures. A very obvious example of this is 'Design Guidelines for Ductal Prestressed Concrete Beams', as will be covered later in this chapter. The French AFGC-SETRA guidelines were aimed at fibre-reinforced UHPC in combination with prestressing and certain types of concrete.

Durability & long-term behaviour

Typically, UHPC is applied for slender structures. To obtain a design as slender as possible, measures such as reducing the concrete cover (e.g. smaller cover than the minimum value prescribed in Eurocode 2) can be taken. If this is done, one should be able to prove that the material is sufficiently dense, so that corrosion of the reinforcement is prevented during the design service life.

Cracking is also related to the durability. A UHPC structure is generally a slender structure. Slender structures loaded in bending and a relatively large variable load may result in microcracks that grow over time. That means that UHPC structures are potentially prone to cracking. The cracking and crack control should be investigated, to be able to show that the durability of the structure is guaranteed during its surface life.

The third aspect related to long term behaviour is fatigue. For a conventional concrete structure this failure criterion is generally not very likely to occur because of the high dead weight of the structure compared to the variable load. This ratio is different for slender UHPC structures though, and as a result, fatigue might become a criterion that has to be taken into consideration.

Resistance to fire

As mentioned before in this report, UHPC has a higher risk of spalling. The higher the tensile strength of the material, the higher the build-up of pressure and the more dangerous spalling might become. Eurocode 2 prescribes measures to prevent spalling above C80/95 or research to prove that it will not occur with the used mixture. This is an additional point of attention.

This subparagraph is concluded by summarizing these points of attention, which has to be kept in mind throughout the remainder of the project:

UHPC is a vastly different material than conventional concrete. Due to its properties and characteristics, it allows for and requires a different way of designing structures (slender design). The material falls beyond the scope of Eurocode 2, this is due to its properties and potentially also due to the dimensions of the structure. In addition, generally applicable and generally accepted codes & guidelines on UHPC are lacking. To compensate for this and to be able to deviate from Eurocode 2, thorough knowledge about the material properties & characteristics, the available codes & guidelines and calculation procedures & structural mechanics is required.

3.2.2 Development of codes

Developments of guidelines is a continuous process, this sub paragraph is written to provide an overview of the development of the guidelines on UHPC up to the point of writing this report. Table 11 provides an overview of the development of different codes, guidelines and other related documents since the first applications of UHPC were reported.

The table and remainder of the paragraph provide a summary of information found from various sources on this topic, among which are (Walraven, Ultra-hogesterktebeton: een materiaal in ontwikkeling, 2006), (Walraven, UHSB op weg naar regelgeving, 2012), (Buitelaar & Quist Batista, 2019), (Wikipedia, sd) and (Aarup, sd).

Table 11 Timeline

Year	Country	Development
1981	Denmark	The development of UHPC started with H.H. Bache who invented a binder with which ultra-high strengths could be achieved, the finding was patented and the first commercial party selling UHPC was founded (Densit). Over the years new products became commonly available, such as silica fume. Developments continued and after the patent had expired other companies started working on their own binders for UHPC.
90's	Worldwide	First applications of UHPC, the need for guidelines becomes obvious.
1997	Canada	First large-scale application of UHPC: The pedestrian bridge in Sherbrooke, Quebec.
2000	Australia	First guideline on UHPC is published: ''Design Guidelines for Ductal Prestressed Concrete Beams''. As the name suggests, it is specifically meant for prestressed beams made using Ductal.
2002	France	A comprehensive guideline (with interim status) is published by AFGC-SETRA: ''Ultra-High Performance Fibre-Reinforced Concretes – Interim Recommendations''.
2005	Germany	In 2005 an extensive research project funded by DFG (Deutschen Forschungsgemeinschaft) started focussing on UHPC, the project ran until 2012.
2006	Japan	Publication of ''Recommendations for Design and Construction of Ultra-High Strength Fibre-Reinforced Concrete Structures (Draft)'', JSCE Guidelines for Concrete No. 9. Draft in 2004, English version in 2006.
2008	Germany	Heft 561 (Sachstandsbericht ''Ultrahochfester Beton'') is published by DAfStb, bringing the community up to date with the recent information from the running research project. Work continues with the goal to publish a DAfStb guideline.
2013	US	In the US, the federal Highway Administration published ''UHPC: A State-of-the-Art Report for the Bridge Community'', a comprehensive document that can be used as a framework to present the possibilities for the use of UHPC in the (US) infrastructure.
2013	France	An updated version is published of the 2002 AFGC-SETRA recommendations, at the moment of publishing the most comprehensive code. This guideline does no longer have an interim status.
2016	Switzerland	In Switzerland the code SIA 2052 ''Ultra-Hochleistungs-Faserbeton (UHFB) – Baustoffe, Bemessung und Ausführung'' is published.

2016	France	In France, the codes NF P18-470 (UHPFRC – Specifications, performance, production and conformity) and NF P18-710 (Design of concrete structures – Specific rules for UHPFRC) were published. These are national annexes to EN 1992-1-1 and EN 206, they replace the AFGC-SETRA 2013 recommendations.
2018	France	In France, the code NF P18-451 (Execution of concrete structures – Specific rules for UHPFRC) is published.

At the moment of writing this report work on the Germany by DAfStb guideline is still in progress, it is expected that it will largely be based on the results of the research programme mentioned in the table. The code will consist of two parts, one for the assessment of the structures (calculations) and one for requirements with regard to the material itself, as is mentioned in (Wachter, Fischer, & Schramm, 2019).

The aforementioned list is not complete, in Canada and Spain guidelines are being prepared as well, according to (Aarup, sd). The same holds for the US where an ACI committee (''committee 239 – UHPC'', formed in 2011) is working on UHPC guidelines.

The summary presented in Table 11 might raise the idea that the development of UHPC guidelines is solely a national process, but in reality, this is not the case. On an international level, ''Fédération internationale du béton'' (fib) is working on a guideline for fibre-reinforced UHPC. The work started in 2004 with the formation of ''Task Group 8.6'' (TG8.6), this group worked in close collaboration with TG8.3, which had a similar task for conventional fibre-reinforced concrete.

At the moment of writing this report, the group is still continuing its work as a part of ''Commission 4'' under the name of TG4.2 (''Task Group 4.2 – Ultra-High-Performance Fibre-Reinforced Concrete''), again in close corporation with TG4.1 (''Task Group 4.1 - Fibre-reinforced concrete''). According to the information found on the Task Group's page on the fib website, a bulletin is in preparation, the work being close to completion.

3.2.3 Overview of available codes

Overview of codes

The following step is to list the state-of-the-art with respect to codes and guidelines on UHPC. Distinction is made between international and Dutch engineering practice.

International engineering practice: The State-of-the-art report of the FHWA (Russell & Graybeal, 2013) describes the recommendations typically used up to the moment of publishing their report. Because the document was meant to present the state-of-the-art in UHPC, and because it is the result of an extensive literature search, the document is used as the starting point for the search of UHPC guidelines in the international engineering practice up to 2013. The following guidelines were identified in the report:

- Australia: Gowripalan, N. and Gilbert, R.I., Design Guidelines for Ductal Prestressed Concrete Beams, The University of New South Wales, May 2000.

- France: SETRA-AFGC, Ultra-High Performance Fibre-Reinforced Concretes - Interim Recommendations, Groupe de travail BFUP, January 2002.

- Japan: Japan Society of Civil Engineers (JSCE), Recommendations for Design and Construction of Ultra-High Strength Fibre Reinforced Concrete Structures (Draft), JSCE Guidelines for Concrete No. 9, 2006.

The reader should note that the publication by Russell & Graybeal refers to the interim recommendations from SETRA-AFGC, but in the meantime a revised version is published (also in 2013).

Dutch engineering practice: Mainly using articles from trade journals, such as (Ketel, Willemse, Van Rijen, & Koolen, Rekenmodel VVUHSB (1), 2011), (Ketel, Willemse, Van Rijen, & Koolen, Dwarskracht- en kolomberekening VVUHSB, 2011), (Bouvy, 2012) and (Falbr, Hunger, & Spiesz, 2016), an overview was

formed of the common practice with respect to UHPC in the Dutch construction industry. As was to expected, mainly the same references were found as in the publication by Russell & Graybeal, but in addition CUR111 is also often mentioned, the most recent revised version being published in 2019:

- CROW-CUR Aanbeveling 111:2018: Staalvezelbeton-bedrijfsvloeren op palen, Maart 2019.

Recent advancements: The sources mentioned are up to the year 2016 and since then new documents have been published, as can be read in for example (Aarup, sd). The following two codes were published in France in 2016:

- NF P18-470: UHPFRC – Specifications, performance, production and conformity
- NF P18-710: Design of concrete structures – Specific rules for UHPFRC

These codes fit within the European code framework, as they are the national annexes to EN 206 and EN 1992 respectively. These codes replace the AFGC-SETRA recommendations and are available in French and English. The set of French codes on UHPC was further completed in 2018, with the issue of:

- NF P18-451: Execution of concrete structures – Specific rules for UHPFRC

In Switzerland a code on UHPC was published as well in 2016:

- Ultra-Hochleistungs-Faserbeton (UHFB) – Baustoffe, Bemessung und Ausführung

Revisions in the form of corrections were issued in 2017. The documents are available in German and French.

Other documents: Other documents are often mentioned in literature as well, albeit not specifically because of UHPC. An example of this is the fib Model Code 2010, which contains sections on fibre-reinforced concrete for all strength classes (from normal strength up to and including ultra-high strength).

3.3 Description of the codes

In the following sections, the different codes and their content are briefly discussed and subsequently it is formulated on which criteria a code will be selected for further use in the project, a decision that will be taken at the start of the design phase.

3.3.1 Design Guidelines for Ductal Prestressed Concrete Beams (2000)

The guideline ''Design Guidelines for Ductal Prestressed Concrete Beams'' was published in 2000 and as the name suggests, it gives guidelines for the design of prestressed concrete beams using the commercial UHPC product 'Ductal', which is a Reactive Powder Concrete (RPC). The document was based on the study of the literature (it is reported that most of the existing literature on RPC and its applications were French sources, codes and specifications) that already existed on the topic and the experiences from the first existing structures constructed using RPC. It is already mentioned in the document that research was still going on in the field and that it was expected that (parts of) the document would have to be revised and expanded. The document fits in the framework of Australian design codes (AS3600 – 1994: Concrete Structures).

In the third chapter design requirements and procedures are described. The procedures are based on structural mechanics and information on the material characteristics. Chapter 4 covers the properties of the material to be used in design (behaviour in tension and compression, design values, idealised stress-strain relations, creep, etc.). Chapters five, six and seven cover the strength in flexure, shear and torsion respectively. Crack control and deflection at service loads are covered in chapters eight and nine. The remaining four chapters describe fire resistance, fatigue, prestress losses and the anchorage zone of the prestressing. The annexes contain material properties of Ductal (annex A), details and examples on behaviour in bending and the $M - \kappa$ diagram (annex B) and examples of design calculations (annex C).

3.3.2 AFGC-SETRA recommendations (2002)

The first comprehensive guideline (with interim status) was the Interim Recommendations on Ultra-High Performance Fibre-Reinforced Concretes, published by the AFGC-SETRA working group for UHPFRC in 2002. The SETRA (Service d'études sur les transports, les routes et leurs aménagements or previously anciennement Service d'études techniques, des routes et autoroutes) is an organization part of the French Ministry of Ecology and is active within the fields of transport, roads and structures in France. The AFGC (Association Française de Génie Civil) is an organization for engineers and researchers active within the field of civil engineering in France.

The document was written as a reference for the use of UHPFRC in practice. The definition of this material in the code is as follows:

"Ultra-High Performance Fibre-Reinforced Concrete" refers to materials with a cement matrix and a characteristic compressive strength in excess of 150 MPa, possibly attaining 250 MPa, and containing steel fibres in order to achieve ductile behaviour under tension and, if possible, to dispense with the need for passive (non-prestressed) reinforcement. They may also contain polymer fibres. (Groupe de travail BFUP, 2002), p.7

The code focusses on the types of UHPFRC that were commercially available at the time the guideline was written (BSI and Ductal products such as RPC). It is stated that the working group based its work on the existing French recommendations for fibre-reinforced concrete (published by AFREM in 1995) and the specifications by EDF for the UHPFRC beams that were used in Nuclear power plants. An early application of UHPFRC in practice was in UHPFRC beams at the Cattenom nuclear powerplant in 1998, this material was selected because of its excellent properties related to durability, which was required because of the aggressive environment in the cooling towers of the power plant (Fehling, Schmidt, Walraven, Leutbecher, & Fröhlich, 2014).

Moreover, the document makes use of laboratory research and experiences obtained through the first applications of the material. The document consists of three parts:

- Part 1: The first part is about the characterization of the material and gives information on how to determine the mechanical performance. Moreover, aspects such as inspection of the product and placement is covered;

- Part 2: Focusses on the design of UHPFRC structures. It is stated that the chapter was written to be in accordance with the existing French code BPEL 91 (''1991 edition of the Rules for Use of Prestressed Concrete at Ultimate Limit State revised in 1999''), which was adjusted to include the effect of the steel fibres and the use of structures without reinforcement;

- Part 3: Focusses on durability of UHPFRC.

The annexes (nine in total) discuss topics such as the compressive behaviour, experimental procedures and characterization of the material, shrinkage, creep and impact strength. Also, more experience-based information is given, such as tests used for design testing for the application of UHPFRC at the Cattenom power plant, characteristics of a number of UHPC mixtures and experience of the Bourg-les-Valance viaduct with respect to design safety factors.

3.3.3 Recommendations for Design and Construction of UHSFRC structures (2006)

In 2004 the Japan Society of Civil Engineers (JSCE) published the JSCE Guideline for Concrete No. 9., which was a draft version titled ''Recommendations for Design and Construction of Ultra-High Strength Fibre-Reinforced Concrete Structures''. The English version was published in 2006. Although many references to this document have been found during the literature study, the document itself could not be obtained. However, it is still deemed valuable to have an idea of the content of the guideline, therefore, the description of the guideline as given in (Russell & Graybeal, 2013) is cited:

"The draft recommendations in Recommendations for Design and Construction of Ultra-High Strength Fibre Reinforced Concrete Structures (Draft), published by the Japan Society of Civil Engineers in 2006, provide basic principles for design and construction using UHPC. The design values for materials include compressive strength, first cracking strength, tensile strength, stress-strain relationships, modulus of elasticity, Poisson's ratio, thermal characteristics, shrinkage, creep, and fatigue. Other chapters address structural safety (strength design), serviceability, fatigue resistance, structural details, prestressed concrete, durability, construction (constituent materials, mix proportions, production, transportation, and inspection), cold-weather concreting, and hot weather concreting. The recommendations build on the Standard Specifications for Concrete Structures prepared by the Japanese Society of Civil Engineers. Both recommendations and extensive commentary are provided.

For flexural design, the use of stress-strain curves rather than an equivalent stress block is recommended. No minimum amount of steel reinforcement is required because the bridging action of the steel fibres provides the strength after cracking.

Shear capacity is calculated as the summation of the shear resistance provided by the matrix, fibre reinforcement, and vertical component of the prestressing force or the shear resistance to diagonal compression failure. The use of shear reinforcement is not recommended. Torsional design is based on the Society's Standard Specifications. An equation is provided for the calculation of punching shear strength.

Serviceability is addressed by checks on stresses, displacements, deformations, vibrations, and other parameters as needed. Verification of fatigue resistance relies on the provisions of the Standard Specifications.

In pretensioned concrete, the clear vertical or horizontal distance between strands may be equal to the strand diameter. A minimum clear cover of 0.8 inches (20 mm) is permitted.

Overall, the document is comprehensive, although it defaults to the Standard Specifications where information is not available to develop different recommendations for UHPC." (Russell & Graybeal, 2013), p.42-43

3.3.4 AFGC-SETRA recommendations (2013)

In 2013 a revised version of the recommendations on Ultra-High Performance Fibre-Reinforced Concrete was published by the AFGC-SETRA working group. At the moment of publishing this was the most comprehensive guideline and no longer had an interim status. The new document incorporates new developments, experience of application of UHPC in practice and feedback, and is written to be consistent with the new Eurocode 2 for design in concrete. It consists of four parts:

- Part 1: Focusses on the constitutive properties and mechanical properties of the UHPFRC;
- Part 2: Focusses on structural design and is revised to be consistent with Eurocode 2;
- Part 3: Focusses on durability of UHPFRC;
- Part 4: Focusses on sustainable development and the use of UHPFRC in this context.

The guideline also includes a total of sixteen annexes. Topics vary from the characteristics of and tests on the material to modelling and a description of structures constructed in UHPFRC from 1997 to 2011. The definition of UHPFRC as given in this document is:

"Ultra-High Performance Fibre-Reinforced Concrete are materials with a cement matrix and a characteristic compressive strength of more than 150 MPa and a maximum of 250 MPa." (Groupe de travail BFUP, 2013), p.8

The code covers only a number of types of UHPFRC, which is important to keep in mind in case this document is used. These are different types of Ductal, BSI/CERACEM and BCV.

3.3.5 SIA 2052 (2016)

In 2016 the Swiss code SIA 2052 (''Ultra-Hochleistungs-Faserbeton (UHFB) – Baustoffe, Bemessung und Ausführung'') was published. The code focusses on two basic concepts for which UHPFRC can be applied:

1. Construction of new structures consisting of components made of UHPFRC, which are usually constructed using prefab elements;

2. Strengthening or repairing existing concrete structures using UHPFRC, thus creating composite elements. It is mentioned that it is also possible to construct new composite structures.

The standard fits within the framework of the SIA standards. Although it is mentioned that UHPFRC is different than conventional concrete, the code refers still to the Swiss version of EN 206, because of testing for example. The definition of UHPFRC given in the code is:

''Composite material made from cement, additives/admixtures, fine aggregates water and short fibres. Its high compactness makes it impermeable to liquids. As a general rule, the characteristic value of the cube compressive strength at 28 days is greater than 120 N/mm^2.'' Translated, after: (Societé suisse des ingénieurs, 2016), p.7

The code consists of the following parts:

- Chapters 0 and 1: General parts such as the scope and terminology;

- Chapter 2: A chapter where the general principles regarding construction in UHPFRC or composite structures using UHPFRC, structural analysis, durability and quality control are covered;

- Chapter 3: A chapter covering the material, including mechanical properties as well as those of UHPFRC with passive reinforcement or prestressed UHPFRC structures;

- Chapter 4: Structural analysis of structures made of UHPFRC and composite structures using UHPFRC;

- Chapter 5: Contains the discussion of connections, including general principles, reinforcement and its cover, prefabricated components composites using UHPFRC;

- Chapter 6: Covers the execution of UHPFRC structures, including the production of the material and casting and curing.

Several annexes are provided as well, among which are annexes regarding properties of UHPFRC, quality control and tests.

3.3.6 NF P18-470, NF P18-710 and NF P18-451 (2016-2018)

In 2016 two new codes were published in France, the NF P18-470 and NF P18-710. In 2018 a third code was published: NF P18-451:

- NF P18-470: UHPFRC – Specifications, performance, production and conformity
- NF P18-710: Design of concrete structures – Specific rules for UHPFRC
- NF P18-451: Execution of concrete structures – Specific rules for UHPFRC

In (Toutlemonde, et al., 2017), further information on the development of these codes is given and their relation to the previous French recommendations from 2013 is also clarified. In France, father standardization started with the AFGC-SETRA recommendations from 2013 as the starting point. Three codes were developed:

- **NF P18-470**: Is a separate code with the same layout as the French version of the EN 206. The code gives the requirements that UHPFRC has to comply to, such as its constituents, mix proportions and properties in fresh and hardened state. In the code, the notion of 'identity card' is also introduced. This is a document which gives the performance of a specific UHPFRC mix with regard to the properties. This 'identity card' can subsequently be used to prove that the material meets certain requirements.

- **NF P18-710**: Is a national annex or complementing document to the Eurocode 2, it focusses specifically on rules for UHPFRC in the design of buildings and bridges. Rules from Eurocode 2 that are not relevant or have to be changed for the use of UHPFRC are indicated. An important difference with conventional concrete is the use of the tensile capacity of the material, which is clearly indicated in the document.

  Important is that the characteristics of the material (e.g. characteristics under tension, stiffness, etc.) cannot be derived as a function of only the concrete compressive strength. For preliminary design, a set of ranges of values is provided in the code. The aforementioned identity cards of mixes can be used to provide more accurate values for design. For the final design however, parameters have to be determined using values from trial production.

- **NF P18-451**: Is a document that complements the current standard for the execution of structures in concrete (the French version of EN 13670) and focusses on UHPFRC.

The starting point for the further standardization process that resulted in these codes was the AFGC-SETRA recommendations from 2013. As mentioned in the article, standardization helps with the acceptability and the quality of UHPFRC structures. These newer codes comprehend product standards, design standards and execution standards, which can be considered a step up and help in widening the use of the material in a reliable way. The added value of this new set of codes with respect to the 2013 recommendation is that the content of these recommendations have been clarified in a more formal way to fit within the European code framework or have been complemented.

3.3.7 Selecting a code for redesign

Although the decision on which code to use in the redesign as elaborated on in this thesis project will be made in a later stage (the start of the design stage), a number of aspects that will be taken into consideration are already mentioned:

- **Year and completeness**: In the introduction of this report, it was stated that the goal is to identify the state-of-the-art standards. The developments within the field of UHPC are very rapid. After all, the first structure in UHPC was only built in 1997, the first guidelines were only introduced in the early 2000's. As can be seen from the previous discussion, more recent guidelines incorporate more experience and results from research. Therefore, they are completer and more accurate;

- **Availability & practicality**: The code itself has to be obtained in order to be able to use the document in the redesign. For example: although the Japanese guideline was commonly mentioned for example, the guideline itself could not be obtained. Another consideration is practicality, having to translate texts is to be avoided. It results in errors and does not contribute to the goal of the project.

- **Completeness**: A single guideline is typically a part of a larger framework of codes and to be used with other documents. The selected guideline has to be able to be used within the framework of the Dutch version of the Eurocodes (NEN-EN). Moreover, if the UHPC guideline requires information from other codes, these have to be able to be found as well.

The final decision on which guideline is to be used in the thesis will be made and justified in a later stage of the project, being the start of the design stage.

3.4 Summary third chapter

The first part of this chapter was dedicated to identifying the challenges that should be kept in mind when designing in UHPC, namely:

- **Validity of Eurocode 2 and the use of codes**: Relying completely on Eurocode 2 is not possible because UHPC falls beyond the range of validity of Eurocode 2. This is because Eurocode 2 only covers concrete up to and including C90/105. Moreover, a UHPC structure may also fall beyond the range of validity because of dimensions.

- **Mix composition**: It is not always clear what the mix composition is of a specific type of UHPC, especially if these are commercial products (premixes). That means that for determining the properties, one should often rely on the documentation belonging to the product.

- **Durability and long-term behaviour**: The concrete cover and cracking behaviour of UHPC structures may also vary from conventional concrete. In addition, fatigue may be a criterion to consider because of slender dimensions.

- **Resistance to fire**: Because of its dense structure, UHPC has a high risk of spalling in case of fire, this should be accounted for in design.

Generally accepted codes & guidelines on UHPC are lacking, although since 2000 different guidelines were introduced on a more national level. To compensate for this and to be able to deviate from Eurocode 2, thorough knowledge about the material properties & characteristics is required. Moreover, a good understanding of the available guidelines and calculation procedures that can be used is essential.

A literature study was performed to identify the different codes, guidelines and recommendations on UHPC that are currently available within the industry, as well as codes that may be expected in the near future. The currently available codes on UHPC that were identified were:

- Design Guidelines for Ductal Prestressed Concrete Beams (Australia, 2000);
- Ultra-High Performance Fibre-Reinforced Concretes - Interim Recommendations (France, 2002);
- Recommendations for Design and Construction of UHSFRC structures (Japan, 2006);
- SIA 2052 (Switzerland, 2016);
- NF P18-470: UHPFRC – Specifications, performance, production and conformity (France, 2016);
- NF P18-710: Design of concrete structures – Specific rules for UHPFRC (France, 2016);
- NF P18-451: Execution of concrete structures – Specific rules for UHPFRC (France, 2018).

Other codes and guidelines might be of interest as well, such as the CUR Aanbeveling 111 and the fib Model Code. The seven identified codes were subsequently described in more detail, this allows for a justified decision to be made on which code to use in the redesign. This decision will be made during the start of the design phase of the project.

3.5 Bibliography

Aarup, B. (sd). *Do we really need another guideline for UHPC?* Opgeroepen op mei 13, 2020, van Hicon: https://www.hi-con.dk/hicon-blog-hoejstyrkebeton/do-we-really-need-another-guideline-for-uhpc

Betoniek. (2017). Da's sterk! *Betoniek Standaard*, 1-12.

Bouvy, L. (2012). Rekenen aan UHSB. *Cement*, 1-5.

Buitelaar, P., & Quist Batista, C. (2019). Nieuwe generatie UHSB. *Cement*, 24-30.

Falbr, J., Hunger, M., & Spiesz, P. (2016). Rekenregels UHSB beproefd. *Cement*, 20-27.

Fehling, E., Schmidt, M., Walraven, J., Leutbecher, T., & Fröhlich, S. (2014). *Ultra-High Performance Concrete UHPC*. Berlin: Wilhelm Ernst & Sohn.

Gowripalan, N., & Gilbert, I. R. (2000, May). Design Guidelines for Ductal Prestressed Concrete Beams. School of Civil and Environmental Engineering, the University of New South Wales.

Groupe de travail BFUP. (2002, January). Interim Recommendations. *Ultra High Performance Fibre-Reinforced Concretes*. Association Francaise de Génie Civil.

Groupe de travail BFUP. (2013, June). Ultra High Performance Fibre-Reinforced Concretes. *Recommendations*. Association Francaise de Génie Civil.

Hunger, M., & Spiesz, P. (2016). Praktijkproef bewijst potentie UHSB. *Betoniek Vakblad*, 12-16.

Ketel, H., Willemse, R., Van Rijen, P., & Koolen, E. (2011). Dwarskracht- en kolomberekening VVUHSB. *Cement*, 86-91.

Ketel, H., Willemse, R., Van Rijen, P., & Koolen, E. (2011). Rekenmodel VVUHSB (1). *Cement*, 50-57.

Russell, H. G., & Graybeal, B. A. (2013). *Ultra-High Performance Concrete: A State-of-the-Art Report for the Bridge Community*. Federal Highway Administration (FHWA), Office of Infrastructure Research and Development.

Societé suisse des ingénieurs. (2016). SIA 2052:2016. *Béton fibré ultra-performant (BFUP) - Matériaux, dimensionnement et exécution*. SIA.

Toutlemonde, F., Kretz, T., Généreux, G., Resplendino, J., Pillard, W., Guérinet, M., & Rougeau, P. (2017). French Standards for Ultra-High Performance Fiber-Reinforced Concrete (UHPFRC). *High Tech Concrete: Where Technology and Engineering Meet - Proceedings of the 2017 fib Symposium* (pp. 1601-1609). Maastricht: Springer.

Van Nalta, R. (2015). Let op bij ontwerpen met UHSB. *Cement*, 38-42.

Wachter, L., Fischer, O., & Schramm, N. (2019). Ultrahochfester Beton (UHPC) in der Anwendung. *NewsletterTechnik*.

Walraven, J. (2006). Ultra-hogesterktebeton: een materiaal in ontwikkeling. *Cement*, 57-61.

Walraven, J. (2012). UHSB op weg naar regelgeving. *Cement*, 50-55.

Wikipedia. (sd). *Ultrahochfester Beton*. Opgeroepen op mei 13, 2020, van Wikipedia.de: https://de.wikipedia.org/wiki/Ultrahochfester_Beton

4

CONCLUSIONS

The goal of this first part of the literature study of the thesis 'Redesign of bridges Twentekanaal in Ultra-High Performance Concrete' was to become familiar to the material behaviour and the more fundamental concepts behind UHPC and to understand how to apply the material in calculations and in practice. By achieving these goals, answers could be formulated to the research questions that were stated at the beginning of this report:

- What are the basic concepts of UHPC from a concrete science & technology point of view?
- What are the basic concepts of design in UHPC in accordance with state-of-the-art standards?

This report started in the first chapter with a (re)collection of relevant knowledge about conventional concrete, i.e. concrete of normal strength. This proved to be helpful in the second chapter, where the basic concepts on UHPC were discussed, as well as different UHPC products, casting, curing and other points of attention. Therefore, the answer to the first research question can therefore be found in this chapter.

In the third chapter, points of attention were given for when UHPC is applied in design. Moreover, an overview was provided on the different UHPC guidelines that are available. The first part of the second question can therefore be answered using this chapter. The decision on which guideline to use will be made in a later phase of the project, the design phase. During this phase, the main features of and design verification in this selected guideline or guidelines will be discussed in more detail as well.

III

LITERATURE STUDY – PART II



Literature Study – Part II

Redesign of bridges Twentekanaal in Ultra-High Performance Concrete

MSc Thesis

14 June 2020

Company	Witteveen+Bos
MSc thesis project	Redesign of bridges Twentekanaal in Ultra-High Performance Concrete
Document	Literature Study – Part II
Status	Final version
Version	D1.0
Date	14 June 2020

Author	ing. M. Dorland
Student id	4719980
Degree programme	MSc Civil Engineering
Track	Structural Engineering – Concrete Structures

Company Supervisors	ing. T. Petersen RC ir. A. ten Voorde
Supervisors TU Delft	Dr. ir. Y. Yang Dr. ir. M.A.N. Hendriks Dr. ir. S. Grünewald

TABLE OF CONTENT

PREFACE 1

DEFINITIONS 2

1 INTRODUCTION TO ARCH BRIDGES 3

1.1 Introduction to arch bridges 3
1.1.1 General introduction 3
1.1.2 Arch bridges in the Netherlands 3
1.2 Classification and structural form 4
1.3 Elements of the structure 8
1.3.1 Load paths of an arch bridge 8
1.3.2 Structural elements of an arch bridge 9
1.3.3 Hanger configuration and bracing between arches 10
1.4 Structural analysis 11
1.4.1 Structural Mechanics: Arches 11
1.4.2 Internal moments and forces 12
1.4.3 Asymmetric and concentrated loads 13
1.4.4 Design verifications 15
1.4.5 Conclusions structural analysis 15
1.5 Bibliography 16

2 INTRODUCTION TO PREFAB BEAM BRIDGES 17

2.1 Introduction to prefab beam bridges 17
2.2 Bridge types, materials and choosing for prefabricated concrete 17
2.2.1 Bridge types 17
2.2.2 Materials 19
2.2.3 Choosing for prefabricated concrete 20
2.3 Design considerations of prefab decks 22
2.3.1 Design 22
2.3.2 Common beam types in the Netherlands 22
2.3.3 Durability 26
2.4 Construction of prefab decks 26
2.5 Structural analysis of prefab deck 28
2.6 Bibliography 29

3 EXAMPLES OF UHPC APPLICATIONS 31

3.1 Introduction examples 31

3.2 General overview 31

3.3 Examples worldwide 32

3.3.1 Sherbrooke pedestrian bridge (Sherbrooke – Canada) 32
3.3.2 Viaduct Bourg-Les-Valance (Bourg-Les-Valance - France) 33
3.3.3 Seonyudo footbridge (Seoul - South Korea) 33
3.3.4 Pont sur l'Huisne (Mans – France) 34
3.3.5 GSE Bridge (Tokyo – Japan) 35

3.4 Examples in the Netherlands 36

3.5 Bibliography 37

4 CONCLUSIONS 38

Final page 38

Annex(es) Number of pages

PREFACE

This document comprises part II of the literature study as part of the thesis 'Redesign of bridges Twentekanaal in Ultra-High Performance Concrete'. The goal of this part of the literature study is to collect basic information regarding arch and prefab beam bridges (design considerations, different types, etc.) and the underlying principles from structural mechanics. This enables to make a start with the design in the subsequent steps of the project, and therefore, attention is paid to examples of the application in UHPC in practice as well. Achieving the aforementioned goal means that an answer can be formulated to the following research question:

- What are the basic concepts of arch bridges and prefab beam bridges with respect to design considerations, the construction phase and principles from structural mechanics?

The literature study in relation to the total thesis project is given in the following figure.

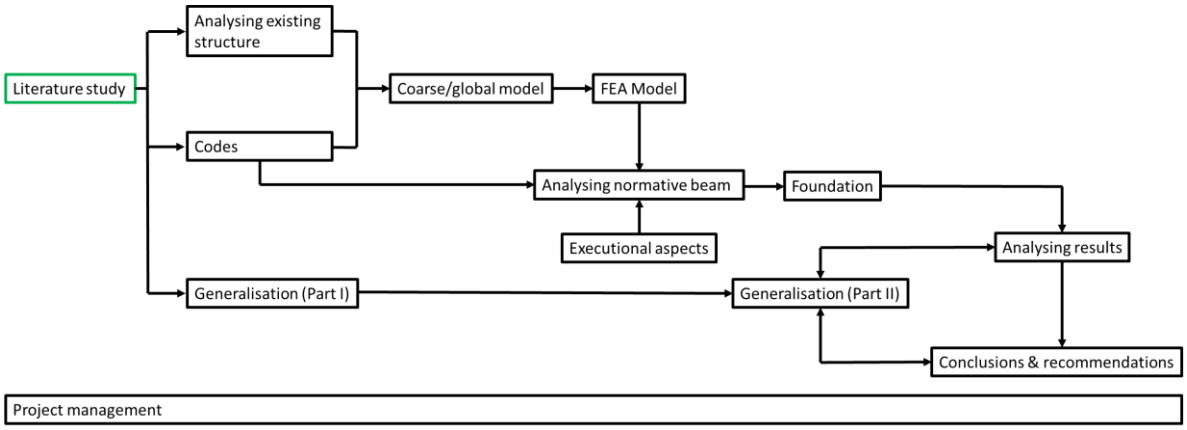


Figure 1 Literature in relation to the project

Reading guide

This report consists of the following chapters:

- Chapter 1: The first chapter contains a discussion of the arch bridge. Its main features, different types of arch bridges, different components of the structure and the basics from structural mechanics are discussed.

- Chapter 2: The second chapter starts with the discussion of basic considerations in bridge design, such as different bridge types, when to choose a specific bridge type and when to choose concrete or steel. After that, the focus is shifted to prefab. Reasons of why to choose for prefab, different types of prefab decks used in the infrastructure and their characteristics are mentioned and discussed. A brief overview of methods of analysis of prefab decks is given as well.

- Chapter 3: The third chapter gives examples of the application of UHPC in the infrastructure. A number of examples are described in greater detail, to illustrate the possibilities of UHPC within the infrastructure, and to serve as inspiration for the subsequent phases of the project.

- Chapter 4: The fourth chapter consists of a brief recap of the research question and goals that are to be answered and achieved via this part of the literature study.

DEFINITIONS

Centre of forces The centre of forces in a cross section is the point of intersection of the resultant force of all normal stresses and the cross section.

Line of pressure The line of pressure (also known as the line of force) is the line obtained by connecting the centre of force for all cross sections.

Isotropic: A material is isotropic if it has the same properties in all directions.

Orthotropic: A material is orthotropic if it has different properties in three perpendicular directions.

1

INTRODUCTION TO ARCH BRIDGES

1.1 Introduction to arch bridges

1.1.1 General introduction

The arch is the oldest structural form used for bridge construction. The principle of the arch is that the loads acting upon the structure are transferred in compression and that there are no tensile stresses in the structure. There are multiple reasons to opt for an arch bridge:

- The forces are transferred in compression (useful if you use certain materials that are unable to resist tensile loads);
- Because of the aesthetics and integrating the bridge into the landscape;
- It is possible to obtain bridges with only small displacements, making these bridges useful for (high-speed) railway lines for example.

Arch bridges (regardless of material type) are generally used for medium to longer spans. For very long spans, other bridge types (cable supported types) are a more economical solution. A bridge type related to the arch bridge is the inclined leg bridge, this can be regarded as a polygonal shaped arch bridge.

Concrete is an ideal material for an arch because of the compression in the structure. However, in practice steel is also often used. One could argue that this is a risky choice, after all, instability phenomenon may occur if steel is loaded in compression. However, steel has other advantages over concrete, such as a lower self-weight. This makes that steel is generally used for larger span bridges than concrete. More details on when to select concrete or steel are given in the second chapter.

There are multiple forms of arch bridges and many aspects to take into consideration when opting for an arch bridge. This will be discussed in the subsequent paragraphs of this chapter.

1.1.2 Arch bridges in the Netherlands

Arch bridges in the Netherlands are typically tied arch bridges. As reported in (Romeijn, Steel Bridges Dictaat CT5125, 2006), the main span for concrete arch bridges in the Netherlands varies between 37 and 68 m while for steel arch bridges this varies between 49 to 295 metres, the ''Van Brienenoordbrug'' being the arch bridge with the longest span in the country. This illustrates indeed that steel is suitable for larger spans because of self-weight of the structure. Moreover, it is reported in the same source that for steel arch bridges the trend can be observed that after 1960 the steel orthotropic decks became widely used for bridges while after 2000 composite decks of steel and concrete became more widely used.

Generally speaking, the type of arch bridge used depends on the type of loading (railway versus highway). The tied arch bridge with stiffening girder is commonly used for railway bridges while bridges for road traffic are commonly constructed using the basic tied arch bridge. Differences between these types and further classification are mentioned in 1.2.

1.2 Classification and structural form

Arch bridges can be found in many different forms and can be classified using different characteristics such as position of the deck, structural form and design of the hangers. Moreover, the arch bridge offers many options for the designer, for example with respect to distributing material between the deck and the arch. In this paragraph, a number of these aspects is considered.

Position of the deck

The first arch bridges were constructed using masonry or stone and the deck was placed on top of the arch. Because there were no materials available that could be used to make elements that could be loaded in tension, other structural types were not possible. Nowadays, this is not a restriction anymore and there are three options:

- Deck on top of the arch (also called ''deck arch'');
- Deck at intermediate position (also called ''half-trough arch'');
- Arch on top of the deck (also called ''through arch'').

The choice of deck position is for a large part determined by the location where the bridge will be placed. A lower deck is a typical solution for flat terrain while a deck on top of an arch can be used when crossing a deep valley, where the arch can be supported. The lower deck is the most common form in the Netherlands, thus the emphasis will be on this type of arch, as will be most of the examples that are shown in the pictures.

The first option is also known as the ''true arch'' and the horizontal forces are restrained by the abutments. If this is not possible because of soil conditions for example, the horizontal force can also be balanced using a tie. This results in the tied-arch bridge. The foundations then primarily have to react to the vertical loads only.

Within the options of the arch on top of the deck, there are also different options. There are two main categories: the basic arch bridge and the tied arch bridge. Within the group of tied arch bridges, one can also distinguish between the basic tied arch bridges and the tied arch bridges with stiffening girders:

- **Classical/Basic arch**: The first option consists of an arch and an independent roadway (not a part of the main load bearing structure) connected to the arch using hangers. The deck only serves as the rolling surface for the traffic, the hangers are loaded in tension by the live load and self-weight and transfer the loads onto the arch. All forces, including horizontal forces, are directly taken up by the pylons and foundation. The arch is subjected to bending, shear forces and axial forces. An example of this bridge type is given in Figure 2.



Figure 2 Waalbrug (Nijmegen)

- **Basic tied arch**: The deck is connected to the ends of the arch to resist the horizontal forces, this way the horizontal forces are internally balanced. Therefore, the foundation only has to restrain the vertical forces from the arch. The arch dominates the behaviour due to its stiffness compared to that of the deck. The hangers are again loaded in tension by live load and self-weight. An example of this bridge type is given in Figure 3.



Figure 3 Oude IJsselbrug (Zwolle)

- **Tied arch with stiffening girder**: A stiffening girders now heavily contributes to the capacity. It is subjected to bending moments and axial forces due to the arch. This type of bridge is often used for railroad bridges. The arch is loaded in compression. A stiffer girder means that the hangers are more uniformly loaded, more uniformly than in the previous two cases. An example of this bridge type is given in Figure 4.



Figure 4 Muiderspoorbrug (Weesp)

These three options may look different if the figures are compared, but the mechanical behaviour is very similar, as will become clear in later sections of this chapter. In the Netherlands, most arch bridges are of the second type (basic tied arch bridge).

Structural form

When it comes to the arch bridges with the deck at the lower position, the four most common structural forms are as follows:

- **Fixed at both ends**: A typical solution when masonry or concrete is used for the structure, because of the continuity of the foundation and arch that can be achieved;

- **Pinned at both ends**: This is a more appropriate solution for steel structures because pinned joints are relatively easy to achieve when using steel;

- **Three-pin arch**: As for the pinned-pinned solution, the three-pin arch is also more appropriate for steel. However, the additional hinged joint can be a complicated joint and increases the required maintenance;

- **Tied arch**: The fourth solution is the tied arch, the ends of the arch are joined using a tensile tie, this balances the horizontal support reactions.

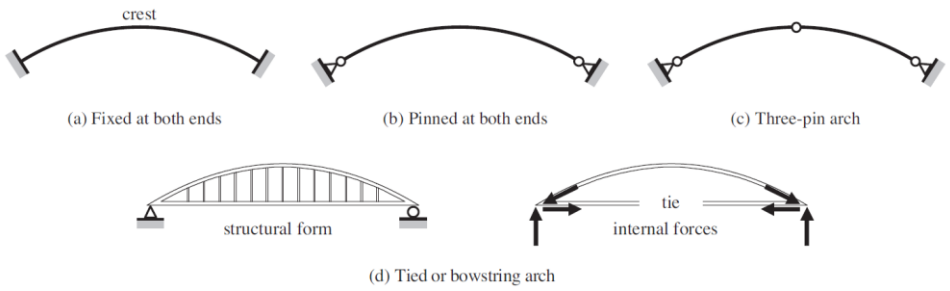


Figure 5 Structural forms - (Lebet & Hirt, 2013), p.464

One can see that the degree of redundancy varies between these options. The fixed-fixed solution has a degree of redundancy of $n = 3$. The pinned-pinned solution has a degree of redundancy of $n = 1$. The three-pin arch is statically determined. The degree of redundancy affects the deformations and force distribution, if the degree n is increased the magnitude of the vertical displacement decreases while the bending moments increase (especially at the arch ends and crest of the arch).

The decision for one of these types is influenced by a number of factors:

- **Construction method**: Certain solutions favour a specific material and allow for different construction methods;

- **Location**: Solutions a-c require good subsoil conditions (e.g. rock) to counter the horizontal forces due to the compression forces in the arch.

In the Netherlands, the subsoil conditions are generally as such that options a-c are not possible. The solution can be found in the form of a tied arch bridge. The horizontal forces at the supports are not balanced externally using the foundation and good subsoil, but internally using a tensile tie. That means that only the vertical component of the compressive force in the arch will have to be transferred by the supports, abutments and foundations. Generally speaking, choosing this bridge type has a number of implications for design:

- The tied-arch bridge is less sensitive to the quality of the soil conditions, which is why this is the arch bridge type typically used in the Netherlands;

- The tied-arch bridge is not very sensitive to settlement of the supports, the structure can follow the deformations without loads being imposed upon it;

- The tied arch bridge is not sensitive to uniform variations in temperature because one of the supports can move without restraint;

- For a tied arch bridge, it holds that the magnitude of the internal forces and the vertical displacements are a function of the flexural stiffness of the arch relative to the flexural stiffness of the tensile tie (deck).

A special form of the arch bridge is also worth mentioning. If a girder bridge does not have sufficient capacity, it can be strengthened by adding an arch. The dead weight is then transferred by the girders, but the additional traffic loads are carried by both the girders and the arch. This system is depicted in Figure 6.

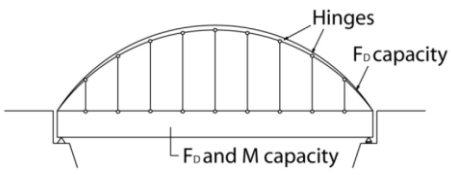


Figure 6 Girder bridge strengthened with arch - (Yang, 2020)

Number of arches

A consideration for design is the number of arches to be used, for example:

- **Single arch**: If a single arch is used, this is typically placed centrically on the bridge, with traffic lanes positioned at both sides of the arch. If a single arch is loaded eccentrically, torsion occurs;

- **Two arches**: If an arch bridge with two arches is constructed, the traffic lanes are typically positioned in between the arches.

Slenderness

A parameter that can be used to describe the bridge in terms of flexibility and material is the term 'slenderness'. The slenderness of an arch bridge may be defined as follows:

$$\lambda_1 = \frac{f}{l}$$

Where:
λ_1: Slenderness given by ratio total rise and span
f: Total rise of the bridge (to the crest of the arch)
l: Span

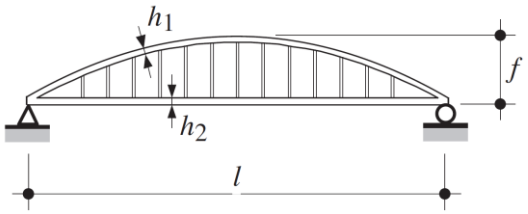


Figure 7 Notations and definitions for slenderness – (Lebet & Hirt, 2013), p.465

A consideration for design is the question what an appropriate value for the slenderness would be. A lower slenderness value means that the flexibility of the bridge will be higher. If the arch is very flat, then the horizontal forces and secondary bending effects can become very large, the result is an uneconomical design. A higher slenderness could imply that the height increases as such that the structure becomes aesthetically unappealing.

The deck and the arch both provide stiffness to the total structure, this should be balanced appropriately. The reason for this is that an arch is efficient in resisting uniform distributed loads over the full span, but concentrated loads can result in larger deformations and bending. Therefore, another slenderness value that may be used is to account for the choice of section sizes and the subsequent distribution of material over the arch and the deck. This may be accounted for using slenderness λ_2:

$$\lambda_2 = \frac{h_1 + h_2}{l}$$

Where:
h_1: Depth of the cross section of the arch
h_2: Depth of the cross section of the deck

Classification bridges arch on top of deck

Up until now, different considerations and options in design have been discussed. The focus now is with an arch bridge with the lower deck position, i.e. an arch on top of the deck. In practice, these bridges can be classified by looking at aspects such as structural form, stiffness of the components and configuration of the hangers. An example of a way of classifying arch bridges is as follows:

- **Two-hinge arch**: The arch as two hinged (i.e. pinned) supports, one at each end of the arch. The deck is connected to the arch via hangers;
- **Three-hinge arch**: The arch has three hinges, not only the supports but also at the middle of the arch. The deck is connected to the arch via hangers;
- **Tied arch**: Using a tensile tie (generally a part of the deck), both of the ends of the arch are connected, balancing the horizontal forces at the supports;
- **Langer arch**: Is a form of the tied arch bridge where the deck has a higher stiffness and the arch is a more slender element. Therefore, the stiffening girders dominate the behaviour. Because of the stiffer deck, this bridge is widely used for arch bridges for railroads;
- **Lohse arch**: Both the deck and the arch are stiff and the arch is positioned out of the vertical plane;
- **Nielsen arch**: An arch bridge with diagonal hangers, where a hanger crosses maximum one other hanger.

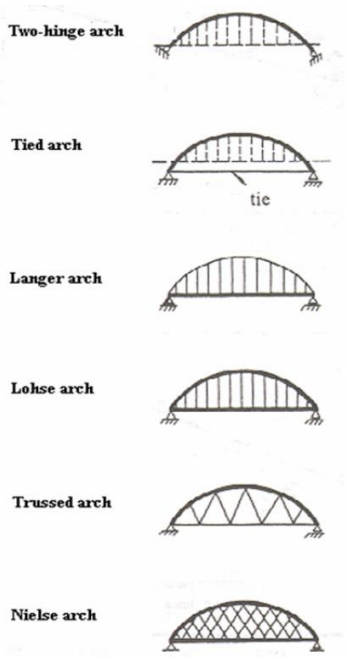


Figure 8 Classification of arch bridges (Romeijn, Steel Bridges Dictaat CT5125, 2006), p.224

A combination of two of the aforementioned types is the Nielsen-Lohse arch: both network hanger configuration and arch positioned out of vertical plane. Not mentioned is the ''network arch bridge'' where the hangers can cross multiple other hangers.

1.3 Elements of the structure

1.3.1 Load paths of an arch bridge

The following figure describes illustrates the load transfer of vertical loads on the deck towards the supports:

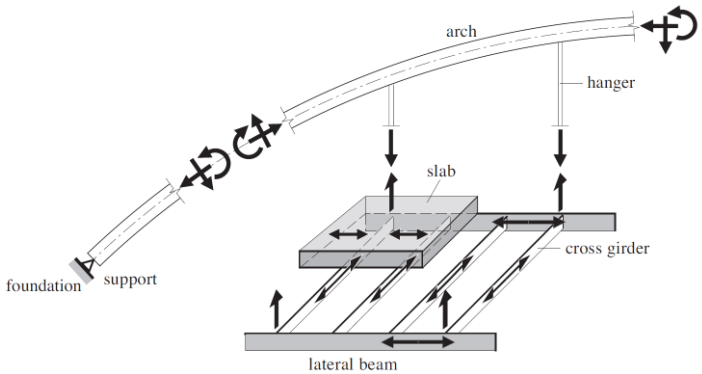


Figure 9 Load parts of an arch bridge - (Lebet & Hirt, 2013), p.466

The vertical loads acting on the deck of the bridge are transferred to the foundation, as described in (Lebet & Hirt, 2013), this is as follows:

- The load is placed on the deck. The deck acts in bending, both in longitudinal and transverse direction, this way the loads are eventually transferred to the lower ends of the hanger;
- The transfer of the load towards the hanger goes via the cross girders and lateral beams. The slab transfers the load to the cross girders mainly via bending. The cross girders are supported by the

main girders (the lateral girders). These lateral beams are connected to the hangers, thus transferring the forces into the hangers;

- The forces are transferred from the hangers onto the arches, which are loaded in compression. The compressive load in the arches is typically accompanied by bending, as will be discussed in later parts of this chapter;

- The arches transfer the forces to the supports. If the bridge is constructed as a tensile tie, the horizontal force is subsequently internally balanced out.

1.3.2 Structural elements of an arch bridge

In this subparagraph the different structural elements of a tied arch bridge are discussed. Roughly speaking, one can distinguish the following structural elements:

- The arch
- The deck/tensile tie/stiffening girders
- Hangers

Arches

The most obvious requirement for arches is that they should be designed as such that compressive forces can be resisted. Typically, these compressive forces are accompanied by bending, which should be accounted for as well. Moreover, instability is to be considered in addition to the strength. The cross-sectional properties (second moment of area) should be sufficiently large about both axes to prevent instability (buckling).

Deck and tensile tie

In the first place, the deck functions as the rolling surface for the traffic. Because of this, the deck has to satisfy requirements with regard to stiffness (deformations should be within limits, therefore, the stiffness should be sufficient – SLS) and resistance (the deck should have sufficient load carrying capacity – ULS).

In the second place, the deck is one of the elements of the load path of the structure, as it transfers the traffic loads from their points of application via the slab and girders to the hangers. The transfer of the loads to the cross girders mainly takes place via bending of the deck (the slab).

In the third place, if the bridge is designed as a tied arch bridge, the deck (or a part of it) may also function as the tensile tie. This results in additional considerations for design, for example: first, the compressive forces in the arch must be able to be guided into the tensile tie as a tensile force. A typical solution is to have the main girders (the longitudinal girders) to function as the tensile tie. Second, the deck must be designed as such that the cracking of the concrete is controlled adequately by proper detailing. If the concrete slab of the deck acts as a part of the tension member, cracks have to be limited. This can be done by prestressing the deck.

Hangers and joints

In arch bridge design, there are many different types of hangers available. The options can be subdivided into bars, cables and rolled sections.

- **Bars**: Bars are often used because they have a number of benefits over cables. For example: the joints are simpler, bars are easier to prestress and the modulus of elasticity is higher than that of cables;

- **Cables**: If longer hangers are required, the use of cables might be more desirable than the use of bars to avoid having to weld multiple bars into a single hanger;

- **Rolled sections**: The use of rolled sections provides bending stiffness to the system. This solution might be used if this bending stiffness is required, for example because of a low out of plane stiffness of the arch. This may be the case if only a single arch is needed, and thus no bracing is provided.

For steel bridges, the most ideal situation is a hanger which is pinned at both of its ends. This prevents restraint. Restraint at the joint causes bending stresses, bending stresses can subsequently result in fatigue related problems at the joints. If the joint is not fully pinned, because of practical reasons for example, then the fatigue resistance is to be considered.

Criteria to consider are static strength, fatigue strength, stiffness and aspects such as aerodynamics. The latter is because hangers may start to vibrate due to various causes, such as traffic, wind, rain, or combinations of these. This can also result in fatigue damage at rigid joints at the end of hangers because of local bending at this zone. This is to be accounted for in design.

1.3.3 Hanger configuration and bracing between arches

Spacing and inclination of the hangers

The arrangement of the hangers can be modified by changing the spacing and inclination of the hangers. Various aspects are affected by doing so:

- Aesthetics (appearance of the bridge)
- Dimensions of the deck
- Stiffness of the bridge
- Resistance of the arches to buckling

The hanger configuration has a large influence on the overall design of the bridge, it highly influences the interaction between the arch and the deck, which will be discussed in more detail in 1.4.3. The use of inclined hangers results in a better distribution of the vertical loads from the deck onto the compressive arch. Especially in the case of asymmetric loading the bending moments in the arches and the deck are smaller if inclined hangers are used instead of vertical hangers. By modifying the hanger arrangement, higher slenderness can be achieved and thus less material is required and construction/erection is therefore influenced as well.

Bracing between the arches

If multiple arches are present, connecting the arches increases the stiffness of the whole structure and contributes to the out of plane stability. If the arches are rigidly connected to the end cross girders at the ends of the deck, then bracing between the arches may not be required. However, if the arches are pinned at their supports about the longitudinal axis, then the bracing is necessary to avoid instability. There are different types of bracing, see figures Figure 10 and Figure 11, for example:

- K-truss bracing
- X-truss bracing
- Vierendeel truss

Triangulated braces (braces with diagonal elements, see a and b in the left figure) provide greater stiffness than braces without diagonal elements (see option c in the left figure). The third option in the left figure acts as a Vierendeel truss. Although the stiffness and therefore stability is less than with the other options, it might be used because of aesthetics. Another option is to make the arches inclined to meet at the crest and support each other, which is close to option c in the right figure.

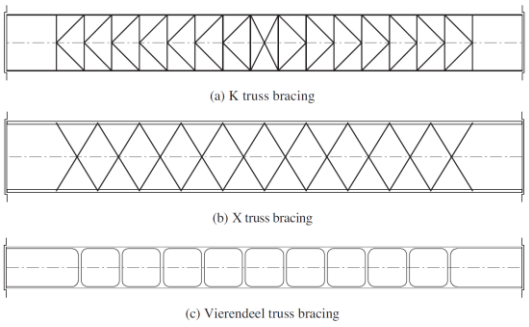


Figure 10 Bracing between arches - (Lebet & Hirt, 2013), p.473

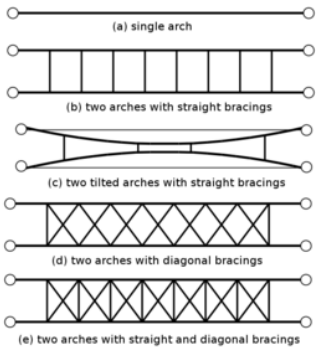


Figure 11 Top view of different types of arches

1.4 Structural analysis

1.4.1 Structural Mechanics: Arches

Arches are structural elements that are primarily loaded in compression. Their shape is retained due to their own bending stiffness. It is important to recognize that arches are susceptible to buckling, which is a point of attention because these elements are primarily loaded in compression. Arches are related to cables, this is depicted below.

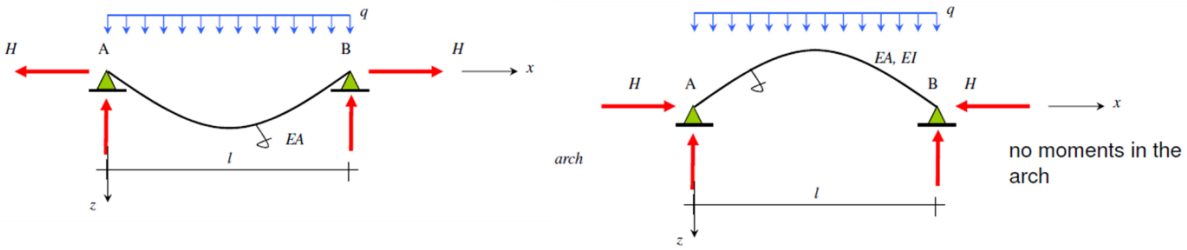


Figure 12 Principle of cables and arches – Edited, after: (Welleman, 2018)

Just like cables, the shape of the arch is in equilibrium with the load. However, where cables are loaded in tension, arches are mainly loaded in compression. In addition, arches possess bending stiffness, which means that they can retain their shape. When designed properly, the shape of the arch is in equilibrium with the load, this is again a difference with a cable, because in case of a cable equilibrium has to be made in the deflected state. When the shape of the arch is in equilibrium with the load, there are no bending moments in the structure. However, to obtain this situation, the axis of the arch must follow the line of force in the structure. Before continuing further discussion of the arch, the definitions 'centre of forces' and 'line of force' are discussed:

Centre of forces: The centre of forces in a cross section is the point of intersection of the resultant force of all normal stresses and the cross section. To obtain the centre of forces, one needs the moment and normal force distributions, after which the position of the centre of forces can be determined according to:

$$e = \frac{M}{N}$$

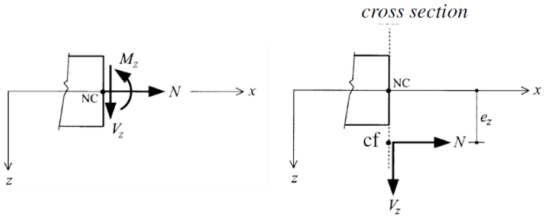


Figure 13 Centre of force – (Welleman, 2018)

Line of force: Connecting the centre of force for all cross sections of a structure results in the line of force, this can be done (piecewise) continuous by formulating a function for '*e*' as a function of the horizontal coordinate.

The line of force is also known as the line of pressure. Theoretically speaking, following the line of force results in the optimal shape of the structure, because the bending moments will be equal to zero. That means that a perfect arch is obtained, which is only subjected to compressive forces. In practice however, this principle will not work. It cannot be achieved in practical situations as will be explained in the remainder of this chapter, however, for studying the behaviour of arches it is still a useful concept.

1.4.2 Internal moments and forces

Line of force

The most ideal case when using an arch is that the form of the arch coincides with the line of force that is defined by the internal forces due to the external loads. If this is the case, a perfect arch is obtained: the loads only result in compressive forces and there is no bending. Therefore, the perfect arch is the most efficient arch structure. Two examples of the perfect arch are as follows:

- Uniformly distributed loads: For a UDL, the perfect arch has a parabolic shape;
- Concentrated loads at hanger positions: The perfect arch has a polygonal shape.

In reality, the imposed loads are not uniformly distributed and arches are generally not polygonal. In other words: in practice the perfect arch is not achieved and therefore the arch is not only subjected to compression but also to bending moments. The bending moment at a certain point along the arch may be defined as the normal force acting on the cross section times the eccentricity relative to the axis of the arch.

Calculating internal moments and forces

For preliminary design of an arch bridge, if problems can be reduced to simple geometry and load cases, analytical expressions can be used. This is for example illustrated in (Lebet & Hirt, 2013) and (Romeijn, Steel Bridges Dictaat CT5125, 2006). In the latter, it is explained that there are four load patterns that are important for the (preliminary) design:

- Full loading
- Full loading over half the length
- One side full loading on the bridge
- Alternate full loading over half the length

The first case, full loading over the whole deck, is further elaborated on. This is a basic case from structural mechanics. Assume a parabolic arch with span l and rise f, the arch is pinned at both ends. A uniformly distributed load q is applied onto the arch, there are no bending moments due to the load. The arch is now subjected to a compressive force with the horizontal component H:

$$H = \frac{ql^2}{8f}$$

Using the horizontal component, the normal force along the axis of the arch can be determined, see Figure 14. The normal force in the arch has angle α, which is the angle between the tangent to the arch axis and the horizontal axis, hence:

$$N = \frac{ql^2}{8f cos\alpha} = \frac{H}{cos\alpha}$$

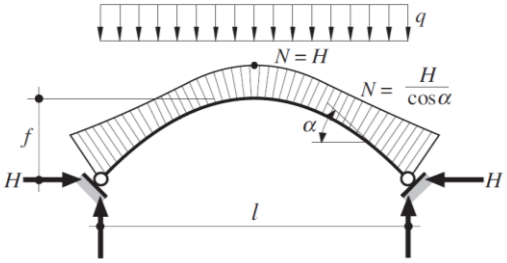


Figure 14 Compression in a parabolic arch - (Lebet & Hirt, 2013), p.478

The horizontal force component of the normal force of the arch stays constant for the whole span length of the bridge. The vertical component in the arch depends on the position along the length.
The bending moments of a beam under a uniformly distributed load can be determined using:

$$M(x) = \frac{1}{2}qx(l-x)$$

Using this equation, the height of a point of the axis of the arch at a certain position along the span can be determined as follows:

$$y = \frac{\frac{1}{2}qx(l-x)}{H} = \frac{1}{2}qx(l-x) * \frac{8f}{ql^2} = \frac{4fx(l-x)}{l^2}$$

If the arch is a perfect arch (the compression line coincides with the axis of the arch), then the aforementioned equations can be used. An example of such a uniformly distributed load is the dead weight of the deck. Note that the self-weight of the arch itself acts along the axis of the arch, not along the horizontal axis. Therefore, the perfect arch in this case would have to be an inverted catenary. The first case has now been analysed. Following the principles of symmetry, the other cases can be analysed as well. This is done by assuming that the total load is made up of superimposed loadings.

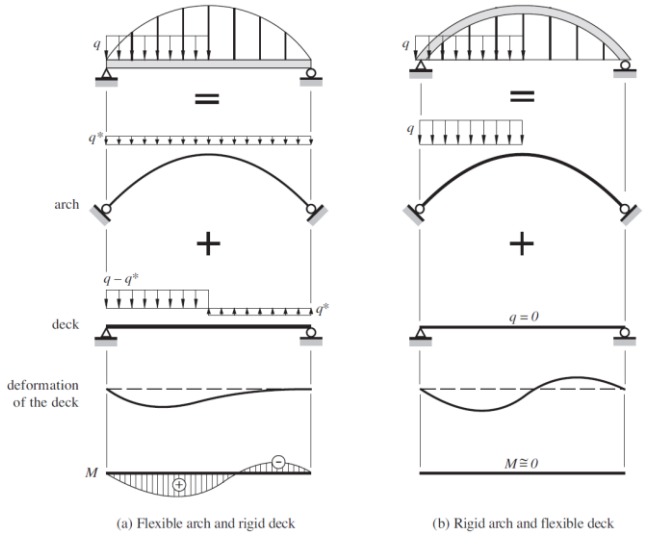
1.4.3 Asymmetric and concentrated loads

If the bridge is subjected to loads and the arch is not a perfect arch, then the arch is subjected to bending in addition to compression. In reality, a perfect arch is never achieved due to the many different load situations that can occur. For example, traffic loads can be asymmetric or concentrated. The occurring bending moments are influenced by many different parameters. A qualitative description will be given on the behaviour of arch bridges subjected to asymmetric or concentrated loads.

Asymmetric loads

Arch only: Suppose that only the arch is studied, loads are directly applied onto it. Compared to a symmetric load, an asymmetric load over half the span results in larger bending moments and smaller normal forces in the arch. This type of loading generally results in the largest deflection of the bridge.

Influence of the deck: In reality, the deck also contributes to the structural behaviour. The bending stiffness of the arch and the deck influence the distribution of the internal forces. After all, stiffness attracts loads. In addition, the axial stiffness of the hangers also has an influence, but this influence is smaller. To study the influence of changing the stiffness of the arch and deck, two cases are presented below.



(a) Flexible arch and rigid deck (b) Rigid arch and flexible deck

Figure 15 Influences of changing the stiffness of the arch and deck - (Lebet & Hirt, 2013), p.480

These are more or less the ''limit cases''. In the first case the arch is very flexible while the deck is very stiff and in the second case this is reversed. The following is observed:

- In case of a flexible arch and stiff deck, only a small portion of the load (q^*) is transferred onto the flexible arch. Most of the load is carried by the deck;

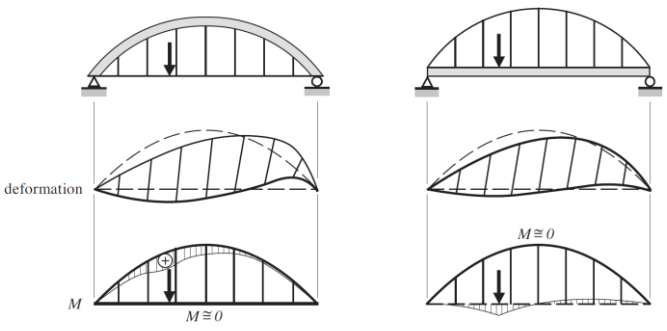
- In case of a stiff arch and flexible deck, most of the load is transferred to the arch because the deck can follow the deformations of the arch without supporting the load.

These results are not surprising: stiffness attracts load. These principles also hold for the tied arch bridge. One can see that the distribution and magnitude of bending moments can be partially controlled by the stiffness of the arch and the deck, this determines which part of the load is taken up by both elements. Therefore, this is an important consideration for design. By providing the required stiffness to the desired element, it can be decided which element takes up the asymmetric load.

Concentrated loads

Distribution of load: A heavy concentrated load can result in significant bending moments in the arch, this effect can be reduced by transferring the load onto the arch using several hangers. This way, the local load is distributed over a larger part of the arch.

Stiffness of the deck: In this case, the stiffness of the deck plays an important role. In the case of a flexible deck, the hanger next to the point where the load is applied is loaded the most. If the deck is stiff, multiple hangers are loaded because of the deformation of the deck, which results in better distribution and therefore less bending. These concepts are illustrated in the following figure.



(a) Flexible deck (b) Rigid deck

Figure 16 Stiffness deck and concentrated load - (Lebet & Hirt, 2013), p.481

Effect of inclined hangers: Another way of distributing the load over a larger part of the deck is by using inclined hangers instead of vertical hangers. The following figure illustrates the effect.

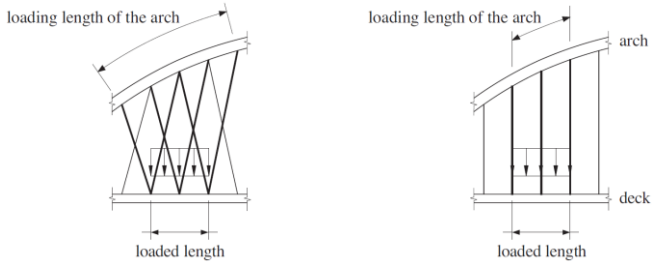


Figure 17 Use of inclined hangers - (Lebet & Hirt, 2013), p.481

Due to the inclination, the length of the arch over which the applied load is introduced is increased. The following figure shows the effect of inclined hangers versus vertical hangers on the distribution of a concentrated load onto the arch. The length over which a given load is introduced onto the arch is increased when the hangers are inclined.

Effect of hanger diameter: Not only the inclination, but also the number and diameter of the hangers influences the behaviour. Suppose that two decks with the same properties are analysed. When it comes to carrying concentrated loads, the deck with a larger number of smaller diameter hangers performs better than a smaller number of larger diameter hangers.

1.4.4 Design verifications

For the verifications in ultimate limit state, the different elements are loaded in the most unfavourable way by positioning the loads accordingly, after which the elements are verified according to the design codes. A number of relevant aspects is listed below:

- **Position of traffic loads**: For design, the traffic loads are positioned as such that the maximum internal forces (bending moments and normal forces) in the arch are obtained. The maximum bending moment can be found either by asymmetric load over half the span or symmetric load over a part of the span. The maximum normal force is found using a uniformly distributed load over the full span.

- **Influence lines**: Traditionally, an important tool in bridge design is the use of the influence lines. These are used to establish a relation between the position of traffic loads and forces in the structural member under consideration. Note that to obtain accurate influence lines, the stiffness of the whole structure is to be taken into consideration. For example, the influence line by assuming that the deck acts as a continuous beam on multiple supports is not accurate enough. This is explained by the relations between the different elements and the influence on the structural behaviour, as described in this paragraph.

- **Hangers and bracings**: The most unfavourable forces in elements such as hangers and bracing elements can be determined by following the influence lines of the elements under consideration.

- **Special load cases**: A final aspect to consider are ''special load cases'', i.e. load cases other than those due to normal use of the structure. Examples are forces during the different stages of construction, accidents and maintenance. An example of the latter two is the situation in which a hanger is not functioning, e.g. due to an accident or because it is being replaced.

1.4.5 Conclusions structural analysis

A number of considerations for the structural analysis of arch bridges has been discussed. It turns out that the behaviour of an arch bridge under loading depends on a number of factors, among which are:

- Stiffness of the deck and the arch;
- Inclination of the hangers;
- Number and diameter of the hangers.

Although basic equations can be used for the first calculations, the load distribution is complex. Influence lines are traditionally also widely used in (arch) bridge design. Because of all the influencing factors and possible loads, for the more refined design calculations it is important to consider all these factors using a 3D model, FEA is a helpful tool for this design phase.

1.5 Bibliography

Sources

Lebet, J.-P., & Hirt, M. A. (2013). *Conceptual and Structural Design of Steel and Steel-Concrete Composite Bridges.* EPFL Press.

Pavlovic, M. (2019). Lecture Notes CIE5125 Steel Bridges.

Romeijn, A. (2002, juni). *Boogbruggen, hoofddraagsystemen en constructief gedrag*. Opgeroepen op 06 09, 2020, van Bruggenstichting: https://www.bruggenstichting.nl/tijdschrift/ouder/67-bruggen-2002/bruggen-juni-2002/569-boogbruggen-hoofddraagsystemen-en-constructief-gedrag?highlight=WyJsb2hzZSJd

Romeijn, A. (2006). *Steel Bridges Dictaat CT5125* (Vol. Parts I and II). Delft: Faculty of Civil Engineering and Geosciences.

Welleman, H. (2018). Lecture notes CIE4190.

Wikipedia. (2020, jan 6). *Boogbrug*. Opgeroepen op 06 09, 2020, van Wikipedia: https://nl.wikipedia.org/wiki/Boogbrug

Yang, Y. (2020). Lecture Notes Concrete Bridges CIE5127.

Figures

Figure 2 From: *https://www.omroepgelderland.nl/nieuws/2415547/Nijmeegse-Waalbrug-gaat-vrijdagnacht-dicht*, on 13-06-2020

Figure 3 From: *https://www.wegenwiki.nl/Oude_IJsselbrug_Zwolle*, on 13-06-2020

Figure 4 From: *https://nl.wikipedia.org/wiki/Muiderspoorbrug*, on 13-06-2020

Figure 11 From: *https://nl.wikipedia.org/wiki/Boogbrug*, on 13-06-2020

Sources of all other figures have been mentioned in the text.

2

INTRODUCTION TO PREFAB BEAM BRIDGES

2.1 Introduction to prefab beam bridges

This chapter covers a number of different general bridge design topics as well as the basics of prefab applied in the infrastructure. This chapter is written with the intent to use it as a source of inspiration for the subsequent phases of the project:

- The second paragraph starts with general considerations: A step prior to designing in prefab is to know when to apply which bridge type and which material (steel or concrete). These are the first points to be discussed. Specific reasons to choose for prefab solutions are also given;

- After that, design considerations of prefab decks are formulated: different prefab solutions commonly applied in the infrastructure Netherlands are discussed;

- The chapter is continued with a brief overview of the construction of prefab bridges and viaducts, from the factory to the finished structure on the construction side;

- The chapter is finalized with a brief overview of different ways to model a prefab deck.

2.2 Bridge types, materials and choosing for prefabricated concrete

2.2.1 Bridge types

Bridges can be seen in all shapes and sizes. There are many different bridge types that can be applied. The choice for a certain bridge type is governed by a number of factors:

- The size and type of the obstacle and required span length;
- The location of the bridge in terms of terrain and the accessibility of the location;
- Methods of construction that can be applied;
- Available construction depth;
- Type of traffic that is expected (nature and magnitude of the loads).

If all bridges are to be categorized, one could use the following distinction that consists of four classes:

- **Beam or girder bridges**: Within this class a distinction can be made of girders and beams of different cross sections and materials (from rolled sections, to prefabricated beams and box girders). The truss bridge also belongs to this class;

- **Arch bridges**: As discussed in the previous chapter, arch bridges can be constructed in accordance with different principles. The different types offer many options for different locations;

- **Inclined leg bridges**: Within the same range of spans as the arch bridges, the inclined leg bridges can be found. These combine the principles of the previous two options;

- **Cable suspended bridges**: For the longer spans, systems in which the deck is suspended by cables can be applied. The two main categories within this class are the cable stayed bridges and the suspension bridges.

For a given span, there might be different bridge types that can be applied. But each bridge type has a certain range within its application is very well feasible from technical and economical perspective. This is illustrated by the following figure. Although this figure is for streel bridges, the general impression is clear: for a given span certain bridge types are more attractive and feasible than others.

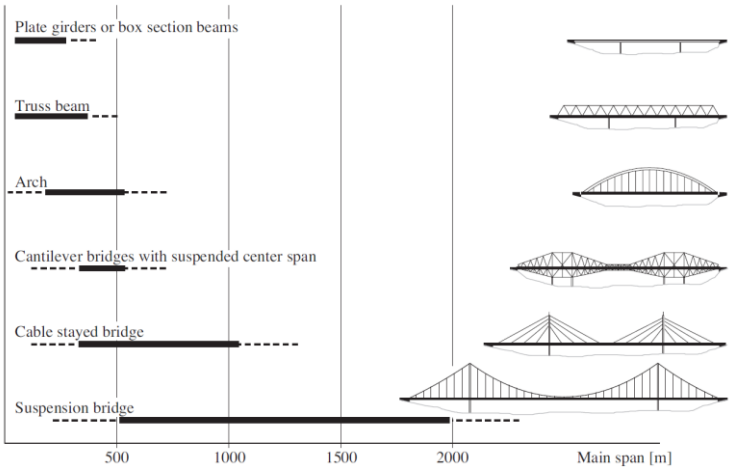


Figure 18 Types of longitudinal structural form and span ranges - (Lebet & Hirt, 2013), p.78

One of the main aspects in determining which bridge type is to be used is the span. Each different bridge type has a certain maximum practical span, this value depends on a number of aspects:

- **Capacity**: Capacity of the bridge is related to its span and dead weight. A bridge is constructed to allow traffic to cross an obstacle, that means that the bridge must be able to support variable load in addition to the dead weight. If the span is increased, the magnitude of the dead weight increases with respect to the other actions (variable loads) acting on the structure. If the span is increased too much, the remaining capacity for variable load becomes so small that the solution is no longer attractive.

  For example: For concrete bridges the dead weight is generally dominant over the variable load. For shorter span bridges (30 to 50 m) about half the capacity is required for carrying the dead weight while for very long bridges (400-2000 m) this can increase up to 80%.

- **Economy**: Within a certain span range, certain solutions are significantly more economical than other solutions.

- **Aesthetics**: Although a certain solution might be technically feasible at a larger span, this might result in a structure that is not aesthetically pleasing.

The exact values at which span certain bridge types are used are no set number. These values depend on many factors and varies between locations. However, there are more typical solutions for certain span ranges:

- **Beam solutions**: At shorter spans, using solutions with (main) beams is a practical and the most traditional solution. Even within this range, there are many different options. Resistance of the beams is provided by bending and shear, and in the case of box type beams, also in torsion.

- **Truss beams**: If the span increases, the beam solution becomes less efficient because the cross section is not fully utilized: only the outer fibres are. Trusses offer a solution in which all members are loaded in tension or compression. This is a more efficient use of material.

- **Arches**: Arches provide solutions for multiple situations. In deep valleys with good soil conditions, arches with a deck on top can be used. The horizontal forces are easily transferred. Smaller spans on flat terrain can be crossed using tied arches. Following the concept of the arches, loads are mainly transferred through compression.

- **Inclined leg bridges**: Within the same span range as arches, inclined leg bridges can be used as well. From a structural point of view, this solution combines features from beams and arches because resistance is provided by bending and compression.

- **Cable suspended bridges**: If the span is increased further, solutions where cables are used to suspend the deck become more economical. One option is the cable stayed bridge, the deck is suspended by the cables in tension, these transfer the loads to the pylon(s). The second option is a cable stayed bridge which offers the largest possible spans. The deck is suspended by cables in tension that transfer the loads onto a primary cable.

The different structural forms are depicted in the following figure. Note that the cable-based bridges support the bridge deck in a more flexible way, while the other shorter span solutions support the deck in a more rigid way by piers and abutments.

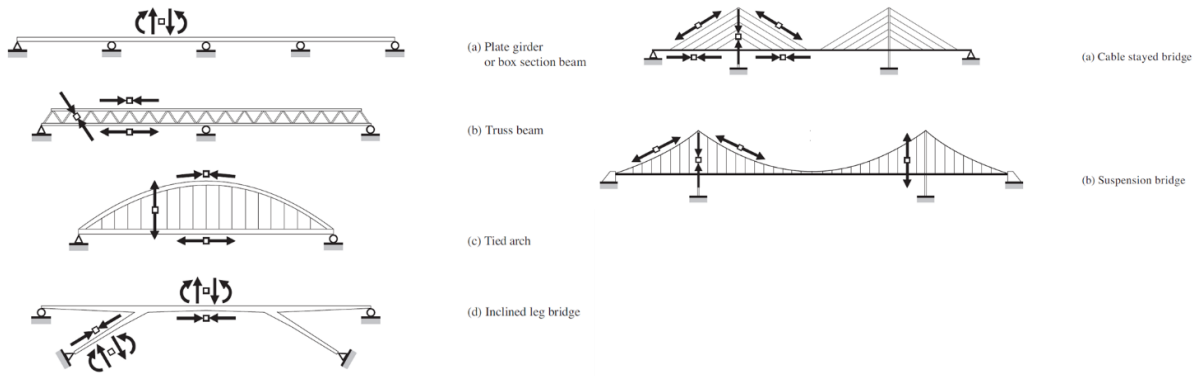


Figure 19 Types of structural form and internal forces – Edited, after: (Lebet & Hirt, 2013), p.80

2.2.2 Materials

Although there are many different materials used in bridge construction (masonry, stone, concrete, timber, steel and FRP), for larger bridges, for larger bridges the choice is usually between concrete and steel. When selecting which material is to be applied, a number of points is of particular interest. For example:

- **Material costs**: Suppose that a span is analysed at which both a concrete and a steel solution can be designed. In this situation, the steel solution is generally more expensive than the concrete solution.

- **Dead weight**: Applying a steel structure results in a lower self-weight than when using concrete. This enables to construct larger spans and smaller foundations. For concrete, the dead weight is a limiting factor for the spans that can be achieved. Steel on the other hand is the traditional solution for larger spans that cannot be constructed in concrete because of this reason. Technological development (new bridge types and construction techniques for example) has opened the possibilities for the application of concrete in larger spans (up to 300 m roughly is possible), but the dead weight remains the limiting factor.

- **Execution**: Related to the dead weight is the construction method. The construction method, and especially the speed of construction related to it, is often considered to be very important in practice. Certain construction methods might be possible in steel, but not in concrete because of the self-weight.

- **Depth of the structure**: The dept of the structure may be defined as the height between the top of the road surface and the bottom of the deck. This is an important parameter in the Netherlands, as it dictates the required height of the abutment, length of the approach bridges, etc to allow traffic to access the bridge. This is also related to the type of traffic, for railroads for example only a small slope can be allowed compared to road traffic. Generally speaking, especially for concrete bridges a minimum construction depth means the lowest total costs. This emphasizes that a slender deck is important.

- **Construction of substructure and approaching bridges**: The substructure is practically always constructed using concrete. If approaching bridges are to be constructed, this is generally done using prestressed concrete. This is a development that started in the 1960's with the introduction of the prestressed prefab beams. If a large part of the project is already constructed in concrete, it might be beneficial to finish the whole project using the same material.

- **Temperature effects**: Steel structures are more prone to problems related to temperature than steel bridges. The reason for this is the relatively low mass and the speed at which the material heats up or cools down.

- **Fatigue**: A steel structure is generally more prone to fatigue related problems than a concrete structure. There are two reasons for this. The first reason is that the stress variation for steel structures is generally higher, because the dead weight is lower compared to the variable load. The second reason is the presence of welded joints, where residual stresses occur along with geometrical effects. This is less of a problem for concrete.

- **Dismounting the structure**: A steel structure is easier to dismount compared to concrete, therefore it is easier to recycle and/or to reuse.

In the end, the choice of the material depends on the situation. It is made individually for a particular case, in which the aforementioned aspects might be taken in consideration, in addition to aspects such as the span. In general, spans smaller than approximately 200 m it holds that most of the market is occupied by the concrete bridges due to costs. Concrete offers more affordable solutions within this span range. Above 200 m, steel is mostly used. There are reasons to use steel for smaller spans or concrete for larger spans, of course. An example being movable bridges that are typically constructed using steel.

2.2.3 Choosing for prefabricated concrete

What is prefab concrete?

Prefabricated concrete (or: prefab) is concrete that is not produced on the construction site (cast in-situ), but on a different location, in an industrial way under controlled conditions.

Prefab concrete is used in all sectors of the construction industry, because it has a number of distinct advantages over cast in-situ concrete, for example:

- Quality of the concrete (higher concrete strengths can easily be achieved, often more easily than in-situ) as well as smaller scatter in strength;

- Elements can be produced with elaborated shapes to optimize the use of the materials and the concept of prefabrication to the full potential;

- Moulds allow for high quality surfaces with respect to shape, texture, tolerances, etc. to be achieved;

- High speed of construction on site because the elements are made on a different location, and no formwork or falsework is required on site;

- Prefabrication is an industrialised production process, which allows for good quality control and planning.

These are aspects that are important throughout the construction industry in general, therefore, prefab is widely applied in practice. Examples from the construction of residential or non-residential buildings are floor elements or balconies. Examples from the construction of foundations are prefab concrete foundation piles or beams. For the infrastructure, different prefab beam solutions are available for the construction of bridges and viaducts.

Development of prefab concrete is an ongoing process. Initially, prefab projects in the infrastructure were based on beam systems with a cast in-situ concrete layer. Later on, more completely prefabricated systems (higher prefabrication index) were developed, e.g. box beams. The potential keeps growing: longer and longer spans can be realised in prefab, which is also because of growth of transport capacity and assembly methods.

There may be some disadvantages as well to prefab. A typical field of application for prefab is projects where a large number of more or less the same types of standardized elements are used. If it is required to deviate from these standardized elements, prefab might be less suitable.

When to use prefab?

Whether prefab or in situ is most suitable depends on the project. There are many criteria that can be taken into consideration by looking at this question, for example:

- Costs
- Quality
- Speed of construction
- Logistics

Applying prefab concrete does not mean that everything of the structure has to be prefabricated. In practice, many structures are built using a combination of in situ concrete and prefab concrete. A part is casted on site, a part is prefabricated. This is generally the most optimal in terms of costs, as is illustrated in the following figure.

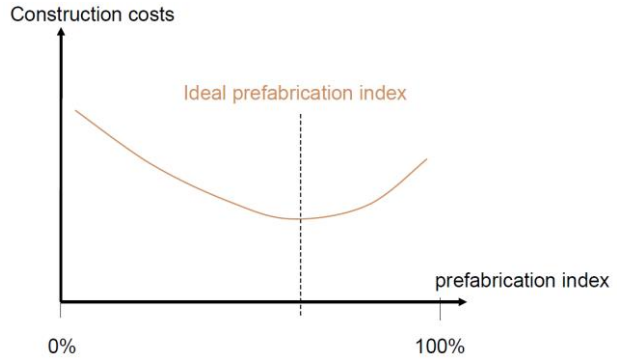


Figure 20 Costs and prefabrication index - (Yang, 2020)

It is also possible to construct a concrete structure completely in situ or almost completely execute it as a prefab structure. Another option is to prefabricate concrete elements at the construction site. What method to apply is a project specific decision. Generally speaking, prefab is especially an attractive solution if the project involves a lot of repetition and where construction time on site is to be kept to a minimum. But if the construction time is not a limiting factor, in situ methods can be economical as well.

Prefab in infrastructure

Prefab solutions are widely used in the Dutch infrastructure. The real break-through for precast was around the 1960's when the prefabrication concept was already initiated and when development of prestressing meant new opportunities. Standard prefab solutions were developed and larger spans and more slender

girders could be prefabricated. Later, standardisation took place. Development of prefab concrete is an ongoing process, size and weight increase and new types of girders are developed for special applications.

About 90% of all bridges in the Netherlands are built using precast elements, a driver for the wide use of prefab in the Dutch infrastructure is that in the infra market a large part of the bridges are the simpler bridge projects with modest spans (prefab with larger spans is difficult) and where speed of construction, minimizing costs and disturbance and good quality and working conditions are important. Prefabrication is very well suited for these projects, because of the characteristics of this building technique, as mentioned at the beginning of this subparagraph.

2.3 Design considerations of prefab decks

2.3.1 Design

For bridges and viaducts prefab beams are a very common solution, especially for the 'simpler' structures of modest span. For the design of a prefab bridge, the same procedure is to be followed as for other concrete bridges. However, there are also some additional aspects that are to be considered:

- Temporary situations during construction of the bridge (manufacture of the elements, storage, transport, erection on simple supports, etc.).

- Transfer of forces between precast elements and in situ concrete, e.g. shear reinforcement at the interface between beams and deck slab.

Another important point is to look for the most optimal cross-section during the design of the precast bridge elements. This is related to the weight and slenderness of the elements, and therefore very important. Prefab designs are therefore often focussed on optimising the dimensions of the elements.

2.3.2 Common beam types in the Netherlands

The following types of prefab elements are commonly used, these elements have in common that they are generally prestressed:

- Solid deck bridges
    - Using solid slab beams
    - Using infill beams
- Inverted T-beam bridges
- Box beam bridges

The characteristics for these three types of decks (and four types of prefab beams) will be discussed. The systems are briefly described and their key figures with respect to prestressing & reinforcement and application are considered as well.

Solid deck bridge using solid slab beams

Description: This solution consists of prestressed solid slab type beams that are placed on site after which an in situ concrete layer is casted.

Prestressing & reinforcement: The plates that require in-situ concrete are prestressed in longitudinal direction, which serves as the longitudinal reinforcement. In transverse direction, additional reinforcement is provided before the in-situ layer is casted.

The additional reinforcement contains reinforcement in longitudinal direction, which is mainly present for practical reasons, and transverse reinforcement, which is required for the bending moments in transverse direction. These occur due to the Poisson effect (ca 20% of longitudinal reinforcement).

Application: This type of prefab beam is used to obtain solid deck bridges and is generally used for bridges with a span of 4 up to a maximum of 8 m and subjected to relatively small traffic loads. The slenderness ratio for this type is 20 – 25.

The advantage of this method that a solid deck is formed and that additional formwork is not needed, the prefab slab already acts as formwork. The prestressing acts as main reinforcement, which means that additional longitudinal reinforcement does not have to be placed, preventing labour intensive activities.

Note: Other prefab plate beam bridges exist as well, for example completely prefabricated beams (these do not require an in-situ concrete layer) that are placed on the construction side and subsequently post-tensioned in transverse direction.

Solid deck bridge using infill beams

Description: Using infill beams is another way of obtaining a solid deck. After the beams have been placed, in situ concrete is casted in between and on top of the beams.

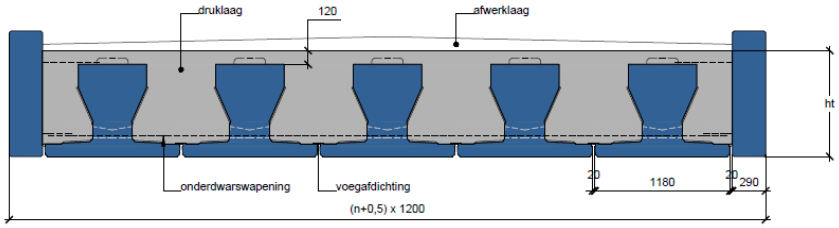


Figure 21 Example of infill beams – Spanbeton

Prestressing & reinforcement: The beams are prestressed in longitudinal direction, which serves as the longitudinal reinforcement. Reinforcement is added in transverse direction by placing reinforcement through the box outs/ducts in the webs of the beams as well as placing it on top of the beams. The transverse reinforcement is again required for the bending moment in transverse direction.

Application: This type of prefab beam is used for spans from 6 up to 20 m. These beams are used together with edge beams, as can be seen in the figure. The slenderness of this system is 20 – 25.

Using this type of beams, the amount of prefabricated concrete is increased compared to the slab beams, and as a result a smaller amount of in situ concrete is required. This increases the maximum span that can be achieved compared to the slab type beams.

Inverted T-beam bridges

Description: For larger spans, inverted T-beams are often used. Using these beams, a deck can be constructed by casting an in-situ layer on top of the formwork that is placed between the webs of the girders. After that the reinforcement is placed in longitudinal and transverse direction and the in-situ layer is casted.

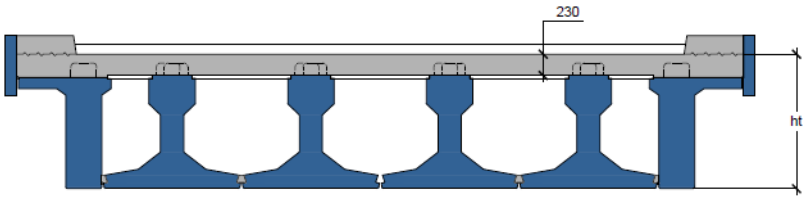


Figure 22 Example of inverted T-beams – Spanbeton

Prestressing & reinforcement: The beams are prestressed in longitudinal direction. In situ, reinforcement is placed for cross beams and for the in-situ layer. The bending stiffness of the in-situ layer is too small to provide sufficient bearing capacity in transverse direction. Therefore, cross beams are required to keep the girders together. To achieve this, reinforcement is guided through the box outs in the girders after which the

cross beams are casted. All reinforcement in transverse direction is this way concentrated in limited number of positions (at the cross beams). This way, the girders are confined.

The slab can be regarded as a continuous slab in transverse direction. Due to the Transverse bending moments reinforcement is required both at the top and the bottom of the slab.

Application: This beam type offers very economical solutions for decks with a span of 20 – 60 m, but requires sufficient height. These beams are commonly used together with edge beams for aesthetic reasons and to increase the resistance against collision. The slenderness is 20 – 28.

A point of attention is the interface of the beam and the cast in situ layer. Moreover, cross beams should be casted to obtain a more solid structure. Another reason for cross beams is for torsion, the girders have only small torsional stiffness by themselves.

Cross beams are placed at the ends. In the past, cross beams were also placed in the middle. This is the most effective place: the longitudinal bending moment is at its maximum at this point, the transverse bending moment then can be expected to be at its maximum at these locations as well. However, nowadays these beams near midspan are not constructed anymore to save in costs.

Box beams

Description: A deck of box beams is formed by placing a number of box shaped prestressed beams next to one another after which the longitudinal joints are casted and prestressing is applied in transverse direction. A benefit of this method is that no cast in situ layer is required. That means that almost the full capacity of the beams can be used to carry the variable loads. Because of the cross-sectional shape, these beams have torsional stiffness and therefore can be produced as curved beams as well.

The box beam has a very high prefabrication index because there is no cast in situ layer needed. This results in reduced height compared to, for example, inverted T-beam bridges.

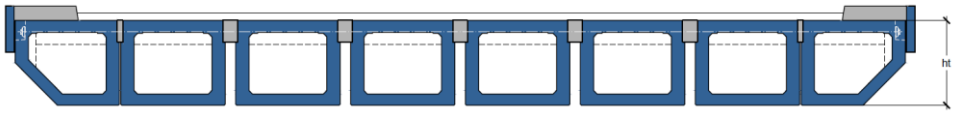


Figure 23 Example of box beams – Spanbeton

Prestressing & reinforcement: The box beams are prestressed in longitudinal direction in the factory. After placing the beams and casting the longitudinal joints, the beams are also prestressed in transverse direction. That means that in the final situation the deck is prestressed in two directions.

Application: Spans constructed using box beams are typically 15 – 68 m. An upper limit is due to the weight of the beam. The slenderness ratio is 28 – 32, which is a higher slenderness than T-girders. For this reason, the more expensive box beams can be used if the structural height is too stringent to use inverted T-beams.

Due to the torsional stiffness, box beams can be curved. Moreover, due to the torsional stiffness, cross girders are not required. Edge beams can be applied but are not required. They can be used to meet specific requirements, e.g. aesthetics, by making adjustments to the mould.

Box beams have a number of distinct advantages over T-beams: a torsion stiff deck, a slender structure, very fast construction because no in-situ layer or edge beams are required. This beam type is therefore suitable for longer spans or reduced construction height compared to the inverted T-beams.

Longest span prefab beams: The current record of longest prefab beams is claimed by Haitsma, the company produced eight prestressed prefabricated concrete box beams with a length of 69 m and a weight of 259 Tons (Haitsma, 2020), for a bridge in Wanssum, beating the old record of 68 m (which was claimed by the same company). Because of the weight and dimensions, these beams had to be transported over water

as road transport was not an option. The beams were transported to and placed on the location in June 2020.





Figure 24 Transport and placement of longest prefab (box) beams

Other beam types

The different aforementioned beam types are widely used in the Netherlands. However, other solutions are also available. For specific projects, special solutions can be designed if the standard solutions do not fulfil the requirements and in other countries other cross-sections can be common practice.

Summary

To summarize the discussion of the mostly applied beam types in the Dutch infrastructure, the following table has been prepared with approximate values for the slenderness and span for all four beam types that have been discussed.

Table 1 Typical slenderness and span for common beam types

Type of beam	**Slenderness**	**Span**
[-]	$[l/h]$	[m]
Solid deck – Solid slab with in-situ layer	20 – 25	4 – 8
Solid deck – Infill beams	20 – 25	6 – 20
Inverted T-beam	20 – 28	15 – 60
Box beam	28 – 32	15 – 69

Prefab in thesis project

For the thesis project, the decision has been made beforehand to strife for a solution in UHPC prefab beams. Although this is a condition that has been set beforehand, this decision can also be justified from an engineering point of view. Given the topics that have already been covered in the literature study up until and including this paragraph, this decision can now be further clarified by means of the following points:

- **Span**: Given the length and span that is to be achieved, a beam type solution (either concrete or steel) is a reasonable solution (see 2.2.1 for more details);

- **Material**: Although being simply defined in the scope of the thesis project, the selection of concrete as construction material can be further substantiated. Given the span range, the fact that a beam type solution is reasonable and that limiting costs and construction speeds are generally considered to be important, a prefabricated solution in concrete is justified.

- **UHPC vs conventional concrete**: A beam of 68 m is at the upper limit of what can be achieved using prefab beams made of conventional concrete, it is proven that it is possible, given the current record of 69 m (see Figure 24). Given the properties of UHPC that are superior to those of conventional concrete (see the first part of the literature study), the use of this material provides new possibilities and further justifies the use of the material in the thesis project.

2.3.3 Durability

Because bridges are designed to function for 100 years under relatively demanding conditions (traffic loads, influence of weather, de-icing salts that are potentially harmful, etc), good performance related to durability is important. According to (fib, 2004), good experiences have been obtained with regard to the durability of prefabricated elements. The reasons for this are that a higher concrete strength, a lower water/cement ratio and good quality of execution can be achieved. The latter is in turn influenced by working indoors under controlled conditions, good workmanship, a high repetition of the work as well as control of the work.

2.4 Construction of prefab decks

Production of prefab elements

The construction using prefab elements starts in the prefab concrete factory. Usually, special moulds are used to produce whole series of elements. Prefab bridge elements are generally produced using the long line system, which means that a very long element is casted and subsequently split (sawn) into elements of the required length. Other production methods may be used as well though. The moulds used are generally made of steel. Smaller products are usually produced according to standard catalogue while larger elements, for which generally special requirements are formulated, are produced by order.

The benefit of prefab is that the production of the elements takes place at a location where the conditions can be controlled. Therefore, there is no influence of the weather conditions for example. This makes it easier to produce concrete of higher strength and to meet other requirements as well, e.g. colour or specific shapes. Note that at the construction site it is also possible to obtain higher concrete strengths, but in prefab factory this is usually easier.

Planning

Production of prefab takes place independently of the work on the construction site. Another benefit of prefab is that due the more industrial way, the production can be planned with quite some accuracy which also gives certainty at the construction site. However, this also means that good planning is very important as the planning of construction and production of elements have to be coordinated.

At the construction site, elements only have to be put in place. That means that the time required at the construction site is limited. Moreover, placing formwork and reinforcement is no longer required or requires less effort than the case where the whole structure would be cast in-situ. However, the preparations do require more effort and work.

Storage of the elements

After the elements have been produced, there are stored for a certain period of time. This allows the concrete to harden further, because after demoulding the concrete is generally not strong enough to take up the loads for which the element is designed.

The storage of the elements is something to consider carefully: the elements are usually placed on supporting blocks and it is to be prevented that this is done in the wrong way. If the elements are loaded in a different way than they were designed for, damage may occur. Other risks are there as well during storage, for example discolouration due to weather effects.

Transportation

After production, hardening and inspection, the elements are transported to the construction site. Transport via road is the most common way. Normal size transport is often sufficient for smaller element, it can also be a decision to design as such that this is possible, for example by producing a long girder in segments and post tensioning the segments together at the construction site.

Normal size transport is limited in terms of dimensions and weight. If this is not sufficient, special transport is an option as it allows for the transportation of larger elements. An alternative is transport via water, which can be more efficient in certain cases. Transport of long and heavy bridge elements might require special

equipment and preparations. The transportation of the elements can be the limiting factor in design of prefab structures.

Although transportation might be a limiting factor in certain cases, the transport of prefab elements to the construction site does not have to be a distinct negative aspect of prefab concrete. For the alternative solution, which is cast in-situ concrete, a larger number of separate transports and activities has to take place (scaffolding, concrete mix trucks, etc.). Prefab means smaller number of truck movements, although the movement is of a heavier element.

Placement of the elements

At the construction site, the prefab elements only have to be placed at the desired position. Erection is typically done using a mobile crane. For elements with larger weight or very long elements, two cranes can be used. Again, the weight of the element is an important parameter. The crane capacity should be sufficient to get the element at the right place. This can be a stringent criterion if the hoisting operation takes place over large distance or large height.

Hoisting requires special measures to be able to pick up the element, which should be kept stable as well. The hoisting operation can result in different loads than for which the element was designed, this is a load combination that is to be taken into consideration during design.

Site work and connecting the elements

The work on the construction site means that in the case of prefab standardised elements are used to erect a structure. This can be seen from the typical layout of the prefab structure, which always requires a capping beam (or a pylon that is wide enough) on which the supports (one support for each beam end) and subsequently the beams themselves can be placed. The work on the construction site for the construction of a prefab beam bridge or viaduct can be summarized as follows:

- Construction of the foundation and columns;
- Construction of the capping beams on top of the columns;
- The bearings (one bearing for each beam end) are placed on the capping beams;
- The prefab beams are placed, depending on the beam type distinct edge beams are required in addition to the ‘standard’ beams;
- The remaining in-situ work is carried out, this depends on the type of beams:
    - **Infill beams**: Reinforcement is placed and the concrete in-situ layer is casted;
    - **Inverted T-beam**: Reinforcement is placed for the cross beams after which the beams are casted. After that, the in-situ layer is constructed by placing the formwork, reinforcement and casting the concrete;
    - **Box beams**: Longitudinal joints are casted and after hardening transverse prestressing is applied.
- After the in-situ concrete is hardened, the remaining work to the bridge can be carried out, such as applying pavement, etc.

In the construction (or better: assembling) of prefab structures an important point are the connections. After all, a prefab structure consists of separate standard elements that should form a single solid structure in the final situation. These connections generally have to be realized on the construction site.

An example of realizing these connections is the inverted T-beam, where cross beams have to be constructed. These fixate the girders and provide also torsional stiffness to the deck. This means that loads

are better distributed in the transverse direction. Contrary to inverted T-beams, infill beams already form a solid slab while box beams form a solid deck after applying transverse post-tensioned prestressing on site.

2.5 Structural analysis of prefab deck

The goal of this paragraph is to give a short overview of possible ways to model a prefab bridge or viaduct, this overview has been prepared to serve as inspiration for the subsequent parts of the project.

''Practical approach''

The first option means that a very practical approach using hand calculation is chosen. After the dimensions of the girders have been established, loads are determined. The variable loads are positioned in the most unfavourable position in transverse and longitudinal direction and the governing internal forces are determined. One can choose to account for load distribution by projecting the area over which the load is applied at the road surface onto the neutral axis of the beams under an angle of 45 degrees.

Plate theory

One can also choose to model the deck using plate theory as an orthotropic plate, which means that it has different stiffness properties in the three perpendicular directions, this is contrary to inotropic material, which has the same properties in all directions. Prefabricated concrete has most stiffness in its longitudinal direction, because of the shape of the beams that make up the deck. Because of the orthotropy, all terms of the constitutive matrix describing the relation between stress and strain of the plate have to be determined individually.

Guyon-Massonet method:

The Guyon-Massonet method is a more old-fashioned way to determine the force distribution in a deck consisting of beams. A 2D differential equation is used to describe the deflection in relation to the load function. Instead of determining this differential equation, it is possible to convert it into a number of sine functions and decouple the deflection in longitudinal and transverse direction. One can construct the function of any load as a combination of infinitely many sine functions in x (axis in longitudinal) direction and infinitely many cosine functions in y (axis in transverse) direction.

In the transverse direction, the proportion of the local deflection and the average deflection do not change over the entire length of the deck, K-values are used to calculate this ratio. The reaction force of the girders in transverse direction can subsequently be determined. In describing the behaviour, two parameters are very important. The stiffness parameter θ (gives the ratio of stiffness in longitudinal and transverse direction and gives information on how the deck deforms under load) and the torsional stiffness α, which can be regarded as a measure for the torsional stiffness of the deck.

Finite element analysis:

The finite element method is a method used in many engineering disciplines, it is a method to solve field problems. In the case of structural engineering, the displacements are the variables of which the distribution is sought for. Discretization of the mechanical model of a structure is applied, it is split up into finite elements, after which the spatial distribution of the displacements is approximated by a piecewise interpolation between nodal values of these elements. The principles are summarized in the following figure.

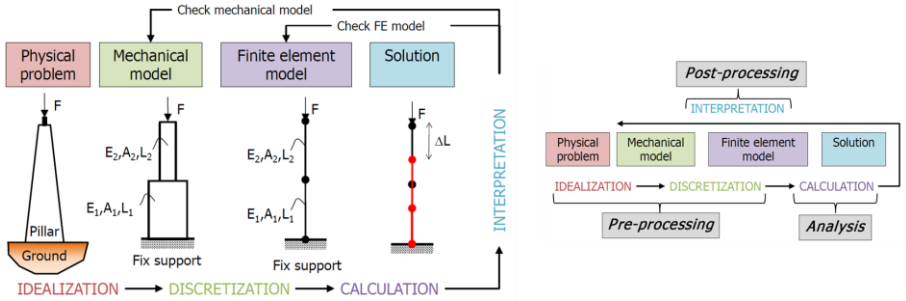


Figure 25 Basic principles and use of FEM – Edited, after (Esposito, Hendriks, & Rots, 2019)

The use of FEA via software gives the possibility to perform detailed calculations and obtain accurate results while incorporating many different load cases and combinations into the model. However, the results are only useful if the structure is modelled and discretized correctly and the results are analysed and interpreted with great care. For comparison, the results of the FEA can be verified with, for example, the results of one of the aforementioned methods.

Considerations for selecting an appropriate method

A number of considerations for selecting an appropriate method are:

- **What is to be determined?** – For example: for the first calculations to obtain insight into required dimensions, a very practical hand calculation could be the best. It gives all the required information without requiring more effort than necessary.

- **How detailed do the results have to be?** – Another question is how accurate the results of the calculation have to be. Suppose that verifications have not been met (for example: fatigue analysis) while performing a hand calculation or 2D FEM model, then it could be useful to choose a more refined method (e.g. 3D FEM model) to obtain more detailed (and less conservative) results. It requires more effort, but this could be justified if this results in satisfying a design criterion.

- **What is the background knowledge?** – Results have to be interpreted, and this requires background knowledge to be able to state whether results are realistic or not. More refined calculation methods, e.g. FEM, require more background knowledge than a simple hand calculation. Therefore, the background knowledge should be sufficient to be able to appropriately analyse and interpret results obtained by using the selected method.

2.6 Bibliography

Sources

Braam, R., Lagendijk, P., Soen, H., & Linssen, J. (2015). *Basiskennis beton.* Aeneas Media.

Esposito, R., Hendriks, M. A., & Rots, J. G. (2019). Lecture notes CIE5148 - Computational Modelling of Structures.

fib. (2004). *Precast concrete bridges.* State-of-art report prepared by Task Group 6.4.

Haitsma. (2020). *'s Wereld langste prefab voorgespannen liggers*. Opgeroepen op 06 12, 2020, van Haitsma beton: https://www.haitsma.nl/nieuws/brugliggers-wanssum/

Lebet, J.-P., & Hirt, M. A. (2013). *Conceptual and Structural Design of Steel and Steel-Concrete Composite Bridges.* EPFL Press.

Pavlovic, M. (2019). Lecture Notes CIE5125 Steel Bridges.

Romeijn, A. (2006). *Steel Bridges Dictaat CT5125* (Vol. Parts I and II). Delft: Faculty of Civil Engineering and Geosciences.

Yang, Y. (2020). Lecture Notes Concrete Bridges CIE5127.

Figures

Figure 21 From: *https://www.spanbeton.nl/content/files/Files/Kennisportaal/Volstortliggers/WEBSITE__SJP-FLEX_NIEUW.pdf*, on 12-06-2020

Figure 22 From: *https://www.spanbeton.nl/content/files/Files/Kennisportaal/Railbalk/WEBSITE__ZIPXL.pdf*, on 12-06-2020

Figure 23 From: *https://www.spanbeton.nl/content/files/Files/Kennisportaal/Kokerbalk/WEBSITE__SKK.pdf*, on 12-06-2020

Figure 24 From: *https://www.haitsma.nl/nieuws/brugliggers-wanssum/*, on 12-06-2020

Sources of all other figures have been mentioned in the text.

3

EXAMPLES OF UHPC APPLICATIONS

3.1 Introduction examples

This chapter gives a number of examples of UHPC applications in the infrastructure. The goal of this chapter is to illustrate the possibilities and to get inspired for the redesign. Also, some of the main features/benefits of using UHPC in design will be highlighted and general trends/impressions observed in the literature are described. The first paragraph is dedicated to giving a general overview of the UHPC applications. This paragraph describes:

- Which types of applications of UHPC are possible and commonly seen;
- Typical forms in which UHPC is applied in the infrastructure;
- The benefits and/or additional value of UHPC in these projects.

The paragraph is followed by a list containing a number of examples of UHPC that have been selected to illustrate the possibilities of UHPC. After that, the last paragraph is dedicated specifically to the application of UHPC in the infrastructure in the Netherlands. Most information in this chapter is from (Russell & Graybeal, 2013) and (Fehling, Schmidt, Walraven, Leutbecher, & Fröhlich, 2014).

3.2 General overview

According to the literature studied, UHPC is applied in infrastructure projects all over the world. In Europe, France and Germany are commonly mentioned, but mention is made of projects in Austria, Croatia, Italy, Slovenia, Switzerland and the Netherlands as well. In North America, UHPC applications can be found in Canada (the first UHPC bridge was constructed in Sherbrooke, Canada) and the US. Furthermore, UHPC is applied in Australia, New Zealand, Japan, Malaysia and South Korea.

From the studied literature it is found that UHPC is commonly applied in projects in one or more of the following forms:

- **Prefabricated beams** for traffic bridges. These beams are often pretensioned and use various types of cross sections, such U-shaped, I-shaped, T-shaped, Pi-shaped or box-type sections;

- **Prefabricated bridge deck segments** that are post tensioned on site to create a UHPC bridge. Various sections are used, such as U-shape or trough-type cross sections. Instead of internal post tensioned prestressing, segments can also be coupled using external prestressing and/or adhesive. Using segments and connecting them on site allows to prefabricate larger structures beyond transportation limits;

- **Joints between prefabricated elements** are also a field of application. Examples are transverse or longitudinal joints between (UHPC) elements. A benefit of UHPC is the relatively short length required for the transfer of forces from steel to concrete. Another application is shear connector pockets used to connect elements;

- **Different types of bridges** such as arch bridges or space trusses apart from beam or girder bridges can also be constructed. This can be done using UHPC only, or by creating a hybrid structure, e.g. by using both steel and UHPC;

- Another application is **strengthening or retrofitting** existing bridges, to add a layer to a bridge deck to function both as protective layer and to contribute to the strength or using a UHPC top layer for the heaviest loaded or most exposed part of new bridges while the remainder of the structure is executed with conventional concrete (hybrid structures).

In the first part of the literature study (see: Literature Study Part I – Ultra-High Performance Concrete), the characteristics and benefits of UHPC were described. In this part of the literature study, many practical applications are listed, from which it can be seen that these benefits are indeed made use of in practice. From the studied literature, it can be concluded that in practice the application of UHPC may result in one or more of the following points:

- UHPC allows for the design of more slender, lightweight and elegant concrete structures;

- UHPC results in a smaller number of beams or girders needed compared to solution in conventional concrete, resulting in overall weight reduction of the structure. The achieved reduction in weight can be very significant;

- UHPC structures have lower weight, which means easier execution (lighter equipment and/or fewer elements) and shorter time at construction site, which can also result in cost savings;

- UHPC is typically prestressed to provide the required resistance, and due to the presence of steel fibres traditional reinforcement can often be omitted (except for transition zones of prestressing or joints).

These features are reasons of why to choose for the application of UHPC in an infrastructural project.

3.3 Examples worldwide

In this paragraph a number of bridges are discussed that are (partially) constructed in UHPC. These projects were selected because these were important for the development of UHPC, because these projects illustrate the possibilities of the application of the material or to serve as inspiration for the later steps in the thesis project.

3.3.1 Sherbrooke pedestrian bridge (Sherbrooke – Canada)

The first bridge constructed in UHPC was the pedestrian/bicycle bridge in Sherbrooke in Quebec province, Canada. It was constructed in 1997 and has a 60 m long span, the structure is shown in Figure 26.



Figure 26 Sherbrooke pedestrian bridge

From the figure it can be seen that the bridge is designed as a space truss with a top chord made of UHPC that serves as the deck. The lower chord is constructed using two continuous prestressed UHPC girders. The diagonals of the truss consist of UHPC encased in hollow steel sections.

The total structure consists of six prefabricated segments, each 10 m long. These segments were match casted to make sure everything would fit during assembly. Using these segments, first two half spans were assembled after which the final structure was assembled. The prefab segments are connected using external prestressing.

3.3.2 Viaduct Bourg-Les-Valance (Bourg-Les-Valance - France)

The first UHPC road bridges in France and perhaps in the world, is constructed in 2001. It consists of two spans, realised with beams of 20,5 m and 22,0 m and made into a continuous structure by a UHPC connection between the spans casted in situ. The beams are pretensioned prefabricated beams with a double T-cross section and bottom flanges. Figure 27 shows the viaduct (left) and the double T-beams that were used (right).



Figure 27 Viaduct and the double T-girders - (Fehling, Schmidt, Walraven, Leutbecher, & Fröhlich, 2014), p.119

The dimensions of the beams used are as follows: the beam depth is 900 mm, the top chord has a width of 2200 mm and the thickness equals 150 mm.

Because of the prestressing and steel fibres, traditional reinforcement was not required, except for the longitudinal and transverse joints. The longitudinal joints were also realised using UHPC. It is reported that the UHPC solution resulted in a reduction of the weight of the required reinforcement and prestressing tendons compared to the solution in conventional concrete. The weight of the superstructure is about a third of the comparable solution in conventional concrete.

3.3.3 Seonyudo footbridge (Seoul - South Korea)

To illustrate possibilities for different shapes and larger spans, the Seonyudo footbridge is added to this report. It is an arch bridge featuring a main span of 120 m. According to (Russell & Graybeal, 2013), this is the longest span UHPC bridge in the world. It is depicted in Figure 28.



Figure 28 Seonyudo pedestrian bridge

The bridge is constructed using six precast prefabricated Pi-shaped cross sections with a height of 1,3 m, the cross section is shown in Figure 29. The cross sections are 1,3 m high, the upper flange (slab) is 30 mm thick and the slab is prestressed in transverse direction. The webs of the section are 160 mm thick and inclined. The deck is 4,3 m wide. Transverse ribs are used to support the slab on regular centre to centre distance, as well as longitudinal ribs at both edges of the slabs.

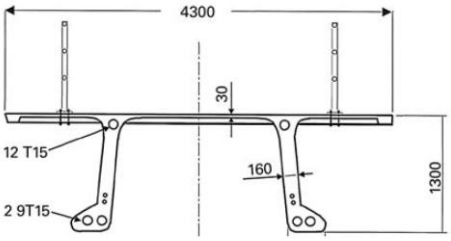


Fig. 7.18 Double-T cross-section and formwork [150]

Figure 29 Cross section - (Fehling, Schmidt, Walraven, Leutbecher, & Fröhlich, 2014), p.130

The transverse ribs are prestressed using strands and small anchors. In longitudinal direction, the segments were post-tensioned together on the construction site. This was done using three prestressing tendons per web, positioned in the haunches.

One can see that the deck is positioned on top of the arch. No tensile tie is present, therefore the horizontal force components are not internally balanced but have to be restrained by the foundation, which is done using vast concrete foundations.

3.3.4 Pont sur l'Huisne (Mans – France)

This example is added to the report because it illustrates another reason why to choose UHPC except for its strength alone. An existing bridge (Pont sur l'Huisne) had to be strengthened (in 2008) and the original solution was to apply external prestressing to the existing bridge. However, this turned out to be impossible: the capacity of the cross-section was already fully utilized. Therefore, the webs of the beams had to be thickened with UHPC.



Figure 30 Placing UHPC through an opening in the bridge deck - (Fehling, Schmidt, Walraven, Leutbecher, & Fröhlich, 2014), p.125

The UHPC used had a high modulus of elasticity, twice that of the conventional concrete of the existing structure. Stiffness attracts load, so the UHPC part of the cross section attracts more normal force, which then does not have to be taken by the existing concrete. This was the main reason for using UHPC in the project, along with its self-compacting properties for execution and because no additional traditional reinforcement was required.

3.3.5 GSE Bridge (Tokyo – Japan)

This example is from the Tokyo Airport, where a bridge had to be built for airport traffic to cross a road. The reason this example is included are the demands that had to be met, being minimum volume and weight for the approach ramps and achieving the required clearance between the bridge and the road.



Figure 31 Picture of the ''Ground Support Equipment'' bridge

A solution was found by lowering the superstructure of the bridge and keeping the depth of the beams as small as possible. For this reason, UHPC was used for the superstructure. By casting the beam in segments, it was possible to comply with the weight limit. The following figure shows a longitudinal section of the bridge, the individual segments can clearly be distinguished.

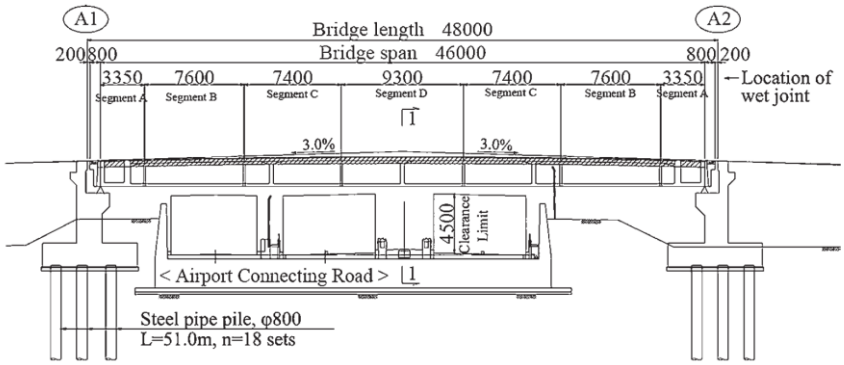


Figure 32 Longitudinal section - (Fehling, Schmidt, Walraven, Leutbecher, & Fröhlich, 2014), p.128

The bridge deck consists of three box type cross sections with a top flange of conventional reinforced concrete. The webs and bottom flange are made of UHPC. The span is 47,6 m and prestressing tendons are positioned inside the box. Because of the steel fibres, traditional reinforcement was not necessary. The flange and the lower UHPC part are connected using shear connectors and the UHPC girders are joined using wet joints with shear keys.

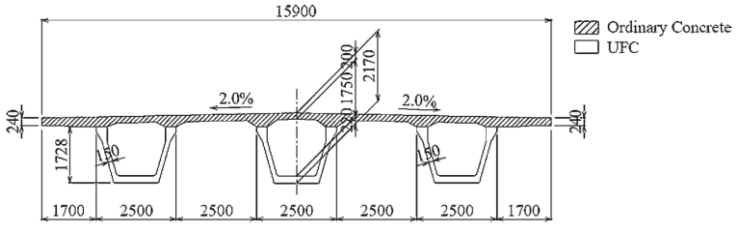


Figure 33 Cross section of the deck - (Fehling, Schmidt, Walraven, Leutbecher, & Fröhlich, 2014), p. 127

3.4 Examples in the Netherlands

This paragraph concludes the chapter by giving a short overview of the application of UHPC in the Netherlands. The first applications of UHPC in the Netherlands was the use for retrofitting a number of existing structures. The first application of UHPC was in 2002: the deck plates of the Kaagbrug were used to be made of timber, but were replaced by UHPC panels of 45 mm thick with a thicker stiffened edge, that were produced using Compacted Reinforced Composite. A material with high strength and high ductility. The plates were placed on the longitudinal steel beams of the bridge and levelled using bolts, see Figure 34.

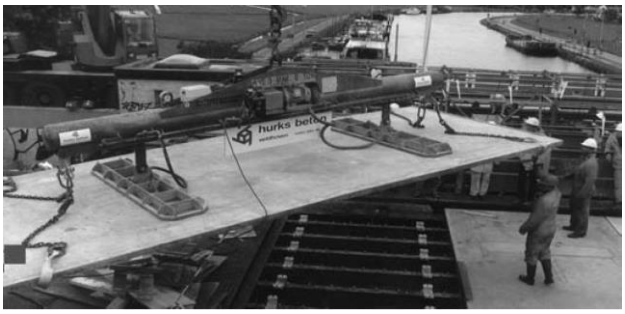


Figure 34 Placing new panels Kaagbrug - (Fehling, Schmidt, Walraven, Leutbecher, & Fröhlich, 2014), p.149

A number of bridges with orthotropic decks have been strengthened using HPC decks (not UHPC). These are examples that show that stronger is not always better: Fatigue cracks were seen in the existing steel deck of these bridges. In these cases, UHPC was not used as it would not solve the fatigue problem. After all, only a very thin UHPC layer with limited weight would be required from a strength point of view. But this does not reduce stress ranges for fatigue sufficiently. In these situations, other mixtures were used with the goal to find an optimum of concrete strength and weight, resulting in thicker deck (60 mm).

A limited number of new bridges has also been constructed in the Netherlands using UHPC. The Wolthuisbrug in Purmerend was the first bridge for which Very-High Strength Concrete was used (2008), the Gooisebrug in Utrecht was the first prestressed bridge in which Very-High Strength Concrete was used (2010). Examples where UHPC has been used are the Brug Zwaaikom in Eindhoven and the Catharinabrug in Leiden (2016), see Figure 35.



Figure 35 Catharinabrug Leiden - (Van Nalta, De Graaff, & Van der Aa, 2016)

For a more extensive list of UHPC applications in practice, reference is made to (Russell & Graybeal, 2013), (Fehling, Schmidt, Walraven, Leutbecher, & Fröhlich, 2014) and Annex 16 of the AFGC-SETRA Recommendations for Ultra-High Performance Fibre-Reinforced Concretes from 2013.

3.5 Bibliography

Sources

Fehling, E., Schmidt, M., Walraven, J., Leutbecher, T., & Fröhlich, S. (2014). *Ultra-High Performance Concrete UHPC*. Berlin: Wilhelm Ernst & Sohn.

Kok, A., Van der Vaart, F., Van der Steen, G., Gonbadani, A. G., & Overbeek, J. (2011). Slanke brug met ZHSB. *Cement*, 62-67.

Lebet, J.-P., & Hirt, M. A. (2013). *Conceptual and Structural Design of Steel and Steel-Concrete Composite Bridges*. EPFL Press.

Russell, H. G., & Graybeal, B. A. (2013). *Ultra-High Performance Concrete: A State-of-the-Art Report for the Bridge Community*. Federal Highway Administration (FHWA), Office of Infrastructure Research and Development.

Van Nalta, R., De Graaff, M., & Van der Aa, J. (2016). Extreme engineering met UHSB. *Cement*, 4-13.

Walraven, J. (2006). Ultra-hogesterktebeton: een materiaal in ontwikkeling. *Cement*, 57-61.

Figures

Figure 26 From: *https://www.researchgate.net/profile/Vic_Perry/publication/340443134/figure/fig2/AS:876812158648320@1586059717555/Sherbrooke-Pedestrian-Bridge-Quebec-Canada-In-2001-the-US-Federal-Highway.jpg*, on 12-06-2020

Figure 28 From: *https://files.structurae.net/files/photos/1/seongyu-bridge_093.jpg*, on 12-06-2020

Figure 31 From: *http://www.jsce.or.jp/committee/concrete/e/newsletter/newsletter19/award.html*, on 12-06-2020

Sources of all other figures have been mentioned in the text.

4

CONCLUSIONS

The goal of this second part of the literature study of the thesis 'Redesign of bridges Twentekanaal in Ultra-High Performance Concrete' was to collect basic information about arch bridges and prefab beam bridges, by considering topics such as the characteristics of the structural systems, design considerations, different bridge types, etc. By achieving this goal, an answer could be formulated to the following research question: What are the basic concepts of arch bridges and prefab beam bridges with respect to design considerations, the construction phase and principles from structural mechanics?

The answer to this research question can be found by looking at the discussions of these topics in the previous three chapters of this report. The first chapter covered the basics of arch bridges. The second chapter started with basic considerations in bridge design, such as when to choose what bridge type or material, after which the focus was placed upon prefab in general and the prefab beam bridges in the infrastructure in particular. In the third chapter, to illustrate the possibilities of UHPC in the infrastructure, general trends and observations in the applications of UHPC in the infrastructure worldwide were discussed. A number of specific projects were highlighted and discussed in more detail, to illustrate the possibilities of UHPC even further and/or to be a source of inspiration for the next phases of the thesis project. The third chapter was finalized by a brief overview of the application of UHPC in the Netherlands.

IV

EXISTING BRIDGES TWENTEKANAAL



Existing bridges Twentekanaal

Redesign of bridges Twentekanaal in Ultra-High Performance Concrete

MSc Thesis

15 June 2020

Company	Witteveen+Bos
MSc thesis project	Redesign of bridges Twentekanaal in Ultra-High Performance Concrete
Document	Existing bridges Twentekanaal
Status	Final version
Version	D1.0
Date	15 June 2020

Author	ing. M. Dorland
Student id	4719980
Degree programme	MSc Civil Engineering
Track	Structural Engineering – Concrete Structures

Company Supervisors	ing. T. Petersen RC ir. A. ten Voorde
Supervisors TU Delft	Dr. ir. Y. Yang Dr. ir. M.A.N. Hendriks Dr. ir. S. Grünewald

TABLE OF CONTENT

PREFACE 1

1 GENERAL DISCRIPTION TWENTEKANAAL 3

1.1 General description and key figures 3

1.2 History 4

1.3 Function of the canal 4

1.4 Engineering structures 5

2 BRIDGES TWENTEKANAAL 6

2.1 Introduction 6

2.2 Overview of bridges across the Twentekanaal 6

2.2.1 Initial construction and second world war 6
2.2.2 Current situation 7
2.2.3 Inventorying the bridges 7

2.3 Characterising the bridges 10

2.4 Bridges Eefde-Enschede 12

2.4.1 Polbrug 12
2.4.2 Spoorbrug Twentekanaal 12
2.4.3 Eefdesebrug 13
2.4.4 Sluis Eefde 14
2.4.5 Almensebrug 14
2.4.6 Ehzerbrug 15
2.4.7 Dochterensebrug 16
2.4.8 Exelsebrug 17
2.4.9 Lochemsebrug 18
2.4.10 Mogezompsebrug 19
2.4.11 Grensbrug 20
2.4.12 Markelosebrug 21
2.4.13 Diepenheimsebrug 23
2.4.14 Weldammerbrug 24
2.4.15 Hengelerbrug 26
2.4.16 Dorrebrug 27
2.4.17 Sluis Delden 28
2.4.18 St. Annabrug 29
2.4.19 Vossenbrinkbrug 30
2.4.20 Loofrietbrug 31
2.4.21 Oelerbrug 32
2.4.22 Boekelosebrug 33

2.4.23 Sluis Hengelo 34
2.4.24 Twekkelerbrug 34
2.4.25 Lonnekerbrug 35
2.5 Bridges Delden-Almelo 36
2.5.1 Spoorbrug Wiene 36
2.5.2 Tankinkbrug 37
2.5.3 Cottwicherbrug 38
2.5.4 Warmtinkbrug 39
2.5.5 Linschotbrug 40
2.5.6 Vredesbrug 40
2.5.7 Hoeselderbrug 41
2.5.8 Brug A35 42
2.5.9 Leemslagenbrug 43
2.5.10 Wierdensebrug 44
2.5.11 Spoorbrug I 45
2.5.12 Spoorbrug II 45
2.6 Analysis 46
2.6.1 Bridge category 46
2.6.2 Year of construction 47
2.6.3 Dimensions, traffic loads and substructure 48
2.7 Conclusions and remarks 53
3 EEFDESEBRUG 54
3.1 Location and description 54
3.2 History 55
3.3 Bridge design 57
3.4 Summary and key figures 64
4 SUMMARY AND CONCLUSIONS 65
5 BIBLIOGRAPHY 66
Final page 69
Annex(es) Number of pages
I Existing bridges Twentekanaal – Summarizing table 1

PREFACE

This document comprises the elaboration of two parts, 'Analysing existing structure' and 'Generalisation (Part I)', of the thesis 'Redesign of bridges Twentekanaal in Ultra-High Performance Concrete'. The goals that are to be achieved in these parts of the project are as follows:

- Goal 'Analysing existing structure': To analyse available information in order to gain insight into the (current state of) the existing structure.

- Goal 'Generalisation': To illustrate the relevance of the project and to generalise the results from the redesign to other existing structures (especially those of the same type).

These goals will be achieved by answering the following related research questions:

- What are the basic details of the Eefdesebrug with regard to geometry, materials, history, loads, etc.?

- What are the characteristics of the different bridges that cross the Twentekanaal?

Answering these research questions allows for completion of the two aforementioned goals. In addition to reaching these two goals, general information on the Twentekanaal is given to provide more background information. To provide an overview, the first part of the generalisation and the analysis of the existing structure in relation to the total project are given in the following figure:

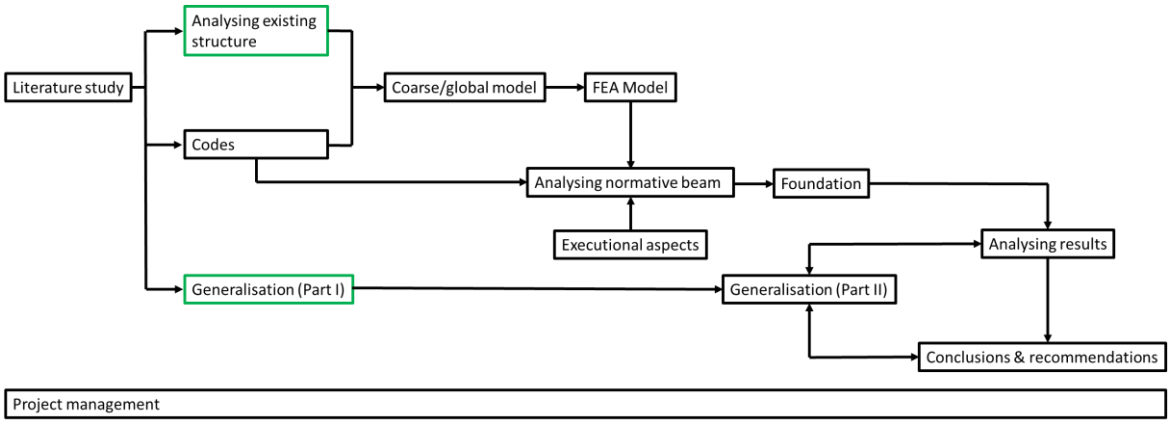


Figure 1 Parts of the project covered in this report in relation to the whole project

Reading guide

This report consists of the following chapters:

- Chapter 1: The first chapter provides the reader with general information about the Twentekanaal. General characteristics, its history and importance are all covered;

- Chapter 2: The second chapter is dedicated to an inventory of all existing bridges crossing the Twentekanaal. First, an overview of all bridges is given after which all bridges are briefly described using publicly available information supplemented by drawings obtained from archives of Rijkswaterstaat. The chapter is concluded by an analysis of the obtained results, to obtain insight into the number of bridges the results of the thesis could be generalised to;

- Chapter 3: The third chapter describes an analysis of the existing Eefdesebrug. Its history and general features are briefly mentioned, followed by a more elaborate description of the structural components of the existing bridge. The chapter is concluded with a summary of the key features of the bridge;

- Chapter 4: The fourth chapter concludes the report with the formulation of the answers to the aforementioned research questions.

An additional remark is made: This report is not only written to answer the research questions, but it is also written to serve as reference material that is to be used in further elaboration of this project. To allow for this, many references to original design drawings from Rijkswaterstaat archives are added, especially in the third chapter. These references are of lesser importance to the reader, but are included to make it easier to look up additional information during further elaboration of this project.

1

GENERAL DISCRIPTION TWENTEKANAAL

1.1 General description and key figures

The Twentekanaal is a canal that connects the larger cities of the Twente region (Almelo, Hengelo and Enschede) to the network of rivers and canals in the Netherlands. The main canal starts at the IJssel river near Zutphen and runs to Enschede while passing towns such as Eefde, Almen, Lochem, Goor, Delden and Hengelo. A second branch starts west of Delden and runs to Almelo. The following figure shows the location of the canal.



Figure 2 Location of Twentekanaal – (Wikipedia, 2020)

A number of key figures of the Twentekanaal have been summarized in Table 1. This table has been prepared using information from (Rijkswaterstaat, sd), (Rijkswaterstaat, 2020) and (Rijkswaterstaat, 2014).

Table 1 Key figures Twentekanaal

Dimension	Value	Units
Length canal (Eefde-Enschede)	47	[km]
Length canal (zijtak Delden-Almelo)	16	[km]
Opened in	1938	[-]
Width	50	[m]
Height to be bridged	21	[m]
Free height for ships	5,5	[m]
Depth (Eefde-Enschede)	-5,0 to -3,30	[m] KP*
Depth (zijtak Delden-Almelo)	-4,2 to -3,5	[m] KP*
Shipping class	CEMT IV / CEMT Va**	[-]

Note:

- *The abbreviation 'KP' stands for 'kanaalpeil', which is used to refer to a height with respect to the water level in the canal. KP can be related to NAP;

- **According to (Rijkswaterstaat, 2020) version 'Mei 2020', the canal from Eefde to a point just past the Dorrebrug is already increased from CEMT IV to CEMT Va standards, the rest of the canal will be upgraded to the same standard as well.

1.2 History

The following table gives an overview of the history of the Twentekanaal. The information is from (Wikipedia, 2020), (Rijkswaterstaat, sd) and (Rijkswaterstaat, 2014).

Table 2 History of the Twentekanaal

Year	Event
1930	Although the first plans were drawn up long before, the construction began at the 12th of March 1930. Before the canals were dug, the construction of the locks and bridges took place, the first would be finished in 1931. After that, canal segments were dug, a large stretch was dug by hand to provide jobs to unemployed workers.
1933	First canal segment is opened and the lock near Eefde is taken into use, followed by the stretch of canal up to Lochem at the end of the year.
1935	The canal is opened all the way to Hengelo.
1936	The main canal up to Enschede is finished and the construction of the side branch from Delden to Almelo starts.
1938	The year 1938 is commonly given as the year in which the Twentekanaal is opened.
40's-50's	During the second world war, a large number of bridges across the canal were damaged or destroyed. During and after the war these bridges had to be rebuilt. These reconstruction works took until the end of the 50's.
1953	The final section of the side branch to Almelo, connecting the Twentekanaal to the ''Overijsselse Kanalen'' was opened in 1953. This concludes the construction of the side branch.
2004-2010	The first phase of the Rijkswaterstaat project to bring the canal up from CEMT IV to CEMT Va standards. The canal is widened and deepened from Eefde to past Lochem (Delden) and is now accessible to ships with a depth up to 3,4 metres. Work was finished in 2010.
2017	Start of the second phase of the Rijkswaterstaat project. The main canal from Delden to Enschede and the side branch are made suitable for CEMT class Va ships with a width up to 2,8 metres. The stretch between the IJssel and Eefde is made suitable for ships up to 3,5 m depth. It is expected the project will be awarded in 2020 and that the project will be finished in 2023.
2017-2020	From 2017 up to 2020 there were multiple projects to strengthen existing bridges crossing the canal or to do maintenance works.

1.3 Function of the canal

There were two reasons for the construction of the Twentekanaal. The first reason was to enable the transport of goods from and to Twente, especially raw materials for the textile industries that were present in the region, as well as coal. The second reason was that the canal would play a role in the water management in the region.

According to (Rijkswaterstaat, 2014) two aspects were especially innovative with respect to the Twentekanalen. The first aspect was that the function of transportation and water management would be

combined, this was considered to be a technical innovation at the time. The second aspect was the effort invested into the aesthetics and integrating the canal into the landscape. This was also something new for the construction of canals and two experts were asked to take care of the aesthetical aspects of the canal and related structures.

It is mentioned in (Rijkswaterstaat, 2014) that during the design of the canal it was already anticipated on future expansion of it. The profile of the canal was designed as such that it would be possible to expand the canal, making it suitable for ships up to 2000 ton instead of the 1350 ton it was originally designed for. Adequate space was reserved for this between the dikes. As was described in the previous paragraph, the canal has indeed been widened since the opening, or plans have been made to do so.

Over time, the economic development related to the construction of the Twentekanaal lagged behind the expectations, but the canal is still used intensively for transport. Nowadays, mainly bulk cargo is transported over the canal, for example: sand, gravel, salt and fodder for animals. Over time the canal has proven to be especially important for water management. In addition to these two main goals the canal was constructed for, it is also used for recreation purposes. In the past the canal was used for the production of drinking water.

1.4 Engineering structures

The construction of the Twentekanaal required comprised the construction of a series of locks and bridges to regulate the water levels and to create a sufficient number of crossing points. Both categories of structures are briefly discussed.

Locks
The elevation drop between Zutphen and Enschede is about 21 metres, to overcome these variations in water levels three locks were constructed. There are three locks located along the main canal (there is no additional lock in the side branch):

- Sluis Eefde: Depending on the IJssel, the rise is approximately 2 to 7,5 m;
- Sluis Delden: Rise of approximately 6 m;
- Sluis Hengelo: Rise of approximately 9 m.

These three locks create three stretches of canal with their own water levels. The water level in the part Eefde-Delden is approximately +10 m NAP, the water level in the part Delden-Hengelo is approximately +16 m NAP and the water level after the lock at Hengelo is approximately +25 m NAP. The canal therefore ends at approximately +25 m NAP at Enschede. The water level between the IJssel and the lock at Eefde depends on the water level in the river.

Bridges
In addition to the locks, a series of bridges was constructed to cross the canal. This will be covered in detail in the next chapter. However, a few points of attention are mentioned. As mentioned in Table 1, the free height for ships should be 5,5 metres. That means that one can already obtain a rough estimation of the required free height by adding up the water level in the sections of the canal and this 5,5 metre margin.

This is more difficult for the stretch of canal between the IJssel and the lock at Eefde, where the water level is controlled by the river (where the Eefdesebrug is located). According to (Rijkswaterstaat, 2020), the free height at the Eefdesebrug is +13,0 m NAP. Subtracting this value by 5,5 metres means that the water level of the IJssel up to + 7,5 m NAP should be accounted for in design. Note that this is just a rough estimation. More detailed information will be collected in subsequent phases of the project.

2

BRIDGES TWENTEKANAAL

2.1 Introduction

In this chapter an inventory will be presented of the bridges crossing the Twentekanaal. This is done to be able to formulate an answer to the research question related to the generalisation. From the previous chapter it is known that a whole series of bridges is constructed over the Twentekanaal. One might already expect that a number of these bridges will be similar with respect to properties such as dimensions, year of construction, etc.

This is already illustrated by the picture on the front page of this report, which is a picture of the Sint Annabrug near Delden. One can see that the bridge has strong similarities with the Eefdesebrug. The goal of this chapter is to quantitatively and qualitatively illustrate the relevance of this project to the bridges over the Twentekanaal.

In paragraph 2.2 the analysis is started by providing a more general overview of the history and characteristics of the bridges across the canal and an overview of all the bridges is given in the form of summarizing tables. In 2.3 it is defined which parameters will be used to characterise the bridges, which will be further elaborated on for each bridge in 2.4 for the main canal (Eefde-Enschede) and in 2.5 for the side branch (Delden-Almelo) respectively. In paragraph 2.6 the results of the inventory are analysed to determine to which extent the results of the project can be generalised to different bridges across the canal. In 2.7 the conclusions are summarized and relevant remarks are given.

2.2 Overview of bridges across the Twentekanaal

2.2.1 Initial construction and second world war

As mentioned in the previous chapter, a whole series of locks and bridges was built during the construction of the Twentekanaal. This was the first phase of the project when it started in 1930, before the different segments of the canal would be dug. The first bridges were finished in 1931 and according to (Rijkswaterstaat, 2014) a total of twenty-nine bridges was constructed:

- Three fixed concrete bridges at the locks;
- Three railroad bridges;
- Eighteen fixed bridges over the main canal (Zutphen-Enschede);
- Five fixed bridges over the side branch to Almelo.

Of the bridges over the main canal, fourteen were constructed in concrete while four were constructed in steel. Most of the bridges were concrete arch bridges what were painted white, a characteristic feature of the bridges crossing the Twentekanaal. Also, characteristic were the bracing elements above the deck between the arches: triangulated concrete bracing elements formed a rhomboidal pattern. Moreover, the bridges were a technical innovation by themselves because these bridges were said to be among the concrete structures with the largest spans in the 1930s.

As will be illustrated in the subsequent parts of this chapter, these concrete arch bridges were very similar in design, and depending on the location and requirements, variations were made in the foundation (e.g. on

grade or on piles) and the width of the deck. For all bridges the minimum free width for ships was 45 m and the free height had to be 5,5 m. As mentioned in the previous chapter, during design it was already anticipated on possible future widening of the canal. This also had implications for the bridges: these were designed as such that if the canal would be widened, the bridges could be jacked upwards to create a larger free height for the ships.

During the war (in 1940 and/or in 1945) many of the bridges across the canal had been destroyed. (Bosch & Van Leeuwen, 2014) reports that twelve bridges were destroyed in 1940: Hoeselderbrug, Middenwegbrug, Dorrebrug, Tankinkbrug, Cottwicherbrug, Warmtinkbrug, Weldammerbrug, Hengelerbrug, Leemslagenbrug, Markelosebrug, Dorrebrug and Railroad bridge Wiene. According to (Rijkswaterstaat, 2014) all bridges were destroyed at the end of the war and would have to be rebuilt, a large number of these for the second time.

In more recent history, the bridges across the canal made the news again in 2013, (NOS Nieuws, 2013) and (Redactie Transport Online, 2013). It was reported that a large number of the bridges across the canal were analysed and a large number of these were found to have insufficient capacity. This was solved by imposing restrictions for maximum traffic loads or by limiting the number of passing vehicles using traffic lights. Maintenance work and or strengthening was carried out to a number of bridges in recent years. Many references to this are included in the upcoming inventory.

2.2.2 Current situation

As mentioned in (Rijkswaterstaat, 2014) all bridges across the canal were destroyed at the end of the war and would have to be rebuilt. According to the same document, eleven bridges were rebuilt in their original design in the period 1948 to 1968. Ten of these bridges are said still to be in service. During the reconstruction, the free height was increased from 5,5 to 6,5 metres.

Other construction projects took place as well. According to the same Rijkswaterstaat document, the Vredesbrug was demolished and replaced by a new concrete girder bridge in the 60's or 70's. The new bridge carries the same name as the old bridge.

In the 70's, the highways A1 and A35 were constructed and as a part of these projects, different bridges were constructed as well. The A1 crosses the side canal near Bornerbroek. The A35 crosses the main canal near Delden and Hengelo and the side branch near Almelo.

In 2005 a new railroad bridge was placed near Eefde, replacing the old one. In 2012 a new traffic bridge was opened there as well (the ''Polbrug''), taking over the role of main traffic bridge from the Eefdesebrug. The Boekelosebrug near Hengelo was replaced in 2019.

This discussion illustrates that the current situation with respect to the bridges across the canal is different than when the canal was opened. As will become clear, nowadays one can distinguish 37 bridges across the canal. All these events and occurrences make that the situation is changed compared to the canal just after opening.

2.2.3 Inventorying the bridges

The first step in the generalisation process is to identify the different bridges across the canal. Note that in this report one or more bridges crossing the canal at or near a lock is also included in the inventory as a ''single'' bridge. This is also done for two bridges positioned directly next to one another, this will be also included as a single bridge.

An overview of the different bridges across the canal has been prepared, it is presented in Table 3 for the main canal and in Table 4 for the branch from Delden to Almelo. It becomes clear that with the aforementioned counting method described, a total of 37 bridges across the canal can be identified.

These two tables have been prepared using (Wikipedia, 2020), (Rijkswaterstaat, 2020), Google Maps and (Rijkswaterstaat, 2014). The bridges are categorised using the following criteria:

- **Nr**: All bridges have been given a number from 1 to 37;
- **Km**: The location of the bridge measured from the start of the canal to its actual location;
- **Name**: Name of the bridge as found in the aforementioned sources, if no name is found a description is given, e.g. ''Spoorbrug'';
- **Road/railroad**: Distinction is made between different roads and railroads. If it is known that the bridge is part of a highway, this is designated with the letter 'A' (e.g. 'A1'). If it is known that the bridge is part of a provincial road, this is designated with 'N' (e.g. 'N346'). The remaining bridges are classified as 'local traffic' for road bridges or as 'railroad' for railroad bridges;
- **Section**: Bridges for road traffic are further classified by roughly denoting the start and endpoint of the road crossing the bridge;
- **Bridge type**: A simple classification is introduced to distinguish between the different types of bridges. The following distinctions are made:
    - Girder bridges (concrete or steel);
    - Truss bridges (steel);
    - Arch bridges (concrete or steel);
    - Other: Cable stayed bridge.

Note: In de 'bridge type' category, no distinction is made between girder or beam bridges at this point. Moreover, the locks are also mentioned in the table because these structures typically also have crossing points. These locks are mentioned in the tables for the sake of completeness, but will not be included in the subsequent analysis, as will be clarified in later parts of this report.

Table 3 Bridges Twentekanaal Eefde-Enschede

Bridges main canal Eefde-Enschede					
Nr.	km	Bridge name	Road/railroad	Section from-to	Bridge type
[-]	[km]	[name]	[-]	[from-to]	[type]
1	1,05	Polbrug	N348	Zutphen-Deventer	Arch bridge (steel)
2	1,80	Spoorbrug Twentekanaal	Railroad	-	Arch bridge (steel)
3	2,05	Eefdesebrug	Local road	Zutphen-Eefde	Arch bridge (concrete)
4	3,30	Sluis Eefde	Lock	Lock	Lock
5	7,43	Almensebrug	N826	Zutphen-Laren	Arch bridge (concrete)
6	9,74	Ehzerbrug	Local traffic	Almen-Laren	Truss bridge
7	11,20	Dochterensebrug	Local traffic	Laren-Klein Dochteren	Girder bridge (steel)
8	14,38	Exelsebrug	N346	Zutphen-Hengelo	Arch bridge (concrete)
9	16,23	Lochemsebrug	N346	Zutphen-Hengelo	Truss Bridge
10	19,30	Mogezompsebrug	Local traffic	Nettelhorst-Armhoede	Girder bridge (steel)
11	21,01	Grensbrug	Local traffic	Markelo-Gelselaar	Girder bridge (steel)
12	23,71	Markelosebrug	N754	Markelo-Stokkum	Truss Bridge
13	25,49	Diepenheimsebrug	Local traffic	Markelo-Diepenheim	Arch bridge (steel)
14	29,04	Weldammerbrug	Local traffic	Goor-Diepenheim	Arch bridge (concrete)
15	30,71	Hengelerbrug	N346	Zutphen-Hengelo	Arch bridge (concrete)
16	33,55	Dorrebrug	Local traffic	Wiene-Zeldam	Girder bridge (steel)
17	36,20	Sluis Delden	Lock	Lock	Lock

18	37,88	St. Annabrug	N740	Delden-Markvelde	Arch bridge (concrete)
19	39,35	Vossenbrinkbrug	Local traffic	Delden-Beckum	Girder bridge (steel)
20	41,67	Loofrietbrug	A35	Zwolle-Enschede	Girder bridge (concrete)
21	42,57	Oelerbrug	Local traffic	Hengelo-Haaksbergen	Arch bridge (concrete)
22	44,08	Boekelosebrug	Local traffic	Industrial area	Truss bridge
23	45,10	Sluis Hengelo	Lock	Lock	Lock
24	46,84	Twekkelerbrug	Other	Pedestrian bridge	Cable stayed bridge
25	48,21	Lonnekerbrug	Local traffic	UT-Havengebied	Arch bridge (concrete)

Table 4 Bridges Twentekanaal Delden-Almelo

Bridges secondary branch Delden-Almelo					
Nr.	km	Bridge name	Road/railroad	Section from-to	Bridge type
[-]	[km]	[name]	[-]	[from-to]	[type]
26	0,35	Spoorbrug Wiene	Railroad	-	Arch bridge (steel)
27	0,76	Tankinkbrug	Local traffic	Local traffic	Arch bridge (steel)
28	1,46	Cottwicherbrug I*	N346	Zutphen-Hengelo	Arch bridge (concrete)
		Cottwicherbrug II*	Local traffic	Local traffic	Girder bridge (concrete)
29	3,93	Warmtinkbrug	Local traffic	Delden-Enter	Arch bridge (steel)
30	6,07	Linschotbrug	A1	Amsterdam-Hengelo	Girder bridge (concrete)
31	7,94	Vredesbrug	Local traffic	Bornerbroek-Enter	Girder bridge (concrete)
32	9,54	Hoeselderbrug	Local traffic	Almelo-Enter	Arch bridge (steel)
33	10,00	Brug in A35	A35	Zwolle-Enschede	Girder bridge (concrete)
34	10,83	Leemslagenbrug	Local traffic	Almelo-Ypelo	Arch bridge (steel)
35	13,28	Wierdensebrug	Local traffic	Almelo-Wierden	Arch bridge (concrete)
36	14,11	Spoorbrug**	Railroad	-	Arch bridge (steel)
37	15,33	Spoorbrug**	Railroad	-	Arch bridge (steel)
*The Cottwicherbrug actually consists of two bridges: the arch bridge in the N346 and a girder bridge for local traffic.					
**No other name is known; hence a description is used as name.					

An overview of the location of the different bridges along the canal can be obtained by the following figure, which was found in (Rijkswaterstaat, 2014). Note that this figure dates back to 2014 and is therefore not entirely correct anymore: The Boekelosebrug has been replaced since publishing the Rijkswaterstaat report (2019), its representation as a truss bridge in the figure is therefore no longer correct.

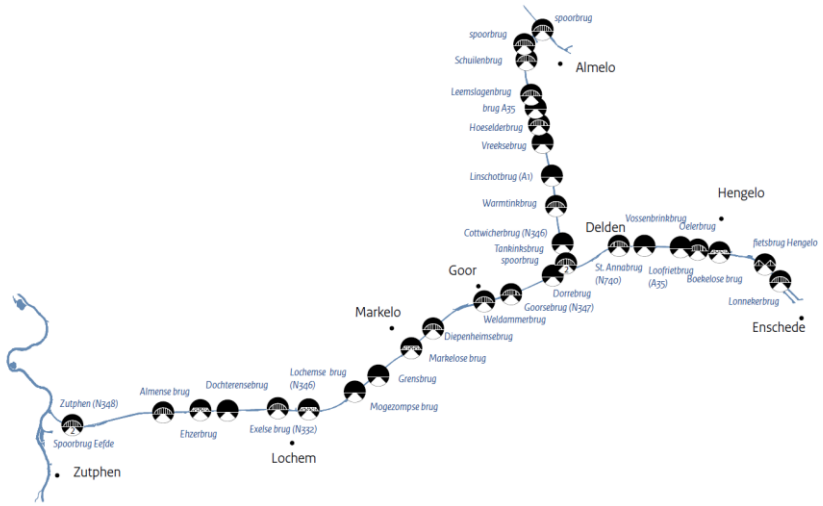


Figure 3 Bridges across the Twentekanaal - (Rijkswaterstaat, 2014)

From the tables and figure, and as described in the report (Rijkswaterstaat, 2014), most of the bridges along the Twentekanaal have similar characteristics and are of one of the following five bridge types:

- Arch bridge concrete
- Arch bridge steel
- Girder bridge concrete
- Girder bridge steel
- Truss bridge

Only one exception to this rule has been identified, which is a cable stayed bridge (Twekkelerbrug). According to the same report, there is more or less a relationship between the type of bridges and their intended function. It is described that the more recently constructed steel arch bridges and concrete arch bridges are typically used for crossings of the canal with the larger provincial and regional roads.

The truss bridges are typically used for the local roads crossing the canal. The steel girder bridges are used for the smaller local roads. These bridges are only one lane wide and have a smaller load bearing capacity than the arch and girder bridges, although the colour and material give similarities to the steel truss bridges. The bridges in the A1 and A35 highway are concrete girder bridges. The exception to these aforementioned bridges is the pedestrian/bicycle bridge at Drienerlo, which is a cable stayed bridge. In the following inventory of the bridges, it will be shown that this classification indeed holds true and forms one of the ways of characterising the bridges and showing the relevance of the project to the other bridges.

2.3 Characterising the bridges

A total of 37 bridges across the canal has been identified. The next step is to characterise these bridges, i.e.: to describe these bridges in more detail. This information will be used for the subsequent analysis. Although not all information could be found from the available sources, the aim was to provide the following information for each bridge:

- **General information**: Information as presented in Table 3 and Table 4;
- **Coordinates**: Coordinates have been provided for easy reference using Google Maps;
- **Span**: The span of the bridge has been given (or estimated, it is explicitly mentioned if this was the case), this is always the main span of the bridge crossing the canal;
- **Width**: The total width of the bridge deck has been given (or estimated, this it is explicitly mentioned if this was the case) as well as the number of traffic lanes;
- **Year of construction**: The year of construction has been determined or, if no sources were available, estimated based on a comparison with similar bridges from the inventory;
- **Pictures**: A picture for overview and a picture of the deck (the latter mostly obtained using Google Maps);
- **General information**: Some general information about the bridge, obtained from generally available sources (e.g. local digital newspapers, websites, etc.), is provided;
- **Additional information**: If available, additional rows are added to the table with additional information from of original (design) documents from Rijkswaterstaat archives. This is used to supplement the aforementioned points.
- **Further clarifications**: Are provided if dimensions or other characteristics had to be estimated. If relevant, this is added as the final row of the table.

These points are summarized into tables, one table is prepared for each bridge. References are mentioned wherever possible. Many of these references are drawings, these are included for easy reference. These design documents were provided along with the information of the Eefdesebrug and were used to give more background information on the different bridges across the canal, the focus was on main characteristics such as span, width and year of construction. Although not complete, it is assumed that it is complete enough for this phase of the project. Paragraphs 2.4 and 2.5 provide the information on the bridges in the canal parts Eefde-Enschede and Delden-Almelo respectively.

2.4 Bridges Eefde-Enschede

2.4.1 Polbrug

Km	Bridge name	Road/railroad	Section from-to	Bridge type
1,05	Polbrug	N348	Zutphen-Deventer	Arch bridge (steel)
Coordinates:		52°09'40.9"N 6°12'10.7"E		
Span:		117 m [1]		
Width:		>15 m – 2 lanes [41]		
Year of construction:		2012 [1]		
				
From: [1]		From: [Google Maps]		
General information: The Polbrug is the replacement of the Eefdesebrug as the main bridge between Zutphen and Eefde for the main traffic, it is part of the new alignment of the N348 around Zutphen [1].				
Additional information: -				
Further clarifications: Width is estimated to be >15 m. This is based on [41], the exact value is unknown.				

2.4.2 Spoorbrug Twentekanaal

Km	Bridge name	Road/railroad	Section from-to	Bridge type
1,80	Spoorbrug Twentekanaal	Railroad	-	Arch bridge (steel)
Coordinates:		52°09'32.9"N 6°12'47.1"E		
Span:		103 [2]		
Width:		2 railroad tracks, width unknown		
Year of construction:		2005 [2]		
				
From: [2]		From: [2]		
General information: The bridge is also known as ''Spoorbrug Eefde'' [2].				
Additional information: -				

2.4.3 Eefdesebrug

Km	Bridge name	Road/railroad	Section from-to	Bridge type
2,05	Eefdesebrug	Local road	Zutphen-Eefde	Arch bridge (concrete)
Coordinates:		52°09'30.9"N 6°12'58.5"E		
Span:		68		
Width:		16,36 m – 2 lanes		
Year of construction:		1955		



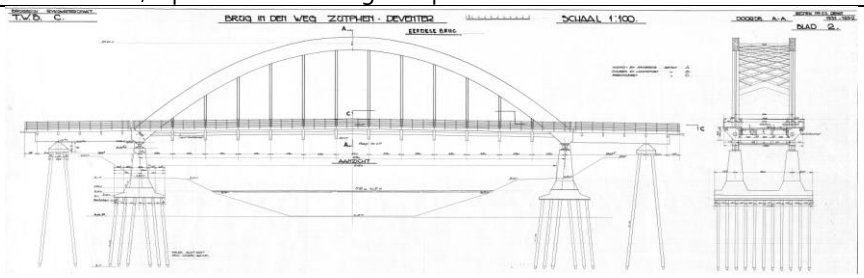
From: -



From: -

General information: The bridge will be covered in more detail in later chapter of this report, see chapter 3 for more details.

Additional information: The first Eefdesebrug, Exelsebrug and Lochemsebrug were very similar in design and part of the same contract: Bestek 69 of 16 February 1931. Drawing B.2790 shows the Eefdesebrug according to this contract, a part of the drawing is depicted below:



2.4.4 Sluis Eefde

Km	Bridge name	Road/railroad	Section from-to	Bridge type
3,30	Sluis Eefde	Lock	Lock	Lock
Coordinates:		52°09'36.6"N 6°14'02.9"E		
Span:		-		
Width:		-		
Year of construction:		1933 [4]		



From: [4] | From: -

General information: A project was started in 2017 to construct a second lock chamber which would be large enough for the CEMT Va class ships. The new lock was opened in April 2020. [4]

Additional information: -

2.4.5 Almensebrug

Km	Bridge name	Road/railroad	Section from-to	Bridge type
7,43	Almensebrug	N826	Zutphen-Laren	Arch bridge (concrete)
Coordinates:		52°09'57.1"N 6°17'36.1"E		
Span:		50,0 – Estimation, see description below		
Width:		10,0 m – 2 lanes – Estimation, see description below		
Year of construction:		1948 [51]		





From: [5] | From: [Google Maps]

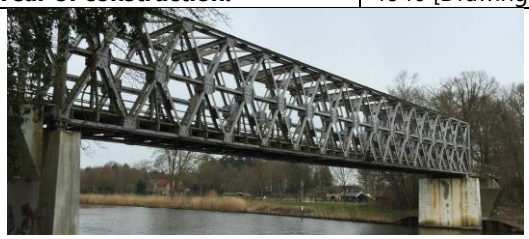
General information: Maintenance work was carried out at the end of 2018 [6].

Additional information: No information was found on the bridge, except for the fact that it was constructed in 1947-1948 on the substructure of the old concrete arch bridge. This suggests, given this is a story similar to many of these bridges across the canal, that it was rebuilt more or less according to original design. Maintenance work was carried out in 2018.

Further clarifications: No detailed information was provided; therefore, the span and width are estimated using Google Maps, (Rijkswaterstaat, 2020) and a comparison with similar bridges from this inventory.

2.4.6 Ehzerbrug

Km	Bridge name	Road/railroad	Section from-to	Bridge type
9,74	Ehzerbrug	Local traffic	Almen-Laren	Truss bridge
Coordinates:		52°09'58.0"N 6°19'37.8"E		
Span:		48,80 [Drawing A.9629]		
Width:		5,2 m – 1 lanes [Drawing A.9629]		
Year of construction:		1946 [Drawing A.9629], [43]		



From: [7]



From: [Google Maps]

General information: In 1946 a bridge (truss bridge, more specific: a Callender-Hamilton type bridge) was constructed on the substructure of the initial concrete arch bridge that was destroyed. This bridge was meant as a temporary solution, but it has been in service until today [43]. The bridge was closed two times in recent years: on one occasion the bridge was strengthened (2017) and in the other periodic maintenance work was carried out (2018) [8].

Additional information: According to information from the Rijkswaterstaat archives, in 1982 a number of elements had to be renewed after damage due to collision.

2.4.7 Dochterensebrug

Km	Bridge name	Road/railroad	Section from-to	Bridge type
11,20	Dochterensebrug	Local traffic	Laren-Klein Dochteren	Girder bridge (steel)
Coordinates:		52°09'58.8"N 6°20'55.1"E		
Span:		47,0 [Drawing 2444]		
Width:		4,86 m – 1 lane [Drawing A.19042]		
Year of construction:		1957 [Drawing A.19042]		



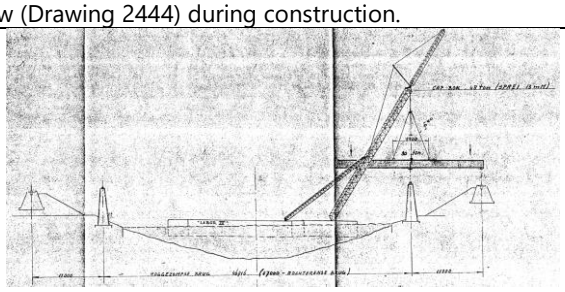
From: [9]



From: [Google Maps]

General information: -

Additional information: Document OO nr. 1960 of the 23rd of August 1957 describes the manufacture and placement of the steel superstructure of the Dochterensebrug (denoted as bridge nr. 4) and the Moggezompsebrug (denoted as bridge nr. 7) on the already existing superstructure, which indicates that older bridges were already present but had to be rebuilt. The bridges are similar in design, the following figure provides an overview (Drawing 2444) during construction.



According to information from the Rijkswaterstaat archive, in 1972 repair works were performed on the pavement layer (asphalt concrete layer).

2.4.8 Exelsebrug

Km	Bridge name	Road/railroad	Section from-to	Bridge type
14,38	Exelsebrug	N346	Zutphen-Hengelo	Arch bridge (concrete)
Coordinates:		52°10'00.2"N 6°23'41.5"E		
Span:		67,09 [Drawing A.16667]		
Width:		16,0 m – 2 lanes – Estimation, see clarification		
Year of construction:		1953-1955 [11]		



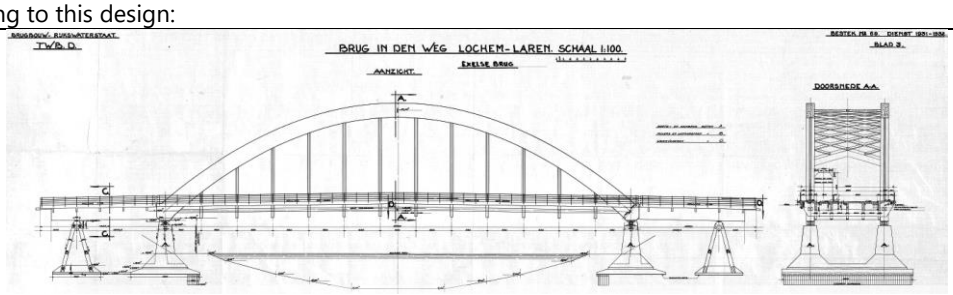
From: [10]



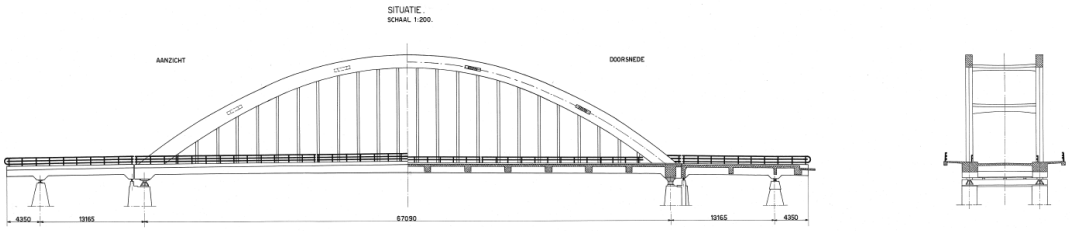
From: [Google Maps]

General information: The original bridge was constructed in the 30's and destroyed in 1945. Between 1953 and 1955 the current bridge was built. In 1992 the bridge was moved 65 metres into its current position to become a part of the new road around the city of Lochem (the current N346). In its old position the bridge became obsolete and moving it was more economical than demolishing the old bridge and constructing a new one [11]. Maintenance work was carried out in the summer of 2018 [12].

Additional information: The first Eefdesebrug, Exelsebrug and Lochemsebrug were very similar in design and part of the same contract: Bestek 69 of 16 February 1931. Drawing B.2791 shows the Exelsebrug according to this design:



Different documents indicate the reconstruction of the bridge between 1953 and 1955. The following drawing (A.16667) provides an overview of the new bridge, it can clearly be seen that the design is changed and is very similar to the second Eefdesebrug, as will become clear in the next chapter.



Further clarifications: No exact dimensions for the width could be found in the provided drawings. Therefore, the width was estimated using the drawings of the joints as given in drawing A.16577.

2.4.9 Lochemsebrug

Km	Bridge name	Road/railroad	Section from-to	Bridge type
16,23	Lochemsebrug	N346	Zutphen-Hengelo	Truss Bridge
Coordinates:		52°09'55.4"N 6°25'19.3"E		
Span:		41.2 [A.30122], (Bosch & Van Leeuwen, 2014)		
Width:		11,0 m – 2 lanes [A.30122], (Bosch & Van Leeuwen, 2014)		
Year of construction:		1947 [14]		



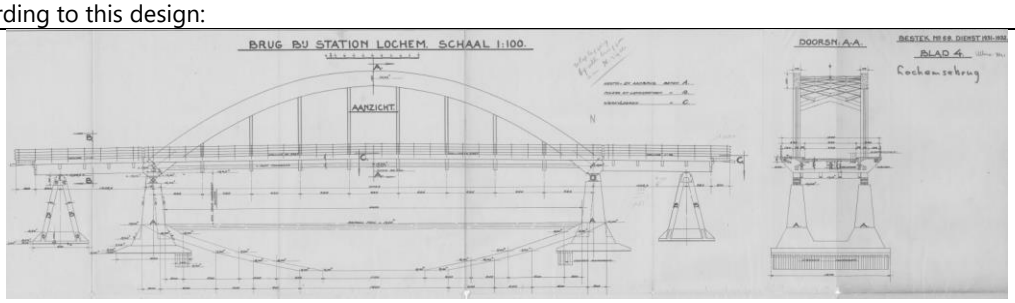
From: [13]



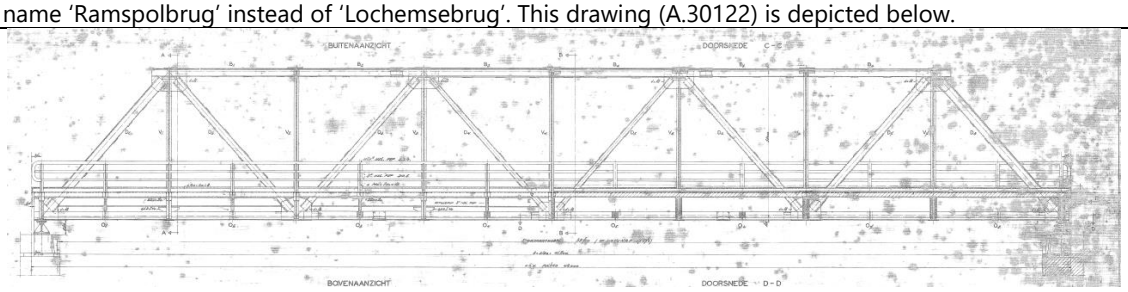
From: [Google Maps]

General information: The original concrete arch bridge was constructed in 1932 and destroyed during the war. A new bridge (a truss bridge this time) was constructed in 1947 [14]. In more recent history, this bridge was found to have insufficient capacity after which traffic lights were placed to limit the passing traffic. Maintenance work was carried out at the end of 2018 [6].

Additional information: The first Eefdesebrug, Exelsebrug and Lochemsebrug were very similar in design and part of the same contract: Bestek 69 of 16 February 1931. Drawing B.2792 shows the Lochemsebrug according to this design:



According to (Bosch & Van Leeuwen, 2014), the concrete arch bridge was rebuilt in 1947. This was done using the superstructure in the form of a truss bridge. This replacing truss bridge was placed in 1947 and was initially meant to be used for Ramspol. However, Lochem had higher priority. The existing foundations and substructure were reused/modified. This explains why provided drawings mention the name 'Ramspolbrug' instead of 'Lochemsebrug'. This drawing (A.30122) is depicted below.



According to the archives from Rijkswaterstaat, in 1978 repair works were performed (a horizontal supporting beam had to be replaced) and in 1984 collision with a ship took place after which a number of elements had to be replaced.

Further clarifications: -

2.4.10 Mogezompsebrug

Km	Bridge name	Road/railroad	Section from-to	Bridge type
19,30	Mogezompsebrug	Local traffic	Nettelhorst-Armhoede	Girder bridge (steel)
Coordinates:		52°10'31.1"N 6°27'44.6"E		
Span:		46,916 m [Drawing 2444]		
Width:		4,86 m – 1 lane [Drawing A.19042]		
Year of construction:		1957 [Drawing A.19042]		



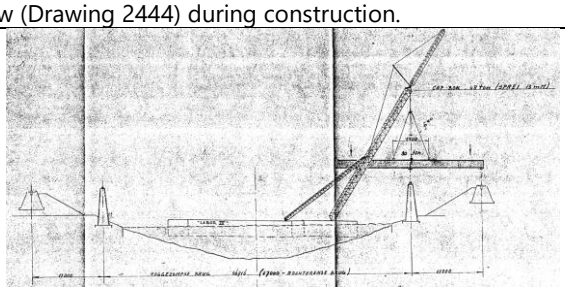
From: [15]



From: [17]

General information: The original bridge was destroyed during the war. The new bridge (see picture) was built in 1957 [15]. Maintenance works were carried out in 2019 [16]. The supports at the South end of the bridge were replaced during maintenance works, see figure top right [17].

Additional information: Document OO nr. 1960 of the 23rd of August 1957 describes the manufacture and placement of the steel superstructure of the Dochterensebrug (denoted as bridge nr. 4) and the Moggezompsebrug (denoted as bridge nr. 7) on the already existing superstructure, which indicates that older bridges were already present but had to be rebuilt. The bridges are similar in design, the following figure provides an overview (Drawing 2444) during construction.



According to information from the Rijkswaterstaat archive, in 1972 repair works were performed on the pavement layer (asphalt concrete layer).

2.4.11 Grensbrug

Km	Bridge name	Road/railroad	Section from-to	Bridge type
21,01	Grensbrug	Local traffic	Markelo-Gelselaar	Girder bridge (steel)
Coordinates:		52°11'06.1"N 6°28'54.9"E		
Span:		28,0 – Estimation, see clarification		
Width:		5,8 m – 1 lanes – Estimation, see clarification		
Year of construction:		Unknown – See clarification		



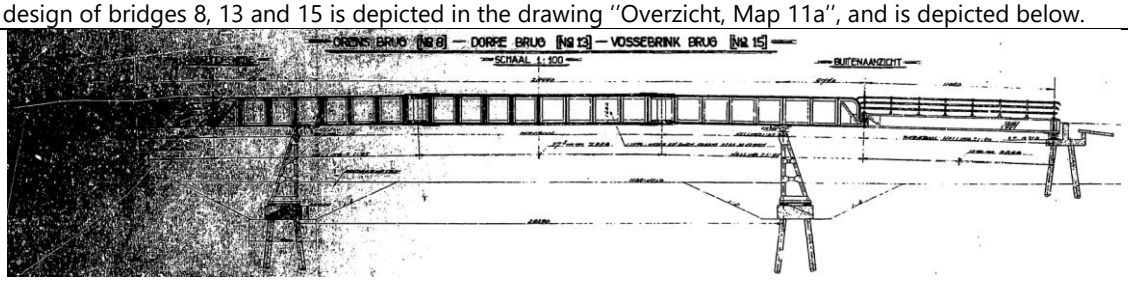
From: [19]



From: [Google Maps]

General information: The bridge is also known as the 'Hungerbrug' [18]. It was destroyed at the end of the war and rebuilt afterwards.

Additional information: The Grensbrug (denoted as: bridge nr 8), Diepenheimsebrug (denoted as: bridge nr 10), Dorrebrug (denoted as: bridge nr 13) and Vossebrinkbrug (denoted as: bridge 15) were similar in design and part of the same contract: Bestek 110 of 28th April 1932. All bridges were made of steel, bridges 8, 13 and 15 were of the same design and consisted of a main span and two side spans. Bridge 10 had a slightly different main span and had to span both the canal and a road. The original design of bridges 8, 13 and 15 is depicted in the drawing ''Overzicht, Map 11a'', and is depicted below.



The superstructure of the Grensbrug was used in 1947 to repair the St. Annabrug.

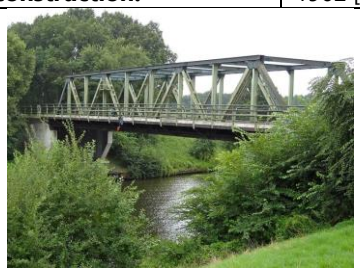
Further clarifications: In the provided information, no details were found regarding the Grensbrug after its superstructure was moved to serve as the new superstructure for the destroyed St. Annabrug. Given the original design drawings and the picture of the current bridge, it might be possible that the superstructure was placed back later after the St. Annabrug was rebuilt in its current form.

Based on drawing ''Overzicht, Map 11a'' of the original design as well as (Rijkswaterstaat, 2020), the span is estimated to be 28,0 m. This estimation is justified by the fact that the original design drawings and the current bridge show large similarities. In the same way, the width is estimated to be 5,8 m.

The year of construction remains unknown because of the aforementioned reasons. The database of the Bruggenstichting (Bruggenstichting, sd) mentions 1932, but it could be that the bridge was built in the 1950's because of the similarity with other bridges. For this reason, it is estimated that the bridge is built in 1950's or earlier because of the similarities to the aforementioned bridges that were rebuilt in the same period.

2.4.12 Markelosebrug

Km	Bridge name	Road/railroad	Section from-to	Bridge type
23,71	Markelosebrug	N754	Markelo-Stokkum	Truss Bridge
Coordinates:		52°11'57.6"N 6°30'48.9"E		
Span:		46,35 [C.10487]		
Width:		10,76 m – 2 lanes [C.10487]		
Year of construction:		1962 [C.10487]		



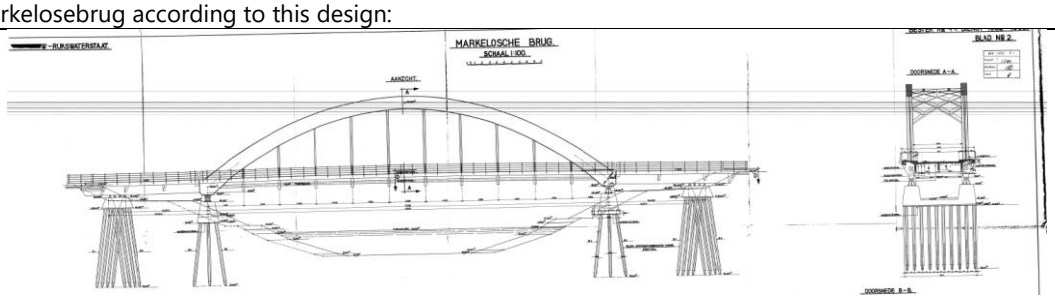
From: [20]



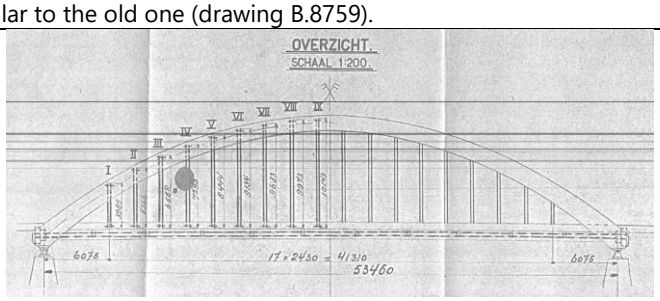
From: [Google Maps]

General information: In 2013 restrictions for traffic loads were imposed upon the bridge, the capacity was deemed insufficient for the heavy lorries and agricultural machinery crossing the structure. These were again lifted after the bridge was strengthened in 2017. The bridge should be able to function safely for another 30 years. [20, 21]

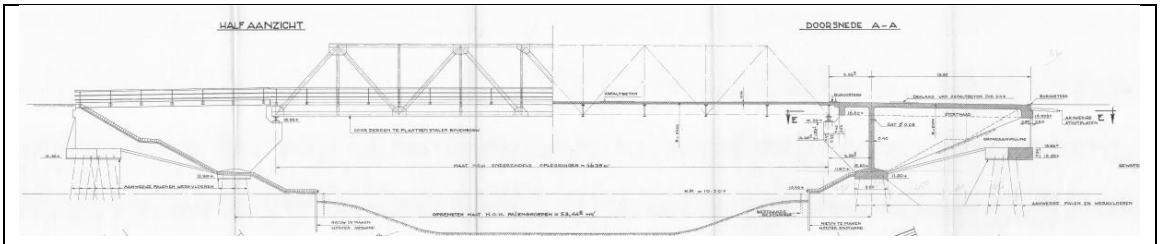
Additional information: The first Markelosebrug, Weldammerbrug and Hengelerbrug were similar in design and part of the same contract: Bestek 44 of 8 februari 1932. Drawing ''Blad 2'' shows the Markelosebrug according to this design:



The document OVK nr. 51 of the 3rd of October 1942 describes the production of tensile ties and hangers for the new bridge, indicating that the bridge had to be rebuilt. A sketch is given below, which shows that the new bridge is similar to the old one (drawing B.8759).



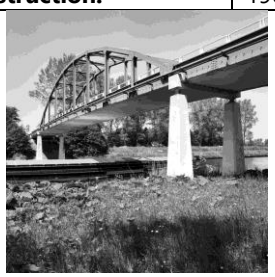
Documents dating from 1961 describe the demolition of the side spans and foundations of the destroyed Markelosebrug (OO nr. 2662 from the 24th of February 1961) and the transport of an old Swing Bridge from Kornewerderzand to the location of the Markelosebrug. On the piles of the destroyed bridge, new supporting structures were constructed on which the modified bridge from Korenewerderzand was placed. The smaller Markelosebrug nearby (an emergency bridge as depicted in drawing C.10487) was taken away, its function being taken over by the larger truss bridge. The bridge from Kornewerderzand was placed at its current position in 1962. This bridge is depicted in the following drawing (C.10487):



The bridge is mentioned in the provided Rijkswaterstaat documents another two times. In 1972 one of the vertical supporting elements of the truss was replaced. In 1987 repair works had to take place.

2.4.13 Diepenheimsebrug

Km	Bridge name	Road/railroad	Section from-to	Bridge type
25,49	Diepenheimsebrug	Local traffic	Markelo-Diepenheim	Arch bridge (steel)
Coordinates:		52°12'34.3"N 6°32'01.3"E		
Span:		41,047 [A.23320]		
Width:		4,87 m – 1 lane [A.23320]		
Year of construction:		1960 [A.23320]		



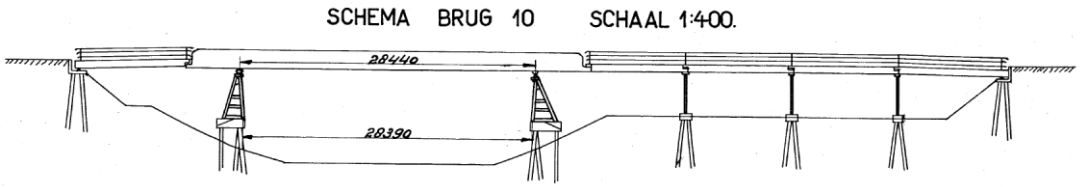
From: [22]



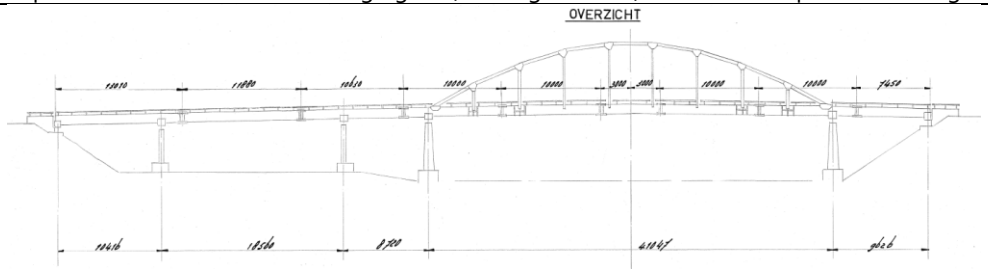
From: [Google Maps]

General information: -

Additional information: The Grensbrug (denoted as: bridge nr 8), Diepenheimsebrug (denoted as: bridge nr 10), Dorrebrug (denoted as: bridge nr 13) and Vossebrinkbrug (denoted as: bridge 15) were similar in design and part of the same contract: Bestek 110 of 28th April 1932. All bridges were made of steel, bridges 8, 13 and 15 were of the same design and consisted of a main span and two side spans. Bridge 10 had a slightly different main span and had to span both the canal and a road. An original design sketch of bridge 10 is given in the following figure (drawing ''A.1143'').



Document OO nr. 2478 from the 8th of July 1960 describes the manufacture and placement of the Hoeselderbrug and Diepenheimsebrug onto the substructure. Both structures have the same main span, the side spans are different. The following figure (drawing A.23320) shows the Diepenheimsebrug.



2.4.14 Weldammerbrug

Km	Bridge name	Road/railroad	Section from-to	Bridge type
29,04	Weldammerbrug	Local traffic	Goor-Diepenheim	Arch bridge (concrete)
Coordinates:		52°13'25.4"N 6°34'44.7"E		
Span:		58,355 [B.6708]		
Width:		9,6 m – 2 lanes – Estimation, see clarification		
Year of construction:		1948 [B.6708]		



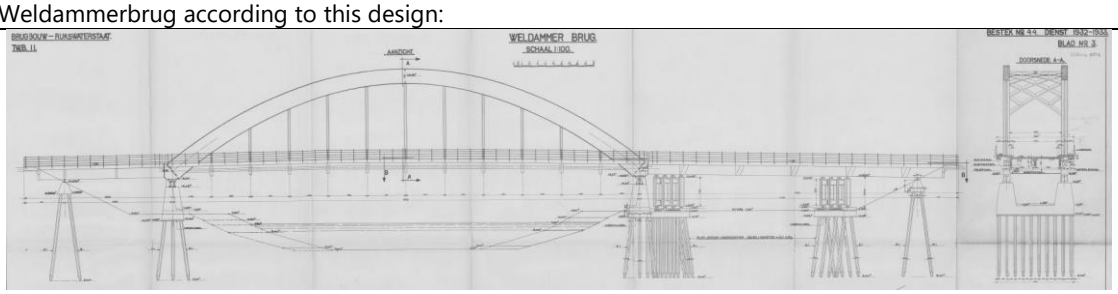
From: [23]



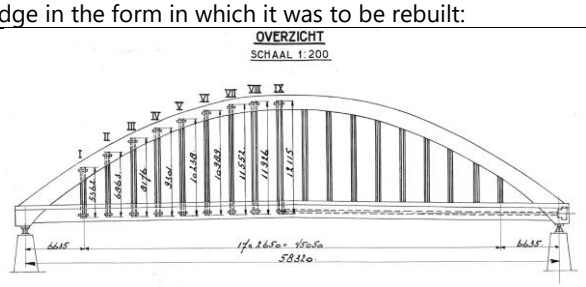
From: [Google Maps]

General information: Maintenance work carried out in 2018 [24].

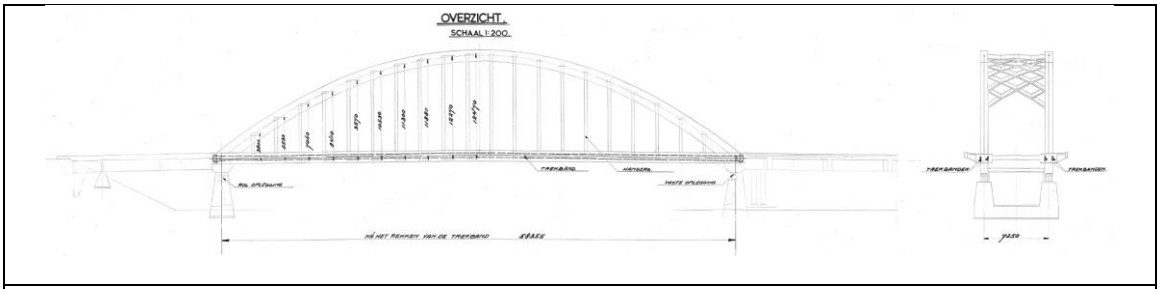
Additional information: The first Markelosebrug, Weldammerbrug and Hengelerbrug were similar in design and part of the same contract: Bestek 44 of 8 February 1932. Drawing ''Blad 3'' shows the Weldammerbrug according to this design:



The bridge was rebuilt in 1940 as described in OVK nr. 67 of the 29th of October 1940. The new design was again a concrete arch bridge. Based on the text in the contract its design was similar to the old design as depicted in the figure above. OVK nr. 80 dating from 19th December 1940 mentions the manufacturing of the tensile ties and hangers for the Weldammerbrug-, Cottwicherbrug and Middenwegbrug (this bridge cannot be traced, it is possibly an old name for the Vredesbrug). This indicates that these were three concrete arch bridges that were damaged/destroyed during the war. The following drawing (A.6760) shows a sketch of the bridge in the form in which it was to be rebuilt:



Document OO nr. 54 of the 5th of April 1948 describes the manufacture of the tensile ties and hangers of the Hengelerbrug and Weldammerbrug. This indicates that both bridges were destroyed in 1945. The following sketch was found in the drawings of the Weldammerbrug (B.6708):



Further clarifications: According to the drawing B.6708, the c.t.c. width between arches is 7,50 m. The total width is not given. Therefore, an estimation is made based on the design from the 1930's, this is justified by the similarities between the designs. The total width is estimated to be 9,0 m.

2.4.15 Hengelerbrug

Km	Bridge name	Road/railroad	Section from-to	Bridge type
30,71	Hengelerbrug	N346	Zutphen-Hengelo	Arch bridge (concrete)
Coordinates:		52°13'37.9"N 6°36'10.1"E		
Span:		63,09 [B.6513]		
Width:		11,80 m – 2 lanes – Estimation, see clarification		
Year of construction:		1948 [B.6513]		



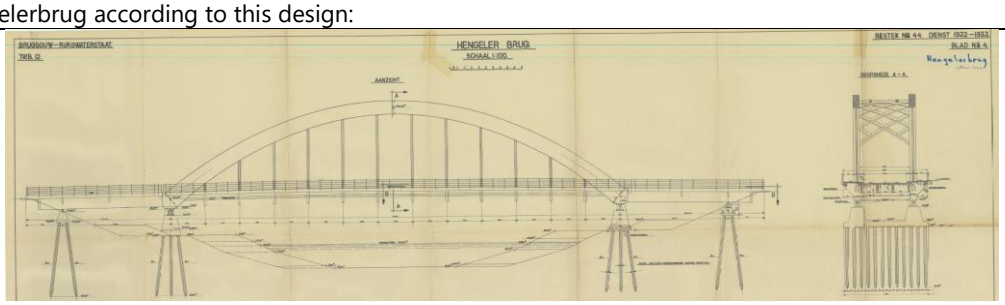
From: [25]



From: [Google Maps]

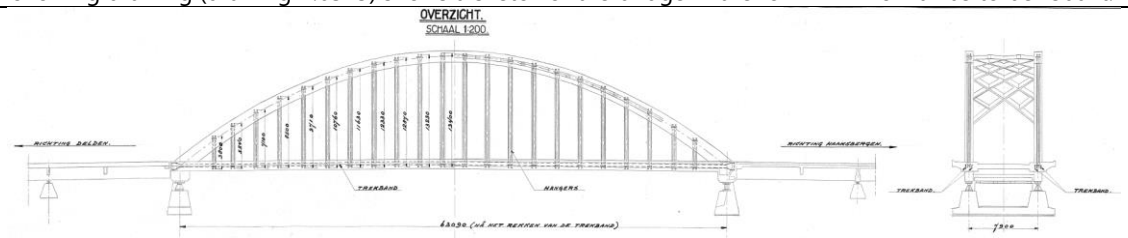
General information: Maintenance work is carried out in 2019 [26].

Additional information: The first Markelosebrug, Weldammerbrug and Hengelerbrug were similar in design and part of the same contract: Bestek 44 of 8 February 1932. Drawing ''Blad 4'' shows the Hengelerbrug according to this design:



The document OVK of the 20th of September 1941 (map 30) describes the repair/reconstruction of the damaged bridge. Based on the description in the document the repaired bridge is similar to the original design.

Document OO nr. 54 of the 5th of April 1948 describes the manufacture of the tensile ties and hangers of the Hengelerbrug and Weldammerbrug. This indicates that both bridges were destroyed in 1945. The following drawing (drawing B.6513) shows a sketch of the bridge in the form in which it was to be rebuilt:



Further clarifications: According to the drawing B.6513, the c.t.c. width of the arches is 7,9 m. The total width is not given. Therefore, an estimation is made based on the design from the 1930's, this is justified by the similarities (the cross section and span are very similar). The total width is estimated to be 11,80 m.

2.4.16 Dorrebrug

Km	Bridge name	Road/railroad	Section from-to	Bridge type
33,55	Dorrebrug	Local traffic	Wiene-Zeldam	Girder bridge (steel)
Coordinates:		52°14'13.6"N 6°38'28.7"E		
Span:		28,86 [A.12798]		
Width:		4,37 m – 1 lane [A.12798]		
Year of construction:		1951 [A.12798]		



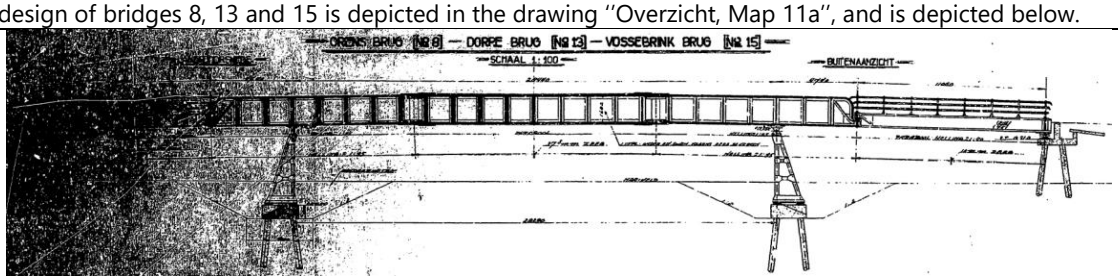
From: [27]



From: [Google Maps]

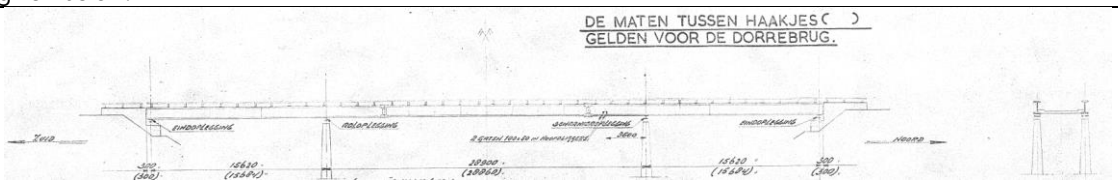
General information: The bridge was strengthened in 2017. Additional work was carried out in 2018 [28].

Additional information: The Grensbrug (denoted as: bridge nr 8), Diepenheimsebrug (denoted as: bridge nr 10), Dorrebrug (denoted as: bridge nr 13) and Vossebrinkbrug (denoted as: bridge 15) were similar in design and part of the same contract: Bestek 110 of 28th April 1932. All bridges were made of steel, bridges 8, 13 and 15 were of the same design and consisted of a main span and two side spans. Bridge 10 had a slightly different main span and had to span both the canal and a road. The original design of bridges 8, 13 and 15 is depicted in the drawing ''Overzicht, Map 11a'', and is depicted below.

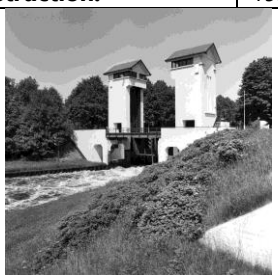


The bridge was repaired in 1940 as mentioned in the document OVK 78 of the 13th of December 1940. Based on the provided drawings the repaired bridge was similar to the initial structure.

The document OO BR nr. 831 from the 15th of May 1951 describes the construction of the superstructure of the Vossebrinkbrug, Dorrebrug and Leemslagenbrug, the first two having a similar design. The superstructures are placed on the already existing substructures. A drawing of the Dorrebrug (A.12798) is given below:



2.4.17 Sluis Delden

Km	Bridge name	Road/railroad	Section from-to	Bridge type
36,20	Sluis Delden	Lock	Lock	Lock
Coordinates:		52°14'46.8"N 6°40'37.0"E		
Span:		-		
Width:		-		
Year of construction:		1936 (Rijkswaterstaat, 2014)		
				
From: [29]			From: -	
General information: -				
Additional information: -				

2.4.18 St. Annabrug

Km	Bridge name	Road/railroad	Section from-to	Bridge type
37,88	St. Annabrug	N740	Delden-Markvelde	Arch bridge (concrete)
Coordinates:		52°15'08.2"N 6°41'56.1"E		
Span:		55,0 – Estimation, see clarification		
Width:		15,0 m – 2 lanes – Estimation, see clarification		
Year of construction:		1965 – Estimation, see clarification		



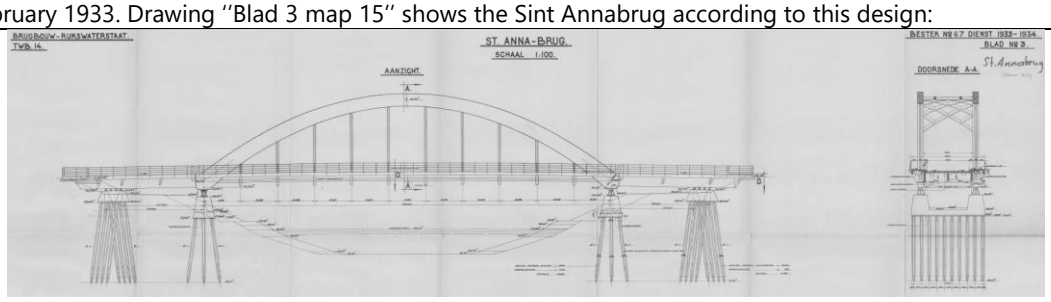
From: Courtesy to R. Bril



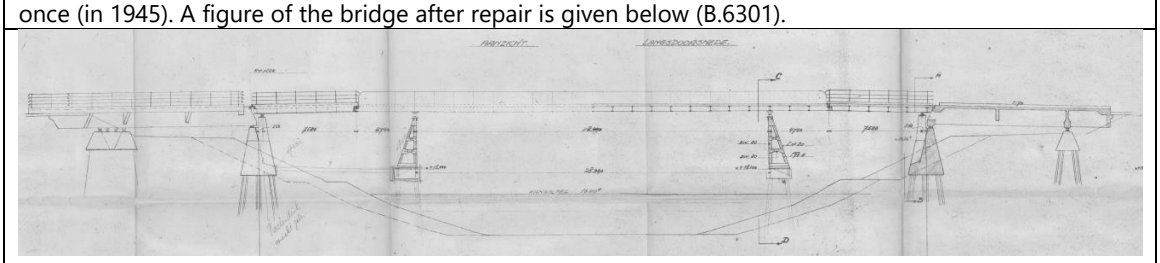
From: Courtesy to R. Bril

General information: The first bridge at this location was built in the 1930's and destroyed during the war. The second bridge was built in 1946, which was removed in the 60's to be replaced by the larger bridge that is present nowadays [30]. Restrictions for the load were imposed in 2013 and again lifted after it was shown that the bridge has sufficient capacity [31].

Additional information: The first Sint Annabrug (bridge nr 14), Oelerbrug (bridge nr 16) and Boekelosebrug (bridge nr 17) were similar in design and part of the same contract: Bestek 67 of 6th of February 1933. Drawing ''Blad 3 map 15'' shows the Sint Annabrug according to this design:



In the document OVK nr. 177 from 25th of November 1947, it is described that the St. Annabrug is repaired using material from the Grensbrug. This indicates that the St. Annabrug was destroyed at least once (in 1945). A figure of the bridge after repair is given below (B.6301).

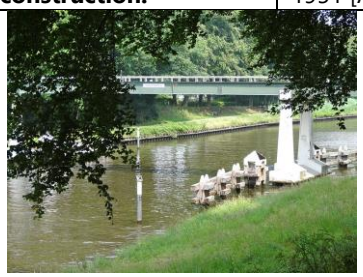


Further clarifications: The current structure indicates that the use of the superstructure of the Grensbrug at this location was only a temporary measure, definitive repairs took place later. However, no details were found regarding these works in the provided information.

The span and width therefore had to be estimated. The estimations for both values are based on Google Maps, Vaarwegen in Nederland and justified by means of a comparison with bridges of similar design (Eefdesebrug & Exelsebrug). The year of construction is also based on a comparison with these other bridges. Given the similarities and the year of construction of these bridges, the year 1965 is assumed as an upper limit, a number of years earlier is also possible.

2.4.19 Vossenbrinkbrug

Km	Bridge name	Road/railroad	Section from-to	Bridge type
39,35	Vossenbrinkbrug	Local traffic	Delden-Beckum	Girder bridge (steel)
Coordinates:		52°15'08.1"N 6°43'13.3"E		
Span:		28,9 m [A.12798]		
Width:		4,37 m – 1 lane [A.12798]		
Year of construction:		1951 [A.12798]		



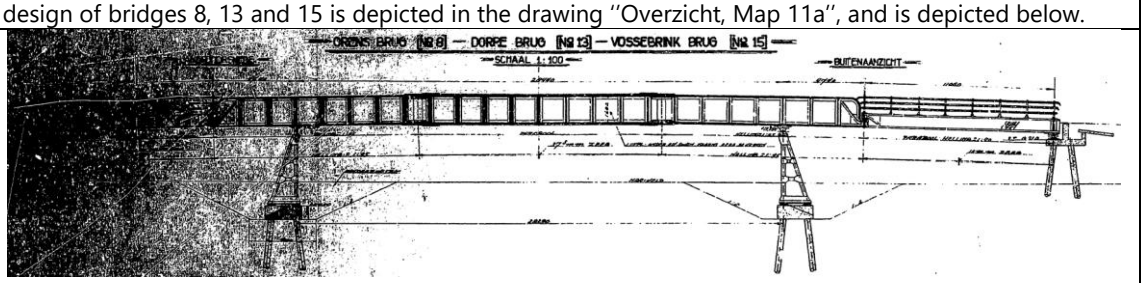
From: [32]



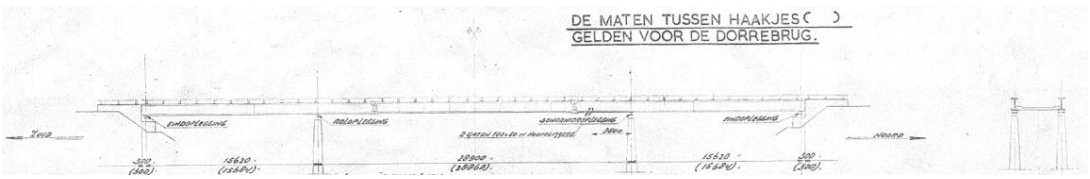
From: [Google Maps]

General information: -

Additional information: The Grensbrug (denoted as: bridge nr 8), Diepenheimsebrug (denoted as: bridge nr 10), Dorrebrug (denoted as: bridge nr 13) and Vossebrinkbrug (denoted as: bridge 15) were similar in design and part of the same contract: Bestek 110 of 28th April 1932. All bridges were made of steel, bridges 8, 13 and 15 were of the same design and consisted of a main span and two side spans. Bridge 10 had a slightly different main span and had to span both the canal and a road. The original design of bridges 8, 13 and 15 is depicted in the drawing ''Overzicht, Map 11a'', and is depicted below.



The document OO BR nr. 831 from the 15th of May 1951 describes the construction of the superstructure of the Vossebrinkbrug, Dorrebrug and Leemslagenbrug, the first two having a similar design. The superstructures are placed on the already existing substructures. A drawing of the Vossenbrinkbrug (A.12798) is given below:



2.4.20 Loofrietbrug

Km	Bridge name	Road/railroad	Section from-to	Bridge type
41,67	Loofrietbrug	A35	Zwolle-Enschede	Girder bridge (concrete)
Coordinates:		52°15'03.9"N 6°45'15.2"E		
Span:		-		
Width:		-		
Year of construction:		1970's (Rijkswaterstaat, 2014)		



From: [Google Maps]

General information: -

Additional information: -

2.4.21 Oelerbrug

Km	Bridge name	Road/railroad	Section from-to	Bridge type
42,57	Oelerbrug	Local traffic	Hengelo-Haaksbergen	Arch bridge (concrete)
Coordinates:		52°15'00.7"N 6°46'02.6"E		
Span:		50,06 [A.30439]		
Width:		18,8 m – 2 lanes – Estimation, see clarification		
Year of construction:		1963 [A.30439]		



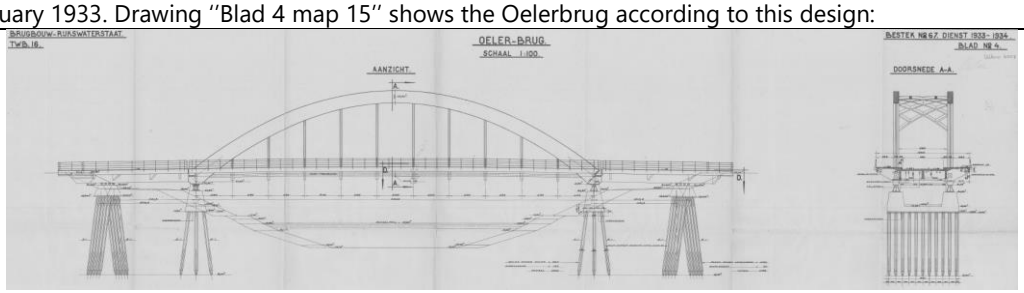
From: [33]



From: [Google Maps]

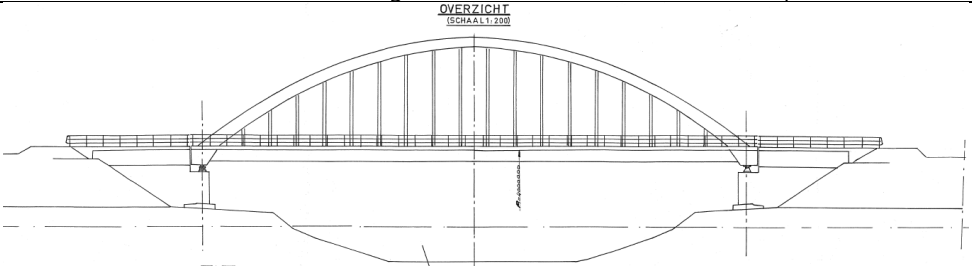
General information: After the war a truss bridge was placed at this location, which was replaced in 1963 by the current concrete arch bridge. The truss bridge was moved to the current location of the Boekelosebrug before being replaced there by an integral bridge in 2019. [34]. Maintenance work was carried out at the Oelerbrug in 2019. [35]

Additional information: The first Sint Annabrug (bridge nr 14), Oelerbrug (bridge nr 16) and Boekelosebrug (bridge nr 17) were similar in design and part of the same contract: Bestek 67 of 6th of February 1933. Drawing ''Blad 4 map 15'' shows the Oelerbrug according to this design:



The document OO nr. 3201 from the 28th of March 1963 describes moving the superstructure from the Oelerbrug to the substructure of the Boekelosebrug. This was a truss bridge, which implies that the arch bridge was destroyed at least once during the war and after the war had to be replaced, which was done by this truss bridge.

The document OVK nr. 3147 from the 17th of May 1963 describes demolishing the supports and abutments of the Oelerbrug after which the bridge was renewed: A new bridge was constructed on the existing pile foundation. Drawings A.30439 and A.31091 provide an overview of this new 1963 bridge, which has features similar to the Eefdesebrug, as will be described in the next chapter.



Further clarifications: In the drawings of the 1963 bridge, no exact value for the total width was given. Therefore, the width is estimated based on drawings of the joints that were given in drawing A.31091. This way, the width is estimated to be 18,8 m.

2.4.22 Boekelosebrug

Km	Bridge name	Road/railroad	Section from-to	Bridge type
44,08	Boekelosebrug	Local traffic	Industrial area	Truss bridge
Coordinates:		52°14'51.9"N 6°47'21.3"E		
Span:		-		
Width:		2 lanes		
Year of construction:		2019 [36]		



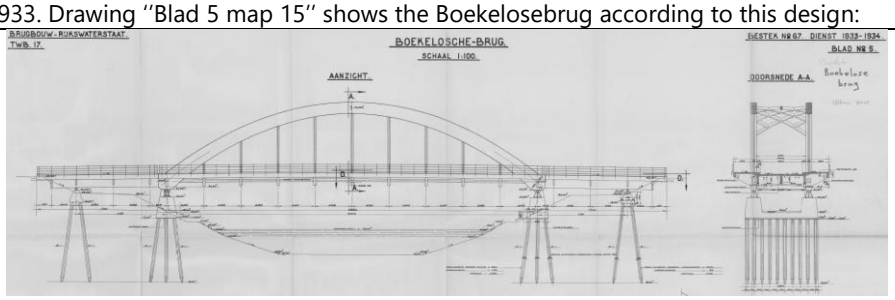
From: [36]



From: [37]

General information: The old truss bridge that was placed in 1963 caused traffic problems and was no longer fit for use in the current form. A new concrete bridge (integral bridge) was constructed, the new bridge at this location was opened in 2019, see the photos [36].

Additional information: The first Sint Annabrug (bridge nr 14), Oelerbrug (bridge nr 16) and Boekelosebrug (bridge nr 17) were similar in design and part of the same contract: Bestek 67 of 6th of February 1933. Drawing ''Blad 5 map 15'' shows the Boekelosebrug according to this design:



The document OVK nr. 2847 from 8th December 1961 describes the work of demolishing the side spans and foundations of the destroyed Boekelosebrug, implying the bridge was destroyed during the war.

The document OO nr. 3201 from the 28th of March 1963 describes moving the superstructure from the Oelerbrug to the substructure of the Boekelosebrug. The superstructure, a truss structure of about 350 T and dimensions 42 by 11 by 6 m (length by width by height) was placed on its new location. This is the old truss bridge as still can be seen on Google Maps:



In the documents used for this project, the truss bridge is mentioned a couple of times after 1963: In 1981 a horizontal supporting element had to be replaced after it was damaged. In 1987 one of the vertical elements had to be replaced.

Further clarification: No further details regarding the width and span of the 2019 bridge have been found.

2.4.23 Sluis Hengelo

Km	Bridge name	Road/railroad	Section from-to	Bridge type
45,10	Sluis Hengelo	Lock	Lock	Lock
Coordinates:		52°14'46.3"N 6°48'13.0"E		
Span:		-		
Width:		-		
Year of construction:		1936 (Rijkswaterstaat, 2014)		
				
From: [38]			From: -	
General information: Directly next to the western lock gate, a traffic bridge and an old railroad bridge are positioned.				
Additional information: -				

2.4.24 Twekkelerbrug

Km	Bridge name	Road/railroad	Section from-to	Bridge type
46,84	Twekkelerbrug	Other	Pedestrian bridge	Cable stayed bridge
Coordinates:		52°14'24.6"N 6°49'39.8"E		
Span:		-		
Width:		-		
Year of construction:		1999 [42]		
				
From: (Wikipedia, 2020)			From: -	
General information: Bicycle/pedestrian bridge crossing the Twentekanaal.				
Additional information: -				

2.4.25 Lonnekerbrug

Km	Bridge name	Road/railroad	Section from-to	Bridge type
48,21	Lonnekerbrug	Local traffic	UT-Havengebied	Arch bridge (concrete)
Coordinates:		52°13'54.2"N 6°50'28.2"E		
Span:		48,2 [A.21630]		
Width:		16,0 m – 2 lanes – Estimation, see clarification		
Year of construction:		1958		



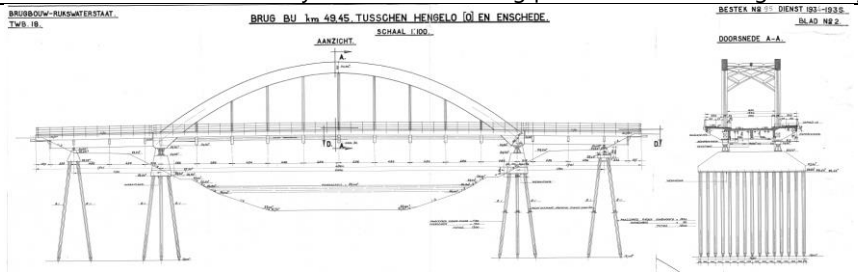
From: [38]



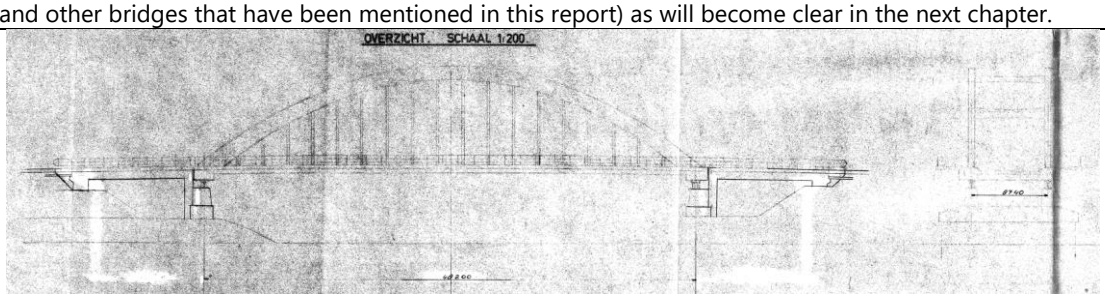
From: [Google Maps]

General information: Maintenance was carried out in 2019 [38].

Additional information: The construction of the original Lonnekerbrug was described by contract document ''Bestek nr. 95'' of 17th February 1934. The following picture shows the original design (B.2793):



Various documents dating back to 1958 describe the demolition of the remnants of the old bridge (indicating it was destroyed in the war) as well as the manufacture and delivery of parts for the new bridge. A drawing of the new bridge (after A.21630) is depicted below. It can be seen that the design is different from the old bridge and is in line with the pictures above. It is similar to the new Eefdesebrug (and other bridges that have been mentioned in this report) as will become clear in the next chapter.



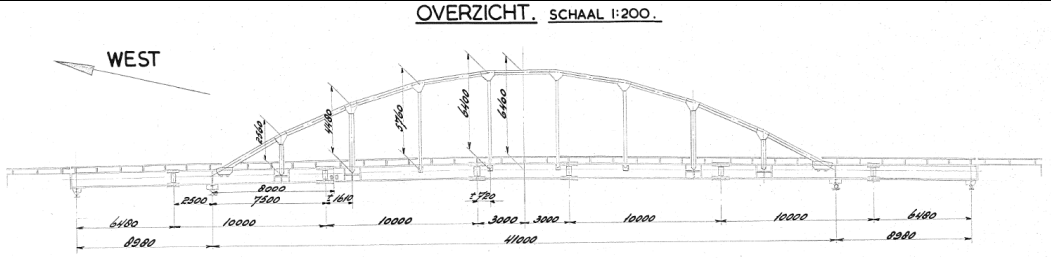
Further clarifications: The total width of the deck has to be estimated. The drawing A.21630 gives a c.t.c. distance of the arches of 8,740 m. Based on Google Maps and the 1930's design drawing, the deck is estimated to be 16,0 m.

2.5 Bridges Delden-Almelo

2.5.1 Spoorbrug Wiene

Km	Bridge name	Road/railroad	Section from-to	Bridge type
0,35	Spoorbrug Wiene	Railroad	-	Arch bridge (steel)
Coordinates:		52°14'31.3"N 6°39'04.2"E		
Span:		-		
Width:		-		
Year of construction:		<1990 [39]		
				
From: [39]			From: -	
General information: The first bridge was constructed during the period in which the branch of the canal from Delden to Almelo was constructed. The bridge was destroyed in 1940, reconstructed and destroyed again in 1945. In 1956 the bridge was reconstructed as a truss bridge. In 1990 a ''new'' bridge was placed at this location, which had first been used as a part of the railroad track near Diemen. [39]				
Additional information: -				

2.5.2 Tankinkbrug

Km	Bridge name	Road/railroad	Section from-to	Bridge type
0,76	Tankinkbrug	Local traffic	Local traffic	Arch bridge (steel)
Coordinates:		52°14'44.6"N 6°39'04.2"E		
Span:		41,0 [A.14659]		
Width:		4,37 m – 1 lane [A.14659]		
Year of construction:		1952 [A.14659]		
				
From: (Wikipedia, 2020)			From: -	
General information: -				
Additional information: Document OO nr. 1104 of the 9th of September 1952 describes the manufacture and transport of the new superstructure, which is to be placed on the existing substructure. As is mentioned on the accompanying letter as well, this is repair works of the previous bridge. The following drawing provides an overview of the new bridge (A.14659):				
				

2.5.3 Cottwicherbrug

Km	Bridge name	Road/railroad	Section from-to	Bridge type
1,46	Cottwicherbrug I	N346	Zutphen-Hengelo	Arch bridge (concrete)
''	Cottwicherbrug II	Local traffic	Local traffic	Girder bridge (concrete)
Coordinates:		52°15'06.8"N 6°38'58.8"E		
Span (bridge I):		42.035 [A.10674]		
Width (bridge I):		12,0 m – 2 lanes – Estimation, see clarification		
Year of construction (bridge I):		1947		



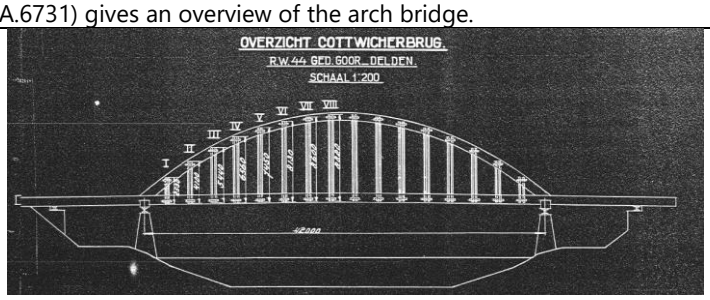
From: [40]



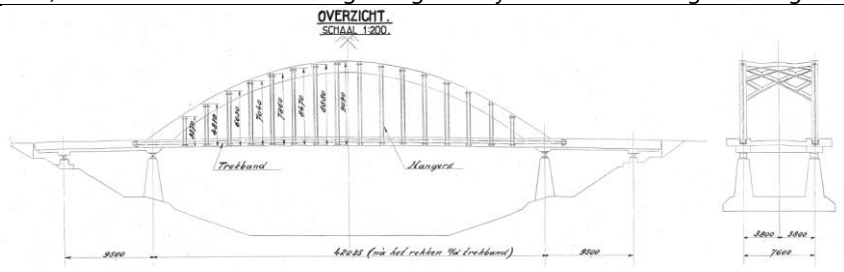
From: [Google Maps]

General information: Maintenance work on the arch bridge was carried out in 2019.

Additional information: The document OVK nr. 80 dating from 19th December 1940 mentions the manufacturing of the tensile ties and hangers for the Weldammerbrug-, Cottwicherbrug and Middenwegbrug (this bridge cannot be traced, it is possibly the old name of the Vredesbrug). This indicates that these three were concrete arch bridges that were damaged/destroyed during the war. The following drawing (A.6731) gives an overview of the arch bridge.



The document OVK nr. 77 of the 7th of July 1947 describes the manufacture of the tensile ties and hangers for the Cottwicherbrug, indicating that the bridge was destroyed at the end of the war. The following drawing (A.10674) shows that the rebuilt bridge is again very similar to the original design.



The arch bridge was mentioned a number of other times in the documents as well. In 1957 work was carried out among which was work done on the joints, this was done again in 1962.

Further clarifications: The total width could not be determined from the design drawings. Following drawing A.10674, the c.t.c. width between the arches is 7,6 m. The total width is estimated to be 12,0 m, this is based on the aforementioned drawing and Google Maps.

Cottwicherbrug II: No information was found on the bridge next to the arch bridge (denoted in this report as: Cottwicherbrug I). Its dimensions are therefore estimated based on first span, Google Maps and

(Rijkswaterstaat, 2020). The estimated dimensions are a span of 42,0 m and a width of 10,0 m. According to (Bruggenstichting, sd), the bridge was constructed in 1975.

2.5.4 Warmtinkbrug

Km	Bridge name	Road/railroad	Section from-to	Bridge type
3,93	Warmtinkbrug	Local traffic	Delden-Enter	Arch bridge (steel)
Coordinates:		52°16'25.7"N 6°38'37.4"E		
Span:		42,0 [A.13807]		
Width:		4,37 m – 1 lane [A.13807]		
Year of construction:		1951 [A.13807]		



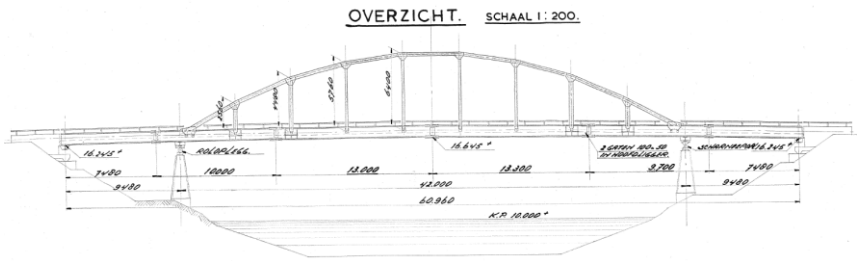
From: (Wikipedia, 2020)



From: [Google Maps]

General information: The bridge was strengthened in 2017. Additional work was carried out in 2018 [28].

Additional information: Document OO BR nr. 981 of the 29th of January 1951 describes the manufacture and delivery of the superstructure of the Warmtinkbrug, which is to be placed on existing substructure, which possibly indicates that a bridge was already present and was destroyed during the war. The following drawing (A.13807) gives an overview of the bridge.



2.5.5 Linschotbrug

Km	Bridge name	Road/railroad	Section from-to	Bridge type
6,07	Linschotbrug	A1	Amsterdam-Hengelo	Girder bridge (concrete)
Coordinates:		52°17'34.3"N 6°38'23.0"E		
Span:		-		
Width:		-		
Year of construction:		1973 (Bruggenstichting, sd)		



From: [Google Maps]

General information: -

Additional information: -

2.5.6 Vredesbrug

Km	Bridge name	Road/railroad	Section from-to	Bridge type
7,94	Vredesbrug	Local traffic	Bornerbroek-Enter	Girder bridge (concrete)
Coordinates:		52°18'33.7"N 6°38'02.3"E		
Span:		-		
Width:		2 lanes		
Year of construction:		60's-70's (Rijkswaterstaat, 2014)		



From: [Google Maps]



From: [Google Maps]

General information: -

Additional information: -

2.5.7 Hoeselderbrug

Km	Bridge name	Road/railroad	Section from-to	Bridge type
9,54	Hoeselderbrug	Local traffic	Almelo-Enter	Arch bridge (steel)
Coordinates:		52°19'24.1"N 6°37'45.4"E		
Span:		41,047 [A.23356]		
Width:		4,37 m – 1 lane [A.23356]		
Year of construction:		1960 [A.23356]		



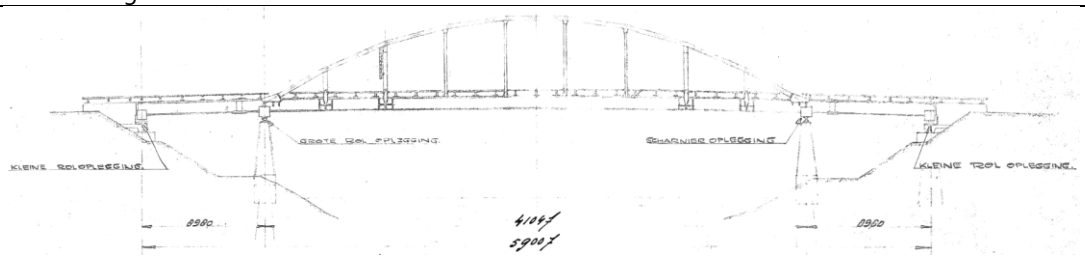
From: [47]



From: [Google Maps]

General information: According to [47, 48] the first bridge at this location was a concrete arch bridge, which was destroyed during the war and replaced by the current steel structure.

Additional information: Document OO nr. 2478 from the 8th of July 1960 describes the manufacture and placement of the superstructure of the Hoeselderbrug and Diepenheimsebrug. Both structures have the same main span, the side spans are different. The following figure, drawing A.23356, shows the Hoeselderbrug.



2.5.8 Brug A35

Km	Bridge name	Road/railroad	Section from-to	Bridge type
10,00	Brug in A35	A35	Zwolle-Enschede	Girder bridge (concrete)
Coordinates:		52°19'33.9"N 6°37'41.1"E		
Span:		-		
Width:		-		
Year of construction:		1970's (Rijkswaterstaat, 2014)		



From: [Google Maps]

General information: -

Additional information: -

2.5.9 Leemslagenbrug

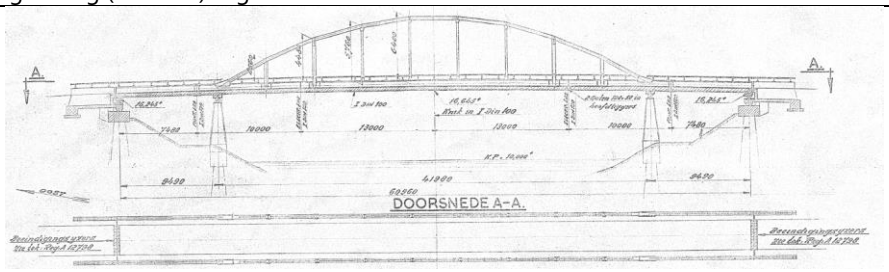
Km	Bridge name	Road/railroad	Section from-to	Bridge type
10,83	Leemslagenbrug	Local traffic	Almelo-Ypelo	Arch bridge (steel)
Coordinates:		52°20'04.3"N 6°37'26.1"E		
Span:		41,98 [A.12831]		
Width:		4,37 m – 1 lane [A.12831]		
Year of construction:		1951 [A.12831]		



From: [-] From: [Google Maps]

General information: -

Additional information: The document OO BR nr. 831 from the 15th of May 1951 describes the construction of the superstructure of the Vossebrinkbrug, Dorrebrug and Leemslagenbrug, the first two having a similar design. The superstructures are placed on the already existing substructures. A drawing of the Leemslagenbrug (A.12831) is given below.



2.5.10 Wierdensebrug

Km	Bridge name	Road/railroad	Section from-to	Bridge type
13,28	Wierdensebrug	Local traffic	Almelo-Wierden	Arch bridge (concrete)
Coordinates:		52°21'21.7"N 6°37'08.4"E		
Span:		44,0 [50]		
Width:		19,0 m [50]		
Year of construction:		1952 [49]		



From: [44]



From: [Google Maps]

General information: According to [49] the bridge was constructed in 1951-1952. According to [50] the bridge was constructed because it became necessary due to the construction of the side branch of the Twentekanaal. After finishing the bridge, the canal was dug. This source also states that it is for the first time that the traditional tensile tie (as seen at the bridges with rhomboidal supporting elements between the arches) were replaced by prestressing cables. From the perspective of aesthetics, new features have also been introduced. The transverse supporting elements between the arches are now in the form of two slightly curved supporting elements. The description in this text shows many similarities with the Eefdesebrug, as will be discussed in chapter 3.

Additional information: -

Further clarifications: -

2.5.11 Spoorbrug I

Km	Bridge name	Road/railroad	Section from-to	Bridge type
14,11	Spoorbrug**	Railroad	-	Arch bridge (steel)
Coordinates:		52°21'47.6"N 6°37'17.4"E		
Span:		-		
Width:		-		
Year of construction:		-		
				
From: (Wikipedia, 2020)			From: -	
General information: -				
Additional information: -				

2.5.12 Spoorbrug II

Km	Bridge name	Road/railroad	Section from-to	Bridge type
15,33	Spoorbrug**	Railroad	-	Arch bridge (steel)
Coordinates:		52°22'11.1"N 6°38'04.4"E		
Span:		-		
Width:		-		
Year of construction:		-		
				
From: (Wikipedia, 2020)			From: -	
General information: -				
Additional information: -				

2.6 Analysis

2.6.1 Bridge category

After inventorying the bridges or the bridges part of larger structures, the results are analysed to determine which bridges are relevant in relation to the thesis project. A total of 37 bridges or bridges part of a larger structure have been identified. Note that Cottwicherbrug is counted as a single bridge, although it consists of two bridges placed next to one another in reality. A lock with multiple bridges (e.g. Hengelo) is still counted for as a single bridge because these are part of the same lock infrastructure.

This total number of bridges of 37 bridges will be categorised and subdivided in a series of steps to qualitatively and quantitatively describe the relevance of the project to these bridges. The first step is to classify the bridges according to a number of categories and to see which bridges are to be taken into consideration. The categories are: Traffic (Highway), Provincial or local traffic, railroad bridges, bridges being part or being near a lock and others. The results are as follows: a total of 37 bridges is identified of which are 3 traffic bridges for highways, 26 bridges for provincial/local traffic, 4 railroad bridges, 3 bridges as part of a lock and 1 classified as 'other'.

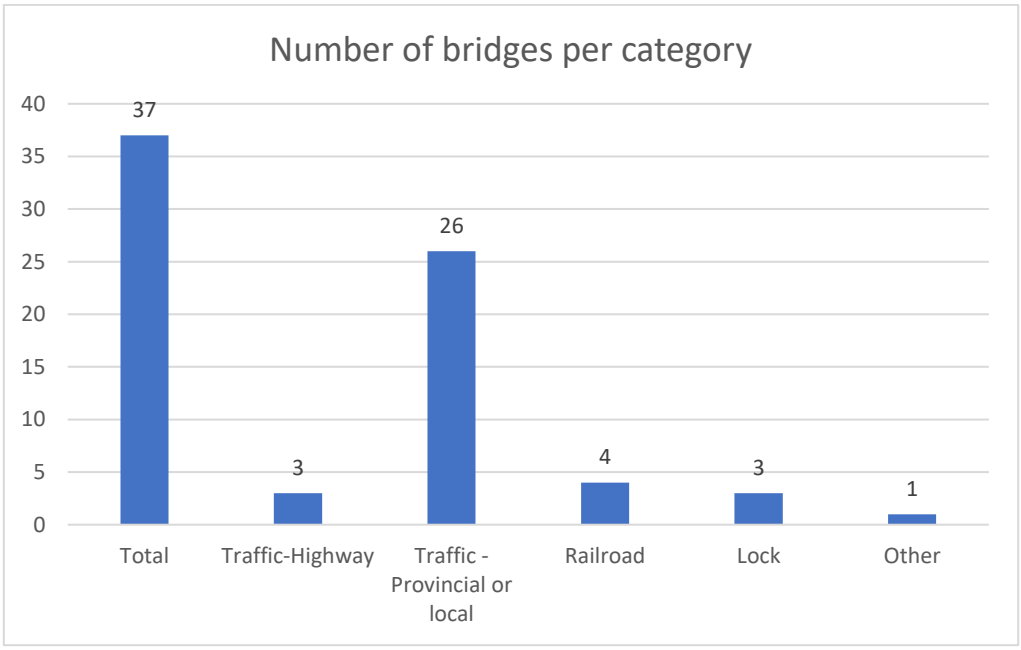


Figure 4 Number of bridges per category

A total of 26 bridges falls within the category ''Traffic – Provincial or local'', these are the bridges that will be included in the remainder of the analysis. The other bridges will be excluded because of the following reasons:

- **Traffic – Highway**: The starting point for the thesis project is the Eefdesebrug, which functioned as a bridge in a provincial road for most of its service life. A typical highway bridge is larger in terms of dimensions and loads compared to a bridge in a provincial road. This can be seen from the images in the inventory of the identified highway bridges. A comparison between the Eefdesebrug and highway bridges is therefore not useful;

- **Railroad bridges**: The characteristics of railroad traffic are different than those of road traffic, this has implications for design. Think of: higher traffic loads on fixed locations (the tracks), high demands for stiffness because of the sensitivity of the tracks to deformations and significant dynamic effects. A successful redesign of a bridge for road traffic therefore does not automatically imply that the same solution can be used for railroad bridges as well. Because of these different characteristics it has been decided to exclude railroad bridges;

- **Bridges part of or near a lock**: Bridges being part of or being near a lock are excluded because these are regarded as part of the lock infrastructure. The geometry of the lock might result in additional boundary conditions that have to be taken into consideration during design, in addition to other requirements to bridge design. Therefore, these bridges have been excluded;

- **Other**: This final category includes only one bridge: the Twekkelerbrug. Designing cable stayed bridges and pedestrian bridges require different points of attention than a traffic bridge using prefabricated girders. Pedestrian bridges are lighter structures with lower loads and a large freedom in design with respect to the structural forms. Another characteristic is the importance of (human induced) vibrations. Moreover, the cable stayed bridge is a completely different structural system compared to an arch or prefab beam bridge. Because of these differences, this bridge is excluded.

2.6.2 Year of construction

By means of categorizing based on the aforementioned categories, the number of bridges is reduced from 37 to 26 bridges for provincial or local traffic. The next distinction that will be made is based on the year of construction. This is done to obtain information on which bridges would be candidates for redesign or replacement in the nearer future. All bridges (1 to 37) are numbered as presented in tables Table 3 and Table 4, and the bridges for provincial and local traffic have been plotted in the following graph. Their number is on the horizontal axis, the year of construction is on the vertical axis.

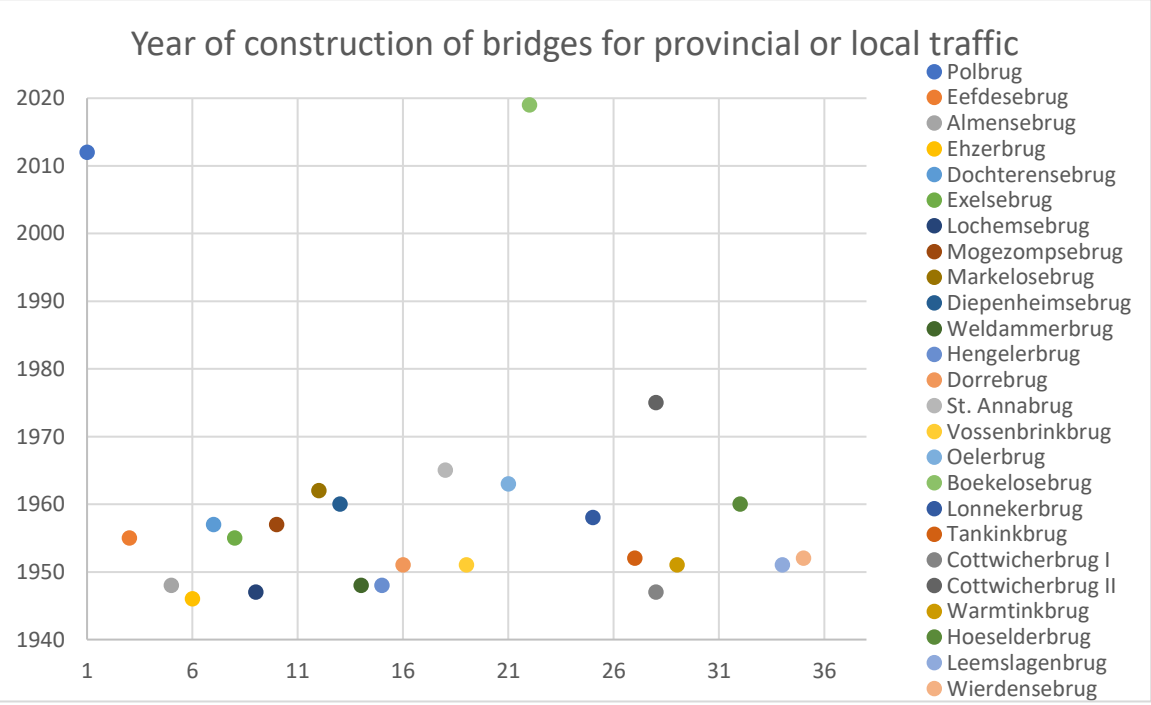


Figure 5 Year of construction of bridges for provincial or local traffic

Some remarks have to be made with respect to the figure:

- The date of construction of the Grensbrug is unknown, as mentioned in the inventory. For this reason, it is not included in the graph. Based on the information obtained via the inventory, it is estimated that the bridge was constructed either before or during the 1950's;

- St. Annabrug: The year of construction of the Sint Annabrug could not be retrieved. However, given the similarities with other bridges such as the Eefdesebrug and Exelsebrug, and the year of construction of these similar bridges, it is estimated that the bridge is constructed either during or before the 1960's. The year of construction is therefore estimated to be 1965 at the latest. This value is included in the graph.

- The Cottwicherbrug is accounted for two times in the graph: the older span (concrete arch bridge) dating from 1947 and the newer span (concrete girder bridge) next to it dates back to 1975. Both spans are represented in the graph and are denoted as bridge number 28;

- According to (Rijkswaterstaat, 2014), the Vredesbrug is constructed in the 60's or 70's, replacing the old bridge of the same name. No more specific information on the year of construction is available and for this reason, the bridge is not represented in the graph.

A total of 24 bridges is represented in the graph. The Grensbrug and Vredesbrug are also to be taken into consideration, bringing the total up to 26. When analysing the result, one can see that a distinction can be made between the bridges constructed before roughly 1970 and after. The bridges of before 1970 are typically the replacements of the original bridges destroyed during the war or the replacements of the temporary bridges constructed after the war. The bridges built after 1970 are of a newer generation and are either parts of new projects (e.g. Polbrug for the new provincial road) or replacements of the pre 1970 generation of bridges.

It is only this first generation of bridges that is deemed to be relevant for the project, as these will be the first candidates for replacement. The post 1970 bridges are therefore no longer taken into consideration. The Polbrug (2012), the second span of the Cottwicherbrug (1975) and Boekelosebrug (2019) can therefore be excluded. The Vredesbrug is also excluded because it is described it was constructed to replace an older bridge of the same name, this suggests it can be included in the second generation. This reduces the number of bridges to be analysed from 26 back to 23, this number still includes the Cotterwicherbrug because of its 1947 span.

2.6.3 Dimensions, traffic loads and substructure

The third step in the analysis is to take dimensions and traffic loads into consideration. The Eefdesebrug is compared to the other bridges using these criteria, to obtain an impression of the number of bridges to which the results could be generalised. Later, the substructure is taken into consideration as well.

- **Dimensions**: Application of the designed solution to structures other than the Eefdesebrug can be justified if the span of the other bridge is equal to or smaller than the span of the Eefdesebrug, under similar loads, thus regarding the Eefdesebrug as an upper limit. Application to larger spans cannot be justified while application to much smaller spans leave room for optimisation.

- **Traffic loads**: Application of the designed solution to structures other than the Eefdesebrug would be most optimal from a load point of view if the load expected on these structures is comparable to the load the new deck of the Eefdesebrug is designed for in terms of dimensions (equal number of lanes) and magnitude and number of vehicles. Application of the redesign to bridges with smaller traffic loads can be justified, although this leaves room for optimisation.

Dimensions

First a distinction is made based on the dimensions. The remaining 23 bridges can be regrouped into two categories: larger bridges for provincial and local traffic and the smaller bridges for local traffic. The inventory already suggests that a practical way of making this distinction is to look at the width of the deck. The following distinction is made:

- **Larger bridges**: Bridges with a deck wide enough for two traffic lanes;

- **Smaller bridges**: Bridges with a deck only wide enough for a single traffic lane.

From the inventory it can be seen that the smaller bridges are all bridges constructed in steel and executed as a girder bridge, truss bridge or smaller arch bridge. The majority of the larger bridges are executed in concrete with the exception of two steel truss bridges. The result is that of the 23 bridges for local traffic 11

can be regarded as smaller bridges and 12 as larger bridges. From these larger bridges 10 are constructed as concrete arch bridge while only 2 are constructed as steel truss bridge, see Figure 6.

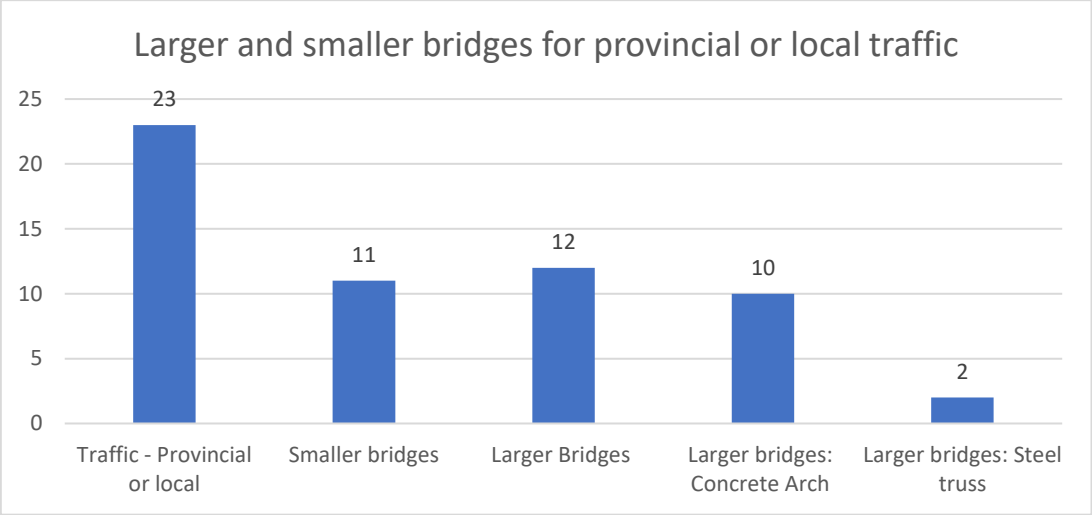


Figure 6 Distinction between one or two traffic lanes

From the inventory the general impression is obtained that these smaller bridges are lighter steel structures and, accordingly, a lighter substructure as well. These bridges are meant for local traffic and agricultural machinery. There where larger traffic loads were expected, a larger bridge was constructed. These larger structures were typically made of concrete, although there are two exceptions.

The Eefdesebrug can be classified as one of the larger bridges. Although it is expected that the engineered solution to the Eefdesebrug can be applied to similar larger bridges, it is not expected that the solution can be applied to the smaller bridges as well. Although a UHPC deck with result in slender and lighter structure compared to an original concrete deck, it is not expected that this same type of UHPC deck will also be lighter than the already very light steel decks of these smaller bridges. It is probable that the substructures of these smaller bridges won't be suitable for decks engineered for application for these larger bridges. Hence the smaller bridges are no longer taken into consideration.

The analysis is continued with the 12 larger bridges, a comparison is made between the spans and widths of the remaining bridges. In the following graphs the number of the bridge is plotted against the span and the width respectively.

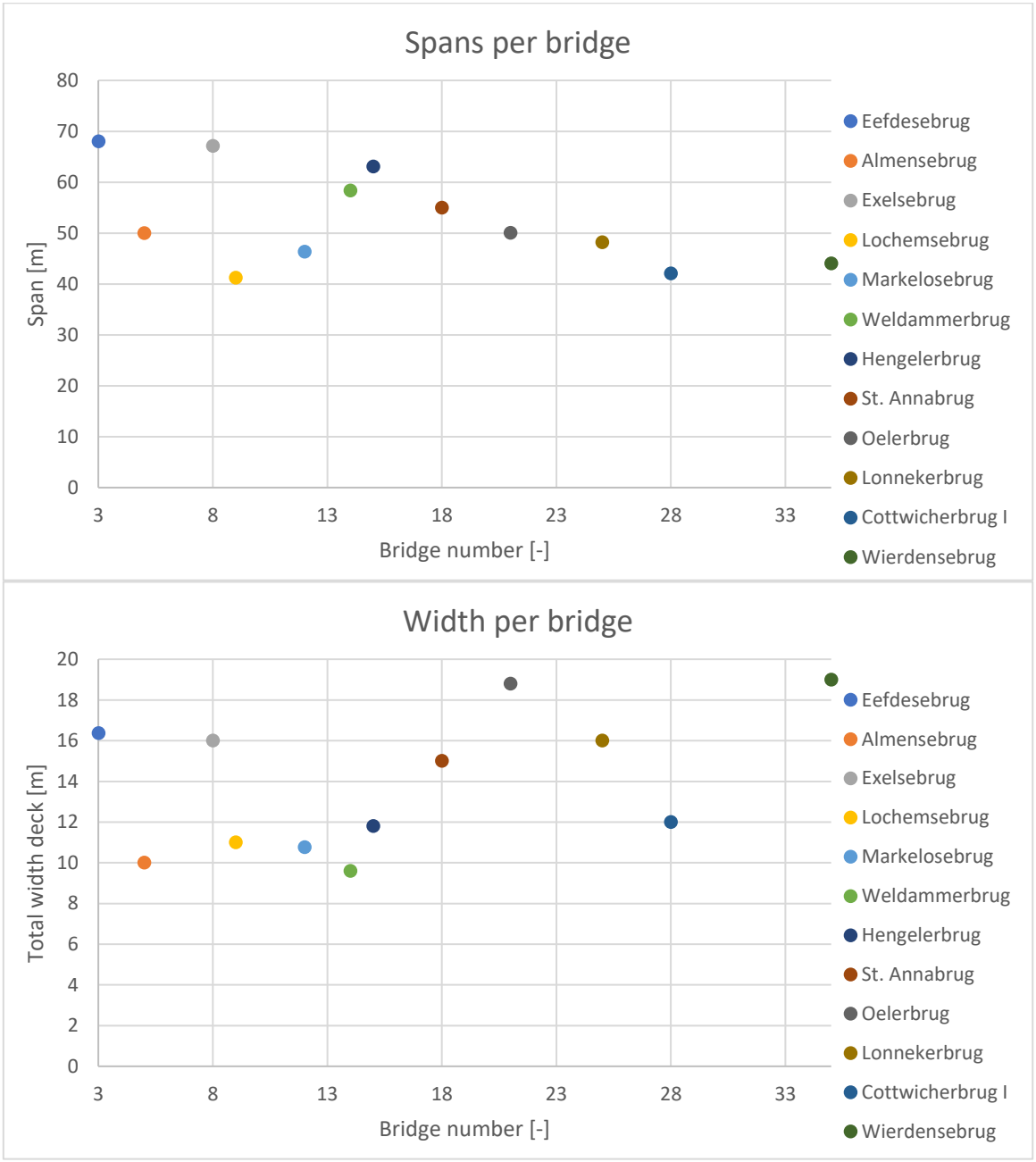


Figure 7 Dimensions of the larger bridges: Span per bridge (upper figure) and width per bridge (lower figure)

Spans of the bridges: When analysing the spans of the bridges, the Eefdesebrug turns out to have the maximum span. This conclusion can be drawn with reasonable certainty: Its span is derived from original design drawings, it is mentioned that the Eefdesebrug at its time the concrete bridge with the longest span (Wegenwiki, 2019) and the spans of bridges that were in the same order of magnitude as the span of the Eefdesebrug were also derived from drawings.

For this reason, it can be stated convincingly enough that the span of the Eefdesebrug can be regarded as an upper limit. If it is possible to design a new deck for the Eefdesebrug (under the same load as the other bridges), then this solution can be applied to other bridges as well, as these spans will be smaller.

Width of the bridges: When it comes to the width of the bridges, one can see that a distinction can be made between two groups of bridges:

- Group 1: The first group is characterised by a width in the range of 10 – 12 metres, characterised by two lanes for traffic and cantilevering parts for pedestrians and cyclists of limited width. These

bridges (Almensebrug, Lochemsebrug, Markelosebrug, Weldammerbrug, Hengelerbrug and Cottwicherbrug) are generally the bridges repaired in the 1940's, often following a similar design to the original 1930's arch bridges.

- Group 2: The second group consists of bridges with a width of about 16 m or wider and are also characterised by two lanes for traffic, but also offer more space for pedestrians and cyclists because of the larger width. These bridges are from the 1950's or 1960's.

The bridges of both groups have in common that they provide room for two traffic lanes. The difference in width is mainly contributed to the room provided to pedestrians and cyclists. Traffic loads are higher than loads for pedestrians. Even though the Eefdesebrug might not be the widest bridge, it is deemed realistic that the designed solution for the Eefdesebrug can be generalised both to bridges with a smaller and a larger width. This is because the two traffic lanes are the common feature of all the remaining bridges. If the beams are suitable for traffic loads, they are definitely suitable for loads due to pedestrians, and depending on the bridge additional beams can be added to obtain the required width. Moreover, the available width will increase because in the new design a concrete arch won't be present.

Note: The aforementioned graphs in Figure 7 are only to be used to obtain an impression of the range of values and not of the exact dimensions. As stated before, a number of values had to be estimated. It can be stated with reasonable certainty that the Eefdesebrug has the largest span. The uncertainty with the width is larger though, especially with respect to the dimensions of the wider bridges from the 50's and 60's, these bridges have a width which is in the same order of magnitude as the Eefdesebrug. However, it is clear that the Eefdesebrug does not have the largest width. It can also be stated with reasonable certainty that the Wierdensebrug is wider, with a width of 19,0 m.

Traffic loads

The distinction based on traffic loads has implicitly already be accounted for by distinguishing smaller bridges and larger bridges for provincial or local traffic. The remaining 12 bridges are presented in the following summarizing table:

Table 5 Larger bridges for provincial or local traffic

Nr.	km	Bridge name	Road	Section from-to	Bridge type	Year
3	2,05	Eefdesebrug	Local road	Zutphen-Eefde	Arch bridge (concrete)	1955
5	7,43	Almensebrug	N826	Zutphen-Laren	Arch bridge (concrete)	1948
8	14,38	Exelsebrug	N346	Zutphen-Hengelo	Arch bridge (concrete)	1955
9	16,23	Lochemsebrug	N346	Zutphen-Hengelo	Truss Bridge	1947
12	23,71	Markelosebrug	N754	Markelo-Stokkum	Truss Bridge	1962
14	29,04	Weldammerbrug	Local traffic	Goor-Diepenheim	Arch bridge (concrete)	1948
15	30,71	Hengelerbrug	N346	Zutphen-Hengelo	Arch bridge (concrete)	1948
18	37,88	St. Annabrug	N740	Delden-Markvelde	Arch bridge (concrete)	1965
21	42,57	Oelerbrug	Local traffic	Hengelo-Haaksbergen	Arch bridge (concrete)	1963
25	48,21	Lonnekerbrug	Local traffic	UT-Havengebied	Arch bridge (concrete)	1958
28	1,46	Cottwicherbrug I	N346	Zutphen-Hengelo	Arch bridge (concrete)	1947
35	13,28	Wierdensebrug	Local traffic	Almelo-Wierden	Arch bridge (concrete)	1950

These bridges are more or less subjected to the same class of traffic: provincial roads or local roads plus agricultural machinery. Designing the Eefdesebrug for traffic corresponding to a provincial road will therefore cover all these bridges and will result in the fact that the results can be projected onto the other bridges with greater confidence as well.

Substructure

Another consideration is the substructure of the bridge. The goal of the project is to design a new deck as such that existing foundations can be used with only limited modification. Only the superstructure is included in the scope of the project. This paragraph is written under the assumption that the substructure therefore won't be included into the project, while at the same time it must be proved that the new deck can be constructed in practice. That means that paying some attention to the substructure cannot be avoided completely.

The redesign of the Eefdesebrug will focus on a prefabricated beam deck. In practice, the standard solution for prefab bridges and viaducts is to construct a capping beam on which bearings are placed, each beam end has its own bearing. Subsequently, the prefab beams are placed on these bearings. That means that a similar sort of solution will have to be sought for in the case of the redesign, and also for the bridges for which a similar solution is to be applied. In the most optimal situation, the beams of the new deck can be placed onto the existing abutments without having to perform modifications other than placing new supports. However, if this is not possible, more modifications will have to be performed and a capping beam has to be constructed first to accommodate the placement of the bearings and prefab beams. The situation varies between the different bridges. The substructure is therefore not a criterion based on which bridges will be included or excluded, but it is mere a point of attention.

Table 6 briefly describes the substructure of the remaining bridges that are being considered, and it illustrates a large variance in design. Although the weight of the capping beam and the prefab deck might not be the problem for these bridges, a practical solution to be able to place it and obtain a stable structure might prove more of a challenge, depending on the design of the bridges. The description is based on the pictures that can be found in the inventory in the preceding paragraphs.

Table 6 Substructure of the relevant bridges

Nr.	km	Bridge name	Description
3	2,05	Eefdesebrug	Reference case – Abutment with buttresses for the supports and a front wall.
5	7,43	Almensebrug	Four pylons, one for each support.
8	14,38	Exelsebrug	Column/wall type structure on which the supports are placed.
9	16,23	Lochemsebrug	Abutment with front wall and extended wing walls for the supports.
12	23,71	Markelosebrug	Abutment with front wall and extended wing walls for the supports.
14	29,04	Weldammerbrug	Pylon type substructure.
15	30,71	Hengelerbrug	Pylon type substructure.
18	37,88	St. Annabrug	Abutment with buttresses for the supports and a front wall.
21	42,57	Oelerbrug	Abutment with buttresses for the supports and a front wall.
25	48,21	Lonnekerbrug	Abutment with buttresses for the supports and a front wall.
28	1,46	Cottwicherbrug I	Pylon type substructure.
35	13,28	Wierdensebrug	Pylon type substructure (four pylons per side).

It is emphasized again that the difference in substructure is not a reason for excluding bridges from the list, but it is a way of describing in a qualitative way to which extent the substructures will have to be modified as such that the engineered solution for the Eefdesebrug can be applied to the other bridges as well. Different substructures that require modifications does not mean that application of the designed solution is impossible but it does mean that it is less optimal. For all cases it is required that supports can be placed for the prefabricated beams. This can be done using a capping beam for example.

The general impression is that the arch bridges following the 1930's design generally have four pylons on which four supports are placed, two under each arch girder. These pylons can be connected using a front wall. The truss bridges (Lochemsebrug and Markelosebrug) have similar substructures, just as the arch bridges from the 1950's (Eefdesebrug, Exelsebrug, St. Annabrug, Oelerbrug and Lonnekerbrug). The Wierdensebrug has a slightly different substructure which consists of four pylons at each side of the deck.

A final remark with respect to the substructure is as follows: From the remaining twelve bridges, ten are constructed in concrete and two in steel. A concrete deck is generally less slender and heavier than an equivalent deck in steel. Replacing a steel deck with a concrete deck might imply that the foundation will not have sufficient capacity for a heavier deck. This could be the case for the two steel truss bridges.
However, based on the inventory, it is concluded that the original bridges at these locations were concrete arch bridges, later replaced by truss bridges still using the original foundation. This suggests that replacing a steel deck by a concrete deck might be still plausible for these two bridges. Therefore, these two bridges are still included into the total of twelve bridges the results could potentially be generalised to.

2.7 Conclusions and remarks

Conclusions based on inventory and analysis

A total number of 37 bridges or bridges as part of a larger piece of infrastructure (e.g. a lock) have been identified. In a number of steps this number has been reduced to a total of 12 bridges for provincial and local traffic. It is expected that there is a large potential to generalise the results of this thesis onto these bridges. This number includes the Eefdesebrug. These remaining 12 bridges have a number of characteristics in common:

- **Bridge category & year of construction**: The remaining bridges are all of the same ''bridge category'', i.e. bridge for provincial or local road, and of roughly the same generation;

- **Dimensions and traffic**: The resulting 12 bridges are among the larger bridges for provincial or local traffic that have been identified. Their cross section generally has two lanes for traffic and remaining area for pedestrians and cyclists. Also, more or less the same traffic loads can be expected;

It is concluded that there is a large potential to generalise the redesign of the Eefdesebrug to these remaining group of 12 bridges because of these comparable characteristics of the bridges. A point of attention is the substructure. The placement of the prefab beams has to be made possible, depending on the exact bridge design this may require more work for certain bridges.

To improve the reliability and the level of confidence with which the results can be generalised, the following aspects should be kept in mind:

- **Dimensions**: The span of the Eefdesebrug can be regarded as the upper limit, it can be stated with confidence that its span is the largest of the remaining twelve bridges. There is a larger level of uncertainty with respect to the width of the twelve bridges, but it is not expected that this will be a problem because of the comparable cross sections (two traffic lanes and remaining area for pedestrians and cyclists);

- **Loads**: Using traffic loads corresponding to provincial roads will improve the reliability of the solution, as this is the maximum traffic load one may expect on the remaining twelve bridges. If a solution can be designed for these loads, this solution will hold for all twelve bridges;

- **Substructure**: A point of attention remains the substructure, it should be proven that it is possible to place the prefab beams onto the existing substructure. It might require more effort for certain bridges to modify the substructure than for others. But given the weight of the existing decks there is a large potential for reusing the existing foundation and (a part of the) substructure.

Remarks

The considerations described in this chapter are all based on the characteristics of the existing bridges. Other aspects such as requirements for design, aesthetics etc. were not taken into consideration.

3

EEFDESEBRUG

3.1 Location and description

The Eefdesebrug is one of the many bridges crossing the Twentekanaal, it is positioned on the road between Zutphen and Eefde. For many years it was part of the main road between Zutphen and Deventer (the provincial road N348). In 2012 the provincial road was diverted and the Polbrug took over this function, but the Eefdesebrug has remained in service for local traffic. Its location is depicted in Figure 8, the alignment of the N238 since 2012 and the location of the Polbrug can be seen as well.

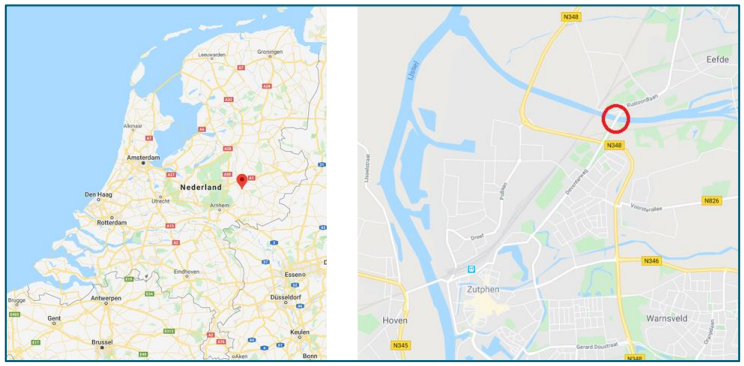


Figure 8 Location Eefdesebrug (After: Google Maps)

The current bridge was constructed in 1955. It is a concrete arch bridge without approach bridges, and two traffic lanes (one for each direction). Recent pictures (made in April 2020) of the current bridge are given below:



Figure 9 Side view of the Eefdesebrug



Figure 10 View of the deck

3.2 History

The current bridge is not the first bridge constructed at this location, the following table provides an overview of the history of the Eefdesebrug, most of the information is taken from (Wegenwiki, 2019) and archive material from Rijkswaterstaat.

Table 7 Summary of the history of the Eefdesebrug

Year	Event
1932	Construction of the first concrete arch bridge at this location as one of a series of new bridges as a part of the construction of the new Twentekanaal.
1945	At the end of the second world war, the first bridge was destroyed.
1946	A temporary bridge (a bailey bridge) was constructed to replace the first bridge.
1955	The temporary bailey bridge is replaced by a new bridge: the current Eefdesebrug.
2019 [45]	In the summer of 2019 maintenance work was carried out which includes (among others): repairing the concrete deck, applying new pavement, maintenance of the steel components such as hangers and the concrete arch.
2020 [46]	Final maintenance work is carried out in April 2020: The joints are replaced and painting work is carried out. It is expected that no major maintenance works will have to be carried out for the next 10 years [46].

The first concrete arch bridge (1932) was of a different design than the current bridge, see the figure below. The Eefdesebrug, Exelsebrug and Lochemsebrug were both of the same design. The Eefdesebrug and Exelsebrug had roughly the same dimensions (both had a span of 67,6 metres), while the Lochemsebrug was smaller (with a span of 47,3 m). The construction of the three bridges was arranged in the same contract (bestek ''no 69''). A drawing of the first bridge is given in Figure 11.

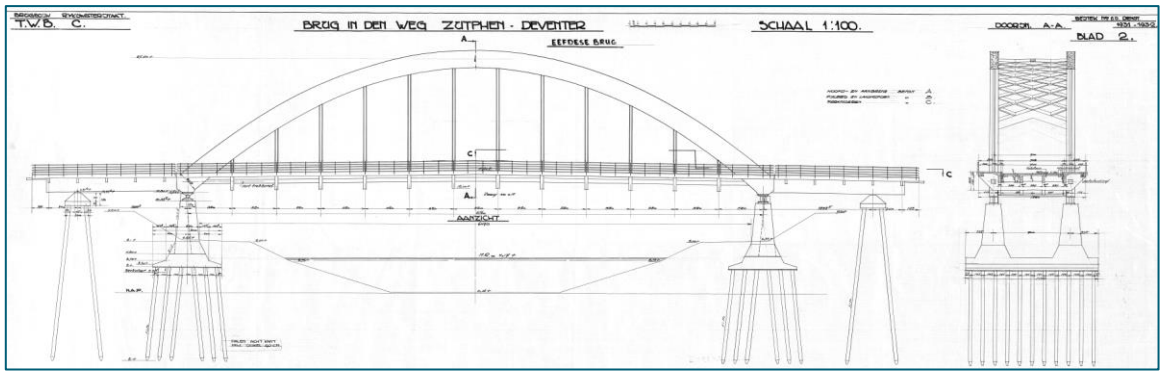


Figure 11 ''First'' Eefdesebrug 1932 - B.2790

The bracing system between the arches with its rhomboidal pattern is very recognizable, it was used for multiple bridges over the Twentekanaal, as could be seen in 2.4 and 2.5.

The bridge was destroyed in 1945. The first reconstruction works took place in 1946, a bailey bridge was constructed as the temporary bridge. It was positioned directly next to the destroyed bridge. In 1955 the ''Second Eefdesebrug'' was constructed at the location of the bailey bridge, this is the bridge that can be seen today.

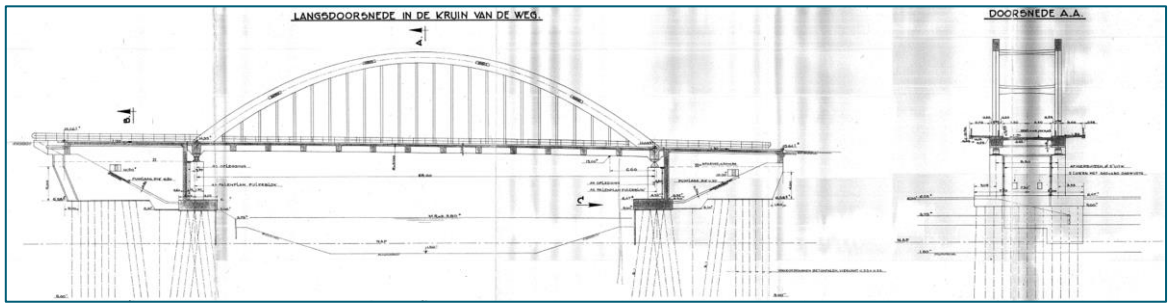


Figure 12 New Eefdesebrug from 1955 - B.5109

Although the second bridge is also an arch bridge, its design is different than the first. Differences are:

- Canal crossed under different angle (new angle slightly larger);
- Span almost the same (67,6 becomes 68,0 m);
- Total width increased (12,5 becomes 16,36 m;
- Dimensions of the arch (height x width: 2,0 x 1,0 at the top becomes 1,6 x 0,9 at the top);
- Different stability system between the arches (rhomboidal pattern replaced by four stability elements);
- Change in design of vertical hangers (2 x 12 encased in concrete) hangers become 2 x 48 steel hangers).

During its service life maintenance and other work has taken place on multiple occasions:

- In 1979 the bridge was equipped with electric installations: the bridge was (along with a number of other bridges across the canal) outfitted with navigation lights.
- In 2019 maintenance work was carried out, it included repairs to the concrete deck, new pavement, maintenance to the steel railing and the steel hangers. Moreover, maintenance took place on the supports and the concrete arch.
- In 2020 the maintenance work was finalized by replacing the joints and painting the bridge. According to Rijkswaterstaat it is expected that no large-scale maintenance work (except for regular maintenance) will have to be carried out to the bridge for the next ten years.

3.3 Bridge design

General description and location

The Eefdesebrug is a tied arch bridge constructed in concrete. It crosses the Twentekanaal north of Zutphen, close to Eefde, as can be seen in the following figure. The northern side of the bridge is at the canal bank at the side of Eefde (and Deventer) and the southern side of the bridge is at the southern canal bank of Zutphen.



Figure 13 Location of the Eefdesebrug (Google Maps)

The bridge consists of the following parts:

- Superstructure consisting of the main span in the form of an arch crossing the canal and two side spans formed by the deck of the abutments;

- Superstructure consisting of box type abutments founded on piles.

To create an overview and for the sake of easy reference for further elaboration on the original design of the Eefdesebrug, the following table is prepared, which gives an overview of the drawings and documents of the bridge from Rijkswaterstaat archives:

Table 8 Provided documents from Rijkswaterstaat archives

General overview	
33F-100.tek-3941	Bouwputten en toegangswegen
B.3806	Herstelling Eefdesebrug 1954-'56 – Blad 1 brief 19-07-1954
B.3807	Herstelling Eefdesebrug 1954-'56 – Bestaande toestand – Blad 2 bij brief 19-07-1954
B.5109	Herstelling Eefdesebrug 1954-'56 – Overzichtstekening met toekomstige kanaalverbreding
Hydraulic structures/canal	
B.3968	Herstelling Eefdesebrug 1954-'56 – Damplanken
B.4026	Herstelling Eefdesebrug 1954-'56 – Remmingwerken
Superstructure: Main span	
B.3622	Herstel Eefdesebrug 1954-'56 – Matentekening hoofdbrug
B.7128	Eefdesebrug Herstelling 1954-'56 – Hoofdliggers rijvloer
B.7125	Eefdesebrug Herstelling 1954-'56 – Rijvloer hoofdbrug
B.7127	Eefdesebrug Herstelling 1954-'56 – Noordelijke aanzetstukken
B.7126	Eefdesebrug Herstelling 1954-'56 – Zuidelijke aanzetstukken
B.7164	Eefdesebrug Herstelling 1954-'56 – Wapening bogen
B.7165	Eefdesebrug Herstelling 1954-'56 – Wapening bogen
B.7166	Eefdesebrug Herstelling 1954-'56 – Windverband

B.7137	Eefdesebrug Herstelling 1954-'56 – Ankerblokken voor trekbandkabels
B.7144	Eefdesebrug Herstelling 1954-'56 – Hangers
Superstructure: Deck of abutments	
B.7212	Eefdesebrug Herstelling 1954-'56 – Rijvloer noordelijk landhoofd
B.7211	Eefdesebrug Herstelling 1954-'56 – Rijvloer zuidelijk landhoofd
Supports	
B.7130	Eefdesebrug Herstelling 1954-'56 – Opleggingen
Substructure: Abutments & foundation	
B.7104	Eefdesebrug Herstelling 1954-'56 – Matentekening landhoofden
B.3625	Herstel Eefdesebrug 1954-'56 – Noordelijk landhoofd wand I
B.7103	Eefdesebrug Herstelling 1954-'56-Noordelijk landhoofd wanden II, III en IV
B.7105	Eefdesebrug Herstelling 1954-'56 – Wanden zuidelijk landhoofd
B.7106	Eefdesebrug Herstelling 1954-'56 – Wanden zuidelijk landhoofd
B.3797	Herstel Eefdesebrug 1954-'56 – Heiplan
B.3623	Herstel Eefdesebrug 1954-'56 – Funderingsblok noordelijk landhoofd
B.3624	Herstel Eefdesebrug 1954-'56 – Funderingsblok zuidelijk landhoofd
Execution: Earthwork, formwork and falsework	
B.7113 TEK 16	Eefdesebrug – Bouwputten en toegangswegen fase 1
B.7113 TEK 56	Eefdesebrug – Bouwputten en toegangswegen fase 1
B.7114 TEK 17	Eefdesebrug – Bouwputten en toegangswegen fase 2
B.7114 TEK 57	Eefdesebrug – Bouwputten en toegangswegen fase 2
B.7100	Eefdesebrug Herstelling 1954-'56 – Bekistingsconstructie
B.7116	Eefdesebrug Herstelling 1954-'56 – Bekistingsconstructie rijvloer
B.7157	Eefdesebrug Herstelling 1954-'56 – Steunconstructies rijvloer hoofdbrug
B.7158	Eefdesebrug Herstelling 1954-'56 – Steunconstructies rijvloer hoofdbrug
B.7167	Eefdesebrug Herstelling 1954-'56 – Steunconstructie bogen
Overig	
B.7107	Eefdesebrug Herstelling 1954-'56 – Steunconstructie fundatieblokken, luiken, afvoerbuizen en roosters
B.7112	Eefdesebrug Herstelling 1954-'56 – Asbest-cementkokers
B.7131	Eefdesebrug Herstelling 1954-'56 – Besteltekening smeedstaal
B.7132	Eefdesebrug Herstelling 1954-'56 – Rijijzers
B.7133	Eefdesebrug Herstelling 1954-'56 – Beëindigingsijzers
B.7140	Eefdesebrug Herstelling 1954-'56 – Hoekbeschermers
B.7143	Eefdesebrug Herstelling 1954-'56 – Leuningen
33F-100.tek-B7303	Waterpassing rijvloer.
Relevant drawings old bridge (1933)	
Bestek	Bestek nr. 69: Drie betonbruggen over Twentekanalen
B.4872	Grondboringen en situatie drie betonbruggen - Bestek nr. 69 blad 1
B.2790	Brug in den weg Zutphen-Deventer (bestek nr. 69 1931-32 blad 2)

Positioning of the bridge

The bridge is built at the location of the temporary Bailey bridge. For the construction of the new Eefdesebrug, another temporary Bailey bridge was constructed just west of the location of the location of the new Eefdesebrug. The Eefdesebrug crosses the canal under an angle of approximately 70° between the axis of the bridge and the canal. According to the original drawings, guiding structures (fenders) were present, positioned middle of the canal at the location of the bridge to guide ships, but in the current situation these are not present anymore.

Superstructure – Main span

The main span is formed by two arch type girders with a tensile tie. The length of the deck (measured from the main girders) is 70,70 m (B.5109 & B.7125), the span between the supports is 68,0 m. The total distance between the front walls of the abutments is 70,86 m (See B.5109 from which this can be derived). Drawing B.7104 gives details on the joints: At the south side, there is an 80 mm gap between the abutment and deck. At the north side, a gap of 80 mm is also present, however, due to a notch on the abutment in the original design drawings, at the top there is a gap of 30 mm left.

Between the main girders a concrete deck is constructed and on both sides of the arches a part is cantilevering out from the main girders, this provides two lanes for pedestrians and cyclists. The arch girders are formed by a main girder of height 1,30 (approximation as the height is variable, see section C-C in B.7125) and width 1,90 and spanning from support to support (B.5109), at the location of the supports the height is increased locally. Above the support the centreline of the arch intersects with the centre line of the main girder. The arches (and supports) are positioned c.t.c. 8,9 m apart in transverse direction. The two arches support one another via four stability elements. These collected values result in a slenderness of the main girder of approximately (because of variation in height of elements):

$$\lambda = \frac{l}{h} = \frac{68{,}0}{1{,}30} \approx 52$$

Following the definition for slenderness as mentioned in the first chapter of the second part of the literature study, the slenderness of the arch bridge is:

$$\lambda_1 = \frac{f}{l} = \frac{14{,}99}{68{,}0} = 0{,}22$$

Where:
f: Total rise of the bridge, i.e.:
Top of the arch at mid span: 27,63 + 0,8 = 28,43 m NAP – See: B.3622
Bottom of deck (lowest point: main girder) at mid span: 13,44 m NAP – See: B.3622
Hence: f = 28,43 – 13,44 = 14,99
l: Span, i.e.: 68,0 m – See: B.B.5109

The concrete arch has a width of 0,9 m (B.5109) and a variable height of 1,6 m at the top to approximately 2,0 metres near the connection with the main girder (B.3622). The arch and the main girder are connected by 24 sets of hangers, each consisting of two steel hangers Ø65 mm, bringing the total of 96 hanger bars for the total bridge. The steel hangers are anchored in the arch and the main girder using anchor plates (see B.3622 and B.7144). The tensile tie is realised by using a number of tensile cables (24 cables for each main girder) that are placed in the main girder (see B.7125, B.7128 and B.7137), the cables are anchored at anchor blocks.

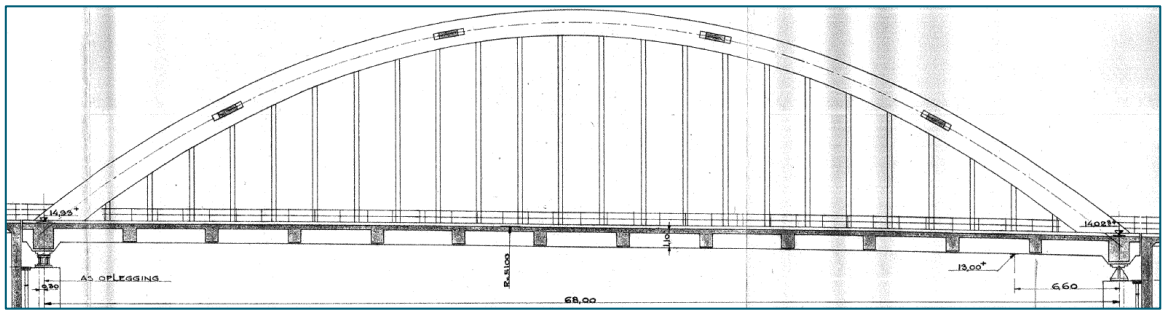


Figure 14 Part of cross section mid of deck – B.5109

The deck between the arch girders is formed by a concrete slab supported by 14 transverse beams between the main girders. The girders at the supports are larger than the girders in between, the girders are positioned 5,2 m centre to centre (and 5,4 at the end supports). The intermediate girders have a width of 0,8 m while the girders near the supports have a width of 1,30 m. The span of the transverse girders (which is equal to the centre-to-centre distance of the arches) is 8,9 m. See B.7125, B.5109 and B.7128.

The slab of the deck is 0,25 m thick and has a slope of 1:70 from the mid span towards the sides where the arches are positioned. Originally, the deck was covered with a 0,05 m thick surfacing layer. The width of the deck area free for traffic, which is the distance between the kerbs formed by the main girders, equals 2 x 3,5 = 7,0 m.

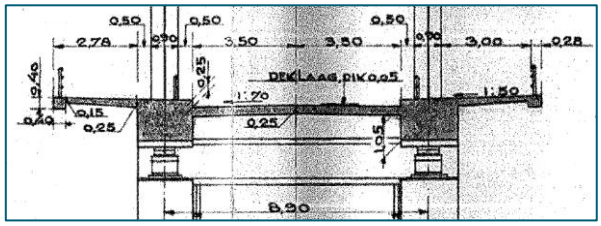


Figure 15 Part of the cross section of the main span – B.5109

The cantilevering parts that from the pedestrian/bicycle lanes extend 2,78 m outward from the edge of the main girders. The total length to the centre of the main girders is 3,73 m. The thickness is 0,25 directly next to the main girder and is reduced gradually to 0,15 m towards the free end. At the free end the cantilevering part is again increased in thickness up to 0,4 m, the railing is positioned at this point. The width of all structural elements brings the total width of the deck up to 16,36 m, see B.5109.

Dimensions: Height

A number of values regarding the height is summarized:

- Lower end of main girders at mid span (is lowest point of deck): 13,44 m + NAP (B.3622);
- Top of arch at mid span: 28,43 m + NAP (B.3622);
- Lower end of support at north side: 11,338 m + NAP (B.3622);
- Top of deck (concrete) at north side: 13,973 m + NAP (B.3622);
- Lower end of support at south side: 12,255 m + NAP (B.3622);
- Top of deck (concrete) at south side: 14,88 m + NAP (B.3806).

Note: According to the drawings, ''top of deck'' means the surface of the concrete, the asphalt layer is not included.

Superstructure – Side spans

The abutments form the connection between the superstructure and embankments, and distribute the forces from the supports to the foundation. In the case of the Eefdesebrug, the decks of the abutments also function as the approaching bridges, both at the north side (Deventer side) and south side (Zutphen side). The following figure shows the plan (from top view) of the deck at the south side. The deck at the north side is of similar design.

The main span has a rectangular plan in top view, both supporting bridges however are not entirely rectangular. At the side of the main span the transverse edge is perpendicular to the axis of the main span and supporting span. At the other side the edge is not perpendicular, but under an angle. Figure 16 gives the op view of the southern abutment. The abutment at the north side has a similar design.

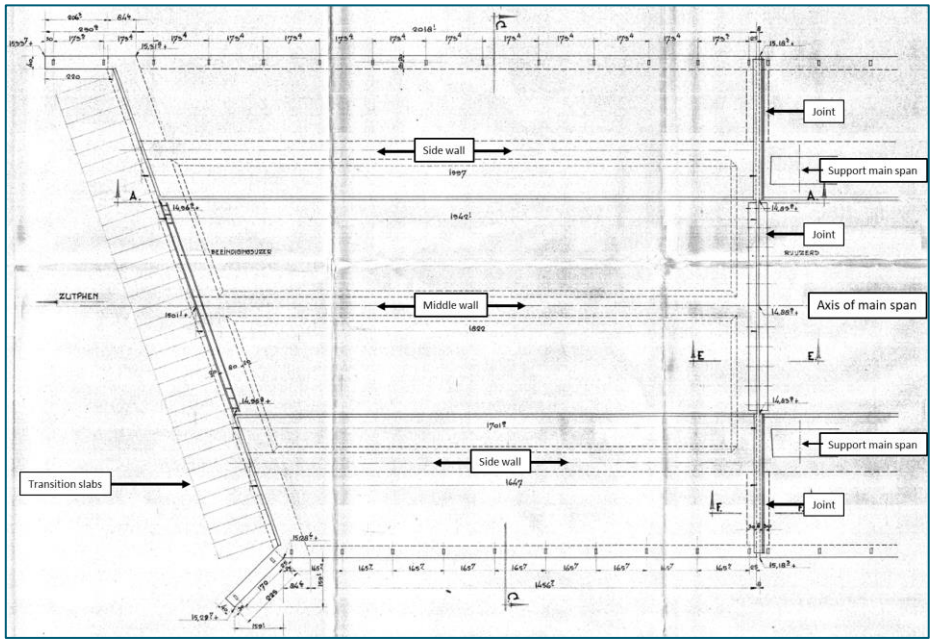


Figure 16 Top view of the deck of the abutment at the south side – Edited, after: B.7104

If a cross section (section C-C in the drawing) is studied, one can see similarities with the cross section of the main span. The profile is practically the same, having a free width of 7,0 m between the curbs, the thickness of the deck being 0,34 m and under the same slope of 1:70. As there is no arch present, the distance from the curb to the edge is 4,68 m. The thickness of the cantilevering part varies from 0,25 at the side walls of the abutment to 0,15 m towards the edge, where the thickness is increased locally. Although this cross section is taken from the abutment at the south side, the abutment of the north side has a similar cross section. The total width of the deck is 16,36 m, just as for the main span.

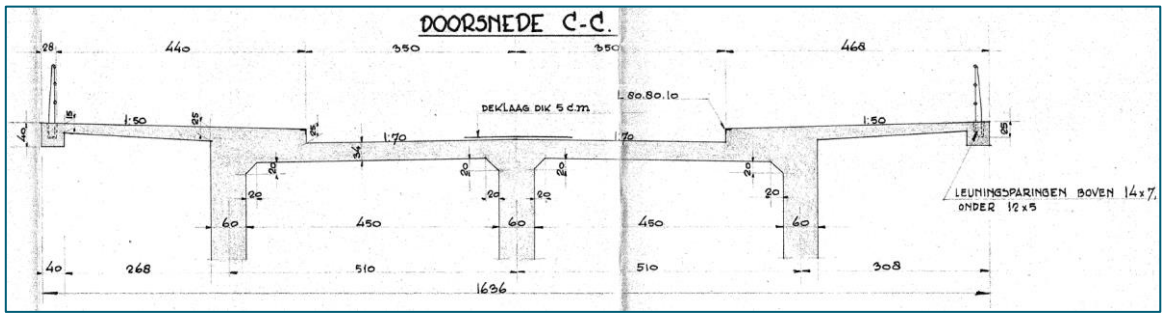


Figure 17 Cross section of approach bridge at the south side – B.7104

Substructure

The main span is supported by a total of four supports, two for each arch girder. The supports are placed at the ends of the main girders, where the main girder is locally increased in height and where the transverse beams are also larger than in the span. The two roller supports are positioned at the southern side of the bridge (Zutphen) while the hinges are positioned below the main girders at the northern side (Deventer).

The supports are depicted in the following figure. The hinged supports are shown at the left picture. The roller supports are shown in the middle and at the right (cross section).

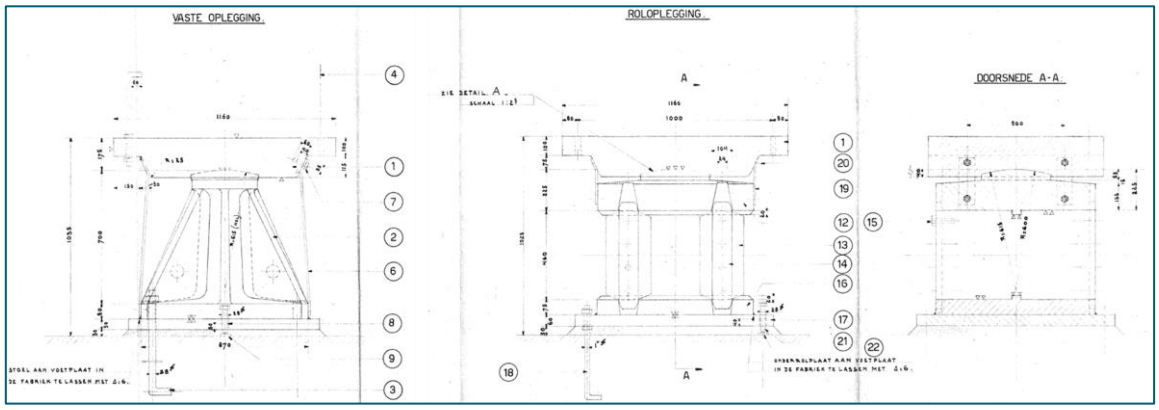


Figure 18 Drawings of the supports - Edited, after: B.7130

The supports are placed at buttresses that are part of the front wall of the abutments. The following picture is a close up of the abutment and support of the northern side of the bridge. One can clearly see the hinges positioned on the buttresses.


Figure 19 Picture of abutment and supports of the north side

The design of both abutments is similar although not all dimensions are exactly the same. One can distinguish the front wall with its distinct buttresses for the supports (dimensions: a width of 1,90 m and a length of 2,43 m - After: B.3625 and B.7105), two wing/side walls and one wall in the middle. The walls are coupled in two ways: a coupling beam about halfway the length and the back wall positioned at the end. The side walls and the wall in the middle are founded on foundation piles (See: B.3806). The approaches slabs are placed on a notch that is part of the back wall. The back wall itself is supported by the walls founded on the subsoil.

Foundation

The front wall and buttresses supporting the supports are founded on a foundation block, which is founded on piles. Both foundation blocks have a width of 15,5 m and a length of 5,75 m. Most of the piles are positioned under these foundation blocks. These piles are 13,6 m long and placed under an angle. The three walls of the abutments that are positioned parallel to the axis of the bridge decks are directly founded on piles (see B.3797). The centre of the supports is placed eccentrically with respect to the centres of the pile groups under the foundation blocks. The eccentricity equals 0,30 m, as can be seen in B.5109.

Subsoil conditions

Drawing B.5109 & B.3807 give the results of two bore holes (''grondboring 1'' and ''grondboring 2'') and two cone penetration tests (''diepsondering 1 and diepsondering 2'') that have been carried out.

'Grondboring 1' and 'diepsondering 1' were carried out at the southern bank of the canal, close to the future location of the southern abutment (Zutphen side):

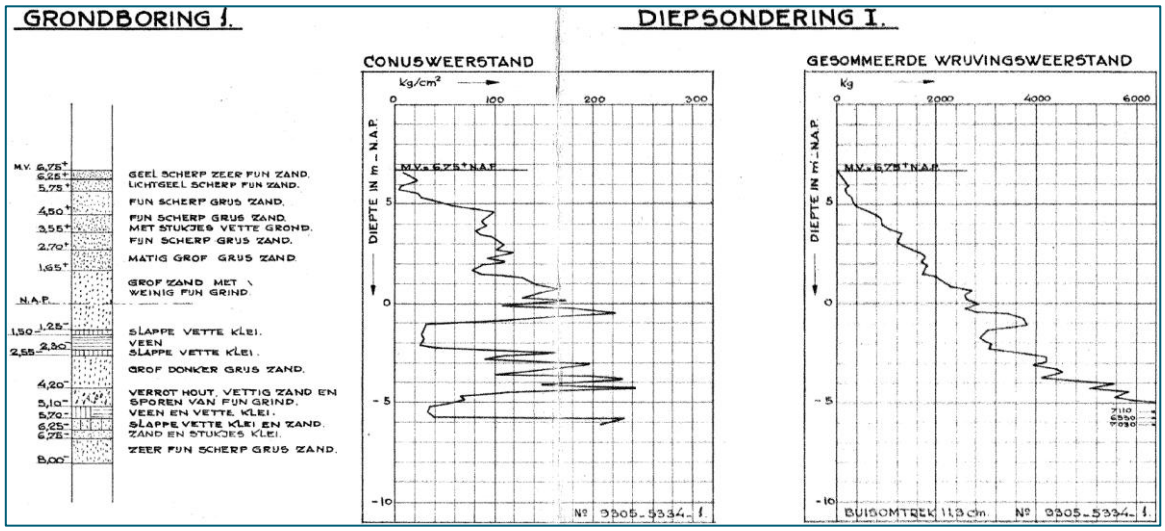


Figure 20 Bore hole and cone penetration test southern bank - B.5109

'Grondboring 2' and 'diepsondering 2' were carried out at the northern bank of the canal (Deventer side) close to the future location of the northern abutment:

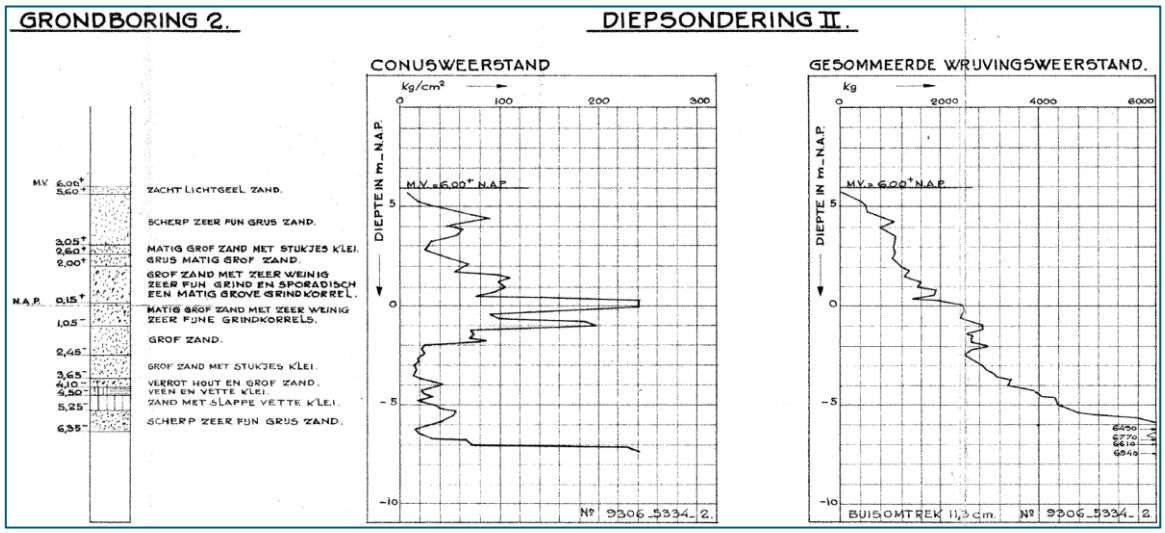


Figure 21 Bore hole and cone penetration test northern bank - B.5109

From drawing B.3797 it can be seen that the dept of the pile tips below the foundation slab of the northern abutment is about 8 m N.A.P. The depth of the pile tips below the foundation slab of the southern abutment shows larger variations and different angles of the piles. The piles of the northern foundation slab are mostly positioned under 8:1.

Original design calculations

On drawing B.3806 it is mentioned that the traffic loads are in accordance with ''Klasse A'' of the ''V.O.S.B.'' (i.e. ''Voorschriften Ontwerp Stalen Bruggen''). No original design calculations have been found in the provided material.

3.4 Summary and key figures

To summarise the most important dimensions of the existing bridge, the following table with key figures has been prepared.

Table 9 Key figures Eefdesebrug

Dimension	Value	Unit	Drawing
Length deck main span	70,70	[m]	B.5109
Span support to support	68,0	[m]	B.5109
Height main girder	1,30	[m]	B.7125
Approximate slenderness girders (λ)	52	[-]	[-]
Slenderness of the arch bridge (λ_1)	0,22	[-]	[-]
Total width main span & abutments	16,36	[m]	B.5109 & B.7104
Width of deck between kerbs	7,0	[m]	B.5109 & B.7104
Width abutment without cantilever*	10,80	[m]	B.7104
''Free height''**	2,3 – 2,8	[m]	[Multiple]**

*This value denotes the width of the abutments without the cantilevering parts of its deck, i.e. that the value is the width between the outer walls.

**This value is introduced in the summary to approximate the height from the bottom of the supports to the upper part of the deck, as an idea of the available room for the redesign. This value is approximated using rounded off values, this is done as follows: Height support (≈ 1,0 m – B.7130) + Height main girder (≈ 1,30 m – B.725) + Extra height girder at support (≈ 0,5 m – B.3622). Note that for the redesign, the drawings have to be consulted because the height of the deck varies over the cross section. The height from the lower side of the support to the top of the deck slab (rolling surface for traffic) is approximately 2,3 m for example. Therefore, the values in the aforementioned table are only suitable for a first indication and not for the final design.

4

SUMMARY AND CONCLUSIONS

Recap of the research questions and goals

In the preface of this report, two goals were introduced that were to be achieved, namely to analyse available information in order to gain insight into the (current state of) the Eefdesebrug and to illustrate the relevance of the project and to generalise the results from the redesign of the Eefdesebrug to other existing structures across the Twentekanaal. Two research questions were introduced related to these goals:

- What are the basic details of the Eefdesebrug with regard to geometry, materials, history, loads, etc.?

- What are the characteristics of the different bridges that cross the Twentekanaal?

Summary and conclusions characteristics bridges Twentekanaal

The first chapter provided general information about the Twentekanaal. The second chapter gave an overview of the different bridges of the Twentekanaal as well as their main characteristics. A total of 37 bridges or bridges as part of a larger piece of infrastructure (e.g. a lock) were identified. An analysis was performed after which it was concluded that the results of the thesis could potentially be generalised to a group of 12 bridges with similar characteristics as the Eefdesebrug. Important for the elaboration of the final steps of this analysis were:

- **Dimensions**: The span of the Eefdesebrug can be regarded as the upper limit, it can be stated with confidence that its span is the largest of the remaining twelve bridges.

- **Loads**: Designing a new bridge using traffic loads corresponding to provincial roads is recommended.

In addition, attention should be paid to the different substructures and more specific on how to place the new deck of prefab beams on the existing substructure. It should be illustrated that this is possible in practice.

The relevance of the project with respect to the other bridges across the Twentekanaal is herewith illustrated.

Summary and conclusions analysis of the Eefdesebrug

In the third chapter of this report the existing Eefdesebrug was studied. A general introduction was given, its history was summarised and the different structural components (superstructure, substructure etc) were explained in more detail. The chapter was finalized with a table that presented a number of key figures of the bridge. A remark was made that no original design calculations were identified. The goal of studying the existing structure is herewith achieved as well.

5

BIBLIOGRAPHY

General sources

Bosch, B., & Van Leeuwen, L. (2014). *De Nieuwe Lochemsebrug.* Afstudeeropdracht, Hogeschool Utrecht. Opgeroepen op 06 07, 2020

Bruggenstichting. (sd). *Bruggen Database*. Opgehaald van Bruggenstichting: https://www.bruggendatabase.nl/

NOS Nieuws. (2013, 07 03). *Bruggen Twentekanaal zijn te zwak*. Opgeroepen op 05 08, 2020, van NOS: https://nos.nl/artikel/525429-bruggen-twentekanaal-zijn-te-zwak.html]

Redactie Transport Online. (2013, 07 03). *Groot aantal bruggen over Twentekanaal kan zwaar vrachtverkeer niet dragen*. Opgeroepen op 06 08, 2020, van Transport Online: https://www.transport-online.nl/site/13701/groot-aantal-bruggen-over-twentekanaal-kan-zwaar-vrachtverkeer-niet-dragen/

Rijkswaterstaat. (2014, oktober). Twentekanaal . *Kijk op de ruimtelijke kwaliteit van kanalen*. (Rijkswaterstaat, Samensteller)

Rijkswaterstaat. (2020). *Vaarwegen in Nederland.* Rijkswaterstaat, CIV. Rijkswaterstaat Centrale Informatievoorziening.

Rijkswaterstaat. (2020, May 28). *Waterdata en waterberichtgeving*. Opgeroepen op May 28, 2020, van Rijkswaterstaat: https://www.rijkswaterstaat.nl/water/waterdata-en-waterberichtgeving

Rijkswaterstaat. (sd). *Twentekanaal*. Opgeroepen op mei 18, 2020, van Rijkswaterstaat: https://www.rijkswaterstaat.nl/water/vaarwegenoverzicht/twentekanalen/index.aspx

Rijkswaterstaat. (sd). *Twentekanalen: verruimen vaarweg*. Opgeroepen op mei 28, 2020, van Rijkswaterstaat: https://www.rijkswaterstaat.nl/water/projectenoverzicht/twentekanalen-verruimen-vaarweg/doelen-en-resultaten.aspx

Wegenwiki. (2019, april 24). *Eefdesebrug*. Opgeroepen op mei 2020, van Wegenwiki: https://www.wegenwiki.nl/Eefdesebrug

Wikipedia. (2013, juni 11). *De Twekkelerbrug over het Twentekanaal*. Opgeroepen op 05 20, 2020, van Wikipedia: https://nl.wikipedia.org/wiki/Lijst_van_bruggen_over_de_Twentekanalen#/media/Bestand:Twekkelerbrug.jpg

Wikipedia. (2020, mei 8). *Lijst van bruggen over de Twentekanalen*. Opgeroepen op 05 19, 2020, van Wikipedia: https://nl.wikipedia.org/wiki/Lijst_van_bruggen_over_de_Twentekanalen

Wikipedia. (2020, mei 7). *Twentekanaal*. Opgeroepen op mei 18, 2020, van Wikipedia: https://nl.wikipedia.org/wiki/Twentekanaal

Bibliography inventory of second chapter

[1] Wikipedia. (2017, juli 15). *Polbrug*. Opgeroepen op 05 19, 2020, van Wikipedia: https://www.wegenwiki.nl/Polbrug

[2] Wikipedia. (2019, juni 11). *Spoorbrug Twentekanaal*. Opgeroepen op 05 19, 2020, van Wikipedia: https://nl.wikipedia.org/wiki/Spoorbrug_Twentekanaal

[3] Wegenwiki. (2019, april 24). *Eefdesebrug*. Opgeroepen op 05 19, 2020, van Wegenwiki: https://www.wegenwiki.nl/Eefdesebrug

[4] Wikipedia. (2020, mei 7). *Sluis Eefde*. Opgeroepen op 05 19, 2020, van Wikipedia: https://nl.wikipedia.org/wiki/Sluis_Eefde

[5] *Almensebrug*. (sd). Opgeroepen op 05 19, 2020, van Brueckenweb.de: https://www.brueckenweb.de/2content/datenbank/bruecken/3brueckenblatt.php?bas=6288

[6] Simons, M. (2018, 10 29). *Lochemse- en Almensebrug weken in onderhoud*. Opgeroepen op 05 19, 2020, van De Stentor: https://www.destentor.nl/achterhoek/lochemse-en-almensebrug-weken-in-onderhoud~a9448b9e/

[7] Koenen, I. (2017, mrt 17). *Jansen Venneboer versterkt bruggen Twentekanaal*. Opgeroepen op 05 19, 2020, van Cobouw: https://www.cobouw.nl/infra/nieuws/2017/03/jansen-venneboer-versterkt-bruggen-twentekanaal-101211658

[8] *Ehzerbrug Almen aan de beurt voor groot onderhoud*. (2018, augustus 15). Opgeroepen op 05 19, 2020, van Lokaal Gelderland.

[9] *Dochterensebrug*. (sd). Opgeroepen op 05 19, 2020, van Brueckenweb.de: https://brueckenweb.de/2content/datenbank/bruecken/3brueckenblatt.php?bas=7040

[10] Bruntink, H. (2018, augustus 30). *Schilderbeurt Exelsebrug blijft voorlopig uit*. Opgeroepen op 05 19, 2020, van Lochems Nieuws: https://www.lochemsnieuws.nl/2018/08/30/schilderbeurt-exelsebrug-blijft-voorlopig-uit/

[11] Exelse brug over Twente-kanaal een stuk verschoven. (1992). *Cement*, 26-29.

[12] *Exelsebrug afgesloten voor groot onderhoud*. (2018, augustus 08). Opgeroepen op 05 19, 2020, van Lokaal Gelderland: https://lokaalgelderland.nl/artikel/6984/exelsebrug-afgesloten-voor-groot-onderhoud

[13] *Lochemsebrug (2)*. (2013, July 7). Opgeroepen op 05 19, 2020, van Wikipedia: https://upload.wikimedia.org/wikipedia/commons/thumb/7/72/Lochemsebrug_%282%29.jpg/727px-Lochemsebrug_%282%29.jpg

[14] *Lochemsebrug*. (2013, juli 7). Opgeroepen op 05 19, 2020, van https://nl.wikipedia.org/wiki/Bestand:Lochemsebrug_(1).jpg

[15] Historisch Genootschap. (sd). *Nieuwe Mogezompsebrug*. Opgeroepen op 05 19, 2020, van Historisch Genootschap: https://hglochem.nl/nl/beeld/nieuwe-mogezompsebrug

[16] Van den Berg, M., & Keukenkamp, S. (2019, 06 04). *Bruggen en sluizen in de regio jarenlang verwaarloosd: 'Sommigen werken nog met een floppy'*. Opgeroepen op 05 19, 2020, van De Stentor: https://www.destentor.nl/apeldoorn/bruggen-en-sluizen-in-regio-jarenlang-verwaarloosd-sommigen-werken-nog-met-een-floppy~a6f1b102/

[17] Freyssinet. (sd). *Trekopleggingen Mogezompsebrug vervangen*. Opgeroepen op 05 19, 2020, van Freyssinet: http://www.freyssinet.nl/freyssinet/wfreyssinet_nl.nsf/sb/over-ons.trekopleggingen-mogezompsebrug-vervangen

[18] *De Hungerbrug of de Grensbrug*. (2017, mei 18). Opgeroepen op 05 19, 2020, van Maarkels Nieuws: https://www.maarkelsnieuws.nl/?p=45483

[19] Schonewille, K. (1978, 1 1). *Twentekanaal Brug ID446495*. Opgehaald van Beeldbank Rijkswaterstaat: https://beeldbank.rws.nl/MediaObject/Details/446495

[20] *Zware vrachtwagens weer over Markelosebrug*. (2018, mei 12). Opgeroepen op 05 19, 2020, van Maarkels nieuws: https://www.maarkelsnieuws.nl/?p=70746

[21] *Markelosebrug komende zomer dicht voor groot onderhoud*. (2017, maart 10). Opgeroepen op 05 19, 2020, van rtv Oost: https://www.rtvoost.nl/nieuws/264629/Markelosebrug-komende-zomer-dicht-voor-groot-onderhoud

[22] *Boogbrug: Exterieur overzicht*. (1985, juli 1). Opgeroepen op 05 19, 2020, van Wikipeida: https://nl.wikipedia.org/wiki/Lijst_van_bruggen_over_de_Twentekanalen#/media/Bestand:Exterieur_overzicht_-_Diepenheim_-_20289522_-_RCE.jpg

[23] Afdeling Multimedia Rijkswaterstaat. (1959, 8 27). *De Weldammerbrug over het Twenthe kanaal nabij Goor ID468742*. Opgeroepen op 05 19, 2020, van Beeldbank Rijkswaterstaat: https://beeldbank.rws.nl/MediaObject/Details/De_Weldammerbrug_over_het_Twenthe_kanaal_nabij_Goor_468742

[24] *Weldammerbrug aantal dagen afgesloten*. (2018, oktober 1). Opgeroepen op 05 19, 2020, van Goors Nieuws: https://www.goorsnieuws.nl/?p=85309

[25] Eissink, J. (2019, July 3). *Hengelerbrug 2*. Opgeroepen op 05 19, 2020, van Wikimedia: https://upload.wikimedia.org/wikipedia/commons/8/82/2019-07-03_Hengelerbrug_2.jpg

[26] Tubantia. (2019, 06 17). *Hengelerbrug Goor in slechte staat: brug langer dicht*. Opgeroepen op 05 19, 2020, van Tubantia: https://www.tubantia.nl/hof-van-twente/hengelerbrug-goor-in-slechte-staat-brug-langer-dicht~a1a8aada/

[27] *Dorrebrug Twentekanaal*. (2013, juli 16). Opgeroepen op 05 20, 2020, van Wikipedia: https://nl.wikipedia.org/wiki/Bestand:2013_07_16_Dorrebrug_Twentekanaal.jpg

[28] Rijkswaterstaat. (2018, april 30). *Dorrebrug en Warmtinkbrug over Twentekanalen in mei 2018 1 week afgesloten*. Opgeroepen op 05 20, 2020, van Rijkswaterstaat: https://www.rijkswaterstaat.nl/nieuws/2018/04/dorrebrug-en-warmtinkbrug-over-twentekanalen-in-mei-2018-1-week-afgesloten.aspx

[29] Wikipedia. (2020, januari 22). *Sluis Delden*. Opgeroepen op 05 20, 2020, van Wikipedia: https://nl.wikipedia.org/wiki/Sluis_Delden

[30] *Update: De geschiedenis van Delden in beeld - Annabrug Delden 1946*. (2015, april 10). Opgeroepen op 05 20, 2020, van Nieuws uit Delden: https://www.nieuwsuitdelden.nl/nieuws/de-geschiedenis-van-delden-in-beeld-annabrug-delden-1946

[31] *Beperkingen zwaar vrachtverkeer Sint Anna brug opgeheven*. (2014, 08 26). Opgeroepen op 05 20, 2020, van Evofenedex: https://www.evofenedex.nl/kennis/actualiteiten/beperkingen-zwaar-vrachtverkeer-sint-anna-brug-opgeheven

[32] *Wikipedia*. (2013, juli 4). Opgeroepen op 05 20, 2020, van https://nl.wikipedia.org/wiki/Bestand:Vossenbrinkbrug2.jpg

[33] Tubantia. (2019, augustus 23). *Werk aan Oelerbrug Hengelo begint week later*. Opgeroepen op 05 20, 2020, van Tubantia: https://www.tubantia.nl/hengelo/werk-aan-oelerbrug-hengelo-begint-week-later~aca8a5aa/

[34] Ankoné, J. (2017, 11 02). *Derde leven voor oude Hengelose brug?* Opgeroepen op 05 20, 2020, van Tubantia: https://www.tubantia.nl/hengelo/derde-leven-voor-oude-hengelose-brug~a7b878e4/

[35] Tubantia. (2019, augustus 23). *Werk aan Oelerbrug Hengelo begint week later*. Opgeroepen op 05 20, 2020, van Tubantia: https://www.tubantia.nl/hengelo/werk-aan-oelerbrug-hengelo-begint-week-later~aca8a5aa/

[36] Smink, G. (2019, mei 31). *Boekelosebrug in Hengelo ondanks forse vertraging eindelijk gebruiksklaar*. Opgeroepen op 05 20, 2020, van Tubantia: https://www.tubantia.nl/hengelo/boekelosebrug-in-hengelo-ondanks-forse-vertraging-eindelijk-gebruiksklaar~a0f00fbd/

[37] *Innovatieve Boekelostebrug Hengelo nu eindelijk geopend voor verkeer*. (2019, mei 31). Opgeroepen op 05 20, 2020, van rtv Oost: https://www.rtvoost.nl/nieuws/313432/Innovatieve-Boekelosebrug-Hengelo-nu-eindelijk-geopend-voor-verkeer

[38] Tubantia. (2019, 07 18). *Lonnekerbrug in Enschede volledig afgesloten voor verkeer*. Opgeroepen op 05 20, 2020, van Tubantia: https://www.tubantia.nl/enschede/lonnekerbrug-in-enschede-volledig-afgesloten-voor-verkeer~af3405d6/

[39] Wikipedia. (2019, november 26). *Spoorbrug bij Wiene*. Opgeroepen op 05 20, 2020, van Wikipedia: https://nl.wikipedia.org/wiki/Spoorbrug_bij_Wiene

[40] Eissink, J. (2019, augustus 5). *Wikipedia*. Opgeroepen op 05 20, 2020, van https://nl.m.wikipedia.org/wiki/Bestand:2019-08-05_Cottwicherbrug_3.jpg

[41] Greisch. (sd). *Polbrug in Zutphen*. Opgeroepen op 05 20, 2020, van Greisch: https://www.greisch.com/nl/projet/polbrug-in-zutphen/

[42] *Fraude bij bouw van Twekkelerbrug*. (2002, feb 7). Opgeroepen op 05 20, 2020, van Cobouw: https://www.cobouw.nl/bouwbreed/nieuws/2002/02/fraude-bij-bouw-van-twekkelerbrug-101135134?_ga=2.116546566.109792361.1590574600-199625789.1590574600

[43] *Wederopbouw in gemeente Lochem*. (2019). Opgeroepen op 05 20, 2020, van Nieuwe tijd Achterhoek: https://nieuwetijdachterhoek.nl/evenementen/omd-lochem/

[44] *Wikipedia*. (2012, juni 2). Opgeroepen op 05 20, 2020, van https://nl.wikipedia.org/wiki/Bestand:Wierdense_brug_(2).jpg

[45] Rijkswaterstaat. (2019). *Onderhoud Eefdesebrug - Doelen en resultaten*. Opgeroepen op 05 22, 2020, van Rijkswaterstaat: https://www.rijkswaterstaat.nl/water/projectenoverzicht/twentekanalen-onderhoud-eefdesebrug/doelen-en-resultaten/index.aspx

[46] Rijkswaterstaat. (2020, maart 30). *Eefdesebrug afgesloten voor gemotoriseerd verkeer; 14-17 april 2020*. Opgeroepen op 05 22, 2020, van Rijkswaterstaat: https://www.rijkswaterstaat.nl/nieuws/2020/03/eefdesebrug-afgesloten-voor-gemotoriseerd-verkeer-14-17-april-2020.aspx

[47] *Hoeselderbrug Twenthekanaal*. (1999, February 13). Opgeroepen op 06 06, 2020, van Flickr: https://www.flickr.com/photos/tomborger23/8501747404

[48] Bouwmeester, A. (2015, april 28). *Hoeselderbrug opgeblazen*. Opgeroepen op 05 20, 2020, van Enters Erfgoed: http://www.enterserfgoed.nl/portfolio_category/2e-wereldoorlog/

[49] Hoogendijk, C. (2009). *De Wierdensche Brug*. Opgeroepen op 06 07, 2020, van Mijn Stad Mijn Dorp: https://mijnstadmijndorp.nl/app/verhalen/de-wierdensche-brug

[50] Sorgdrager, H. (1953). De ''Wierdense Brug'' te Almelo. *Cement*, 167-169. Opgeroepen op 06 07, 2020

[51] Stenvert, R., Kolman, C., Broekhoven, S., Olde Meierink, B., & Tenten, M. (2000). *Monumenten in Nederland. Gelderland*. Zwolle: Waanders Uitgevers. Opgehaald van https://www.dbnl.org/tekst/sten009monu05_01/sten009monu05_01.pdf

Archive material

Throughout this report many references have been made to original design documents and drawings of bridges crossing the Twentekanaal, these have been provided by Rijkswaterstaat

Pictures of Sint Annabrug & Eefdesebrug

Pictures of the Sint Annabrug and frontpage: Courtesy to R. Bril.
All Pictures of the Eefdesebrug (Figure 9, Figure 10 and Figure 19): Own work.

Annex(es)

ANNEX: EXISTING BRIDGES TWENTEKANAAL – SUMMARIZING TABLE

Existing bridges Twentekanaal - Summarizing table

Name: M. Dorland
Date: 07-06-2020
Version: D1.0

	Nr. [-]	km [km]	Bridge name [name]	Number RWS [-]	Road/railroad [-]	Section from-to [from-to]	Bridge type [type]	Span [m]	Width [m]	Lanes [-]	Year [-]	Remarks/sources of span, width, lanes and year [-]
Eefde-Enschede	1	1,05	**Polbrug**	-	N348	Zutphen-Deventer	Arch bridge (steel)	117	>15	2	2012	Span: [1] - Width: [41], exact width unknown - Year: [1]
	2	1,80	**Spoorbrug Twentekanaal**	-	Railroad	-	Arch bridge (steel)	103	[-]	[-]	2005	Span: [2] - Year: [2]
	3	2,05	**Eefdesebrug**	Brug nr. 1	Local road	Zutphen-Eefde	Arch bridge (concrete)	68	16,36	2	1955	See chapter third chapter of report
	4	3,30	**Sluis Eefde**	-	Lock	Lock	Lock	[-]	[-]	[-]	1933	Year: [4]
	5	7,43	**Almensebrug**	brug nr. 2	N826	Zutphen-Laren	Arch bridge (concrete)	50	10	2	1948	Span and width: Estimation - Year: [51]
	6	9,74	**Ehzerbrug**	Brug nr. 3	Local traffic	Almen-Laren	Truss bridge	48,8	5,2	1	1946	Span, width and year: drawing A.9629 and [43]
	7	11,20	**Dochterensebrug**	Brug nr. 4	Local traffic	Laren-Klein Dochteren	Girder bridge (steel)	47	4,86	1	1957	Span: drawing 2444 - Width: drawing A.19042 - Year: drawing 2444
	8	14,38	**Exelsebrug**	Brug nr. 5	N346	Zutphen-Hengelo	Arch bridge (concrete)	67	16	2	1955	Span: drawing A.16667 - Width: Estimation - Year: [11]
	9	16,23	**Lochemsebrug**	Brug nr. 6	N346	Zutphen-Hengelo	Truss Bridge	41,2	11	2	1947	Span and width: drawing A.30122 & (Bosch & Van Leeuwen, 2014) - Year: [14]
	10	19,30	**Mogezompsebrug**	Brug nr. 7	Local traffic	Nettelhorst-Armhoede	Girder bridge (steel)	46,916	4,86	1	1957	Span: drawing 2444 - Width: drawing A.19042 - Year: drawing A.19042
	11	21,01	**Grensbrug**	Brug nr. 8	Local traffic	Markelo-Gelselaar	Girder bridge (steel)	28	5,8	1	[?]	Span and width: Estimation - Year: Unknown, estimation has been made
	12	23,71	**Markelosebrug**	Brug nr. 9	N754	Markelo-Stokkum	Truss Bridge	46,35	10,76	2	1962	Span, width and year: Based on drawing C.10487
	13	25,49	**Diepenheimsebrug**	Brug nr. 10	Local traffic	Markelo-Diepenheim	Arch bridge (steel)	41,047	4,87	1	1960	Span, width and year: Based on drawing A.23320
	14	29,04	**Weldammerbrug**	Brug nr. 11	Local traffic	Goor-Diepenheim	Arch bridge (concrete)	58,355	9,6	2	1948	Span: drawing B.6708 - Width: Estimation - Year: drawing B.6708
	15	30,71	**Hengelerbrug**	Brug nr. 12	N346	Zutphen-Hengelo	Arch bridge (concrete)	63,09	11,8	2	1948	Span: drawing B.6513 - Width: Estimation - Year: drawing B.6513
	16	33,55	**Dorrebrug**	Brug nr. 13	Local traffic	Wiene-Zeldam	Girder bridge (steel)	28,86	4,37	1	1951	Span, width and year: drawing A.12798
	17	36,20	**Sluis Delden**	-	Lock	Lock	Lock	[-]	[-]	[-]	1936	(Rijkswaterstaat, *Kijk op de ruimtelijke kwaliteit van kanalen - Twentekanaal* , 2014)
	18	37,88	**St. Annabrug**	brug nr. 14	N740	Delden-Markvelde	Arch bridge (concrete)	55	15	2	1965	Span, width and year: Estimation
	19	39,35	**Vossenbrinkbrug**	Brug nr. 15	Local traffic	Delden-Beckum	Girder bridge (steel)	28,9	4,37	1	1951	Span, width and year: drawing A.12798
	20	41,67	**Loofrietbrug**	KW 2	A35	Zwolle-Enschede	Girder bridge (concrete)	[-]	[-]	[-]	70's	(Rijkswaterstaat, *Kijk op de ruimtelijke kwaliteit van kanalen - Twentekanaal* , 2014)
	21	42,57	**Oelerbrug**	Brug nr. 16	Local traffic	Hengelo-Haaksbergen	Arch bridge (concrete)	50,06	18,8	2	1963	Span: drawing A.30439 - Width: Estimation - year: drawing A.30439
	22	44,08	**Boekelosebrug**	Brug nr. 17	Local traffic	Industrial area	Truss bridge	[-]	[-]	2	2019	Year: [36]
	23	45,10	**Sluis Hengelo**	-	Lock	Lock	Lock	[-]	[-]	[-]	1936	(Rijkswaterstaat, *Kijk op de ruimtelijke kwaliteit van kanalen - Twentekanaal* , 2014)
	24	46,84	**Twekkelerbrug**	-	Other	Pedestrian bridge	Cable stayed bridge	[-]	[-]	[-]	1999	Year: [42]
	25	48,21	**Lonnekerbrug**	Brug nr. 18	Local traffic	UT-Havengebied	Arch bridge (concrete)	48,2	16	2	1958	Span: drawing A.21630 - Width: Estimation - Year: drawing A.21630
Delden-Almelo	26	0,35	**Spoorbrug Wiene**	-	Railroad	-	Arch bridge (steel)	[-]	[-]	[-]	[-]	Year: [39]
	27	0,76	**Tankinkbrug**	Brug nr. 19	Local traffic	Local traffic	Arch bridge (steel)	41	4,37	1	1952	Span, width and year: drawing A.14659
	28	1,46	**Cottwicherbrug I**	Brug nr. 20	N346	Zutphen-Hengelo	Arch bridge (concrete)	42,035	12	2	1947	Span: drawing A.10674 - Width: Estimation - Year: drawing A.10674
	28	''	**Cottwicherbrug II**	''	Local traffic	Local traffic	Girder bridge (concrete)	42	10	2	1975	Span and width: Estimation - Year: Database Bruggenstichting
	29	3,93	**Warmtinkbrug**	Brug nr. 21	Local traffic	Delden-Enter	Arch bridge (steel)	42	4,37	1	1951	Span, width and year: drawing A.13807
	30	6,07	**Linschotbrug**	KW 29	A1	Amsterdam-Hengelo	Girder bridge (concrete)	[-]	[-]	[-]	1973	Year: (Rijkswaterstaat, *Kijk op de ruimtelijke kwaliteit van kanalen - Twentekanaal* , 2014) & Database Bruggenstichting
	31	7,94	**Vredesbrug**	-	Local traffic	Bornerbroek-Enter	Girder bridge (concrete)	[-]	[-]	[-]	60's-70's	Year: (Rijkswaterstaat, 2014)
	32	9,54	**Hoeselderbrug**	Brug nr. 23	Local traffic	Almelo-Enter	Arch bridge (steel)	41,047	4,37	1	1960	Span, width and year: drawing A.23356
	33	10,00	**Brug in A35**	-	A35	Zwolle-Enschede	Girder bridge (concrete)	[-]	[-]	[-]	70's	Year: (Rijkswaterstaat, *Kijk op de ruimtelijke kwaliteit van kanalen - Twentekanaal* , 2014)
	34	10,83	**Leemslagenbrug**	Brug nr. 24	Local traffic	Almelo-Ypelo	Arch bridge (steel)	42	4,37	1	1951	Span, width and year: drawing A.12831
	35	13,28	**Wierdensebrug**	Brug nr. 25	Local traffic	Almelo-Wierden	Arch bridge (concrete)	44	19	2	1952	Span and width: [50] - Year: [49]
	36	14,11	**Spoorbrug****	-	Railroad	-	Arch bridge (steel)	[-]	[-]	[-]	[-]	[-]
	37	15,33	**Spoorbrug****	-	Railroad	-	Arch bridge (steel)	[-]	[-]	[-]	[-]	[-]

V

PRELIMINARY DESIGN



Preliminary Design

Redesign of bridges Twentekanaal in Ultra-High Performance Concrete

MSc Thesis

12 August 2020

Company	Witteveen+Bos
MSc thesis project	Redesign of bridges Twentekanaal in Ultra-High Performance Concrete
Document	Preliminary Design
Status	Final version
Version	D1.0
Date	12 August 2020

Author	ing. M. Dorland
Student id	4719980
Degree programme	MSc Civil Engineering
Track	Structural Engineering – Concrete Structures

Company Supervisors	ing. T. Petersen RC ir. A. ten Voorde
Supervisors TU Delft	Dr. ir. Y. Yang Dr. ir. M.A.N. Hendriks Dr. ir. S. Grünewald

TABLE OF CONTENT

PREFACE 1

1 GOAL & SCOPE OF PRELIMINARY DESIGN 3

1.1 Goal of preliminary design 3

1.2 Scope preliminary design 3

2 FRAMEWORK OF THE DESIGN STAGE 5

2.1 Assumptions 5

2.2 Boundary conditions and requirements 5

3 CODES & GUIDELINES 7

3.1 General codes and guidelines 7

3.2 UHPC guidelines 8

3.2.1 Recap of identified codes and considerations 8

3.2.2 Selecting appropriate guideline 8

4 AFGC-SETRA 2013 – REVIEW PART 1 10

4.1 Introduction 10

4.1.1 Introduction to the AFGC-SETRA 2013 guideline 10

4.2 Characterisation of UHPC at different stages of a project 11

4.2.1 General 11

4.2.2 Overall design approach 11

4.2.3 Compressive strength 13

4.2.4 Tensile strength 13

4.2.5 Static modulus of elasticity 17

4.2.6 Poisson's ratio 17

4.2.7 Coefficient of thermal expansion 18

4.2.8 Effect of heat treatment 18

4.2.9 Shrinkage and creep 18

4.2.10 Impact strength 19

4.2.11 Design, batching, and placement of UHPC 19

4.2.12 Tests 20

4.3 Bibliography chapter four 20

5 AFGC-SETRA 2013 – REVIEW PART 2 21

5.1 General provisions 21

5.2 Material constitutive law for design (AFGC guideline) 23

5.2.1 Constitutive law for concrete in compression 23
5.2.2 Constitutive laws for concrete in tension 25

5.3 Provisions Eurocode 2 on material properties 30

5.3.1 Partial material factors 30
5.3.2 Concrete 30
5.3.3 Reinforcing steel 34
5.3.4 Prestressing steel 37

5.4 ULS verifications – Bending 40

5.4.1 Provisions from the AFGC guideline 40
5.4.2 Calculation procedures bending moment capacity 41

5.5 ULS verifications – Shear 50

5.5.1 Provisions from the AFGC guideline 50
5.5.2 Calculation procedures shear capacity 53

5.6 Provisions Eurocode 2 on ULS verifications 56

5.6.1 Calculation procedures bending moment capacity Eurocode 2 56
5.6.2 Calculation procedures shear capacity Eurocode 2 56

5.7 Bibliography chapter five 59

6 PRELIMINARY DESIGN: DIMENSIONING AND LOADS 61

6.1 Dimensioning 61

6.1.1 Main dimensions 61
6.1.2 Dimensions of the cross-section 61

6.2 Description of the deck geometry and layout 63

6.3 Determining cross-sectional properties 64

6.4 Loads and load combinations 65

6.4.1 Identifying different loads 65
6.4.2 Permanent loads 66
6.4.3 Variable loads 66
6.4.4 Load combinations 68

6.5 Modelling and governing beam 71

6.5.1 Principle of the model 71
6.5.2 Transverse direction 71
6.5.3 Longitudinal direction 74
6.5.4 Determining internal forces 75

6.6 Performing the calculations 76

6.7 Bibliography chapter six 77

7 PRELIMINARY DESIGN: DESIGN VERIFICATIONS 78

7.1 Approach and parameters 78
7.2 Design of prestressing 80
7.3 Verifications 83
7.3.1 ULS verifications - Bending moment capacity 83
7.3.2 ULS verifications - Shear force capacity 84
7.3.3 SLS verifications – Deflection 84
7.4 Summary & Conclusions 85
7.5 Bibliography chapter seven 86

8 WEIGHT COMPARISON 87

8.1 Weight comparison 87
8.1.1 Goal of the comparison 87
8.1.2 Approach 87
8.1.3 Elaboration of the comparison and results 88
8.1.4 Conclusions 89
8.2 Bibliography chapter eight 89

9 SENSITIVITY ANALYSIS 90

9.1 Goal of sensitivity analysis 90
9.2 Approach 90
9.2.1 RFEM model 90
9.2.2 Material and stiffness parameters 91
9.2.3 Comparison and expected results 92
9.3 Analysis of results, interpretation and conclusions 93
9.3.1 Overview of results 93
9.3.2 Interpretation of results 93
9.3.3 Validation of the model 94
9.3.4 Conclusion 95
9.4 Bibliography chapter nine 96

10 CONCLUSIONS AND PROSPECTS 97

Final page 98

Annex(es) Number of pages

I Drawing cross-section preliminary design 1
II Preliminary design calculations 6
III Derivations concrete compressive zone over variable width 3
IV Drawings preliminary design 1

V	Drawing existing bridge	1
VI	Weight comparison	1
VII	Input RFEM model	3
VIII	Calculations sensitivity analysis	1

PREFACE

This report is titled 'preliminary design' and it contains different parts of the thesis project, namely the parts denoted as 'codes' and 'coarse/global model'. The goal of all the work in this report is to finalize the preparatory work for design (by formulating boundary conditions & requirements, collecting relevant codes & guidelines and selecting which UHPC specific code/guideline will be used), to set up a preliminary design (to become familiar with designing in UHPC and getting an impression of required dimensions for the bridge), to set up a weight comparison using the preliminary design (to investigate whether reaching the project goal is feasible) and to identify possibilities for later design and optimization stages.

In relation to the work plan, achieving all these different goals means that an answer can be formulated to the following research questions:

- What are the current Dutch codes and standards the redesign has to comply with?
- What additional (foreign) codes and standards are to be considered to compensate for lack of information in current Dutch codes and standards?
- What are the main concepts of force distribution in a prefab beam bridge deck and the required dimensions?
- In which ways can one model a prefab beam bridge and which is the most appropriate way for this stage of the project?
- What are the required assumptions that have to be made in order to model the bridge and what are the consequences/implications of these assumptions?

The content of this report in relation to the total thesis project is given in the following figure:

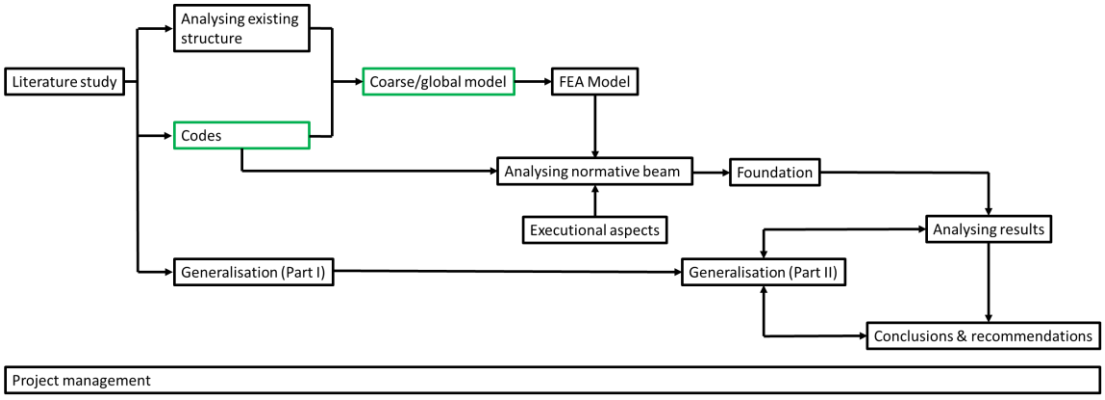


Figure 1 Preliminary design report in relation to the project

Reading guide

This report consists of the following chapters:

- Chapter 1: The first chapter covers the goal and the scope of the preliminary design as presented in this report;
- Chapter 2: The second chapter covers assumptions and boundary conditions & requirements imposed upon the design. These hold for the total project and not just for the preliminary design;
- Chapter 3: The third chapter comprises an overview of all relevant codes and guidelines that have been collected for the design stages of the thesis project, as well as the selection of the UHPC specific guideline that will be used in the further elaboration of this project;
- Chapter 4: The fourth chapter comprises a review of the contents of the first part of the selected UHPC guideline;

- Chapter 5: The fifth chapter covers parts of the selected UHPC guideline that are relevant for the design. Other codes (Eurocode 2) and literature is also used to add additional information wherever required, and to formulate calculation procedures that can be used in design;

- Chapter 6: The sixth chapter is the start of the preliminary design and covers both the dimensioning of the new bridge as well as the calculation of the loads that will be considered in the preliminary design. A simple model is proposed that will be used for the preliminary design to determine the internal forces;

- Chapter 7: The seventh chapter covers the preliminary design verifications, using the loads determined from chapter 6 and the calculation procedures from chapter 5 as input;

- Chapter 8: The eight chapter comprises a brief comparison of the weight of the existing bridge and the preliminary design, to determine if it is realistic to achieve the project goals;

- Chapter 9: The ninth chapter comprises a more in-depth analysis of the force distribution in the bridge by exploring limitations of the model proposed in chapter 6;

- Chapter 10: The tenth and final chapter summarizes the results of the previous chapters and gives prospects and an overview of possibilities for the later design and optimization stages.

1

GOAL & SCOPE OF PRELIMINARY DESIGN

1.1 Goal of preliminary design

In this chapter two topics are discussed, namely the goal and the scope of the preliminary design. From the perspective obtained by defining these, the necessary information will be collected and the preliminary design will be elaborated on in the subsequent chapters. The goals to be achieved in this report are as follows:

- *Collecting all missing relevant information for designing, such as the appropriate design codes and guidelines and calculation procedures;*
- *Defining the requirements for the preliminary design and refined design in later project stage;*
- *Understanding the force distribution in the prefab UHPC beam deck;*
- *By performing the first design verifications, obtaining an idea of the required dimensions for the prefab UHPC beams.*

In addition, an analysis is made of the weight of the new preliminary design versus the existing bridge to verify the feasibility of the project goal and suggestions for further refinement and optimisation of the design in later stages are collected. This way, a basis is formed for the more refined modelling and analysis in later project phases.

1.2 Scope preliminary design

The following points discuss what is and what is not taken into consideration in the elaboration of the preliminary design. Aspects that are not considered are often dealt with by making assumptions, these are also included in the following considerations. Other assumptions will be made during the elaboration of the preliminary design if required, these will be clearly mentioned.

Included verifications

- *The following validations are included in the preliminary design: Bending moment capacity, shear capacity and deflections of the beams. In addition, the boundary conditions and requirements formulated in this report have to be met.*

These aforementioned verifications are the most elementary verifications, verifying these will contribute the most to obtaining an idea of the required dimensions for the structure, as a basis for the next design phases. Other verifications and effects such as the fatigue capacity under cyclic loading, ship collision or imposed deformations due to temperature are not be considered at this design stage.

Different beams

- *Only one beam type will be considered in the preliminary design. No optimizations are carried out in this design stage.*

The goal of the preliminary design is to understand the force distribution in the deck and to obtain an idea of the required dimensions. These goals do not require optimizations. Therefore, it is assumed that the

whole deck consists of a number of identical beams. The most unfavourable situation will be determined, after which the heaviest loaded beam will be designed. Optimizations that result in saving material (e.g. smaller beams below pedestrian lanes) or aesthetics (e.g. edge beams) are not considered in this phase.

Optimizing dimensions

- *No optimization of dimensions of the cross section are taken into consideration in the preliminary design.*

Because the cross section is altered only to obtain an indication of the required dimensions, complicating factors such as chamfers for reducing the amount of material required or for the formwork are not included in this design stage. The cross sections will be constructed of simple forms, such as rectangles.

Considered loads and situations

- *For the preliminary design, only the final situation (with the exception of the design of the prestressing) is taken into consideration when performing the design verifications. For the loads only the permanent loads and vertical traffic loads are taken into consideration.*

For the preliminary design stage, only the most predominant loads and situations are considered, because the goal is to obtain a first indication of the required dimensions. This preliminary design will be the basis for the next design phase, in which all relevant loads will be included.

2

FRAMEWORK OF THE DESIGN STAGE

2.1 Assumptions

A number of assumptions have been formulated that hold for all design work of the project, these have been made to simplify calculations or to rule out aspects that are of lesser importance for the design work.

Horizontal levelling of the deck

- *For designing the differences in vertical height of the abutments, causing the deck surface not to be horizontal, are not considered.*

From the analysis of the existing bridge, it is known that the bridge deck is not levelled horizontally, because the abutment at the south side is higher than the abutment at the north side. This is not taken into consideration; it is assumed the deck is flat in the horizontal plane.

Span and width of the deck

- *For the design, the prefab UHPC beams are assumed to be of the same span as the existing bridge, namely: 68,0 m. In the new situation the width has to be the same as in the existing situation.*

For the design calculations, the span and total width are assumed to be of the same value as that of the existing bridge.

Minimum clearance

- *Minimum clearance is assumed to be guaranteed by placing the new deck as such that the lower side of the deck in the new situation is at the same height as that in the existing situation.*

By the aforementioned assumption the clearance is guaranteed. Limiting the height of the beam is not a project goal by itself, but the goal is to optimize the deck throughout the design stage.

2.2 Boundary conditions and requirements

From the start of the project, a number of requirements and boundary conditions have been formulated. These are originating from the work plan, derived from the results of the generalisation study (see report ''existing bridges Twentekanaal''), etc. For the sake of completeness, these conditions and requirements are formulated in this section. Note that these hold for all the phases in the project. Mentioning these conditions and requirements here does not mean that these will be elaborated on in this report already.

Analysing substructure and superstructure

- *The focus of the redesign is on the deck and the substructure should only be considered if this is required to show that the prefab beam deck can be constructed, i.e. include solution such as capping beam for placement of the prefab beams.*

Conforming the work plan the focus of the design is on the superstructure. However, it should be proven that the new deck can actually be constructed in practice, thus paying attention to the substructure cannot

be avoided completely. Modifications to the abutment are allowed only as such that these demonstrate that the construction of the prefab beam deck is possible in practice. If there is more time at the end of the project, the scope can be widened in later stages.

Layout of the bridge deck and positioning of the loads

- *Conditions imposed on the layout of the deck and load positioning consist of two parts:*
    - *For the redesign, the existing layout of the bridge deck (traffic lanes and lanes for cyclists) will be retained;*
    - *The traffic lanes and lanes for pedestrians/cyclists are separated by a sufficiently high kerb, as such that the traffic loads only have to be positioned between these kerbs.*

There are two reasons that justify this condition. The first reason has to do with the existing road. The new bridge will be part of an existing road, a sudden change in road alignment is deemed to be unwanted and potentially dangerous for traffic. Therefore, the existing layout is retained.

The second reason is related to ''future-proof'' designs. In codes the positioning of traffic loads is often based on the idea that in the distant future the layout of the traffic lanes might be changed, in which case the structure still has to function. However, given that the Eefdesebrug has been functioning as a link in an existing road for decades, it is deemed to be justified to apply the 'real' traffic situation. Positioning the traffic loads between the curbs is therefore deemed to be sufficient whilst complying to the ''future-proof'' design concept is unnecessarily conservative.

Number of vehicles

- *For the redesign traffic loads corresponding to traffic on provincial roads should be applied, this has implications for the number of vehicles that are to be accounted for (fatigue).*

Conforming to the findings from the report 'Existing bridges Twentekanaal', the new deck should be designed for traffic corresponding to provincial roads. This affects the number of vehicles for the fatigue analysis.

3

CODES & GUIDELINES

3.1 General codes and guidelines

Where the literature study stopped by only mentioning and briefly describing different (UHPC related) codes and guidelines, this chapter lists the codes and guidelines that will be actually considered during the remainder of the project. This chapter lists both the general codes and guidelines as well as the selection of the most appropriate UHPC specific guideline.

Note that the considerations made and the codes and guidelines selected in this chapter hold for the total project. Not all codes & guidelines mentioned in this chapter will be considered for the preliminary design already. Codes & guidelines that are not taken into consideration yet will be accounted for in later design stages.

The following general codes and guidelines relevant for the design of concrete bridges have been identified:

Table 1 Codes and guidelines

Eurocode – Basis of structural design (EC0)	
NEN-EN 1990+A1+A1/C2	Eurocode: Grondslagen voor het constructief ontwerp
Eurocode – Actions on structures (EC1)	
NEN-EN 1991-1-1+C1+C11	Eurocode 1: Belastingen op constructies – Deel 1-1: Algemene belastingen – Volumieke gewichten, eigen gewicht en gebruiksbelastingen voor gebouwen
NEN-EN 1991-1-3+C1+A1	Eurocode 1: Belastingen op constructies – Deel 1-3: Algemene belastingen – Sneeuwbelasting
NEN-EN 1991-1-4+A1+C2	Eurocode 1: Belastingen op constructies - Deel 1-4: Algemene belastingen – Windbelasting
NEN-EN 1991-1-5+C1	Eurocode 1: Belastingen op constructies - Deel 1-5: Algemene belastingen – Thermische belasting
NEN-EN 1991-1-6 (en)	Eurocode 1: Belastingen op constructies – Deel 1-6: Algemene belastingen - Belastingen tijdens uitvoering
NEN-EN 1991-1-7+C1+A1	Eurocode 1: Belastingen op constructies - Deel 1-7: Algemene belastingen – Buitengewone belastingen: stootbelastingen en ontploffingen
NEN-EN 1991-2+C1	Eurocode 1: Belastingen op constructies – Deel 2: Verkeersbelasting op bruggen
Eurocode – Design of concrete structures	
NEN-EN 1992-1-1+C2	Eurocode 2: Ontwerp en berekening van betonconstructies - Deel 1-1: Algemene regels en regels voor gebouwen
NEN-EN 1992-2+C1	Eurocode 2: Ontwerp en berekening van betonconstructies - Betonnen bruggen – Regels voor ontwerp, berekening en detaillering
All national annexes to the codes listed in the table are also included, although not mentioned here.	

Additional codes and guidelines have been identified as well. The Eefdesebrug, being a structure from Rijkswaterstaat, means that the following guidelines are also of relevance:

Table 2 Guidelines Rijkswaterstaat

Rijkswaterstaat	
RTD 1001:2017	Richtlijnen Ontwerp Kunstwerken ROK 1.4 (Including annexes A and B)
RTD 1006:2013	Richtlijnen Beoordeling Kunstwerken RBK 1.1

3.2 UHPC guidelines

3.2.1 Recap of identified codes and considerations

In the first part of the literature study (See: Literature study part I – Chapter 3) available guidelines on UHPC were identified. A summarizing table with the UHPC specific guidelines is given below:

Table 3 Codes & Guidelines UHPC

Year	**Country**	**Description**
2000	Australia	Design Guidelines for Ductal Prestressed Concrete Beams
2002	France	Ultra-High Performance Fibre-Reinforced Concretes - Interim Recommendations
2006	Japan	JSCE Guidelines for Concrete No. 9 – Recommendations for Design and Construction of Ultra-High Strength Fibre Reinforced Concrete Structures (Draft)
2013	France	Ultra-High Performance Fibre-Reinforced Concretes – Recommendations (Revised edition)
2016	Switzerland	SIA 2052 (Ultra-Hochleistungs-Faserbeton (UHFB) – Baustoffe, Bemessung und Ausführung)
2016-2018	France	NF P18-470 (UHPFRC – Specifications, performance, production and conformity), NF P18-710 (Design of concrete structures – Specific rules for UHPFRC) and NF P18-451(Execution of concrete structures – Specific rules for UHPFRC)

In addition, a number of criteria for the selection of the code that is to be used was also mentioned in the literature study:

- **Year and completeness**: Due to rapid developments in the field of UHPC, more recent guidelines are deemed to be completer and more comprehensive and include more results from research and applications in practice, compared to more dated guidelines.

- **Availability & practicality**: The text of the guideline itself should be able to be found and in addition it should be able to be used without having to translate large amounts of text.

- **Completeness**: A single code or guideline is typically part of a larger framework of codes. The code or guideline should be able to be used within the framework of the Dutch Eurocodes and if additional information is required from other guidelines, these should be able available as well.

3.2.2 Selecting appropriate guideline

Year and completeness

From the table it can be seen that there are roughly two 'generations' of guidelines. The first guidelines, from the early 2000's are the first guidelines on UHPC. From the literature study it is known that these documents

commonly make use of the same sources and are the first attempts to cover the lack of guidance in design of UHPC structures.

The second set of guidelines is more comprehensive. From the AFGC guideline of 2013 it is known that a lot of experience from the use of UHPC in practice and ongoing research was included into the document. About the series of French codes from 2016-2018 it is known that this is a further continuation of this development, and contributes to further formalized standardization. The Swiss code is deemed to fulfil a similar role, as the basis of UHPC design in Switzerland. These three (sets of) guidelines are therefore deemed to be better established and comprehensive than documents from the first generation of guidelines.

Given this information, the focus is on the more recent codes: The AFGC guideline from 2013, the Swiss code from 2016 and the set of French codes from 2016-2018.

Availability & practicality

From these three codes or sets of codes, the following documents were acquired:

- Ultra-High Performance Fibre-Reinforced Concretes – Recommendations, from 2013;
- The French version of the SIA 2052;
- English version of NF P18-710.

The NF P18-470 and NF P18-451 could not be acquired.

The AFGC-SETRA recommendations from 2013 are written to be in accordance with the framework of the EC2 for design and are therefore readily applicable. From the SIA 2052, only the French version could be acquired, which is to be used within the framework of the Swiss codes. This is not practical, and will not be used except for additional reference. The other two options therefore remain. However, of the most recent French set of codes, only the NF P18-710 was found.

Completeness

Of the more recent French codes, only the NF P18-710 could be acquired. After studying its content, it was concluded that many references are made to the NF P18-470 for determining material parameters.

Remaining codes & Decision

The P18-710 is deemed not to be used on its own because this document was never meant to be used in that way. This is explicitly stated. Therefore, the decision has been made to use the AFGC-SETRA from 2013. This is justified as follows:

- The AFGC-SETRA was the base for further normalization that resulted in the 470, 710 and 451, it is expected that substantive differences will be acceptably small;

- The most important reason to choose for the AFGC-SETRA is that it is a complete guideline that can be used together with Eurocode 2, contrary to the 710 that requires two other codes. Using a complete guideline, although a few years older, gives a more transparent design procedure and avoids uncertainty because relevant documents are missing.

4

AFGC-SETRA 2013 – REVIEW PART 1

4.1 Introduction

4.1.1 Introduction to the AFGC-SETRA 2013 guideline

This chapter gives a general introduction to the AFGC-SETRA guideline and discusses the first part of this document in detail. The goal is to become familiar with the setup of the AFGC guideline and specifically with the sections of the first part that are relevant for the thesis project. In this sense, this chapter continues where the discussion of the AFGC in Chapter 3 of the literature study part I stopped. Because of the contents of this chapter, it also provides the required background for the next chapter in which the second part of the AFGC guideline will be discussed.

The AFGC 2013 guideline is the revised version from 2002. It is complemented and improved on compared to the 2002 version and comprises four different parts.

- Part 1. UHPFRC material characterisation – Deals with characterising the material, mechanical properties and quality control;
- Part 2. Design of UHPFRC structures – Deals with the design of UHPFRC structures, following the EC2 with adjustments to include contribution of fibres and elements without prestressing and/or reinforcing steel;
- Part 3. Durability of UHPFRC – Deals with one of the main advantages of the material: its durability;
- Part 4. Sustainable development – Comprises feedback on the use of material from a sustainable development point of view.

In the introduction, a definition is given of Ultra-High Performance Fibre-Reinforced Concrete (UHPFRC):

- *"UHPFRC are materials with a cement matrix and a characteristic compressive strength of more than 150 MPa and a maximum of 250 MPa."*

This type of material described in the guideline sets itself apart from high-performance and very high-performance concrete because of a number of reasons:

- The high post-cracking tensile strength, due to a high percentage of steel fibres, these are added to achieve ductile behaviour in tension;
- Mix design with a high binder content, which results in the elimination of capillary porosity resulting in good durability, especially also of the fibres in the material;
- The material has a capacity of self-healing of the cracks, this means that the tensile strength of the material may be retained on the longer-term. This is provided that crack width limits are met;
- The direct tensile strength of the matrix is greater than 7 MPa.

These points already give an idea of what the reader may expect form the guidelines, which can now be expected to be different than EC2. Fibres play an important role in the guideline and result in achieving high tensile strengths, this will often result in not having to provide conventional reinforcement for the total structure.

The guidelines are heavily influenced by the concrete/construction industry in France and are based on application of certain materials in practice, as well as the laboratory research in developing and applying the materials. As a result of this, the guideline only covers certain specific types of UHPFRC, mentioned are:

- Ductal mixtures (including Reactive Powder Concrete)
- BSI/CERACEM mixtures
- BCV mixtures

Note that in the guideline, this type of concrete used in the elaboration of the thesis is consistently denoted as 'UHPFRC'. However, to be in accordance with the rest of the work, in this report it will be denoted as 'UHPC'.

4.2 Characterisation of UHPC at different stages of a project

4.2.1 General

The first part of the recommendations covers the characterisation of the material by looking at the main properties of the material, as well as experiments to determine these. An important notion related to the characterisation of the material is the ''technical description'', which is often also denoted as the ''identity card'' of the material. This might be defined as follows:

- **A technical description of UHPC** (a.k.a. ''identity card''): A description of a specific UHPC mix which includes all its properties guaranteed by its supplier. These descriptions have to be confirmed by performing tests.

The technical description (identity card) is based on the documents that provide evidence of the material properties or its performance, examples are test reports or assessment reports. This is important information in order to be able to meet the project requirements.

4.2.2 Overall design approach

UHPC is characterized using a constitutive law, this law is largely influenced by the presence of steel fibres in the mixture. An accurate characterization of the material behaviour in tension is vital. Appropriate ways of determining the material properties are to be used, this is influenced by the geometry of the structure and the conditions under which the material will be placed.

In the guideline it is described that a UHPC project consists of three phases. During each phase, characteristics of the material have to be defined or have to be tested for. This information has to be sufficiently accurate for each stage of the project, to confirm that the assumed properties of the material are indeed achieved. Testing therefore plays an important role throughout the guideline. Three phases are distinguished:

Project design stage: For the (first) design, certain characteristics of the material have to be known, as these are input parameters. This information serves as the background for the first design calculations. There are two options to define these properties:

- A specific UHPC mixture is available which has already been characterized. The supplier has a full technical description including the constitutive laws;

- There is no technical description available, because the material has not been predefined just yet. The design is therefore based on standard constitutive laws defined beforehand.

Concrete design-test stage: The concrete mixture is produced in a concrete laboratory and then characterized by tests, to obtain the characteristics that are required by the designer. These results are then used for refined design calculations.

The tests that will be performed depend on the intended use of the material. Structural effects and effects of placement method are also taken into consideration (using mock-ups or test specimen). Eventually a technical description of the material can be formulated. If a known material is used, which already has a full technical description, these experiments are not required. It is sufficient if the manufacturer hands over the test results to prove the characteristics as presented in the technical description of the product.

Concrete suitability-test stage: For new applications with known mixtures, or for applications of new mixtures, suitability-tests are to be carried out as well. In this test stage, full scale tests are carried out. The concrete is placed on a representative mock-up of the structure under real site conditions. If the application is not new and the geometry isn't either, results of tests confirming the construction of similar structures can be provided.

The results of the design tests and/or suitability tests are used to adjust the constitutive laws if this proves to be necessary. This way the design can be further refined using more accurate values.

Batch control testing: During the actual production stage, tests are needed as well, to control the concrete production itself.

The total approach to a project involving UHPC is given in the following figure. It illustrates that testing plays a vital role in UHPC applications in accordance with the AFGC guideline.

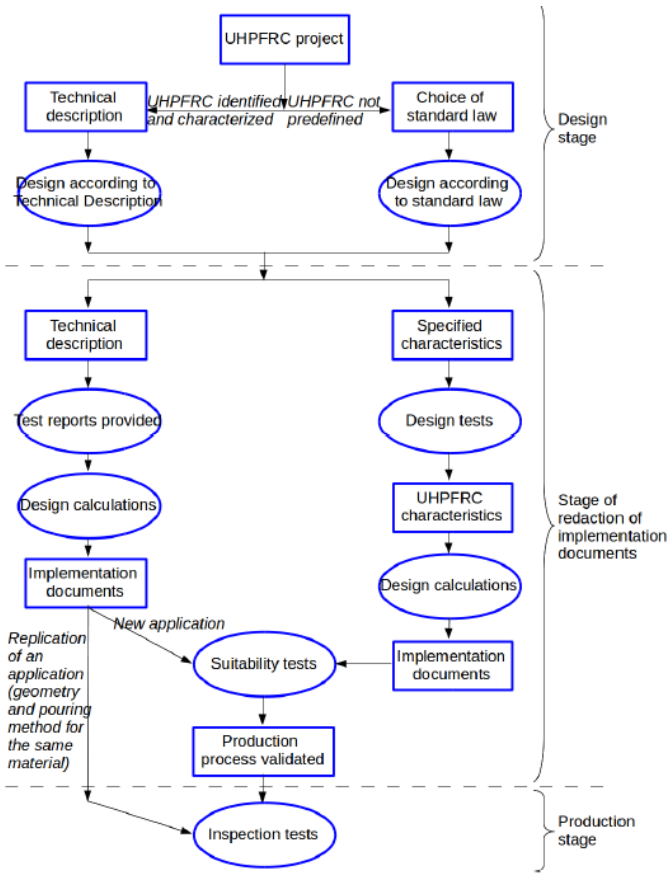


Figure 2 Overall approach to a UHPC project – (AFGC-SETRA 2013), p.19

4.2.3 Compressive strength

For the structural calculations, the constitutive law of concrete in compression is defined using the characteristic compressive strength (f_{ck}) and the mean modulus of elasticity (E_{cm}). The UHPC mixtures covered by the guidelines have a compressive strength between the 150 and 250 N/mm^2.

Constitutive laws used for design are idealized graphs. Constitutive laws established through experiments can be as in the following figure. If this type of characterization is required, predefined test procedures are described in the guideline. A reference specimen (cylinder is given), but tests can be carried out on cylinders or on cubes of other dimensions as well. The characteristic compressive strength value is subsequently obtained using statistics.

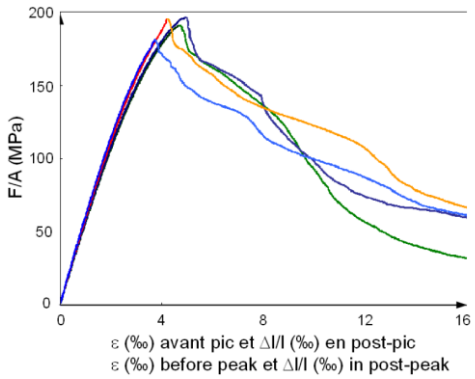


Figure 3 Experimental constitutive law of UHPC in compression – (AFGC-SETRA 2013), p.22

From the experimental results it can be seen that in compression the material behaves elastically until a maximum is reached. This is at relatively large strain value. A decrease in capacity then occurs while the strain still increases (post-peak behaviour). This decrease can occur very sudden (brittle) if there is a low fibre content (2% by volume is the recommended minimum).

4.2.4 Tensile strength

UHPC in tension & Strain hardening versus strain softening behaviour

In tension, UHPC initially exhibits linear elastic behaviour up to a certain limit value, the resistance of the matrix: $f_{ct,el}$. Note that this value is not only due to the matrix, the fibres present in the material also contribute to this up to a certain limited extent.

As long as the material behaves linear elastically, the E-modulus is the same in both tension and compression. After reaching the limit value $f_{ct,el}$ however, the material cracks but the tensile strength of the material does not become zero. This is due to the fibres that are present, this is an obvious difference with conventional concrete and the presence of fibres plays a vital role in the guideline.

After cracking, the fibres take over the role of the cracked cement matrix in transferring forces. The tensile strength provided by the fibres is usually translated into a stress σ_f, which denotes the post-cracking strength contributed by the fibres:

$$\sigma_f = \frac{F}{A}$$

Where:
F: Force
A: Surface area of the cross-section of the concrete

If the load is increased, the crack opens further and the fibres are pulled out of the matrix. The apparent stress in the material decreases as a result of this. Note that the failure of the fibres in tension is usually due to the loss of the bond with the matrix (pull-out failure) and not due to the failure of the fibres themselves,

because very high steel grades are usually used for the fibres. At a certain point almost all fibres failed and no tensile capacity is left.

The behaviour of a specific UHPC in tension depends on multiple parameters, among which are fibre quantity, fibre length, ratio of length and width of the fibre, the diameter, etc. This results in the fact that different types of tensile constitutive laws can be distinguished. The main two types of behaviour are:

- Strain-hardening: The resistance after cracking (post-cracking) is higher than the resistance of the matrix;

- Strain-softening: The resistance after cracking (post-cracking) is lower than the resistance of the matrix.

Among the UHPC types displaying hardening behaviour, one can distinguish low and high strain-hardening behaviour. The following figures gives an overview of the different possibilities that can be encountered in practice.

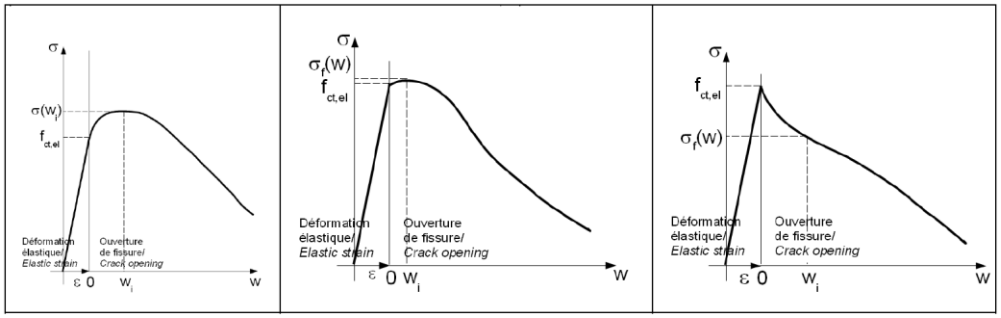


Figure 4 Strain-hardening (left), low strain-hardening (middle) and strain-softening (right) – (AFGC-SETRA 2013), p.25

Using an appropriate tensile constitutive law is a very important piece of information for the design of UHPC structures. The constitutive law of a UHPC in tension is characterized by two parameters/stages:

1. A linear elastic stage – The linear elastic stage is limited by a certain maximum stress value $f_{ct,el}$;

2. A post-cracking stage – The post-cracking part is characterized either by a stress-crack width law ($\sigma_f - w$ law) or a stress-strain law ($\sigma_f - \varepsilon$ law), depending on the behaviour of the material.

Effect of fibre orientation

The pre-cracking behaviour can be predicted with reasonable accuracy, because for the maximum value $f_{ct,el}$ reasonably low scatter can be achieved when mixing and placing the concrete. For the post-cracking behaviour this does not hold.

The post-cracking strength due to the fibres, σ_f, is largely determined by the way the UHPC is placed. This is because it is known that during placement of the concrete the fibres can be aligned in certain directions. The orientation of the fibres influences the material behaviour, therefore, it has to be accounted for. The alignment of the fibres can occur due to different processes:

- Process 1: The flow of the material during concreting aligns the fibres with the direction of the flow of the concrete;

- Process 2: Fibres near the formwork are aligned parallel to it. This effect occurs within a distance from the formwork equal to the length of the fibres. Therefore, the closer the thickness of the element to the fibre length, the greater this effect on the tensile strength;

- Process 3: Preferential gravitational orientation of the fibres can also occur.

To account for the impact of the fibre orientation on the behaviour of the structure, the AFGC guideline introduces different K-factors, these can be determined during the suitability test stage via tests that are carried out in conditions that are representative of the real structure. This way, this situation can be simulated and most accurate results are achieved.

The values of the K-factors are verified using experiments, by analysing the tensile strength of test specimen taken from a casted full scale UHPC element that represents the conditions under which the real structure will be casted. The tensile strength is analysed in the principal directions of the tensile stresses in the structure, an example is given in the following figure. The AFGC guideline also gives calculation methods for the factor.

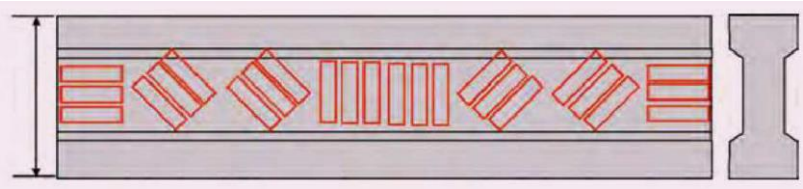


Figure 5 Example of specimen to determine the K-factor in different directions – (AFGC-SETRA 2013), p.27

The guideline distinguished a local value and a global value for the K-factor. This distinction is made to account for that the fact that the cross-sectional dimensions may or may not enable the redistribution of stresses:

- **Local value K_{local}**: For local effects, which corresponds to local stresses that require fibre resistance in very local areas (given example: stress distribution due to prestressing);

- **Global value K_{global}**: For the overall effects, which corresponds to stresses that require fibre resistance in larger areas, which is not affected by local defects (given example: shear or bending of a slab).

Scatter of the fibres cannot be avoided. For smaller elements, the consequences can be more severe though because there is no option to redistribute stresses, while this is generally possible for larger elements.
Note that the K-factor is only applicable to the post-cracking part of the tensile law, because only in this stage the fibres become active. An example of its application is given below. As will become clear in the later stages of the discussion, the K-factor is used to reduce the allowable stresses.

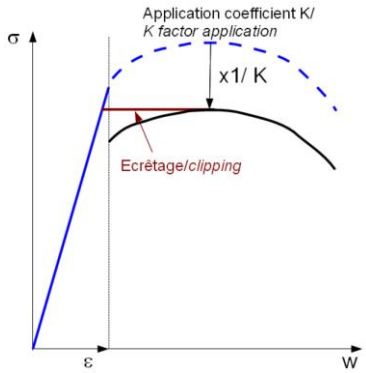


Figure 6 Application of the K-factor – (AFGC-SETRA 2013), p.28

Different tensile constitutive laws

From experiments, different types of behaviour in tension can be obtained, resulting in different tensile constitutive laws. The AFGC guideline distinguishes between three types, the UHPC can be classified as one of these types, depending on the material itself but also on how it is placed on the construction site. This classification influences for example the way the predefined constitutive law in tension that may be used during the structural analysis.

- **Strain-softening material (Type 1)**: This type corresponds to UHPC with an average and characteristic constitutive law that is strain-softening. Typical behaviour of this type of material is that if a tensile force is applied and the matrix strength is reached, the crack localizes, for this reason a stress-crack width law is applied. This type of constitutive law can be found in material with either a low fibre content, or inefficient use of fibres.

- **Low strain-hardening material (Type 2)**: This type corresponds to UHPC with a strain-hardening average constitutive law, but a strain-softening characteristic law. Most of the UHPC materials on the market fall within this category. For material characterisation and design, these materials are analysed as strain-softening material.

- **Strain hardening material (Type 3)**: This third type corresponds to a UHPC with a post-cracking peak that remains higher than $f_{ct,el}$, even after the characteristic constitutive law is considered and the fibre orientation has been accounted for. This only occurs in the case of materials having a high fibre content.

  Once the elastic strength is reached, a large number of fine cracks develop. These are micro-cracks, and in the calculations, these can be treated as strain. Therefore, a stress-strain type of constitutive law (also denoted as an ''intrinsic'' law) can be used instead of a stress-crack width law.

The following table gives an overview of the information according to the AFGC (section 1.4.2.).

Table 4 Overview of constitutive laws for different material types

	Average law	Characteristic law	Design law	Type post-cracking law
Type 1 – Strain-softening	Softening	Softening	Softening	$\sigma_f - w$
Type 2 – Low strain-hardening	Hardening	Softening	Softening	$\sigma_f - w$
Type 3 – Strain-hardening	Hardening	Hardening	Hardening	$\sigma_f - \varepsilon$

Thin versus thick

In addition to the three types of material, the guideline distinguishes two different ''types'' of structures: thin structures and thick structures. An element is considered thin if:

$$e \leq 3 * l_f$$

Where:
e: Thickness of the element
l_f: Length of individual fibre

It is important to make this distinction, because this influences the characterisation and the constitutive law that is to be applied. Fibre orientation has a more predominant effect in the case of thin members than in the case of thick members, as will be explained in the next section.

Characterisation of tensile constitutive laws

Subsequently the guideline covers the characterisation of the tensile constitutive law of thick or thin elements that can be of any of the three types discussed before. Performing tests play an essential role in determining these tensile constitutive laws, the guideline prescribes the procedures to determine these laws. These characterisation procedures are summarized as follows:

- **Thick elements of types 1 and 2**: For type 1 and type 2 materials, materials that are treated as strain-softening, first the strength of the matrix is determined using the prescribed testing methods (a number of four-point bending tests or direct tensile tests). It is assumed that a crack has formed as soon as this limit $f_{ct,el}$ has been exceeded. The crack width is assumed to be localized in this crack.

Subsequently, the post-cracking curve, which is a stress-crack width curve (a $\sigma_f - w$), is determined. This can be done by subjecting a number of notched specimen (prisms) to a three-point bending test to obtain the moment-crack width law, after which a prescribed back analysis procedure is performed to determine the stress-crack width law. The alternative is loading a number of specimens in tension and directly measuring the crack width.

Procedures to determine the K-factor are also given. The essence is that the ratio of the mean value of the peaks of the force-crack width or moment-crack width curves obtained with the specimen cast during suitability tests to the mean (or lowest value, for the global or local value respectively) value of the peaks of the $F - w$ or $M - w$ curves obtained from the specimen sawn during suitability tests.

- **Thick elements of type 3**: For a strain-hardening material, the strain of the micro-cracked material can be used (a $\sigma_f - \varepsilon$ constitutive law). There is no crack localization before the maximum strength is reached. The relevant characterization tests and calculations are described in the guideline.

  The basis for determining the $f_{ct,el}$ and the intrinsic post-cracking stress-strain law are either a series of four-point bending tests or a series of direct tensile tests. Following the prescribed procedures, a stress-strain law is obtained for the post-cracking part. If four-point bending tests are carried out, back analysis has to be performed. If direct tensile tests are performed, the stress-strain law is determined directly.

  Procedures to determine the K-factor are also given. The essence is to determine the ratio between the average peak of the force-strain or moment-strain curves obtained with the specimen cast during suitability tests to the mean (or lowest value, for the global or local value respectively) peak value of the $F - \varepsilon$ or $M - \varepsilon$ curves obtained from the specimen sawn during suitability tests.

- **Thin elements**: For thin elements, the effect of the fibre orientation is very evident because of the small dimensions of the element compared to the dimensions of the fibre. It is assumed that the fibres have a nearly 2D orientation. As a result, their constitutive law is similar to that of strain hardening material, with a large number of fine cracks very close together (no localization). A constitutive law in the form of $\sigma_f - \varepsilon$ can therefore be used.

  The relevant characterization tests and calculations are described in the guideline. A series of four-point bending tests or direct tensile tests can be applied. If the four-point bending test method is applied, back analysis has to be performed. There are two ways to do this: a simplified method resulting to an elasto-plastic law (graph with a horizontal plateau) or a more elaborate method resulting in a more exact graph. Both types of laws will be encountered in the next chapter. Direct tensile tests directly result in the constitutive law.

4.2.5 Static modulus of elasticity

According to the guideline, there is no formula that directly links the modulus of elasticity to the compressive strength of the material. It is prescribed that tests should be applied to determine the modulus of elasticity during more detailed design stages. At a preliminary design stage, provided nothing is known, a value of 50.000 N/mm^2 can be used as a guiding value.

4.2.6 Poisson's ratio

If no other value is available, a value of $\nu = 0{,}2$ can be used. This is in accordance with the value for different UHPC types as presented in one of the annexes (annex 9) of the guideline.

4.2.7 Coefficient of thermal expansion

Different UHPC types as presented in one of the annexes (annex 9) of the guideline give values of $10{,}4 * 10^{-6}$ to $12 * 10^{-6}$. According to the guideline, a value of $1{,}1 * 10^{-5}$ can be used as a guiding value, if nothing is known beforehand.

4.2.8 Effect of heat treatment

From the second chapter of the literature study part I, it is known that heat treatment can be applied to UHPC, influencing the properties of the material. This is also taken into consideration in the AFGC guideline, which mentions the following main effects of heat treatment:

- More rapid strength development
- Decrease of shrinkage and creep after treatment
- Improvement of the durability

In the guideline it is mentioned that in practice one can distinguish between two types of heat treatment, these two types can be applied separately of one another:

- **Type 1**: The first type is applied during the first few hours after casting the UHPC. It is applied at moderate temperatures and the goal is to accelerate the initial hardening of the material.

- **Type 2**: The second type is applied after the concrete has hardened, relatively high temperatures (90 degrees) and adequate moisture content are used. The goal of this type of heat treatment is to develop new hydrates, which results in a further increase of the material strength. The following effects of this type are mentioned in the guideline:

    - After treatment the components have reached their final maturity, which means that waiting 28 days (as is standard to reach the 28-day strength) is not required;

    - The compressive strength and tensile strength are higher than 28-day strength with storage in water;

    - The total shrinkage after the treatment is zero, while the creep after treatment is significantly reduced (the creep coefficient goes from 0,8 without heat treatment to 0,2);

    - The porosity is further reduced, leading to improved durability.

- The remark is made in the guideline that the heat treatment applied has to be adapted and optimized for each specific concrete mixture. In addition to that, one has to balance the short-term strength versus the long-term strength because heat treatment applied in a stage too early (resulting in higher short-term strength) can result in a lower long-term strength.

4.2.9 Shrinkage and creep

Shrinkage

From the first part of the literature study (chapter 2) it is known that in the case of UHPC the autogenous shrinkage is the predominant type of shrinkage, this is due to the large amount of fine material and low water/cement ratio. This is also acknowledged in the AFGC guideline, where the shrinkage of UHPC is described as being mainly an endogenous (i.e. ''internal'') process. In addition, the shrinkage is influenced by the application of heat treatment:

- Heat treatment – Type 1: Shrinkage occurs partly during the treatment; a part remains afterwards;

- Heat treatment – Type 2: There will be no further shrinkage after application of the treatment.

The following figure, taken from the AFGC guideline, gives an example of a comparison between the type 2 heat treatment and a case where no heat treatment is applied. The straight horizontal line clearly indicates that no remaining shrinkage occurs after the treatment, versus a slower occurrence if no treatment is applied.

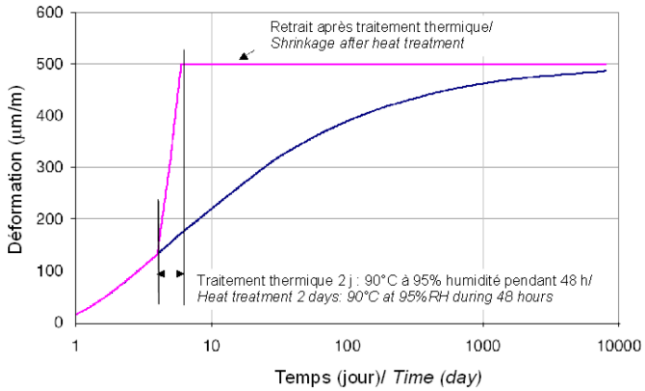


Figure 7 Shrinkage of UHPC with and without heat treatment – (AFGC-SETRA 2013), p.51

The guideline also gives a number of values that can be used during the preliminary design to describe the long-term shrinkage effects, if nothing is known.

- **No heat treatment applied**: A value of 550 $\mu m/m$ for endogenous shrinkage and 150 $\mu m/m$ for drying shrinkage (outdoor environment with relative humidity of 50-70%) may be used;
- **Type 1 heat treatment applied**: A total shrinkage value of 550 $\mu m/m$ (outdoor environment with relative humidity of 50-70%) may be used;
- **Type 2 heat treatment applied**: A total shrinkage value of 550 $\mu m/m$ may be expected before the end of the treatment, after the treatment the shrinkage equals zero.

Creep

In the guideline it is stated that creep of UHPC is similar to that of high performance concrete if no heat treatment is applied. The application of heat treatment reduces the creep. The guideline presents the following values that can be used as indicative values for the preliminary design, if nothing is known:

Table 5 Values for creep factor with and without heat treatment

	No heat treatment	Type 1 heat treatment	Type 2 heat treatment
Creep factor φ [-]	0,8	0,4	0,2

Long-term strength under load

In the guideline information is given on the long-term strength of UHPC under sustained load. In the AFGC it is assumed that the long-term reduction of the strength under high constant stresses is in the same order of magnitude as for conventional and high-performance concrete, resulting in a reduction factor of 0,85.

4.2.10 Impact strength

UHPC has, like many other fibre-reinforced concretes, a high energy-dissipation capacity as well as a relatively high tensile capacity, even after cracking. Along with its high strength in general, this makes UHPC into a useful option in the case of impact loads. Although not further discussed in this report, such properties can be of relevance in case of accidental situations such as ship collision. The reader is referred to 1.10 of the AFGC 2013 guideline for more information.

4.2.11 Design, batching, and placement of UHPC

The first part of the AFGC guideline also discusses more practical aspects of the application of UHPC, although no complete review is given in this report, the topics discussed in the guideline are:

- **General requirements**: Composition of the mix (low water/binder-ratio), the necessity of carefully controlling of the amount of water and regularity of ingredients;

- **Mix design**: Requirements regarding defining a specific mix design and the information the mix design should contain;

- **Batching of UHPC**: Requirements and allowable values with respect to tolerances for the premix or raw materials and requirements for the equipment used;

- **Transporting UHPC**: Requirements regarding the transportation of the UHPC between batching and placing;

- **Placement of UHPC**: Considerations regarding vibration, concreting in warmer or colder temperatures, concrete curing and the hardening process are addressed and discussed.

The essence of this section of the guideline is that raw materials of and complete UHPC mixtures should be handled with care during all phases, and especially during placement. Large tolerances in the mixture cannot be allowed for example. The flowability of some mixes, or even self-compacting properties, is a point of attention for the placement of the concrete. The curing requires attention because of the low bleeding of this material, or even the absence of this phenomenon. The temperature during the casting operations has to be taken into consideration as well: at lower temperatures, concreting is not recommended unless additional precautions are made. At higher temperatures, measures should be taken to prevent too high temperature inside thick components.

4.2.12 Tests

From the previous discussions in this chapter, it may be clear that testing plays an essential role in de AFGC guideline. Proving that the material meets the specifications and behaves in practice as expected during design has to be proven. The final paragraph of the first part of the guideline therefore describes the different categories of tests:

Design tests: The goal of the design tests is to confirm that the mix design satisfies the desired specifications for the project. For a UHPC with a complete identity card (''technical description''), the design tests only comprise handing over the test results confirming the characteristics in its identity card. If certain requirements cannot be confirmed this way, additional tests are to be carried out.

The design testing has another goal as well, namely to check that the requirements are still met if the proportions of constituents reach the tolerance limit values. Design tests can be considered to be conclusive if the consistency results are within the tolerances, and if the acceptance criteria of compressive and tensile strength tests are met.

Suitability test: Suitability tests are carried out to verify if the concrete produced using nominal mix design, and the materials and equipment used on site is within the tolerances of the design tests. It is prescribed in the guideline that at least one mix of a volume representative of the actual production is to be used to take samples and carry out a series of tests.

Control tests: Control tests are performed to verify that the concrete produced in the execution phase of the project complies with the project specifications. These tests are carried out on samples of the fresh concrete, these are taken during placement operations. Using these samples, a series of tests is to be performed.

4.3 Bibliography chapter four

Fehling, E., Schmidt, M., Walraven, J., Leutbecher, T., & Fröhlich, S. (2014). *Ultra-High Performance Concrete UHPC*. Berlin: Wilhelm Ernst & Sohn.

Groupe de travail BFUP. (2013, June). Ultra-High Performance Fibre-Reinforced Concretes. *Recommendations*. Association Francaise de Génie Civil.

5

AFGC-SETRA 2013 – REVIEW PART 2

5.1 General provisions

This chapter of the report discusses relevant parts of the second part of the AFGC-SETRA 2013 recommendations, which comprises the structural analysis of UHPC structures. Not all provisions immediately result in clear calculation procedures. Therefore, in this chapter calculation procedures are also formulated, making use of other sources wherever required.

In the beginning of the second part of the guideline, its relation to Eurocode 2 is explained. The guideline is written to be in accordance with the structure of EC2-1-1 (General rules and rules for buildings) and EC2-2 (Concrete bridges – Design and detailing rules). Articles from the original Eurocode that have to be changed for the application of UHPC are explained in the guideline, while for articles that remain unchanged can be found in the original Eurocode. Because of this, several parts of Eurocode 2 are also briefly discussed in this chapter wherever required, or to make a comparison with provisions from the AFGC guideline.

At the start of the second part of the guideline, a number of concepts that play an important role in the design of UHPC structures are introduced:

- Scatter in fibre distribution
- New partial safety factors
- Characteristic length
- Minimum ductility
- Condition for non-brittleness

These concepts will be covered in the subsequent paragraphs.

Scatter in fibre distribution

As discussed in the literature study and the previous chapter of this report, scatter in fibre orientation may occur due to the preferential orientation of fibres that occurs during the casting operations. Fibre orientation influences the behaviour of the material. To account for this effect, the so-called ''orientation factor'' $1/K$ is introduced in design and a distinction is made between the local and global values:

- Global coefficient K_{global}: For general stress distribution (larger elements);

- Local coefficient K_{local}: For smaller components or specific situations (smaller elements or details).

In the verifications, the ''K'' is positioned in the denominator of the orientation factor. A value larger than 1 therefore implies unfavourable effects due to the preferential orientation of the fibres while a value smaller than 1 implies a favourable effect. The minimal value therefore equals 1. Starting values for the K are given in the guideline ($K_{global} = 1{,}25$ and $K_{local} = 1{,}75$), and as described in the first chapter the real value can be determined using tests.

Partial safety factors

For the concrete compressive strength and the tensile strength of reinforcing steel and prestressing steel, partial factors as defined in EC2-1-1 are to be applied. In addition to these values, an additional factor is introduced for fibre-reinforced concrete loaded in tension: γ_{cf}. This factor accounts for manufacturing defects in ULS verifications. Its value is 1,3 for permanent/transient situations while 1,05 is prescribed for accidental situations.

Characteristic length

A notion related to the tensile strength of concrete is the characteristic length, which is used for strain softening UHPC or low strain hardening UHPC. The characteristic length is used to convert from a stress-crack width type constructive law to a stress-strain type constitutive law. The following relation is defined in the guideline:

$$\varepsilon = \frac{f_{ct,el}}{E_{cm}} + \frac{w}{l_c}$$

Where:
$f_{ct,el}$: Limit of elasticity in tension
E_{cm}: Mean modulus of elasticity
w: Crack width
l_c: Characteristic length

The value for the characteristic length depends on the cross section. As an example: for a rectangular section or T-section $l_c = 2/3 * h$, where h is the height.

Ductility requirement

Adding fibres to UHPC results in more ductile behaviour, for safe application of the material it has to be guaranteed that the material has sufficient ductility when imposed to bending. This can be done by imposing a ductility requirement. According to the guideline, the following criterion has to be satisfied for strain softening or low strain hardening UHPC:

$$\frac{1}{w_{lim}} \int_0^{w_{lim}} \frac{\sigma(w)}{K_{global}} dw \geq \max\left(0{,}4 * f_{ctm,el}; 3\ MPa\right)$$

Where:
w_{lim}: Crack width that can be chosen equal to 0,3 mm
$f_{ctm,el}$: Mean limit of elasticity in tension
$\sigma(w)$: Characteristic post-cracking stress

Note that in the guideline the remark is made that this criterion does not hold for elements with strain-hardening behaviour (thin slabs or thick elements of strain-hardening UHPC). The reason for this is that by definition the maximum post-cracking stress is higher than the elastic limit.

Non-brittleness condition

The guideline also prescribes that the non-brittleness of the cross-section has to be ensured. For this criterion it has to be verified that the ULS load conditions are higher than the load that results in cracking.

The verification means that it has to be checked that the elastic force domain (loads calculated with elastic constitutive law) is within the ultimate force domain (the resisting forces at ULS). In the case of pure bending for example, this means that it has to be verified that the elastic moment, in an uncracked cross-section, is less than the ultimate bending moment.

This is a condition described under 7.3.2. (6) of the AFGC. This corresponds to 7.3.2 in EC2. This is a paragraph dedicated to minimum reinforcement. For conventional concrete under tension, a certain minimum amount of reinforcement has to be provided. As soon as the concrete cracks, the reinforcement balances the tensile forces. Therefore, this amount of reinforcement has to be sufficiently large to balance these tensile forces, this prevents that the cross section suddenly fails (brittle failure) at the moment of cracking.

In the case of UHPC, the design principles are different: as soon as the concrete cracks, the fibres balance the tensile forces and conventional reinforcement is often not even provided. Strain hardening UHPC never requires a minimum amount of reinforcement. In the case of strain-softening UHPC it is not required if a number of requirements is met, namely:

- A minimum percentage of fibres is provided (verified by means of the aforementioned ductility condition);
- The aforementioned non-brittleness condition is met;
- Maximum crack width w_{max} is not exceeded (this ensures the durability of the steel fibres, and of the reinforcement if provided). For the recommended values reference is made to table 7.1 of the AFGC guideline.

5.2 Material constitutive law for design (AFGC guideline)

In EC2, material properties of concrete are described in paragraph 3.1 and it is valid for normal concrete and high strength concrete (up to C90/105). Many parameters are deduced from the characteristic compressive strength of the material. For UHPC, which is a different material, these provisions are not valid and have to be replaced completely by the provisions from the AFGC. Important changes with respect to the Eurocode are:

- Mechanical properties such as the tensile strength and modulus of elasticity have to be determined via material characterisation tests (reference is made to chapter 1 and annexes 2, 3 and 4 of the guideline). This is contrary to EC2, where these values are determined directly from the characteristic compressive strength;
- Creep and shrinkage of the material has to be determined via tests performed on the material that will be used for the actual structure (reference made to annex 5 which describes the tests to be carried out). Equations given in the EC2 to determine the creep and shrinkage as a function of time are no longer valid.

The following subparagraphs cover the constitutive laws for UHPC in compression and tension according to the AFGC guidelines.

5.2.1 Constitutive law for concrete in compression

Concrete constitutive law in compression

In the following figure the constitutive law for concrete in compression is given for the SLS (left) and the ULS (right). In addition, equations from the AFGC to determine the quantities given in the figures are given as well.

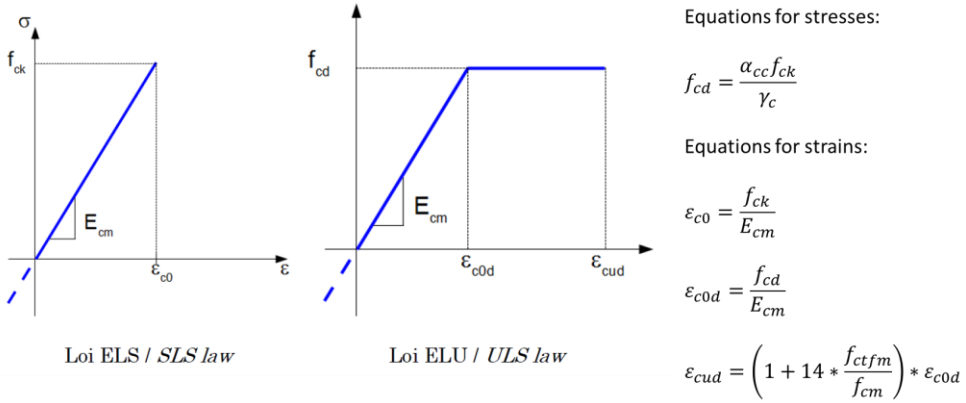


Figure 8 Constitutive laws and equations for concrete in compression - Edited, after (AFGC-SETRA 2013), p.83

Where:
f_{ck}: Characteristic compressive strength
E_{cm}: Mean modulus of elasticity
f_{cd}: Design compressive strength
f_{ctfm}: The maximal mean post-cracking stress in tension
f_{cm}: The mean compressive strength

ε_{c0}: Strain belonging to reaching characteristic compressive strength
ε_{c0d}: Strain belonging to reaching design compressive strength
ε_{cud}: Maximum compressive strain at ULS

Remarks:

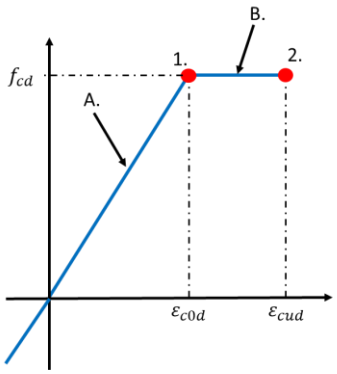
- The parameter α_{cc} denotes a coefficient that accounts for the long-term effects on the compressive strength of the material and unfavourable effects associated to the application of the loads. In the guideline a value of 0,85 is recommended for UHPC.

- The partial factor γ_c is the partial factor for concrete, and is to be determined according to the Dutch national annex to EC2-1-1.

- In the guideline the comment is made that the coefficient used to multiply ε_{c0d} with is deduced from analysing numerous test results on fibre-reinforced high performance and ultra-high performance concrete, after which it was based on the most pessimistic results.

- In this section of the guideline, recommended values are given for f_{cm}, f_{ck}, f_{cd}, f_{ctfm} and ε_{cud} that can be used for a preliminary design. All recommended values will be summarized later on in this chapter.

- The behaviour of concrete in compression is as follows:



Branches:
A. Linear elastic branch
B. Plastic stage, increase of strain until failure

Points:
1. Elastic limit reached
2. Failure of concrete at limit strain in compression

Figure 9 Behaviour of concrete in compression

Modulus of elasticity:

According to the guideline, the secant modulus E_{cm} can be considered directly for determining stresses. Creep effects can be accounted for when calculating the deformation, by using the effective modulus of elasticity:

$$E_{c,eff} = \frac{E_{cm}}{1+\varphi}$$

Where:
E_{cm}: Mean modulus of elasticity
$E_{c,eff}$: Effective modulus of elasticity
φ: Creep coefficient

A recommended value for E_{cm} is given that can be used for the preliminary design. All recommended values will be summarized later on in this chapter.

5.2.2 Constitutive laws for concrete in tension

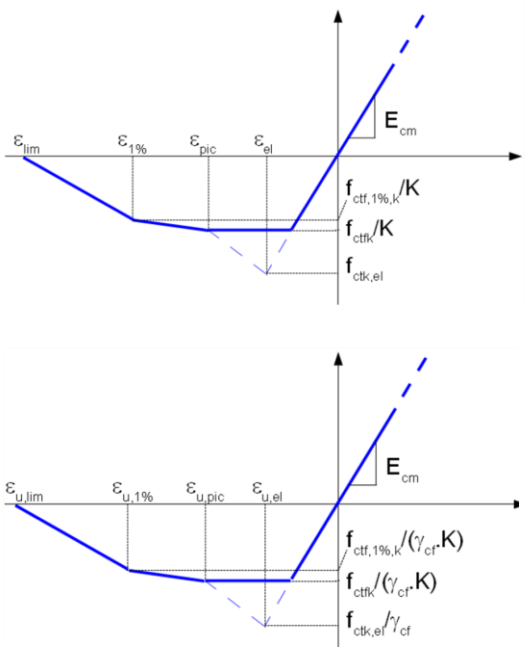
Steel fibres give ductility and tensile strength to the UHPC material. This is a key concept in the AFGC guideline, which is where designing in UHPC differs substantially from the provisions for conventional concrete in EC2. In order to account for the presence of fibres in tension, different simplified constitutive laws are presented for concrete that can be used to describe the behaviour of the fibre-reinforced material in tension. In the previous chapter, the importance of testing in the guideline was already illustrated, and indeed the option is also given to replace these simplified laws (later on) for UHPC in tension by more realistic laws obtained through testing.

For selecting an appropriate simplified law for concrete in tension, a distinction is made between thick cross sections and thin cross sections. In the previous chapter an equation was discussed that is used to distinguish between these two types of cross sections. For the thin sections, two types of tension laws are available (''simplified'' and ''realistic law''). First the tensile laws for thick elements are discussed. After that, the thin elements are discussed.

Constitutive laws for thick elements in tension

Within the group of ''thick elements'', distinction is made between two categories, namely strain softening or low strain hardening law and a strain hardening law.

Strain softening/low strain hardening law: The following figure gives the SLS and ULS law and corresponding equations for the strains of the constitutive law of strain softening/low strain hardening material in tension.



Serviceability limit state

$$\varepsilon_{lim} = \frac{l_f}{4l_c}$$

$$\varepsilon_{1\%} = \frac{w_{1\%}}{l_c} + \frac{f_{ctk,el}}{E_{c,eff}}$$

$$\varepsilon_{peak} = \frac{w_{peak}}{l_c} + \frac{f_{ctk,el}}{E_{c,eff}}$$

With: $w_{1\%} = 0{,}01 * H$ and $l_c = 2/3 * h$

Ultimate limit state

$$\varepsilon_{u,lim} = \frac{l_f}{4l_c}$$

$$\varepsilon_{u1\%} = \frac{w_{1\%}}{l_c} + \frac{f_{ctk,el}}{\gamma_{cf} E_{c,eff}}$$

$$\varepsilon_{u,peak} = \frac{w_{peak}}{l_c} + \frac{f_{ctk,el}}{\gamma_{cf} E_{c,eff}}$$

With: $w_{1\%} = 0{,}01 * H$ and $l_c = 2/3 * h$

Figure 10 Constitutive law and equations of type 1 and 2 materials in tension – Edited, after (AFGC-SETRA 2013), p.85

In addition, the strain ε_{el} (i.e. the elastic tensile strain) can be determined by dividing the tensile strength by the modulus of elasticity:

$$\varepsilon_{el} = \frac{f_{ctk,el}}{E_{cm}}$$

In the graphs the symbols for the stresses are as follows:
$f_{ctf,1\%,k}$: Characteristic post cracking stress corresponding to a crack width of $0{,}01 * H$
f_{ctfk}: Characteristic maximal post cracking stress
$f_{ctk,el}$: Characteristic limit of elasticity under tension

The corresponding symbols for the strain then are as follows:

$\varepsilon_{u,el}$: Elastic tensile strain at ULS
$\varepsilon_{u,pic}$: ULS equivalent strain corresponding to the local peak in post-cracking phase or to a crack width equal to 0,3 mm if there is no peak.
$\varepsilon_{u,1\%}$: Equivalent strain corresponding to a crack width of $0{,}01 * H$ where H is the depth of the tested prism with dimensions complying with the structure's dimensions at ULS.
$\varepsilon_{u,lim}$: Ultimate strain beyond which fibres participation is no longer taken into account at ULS

The other symbols are:
γ_{cf}: Partial safety factor on fibres in fibre reinforced concrete under tension
K: Fibre orientation factor
w_{peak}: Crack opening corresponding to the local peak, or 0,3 mm if there is no peak
H: The height of the prism tested under flexure corresponding to the thickness of the structure
l_f: Length of a fibre
l_c: Characteristic length

Remarks:

- The tensile strength of the material (the stresses on the vertical axis) are generally derived using tests, using the equations for the strains as mentioned next to the figures the full figures can be constructed.

- From the graphs and equations, it can be seen that the stress corresponding to a crack width of 0,3 mm plays an important role. In addition, it is assumed that fibres do not longer contribute when a crack width is reached equal to a quarter of the length of the individual fibre;

- As mentioned in the previous chapter of this report, both softening and low strain-hardening materials are in the AFGC guideline regarded as softening material when selecting a design law. From the dotted lines in the previous curves, it can be seen that the design curves for these materials are obtained by truncating the actual curves.

- The actual curve is truncated at a value of f_{ctf} (i.e. maximal post-cracking stress) to obtain a curve suitable for design. This can be done in two ways, depending on the type of material.

    - Case 1: Local peak (low strain-hardening) – After the initial crack a local peak can be observed due to the occurrence of limited strain-hardening. In this case a plateau is formed by truncating the real curve at the value of the local maximum;

    - Case 2: No local peak (softening) – After the initial crack occurs the material shows softening behaviour. Not local peak is observed. In this case a plateau is formed by truncating the real curve at a stress value corresponding to a crack opening of 0,3 mm (right graph).

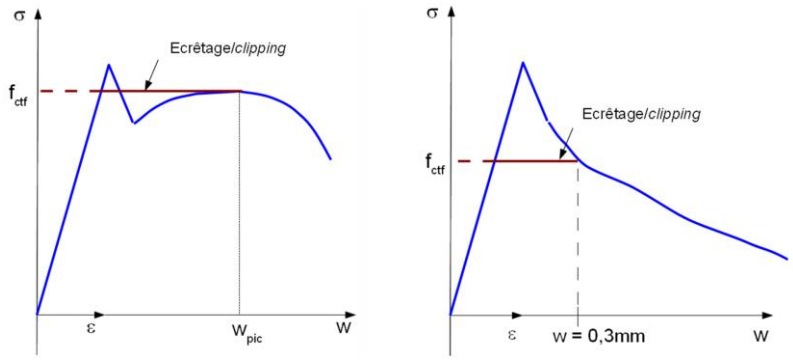
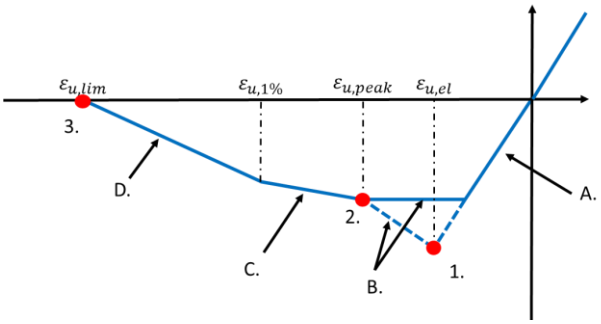


Figure 11 Truncating actual curves – Edited, after (AFGC-SETRA 2013), p.86

- The aforementioned curves can be interpreted as follows, in order to gain more insight into the behaviour of the material in different stages of it being subjected to tensile loads. Note that the dotted line is truncated in accordance with the guideline, but depicted in the next picture for the sake of completeness.



Branches:
- A. Linear elastic branch
- B. Cracking of the matrix and activation of the fibres
- C. Increase of crack width and failure of first fibres
- D. Gradual failure of the fibres (pull-out failure)

Points:
1. First crack of the matrix, start plastic stage
2. Fully developed crack pattern reached
3. No remaining fibre contribution

Figure 12 Behaviour of type 1 and type 2 material in tension

Note: In theory for low strain hardening material there would be an increase of apparent stress between $\varepsilon_{u,el}$ and $\varepsilon_{u,peak}$, the guideline does not consider this though for type 2 materials and assesses them as softening material.

Strain hardening law: The following figure gives the SLS and ULS law and corresponding equations for the strains of the constitutive law of strain hardening material in tension.

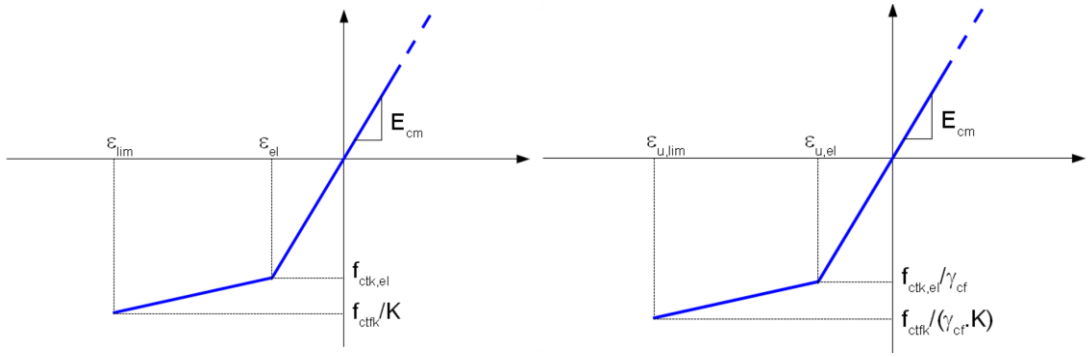
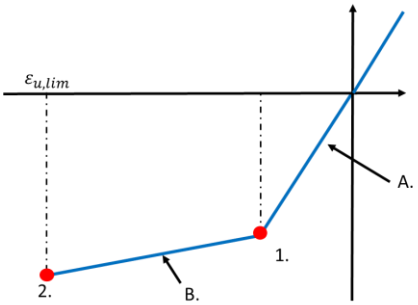


Figure 13 Constitutive law and equations of type 3 material in tension – (AFGC-SETRA 2013), p.85

The different stress and strain values on the graph are determined as follows:

- Elastic strain value ε_{el}: The elastic strain value under tension is calculated as mentioned for the softening/low-strain hardening materials;
- Ultimate strain $\varepsilon_{u,lim}$: The limit strain value for strain hardening materials is derived from characterisation tests. The permissible maximum value is set equal to 2,5 permille, except if the characterisation was carried out using direct tensile tests;
- The other symbols are defined in the same way as for softening/low strain hardening material.

The figure for strain-hardening material may be interpreted as follows:



Branches:
- A. Linear elastic branch
- B. Strain-hardening: increase of apparent stress due to further cracking of the concrete and activation of the fibres

Points:
1. First crack of the matrix
2. Maximum capacity of the strain-hardening material is reached

Figure 14 Behaviour of type 3 material in tension

Constitutive laws for thin elements in tension

Within the category of ''thin elements'', two options are given for the constitutive tensile law, namely: a simplified law and a realistic law. This was explained before in the previous chapter, where two different ways were mentioned to obtain the constitutive law for plates via back analysis of characterization test results.

Simplified law: The simplified law (results from simplified back analysis of test results) is an elasto-plastic law with a horizontal plateau and it can only be used for elements subjected to pure bending or bending and compression. The following figure gives the graph for the SLS at the left, and for the ULS at the right.

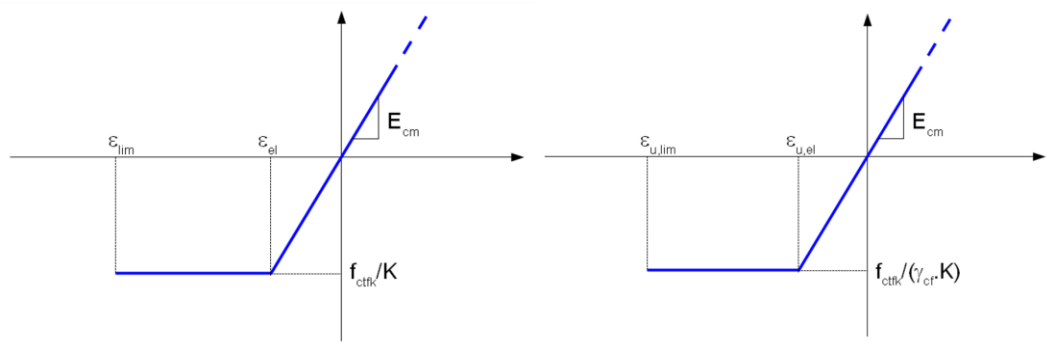


Figure 15 Simplified constitutive law for thin elements in tension – (AFGC-SETRA 2013), p.88

Where:
f_{ctfk}: Tensile stress resulting from tensile tests
$\varepsilon_{u,lim}$: Maximum tensile strain, resulting from tensile tests. The maximum value is 2,5 permille

Realistic law: This law (results from more elaborate back analysis of test results or direct tensile tests) depicts more realistic behaviour of the material, it is very similar to the graph of strain-hardening thick elements. This type of behaviour is to be expected because of the fibre alignment in thin elements. The realistic law may be used for any type of loading, if and only if the material is strain-hardening. The following figure gives the graph for the SLS at the left, and for the ULS at the right.

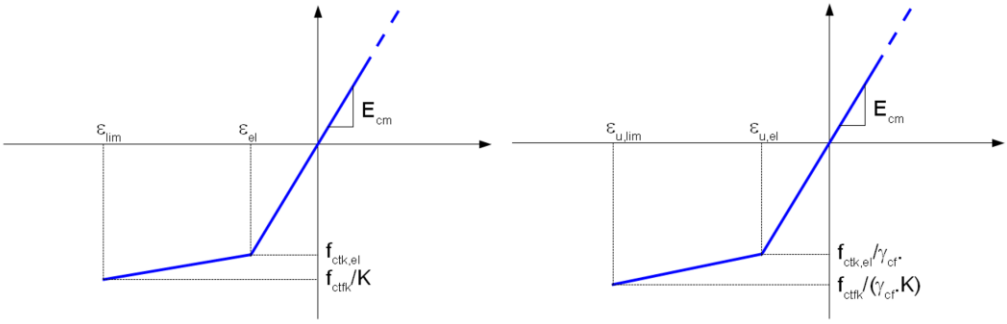


Figure 16 Realistic constitutive law for thin elements in tension – after (AFGC-SETRA 2013), p.88

The symbols used for both graphs are:

f_{ctfk}: Tensile stress derived from the tensile tests
$f_{ctk,el}$: Characteristic elastic tensile strength
$\varepsilon_{u,lim}$: Maximum tensile strain derived from tensile tests, which is limited to 2,5 permille except if direct tensile tests were performed for the characterisation

Selecting appropriate law: Which law is to be used for thin elements depends on the situation. According to the guideline the following holds:

1. The material is strain softening in pure bending: The same stress-crack width law as for thick elements is to be used;

2. The material is strain hardening in pure bending, but strain softening in direct tension:
   a. The element can be subjected to tension: The same stress-crack width law as for thick elements is to be used;

   b. The element is subjected to pure bending or bending compression: a simplified stress-crack width of thin elements is used;

3. The material is strain hardening in pure bending or direct tension: Two options

   a. Only if the element is never subjected to tension: Simplified law can be used

   b. Realistic law: valid in all cases

Parameters for preliminary design

Throughout the first and second part of the guideline, different values are given that are recommended to be used as guiding values in the preliminary design (if no other values are known). These values are summarized in the following tables.

Table 6 Recommended guiding values for preliminary design (1)

Parameter		**Value**	**Unit**	**Remarks**
Poisson ratio	v	0,2	[-]	
Coefficient of thermal expansion	α	$1{,}1 * 10^{-5}$	$[K^{-1}]$	
Endogenous shrinkage	ε_{shr}	$550 * 10^{-6}$	[-]	Value without heat treatment
Drying shrinkage	ε_{shr}	$150 * 10^{-6}$	[-]	Value without heat treatment
Creep	φ	0,8	[-]	Value without heat treatment

For the constitutive law in compression the following values are recommended for preliminary design:

Table 7 Recommended guiding values for preliminary design (2)

Parameter	**Value**	**Unit**	**Remarks**
E_{cm}	50.000	[N/mm^2]	
f_{cm}	180	[N/mm^2]	
f_{ck}	150	[N/mm^2]	
f_{cd}	85	[N/mm^2]	Under the assumption that for UHPC $\alpha_{cc} = 0{,}85$ and $\gamma_C = 1{,}5$.
ε_{cud}	2,7*10^{-3}	[-]	Under the assumption that $f_{ctfm} = 9$ N/mm^2

The following table gives recommended values for tension. Note that only the values for thick elements are given. Values for thin elements (both simplified and realistic law) can be found in the guideline.

Table 8 Recommended guiding values for preliminary design (3)

Parameter	Value	Unit	Remarks
$f_{ctk,el}$	9	[N/mm^2]	A low strain hardening UHPC can be taken for preliminary design
f_{ctfk}	9	[N/mm^2]	A low strain hardening UHPC can be taken for preliminary design
K_{global}	1,25	[-]	A low strain hardening UHPC can be taken for preliminary design
K_{local}	1,75	[-]	A low strain hardening UHPC can be taken for preliminary design

5.3 Provisions Eurocode 2 on material properties

Throughout the sections of the AFGC on constitutive laws and material properties, several references to the Eurocode 2 are made. Therefore, the relevant parts of the Eurocode are very briefly discussed to fill in the missing information (e.g. partial factors or properties of reinforcing and prestressing steel) not covered in the AFGC guideline as well as provide some background information on the parts replaced by the AFGC (e.g. the concrete part).

5.3.1 Partial material factors

For the concrete compressive strength and the tensile strength of reinforcing steel and prestressing steel, partial factors as defined in EC2-1-1 are to be applied. Conforming 2.4.2.4 and the national annex, the partial factors for concrete and reinforcing and prestressing steel in the ULS are as follows:

Table 9 Partial factors Eurocode 2-1-1 + National Annex

Situation	**Concrete (γ_C)**	**Reinforcing steel (γ_S)**	**Prestressing steel (γ_S)**
Permanent or transient	1,5	1,15	1,1
Accidental	1,2	1,0	1,0

For verifications in the serviceability limit state, conforming the national annex γ_C and γ_S are to be taken equal to 1,0.

5.3.2 Concrete

Definitions

The material properties of concrete are discussed in paragraph 3.1 of EC2-1-1. In the Eurocode 2, the strength of concrete is expressed by using strength classes in the following notation:

CX/Y

Where:
X: Characteristic value of the cylindric compressive strength
Y: Characteristic value of the cube compressive strength

The Eurocode 2 is valid from strength classes C12/15 to C90/105.

Compressive strength

The strength is determined by performing compression tests on cylinders or cubes with prescribed dimensions after being stored under controlled conditions.

Mean value cylinder compressive strength: The mean value for the cylinder compressive strength can be determined directly from the characteristic value:

$$f_{cm} = f_{ck} + 8\ N/mm^2$$

Design value compressive strength: The design value for the compressive strength is as follows:

$$f_{cd} = \frac{\alpha_{cc} * f_{ck}}{\gamma_c}$$

f_{cd}: Design value compressive strength
f_{ck}: Characteristic value compressive strength
α_{cc}: Coefficient accounting for long term effects on the compressive strength and unfavourable effects due to the way the loads are applied (national annex sets the value equal to 1,0).

For conventional concrete the increase in strength after 28 days can be in the order of magnitude of 10 to 30%, this is accounted for in the calculation by setting $\alpha_{cc} = 1{,}0$ in accordance with the national annex.

Tensile strength

Axial and splitting tensile strength: The tensile strength can be determined via a direct tensile test (results in the axial tensile strength f_{ct}) or the splitting tensile test (results in the splitting tensile strength value $f_{ct,sp}$), the latter is more practical to deform. These two values can be related through:

$$f_{ct} = 0{,}9 * f_{ct,sp}$$

Mean axial tensile strength: The mean tensile strength can, for strength classes up to and including C50/60, be determined directly from the characteristic compressive strength:

$$f_{ctm} = 0{,}30 * f_{ck}^{\left(\frac{2}{3}\right)}$$

For strength classes from C50/60 up to and including C90/105 the value is determined from the mean compressive strength:

$$f_{ctm} = 2{,}12 * \ln\left(1 + \frac{f_{cm}}{10}\right)$$

5% fractile of axial tensile strength: The 5% fractile of the axial tensile strength of concrete, which is the lower bound value of the tensile strength, can be determined from the mean axial tensile strength:

$$f_{ctk,0,05} = 0{,}7 * f_{ctm}$$

Design value tensile strength: Using the lower bound value of the axial tensile strength, the design value for the tensile strength can subsequently be determined:

$$f_{ctd} = \frac{\alpha_{ct} * f_{ctk,0,05}}{\gamma_c}$$

f_{ctd}: Design value tensile strength
$f_{ck,0,05}$: 5% fractile of axial tensile strength
α_{ct}: Coefficient accounting for long term effects on the tensile strength and unfavourable effects due to the way the loads are applied

Conforming the national annex, a value of 1,0 is prescribed for α_{ct}, following the same line of reasoning as was done for α_{cc}.

Modulus of elasticity

The modulus of elasticity, E_{cm}, can be determined directly from the mean value of the compressive strength:

$$E_{cm} = 22.000 * \left[\frac{f_{cm}}{10}\right]^{0,3}$$

Note that values such as the compressive strength, tensile strength and modulus of elasticity are load rate dependent. If loads during tests are applied slowly, the values that are found are lower than the values found for more rapid applied loads.

Following the aforementioned definitions, the following values of the most important quantities can be found and determined for all strength classes defined in Eurocode 2:

Table 10 Material properties concrete in accordance with Eurocode 2

	Strength class	f_{ck}	f_{cm}	f_{cd}	f_{ctm}	f_{ctd}	E_{cm}
		[N/mm^2]	[N/mm^2]	[N/mm^2]	[N/mm^2]	[N/mm^2]	[N/mm^2]
NSC	C12/15	12	20	8,0	1,57	1,05	27.000
	C16/20	16	24	10,7	1,90	1,27	29.000
	C20/25	20	28	13,3	2,21	1,47	30.000
	C25/30	25	33	16,7	2,56	1,71	31.000
	C30/37	30	38	20,0	2,90	1,93	33.000
	C35/45	35	43	23,3	3,21	2,14	34.000
	C40/50	40	48	26,7	3,51	2,34	35.000
	C45/55	45	53	30,0	3,80	2,53	36.000
	C50/60	50	58	33,3	4,07	2,71	37.000
HSC	C55/67	55	63	36,7	4,21	2,81	38.000
	C60/75	60	68	40,0	4,35	2,90	39.000
	C70/85	70	78	46,7	4,61	3,07	41.000
	C80/95	80	88	53,3	4,84	3,23	42.000
	C90/105	90	98	60,0	5,04	3,36	44.000

Constitutive law in compression

The stress-strain diagrams of concrete obtained from experiments are non-linear graphs that are close to a parabola. According to EC2, for calculations a simplified stress-strain curve consisting of a parabolic part and a rectangular part may be used (next figure on the left). It is also allowed to use a more simplified relation as long as the relation is equivalent or more conservative than the aforementioned one. An example of this is the bi-linear stress-strain diagram, which is most widely used for calculations (next figure on the right).

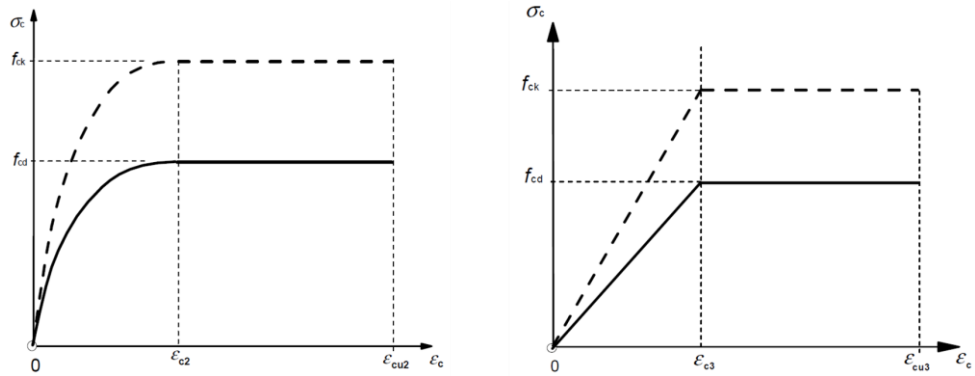


Figure 17 Stress-strain diagrams concrete in compression - after Eurocode 2-1-1 p.36-37

The bi-linear stress-strain diagram consists of two branches. The first part up to strain value ε_{c3} is the elastic part, which is described following Hooke's law. The second part is the plastic branch, deformations are permanent and is described using the stress value $\sigma_c = f_{cd}$ and the ultimate strain value for concrete under compression, ε_{cu3}.

In addition to the strain values, the parameters α and β are also commonly used in design calculations to describe the shape of the figure for cross section verifications. The parameter α is a ''shape factor'', describing the shape of the compressive zone that differs from a rectangle. The parameter β is used to determine the location of the centre of gravity of the compressive zone. These two parameters can be derived by considering the cross-sectional area and centre of gravity of the concrete compressive zone. The following table summarizes the values for ε_{c3}, ε_{cu3}, α and β for all strength classes covered by the Eurocode.

Table 11 Parameters concrete compressive zone in accordance with Eurocode 2-1-1

	α	β	ε_{c3}	ε_{cu3}
	[-]	[-]	[‰]	[‰]
≤C50/60	0,75	0,39	1,75	3,5
C55/67	0,71	0,37	1,8	3,1
C60/75	0,65	0,36	1,9	2,9
C70/85	0,62	0,35	2	2,7
C80/95	0,58	0,34	2,2	2,6
C90/105	0,56	0,34	2,3	2,6

The shape of the stress-strain figure (and thus the shape of the concrete compressive zone in cross sections) depends on the concrete compressive strength. Above C50/60 the elastic branch becomes larger while the plastic branch becomes smaller. In other words, the higher the strength class the more brittle the behaviour of the concrete in compression. This can be seen from the following graph.

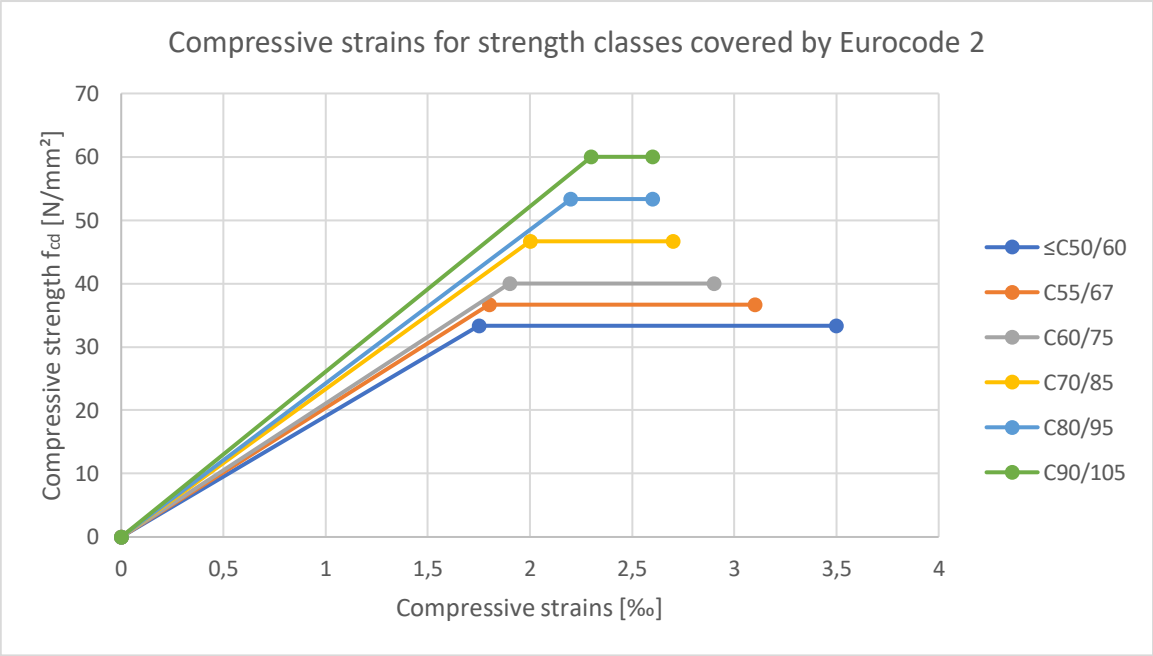


Figure 18 Maximum compressive strains for all strength classes covered by Eurocode 2

The Eurocode also allows for the use of a rectangular stress distribution of the compressive stresses in the concrete, as depicted in the following figure. Two factors are introduced to describe this compressive zone: the factor λ defines the effective height of the compressive zone while the factor η defines the effective strength.

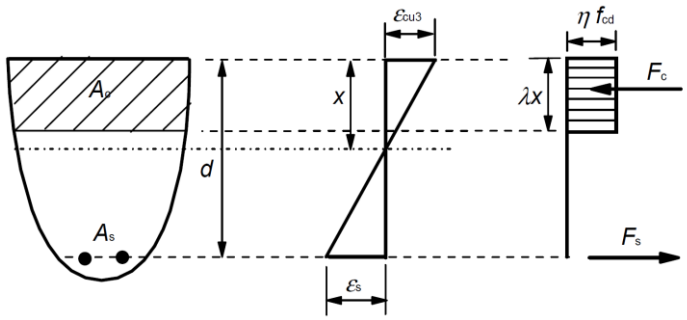


Figure 19 Rectangular stress distribution - Eurocode 2-1-1, p.37

Although the Eurocode 2 does not use the term 'High strength concrete' explicitly, these two parameters are used to account for the more brittle behaviour of concrete with higher strength (above C50/60) by means of reducing the η factor for the more brittle behaviour.

- For $f_{ck} \leq 50$ N/mm^2:

$\lambda = 0{,}8$ and $\eta = 1{,}0$

- For $50 < f_{ck} \leq 90$ N/mm^2:

$$\lambda = 0{,}8 - \frac{f_{ck} - 50}{400}$$

$$\eta = 1{,}0 - \frac{f_{ck} - 50}{200}$$

In addition, if the width of the compressive zone decreases in the direction of the most outer fibre under compression, the value of ηf_{cd} has to be reduced by 10%.

Remark: Post-peak behaviour of UHPC

Concrete of higher strength exhibits post-peak behaviour, which becomes apparent starting with strength class C55. UHPC therefore also exhibits this behaviour. Post-peak behaviour means that in compression the strain of the concrete increases while the compressive stress (the load carrying capacity of the material) reduces, see the following figure. This is also related to the strength class, with an increase of the strength class the limit value for the compressive strain decreases to 2,6 permille.

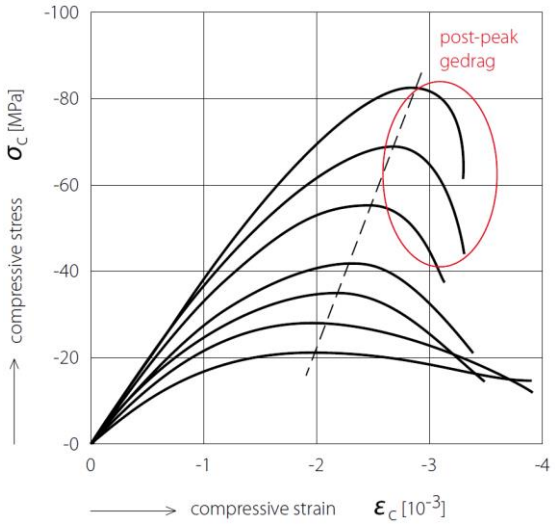


Figure 20 Post-peak behaviour – (Ketel, Willemse, Van Rijen, & Koolen, Rekenmodel VVUHSB (1), 2011), p.54

To account for the post-peak behaviour, maximum values can be imposed upon the strain values. In Eurocode 2 limits are given for the strains, as can be seen in Figure 18.

5.3.3 Reinforcing steel

The material properties of reinforcing steel are discussed in paragraph 3.2 of EC2-1-1. The behaviour of the steel is specified using various properties as mentioned in section 3.2.2. For design calculations the yield strength, tensile strength and ductility are most important.

Material properties are determined via tensile tests, usually the reinforcing steel shows typical steel behaviour, i.e. three different branches can be distinguished: elastic stage, yield stage and hardening stage. Via composition or treatment material properties can be modified, this could result in the loss of a clear yield stage.

In the Eurocode notation the reinforcing steel is classified using the following notation:

BXY

Where:
X: Characteristic yield strength f_{yk}
Y: Ductility class (can be A, B or C)

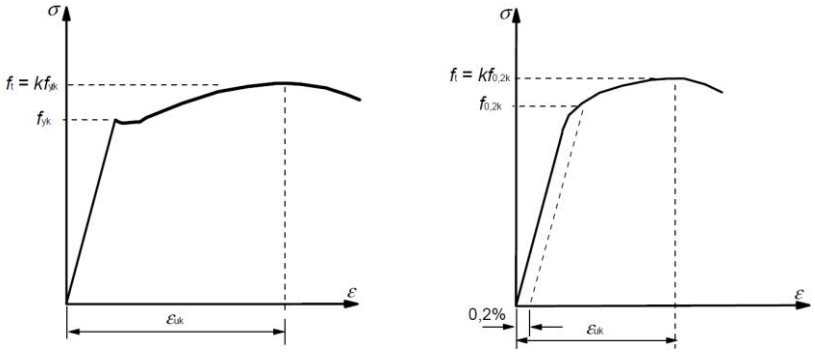
For describing strength two parameters are important:

- Yield strength f_{yk}: Characteristic value of the yield force under axial tensile force divided by the nominal area of the cross section. The rules in the EC2 are valid for $400 < f_{yk} < 600$ N/mm^2, the most common value is 500 N/mm^2.

  Depending on certain treatment types applied to the steel, it may occur that the reinforcing steel does not have a clear yield plateau. In that case the 0,2%-strain value$f_{0,2k}$ is used as an imaginary yield limit.

- Tensile strength f_{tk}: Characteristic value of the maximum force under axial tensile load divided by the nominal area of the cross section.

The reinforcement has to have sufficient ductility. In the code this is defined through the ratio k between the tensile strength f_{tk} and the yield strength f_{yk} and ε_{uk}, which is the characteristic deformation (strain) at maximum force. The following figure shows two typical stress-strain curves for reinforcing steel.



a) warmgewalst staal **b) koudvervormd staal**

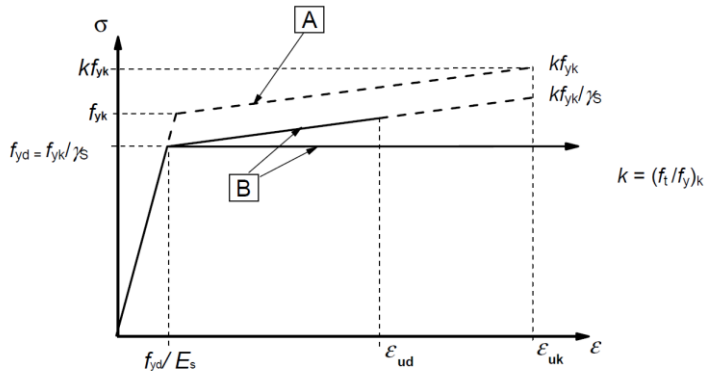
Figure 21 Stress-strain diagrams for reinforcing steel - Eurocode 2-1-1, p.40

Three different ductility classes are distinguished that prescribe different values for the k ratio and ε_{uk}. According to annex C the minimum values are as follows:

Table 12 Ductility classes reinforcing steel

Class	ε_{uk} **[%]**	k **[-]**
A	2,5	1,05
B	5,0	1,08
C	7,5	1,15

For the calculation the following bi-linear schematized graph can be used.



Verklaring

A geschematiseerd
B berekening

Figure 22 Schematized stress-strain diagram - Eurocode 2-1-1, p.42

This graph gives two options for design calculations:

- Option 1: The inclined upper branch is used with a maximum strain of ε_{ud} (defined in national annex to be taken as $\varepsilon_{ud} = 0{,}9 * \varepsilon_{uk}$) and a maximum stress $k * f_{uk}/\gamma_S$ at a strain of ε_{uk};

- Option 2: A horizontal upper branch is used, in this case the maximum strain does not have to be verified.

The design value of the yield strength f_{yd} is determined as follows:

$$f_{yd} = \frac{f_{yk}}{\gamma_s}$$

Where:
f_{yd}: Design value of the yield strength
f_{yk}: Characteristic value of the yield strength
γ_s: Material factor

Note that the material factor for reinforcing steel is smaller than the factor for concrete (1,15 versus 1,5) because of the smaller scatter in the steel strength compared to that of concrete compressive strength. The factor k is defined as follows:

$$k = \frac{f_{tk}}{f_{yk}}$$

In addition, the code gives the following values that may be used in design:

- Volumetric mass: 7850 kg/m^3

- Modulus of elasticity E_s: 200.000 N/mm^2

5.3.4 Prestressing steel

The material properties of prestressing steel are discussed in paragraph 3.3 of EC2-1-1. According the code prestressing elements can be:

- Wires
- Strands
- Bars

Prestressing elements are classified regard strength, relaxation classes, dimensions and properties of the surface.

Strength: For the classification regarding strength, the following three characteristics of the steel are specified:

- Characteristic tensile strength f_{pk}: Characteristic maximum load under axial tension divided by the cross-sectional area of the cross section;
- Characteristic value of the 0,1%-strain limit $f_{p0,1k}$: Characteristic value of the force at 0,1% strain divided by the cross-sectional area of the cross section;
- The strain at maximum loading ε_{uk}

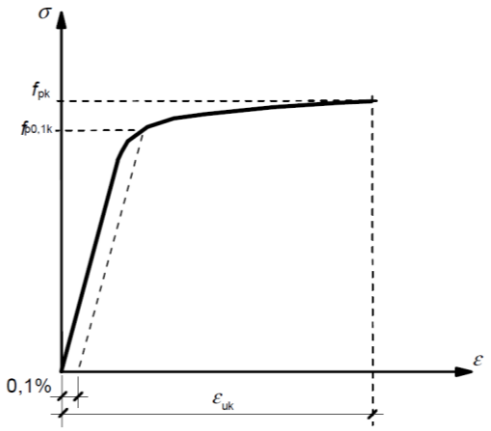


Figure 23 Stress-strain diagram prestressing steel, Eurocode 2-1-1, p.45

Ductility: Prestressing elements have to have sufficient ductility. It may be assumed that the elements have sufficient ductility in tension if the following relationship is satisfied:

$$\frac{f_{pk}}{f_{p0,1k}} \geq k$$

The value of k is, in accordance with the national annex, equal to 1,05.

Relaxation: The code defines three relaxation classes. Relaxation losses can be determined using certificates of manufacturers or, alternatively, using the following equations:

- Class 1: Wires or strands and normal relaxation

$$\frac{\Delta\sigma_{pr}}{\sigma_{pi}} = 5{,}39 * \rho_{1000} * e^{6{,}7\mu} * \left(\frac{t}{1000}\right)^{0{,}75(1-\mu)} * 10^{-5}$$

- Class 2: Wires or strands and low relaxation

$$\frac{\Delta\sigma_{pr}}{\sigma_{pi}} = 0{,}66 * \rho_{1000} * e^{9{,}1\mu} * \left(\frac{t}{1000}\right)^{0{,}75(1-\mu)} * 10^{-5}$$

- Class 3: Hot rolled bars

$$\frac{\Delta\sigma_{pr}}{\sigma_{pi}} = 1{,}98 * \rho_{1000} * e^{8\mu} * \left(\frac{t}{1000}\right)^{0{,}75(1-\mu)} * 10^{-5}$$

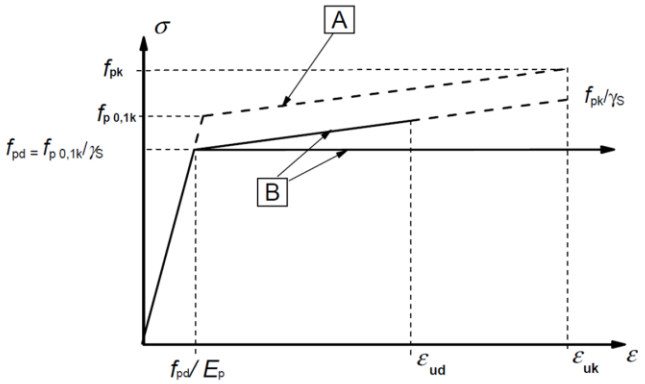
Where:
$\Delta\sigma_{pr}$: Absolute value of relaxation losses of the prestressing
σ_{pi}: For post tensioned steel the absolute value of the initial prestressing ($\sigma_{pi} = \sigma_{pm0}$). For pretensioned steel the maximum tensile stress in the prestressing element minus the direct losses occurring during the stressing
t: Time after stressing
μ: Equals σ_{pi}/f_{pk}
ρ_{1000}: The value of the relaxation loss (in %) at 1000 h after stressing at an average temperature of 20 °C.

The value for ρ_{1000} can be taken equal to 8% for class 1, to 2,5% for class to and to 4% for class 3. The value for t can be taken equal to 500.000 hours for determining the final value of the relaxation losses.

Calculation procedure: For the calculation procedure the following curve is given. The calculations are performed making use of the aforementioned characteristic values: $f_{p0,1k}$, f_{pk} and ε_{uk}. Using this curve to design cross sections gives two options:

- Option 1: An ascending upper branch with a maximum strain value of ε_{ud}, which is according to the national annex equal to $0{,}9 * \varepsilon_{uk}$;

- Option 2: A horizontal upper branch without maximum strain value.



Equations:

$$f_{pd} = \frac{f_{p0,1k}}{\gamma_S}$$

$$\varepsilon_{ud} = 0{,}9 * \varepsilon_{uk}$$

$$\varepsilon_{pd} = \frac{f_{pd}}{E_p}$$

Verklaring

A geschematiseerd
B berekening

Symbols:
f_{pk}: Characteristic tensile strength
$f_{p0,1k}$: Characteristic stress value at 0,1% strain
f_{pd}: Design value of the steel stress
ε_{uk}: Characteristic strain at maximum load
ε_{ud}: Design value of the maximum strain
E_p: Modulus of elasticity
γ_S: Partial safety factor

Figure 24 Schematized stress-strain diagram and equations prestressing steel - Edited, after Eurocode 2-1-1, p.46

Other values given in the code are:

- Modulus of elasticity E_p for wires and bars: 205.000 N/mm^2

- Modulus of elasticity E_p for strands: 195.000 N/mm^2

- Average volumetric mass of prestressing elements: 7850 kg/m^3

- According to EN 10138 the minimum value of ε_{uk} is 3,5%

Other values: The following figure, taken from (Walraven & Braam, 2019), depicts a number of stress-strain diagrams for different steel types. It can be seen that for the prestressing steels there is often no clear yield plateau, this is why the stress that causes a plastic strain of 0,1% ($f_{p0,1k}$) is typically used as an alternative for the yield stress. These graphs are schematized to be used in the calculations.

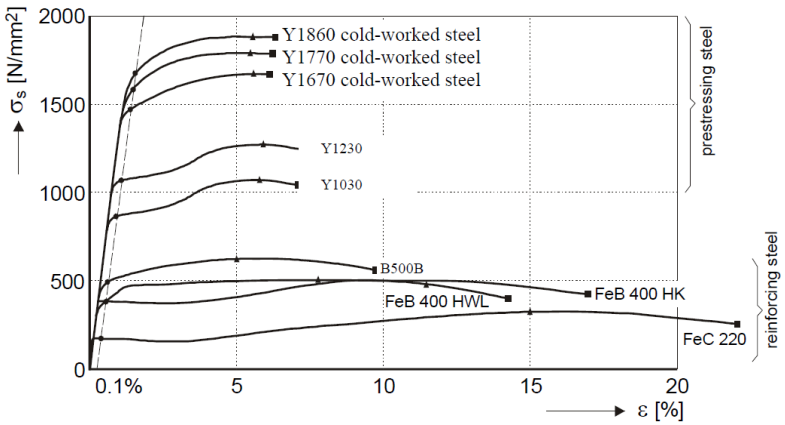


Figure 25 Stress-strain relationships of reinforcing and prestressing steel - (Walraven & Braam, 2019), p.2-6

Commonly used prestressing elements are the strands made of seven wires of steel type Y1860S7. Its properties are summarized in the following table, which is taken from (Walraven & Braam, 2019):

Table 13 Data of prestressing strands used in tendons - (Walraven & Braam, 2019), p.2-7

steel type	Y1860S7	
characteristic diameter (mm)	13,0	15,2
cross-section of steel (mm^2)	100	140
design value of failure load ($A_p f_{pk} / \gamma_s$) (kN)	169	235
Maximum prestressing force after tensioning (kN) $\sigma_{pm0} = 0{,}75\, f_{pk}$ =0,75·1860 = 1395 MPa	140	194
Maximum prestressing force during tensioning (kN) $\sigma_{p,max} = 0{,}80\, f_{pk}$ = 0,80·1860 = 1488 MPa	149	207

Throughout the Eurocode a number of different maximum allowable stress values is imposed:

- During stressing a maximum stress is allowed at the anchorage side of (see 5.10.2.1 (1)):

$$\sigma_{p,max} = \min\{0{,}8 * f_{pk}; 0{,}9 * f_{p0,1k}\}$$

- Directly after tensioning (i.e. applied prestressing force minus direct losses) is not allowed to be larger than (see 5.10.3 (2)):

$$\sigma_{pm0} = \min\{0{,}75 * f_{pk}; 0{,}85 * f_{p0,1k}\}$$

- According to 5.10.2.2 (5), during stressing the concrete compressive stress due to the prestressing and other loads should not exceed $0{,}60 * f_{ck}(t)$

- For pre-tensioned steel this value can be increased, in that case the concrete compressive stress due to the prestressing and other loads should not exceed $0{,}70 * f_{ck}(t)$

- Permanent compressive concrete stress greater than $0{,}45 * f_{ck}(t)$ is allowed if non-linear creep is accounted for in the design.

The following table, taken from (Walraven & Braam, 2019) summarizes characteristics of frequently used types of prestressing steel, the information is determined in accordance with EC2-1-1.

Table 14 Mechanical properties of prestressing steel - (Walraven & Braam, 2019), p.2-21

steel type	type	tensile strength		fracture strain	0,1% proof-stress	maximum tensile stress			slope discontinuity in the σ-ε diagram (ULS)	modulus of elasticity
						during pre-stressing	during pre-stressing with accurate jack	initial stress		
		f_{pk}	f_{pk}/γ_s	ε_{pu}	$f_{p0,1k}$	$\sigma_{p,max}$	$\sigma_{p,max}$	σ_{pm0}	f_{pd}	E_p
		MPa	MPa	‰	MPa	MPa	MPa	MPa	MPa	GPa
Y1030H	bar	1030	936	35	927	773	773	773	843	205 or 170
Y1670C	wire	1670	1518	35	1503	1336	1428	1253	1366	205
Y1770C	wire	1770	1609	35	1593	1416	1513	1328	1448	205
Y1860S7	strand	1860	1691	35	1674	1488	1590	1395	1522	195

5.4 ULS verifications – Bending

5.4.1 Provisions from the AFGC guideline

Scope: In 6.1 of the AFGC guideline, verification of the bending moment capacity of cross sections is covered. The capacity of the cross section is verified by determining the maximum bending moment under an axial force imposed on the cross section. The section applies to elements which cross sections remain approximately plane (undisturbed regions of elements such as beams). For disturbed regions of members, strut and tie models can be used for design.

Assumptions: UHPC cross sections can be regarded as a specific case of fibre-reinforced concrete cross sections. According to the guideline under (2), a number of assumptions is made when calculating the bending moment capacity of FRC cross sections (the cross sections can be reinforced, prestressed or neither). It is assumed that:

1. The plane cross sections remain plane;
2. The strain in bonded reinforcement or prestressing tendons is the same as the strain in the surrounding concrete (both for tension and compression);
3. The stresses in the concrete in compression and tension are derived from the stress-strain diagrams as described in the guideline;
4. The stresses in the reinforcing/prestressing steel are derived from the stress-strain relations as given in EC2-1-1;
5. The initial strain in the prestressing tendons is taken into account when assessing the stresses in the tendons.

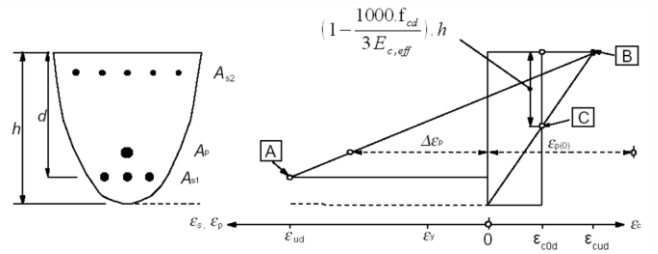
Strain limits: According to (3) and (5) strain limits are to be imposed on the cross section in bending:

- Concrete compressive strain is to be limited to ε_{cud};
- Strain in reinforcing and prestressing steel is to be limited to ε_{ud} in accordance with EC2-1-1;
- Parts of a cross section can be subjected to (approximately) concentric loading, which is the case if $e/h < 0{,}1$. Given examples are compression flanges of box girders. In such a case the mean compressive strain in this cross-sectional part is to be limited to ε_{c0d}.

Minimum eccentricity: The guideline prescribes a minimum eccentricity e_0 to cross sections in compression, the required minimum eccentricity equals:

$$e_0 = \max\left\{\frac{h}{30}; 20\ mm\right\}$$

Ultimate strain rule: The guideline describes that the ultimate strain rule can be used to determine the cross-sectional capacity, this means that the capacity is verified by determining the maximum allowable bending moment under an axial force within the limits of a prescribed stress-strain diagram. This stress-strain diagram is given in the following figure.



Where:

A. Reinforcing steel tension strain limit
B. Concrete compression strain limit
C. Concrete strain limit under pure compression

Figure 26 Acceptable strain distributions in ULS - (AFGC-SETRA 2013), p.101

A number of ultimate strain values are depicted in the figure. These are defined as follows:

- **Point *A***: Corresponds to a 10‰ increase in elongation of the outer most reinforcement from the centre of the cross section, after the strain in the adjacent concrete returns to zero. If:

$$\frac{l_f}{4l_c} + \frac{f_{tj}}{E_{ij}} < 10‰,$$

  then the participation of the fibres (this is in the post-cracking domain) is ignored. This could be the case for deep beams.

- **Point *B***: This point corresponds a shortening of ε_{cud} at the most compressed fibre of the cross-section.

- **Point *C***: This is the compressive strain$\varepsilon_{c0d} = f_{cd}/E_{cm}$ of the concrete at a distance of $(1 - 1000f_{cd}/3E_{cm}) * h$ from the most compressed outermost fibre.

Remarks: For strain hardening material al ultimate strain value $\varepsilon_{u,lim}$ for the fibre resistance can be taken into consideration while in some cases the steel strain can be taken equal to the elastic limit.

Application ultimate strain rule: It is mentioned that the ultimate strain rule can be applied for strain hardening material or for thin plates (because these also behave as strain hardening material). For softening/low strain-hardening material the rule can only be applied if the concrete strength in the cracked part is ignored, meaning that there is no ultimate strain imposed but that the constitutive laws for tension and compression as defined before are applied.

Bending and tensile forces: An additional clause, clause (9), is added to introduce a safety margin in the case of members subjected to high tensile forces. The clause prescribes that for thick members of strain-hardening material or for thin slabs the mean strain in the whole cross-section must not be less than $\varepsilon_{u,lim}/2$ (or in absolute terms: the mean strain in the cross section must be lower than $\varepsilon_{u,lim}/2$).

5.4.2 Calculation procedures bending moment capacity

Although the AFGC guideline gives plenty of information on determining the bending moment capacity, there is no specific calculation procedure. Therefore, such a procedure will be formulated which will be based on various sources such as the AFGC guideline, theory on prestressed concrete and other relevant pieces of literature.

Formulating the stress-strain diagram

The starting point for the bending moment calculation is formulating an appropriate constitutive law in the form of a stress-strain diagram in accordance with the AFGC guideline. In the first part of the guideline, it was mentioned that most UHPC materials fall within the category of low-strain hardening materials. It is

therefore deemed to be appropriate to assume that, up to a certain degree, strain-hardening behaviour may be expected in any case. A practical and simplified stress-strain diagram will be formulated that can be used to describe UHPC displaying strain-hardening behaviour with symbols in accordance with Eurocode 2.

In (Ketel, Willemse, Van Rijen, & Koolen, Rekenmodel VVUHSB (1), 2011) a practical diagram and approach is presented, which is applied in (Van Geffen & Attahiri, 2016) for example. The simplifications to the stress-strain diagram as proposed in the article is based on the constitutive law for strain hardening material from the AFGC-SETRA recommendations from 2002. The Cement article presents the following stress-strain diagram as the starting point.

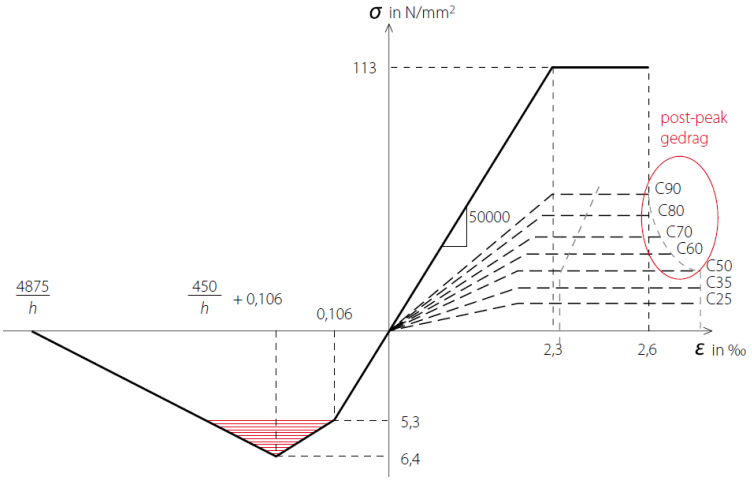


Figure 27 Idealized stress-strain diagram in ULS - (Ketel, Willemse, Van Rijen, & Koolen, Rekenmodel VVUHSB (1), 2011), p.54

After comparison the simplified approach is deemed to be applicable to the calculations as presented in this report as well. The final model, which is presented in Figure 28, can be applied to strain-hardening material. The prerequisite is that the value of the characteristic maximal post cracking stress divided by the fibre orientation factor is above or at least equal to the characteristic elastic tensile strength (cracking of the matrix). The model is not applicable to material displaying softening behaviour.

The symbols between the Eurocode, the guideline and the aforementioned article are not always consistent. Therefore, the following table gives definitions, symbols from the AFGC guideline and EC2 and the symbols that have been adopted.

Table 15 Symbols according to AFGC-SETRA, Eurocode 2 and adopted symbols

Definition	**Symbol**		
	AFGC	EC2	Adopted
Strain at reaching design compressive strength	ε_{c0d}	ε_{c3}	ε_{c3}
Maximum compressive strain at ULS	ε_{cud}	ε_{cu3}	ε_{cu3}
Characteristic value compressive stress	f_{ck}	f_{ck}	f_{ck}
Design value compressive strength	f_{cd}	f_{cd}	f_{cd}
Modulus of elasticity	E_{cm}	E_{cm}	E_{cm}
Characteristic elastic (5% percentile value) tensile strength	$f_{ctk,el}$	$f_{ctk;0,05}$	$f_{ctk,el}$
Design value of tensile strength (tensile strength 1st crack)	-	f_{ctd}	f_{ctd}
Characteristic maximal post cracking stress (stress at $w = 0{,}30$)	f_{ctfk}	-	f_{ctfk}
Design value maximal post cracking stress (stress at $w = 0{,}30$)	$f_{ctfk}/(\gamma_{cf}*K)$	$f_{ctd;2}$	$f_{ctd;2}$
Elastic strain (strain at the first crack)	$\varepsilon_{u,el}$	ε_{ct}	ε_{ct}
Strain corresponding to local peak or crack width $w = 0{,}30$ mm	$\varepsilon_{u,peak}$	-	$\varepsilon_{u,peak}$
Strain corresponding to crack width of $0{,}01 * H$	$\varepsilon_{u,1\%}$	-	$\varepsilon_{u,1\%}$
Ultimate strain for fibre participation	$\varepsilon_{u,lim}$	ε_{ctu}	$\varepsilon_{u,lim}$
Characteristic length	l_c	-	l_c
Fibre length	l_f	-	l_f

Note that for type 1 and 2 materials the characteristic maximal post cracking stress is achieved at the equivalent strain value $\varepsilon_{u,peak}$, which corresponds to a local peak in the post-cracking stage or to an equivalent strain corresponding to a crack width of $w = 0{,}30$ mm if there is no peak. In this design the value of 0,3 mm is therefore used. Following the guideline, for type 3 material this stress corresponds to the ultimate strain $\varepsilon_{u,lim}$, which results from characterisation tests with a maximum of 2,5‰, except when direct tensile tests were applied.

To obtain the simplified curve as presented in (Ketel, Willemse, Van Rijen, & Koolen, Rekenmodel VVUHSB (1), 2011) as presented in Figure 27, the following simplifications are made. First, the declining line from the strain at $w = 0{,}30$ is drawn directly to the ultimate strain value. The graph is, for the sake of simplicity, truncated at the value of the concrete tensile strength (the stress value where the first crack occurs). Above this value no contribution is taken into consideration, the graph is therefore on the conservative side.

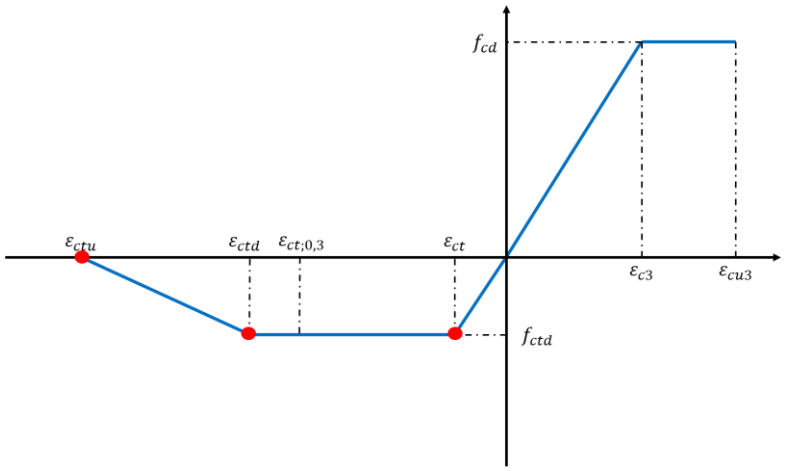
This simplification results in a simpler calculation to determine the contribution of the fibre-reinforced material in tension and is justified by the fact that the neglected area (red area in Figure 27) is relatively small compared to the declining branch of the figure.

To determine the strain value at the point where the horizontal line at stress value f_{ctd} intersects the declining branch, a strain value ε_{ctd} is introduced. An equation for this strain value can be deduced by considering the geometry of the stress-strain diagram.

$$\Delta\varepsilon = \frac{f_{ctd}}{f_{ctd;2}} * \left(\varepsilon_{ctu} - \varepsilon_{ct;0,3}\right)$$

$$\varepsilon_{ctd} = \varepsilon_{ctu} - \Delta\varepsilon$$

The simplified (truncated) stress-strain figure now becomes:



Calculating stresses:

$$f_{cd} = \frac{\alpha_{cc} * f_{ck}}{\gamma_C}$$

$$f_{ctd} = \frac{\alpha_{ct} * f_{ctk,el}}{\gamma_C}$$

Calculating strains:

$$\varepsilon_{ct} = \frac{f_{ctd}}{E_{cm}} = \frac{f_{ctk,el}}{\gamma_c * E_{cm}}$$

$$\varepsilon_{ct;0,3} = \frac{w_{0,3}}{l_c} + \varepsilon_{ct}$$

$$\varepsilon_{ctd} = \varepsilon_{ctu} - \frac{f_{ctd}}{f_{ctd;2}} * \left(\varepsilon_{ctu} - \varepsilon_{ct;0,3}\right)$$

$$\varepsilon_{ctu} = \frac{l_f}{4 * l_c}$$

Figure 28 Adopted simplified stress-strain relationship and equations for the ULS verifications

Remarks:

- In accordance with the AFGC guideline the crack width value $w_{0,3}$ is taken equal to 0,30 mm;
- In case of material with predominant strain hardening behaviour and having to determine the tensile stress at the peak value $w = 0{,}30$ mm, the following equation may be used to calculate the design value for the stress. Note that f_{ctfk} here denotes the characteristic value of the characteristic maximal post cracking stress, which is the stress at a crack width of 0,3 mm (alternative symbol: $\sigma_{w0,3}$).

$$f_{ctd;2} = \frac{f_{ctfk}}{K * \gamma_c}$$

- For the recommended preliminary design values for type 2 material (low strain hardening) as given in the AFGC guideline, the peak is not present and the elastic tensile strength $f_{ctk,el}$ and maximal post cracking stress f_{ctfk} are equal. In that case $\varepsilon_{ctd} = \varepsilon_{ct;0,3}$;

- In the AFGC guideline, the partial factor γ_{cf} is introduced for fibre-reinforced concrete loaded in tension. However, to use the same factors for concrete for the total strain figure, in these calculations this factor is replaced by the partial factor for concrete from the Eurocode;

- The ultimate strain value ε_{ctu} will be limited to a maximum of 2,5 permille, which is in correspondence with the guideline, which prescribes this maximum value except for the cases where direct tensile tests were applied.

Calculation procedure prestressed UHPC

Now a suitable stress-strain diagram has been defined, the procedure for the cross-sectional capacity can be further elaborated on. A calculation procedure based on the equilibrium method for prestressed cross sections of conventional concrete will be formulated, under the assumption that the cross section is rectangular. The main principles of the approach, as for conventional prestressed cross sections, are as follows:

- It is assumed that Bernoulli's hypothesis is valid, in other words: plane sections remain plane and therefore a linear relationship can be used to determine the strains of the fibres over the height of the cross-section;

- The cross section is in equilibrium, which means that the summation of internal and external horizontal forces and bending moments acting on the cross section both equal zero;

- Appropriate stress-strain relationships are used for the different materials, see the simplified stress-strain diagram for the concrete (Figure 28) and those for the reinforcing and/or prestressing steel in the paragraphs 5.3.3 and 5.3.4).

As for prestressed cross sections of conventional concrete the main principle is to start with making an estimation of the height of the concrete compressive zone (which can be done either directly or by using an initial assumption for total steel stress in prestress steel) after which the strains and stresses belonging to this height are determined, all forces are calculated and the equilibrium is checked. This is an iterative process. If no equilibrium is found, a new estimation is made for the height of the concrete compressive zone.

What is different compared to conventional concrete is that for UHPC the contribution of steel fibres is taken into consideration, whereas conventional concrete the tensile strength of the material is generally neglected. This requires a number of modifications to the standard approach for prestressed cross sections of conventional concrete. In the following steps the full procedure will be explained.

Step 1. Identifying all horizontal forces: Based on the (simplified) stress-strain diagrams and the aforementioned assumptions, the following graphs depicted all forces, strains and stresses over the prestressed UHPC cross section can be constructed.

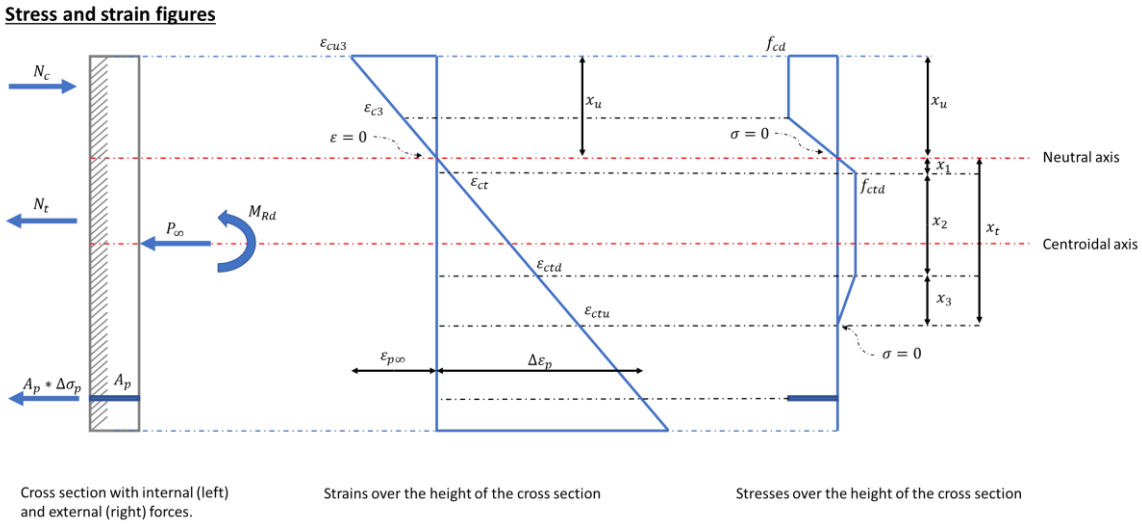


Figure 29 Forces and stresses and strains over the prestressed UHPC cross section

Note that the upward bending moment due to prestressing is accounted for as a load case and is therefore not included in the figure. The horizontal forces acting on the cross section are:

- **Compressive force in the concrete**: Horizontal force due to concrete in compression, important parameters are the height of the compressive zone x_u and its shape described using the α factor:

$$N_c = \alpha * b * x_u * f_{cd} \quad \text{Equation (1)}$$

- **Tensile force in reinforcement (if provided)**: If provided the reinforcing steel contributes to the capacity, in practice it usually yields. Although it is not expected that conventional reinforcement will have to be provided, it is mentioned here for completeness.

$$N_s = A_s * f_{yd} \quad \text{Equation (2)}$$

- **Tensile force in prestressing steel**: The prestressing contributes in two ways to the capacity of the cross section: through an active and a passive contribution. The summation of these two is the total contribution. If it is initially assumed that the total stresses in the prestressing steel in the ULS stage are $\sigma_{pu} = f_{pd}$ and the working prestressing stress is $\sigma_{p,\infty}$, then the two components are:

  - Active contribution: Tensile force in the steel due to the prestressing force that is applied, the working prestressing stress is used to determine this force and it is accounted for as a load (and not at the resistance side):

$$P_{m,\infty} = A_p * \sigma_{p,\infty} \quad \text{Equation (3)}$$

  - Passive contribution: In the use phase the member is loaded and deforms. As a result, the prestressing tendon, which was already stretched due to the prestressing, will be stretched further. The material resists this additional elongation, resulting in an increase of the forces in the prestressing steel. This is the passive contribution. The capacity of the prestressing cable remaining after applying the prestressing can be used for this passive contribution:

$$\Delta N_p = A_p * \left(f_{pd} - \sigma_{p,\infty}\right) \quad \text{Equation (4)}$$

- **Tensile force in the concrete**: UHPC has a considerable tensile capacity. Contrary to conventional concrete cross sections, this tensile capacity is taken into consideration as well. In Figure 28 and Figure 29 it can be seen that the tensile zone can be divided into three parts (to triangles and one rectangle), which means that the total tensile force in the concrete is as follows:

$$N_t = N_{t1} + N_{t2} + N_{t3}$$ Equation (5)

Using Figure 29, the following equations are formulated to determine the individual components of the concrete tensile force:

$$N_{t1} = \frac{1}{2} * x_1 * b * f_{ctd}$$

$$N_{t2} = x_2 * b * f_{ctd}$$

$$N_{t3} = \frac{1}{2} * x_3 * b * f_{ctd}$$

Step 2. Height of concrete compressive and tensile zone: The next step is formulating an equation to determine the height of the concrete compressive zone x_u, which can be done by considering the horizontal equilibrium of the cross section. It should hold that:

$$N_c = N_t + P_{m,\infty} + \Delta N_p$$ Equation (6)

However, in addition to x_u, the height of the individual concrete tensile zones (values x_1, x_2 and x_3) are unknown as well. To solve this problem three additional equations have to be formulated. Using these equations, the height of the individual tensile zones is related to the height of the concrete compressive zone, this way only one unknown value remains: x_u. The additional equations can be derived from Figure 29 and are as follows:

$$x_1 = \frac{\varepsilon_{ct}}{\varepsilon_{cu3}} * x_u$$

$$x_2 = \frac{\varepsilon_{ctd} - \varepsilon_{ct}}{\varepsilon_{cu3}} * x_u$$

$$x_3 = \frac{\varepsilon_{ctu} - \varepsilon_{ctd}}{\varepsilon_{cu3}} * x_u$$

The internal equilibrium can now be considered. By substituting equations (1) and (5) into (6), the following is obtained:

$$\alpha * b * x_u * f_{cd} = \frac{1}{2} * x_1 * b * f_{ctd} + x_2 * b * f_{ctd} + \frac{1}{2} * x_3 * b * f_{ctd} + P_{m,\infty} + \Delta N_p$$

By expressing the unknowns x_1, x_2 and x_3 as functions of x_u the following is obtained:

$$\alpha * b * x_u * f_{cd} = \left(\frac{1}{2} * \frac{\varepsilon_{ct}}{\varepsilon_{cu3}} + \frac{\varepsilon_{ctd} - \varepsilon_{ct}}{\varepsilon_{cu3}} + \frac{1}{2} * \frac{\varepsilon_{ctu} - \varepsilon_{ctd}}{\varepsilon_{cu3}}\right) * x_u * b * f_{ctd} + P_{m,\infty} + \Delta N_p$$

Rewriting results in:

$$\alpha * b * x_u * f_{cd} - \left(\frac{1}{2} * \frac{\varepsilon_{ct}}{\varepsilon_{cu3}} + \frac{\varepsilon_{ctd} - \varepsilon_{ct}}{\varepsilon_{cu3}} + \frac{1}{2} * \frac{\varepsilon_{ctu} - \varepsilon_{ctd}}{\varepsilon_{cu3}}\right) * x_u * b * f_{ctd} = P_{m,\infty} + \Delta N_p$$

Taking x_u out of the brackets yields the equation for the height of the concrete compressive zone:

$$x_u = \frac{P_{m,\infty} + \Delta N_p}{\alpha * b * f_{cd} - \left(\frac{1}{2} * \frac{\varepsilon_{ct}}{\varepsilon_{cu3}} + \frac{\varepsilon_{ctd} - \varepsilon_{ct}}{\varepsilon_{cu3}} + \frac{1}{2} * \frac{\varepsilon_{ctu} - \varepsilon_{ctd}}{\varepsilon_{cu3}}\right) * b * f_{ctd}}$$ Equation (7)

Step 3. Determining the strains: The height of the compressive zone is now known and the linear distribution of the strains over the cross-section has been shown in Figure 29. Assuming a strain of ε_{cu3} at the outer most compressed concrete fibre, expressions for all other strains can be determined as well:

- **Reinforcing steel**: Although not expected to be required, the expression for the strains in reinforcing steel is given below:

$$\frac{\varepsilon_{cu3}}{x_u} = \frac{\varepsilon_{cu3} + \varepsilon_s}{d_s} \leftrightarrow \varepsilon_s = \varepsilon_{cu3} * \left(\frac{d_s}{x_u} - 1\right)$$

- **Prestressing steel**: The increase of the strains in the prestressing steel due to the elongation during loading (passive contribution) is as follows:

$$\frac{\varepsilon_{cu3}}{x_u} = \frac{\varepsilon_{cu} + \Delta\varepsilon_p}{d_p} \leftrightarrow \Delta\varepsilon_p = \varepsilon_{cu3} * \left(\frac{d_p}{x_u} - 1\right)$$

The applied prestressing also caused strains in the material (initial prestressing):

$$\varepsilon_{p,\infty} = \frac{\sigma_{p,\infty}}{E_p}$$

This makes that the total strain in the prestressing steel, i.e. the summation of the strains due to active and passive contribution, is as follows:

$$\varepsilon_p = \varepsilon_{p,\infty} + \Delta\varepsilon_p \rightarrow \varepsilon_{cu3} * \left(\frac{d_p}{x_u} - 1\right) + \frac{\sigma_{p,\infty}}{E_p}$$

- **Concrete under tension**: The strains in the concrete under tension can be calculated using the equations given in Figure 28. By determining the strains, the height over which the steel fibres contribute to the cross-sectional capacity can be determined.

Step 4. Calculating all stresses & forces: Now the strains have been calculated the stresses and subsequently the forces in the reinforcing steel, prestressing steel and concrete under tension can be determined.

- **Reinforcing steel**: Although not expected to be required, the expression for the strains in reinforcing steel is given below. In practice, the reinforcement usually yields, which means that $\sigma_s = f_{yd}$ and:

$$N_s = A_s * f_{yd}$$

- **Prestressing steel**: For the start of the calculation, a value for the total stress σ_{pu} in the prestressing steel was assumed. Because the strains are now known, the 'real' occurring stresses can now be calculated. Taking the sloping branch for the prestressing steel, the stresses can be calculated as follows:

$$\sigma_{pu} = f_{pd} + \frac{\varepsilon_p - \frac{f_{pd}}{E_p}}{\varepsilon_{uk} - \frac{f_{pd}}{E_p}} * \left(\frac{f_{pk}}{\gamma_s} - f_{pd}\right)$$

The increase of the force (passive contribution) in the prestressing steel now is:

$$\Delta N_p = A_p * \left(\sigma_{pu} - \sigma_{p,\infty}\right)$$

- **Concrete under tension**: Using equation (5) the tensile forces in the concrete can now be determined as well, by substituting the values for x_1, x_2 and x_3. To simplify later stages of the calculation procedure, the resulting force of the individual tensile forces can be determined. Taking the neutral axis as the reference point of the resulting force N_t (see Figure 29):

$$x_{Nt} = \frac{\sum N_{ti} * x_i}{\sum N_{ti}} = \frac{N_{t1} * \frac{2}{3} * x_1 + N_{t2} * \left(x_1 + \frac{1}{2} * x_2\right) + N_{t3} * \left(x_1 + x_2 + \frac{1}{3} * x_3\right)}{N_{t1} + N_{t2} + N_{t3}}$$

Where:
N_{ti}: Tensile capacity of part 'i', i being 1, 2 or 3
x_i: Distance between centre of gravity of part 'i' and the neutral axis of the cross section

Step 5. Check horizontal equilibrium: At the start of the calculation an estimation was made for the total stress in the prestressing steel and the height of the concrete compressive zone. Now it should be verified whether these assumptions were correct and, if so, equilibrium is found in the cross section. There are two ways to verify equilibrium:

- Option 1 – Stresses prestressing steel: In step 1 at the beginning of the procedure an estimate was made for the total stresses in the prestressing, which was used to determine the height of the concrete compressive zone. The total stress in the prestressing steel is determined in step 4, based on the strain based on the assumed stress. If the assumed stress for σ_{pu} equals the estimated value the estimation was correct.

- Option 2 – Height x_u: Now all forces have been determined, the horizontal equilibrium can be verified following equation (6) using the height of the compressive zone as the parameter. There are three possible outcomes, the benefit of this method is that it gives more insight:

Table 16 Height of concrete compressive zone

x_u too large if:	$N_t + P_{m,\infty} + \Delta P < N_c$
x_u assumed correctly if:	$N_c = N_t + P_{m,\infty} + \Delta P$
x_u assumed too small if:	$N_c < N_t + P_{m,\infty} + \Delta P$

If equilibrium is not found, the total calculation procedure has to performed again using a new estimate for the total stress in the prestressing steel or the height of the concrete compressive zone. This is an iterative process.

Step 6. Bending moment capacity: If horizontal equilibrium has been found, the bending moment resistance M_{Rd} can be determined around the selected reference point. Any reference point can be used for this, in this case the top fibre is chosen. Note that the following table only holds for rectangular cross sections (equal width over the full height).

Table 17 Determining bending moment capacity

Component	Force	Lever arm
Concrete compressive force	N_c	$\beta * x_u$
Prestressing (active contribution)	$P_{m\infty}$	e_t
Prestressing (passive contribution)	ΔN_p	d_p
Concrete tensile force	N_t	x_{Nt}

Now the bending moment capacity can be determined:

$$M_{Rd} = -\beta * x_u * N_c + P_{m\infty} * e_t + \Delta N_p * d_p + N_t * x_{Nt}$$

Where:
e_t: Distance top fibre to centroidal axis
d_p: Effective height of the cross section
x_{Nt}: Distance resultant of tensile concrete forces to top fibre

Step 7. Verify rotational capacity: After calculating the bending moment capacity the final step is to verify the rotational capacity of the cross section. Theoretically, if reinforcement reaches the yield stress it starts to yield and the cross section rotates (behaves as a hinge). The capacity of a cross section to do so is the rotational capacity. The rotational capacity is of importance because the deformations give a warning effect (yielding before crushing of the concrete results in cracking and deformations before failure), it is required

for redistribution of forces and for statically indeterminate structures it contributes to resisting imposed deformations.

The height of the concrete compression zone can be seen as a measure for the curvature of the cross section. Therefore, the rotational capacity depends on the height of the concrete compressive zone and a maximum is to be imposed on this value. As the AFGC guideline does not give provisions for determining the rotation capacity, this is taken from the EC2 and the national annex. According to article 5.5 of EC2-1-1 and national annex, the following relation has to be satisfied for concrete for which $f_{ck} > 50$ N/mm^2:

$$\delta \geq \frac{7f}{\varepsilon_{cu} * 10^6 + 7f} + \frac{x_u}{d}$$

$$f = \frac{\left(\frac{f_{pk}}{\gamma_s} - \sigma_{pm,\infty}\right) A_p + f_{yd} A_s}{A_p + A_s}$$

Where:
x_u: Height of concrete compressive zone
d: Effective height ($d \approx 0{,}9 * h$)
ε_{cu}: Strain at failure of concrete
δ: Ratio of the redistributed moment to the elastic bending moment
f: Factor accounting for the ''weighed contribution'' of both the reinforcing and prestressing steel

Under the assumption that there is no redistribution this results in the following requirement:

$$\frac{x_u}{d} \leq \frac{\varepsilon_{cu} * 10^6}{\varepsilon_{cu} * 10^6 + 7f}$$

Performing iterations and summary of the calculation procedure

As mentioned before, determining the bending moment capacity of the prestressed cross section is an iterative procedure. For the first calculation a certain total steel stress in the prestressing steel is assumed which is used to determine the height of the compressive zone, or this value is directly assumed after which the full calculation procedure is performed and horizontal equilibrium is checked. If horizontal equilibrium is not achieved, a new estimate for the total stress in the prestressing steel or the height of the concrete compressive zone. This is repeated until equilibrium is found. Spreadsheets can be used to perform this iterative procedure. The procedure used for the calculations can be summarized schematically as follows:

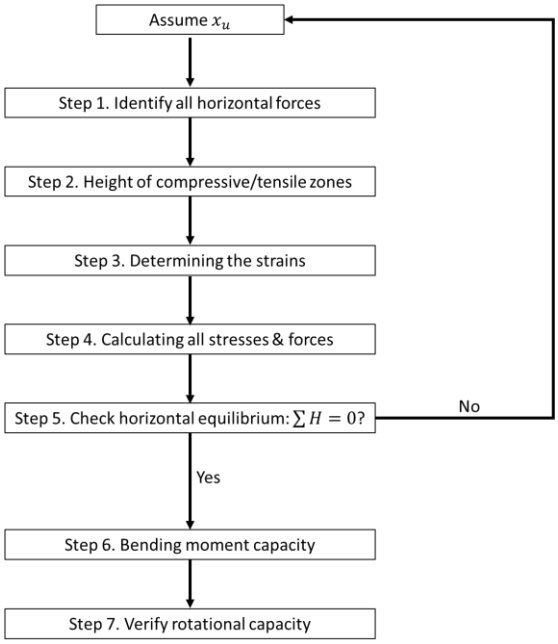


Figure 30 Calculating the bending moment capacity

5.5 ULS verifications – Shear

5.5.1 Provisions from the AFGC guideline

In 6.2 of the AFGC guideline, verification of the shear capacity is covered, which replaces sections 6.2.1 up to 6.2.3 of Eurocode 2. The shear capacity is to be taken as follows, note that similar to EC2, the failure of the concrete compressive strut is the upper bound for the shear capacity.

$$\min(V_{Rd}; V_{Rd,max}) \qquad \text{Equation (8)}$$

Where:
V_{Rd}: Tensile resistance of the ties in the concrete
$V_{Rd,max}$: The resistance of the concrete compressive strut

Tensile resistance of the concrete ties

The tensile resistance of the concrete ties is determined as the summation of three individual components:

$$V_{Rd} = V_{Rd,c} + V_{Rd,s} + V_{Rd,f} \qquad \text{Equation (9)}$$

Where:
$V_{Rd,c}$: Concrete contribution
$V_{Rd,s}$: Shear reinforcement contribution
$V_{Rd,f}$: Fibre contribution

Concrete contribution $V_{Rd,c}$: The expression for the concrete contribution to the shear capacity depends on the type of cross section.

- Reinforced cross section:

$$V_{Rd,c} = \frac{0{,}21}{\gamma_{cf}\gamma_E} k f_{ck}^{\frac{1}{2}} b_w d$$

- Prestressed cross section (both for cross sections with or without reinforcement):

$$V_{Rd,c} = \frac{0{,}24}{\gamma_{cf}\gamma_E} k f_{ck}^{\frac{1}{2}} b_w z$$

- Cross section without prestressing and without reinforcement:

$$V_{Rd,c} = \frac{0{,}18}{\gamma_{cf}\gamma_E} k f_{ck}^{\frac{1}{2}} b_w h = \frac{0{,}21}{\gamma_{cf}\gamma_E} k f_{ck}^{\frac{1}{2}} b_w 0{,}875h$$

Where:

$$k = 1 + \begin{cases} 3 * \frac{\sigma_{cp}}{f_{ck}}, \sigma_{cp} \geq 0 \\ 0{,}7 * \frac{\sigma_{cp}}{f_{ctk,0.05}}, \sigma_{cp} < 0 \end{cases}$$

$$\sigma_{cp} = N_{Ed}/A_c$$

f_{ck}: Characteristic compressive strength
k: Factor accounting for presence of axial force
b_w: Smallest width of the cross-section in the tensile area
z: Inner lever arm corresponding to the bending moment in the element under consideration
d: Distance from the most severely compressed outermost point to the longitudinal reinforcement

N_{Ed}: Axial force in the cross section due to loading or prestressing ($N_{Ed} > 0$ for compression)
A_c: Area of the concrete cross section
γ_E: Safety coefficient as such that $\gamma_{cf} * \gamma_E$ is equal to 1,5.

The following remarks are made in the guideline:

- The afore mentioned formulas are coherent if $z = 0{,}9 * d$ and $d = 7/8h$ in the case of passive reinforcement;
- The influence of imposed deformations on N_{Ed} may be ignored when calculating σ_{cp};
- The coefficient γ_E accounts for the uncertainty at the time of developing the guidelines about extrapolating high performance concrete formulas for which $f_{ck} \leq 90$ MPa, to values for UHPC. It is stated in the guideline that studies have shown that safety is provided by the coefficient, but that this is a hypothesis that still has to be verified by experimental results.

Contribution of the fibres $V_{Rd,f}$: Design value for the fibre contribution to the shear capacity is:

$$V_{Rd,f} = \frac{A_{fv}\sigma_{Rd,f}}{tan\theta}$$

Where:

$A_{fv} = b_w * z$ (for rectangular or T-sections)

$z \approx 0{,}9 * d$

A_{fv}: Area of the fibre effect
z: Inner lever arm corresponding to the bending moment in the element under consideration
$\sigma_{Rd,f}$: Residual tensile strength of the fibre-reinforced cross-section
θ: Angle between the principal compression stress and the beam axis, recommendation: take $\theta \geq 30^o$

- For type 1 and type 2 UHPC (softening or low strain-hardening):

$$\sigma_{Rd,f} = \frac{1}{K\gamma_{cf}} \frac{1}{w_{lim}} \int_0^{w_{lim}} \sigma_f(w)\, dw$$

$$w_{lim} = \max(w_u; w_{max})$$

Where:
w_u: Ultimate crack width attained at the ULS for bending combined with axial forces, on the outer fibre, under the moment exerted in the section
w_{max}: Maximum admissible crack width, with reference made to 7.3.1.

- For type 3 UHPC (strain-hardening):

$$\sigma_{Rd,f} = \frac{1}{K\gamma_{cf}} * \frac{1}{\varepsilon_{lim} - \varepsilon_{el}} \int_{\varepsilon_{el}}^{\varepsilon_{lim}} \sigma_f(\varepsilon)\, d\varepsilon$$

With:

$$\varepsilon_{lim} = \max(\varepsilon_u; \varepsilon_{max})$$

Where:
ε_u: The ultimate strain attained at the ULS for bending combined with axial forces, on the outer fibre, under the moment exerted in the section
ε_{max}: Maximum strain to be taken equal to ε_{lim}

Remarks:

- When calculating the shear capacity of reinforced concrete without axial force, when calculating the area of the fibre effect A_{fv} one can use $z \approx 0{,}9 * d$;
- The remark is made that the value for $\sigma_{Rd,f}$ is calculated by considering the vertical component of the force provided by the fibres along a bending crack;
- For the K-value the value for K_{global} will be used, except for very small elements;
- For shear analysis an element can be considered to be very small if the width b_w and the height h are both less than $5 * l_f$. Note that l_f is the length of an individual fibre.

Contribution of the shear reinforcement $V_{Rd,s}$: The contribution of the shear reinforcement ($V_{Rd,s}$) to the shear capacity is:

- Vertical reinforcement:

$$V_{Rd,s} = \frac{A_{sw}}{s} z f_{ywd} \cot\theta$$

- Inclined reinforcement:

$$V_{Rd,s} = \frac{A_{sw}}{s} z f_{ywd} (cot\theta + cot\alpha) sin\alpha$$

Where:
A_{sw}: Cross-sectional area of the shear reinforcement
s: Spacing of the stirrups
f_{ywd}: Design yield strength of the shear reinforcement
α: The angle between the passive shear reinforcement and the beam axis

Ultimate strength of the concrete compressive strut $V_{Rd,max}$

The strength of the concrete compressive strut is as follows:

$$V_{Rd,max} = 2 * 1{,}14 * \frac{\alpha_{cc}}{\gamma_c} b_w z f_{ck}^{\frac{2}{3}} * \frac{1}{cot\theta + tan\theta} \qquad \text{Equation (10)}$$

Where:
θ: Angle between the principal compressive stress and the beam axis

Remarks:

- In the interim recommendations, a coefficient γ_E was present in this equation (10) to account for the fact that there were limited experimental results for this equation. This coefficient is no longer taken into account in the equation because in the guideline it is stated that test results have shown the robustness of the formula and that it is considered to be safe if there are enough fibres and a moderate K-value.

- Moreover, it is explained in the guideline that the term for the compressive strut resistance results from extrapolation of the BPEL rules (previous French guideline on prestressed concrete) for HPC to UHPC. It was verified during shear tests carried out in 2009.

Reduction prestressing ducts

In clause (5) it is stated that in the case the web contains grouted or non-grouted ducts, the duct diameter should be deduced from the web thickness b_w, the width must be reduced to the nominal width $b_{w,nom}$:

$$b_{w,nom} = b_w - \sum \emptyset$$

Remarks:

- Even if the duct is grouted, the width has to be reduced because of the fibre efficiency. The grout has a considerably lower strength than UHPC (it is mentioned that a compressive strength of more than 30 MPa is required by guidelines), therefore it is safe to ignore the compressive strength of the grout when verifying the compressive strength of the struts.

- In EC2 a factor 1,2 is applied to the duct diameter in the case of non-grouted ducts, grouted plastic ducts and unbonded tendons. For UHPC this is reduced in the AFGC to 1,0 because the fibres are considered to be replacing the transverse reinforcement in preventing the splitting of the struts.

Clauses (6) and (7) give information on the bending moment correction rule and reduction of loads to the shear force in case these loads are applied within a certain distance from the supports. See, if relevant, the AGFC (and EC2) for more details.

5.5.2 Calculation procedures shear capacity

Further elaboration

In this subparagraph the calculation procedure will be formulated that is to be used in the (preliminary) design, this will be done based on the aforementioned provisions from the AFGC guideline together with information from additional sources.

As shown in equation (9) the shear capacity is split up into three components. According (Falbr, Hunger, & Spiesz, 2016) to this approach does not correspond to the failure mechanism that occurs in reality but this is done because of lack of experimental results, because this approach. At the same time, this approach is said to be conservative. Also, a maximum allowable shear force is defined, determined by the failure of the concrete compressive strut, see equation (10).

Concrete component: For the concrete contribution a distinction is made between different types of cross sections. This is an important distinction because by prestressing the UHPC, a higher capacity can be reached.

Given the fact that the cross section is prestressed, the following equation is taken:

$$V_{Rd,c} = \frac{0{,}24}{\gamma_{cf}\gamma_E} k f_{ck}^{\frac{1}{2}} b_w z$$ Equation (11)

Because of the application of prestressing (compressive stress):

$$k = 1 + 3 * \frac{\sigma_{cp}}{f_{ck}}$$

Moreover: $\sigma_{cp} = N_{Ed}/A_c$ and $z = 0{,}9 * d$

Fibre component: The big difference compared to conventional concrete is the contribution of steel fibres, which is known to result in a significant of capacity compared to cross sections without. This was already

concluded from the reference projects in the literature study, examples of larger structures were given that were executed without additional conventional shear reinforcement. In (Bouvy, 2012) in which FEM was used to simulate experimental results, significant increases in shear force capacity were obtained for only adding 0,8% by volume of steel fibres. The capacity went up to a factor five if no conventional shear reinforcement (thus only the concrete capacity was considered) was provided.

It is assumed that the material is low strain-hardening (type 2), therefore the equations from the AFGC guideline are as follows (note that the partial factor γ_{cf}) is moved from the expression for $\sigma_{Rd,f}$ to $V_{Rd,f}$.

$$V_{Rd,f} = \frac{A_{fv}\sigma_{Rd,f}}{\gamma_{cf} * tan\theta}$$ Equation (12)

$$\sigma_{Rd,f} = \frac{1}{K}\frac{1}{w_{lim}}\int_0^{w_{lim}} \sigma_f(w)\, dw$$ Equation (13)

For the fibre contribution two factors are of particular interest:

- Area A_{fv} is the area of the cross section which is corrected (reduced) to determine the area over which the fibres are effective. The guideline proposes $A_{fv} \approx b_w * z = b_w * 0{,}9 * d$.
- The residual tensile strength $\sigma_{Rd,f}$ is more difficult to determine, it describes the remaining tensile strength of the material after cracking. The integral complicates the calculations and in reality, experiments should be performed. In available literature different ways were found to deal with the residual tensile strength and/or the integral in particular.
    - In (Falbr, Hunger, & Spiesz, 2016) the assumption was made that the residual tensile strength at a crack width of 0,30 mm is approximately 70% of the original tensile strength, after which this value was used in calculations.
    - In (Bouvy, 2012) it was found that a conservative assumption is included in the equation (13) for the fibre contribution in the AFGC. In the guideline the maximum crack width is limited to 0,30 mm because the equations were developed for a mixture with a maximum grain size of 0,30 mm. For the equation it was assumed that the fibres no longer contribute if the crack width exceeds 0,30 mm. It was concluded in the article that the maximum allowable crack width for this equation can be, depending on the grain size, increased to 0,37 mm for a more accurate but still safe result.
    - In (Ketel, Willemse, Van Rijen, & Koolen, Dwarskracht- en kolomberekening VVUHSB, 2011) more insight was given into the residual tensile strength. The residual tensile strength is the remaining tensile strength of the material after the first crack. The integral used to determine this value describes the area under the tensile part of the stress-strain diagram between the point of cracking ($w = 0$) and w_{lim}, as depicted in the following figure:

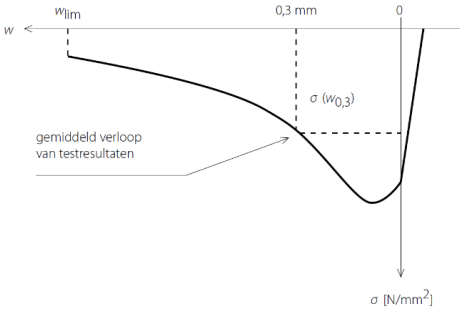


Figure 31 Experimentally obtained stress-strain relation of UHPC in tension – (Ketel, Willemse, Van Rijen, & Koolen, Rekenmodel VVUHSB (1), 2011), p.88

By dividing the area under the curve by the crack width w_{lim} an average residual tensile strength value is obtained. The integral complicates the calculation and depends on the mixture that is applied, because the stress-strain diagram is constructed is obtained from test results.

Based on literature it was concluded in the article that a safe approximation is obtained by setting the residual tensile strength equal to the stress value $\sigma(w_{0,30})$, which is the stress corresponding to a crack width of 0,30 mm.

The latter approach will be used in further elaboration. For the symbol $\sigma(w_{0,30})$ also the symbol $f_{ctfk}/(\gamma_{cf}K)$ is used in the AFGC guideline (and the symbol $f_{ctd;2}$ is used in this report as well, see Table 15). That means that equation (13) changes into:

$$\sigma_{Rd,f} = \frac{f_{ctfk}}{\gamma_{cf} * K} = f_{ctd;2}$$

And equation (12) therefore changes into:

$$V_{Rd,f} \approx \frac{A_{fv} * f_{cftk}}{K_{global} * \gamma_{cf} * tan\theta} = \frac{A_{fv} * f_{ctd;2}}{tan\theta} \qquad \text{Equation (14)}$$

Reinforcement component: Based on all previously collected information it is expected no reinforcement will be required, therefore, this term is omitted.

Summary

All required information from the AFGC is now collected and further terms have been defined wherever required. Using equations (10), (11) and (14), the following figure is composed, which summarizes the verification for the shear capacity. Note that the assumptions made throughout the previous considerations are listed as well.

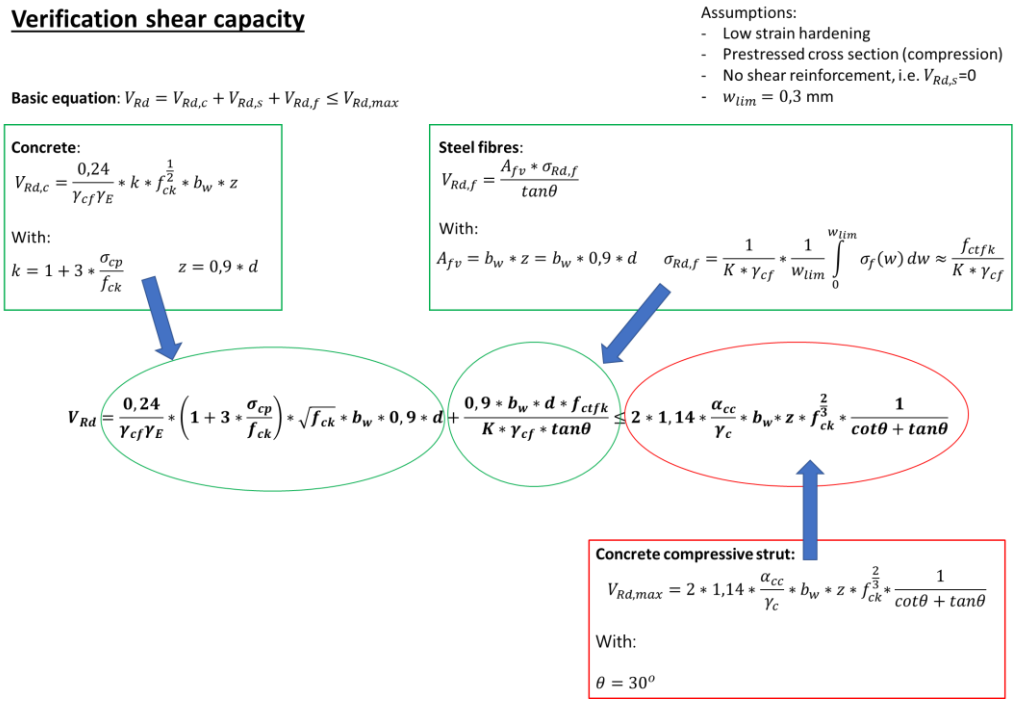


Figure 32 Overview calculation procedure shear capacity

Remarks - Conservative approach AFGC

In the literature studied many sources illustrated that UHPC has a significantly larger shear force capacity compared to conventional concrete. Although the higher strength of the concrete itself results in an increase, it is predominantly the contribution of the steel fibres that gives the high capacity.

Many different sources among which are (Falbr, Hunger, & Spiesz, 2016) and (Russell & Graybeal, 2013), suggest that the provisions from the AFGC guideline are on the safe side when it comes to shear capacity of beams.

The AFGC calculates the total shear force capacity by adding up the three individual components. In (Bouvy, 2012) for example this approach was analysed. It was concluded that the capacity found using the guideline was smaller than the capacity found from FEM simulations of experimental results. This was because of the conservative assumption for the fibre contribution (crack width allowed) and in addition it was concluded that synergy occurs if both fibres and reinforcement are applied, the total capacity then is greater than the summation of the individual components.

5.6 Provisions Eurocode 2 on ULS verifications

5.6.1 Calculation procedures bending moment capacity Eurocode 2

The bending moment capacity of prestressed cross sections of the concrete types as covered by the Eurocode 2 can be determined in a way similar to the approach described in 5.4.2. The only differences are:

- For concrete types covered by Eurocode 2 the contribution of concrete in tension is neglected;
- Material properties of the concrete are in accordance to what is discussed in 5.3.2.

5.6.2 Calculation procedures shear capacity Eurocode 2

Discussion of Eurocode 2

The Eurocode 2 covers conventional normal strength concrete and, although not explicitly mentioned as such, high strength concretes up to and including strength class C90/105. This section covers the paragraphs of Eurocode 2 that correspond to the paragraphs of the AFGC guideline on shear force capacity that were discussed in 5.5 (i.e. Eurocode 2 paragraphs. 6.2.1-6.2.3). The code introduces three definitions in 6.2.1:

- $V_{Rd,c}$: Shear force capacity of elements without shear reinforcement
- $V_{Rd,s}$: Shear force capacity of the shear reinforcement
- $V_{Rd,max}$: Maximum shear force capacity of the element, limited by failure of the concrete compressive strut

The main principles for the shear force verification as mentioned in 6.2.1 are:

- For elements where $V_{Ed} \leq V_{Rd,c}$ no shear reinforcement is required, except for minimum reinforcement if required by (4) in 6.2.1. This minimum requirement is related to execution, redistribution capacity of forces in transverse direction, etc.
- For elements where $V_{Ed} > V_{Rd,c}$ shear reinforcement is to be provided as such that $V_{Ed} \leq V_{Rd}$. The maximum value $V_{Rd,max}$ cannot be exceeded by load V_{Ed}.
- If shear reinforcement is to be provided, the concrete capacity has to be neglected. The shear force has to be restrained completely by the reinforcement $V_{Rd,s}$.

Elements without shear reinforcement

Concrete capacity: Section 6.2.2. describes elements without shear reinforcement. According to (1) the shear force capacity of elements without shear reinforcement is:

$$V_{Rd,c} = \left[C_{Rd,c} * k * (100 * \rho_l * f_{ck})^{\frac{1}{3}} + k_1 * \sigma_{cp}\right] * b_w * d \qquad \text{Equation (15)}$$

Equation (15) may be regarded as an upper limit of the concrete capacity, but this equation also has a minimum value:

$$V_{Rd,c} = \left[v_{min} + k_1 * \sigma_{cp}\right] * b_w * d$$

If no axial forces are present, the minimum value is determined according to the following equation. This is a lower bound value which can always be applied.

$$V_{Rd,c} = v_{min} * b_w * d = 0{,}035 * k^{\frac{3}{2}} * \sqrt{f_{ck}}$$

Where:

$$k = 1 + \sqrt{\frac{200}{d}} \leq 2{,}0$$

$$\rho_l = \frac{A_{sl}}{b_w * d}$$

$$\sigma_{cp} = \frac{N_{Ed}}{A_c} < 0{,}2 * f_{cd}$$

f_{ck}: Characteristic value of the compressive strength
A_{sl}: Cross section of the longitudinal reinforcement at the cross section under consideration
b_w: Smallest width of the cross section in the tensile zone
σ_{cp}: Factor accounting for presence of normal forces due to loading or prestressing (compression: $N_{Ed} > 0$)
A_c: Cross sectional area
k: Scale factor

Conforming the national annex, $C_{Rd,c} = 0{,}12$ and $k_1 = 0{,}15$.

Remark regarding UHPC: As the previous equations may already suggest the capacity of the concrete element without shear reinforcement is influenced by multiple factors, among which are:

- Uncracked compressive zone, depending on the concrete strength class this can contribute significantly to the shear capacity;
- Friction forces in the crack due to rough edges of the crack surface, this is called the aggregate interlocking effect;
- Dowel action of the longitudinal reinforcement;
- The presence of prestressing;
- Dimensions of the cross section.

Because there are multiple factors involved, the equations in the Eurocode are empirically determined. However, using these aforementioned influencing factors it is possible to describe qualitatively an important difference between concrete of normal and higher strength.

The main difference between concrete of normal strength and higher strength is the way in which cracking occurs. The crack develops through the weakest parts of the material. For normal strength concrete this is these are the interfaces between the aggregate and the paste. For high strength concrete the crack propagates through the aggregate, due to the strong matrix the aggregate particles have become the weakest links in the material. This can be seen in the following figure:

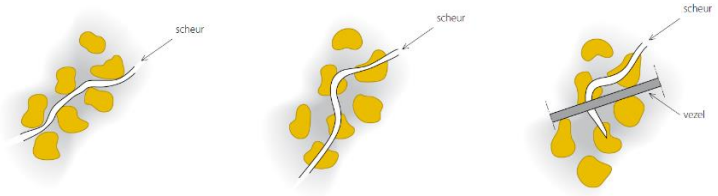


Figure 33 Cracking of conventional concrete (left), UHPC (middle) and fibre-reinforced UHPC (right) – (Ketel, Willemse, Van Rijen, & Koolen, Dwarskracht- en kolomberekening VVUHSB, 2011), p.87

As a result of this the surface of the cracks in high strength concrete, and UHPC in particular, are very smooth compared to the surface of the cracks in conventional concrete. As a result, the contribution of the interlocking effect is very low and when compared relatively to normal strength concrete the shear force capacity of the higher strength concrete is less. The option to add steel fibres increases the shear force capacity.

Tensile splitting shear failure: The aforementioned equations (equation (15)) may be used to determine the shear force capacity of the parts of single span prestressed element without shear reinforcement, that are cracked due to bending.

In parts that are uncracked (if the bending tensile stresses are smaller than $f_{ctd} = f_{ctk;0,05}/\gamma_c$) the concrete capacity is limited by the tensile strength of the concrete. In these uncracked parts the shear force capacity is determined using principal stresses, which is as follows:

$$V_{Rd,c} = \frac{I * b_w}{S} * \sqrt{(f_{ctd})^2 + \alpha_l * \sigma_{cp} * f_{ctd}} \qquad \text{Equation (16)}$$

Where:
I: Second moment of area
b_w: Width of the cross section at the height of the centroid, whilst accounting for prestressing ducts
S: First moment of area of the top part with respect to the centroidal axis
α_l: For elements with pretensioned steel $l_x/l_{pt2} \leq 1{,}0$ and for other type of prestressing 1,0
l_x: Distance from the cross section considered to the start of the transmission length
l_{pt2}: Upper limit value of the transmission length of the prestressing element
σ_{cp}: Concrete compressive stress at the height of the centroidal axis due to loading and/or prestressing

Elements with shear force reinforcement

Using a truss model, the capacity of elements with shear reinforcement can be calculated. An important parameter is the angle θ of the concrete compressive strut, which is between 21,8 and 45°. According to 6.2.3, for elements with vertical reinforcement:

$$V_{Rd,s} = \frac{A_{sw}}{s} * z * f_{ywd} * \cot(\theta) \qquad \text{Equation (17)}$$

Where:
A_{sw}: The cross-sectional area of the shear reinforcement
s: Centre-to-centre distance of the shear reinforcement
f_{ywd}: Design value of the yield strength of the shear reinforcement
v_1: Reduction factor for concrete cracked due to shear force
α_{cw}: Factor accounting for stress state in the compression strut

According to the national annex, the values for v_1 equals $v = 0{,}6 * [1 - f_{ck}/250]$ and α_{cw} is as follows:

$\alpha_{cw} = 1$ — Structures without prestressing

$\alpha_{cw} = \left(1 + \frac{\sigma_{cp}}{f_{cd}}\right)$ — For $0 < \sigma_{cp} \leq 0{,}25 * f_{cd}$

$\alpha_{cw} = 1{,}25$ — For $0{,}25 < \sigma_{cp} \leq 0{,}5 * f_{cd}$

$\alpha_{cw} = 2{,}5 * \left(1 - \frac{\sigma_{cp}}{f_{cd}}\right)$ — For $0{,}5 * f_{cd} < \sigma_{cp} < 1{,}0 * f_{cd}$

In addition, the national annex prescribes that if the stresses in the shear reinforcement in the calculation smaller is than 80% of the characteristic yield strength f_{yk}, the following more favourable values may be used for v_1:

$v_1 = 0{,}6$ For $f_{ck} \leq 60$ N/mm^2

$v_1 = 0{,}9 - \frac{f_{ck}}{200} > 0{,}5$ For $f_{ck} \geq 60$ N/mm^2

Note that if $V_{Ed} > V_{Rd,c}$ the full load has to be restrained by the shear reinforcing steel. Although this might seem conservative, the Eurocode compensates for this by allowing a relatively small minimum angle $\theta = 21{,}8^o$ for the compressive strut. By allowing a small angle, more reinforcement crosses a shear crack, resulting in a larger capacity.

Failure of the concrete compressive strut
The upper limit of the shear force capacity is dictated by failure of the concrete compressive strut, which is determined as follows:

$$V_{Rd,max} = \alpha_{cw} * b_w * z * v_1 * f_{cd} * \frac{1}{\cot(\theta) + \tan(\theta)} \quad \text{Equation (18)}$$

Note that shear reinforcement can also be provided under an angle. In that case the equations (17) and (18) have to be modified according to (4) as given in 6.2.3.

Other provisions – Reduction due to prestressing ducts

In case of the presence of prestressing ducts in the webs, the width of the web has to be reduced to a nominal width. This is as follows:

- Grouted metal ducts and $\phi > b_w/8$:

$$b_{w,nom} = b_w - 0{,}5 * \sum \phi$$

- Grouted metal ducts and $\phi < b_w/8$:

$$b_{w,nom} = b_w$$

- Ducts not grouted, grouted plastic ducts and unbonded tendons:

$$b_{w,nom} = b_w - 1{,}2 * \sum \phi$$

The factor 1,2 is introduced to account for the splitting of the concrete compressive struts due to tensile forces occurring in transverse direction, which may become governing over the concrete compressive strength.

5.7 Bibliography chapter five

Bouvy, L. (2012). Rekenen aan UHSB. *Cement*, 1-5.

Falbr, J., Hunger, M., & Spiesz, P. (2016). Rekenregels UHSB beproefd. *Cement*, 20-27.

Fehling, E., Schmidt, M., Walraven, J., Leutbecher, T., & Fröhlich, S. (2014). *Ultra-High Performance Concrete UHPC*. Berlin: Wilhelm Ernst & Sohn.

Groupe de travail BFUP. (2013, June). Ultra-High Performance Fibre-Reinforced Concretes. *Recommendations*. Association Francaise de Génie Civil.

Ketel, H., Willemse, R., Van Rijen, P., & Koolen, E. (2011). Dwarskracht- en kolomberekening VVUHSB. *Cement*, 86-91.

Ketel, H., Willemse, R., Van Rijen, P., & Koolen, E. (2011). Rekenmodel VVUHSB (1). *Cement*, 50-57.

Lagendijk, P., & Braam, C. (2011). *Cement en beton 2 Constructieleer Gewapend Beton* (Zevende gewijzigde druk 2011 ed.). Aeneas.

NEN. (2011, november). NEN-EN 1992-1-1+C2. *Eurocode 2: Ontwerp en berekening van betonconstructies - Deel 1-1: Algemene regels en regels voor gebouwen*.

NEN. (2020, februari). NEN-EN 1992-1-1+C2/NB+A1. *Nationale bijlage bij NEN-EN 1992-1-1+C2 Eurocode 2: Ontwerp en berekening van betonconstructies - Deel 1-1: Algemene regels en regels voor gebouwen*.

Russell, H. G., & Graybeal, B. A. (2013). *Ultra-High Performance Concrete: A State-of-the-Art Report for the Bridge Community*. Federal Highway Administration (FHWA), Office of Infrastructure Research and Development.

Van Geffen, L., & Attahiri, M. (2016). UHSB als alternatief voor hout. *Cement*, 28-34.

Walraven, J., & Braam, C. (2019, February). Prestressed Concrete.

6

PRELIMINARY DESIGN: DIMENSIONING AND LOADS

6.1 Dimensioning

6.1.1 Main dimensions

In this chapter the dimensions of the deck for the loads and first preliminary design verifications are established. Based on what is defined in the first chapters of this report the dimensions of the deck are as follows:

- Span: $l = 68{,}0$ m
- Total width: $b_{tot} = 16{,}36$ m
- Total length: $l_{tot} = 70{,}70$ m

These values are the same as the dimensions of the existing bridge.

6.1.2 Dimensions of the cross-section

Type of cross section

The span of the bridge is at the edge of what can be achieved with (conventional) prefab beams (See: Literature Study part II). Beams at this span range are typically box beams, these are most suitable because they combine the following properties and characteristics:

- High slenderness ratio due to relatively small structural height
- High prefabrication index
- Large torsional stiffness meaning that cross beams are not required
- Edge beams are not required from a structural point of view

This makes the box beam into the most ideal type of prefab beam for the given project, which is why box beams will be used.

Height of beam

Using the following rule of thumb the required height of the beams is estimated:

$$\frac{l}{h} = 30$$

Where:
l: Span
h: Height

$$\frac{68{,}0}{h} = 30 \rightarrow h = \frac{68{,}0}{30} \approx 2{,}3\ m$$

For beams and slabs the slenderness is typically within this range. For box beams in particular the slenderness is typically between 28 – 32.

Cross sectional dimensions

Within the class of box type cross sections, different options are possible. Given the mechanical properties of the concrete it is expected that less material is required compared to conventional concrete, and the decision is therefore made to start with box beams with widened top flanges (''top hat beams''). This saves material for the webs compared to a more 'conventional' rectangle cross section commonly used in prefab box beams.

For the first design a total of five beams is assumed, this is deemed to be a compromise between performance (i.e. bending moment capacity, shear capacity and bending stiffness), execution (practical dimensions for execution) and saving material (because of the high capacity). Although the shape is that of an inverted top hat beam, for simplicity the beams will be called box beams in the remainder of this report.

The deck consists of these beams, the top height being 2,3 m and the total deck width being 16,36 m. By means of the longitudinal joints between the different beams practical dimensions can be chosen for the width of the beams. For the box beams the following dimensions have to be defined:

- t_{ft}: Thickness of the top flange
- t_{fb}: Thickness of bottom flange
- t_w: Thickness of the web
- w_b: Width of the box
- w_f: Width of a single flange
- h_b: Internal height of the box

The total dimensions are:

w: Total width of the beam, $w = 2 * w_f + 2 * t_w + w_b$
h: Total height of the cross section, $h = t_{ft} + h_b + t_{fb}$

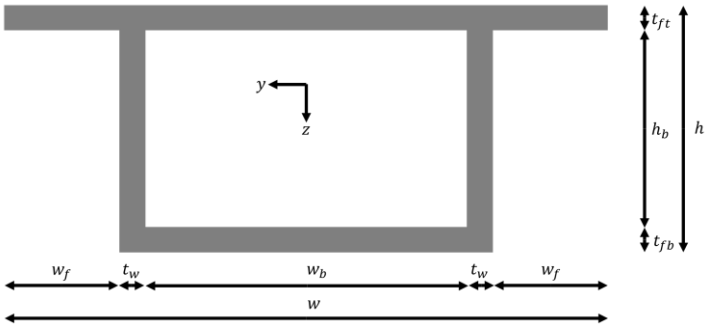


Figure 34 Definition of the cross-sectional dimensions

Thickness top flange t_{ft}: The top flanges of the beams can be regarded as continuous slabs, for a continuous slab a slenderness of 35 is an appropriate value. However, prestressing has to be accommodated at the top flange as well. Therefore, a thickness of 250 mm is taken as the starting value.

Thickness bottom flange t_{fb}: The bottom flange is required to obtain a box cross section, by keeping the elements together. In addition, they accommodate prestressing. A practical value of 150 mm is taken as the starting point.

Thickness of web t_w: The web provides shear capacity to the cross section. Although the capacity of the material is high, a sufficiently large cross-sectional area has to be provided. In addition, it might be the case that the webs have to accommodate prestressing. Therefore, a width of 150 mm is selected as the starting value.

Internal height of box h_b: With the aforementioned dimensions the internal height of the box can be determined.

$h_b = h - t_{ft} - t_{fb} \rightarrow 2300 - 250 - 150 = 1900$ mm

Width of flange and w_f and internal width box w_b: Given the width of the bridge deck and the number of beams, each beam would have to be $16{,}36/5 = 3{,}272$ m wide. This is not a practical value though, and joints are present in reality as well. Therefore, the decision has been made to make each beam 3,2 m wide, the remaining area determine the width of the joints.

A part of the flanges is cantilevering outwards, this length is limited to less than half the width of the box, this is done to limit the bending moments due to the cantilevering flanges. The width is taken as $w_f = 500$ mm. The webs are both 150 mm, that means that the width between the webs equals:

$$w_b = 3200 - 2 * 150 - 2 * 500 = 1900 \text{ mm}$$

The remaining width is realised using in situ joints between the UHPC box beams. Given these widths, four joints of 90 mm will be present between the five beams of the deck.

6.2 Description of the deck geometry and layout

The UHPC deck consists of five UHPC box beams and four longitudinal joints in between. The total span is 68,0 m and the total width is 16,36 m. To construct this deck, a capping beam is constructed on the existing buttresses. On top of this beam five bearings are placed on which the prefab UHPC box beams are positioned to construct the new deck. Using post tensioning of the slab in transverse direction, a solid deck is obtained. A cross section of the deck is given in the following figure. The drawing of the cross section can be found in the annexes to this report (annex I).

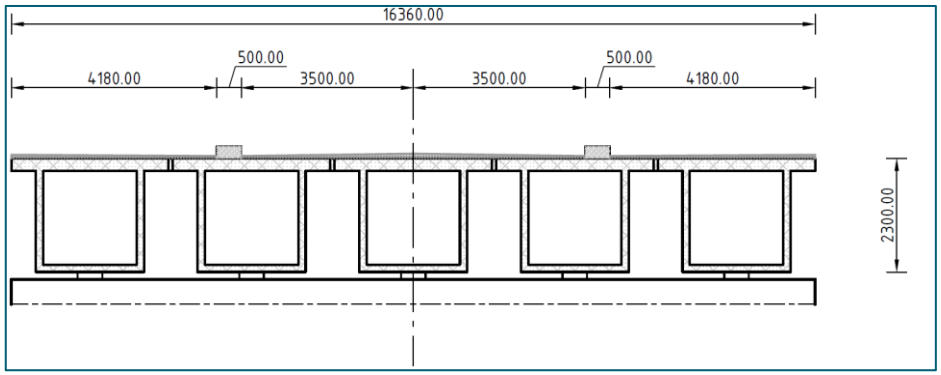


Figure 35 Drawing of the cross section with main dimensions

The layout of the deck for traffic can be seen in the figure as well. The cross section of the deck consists of a single carriageway comprised of two traffic lanes (one lane for each direction) between curbs. On both sides of the carriageway a footway/bicycle lane is positioned, which is separated from the main carriageway by means of these kerbs.

For this preliminary design calculation, it is assumed that an asphalt layer is placed on top of the deck. Although not required from a structural point of view, this accounts for different situations that could be carried out in practice, such as creating a profiled cross section (cross slope for dewatering). Conforming the ROK 1.4 from Rijkswaterstaat, a thickness of 140 mm is taken into account. It is assumed that pavement material is present over the full width of the deck.

Conforming the national annex to EN 1991-2, the kerbs have to be at least 200 mm high to be able to be used as a traffic obstacle. Taking into consideration the height of 140 mm of the pavement, a height of 340 mm is proposed.

6.3 Determining cross-sectional properties

Using the established cross-sectional dimensions, the cross-sectional properties are determined.

Cross-sectional area

By definition, the area of the cross section is as follows:

$$A = \int dA$$

The area is calculated by adding up the areas of the separate parts of the cross section:

$$A = \left(2 * w_f + 2 * t_w + w_b\right) * t_{ft} + 2 * h_b * t_w + (2 * t_w + w_b) * t_{fb}$$

Centre of gravity

The centre of gravity of the cross section is a point that is defined as such that when the origin of the reference system is taken at this point, the first moments of area about the horizontal and vertical axis will be equal to zero. The definitions of the first moments of area are as follows:

$$S_y = \int ydA$$

$$S_z = \int zdA$$

By applying this principle and using the top of the cross section as the reference level, the vertical coordinate of the centre of gravity can be determined as follows:

$$\overline{z} = \frac{S_{\overline{z}}}{A} = \frac{\sum A_i * \overline{z}_i}{\sum A_i}$$

Where:
$S_{\overline{z}}$: A first moment of area of the cross section with respect to the top of the cross section
A_i: Area of segment 'i' of the cross section
$\overline{z}_i$: Distance centre of gravity of segment 'i' with respect to the top of the cross section
$\overline{z}$: Vertical coordinate of the centre of gravity, with respect to the top of the cross section as reference

Because of symmetry, the horizontal coordinate $\overline{y}$ is at the middle of the cross section. Two additional definitions are introduced:

- The distance between the top fibre of the cross section and the centre of gravity:

$$e_t = h - e_b = \overline{z}$$

- The distance between the bottom fibre of the cross section and the centre of gravity:

$$e_b = h - \overline{z}$$

Second moment of area

The second moment of area for bending around the y-axis (horizontal axis) is by definition:

$$I_{zz} = I_{y-y} = \int z^2\, dA$$

For the given cross section, which consists of several parts, Steiner's rule can be applied to determine the second moment of area of the total cross section:

$$I_{zz} = I_{y-y} = \sum I_{zz,i} + A_i * a_i^2$$

Where:
$I_{zz,i}$: Second moment of area of area of component 'i' of the cross section
A_i: Area of component 'i' of the cross section
a_i: Distance between centre of gravity of component 'i' and the centre of gravity of the cross-section

NOTE: In practice different ways of denoting the second moment of area can be used for the same quantity, in structural mechanics I_{zz} is often used while I_{y-y} (or I_y) is often used within the field of steel structures to denote one and the same property: the second moment of area determined along the z-coordinate (i.e. for bending around the horizontal y-axis). The same goes for the second moment of area determined along the y-coordinate (i.e. for bending around the vertical z-axis), for which I_{yy} is often used in structural mechanics while I_{z-z} (or: I_z) is often used in other fields.

Section moduli

Subsequently the section moduli around the horizontal axis are determined:

$$W_{y,t} = \frac{I_{y-y}}{e_t}$$

$$W_{y,b} = \frac{I_{y-y}}{e_b}$$

6.4 Loads and load combinations

6.4.1 Identifying different loads

The following loads are considered in the preliminary design calculations:

- Permanent loads
    - Self-weight of the UHPC beams
    - Concrete kerbs
    - Pavement (asphalt layer)
- Variable loads
    - Traffic loads: Traffic on main carriageway
    - Traffic loads: Traffic (bicycle/pedestrians) on bicycle/pedestrian lanes

Not all relevant loads are considered, this is for simplicity, which is in line with the goal of the preliminary design. In the later design stages all relevant loads will be considered.

The magnitude of the loads that are taken into consideration is determined in accordance with the relevant parts of the Eurocode, this will be elaborated on in the following sections. For convenience the beams are numbered 1 to 5 as well as the joints, that are numbered 1 to 4. In addition, the ''effective widths'' of the outer and inner beams are determined, which equals the width of each of the beams with half the width of the adjacent joint(s).

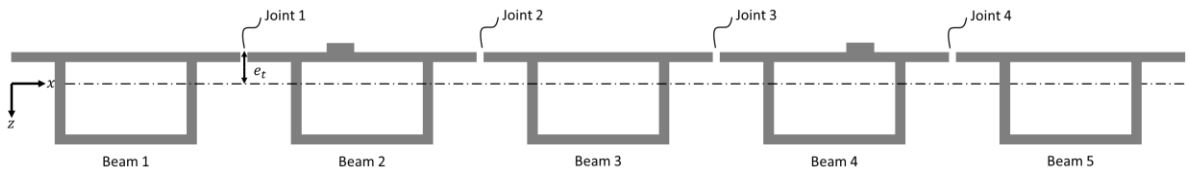


Figure 36 Numbering beams and joints

The effective width of the outer beams (beams 1 and 5):

$$b_{eff,o} = w + \frac{w_{joint}}{2}$$

The effective width of the inner beams (beams 2 – 4):

$$b_{eff,i} = w + 2 * \frac{w_{joint}}{2}$$

6.4.2 Permanent loads

Self-weight of the UHPC beams

In rule (5) of 4.1.2. of Eurocode 0 it is mentioned that the self-weight of the structure may be represented by a single characteristic value and reference is made to NEN-EN 1991-1-1, of which annex A gives average values for various materials. UHPC is not listed in the table though. A whole range of values of UHPC material properties has been obtained, including from annex 9 of the AFGC recommendations. The volumetric weight of UHPC is determined by taking the upper value of the range of values, which is deemed sufficiently accurate for this project stage:

$\gamma_{UHPC} = 28{,}0$ kN/m^3

Permanent loads – Asphalt surfacing

An asphalt layer is assumed to be present on the deck. Conforming ROK 1.4 a thickness of 140 mm is assumed. According to table A.6 of NEN-EN 1991-1-1 for hot rolled asphalt:

$\gamma_{asphalt} = 23{,}0$ kN/m^3

Note: Although considered as self-weight in 5.1 of Eurocode 1, non-structural elements of the bridge are mentioned here as permanent loads (e.g. kerbs).

Permanent loads – Kerbs

The kerbs are assumed to be made of reinforced concrete, which according to annex A of NEN-EN 1991-1-1 has a weight of:

$\gamma_{kerbs} = 25{,}0$ kN/m^3

Dimensions of 500 by 340 mm (width by height) are assumed.

6.4.3 Variable loads

Traffic loads are described in NEN-EN 1991-2. For the global design calculation load model 1 is applied to account for normal traffic on the traffic lanes while model 4 is applied to account for pedestrians and cyclists on the pedestrian lanes.

Traffic loads – Traffic on main carriageway (Load model 1)

According to (1) of 4.2.3, the width of the carriageway is the width between the kerbs. According to the national annex, these kerbs have to be at least 200 mm high, this criterion has been satisfied. This means that the width w equals 7,0 m.

Following (2) of the same paragraph, the total width of the carriageway is divided into a number n_1 of theoretical lanes with width w_1 and remaining area. This is done in accordance with table 4.1.

Breedte van de rijweg w	Aantal theoretische rijstroken	Breedte van een theoretische rijstrook w_l	Breedte van het resterende oppervlak
$w < 5{,}4$ m	$n_1 = 1$	3 m	$w - 3$ m
$5{,}4$ m $\leq w < 6$ m	$n_1 = 2$	$\frac{w}{2}$	0
6 m $\leq w$	$n_1 = Int\left(\frac{w}{3}\right)$	3 m	$w - 3 \times n_1$
OPMERKING Bijvoorbeeld geldt voor een breedte van de rijweg gelijk aan 11 m, dat: $n_1 = Int\left(\frac{w}{3}\right) = 3$ *) en dat de breedte van het resterende oppervlakte gelijk is aan: $11 - 3 \times 3 = 2$m.			

Figure 37 Determining number and width of theoretical lanes – NEN-EN 1991-2, p.35

The number of theoretical lanes is:

$$n_1 = Int\left(\frac{7{,}0}{3}\right) = 2$$

The width of the theoretical lanes w_1 equals 3,0 m. The width of the remaining area is:

$$7{,}0 - 3 * 2 = 1{,}0 \text{ m}$$

Load model 1 (LM1) is described in 4.3.2. and consists of tandem axles (TS) with load per axle of $\alpha_Q Q_k$ and a uniformly distributed load (UDL) of $\alpha_q q_k$. The values for Q_k and q_k depend on the traffic lane 'i' that is under consideration and are determined according to the following table (this includes dynamic amplification):

Positie	Tandemstelsel *TS*	Gelijkmatig verdeelde belasting (GVB)
	Aslast Q_{ik} (kN)	q_{ik} (of q_{rk}) (kN/m^2)
Rijstrook nummer 1	300	9
Rijstrook nummer 2	200	2,5
Rijstrook nummer 3	100	2,5
Overige rijstroken	0	2,5
Resterende oppervlakte (q_{rk})	0	2,5

Figure 38 Characteristic values of the traffic loads – NEN-EN 1991-2, p.39

The α_Q and α_q are correction factors that can be used to account for the type of traffic expected to cross the bridge, which depends on the type of road (e.g. highway vs rural road). According to 4.3.2 of the national annex, the load may be reduced via these factors if the number of trucks per year at the lane for heavy traffic is smaller than $N_{obs} = 2\ M$. This will definitely be the case for the Eefdesebrug, but it has been decided to keep the correction factors equal to 1,0 because this is only the preliminary design stage. These considerations result in the following:

- Theoretical lane 1: $\alpha_{Q1} * Q_{1k} = 1{,}0 * 300$ kN per axle, $\alpha_{q1} * q_{1k} = 1{,}0 * 9{,}0 = 9{,}0$ kN/m^2
- Theoretical lane 2: $\alpha_{Q2} * Q_{2k} = 1{,}0 * 200$ kN per axle, $\alpha_{q2} * q_{2k} = 1{,}0 * 2{,}5 = 2{,}5$ kN/m^2
- Remaining area: $\alpha_{qr} * q_{rk} = 1{,}0 * 2{,}5 = 2{,}5$ kN/m^2

Subsequently the load model is applied to the deck. According to 4.2.4 and 4.3.2, this should be done in such a way that the tandems are positioned along the centre of the theoretical lane and the most unfavourable situation is obtained. This can be done by shifting the theoretical lanes and loads over the width and length of the deck. The UDL is only applied at positions where this has an unfavourable effect. The principle of applying the load model is given in the following figure (the transverse width between the axles is 1,20 m while the contact areas of the wheels are 0,4 by 0,4 m):

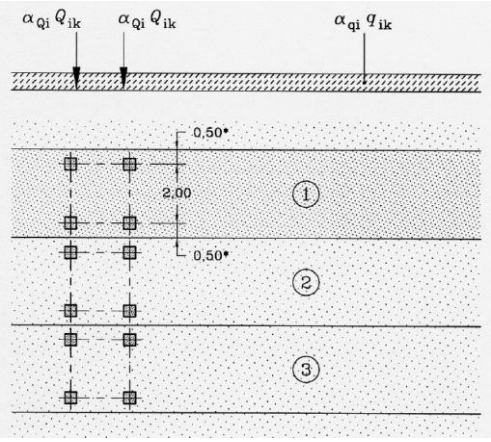


Figure 39 Applying LM1 – NEN-EN 1991-2, p.40

Traffic loads – Bicycle/pedestrian lanes (Load model 4)

This load model is described in 4.3.5 and it resembles a crowd loading with a basic value of 5 kN/m^2, this includes a factor for dynamic effects. This load model is relevant because of the presence of two pedestrian lanes on the bridge, in accordance with the national annex this is accounted for by applying this load model on the respective lanes. According to the national annex (see 5.3.2.1 (3)) for bridges longer than 10 m the load may be reduced:

$$q_{fk} = 2{,}0 + \frac{120}{L+3}, 2{,}5 \leq q_{fk} \leq 5{,}0\ kN/m^2$$

Assuming L equals the span of the bridge, this gives:

$$q_{fk} = 2{,}0 + \frac{120}{68+3} = 3{,}7\ kN/m^2$$

Details on the application of LM1 and LM4 are given in later paragraphs of this chapter.

Prestressing

The loads due to the prestressing forces will be calculated in the next chapter.

6.4.4 Load combinations

Provisions from EN 1990 and EN 1991

The verification of the ultimate limit state is described in 6.4 of EN 1990. The ultimate limit state STR is considered, which means that it must be validated that:

$$E_d \leq R_d$$

E_d: Design value of the effects of actions
R_d: Design value of the corresponding resistance.

To determine the effects of the actions, load combinations have to be formulated. According to 6.4.3.2, for the STR-limit state the least favourable of the following two expressions should be applied:

- Eq. 6.10a.

$$E_d = \sum_{j\geq 1} \gamma_{G,j} G_{k,j} + \gamma_P P + \gamma_{Q,1}\psi_{0,1} Q_{k,1} + \sum_{i>1} \gamma_{Q,i}\psi_{0,i} Q_{k,i}$$

- Eq. 6.10b.

$$E_d = \sum_{j\geq 1} \zeta_j \gamma_{G,j} G_{k,j} + \gamma_P P + \gamma_{Q,1} Q_{k,1} + \sum_{i>1} \gamma_{Q,i}\psi_{0,i} Q_{k,i}$$

Where (after: EN 1990):
E_d: Design value of effect of actions
γ_G: Partial factor for permanent actions, also accounting for model uncertainties and dimensional variations
G_k: Characteristic value of a permanent action
γ_P: Partial factor for prestressing actions (reference made to EN 1992)
P: Relevant representative value of a prestressing action (reference made to EN 1992)
γ_Q: Partial factor for variable actions, also accounting for model uncertainties and dimensional variations
ψ_0: Factor for combination value of a variable action
Q_k: Characteristic value of a single variable action
ζ: Reduction factor for unfavourable permanent actions G

According to 6.4.4 the partial factors γ and combination factors ψ for the load have to be taken from NEN-EN 1991 and annex A of NEN-EN 1990.

According to (4) and the national annex, table NB.15 – A2.4(B), the following table is to be used for the design of the structural elements.

Tabel NB.15 – A2.4(B) — Rekenwaarden voor de belastingen (STR/GEO) (groep B)

Blijvend en tijdelijke ontwerpsituaties	Blijvende belastingen		Voor-spanning	Overheersende veranderlijke belasting [a)]	Tegelijkertijd optredende veranderlijke belastingen [a]	
	Ongunstig	Gunstig			Belangrijkste (indien aanwezig)	Andere
(Vgl. 6.10a)	$\gamma_{G,j,sup}G_{k,j,sup}$	$\gamma_{G,j,inf}G_{k,inf}$	$\gamma_P P$		$\gamma_{Q,1}\psi_{0,1}Q_{k,1}$	$\gamma_{Q,i}\psi_{0,i}Q_{k,i}$
(Vgl. 6.10b)	$\xi\gamma_{G,j,sup}G_{k,j,sup}$ waarbij $\xi = 0{,}89$	$\gamma_{G,j,inf}G_{k,j,inf}$	$\gamma_P P$	$\gamma_{Q,1}Q_{k,1}$		$\gamma_{Q,i}\psi_{0,i}Q_{k,i}$
[a] Veranderlijke belastingen zijn die, die zijn beschouwd in tabellen NB.12 – A2.1, NB.13 – A2.2 en A2.3.						

Figure 40 Design values for the loads (STR/GEO, group B) – NA to NEN-EN 1990, p.31

In addition, again according to the national annex, the values for γ are to be taken from the following table:

Gevolgklasse	β	G			Verkeer (met $\psi = 1$)	Overig veranderlijk (met $\psi = 1$)
		$\gamma_{G,j,sup}$		$\gamma_{G,j,inf}$		
		6.10a	6.10b (incl. ξ)	6.10a en 6.10b		
CC1	3,3	1,20	1,10	0,9	1,20	1,35
CC2	3,8	1,30	1,20	0,9	1,35	1,5
CC3	4,3	1,40	1,25	0,9	1,5	1,65

$\gamma = 0$ voor gunstig werkende veranderlijke belastingen

Voor γ_P zie de aanbevelingen in de desbetreffende materiaalgebonden Eurocodes 1992 t/m 1999.

Voor de berekening van het effect van ongelijkmatige zettingen geldt dat $\gamma_{G,set} = 1{,}20$ in het geval van een lineaire berekening en $\gamma_{G,set} = 1{,}35$ in het geval van een niet lineaire berekening. Gunstig werkende zettingsverschillen worden niet in rekening gebracht. De grootte van de zettingen is bepaald op basis van de karakteristieke belastingscombinatie en de karakteristieke waarden voor de grondeigenschappen.

OPMERKING De factor K_{FI} volgens B 3.3 is in de waarden van γ verwerkt; voor de zettingsberekening blijft de betrouwbaarheidsdifferentiatie achterwege.

Figure 41 Load factors for traffic bridges (STR/GEO, group B) – NA to NEN-EN 1990, p.33

Values for the ψ-factors for bridges for road traffic are given in A.2.2.6 table NB.12 - A2.1 from the national annex to EN 1990. This table is given in the following figure.

Belasting	Symbool		ψ_0	ψ_1	ψ_2
Verkeersbelastingen (zie NEN-EN 1991-2+C1:2015, tabel 4.4)	gr1a (LM1 + voetgangers- of fietspad-belastingen)	TS	0,8	0,8	0,4
		UDL		0,8	
		Horizontale belasting		0,8	
		Voetgangers- + fietspad-belastingen		0,8 [d]	
	gr1b (enkele as)		0	0,8 [b]	0
	gr2 (horizontale krachten dominant)		0,8	0,8 [c]	0
	gr3 (voetgangersbelastingen)		0	0,8 [b]	0
	gr4 (LM4 – belasting door een menigte)		0	0,8 [b]	0
	gr5 (LM3 – speciale voertuigen)	TS	0	0,8 [b]	0
		UDL		0,8 [b]	
		Horizontale belastingen		0,8 [b]	
		Speciaal voertuig		1,0 [b]	
Windkrachten	F_{wk}	blijvende ontwerpsituatie	0,3	0,6 [b]	0
		Uitvoering	0,8	0	0
	F_w*		1,0	0	–
Thermische belastingen	T_k		0,3	0,8 [b]	0,3 [a]
Sneeuwbelastingen	$Q_{Sn,k}$	blijvende ontwerpsituatie	0	0	0
		Uitvoering	0,6	0	0
Belastingen tijdens de bouw	Q_c		1,0	0	1,0

[a] In de uiterste grenstoestand mag voor ψ_2 voor thermische belasting de waarde 0 zijn aangehouden.

[b] Voor aanrijding op of onder de brug en aanvaring is $\psi_2 = 0$.

[c] Voor scheurvomingsberekeningen van beton zijn de verschillende waarden van ψ_2 gelijk aan de waarden behorend bij gr1a (zie voor de waarden van ψ Tabel NB.19).

[d] Voor scheurvormingsberekeningen van beton moet $\psi_2 = 0{,}4$ zijn aangehouden.

OPMERKING Groepen verkeersbelastingen hoeven niet met elkaar te zijn gecombineerd.

Figure 42 ψ-factors for traffic bridges – NA to NEN-EN 1990, p.29

NEN-EN 1991 gives additional rules regarding combining different load models for traffic with other loads. According to 4.5.1, the presence of the different load models and load on bicycle/pedestrian lane at the same time is accounted for using so-called ''load groups''. For the formulation of load combinations, each of these ''load groups'' is to be considered as a single characteristic load. The national annex provides table NB.3 – 4.4a, which formulates these ''load groups'', this table is given in the following figure.

Belastings-type		Rijweg						Voet- en fietspaden
		Verticale krachten				Horizontale krachten		Alleen verticale krachten
Verwijzing		4.3.2	4.3.3	4.3.4	4.3.5	4.4.1	4.4.2	5.3.2.1
Belastings-systeem		BM1 (TS en UDL)	BM2 (enkele as)	BM3 (bijzondere voertuigen)	BM4 (mensen-menigte)	Rem- en versnellings-krachten	Centrifugaal-krachten en krachten in dwarsrichting	Gelijkmatig verdeelde belastingen
Groepen van belastingen	gr1a	Karakteristieke waarde				0,8 × karakte-ristieke waarde	0,8 × karakte-ristieke waarde	0,4 × karakte-ristieke waarde
	gr1b		Karakteristieke waarde					
	gr2	0,8 × karakteristieke waarde				Karakteristieke waarde	Karakteristieke waarde	0,4 × karakte-ristieke waarde
	gr3							Karakteristieke waarde [a]
	gr4				Karakteristieke waarde [b]			
	gr5	0,8 × karakteristieke waarde [c]		Karakteristieke waarde		0,8 × karakteristieke waarde [c]	0,8 × karakteristieke waarde [c]	
		De gearceerde vakken zijn de overheersende belastingscomponent (aangeduid als component behorend bij de groep)						

[a] Zie 5.3.2.1. Er behoort slechts één voetpad als belast te zijn beschouwd, indien het effect hiervan ongunstiger is dan bij belasting op twee voetpaden.
[b] Inclusief de belasting op voet- en fietspaden.
[c] Vast te stellen voor afzonderlijke projecten.

Figure 43 Determining groups of traffic loads (characteristic values) – NA to NEN-EN 1991-2 p.15

In accordance with the table, the characteristic values of LM1 are combined with the characteristic values of LM4 that are multiplied with a factor of 0,4. Together, these loads form the load group ''gr1a''.

Formulating the load combinations

The different loads, partial factors and combination factors have been determined. An overview of the obtained parameters is given, after which load combinations are formulated.

Permanent loads: The partial factors for the permanent loads are determined in accordance with table NB.16 – A2.4(B):

- For equation 6.10a: $\gamma_G = 1{,}40$
- For equation 6.10b: $\gamma_G * \zeta = 1{,}25$

The different permanent loads are:

- Self-weight of the beams: $G_{k,beams}$
- Asphalt layer: $G_{k,asphalt}$
- Kerbs: $G_{k,kerbs}$

Variable loads: In this preliminary design calculation only the vertical traffic loads due to LM1 on the traffic lane and LM4 on the pedestrian lanes is taken into consideration. In accordance with table NB.3 – 4.4a from the national annex to EN 1991, this results in (group gr1a):

$Q_k = 1{,}0 * Q_{k,LM1} + 0{,}4 * Q_{k,LM4}$.

- Both 6.10a and 6.10b: $\gamma_Q = 1{,}50$ for traffic loads.

Where:
$Q_{k,LM1}$: Effects due to LM1 on the traffic lane
$Q_{k,LM4}$: Effect of LM4 on the pedestrian lanes

According to table NB.12 - A2.1, the ψ_0-factor for this load group equals 0,8. In accordance with table NB.16 – A2.4(B) of EN 1990, the partial factor for variable traffic loads equals 1,5.

Note that for the design calculations the characteristic values of LM1 $Q_{k,LM1}$ have to be split into the characteristic values of the uniformly distributed loads $Q_{k,ULD,LM1}$ and of the concentrated loads $Q_{k,axle,LM1}$.

Combinations: The different characteristic loads can now be determined and all other relevant parameters have been obtained (partial factors and combination factors). Substituting all values into the equations for 6.10a and 6.10b, the following equations are found:

- Eq. 6.10a:

$$E_d = 1{,}40 * \left(G_{k,beams} + G_{k,asphalt} + G_{k,kerbs}\right) + \gamma_P P + 0{,}8 * 1{,}5 * Q_k$$

- Eq. 6.10b:

$$E_d = 1{,}25 * \left(G_{k,beams} + G_{k,asphalt} + G_{k,kerbs}\right) + \gamma_P P + 1{,}5 * Q_k$$

These equations will be elaborated on in the remainder of this chapter by formulating the loads and determining the governing beam and its internal forces.

Serviceability limit state (SLS): The code prescribes different combinations for verifying the serviceability limit state. Details on the serviceability limit state for road traffic bridges can be found in 3.4, 6.5, A2.4.1 and A.2.4.2 of NEN-EN 1990 and the national annex. The frequent combination is used (reversible limit state). The combination is defined as follows:

$$\sum_{j\geq 1} G_{k,j} + P + \psi_{1,1} Q_{k,1} + \sum_{i>1} \psi_{2,i} Q_{k,i}$$

All γ-factors for the loads are set equal to '1,0'. This is in accordance with the national annex. According to table NB.12 – A2.1 of the national annex, the ψ_1 value for gr1a traffic loads is 0,8. If all relevant symbols and values are plugged into the equation, the result is:

$$G_{k,beams} + G_{k,asphalt} + G_{k,kerbs} + P + 0{,}8 * Q_k$$

6.5 Modelling and governing beam

6.5.1 Principle of the model

A simple model is proposed that will be used to determine the governing beam, cross sectional forces and deflection. The transverse and longitudinal direction are studied separately.

- First the transverse direction is analysed: all loads are positioned on the deck and the traffic loads are positioned as such that the most unfavourable situation in transverse direction and the governing beam are obtained and determined;

- Second the longitudinal direction is considered by the axle loads again as such that the most unfavourable position or positions in longitudinal direction are obtained for the governing beam.

The third step then is to determine the internal forces and deflections for the governing beam for the loads in these most unfavourable positions.

6.5.2 Transverse direction

The different loads are positioned onto the deck. Special attention goes to the variable loads (LM1), these loads have to be positioned as such that the most unfavourable situation is obtained. For this calculation a conservative assumption is made: it is assumed that there is no interaction between the different beams. If a concentrated load or an (part of an) uniformly distributed load is placed onto a beam, the beam carries this entire force.

In reality there is a certain interaction between the UHPC beams, which is obtained via post tensioning of the beams in transverse direction. The reason that this effect is neglected in this stage of the project is because for a simple model it cannot be quantified what the magnitude of this effect will be, especially because the components of the box beams are relatively slender. The effect of this assumption will be analysed in more detail in chapter 8.

Note that this is a conservative approach, but in the preliminary design stage this is still justifiable, as on the of the goals is to obtain a first impression of the required dimensions. In later design stages more detailed calculation procedures are carried out after which the design will be optimised. For the preliminary design the positioning of the loads onto the deck in transverse direction will now be further clarified.

Self-weight of the UHPC beams

The self-weight of the beam is modelled as a line load along the axis of the beam.



Figure 44 Self-weight of the beams

With a cross section of 1,7 m^2 and the weight of 28 kN/m^2 this results in a line load of:

$G_{k,beams} = 1{,}7 * 28 = 47{,}6$ kN/m^1

Permanent loads – Asphalt surfacing

The asphalt layer is assumed to be present over the full area of the deck and it can be modelled as a line load over the full length of the beams.

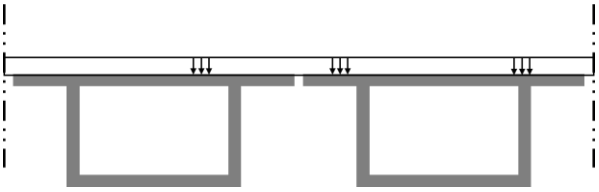


Figure 45 Permanent load due to the asphalt layer

With the dimensions as defined earlier the uniformly distributed force has a magnitude of:

$q_{k,asphalt} = 0{,}14 * 23 = 3{,}22$ kN/m^2

By multiplying this uniformly distributed load with the effective width of the beams, a line load is found of:

$G_{k,asphalt} = 3{,}245 * 3{,}22 = 10{,}45$ kN/m^1 for the outer beams

$G_{k,asphalt} = 3{,}290 * 3{,}22 = 10{,}59$ kN/m^1 for the inner beams

Permanent loads – Kerbs

Kerbs are positioned to mark the main carriageway, the kerbs are placed on beams 2 and 4:

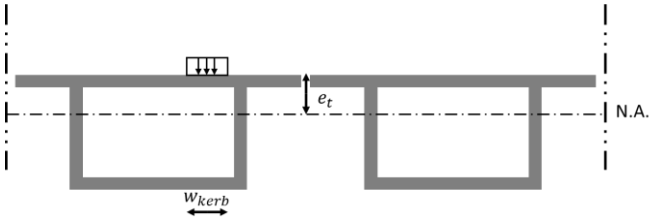


Figure 46 Permanent load due to the kerbs

By considering the dimensions of the kerbs and the weight of concrete, these kerbs can be taken into consideration as (eccentric) line loads on the respective beams:

$$G_{k,kerbs} = h_{kerbs} * w_{kerbs} * \gamma_c$$

$$G_{k,kerbs} = 0{,}34 * 0{,}50 * 25 = 4{,}25 \text{ kN/m}^1$$

Traffic loads – Bicycle/pedestrian lanes (Load model 4)

A uniformly distributed load is applied onto the bicycle/pedestrian lanes, from the edge of the deck to the kerb, to account for the presence of this kind of traffic.

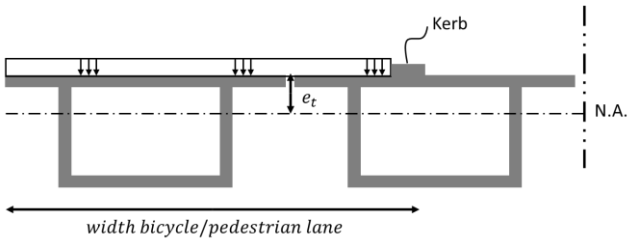


Figure 47 Variable load on the pedestrian lanes

Conforming EN 1991 a uniformly distributed load $q_{fk} = 3{,}7$ kN/m^2 is determined. By multiplying this value with the width over which the outer two beams are loaded, the magnitude of (eccentric) line loads is obtained. In addition, these values are multiplied by a factor 0,4 to account for the simultaneous presence of LM1 and LM4 (gr1a).

- For the outer beams (beams 1 and 5):

$$0{,}4 * Q_{k,LM4} = 0{,}4 * q_{fk} * b_{eff,o} = 0{,}4 * 3{,}7 * 3{,}245 = 4{,}80 \text{ kN/m}^1$$

- For the inner beams (beams 2 and 4):

$$0{,}4 * Q_{k,LM4} = 0{,}4 * q_{fk} * (w_{ped} - b_{eff,o}) = 0{,}4 * 3{,}7 * (4{,}18 - 3{,}245) = 1{,}38 \text{ kN/m}^1$$

Where:
w_{ped}: Total width of the bicycle/pedestrian lanes

Traffic loads – Traffic on main carriageway (Load model 1)

LM1 is positioned as such that the most unfavourable situation is obtained in transverse direction, three different load configurations are possible:

- Configuration 1: Lane 1 directly next to the kerb, lane 2 next to it and after that the remaining area (from right to left).

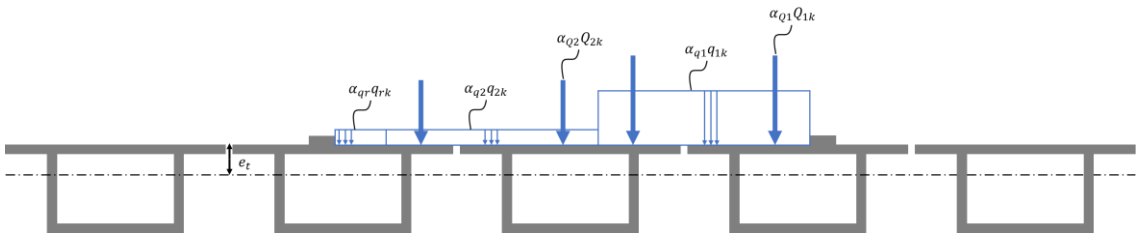


Figure 48 Load model 1 – First possible load configuration

- Configuration 2: The second lane is shifted to the left kerb, the remaining area is now positioned between the heaviest lane and the rightmost kerb.

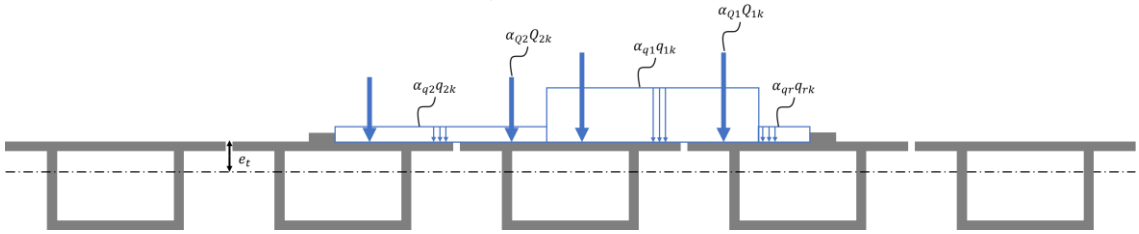


Figure 49 Load model 1 – Second possible load configuration

- Configuration 3: Lane 1 is positioned centrically onto the middle beam (beam 3), the remaining width of the carriageway is regarded as remaining area.

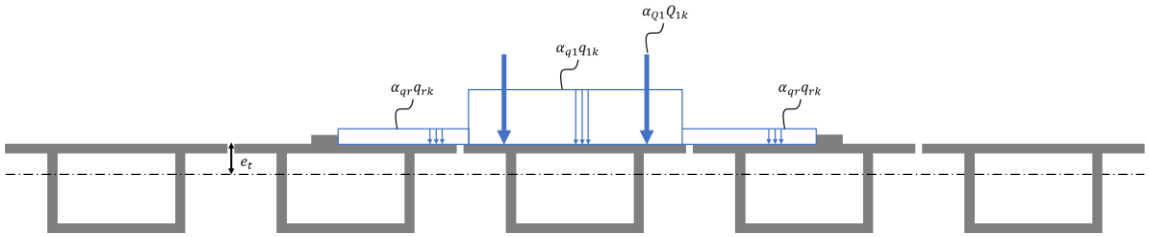


Figure 50 Load model 1 – Third possible load configuration

Under the assumption that there is no interaction between the beams, the third configuration gives the most unfavourable situation of the three, because the full load of the heaviest traffic lane (lane 1) is to be carried by a single beam. All loads considered this makes beam 3 the governing beam if both permanent and variable loads are considered. Therefore, it is this beam that will be considered for the remainder of the elaboration of the preliminary design.

The line load on beam 3 due to the uniformly distributed loads is:

$$Q_{k,UDL,LM1} = w_1 * \alpha_{Q1} Q_{1k} + (b_{eff,i} - w_1) * \alpha_{qr} q_{rk}$$

$$Q_{k,UDL,LM1} = 3{,}0 * 9{,}0 + (3{,}29 - 3{,}0) * 2{,}5 = 27{,}74 \text{ kN/m}^1$$

In addition, two sets (axles) of concentrated loads are present, representing axle loads due to heavy traffic:

$Q_{k,axle,LM1} = 300$ kN per axle, two axles in total

In the next sub paragraph these axle loads are positioned in longitudinal direction as such that the most unfavourable situation is obtained.

6.5.3 Longitudinal direction

Line loads

In longitudinal direction the self-weight, permanent loads and uniformly distributed loads due to the traffic are schematized as line loads over the full span.

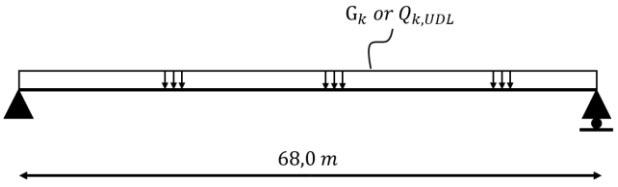


Figure 51 Line load on the UHPC beams

Axle loads

Bending moments: The concentrated loads of LM1 require additional attention. By positioning the concentrated loads as depicted in Figure 52 the most unfavourable situation for the bending moment and deflection is obtained, which will occur at midspan. This coincides with the load effects due to the uniformly distributed load.

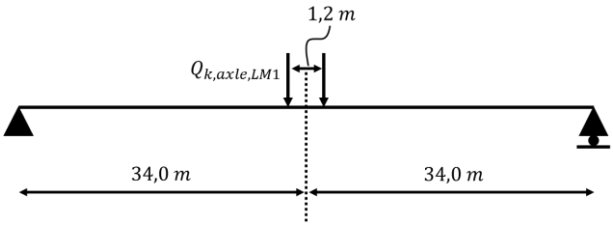


Figure 52 Axle loads on the UHPC beams

In this situation the bending moment due to axle load Q can be determined as follows:

$$M = \frac{68 - 1{,}2}{2} * Q_{k,axle,LM1} = 33{,}4 * Q_{k,axle,LM1} = \frac{1}{4} * 2 * Q_{k,axle,LM1} * l$$

Where:
$Q_{k,axle,LM1}$: Axle load according to LM1

Shear forces: To obtain the most unfavourable situation for the shear forces the axle loads should be positioned close to one of the supports.

6.5.4 Determining internal forces

Load combinations

The characteristic values of the loads, as were determined in the previous paragraphs, were multiplied with the appropriate factors to obtain the design values. Using these design values, the internal forces were determined for each load individually. These initial forces were subsequently added up to determine the total internal forces in accordance with the load combinations. Both equations 6.10a and 6.10b are considered, the governing values are subsequently selected to be used as input for the verifications.

The equations to determine the internal forces in the governing beam (beam 3) are briefly summarized in this paragraph.

Bending moments

- For the line loads (all permanent loads and uniformly distributed traffic loads):

$$M_{Ed,UDL} = \frac{1}{8} * q_d * l^2$$

- For axle loads:

$$M_{Ed,axle} = \frac{1}{4} * 2Q_{d,axle,LM1} * l$$

Shear forces

- For the line loads (all permanent loads and uniformly distributed traffic loads):

$$V_{Ed,UDL} = \frac{1}{2} * q_d * l$$

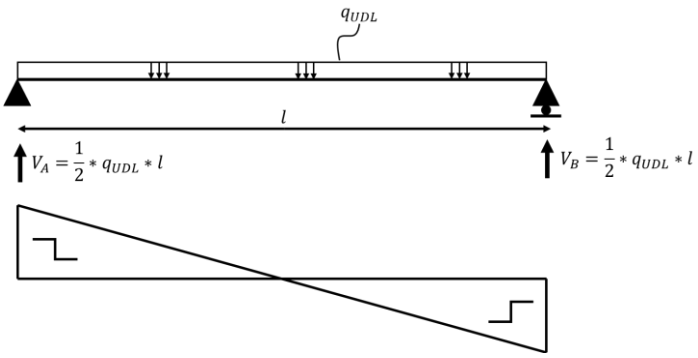


Figure 53 Shear force distribution due to line loads

- For axle loads:

$$V_{Ed,axle} = 2 * Q_{d,axle,LM1}$$

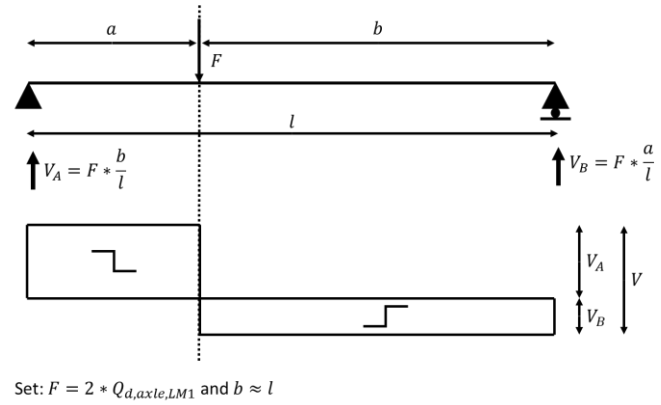


Figure 54 Shear force distribution due to axle loads

For axle loads the forces are positioned close to the supports.

6.6 Performing the calculations

Excel calculations

An Excel sheet has been prepared in which the preliminary design calculations have been performed. Calculating the loads, load combinations and verifications have been elaborated on in this document. In addition, the verifications that will be discussed in chapter 7 are covered there as well. The Excel sheet is included in the annexes (annex II) to this report.

Calculation results

For the calculation results of the calculations as described in this chapter reference is made to the Excelsheet. The overall impression of the results are as follows:

- If only permanent loads are considered load combination 6.10a is governing, while 6.10b is governing if both permanent and variable loads are considered. The latter is the case for the verifications that will be performed in the next chapter;

- The governing beams if only permanent loads are considered are beams 2 and 4 because of the presence of the kerbs;

- However, the verifications are performed for the combination of permanent and variable loads because that way larger internal forces and deflections are obtained. In that case beam 3 is governing because the first traffic lane (i.e. the traffic lane with the largest loads) is positioned on top of this beam, while at the same time interaction (and therefore the load distribution) between the beams is neglected.

Verifications and remarks

In this chapter the loads, load combinations, the governing beam and the internal forces in the governing beam have been determined. Using a very basic model the load distribution is analysed. Using the obtained results as input, verifications of the governing beam will be discussed in chapter 7. An important remark is that the results were obtained under a number of assumptions:

- For the loads three permanent loads (self-weight, asphalt layer and kerbs) have been taken in consideration. For the variable loads, only the vertical traffic loads due to LM1 on the carriageway and LM4 on the bicycle/pedestrian lanes were considered;

- The assumption was made that the deck would consist of five beams, with the aforementioned dimensions;

- LM1 was positioned as such that beam 3 would become governing. No other traffic load configurations were taken into consideration;

- The conservative assumption was made that there would be no interaction and therefore no load distribution between the beams, i.e. each beam carries all the loads that are acting upon it.

All these assumptions were justified by the goal of the preliminary design calculations as presented in this report: to obtain an idea of the required dimensions for the beams, as starting point for the more refined design procedure in the later stages of the project, as well as familiarizing with the procedures for the verifications. In chapter 9 the influence of the assumption that there is no interaction between the beams will be analysed in greater detail to obtain insight into the consequences of this assumption.

6.7 Bibliography chapter six

Groupe de travail BFUP. (2013, June). Ultra-High Performance Fibre-Reinforced Concretes. *Recommendations*. Association Francaise de Génie Civil.

Hartsuijker, C. (2016). *Mechanica Spanningen, vervormingen, verplaatsingen* (2e druk ed.). Boom.

NEN. (2015, oktober). NEN-EN 1991-2+C1. *Eurocode 1: Belastingen op constructies – Deel 2: Verkeersbelasting op bruggen*.

NEN. (2019, november). NEN-EN 1990+A1+A1/C2. *Eurocode: Grondslagen voor het constructief ontwerp*.

NEN. (2019, november). NEN-EN 1990+A1+A1/C2/NB. *Nationale bijlage bij NEN-EN 1990+A1:2006+A1:2006/C2:2019 Eurocode: Grondslagen van het constructief ontwerp*.

NEN. (2019, november). NEN-EN 1991-1-1+C1+C11. *Eurocode 1: Belastingen op constructies – Deel 1-1: Algemene belastingen – Volumieke gewichten, eigen gewicht en gebruiksbelastingen voor gebouwen*.

NEN. (2019, november). NEN-EN 1991-1-1+C1+C11/NB. *Nationale bijlage bij NEN-EN 1991-1-1+C1+C11: Eurocode 1: Belastingen op constructies - Deel 1-1: Algemene belastingen – Volumieke gewichten, eigen gewicht en gebruiksbelastingen voor gebouwen*.

NEN. (2020, februari). NEN-EN 1992-1-1+C2/NB+A1. *Nationale bijlage bij NEN-EN 1992-1-1+C2 Eurocode 2: Ontwerp en berekening van betonconstructies - Deel 1-1: Algemene regels en regels voor gebouwen*.

7

PRELIMINARY DESIGN: DESIGN VERIFICATIONS

7.1 Approach and parameters

In the previous paragraph the force distribution in the bridge deck was analysed, the governing beam was determined and the internal forces (bending moments and shear forces) were calculated. In this chapter the design verifications will be carried out to find out whether the beams have sufficient capacity to withstand these internal forces. In addition, several SLS criteria will be checked. The verifications are discussed in 0. However, first the prestressing has to be designed, which is discussed in 0.

The starting point is collecting relevant material parameters that are required as input. For convenience, all assumed material parameters are listed in the following tables. The majority of the concrete parameters are the recommended values for preliminary design from the AFGC guideline.

Table 18 Input parameters preliminary design calculations – Concrete

Parameters concrete compression			
Definition	**Symbol**	**Value**	**Unit**
Characteristic value compressive stress	f_{ck}	150	[N/mm^2]
Design value compressive strength	f_{cd}	85	[N/mm^2]
Modulus of elasticity	E_{cm}	50.000	[N/mm^2]
Maximum compressive strain at ULS	ε_{cu3}	2,7	[‰]
Strain at reaching concrete compressive strength	ε_{c3}	1,7	[‰]
Parameters concrete tension			
Definition	**Symbol**	**Value**	**Unit**
Characteristic elastic (5% percentile value) tensile strength	$f_{ctk,el}$	9	[N/mm^2]
Design value of tensile strength (tensile strength 1st crack)	f_{ctd}	6,0	[N/mm^2]
Design value maximal post cracking stress (stress at $w = 0{,}30$)	$f_{ctd;2}$	6,0	[N/mm^2]
Fibre orientation factor (global)	K_{global}	1,25	[-]
Fibre orientation factor (local)	K_{local}	1,75	[-]
Parameters concrete other			
Definition	**Symbol**	**Value**	**Unit**
Factor for shape of concrete compressive zone	α	0,69	[-]
Factor for position centre of gravity of concrete compressive zone	β	0,37	[-]
Factor for long term effects and unfavourable loading (compression)	α_{cc}	0,85	[-]
Factor for long term effects and unfavourable loading (tension)	α_{ct}	1,0	[-]
Fibre length	l_f	30	[mm]
Creep	φ	0,8	[-]

The AFGC recommends a strain value $\varepsilon_{cu3} = 2{,}7$ ‰ and a value for ε_{c3} of $f_{cd}/E_{cm} = 1{,}7$ ‰. By analysing the stress-strain figure of concrete in compression, and taking the factors x_u and f_{cd} outside the brackets, one can derive the following expressions for the factors related to the shape of the stress-strain diagram of concrete in compression (α and β). Using values of $\varepsilon_{cu3} = 2{,}7$ ‰ and $\varepsilon_{c3} = f_{cd}/E_{cm} = 1{,}7$ ‰ equations (19) and (20) result in $\alpha = 0{,}69$ and $\beta = 0{,}37$.

$$\alpha = \frac{1}{\varepsilon_{cu3}} * (\varepsilon_{cu3} - \varepsilon_{c3}) + \frac{1}{2} * \frac{1}{\varepsilon_{cu3}} * \varepsilon_{c3}$$ Equation (19)

$$\beta = \frac{\frac{1}{2}\left(\frac{1}{\varepsilon_{cu3}}(\varepsilon_{cu3} - \varepsilon_{c3})\right)^2 + \frac{1}{2} * \frac{1}{\varepsilon_{cu3}} \varepsilon_{c3} * \left(\frac{1}{\varepsilon_{cu3}}(\varepsilon_{cu3} - \varepsilon_{c3}) + \frac{1}{3} * \frac{1}{\varepsilon_{cu3}} \varepsilon_{c3}\right)}{\frac{1}{\varepsilon_{cu3}} * (\varepsilon_{cu3} - \varepsilon_{c3}) + \frac{1}{2} * \frac{1}{\varepsilon_{cu3}} * \varepsilon_{c3}}$$ Equation (20)

For the concrete in tension, values corresponding to thick elements of low strain-hardening material are taken. Based on the recommended values from the AFGC guideline the values of f_{ctd} and $f_{ctd;2}$ are both taken equal to 6,0 N/mm^2. The values of the fibre-orientation factors are the recommended default values from the guideline for preliminary design.

The length of an individual fibre, l_f, is assumed to be equal to 30 mm. This is a 'compromise' between the different values identified in the literature study. For the creep factor it is assumed that no heat treatment is applied to the material, this results in the largest value for the creep factor.

The following table gives the values adopted for the prestressing steel. Steel type Y1860 is assumed to be used.

Table 19 Input parameters preliminary design calculations – Prestressing steel

Parameters prestressing steel			
Definition	**Symbol**	**Value**	**Unit**
Characteristic value tensile strength	f_{pk}	1860	[N/mm^2]
Design value steel stress	f_{pd}	1522	[N/mm^2]
Maximum allowed stress directly after tensioning	σ_{pm0}	1395	[N/mm^2]
Modulus of elasticity	E_p	195.000	[N/mm^2]
Characteristic value strain at failure	ε_{uk}	35	[‰]

The following table gives the details on the individual prestressing strands that were selected to be applied.

Table 20 Input parameters preliminary design calculations – Prestressing strands

Prestressing strands			
Characteristic diameter	D_{strand}	15,2	[mm]
Cross-sectional area	$A_{p,strand}$	140	[mm^2]

The following table gives all partial safety factors (material factors) used in the verifications.

Table 21 Input parameters preliminary design calculations – Partial factors

Partial factors			
Definition	**Symbol**	**Value**	**Unit**
Partial factor concrete (cf EC2)	Yc	1,5	[-]
Partial factor for fibre reinforced concrete in tension (cf AFGC)	Y_{cf}	1,3	[-]
Product of partial factor for uncertainty in extrapolation * factor Y_{cf}	Y_E*Y_{cf}	1,5	[-]
Partial factor prestressing steel (cf EC2)	Ys	1,1	[-]

7.2 Design of prestressing

Before the verifications of the cross-sectional capacity can be carried out, the prestressing has to be designed. This will be done in this paragraph. In order to do so, the following assumptions have been made:

- The prestressing is designed in the serviceability limit state, therefore the partial load factors are all set equal to 1,0. The criterion is used that no tensile stresses in the cross section are allowed (''full prestressing''), that means that the maximum stress is 0 N/mm^2. This is a conservative approach, because UHPC is known to have a relatively high tensile capacity, but this is justified in the preliminary design stage because no specific UHPC mixture with known properties has been chosen yet, and therefore this leaves room for optimization in later stages;

- The prestressing consists of straight pretensioned prestressing strands, positioned in the bottom flange of the cross section because there is relatively large cross-sectional area available. It is assumed that the centre of gravity of the prestressing strands is at half the thickness of the bottom flange (75 mm from the bottom fibre). Note that this will result in an upward bending moment constant over the span of the beams;

- It is assumed that the stresses in the prestressing steel directly after tensioning are equal to the maximum allowable stress (σ_{pm0}) and that the total prestress losses at $t \rightarrow \infty$ equal 20 %. This assumption is deemed to be reasonable for pretensioned steel, which is typically used for prefabricated elements.

When considering all loads acting on the structure, the situation as in Figure 55 occurs:

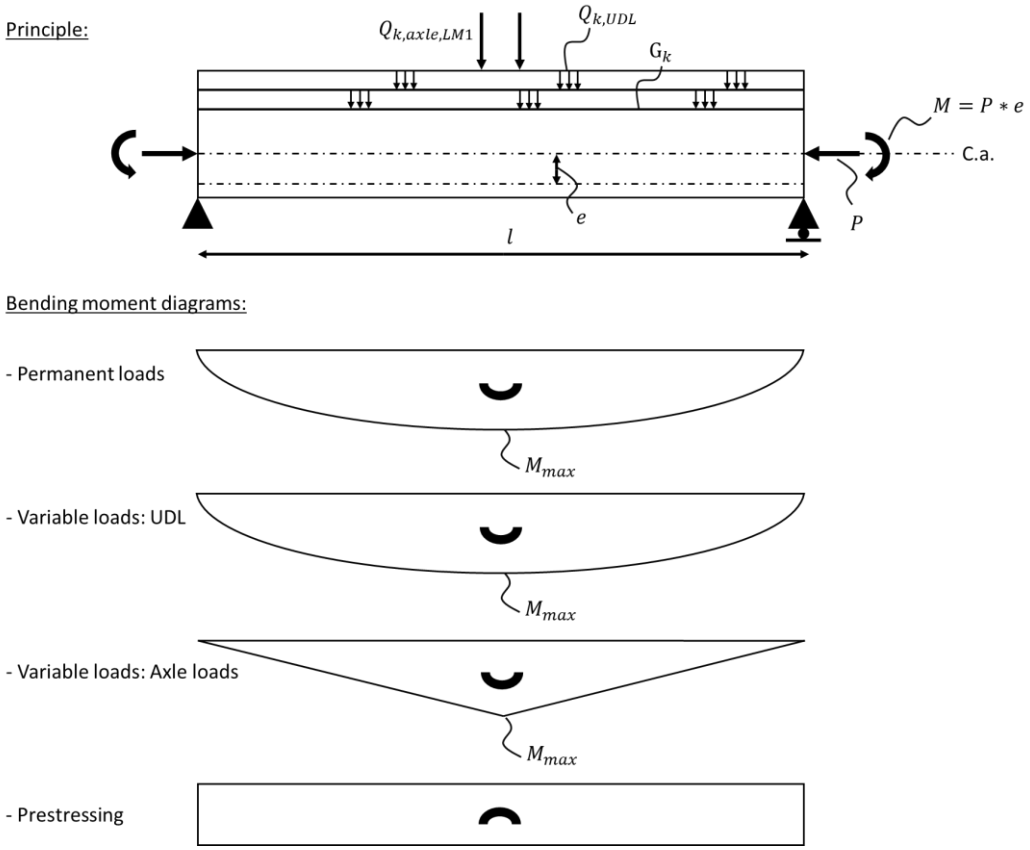


Figure 55 Bending moment distribution due to different loads acting on the governing beam

For designing the prestressing, the outer fibres are analysed as these are governing, the maximum stresses occur at these fibres. Since no tensile stresses are allowed, the concrete is uncracked and the stress distributions therefore are linear over the height of the cross section. Two situations are analysed. The first situation is just after construction ($t = 0$) where the beams are at their final position while variable loads are not present yet. The second situation is the use phase ($t \rightarrow \infty$) where variable loads are also present.

Situation 1 (After construction, $t = 0$) – The following figure gives the stresses over the cross section due to the acting loads (permanent load and prestressing load without prestress losses). Note that due to the positioning of the tendons the prestressing results both in a centric compressive force and an upward bending moment.

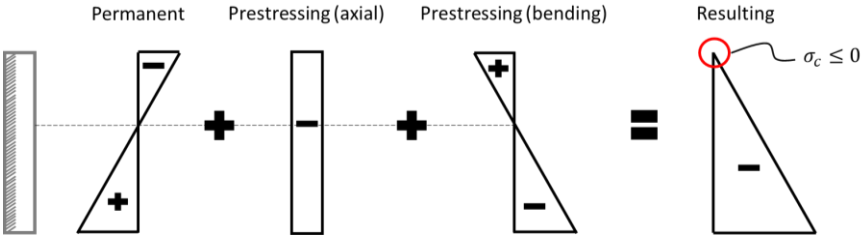


Figure 56 Stresses over the cross section – Situation 1

- Concrete stress at the top fibre:

$$\sigma_c = -\frac{M_G}{W_t} - \frac{P_0}{A_c} + \frac{P_0 * e}{W_t}$$

- Concrete stress at the bottom fibre:

$$\sigma_c = +\frac{M_G}{W_b} - \frac{P_0}{A_c} - \frac{P_0 * e}{W_b}$$

Situation 2 (Use phase, $t \to \infty$) – The following figure gives the stresses over the cross section in the use phase, which means that variable loads are also included. The assumption is that prestressing losses are 20% of the initial prestressing force, hence $P_\infty = 0{,}8 * P_0$.

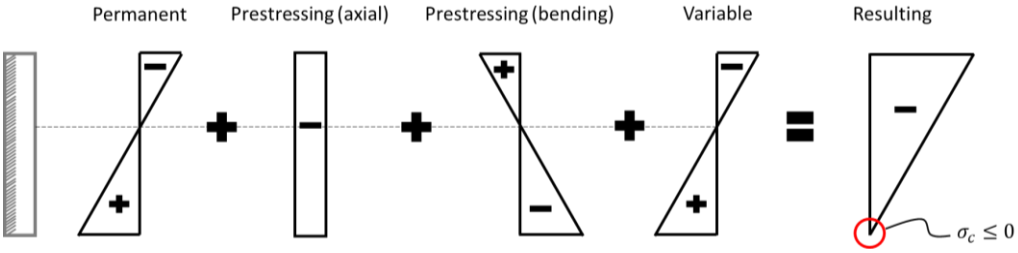


Figure 57 Stresses over the cross section – Situation 2

- Concrete stress at top fibre:

$$\sigma_c = -\frac{M_G}{W_t} - \frac{0{,}8 * P_0}{A_c} + \frac{0{,}8 * P_0 * e}{W_t} - \frac{M_Q}{W_t}$$

- Concrete stress at the bottom fibre:

$$\sigma_c = +\frac{M_G}{W_b} - \frac{0{,}8 * P_0}{A_c} - \frac{0{,}8 * P_0 * e}{W_b} + \frac{M_Q}{W_b}$$

In the Excel sheet the concrete stresses at the outer fibres are calculated for both situations, after which the required prestressing force at $t \to 0$, P_0, is required to keep the cross section under compression. This is an iterative procedure, and the largest required compressive force is subsequently selected, this value is then used to calculate the required prestressing tendons, etc.

Requirements cover and spacing: According to the calculation, a total of 214 strands are required, each with a diameter of 15,2 mm. These have to be distributed over the bottom flange of the cross section. An important consideration is what the required spacing between the strands and the required concrete cover would be. Given the superior mechanical properties of UHPC compared to conventional concrete, it is expected that the minimum concrete cover and spacing for conventional concrete will be more than sufficient for UHPC.

More information can be found in (Russell & Graybeal, 2013) (which gives an overview of various sources) and (Bertram & Hegger, 2012) (where the bond behaviour of prestressing strands in UHPC was investigated, resulting in recommendations for minimum concrete cover and minimum clearance between the strands). Higher bond stresses result in a shorter transfer length, while higher bond stresses also lead to an increase of tensile stresses in the concrete around the strands.

According to these sources, a cover of $2{,}5 * d$ was applied. The different sources referred to in (Russell & Graybeal, 2013) varied between spacing of $2{,}0 - 2{,}5 * d$. For this design stage the value of $2{,}0 * d$ (i.e. 30,4 mm) is assumed to be sufficient.

Changing dimensions: Positioning all the tendons within the cross section proved to be the most stringent criterion and the dimensions of the cross section were modified to allow for this. Tendons were changed from diameter 15,2 to diameter 13,0 and the height was increased to 2325 mm, the top flange remained 250 while the bottom flange was increased to 273 mm. The internal height (height of the webs) therefore became 1802 mm.

The centre of gravity of the strands is at half the thickness of the bottom flange and eventually 332 strands were applied to keep the cross section symmetric. A detail of the positioning of the tendons is given in Figure 58 and can also be found in the preliminary design drawings, these are included in the annexes (annex IV) of this report.

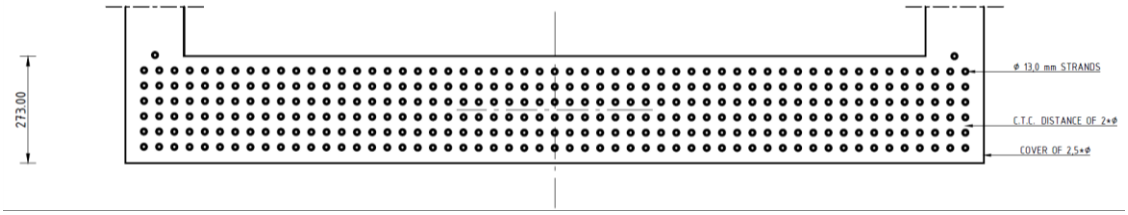


Figure 58 Positioning of prestressing strands in bottom flange

Bending moments near supports: A point of attention is that the stress verifications as described in this paragraph are performed at mid span. However, near the supports the bending moment due to loads is much smaller while the bending moment due to prestressing is constant over full span. This may cause cracking near supports. In general, different measures can be taken. These are not worked out in detail, but are described briefly:

- Option 1 – Bending tendons upwards: For a number of tendons (those positioned within the width of the web of the cross section) it is possible to bend these upwards near the supports, thus reducing the bending moment;

- Option 2 – Manipulate bond of tendons: Another way is hindering the bond of a number of tendons near the supports, e.g. by wrapping these or by using grease. The transfer of prestressing forces of these tendons than happens more inwards, away from the supports.

The results of both measures are that the bending moment near the supports due to the prestressing decreases and as a result the tensile stresses at these cross sections decreases as well. The bending moment curve becomes more ''smooth'', as is illustrated in the following figure. Note that this is not to scale.

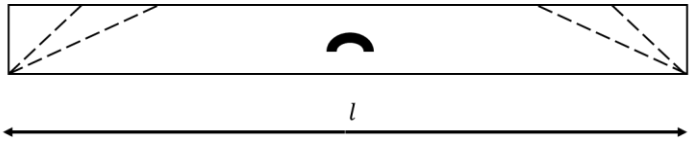


Figure 59 ''Smoothening'' the bending moment distribution at the beam ends

For the full calculation of the prestress design, reference is made to the Excelsheet in the annexes (annex II).

7.3 Verifications

7.3.1 ULS verifications - Bending moment capacity

ULS requirement bending moment capacity

Prestressed cross sections are generally designed in the serviceability limit state, no tensile stresses were allowed in the cross section. In addition, the cross section has to be verified in the ultimate limit state as well in which case it is assumed that the cross section is cracked ($M_{Ed} > M_{cr}$) and the situation as in Figure 29 is achieved. In the ultimate limit state, the following criterion has to be satisfied:

$$M_{Ed} \leq M_{Rd}$$

Effective width top flange

Given the shape of the cross section, first the effective width of the top flange should be determined. This is done in accordance with 5.3.2.1 of NEN-EN 1992-1-1. Required parameters are given in the following figures.

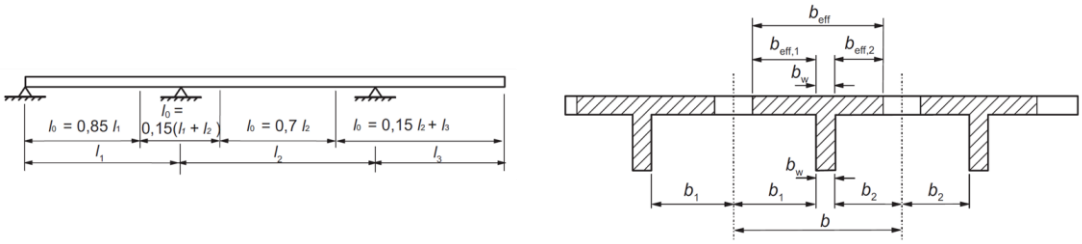


Figure 60 Determining effective flange width – NEN-EN 1992-1-1, p.61-62

- Because the beams are statically determined, the distance between the points where the bending moment equals zero (l_0) equals the span, which is 68,0 m.

- The effective flange width b_{eff} is calculated as follows:

$$b_{eff} = \sum b_{eff,i} + b_w \leq b$$

- First the internal width is analysed, which beams that $b_1 = w_b/2 = 0{,}95$ m. Plugging in the values:

$$b_{eff,i} = 0{,}2 * b_i + 0{,}1 * l_0 \leq 0{,}2 * l_0 \rightarrow b_{eff,1} = 0{,}2 * b_1 + 0{,}1 * l_0 \leq 0{,}2 * l_0$$

$$b_{eff,1} = 0{,}2 * 0{,}95 + 0{,}1 * 68{,}0 \leq 0{,}2 * 68{,}0$$

- Given the large span (distance between points of zero bending moment), using these equations it can easily be seen that the whole top flange can be assumed to be part of the effective width.

Height of concrete compressive zone and varying width

In 5.4.2 the calculation procedure for determining the bending moment capacity is covered. However, this procedure was based on a rectangular cross section. Therefore, some modifications have to be made to include variable width of the cross section in relation to the height of the concrete compressive zone. Three cases can be distinguished, this is illustrated in the following figure.

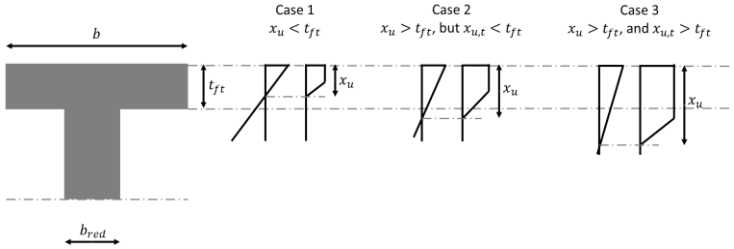


Figure 61 Height of concrete compressive zone and variable width of the cross section

These modifications are included in the Excelsheet. The derivations are given in annex III. Note that the contribution of concrete in tension is calculated only by considering the width of the webs, because it is assumed that if the neutral axis is positioned within the top flange, the height of the top flange part in tension will be small.

Performing calculations and unity check

The bending moment capacity is calculated following the procedure given in 5.4.2 while also accounting for the effective width and the varying width over the height of the cross section as discussed in this paragraph. The full calculation can be found in the annexes (annex II) to this report. Only the results are given in this text. For the bending moment capacity, the unity check is:

$$UC = \frac{M_{Ed}}{M_{Rd}} \leq 1{,}0 \rightarrow \frac{44.176}{69.130} = 0{,}64$$

The rotational capacity also is to be verified:

$$\frac{x_{u,prov}}{d} \leq \frac{x_{u,max}}{d} \rightarrow \frac{0{,}14}{0{,}40}$$

The criteria regarding bending moment capacity and rotational capacity are therefore satisfied.

7.3.2 ULS verifications - Shear force capacity

The shear force capacity is verified in accordance with the procedure as 5.5.2. The width of the shear cross section is taken equal to the summation of both webs: $b_w = 2 * t_w$. The angle of the concrete compressive strut with the beam axis, the angle θ, is taken equal to the minimum angle: 30^o. The full calculating procedure can be found in the annexes (annex II) to this report.

$$UC = \frac{V_{Ed}}{V_{Rd}} \leq 1{,}0 \rightarrow \frac{5074}{7739} = 0{,}66$$

The criteria regarding shear force capacity are therefore satisfied.

7.3.3 SLS verifications – Deflection

Load combination

Deformation of the bridge deck is verified in the serviceability limit state. The frequent load combination (reversible situations) is used, this results in the following combination:

$$G_{k,beams} + G_{k,asphalt} + G_{k,kerbs} + P + 0{,}8 * Q_k$$

Long term effects

The increase of the deformation due to long term effects (i.e. creep) is taken into consideration using the approach given in the AFGC guideline, it prescribes that creep may be accounted for by using an effective modulus of elasticity.

$$E_{c,eff} = \frac{E_{cm}}{1 + \varphi}$$

Given the values from the first part of the literature study and the values from the AFGC guideline, a value of $\varphi = 0{,}8$ is applied. The reduction is applied both to all loads to account for all possible effects that may occur over time, such as creep, cracking of the concrete, etc.

Deflection calculations

Also, for the verification of the deflections the governing beam (beam 3) is considered, while considering full loads and the axle loads positioned at mid span. This results in the maximum values for the deformations. Engineering formulas (''vergeetmenietjes'') are used to calculate the deflections for each load case, after which the results are superimposed to obtain the total deformation. This approach is justified because a frequent load combination is assumed (reversible situation) and prestressing is designed for uncracked

concrete, implying no resulting deformation after unloading (except for creep effects). The deflection due to the individual load cases is as follows:

- Downward deformation due to self-weight and permanent loads:

$$\delta_G = \frac{5 * G_{k,total} * l^4}{384 * E_{c,eff} * I}$$

- Upward deformation due to the prestressing:

$$\delta_P = \frac{P_\infty * e * l^2}{8 * E_{c,eff} * I}$$

- Downward deformation due to the uniformly distributed variable loads:

$$\delta_{Q,UDL} = \frac{5 * 0{,}8 * Q_{k,UDL,tot} * l^4}{384 * E_{c,eff} * I}$$

- Downward deformation due to the axle loads:

$$\delta_{Q,axle} = \frac{2 * 0{,}8 * Q_{k,axle,LM1} * l^3}{48 * E_{c,eff} * I}$$

The equation for the prestressing can be found by adding up two standard cases of a statically determined beam with a bending moment at one of its supports. It can also be derived directly using Euler beam theory and appropriate boundary conditions.

Verification

The total deformation can now be found by adding up the different components, while taking into consideration whether the deformation is upwards or downwards:

$$\delta_{tot} = \delta_G - \delta_P + \delta_{Q,UDL} + \delta_{Q,axle}$$

In the codes no requirements with regard to maximum allowable deformations are given, these are often defined individually for each project. Therefore, an appropriate value had to be defined:

$$\delta_{max} = \frac{l}{300}$$

Without variable loads the result is upward bending of 139 mm, while including variable loads results in downward bending of 68 mm. The maximum deflection is 227 mm. Therefore, the criterion is satisfied.

7.4 Summary & Conclusions

Based on the cross-sectional dimensions assumed and the loads determined in chapter 6, the deck has been verified in this chapter based on three conditions. First the prestressing was designed after which the bending moment capacity, shear force capacity and deflection were verified.

A number of modifications had to be made to the assumed dimensions and values to be able to accommodate the prestressing strands. After trial and error, it was found that all the prestressing could be placed and the verifications could be satisfied by changing the strands from diameter 15,2 to diameter 13,0, by increasing the height to 2325 mm, keeping the top flange at 250 mm and increasing the thickness of the bottom flange to 273 mm. The internal height therefore became 1802.

After the design of the prestressing the bending moment capacity, shear force capacity and deflection were calculated. For the first two verifications the procedures as formulated in 5.4.2 and 5.5.2 were applied, although modifications were required for the verification of the bending moment capacity, because of the

varying width over the height of the cross section. The deflections were verified using standard engineering formulas while taking long term effects (creep) into consideration as well.

All three criteria were satisfied, and therefore the preliminary design is finalized. The result with the adjusted cross-sectional dimensions is presented in the drawings in the annexes (annex IV) to this report. In the following chapters of this report the obtained preliminary design will be used to make a brief comparison with the weight of the existing bridge, to have an impression on the feasibility of the project goal. Furthermore, it will be analysed what the impact is of the way in which the force distribution was modelled (assumption was no interaction between the beams).

7.5 Bibliography chapter seven

Bertram, G., & Hegger, J. (2012). Bond Behavior of Strands in UHPC - Test and Design. In E. Schmidt, E. Fehling, C. Glotzbach, S. Fröhlich, & S. Piotrowski (Red.), *Ultra-High Performance Concrete and Nanotechnology in Construction* (pp. 525-532). Kassel: kassel university press.

Groupe de travail BFUP. (2013, June). Ultra-High Performance Fibre-Reinforced Concretes. *Recommendations*. Association Francaise de Génie Civil.

Ketel, H., Willemse, R., Van Rijen, P., & Koolen, E. (2011). Rekenmodel VVUHSB (1). *Cement*, 50-57.

NEN. (2011, november). NEN-EN 1992-1-1+C2. *Eurocode 2: Ontwerp en berekening van betonconstructies - Deel 1-1: Algemene regels en regels voor gebouwen*.

NEN. (2020, februari). NEN-EN 1992-1-1+C2/NB+A1. *Nationale bijlage bij NEN-EN 1992-1-1+C2 Eurocode 2: Ontwerp en berekening van betonconstructies - Deel 1-1: Algemene regels en regels voor gebouwen*.

Russell, H. G., & Graybeal, B. A. (2013). *Ultra-High Performance Concrete: A State-of-the-Art Report for the Bridge Community*. Federal Highway Administration (FHWA), Office of Infrastructure Research and Development.

Walraven, J., & Braam, C. (2019, February). Prestressed Concrete.

8

WEIGHT COMPARISON

8.1 Weight comparison

8.1.1 Goal of the comparison

With the verifications as described in the previous chapter the preliminary design has been finalized, which means that a substantiated estimate of the required dimensions has been obtained. Although this is just the preliminary design, these dimensions can be used for a simple weight comparison with the existing bridge. A goal of the comparison is to obtain insight into the contribution to the total self-weight per element, which can be useful for optimization later on. But the most important goal is that using this comparison it can be judged whether the project goal is still realistic or not.

- If the preliminary design results in a significantly larger self-weight than the existing bridge the project goal and intended approach should be reconsidered.

- If the difference in weight is only limited, the project goal and intended approach are considered realistic because the design will be refined and optimized in later design stages (resulting in a reduction of the weight).

- If the preliminary design results in a smaller self-weight than the existing bridge, then it may be expected that the project goal can be achieved without great difficulty, although further design and optimization work will be carried out to obtain a structure as optimized as possible.

In any case it is important to note that the comparison in this chapter is only a rough comparison.

8.1.2 Approach

An Excelsheet has been prepared in which the weight comparison has been carried out. The main structural components of both bridges are listed after which the dimensions and self-weight of these elements was calculated and/or estimated. Subsequently the weight all the separate parts are added up to obtain the total values. Reference is made to the annexes (annexes V and VI) of this report for the full analysis and the drawing of the existing bridge that was used to determine certain dimensions.

For the existing bridge the dimensions as reported in ''Existing Bridges Twentekanaal'' (chapter 3) are used and supplemented by information from design drawings from Rijkswaterstaat archives wherever required.

For the preliminary design, the adjusted dimensions as given in 7.4 and drawn in the preliminary design drawings (annex IV) are applied. Note that the preliminary design calculations only involved the design of the main load bearing elements (the beams) and the dimensioning of the kerbs and asphalt layer. Two essential elements of the deck are missing: the end cross beams and the capping beams. To overcome this, assumed dimensions and properties for these elements will be used in the analysis:

- **End cross beams**: It is assumed that the end cross beams will be constructed using prestressed conventional concrete (infill between the ends of the prefab UHPC beams and prestressing tendons guided through box outs in the beam ends), therefore a volumetric weight of 25 kN/m^3 is assumed. In addition, it is assumed that the height and width of the end cross-beams are equal to the height of the beams and that the length will be equal to the full width of the deck. This results in a beam

with dimensions 2,325 by 2,325 by 16,36 m (height, width, length). This results in a solid beam element at both ends of the deck.

- **Capping beam**: It is assumed that the capping beam will a prestressed concrete beam of conventional concrete, therefore a volumetric weight of 25 kN/m^3 is assumed. The length is taken equal to the full width of the deck. The required height is estimated using rules of thumb for prestressed concrete beams, applied to the centre-to-centre distance of the existing buttresses of the Eefdesebrug (see chapter 3 of ''Existing bridges Twentekanaal''):

$$h = \frac{8{,}90}{15} = 0{,}59 \approx 0{,}60\ m$$

This value is deemed to be fairly small given the large expected loads, therefore a height of 1,0 m is assumed. To obtain a stable element and enough space to position the bearings, a width of 0,75 m is assumed. The result is a beam with dimensions 1,0 by 0,75 by 16,36 m (height, width, length). A possible reduction of the height of the existing buttresses because of the placement of the capping beams is not considered in the calculation.

Some additional simplifications are made by not considering a number of ''smaller'' elements:

- Bearings
- Railings
- Joints
- Hangers of the existing bridge

It is not expected that these elements will be a decisive factor for the weight comparison. Given the small diameters the hangers of the existing bridge will hardly contribute on the whole. For the bearings, railings and joints it is expected that the weight in the existing and new situation will be approximately the same (thus cancelling out).

8.1.3 Elaboration of the comparison and results

Following the approach as described in the previous two sections, an Excelsheet is prepared in which the weight of both the new and old bridge is roughly calculated. Reference is made to the annexes to this report for the complete calculation (annex VI).

According to the performed comparison of the preliminary design and the existing bridge, the new design would result in a weight increase of 26% compared to the current situation. Although this might seem as a considerable increase, there is a number of remarks that can be made:

- The comparison itself is incomplete (adjustment of the existing buttresses is neglected for example) and at some situations material has been counted double (the cross beams and the ends of the prefab beams overlap; material is counted two times at these points). Including this probably saves already a few percent;

- The preliminary design is carried using 'traditional principles', an example is the application of an asphalt layer. This is described by the ROK but for UHPC this is not required from a structural point of view, this is for example illustrated in (Braam, Kaptijn, & Buitelaar, 2003) and examples in (Fehling, Schmidt, Walraven, Leutbecher, & Fröhlich, 2014). Leaving out the asphalt layer results in a weight increase of 10% instead of the 26% increase when including it.

These two remarks already illustrate that without extensive further design calculations the apparent increase in weight can already be mitigated considerably.

The most important remark however is the way in which the preliminary design has been worked out. The dimensions were chosen and adjusted using practical rules of thumb, the material parameters were mostly taken from the AFGC guideline and in the modelling and further design and verification calculations generally the more conservative approaches were chosen. In addition, dimensions such as those of the end cross

beams are simply not known yet and where therefore estimated. Such dimensions are another possibility for further optimization.

8.1.4 Conclusions

Considering the results of the comparison it is concluded that the preliminary design as elaborated on in this report results in an increase of the weight compared to the existing structure. At the same time many possibilities are identified to refine and optimize the redesign. The potential to reduce the weight of the new bridge, either by optimizing and refining the design (which will be done in later design stages) or by changing the ''design philosophy'' (e.g. leaving out the asphalt layer), is deemed to be large enough to obtain a design with a weight equal to or lower than the existing bridge. The next phase of the project will therefore be to work on a more refined and optimized design. In chapter 10 different options for optimizing and refining the design will be discussed, as a prospect to the next project phase.

8.2 Bibliography chapter eight

Braam, C., Kaptijn, N., & Buitelaar, P. (2003). Hogesterktebeton als brugdekoverlaging. *Cement*, 86-91.

Fehling, E., Schmidt, M., Walraven, J., Leutbecher, T., & Fröhlich, S. (2014). *Ultra-High Performance Concrete UHPC*. Berlin: Wilhelm Ernst & Sohn.

9

SENSITIVITY ANALYSIS

9.1 Goal of sensitivity analysis

In the calculation model of the preliminary analysis, it was assumed that there would be no distribution of the variable loads between the bridge beams. This was already known to be a conservative assumption, but in this chapter the effect of this assumption will be studied more closely.

A so-called ''sensitivity analysis'' will be carried out, in which it will be analysed to what extent the results would change if various degrees of load distribution would be taken into consideration. To analyse this, a model is set up in RFEM with an orthotropic plate functioning as the ''distribution element''. This element determines the load distribution over the various beams and resembles the top flange of the box beams that would be prestressed in reality, in order to form one solid deck.

To analyse to what extent the results would have changed, the stiffness of the plate is varied in transverse direction. Multiple situations are analysed:

- $E_y = 0$: A limit case where no stiffness in transverse direction is assumed, the results should correspond to the calculations made in the preliminary design;
- $E_y = E_x$: The second limit case where the stiffness in transverse direction is assumed to be equal to the stiffness in longitudinal direction and where maximum distribution is expected;
- $E_y = \alpha * E_x$: Various intermediate values where the transverse stiffness is taken as 25%, 50% and 75% of the longitudinal stiffness;
- $E_y = 1/3 * E_x$: Additionally, 1/3 of longitudinal stiffness is checked, because this is a very common assumption for the stiffness of cracked concrete.

Results of these different situations will show how sensitive the results of the calculation are to changes in the stiffness of the plate in transverse direction, and thus to a change of load distribution of the cross section. Further outline of the approach and the analysis of the results is covered in the following sections.

9.2 Approach

9.2.1 RFEM model

To perform the analysis a finite element model is prepared using the programme RFEM. The x-direction in the RFEM model coincides with the longitudinal axis of the bridge deck while the y-direction in the RFEM model coincides with the transverse direction of the bridge deck.

Five beams are modelled (element type used: ''beam''), each beam has a span of 68,0 m and there is a centre-to-centre distance of 3,29 m, resulting in a total width of 16,36 m. This way there is some free space between the beams, where the joints would be in reality.

Four nodes are added corresponding to the corner points of the top surface of the deck, these nodes are used to model a plate element in between, which is positioned this way at the centre of gravity of the beams.

The beams are supported on one side using hinges and on the other side using sliding supports in x-direction.

Because it is the distribution of the variable loads over the beams that is to be analysed, only the variable loads are modelled. No partial factors are taken into consideration. The loads are modelled in accordance with configuration 3 as presented in Figure 50 in section 6.5.2. The loads are modelled as two separate load cases, but combined into one load combination for the purpose of calculations and are positioned on the surface. The axle loads are positioned at mid span to simulate maximum bending moment and deflection.

The cross sections of the beams are in accordance with the cross section of the preliminary design as discussed in 7.4 and the thickness of the slab is 250 mm, which is equal to the thickness of the top flange of the beams. For all other settings (e.g., mesh of the plate), the default values are used. The following figure gives an overview of the model and the different load cases.

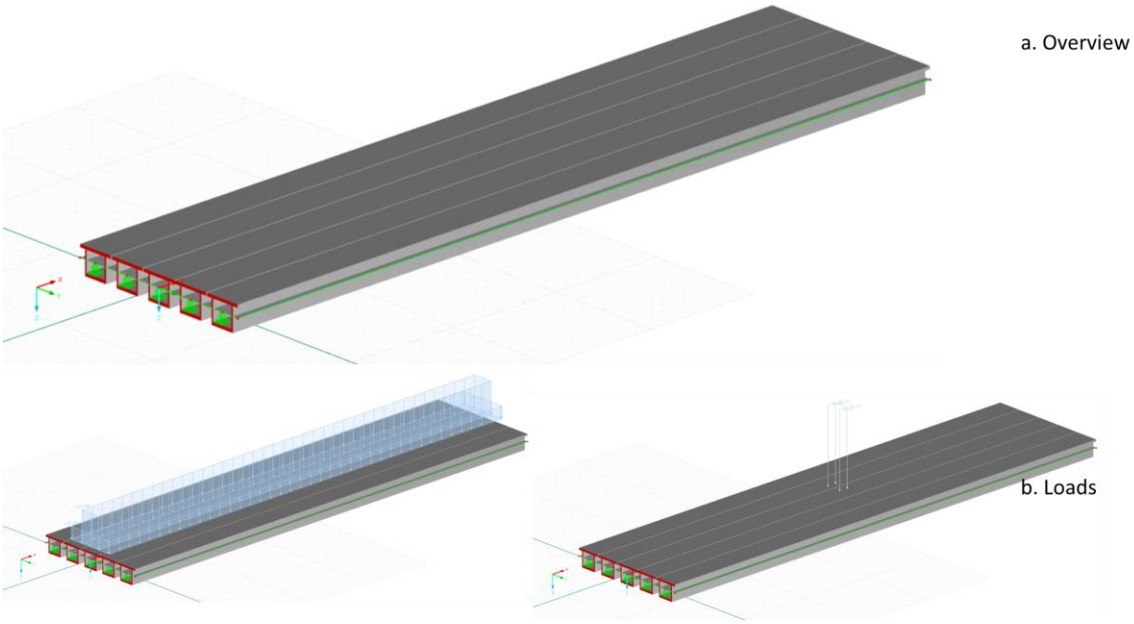


Figure 62 Overview of the RFEM model and the modelled load configurations

To enable easy remodelling of the RFEM model, all input parameters have been listed in a separate document, which has been attached to this report as an annex (annex VII). Reference is made to this document for all RFEM input parameters.

9.2.2 Material and stiffness parameters

Material

The starting point for the RFEM model is that only a single material is defined, for which the default option of C30/37 concrete is used, which is then applied to the beams and the plate. The calculation is elastic and only the force distribution is analysed. Therefore, it does not make a difference which material is used. For the plate, this material only dictates the starting values but as explained in the next subsection its material parameters will be modified to account for orthotropic behaviour.

Orthotropic plate

For the orthotropic plate the material properties are adjusted to obtain an orthotropic material, the following parameters are plugged into the RFEM model:

- Modulus of elasticity in longitudinal direction E_x
- Modulus of elasticity in transverse direction E_y
- Shear stiffnesses G_{xz}, G_{yz} and G_{xy}
- Poisson ratio v_{xy}

The shear stiffnesses are calculated using the moduli of elasticity and Poisson ratio:

$$v_{yx} = v_{xy} * \frac{E_y}{E_x}$$

$$G_{yz} = \frac{E_y}{2 * (1 + v_{yx})}$$

$$G_{xz} = \frac{E_x}{2 * (1 + v_{xy})}$$

$$G_{xy} = \frac{\sqrt{(E_x * E_y)}}{2 * (1 + \sqrt{v_{xy} * v_{yx}})}$$

The following values for the moduli of elasticity in both directions are used as input values:

Table 22 Input parameters for the moduli of elasticity

Calculation No.	Modulus of elasticity E_x	Modulus of elasticity E_y	Percentage of E_x in y-direction
[-]	[N/mm^2]	[N/mm^2]	[%]
1	33.000	0	0
2	33.000	8250	25
3	33.000	11.000	33
4	33.000	16.500	50
5	33.000	24.750	75
6	33.000	33.000	100

Reference is made to the Excelsheet in the annexes (annex VIII) to this report for all calculated values.

9.2.3 Comparison and expected results

Comparison

A comparison will be carried out by determining the support reaction and maximum bending moment at mid span of the middle beam (beam 3). These values will be used as a measure for the amount of interaction and force distribution between the beams.

Expected results

It is expected that there will be two limit cases in the calculation results. The first limit case is the situation in which $E_y = 0$, as this should give the same results as the calculations performed in the preliminary design. These are as follows:

- **Support reaction**: Half of the traffic loads is carried by each support of beam 3:

$$R = (3{,}0 * 9{,}0 + (3{,}29 - 3{,}0) * 2{,}5) * 34{,}0 + 300 = 1242{,}65\ kN$$

- **Bending moment at mid span**: The bending moment at midspan is:

$$M_{UDL} = \frac{1}{8} * (3{,}0 * 9{,}0 + (3{,}29 - 3{,}0) * 2{,}5) * 68{,}0^2 = 16.025\ kNm$$

$$M_{axles} = \frac{1}{4} * 2 * 300 * 68{,}0 = 10.200\ kNm$$

$$M = 16.025 + 10.200 = 26.225\ kNm$$

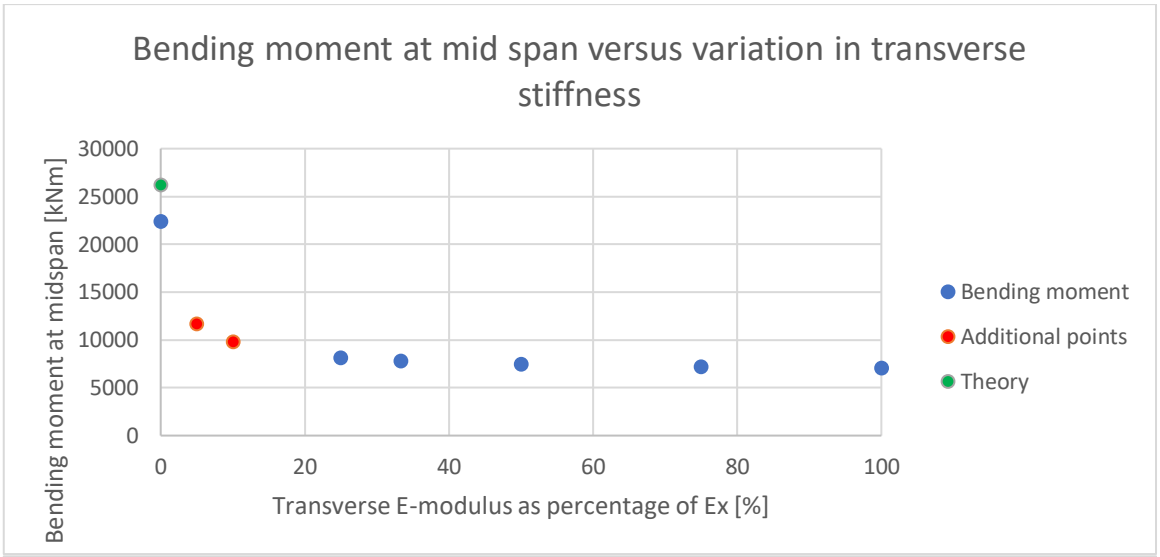
The second limit case is where $E_y = E_x$, in this situation the maximum distribution is expected and the results should be the same as for an isotropic plate.

These limit cases are used to verify the results. The first limit case should correspond to the hand calculations preliminary design calculation. The second case should be the same as for an isotropic plate. All other cases should fall in between the limit cases.

9.3 Analysis of results, interpretation and conclusions

9.3.1 Overview of results

The results are summarized in the following two graphs.



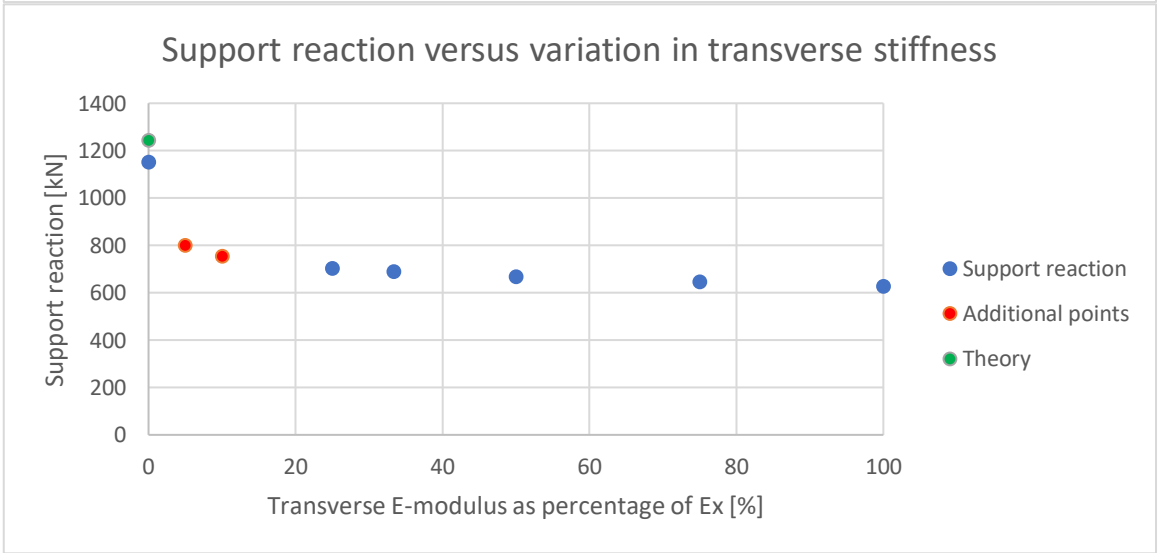


Figure 63 Bending moment and support reactions for varying transverse stiffness

9.3.2 Interpretation of results

Three groups of values are given in the graphs:

- The blue dots represent the bending moment and support reaction respectively, for a varying value for the transverse modulus of elasticity. For both graphs it can be seen that a sudden decrease in the bending moment/support reaction takes place between a transverse E-modulus of 0% and 25% of E_x. Therefore, two additional points were introduced;

- The red points represent these additional points. The bending moments and support reactions were calculated for a transverse modulus of elasticity of 5% and 10% of E_x;

- The green dots represent the values determined by a hand calculation in the previous paragraph.

It can be seen that a large reduction in bending moment and support reaction can already be achieved by a applying an orthotropic plate with a transverse E-modulus of a few percent of the E-modulus in longitudinal direction. The largest reduction is obtained with a transverse E-modulus equal to 25 – 33% of the E-modulus in transverse direction, further decrease of the bending moment/support reaction by increasing the transverse stiffness is limited.

In addition, it can be concluded that even if the modulus of elasticity in transverse direction is set equal to zero, there is still a certain amount of redistribution of the loads, because even in limit case 1 the theoretical value has not been achieved. The decrease in value between the hand calculation and the FEM model are a decrease of 15% for the bending moment and 7% for the support reaction.

Limit case 1 is found for $E_y = 0$ and case 2 is found for $E_y = E_x$, in the latter case an isotropic plate is modelled. The total reduction of the determined forces between the two limit cases of the FEM model are 68% for the bending moment and 46% for the support reactions.

9.3.3 Validation of the model

To verify the results, it is analysed how RFEM calculates the properties of the orthotropic plate. In order to do so, one of the analysed cases is selected (selected case is $E_y = 0{,}5 * E_x$) and the orthotropic plate is modelled again, but this time the stiffness parameters are directly entered into the stiffness matrix. The parameters are calculated as follows:

- Bending components:

$$D_{11} = \frac{E_x * h^3}{12 * \left(1 - \left(v_{xy} * v_{yx}\right)\right)}$$ Equation (21)

$$D_{22} = \frac{E_y * h^3}{12 * \left(1 - \left(v_{xy} * v_{yx}\right)\right)}$$ Equation (22)

$$D_{12} = v_{yx} * D_{11}$$ Equation (23)

$$D_{33} = \frac{G_{xy} * h^3}{12}$$ Equation (24)

Where:
D_{11}: Bending in x-direction
D_{22}: Bending in y-direction
D_{12}: Coupling of bending in x and y-direction
D_{33}: Torsion

- Shear components:

$$D_{44} = G_{xz} * h$$ Equation (25)

$$D_{55} = G_{yz} * h$$ Equation (26)

Where:
D_{44}: Shear in x-direction
D_{55}: Shear in y-direction

Reference is made to the Excelsheet (annex VIII) for the calculation of these parameters for all used values for E_y. For a comparison it can be seen that the calculated values using the aforementioned equations and the values calculated for the case $E_y = 0{,}5 * E_x$ by RFEM coincide, except for two differences.

- Equations (21) up to and including (24) are in exact accordance with the calculations of RFEM. The equations (25) and (26) result in larger values than the values calculated by RFEM, this is due to the fact that in RFEM both values are multiplied with a factor $5/6$, this term being a factor associated with the shear of a rectangular cross section;

- In addition, RFEM includes membrane forces. To analyse the influences of this, the values for the case $E_y = 0{,}5 * E_x$ are used again. The terms associated to membrane action are set equal to zero while the other aforementioned terms D_{11} up to D_{55} are kept. The results are a maximum bending moment of 7455 kNm and the support reactions are 667 kN, the differences are therefore negligible.

The expressions and default approach in RFEM has herewith been explained. A final point worth considering is the fact that the limit value where E_y results in lower values for the bending moment and the support reactions. The question is what causes this difference. It could be that the bending stiffness in longitudinal direction is overestimated by adding a plate element. After all, the top flange of the box beam is accounted for twice: once via the beam elements representing the box beams and once via the plate element.

Reduce the bending stiffness in longitudinal direction to analyse this. $E_x = 11.000$ whilst keeping $E_y = 0$ results in a bending moment of 22.571 kN and a support reaction of 1151 versus the limit case where the bending moment was 22.406 and the support reaction 1151 (for $E_x = 33.000$ and $E_Y = 0$). It can be seen that at least the bending moment shifts towards the theoretical value. The remaining difference in the theoretical value and the value from the RFEM model can be explained by the behaviour of the model. The adjacent beams will be ''activated'' due to the plate being present and the loads acting on these beams via the plate. As a result, the interaction cannot be avoided completely. That means that with the given load configuration the theoretical value can be approached, but not exactly reached.

9.3.4 Conclusion

In this chapter the influence of the assumption that there would be no interaction to the beams on the results of the calculation has been analysed by comparing the values for the maximum bending moment at midspan and the support reactions due to the traffic loads, for a varying value for the transverse modulus of elasticity.

It has been concluded that already for a relatively small value for the modulus of elasticity a large reduction of the bending moment and support reaction can be achieved. As it turns out there is a significant interaction between the different beams. Previously it was stated that the interaction between the beams would be neglected because it could not be quantified what the magnitude of this effect would be, especially because of the relatively slender cross sections. As it turns out this assumption was on the safe side, but overly conservative.

Although exact values cannot be given because modelling only the variable loads in a specific configuration does not give the complete force distribution and because other situations might turn out to be governing when accounting for the interaction between the beams, based on the results in this chapter it can be safely assumed that using a FEM model that includes the interaction between the beams will result in a more economical design compared to the hand calculations from the preliminary design.

9.4 Bibliography chapter nine

Dlubal Software. (2018, June 27). *Orthotropic Material Laws*. Opgeroepen op August 10, 2020, van Dlubal Software - Support and learning: https://www.dlubal.com/en/support-and-learning/support/knowledge-base/001525

Dlubal Software. (2018, July 10). *Thin Rectangular Orthotropic Plate Under Uniform Load*. Opgeroepen op August 10, 2020, van Dlubal Software - Downloads and information: https://www.dlubal.com/en-US/downloads-and-information/examples-and-tutorials/verification-examples/000091

Dlubal Software. (2019, December). User Manual RFEM 5. *Spatial Models Calculated According to Finite Element Method*.

SCIA. (sd). *Orhotrope eigenschappen van plaatelementen*. Opgehaald van Scia Engineer: https://help.scia.net/17.0/nl/rb/modelling/orthotropic_properties_of_slab_members.htm

Welleman, H. (2018). Lecture notes CIE4190.

10

CONCLUSIONS AND PROSPECTS

Conclusions

This report covered many topics considering preparatory work for the design phase as well as the elaboration of the preliminary design. By achieving the goal of the work presented in this report an answer can be formulated to the different research questions that were introduced in the preface of this report, the answers can be found in the corresponding chapters.

After the goal and scope as well as the assumptions, boundary conditions and requirements were covered, an overview was given of the collected codes & guidelines. In addition, the AFGC-SETRA recommendations from 2013 were selected to be used as the UHPC specific guideline. The reasoning behind this was explained as well.

Subsequently the AFGC-SETRA guideline itself was considered. In the fourth chapter the first part of the guideline was discussed, revealing main principles of the guideline and its reliance on testing. In the fifth chapter the review continued with relevant sections from the second part, which covers the structural design in UHPC. Using the guideline and other sources of literature, calculation procedures were formulated for bending moment and shear force capacity. In addition, relevant parts from Eurocode 2 were also given. Either to supplement missing information from the AFGC guideline, or as a brief comparison with the provisions from the AFGC.

In the sixth and seventh chapter a preliminary design was dimensioned, loads were calculated and the verification was subsequently carried out based on the procedures formulated in the preceding chapters. A simple model was proposed to analyse the force distribution. Although some of the initial dimensions had to be changed to satisfy the requirements with regard to the prestressing, it was proven that the preliminary design has sufficient bending moment and shear force capacity and that the deflection is within appropriate limits. This preliminary design is the starting point for the next phases of the project and gives the order of magnitude of the required dimensions.

In chapter eight a rough comparison was made between the weight of the existing bridge and the preliminary design. Although it was concluded that the preliminary design results in higher self-weight, the potential to reduce the weight of the new bridge by further optimizations was also deemed large enough to obtain a design with a weight equal to or lower than the bridge. In the ninth chapter the force distribution was analysed further by considering the interaction between the different beams. This analysis demonstrated that the hand calculation model used in chapters six and seven has shortcomings as it yielded very conservative results. Using FEM in the next design stage has a large potential to contribute to a more economical design in terms of weight.

Considering this report as a whole it has been proven that there is potential to, after further design and optimizations, obtain a design that meets the goal of the thesis project. The next phase of the project will therefore be to work on a more refined and optimized design.

Prospects

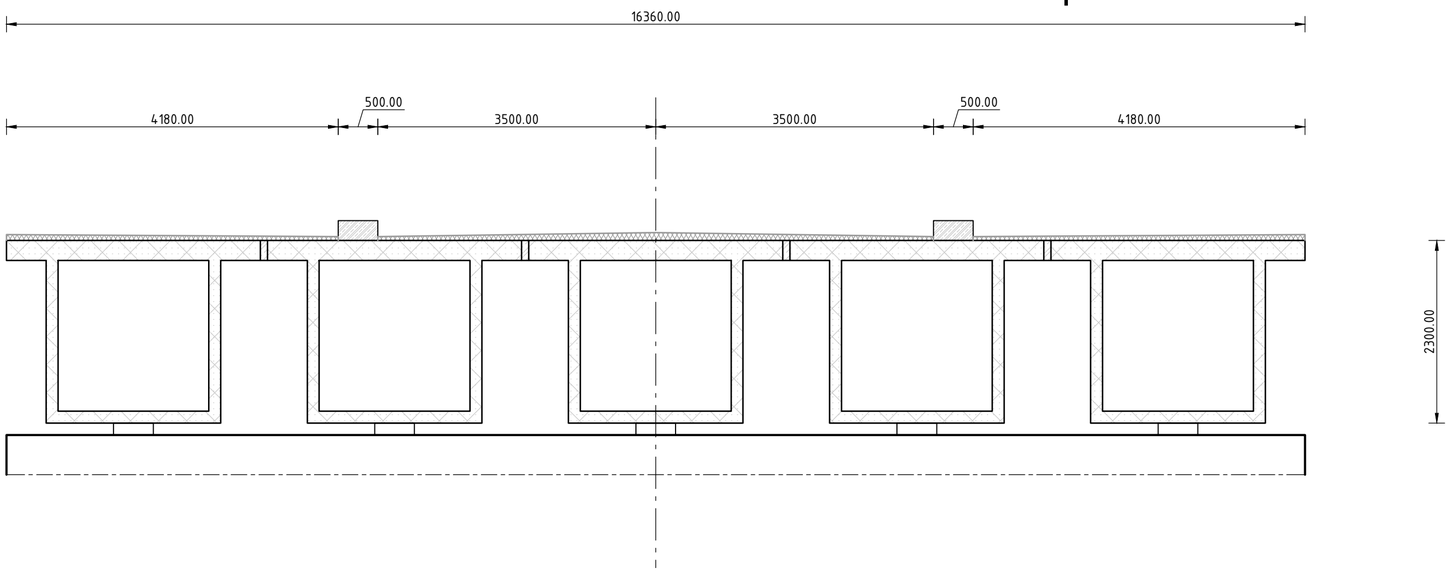
In addition to proving the potential of meeting the goal of the project, the elaboration of the preliminary design and further analysis of the results have provided insight into the many opportunities to further refine and optimize the design within the framework of the project. To conclude this report an overview of these points is given.

- **Material parameters**: More accurate values so the UHPC mixture can be used to its full potential;
- **More accurate model**: Chapter nine has illustrated the importance of an accurate model. Using a more accurate FEM model instead of more practical hand calculations has large potential to result in a more optimized design;
- **Beam design**: The number and shape of the beams has been established based on rules of thumb, examples from the literature study, etc. Optimizing for the number and shape of the beams may result in more a more economical design;
- **Prestressing**: The design of the prestressing also offers possibilities for optimization. For example, external prestressing could result in more slender cross sections because the concrete cross section no longer has to accommodate the prestressing tendons. Calculating the prestressing losses might also result in more economical solutions instead of using estimations for the losses.
- **Adjusting requirements**: In the preliminary design the most conservative solution was often chosen, an example was to opt for ''full prestressed'' beams. However, one of the benefits of UHPC is its high tensile strength. Relaxing this requirement and allowing for a certain tensile stress could therefore result in savings for the required prestressing;
- **Evaluating the loads**: In the following design phases all relevant loads will be considered (contrary to this preliminary design), but these should also be evaluated critically. For example, in the preliminary design an asphalt layer was included as this was described by the ROK. However, from a structural point of view this is not required for UHPC while at the same time it accounts for a significant portion of the permanent loads. It can be substantiated that reducing or leaving out the asphalt layer will result in a more economical design.

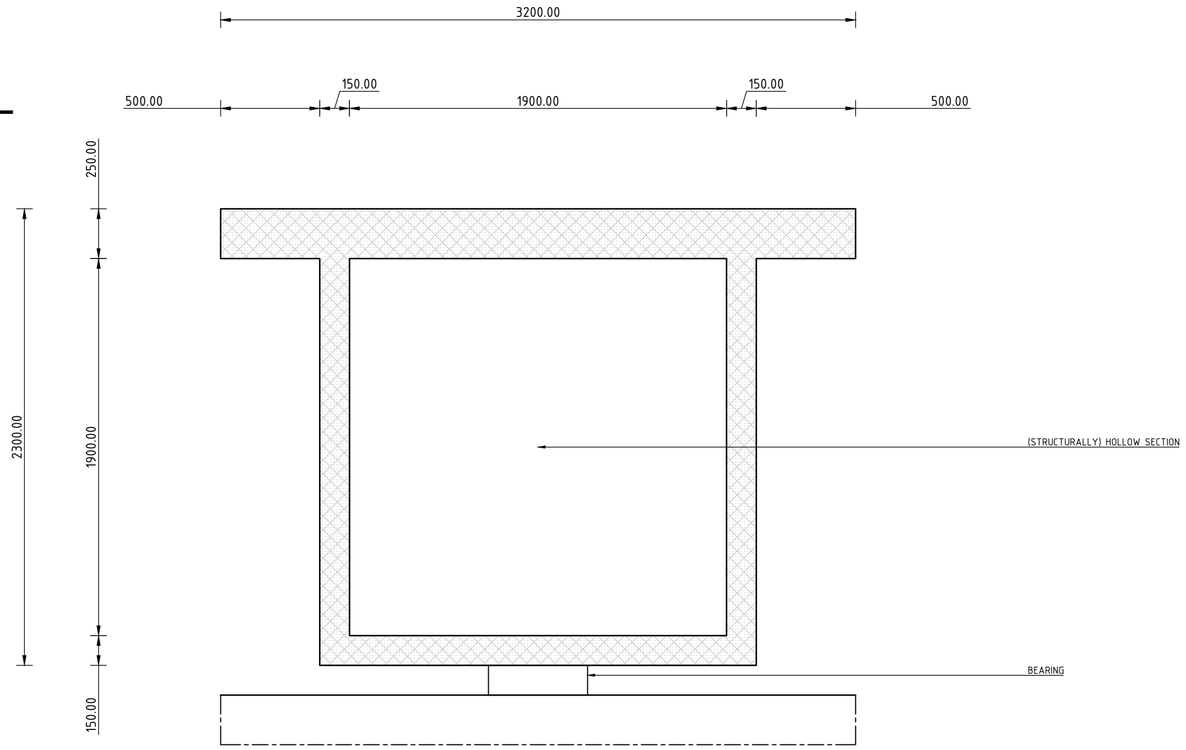
In addition to these opportunities for design, a number of points have simply not been considered in the preliminary design. For example, certain load situations (execution phase), limitations in terms of execution (transport or maximum prestressing forces in a prefab factory) or verifications (e.g. local verifications of joints). These points will have to be considered nonetheless, and in the next design phase a more comprehensive and detailed design will therefore be elaborated.

Annex(es)

ANNEX: DRAWING CROSS-SECTION PRELIMINARY DESIGN



DECK CROSS SECTION AND POSITIONING OF TRAFFIC LANES
SCHAAL 1 : 50



CROSS SECITONAL DIMENSIONS OF SINGLE PREFAB BEAM
SCHAAL 1 : 20

REMARKS:

- ALL UNITS IN mm

- CAPPING BEAM AND BEARINGS ONLY FOR INDICATION

OPDRACHTGEVER
–

PROJECTOMSCHRIJVING
MSC THESIS
REDESIGN OF BRIDGES TWENTEKANAAL IN UHPC

TEKENINGOMSCHRIJVING
PRELIMINARY DESIGN
DRAWING CROSS-SECTION PRELIMINARY DESIGN

DOCUMENTSOORT
DRAWING

STATUS
FINAL VERSION

TEKENAAR

SCHAAL
1:50/1:20

PROJECTLEIDER

FORMAAT
A2

BLAD IN BLADEN
1 IN 1

TEKENINGNUMMER

WIJZ.NR

Plaats hier uw logo

ANNEX: PRELIMINARY DESIGN CALCULATIONS

Preliminary Design Calculations - Geometry & Loads

Project: MSc thesis "Redesign of bridges Twentekanaal in UHPC"
Name: M. Dorland
Date: 9-8-2020
Version: D1.0

Legend:
Input
Output

Input: Prefab UHPC beams

Geometry of the beams

w	3200	[mm]	*Total width*
h	2325	[mm]	*Total height*
t_{ft}	250	[mm]	*Thickness top flange*
t_{fb}	273	[mm]	*Thickness bottom flange*
t_w	150	[mm]	*Thickness of web*
h_b	1802	[mm]	*Internal height of the box*
w_f	500	[mm]	*Width of the flanges*
w_b	1900	[mm]	*Internal width of the box*
Check 1	OK	[-]	*Check: w=2*wf+2*tw+wb?*
Check 2	OK	[-]	*Check: h=tft+hb+tfb?*

Modelling parameters

δ	0,0	[-]	

Material properties UHPC

f_{ck}	150	[N/mm²]	
α_{cc}	0,85	[-]	
E_{cm}	50000	[N/mm²]	
ε_{cu3}	0,0027	[-]	
ε_{c3}	0,0017	[-]	
f_{ctd}	6	[N/mm²]	
$f_{ctd;2}$	6	[N/mm²]	
K_{global}	1,25	[-]	
α	0,69	[-]	
β	0,37	[-]	
θ	30	[º]	
φ	0,8	[-]	
γ_{UHPC}	28	[kN/m³]	
γ_c	1,5	[-]	
$\gamma_{cf}\gamma_E$	1,5	[-]	
γ_{cf}	1,3	[-]	

Properties steel fibres

l_f	30	[mm]	Length of fibre (assumption)

Material properties prestressing

f_{pk}	1860	[N/mm²]	
f_{pd}	1522	[N/mm²]	Slope discontinuity.
σ_{pm0}	1395	[N/mm²]	Max. prestressing force after tensioning.
$\sigma_{pu,est}$	1606	[N/mm²]	
E_p	195000	[N/mm²]	
ε_{uk}	0,035	[-]	
γ_s	1,1	[-]	

Parameters prestressing

$A_{p,strand}$	100	[mm²]	
Depth	136,5	[mm]	Position in bottom flange from bottom
ΔP	20	%	Estimated prestress loss
σ_{max}	0	[N/mm²]	

Other material properties

γ_C	25	[kN/m³]	*Concrete used for the kerbs.*
$\gamma_{asphalt}$	23	[kN/m³]	*Asphalt layer on top of the concrete deck.*

Calculation parameters

Rgoal	1,0000	[-]	*Required for calculations using Macro.*

Input: Geometry of the deck

Geometry of the deck: Cross section

l	68,00	[m]	*Span of the bridge*
b_{tot}	16,36	[m]	*Total width of the bridge*
w_{ped}	4,18	[m]	*Width of a single bicycle/pedestrian lane*
w_{tl}	7,00	[m]	*Width of the carriageway*
w_{kerbs}	0,50	[m]	*Width of single kerb*
Check	OK	[-]	*Check: Total width has to be 16,36 m*

Geometry of the deck: Beams

N	5	[-]	*Number of beams*
w	3,2	[m]	*Total width of the beam*
w_{joint}	0,09	[m]	*Width of the joint*

Coordinates of the elements

Element	From	To
[-]	[m]	[m]
Beam 1	0,00	3,20
Joint 1	3,20	3,29
Beam 2	3,29	6,49
Joint 2	6,49	6,58
Beam 3	6,58	9,78
Joint 3	9,78	9,87
Beam 4	9,87	13,07
Joint 4	13,07	13,16
Beam 5	13,16	16,36

Input: Loads

Input static loads

$t_{asphalt}$	140	[mm]	*Thickness based on RBK 1.4*
h_{kerbs}	340	[mm]	*Based on NA to EN 1991-2 and t asphalt*

Input traffic load pedestrian lanes (LM4)

p_{LM4}	3,7	[kN/m²]	

Input traffic load traffic lane (LM1)

w_1	3,0	[m]	*Width of lane 1*
w_2	3,0	[m]	*Width of lane 2*
w_r	1,0	[m]	*Width of remaining area*
$\alpha_{Q1}Q_{1k}$	300	[kN/axle]	*Axle load lane 1*
$\alpha_{q1}q_{1k}$	9	[kN/m²]	*Uniformly distributed load lane 1*
$\alpha_{Q2}Q_{2k}$	200	[kN/axle]	*Axle load lane 2*
$\alpha_{q2}q_{2k}$	2,5	[kN/m²]	*Uniformly distributed load lane 2*
$\alpha_{qr}q_{rk}$	2,5	[kN/m²]	*Uniformly distributed load remaining area*

Load and combination factors 6.10a

γ_G	1,4	[-]	*Tabel NB.16 – A2.4(B)*
ψ_0	0,8	[-]	*Tabel NB.12 – A2.1*
γ_Q	1,5	[-]	*Tabel NB.16 – A2.4(B)*

Load and combination factors 6.10b

$\zeta * \gamma_G$	1,25	[-]	*Tabel NB.16 – A2.4(B)*
ψ_0	-	[-]	*Tabel NB.12 – A2.1*
γ_Q	1,5	[-]	*Tabel NB.16 – A2.4(B)*

Load group traffic loads

gr1a is applied (cf NEN-EN 1991-2 +NA), which means that for LM1 the characteristic load is used while LM4 is multiplied with a factor 0,4.

Output: Determining cross-sectional properties

Cross-sectional area

A	1941200	[mm²]	$A = (2w_f + 2t_w + w_b) * t_{ft} + 2h_b t_w + (2t_w + w_b) * t_{fb}$

Centre of gravity

Part	A_i	$\overline{z}_i$	$S_{\overline{z}}$
[-]	[mm²]	[mm]	[mm³]
Top flange	800000	125	100000000
Webs	540600	1151	622230600
Lower flange	600600	2188,5	1314413100
Total	1941200	-	2036643700

$$\overline{z} = \frac{S_{\overline{z}}}{A} = \frac{\sum A_i * \overline{z}_i}{\sum A_i}$$

$\overline{z}$	1049	[mm]	*Vertical coordinate of centroid measured from top of the CS.*
e_t	1049	[mm]	$e_t = h - e_b = \overline{z}$
e_b	1276	[mm]	$e_b = h - \overline{z}$

Second moment of area

Part:	$I_{zz,i}$	A_i	a_i^2	$I_{zz,i}+A_i*a_i^2$
	[mm⁴]	[mm²]	[mm]	[mm⁴]
Top flange	4166666667	800000	924,1673707	6,87435E+11
Webs	1,46287E+11	540600	101,8326293	1,51892E+11
Lower flange	3730176450	600600	1139,332629	7,83356E+11
Total	-	-	-	1,62268E+12

I_{zz}	1,623E+12	[mm⁴]

Section modulus

$W_{y,t}$	1,55E+09	[mm³]	$W_{y,t}=I_{zz}/e_t$
$W_{y,b}$	1,27E+09	[mm³]	$W_{y,b}=I_{zz}/e_b$

Output: Elaboration of the loads

Load case: Self-weight

$q_{k,sw}$	54,3536	[kN/m]

Load case: Asphalt layer

$q_{k,asphalt}$	3,22	[kN/m²]

Load case: Kerbs

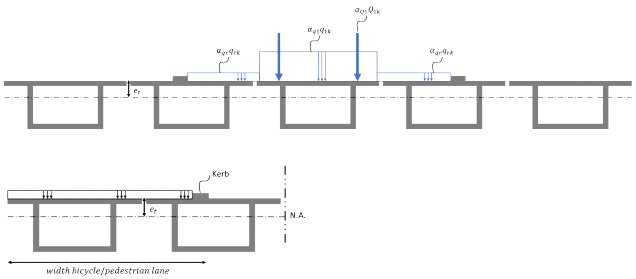
$q_{k,kerbs}$	4,25	[kN/m]

Load case: Traffic loads (LM1)

$\alpha_{q1}q_{1k}$	9,00	[kN/m²]
$\alpha_{Q1} * Q_{1k}$	300,00	[kN/axle]
w_1	3,00	[m]
$\alpha_{q2}q_{2k}$	2,50	[kN/m²]
$\alpha_{Q2}Q_{2k}$	200,00	[kN/axle]
w_2	3,0	[m]
$\alpha_{qr}q_{rk}$	2,50	[kN/m²]

Load case: Pedestrian loads (LM4)

q_{fk}	3,7	[kN/m²]
w_{ped}	4,18	[m]



Output: Load combinations ultimate limit state

Effective width of the beams

$b_{eff,o}$	3,245	[m]	*Effective width outer beams*
$b_{eff,i}$	3,290	[m]	*Effective width inner beams*

Force distribution over the beams

UDL LM1	100	[%]	*Percentage of load carried by the beam.*
Axles LM1	100	[%]	*Percentage of load carried by the beam.*
UDL rest	100	[%]	*Percentage of load carried by the beam.*
UDL LM4	100	[%]	*Percentage of load carried by the beam.*

Adding up characteristic values of the loads

	Permanent loads				Variable loads				Prestressing
Beam	$G_{k,beams}$	$G_{k,asphalt}$	$G_{k,kerbs}$	$G_{k,total}$	$Q_{k,UDL,LM1}$	$0.4 * Q_{k,LM4}$	$Q_{k,UDL,total}$	$Q_{k,axle,LM1}$	$M_{P,\infty}$
[-]	[kN/m1]	[kN/m1]	[kN/m1]	[kN/m1]	[kN/m1]	[kN/m1]	[kN/m1]	[kN/axle]	[kNm]
Beam 1	54,35	10,45	0,00	64,80	0,00	4,80	4,80	0,00	-42086
Beam 2	54,35	10,59	4,25	69,20	4,64	1,38	6,02	0,00	-42086
Beam 3	54,35	10,59	0,00	64,95	27,73	0,00	27,73	300,00	-42086
Beam 4	54,35	10,59	4,25	69,20	4,64	1,38	6,02	0,00	-42086

Beam 5	54,35	10,45	0,00	64,80	0,00	4,80	4,80	0,00	-42086

Formulating the load combinations (Eq. 6.10a and Eq. 6.10b)

Load combination 6.10a			Load combination 6.10b		
$G_{d,total}$	$Q_{d,UDL,total}$	$Q_{d,axle}$	$G_{d,total}$	$Q_{d,UDL,total}$	$Q_{d,axle.LM1}$
[kN/m1]	[kN/m1]	[kN/axle]	[kN/m1]	[kN/m1]	[kN/axle]
90,72	5,76	0,00	81,00	7,20	0,00
96,88	7,23	0,00	86,50	9,03	0,00
90,93	33,27	360,00	81,18	41,59	450,00
96,88	7,23	0,00	86,50	9,03	0,00
90,72	5,76	0,00	81,00	7,20	0,00

Eq. 6.10a $E_d = 1{,}40 * (G_{k,beams} + G_{k,asphalt} + G_{k,kerbs}) + \gamma_P P + 0{,}8 * 1{,}5 * Q_k$

E1. 6.10b $E_d = 1{,}25 * (G_{k,beams} + G_{k,asphalt} + G_{k,kerbs}) + \gamma_P P + 1{,}5 * Q_k$

Determining bending moments acc. Eq. 6.10a and Eq. 6.10b

	$M_{Ed,G}$	$M_{Ed,Q,UDL}$	$M_{Ed,Q,Axle}$	$M_{P,\infty}$	$M_{Ed,total}$	**Beams**	**Equation**
	[kNm]	[kNm]	[kNm]	[kNm]	[kNm]	[Nr.]	[Nr.]
	52438	3331	0	-42086	13683	Beam 1	**6.10a**
	55995	4176	0	-42086	18084	Beam 2	**6.10a**
Eq. 6.10a	52555	19230	12240	-42086	41939	Beam 3	**6.10a**
	55995	4176	0	-42086	18084	Beam 4	**6.10a**
	52438	3331	0	-42086	13683	Beam 5	**6.10a**
	46820	4164	0	-42086	8897	Beam 1	**6.10b**
	49995	5220	0	-42086	13129	Beam 2	**6.10b**
Eq. 6.10b	46924	24038	15300	-42086	44176	Beam 3	**6.10b**
	49995	5220	0	-42086	13129	Beam 4	**6.10b**
	46820	4164	0	-42086	8897	Beam 5	**6.10b**
Maximum:	55995	24038	15300	-42086	44176	-	-
Beam:	Beam 2	Beam 3	Beam 3	-	Beam 3	-	-
Equation:	6.10a	6.10b	6.10b	-	6.10b	-	-

For any uniformly distributed load q_d, the bending moment is determined using:

$$M_{Ed,UDL} = \frac{1}{8} * q_d * l^2$$

For the concentrated axle loads, the bending moment is determined using:

$$M_{Ed,axle} = \frac{1}{4} * 2Q_{d,axle,LM1} * l$$

For the bending moment due to the prestressing (see next page):

$$M_{P,\infty} = P_\infty * e * l$$

Determining shear forces acc. Eq. 6.10a and Eq. 6.10b

	$V_{Ed,G}$	$V_{Ed,Q,UDL}$	$V_{Ed,Q,Axle}$	$V_{P,\infty}$	$V_{Ed,total}$	**Beams**	**Equation**
	[kN]	[kN]	[kN]	[-]	[kN]	[Nr.]	[Nr.]
	3085	196	0	0	3281	Beam 1	**6.10a**
	3294	246	0	0	3539	Beam 2	**6.10a**
Eq. 6.10a	3091	1131	720	0	4943	Beam 3	**6.10a**
	3294	246	0	0	3539	Beam 4	**6.10a**
	3085	196	0	0	3281	Beam 5	**6.10a**
	2754	245	0	0	2999	Beam 1	**6.10b**
	2941	307	0	0	3248	Beam 2	**6.10b**
Eq. 6.10b	2760	1414	900	0	5074	Beam 3	**6.10b**
	2941	307	0	0	3248	Beam 4	**6.10b**
	2754	245	0	0	2999	Beam 5	**6.10b**
Maximum:	3294	1414	900	0	5074	-	-
Beam:	Beam 2	Beam 3	Beam 3	-	Beam 3	-	-
Equation:	6.10a	6.10b	6.10b	-	6.10b	-	-

For any uniformly distributed load q_d, the shear force is determined using:

$$V_{Ed,UDL} = \frac{1}{2} * q_d * l$$

For the concentrated axle loads, the shear force is determined using:

$$V_{Ed,axle} \approx 2 * Q_{d,axle,LM1}$$

For the shear force due to the prestressing (see next page):

$$V_{P,\infty} = 0$$

Preliminary Design Calculations - Preliminary design verifications

Project: MSc thesis "Redesign of bridges Twentekanaal in UHPC"
Name: M. Dorland
Date: 9-8-2020
Version: D1.0

Input overview

Cross sectional properties		
h	2325	[mm]
b	3200	[mm]
bweb	300	[mm]
dp	2188,5	[mm]

Properties concrete		
f_{ck}	150	[N/mm²]
α_{cc}	0,85	[-]
E_{cm}	50000	[N/mm²]
ε_{cu3}	0,0027	[-]
ε_{c3}	0,0017	[-]
f_{ctd}	6	[N/mm²]
$f_{ctd;2}$	6	[N/mm²]
K_{global}	1,25	[-]
α	0,69	[-]
β	0,37	[-]
θ	30	[°]
φ	0,8	[-]
γ_c	1,5	[-]
$\gamma_{cf}\gamma_E$	1,5	[-]
γ_{cf}	1,3	[-]

Properties prestressing		
f_{pk}	1860	[N/mm²]
f_{pd}	1522	[N/mm²]
σ_{pm0}	1395	[N/mm²]
$\sigma_{pu,est}$	1606	[N/mm²]
E_p	195000	[N/mm²]
ε_{uk}	0,035	[-]
γ_s	1,1	[-]
$A_{p,strand}$	100	[mm²]
Depth	136,5	[mm]
ΔP	20	[%]
σ_{max}	0	[N/mm²]

Properties steel fibres		
l_f	30	[mm]

Accuracy		
Rgoal	1,0000	[-]

Prestressing

Input parameters for prestressing design

Input loads			
ME,perm	39996	[kNm]	*Bending moment permanent loads SLS*
ME,var	26225	[kNm]	*Bending moment variable loads SLS*

Relevant cross sectional properties		
A	1941200	[mm²]
$W_{y,t}$	1,55E+09	[mm³]
$W_{y,b}$	1,27E+09	[mm³]
I	1,623E+12	[mm⁴]

Determining bending moment prestressing		
e	1139	[mm]

Designing the prestressing

Stresses - Analysing situation 1

	Perm	P axial	P moment	Resulting
Case	[N/mm²]	[N/mm²]	[N/mm²]	[N/mm²]
Top fibre	-25,86	-11,48	16,42	-20,92
Bottom fibre	31,45	-11,48	-19,97	0,00

Max 0,00 [N/mm²]

Stresses - Analysing situation 2

	Perm	P axial	P moment	Variable	Resulting
Case	[N/mm²]	[N/mm²]	[N/mm²]	[N/mm²]	[N/mm²]
Top fibre	-25,86	-19,01	27,18	-16,96	-34,64
Bottom fibre	31,45	-19,01	-33,06	20,62	0,00

Max 0,00 [N/mm²]

Prestressing force

Preq kN 1	22287,82616	[kN]	*Required to obtain prescribed maximum stress*
Preq kN 2	46127,1699	[kN]	*Required to obtain prescribed maximum stress*
Preq	46127,1699	[kN]	*Governing value of required prestressing force*

Prestressing elements

$A_{p,req}$	33066	[mm2]	*Required cross secitonal area of prestressing elements*
$N_{strands}$	331	[-]	*Required number of prestressing strands*
A_p	33100	[mm2]	*Provided cross sectional area of prestressing elements*
P_0	46175	[kN]	*Provided initial prestressing force*
P_∞	36940	[kN]	*Provided working prestressing force with estimated losses*

Bending moment capacity

Step 1. Identifying all horizontal forces

Passieve bijdrage wapening hier nog niet berekend.

Concrete		
α	0,69	[-]
b	3200	[mm]
fcd	85	[N/mm²]
xu	296,2402264	[mm]

Active contribution prestressing		
A_p	33100	[mm²]
$\sigma_{p,\infty}$	1116	[N/mm²]

Contribution concrete under tension		
f_{ctd}	6	[N/mm²]
$f_{ctd;2}$	6	[N/mm²]
b	300	[mm]

Auxiliary parameters			
lc	1550	[mm]	*Characteristic length*

Step 2. Height of concrete compressive and tensile zone

Parameters compressive zone	Concrete compressive forces	Lever arm (from top fibre)	Eccentricity with respect to top fibre

ε_{c3}	0,0017	[-]	Case 1: Nc1	0	[N]	S1	N.A.	[Nmm]	Case 1: et	0 [mm]
ε_{cu3}	0,0027	[-]	Case 1: Nc2	0	[N]	S2	N.A.	[Nmm]		
fcd	85	[N/mm²]	Case 1: Nc3	0	[N]	S3	N.A.	[Nmm]		
b	3200	[mm]	Case 2: Nc1	29843460	[N]	S1	1637191352	[Nmm]	Case 2: et	110,7496778 [mm]
tft	250	[mm]	Case 2: Nc2	23807928	[N]	S2	4282077342	[Nmm]		
bred	300	[mm]	Case 2: Nc3	146157	[N]	S3	38792142	[Nmm]		
xu,t	109,72	[mm]	Case 3: Nc1	0	[N]	S1	0	[Nmm]	Case 3: et	0 [mm]
xu,b	186,52	[mm]	Case 3: Nc2	0	[N]	S2	0	[Nmm]		
$\varepsilon_{c,fl}$	0,000421	[-]	Case 3: Nc3	0	[N]	S3	0	[Nmm]		
$\sigma_{c,fl}$	21,07	[N/mm²]								
			Nc	53797545,55	[N]				et	110,7496778 [mm]

Parameters tensile zone			Concrete tensile forces			Lever arm (from top fibre)			Eccentricity with respect to top fibre	
ε_{ct}	0,00012	[-]	Nt1	11849,60906	[N]	S1	3614340,673	[Nmm]		
$\varepsilon_{ct;0,3}$	0,00031	[-]	Nt2	38224,54534	[N]	S2	12232786,73	[Nmm]		
ε_{ctd}	0,00031	[-]	Nt3	215904,9736	[N]	S3	88652119,89	[Nmm]		
ε_{ctu}	0,00250	[-]								
x1	13,16623228	[mm]								
x2	21,23585852	[mm]								
x3	239,8944151	[mm]	Nt	265979,128	[N]				et	392,8851413 [mm]

Step 3. Determining the strains

$\Delta\varepsilon_p$	0,017246481	[-]
$\varepsilon_{p,\infty}$	0,005723077	[-]
ε_p	0,022969558	[-]

Step 4. Steel stresses

f_{pd}	1522	[N/mm²]	σ_{pu}	1616	[N/mm²]
f_{pk}/γ_s	1691	[N/mm²]	$\sigma_{p,\infty}$	1116	[N/mm²]
ε_{uk}	0,035	[-]			
f_{pd}/E_p	0,007804196	[-]	P_∞	36939600	[N]
A_p	33100	[mm²]	ΔN_p	16553620	[N]

Step 5. Check equilibrium

N_c	53797546	[N]	R	1,000713294	[-]
N_t	265979	[N]			
P_∞	36939600	[N]			
ΔN_p	16553620	[N]			
Total	53759199	[N]			

Step 6. Determine bending moment capacity

Remark:
- Bending moment is calculated using the top fibre as point of reference

	Force [N]	Lever arm [mm]	Moment [Nmm]
N_c	-53797546	111	-5958060836
N_t	265979	393	104499247
P_∞	36939600	1049	38755823007
ΔN_p	16553620	2189	36227598089

M_{Rd} 69130 [kNm]

Verification:

M_{Ed}	44176	[kNm]
M_{Rd}	69130	[kNm]
UC	0,64	[-]

Step 7. Verifying the rotational capacity

δ	0,0	[-]
ε_{cu}	0,00270	[-]

d	2188,50	[mm]
f	574,91	[N/mm²]
$x_{u,max}/d$	0,40	[-]
$x_{u,prov}/d$	0,14	[-]
Verification	OK	

Shear force capacity

Remarks
- It is assumed the concrete is loaded in compression due to the prestressing, not under tension.
- It is assumed that the cross section is prestressed, but that no reinforcement is present.
- No reduction is taken into consideratoin to account for ducts, etc.

Contribution of the concrete

N_{Ed}	36940	[kN]	Axial force is taken as $N_{Ed} = P_\infty$
A_c	1941200	[mm²]	*Cross sectional area*
fck	150	[N/mm²]	
bw	300	[mm]	*Summation of width of both webs*
h	2325	[mm²]	*Height of cross section*
σ_{cp}	19,02926025	[N/mm²]	*Compressive stress due to axial prestressing*
k	1,380585205	[-]	*Factor depending on compressive stress and fck*
z	1969,65	[mm]	*cf AFGC: z = 0,9 * d*
$V_{Rd,c}$	1599	[kN]	

Concrete compressive strut

α_{cc}	0,85	[-]	$\tan(\theta)$	0,577350269	[-]
γ_c	1,5	[-]	$\cot(\theta)$	1,732050808	[-]
bw	300	[mm]			
z	1969,65	[mm]			
fck^(2/3)	28,23108087	[N/mm²]			
VRd,max	9333	[kN]			

Shear capacity and verification

Vtot	7739	[kN]
VRd,max	9333	[kN]
VEd	5074	[kN]
VRd	7739	[kN]
UC	0,66	[kN]

Contribution of the steel fibres

Afv	590895	[mm²]	*Area of fibre effect (bw*z)*
$f_{ctd;2}$	6	[N/mm²]	
θ	30	[°]	
Vf	6141	[kN]	

Total concrete capacity

Vtot	7739	[kN]

Deformations

Determining (effective) bending stiffness

l	68000	[mm]
φ	0,8	[-]
E_{cm}	50000	[N/mm²]
$E_{c,eff}$	27778	[N/mm²]
I	1,62268E+12	[mm4]
$E_{c,eff} * I$	4,50745E+16	[Nmm²]

Loads to be considered

$G_{k,total}$	64,95	[kN/m1]
$Q_{k,UDL,total}$	27,73	[kN/m1]
$Q_{k,axle.LM1}$	300,00	[kN]
$P_\infty * e$	42086	[kNm]

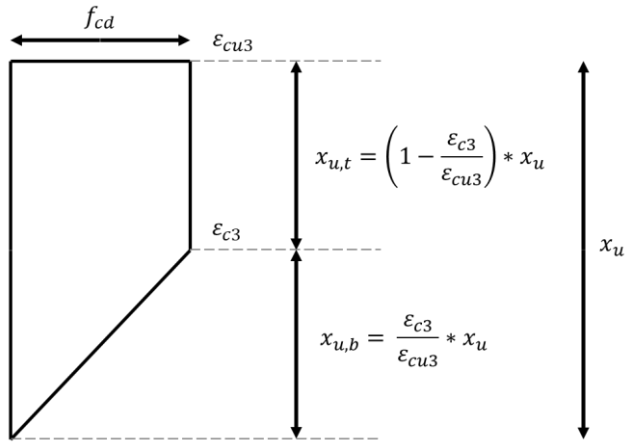
Verification

δ_G	401	[mm]
δ_P	540	[mm]
$\delta_{Q,UDL}$	137	[mm]
$\delta_{Q,axle}$	70	[mm]
δ_{tot}	68	[mm]
δ_{max}	227	[mm]
Verification	0,30	[-]

ANNEX: DERIVATIONS CONCRETE COMPRESSIVE ZONE OVER VARIABLE WIDTH

Derivations concrete compressive zone over variable width

The principle of the stress-strain figure (schematically) of concrete under compression is as follows:



Where:

$$x_{u,t} = \left(1 - \frac{\varepsilon_{c3}}{\varepsilon_{cu3}}\right) * x_u$$

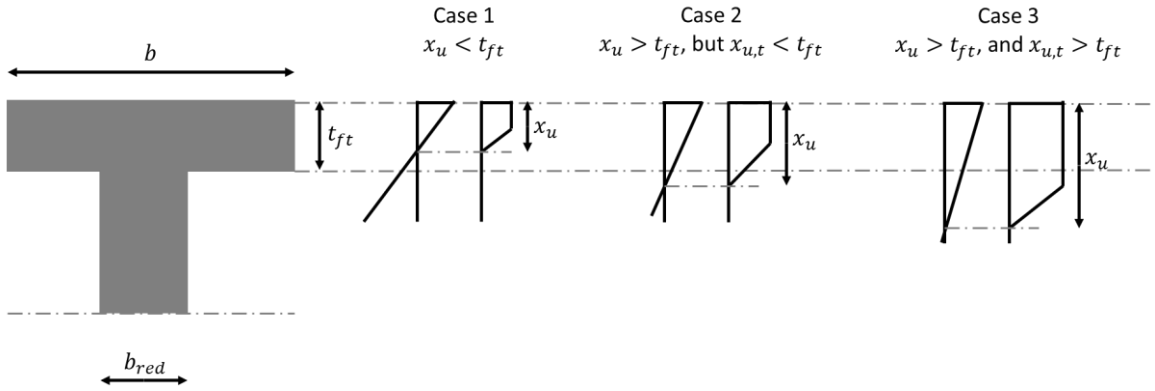
$$x_{u,b} = \frac{\varepsilon_{c3}}{\varepsilon_{cu3}} * x_u$$

The basic equations as presented in the main report are for rectangular cross sections. The width of the cross section could be varied over the height of the cross section though, an example is a box beam. Equations are formulated to calculate the normal force of the concrete compressive zone for such cases.

Definitions:

- Thickness top flange: t_{ft}
- Width top flange: b
- Reduced width: b_{red}

For a T-section three different ''scenarios'' can be distinguished:



- Scenario 1: $x_u < t_{ft}$ – Because the height of the compressive zone is smaller than the height of the top flange, standard equations for rectangular cross sections can be applied;

- Scenario 2: $x_u > t_{ft}$ maar $x_{u,t} < t_{ft}$ – Equations are to be modified to account for a reduced effective width over the web of the section;

- Scenario 3: $x_u > t_{ft}$ en $x_{u,t} > t_{ft}$ – Equations are to be modified to account for a reduced effective width over the web of the section.

The equations will now be formulated/derived for each of these three cases.

Scenario 1: The height of the compressive zone is smaller than the height of the top flange. Therefore the ''basic equations'' for rectangular cross sections can be applied:

$$N_c = \alpha * b * f_{cd} * x_u$$

The position of the resulting force of the concrete compressive zone with respect to the top fibre (most compressed fibre) is:

$$e_t = \beta * x_u$$

Scenario 2: The height of the compressive zone is larger than the thickness of the top flange, a part of the ascending part is positioned at the part of het cross section with reduced width. Therefore the equations have to be modified. The stress diagram and cross section are divided into multiple parts to calculate the compressive force.

- Part 1: Part over the full width of the top flange with a constant compressive force:

$$N_{c,1} = x_{u,t} * b * f_{cd}$$

- Part 2: Ascending part of the stress diagram within the height of the concrete compressive zone. The first term in the equation gives the height of this zone, the second term the average compressive stress.

$$N_{c,2} = \left(t_{ft} - x_{u,t}\right) * b * \frac{1}{2} * \left(\sigma_{c,fl} + f_{cd}\right)$$

- Part 3: Ascending part within the web with reduced width. The first term gives the height of this zone, the second part gives the average compressive stress.

$$N_{c,3} = \left(x_u - t_{ft}\right) * b_{red} * \frac{1}{2} * \left(0 + \sigma_{c,fl}\right)$$

- Other relevant expressions: From the stress-strain figure it can be deduced that the strain and stress at the lower side of the compressed flange are as follows:

$$\varepsilon_{c,fl} = \left(\frac{x_u - t_{ft}}{x_u}\right) * \varepsilon_{cu3}$$

$$\sigma_{c,fl} = \frac{\varepsilon_{c,fl}}{\varepsilon_{c3}} * f_{cd}$$

To determine the bending moment capacity the position of the resulting force has to be determined. In order to do so, analogous to calculating the centre of gravity of a cross section, the first moment with respect to a reference point (the upper fibre) of the three separate parts is determined. Because average values are used for the first two zones, the resulting forces of these individual parts act at half the height of these parts.

$$S_1 = N_{c,1} * \frac{x_{u,t}}{2}$$

$$S_2 = N_{c,2} * \left(x_{u,t} + \frac{t_{ft} - x_{u,t}}{2}\right)$$

$$S_3 = N_{c,3} * \left(x_{u,t} + \left(t_{ft} - x_{u,t}\right) + \frac{x_u - t_{ft}}{3}\right)$$

The centre of gravity (position of the resulting force) of the compressive zone is positioned at a distance e_t with respect to the top fibre:

$$e_t = \frac{S_1 + S_2 + S_3}{N_{c,1} + N_{c,2} + N_{c,3}}$$

Scenario 3: The height of the compressive zone is larger than the thickness of the top flange, the complete ascending part is positioned at the part of the cross section with the reduced width. The equations have to be modified. The stress diagram and cross section are divided into multiple parts to calculate the compressive force.

- Part 1: Over the full height of the top flange the stress value f_{cd} is reached;

$$N_{c,1} = t_{ft} * b * f_{cd}$$

- Part 2: Also over a limited part of the web the stress value f_{cd} is reached;

$$N_{c,2} = \left(x_{u,t} - t_{ft}\right) * b_{red} * f_{cd}$$

- Part 3: The third contribution is due to the ascending part of the compressive zone, with height $x_{u,b}$:

$$N_{c,3} = \frac{1}{2} * x_{u,b} * b_{red} * f_{cd}$$

To determine the bending moment capacity the position of the resulting force has to be determined. In order to do so, the first moment with respect to a reference point (the upper fibre) of the three separate parts is determined.

$$S_1 = N_{c,1} * \frac{t_{ft}}{2}$$

$$S_2 = N_{c,2} * \left(t_{ft} + \frac{x_{u,t} - t_{ft}}{2}\right)$$

$$S_3 = N_{c,3} * \left(t_{ft} + (x_{u,t} - t_{ft}) + \frac{x_{u,b}}{3}\right)$$

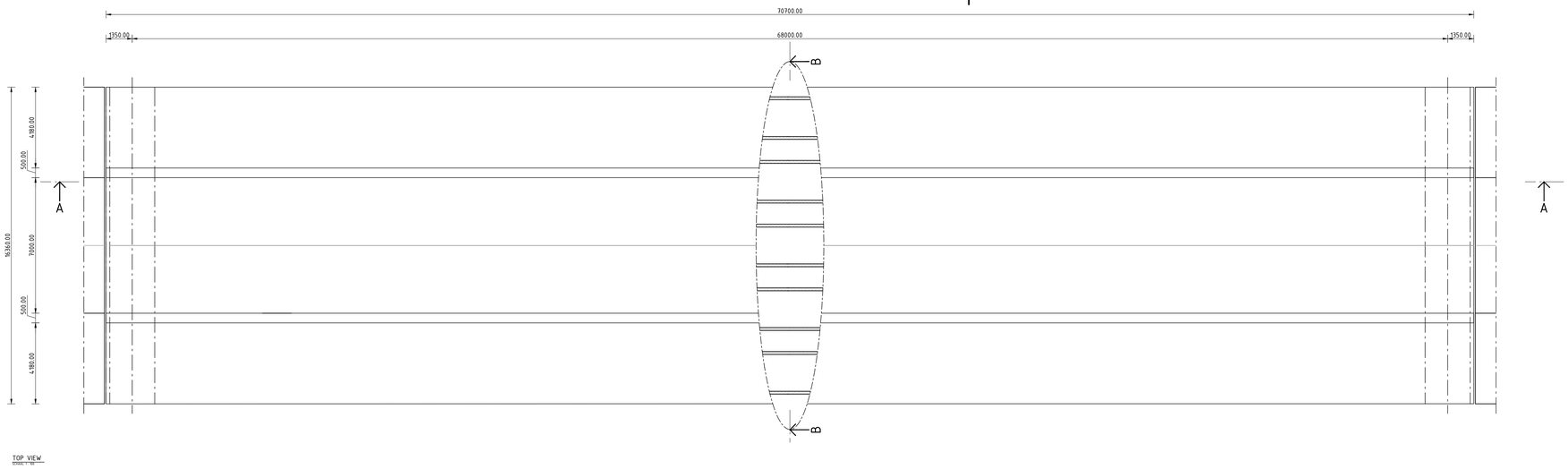
The position of the centre of gravity (position of the resulting force) of the compressive zone with respect to the outer fibre can now be determined as follows:

$$e_t = \frac{S_1 + S_2 + S_3}{N_{c,1} + N_{c,2} + N_{c,3}}$$

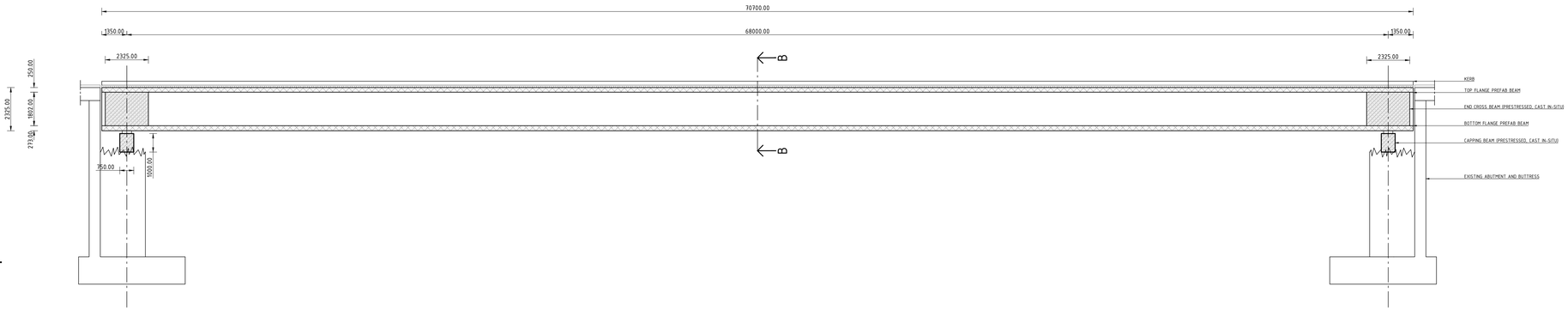
REMARK: The equations can be simplified for concrete strength classes up to and including C50/60, in these cases it holds that: $x_{u,t} = x_{u,b} = \frac{1}{2} * x_u$.

IV

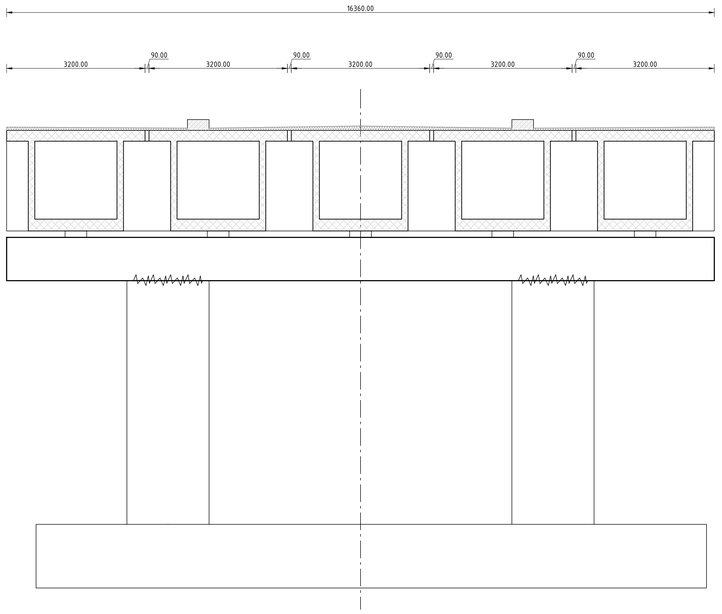
ANNEX: DRAWINGS PRELIMINARY DESIGN



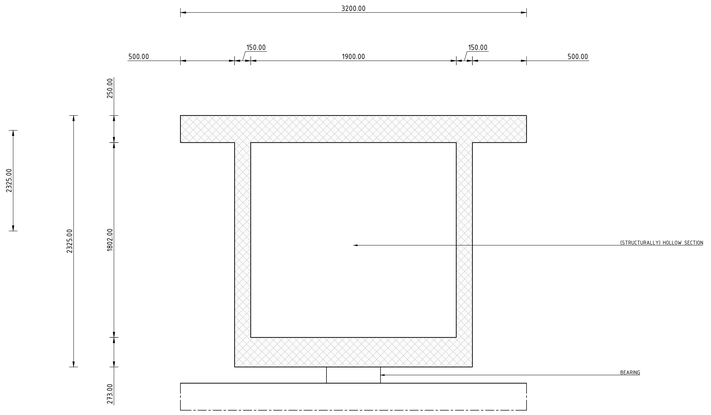
TOP VIEW
SCALE 1 : 50



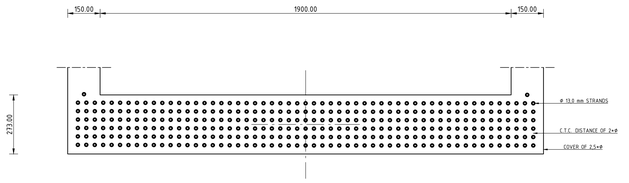
SECTION A-A: LONGITUDINAL SECTION
SCALE 1 : 50



SECTION B-B: CROSS SECTION AND POSITIONING OF TRAFFIC LANES
SCALE 1 : 50



DIMENSIONS OF PREFAB BEAM
SCALE 1 : 50



DETAIL POSITIONING PRESTRESSING STRANDS IN BOTTOM FLANGE
SCALE 1 : 10

REMARKS:

- ALL UNITS IN mm
- ABUTMENTS AND BEARINGS ONLY FOR INDICATION
- SEE REPORT FOR PRELIMINARY DESIGN AND ASSUMPTIONS, BOUNDARY CONDITIONS & REQUIREMENTS

OPDRACHTGEVER
–

PROJECTOMSCHRIJVING
MSC THESIS
REDESIGN OF BRIDGES TWENTEKANAAL IN UHPC

TEKENINGOMSCHRIJVING
PRELIMINARY DESIGN
DRAWINGS PRELIMINARY DESIGN

DOCUMENTSOORT
DRAWING

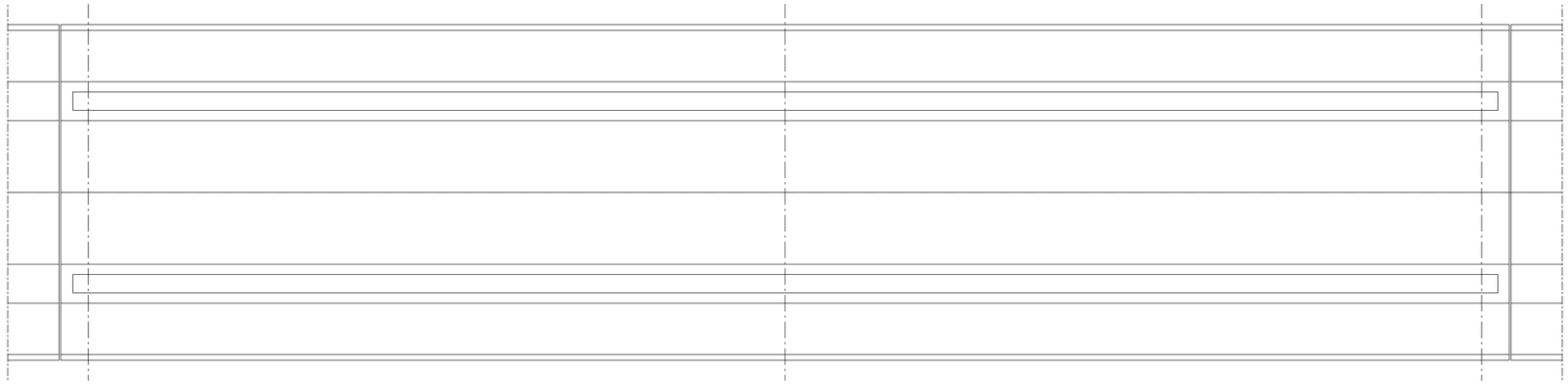
STATUS
FINAL VERSION

TEKENAAR
SCHAAL
SEE DRAWINGS
PROJECTLEIDER
FORMAAT
A0
BLAD IN BLADEN
1 IN 1
TEKENINGNUMMER
WIJZ NR

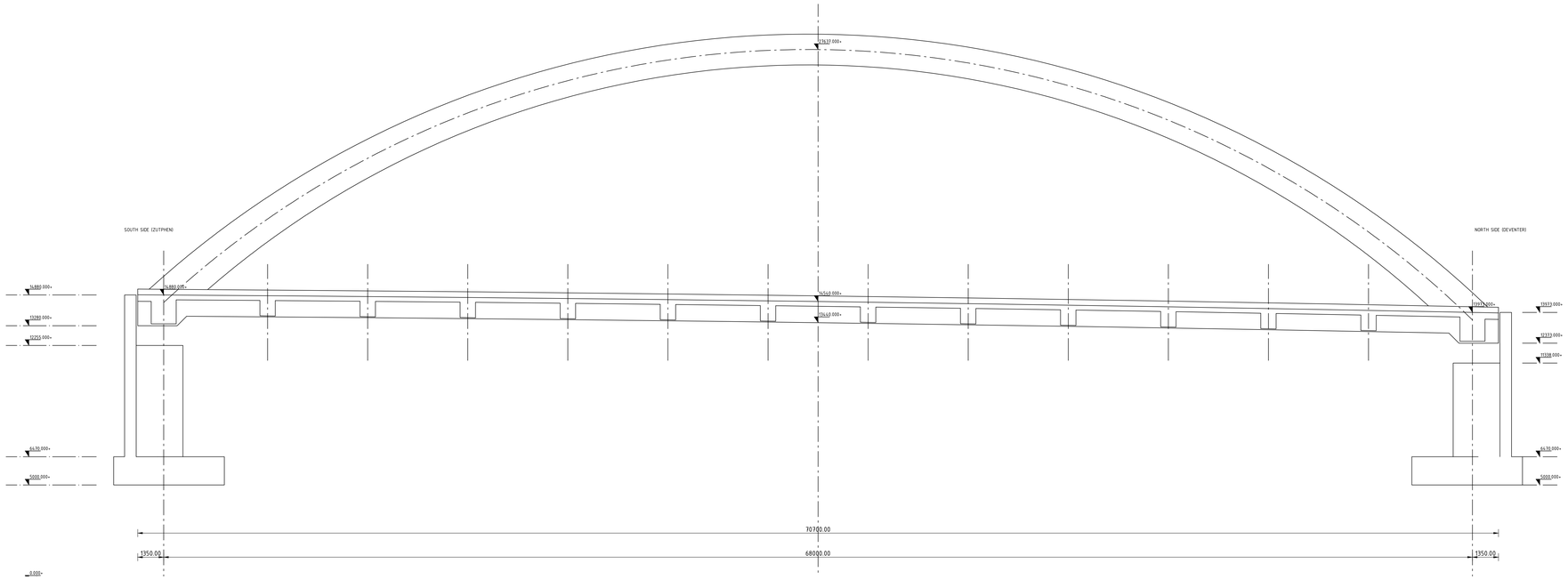
Plaats hier uw logo

V

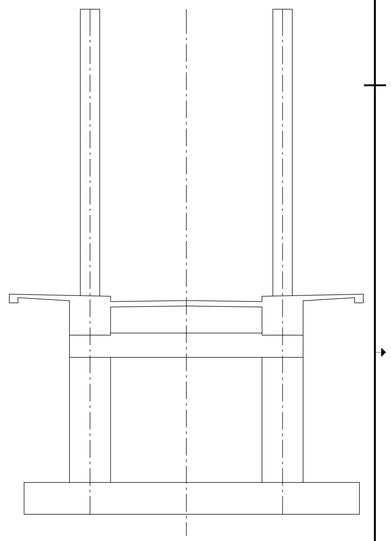
ANNEX: DRAWING EXISTING BRIDGE



TOP VIEW EXISTING BRIDGE
SCALE 1: 500



LONGITUDINAL SECTION OF THE DECK
SCALE 1: 500



CROSS SECTION AND ABUTMENT SOUTH SIDE
SCALE 1: 100

REMARKS:

- ALL UNITS IN mm
- DIMENSIONS BASED ON ORIGINAL DESIGN DOCUMENTS
- SEE REPORT "EXISTING BRIDGES TWENTEKANAAL" FOR MORE DETAILS REGARDING THE EXISTING BRIDGE

OPDRACHTGEVER: –	TEKENAAR
PROJECTOMSCHRIJVING: MSC THESIS REDESIGN OF BRIDGES TWENTEKANAAL IN UHPC	SCHAAL: 1:100
TEKENINGOMSCHRIJVING: PRELIMINARY DESIGN DRAWING EXISTING BRIDGE	PROJECTLEIDER FORMAAT: A0
DOCUMENTSOORT: DRAWING	BLAD IN BLADEN: 1 IN 1
STATUS: FINAL VERSION	TEKENINGNUMMER WIJZ.NR

Plaats hier uw logo

VI

ANNEX: WEIGHT COMPARISON

Preliminary Design Calculations - Weight comparison

Project: MSc thesis ''Redesign of bridges Twentekanaal in UHPC''
Name: M. Dorland
Date: 9-8-2020
Version: D1.0

Description	Length [m]	Height/depth [m]	Width [m]	Cross-section [m²]	Number [-]	Weight [kN/m³]	Result [-]	Units [-]	Remarks/notes
Preliminary design prefab UHPC deck									
Prefab UHPC beams	70,70			1,94	5	28,0	19214	[kN]	
In-situ UHPC joints	70,70	0,25	0,09		4	28,0	178	[kN]	
Cross beams	16,36	2,325	2,325		2	25,0	4422	[kN]	*See chapter ''Weight Comparison''.*
Asphalt layer	70,70	0,14	16,36			23,0	3724	[kN]	
Kerbs	70,70	0,34	0,50		2	25,0	601	[kN]	
Capping beam	16,36	1,00	0,75		2	25,0	614	[kN]	*See chapter ''Weight Comparison''.*
Total							**28753**	[kN]	
Existing concrete arch bridge - Eefdesebrug									
Arches	75,00	1,80	0,90		2	25,0	6075	[kN]	*Arch length is measured using AutoCAD.*
Supporting elements arches (''windverband'')	8,00	0,36	1,60		4	25,0	461	[kN]	*See drawing B.3622*
Main girders	70,70	1,30	1,90		2	25,0	8731	[kN]	
Cross beams	7,00	0,80	0,80		12	25,0	1344	[kN]	
end cross beams	7,00	1,20	1,30		2	25,0	546	[kN]	*Average height, see ''detail B-B'' of B.7125*
Deck between main girders	70,70	0,25	7,00			25,0	3093	[kN]	
Deck pedestrian lanes	70,70	0,20	2,78		2	25,0	1965	[kN]	*An verage height of 0,20 m is assumed.*
Asphalt layer	70,70	0,05	7,00			23,0	569	[kN]	*Assumption: layer of 50 mm acc to B.5109.*
Total							**22785**	[kN]	
Comparison									
Percentual change of weight	26	[%]							

VII

ANNEX: INPUT RFEM MODEL

Input RFEM model

Nodal coordinates
The following nodes have been defined:

Node No.	Node Type	Reference Node	Coordinate System	X [m]	Y [m]	Z [m]
1	Standard	0	Cartesian	0	-8,18	0
2	Standard	0	Cartesian	0	-6,58	0
3	Standard	0	Cartesian	0	-3,29	0
4	Standard	0	Cartesian	0	0	0
5	Standard	0	Cartesian	0	3,29	0
6	Standard	0	Cartesian	0	6,58	0
7	Standard	0	Cartesian	0	8,18	0
8	Standard	0	Cartesian	68,0	-8,18	0
9	Standard	0	Cartesian	68,0	-6,58	0
10	Standard	0	Cartesian	68,0	-3,29	0
11	Standard	0	Cartesian	68,0	0	0
12	Standard	0	Cartesian	68,0	3,29	0
13	Standard	0	Cartesian	68,0	6,58	0
14	Standard	0	Cartesian	68,0	8,18	0

Lines
For the beams the following lines have been defined:

Line No.	Line Type	Nodes No.	Line Length L [m]
1	Polyline	2,9	68,0
2	Polyline	3,10	68,0
3	Polyline	4,11	68,0
4	Polyline	5,12	68,0
5	Polyline	6,13	68,0

To act as the boundary lines for the surface element (to be modelled as an orthotropic plate), the following boundary lines have been defined:

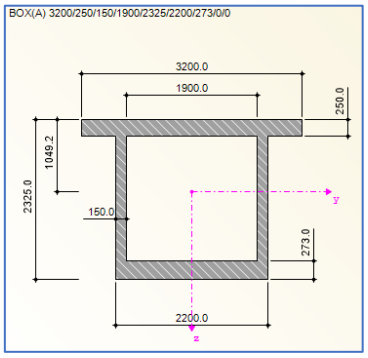
Line No.	Line Type	Nodes No.	Line Length L [m]
6	Polyline	1,2	1,6
7	Polyline	2,3	3,29
8	Polyline	3,4	3,29
9	Polyline	4,5	3,29
10	Polyline	5,6	3,29
11	Polyline	6,7	1,6
12	Polyline	7,14	68,0
13	Polyline	14,13	1,6
14	Polyline	13,12	3,29
15	Polyline	12,11	3,29
16	Polyline	11,10	3,29
17	Polyline	10,9	3,29
18	Polyline	9,8	1,6
19	Polyline	8,1	68,0

Defining cross section of the beams

Cross-sections are defined for and assigned to the different line segments to model the beams. The cross sections of the beams are identical to the cross section defined in the main report. A thin walled cross section (Type A) is applied to model the beams:

BOX(A) 3200/250/150/1900/2325/2200/273/0/0

Parameters		
b_t	3200	[mm]
t_t	250	[mm]
s	150	[mm]
b_i	1900	[mm]
h	2325	[mm]
b_b	2200	[mm]
t_b	273	[mm]
a_t	0	[mm]
a_b	0	[mm]



Assigning members

Assigning member types and cross sections to the lines for the beams:

Line No.	Member Type	Cross-Section No.	
		Start	End
1	Beam	1	1
2	Beam	1	1
3	Beam	1	1
4	Beam	1	1
5	Beam	1	1

Surface

The surface is modelled using the following parameters:

Geometry	Stiffness	Boundary Lines No.	Material No.	Thickness		Eccentricity
				Type	e [mm]	ez [mm]
Plane	Standard	6-19	1	Constant	250.0	0.0

Nodal supports

Two types of supports are modelled, namely hinges and sliding supports in x-direction:

Support No.	On Nodes No.	Axis system	Column in Z	Support			Rotational restraint		
				u_x	u_y	u_z	φ_x	φ_y	φ_z
1	2-6	Global X,Y,Z	-	+	+	+	-	-	+
2	9-13	Global X,Y,Z	-	-	+	+	-	-	+

Load cases

Two load cases are created, one for the uniformly distributed loads and one for the axle loads.

Load Case	Load Case Description	To Solve	Action Category	Self-weight active
LC1	Traffic load LM1 - UDL	+	Permanent	-
LC2	Traffic Load LM1 - Axles	+	Permanent	-

Defining the loads

The loads are entered into RFEM. The uniformly distributed loads (Load Case 1) are modelled as ''Free Rectangular Load''.

					Load position				Magnitude	
No.	On Surface No.	Projection	Load Distribution	Load Direction	X1	Y1	X2	Y2	P1	P2
	[-]	[-]	[-]	[-]	[m]	[m]	[m]	[m]	[kN/m2]	[kN/m2]
1	1	XY	Uniform	ZL	0.000	-3,5	68,0	3,5	2,5	
2	1	XY	Uniform	ZL	0.000	-1,5	68,0	1,5	6,5	

The axle loads (Load Case 2) are modelled as ''Free Concentrated Load''.

No.	On Surfaces No.	Projection	Load Type	Load Direction	Load Position		Magnitude
					X	Y	P
[-]	[-]	[-]	[-]	[-]	[m]	[m]	[kN]
1	1	XY	Force	Z	33,4	-1,0	150
2	1	XY	Force	Z	33,4	1,0	150
3	1	XY	Force	Z	34,6	-1,0	150
4	1	XY	Force	Z	34,6	1,0	150

The separate load cases are combined into one load combination, which will be used to perform the analysis as described in the main report.

VIII

ANNEX: CALCULATIONS SENSITIVITY ANALYSIS

Preliminary Design Calculations - Sensitivity analysis

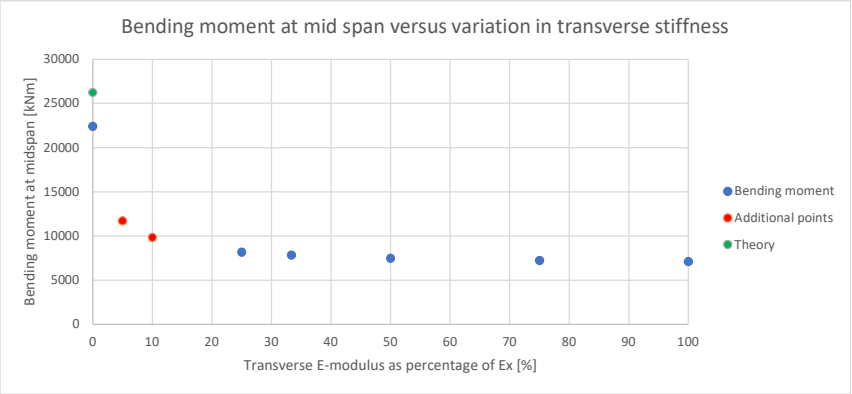
Project: MSc thesis "Redesign of bridges Twentekanaal in UHPC"
Name: M. Dorland
Date: 10-8-2020
Version: D1.0

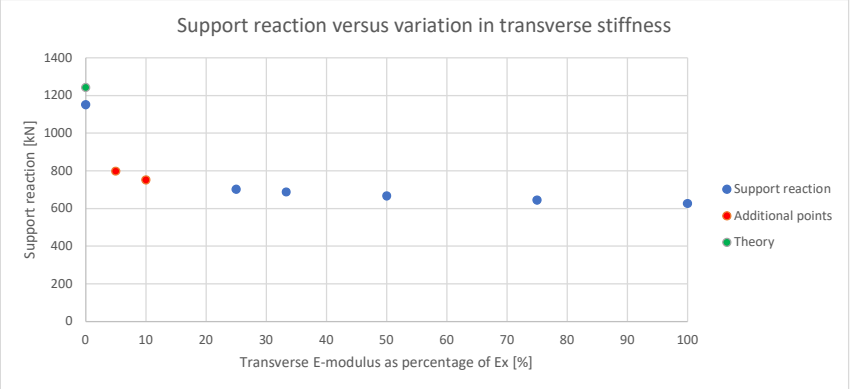
h	[mm]	250
v_{xy}	[-]	0,2

		Case						Additional cases analysis			
Parameter	Units	1	2	3	4	5	6	Extra 1	Extra 2	Theory	Comparison
E_x	[N/mm²]	33000	33000	33000	33000	33000	33000	33000	33000	-	11000
E_y	[N/mm²]	0	8250	11000	16500	24750	33000	1650	3300	-	0
v_{xy}	[-]	0,2	0,2	0,2	0,2	0,2	0,2	0,2	0,2	-	0,2
v_{yx}	[-]	0	0,05	0,067	0,1	0,15	0,2	0,01	0,02	-	0
G_{yz}	[N/mm²]	0	3929	5156	7500	10761	13750	817	1618	-	0
G_{xz}	[N/mm²]	13750	13750	13750	13750	13750	13750	13750	13750	-	4583
G_{xy}	[N/mm²]	0	7500	8540	10222	12180	13750	3532	4907	-	0
D_{11}	[MNm]	43,0	43,4	43,5	43,8	44,3	44,8	43,1	43,1	-	14,3
D_{12}	[MNm]	0,0	2,2	2,9	4,4	6,6	9,0	0,4	0,9	-	0,0
D_{22}	[MNm]	0,0	10,9	14,5	21,9	33,2	44,8	2,2	4,3	-	0,0
D_{33}	[MNm]	0,0	9,8	11,1	13,3	15,9	17,9	4,6	6,4	-	0,0
D_{44}	[MN/m]	3437,5	3437,5	3437,5	3437,5	3437,5	3437,5	3437,5	3437,5	-	1145,8
D_{55}	[MN/m]	0,0	982,1	1289,1	1875,0	2690,2	3437,5	204,2	404,4	-	0,0

Output RFEM: Bending moments at mid span and reaction forces											
		1	2	3	4	5	6	Extra 1	Extra 2	Theory	Comparison
M	[kNm]	22406	8157	7814	7456	7214	7094	11686	9838	26225,05	22571
R	[kN]	1151	702	688	667	645	627	798	752	1242,65	1151
E%	[%]	0	25	33	50	75	100	5	10	0	0

Percentual decrease of forces		
Case	M [%]	R [%]
Theory versus FEM	-15	-7
Limit cases REM	-68	-46





VI

DETAILED DESIGN



Detailed Design

Redesign of bridges Twentekanaal in Ultra-High Performance Concrete

MSc Thesis

20 November 2020

Company	Witteveen+Bos
MSc thesis project	Redesign of bridges Twentekanaal in Ultra-High Performance Concrete
Document	Detailed Design
Status	Final version
Version	D1.0
Date	20 November 2020

Author	ing. M. Dorland
Student id	4719980
Degree programme	MSc Civil Engineering
Track	Structural Engineering – Concrete Structures

Company Supervisors	ing. T. Petersen RC ir. A. ten Voorde
Supervisors TU Delft	Dr. ir. Y. Yang Dr. ir. M.A.N. Hendriks Dr. ir. S. Grünewald

TABLE OF CONTENT

PREFACE 1

1 OUTLINE OF THE DETAILED DESIGN PHASE 3

2 GEOMETRY, DIMENSIONS AND MATERIALS 5

2.1 Description of the structure 5
2.1.1 Geometry of the bridge 5
2.1.2 Phased description 6
2.2 Dimensioning the structural elements 7
2.2.1 Main beams 7
2.2.2 End cross beams 9
2.2.3 Longitudinal joints 10
2.2.4 Capping beams 10
2.3 Materials 11
2.3.1 Main beams 11
2.3.2 End cross beams 12
2.3.3 Longitudinal joints 13
2.3.4 Prestressing steel 14
2.3.5 Other parameters 16
2.4 Bibliography chapter two 17

3 PRINCIPLES FOR THE DETAILED DESIGN 18

3.1 Eurocode 0 – Basis of Design 18
3.1.1 Reliability 18
3.1.2 Design service life 19
3.2 Eurocode 2 – Durability and concrete cover 19
3.2.1 Background 19
3.2.2 Provisions chapter 4 Eurocode 2 20
3.2.3 Provisions AFGC-SETRA 2013 24
3.2.4 Determining exposure classes & concrete cover – Main beams 25
3.2.5 Determining exposure classes & concrete cover – End beams 27
3.3 Bibliography chapter three 28

4 LOADS AND LOAD COMBINATIONS 29

4.1 Identifying relevant loads 29
4.2 Determining the actions 30
4.2.1 Permanent actions (G) 30
4.2.2 Prestressing actions (P) 31
4.2.3 Variable actions (Q) 31
4.2.4 Accidental actions (A) 36
4.3 Provisions on limit states 37
4.4 Provisions on combinations of actions 38
4.4.1 Combination of actions ULS – Fundamental combinations 38
4.4.2 Combination of actions ULS – Fatigue 39
4.4.3 Combination of actions ULS – Accidental design situations 39
4.4.4 Combination of actions SLS – Frequent combination 39
4.4.5 Partial and combination factors 39
4.4.6 Remarks and background 43
4.5 Elaborating the combinations of actions 44
4.5.1 Elaboration fundamental combinations (ULS) 44
4.5.2 Elaboration combination fatigue (ULS) 45
4.5.3 Elaboration combination of actions accidental design situations (ULS) 45
4.5.4 Elaboration frequent combination of actions (SLS) 46
4.6 Bibliography chapter four 46

5 FEA CALCULATION MODEL 47

5.1 RFEM model 47
5.2 Modelling the structure 47
5.2.1 Geometry of the structure 47
5.2.2 Cross sections and materials 48
5.3 Load cases and load combinations 49
5.3.1 Permanent actions (G) 50
5.3.2 Variable loads (Q) 50
5.3.3 Accidental loads (A) 51
5.3.4 Fatigue loads 52
5.4 Performing the calculation 52
5.4.1 Calculation parameters 52
5.4.2 Combinations of actions and results for ULS - STR 52
5.4.3 Combinations of actions and results for ULS – FAT 54
5.4.4 Combinations of actions and results for SLS – Characteristic combination 54
5.4.5 Combinations of actions and results for SLS – Frequent combination 56
5.5 Validation of the model 56
5.5.1 Qualitative verification – Boundary conditions 56
5.5.2 Quantitative verification – Internal forces 57
5.6 Bibliography chapter five 59

6 DESIGN OF MAIN BEAMS – MAIN PRESTRESSING AND ULS (STR) 60

6.1 Design approach 60
6.1.1 Design of main prestressing and global design verifications 60
6.1.2 General principles AFGC-SETRA 2013 guideline 60
6.2 Design of the main prestressing 61
6.2.1 General provisions prestressing – Eurocode 2 61
6.2.2 Positioning and assumed number of strands 66
6.2.3 Calculating prestress losses 66
6.2.4 Determining stresses and required prestressing force at midspan 69
6.3 Detailing beam ends 71
6.3.1 Aspects of the detailing 71
6.3.2 Bond stresses and transmission length 71
6.3.3 Tensile stresses at top fibre 73
6.3.4 Positioning of strands in the bottom flange 75
6.3.5 Splitting reinforcement – Vertical distribution 77
6.4 Verification bending moment capacity 79
6.4.1 Parameters & assumptions 79
6.4.2 Calculation procedure 80
6.5 Verification shear force capacity 81
6.5.1 Parameters & assumptions 81
6.5.2 Calculation procedure 82
6.6 Torsion 83
6.6.1 Provisions from codes 83
6.6.2 Calculation procedure 85
6.7 Ship collision 87
6.7.1 Global verification 87
6.7.2 Local verifications 88
6.8 Bibliography chapter six 88

7 DESIGN OF MAIN BEAMS – TOP FLANGE AND TRANSVERSE PRESTRESSING 89

7.1 Analysis of top flange 89
7.1.1 Beam interaction and local verifications 89
7.1.2 Design approach 89
7.2 Design of transverse prestressing 90
7.2.1 Positioning and assumed number of strands 90
7.2.2 Calculating prestress losses 90
7.2.3 Forces acting on top flange and joint 94
7.2.4 Verifying stresses over joint height 95
7.2.5 Detailing 96
7.3 Local verifications top flange 98
7.3.1 Capacity longitudinal joint 98
7.3.2 Capacity of top flange – Transverse direction 99
7.3.3 Capacity of top flange – Longitudinal direction 100

7.4 Bibliography chapter seven 102

8 DESIGN OF MAIN BEAMS – FATIGUE VERIFICATION 103

8.1 Fatigue verification 103
8.1.1 Importance of fatigue verification and approach 103
8.1.2 Load model & force distribution 103
8.1.3 Verification prestressing steel 104
8.1.4 Verification concrete 106
8.2 Bibliography chapter nine 109

9 DESIGN OF MAIN BEAMS – SERVICEABILITY LIMIT STATE 110

9.1 Serviceability limit state 110
9.1.1 Deflections 110
9.1.2 Crack width 112
9.1.3 Cracking bending moment 113
9.1.4 Vibrations 113
9.2 Bibliography chapter nine 113

10 DESIGN OF END CROSS BEAM 114

10.1 Design of the end cross beam 114
10.1.1 Goal and assumptions 114
10.1.2 Input parameters 114
10.2 Design of the prestressing 116
10.2.1 Calculating prestress losses 116
10.2.2 Determining stresses over beam height 118
10.3 Ultimate limit state verifications 118
10.3.1 Verification bending moment capacity 118
10.3.2 Verification shear force capacity 119
10.3.3 Force introduction 120
10.4 Bibliography chapter ten 121

11 WEIGHT CALCULATION 122

11.1 Weight calculation 122
11.1.1 Setup of the calculation 122
11.1.2 Results and comparison with the preliminary design 122
11.1.3 Conclusion 123

12 EXECUTIONAL ASPECTS 124

12.1 Considering executional aspects 124

12.2 Phased description of the main beams 124
12.2.1 Production of the beams 124
12.2.2 Storing the beams 126
12.2.3 Transport to and placement on site 126
12.2.4 On site construction work 128
12.2.5 Use phase 128
12.3 Implications for design 128
12.3.1 Prestressing capacity 128
12.3.2 Transportation and placement 128
12.4 Bibliography chapter twelve 129

13 CONCLUSIONS AND PROSPECTS 131

Final page 132

Annex(es)

		Number of pages
I	Determining Material Parameters – Ductal FM	10
II	Product Sheet Ductal JS1000	2
III	Calculations Detailed Design	13
IV	Overview Design Calculations	60
V	Input RFEM Model	13
VI	Derivations concrete compressive zone over variable width	3
VII	Unreinforced UHPC beams with and without prestressing	18
VIII	Drawing Detailed Design	1

PREFACE

This report comprises the detailed design as a part of the thesis 'Redesign of bridges Twentekanaal in Ultra-High Performance Concrete'. The goal of this design is to perform a more complete and accurate analysis to obtain better insight into the structural behaviour of the bridge, as well as to identify the best options for optimization. Achieving these goals means that an answer can be formulated to (a part of) the following research questions:

- In which ways can one model a prefab beam bridge using FEM and which way is most appropriate to apply in order to generate the required numerical data?
- What are the required assumptions that have to be made in order to model the bridge using FEM and what are the consequences/implications of these assumptions?
- What is/are the normative beam(s) and the corresponding cross-sectional forces according to the FEA model?
- What should the dimensions of the beams (and/or superstructure in general) be in order to obtain the most optimal (i.e. the least amount of material) redesign which complies with the relevant codes and standards?

The relation between the activities (partially) covered in the detailed design and the total project is given in the following figure.

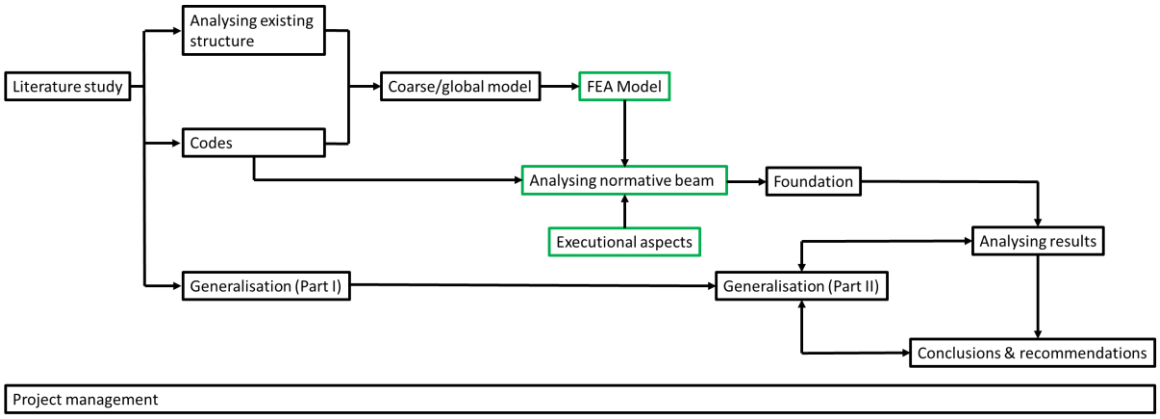


Figure 1 Detailed design in relation to the project

Reading guide

This report consists of the following chapters:

- Chapter 1: The report starts with a chapter in which the outline of the detailed design phase is covered;
- Chapter 2: In the second chapter the main assumptions of the design are listed, i.e. the overall geometry, main dimensions and materials;
- Chapter 3: In the third chapter a number of principles from the Eurocode and AFGC-SETRA 2013 are discussed that are relevant for the design and have not been covered in previous project parts: reliability, design service life and concrete cover;
- Chapter 4: In the fourth chapter all relevant loads and load combinations are identified and elaborated on;
- Chapter 5: Subsequently the setup of the FEA model is covered as well as the main results and a brief validation of the model;

- Chapter 6: In the sixth chapter the main prestressing of the prefab beams is designed and the global design verifications are performed using the input from previous chapters;

- Chapter 7: After that the transverse prestressing in the top flanges is designed and a number of local verifications of the top flange are performed;

- Chapter 8: In the eight chapter a fatigue verification of the main prestressing and concrete of the prefab beams is discussed;

- Chapter 9: The ninth chapter covers the verification of the deflections of the bridge;

- Chapter 10: The tenth chapter subsequently covers a brief analysis of the end cross beams. The post-tensioned prestressing is designed and the bending moment and shear force capacity are calculated;

- Chapter 11: After the different design calculations have been performed, a weight calculation is added in chapter eleven;

- Chapter 12: The twelfth chapter covers various executional aspects that have to be taken into consideration;

- Chapter 13: The final chapter gives a summary of the results of the detailed design as well as prospects for the next project phases.

1

OUTLINE OF THE DETAILED DESIGN PHASE

In the previous design stage (preliminary design) a first design was set up, the goals were to gain insight into the required dimensions of the structure and to determine the feasibility of the project goal based on the structures self-weight. Based on the self-weight of this first design achieving the project goal was deemed to be feasible.

However, a number of remarks had to be made. The conclusion was drawn based on the self-weight of the structure only and, although being justifiable for the project stage, the preliminary design did not cover all relevant aspects & criteria and it was on the more conservative side.

These aforementioned points mean that the preliminary design give a rough estimation and that for the following project stages attention will have to be paid to other aspects & criteria and that the design requires refining and optimisation to reduce the weight of the structure further. Therefore, the report on the preliminary design was finalized (see chapter 10 of this report) with a number of possibilities for further elaboration and optimization.

This leads to the detailed design, which may be regarded as a continuation of the preliminary design and in which many of the given options for refinement and optimization will already be implemented. The goals of this design stage are to obtain better insight into the structure and its behaviour and to identify options for optimization. The following four factors set the detailed design apart from the preliminary design and contribute to achieving this goal:

- **More accurate assumptions**: The detailed design is based on more accurate input compared to the preliminary design, for example:
    - The cross-sectional dimensions are largely based on the results of the preliminary design instead of rules of thumb;
    - Material properties are based on actual commercially available UHPC mixtures, making it possible to take full benefit of the properties of these materials;
    - Certain requirements are relaxed in accordance with the guidelines (e.g. full prestressing is not required according to the AFGC-SETRA 2013 guideline) to achieve a more economical design.
- **More complete and accurate model**: All relevant loads & situations are identified and determined in accordance with Eurocode 1. In addition, the loads are evaluated critically, loads that are not required from a structural point of view (e.g. asphalt) are reduced. A FEM model is used to determine the force distribution, this will contribute to a more economical design.
- **More elaborate verifications**: Where the preliminary design only included basic global design verifications (bending moment, shear and deflection) the detailed design covers other relevant global and local verifications, e.g. torsion, fatigue, local verifications, etc. In addition, the prestressing is redesigned including the option of applying centrically positioned prestressing

strands in the main beams and including the calculation of the prestress losses instead of making assumptions.

- **Boundary conditions from practice**: Executional aspects such as transportation or the prestressing capacity in the prefabrication factory may prove to be boundary conditions for the project. These are therefore discussed in a separate chapter.

By implementing these points, the detailed design will give a more complete overview of the structure and its behaviour and of opportunities for optimization. The programme RFEM will be used to determine the (global) force distribution while an Excelsheet will be developed to perform all verifications. All assumptions of the preliminary design not mentioned or changed by the aforementioned points still hold, they will remain to be used for this detailed design phase.

2

GEOMETRY, DIMENSIONS AND MATERIALS

2.1 Description of the structure

2.1.1 Geometry of the bridge

The bridge deck is a beam type structure and made up of five prestressed prefabricated UHPC box beams and four longitudinal joints in between, the total dimensions of the bridge are:

- Span l: 68,0 m;
- Total width w_{tot}: 16,36 m;
- Total length l_{tot}: 70,7 m.

These dimensions are the same as the preliminary design and the existing deck. The beams are hollow box beams except for the beam ends, at the ends the beams are solid. The beams are positioned on bearings that are placed on capping beams. These beams are placed on the (modified) existing buttresses of the existing bridge and are prestressed. Because of this layout the bridge deck is analysed as a statically determinate structure. Reference is made to annex VIII for a drawing of the structure.

After the beams are placed on their bearings end cross beams are constructed at both ends of the deck. This is done by casting in-situ concrete in between the prefab beams, after which prestressing is applied in transverse direction (post-tensioned steel). In addition, the longitudinal joints between the beams are filled and after which the beams are post tensioned through the top flanges. This way a solid structure is obtained.

The following figure gives the layout of the deck. In the final stage one can distinguish the main carriageway (two lanes, one for each direction) and two pedestrian/bicycle lanes on the outer sides, these are separated from the main carriageway by kerbs with dimensions assumed to be 340 by 500 mm (height by width).

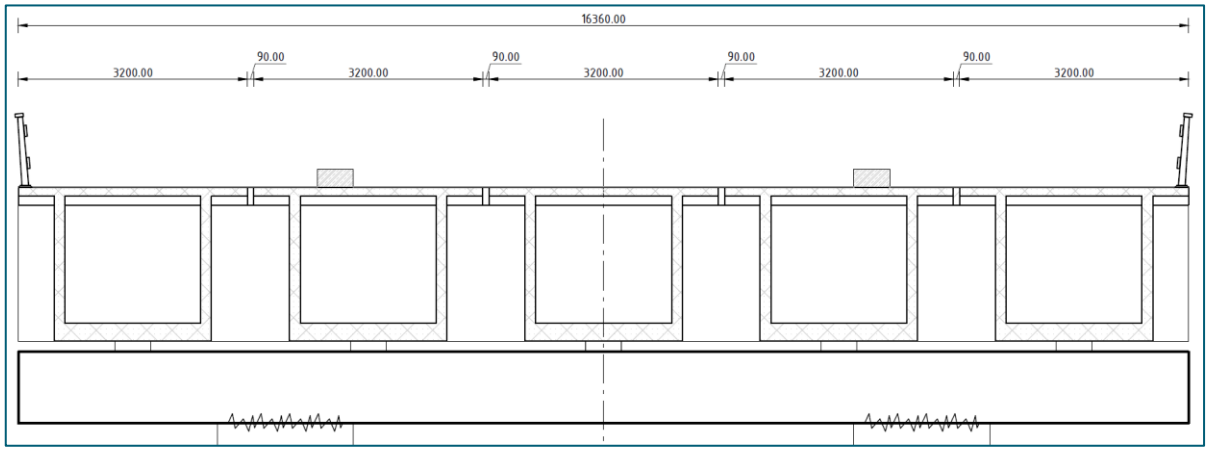


Figure 2 Cross section of the bridge deck

2.1.2 Phased description

The most important components of the bridge are the prefab beams. Especially for prefab structures it is important to have an overview of the different stages from production to use phase, because in each stage the elements could be subjected to different circumstances (e.g. weather conditions), loads (e.g. due to changing support conditions or imposed loads) and limitations & boundary conditions (e.g. transportation).

A more detailed phased description including all executional aspects is covered in a separate chapter (see chapter 12), but because some information regarding execution is required earlier this chapter gives a brief overview of the different stages. The focus is placed on possible load cases and boundary conditions from practice.

Production

The box beams are produced in the prefab factory using pretensioned steel, which is done in three steps. First the prestressing steel is placed at the formwork, anchored and stressed. Then the concrete is casted and starts to harden. After a certain amount of time the strands are released, the element is then prestressed and taken out of its formwork. Note that at this point the tensile stresses at the top of the beam near the beam end might be too high resulting in cracking as the downward bending moment due to self-weight might be insufficient at these locations to compensate for the upward bending moment due to prestressing.

An important assumption is that heat treatment will be applied to the UHPC, this improves mechanical properties but more importantly it helps in controlling and/or reducing the shrinkage and creep of the material. This is denoted as type 2 heat treatment in the AFGC-SETRA 2013 guideline, for which the elements are taken to a temperature of 90 °C for 48 hours.

An important boundary condition is the maximum prestressing capacity in the prefab factory. The upper limit has been established by contacting a firm that produces prefab concrete elements. The limit is approximately 2500 tons (i.e. about 25.000 kN), which corresponds to 120 strands with diameter Ø15,7, loaded with 21 tons each (i.e. about 210 kN). In chapter 12 this limit will be compared with the design.

Storage

After taking the beam out of the formwork the beams are usually stored at a storage site. Therefore, the element should be able to carry at least its own weight after prestressing, so it can be hoisted and transported.

Transportation and placement

At a certain moment in time the beams are moved from the storage location at the prefab factory to the construction site where these will be hoisted into place. Especially for larger elements the transportation or hoisting capacity can become stringent. In chapter 12 a two reference projects will be discussed to determine the feasibility of the project with respect to these criteria.

On site construction

Once the beams are placed on their bearings the remaining in-situ work can be carried out. This comprises structural work (constructing and post tensioning the end cross beams and filling and post-tensioning the longitudinal joints) and the non-structural work (placing a surface layer, railings, etc.). These are additional permanent loads acting on the structure.

Use phase

After constructing and finishing the structure the bridge is ready for use. This means that the use phase starts. During this phase the bridge should be able to function without requiring excessive repairs or maintenance under the anticipated use. A point to keep in mind for the design is that as time progresses, time dependent effects of the materials occur. Examples are relaxation of the prestressing steel and creep of the concrete. This should be included in the design of the prestressing and verifications of the beam.

Use phase – accidental situations

During the use phase of the bridge, accidental situations could occur. An example is ship collision, and such situations have to be taken into consideration. This is done by determining the relevant loads and verifying the structure for these accidental situations conforming the relevant codes and guidelines.

2.2 Dimensioning the structural elements

In the following sub sections the dimensions of the various structural elements of the deck are given. The starting point for the dimensions were the results from the preliminary design, because the goal of the preliminary design was to obtain insight into the require dimensions. However, various modifications have been made to obtain a more economical design and satisfy all relevant verifications.

2.2.1 Main beams

Cross sectional dimensions

The cross section of the box beams is given in the following figure.

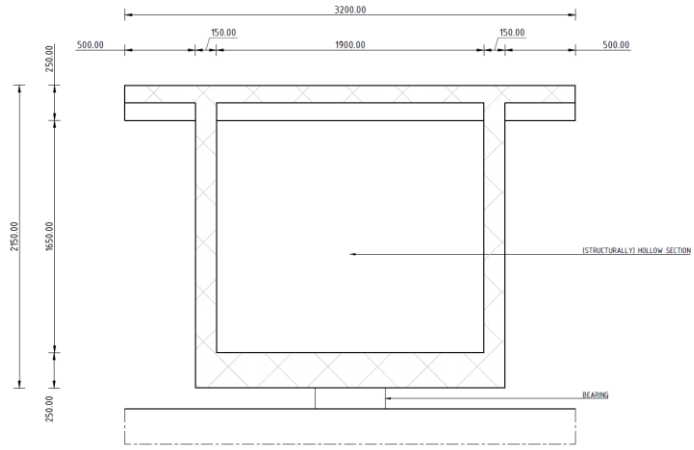


Figure 3 Cross section of the main beams

For the analysis of the deck the following parameters were assumed:

- Total width w: 3200 mm
- Total height h: 2150 mm
- Thickness of bottom flange t_{fb}: 250 mm
- Thickness of the web t_w: 150 mm
- Width of a single flange w_f: 500 mm
- Width of the box w_b: 1900 mm

Note that the cross section is symmetric. In the calculation the option was also included to apply chamfering of the flanges, although for simplification this was not used at this stage.

To save material and thus weight the thickness of the top flange has been made variable in transverse direction by applying prestressing ribs with a certain centre to centre distance. The parts of the top flange spanning these ribs have a reduced thickness. This principle can be seen in the following figure:

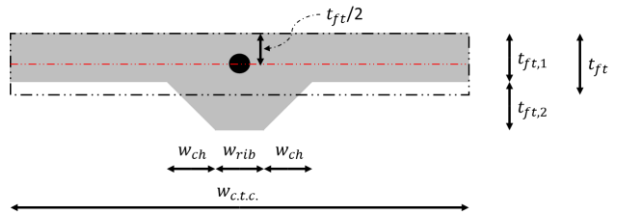


Figure 4 Principle of prestressing rib and variable thickness of top flange

The following dimensions have been assumed:

- Centre to centre distance of the transverse prestressing ribs $w_{c.t.c.}$: 1000 mm
- Continuous thickness of the top flange $t_{ft,1}$: 125 mm
- Local increase thickness top flange at transverse rib $t_{ft,2}$: 125 mm
- Width of transverse prestressing rib w_{rib}: 250 mm
- Width of chamfer next to the transverse prestressing rib w_{ch}: 250 mm

Using these dimensions different cross-sectional properties of the beams were calculated, reference is made to annexes III (Excel sheet) and IV (overview of the calculations) for all details. For the calculation the following schematic representation of the cross section was used:

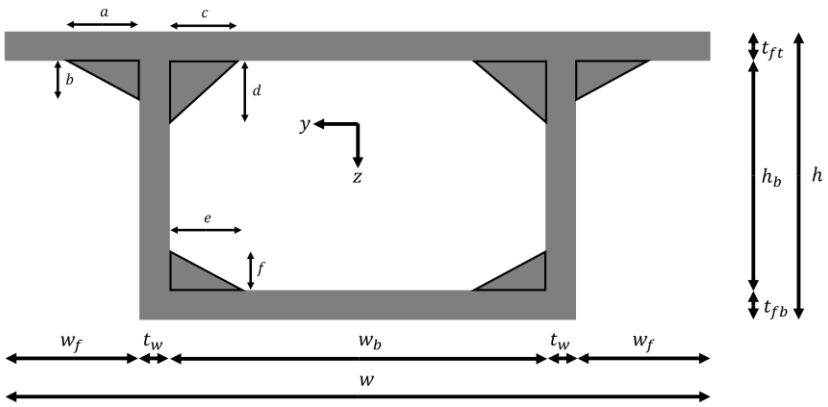


Figure 5 Schematic representation of the cross section

An important feature of these calculations is the introduction of the ''mean value'' of the thickness of the top flange, which is used to take the variable thickness of the top flange into consideration. It is calculated as follows:

$$t_{ft} = \frac{w_{c.t.c.} * t_{ft,1} + w_{rib} * t_{ft,2} + 2 * 0{,}5 * w_{ch} * t_{ft,2}}{w_{c.t.c.}} \qquad \text{Equation (1)}$$

In all further calculations where the thickness of the top flange is involved this mean value will be used, this is a practical way of taking the variable thickness into consideration. Given the limited centre to centre distance between the prestressing ribs this is deemed to be a justifiable approach.

Using the defined dimensions and the calculated mean thickness of the top flange the internal height of the box h_b can be calculated as well. The relevant cross-sectional properties of the beam are subsequently calculated in Excel and are given in the following table.

Table 1 Cross sectional properties main beams

Symbol	Value	Units	Definition
A_c	1663750,0	[mm^2]	Cross sectional area of total cross section
z	1025,5	[mm]	Position centre of gravity from the top flange
I_y	1,201E+12	[mm^4]	Second moment of area of the combined cross section
e_t	1025,5	[mm]	Distance from centre of gravity to top fibre
e_b	1124,5	[mm]	Distance from centre of gravity to bottom fibre
$W_{y,t}$	1,171E+09	[mm^3]	Section modulus with respect to top fibre
$W_{y,b}$	1,068E+09	[mm^3]	Section modulus with respect to bottom fibre

To aid in the further analysis of the deck the beams are numbered from 1 to 5 and the joints are numbered from 1 to 4. Note that the deck is symmetric with respect to the vertical axis through beam 3.

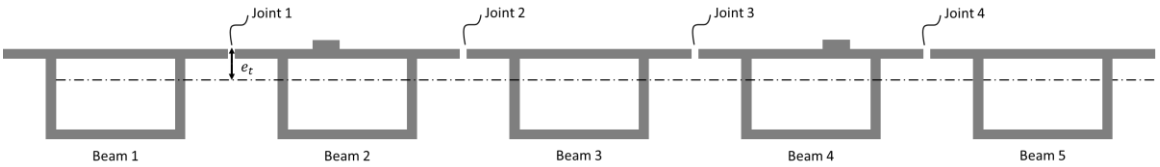


Figure 6 Numbering of the beams and joints

To determine distributed loads acting on the different beams the ''effective widths'' of the outer and inner beams are determined, which equals the width of each of the beams with half the width of the adjacent joint(s):

- The effective width of the outer beams (beams 1 and 5):

$$b_{eff,o} = w + \frac{w_{joint}}{2} \quad \text{Equation (2)}$$

- The effective width of the inner beams (beams 2 – 4):

$$b_{eff,i} = w + 2 * \frac{w_{joint}}{2} \quad \text{Equation (3)}$$

2.2.2 End cross beams

End cross beams are present at both ends of the bridge deck, these are constructed in situ and post tensioned. The beams have a total length equal to the width of the bridge deck. The main function of the end beam is to fixate the main beams, therefore large cross-sectional dimensions are chosen. It is assumed that the height of the beams is equal to the height of the prefab beams and that their width is equal to their height, hence:

- Height of the cross beam h_{cb}: 2150 mm
- Width of the cross beam w_{cb}: 2150 mm

The following figure gives an indication of the position of the beams near the beam ends.

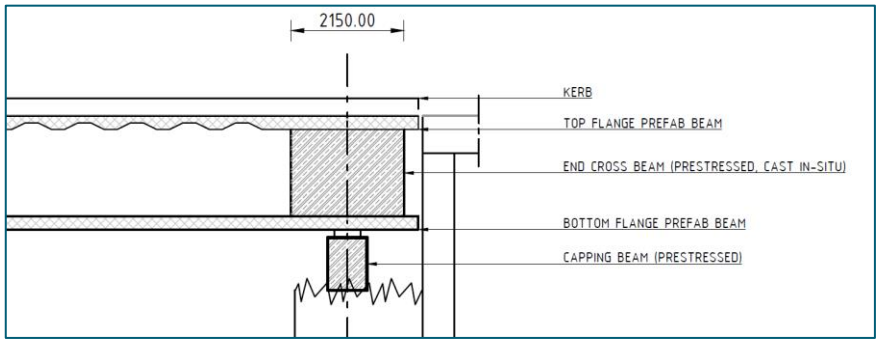
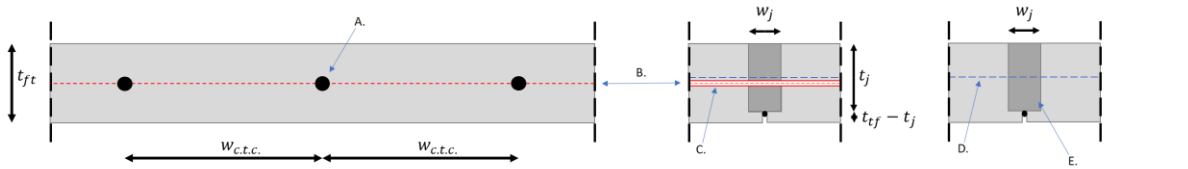


Figure 7 End cross beam

For the verifications of the end cross beams and FEA model two assumptions are made. First it is assumed that the centre of the cross beam coincides with the centre of the support, and thus that the beams are 68,0 m apart centre to centre. Second it is assumed that the beams are continuous and solid over their full length while this in reality would not be the case because that means that the end beams overlap the beam ends of the prefab beams.

2.2.3 Longitudinal joints

For the analysis of the longitudinal joints use is made of the mean value t_{ft} for the thickness of the top flange. The following sketch shows all relevant dimensions.



Side view part of the deck | Cross section joint with tendon | Cross section joint without tendon

Symbols:
A. Position prestressing tendon
B. Centre of gravity of prestressing tendon
C. Prestressing tendon
D. Centre of gravity of the joint
E. In-situ concrete (joint)

Figure 8 Longitudinal joint

The following additional dimensions have to be defined. Note that the latter dimension is based on the principle that in-situ concrete has to be placed, for this purpose small edges can be applied to the prefab beams to facilitate this. This can be seen in the middle and rightmost sketches of Figure 8, it is assumed that the edge is 25 mm high, hence $t_j = t_{ft} - 25$ mm.

- Width of the joint w_j: 90 mm (follows from w_{tot} and number of beams)
- The height of the joint t_j: 162,5 mm

In the analysis of the longitudinal joint two main assumptions are made. First it is assumed that all dimensions are related to the mean value t_{ft} of the thickness of the top flange. Second it is assumed that the transverse prestressing is positioned as such that the centre of the tendons coincides with half the mean value of the top flange.

Because of this latter assumption and because the thickness of the joint t_j is always smaller than the thickness t_{ft} of the top flange the prestressing tendon is positioned centrically with respect to the top flange but always eccentric with respect to the centre of the joint. The eccentricity is:

$$e_j = \frac{1}{2} * t_{tf} - \frac{1}{2} * t_j \; [mm]$$ Equation (4)

2.2.4 Capping beams

Capping beams are not considered in the structural analysis, but required for the weight. Therefore, these beams are briefly mentioned in this section. The same dimensions are applied as were assumed for the preliminary design:

- Length: 16,36 m
- Height: 1,0 m
- Width: 0,75 m

Furthermore, the beam is assumed to be made of prestressed concrete, this implies a volumetric weight of 25 kN/m^3. The beam can either be prefabricated or constructed in-situ.

2.3 Materials

Different types of concrete (different UHPC mixtures and conventional concrete) and ways of prestressing (pretensioning and post tensioning) will be used in the design. The following table gives an overview of the materials used per element, after which each will covered in more detail.

Table 2 Different materials applied in the detailed design

Element	Material	Description
Main beams	UHPC	Prefabricated pretensioned elements. Material properties are based on heat treated Ductal FM.
End cross beams	Conventional concrete	In situ elements made of conventional C30/37 concrete, post tensioned.
Longitudinal joints	UHPC	Joints filled using in situ UHPC (based on Ductal JS1000) and subsequently post tensioned.
Prestressing elements	Steel grade Y1860	Prestressing elements are used for the pretensioned and post tensioned elements. Steel quality is Y1860.

2.3.1 Main beams

A key feature of the project is the use of UHPC for the main beams and for the detailed design material parameters are used that correspond to a specific UHPC mixture. However, defining these parameters is not straightforward because, although there are certain commercial products, there is not a single specific formulation for a UHPC mixture.

UHPC mixtures are generally adjusted on a project-to-project basis to optimally meet the requirements for that specific project: the material is ''tailor made'' to meet project specifications. That means that in literature one usually only finds a range of typical values instead of specific values. The following approach is used to work around this:

- First a number of requirements for the material (e.g. mechanical properties and strain-hardening behaviour) have been listed as well as a description of how the material will be applied (e.g. heat treatment will be applied).

- Subsequently the parameters of a ''fictitious mixture'' are formulated and substantiated by taking into account these conditions and requirements.

This way specific values for material properties required for the design can be assumed in a more substantiated way and this approach will be used for the detailed design. The assumed properties are based on the range of materials called Ductal FM, and will be deduced from and substantiated by available information of various sources. These assumed properties will subsequently be used in the elaboration of the design.

Some of the values assumed for the detailed design are on the more favourable side of the range that can be found in the literature considered. The decision to assume more optimistic values is justified by the following two arguments:

1. Technological advancement: The values range of values found in the literature are sometimes based on partially dated information. Upper values reached with difficulty some years ago might have become more common over time due to technological advancements in the construction industry;

2. Challenging the industry: Formulating requirements that may provide a challenge to manufacturers and contractors may function as an incentive to innovate. This results in shifting boundaries of what is possible, thus contributing to further technological advancements in the construction industry.

Following this approach, the following material parameters, based on heat treated Ductal FM, have been adopted.

Table 3 Assumed parameters Ductal FM

Parameters mixture composition				
Definition	**Symbol**		**Value**	**Unit**
Density	ρ		2500	[Kg/m^3]
Fibre length	l_f		13	[mm]
Parameters concrete in compression				
Definition	**AFGC**	**Symbol**	**Value**	**Unit**
Characteristic value compressive strength	f_{ck}	f_{ck}	200	[N/mm^2]
Design value compressive strength	f_{cd}	f_{cd}	113	[N/mm^2]
Strain at reaching concrete compressive strength	ε_{c0d}	ε_{c3}	2,3	[‰]
Maximum compressive strain at ULS	ε_{cud}	ε_{cu3}	2,6	[‰]
Parameters concrete in tension				
Definition	**AFGC**	**Symbol**	**Value**	**Unit**
Characteristic elastic (5% percentile value) tensile strength	$f_{ctk,el}$	$f_{ctk,el}$	9	[N/mm^2]
Design value of tensile strength (tensile strength 1st crack)	-	f_{ctd}	6,0	[N/mm^2]
Characteristic value maximal post cracking stress ($w = 0{,}30$)	f_{ctfk}	-	10,0	[N/mm^2]
Design value maximal post cracking stress (at $w = 0{,}30$)	f_{ctfk}/(Y *K)	$f_{ctd;2}$	6,15	[N/mm^2]
Fibre orientation factor (global)	K_{global}	K_{global}	1,25	[-]
Fibre orientation factor (local)	K_{local}	K_{local}	1,75	[-]
Parameters stiffness and deformations (temperature, creep and shrinkage)				
Definition	**Symbol**		**Value**	**Unit**
Modulus of elasticity	E_{cm}		50.000	[N/mm^2]
Shear modulus	G		20.833	[N/mm^2]
Poisson ratio	v		0,2	[-]
Coefficient of thermal expansion	α		12*10^{-6}	[K^{-1}]
Creep	φ		0,3	[-]
Autogenous shrinkage (during HT)	ε_{shr}		0,8	[‰]
Parameters concrete other				
Definition	**Symbol**		**Value**	**Unit**
Factor for shape of concrete compressive zone	α		0,56	[-]
Factor position centre of gravity concrete compressive zone	β		0,34	[-]
Long term effects and unfavourable loading (compression)	α_{cc}		0,85	[-]
Long term effects and unfavourable loading (tension)	α_{ct}		1,0	[-]

These parameters will be applied in all subsequent phases of the design. For the full background behind the adoption of these values reference is made to annex I. Note that the symbols are in accordance to those adopted in the preliminary design.

2.3.2 End cross beams

For the end cross beams, the application of conventional concrete is deemed sufficient given the large dimensions and function of the end cross beams. This results in a more economical solution than when applying UHPC without technical reason, given the higher costs of the latter. The concrete will be applied in-situ and after sufficient hardening the beams will be post-tensioned.

For the calculations concrete strength class C30/37 is assumed, which is a common strength class for in-situ concrete and which can be achieved without requiring additional measures or provisions. The material

properties are deduced from Eurocode 2 and an overview of all adopted parameters can be found in the following table. The values adopted for the modulus of elasticity and concrete in tension and compression are in accordance with the properties given in table 3.1 of chapter 3, NEN-EN 1992-1-1.

Table 4 Adopted parameters concrete of end cross beams

Parameters mixture composition			
Definition	**Symbol**	**Value**	**Unit**
Density	ρ	2500	[Kg/m^3]
Parameters concrete compression			
Definition	**Symbol**	**Value**	**Unit**
Characteristic cylinder compressive strength at 28 days	f_{ck}	30	[N/mm^2]
Characteristic cube compressive strength	$f_{ck,cube}$	37	[N/mm^2]
Mean value cylinder compressive strength	f_{cm}	38	[N/mm^2]
Strain at reaching concrete compressive strength	ε_{c3}	1,75	[‰]
Maximum compressive strain at ULS	ε_{cu3}	3,5	[‰]
Parameters concrete tension			
Definition	**Symbol**	**Value**	**Unit**
Mean value axial tensile strength	f_{ctm}	2,9	[N/mm^2]
5%-fractile of the axial tensile strength	$f_{ctk;0,05}$	2,0	[N/mm^2]
Parameters stiffness and deformations (temperature, creep and shrinkage)			
Definition	**Symbol**	**Value**	**Unit**
Secant modulus of elasticity	E_{cm}	33.000	[N/mm^2]
Creep	φ	1,75	[-]
Rate of hydration: Rapid (R), Normal (N) or slow (S)	Hydration	Normal (N)	[-]
Relative humidity	RH	80,0	[%]
Parameters concrete other			
Definition	**Symbol**	**Value**	**Unit**
Factor for shape of concrete compressive zone	α	0,75	[-]
Factor position centre of gravity concrete compressive zone	β	0,39	[-]
Long term effects and unfavourable loading (compression)	α_{cc}	1,0	[-]

2.3.3 Longitudinal joints

The concrete of the main beams will be casted under controlled conditions in a prefab factory and subjected to heat treatment. This justifies the assumption of the relatively high values as given in Table 3. The joints will be made of a UHPC mixture as well, because the joints are critical points in the structure and it is not expected that conventional concrete could provide the required capacity.

However, the concrete of the joints will be poured in-situ. When casting in-situ the conditions are generally not as optimal as those in a prefab factory and the application of heat treatment is not expected to be possible, thus resulting in lower performance compared to the material of the main beams. Applying the same parameters for both the main beams and the joints is therefore deemed to be unrealistic, thus different parameters will be adopted for the joints.

These material properties are based on Ductal JS1000, a product specifically developed for connections and joints in prefab structures. The decision has been made for this Ductal product because more accurate complete information is available, see the product sheet in annex II, from which various parameters have been deduced. The adopted material properties are summarized in the following table:

Table 5 Material properties longitudinal joints

Parameters mixture composition – Joint filling				
Definition	**Symbol**		**Value**	**Unit**
Density	ρ		2500	[Kg/m^3]
Parameters concrete in compression				
Definition	**AFGC**	**Symbol**	**Value**	**Unit**
Characteristic value compressive strength (4 days)	f_{ck}	f_{ck}	100	[N/mm^2]
Maximum compressive strain at ULS	ε_{cud}	ε_{cu3}	2,6	[‰]
Parameters stiffness and deformations (temperature, creep and shrinkage)				
Definition	**Symbol**		**Value**	**Unit**
Modulus of elasticity (28 days)	E_{cm}		45.000	[N/mm^2]
Creep	φ		0,8	[-]
Shrinkage (long term)	ε_{shr}		0,8	[‰]
Parameters concrete other				
Definition	**Symbol**		**Value**	**Unit**
Factor for shape of concrete compressive zone	α		0,56	[-]
Factor position centre of gravity concrete compressive zone	β		0,34	[-]
Long term effects and unfavourable loading (compression)	α_{cc}		0,85	[-]

Various parameters can be deduced directly from the product sheet while other parameters require additional remarks or assumption. A number of remarks regarding the parameters in the aforementioned table are:

- **Compressive strength**: According to the product sheet the compressive strength can reach 100 N/m^2 in four days, which is the parameter used in the table. At 28 days the compressive strength increases to at least 150 N/mm^2 but the strength at four days is applied because this is a beneficial property for the given application: the transverse prestressing can be applied shortly after filling the joints.

- **Tensile strength**: Although the material has a tensile capacity of at least 5 N/mm^2 after 28 days this is neglected in the calculation.

- **Modulus of elasticity**: For the modulus of elasticity a value of at least 45.000 N/mm^2 is given for 28 days. Although transverse prestressing may be applied earlier, this value is still used to calculate the initial prestress losses. This is justified by the fact that in transverse direction the top flanges of the main beams are also present. These have a higher E-modulus and because these make up most of the length over which the transverse prestressing is stressed, the application of a lower E-modulus would be unnecessarily conservative.

- **Creep and shrinkage**: For long-term shrinkage an upper limit of 800 microstrain, i.e. 0,8 ‰, is given on the data sheet. No value for the creep coefficient is given, thus a value of 0,8 has been assumed (upper limit value for UHPC without heat treatment).

- **Other parameters**: Since no information is given for the parameters α, β and α_{cc}, values have been assumed of $0{,}56$, $0{,}34$ and $0{,}85$ respectively. This is in accordance with the parameters assumed for the main beams.

2.3.4 Prestressing steel

For all prestressed elements 7-wire strands Ø15,2 of steel quality Y1860 will be applied. For the pretensioned prestressing these are applied as strands while for the post-tensioned prestressing several strands will be combined into tendons. The main parameters of this material are summarized in the following table.

Table 6 Parameters Ø15,2 strands grade Y1860 prestressing steel

Symbol	Value	Unit	Definition
f_{pk}	1860	[N/mm^2]	Characteristic value tensile strength
f_{pd}	1522	[N/mm^2]	Design value steel stress
σ_{pm0}	1395	[N/mm^2]	Maximum allowed stress directly after tensioning
$\sigma_{p,max}$	1488	[N/mm^2]	Maximum prestressing stress during tensioning
E_p	195.000	[N/mm^2]	Modulus of elasticity
ε_{uk}	35	[‰]	Characteristic value strain at failure
$D_{strand,c}$	15,2	[mm]	Diameter of strands positioned centrically
$A_{p,strand,c}$	140	[N/mm^2]	Cross sectional area per strand

Details regarding each specific application are summarized in the remainder of this section.

Main prestressing (pretensioned)

The main beams are prestressed in longitudinal direction using pretensioned steel. Centric prestressing is applied by using strands positioned in the web with the centre of gravity of the group of strands coinciding with that of the cross section, the strands are divided over both webs. The following table gives information regarding the centric prestressing.

Table 7 Parameters centric prestressing

n_c	10	[pcs]	Assumed number of strands positioned centrically in cross section
$\sigma_{p,max,prov,c}$	1390	[mm^2]	Assumed maximum stress applied to centrically positioned strands
Relaxation	Class 2	[-]	Selected relaxation class: low relaxation
t	500.000	[h]	The value of the relaxation loss (in %) at 1000 h
ρ	2,5	[%]	Time after stressing (to determine final value of the relaxation loss)

In addition, eccentric prestressing is applied, these strands are positioned in the bottom flange. The strands are positioned as such that the centre of gravity of the group of strands coincides with the centre of the bottom flange. The following table gives the parameters of the eccentric prestressing.

Table 8 Parameters eccentric prestressing

n_{fb}	120	[pcs]	Assumed number of strands positioned in bottom flange
$\sigma_{p,max,prov,fb}$	1450	[mm^2]	Assumed maximum stress applied to strands in bottom flange
Relaxation	Class 2	[-]	Selected relaxation class: low relaxation
t	500.000	[h]	The value of the relaxation loss (in %) at 1000 h
ρ	2,5	[%]	Time after stressing (to determine final value of the relaxation loss)

Transverse prestressing top flange (post-tensioned)

The top flange is post-tensioned in transverse direction using tendons positioned in the prestressing ribs, these tendons are made up of several 7-wire strands Ø15,2. Parameters regarding the tendons are as follows:

Table 9 Parameters tendons prestressing top flange

n	5	[pcs]	Assumed number of strands per tendon
$\sigma_{p,max,prov}$	1400	[N/mm^2]	Assumed maximum stress applied to prestressing element
μ	0,23	[-]	Friction coefficient
k	0,009	[rad]	Unintentional angular rotation due to the Wobble-effect
w_{set}	3	[mm]	Estimated wedge set
Relaxation	Class 2	[-]	Selected relaxation class: low relaxation
t	500.000	[h]	The value of the relaxation loss (in %) at 1000 h
ρ	2,5	[%]	Time after stressing (for final value of the relaxation loss)

The values for 'μ' and 'k' are based on the values given in 5.10.5.2 of the ROK. The estimated value of the wedge set is based on the assumption that a small anchor will be used to limit this contribution to the direct losses, by keeping the influence length limited.

Prestressing end cross beam (post-tensioned)

The end beams are post-tensioned using prestressing tendons. The position of the tendons is defined with respect to the centre of the beam and the tendons at both halves are positioned symmetrically:

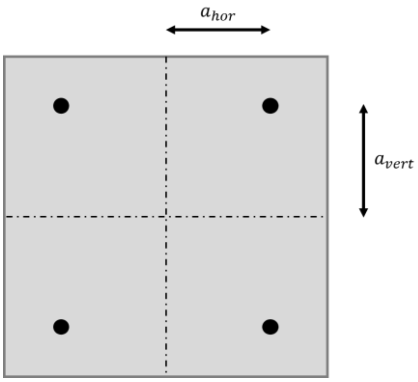


Figure 9 Position of the prestressing ducts in the end cross beams

A total of four tendons is used with their centre of gravity coinciding with that of the beam. This way the anchor forces are kept relatively limited to allow for the use of smaller anchors with smaller wedge set while a relatively large resulting centric prestressing force is imposed onto the beam. The tendons are made up of several 7-wire strands Ø15,2. Parameters regarding the tendons are as follows:

Table 10 Parameters tendons prestressing end cross beams

n_{ducts}	4	[pcs]	Number of ducts in total
a_{vert}	500	[mm]	Vertical position centre of duct from centre of beam
a_{hor}	750	[mm]	Horizontal position centre of duct from centre of beam
n_{strand}	7	[pcs]	Assumed number of strands per tendon
$\sigma_{p,max,prov}$	1400	[N/mm^2]	Assumed maximum stress applied to prestressing element
$Ø_{Duct}$	65	[mm]	Outer diameter of prestressing ducts
μ	0,23	[-]	Friction coefficient
k	0,009	[rad]	Unintentional angular rotation due to the Wobble-effect
w_{set}	3	[mm]	Estimated wedge set
Relaxation	Class 2	[-]	Selected relaxation class: low relaxation
t	500.000	[h]	The value of the relaxation loss (in %) at 1000 h
ρ	2,5	[%]	Time after stressing (for final value of the relaxation loss)

The values for 'μ' and 'k' are based on the values given in 5.10.5.2 of the ROK. The estimated value of the wedge set is based on the assumption that a small anchor will be used for each tendon to limit this contribution to the direct losses, by keeping the influence length limited.

2.3.5 Other parameters

The following table summarizes other parameters that will be used for the calculation, these factors are determined in accordance with the Eurocode 2 and the AFGC-SETRA 2013 guideline.

Table 11 Other parameters

Partial factors			
Definition	**Symbol**	**Value**	**Unit**
Partial factor concrete (cf EC2)	Yc	1,5	[-]
Partial factor for fibre reinforced concrete in tension (cf AFGC)	Y_{cf}	1,3	[-]
Product of partial factor for uncertainty in extrapolation * factor Y_{cf}	Y_E*Y_{cf}	1,5	[-]
Partial factor prestressing steel (cf EC2)	Ys	1,1	[-]

2.4 Bibliography chapter two

Braam, C. (2012). *Cement en beton 3 Constructieleer Voorgespannen Beton* (Vijfde herziene druk 2012 ed.). Aeneas.

Braam, R., Lagendijk, P., Soen, H., & Linssen, J. (2015). *Basiskennis beton.* Aeneas Media.

Groupe de travail BFUP. (2013, June). Ultra High Performance Fibre-Reinforced Concretes. *Recommendations*. Association Francaise de Génie Civil.

Hartsuijker, C. (2016). *Mechanica Spanningen, vervormingen, verplaatsingen* (2e druk ed.). Boom.

Lafarge North America Inc. (sd). JS1000. *Field-cast UHPC closure pour solutions for prefabricated bridge element connections*. USA.

NEN. (2011, november). NEN-EN 1992-1-1+C2. *Eurocode 2: Ontwerp en berekening van betonconstructies - Deel 1-1: Algemene regels en regels voor gebouwen*.

NEN. (2020, februari). NEN-EN 1992-1-1+C2/NB+A1. *Nationale bijlage bij NEN-EN 1992-1-1+C2 Eurocode 2: Ontwerp en berekening van betonconstructies - Deel 1-1: Algemene regels en regels voor gebouwen*.

Rijkswaterstaat. (2017, April). Richtlijnen Ontwerp Kunstwerken. *ROK 1.4*.

Walraven, J., & Braam, C. (2019, February). Prestressed Concrete.

3

PRINCIPLES FOR THE DETAILED DESIGN

In this chapter principles for the design that have not been covered previously are discussed. In the first paragraph the notions of consequence class and design service life from Eurocode 0 are introduced. In the second chapter provisions from Eurocode 2 and the AFGC-SETRA 2013 guideline are covered regarding durability, exposure classes and concrete cover. This information will be used in later paragraphs.

3.1 Eurocode 0 – Basis of Design

Eurocode 0 covers the basis of the design. In the second chapter requirements regarding the structure can be found. The most basic or fundamental and essential requirement (the whole design revolves around achieving this) is that the structure should be designed and executed as such that during the intended service life all actions and influences that may occur can be withstood while satisfying the requirements regarding the use of the structure. This basic requirement should be met by providing sufficient reliability, which should be achieved in an economical way.

Two concepts related to this, and that are important for the design phase, are discussed in greater detail, namely the reliability management and the service life, because these are important for the design.

3.1.1 Reliability

Reliability is first discussed in 2.2 of Eurocode 0. In Eurocode 0 the notion of ''reliability differentiation'' is introduced, in practical terms this means that structures (or if relevant: parts of structures) are classified according to different consequence classes and corresponding reliability classes. Annex B to Eurocode 0 gives more information regarding reliability and according to the national annex, the definitions for the consequence classes are as follows:

Tabel NB.23 - B1 — Definitie van gevolgklassen

Gevolgklasse [a]	Omschrijving
CC3	**Grote** gevolgen ten aanzien van het verlies van mensenlevens [b], of **zeer grote** economische of sociale gevolgen of gevolgen voor de omgeving
CC2	**Middelmatige** gevolgen ten aanzien van het verlies van mensenlevens, of **aanzienlijke** economische of sociale gevolgen of gevolgen voor de omgeving
CC1 nader onderverdeeld in:	
CC1b	**Geringe** gevolgen ten aanzien van het verlies van mensenlevens en **kleine** of **verwaarloosbare** economische of sociale gevolgen of gevolgen voor de omgeving
CC1a	**Nagenoeg uitgesloten** verlies van mensenlevens en **zeer kleine** of **verwaarloosbare** economische of sociale gevolgen of gevolgen voor de omgeving

[a] Projectspecifieke indeling mag worden gedaan op basis van een risicoanalyse, volgens 2.2 van NEN-EN 1990+A1+A1/C2:2019. Voorbeelden voor de toepassing van de gevolgklassen staan in tabel NB.24 – B1.
[b] Bedoeld zijn situaties van bouwwerken, waarin zich tegelijkertijd veel mensen kunnen ophouden en waarbij bij bezwijken van een essentieel onderdeel ineens een groot aantal mensen kan worden getroffen.

Figure 10 Definition of consequence classes – after NA to Eurocode 0, p.42

Which consequence class is to be selected depends on the consequences of failure or misfunctioning of the structure. The main load bearing structure of the Eefdesebrug is classified to fall within consequence class CC3, meaning large consequences in case of failure. Separate elements (e.g. railing) can be classified into lower class if it can be proven that failure has consequences of a lower order. This is not considered though as primarily the main load bearing structure is assessed.

In the same annex, the notions of reliability class and corresponding reliability index are also introduced. Consequence classes and reliability classes correspond to one another because probability of failure and consequences of failure are both important for assessing a structure. The required reliability of a structure (reliability class) can therefore be determined by means of classification of the consequences of failure of the structure (consequence class). The values of the partial factors for the loads depend on the classification as well.

The reliability classes determine the required reliability index β, which can be regarded as a measure for the required safety of the structure throughout the period in which it is in service, therefore it depends on the period of time for which the structure is designed. A larger value for the reliability index means a smaller probability of failure of the structure.

3.1.2 Design service life

According to Eurocode 0 the design service life has to be specified as well, which is the period of time over which the structure has to meet the requirements regarding its reliability. Reference is made to annex A for the minimum values of design service life of bridges. For the Eefdesebrug the design service life is 100 years, which corresponds to consequence class CC3.

Tabel NB.11 – 2.1 — Ontwerplevensduur bruggen – minimumwaarden

Ontwerplevensduur		Bruggen in gevolgklasse [c]
Klasse [a]	Jaren [b]	
3	50	CC1
3	50	CC2
4	100	CC3

[a] De aangegeven ontwerplevensduurklasse heeft betrekking op de constructieve en dragende onderdelen van de brug.

[b] De ontwerplevensduur is gedefinieerd in 1.5.2.8.
De referentieperiode is gedefinieerd in 1.5.3.15.
Voor aanpassing van de karakteristieke waarde, zie 4.1.2(7).

[c] De gevolgklasse is gedefinieerd in tabel NB.23 – B1.

Figure 11 Minimum value design service life of bridges - after NA to Eurocode 0, p.25

The structure has to function in a safe and durable way throughout the design service life. It is an important factor because if the time over which the structure has to function increases, the probability of the maximum load actually occurring during this period also increases. The characteristic value of the load only occurs once during the reference period. A shorter reference period (intended service life) therefore results in a lower load value while a longer reference period results in a larger load.

3.2 Eurocode 2 – Durability and concrete cover

When designing concrete structures, the exposure classes and the concrete cover are important notions because these are related to the durability of the structure. Chapter 4 of Eurocode 2 and the corresponding sections of the AFGC-SETRA 2013 guideline give the relevant provisions, these will be discussed in this paragraph and put into practice by determining the exposure classes and required concrete cover for different elements of the bridge.

In the first subparagraph, the background behind concrete cover and exposure classes is given. In the second subparagraph the provisions from Eurocode 2 are covered. Those from the AFGC-SETRA 2013 guideline are given in the third one. In the fourth subparagraph the required cover is determined.

3.2.1 Background

Concrete cover

For conventional concrete the concrete cover is an important measure to obtain durable structures. The cover has multiple functions. It protects the reinforcement against outside influences that could cause

corrosion of the steel, as well as against fire. In addition, by covering the rebars it also facilitates good transfer of stresses between the concrete and the steel via bond.

The concrete cover required for a specific application depends on multiple factors, one of them being related to the environment which the structure will be exposed to. This environment is described using exposure classes.

Exposure classes

In the Eurocode a total of six main groups is distinguished. By means of subdivision within these main groups a total of eighteen expose classes can be defined. The main groups are:

- **Group X0** – No risk of corrosion or attack: This is of relevance for situations where the concrete is shielded off from potential harmful influences. For example, concrete inside a building;

- **Group XC** – Corrosion induced by carbonation: Carbonation results in a decrease of the pH within the concrete which could facilitate other degradation processes. Within this group distinction is made between the humidity the concrete is exposed to, as this influences the carbonation process;

- **Group XD** – Corrosion induced by chlorides (not from seawater): Chloride from sources other than seawater could result in corrosion of the reinforcement. Different subgroups are given to distinguish between different degrees of humidity;

- **Group XS** – Corrosion induced by chlorides (from seawater): Chloride could cause corrosion of the reinforcement, and chlorides from the sea are in a separate group because structures to which this applies are commonly also exposed to other related influences such as other salts from seawater and current from the sea. Different subgroups distinguish between the degree to which the structure is exposed to the water (not direct, permanently submerged, etc.).

- **Group XF** – Freeze/thaw attack: Is of relevance for structures that could be exposed to freeze/thaw cycles. A distinction is made between groups to account for the water saturation and the potential presence of de-icing agents.

- **Group XA** – Chemical attack: Is of relevance to structures that could be subjected to chemical attack. Three subgroups are defined to distinguish between the aggressiveness of the environment.

The last five main groups have different subgroups. Using a number behind the two letters ('X' stands for 'exposure' and the second letter stands for the type of degradation mechanism) the degree of humidity or aggressiveness of the environment within the main group can be classified. The number is 1 to 3 or 1 to 4. The higher the number, the more aggressive or harmful the environment is to the structure.

Using this total of eighteen environmental classes the environment in which a structure or part of a structure will have to function can be described accurately. Relevant environmental classes are assigned to a part of the structure or to the structure as a whole. If multiple classes are of relevance, one will be the governing environmental class which will dictate several aspects of design, for example for the mixture composition, crack width criterion or required concrete over.

3.2.2 Provisions chapter 4 Eurocode 2

Environmental classes

This section describes the provisions chapter 4 of Eurocode 2, which covers durability and concrete cover. General requirements regarding durability and functioning of the structure are covered in 4.1. In paragraph 4.2 the environmental conditions are covered. The following table gives the exposure classes and environmental conditions to which these are related.

Klasse-aanduiding	Beschrijving van het milieu	Informatieve voorbeelden waar de milieuklassen zich kunnen voordoen
1 Geen risico op corrosie of aantasting		
X0	Voor beton zonder wapening of ingestorte metalen: alle milieus, behalve bij vorst/dooi, afslijting of chemische aantasting. Voor beton met wapening of ingesloten metalen: zeer droog	Beton binnen gebouwen met zeer lage luchtvochtigheid
2 Corrosie ingeleid door carbonatatie		
XC1	Droog of blijvend nat	Beton binnen gebouwen met lage luchtvochtigheid Beton blijvend onder water
XC2	Nat, zelden droog	Betonoppervlakken langdurig in contact met water Veel funderingen
XC3	Matige vochtigheid	Beton binnen gebouwen met matige of hoge luchtvochtigheid Beton buiten beschut tegen regen
XC4	Wisselend nat en droog	Betonoppervlakken in contact met water, maar die niet onder milieuklasse XC2 vallen
3 Corrosie ingeleid door chloriden *		
XD1	Matige vochtigheid	Betonoppervlakken blootgesteld aan chloriden uit de lucht
XD2	Nat, zelden droog	Zwembaden Beton blootgesteld aan chloridehoudend industriewater
XD3	Wisselend nat en droog	Brugdelen blootgesteld aan chloridehoudend spatwater Verhardingen Vloeren van parkeerplaatsen voor voertuigen
4 Corrosie ingeleid door chloriden afkomstig uit zeewater		
XS1	Blootgesteld aan zout uit de lucht, maar niet in direct contact met zeewater	Constructies bij of aan de kust
XS2	Blijvend onder zeewater	Delen van constructies in zee
XS3	Getijde-, spat- en stuifzones	Delen van constructies in zee
5 Aantasting door vorst/dooi-wisselingen		
XF1	Niet volledig verzadigd met water, zonder dooizouten	Verticale betonoppervlakken blootgesteld aan regen en vorst
XF2	Niet volledig verzadigd met water, met dooizouten	Verticale betonoppervlakken van wegconstructies blootgesteld aan vorst en met de lucht meegevoerde dooizouten
XF3	Verzadigd met water, zonder dooizouten	Horizontale betonoppervlakken blootgesteld aan regen en vorst
XF4	Verzadigd met water, met dooizouten of zeewater	Wegen en brugdekken blootgesteld aan dooizouten Betonoppervlakken blootgesteld aan direct gesproeide dooizouten en vorst Spatzones van constructies in zee blootgesteld aan vorst
6 Chemische aantasting		
XA1	Zwak agressief chemisch milieu volgens tabel 2 van EN 206-1	Natuurlijke grond en grondwater
XA2	Matig agressief milieu volgens tabel 2 van EN 206-1	Natuurlijke grond en grondwater
XA3	Sterk agressief milieu volgens tabel 2 van EN 206-1	Natuurlijke grond en grondwater

Figure 12 Exposure class and environment – Eurocode 2-1-1, p.50

Determining the concrete cover

After a number of requirements regarding durability (given in section 4.3, prescribing that appropriate measures should be taken to protect the structural elements against the relevant environmental conditions in order to reach the design service life) the concrete cover is discussed in 4.4. The steps of determining the cover are given below.

Nominal cover: The concrete cover is defined as the distance between the surface of the rebar and the closest concrete surface. The nominal cover is the value that is to be applied and to be specified. It is calculated as follows:

$$c_{nom} = c_{min} + \Delta c_{dev} \qquad \text{Equation (5)}$$

Where:
c_{min}: Minimum cover
Δc_{dev}: Tolerance for execution

Minimum cover: The minimum concrete cover ensures protection of the steel against corrosion and fire and transmission of forces. These two aspects are taken into consideration by calculating it as follows:

$$c_{min} = \max\{c_{min,b}; c_{min,dur}; 10\} \qquad \text{Equation (6)}$$

Where:
$c_{min,b}$: Minimum cover for bond
$c_{min,dur}$: Minimum cover for durability (environmental conditions)

Minimum cover for bond: The minimum cover should at least be equal to the minimum cover for bond in order to ensure that the rebar is well embedded in the concrete, this way forces can be transferred properly from the steel to the surrounding concrete. This is given in the following picture:

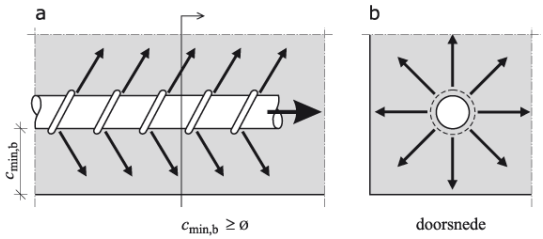


Figure 13 Force transfer steel to concrete – (Lagendijk & Braam, 2011), p.42

To ensure this, the code gives the following requirements under (3) of 4.4.1.2 and the national annex:

- Single rebar: $c_{min,dur} \geq \emptyset$;
- Bundle of rebars: $c_{min,dur} \geq \emptyset_n$, where $\emptyset_n$ is the equivalent diameter;
- Maximum grain size > 32 mm: Increase $c_{min,dur}$ by +5 mm;
- Post tensioned steel with circular ducts: $c_{min,dur} \geq \emptyset_n$, where $\emptyset_n$ is the equivalent diameter of the prestressing steel in the duct with a minimum of 25 mm (maximum is 80 mm);
- Post tensioned steel with rectangular ducts: $c_{min,dur}$ is the maximum value of the smallest dimension and half of the largest dimension;
- Pretensioned steel, smooth wires or strands: $c_{min,dur} = 1{,}5 * \emptyset$;
- Pretensioned steel, ribbed wires: $c_{min,dur} = 2{,}5 * \emptyset$.

Minimum cover for durability: The minimum cover required to meet durability requirements depends on multiple parameters that have to be determined first:

- Environmental class
- Concrete strength class
- Design service life
- Type of structure
- Measures for quality control

Using the following table from the national annex, one determines the structural classification. For a design service life of 50 years structural class S4 is prescribed. The minimum class is S1. Note that the five aforementioned criteria are considered in the table, for example:

- One aspect that is of relevance for determining the minimum cover for durability is the potential within a structure to redistribute loads in case of damage. For a plate element the cover is therefore smaller because redistribution is possible, while this is not the case for e.g. beams (for the bridge deck);
- In case of quality control, the structure class can be reduced as well. A case where this could be applied is for prefab elements but not for in-situ concrete.

Tabel 4.3N — Constructieve classificatie

Criterium	Constructieklasse: Milieuklasse volgens tabel 4.1						
	X0	XC1	XC2 / XC3	XC4	XD1	XD2 / XS1	XD3 / XS2 / XS3
Ontwerplevensduur 100 jaar	vermeer-dering met 2 klassen	vermeer-dering met 2 klassen	vermeer-dering met 2 klassen	vermeer-dering met 2 klassen	vermeer-dering met 2 klassen	vermeer-dering met 2 klassen	vermeerdering met 2 klassen
Ontwerplevensduur 75 jaar	vermeer-dering met 1 klasse	vermeer-dering met 1 klasse	vermeer-dering met 1 klasse	vermeer-dering met 1 klasse	vermeer-dering met 1 klasse	vermeer-dering met 1 klasse	vermeerdering met 1 klasse
Sterkteklasse [1), 2)]	≥ C30/37 vermindering met 1 klasse	≥ C30/37 vermindering met 1 klasse	≥ C35/45 verminde-ring met 1 klasse	≥ C40/50 verminde-ring met 1 klasse	≥ C40/50 verminde-ring met 1 klasse	≥ C40/50 verminde-ring met 1 klasse	≥ C45/55 vermindering met 1 klasse
Element met plaat-geometrie (plaats van de wapening niet beïnvloed door het bouwproces)	vermindering met 1 klasse	vermindering met 1 klasse	verminde-ring met 1 klasse	verminde-ring met 1 klasse	verminde-ring met 1 klasse	verminde-ring met 1 klasse	vermindering met 1 klasse
Specifieke kwaliteits-beheersing van de betonproductie gewaarborgd	vermindering met 1 klasse	vermindering met 1 klasse	verminde-ring met 1 klasse	verminde-ring met 1 klasse	verminde-ring met 1 klasse	verminde-ring met 1 klasse	vermindering met 1 klasse

1) Aangenomen is dat de sterkteklasse en de w/c-factor met elkaar verband houden. Een specifieke samenstelling (type cement, w/c-factor, fijne vulmiddelen) met de bedoeling een lage permeabiliteit te verkrijgen, mag zijn overwogen.

2) De grens mag zijn verminderd met één sterkteklasse indien luchtinsluiting van meer dan 4 % is toegepast.

Figure 14 Structural classification – NA to Eurocode 2-1-1, p.8

Using the determined structural class, the minimum cover required for durability, $c_{min,dur}$, can subsequently be determined using the following two tables from the national annex for reinforcement and prestressing steel respectively.

Tabel 4.4N — Waarden van de minimale dekkingseisen, $c_{min,dur}$, met betrekking tot duurzaamheid voor betonstaal volgens NEN-EN 10080

Constructie-klasse	Omgevingseisen voor $c_{min,dur}$ mm: Milieuklasse volgens tabel 4.1						
	X0	XC1	XC2/XC3	XC4	XD1/XS1	XD2/XS2	XD3/XS3
S1	10	10	10	15	20	25	25
S2	10	10	15	20	25	30	30
S3	10	10	20	25	30	35	35
S4	10	15	25	30	35	40	40
S5	15	20	30	35	40	45	45
S6	20	25	35	40	45	50	50

Tabel 4.5N — Waarden van de minimale dekkingseisen, $c_{min,dur}$, met betrekking tot duurzaamheid voor voorspanstaal

Constructie-klasse	Omgevingseisen voor $c_{min,dur}$ mm: Milieuklasse volgens tabel 4.1						
	X0	XC1	XC2 / XC3	XC4	XD1 / XS1	XD2 / XS2	XD3 / XS3
S1	10	15	15	20	25	30	30
S2	10	15	20	25	30	35	35
S3	10	15	25	30	35	40	40
S4	10	20	30	35	40	45	45
S5	15	25	35	40	45	50	50
S6	20	30	40	45	50	55	55

Figure 15 Minimum cover for durability for reinforcing steel (left) and prestressing steel (right) – NA to Eurocode 2-1-1, p.9

Additional provisions are given in the code as well:

- For concrete casted on other concrete surfaces or prestressing elements using unbonded tendons, other rules apply, see (9) and (10) respectively in the code;
- In case of uneven surfaces, c_{min} should be increased with +5 mm.

Tolerances for execution: The last step is to determine the tolerances related to execution, Δc_{dev}. The minimum cover has to be increased by this value to account for possible tolerances that occur during the execution phase.

The national annex prescribes $\Delta c_{dev} = 5$ mm;

Under (4) and in the national annex additional provisions are given:

- For uneven surface due to surface finishing: increase c_{min} with +5 mm (also see 4.4.1.2 (11);
- Concrete casted against uneven surfaces (work floor): $c_{nom} \geq c_{min,dur} + 10mm$

- Concrete casted against soil (directly on grade): $c_{nom} \geq c_{min,dur} + 50mm$

Remark Eurocode 2-2 and national annex: In the concrete code focussing on bridges a number of additional provisions is given in chapter 4, that are relevant for the design.

- In case de-icing salts are used all concrete services within 6,0 m from the carriageway in horizontal direction and 6 m above the carriageway have to be considered as directly exposed to de-icing salts. Top surfaces of supports below expansion joints also have to be considered as directly exposed.

- Concrete surfaces below grade within a distance of 6 m have to be considered as directly exposed up to 1 m below grade.

- Exposure classes for surfaces directly exposed to de-icing salts have to be determined as XD3, XF2 or XF4, depending on the situation.

3.2.3 Provisions AFGC-SETRA 2013

Section 4 in part 2 of the AFGC-SETRA 2013 covers the same topics as the corresponding chapter 4 in Eurocode 2-1 and 2-2. The guideline gives additional provisions for the environmental conditions and determining the concrete cover.

Environmental classes

The table from Eurocode 2-1 containing examples is rendered normative with the addition of a number of notes regarding the implementation of the table. This mainly involves detailed information on the implementation of the table and changes compared to Eurocode 2-1, for XF classes for example the cover is first related to exposure classes XC or XD. Reference is made to the guideline for all details.

Determining the concrete cover

Minimum cover: The equation to determine the minimum cover is modified to include an additional term to account for the minimum cover due to placement conditions:

$$c_{min} = \max\{c_{min,b}; c_{min,dur}; c_{min,p}; 10\ mm\} \quad \text{Equation (7)}$$

Where:

$$c_{min,p} = \max\{1{,}5 * l_f; 1{,}5 * D_{max}; \emptyset\} \quad \text{Equation (8)}$$

l_f: Fibre length
D_{max}: Maximum aggregate size
$\emptyset$: Diameter of the reinforcement or prestressing elements (whichever is relevant)

Minimum cover for bond: Although the requirements for the rebars are kept the same as in Eurocode 2, the values for $c_{min,b}$ for prestressing elements has been modified:

- Post tensioning:
    - Circular ducts: $c_{min,b} = \emptyset \leq 80$ mm, where $\emptyset$ is the diameter of the duct
    - Flat ducts: The maximum of the smallest dimension or half the largest dimension

- Pretensioning: $c_{min,b} = \max\{2 * \emptyset; 2 * D_{max}\}$, where $\emptyset$ is the diameter of the wire or strand and D_{max} the maximum aggregate size.

Minimum cover for durability: The table from Eurocode 2-1 to determine the structural class does no longer apply. The AFGC-SETRA 2013 guideline prescribes the following:

- Use S4 for current buildings and structures;
- Increase the class by 2 when the design service life is 100 years;
- Reduce the class by 1 when the design service life is 25 years or less;
- The minimum structural class is S1.

Subsequently the values for $c_{min,cur}$ are determined using the following two tables for reinforcing steel and prestressing steel respectively.

Tableau 4.4NF* : Valeurs de l'enrobage minimal $c_{min,dur}$ requis vis-à-vis de la durabilité dans le cas des armatures de béton armé conformes à l'EN 10080

Table 4.4NF : Values of minimum cover, $c_{min,dur}$, requirements with regard to durability for reinforcing steel in accordance with EN 10080.*

Exigence environnementale pour $c_{min,dur}$ (mm)/ *Environmental requirement for $c_{min,dur}$ (mm)*							
Classe structurale / *Structural class*	*Classe d'exposition suivant le tableau 4.1/ Exposure class according to Table 4.1*						
	X0	XC1	XC2/XC3	XC4	XD1/XS1	XD2/XS2	XD3/XS3
S1	5	5	5	10	10	15	15
S2	5	5	10	10	15	15	20
S3	5	5	10	15	15	20	20
S4	5	10	15	15	20	20	20
S5	10	10	15	20	20	20	25
S6	10	15	20	20	20	25	25

Tableau 4.5NF* : Valeurs de l'enrobage minimal $c_{min,dur}$ requis vis-à-vis de la durabilité dans le cas des armatures de précontrainte

Tableau 4.5NF: Values of minimum cover, $c_{min,dur}$, requirements with regard to durability for prestressing steel.*

Exigence environnementale pour $c_{min,dur}$ (mm)/ *Environmental requirement for $c_{min,dur}$ (mm)*							
Classe structurale / *Structural class*	*Classe d'exposition suivant le tableau 4.1/ Exposure class according to Table 4.1*						
	X0	XC1	XC2/XC3	XC4	XD1/XS1	XD2/XS2	XD3/XS3
S1	irrelevant	5	10	15	15	20	20
S2		10	15	15	20	20	20
S3		10	15	20	20	20	25
S4		15	20	20	20	25	25
S5		15	20	20	25	25	30
S6		20	20	25	25	30	30

Figure 16 Minimum cover for durability for reinforcing steel (left) and prestressing steel (right) – AFGC-SETRA 2013, p.95-96

Note: In the AFGC-SETRA 2013 guideline the remark is made that these tables are based on the tables in the Eurocode 2, but the values are modified by taking into account the diffusion coefficient for UHPC, which is significantly lower than the value for conventional concretes (a factor five). The values in the guideline are, as a result of this, the values in the Eurocode divided by a factor $\sqrt{5}$.

In case the in-situ concrete is in contact with other concrete (prefab or in-situ), then the minimum cover can be reduced provided a number of criteria has been met. See the guideline (point (9) of 4.4.1.2) for more details.

Tolerances for execution: Under (3) the guideline gives options to reduce the tolerance Δc_{dev} to 5 mm if a quality assurance system is used to monitor the production, including measuring the concrete cover. If additional conditions (more stringent quality control measures) are met the tolerance can be reduced to 0 mm. Reference is made to the guideline for all requirements.

3.2.4 Determining exposure classes & concrete cover – Main beams

Determining exposure classes

The prefab beams are exposed on multiple sides. The top side acts as the rolling surface of the deck and is fully exposed to the elements. Although in practice there is always a small inclination to allow the water to run off, the deck may be exposed to water for a longer period of time in case of rain. It may also be directly exposed to de-icing salts. That makes that the exposure classes of the top side are more severe than those for the sides of the beam. The sides of the beam are also exposed, but more sporadically (cyclic) than the top surface of the deck. Therefore, the practical approach is chosen to determine the exposure classes for the top surface of the beam and subsequently apply this to the whole beam.

The table from Eurocode 2 is used to determine the exposure classes together with the additional remarks from the AFGC-SETRA 2013 guideline, which suggest that applying the provisions for conventional concrete directly to UHPC is on the conservative side. For the top surface the following exposure classes are selected:

- Carbonation induced corrosion: XC4 – The top surface is cyclic wet and dry, e.g. due to rain. The water subsequently runs off;

- Chloride induced corrosion: XD3 – The top surface is cyclic wet and dry, the water may contain chlorides;

- Freeze/thaw: XF4 – The bridge deck is directly exposed to de-icing salts and water may be present for longer periods of time (before it flows off or evaporates completely).

The AFGC-SETRA 2013 prescribes that special attention to the mix design is required in case XF classes are relevant, though this is not taken into consideration for the design. In addition, the cover for XF classes is to be determined by selecting an appropriate XC of XD reference class. In order to do so the AFGC-SETRA 2013 presents the following table:

		Classe d'exposition/*Exposure class*			
		XF1	XF2	XF3	XF4
Type de salage (cf. recommandations GEL 2003) / *Type of de-icing (see freeze recommendations 2003)*	Peu fréquent / *Not very frequent*	XC4	Sans objet / *Not applicable*	XD4 si le béton est formulé sans entraîneur d'air / *XD4 if the concrete does not contain an air-entraining admixture* XD1 si le béton est formulé avec entraîneur d'air / *XD1 if the concrete contains an air-entraining admixture*	Sans objet / *Not applicable*
	Fréquent / *Frequent*	Sans objet / *Not applicable*	XD1, XD3 pour éléments très exposés (*) / *XD1, XD3 for highly exposed elements*	Sans objet / *Not applicable*	XD2, XD3 pour éléments très exposés (*) / *XD2, XD3 for highly exposed elements (*)*
	Très fréquent / *Very frequent*	Sans objet / *Not applicable*	Sans objet / *Not applicable*	Sans objet / *Not applicable*	XD3

Figure 17 Reference classes to XF exposure classes – AFGC-SETRA 2013, p.92

For XF4, the reference class XD3 is selected, this is on the conservative side as it corresponds to very frequent de-icing and direct exposure of the deck.

Determining concrete cover

The concrete cover is determined for XC4 and XD3. A different value is determined for the bottom flange (pretensioned prestressing strands are present here) and the top flange (where a larger duct for the post-tensioning is used).

Minimum cover for bond: For the top flange circular ducts are assumed for pretensioning. According to the guideline $c_{min,b} = \emptyset$ with a maximum of 80 mm. As a diameter $\emptyset 40$ mm is assumed, resulting in a value for $c_{min,b}$ of 40 mm.

For the bottom flange pretensioned strands with $\emptyset 15{,}2$ are assumed and the minimum cover for bond is:

$$c_{min,b} = \max\{2 * \emptyset; 2 * D_{max}\}$$

The value D_{max} is neglected because a UHPC of the type Reactive Powder Concrete is assumed, which is significantly smaller than the strand diameter. Hence: $c_{min,b} = 2 * 15{,}2 \approx 30$ mm.

Minimum cover for durability: According to the AFGC guideline S4 is the standard value for the structural class and it has to be increased to S6 for a design service life of 100 years. For both the top and bottom flange this results in: XC4: $c_{min,dur} = 25$ mm and XD3: $c_{min,dur} = 30$ mm.

Minimum cover for placement conditions: For the top flange where transverse post tensioned tendons are used a value of $\emptyset = 40$ mm was already assumed for the ducts. When keeping the other parameters equal, applying equation (8) yields: $c_{min,p} = \max\{1{,}5 * 13; 40\} = 40$ mm.

For the bottom flange the fibre length is 13 mm, the assumed strand diameter is $\emptyset 15{,}2$ and D_{max} is neglected (particle size of RPC type UHPC). Hence: $c_{min,p} = \max\{1{,}5 * 13; 15{,}2\} \approx 20$ mm.

Minimum cover: By applying equation (7) the following values are found for the top and bottom flanges:

- Top flange: $c_{min} = \max\{40; 30; 40; 10\ mm\} = 40$ mm
- Bottom flange: $c_{min} = \max\{30; 30; 20; 10\ mm\} = 30$ mm

Tolerances for execution: The tolerance is taken as $\Delta c_{dev} = 5$ mm, both for the top and bottom.

Nominal cover: The nominal cover for the top flange becomes:

$c_{nom} = 40 + 5 = 45$ mm

The nominal cover for the bottom flange becomes:

$c_{nom} = 30 + 5 = 35$ mm

Application
A cover of 35 mm will be applied onto the strands in the bottom flange.

3.2.5 Determining exposure classes & concrete cover – End beams

Determining exposure classes
The cross beams are constructed in conventional concrete. Although different parts of the beam are very well protected (fully covered), other parts are not. Exposure classes are determined for the most unfavourable (most exposed) parts of the beam and then applied to all surfaces.

They are positioned near the ends of the decks, near the joints with the abutments. While the top surface is covered by the deck of the bridge, due to its sides the beam is partially exposed. Due to this position, parts of the beam could also be exposed to water containing chlorides, due to de-icing salts. Given this description, the following environmental classes are selected:

- Carbonation induced corrosion: XC4 – Element is cyclic wet and dry, e.g. due to direct exposure to rain or water running down along the beam;
- Chloride induced corrosion: XD3 – Element is cyclic wet and dry and exposed to water containing chlorides, e.g. water running down the sides along the beam;
- Freeze/thaw: XF2 – Vertical element of the bridge which is both exposed to freeze/thaw (as it is partly exposed) and exposed to de-icing salts.

Determining concrete cover
Using the aforementioned exposure classes the concrete cover is determined. This will be applied to all sides of the beam, for simplicity no distinction is made between different parts. As discussed in 2.3.4 the tendons are positioned as such that the cover will be sufficient for the post tensioning tendons. Although no further passive reinforcement will be considered in the design calculations of the end beam, for the sake of completeness a calculation is made of the required cover if reinforcement would be applied. For this calculation a diameter of $\emptyset 40$ mm is assumed, the maximum value used for rebars.

Minimum cover for bond: Given the assumed diameter $c_{min,b}$ would be 40 mm.

Minimum cover for durability: For both exposure classes the minimum cover for durability is as follows:

- For XC4: The initial value for the structural class is S4. Because the design service life is 100 years the structural classification is increased by 2. There is no plate geometry and no specific quality control is assumed. Hence the class is S6. For reinforcement the cover $c_{min,dur}$ is 40 mm.

- For XD3, following the same line of reasoning, the class would be again S6. For reinforcement the cover $c_{min,dur}$ is 50 mm.

The value for XD3 is governing over XC4. Hence $c_{min,dur}$ is 50 mm.

Minimum cover: Given the different values for minimum cover for durability and bond, $c_{min} = 50$ mm.

Tolerances for execution: The basic value is 5 mm. The beam is casted on formwork or against the UHPC beams. These are even surfaces and no surface finishing is assumed to be used. Therefore, the value for the tolerances is taken as $\Delta c_{dev} = 5$ mm.

Nominal cover: The nominal cover can now be determined, which is done as follows: $c_{nom} = c_{min} + \Delta c_{dev}$. Hence: $c_{nom} = 50 + 5 = 55$ mm. This value would be applied to all sides of the beam.

Application

Given the positioning of the tendons as discussed in 2.3.4 the cover is sufficient. Passive reinforcement for the end beams is not considered in the remainder of the elaboration of the design.

3.3 Bibliography chapter three

Groupe de travail BFUP. (2013, June). Ultra High Performance Fibre-Reinforced Concretes. *Recommendations*. Association Francaise de Génie Civil.

Lagendijk, P., & Braam, C. (2011). *Cement en beton 2 Constructieleer Gewapend Beton* (Zevende gewijzigde druk 2011 ed.). Aeneas.

NEN. (2011, november). NEN-EN 1992-1-1+C2. *Eurocode 2: Ontwerp en berekening van betonconstructies - Deel 1-1: Algemene regels en regels voor gebouwen*.

NEN. (2011, december). NEN-EN 1992-2+C1. *Eurocode 2: Ontwerp en berekening van betonconstructies - Betonnen bruggen - Regels voor ontwerp, berekening en detaillering*.

NEN. (2016, november). NEN-EN 1992-2+C1/NB. *Nationale bijlage bij NEN-EN 1992-2+C1 Eurocode 2: Ontwerp en berekening van betonconstructies - Betonnen bruggen - Regels voor ontwerp, berekening en detaillering*.

NEN. (2019, november). NEN-EN 1990+A1+A1/C2. *Eurocode: Grondslagen voor het constructief ontwerp*.

NEN. (2019, november). NEN-EN 1990+A1+A1/C2/NB. *Nationale bijlage bij NEN-EN 1990+A1:2006+A1:2006/C2:2019 Eurocode: Grondslagen van het constructief ontwerp*.

NEN. (2020, februari). NEN-EN 1992-1-1+C2/NB+A1. *Nationale bijlage bij NEN-EN 1992-1-1+C2 Eurocode 2: Ontwerp en berekening van betonconstructies - Deel 1-1: Algemene regels en regels voor gebouwen*.

Snijder, H., & Steenbergen, H. (2011). *Krachtswerking.* Zoetermeer: Bouwen met Staal.

4

LOADS AND LOAD COMBINATIONS

4.1 Identifying relevant loads

In the preliminary design only a few load cases were taken into consideration (self-weight, imposed permanent loads and LM1 and LM4 for vertical traffic loads). In reality many more different loads can be distinguished and in the most general case, the following load cases may be taken into consideration for a prefab concrete bridge or viaduct:

- Permanent action (G):
    - Self-weight of the structure: The self-weight of the main load bearing elements, such as the prefab UHPC beams and end cross beams;
    - Kerbs: Many different types of ''street furniture'' may be present on a bridge. In the bridge under consideration concrete kerbs are present to keep traffic within the carriageway;
    - Railing: A railing is positioned at the edges of the outer beams;
    - Road surface (e.g. asphalt layer): Road surfacing is also typically applied to the concrete deck, typically this is a layer of bituminous material or asphalt;
    - Imposed deformation (settlements, shrinkage and creep): Due to settlements of the substructure deformations can be imposed upon the structure, if these are restraint this causes loads. In addition, imposed deformations may also be caused by shrinkage and creep.
- Prestressing action (P):
    - Action due to the prestressing strands and/or tendons on the beam.
- Variable action (Q):
    - Vertical traffic loads: Different load models are used to describe the vertical traffic loads due to traffic and pedestrians. Loads can be distinguished for global and local verifications;
    - Horizontal traffic loads: The variable traffic loads also result in horizontal actions, for example due to braking of the vehicles;
    - Actions due to rain, wind and snow loads: Different actions can be imposed upon the structure due to factors such as rain, snow and wind;
    - Imposed deformations due to temperature: Temperature and temperature cycles may result into superimposed deformations. If restrained, these deformations cause forces.

- Accidental actions (A):
    - Traffic accidents: Due to accidents truck loads may be positioned outside the traffic lanes, this is modelled by wheel loads at the edges of the bridge deck;
    - Collision loads (ships): A possible accidental scenario for a bridge is a collision with a ship, this is also to be accounted for in the analysis.

Before the loads are discussed in more detail it has to be determined which are of relevance and which are not. The following loads are not taken into consideration:

- Imposed deformation (settlements, shrinkage and creep): Because the structure is statically determinate, imposed deformations are not restrained. The structure can deform freely, thus preventing forces to occur. In addition, the structure has functioned for decades. Provided that the load on the substructure is not increased compared to the current situation, additional settlements are not expected. Shrinkage and creep will have to be considered for the calculation of prestressing losses though.

- Horizontal traffic loads: Horizontal loads are especially relevant if the substructure is analysed, as the horizontal loads have to be restrained by the substructure and foundation. However, the design focusses on the superstructure, for which the horizontal loads are of lesser importance. Therefore, these are not taken into consideration at this design stage.

- Actions due to rain, wind and snow loads: Although variable loads due to rain, wind and snow can be determined it is expected that the influence of these loads on the whole will be very limited. The magnitude of these loads is small compared to the self-weight and traffic loads on the bridge for example, and in addition these loads will be combined using the combination factors ψ, which means that the characteristic values that are already relatively small will be reduced even further.

- Imposed deformations due to temperature: Following the same line of reasoning as for the afore-mentioned causes of imposed deformations, imposed deformations due to temperature are not relevant because the structure can deform freely (statically determinate structure).

All other loads from the list are relevant and will be taken into consideration. These loads will be determined in next paragraph, which will be done accordance with the relevant parts of the Eurocode.

4.2 Determining the actions

4.2.1 Permanent actions (G)

Self-weight prefab beams

The self-weight of the prefab beams (as a line load) is determined by multiplying the area of the cross section with the specific weight γ_{UHPC}. The load per meter of length is:

$$G_{k,beams} = A_c * \gamma_{UHPC}$$

$$G_{k,beams} = 1{,}66 * 25 = 41{,}59 \text{ kN/m}$$

Self-weight in-situ end cross-beams

The self-weight of the prefab beams (as a line load) is determined by multiplying the area of the cross section with the specific weight γ_C. The end beams will be constructed in conventional (assumed to be prestressed) concrete. The load per meter of length:

$$G_{k,cb} = A_{cb} * \gamma_C$$

$$G_{k,cb} = 4{,}62 * 25 = 115{,}56 \text{ kN/m}$$

Longitudinal joint

The longitudinal joints result in line loads along the length of the deck. Its cross section is calculated by multiplying the mean value of the thickness of the top flange with the width of the joint (note that ff only the height of the in-situ part would be included the outstand prefab parts would be missed). The calculation is as follows:

$$G_{k,j} = t_{ft} * w_j * \gamma_{UHPC}$$

$$G_{k,j} = 0{,}019 * 25 = 0{,}42 \text{ kN/m}$$

Road surface

In the preliminary design report the influence of the asphalt layer on the weight increase was discussed. Although not required from a structural point of view an asphalt layer was still applied, and contributed heavily to the total weight of the structure. To obtain a more economical design it has been decided to reduce the asphalt layer significantly, only to account for the presence of a protective layer. To account for this a layer of 10 mm with a density $\gamma_{asphalt}$ of 23 kN/m^3 is assumed.

$$G_{k,surf} = t_{surf} * \gamma_{asphalt}$$

$$G_{k,surf} = 10 * 10^{-3} * 23 = 0{,}23 \text{ kN/m}^2$$

Kerbs

The permanent load due to the kerbs (as a line load) is calculated by multiplying the area of the cross section with the specific weight. Reinforced concrete is assumed for the kerbs. The load then is per metre of length:

$$G_{k,kerbs} = A_{kerbs} * \gamma_C$$

$$G_{k,kerbs} = 0{,}17 * 25 = 4{,}25 \text{ kN/m}$$

Railing

The load of the railing is determined by calculating the railing of the existing bridge. The assumed weight of steel is 78,50 kN/m^3. Based on original design drawings (drawing number B.7143) the weight is assumed to be 0,31 kN/m. This value is rounded off to $q_{k,rail} = 0{,}50$ kN/m to include margin, hence:

$$G_{k,rail} = q_{k,rail} = 0{,}50 \text{ kN/m}$$

4.2.2 Prestressing actions (P)

The prestressing actions will be determined in later chapters of this report. These loads will not be included in the RFEM model but the output from the programme is used to design the prestressing.

4.2.3 Variable actions (Q)

Traffic lanes

Section 4.2.3 of NEN-EN 1991-2 covers the division of the carriageway into theoretical traffic lanes. The kerbs are higher than 200 mm, therefore, according to the national annex, the width w of the carriageway is the width between the kerbs: 7,0 m.

- According to table 4.1 of the code, the number of theoretical lanes, n_1, is:

$$n_1 = Int\left(\frac{7{,}0}{3}\right) = 2$$

- According to the same table, the width of a theoretical lane, w_1, equals 3,0 m and the remaining area then equals $7{,}0 - 2 * 3{,}0 = 1{,}0$ m. The width of the pedestrian lanes equals 4,18 m.

Load model 1 – ULS

Use of Load Model 1 (LM1): Characteristic values of the vertical traffic loads are found in section 4.3 of Eurocode 1-2. According to (1) of 4.3.1 load model 1 is to be used for global and local verifications.

Values for global verifications: Load model 1 consists of tandem axles (TS) with load per axle of $\alpha_Q Q_k$ and a uniformly distributed load (UDL) of $\alpha_q q_k$. The values for Q_{ik} and q_{ik} for traffic lane 'i' are taken from table 4.2 of the code:

Positie	Tandemstelsel *TS*	Gelijkmatig verdeelde belasting (GVB)
	Aslast Q_{ik} (kN)	q_{ik} (of q_{rk}) (kN/m^2)
Rijstrook nummer 1	300	9
Rijstrook nummer 2	200	2,5
Rijstrook nummer 3	100	2,5
Overige rijstroken	0	2,5
Resterende oppervlakte (q_{rk})	0	2,5

Figure 18 Characteristic values of the traffic loads – NEN-EN 1991-2, p.39

In addition, the values Q_{ik} and q_{ik} are multiplied with correction factors α_Q and α_q respectively, these can be used to account for the expected traffic crossing the bridge (i.e. different traffic categories), which depends on the type of road. The values for these factors can be found in the national annex.

Reduction factors and values: According to the national annex, the loads can be reduced through these factors if the number of trucks per year on the lane for the heavy traffic (N_{obs}) is smaller than 2 M. For the Eefdesebrug this will definitely be the case, because at most traffic corresponding to a provincial road is expected, because in the report 'Existing Bridges Twentekanaal' it was recommended to design for provincial traffic.

Theoretically speaking, a reduction would therefore be justified, which has to be applied in accordance with the following table. At the same time the exact extent of such a reduction is difficult to quantify because different bridges could vary in intensity. It has been decided to apply the values corresponding to a span $l = 50$ m and number of trucks for heavy traffic equal to 200.000. This results in $\alpha_{Qi} = \alpha_{qi} = 0{,}97$ (to be applied onto all lanes) and $\alpha_q = 0{,}90$.

Aantal vrachtwagens per jaar per rijstrook voor zwaar verkeer N_{obs} [a]	α_{Q1} en α_{q1}				α_{qr}
	Lengte van de overspanning of invloedslengte (L)				
	20 m	50 m	100 m	≥ 200 m	
≥ 2 000 000	1,0	1,0	1,0	1,0	
200 000	0,97	0,97	0,95	0,95	0,90
20 000	0,95	0,94	0,89	0,88	0,80
2 000	0,91	0,91	0,82	0,81	0,70
200	0,88	0,87	0,75	0,74	0,60

[a] Tussengelegen waarden mogen worden geïnterpoleerd.

Figure 19 Correction factors for LM1 – NA to Eurocode 1-2, p.9

This results in the following values:

- Theoretical lane 1: $\alpha_{Q1} * Q_{1k} = 0{,}97 * 300 = 291$ kN per axle, $\alpha_{q1} * q_{1k} = 0{,}97 * 9{,}0 = 8{,}73$ kN/m^2
- Theoretical lane 2: $\alpha_{Q2} * Q_{2k} = 0{,}97 * 200 = 194$ kN per axle, $\alpha_{q2} * q_{2k} = 0{,}97 * 2{,}5 = 2{,}425$ kN/m^2
- Remaining area: $\alpha_{qr} * q_{rk} = 0{,}9 * 2{,}5 = 2{,}25$ kN/m^2

Positioning on deck for global verification: To obtain the load effects for the global verification, the axles have to be placed centrically at the theoretical lane. The contact area of a single wheel is 0,4 by 0,4 m while the distance between the axles is 1,2 m. More information is given in the following figure.

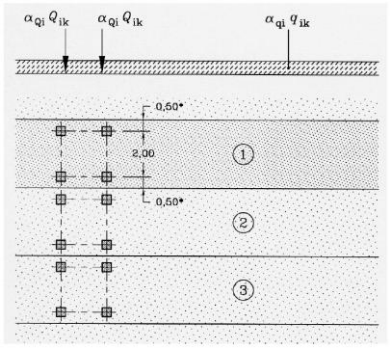


Figure 20 Applying LM1 – NEN-EN 1991-2, p.40

According 4.2.4 and 4.25 the number of loaded lanes, their positioning and the remaining areas should be as such that the load effects are most unfavourable. Therefore, various load configurations have been determined. In transverse direction (and the same as for preliminary design) these are as follows:

- Configuration 1: Lane 1 directly next to the kerb, lane 2 next to it and after that the remaining area (from right to left).

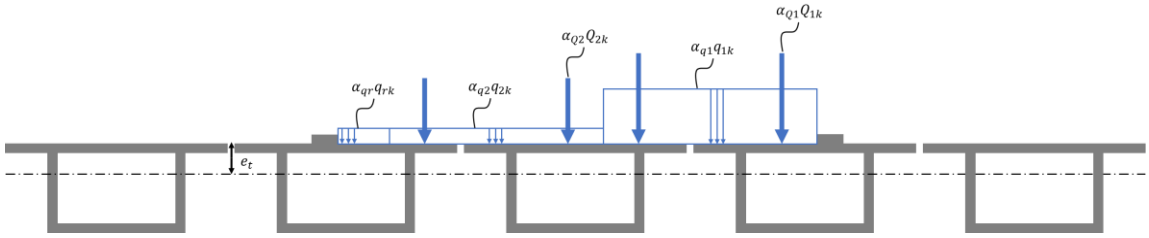


Figure 21 LM1 – First possible load configuration

- Configuration 2: The second lane is shifted to the left kerb, the remaining area is now positioned between the heaviest lane and the rightmost kerb.

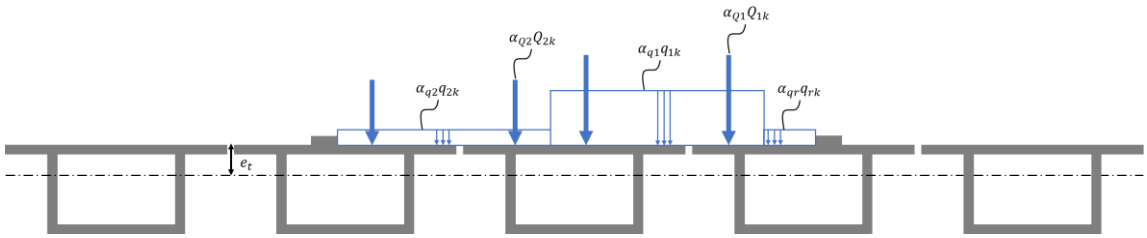


Figure 22 LM1 – Second possible load configuration

- Configuration 3: Lane 1 is positioned centrically onto the middle beam (beam 3), the remaining width of the carriageway is regarded as remaining area.

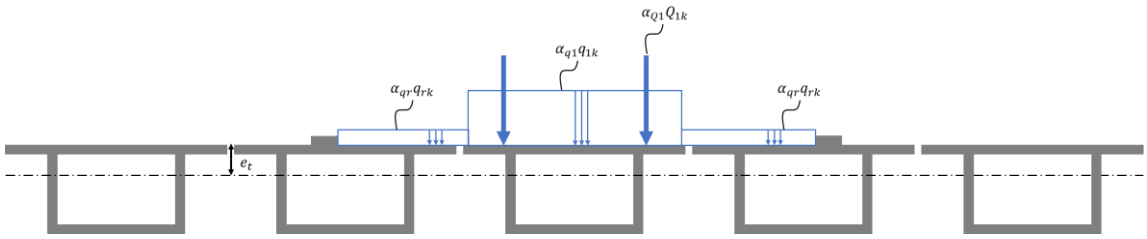


Figure 23 LM1 – Third possible load configuration

In longitudinal direction the loads could be modelled both at mid span (to obtain the maximum bending moment) and near the supports (for the maximum shear force). This positioning will be covered in the chapter on modelling the RFEM model.

Load model 2 – ULS (local verification)

Magnitude of the load: For local verifications LM2 is applied instead of LM1. This load model consists of a single axle with value $\beta_Q Q_{ak}$. The value of Q_{ak} is 400 kN (includes magnification factor for dynamic effects). According to the national annex, the value of β_Q equals that of α_{Q1}, which is 0,97 in this case, resulting in $\beta_Q Q_{ak} = 0{,}97 * 400 = 388$ kN.

Application of the load: The axle load can be positioned at any point of the carriageway. The contact area with the road surface is 0,6 m in transverse direction and 0,35 m in longitudinal direction (note the difference with the contact surface of LM1, LM2 represents double tires):

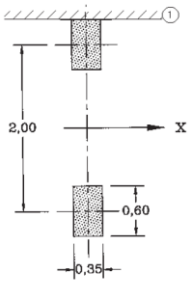


Figure 24 LM2 – Eurocode 1-2, p.42

Additional provisions on the local distribution of forces can be found in 4.3.6 of the code in case LM1 or LM2 is applied for local verifications. Note that the loads for the local distributions will not be included in the RFEM model. The force distribution for the local verifications will be determined manually in the respective sections of the report.

Load model 4 – ULS

To account for the presence of pedestrians and/or cyclists on the pedestrian/bicycle lanes load model 4 is applied. This is only applied for the global verifications and is applied there where it results in an unfavourable load effect in transverse and longitudinal direction.

In the main text in 4.3.5 a standard value for the uniformly distributed load of 5 kN/m^2 is given. The national annex refers to 5.3.2.1 (3), which allows for this bridge that the load is determined as follows (full load is not required, it is not expected that the bridge is fully loaded by crowd load, so the 5 kN/m^2 may be reduced):

$$q_{fk} = 2{,}0 + \frac{120}{L + 30}\ [kN/m^2]$$

In addition: 2,5 kN/m^2 $\leq q_{fk} \leq$ 5,0 kN/m^2

$$q_{fk} = 2{,}0 + \frac{120}{68 + 30} = 3{,}22\ [kN/m^2]$$

Load on railing

Loads on the railing is covered in 4.8. of Eurocode 1-2. The loads on the railing comprise a horizontal and a vertical line load. According to (2) the horizontal loads are to be considered simultaneously with the uniformly distributed load due to the pedestrians (LM4). Given the fact that the kerbs at the outer sides of the carriage way are present, the railing is assumed to be protected from collision with vehicles from the main traffic lanes.

The magnitudes of the loads can be found in the national annex, according to (1) of this document the loads transferred by the railing onto the bridge deck are line loads and these have to be considered once both horizontally and vertically, as a variable load acting at the upper side of the railing. The appropriate value for the Eefdesebrug is a line load of 3,0 kN/m.

$Q_{k,rail,h} = 3$ kN/m

$Q_{k,rail,v} = 3$ kN/m

Fatigue load model (FLM1)

Different load models: Eurocode 1-2 gives five different load models for fatigue due to vertical traffic loads, these are given in paragraph 4.6. Note however that according to the national annex to Eurocode 2-2 not all models are allowed for all verifications. In this stage a simple model, FLM1, will be used to determine the maximum and minimum stresses that occur in the bridge. These stresses are then used to determine whether the fatigue life can be regarded as infinite or not. If this is not the case and the fatigue life have to be determined as a result of this, a different model can be used.

Number of vehicles: Eurocode 1-2 prescribes that number of heavy vehicles per year (N_{obs}) has to be estimated or counted. According to the national annex every lane has to be regarded as a lane for heavy traffic, and indicative values can be found in the following table. Values corresponding to provincial roads are used:

Tabel NB.5 – 4.5(n) — Aantal verwachte zware voertuigen per jaar en per rijstrook voor zwaar verkeer

	Verkeerscategorie	$N_{obs,a,sl}$ per jaar en per rijstrook voor zwaar verkeer
1	Autosnelwegen (A-wegen) en wegen met twee of meer rijstroken per rijrichting en met intensief vrachtverkeer	$2{,}0 \times 10^6$
2	(Auto)wegen met gemiddeld vrachtverkeer (zoals N-wegen)	$0{,}5 \times 10^6$
3	Wegen met weinig vrachtverkeer	$0{,}125 \times 106$
4	Wegen met weinig vrachtverkeer en bovendien uitsluitend bestemmingsverkeer	$0{,}05 \times 10^6$
OPMERKING	De aantallen zware voertuigen per jaar en per rijstrook voor zwaar verkeer $N_{obs,a,sl}$ zijn inclusief de trend.	

Figure 25 Number of heavy vehicles – NA to Eurocode 1-2, p.17

Fatigue Load Model 1 (FLM1): The FLM1 itself is described in 4.6.2. and is comparable to LM1, only the magnitude of the vertical loads is different:

- Axle loads: $0{,}7 * Q_{ik}$
- Uniformly distributed load: $0{,}3 * q_{ik}$
- Remaining area: $0{,}3 * q_{rk}$

Hence: for lane 1 and 2 the axle loads are 210 and 140 kN respectively. The uniformly distributed loads are 2,7 kN/m^2 and 0,75 kN/m^2 for lanes 1 and 2 respectively, while the remaining area is also loaded by 0,75 kN/m^2.

Using these values, the maximum stresses ($\sigma_{FLM,max}$) and minimum stresses ($\sigma_{FLM,min}$) are determined while accounting for the different positions of this load model on the bridge as defined for load model 1.

Throughout the paragraph 4.6 different comments are made on what FLM1 actually represents. The model is used to verify if the fatigue life can be regarded as infinite and the model is said to be conservative in most cases. The values of the load model correspond to the effect of the heavy traffic on European main roads (traffic category 1) and are comparable to those the model for frequent loads.

Positioning of FLM1: For the positioning of the load model provisions can be found in the main codes 1-2 and 2-2, as well as their national annexes. For this design a practical approach has been chosen by following the transverse positioning as worked out for LM1.

Dynamic effects: FLM1 already includes a magnification factor for dynamic effects which is applicable to road surfaces of good quality. However, close to expansion joints an additional magnification factor has to be applied in accordance to:

$$\Delta\varphi_{fat} = 1{,}30 * \left(1 - \frac{D}{26}\right) \geq 1$$

Where:
D: Distance between cross section under consideration and the expansion joint

According to the national annex to Eurocode 1-2 the maximum value of $\Delta\varphi_{fat}$ may be taken equal to 1,15 if a road surface of good quality is present near the joint. If at least one axle of a vehicle is within the 6,0 m zone from a joint, the magnification factor has to be applied to all axles of the vehicle. In addition, the value $\Delta\varphi_{fat}$ has to be taken constant over the full 6,0 m zone.

4.2.4 Accidental actions (A)

In the case of the Eefdesebrug accidental situation can occur due to road traffic (traffic accident) or due to ships passing the bridge (collision). These loads are discussed next.

Accidental actions due to road traffic

Accidental situations may occur resulting in (heavy) vehicles being positioned outside the main carriageway. Provisions on this situation are given in 4.7.3.1 of Eurocode 1-2 and 4.7.1 of the ROK. As the latter is more stringent, this will be applied. Regardless of a guiding structure being present or not, the possibility of a traffic accident resulting in an accidental action has to be accounted for.

For this accidental situation the outer wheels of the heaviest concentrated loads $2 * Q_{1k}$ have to be assumed to be positioned at the edge of the bridge. The remainder of the bridge is loaded by a load with the magnitude of the representative value of the traffic load. The outer side of the structure has to be taken as the edge of the bridge deck. This is modelled by placing lane 1 at the outermost part of the bridge, while loading the rest of the carriageway by the loads corresponding to the remaining area.

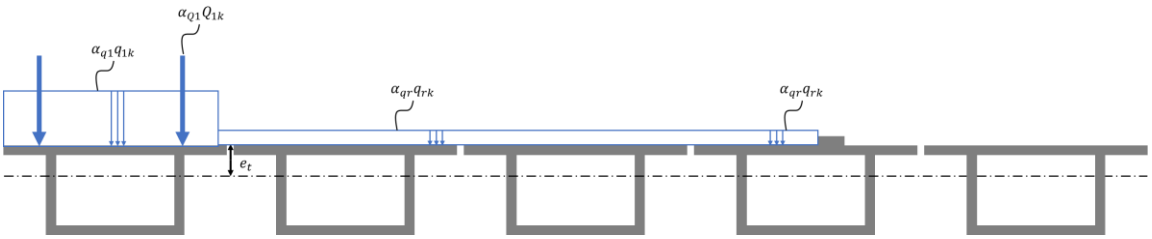


Figure 26 Load configuration traffic accident

Another possible accidental situation is a collision with a kerb. Provisions on this load case are given in 4.7.3.2 of Eurocode 1-2. Additional provisions are given in 4.7.3.2 and 4.7.3.3 of the ROK. Given the magnitude of this load case it is not expected to be governing and therefore omitted.

Accidental actions due to shipping

Load models for accidental actions due to collision with ships are given in section 4.6 of Eurocode 1-1-7 and the national annex. Most of the provisions are focussed on the collision between ships and the substructure of a bridge and to determine the loads the CEMT classification of the waterway is used as input. The substructure is positioned outside the waterway behind guiding structures, such verifications are therefore not of importance.

What is of relevance is the collision of a ship and the bridge deck. According to (4) of 4.6.2 the deck of the bridge should, if this situation is relevant, be designed as such that it can withstand the equivalent static load due to the impact of a ship collision in the direction perpendicular to the longitudinal axis of the deck.

According to the national annex the equivalent static force has a magnitude of 1 MN and an impact area with dimensions $a = 0{,}25$ and $b = 3{,}0$ m.

4.3 Provisions on limit states

Ultimate limit states

Limit states are situations where the structure cannot fulfil one or more of its functions, as a result it does no longer fulfil the requirements regarding reliability. Distinction is made between ultimate limit states (associated to structural failure and thus safety) and serviceability limit state (associated to requirements regarding the functioning of the structure, aesthetics, durability and comfort).

It has to be verified that the limit states are not exceeded in any of the relevant design situations and load cases that can occur during the intended service life of the structure. In the Eurocode the method of partial factors is used for these verifications.

In paragraph 6.4 of Eurocode 0, various ultimate limit states are defined for which the appropriate load combinations have to be formulated. The limit states relevant for the design of the Eefdesebrug are discussed below.

STR: Failure or excessive deformation of the structure or elements of the structure where the strength of the material is governing. It has to be verified that:

$$E_d \leq R_d$$

Where:
E_d: Design value of the effect of actions
R_d: Design value of the resistance

FAT: Failure of the structure or elements of the structure due to fatigue. Details are found in the material specific code (in this case Eurocode 2). It has to be verified that:

$$E_{d,fat} \leq R_{d,fat}$$

Where:
$E_{d,fat}$: Design value of the effect of fatigue actions
$R_{d,fat}$: Design value of the fatigue resistance

Combinations of actions for the ULS

To verify these ultimate limit states the appropriate load combinations have to be formulated so the effect of the actions can be calculated. The following load combinations have to be formulated:

- **Fundamental combinations**: These combinations are for persistent or transient design situations and will be used to verify the ULS STR;
- **Combinations for fatigue**: These are defined in the material specific codes and will be used to verify the ULS FAT;
- **Combinations for accidental situations**: These combinations are for accidental design situations and will be used to verify the resistance of the structure under these situations.

Serviceability limit states

In paragraph 6.5 of Eurocode 0 the serviceability limit state is discussed, which will be verified to determine whether deflections will remain between acceptable limits. It has to be verified that:

$$E_d \leq C_d$$

Where:
E_d: Design value of the effects of actions specified in the serviceability criterion
C_d: Limiting design value of the relevant serviceability criterion

Combinations of actions for the SLS
To verify the serviceability limit state, again load combinations have to be formulated to determine the effects of the actions. The code distinguishes between three different combinations for the serviceability limit state:

- Characteristic combination
- Frequent combination
- Quasi-permanent combination

Which combination is to be used depends on the limit state under consideration. The characteristic combination is used for irreversible situations (e.g. plastic deformation after overloading). The frequent combination is for reversible situations (e.g. elastic deformation to verify cracking or deflection). The quasi-permanent combination is used for long-term effects (e.g. shrinkage or increase of deflection due to creep). Because deflection and crack width are to be assessed as separate criterions, the frequent combination will be used.

4.4 Provisions on combinations of actions

The design values of the individual action effects of actions that occur at the same time are combined to obtain combinations of actions for the critical situations. Each combination contains either a dominant variable load or an accidental load.

4.4.1 Combination of actions ULS – Fundamental combinations

Combinations of actions for the permanent or transient design situations (fundamental combinations) are given in 6.4.3.2. For the STR limit state, the most unfavourable of the following two equations is to be used (equations 6.10a and 6.10b):

- Eq. 6.10a.

$$E_d = \sum_{j\geq 1} \gamma_{G,j} G_{k,j} + \gamma_P P + \gamma_{Q,1} \psi_{0,1} Q_{k,1} + \sum_{i>1} \gamma_{Q,i} \psi_{0,i} Q_{k,i}$$

- Eq. 6.10b.

$$E_d = \sum_{j\geq 1} \zeta_j \gamma_{G,j} G_{k,j} + \gamma_P P + \gamma_{Q,1} Q_{k,1} + \sum_{i>1} \gamma_{Q,i} \psi_{0,i} Q_{k,i}$$

Where (after: Eurocode 0):
E_d: Design value of effect of actions
γ_G: Partial factor for permanent actions, also accounting for model uncertainties and dimensional variations
G_k: Characteristic value of a permanent action
γ_P: Partial factor for prestressing actions (reference made to Eurocode 2)
P: Relevant representative value of a prestressing action (reference made to Eurocode 2)
γ_Q: Partial factor for variable actions, also accounting for model uncertainties and dimensional variations
ψ_0: Factor for combination value of a variable action
Q_k: Characteristic value of a single variable action
ζ: Reduction factor for unfavourable permanent actions G

4.4.2 Combination of actions ULS – Fatigue

Information on the load combinations for the ULS verification FAT can be found in 6.8.3 of Eurocode 2-1-1. The main principle is that the load has to be divided into non-cyclic actions that do not result in fatigue (constant magnitude, so non-cyclic) and cyclic loads that do result in fatigue.

- Non-cyclic (constant) loads: The combination for the non-cyclic load is equal to the frequent combination for the SLS:

$$E_d = \sum_{j\geq 1} G_{k,j} + P + \psi_{1,1} Q_{k,1} + \sum_{i>1} \psi_{2,i} Q_{k,i}$$

- Cyclic loads: The cyclic load has subsequently to be combined with the most unfavourable combination of the non-cyclic loads:

$$E_d = \sum_{j\geq 1} G_{k,j} + P + \psi_{1,1} Q_{k,1} + \sum_{i>1} \psi_{2,i} Q_{k,i} + Q_{fat}$$

Where:
Q_{fat}: Fatigue load (i.e. traffic load in this case)

During the verification these two combinations will be used to determine the stress range to be used for the fatigue analysis.

4.4.3 Combination of actions ULS – Accidental design situations

Combinations of actions for accidental situations are given in 6.4.3.3. of Eurocode 0. These include an accidental action (e.g. an impact load for example) while the other variable actions are reduced by applying $\psi_{1,1}$ and/or $\psi_{2,1}$. These combinations of actions may be formulated as follows:

$$E_d = \sum_{j\geq 1} G_{k,j} + P + A_d + (\psi_{1,1} \text{ or } \psi_{2,1}) Q_{k,1} + \sum_{i>1} \psi_{2,i} Q_{k,i}$$

Following (9)P of A.2.2.1, whenever variable traffic loads are combined with another variable loads each group of loads as given in Eurocode 1-2 has to be considered as a single variable load.

According A2.2.5, if accidental situations are considered only one accidental load has to be considered in an accidental load combination.

4.4.4 Combination of actions SLS – Frequent combination

According to 6.5.3, the frequent combination is formulated as follows:

$$E_d = \sum_{j\geq 1} G_{k,j} + P + \psi_{1,1} Q_{k,1} + \sum_{i>1} \psi_{2,i} Q_{k,i}$$

Typically for all combinations of actions in the SLS is that the partial factors for the loads are taken equal to 1,0.

4.4.5 Partial and combination factors

Design values of loads & partial factors
Eurocode 0 and its national annex gives more information regarding design values of actions and partial factors for the formulation of load combinations. Annex A.2 is especially important, as this covers the rules and methods to formulate load combinations for ULS and SLS verifications of bridges.

Design value of actions – Permanent and variable: Design values and partial factors for the loads in the ultimate limit state can be found in section A.2.3. of Eurocode 0 and the national annex. For structural elements (ULS STR) where geotechnical loads are not considered (this is the case for the superstructure of the Eefdesebrug) the design value of the loads should be determined in accordance with table NB.15 – A2.4(B) from the national annex:

Tabel NB.15 – A2.4(B) — Rekenwaarden voor de belastingen (STR/GEO) (groep B)

Blijvend en tijdelijke ontwerpsituaties	Blijvende belastingen		Voor-spanning	Overheersende veranderlijke belasting [a)]	Tegelijkertijd optredende veranderlijke belastingen [a]	
	Ongunstig	Gunstig			Belangrijkste (indien aanwezig)	Andere
(Vgl. 6.10a)	$\gamma_{G,j,sup}G_{k,j,sup}$	$\gamma_{G,j,inf}G_{k,,inf}$	$\gamma_P P$		$\gamma_{Q,1}\psi_{0,1}Q_{k,1}$	$\gamma_{Q,i}\psi_{0,i}Q_{k,i}$
(Vgl. 6.10b)	$\xi\gamma_{G,j,sup}G_{k,j,sup}$ waarbij $\xi = 0{,}89$	$\gamma_{G,j,inf}G_{k,j,inf}$	$\gamma_P P$	$\gamma_{Q,1}Q_{k,1}$		$\gamma_{Q,i}\psi_{0,i}Q_{k,i}$

[a] Veranderlijke belastingen zijn die, die zijn beschouwd in tabellen NB.12 – A2.1, NB.13 – A2.2 en A2.3.

Figure 27 Design values of loads – NA to Eurocode 0, p.32

Partial factors: The values for the partial load factors for bridges designed for road traffic are to be taken in accordance with table NB.16 – A2.4 of the national annex:

Tabel NB.16 – A2.4(B) — Belastingsfactoren voor wegverkeersbruggen en bruggen voor langzaam verkeer en voetgangers- en fietsbruggen STR/GEO) (groep B)

Gevolgklasse	β	G			Verkeer (met $\psi = 1$)	Overig veranderlijk (met $\psi = 1$)
		$\gamma_{G,j,sup}$		$\gamma_{G,j,inf}$		
		6.10a	6.10b (incl. ξ)	6.10a en 6.10b		
CC1	3,3	1,20	1,10	0,9	1,20	1,35
CC2	3,8	1,30	1,20	0,9	1,35	1,5
CC3	4,3	1,40	1,25	0,9	1,5	1,65

$\gamma = 0$ voor gunstig werkende veranderlijke belastingen

Voor γ_P zie de aanbevelingen in de desbetreffende materiaalgebonden Eurocodes 1992 t/m 1999.

Voor de berekening van het effect van ongelijkmatige zettingen geldt dat $\gamma_{G,set} = 1{,}20$ in het geval van een lineaire berekening en $\gamma_{G,set} = 1{,}35$ in het geval van een niet lineaire berekening. Gunstig werkende zettingsverschillen worden niet in rekening gebracht. De grootte van de zettingen is bepaald op basis van de karakteristieke belastingscombinatie en de karakteristieke waarden voor de grondeigenschappen.

OPMERKING De factor K_{FI} volgens B 3.3 is in de waarden van γ verwerkt; voor de zettingsberekening blijft de betrouwbaarheidsdifferentiatie achterwege.

Figure 28 Applied partial factors – NA to Eurocode 0, p.33

For equation 6.10a the factor for permanent actions equals 1,40 while for equation 6.10 b it equals 1,25 (including ζ). The factor for traffic loads equals 1,5 if ψ equals 1,0 (equation 6.10 b).

Design value of actions – Accidental: For accidental load combinations the factors can be found in A2.3.2. of Eurocode 0. According to the national annex the design values as given in table NB.22 – A2.5 should be used:

Tabel NB.22 – A2.5 — Rekenwaarden voor belastingen voor gebruik in buitengewone en aardbevingsbelastingscombinaties

Blijvende en tijdelijke ontwerpsituaties	Blijvende belastingen		Voor-spanning	Buitengewone of aardbevings-belasting	Begeleidende veranderlijke belastingen [b]	
	Ongunstig	Gunstig			Belangrijkste (indien aanwezig)	Andere
Buitengewoon [a]	$G_{k,j,sup}$	$G_{k,j,inf}$	P	A_d	$\psi_{1,1}\ Q_{k,1}$	$\psi_{2,i}\ Q_{k,i}$ $i > 1$
Aardbeving [c]	$G_{k,j,sup}$	$G_{k,j,inf}$	P	$A_{Ed} = \gamma_I A_{Ek}$	$\psi_{2,1}\ Q_{k,1}$	$\psi_{2,i}\ Q_{k,i}$ $i \geq 1$

[a] Bij een buitengewone ontwerpsituatie moet de belangrijkste veranderlijke belasting zijn genomen met zijn frequente waarde en de overige veranderlijke belastingen met de quasi-blijvende waarde. Indien de buitengewone ontwerpsituatie een aardbevingbelastingscombinatie is, dan moet de belangrijkste veranderlijke belasting en alle overige veranderlijke belastingen zijn genomen met hun quasi-blijvende waarde.

[b] De veranderlijke belastingen zijn de beschouwde in tabel NB.12 – A2.1, A2.2 en A2.3.

[c] Er is geen bijzondere aardbevingsontwerpsituatie voorgeschreven.

De ontwerpwaarde voor γ voor alle niet-aardbevingsbelastingen moet gelijk zijn genomen aan 1,0.

Figure 29 Design values of loads in accidental combinations - NA to Eurocode 0, p.39

ψ-factors

For the and ψ reference is made to A2.2.6. of Eurocode 0. For bridges for road traffic the combination factors (ψ-factors) are given in table NB.12-A.2.1 of the national annex. For the traffic loads considered both for ψ_0 and ψ_1 the value of 0,8 is used.

Belasting	Symbool		ψ_0	ψ_1	ψ_2
Verkeersbelastingen (zie NEN-EN 1991-2+C1:2015, tabel 4.4)	gr1a (LM1 + voetgangers- of fietspad-belastingen)	TS	0,8	0,8	0,4
		UDL		0,8	
		Horizontale belasting		0,8	
		Voetgangers- + fietspad-belastingen		0,8 [d]	
	gr1b (enkele as)		0	0,8 [b]	0
	gr2 (horizontale krachten dominant)		0,8	0,8 [c]	0
	gr3 (voetgangersbelastingen)		0	0,8 [b]	0
	gr4 (LM4 – belasting door een menigte)		0	0,8 [b]	0
	gr5 (LM3 – speciale voertuigen)	TS	0	0,8 [b]	0
		UDL		0,8 [b]	
		Horizontale belastingen		0,8 [b]	
		Speciaal voertuig		1,0 [b]	
Windkrachten	F_{Wk}	blijvende ontwerpsituatie	0,3	0,6 [b]	0
		Uitvoering	0,8	0	0
	F_W^*		1,0	0	–
Thermische belastingen	T_k		0,3	0,8 [b]	0,3 [a]
Sneeuwbelastingen	$Q_{Sn,k}$	blijvende ontwerpsituatie	0	0	0
		Uitvoering	0,6	0	0
Belastingen tijdens de bouw	Q_c		1,0	0	1,0

[a] In de uiterste grenstoestand mag voor ψ_2 voor thermische belasting de waarde 0 zijn aangehouden.

[b] Voor aanrijding op of onder de brug en aanvaring is $\psi_1 = 0$.

[c] Voor scheurvomingsberekeningen van beton zijn de verschillende waarden van ψ_1 gelijk aan de waarden behorend bij gr1a (zie voor de waarden van ψ Tabel NB.19).

[d] Voor scheurvormingsberekeningen van beton moet $\psi_1 = 0,4$ zijn aangehouden.

OPMERKING Groepen verkeersbelastingen hoeven niet met elkaar te zijn gecombineerd.

Figure 30 ψ-factors for traffic bridges – NA to Eurocode 0, p.29

For the limit state STR the following table (table NB.19 from the national annex) gives more detailed information on the formulation of load combinations for the limit state ULS – STR.

Tabel NB.19 — ψ-waarden voor belastingscombinaties STR – wegverkeersbruggen en bruggen voor langzaam verkeer

Belasting	Belastingscombinaties												
	gr1a	gr1b	gr2	gr3	gr4	gr5	W [b]		T [b]		S	A1 [a,b]	
TS	1	0	0,8	0	0	0,8	0,8	0,64	0,8	0,64	0	0,8	0,64
UDL	1	0	0,8	0	0	0,8	0,8	0,64	0,8	0,64	0	0,8	0,64
Enkele as	0	1	0	0	0	0	0	0	0	0	0	0	0
Horizontale belasting	0,8	0	1	0	0	0,8	0,64	0,8	0,64	0,8	0	0,64	0,8
Voetpaden	0,4	0	0,4	1	1	0	0,32	0,32	0,32	0,32	0	0,32	0,32
Mensenmenigte	0	0	0	0	1	0	0	0	0	0	0	0	0
Bijzondere voertuigen	0	0	0	0	0	1	0	0	0	0	0	0	0
Wind [c] F_{wk}	0,3	0	0,3	0	0	0,3	1	1	0,3	0,3	0	0	0
F^*_w	1	0	1	0	0	1	0	0	0	0	0	0	0
Temperatuur	0,3	0	0,3	0	0,3	0,3	0,3	0,3	1	1	0	0	0
Sneeuw	0	0	0	0	0	0	0	0	0,	0	1	0	0
Impact op of onder de brug	0	0	0	0	0	0	0	0	0	0	0	1	1
Aardbevingsbelasting	0	0	0	0	0	0	0	0	0	0	0	0	0

[a] A1 = aanrijding op of onder de brug en aanvaring.

[b] Bij deze combinaties is in eerste kolom gr1a × Ψ_0 en de tweede kolom gr2 × Ψ_0 .Voor de definitie van de groep verkeersbelasting gr1a en gr2 zie NEN-EN 1991-2+C1.

[c] Waar verkeersbelasting op (delen van) de brug aanwezig is, mag zijn gerekend met F^*_w in plaats van F_{wk}.

Figure 31 ψ-factors for load combinations – NA to Eurocode 0, p.37

Load groups

In 4.5 of Eurocode 1-2 groups of variable traffic loads on bridges for road traffic are introduced to account for the simultaneous occurrence of different traffic loads. In combining such a group with loads other than traffic loads, these load groups are to be considered as a single characteristic load. This is given in table NB.3-4.4a of the national annex:

Tabel NB.3 – 4.4a — Bepaling van groepen verkeersbelastingen (karakteristieke waarden van de belastingen met verschillende componenten)

Belastings-type		Rijweg						Voet- en fietspaden
		Verticale krachten				Horizontale krachten		Alleen verticale krachten
Verwijzing		4.3.2	4.3.3	4.3.4	4.3.5	4.4.1	4.4.2	5.3.2.1
Belastings-systeem		BM1 (TS en UDL)	BM2 (enkele as)	BM3 (bijzondere voertuigen)	BM4 (mensen-menigte)	Rem- en versnellings-krachten	Centrifugaal-krachten en krachten in dwarsrichting	Gelijkmatig verdeelde belastingen
Groepen van belastingen	gr1a	Karakteristieke waarde				0,8 × karakte-ristieke waarde	0,8 × karakte-ristieke waarde	0,4 × karakte-ristieke waarde
	gr1b		Karakteristieke waarde					
	gr2	0,8 × karakteristieke waarde				Karakteristieke waarde	Karakteristieke waarde	0,4 × karakte-ristieke waarde
	gr3							Karakteristieke waarde [a]
	gr4				Karakteristieke waarde [b]			
	gr5	0,8 × karakteristieke waarde [c]		Karakteristieke waarde		0,8 × karakteristieke waarde [c]	0,8 × karakteristieke waarde [c]	
		De gearceerde vakken zijn de overheersende belastingscomponent (aangeduid als component behorend bij de groep)						

[a] Zie 5.3.2.1. Er behoort slechts één voetpad als belast te zijn beschouwd, indien het effect hiervan ongunstiger is dan bij belasting op twee voetpaden.

[b] Inclusief de belasting op voet- en fietspaden.

[c] Vast te stellen voor afzonderlijke projecten.

Figure 32 Groups of traffic loads – NA to Eurocode 1-2, p.15

In the case of this design, the simultaneous occurrence of LM1 on the main carriageway and LM4 on the bicycle lanes are of relevance. Together they form load group gr1a, comprising the characteristic value of LM1 plus the combination value of LM4. According to the national annex this is 0,4 times the characteristic value, which is schematically written as:

$$gr1a = 1{,}0 * LM1 + 0{,}4 * LM4$$

Partial factors ULS (material)

The partial factors for the material resistance are given in the material specific codes and therefore not covered in this chapter, various factors are listed in 0 of this report.

Partial factors SLS (loads & material)

Values for the partial factors for the SLS are discussed in A2.4.1. of Eurocode 0 and the national annex. Conforming these, the partial factors for the loads are taken equal to 1,0 for the SLS. The partial factors for the materials are typically also taken equal to 1,0 except when prescribed otherwise in the material specific codes.

4.4.6 Remarks and background

To aid in the understanding, some additional information is given on the different concepts that were used in this chapter.

Different representative values of the (variable) load

Loads have different representative values. Which one is relevant depends on the period of time over which the load is present. Something that was not covered before is the period of time over which the load is present, this explains the different ψ factors in the aforementioned equations.

- **Permanent load G_k**: By definition the permanent loads are always present and are therefore mentioned in all load combinations. For calculations the characteristic value is used.

- **Variable load**: The magnitude of the variable load varies in time, therefore this influence has to be considered when determining the value for a variable load. Distinction is made between the four different representative values of the load: the characteristic value, combination value, the frequent value and the quasi-permanent value.

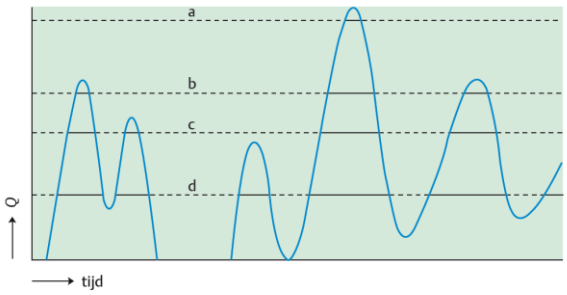
    - Characteristic value Q_k: The value of the variable load for which the probability of being exceeded during the service life of the structure is very small. This implies that the time is of lesser important. The mere fact that this load could be present at some point during the service life is what matters, the structure has to satisfy its requirements also at this moment of time.

    - Combination value $\psi_0 Q_k$: It accounts for the probability of simultaneous occurrence of two or more variable loads. The value of the characteristic load as such that the probability of the effects of the load combination being exceeded is about the same as the probability of exceeding the effect of an individual characteristic load. It is used for the ULS.

    - Frequent value $\psi_1 Q_k$: The value of the variable load that will be present for a short period of time (a part of the design service life). Time starts to play a role here and this value will only be exceeded for limited periods of time. It is used for accidental situations in the ULS and reversible situations in the SLS.

    - Quasi-permanent value $\psi_2 Q_k$: Value of the variable load of which the probability of it being present at a certain moment of time is very large. It can be considered as the average variable load being present in time and can therefore be expected to be exceeded for substantial periods of time. It is used for accidental situations in the ULS and for the study of long-term effects in the SLS.

These different values are schematically given in the following figure. The horizontal axis represents time while the vertical axis represents the magnitude of the value of the load.



1.3 | **Representatieve waarden van variabele belastingen**
a. karakteristieke waarde of Q_k
b. combinatiewaarde of $\psi_0 Q_k$
c. frequente waarde of $\psi_1 Q_k$
d. quasi-blijvende waarde of $\psi_2 Q_k$

Figure 33 Different representative values of variable loads – (Cement&BetonCentrum, 2008)

The combination, frequent and quasi-permanent values are determined from the characteristic value via the factors ψ_0, ψ_1 and ψ_2. The value of these factors depends on the use of the structure, the probability of a load being present depends on the type of structure after all.

In the previous expressions for the load combinations, it can be seen that typically one variable load is chosen to be taken as the leading/predominant variable load (for which its characteristic value is used) and then combined with the accompanying values of other variable loads that can be present simultaneously (can be $\psi_0 Q_k$, $\psi_1 Q_k$ or $\psi_2 Q_k$ depending on the combination).

The reason behind this is that the occurrence of the characteristic value of the load at a given moment in time is small. The simultaneous presence of the characteristic values of two separate variable loads is therefore very unlikely, as is the simultaneous presence of one characteristic value of a variable load and an accidental load. Therefore, these values of the loads do not have to be combined.

Combinations for the SLS

One should be careful not to confuse the combinations for the SLS with the different representative values of the variable loads, as these have the same names. The difference is that the representative values of the variable loads are used to compose the serviceability limit state combinations of actions (and these describe the magnitude of the individual variable loads). To emphasize the difference, the meaning and use of the different combinations for the SLS are repeated.

- **Characteristic combination**: The characteristic combination in the SLS is to be used for irreversible situations, for example plastic deformation due to overloading the structure;

- **Frequent combination**: The frequent combination in the SLS is to be used for reversible situations, for example the deflection of a structure in the elastic stage or cracking of the structure;

- **Quasi-permanent combination**: The quasi-permanent combination in the SLS is used if long term effects are to be considered, for example the increase of deflection due to creep caused by the presence of the load over a long period of time.

4.5 Elaborating the combinations of actions

In the previous sections all relevant loads and equations & provisions from the codes have been determined and/or listed. The next step is to combine these into the required combinations of actions. Although this will be worked out to full extent in the next chapter (the calculation model itself) the equations for the combinations of actions are further completed by plugging in the partial load and ψ factors.

4.5.1 Elaboration fundamental combinations (ULS)

When applying the design values for the loads, the partial load factors and the ψ factors as determined in the previous sections, then the equations for the fundamental load combinations are as follows:

- Equation 6.10a:

$$E_d = \sum_{j\geq 1} \gamma_j G_{k,j} + \gamma_P P + \gamma_{Q,1}\psi_{0,1}Q_{k,1} + \sum_{i>1} \gamma_{Q,i}\psi_{0,i}Q_{k,i} \rightarrow$$

$$E_d = \sum_{j\geq 1} 1{,}40 * G_{k,j} + 1{,}0 * P + 1{,}50 * 0{,}8 * Q_{k,1} + 1{,}50 * 0{,}8 * Q_{k,2}$$

- Equation 6.10b:

$$E_d = \sum_{j\geq 1} \zeta_j \gamma_{G,j} G_{k,j} + \gamma_P P + \gamma_{Q,1} Q_{k,1} + \sum_{i>1} \gamma_{Q,i}\psi_{0,i}Q_{k,i} \rightarrow$$

$$E_d = \sum_{j\geq 1} 1{,}25 * G_{k,j} + 1{,}0 * P + 1{,}50 * Q_{k,1} + 1{,}50 * 0{,}8 * Q_{k,2}$$

In these equations the term $G_{k,j}$ represents the different components of the permanent actions while $Q_{k,1}$ represents load group gr1a of the variable loads and $Q_{k,2}$ represents the variable load acting on the railing of the bridge.

4.5.2 Elaboration combination fatigue (ULS)

When applying the design values for the loads, the partial load factors and the ψ factors as determined in the previous sections, then the equations for the fatigue combinations are as follows:

- Non-cyclic (constant) loads:

$$E_d = \sum_{j\geq 1} G_{k,j} + P + \psi_{1,1}Q_{k,1} + \sum_{i>1} \psi_{2,i}Q_{k,i} \rightarrow E_d = \sum_{j\geq 1} G_{k,j} + P + 0{,}4 * Q_{k,2}$$

- Cyclic loads:

$$E_d = \sum_{j\geq 1} G_{k,j} + P + \psi_{1,1}Q_{k,1} + \sum_{i>1} \psi_{2,i}Q_{k,i} + Q_{fat} \rightarrow E_d = \sum_{j\geq 1} G_{k,j} + P + 0{,}4 * Q_{k,2} + Q_{fat}$$

Here $Q_{k,2}$ denotes the loads due to pedestrians on the pedestrian lanes and railings, factor ψ_2 is applied in accordance with Figure 30. The symbol Q_{fat} denotes fatigue load model 1. Load $Q_{k,1}$ is not of importance because LM1 is replaced by FLM1.

4.5.3 Elaboration combination of actions accidental design situations (ULS)

When applying the design values for the loads, the partial load factors and the ψ factors as determined in the previous sections, then the equations for the combinations of accidental design situations are as follows:

$$E_d = \sum_{j\geq 1} G_{k,j} + P + A_d$$

In this equation the term A_d represents the accidental load. For the load case representing a traffic accident on the bridge, the accidental load is present over almost the full width of the deck (see Figure 26) and therefore it is not combined with the combination values of other variable loads. In case of ship collision, a different type of verification is performed (static equilibrium, see 6.7) and therefore no combination value of other variable loads is included in this case either.

4.5.4 Elaboration frequent combination of actions (SLS)

According to 6.5.3, the frequent combination is formulated as follows:

$$E_d = \sum_{j\geq 1} G_{k,j} + P + \psi_{1,1} Q_{k,1} + \sum_{i>1} \psi_{2,i} Q_{k,i} \rightarrow E_d = \sum_{j\geq 1} G_{k,j} + P + 0{,}8 * Q_{k,1} + 0{,}4 * Q_{k,2}$$

In this equation the term $G_{k,j}$ represents the different components of the permanent actions while $Q_{k,1}$ represents load group gr1a of the variable loads and $Q_{k,2}$ represents the variable load acting on the railing of the bridge. The values of ψ_1 and ψ_2 are in accordance with Figure 30.

4.6 Bibliography chapter four

Cement&BetonCentrum (Red.). (2008). *Ontwerpen en berekenen - Eurocode 2* (Eerste druk ed.). Boxtel: Aeneas.

Lagendijk, P., & Braam, C. (2011). *Cement en beton 2 Constructieleer Gewapend Beton* (Zevende gewijzigde druk 2011 ed.). Aeneas.

NEN. (2011, november). NEN-EN 1992-1-1+C2. *Eurocode 2: Ontwerp en berekening van betonconstructies - Deel 1-1: Algemene regels en regels voor gebouwen*.

NEN. (2011, december). NEN-EN 1992-2+C1. *Eurocode 2: Ontwerp en berekening van betonconstructies - Betonnen bruggen - Regels voor ontwerp, berekening en detaillering*.

NEN. (2015, oktober). NEN-EN 1991-1-7+C1+A1. *Eurocode 1: Belastingen op constructies - Deel 1-7: Algemene belastingen - Buitengewone belastingen: stootbelastingen en ontploffingen*.

NEN. (2015, oktober). NEN-EN 1991-2+C1. *Eurocode 1: Belastingen op constructies – Deel 2: Verkeersbelasting op bruggen*.

NEN. (2016, november). NEN-EN 1992-2+C1/NB. *Nationale bijlage bij NEN-EN 1992-2+C1 Eurocode 2: Ontwerp en berekening van betonconstructies - Betonnen bruggen - Regels voor ontwerp, berekening en detaillering*.

NEN. (2019, november). NEN-EN 1990+A1+A1/C2. *Eurocode: Grondslagen voor het constructief ontwerp*.

NEN. (2019, november). NEN-EN 1990+A1+A1/C2/NB. *Nationale bijlage bij NEN-EN 1990+A1:2006+A1:2006/C2:2019 Eurocode: Grondslagen van het constructief ontwerp*.

NEN. (2019, november). NEN-EN 1991-1-7+C1+A1/NB. *Nationale bijlage bij NEN-EN 1991-1-7+C1+A1: Eurocode 1: Belastingen op constructies - Deel 1-7: Algemene belastingen - Buitengewone belastingen*.

NEN. (2019, november). NEN-EN 1991-2+C1/NB. *Nationale bijlage bij NEN-EN 1991-2+C1: Eurocode 1: Belastingen op constructies – Deel 2: Verkeersbelasting op bruggen*.

NEN. (2020, februari). NEN-EN 1992-1-1+C2/NB+A1. *Nationale bijlage bij NEN-EN 1992-1-1+C2 Eurocode 2: Ontwerp en berekening van betonconstructies - Deel 1-1: Algemene regels en regels voor gebouwen*.

Rijkswaterstaat. (2017, April). Richtlijnen Ontwerp Kunstwerken. *ROK 1.4*.

Snijder, H., & Steenbergen, H. (2011). *Krachtswerking*. Zoetermeer: Bouwen met Staal.

5

FEA CALCULATION MODEL

5.1 RFEM model

The global force distribution in the bridge deck is calculated using a fine element model. In the preliminary design report, it was already concluded that using such a model would contribute to a more economical design compared to hand calculations, because a finite element model includes the distribution of loads due to interaction between different structural elements.

This chapter covers the setup of a finite element model that will be used to determine the global force distribution in the structure, for this the finite element analysis programme RFEM is used. The governing values of the internal forces determined using this model will be used as input for the verifications performed in the subsequent parts of the design.

All input parameters have been collected in a separate document which is attached to this report as an annex (see annex V). Reference is made to this document for more detailed information regarding the RFEM input.

5.2 Modelling the structure

5.2.1 Geometry of the structure

A 3D FEM model is set up where the x-axis in the programme coincides with the longitudinal axis of the bridge and the y-axis coincides with the transverse direction of the bridge. Using nodes and line segments the main geometry of the bridge is modelled:

- The five main beams are modelled using line segments with a length equal to the span of the beams, which is 68 m, and they are placed centre of centre 3,29 m in between. This way the total width is 16,36 m;

- Between the beams free space is present. This represents the longitudinal joints between the main beams, these will be included as permanent loads acting on the structure;

- The end cross beams are modelled as line segments between the end nodes of the outer two beams;

- In addition, nodes are added corresponding to the corner points of the top surface of the bridge deck, connected with lines in between. This represents the outer boundaries of the surface element, which will be modelled, and which mid plane coincides with the centre of gravity of the beams.

Reference is made to annex V for more details regarding the input parameters.

Nodal supports are added to the model to support the beams. The beams are supported by hinges on one side and sliding supports in x-direction on the other. The following figure gives an overview of the line and surface elements of the model:

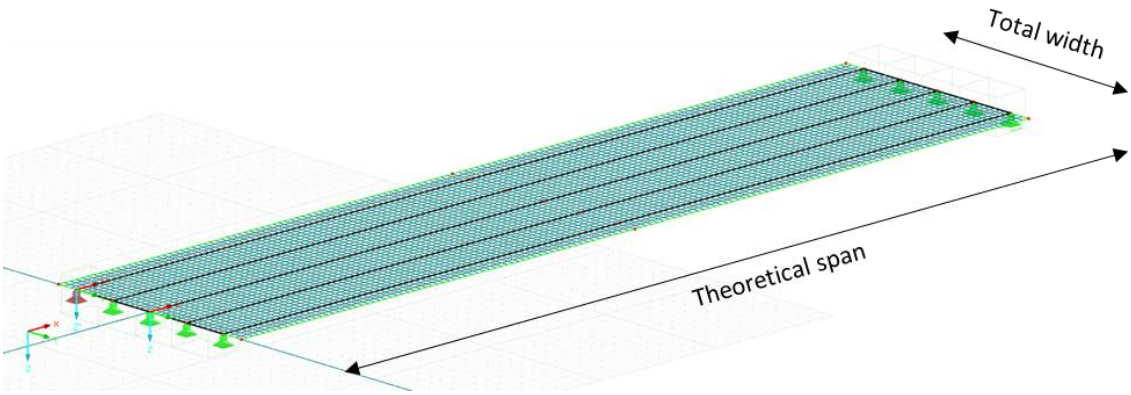


Figure 34 Finite element model of the bridge

5.2.2 Cross sections and materials

By assigning member types, cross sections and material parameters to the line segments, the beams and distribution element (surface) can be modelled.

Main beams

Cross section: Cross sectional dimensions are in accordance to those given in 2.2.1. To represent the cross section as closely as possible, a predefined RFEM cross section (thin-walled cross section – Type A) is used and modified. Subsequently the cross sections are assigned to the lines to create the members representing the prefab elements.

Member type: As member types the type 'beam' is selected. This means that a member is modelled that can transfer all internal forces. Connections with other beams are assumed to be rigid (i.e. bending resistant), which is of relevance for the cross beams.

Material parameters: UHPC is not one of the standard materials from the RFEM Material Library and therefore the properties have to be defined. To define a material in RFEM one has to define:

- Material constants: The material constants in RFEM are defined using main properties and additional properties, the latter is optional;

- Material model: In addition, a material model is to be selected (e.g. isotropic linear, orthotropic linear, plastic, etc.).

The following table gives an overview of the main properties as entered into the programme.

Table 12 Main material properties main beams

Modulus of elasticity (E)	50.000	[N/mm^2]
Shear modulus (G)	20.833	[N/mm^2]
Poisson ratio (v)	0,2	[-]
Specific weight (γ)	25	[kN/m^3]
Coefficient of thermal expansion (α)	1,2*10^{-5}	[K^{-1}]
Partial safety factor (γ_M)	1,0	[-]

Remarks:

- Specific weight and coefficient of thermal expansion: These parameters are important for self-weight function or for temperature loads. Loads are all entered manually but the parameters are nonetheless defined for the sake of completeness.

- Partial factor: In RFEM this factor is the safety factor for the material resistance and according to the manual it reduces the stiffness for calculation. If required, this will be accounted for manually, so this factor is set equal to 1,0.

In addition to the aforementioned main properties, RFEM gives the option to define multiple ''additional properties'', mainly strength and strain values to describe constitutive relations. This will be included in verifications in Excel and not in RFEM, as these parameters are not required for determining the force distribution these values are therefore kept equal to zero.

Material model: To complete the material description a material model has to be selected as well, of which 12 are available in the programme. For the analysis of the bridge 'isotropic linear elastic' material model is selected. This means that the linear elastic behaviour defined using the values in the table is independent from the directions. These material properties (denoted as ''material 1'' in RFEM) are subsequently assigned to cross section of the main beams.

End cross beams

Cross section: The cross section of the end cross beams is subsequently entered into the programme. The cross section is as described in 2.2.2 and rectangular of shape.

Member type: As the members are connected without any additional releases at the ends, these are rigidly connected, forming one beam. Subsequently the cross section and member type are assigned to the appropriate lines for model the cross beams.

Material parameters: For the conventional concrete, the concrete type C30/37 is selected. The material constants of this concrete type are readily available from the RFEM material library. As was done for the main beams again isotropic linear elastic material model is assumed, which is readily available from the material library. These material properties (denoted as ''Material 2'' in RFEM) are subsequently assigned to cross section 2.

Surface element

To take the beam interaction into consideration a ''distribution element'' is modelled: the surface element. Such an element is defined by assigning the geometry, stiffness parameters and material properties.

Geometry: A plane (i.e. flat) surface is modelled using the outer lines as its boundary. This corresponds with the outer dimensions of the top flange of the bridge.

Stiffness properties: As stiffness the option 'standard' is selected. This means that the plate is assumed to be of a homogeneous and isotropic material and transferring bending moments and membrane forces. The deck is prestressed in both longitudinal and transverse direction in the final situation, thus it is a valid assumption to assume that the concrete is uncracked in both directions. Therefore, this stiffness option is justified.

Material model: For the plate it is also assumed that it is made of UHPC (defined in RFEM as 'Material No. 1'), because it represents the distribution of forces due to the top flanges of the beams that are post-tensioned on site. In practice there is a small inaccuracy because the joints are made of a different UHPC mixture, but given the small dimensions of the joint this is neglected.

Thickness: For the thickness of the surface a constant thickness is assumed, equal to the mean value t_{ft} for the thickness of the top flange.

5.3 Load cases and load combinations

In the following sub sections a brief overview is given of the different load cases defined in the RFEM model, for more detailed elaboration on the modelling of the loads reference is made to annex V.

5.3.1 Permanent actions (G)

The following load cases are entered in RFEM to model the permanent actions:

- **Load case 1 – Self-weight prefab beams**: The self-weight of the beams is modelled as member loads over the full span of the main beams.

- **Load case 2 – Self-weight end cross beams**: The self-weight of the end cross beams is modelled as member loads over the full span of the end cross beams.

- **Load case 3 – Self weight longitudinal joints**: The joints are taken into consideration by placing free line loads on top of the surface, positioned on locations corresponding with the centre line of the joints.

- **Load case 4 – Road surface**: The road surface is modelled as a surface load acting over the entire surface of the deck.

- **Load case 5 – Kerbs**: The kerbs are modelled as two free rectangular loads acting on the surface of the deck.

- **Load case 6 – Railing**: To represent the railing a value for a line load was determined and when modelling this load it should be noted that in reality it acts eccentrically with respect to the beam axis. In the FEA model the railing can be modelled by replacing the eccentric line load by a centric line load and bending moment, both acting over the full beam length.

- **Load case 7 – Permanent loads**: For practical reasons all aforementioned loads have been combined into a single load case as well.

5.3.2 Variable loads (Q)

The following section gives an overview of the load cases entered into RFEM to model the variable loads. In order to model the variable loads of load group 1 (gr1a) the group is decomposed into sets of uniformly distributed loads and axle loads.

For the uniformly distributed loads there are three possible load cases corresponding to the three configurations of load model 1 as discussed in 4.2.3, the uniformly distributed load on the pedestrian lanes is already included in these load cases as well.

For the axle loads there are six possible load cases, because within each configuration of LM1 as discussed in 4.2.3 the axles can be positioned around mid-span (to achieve maximum bending moment) or near the supports (to achieve the maximum shear force).

The different load cases are as follows, for more detailed information reference is made to annex V.

- **Load Case 8 – gr1a configuration 1 – UDL**: The positioning of the uniformly distributed load corresponds to configuration 1 of load model 1, as discussed in 4.2.3. The loads on the pedestrian lanes have also been added while already including the combination value of 0,4 for load group gr1a. The forces are modelled as free rectangular loads acting on the surface.

- **Load Case 9 – gr1a configuration 2 – UDL**: The positioning of the uniformly distributed load corresponds to configuration 2 of load model 1, as discussed in 4.2.3. The loads on the pedestrian lanes have also been added while already including the combination value of 0,4 for load group gr1a. The forces are modelled as free rectangular loads acting on the surface.

- **Load Case 10 – gr1a configuration 3 – UDL**: The positioning of the uniformly distributed load corresponds to configuration 3 of load model 1, as discussed in 4.2.3. The loads on the pedestrian

lanes have also been added while already including the combination value of 0,4 for load group gr1a. The forces are modelled as free rectangular loads acting on the surface.

- **Load case 11 – gr1a configuration 1 – Axle – Moment**: In transverse direction the positioning of the concentrated loads corresponds to configuration 1 of load model 1, as discussed in 4.2.3. while in longitudinal direction the forces have been centred around mid-span to achieve the maximum bending moment. The forces are modelled as free concentrated loads acting on the surface.

- **Load case 12 – gr1a configuration 1 – Axle – Shear**: In transverse direction the positioning of the concentrated loads corresponds to configuration 1 of load model 1, as discussed in 4.2.3. while in longitudinal direction the forces have been placed near the supports with one axle directly above the end cross beam to achieve the maximum shear force. The forces are modelled as free concentrated loads acting on the surface.

- **Load case 13 – gr1a configuration 2 – Axle – Moment**: In transverse direction the positioning of the concentrated loads corresponds to configuration 2 of load model 1, as discussed in 4.2.3. while in longitudinal direction the forces have been centred around mid-span to achieve the maximum bending moment. The forces are modelled as free concentrated loads acting on the surface.

- **Load case 14 – gr1a configuration 2 – Axle – Shear**: In transverse direction the positioning of the concentrated loads corresponds to configuration 2 of load model 1, as discussed in 4.2.3. while in longitudinal direction the forces have been placed near the supports with one axle directly above the end cross beam to achieve the maximum shear force. The forces are modelled as free concentrated loads acting on the surface.

- **Load case 15 – gr1a configuration 3 – Axle – Moment**: In transverse direction the positioning of the concentrated loads corresponds to configuration 3 of load model 1, as discussed in 4.2.3. while in longitudinal direction the forces have been centred around mid-span to achieve the maximum bending moment. The forces are modelled as free concentrated loads acting on the surface.

- **Load case 16 – gr1a configuration 3 – Axle – Shear**: In transverse direction the positioning of the concentrated loads corresponds to configuration 3 of load model 1, as discussed in 4.2.3. while in longitudinal direction the forces have been placed near the supports with one axle directly above the end cross beam to achieve the maximum shear force. The forces are modelled as free concentrated loads acting on the surface.

- **Load case 17 – Variable load Railing**: To model the variable load acting on the railing the same approach is used as done for the self-weight of the railing. The vertical and horizontal component have to be considered separately, but given the lever arm and combination with other loads only the vertical component is considered because this gives the most unfavourable result.

5.3.3 Accidental loads (A)

Two accidental load cases are included in the model:

- **Load case 18 – Traffic accident – Moment**: In this load case a traffic accident is simulated that caused a heavy vehicle to be positioned directly at the edge of the bridge. The load values corresponding to load model 1 were used and the axle loads were positioned centred around mid-span to give the largest possible bending moment for the outer beam.

- **Load case 19 – Traffic accident – Shear**: For this load case the same input has been used as for load case 18, the only difference being the positioning of the concentrated loads. These have been placed close to the supports to obtain maximum shear force, with one axle placed directly at the centre of the edge beam.

For more detailed information reference is made to annex V. Note that given the magnitude of the load the accidental action resembling collision of vehicles with the kerbs on the bridge are not taken into consideration. The action resembling ship collision is also not included in RFEM, but will be considered during the verifications.

5.3.4 Fatigue loads

The force distribution for the fatigue verifications is also determined using RFEM, only the modelling of the loads and the results are covered in this chapter, for more information reference is made to chapter 8. To determine the force distribution required for the fatigue verification two additional load cases have been added to the model. One is for non-cyclic variable loads that do not cause stress cycles while one is for variable loads that do cause stress cycles.

- **Load case 20 – Fatigue – Non-cyclic**: The non-cyclic variable fatigue loads refer to the variable loads acting on the railing of the bridge (modelled as member loads, i.e. line loads and bending moments along the length of the outer main beams) and the load on the pedestrian lanes (modelled as a free rectangular load).

- **Load case 21 – Fatigue – Cyclic**: The load case for cyclic fatigue loads is composed of uniformly distributed loads (modelled as free rectangular loads) and axle loads (modelled as free concentrated loads) in accordance with fatigue load model 1. The positioning of the loads is the same as configuration 2 of load model 1, with the axle loads at midspan.

For the input parameters of the fatigue loads reference is made to annex V.

5.4 Performing the calculation

5.4.1 Calculation parameters

Using RFEM a geometrically linear analysis is performed, which means that equilibrium is determined based on the undeformed structure. Given the type of structure and the loads applied upon it this is an appropriate decision. Note that the material laws adopted in the model are also linear. Linear elastic means that stresses and strains are directly related through a linear relationship (Hooke's law), this resembles the situation where the structure does not crack. This situation corresponds to the serviceability limit state, in which cracking of the structure will not be allowed. This will be covered in subsequent chapters of this report, and to achieve this situation the tensile stresses in the element will be kept limited. For the 1D elements, i.e. the beams in the model, it is assumed in RFEM that the cross sections remain plane.

Before the calculation can be performed the surface has to be discretized into a finite element mesh. For the meshing the default values of the programme are used. Quadrangle 2D elements are used to mesh the surface, with a target length of 0,5 m for the finite elements. Given the plate thickness of 0,188 m and the total area of the surface this is deemed to be a good compromise between accuracy and computation time. Given the small thickness compared to the dimensions the surface is regarded as a thin plate, which is why Kirchhoff plate theory has been selected. For all parameters not discussed in this section the default settings of RFEM are used.

5.4.2 Combinations of actions and results for ULS - STR

Combinations of actions for ULS – STR

To obtain the governing values of the internal forces for the ULS verification of the main beams and end cross beams a total of fourteen load combinations have been formulated. The first twelve combinations comprise permanent loads (combined in load case 7), the different configurations of variable traffic loads (LM1 and LM4 combined as gr1a, covered in load cases 8-14).

These equations cover the permanent or transient design situations and are the fundamental combinations. One can distinguish combinations according to equation 6.10a and 6.10b from the Eurocode. Because the most unfavourable of the two has to be applied all combinations are formulated once using the factors according to equation 6.10a and once using the factors of equation 6.10b.

In addition, two combinations comprise the permanent loads and the accidental loads (load cases 18 and 19), because these are combinations of actions for accidental design situations the partial factors are different from those of the fundamental combinations. The following table summarizes the RFEM input for the formulation of the load combinations.

Table 13 Formulation of load combinations in RFEM for ULS - STR

	Load Combinations ULS – STR													
	CO1	CO2	CO3	CO4	CO5	CO6	CO7	CO8	CO9	CO10	CO11	CO12	CO13	CO14
LC7	1,40	1,25	1,40	1,25	1,40	1,25	1,40	1,25	1,40	1,25	1,40	1,25	1,00	1,00
LC8	1,20	1,50					1,20	1,50						
LC9			1,20	1,50					1,20	1,50				
LC10					1,20	1,50					1,20	1,50		
LC11	1,20	1,50												
LC12							1,20	1,50						
LC13			1,20	1,50										
LC14									1,20	1,50				
LC15					1,20	1,50								
LC16											1,20	1,50		
LC17	1,20	1,50	1,20	1,50	1,20	1,50	1,20	1,50	1,20	1,50	1,20	1,50		
LC18													1,00	
LC19														1,00

Results for ULS – STR

To determine the governing design values of the internal forces for the main beams and end cross beams a result combination (RC1) has been set up. This combination combines load combinations CO1 up to and including CO14 to obtain enveloping force distribution diagrams. This way the governing values can be determined in a practical way.

Main beams: Using this result combination the following governing design values were found for the global ULS verification of the main beams:

- Bending moment M_{Ed}: 48.426 kNm – This value is found at mid span of beam 3 for load combination CO3 (using equation 6.10a and configuration 2 of the variable loads, with the axle loads at midspan);

- Shear force V_{Ed}: 4090 kN – As a conservative assumption the maximum support reaction is taken as the design value of the shear force, this value is found at the support of beam 3 for load combination CO10 (using equation 6.10b and configuration 2 of the variable loads, with the axle loads near the supports);

- Torsional moment T_{Ed}: 1222 kNm – This value is found at beam 3 for load combination CO13 (traffic accident with the axle loads at midspan).

Note that for the torsional moment a higher value is found at beam 2, which is 1516 kNm. However, in the verification that will be discussed in chapter 6 the maximum shear force and maximum torsional moment will be combined (a conservative approach), in which case beam 3 is still governing over beam 2 because of the higher shear force (4090 kN of beam 3 versus 3291 kN of beam 2).

End cross beams: Using the result combination the following governing design values were found for the ULS verification of the end cross beams:

- Hogging bending moment $M_{Ed,hog}$: 1212 kNm – This value is found at the support of beam 1 for combination CO13 (traffic accident with axle loads at midspan);

- Sagging bending moment $M_{Ed,sag}$: 436 kNm – This value is found at the beam segment spanning between the supports of beams 3 and 4 for load combination CO8 (using equation 6.10b and configuration 1 of the variable loads with the axle loads near the supports);

- Shear force V_{Ed}: 837 kNm – This value is found at the support of beam 1 for load combination CO14 (traffic accident with axle loads near the supports).

Note: In denoting hogging and sagging bending moments absolute values have been used.

5.4.3 Combinations of actions and results for ULS – FAT

Combinations of actions for ULS – FAT

In accordance with the provisions from Eurocode 2 two combinations of actions are formulated, one for non-cyclic loads and one including both variable and cyclic loads.

Table 14 Formulation of load combinations in RFEM for ULS - FAT

	Load Combinations ULS – FAT	
	CO15	CO16
LC7	1,0	1,0
LC20	1,0	1,0
LC21		1,0

Results for ULS – FAT

For combination CO15 all five beams have an approximately equal bending moment at mid span, for beam 3 the value is 27.183 kNm. For combination CO16 the difference in bending moment at mid span is more pronounced and beam 3 is governing with a value of 31.539 kNm.

5.4.4 Combinations of actions and results for SLS – Characteristic combination

Combinations of actions for SLS – Characteristic combination

Characteristic combinations of actions in the serviceability limit state are formulated for the design of the main prestressing of the prefab beams and the prestressing of the end cross beams.

Prefab beams: For the design of the prefab beams the maximum bending moments due to superimposed permanent loads and variable loads are required. To determine the bending moment due to the superimposed permanent loads the following combination is formulated:

Table 15 Formulation of load combinations in RFEM for SLS - Characteristic combination (permanent loads)

	SLS – Characteristic combination – Permanent loads
	CO17
LC3	1,0
LC4	1,0
LC5	1,0
LC6	1,0

To determine the maximum bending moments due to the variable loads three combinations are formulated to combine the uniformly distributed loads of the three possible configurations of LM1 and the corresponding axle loads at mid span.

Table 16 Formulation of load combinations in RFEM for SLS - Characteristic combination (variable loads)

	SLS – Characteristic combination – Variable loads		
	CO19	CO20	CO21
LC8	1,0		
LC9		1,0	
LC10			1,0
LC11	1,0		
LC13		1,0	
LC15			1,0

End cross beams: As input for the design of the prestressing of the end cross beams characteristic combinations of actions have been formulated to determine the maximum hogging and sagging bending moments. Each combination includes the permanent loads and the variable loads, for each combination a different configuration of the variable loads is applied.

Table 17 Formulation of load combinations in RFEM for SLS - Characteristic combination (End beam)

	SLS – Characteristic combination – End beam					
	CO24	CO25	CO26	CO27	CO28	CO29
LC7	1,0	1,0	1,0	1,0	1,0	1,0
LC8	1,0			1,0		
LC9		1,0			1,0	
LC10			1,0			1,0
LC11	1,0					
LC12				1,0		
LC13		1,0				
LC14					1,0	
LC15			1,0			
LC16						1,0
LC17	1,0	1,0	1,0	1,0	1,0	1,0

Results for SLS – Characteristic combination

The governing values for the design of the prestressing of the main beam and end cross beam are as follows.

Main beams: The governing values are determined by looking at the relevant load cases, the point under consideration is mid span.

- Bending moment permanent loads in SLS at midspan $M_{E,G,perm}$: The bending moment at midspan of the three beams is approximately equal, the value of beam 3 is 1727 kNm;

- Bending moment variable loads in SLS at midspan $M_{E,Q}$: The highest value at mid span is found at beam 3 for configuration 2 of the variable loads and is 9694 kNm.

End cross beams: The governing values are determined using a result combination (Result combination 3) combining load cases CO24 up to and including CO29.

- Maximum hogging bending moment in SLS $M_{E,hog}$: 469 kNm – This value is found at the support of beam 3 for combination CO24 (configuration 1 of the variable loads with the axle loads at midspan);

- Maximum sagging bending moment in SLS $M_{E,sag}$: 298 kNm – This value is found in the field spanning the supports of beams 3 and 4 for combination CO27 (configuration 1 of the variable loads with the axle loads near the supports).

5.4.5 Combinations of actions and results for SLS – Frequent combination

Combinations of actions for SLS – Frequent combination

For the verification of the deflections of the bridge three combinations have been formulated combining the permanent loads and the different configurations of the variable load, each with the axle loads at midspan. In addition, the modulus of elasticity of the prefab beams has been reduced to account for long term effects, for all details regarding the verification of deflections reference is made to chapter 9. The combinations are as follows.

Table 18 Formulation of load combinations in RFEM for SLS - Frequent combination

	SLS – Frequent combination		
	CO21	CO22	CO23
LC7	1,0	1,0	1,0
LC8	0,8		
LC9		0,8	
LC10			0,8
LC11	0,8		
LC13		0,8	
LC15			0,8
LC17	0,4	0,4	0,4

Results for SLS – Frequent combination

Using a result combination (result combination 3) combining the load combinations CO21 up to and including CO23 the maximum deflection is determined. The maximum deflection δ_{max} is 344,4 mm, it is found at beam 3 for configuration 2 of the variable loads.

5.5 Validation of the model

In this paragraph the model is validated to confirm that the results used for further design are realistic. For this validation the following load cases from RFEM are compared with hand calculations:

- Self-weight prefab beams
- Permanent load due to surface layer
- UDL gr1a with lane 1 positioned on the middle beam (configuration 3)
- Corresponding concentrated loads at mid span, simulating the axle loads

5.5.1 Qualitative verification – Boundary conditions

The first part of the validation takes place by looking at the boundary conditions of the model. Because of the supports the displacements at the edges of the deck where the edge beams are positioned should be equal to zero while the maximum deformations are expected at mid span. The following figure gives the displacements due to the axle loads for example (load case LC15).

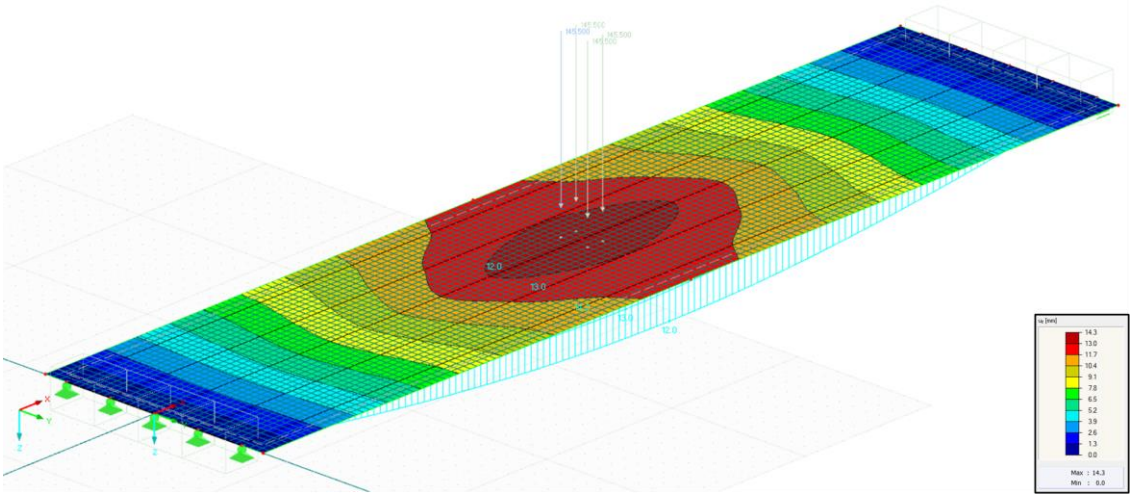


Figure 35 Deflections bridge deck due to axle loads at midspan

The results observed in the model are as to be expected. The boundary conditions are correct, i.e. the deformations at the supports are equal to zero while indeed the maximum displacement is found at midspan. The other load cases analysed confirm this impression. Based on the qualitative aspects considered the results from the model are deemed to be correct.

5.5.2 Quantitative verification – Internal forces

A brief quantitative verification is also performed by comparing the bending moments at mid span calculated using hand calculations and those calculated in the RFEM model for the four load cases mentioned previously. No partial load factors are applied.

Hand calculation

In the preliminary design a sensitivity analysis was carried out showing the importance of considering the interaction between the beams made possible by the surface (a ''distribution element''). A substantiated assumption for the interaction between the beams is essential to make a comparison with the results from RFEM.

In the sensitivity analysis it was found that when two limit cases were compared (case 1 being a surface element without transverse stiffness, which implies no interaction and thus no redistribution of loads between the beams and case 2 being an isotropic plate, meaning maximum redistribution of the beams) the bending moment at mid span in limit case 2 was only approximately 33% of the bending moment at mid span for case 1.

Because in this calculation the thickness of the surface compared to the total dimensions of the beams is lower than for the model in the sensitivity analysis, it is assumed that the observed redistribution will also be a bit lower. Therefore, it is assumed that approximately 50% of the variable loads is redistributed.

- First the contribution of the self-weight of the beam and the road surface to the bending moment at mid span is calculated:

$$M_G = \frac{1}{8} * \left(G_{k,beams} + b_{eff,i} * G_{k,surf}\right) * l^2$$

$$M_G = \frac{1}{8} * (41{,}59 + 3{,}29 * 0{,}23) * 68{,}0^2 = 24.476\ [kNm]$$

- The contribution of the uniformly distributed loads and axle loads to the bending moment at mid span are:

$$M_Q = \frac{1}{8} * \left(\alpha_{q1} q_{1k} * w + \left(b_{eff,1} - w\right) * \alpha_{rk} q_{rk}\right) * l^2 + \frac{1}{4} * 2 * \alpha_{Q1} Q_{1k} * l$$

$$M_Q = \frac{1}{8} * 50\% * (8{,}73 * 3{,}0 + (3{,}29 - 3{,}0) * 2{,}25) * 68{,}0^2 + \frac{1}{4} * 50\% * 2 * 291 * 68{,}0 = 12.705\ [kNm]$$

Total bending moment:

$$M_{tot} = M_G + M_Q = 24.476 + 12.705 = 37.181\ [kNm]$$

RFEM results

Using RFEM the following bending moments have been determined:

- Self-weight prefab beams (LC1): 23.997 kNm
- Self-weight road surface (LC4): 434 kNm
- Uniformly distributed load – configuration 3 (LC10): 5465 kNm
- Axle loads – configuration 3 (LC11): 2769 kNm

The total bending moment at mid span is 32.665 kNm.

Comparison & conclusion

The difference between the hand calculation and RFEM is approximately $((37.181 - 32.665)/32.665 * 100\%) \approx 14\%$. This is within the limits of what is acceptable when comparing a hand calculation and a FEM model, but the question remains if this difference can be explained.

The result if only the self-weight and asphalt layer are taken into consideration are almost identical, if the values are compared it turns out that the difference is negligible. That means that the difference has to be in the variable load, where the difference is indeed larger.

The total bending moment calculated using RFEM equals $5465 + 2769 = 8234$ kNm. That means that there is a difference of $(12.705 - 8234)/8234 * 100\% \approx 54\%$. This is a significant difference, which could be explained by the following two factors:

1. The hand calculation does not include all the same loads the RFEM model contains, the load case comprising the uniformly distributed loads also contains the variable loads on the pedestrian lanes;

2. The distribution of the loads by the surface is perhaps underestimated and could be higher than the assumed 50%.

This latter cause is expected to have the largest influence because the effects of the loads on the outermost beams should be limited to the innermost beam. In addition, this contribution is relatively easy to verify. If only the axle loads at midspan without reduction are assessed, then the bending moment is:

$$M_Q = \frac{1}{4} * 100\% * 2 * 291 * 68{,}0 = 9894\ [kNm]$$

The RFEM model gives a bending moment of 2769 kNm. That means that the reduction due to accounting for the force redistribution is: $(2769 - 9894)/9894 * 100\% \approx -70\%$. That means that only 30% remains at the beam itself, which is close to the value initially found in the sensitivity analysis as part of the preliminary design. If this value is plugged into the hand calculation to determine the bending moments due to the variable loads:

$$M_Q = \frac{1}{8} * 30\% * (8{,}73 * 3{,}0 + (3{,}29 - 3{,}0) * 2{,}25) * 68{,}0^2 + \frac{1}{4} * 30\% * 2 * 291 * 68{,}0 = 7622\ [kNm]$$

This value is closer to the value found using RFEM, which is a total bending moment of 8234 kNm (5465 kNm due to the UDL and 2769 kNm due to the axle loads). The differences between the hand calculation

and RFEM results are herewith explained, the redistribution of the forces in the deck due to the surface element is in the same order of magnitude as found during the elaboration of the sensitivity analysis. Therefore, the RFEM model is considered to be modelled correctly and produce results in the right order of magnitude.

5.6 Bibliography chapter five

Dlubal Software. (2019, December). User Manual RFEM 5. *Spatial Models Calculated According to Finite Element Method*.

Esposito, R., Hendriks, M. A., & Rots, J. G. (2019). Lecture notes CIE5148 - Computational Modelling of Structures.

Groupe de travail BFUP. (2013, June). Ultra High Performance Fibre-Reinforced Concretes. *Recommendations*. Association Francaise de Génie Civil.

6

DESIGN OF MAIN BEAMS – MAIN PRESTRESSING AND ULS (STR)

6.1 Design approach

6.1.1 Design of main prestressing and global design verifications

To complete and verify the design of the bridge one can distinguish different calculations and verifications, the following figure gives an overview of the calculations and verifications of the main beams that have been identified and will be performed in the following chapters of the report.

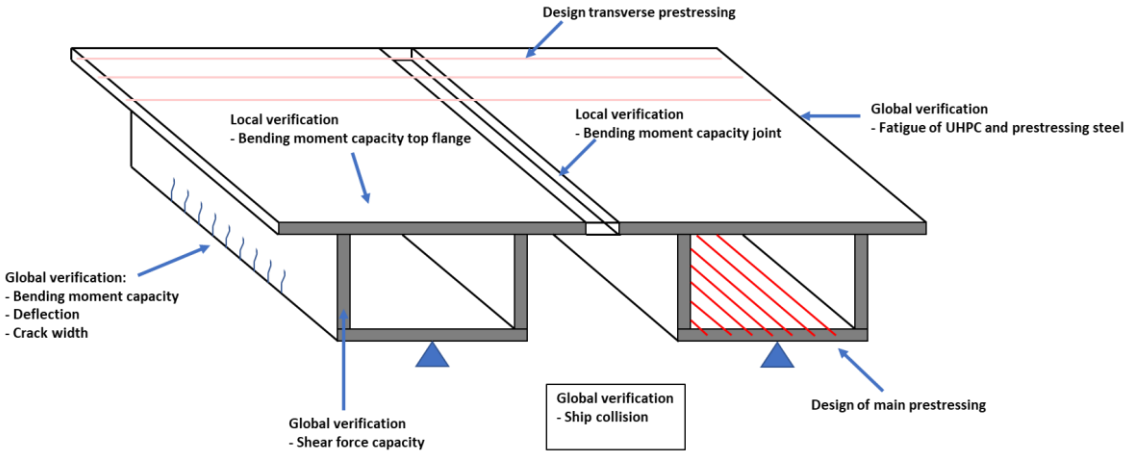


Figure 36 Calculations and design verifications of the main beams

This chapter starts with general provisions from the AFGC-SETRA 2013 guideline and the design of the main prestressing of the beam after which the global design verifications (bending moment capacity, shear force capacity and torsional capacity) will be covered. In addition, detailing aspects related to the design of the main prestressing and the global verification of the accidental situation of ship collision are also discussed. If topics have not been covered before in previous stages of the project provisions from codes and other sources will be discussed first to provide the background information required for further elaboration of those particular topics. All required material and geometrical parameters can be found in chapter 2 while the required input from RFEM is given in chapter 5.

6.1.2 General principles AFGC-SETRA 2013 guideline

The section of the AFGC-SETRA 2013 regarding design verifications starts with a number of general considerations that have to be taken into consideration. A number of these are already covered implicitly in previous chapters of this report: The fibre distribution is taken into consideration by adopting values for the orientation factors. The partial factor γ_{cf} is applied if required and the notion of characteristic length (used to go from constitutive stress-crack width laws to stress-strain laws) are included in the calculation procedures wherever relevant.

Additionally, the minimum ductility condition and non-brittleness requirement have to be taken into consideration. Because these have not been covered before this is included in this section of the report.

Minimum ductility condition

The guideline prescribes that for strain softening or low strain hardening material it has to be verified that sufficient ductility in bending is provided, which is done using the ductility requirement:

$$\frac{1}{w_{lim}} \int_0^{w_{lim}} \frac{\sigma(w)}{K_{global}} dw \geq \max(0{,}4 * f_{ctm,el}; 3\ MPa)$$

Where:
w_{lim}: Crack width that can be chosen equal to 0,3 mm
$f_{ctm,el}$: Mean limit of elasticity in tension
$\sigma(w)$: Characteristic post-cracking stress

For elements showing strain hardening behaviour this does not have to be verified. Ductal FM is known to show strain hardening behaviour, which is also assumed as one of its properties. It therefore may be achieved that this will be achieved in practice.

However, for the sake of completeness, this ductility criterion is analysed once using the parameters from the tables in 2.3.1. The crack width limit $w_{lim} = 0{,}30$ mm. By taking the characteristic post cracking stress equal to the maximum value $\sigma(w) = f_{ctfk} = 10{,}0$ N/mm^2 and $K_{global} = 1{,}25$. No elastic mean limit is specified, but according to (Fehling, Schmidt, Walraven, Leutbecher, & Fröhlich, 2014) this value can be estimated using:

$$f_{ctm} = 0{,}3 * f_{ck}^{\frac{2}{3}} \rightarrow 0{,}3 * 200^{\frac{2}{3}} \approx 10\ [N/mm^2]$$

Hence it has to be verified that:

$$\frac{1}{0{,}3} * \int_0^{0{,}3} \frac{10{,}0}{1{,}25} dw \geq \max(0{,}4 * 10; 3\ MPa) \rightarrow \frac{1}{0{,}3} * \frac{10{,}0}{1{,}25} * (0{,}3 - 0) \geq 4{,}0 \rightarrow 8{,}0 > 4{,}0$$

The criterion is therefore satisfied.

Non-brittleness condition

In addition, the non-brittleness condition has to be verified, which prescribes that the ULS loads are higher than the loads resulting in cracking. In practical terms for bending this means that the elastic bending moment in the uncracked section is smaller than the ultimate bending moment capacity. In later sections of this report, it will be demonstrated that this is indeed the case, which means this condition is satisfied.

6.2 Design of the main prestressing

6.2.1 General provisions prestressing – Eurocode 2

Before any design verifications are performed the main prestressing of the beams is designed. Contrarily to the preliminary design stage the prestress losses will be calculated, which is why this paragraph starts with a discussion of provisions from Eurocode 2 regarding prestressing.

Prestressing forces during prestressing

Prestressing is covered in 5.10 of Eurocode 2. In section 5.10.2 two limitations are given regarding the force that can be applied during the prestressing operation.

Maximum prestressing force (5.10.2.1): During the prestressing operation there is a maximum value for the force P_{max} that is allowed to be applied onto the prestressing element, this value is limited to (values k_1 and k_2 follow from the national annex):

$$P_{max} = A_p * \sigma_{p,max}$$

$\sigma_{p,max} = \min\{k_1 * f_{pk}; k_2 * f_{p0,1k}\} \rightarrow \min\{0{,}8 * 1860 = 1488; 0{,}9 * 0{,}9 * 1860 = 1507\} = 1488$

Where:
P_{max}: Force acting on the active end of the prestressing element during the prestressing operation
A_p: Cross section of the prestressing element
$\sigma_{p,max}$: Maximum stress acting on the prestressing element

Maximum compressive concrete stress (5.10.2.2): In addition to the previous point, a maximum concrete compressive stress (caused by prestressing and other forces acting during this stage) is also defined that should not be exceeded during the prestressing operation releasing the force:

$\sigma_c \leq 0{,}7 * f_{ck}(t)$

Where:
$f_{ck}(t)$: The characteristic compressive strength of the concrete at moment t at which it is prestressed

Note that for post tensioned steel the maximum value is 0,6 but for pretensioned steel the national annex allows the value of k_6 to be increased to 0,7. In addition, a minimum concrete strength is also given that has to be reached before the prestressing can be applied (this is 50% of the required strength for full prestressing as given in the certificate of the prestressing system).

Prestressing force

During the service life of the structure the value of the prestressing force is not constant, different values should be used at different moments in time. This is discussed in section 5.10.3.

Prestressing force: Suppose that at a location at distance x from the active end of the prestressing element is analysed at any given moment of time t. The mean prestressing force at this point, $P_{m,t}(x)$, is:

$P_{m,t}(x) = P_{max} - \Delta P_i - \Delta P_{c+s+r}$

Where:
$P_{m,t}(x)$: Mean prestress force at time t and position x
P_{max}: Maximum prestressing force acting at the active end
ΔP_i: Direct prestress losses
ΔP_{c+s+r}: Time dependent losses

Initial prestress force: The initial prestress force at $t = 0$, $P_{m0}(x)$, is the prestressing force applied to the concrete immediately after stressing and anchoring (post tensioned steel) or transferring the prestressing onto the concrete via bond (pretensioned steel). It equals the maximum value of the prestressing force minus the direct prestressing losses:

$P_{m0}(x) = P_{max} - \Delta P_i(x)$

This value is limited to (values for k_7 and k_8 are according to the national annex):

$P_{m0}(x) = A_p * \sigma_{pm0}(x)$

$\sigma_{pm0}(x) = \min\{k_7 * f_{pk}; k_8 * f_{p0,1k}\} \rightarrow \min\{0{,}75 * 1860 = 1395; 0{,}85 * 0{,}9 * 1860 = 1423\} = 1395$

Where:
$P_{m0}(x)$: Initial prestress force
P_{max}: Maximum prestress force acting at the active end
$\Delta P_i(x)$: Initial losses
$\sigma_{pm0}(x)$: Initial prestressing stress (stress immediately after transfer of the prestressing onto the concrete)

Remark: Note that $P_{m0}(x)$, $\Delta P_i(x)$ and $\sigma_{pm0}(x)$ are given as functions of the coordinate 'x'. This implies that the values are not constant over the length of the element.

Prestress losses

Due to various losses the maximum prestressing force that was applied is reduced over time:

- At the moment the prestressing force is transferred onto the concrete the direct losses take place and P_{max} is reduced to the initial prestressing force $P_{m0}(x)$;
- As time passes the time dependent losses occur and the initial prestressing force $P_{m0}(x)$ is further reduced to the mean value of the prestressing force at $t > 0$, denoted as $P_{m,t}(x)$;
- If $t \to \infty$ the maximum value of the time dependent losses is reached, the remaining prestressing force is the working prestressing force $P_{m,\infty}$.

An overview of the different values of the prestressing force as well as stress limitations is given in the following figure.

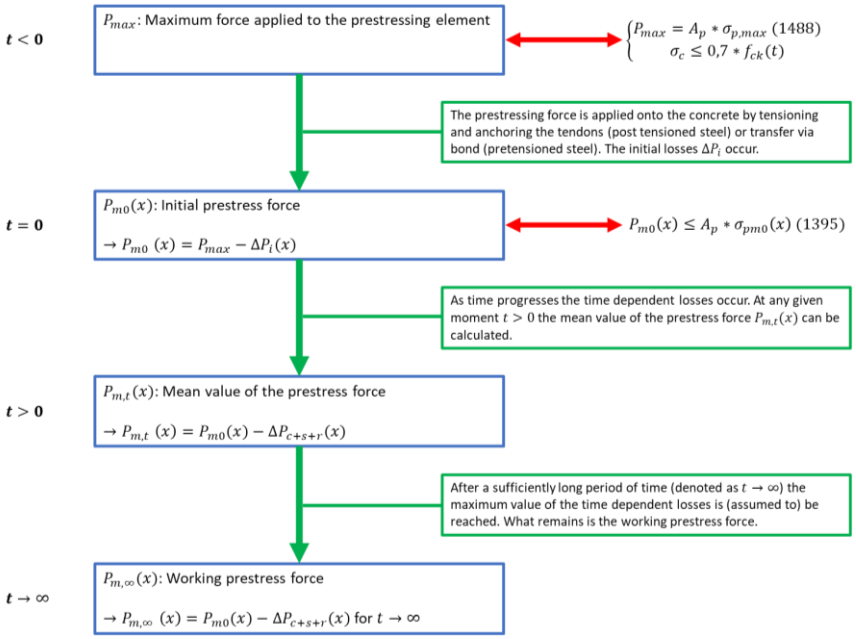


Figure 37 Different values of prestressing force

The type of prestressing losses that occur depend on the prestressing method. For the design calculation using pretensioned steel the following losses are of relevance:

- Direct losses ΔP_i (acting at $t = 0$)
  - Elastic shortening of the concrete ΔP_{el}
- Time dependent losses ΔP_{c+s+r} (acting at $t > 0$)
  - Creep of the concrete ΔP_c
  - Shrinkage of the concrete ΔP_s
  - Relaxation of the prestressing steel ΔP_r

For post tensioned steel two additional direct losses occur, namely friction and wedge set. The latter also occurs in the case of pretensioned steel, but this is considered during the detailing.

Direct losses

Provisions from the code: Direct losses of pretensioned steel are covered in 5.10.4. The loss due to elastic shortening of the concrete during the transfer of the prestressing forces onto the element has to be included in the calculation, but no explicit equations are given in the code.

Information on calculating the losses can be found in sources such as (Walraven & Braam, 2019). When the prestressing force is transferred from the pretensioned steel to the concrete, the concrete element shortens. As a result, the tendon shortens as well, causing the prestress loss and the steel stress is reduced from σ_{pmax} to σ_{pm0}. The principle is given in the following figure.

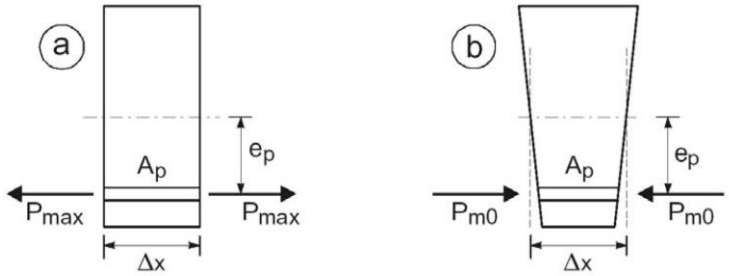


Figure 38 Situation before (left) and after (right) loading the concrete - (Walraven & Braam, 2019), p.4-13

From calculating the shortening of the concrete at steel level, Δl_c, and the shortening of the steel, Δl_p, and requiring that these are equal, $\Delta l_c = \Delta l_p$, it can be derived that the prestress loss is:

$$\Delta P_{el} = \frac{\alpha_e \rho_p f}{1 + \alpha_e \rho_p f} * P_{max}$$ Equation (9)

Where:

$$\alpha_e = \frac{E_p}{E_c}$$

$$\rho_p = \frac{A_p}{A_c}$$

$$f = \left(1 + \frac{A_c e_p^2}{I_c}\right)$$

e_p: Eccentricity of the tendons

Time dependent losses

Equation for time dependent losses: For both pretensioned and post tensioned steel the time dependent losses are given in 5.10.6., the code gives a simplified approach to determine the time dependent losses under permanent load at location x:

$$\Delta P_{c+s+r} = A_p * \Delta\sigma_{p,c+s+r} = A_p * \frac{\varepsilon_{cs} E_p + 0{,}8\Delta\sigma_{pr} + \frac{E_p}{E_{cm}}\varphi(t,t_0)\sigma_{c,QP}}{1 + \frac{E_p}{E_{cm}}\frac{A_p}{A_c}\left(1 + \frac{A_c}{I_c} z_{cp}^2\right)[1 + 0{,}8 * \varphi(t,t_0)]}$$ Equation (10)

Where:
$\Delta\sigma_{p,c+s+r}$: The time dependent prestress loss in the prestressing elements at point x and time t
ε_{cs}: Shrinkage strain (absolute value)
E_p: Modulus of elasticity of the prestressing steel
E_{cm}: Modulus of elasticity of the concrete

$\Delta\sigma_{pr}$: Stress variation in the tendon at location x and time t due to relaxation, determined at stress $\sigma_p = \sigma_p(G + P_{m0} + \psi_2 Q)$, which is the initial stress in the prestressing element due to initial prestressing and quasi-permanent loads
$\varphi(t, t_0)$: Creep coefficient at time t and load application time t_0
$\sigma_{c,QP}$: Stress in the concrete adjacent to the prestressing element due to self-weight, initial prestress and other quasi-permanent actions where relevant
A_p: Area of the prestressing tendons at location x
A_c: Cross sectional area of the concrete
I_c: Second moment of area of the concrete cross section
z_{cp}: The distance between the centre of gravity of cross section of the concrete and the tendons

If the equation is studied more closely one can distinguish the contributions of creep and shrinkage of the concrete and relaxation of the prestressing steel. The positioning of the prestressing elements is also included:

- In the numerator from left to right terms for shrinkage of the concrete, relaxation of the prestressing steel and creep of the concrete can be distinguished. Note that the term for relaxation is multiplied with a factor 0,8 to account for the interaction between the relaxation of the prestressing steel and the creep and shrinkage of the concrete;

- The equation for the relaxation uses the stresses in the prestressing steel after applying the prestressing (initial prestressing stress) while creep and shrinkage reduce the stresses over time. As a result, the shrinkage losses are reduced as well, which is accounted for by using this factor;

- The denominator accounts for two effects. The first effect is that the prestressing steel tries to restrain the deformation of the concrete. As a result, the concrete does not deform freely under the time dependent effects. The term z_{cp} accounts for possible eccentricity of the prestressing elements within the cross section. If the prestressing elements are positioned centrically the denominator can be rewritten into a simplified expression;

- The rightmost term accounts for the second effect, which is the influence of the time dependent deformation and age on the modulus of elasticity of the concrete and the load history. The creep factor is used to reduce the modulus of elasticity. In addition, the creep factor is multiplied with a correction factor of 0,8. Using this equation only one creep function is used on the summation of all load increments (i.e. the total load) for the global analysis while in reality each load increment would follow its own creep curve. This is corrected for by using this factor.

For bonded elements equation (10) is valid if the local values for the stresses are used. That means that if the prestress losses are to be calculated at a specific point $x = x_1$, then the prestressing stresses and losses should be calculated on that specific point.

Increase relaxation due to temperature: Increasing temperature during the hardening of the concrete affects the relaxation loss of pretensioned steel, this is covered in 10.3.2.1 of Eurocode 2-1-1. This is taken into consideration by adding up an equivalent time 't_{eq}' to the time 't' in the equations for the relaxation loss, which is calculated as follows:

$$t_{eq} = \frac{1{,}14^{T_{max}-20}}{T_{max}-20} * \sum_{i=1}^{n} (T_{(\Delta t_i)} - 20)\Delta t_i \qquad \text{Equation (11)}$$

Where:
t_{eq}: Equivalent time [in hours]
$T_{(\Delta t_i)}$: Temperature during time interval Δt_i
T_{max}: Maximum temperature during the heat treatment

6.2.2 Positioning and assumed number of strands

The principles regarding the design of prestressing in accordance with the code have now been covered and the actual prestressing can be designed. The main beams are prestressed using pretensioned steel, strands are applied both centrically and eccentrically, this is depicted in the following figure. The parameters of the prestressing are given in 2.3.4.

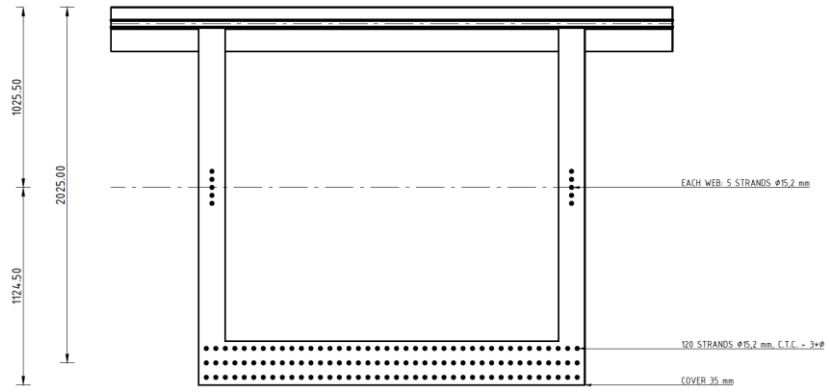


Figure 39 Positioning of the pretensioned strands in the prefab beams

The centric prestressing strands are collectively referred to using the subscript 'n' while the eccentric strands are collectively referred to using the subscript 'fb'. Important assumptions are that:

- Strands in the web are positioned as such that the centre of gravity of the strand group coincides with the centre of gravity of the cross section;

- The strands in the bottom flange are positioned as such that the centre of gravity of the strand group coincides with the centre of gravity of the bottom flange, the eccentricity between this strand group and the centre of gravity of the cross section is:

$$e_p = e_b - \frac{1}{2} * t_{fb}$$ Equation (12)

6.2.3 Calculating prestress losses

With the aforementioned assumptions the prestressing losses are calculated. The calculation is performed for the mid-span position of the bridge because this is the point where the maximum bending moments occur. For the full elaboration of the calculation reference is made to annexes III (Excelsheet with the calculation) and IV (overview of all equations), the most relevant points of the calculation are highlighted in the remainder of this subparagraph.

Applied maximum force onto prestressing element and stress verification

The provided maximum prestressing forces by the centric and eccentric group of strands have to be compared to the maximum value. In addition, it should be verified that during the transfer of the prestressing force onto the concrete the maximum allowed concrete compressive stress caused by the prestressing and other relevant forces is not exceeded. Forces to consider are the prestressing and the self-weight, which is activated when applying the prestressing because the beam bends upwards.

The cross section to consider is the end of the beam, because the self-weight does not compensate the prestressing there, hence the highest compressive stress is found at the bottom fibre at this point. Because heat treatment will be applied it is assumed that the full 28-day strength of the concrete is reached at the moment the strands are released. It has thus to be verified that:

$$\sigma_c = \frac{P_{max,c}}{A_c} + \frac{P_{max,fb}}{A_c} + \frac{P_{max,fb} * e_p}{W_b} \leq 0{,}7 * f_{ck}$$

Direct losses

For the calculation of the direction losses, it has to be remembered that the different strand groups have different values for the eccentricity. By definition the centric strand group has an eccentricity of zero with respect to the centre of gravity of the cross section. That means that $e_{p,c} = 0$ and $f_c = 1$ and equation (9) can be rewritten to:

$$\Delta P_{el,c} = \frac{\alpha_e \rho_p}{1 + \alpha_e \rho_p} * P_{max,c}$$

Where:

$$\alpha_e = \frac{E_p}{E_c}, \rho_{p,c} = \frac{A_{p,c}}{A_c}$$

For the eccentric prestressing applying equation (9) leads to:

$$\Delta P_{el,fb} = \frac{\alpha_e \rho_p f_{fb}}{1 + \alpha_e \rho_p f_{fb}} * P_{max,fb}$$

Where:

$$\rho_{p,fb} = \frac{A_{p,fb}}{A_c}$$

Determining initial prestressing force and stress verification

Using the values of the direct losses the initial prestressing can be calculated, for the centric and eccentric prestressing this value is respectively:

$$P_{m0,c} = P_{max,c} - \Delta P_{el,c}$$

$$P_{m0,fb} = P_{max,fb} - \Delta P_{el,fb}$$

Using these values, it is subsequently verified that the maximum allowable value σ_{pm0} is not exceeded.

Time dependent losses

The time dependent losses are calculated for $t \to \infty$, in other words: their maximum value is determined. The losses are calculated separately for the centric and eccentric prestressing, but one aspect that both groups have in common is that the effects of applying heat treatment have to be taken into consideration.

Effect of heat treatment: The effect of heat treatment is included in two ways. First of all, a suitable value for the creep factor and shrinkage value have been chosen, these values include the effect of heat treatment on the creep and shrinkage of UHPC, see 2.3.1. The second way is by considering the effect on relaxation by calculating the equivalent time following equation (11). This equivalent time is subsequently included in the calculation of the relaxation losses.

One interval is taken into consideration for the heat treatment, during which the elements are heated up to approximately 90 °C for a period of 48 hours. Hence $\Delta t_1 = 48$ h, $T_{(\Delta t_1)} = 90$ °C and $T_{max} = 90$ °C, and this results in:

$$t_{eq} = \frac{1{,}14^{90-20}}{90 - 20} * (90 - 20) * 48 = 461.935\ h$$

Calculating time dependent loss: The basic equation for the time dependent loss as given in Eurocode 2-1-1 is given in equation (10). For the centric prestressing this equation can be simplified because the eccentricity equals zero. For the centric and eccentric prestressing, the total time dependent losses can therefore be calculated using the following equations:

$$\Delta P_{c+s+r,c} = A_{p,c} * \Delta\sigma_{p,c+s+r,c} = A_{p,c} * \frac{\varepsilon_{cs}E_p + 0{,}8\Delta\sigma_{pr,c} + \frac{E_p}{E_{cm}}\varphi(\infty,t_0)\sigma_{c,QP,c}}{1 + \frac{E_p}{E_{cm}}\frac{A_{p,c}}{A_c}[1 + 0{,}8 * \varphi(\infty,t_0)]}$$

$$\Delta P_{c+s+r,fb} = A_{p,fb} * \Delta\sigma_{p,c+s+r,fb} = A_{p,fb} * \frac{\varepsilon_{cs}E_p + 0{,}8\Delta\sigma_{pr,fb} + \frac{E_p}{E_{cm}}\varphi(\infty,t_0)\sigma_{c,QP,fb}}{1 + \frac{E_p}{E_{cm}}\frac{A_{p,fb}}{A_c}\left(1 + \frac{A_c}{I_c}z_{cp}^2\right)[1 + 0{,}8 * \varphi(\infty,t_0)]}$$

The required values for shrinkage and creep have already been defined in section 2.3.1. For the prestressing steel of both strand groups relaxation class 2 is assumed, which implies low relaxation. The following basic equation is used to calculate the relaxation loss, it can be applied to the centric and eccentric strands by plugging in the relevant numerical values:

$$\frac{\Delta\sigma_{pr}}{\sigma_{pi}} = 0{,}66 * \rho_{1000} * e^{9{,}1\mu} * \left(\frac{t}{1000}\right)^{0{,}75(1-\mu)} * 10^{-5}$$

In this equation σ_{pi} is the initial prestressing stress $\sigma_{pm,0}$ and the factor $\mu = \sigma_{pm,0}/f_{pk}$. The parameter '$t$' includes the equivalent time and is calculated as follows:

$$t = 500.000 + t_{eq}$$

To determine the losses due to creep the stress in the concrete adjacent to the centric and eccentric strands has to be calculated. Following the code this stress involves actions that could contribute to creep losses, such as self-weight, initial prestressing and possibly other quasi-permanent actions.

For the centric strands the only contributing forces are the axially acting prestressing forces due to the centric and eccentric prestressing (note that compression is positive):

$$\sigma_{c,QP,c} = \frac{P_{m0,c}}{A_c} + \frac{P_{m0,fb}}{A_c}$$

For the eccentric strands other loads have to be included as well, because the time dependent losses are calculated for $t \to \infty$ the self-weight, permanent loads and prestressing are included. The stress at the centre of the bottom flange is calculated as follows (note that in this equation compression is positive):

$$\sigma_{c,QP,fb} = \frac{P_{m0,c}}{A_c} + \frac{P_{m0,fb}}{A_c} + \frac{P_{m0,fb} * e_p * z_{cp}}{I_c} - \frac{M_{G,sw} * z_{cp}}{I_c} - \frac{M_{G,perm} * z_{cp}}{I_c}$$

$$M_{G,sw} = \frac{1}{8} * G_{k,beams} * l^2$$

Where:
$M_{G,sw}$: Bending moment at mid span due to self-weight of the prefab beams only
$M_{G,perm}$: Bending moment at mid span due to all other permanent loads (determined using RFEM)

Note that although a contribution of the traffic load ($\psi_2 * Q$) could be included to obtain the quasi-permanent load combination this is not used because: the contribution would be relatively small given the combination factor ψ_2, because the generally has a relatively local effect and because traffic is present only for relatively short time.

Working prestress force

The working prestressing force can now be calculated at mid span. The values for the initial and working prestressing will be used in the subsequent phases of the design of the main beams. The following table gives an overview of the results.

Table 19 Summary of results calculating prestressing forces and losses

	Prestressing forces			Prestress losses forces			
	P_{max}	P_{m0}	$P_{m,\infty}$	ΔP_i	ΔP_{c+s+r}	ΔP_{tot}	$\Delta P_{\%}$
Prestressing:	[kN]	[kN]	[kN]	[kN]	[kN]	[kN]	[%]
Centric	1946	1940	1615	6	325	331	17,0
Eccentric	24.360	22.269	18.581	2091	3688	5779	23,7

6.2.4 Determining stresses and required prestressing force at midspan

In the previous subparagraph the prestressing forces were calculated based on the assumed number of strands. As will be covered in more detail in chapter 9, the tensile stresses at the governing cross section have to be kept to a certain maximum value in the serviceability limit state. In this subsection it will be verified if the prestressing forces are sufficient to achieve this.

The cross section under consideration is mid span, bending moments due to permanent and variable loads achieve their maximum here, making it the governing cross section. The verification is performed by considering to ''limit cases'' that occur at different moments of time:

- Situation 1: Self-weight and prestressing only (at $t = 0$)
- Situation 2: Use phase (at $t \to \infty$)

These are the two most unfavourable situations that can occur during all stages of the service life of the bridge, and therefore satisfying the tensile stress criterion in these two cases covers all other possible situations that may occur during the service life of the bridge. For both situations the stresses in the outer fibres are determined.

Self-weight and prestressing only ($t = 0$): This limit case covers all situations where only the self-weight and prestressing force are present, for example:

- The beam just after demoulding in the factory;
- Storing the beam at the storage site;
- Hoisting the beam into position;
- The beam in the final position without other permanent loads being present.

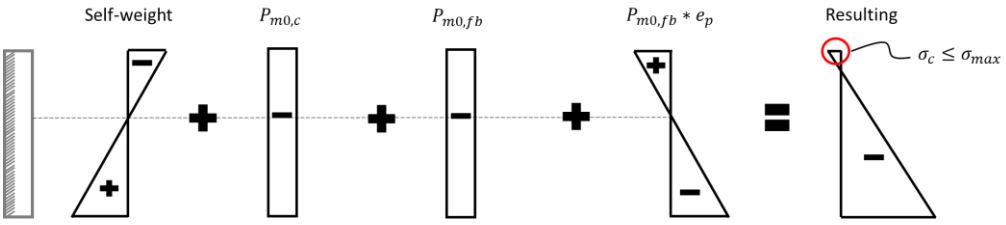


Figure 40 Stresses over the height of the cross section - Situation 1

By applying the prestressing value at $t = 0$ the most unfavourable situation is obtained because the largest prestressing acting prestressing forces (P_{m0}) causing compression and upward bending is combined with the smallest value of the permanent loads (only the self-weight of the beam) causing downward bending, which is why it is expected that the top fibre will be governing. The stresses in the top and bottom fibre are as follows:

$$\sigma_{c,t} = -\frac{M_{G,sw}}{W_t} - \frac{P_{m0,c}}{A_c} - \frac{P_{m0,fb}}{A_c} + \frac{P_{m0,fb} * e_p}{W_t} \leq \sigma_{max} \qquad \text{Equation (13)}$$

$$\sigma_{c,b} = +\frac{M_{G,sw}}{W_b} - \frac{P_{m0,c}}{A_c} - \frac{P_{m0,fb}}{A_c} - \frac{P_{m0} * e_p}{W_b} \leq \sigma_{max} \qquad \text{Equation (14)}$$

Use phase ($t \rightarrow \infty$): The second limit case covers the situation where the bridge has been in service for a long time (denoted as $t \rightarrow \infty$), the prestressing force is reduced to the working prestress $P_{m,\infty}$ which is combined with a fully loaded bridge.

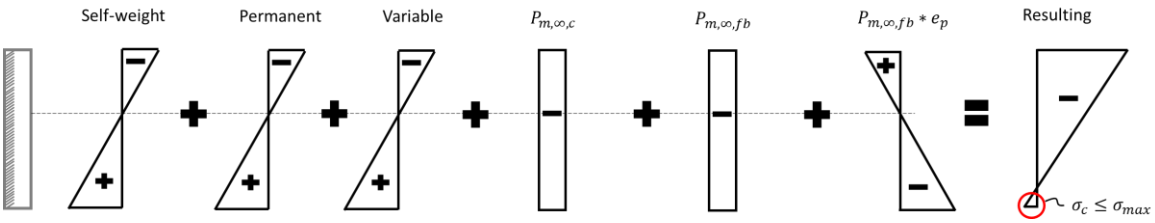


Figure 41 Stresses over the height of the cross section - Situation 2

The prestressing force causes compression and upward bending, because the working prestressing force is applied this gives the smallest possible prestressing force. This is combined with the highest possible downward bending by the summation of self-weight, permanent loads and variable loads, which is why it is expected that the bottom fibre will be governing. The stresses at the top and bottom fibre are as follows:

$$\sigma_{c,t} = -\frac{M_{G,sw}}{W_t} - \frac{M_{G,perm}}{W_t} - \frac{M_Q}{W_t} - \frac{P_{m,\infty,c}}{A_c} - \frac{P_{m,\infty,fb}}{A_c} + \frac{P_{m,\infty,fb} * e_p}{W_t} \leq \sigma_{max} \qquad \text{Equation (15)}$$

$$\sigma_{c,b} = +\frac{M_{G,sw}}{W_b} + \frac{M_{G,perm}}{W_t} + \frac{M_Q}{W_b} - \frac{P_{m,\infty,c}}{A_c} - \frac{P_{m,\infty,fb}}{A_c} - \frac{P_{m,\infty,fb} * e_p}{W_b} \leq \sigma_{max} \qquad \text{Equation (16)}$$

Stress verification: Using equations (13) to (16) the stresses in the outer fibres are calculated and the largest stress values of both situations at the top and bottom are the governing values. Graphs showing the stresses due to permanent loads, variable loads and the total stresses for both situations are given below.

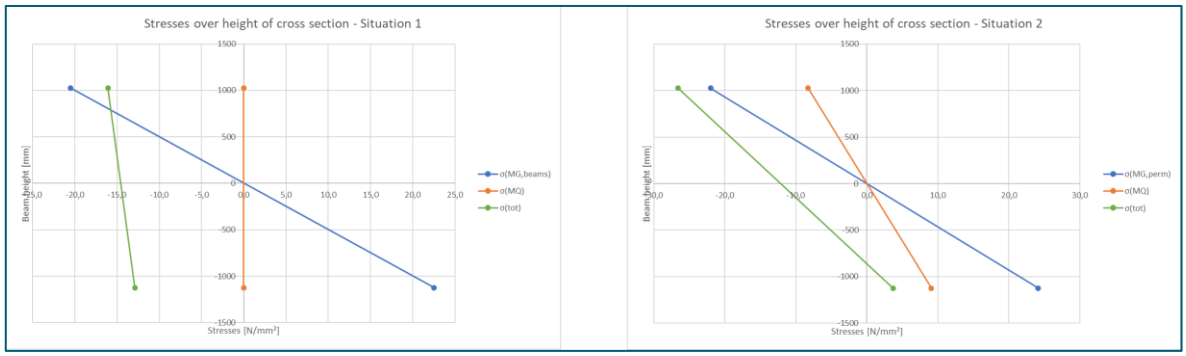


Figure 42 Calculated stresses over the beam height

The only situation where a resulting tensile stress is found is for the section situation (use phase) and the tensile stress has a value of 3,7 N/mm^2. According to the provisions of the AFGC-SETRA 2013 guideline the maximum tensile stress should be limited to a value of:

$$\sigma_{max} = \frac{2}{3} * \min\left\{f_{ctm,el}; \frac{f_{ctfm}}{K}\right\} \qquad \text{Equation (17)}$$

This results in a value of 6,7 N/mm^2, which means that the provided prestressing is sufficient to meet this criterion. Reference is made to chapter 9 for a more elaborate explanation on how this maximum tensile stress value has been determined.

6.3 Detailing beam ends

6.3.1 Aspects of the detailing

The prestressing has been designed and is sufficient to meet the maximum tensile stress requirement at midspan. However, additional attention has to be paid to the detailing of the beam where the prestressing forces are introduced from the steel onto the concrete. The following aspects will be covered:

- **Transmission length**: Because pretensioned steel is applied for the prestressing the forces are applied onto the concrete via bond. This requires a certain transmission length, which will be calculated;
- **Tensile stresses at the top fibre**: The eccentric prestressing causes an upward bending moment which may cause tensile stresses near the supports, the maximum tensile stress has to be verified;
- **Positioning of strands**: The strands have to be positioned in the bottom flange as such that the requirements regarding cover and spacing are met;
- **Splitting action**: At the anchorage zone various tensile stresses occur that may result in different types of cracking (splitting action), in the case of pretensioned steel these are bursting, spalling and splitting. If the concrete capacity is insufficient, splitting reinforcement has to be designed.

6.3.2 Bond stresses and transmission length

Introduction of prestressing forces onto the concrete

In the case of pretensioned steel the prestressing forces are transferred from the steel onto the concrete via bond, this requires a certain length (the transmission length). The prestressing forces subsequently distribute themselves over the cross section until a linear stress distribution is achieved. This is depicted in the following figure.

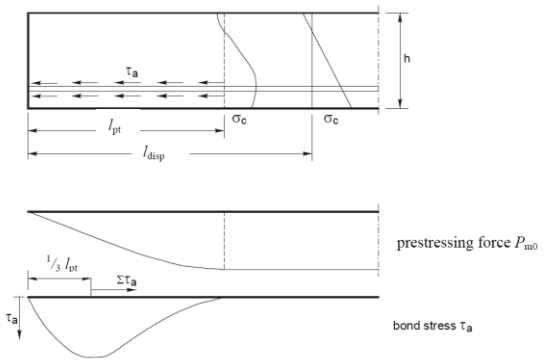


Figure 43 Transmission and dispersion length - (Walraven & Braam, 2019), p.10-7

One can distinguish two notions:

- Transmission length l_{pt}: The length that is required to transfer all forces from the strands onto the concrete via bond;
- The dispersion length l_{disp}: The length that is required to obtain a linear stress distribution of the compressive stresses due to the prestressing over the heigh of the cross section, where $l_{disp} \geq l_p$.

The analysis of the force transfer in the case of pretensioned strands is covered in 8.10.2.2 of Eurocode 2-1-1 and the accompanying sections of the AFGC-SETRA 2013 guideline.

Provisions Eurocode 2-1-1 and AFGC-SETRA 2013 – Bond stress

The stresses are transferred from steel to concrete via bond, therefore the bond stress has to be calculated first. According to the codes the bond stress may be assumed to be a constant value, and is calculated using the following equation from the AFGC-SETRA 2013 guideline:

$$f_{bpt} = \eta * \eta_1 * \kappa * \frac{f_{ctk,el}(t)}{\gamma_c}$$ Equation (18)

Where:
Bond factor η: The bond factor is defined in the following table from the guideline:

Armatures *Bars*	Béton armé ou béton précontraint par pré-tension η_s ou η_p *Reinforced concrete or pretensioned concrete η_s or η_p*	Béton précontraint à armatures post-tendues adhérentes (gaines injectées au coulis de ciment) η'_p *Prestressed concrete with post-tensioned bonded tendons (grouted ducts) η'_p*
Béton armé/ *reinforced concrete* Barres HA/*rebars (ribbed)* Barres lisses/*smooth bars*	 2,25 1	 -- --
Béton précontraint *prestressed concrete* Barres HA/*rebars (ribbed)* Fils crantés/ *indented wires* Torons/ *strands* Barres ou fils lisses/ *smooth bars and wires*	 1,8 1,6 1,35 (0,8)	 0,55 0,5 0,4 0,25

Figure 44 Bond factors - AFGC-SETRA 2013, p.127

Factor accounting for bond conditions η_1: To determine the factor for bond conditions reference is made to Eurocode 2-1-1, which prescribes:

- Good bond: $\eta_1 = 1{,}0$
- Otherwise: $\eta_1 = 0{,}7$

Factor for bond strength improvement due to the presence of fibres κ: The factor κ is calculated as follows:

$$\kappa = 1 + 0{,}5 * \frac{f_{ctfm}}{f_{ctm,el}} \leq 1{,}5$$

$f_{ctm,el}$: Mean value tensile strength of the matrix (limit of elasticity under tension)
f_{ctfm}: Mean value maximum post-cracking stress

Tensile strength $f_{ctk,el}(t)$: The value $f_{ctk,el}$ is the characteristic value of the tensile strength (characteristic value of limit of elasticity under tension) at moment 't', which is the date of the transfer of the prestressing onto the concrete.

Calculating bond stress

Using equation (18) the bond stress can now be calculated, this value will be equal for the centric and eccentric strands as the same parameters are used for both.

- For the factor η a value of 1,35 (strands) is selected. Good bond is assumed, which is why η_1 is taken equal to 1,0;

- The factor κ accounts for the improvement of the bond strength due to the presence of fibres. No specific value has been assumed for f_{ctfm}, but because a strain hardening material is applied the value should be at least be equal to $f_{ctm,el}$. This implies a maximum post-cracking stress higher than the elasticity limit, which is why κ is taken equal to 1,5;

- For the value $f_{ctk,el}(t)$ the value at 28 days is assumed because of the application of heat treatment.

This results in the following equation:

$f_{bpt} = 1{,}35 * 1{,}0 * 1{,}5 * 6{,}0 = 12{,}15$ N/mm^2

Provisions Eurocode 2-1-1 and AFGC-SETRA 2013 – Transfer length

Both codes give the same equation for the transfer length:

$$l_{pt} = \alpha_1 * \alpha_2 * \emptyset * \frac{\sigma_{pm0}}{f_{bpt}} \qquad \text{Equation (19)}$$

Where:
α_1: Factor depending on way of releasing the strands: 1,0 for gradual and 1,25 for sudden
α_2: Factor depending on the type of tendon: 0,25 for circular cross section and 0,19 for 3- or 7-wire strands
$\emptyset$: Diameter of the tendon
σ_{pm0}: Stress in the tendon just after release

Depending on the analysis the codes distinguish two design values for the transmission length:

$l_{pt1} = 0{,}4 * l_{pt}$

$l_{pt2} = 1{,}2 * l_{pt}$

Generally speaking, the lower value is used for local stress verifications (e.g. splitting action and stresses during release of the strands) and the higher value for the ULS verifications (e.g. shear force capacity or anchorage capacity). Note that Eurocode 2 uses factor 0,8 for l_{pt1}.

Calculating transmission length

For both the centric and eccentric prestressing it is assumed that the strands are released gradually, hence $\alpha_1 = 1{,}0$. Because 7-wire strands Ø15,2 are applied $\alpha_2 = 0{,}19$. The transfer length for both sets of strands are:

$$l_{pt,c} = 1{,}0 * 0{,}19 * 15{,}2 * \frac{\sigma_{pm0,c}}{f_{bpt}}$$

$$l_{pt,fb} = 1{,}0 * 0{,}19 * 15{,}2 * \frac{\sigma_{pm0,fb}}{f_{bpt}}$$

This results in 0,132 m for the centric and 0,126 m for the eccentric prestressing respectively.

6.3.3 Tensile stresses at top fibre

Near the supports the situation may occur that in the top fibres the compressive stresses due to a downward bending moment caused by the self-weight are smaller than the tensile stresses due to an upward bending moment caused by the eccentric prestressing. If the tensile stresses are higher than the material tensile strength, cracking occurs and measures have to be taken. Therefore, the stresses in the top fibre near the supports have to be calculated.

Introduction of prestressing forces

The following graph presents the introduction of the centric and eccentric prestressing forces near the supports as well as the total introduced force.



Figure 45 Introduction of prestressing forces near support

This graph is prepared under the following assumptions:

- The start of the transfer length of all strands, both centric and eccentric, is at the support and the force transfer follows a linear relationship over the transmission length;
- Because a local stress verification is performed, the lower design value $l_{pt1} = 0{,}4 * l_{pt}$ is applied for all strands.

By introducing the forces of all strands within the same region and by selecting the lower design value of the transmission length the most unfavourable situation is considered because the maximum bending moment value is reached within the shortest distance of the support possible.

Development of stresses at top fibre

Subsequently the development of the stresses at the top fibre is analysed. In reality one should distinguish between the transmission and dispersion length, outside the dispersion length a linear distribution of the concrete stresses may be assumed. However, for this analysis it is assumed that the tensile stresses are at their maximum at the end of the transmission length, again to obtain the most unfavourable situation by combining maximum eccentric prestressing force with minimum bending moment due to self-weight.

A single beam is analysed with only the self-weight and prestressing (initial value) acting upon it, this corresponds to the situation in the factory just after demoulding for example, which is the critical situation for tensile stresses at the top fibre. The stresses in the top fibre are calculated at different points along the longitudinal axis of the beam, described with the x coordinate, starting at the support. This results in the following graph.

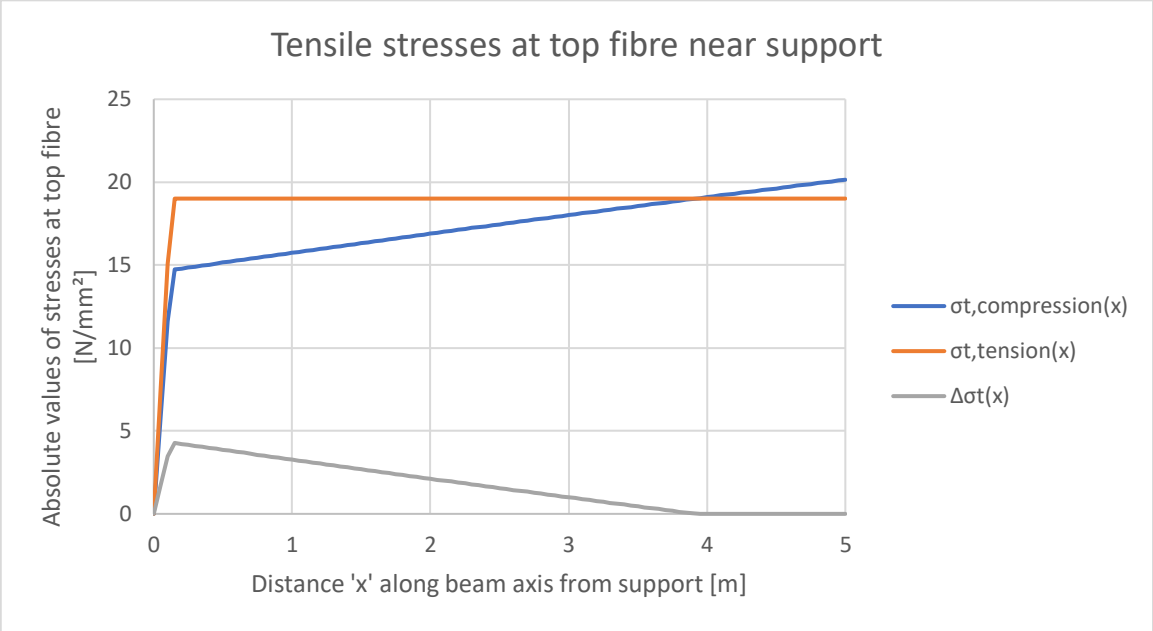


Figure 46 Tensile stresses at top fibre near the support

One can distinguish three curves. The first curve gives the compressive stresses due to the bending moment due to the self-weight and the axial prestressing components, this may be regarded as an ''enveloping curve''. The second curve gives the tensile stresses due to the upward bending moment caused by the eccentric prestressing. If the tensile stress curve falls outside the ''enveloping'' compression curve, then a tensile stress remains, which is given by the third curve.

In the calculation a maximum tensile stress value is found of $\Delta\sigma_t = 4{,}3$ N/mm^2, which should be smaller than the maximum allowable tensile stress value. For consistency the same upper limit of the tensile stress is used as done for the design of the prestressing, see equation (17). This means that the σ_{max} is 6,7 N/mm^2 and this verification is therefore satisfied.

For all equations used to plot the aforementioned curves reference is made to annexes III, which gives the calculation, and IV, which gives an overview of all equations used.

Should the tensile stress have exceeded the maximum allowable value, then two different measures could have been taken:

- **Repositioning tendons**: The first option is to bend a number of tendons upward to reduce the bending moment, or apply a number of centric strands (already applied in the design);

- **Debonding tendons**: The second option is to take measures (debonding) to prevent all eccentric strands from transferring their forces onto the concrete directly at the beam end.

6.3.4 Positioning of strands in the bottom flange

For further elaboration and preparing drawings of the bridge it is required to verify that the assumed number of strands fits within the cross section while keeping sufficient spacing and concrete cover. Two ''boundary conditions'' for determining the positioning and number of strands are the required concrete cover and bar spacing.

Cover

A minimum cover for bond is prescribed in (3) of 4.4.1.2. of Eurocode 2-1-1 and the AFGC-SETRA 2013 guideline, the latter allows a smaller value for UHPC:

$$c_{min,b} = \max\{2 * \emptyset; 2 * D_{max}\}$$

In 3.2.4 the nominal cover has been calculated for the bottom flange of the main beams. This is 35 mm and thus exceeds the cover for bond. Therefore, this value will be applied in the calculations.

Spacing

A second requirement is the clear spacing between the pretensioned strands. Both guidelines refer to the requirements in the figure, which is taken from section 8.10.1.2 of Eurocode 2-1-1.

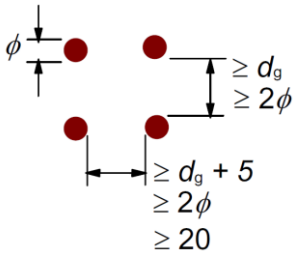


Figure 47 Minimum spacing between prestressing elements - Eurocode 2-1-1, p.156

Note that in addition the AFGC-SETRA 2013 guideline also requires that (because of flow of the material) the spacing should be at least $1{,}5 * l_f$, however, given the assumed fibre length of 13 mm and diameter of 15,2 mm this aspect is not of importance.

Positioning of the strands in the bottom flange

To summarize the boundary conditions to determine the maximum number and positioning of the strands is:

- Minimum cover bottom flange: c_{nom} (35 mm);
- Minimum horizontal and vertical spacing: $s_{min} = 2 * \emptyset$.

With the assumption of strands with a diameter of 15,2 mm all required information has been defined. In the calculation sheet first the maximum allowable number of strands in the bottom flange has been calculated. This is done by calculating the available area using the minimum concrete cover and subsequently applying the minimum spacing to obtain the maximum number of strands.

From this calculating the maximum number of strands in the bottom flange is 138 strands, this is lower than the applied number of strands (120 strands) and thus the required number of strands can be accommodated in the bottom flange.

With the applied number of strands the actual horizontal and vertical spacing is subsequently calculated by keeping the cover equal to c_{nom} and distributing the strands over a number of rows with equal horizontal and vertical distance. This distribution is as such that the centre of gravity of the strand group coincides with the centre of gravity of the bottom flange. The full elaborated calculation and an overview of the equations can be found in annexes III and IV respectively.

Positioning of the strands in the web

The positioning of the strands in the web is as follows:

- The strands are equally divided over both webs and positioned as such that the centre of gravity of the strand group coincides with that of the cross section;

- The strands are positioned at the centre lines of the webs, this way the cover exceeds the required nominal cover;

- The spacing is taken equal to the required value of $2 * \emptyset$.

6.3.5 Splitting reinforcement – Vertical distribution

Splitting action in anchorage zone

In the anchorage zone high concentrated forces are imposed onto the concrete and distribute themselves, in this anchorage zone different transverse tensile stresses occur that may result in splitting action of the concrete.

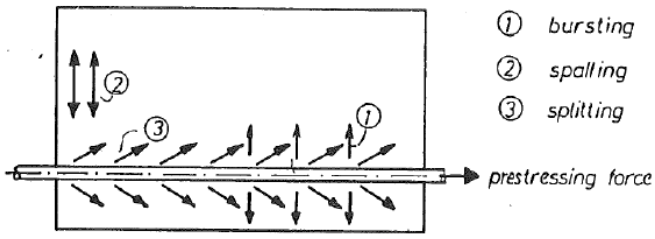


Figure 48 Tensile stresses in concrete with pretensioned steel – (Walraven & Braam, 2019), p.10-9

In the case of pretensioned steel one can distinguish the following stresses:

- **Spalling stresses**: The spalling stresses are caused by the eccentricity with which the prestressing force is applied onto the cross section. A typical spalling crack is parallel to the prestressing tendon, but at some distance away from it (in case of a single tendon) or in between multiple tendons if there are more than one;

- **Bursting stresses**: Bursting stresses are generated due to the prestressing force distributing itself over the cross section. As a result of this a transverse stress distribution develops perpendicular to the beam axis. Near the edge of the element these stresses are compressive while away from the edge these are tensile stresses, these stresses are in equilibrium. Bursting cracks therefore occur at a certain distance away from the crack;

- **Splitting stresses**: These stresses occur when the prestressing strands are released. The strands that were elongated during stressing shorten and their diameter increases again (loss of the contraction). The latter is called the 'wedge effect' and causes internal pressure onto the concrete along the transmission length, resulting in tangential tensile stresses.

These stresses have to be considered and compared with the concrete capacity. If the capacity is insufficient, reinforcement has to be provided to control cracks. In these verifications the partial factor γ_{spl}, which is taken equal to 1,2, is applied because these ultimate limit state verifications. A brief overview is given of the verifications that have been performed.

Vertical distribution

To analyse the vertical distribution of the prestressing forces the spalling stresses and bursting stresses have been calculated. The verification of the spalling stresses was performed using equivalent prism analogy, which is described in (Walraven & Braam, 2019) for example:

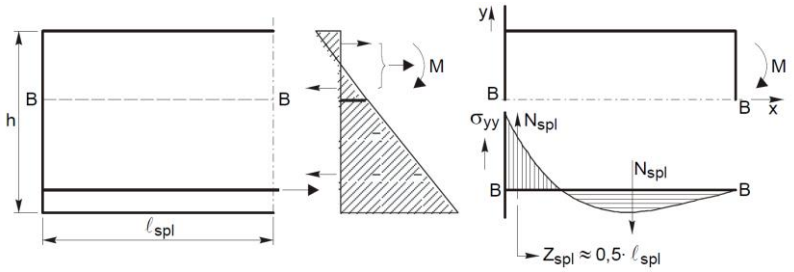


Figure 49 Prism analogy to determine spalling stresses – (Walraven & Braam, 2019), p.10-11

To determine the bursting stresses the procedure found in section 7.13.6.5.2 of the fib Model Code 2010 was applied, which makes use of a symmetric analogous prism:

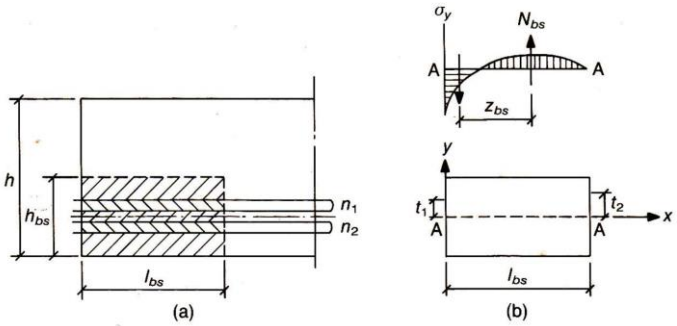


Figure 50 Calculating bursting forces – fib Model Code 2010 (Volume 2), p.273

For both calculations it was concluded that the concrete capacity was sufficient, therefore no additional measures were required. The full elaborated calculation and an overview of the equations can be found in annexes III and IV respectively.

The splitting stresses are not verified separately. Be applying the minimum required spacing and concrete cover splitting is prevented, see (Walraven & Braam, 2019) for example. Because these minimum values are applied in the calculation, this criterion is accounted for automatically.

Horizontal distribution

The horizontal distribution of the prestressing force over the bottom flange is also analysed as it is expected that this also involves tensile forces. This is done by applying a strut and tie model. A large number of prestressing forces is applied onto the cross section. Given the close spacing between these forces these can be modelled as a q-load acting on a part of the top flange.

These forces distribute themselves until uniformly distributed over the full width $b = t_w + w_b + t_w$. The disturbance length is therefore taken equal to this width of the beam while it is assumed that each force distributes itself over approximately the centre-to-centre distance between the tendons. The situation of a single strand is given below.

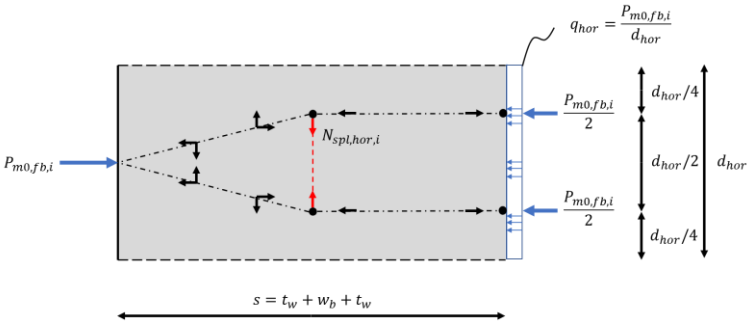


Figure 51 Force distribution of a single tendon

A single strand in the bottom flange with initial prestressing force $P_{m0,fb,i}$ results, in a horizontal splitting force of:

$$N_{spl,hor,i} = \frac{1}{4} * \gamma_{spl} * P_{m0,fb,i} * \frac{b_{hor}}{2 * t_w + w_b}$$

Despite the fact that UHPC has a relatively high tensile capacity which may be applied in strut and tie models, it is still expected that splitting reinforcement is required given the magnitude of the forces. The minimum required capacity of the reinforcement is determined by multiplying the number of strands applied in the bottom flange with the splitting force of an individual strand:

$$N_{spl,hor} = n_{fb} * N_{spl,hor,i}$$

For splitting reinforcement, the allowed stress value is generally taken smaller than the yield strength of reinforcing steel to limit the crack width. This way both the equilibrium requirement is met (ULS) and at the same time the crack width remains acceptable (SLS).

The stress that can be allowed depends on the diameter of the rebars and allowable crack width. Indicative values can be found in the codes, for example in the sections of Eurocode 2 on crack width. A practical formula that can be used as a rule of thumb is:

$$f_s = \frac{3000}{\emptyset_k} \leq 360\ [MPa]$$ Equation (20)

The minimum required diameter of the reinforcement follows from:

$$A_{s,min} = \frac{N_{spl,hor}}{f_s}$$

6.4 Verification bending moment capacity

6.4.1 Parameters & assumptions

For the calculation of the bending moment capacity largely the same procedure is followed as was applied in the preliminary design. However, a number of changes have been made to account for the centric and eccentric prestressing and change in dimensions compared to the preliminary design. The main assumptions are briefly summarized in this section.

Stress-strain diagram: The following graphs give the assumed distribution of the strains and stresses over the height of the cross section in the ultimate limit state.

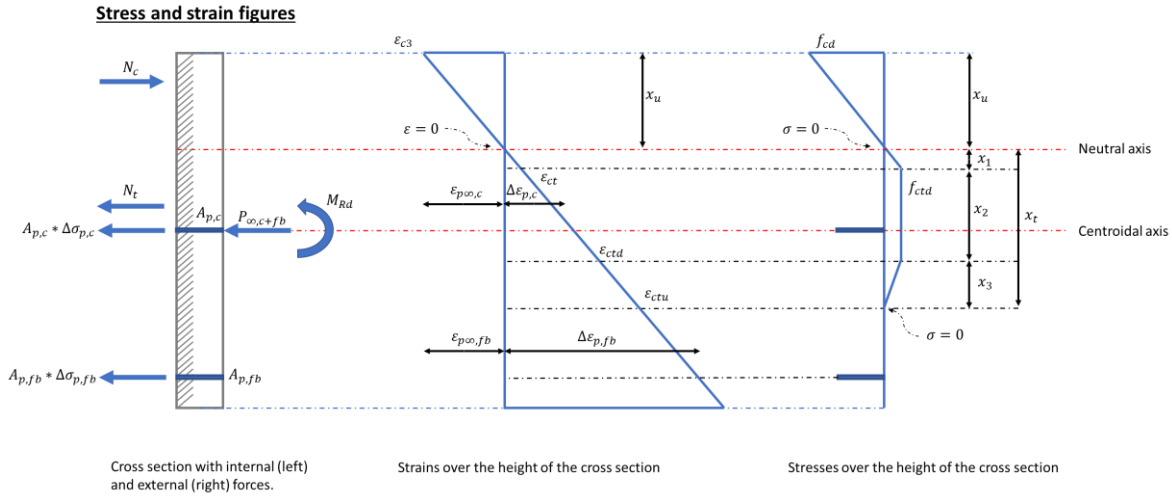


Figure 52 Assumed stress and strain distributions in the ULS

Note that compared to the preliminary design the bi-linear stress diagram of concrete in compression has been truncated at the strain ε_{c3} and that the plastic zone is not taken into consideration. The reason for this is that the number of applied strands is lower compared to the preliminary design, and as a result the tensile strains in the prestressing steel turn out to be governing over the compressive strains in the concrete.

Because of the high capacity of the concrete only a limited height x_u is required to obtain horizontal equilibrium. At the same time the effective height is relatively large because of the cross-sectional dimensions. The strains in the steel required to achieve the bi-linear stress figure typical for concrete in compression in the ultimate limit state exceeds the maximum allowable strain ε_{ud} (i.e. design value of strain

at failure) as a result of this. The assumed stress and strain diagrams have therefore been modified accordingly.

Effective height strands: Two values for the effective height of the prestressing tendons are used because of the positioning of two different groups of strands. The effective height of the centric and eccentric prestressing is respectively:

$$d_{p,c} = e_t$$

$$d_{p,fb} = h - \frac{1}{2} * t_{fb}$$

Height of compressive zone: Depending on the value of x_u the width of the compressive zone could vary over its height. Because of the triangular compressive zone two different cases are included in the Excelsheet to allow for this distinction to be made.

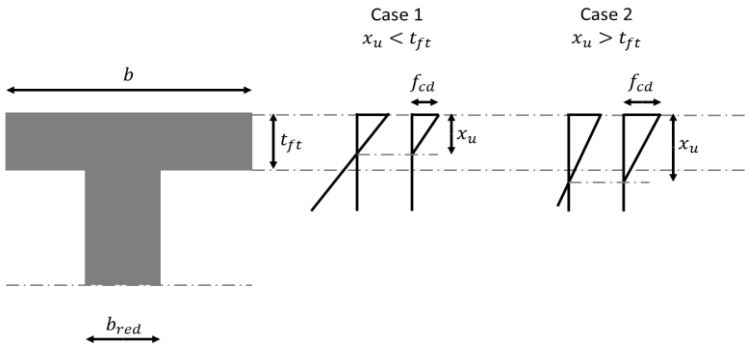


Figure 53 Height of concrete compressive zone in case of a cross section with variable width

Reference is made to annex VI where all related derivations are given. Note that for the capacity of the concrete tensile zone only the width of the webs (b_{red}) has been taken into consideration.

Effective width: Based on the check performed for the preliminary design the whole width of the top flanges is assumed to be part of the effective width of the beams in bending.

Redistribution: For the calculation of the rotational capacity, it is assumed that no redistribution takes place, hence $\delta = 1{,}0$.

Design value bending moment: The design value of the bending moment is calculated by taking the governing bending moment value at midspan from RFEM (denoted as $M_{Ed,RFEM}$) and subtracting it with the upward bending moment due to the prestressing:

$$M_{Ed} = M_{Ed,RFEM} - P_{m,\infty,fb} * e_p$$

This way the prestressing is accounted for as an external load acting on the structure, this is the 'equivalent prestressing load method', and only the passive contribution is allowed to be included in the calculation of the bending moment capacity.

6.4.2 Calculation procedure

Outline of the procedure: The bending moment capacity is verified for the governing cross section, which is at mid span. The calculation procedure applied in the Excelsheet is summarized in the following figure.

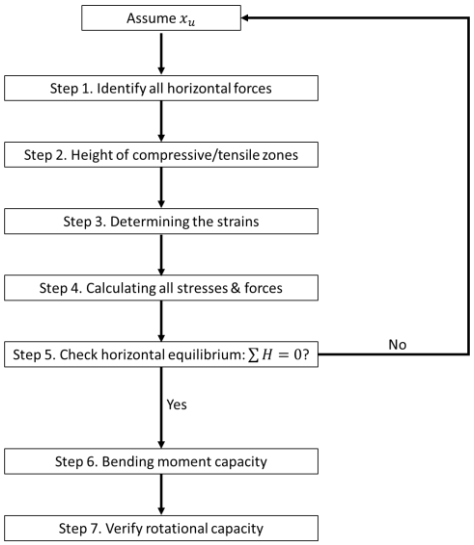


Figure 54 Calculating the bending moment capacity

For a more detailed description reference is made to annexes III for the complete calculations and IV for an overview of the equations used.

Verification bending moment capacity: The following unity check is performed to verify the bending moment capacity.

$$UC = \frac{M_{Ed}}{M_{Rd}} \leq 1{,}0 \rightarrow \frac{29.855}{38.756} = 0{,}77$$

Verification rotational capacity: The following verification is performed to check the rotational capacity of the cross section:

$$\frac{x_u}{d_{p,ave}} \leq \frac{\varepsilon_{cu} * 10^6}{\varepsilon_{cu} * 10^6 + 7f} \rightarrow \frac{0{,}09}{0{,}36} = 0{,}24$$

Note that because both centric and eccentric prestressing is used, use has been made of weighted average values to verify the rotational capacity. The weighted average value of the effective height is calculated as follows:

$$d_{p,ave} = \frac{n_c * d_{p,c} + n_{fb} * d_{p,fb}}{n_c + n_{fb}}$$

A similar approach is used for the cross section of the prestressing steel and the working prestressing stress in the strands.

6.5 Verification shear force capacity

6.5.1 Parameters & assumptions

For the verification of the shear force capacity the same approach is used as done for the preliminary design, the main assumptions are briefly summarized.

Type of section: The calculation is performed under the assumption that the cross section is loaded in compression due to prestressing. In addition, no additional conventional reinforcement is assumed to be present.

Width of the shear cross section: For the width of the shear cross section, it is assumed that no ducts are present, and thus the width is taken as twice that of a single web:

$b_w = 2 * t_w$

Angle compressive strut: The angle of the concrete compressive strut is taken equal to the minimum value of 30°.

Residual tensile strength: As was done in the preliminary design it is assumed that the residual tensile strength can be approximated by applying the value for the stress at a crack width of 0,30 mm:

$$\sigma_{Rd,f} = \frac{1}{K * \gamma_{cf}} * \frac{1}{w_{lim}} \int_0^{w_{lim}} \sigma_f(w) dw \approx \frac{1}{K * \gamma_{cf}} * f_{ctfk}$$

Where f_{ctfk} is the characteristic post cracking stress and for K the global value is used. Note that for this stress the symbol $f_{ctd;2}$ was introduced. The equation for the fibre contribution can then be written as:

$$V_{Rd,f} \approx \frac{A_{fv} * f_{cftk}}{K_{global} * \gamma_{cf} * tan\theta} = \frac{A_{fv} * f_{ctd;2}}{tan\theta}$$

Area of fibre effect: The area of the fibre effect, A_{fv}, has been calculated using the effective height of the eccentric tendons, because shear is many restrained through the web of the cross section.

6.5.2 Calculation procedure

Outline of the procedure: The shear force capacity is verified for the governing cross section which is near the supports. As a conservative assumption the support reactions are applied as the governing value for the shear force, these are calculated using RFEM. The following figure summarizes the calculation procedure:

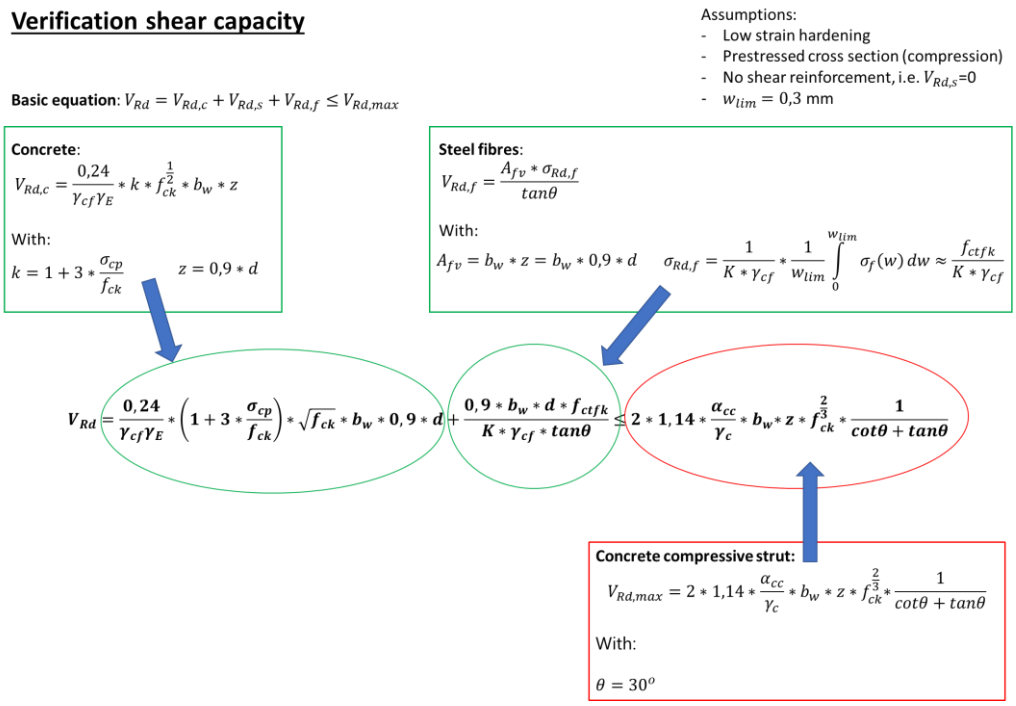


Figure 55 Verification shear force capacity

Verification shear force capacity: The following unity check is performed to verify the shear force capacity.

$$UC = \frac{V_{Ed}}{V_{Rd}} \leq 1,0 \rightarrow \frac{4090}{7290} = 0,56$$

The verification of the shear force capacity is therefore satisfied.

6.6 Torsion

6.6.1 Provisions from codes

In this section the verification of the torsion capacity and capacity under the combination of shear and torsion is verified. These verifications have not been performed before in the project, therefore the relevant provisions from the codes are summarized first. Torsion is covered in section 6.3 of Eurocode 2-1-1, Eurocode 2-2 and the AFGC-SETRA 2013 guideline. The relevant provisions of each code are summarized below.

NEN-EN 1992-1-1

The basic provisions for torsion design of conventional concrete structures are given in Eurocode 2-1-1. The design rules have to be modified for verifications of UHPC structures and therefore these cannot be applied directly, however the code does given insight into when torsion design is required, as well as the main outline of it.

A verification has to be performed if the equilibrium of the structure depends on the torsion resistance of its components. The verification is based on thin-walled closed cross sections in which equilibrium is made using a closed flow of stresses. More complicated cross sections can be divided into a number of sub sections.

NEN-EN 1992-2

The code on concrete bridges gives additional provisions that are of relevance for the design. It is stated that the effects of torsion and shear for hollow elements may be superimposed, after which the maximum capacity of an element subjected to both torsion and shear is determined. The prerequisite is that the same angle of the concrete compressive strut is used for both calculations.

In addition, it is required that for box type cross sections the cross section has to be divided into separate elements, after which the capacity of each separate element to the combined effect of torsion and shear is assessed. The combined internal effect due to torsion and shear is given schematically in the following figure.

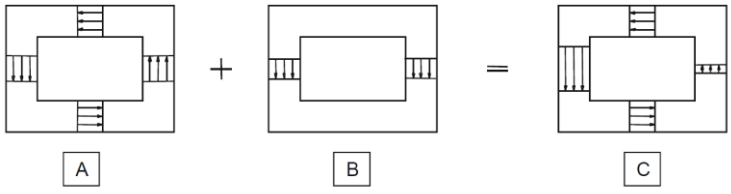


Figure 56 Combined effect shear and torsion - Eurocode 2-2, p.32

AFGC-SETRA 2013

The AFGC-SETRA 2013 guideline follows largely the same principle as the Eurocode, but the approach is modified on several occasions to allow for the fibre contribution to be taken into account.

Shear stress and shear force: The shear stress $\tau_{t,i}$ and shear force $V_{Ed,i}$ in wall 'i' which is subjected to torsion are calculated as follows:

$$\tau_{t,i} * t_{ef,i} = \frac{T_{Ed}}{2 * A_k}$$

$$V_{Ed,i} = \tau_{t,i} * t_{ef,i} * z_i$$

Where:
T_{Ed}: Design value of the torsional moment
A_k: Area enclosed by the centre lines of the connected walls, including enclosed hollow parts
$\tau_{t,i}$: Shear stresses due to torsion in wall 'i'
$t_{ef,i}$: Effective wall thickness
z_i: Length of wall 'i' defined as the distance between the intersections with the adjacent walls

Effective wall thickness: The effective wall thickness may be taken as (note that for hollow sections the actual thickness is the upper limit of the effective wall thickness):

$$t_{ef,i} = \frac{A}{u}$$

Where:
A: Total area of the cross section within the outer circumference, including enclosed hollow parts
u: Outer circumference of the cross section

Combination of shear and torsion: The effects of torsion and shear may be superimposed, provided that the same value for the angle of the compressive struts, θ, is used. For box girders or hollow sections each segment 'i' has to be checked separately for the combined effect of shear and torsion. The following equation can be applied to check the capacity of each segment:

$$V_{Rd,c} + V_{Rd,f} + V_{Rd,s} \geq V_{Ed,i} + \frac{T_{Ed}}{2 * A_k} * z_i \quad \text{Equation (21)}$$

Failure of concrete compressive strut: The resistance of an element submitted to shear and torsion is limited by the strength of the concrete compressive strut, this capacity should not be exceeded. For solid or open profiles this is verified by satisfying the following condition:

$$\frac{T_{Ed}}{T_{Rd,max}} + \frac{V_{Ed}}{V_{Rd,\max}} \leq 1{,}0 \quad \text{Equation (22)}$$

Where:
T_{Ed}: Design value of the acting torsional moment
V_{Ed}: Design value of the acting shear force
The design values of the torsional moment resistance ($T_{Rd,max}$) and maximum shear resistance ($V_{Rd,max}$) are:

$$T_{Rd,max} = 2 * 1{,}14 * \frac{\alpha_{cc}}{\gamma_C} * 2 * A_k * t_{ef,i} * sin\theta * cos\theta \quad \text{Equation (23)}$$

$$V_{Rd,max} = 2 * 1{,}14 * \frac{\alpha_{cc}}{\gamma_C} * b_w * z * f_{ck}^{\frac{2}{3}} * \frac{1}{cot\theta + tan\theta} \quad \text{Equation (24)}$$

For box beams a different procedure is to be applied. Each segment is verified separately to confirm that the equivalent shear force due to the combination of torsion and shear is smaller than $V_{Rd,max}$:

$$V_{Ed,i} + \frac{T_{Ed}}{2 * A_k} * z_i \leq V_{Rd,max,i} \quad \text{Equation (25)}$$

In this equation the capacity of the concrete compressive strut is calculated in accordance with equation (24), where the terms 'b_w' and 'z' should correspond to the dimensions of the segment 'i' under consideration by taking $b_w = t_{ef,i}$ and $z = z_i$.

6.6.2 Calculation procedure

Approach

For the verification of the torsion capacity the cross section is simplified by leaving out the flanges, this results in the following figure. Note the red centre lines of the separate elements.

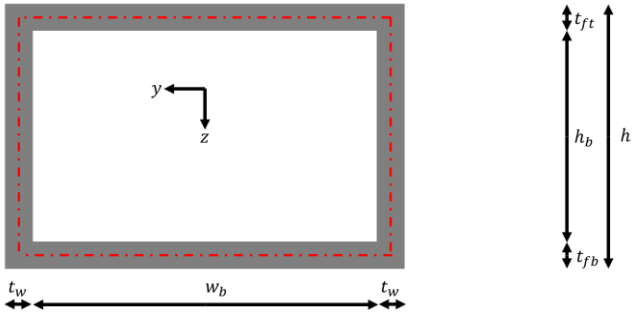


Figure 57 Simplified cross section for torsion design

Using RFEM the force distribution in the structure is determined and the design values of the shear force and torsional moment are obtained. Subsequently two sets of verifications are carried out.

- First the torsional moment capacity of the box beam as a whole is verified to determine whether the cross section can withstand the torsional moment;
- Second the resistance under the combined action of torsion and shear is verified for which each segment of the box beam is assessed separately.

Torsional moment capacity

First it is verified that the cross section as a whole can resist the torsional moment, by calculating the torsional cracking moment. This is found by taking $\tau_{t,i} = f_{ctd}$:

$$T_{Rd,c} = f_{ctd} * t_{ef} * 2 * A_k \qquad \text{Equation (26)}$$

Where:
A_k: Area enclosed by the centre lines of the connected walls, including enclosed hollow parts
t_{ef}: Effective wall thickness

The effective wall thickness is calculated by assessing the cross section as a whole, and is thus limited by the smallest actual cross-sectional dimension:

$$t_{ef} = \frac{A}{u} \leq \min\{t_w; t_{ft}; t_{fb}\}$$

$$A_k = \left(\frac{1}{2} * t_w + w_b + \frac{1}{2} * t_w\right) * \left(\frac{1}{2} * t_{ft} + h_b + \frac{1}{2} * t_{fb}\right)$$

Where:
A: Total area of the cross section within the outer circumference, including enclosed hollow parts
u: Outer circumference of the cross section

Using the governing value for the torsional moment as determined using RFEM, the following verification is performed:

$$UC = \frac{T_{Ed}}{T_{Rd,c}} \leq 1{,}0 \rightarrow \frac{1222}{7126} = 0{,}17$$

The verification of the torsional capacity of the cross section is therefore satisfied.

Combined effect of torsion and shear

In order to verify the resistance to the combined effect of torsion and shear the total cross section has to be decomposed into separate elements. The combined effect (an equivalent shear force) of shear and torsion is calculated for each separate element, after which the capacity of each separate element is verified. In addition, the upper limit due to the failure of the concrete compressive strut is calculated as well. The four separate parts of the section are:

- Left web – Part 1
- Bottom flange – Part 2
- Right web – Part 3
- Top flange – Part 4

Determining the forces: For each element the shear forces due to shear and torsion are calculated separately and added up to determine the total effect. One section will be governing with regard to the magnitude of the equivalent shear force. Figure 56 already indicates that one of the webs will be governing.

- The design value of the shear force that acts upon the beam can be decomposed into two shear forces of equal magnitude in the vertical webs:

$$V_{Ed,V,1} = V_{Ed,V,3} = \frac{V_{Ed}}{2}$$

$$V_{Ed,V,2} = V_{Ed,V,4} = 0$$

- The shear force $V_{Ed,T,i}$ in wall 'i' due to torsion is calculated as follows, note that 'z_i' indicates the length of segment 'i' (the red centrelines in Figure 57 indicate the lengths of the segments):

$$V_{Ed,T,i} = \tau_{t,i} * t_{ef,i} * z_i = \frac{T_{Ed}}{2 * A_k} * z_i$$

- The combined effect of shear and torsion is found by adding up the individual components, note the subtraction in the equation of segment 3, which is in accordance with Figure 56:

$$V_{Ed,T+V,1} = V_{Ed,V,1} + V_{Ed,T,1}$$

$$V_{Ed,T+V,2} = V_{Ed,T,2}$$

$$V_{Ed,T+V,3} = V_{Ed,V,3} - V_{Ed,T,3}$$

$$V_{Ed,T+V,4} = V_{Ed,T,4}$$

Capacity of each wall: For each section it has to be verified separately that the capacity is sufficient. Because there is no shear reinforcement equation (21) is rewritten as:

$$V_{Ed,i} + \frac{T_{Ed}}{2 * A_k} * z_i \leq V_{Rd,c,i} + V_{Rd,f,i} \qquad \text{Equation (27)}$$

The capacity is calculated following the equations given for the shear capacity (see Figure 55), while the values for the dimensions b_w and z are adjusted in accordance with the dimensions of each segment. To determine the area over which the fibres are active the width b_w is taken equal to the width $t_{ef,i}$ while z is taken equal to the length z_i of the element under consideration.

Failure of the concrete compressive strut: The resistance of the section to the combined effect of shear and torsion is limited by the failure of the concrete compressive strut, the capacity of which should therefore not be exceeded, see equation (25). This verification is performed for each section separately, with one of the webs expected to be the governing section due to the equivalent shear force. For each segment should hold:

$$V_{Ed,i} + \frac{T_{Ed}}{2 * A_k} * z_i \leq V_{Rd,max,i}$$ Equation (28)

Where:

$$V_{Rd,max,i} = 2 * 1{,}14 * \frac{\alpha_{cc}}{\gamma_C} * b_{w,i} * z_i * f_{ck}^{\frac{2}{3}} * \frac{1}{cot\theta + tan\theta}$$ Equation (29)

$$b_{w,i} = t_{ef,i}$$

$$t_{ef,i} = \frac{A}{u} \leq t_i$$

Results: The combined effect of shear and torsion is analysed using equation (27), one of the webs (which is element 1) is governing with a unity check of 0,61. For the verification of the concrete compressive strut, following equations (28) and (29), the same element is governing, with a unity check of 0,42. Based on these results it is concluded that the verification of the resistance to the combined effect of shear and torsion is satisfied.

6.7 Ship collision

6.7.1 Global verification

As discussed in 4.2.4 the deck should be designed as such that it can withstand the impact due to a collision, which is accounted for using an equivalent static force. This force acts perpendicular to the longitudinal axis of the deck, has a magnitude of 1000 kN (1 MN) and an impact area of $a = 0{,}25$ by $b = 3{,}0$ m. Two sets of verifications can be performed to verify the resistance of the deck to such an impact: a global verification and a local verification.

The first verification follows from an additional rule given in 6.4 of the ROK, which considers the stability of the deck in case of collision: it has to be verified that the deck will not lose its support in case of collision, which can be done by considering its static equilibrium. It has to be verified that:

$$F_{eq} \leq \mu * F_{sw}$$

Where:
F_{eq}: Equivalent static force caused by ship collision (1000 kN, see 4.2.4)
μ: Friction coefficient for friction between the concrete beams and its supports
F_{sw}: Self-weight of the deck

For the friction coefficient a value of 0,5 is applied, which is a value found in the ROK for friction between supports and concrete. For simplicity the self-weight of the deck is calculated by only considering the weight of the UHPC beams. This value is found by multiplying the number of beams, total beam length, their cross-sectional area and specific weight of the UHPC:

$$F_{sw} = n_{beams} * l_{tot} * A_c * \rho$$

This results in:

$$UC = \frac{F_{eq}}{\mu * F_{sw}} \leq 1{,}0 \rightarrow \frac{1000}{0{,}5 * 14.703} = 0{,}14$$

The stability criterion is therefore satisfied.

6.7.2 Local verifications

The local verification comprises a number of checks to ensure that the different relevant sections of the box beam have sufficient capacity to withstand the static equivalent load due to ship collision. Detailed elaboration of these verifications is beyond the scope of this design. However, the importance of this design aspect has to be acknowledged: in the engineering practice these verifications would be part of the design if the bridge would be constructed.

In practice such local verifications will involve extensive detailing but these aspects can be solved very well. One way of doing so is reinforcing the edge beams by applying slender diaphragms (transverse stiffening walls within the box beam) placed with a certain centre to centre distance apart. Using these elements, the effects of ship collision can be mitigated because these increase stiffness and restrain and redistribute (parts of) the collision force.

At the same time, it is expected that such a solution would have a negligible effect on the results of the project. Even the application of very slender diaphragm elements to the edge beams will already have large effects on the force distribution, while the overall increase of the self-weight of the structure is kept to an absolute minimum.

6.8 Bibliography chapter six

Braam, C. (2012). *Cement en beton 3 Constructieleer Voorgespannen Beton* (Vijfde herziene druk 2012 ed.). Aeneas.

Braam, R. (2010). *Rekenvoorbeelden Eurocode 2* (Eerste druk ed.). (Cement&BetonCentrum, Red.) 's-Hertogenbosch: Aeneas.

Groupe de travail BFUP. (2013, June). Ultra High Performance Fibre-Reinforced Concretes. *Recommendations*. Association Francaise de Génie Civil.

International Federation for Structural Concrete (fib). (2012, April). Model Code 2010 - Volume 2.

Jongenelen, A. (2016). Lecture notes - Voorgespannen beton in de Prefab Beton Industrie.

NEN. (2011, november). NEN-EN 1992-1-1+C2. *Eurocode 2: Ontwerp en berekening van betonconstructies - Deel 1-1: Algemene regels en regels voor gebouwen*.

NEN. (2011, december). NEN-EN 1992-2+C1. *Eurocode 2: Ontwerp en berekening van betonconstructies - Betonnen bruggen - Regels voor ontwerp, berekening en detaillering*.

NEN. (2016, november). NEN-EN 1992-2+C1/NB. *Nationale bijlage bij NEN-EN 1992-2+C1 Eurocode 2: Ontwerp en berekening van betonconstructies - Betonnen bruggen - Regels voor ontwerp, berekening en detaillering*.

NEN. (2020, februari). NEN-EN 1992-1-1+C2/NB+A1. *Nationale bijlage bij NEN-EN 1992-1-1+C2 Eurocode 2: Ontwerp en berekening van betonconstructies - Deel 1-1: Algemene regels en regels voor gebouwen*.

Rijkswaterstaat. (2017, April). Richtlijnen Ontwerp Kunstwerken. *ROK 1.4*.

Walraven, J., & Braam, C. (2019, February). Prestressed Concrete.

7

DESIGN OF MAIN BEAMS – TOP FLANGE AND TRANSVERSE PRESTRESSING

7.1 Analysis of top flange

7.1.1 Beam interaction and local verifications

In the preliminary design it was assumed that there is no interaction between the separate beams: the beams were assumed to carry the full load applied onto it. In reality this is not the case: The joints between the prefab beams are filled with in-situ concrete after which the beams are post tensioned in transverse direction. This creates a solid deck and as a result interaction occurs. As a result, applied loads are distributed over the different beams. In the FEM model this is simulated instead by adding a surface element.

Only global verifications (i.e. the beams were assessed as a whole) were performed in the preliminary design and the previous chapter. Although this is the first step in the verification process in practice local verifications should be performed as well to verify that the individual segments of the beams have sufficient capacity.

These two points, the beam interaction and the importance of local verifications, will be studied more closely in this chapter. The transverse prestressing will be designed and various local verifications of the top flange will be performed.

7.1.2 Design approach

The following calculations and local verifications are included in this chapter:

- **Design of transverse prestressing**: The occurrence of force distribution between the prefab beams implies that in addition to the longitudinal bending moments (verifications of which have been performed in 6.4) transverse bending moments occur. To enable the transfer of these bending moments continuity between the beams is required, which is achieved by applying transverse prestressing. This prestressing is designed with the requirement that no tensile stresses may occur at the weakest point of the top flange: the longitudinal joints.

- **Capacity of longitudinal joint**: It has to be verified that the prestressed longitudinal joint has sufficient capacity to transfer the transverse bending moments between the beams that are caused by the beam interaction.

- **Capacity of top flange – transverse direction**: In addition to the longitudinal joints the prestressed top flanges should also be able to transfer the transverse bending moments. Therefore, their bending moment capacity at the beam webs and in between the webs will be verified.

- **Capacity of top flange – longitudinal direction**: The top flanges of the beams are provided with prestressing ribs in order to decrease the thickness of the top flange, saving material and thus weight. These ribs act as supporting elements and the capacity of the top flange spanning these ribs has to be verified as well.

Note that these verifications are local design verifications, these are carried out almost separately from the global verifications:

- For the elaboration of the local verifications different load models are applied compared to the global verification;

- In addition, where the force distribution for the global verification was determined using a finite element model the force distributions for the local verifications are calculated using simpler models: the structural elements will be schematized as beams with clamped or hinged supports.

In the subsequent sections the transverse prestressing will be designed after which the various local verifications will be performed.

7.2 Design of transverse prestressing

7.2.1 Positioning and assumed number of strands

The top flanges are prestressed using post-tensioned prestressing tendons positioned in the ducts at the prestressing ribs. The parameters of the prestressing are given in 2.3.4.

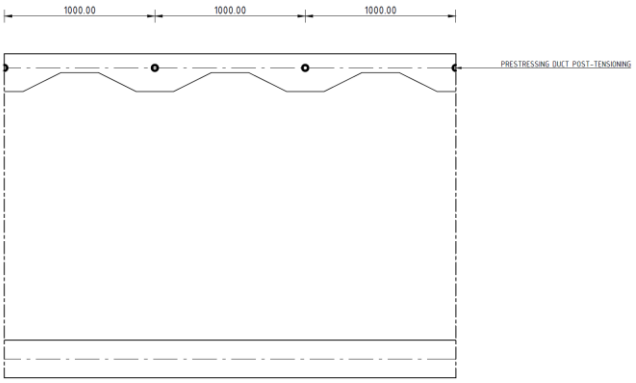


Figure 58 Side view of beam section with prestressing ducts

The analysis is based on the following points:

- A strip of the top flange is analysed with width $w_{c.t.c.}$ and average thickness t_{ft}, the strip is centred in horizontal direction around the centre of the prestressing duct;

- The prestressing tendon is positioned in vertical direction at a height $0{,}5 * t_{ft}$, the top flange is therefore prestressed centrically;

- The joint has a thickness $t_j$which is smaller than the thickness t_{ft}. As a result, an upward bending moment is caused in the joint because of an eccentricity of:

$$e_j = 0{,}5 * t_{ft} - 0{,}5 * t_j$$

7.2.2 Calculating prestress losses

With the aforementioned assumptions the prestressing losses are calculated at different positions along the width of the deck. For the full elaboration of the calculation reference is made to annexes III (Excelsheet with the calculation) and IV (overview of all equations), the most relevant points of the calculation are highlighted in the remainder of this subparagraph.

Applied maximum force onto prestressing element and stress verification

It has to be verified that the maximum stress applied to the prestressing strands does not exceed the maximum value. In addition, it should be verified that during the transfer of the prestressing force onto the concrete the maximum allowed concrete compressive stress is not exceeded.

The point under consideration is the edge of the deck and the prestressing acts centrically. Note the factor '0,6' instead of '0,7' because post-tensioned steel is used for the transverse prestressing.

$$\sigma_c = \frac{P_{max}}{A_{tf}} = \frac{\sigma_{p,max} * n * A_{p_{strand}}}{w_{c.t.c.} * t_{ft}} \leq 0{,}6 * f_{ck}$$

Direct losses

The direct prestressing losses are subsequently calculated. Because post-tensioned steel is applied the following three losses are of relevance:

- Elastic shortening: Prestressing of the concrete results in elastic shortening of the material. As a result, the tendons are shortened as well and as a result the prestressing force is reduced as well.

- Friction: When stressing the tendon, it is then pulled towards the jack and the inner side of the duct resists this motion in the form of friction into the other direction. As a result, at each point along the tendon the cable force is equal to the maximum force minus the friction that occurs between the jack and the point under consideration. Due to factors such as deflection of the tendon, curvature of the ducts, execution of the work, etc. there turns out to be an additional ''unintentional'' angular rotation (Wobble-effect), thus increasing the loss.

- Wedge set: When the required prestressing force is reached, the tendon is anchored using wedges. As the jack is released the wedge slips until sufficient anchorage force is generated. As a result, the tendon shortens and a local prestress loss occurs. The direction of the slip is opposite to the direction of the tensioning, thus the friction that develops is in the other direction (and is assumed to be linear). As a result, the maximum prestressing force is found at some distance from the active end from where the tendon was stressed.

Elastic shortening: The elastic losses in case of a single tendon is as follows:

$$\Delta P_{el} = P_{max} * \frac{E_p A_p}{E_{cm} A_c} = P_{max} * \frac{E_p * A_p}{E_{cm} * w_{c.t.c.} * t_{ft}} \qquad \text{Equation (30)}$$

Friction: According to 5.10.5.2 of Eurocode 2-1-1 the frication losses are calculated as follows:

$$\Delta P_\mu(x) = \left(1 - e^{-\mu(\theta + k*x)}\right) * P_{max}$$

Where:
θ: Total angular rotation over a distance x
μ: Friction coefficient between the prestressing tendon and the duct
k: The unintentional angular rotation of the tendon (Wobble-effect) per unit of length
x: Distance between the jack to the cross section under consideration
P_{max}: Maximum prestress force

Because the tendons are straight the total angular rotation θ equals zero:

$$\theta = \left|\frac{x}{R}\right| \rightarrow \theta = \lim_{R \to \infty} \left|\frac{x}{R}\right| = 0$$

The remaining equation for the friction loss at coordinate 'x' along the beam length therefore is:

$$\Delta P_\mu(x) = (1 - e^{-\mu * k * x}) * P_{max} \qquad \text{Equation (31)}$$

Wedge set: The losses due to wedge set are calculated under the assumption that friction develops linear over the full width of the deck. The principle is given in the following figure.

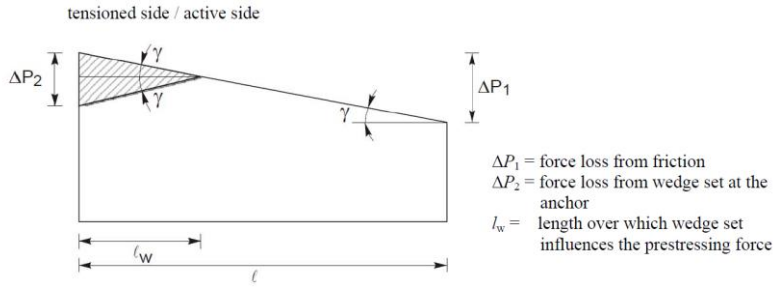


Figure 59 Wedge set – (Walraven & Braam, 2019), p.4-26

The prestress loss due to wedge set at the position of the anchor is calculated as follows:

$$\Delta P_{set} = 2 * A_p * \frac{\Delta\sigma_{p\mu,m}}{\Delta x} * l_w \qquad \text{Equation (32)}$$

In this equation the term $\Delta\sigma_{p\mu,m}/\Delta x$ denotes the stress reduction due to friction per unit of length. The influence length over which the wedge set influences the prestressing force is calculated as follows:

$$l_w = \sqrt{\frac{w_{set} * E_p}{\left(\frac{\Delta\sigma_{p\mu,m}}{\Delta x}\right)}}$$

Determining initial prestressing force and stress verification

The initial prestressing force at position 'x' along the width of the deck is calculated as follows:

$$P_{m0}(x) = P_{max} - \Delta P_{el} - \Delta P_{\mu}(x) - \Delta P_{set}(x)$$

Because the losses due to friction and wedge set depend on the coordinate 'x' along the width of the deck the initial prestressing force depends on the coordinate as well. The prestressing forces and losses have been calculated on a large number of points, for which the beam has been divided into one hundred equal intervals. The following graph shows the direct prestress losses along the beam length:

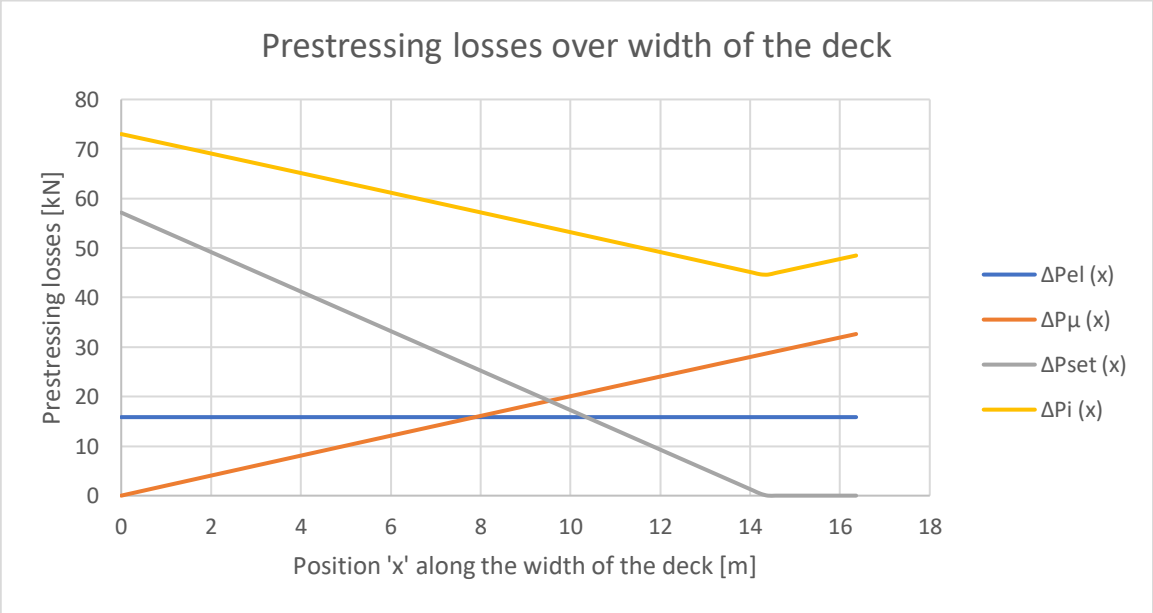


Figure 60 Initial prestress losses along the beam length

It has to be verified that the stresses in the strands are not larger than the maximum allowable value, for this the maximum value of the initial prestressing force along the width has been applied:

$$\frac{\max\{P_{m0}(x)\}}{A_p} \leq \sigma_{pm0}$$

Time dependent losses

The initial prestressing force $P_{m0}(x)$ is a function of 'x' but for the further calculations it is deemed sufficiently accurate to apply a simplification by using the mean value of all values $P_{m0,i}$ calculated at the end points of the intervals on which the prestress losses were calculated. For a total number of end points 'j' this is written as:

$$P_{m0} = \frac{1}{j} * \sum_{i=1}^{i=j} P_{m0,i} \qquad \text{Equation (33)}$$

This mean value P_{m0} will be used to calculate the time dependent losses, note that by using this mean value the time dependent losses are calculated independently of 'x' and thus one constant value is found. The time dependent losses are calculated for $t \to \infty$ (i.e. their maximum values are calculated).

The top flange is centrically prestressed and the basic equation for time dependent losses according to Eurocode 2-1-1, see equation (10), is therefore simplified to:

$$\Delta P_{c+s+r} = A_p * \Delta\sigma_{p,c+s+r} = A_p * \frac{\varepsilon_{cs}E_p + 0{,}8\Delta\sigma_{pr} + \frac{E_p}{E_{cm}}\varphi(\infty,t_0)\sigma_{c,QP}}{1 + \frac{E_p}{E_{cm}}\frac{A_p}{A_c}[1 + 0{,}8 * \varphi(\infty,t_0)]}$$

For the prestressing steel relaxation class 2 is assumed, which implies low relaxation. The relaxation loss is calculated as follows:

$$\frac{\Delta\sigma_{pr}}{\sigma_{pi}} = 0{,}66 * \rho_{1000} * e^{9{,}1\mu} * \left(\frac{t}{1000}\right)^{0{,}75(1-\mu)} * 10^{-5}$$

The parameter μ is defined as $\mu = \sigma_{pi}/f_{pk}$, in which σ_{pi} equals the initial stress value σ_{pm0} which is calculated using the mean value of the initial prestressing over the beam width:

$$\sigma_{pm0} = \frac{P_{m0}}{A_p}$$

To determine the losses due to creep the stress $\sigma_{c,QP,c}$ has to be calculated as well, this is the stress in the concrete adjacent to the prestressing element due to loads that contribute to the creep losses. Only the prestressing contributes because the tendons are positioned centrically, hence:

$$\sigma_{c,QP} = \frac{P_{m0}}{w_{c.t.c.} * t_{ft}}$$

Working prestress force

The following graph shows the maximum prestressing force P_{max}, the initial prestressing force $P_{m0}(x)$ (as a function of the coordinate 'x'), the mean value of the initial prestressing force P_{m0} and the working prestressing force $P_{m,\infty}$ (calculated using the mean value of the initial prestressing force). The working prestressing force equals 776 kN, which implies a working prestress of 1108 N/mm^2 in the steel and a loss of approximately 21 %.

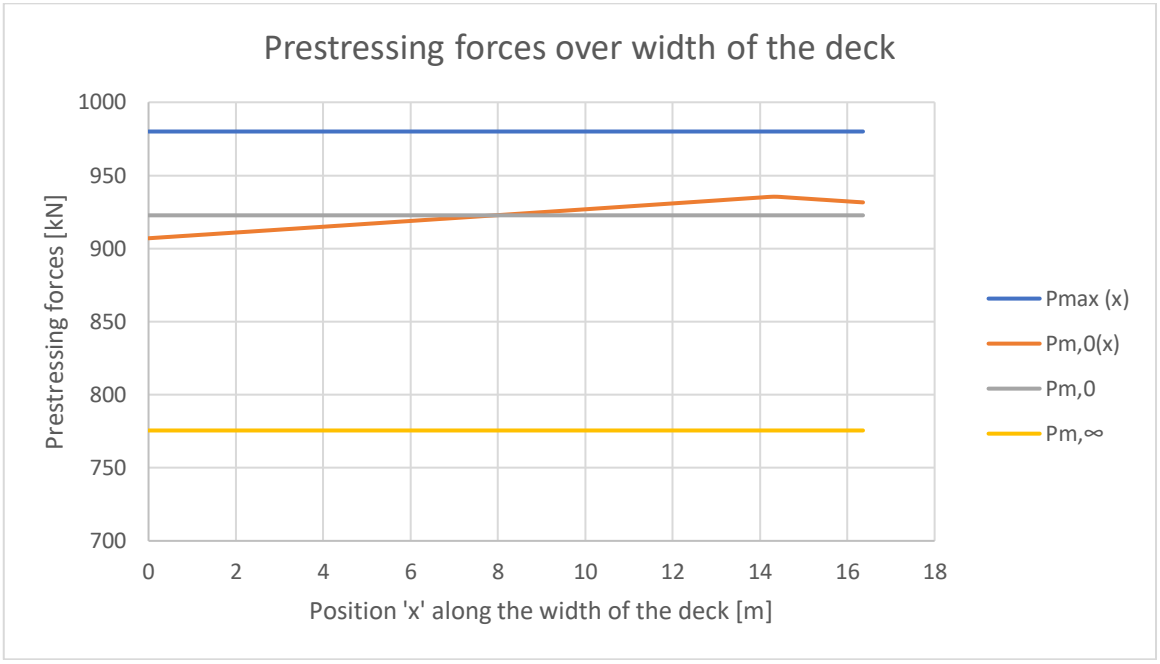


Figure 61 Prestressing forces over the width of the deck

7.2.3 Forces acting on top flange and joint

The prestressing forces and losses have been calculated and these will be used to verify if the prestressing is sufficient to keep the longitudinal joints under compression. To analyse this a strip of the deck in transverse direction with a width of 1,0 m is considered. Because a local verification is performed the loads used for these verifications have to be determined first. The following loads are of relevance:

- **Self-weight & permanent load**: The self-weight of the concrete top flange and the asphalt layer are calculated for a strip with 1,0 m width. The line load found is:

$G_k = t_{tf} * \rho_{UHPC} + t_{asphalt} * \rho_{asphalt}$ [kN/m]

- **Variable load**: For the variable loads load model 2 (LM2) is applied, which consists of a single axle with force $\beta_Q Q_{ak} = 388$ kN. To obtain the most unfavourable situation for the joint half an axle load is positioned directly above the joint while the other wheel load is neglected:

$Q_k = 194$ [kN]

- **Prestressing forces**: The axial prestressing force $P_{m,\infty}$ has been calculated in the previous section at the location of the longitudinal joint it causes and an upward bending moment due to the eccentricity between the tendon and centre of the joint:

$$M_P = \frac{P_{m,\infty} * e_j}{w_{c.t.c.}}$$

Calculation model longitudinal joint

For the assessment of the joint and designing the transverse prestressing a simple model is proposed to calculate the required bending moments: The top flange is schematized using simple models of beams with clamped supports and uniformly distributed or point loads. The joint is positioned at mid span, the span is:

$l = 2 * w_f + w_j + t_w$

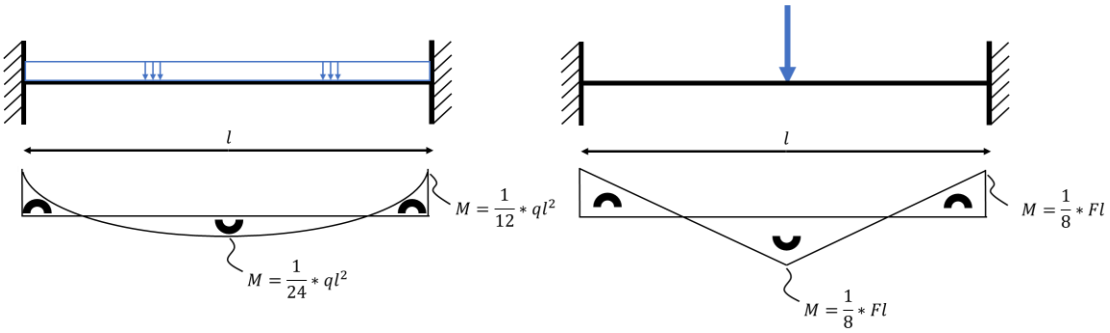


Figure 62 Calculation model top flange

7.2.4 Verifying stresses over joint height

The joint is designed for the criterion that no tensile stresses are allowed, the working prestressing force should be sufficient to keep the joint under compression. This criterion has to be verified by calculating the stresses over the height of the joint. Two different situations are assessed and for both cases the stresses at the top and bottom fibre of the joint are calculated:

Situation with traffic loads – Including the effects of the prestressing the stresses at the top and bottom fibre of the joint are as follows:

$$\sigma_{j,t} = -\frac{\frac{1}{24} * G_k * l^2}{W_j} - \frac{\frac{1}{8} * Q_k * l}{W_j} - \frac{P_{m,\infty}}{w_{c.t.c.} * A_j} + \frac{P_{m,\infty} * e_j}{w_{c.t.c.} * W_j} \leq 0$$

$$\sigma_{j,b} = +\frac{\frac{1}{24} * G_k * l^2}{W_j} + \frac{\frac{1}{8} * Q_k * l}{W_j} - \frac{P_{m,\infty}}{w_{c.t.c.} * A_j} - \frac{P_{m,\infty} * e_j}{w_{c.t.c.} * W_j} \leq 0$$

Situation without traffic loads – Including the effects of the prestressing the stresses at the top and bottom fibre of the joint are as follows:

$$\sigma_{j,t} = -\frac{\frac{1}{24} * G_k * l^2}{W_j} - \frac{P_{m,\infty}}{w_{c.t.c.} * A_j} + \frac{P_{m,\infty} * e_j}{w_{c.t.c.} * W_j} \leq 0$$

$$\sigma_{j,b} = +\frac{\frac{1}{24} * G_k * l^2}{W_j} - \frac{P_{m,\infty}}{w_{c.t.c.} * A_j} - \frac{P_{m,\infty} * e_j}{w_{c.t.c.} * W_j} \leq 0$$

The resulting stresses over the joint height are given in the following figure.

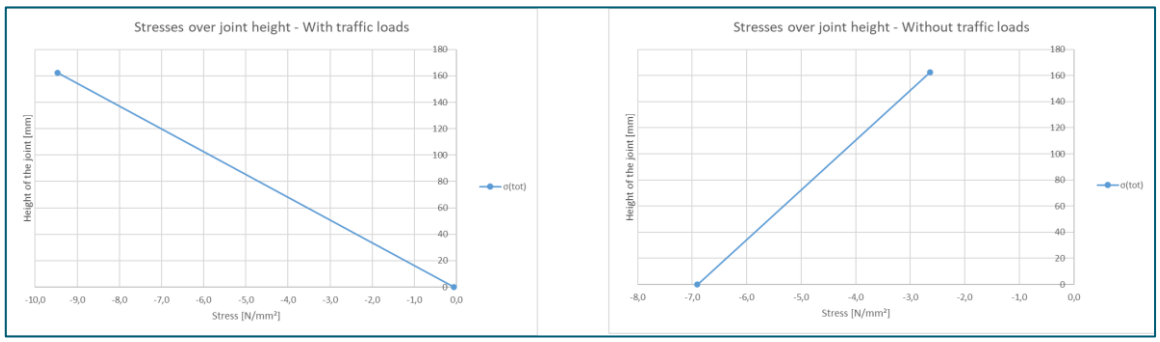


Figure 63 Stresses over the joint height for both situations

It can be seen that the working prestressing force is sufficient to keep the joints under compression, this criterion is therefore satisfied.

7.2.5 Detailing

Strut and tie models

In this section the transfer of the prestressing forces onto the top flange is analysed to determine if splitting reinforcement is required. Note that this verification is different than for the pretensioned steel in the previous chapter because in the case of post-tensioned prestressing the forces are applied locally at the anchor instead of over a certain length using bond. A similarity is that in the case of post-tensioned steel also bursting stresses occur.

At the anchorage zones prestressing forces of post tensioned tendons are introduced as a concentrated force using anchors and over a certain distance, which is known as the disturbance length or St.-Venant length, these forces distribute themselves over the cross section until a uniform stress distribution is achieved. As a rule of thumb the disturbance length is equal to the height or width of the element over which the force distributes, this parameter is therefore only dependent on geometry (and not on the magnitude of the force).

For the analysis of beams generally the assumption is used that plane cross sections remain plane, but this does not hold for the disturbance length. The force distribution at this zone can be analysed using strut and tie models, in which often large tensile forces (in tensile ties) are required to obtain equilibrium. Using basic strut and tie models the introduction of the prestressing forces onto the top flange will be discussed.

Distribution prestressing force over the width

First the distribution of the prestressing force over the width of the top flange is analysed. It is assumed that a square anchor plate with dimensions h_1 is applied. The principle is given in the following figure.

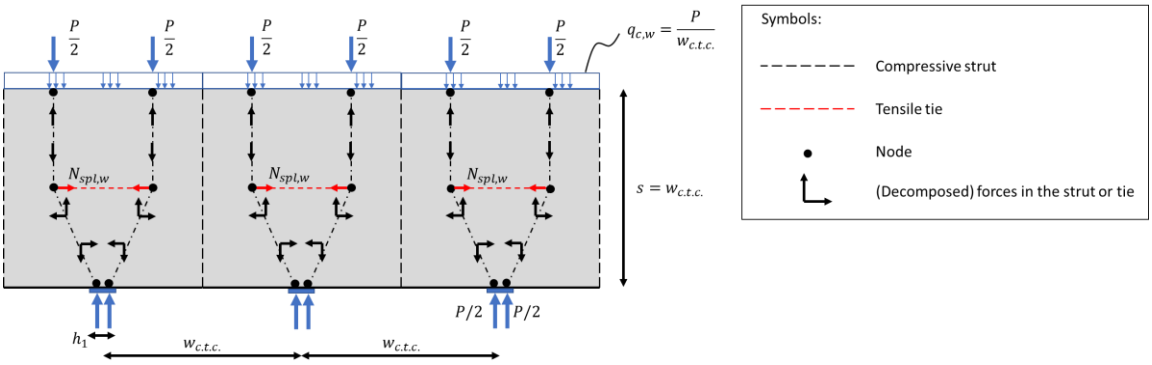


Figure 64 Force distribution in width direction

The prestressing is applied at the anchor plate located at the centre of the prestressing ribs, these ribs are positioned on a centre-to-centre distance of $w_{c.t.c.}$ metres. The forces distribute over a distance s until a uniform distribution is achieved. It is assumed that this disturbance length is equal to $w_{c.t.c.}$ metres. Using the figure, it can be derived that the splitting force is:

$$N_{spl,w} = \frac{1}{4} * \gamma_{spl} * P_{m0} * \left(1 - \frac{w_{c.t.c.}}{h_1}\right)$$

If the tensile capacity of the UHPC is neglected the splitting reinforcement can be calculated using:

$$A_{s,req} = \frac{N_{spl}}{f_s}$$

Where f_s is calculated using equation(20). The splitting force is 249 kN. If a diameter $\emptyset_{spl,ft}$ of 10 mm is assumed the stress f_s would be 300 N/mm^2, resulting in a minimum of 11 bars.

Distribution prestressing force over the height

Subsequently the distribution of the prestressing forces over the height of the flange is analysed. The principle is sketched in the following figure.

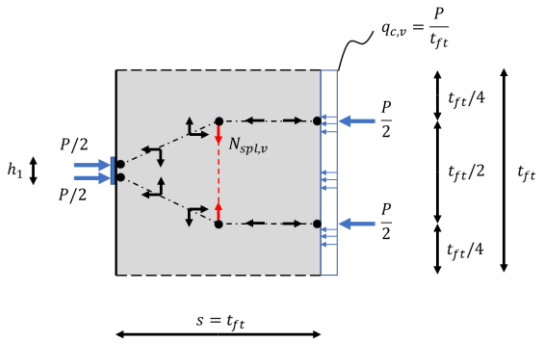


Figure 65 Force distribution in vertical direction

The disturbance length is taken equal to the height, hence $s = t_{ft}$. The splitting force is:

$$N_{spl,w} = \frac{1}{4} * \gamma_{spl} * P_{m0} * \left(1 - \frac{t_{ft}}{h_1}\right)$$

The splitting force is 129 kN. If the tensile capacity of the UHPC is neglected and the same assumption for the rebar diameter is used as for the distribution over the width the stress f_s would be 300 N/mm^2 and the number of rebars required would be 6 bars.

Concrete contribution tensile ties

In the calculations of the splitting reinforcement the tensile capacity of the concrete is not taken into consideration. However, the AFGC-SETRA 2013 guideline states that a tensile tie can be realised using reinforcing steel and/or steel fibres present in the concrete. Strut and tie models are covered in 6.5 of the guideline, for tensile ties formed by the concrete the capacity is as follows:

$$A_t * \sigma_{Rd,f}$$

Where:
A_t: Area of the tie
$\sigma_{Rd,f}$: Residual strength of the fibre-reinforced cross-section

In this case the residual tensile strength has to be calculated using the local fibre orientation factor because the analysis using strut and tie models is considered to be a 'local verification'.

Two remarks are made regarding the realisation of a tensile tie using the concrete:

- **Dimensions**: A point of consideration is the required dimensions A_t and if this value is realistic. For the residual tensile strength, a value is assumed of:

$$\sigma_{Rd,f} = \frac{f_{ctfk}}{\gamma_{cf} * K_{local}} = \frac{10}{1{,}3 * 1{,}75} = 4{,}4\ [MPa]$$

  The distribution over the width is analysed with a tensile force of 249 kN. The required area of the tensile tie would be:

$$A_t = \frac{N_{spl,w}}{\sigma_{Rd,f}} \rightarrow \frac{249 * 10^3}{4{,}4} = 56.590\ [mm^2]$$

  If the top flange contributes over the full height, then the required width of the tensile tie would be:

$$A_t = 56.590 = t_{ft} * w_t \rightarrow w_t = \frac{56.590}{187{,}5} = 302\ [mm]$$

Given the dimensions from Figure 64 this is a reasonable value for the width of the tensile tie.

- **Stress state in top flange**: A second point of consideration are the stresses in the top flange along the beam length. Although the required dimensions for the tensile tie can be estimated the question remains of the full capacity of the steel fibres can actually be mobilised for this purpose.

  The participation of the fibres depends on the forces in the beam, if the beam is in compression a larger contribution of the fibres to the tensile capacity is available while if the beam is in tension this contribution reduces or equals zero. The stresses in the top flange in longitudinal direction are not constant along the beam length, this can be seen from the bending moment diagrams for different loads. That means that the available stress $\sigma_{Rd,f}$ is not constant either along the beam length.

Given these two remarks the splitting reinforcement has been calculated assuming no contribution of the steel fibres. This is a conservative assumption and the calculated amount of reinforcement should thus be interpreted as an upper bound value.

7.3 Local verifications top flange

7.3.1 Capacity longitudinal joint

To verify the capacity of the longitudinal joint a strip of 1,0 m width is analysed with the loads as determined in 7.2.3. The bending moments are calculated following Figure 62. To determine the design value of the bending moments two combinations are formulated (using equations 6.10a and 6.10b of the Eurocode 0) and the governing value is applied:

$$M_{Ed} = \max\{\gamma_G * M_G - \gamma_P * M_P + \psi_0 * \gamma_Q * M_Q; \zeta * \gamma_G * M_G - \gamma_P * M_P + \gamma_Q * M_Q\}$$

This value is compared with the bending moment capacity of the joint. The following strain and stress relations over the joint height in the ultimate limit state are assumed.

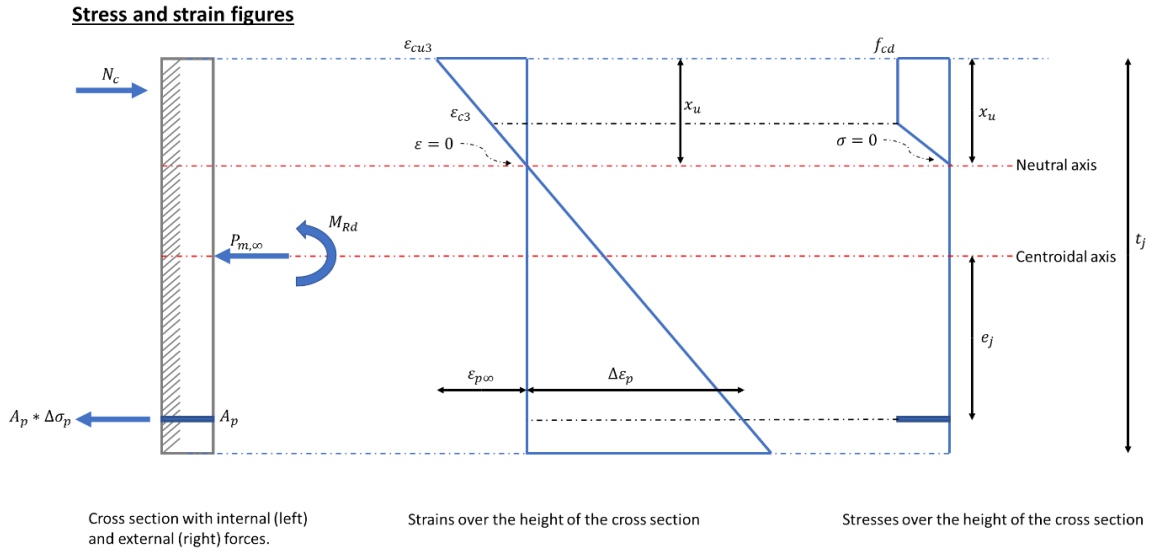


Figure 66 Assumed stress and strain distributions longitudinal joint in the ULS

The general calculation procedure is the same as applied for the bending moment capacity of the main beams. The following unity check has to be satisfied:

$$UC = \frac{M_{Ed}}{M_{Rd}} \leq 1{,}0 \rightarrow \frac{35{,}8}{78{,}8} = 0{,}45$$

The bending moment capacity of the joint is sufficient. For a more detailed elaboration reference is made to annexes III and IV.

7.3.2 Capacity of top flange – Transverse direction

The bending moment capacity of the prefab beams in transverse direction are also verified using the same loads and approach as applied for the longitudinal joint. First the actions on the joints have to be calculated. The same model is used as given in Figure 62, but with a different span:

$$l = 2 * t_w + w_b$$

Using these models, the hogging and sagging bending moment in the ULS are calculated, these will be compared with the bending moment capacity of the centrically prestressed top flange. The following strain and stress relations over the height of the top flange in the ULS are assumed:

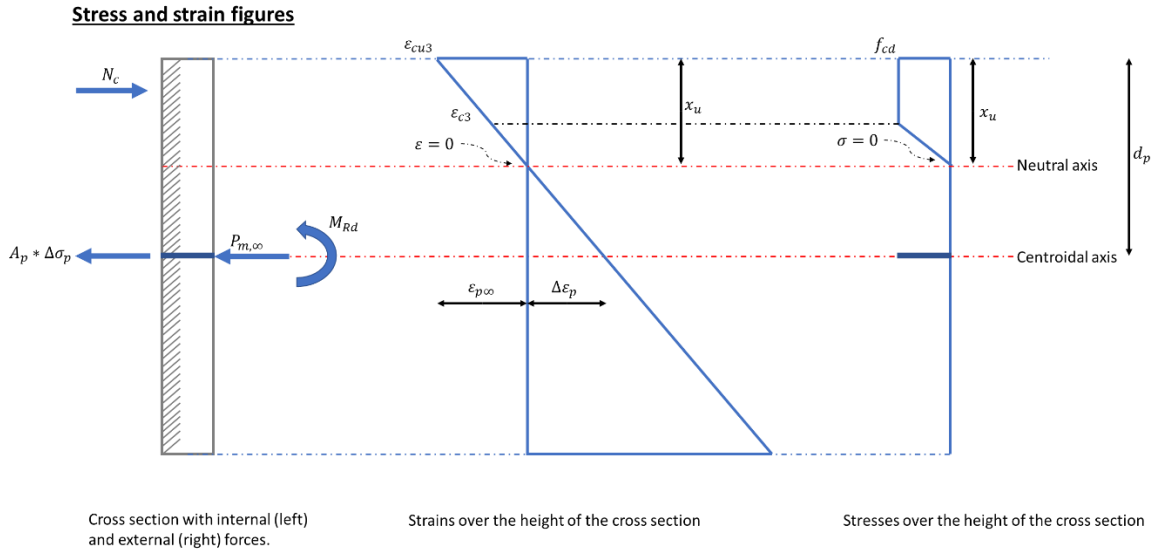


Figure 67 Assumed stress and strain distributions top flange in the ULS

Two unity checks have to be performed, one for the sagging and one for the hogging bending moment:

$$UC = \frac{M_{Ed,sag}}{M_{Rd}} \leq 1{,}0 \rightarrow \frac{75{,}6}{97{,}1} = 0{,}78$$

And:

$$UC = \frac{M_{Ed,hog}}{M_{Rd}} \leq 1{,}0 \rightarrow \frac{76{,}7}{97{,}1} = 0{,}79$$

The capacity of the top flange is therefore sufficient with respect to the bending moment capacity. For a more detailed elaboration reference is made to annexes III and IV.

7.3.3 Capacity of top flange – Longitudinal direction

Model top flange in longitudinal direction

The final local verification included in the design is the bending moment of the top flange in longitudinal direction. The top flange is modelled as a 1,0 m wide beam spanning between two adjacent prestressing ribs. It is prestressed by external axial forces due to the prestressing (see 6.2) and self-weight of the main beams. The model is as follows:

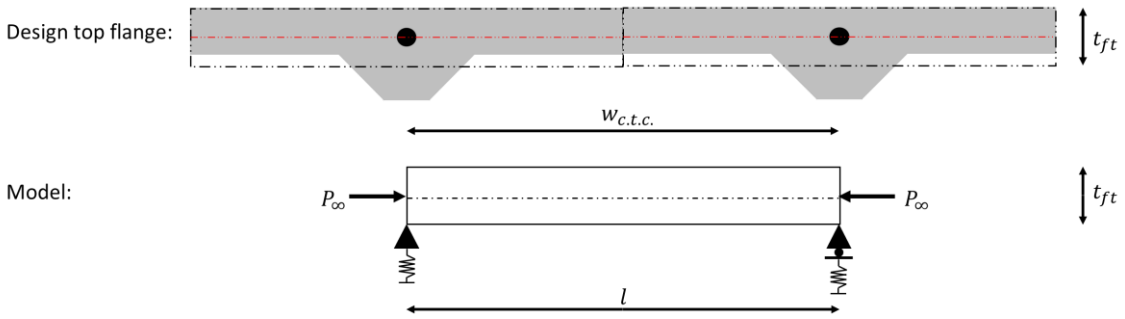


Figure 68 Model local verification top flange in longitudinal direction

The model is based on the following assumptions:

- The beam is modelled as in Figure 68 with a height of t_{ft}, a width of 1,0 m and a span equal to the centre-to-centre distance between the ribs: $l = w_{c.t.c.}$;
- No conventional longitudinal reinforcement is provided, the only reinforcement is from the steel fibres;
- The beam is prestressed by external prestressing force P_∞, which is assumed to act centrically on the top flange.

Note that the external prestressing force acting on the top flange depends on the self-weight of the beam and the prestressing force. For this reason, the compressive force is not constant over the beam length. It is at its maximum at mid span and at its minimum near the supports. If there is a tensile force present, which may occur at the supports, P_∞ is taken equal to zero.

Force distribution

To calculate the force distribution the same values for the loads are applied as in 7.2.3. To determine the bending moments the beam is regarded as a simply supported beam. In reality one could regard these supports as springs because the main beams deform as a whole, but this is not taken into consideration. The maximum bending moments occur at mid span and are:

$$M_G = \frac{1}{8} * G_k * l^2$$

$$M_Q = \frac{1}{4} * Q_k * l$$

The design value of the bending moments is calculated by assessing both equations 6.10a and 6.10b of Eurocode 0:

$$M_{Ed} = \{\gamma_G * M_G + \psi_0 * \gamma_Q * M_Q; \zeta * \gamma_G * M_G + \gamma_Q * M_Q\}$$

Assumptions

The verification in this section is based on the equations that have been derived to determine the bending moment capacity of unreinforced (i.e. no passive reinforcing steel) UHPC cross sections with or without external compressive force. Reference is made to annex VII for all derivations.

For unreinforced UHPC cross sections the maximum capacity is reached at the moment the outermost tensile fibre reaches a strain value of ε_{ctd}. The corresponding strain and stress distributions over the height of the cross section are as follows:

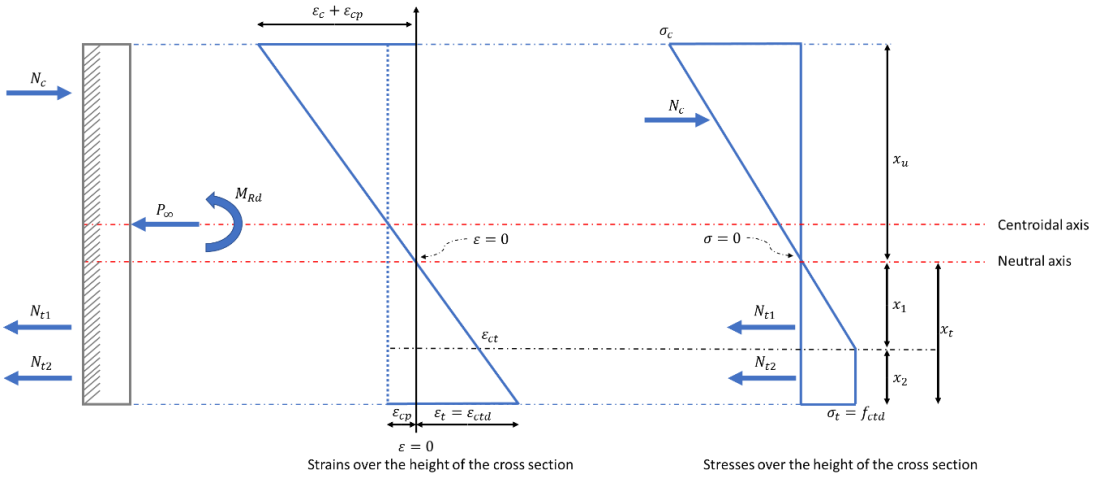


Figure 69 Stress and strain diagram in ULS for unreinforced UHPC beam with external compressive force

By including a compressive force, a larger bending moment can be achieved before the strain value of ε_{ctd} is reached in the outermost tensile fibre. Because the external axial force depends on the position along the beam, the capacity depends on it as well. For this reason, the verification is performed by analysing a section of the beam directly next to the support. The capacity is calculated on a number of intervals of 0,25 m apart. As a simplification it is assumed that the full prestressing forces $P_{m0,c}$ and $P_{m0,fb}$ are applied directly from the support, thus the transfer length is not taken into consideration.

Capacity at each point under consideration

At each point where the bending moment capacity is calculated a set of calculations is carried out. First the stresses at the centre of the top flange due to the self-weight of the beam and the prestressing are determined. This results in the external prestressing force at the point under consideration. If this force is a compressive force, this value will be included in further calculations while tensile forces are neglected, in such a case the capacity is calculated for a section without external forces.

At the moment the maximum capacity is reached the total compressive strain at the outermost compressed fibre is calculated using the following equation.

$$(\varepsilon_c + \varepsilon_{cp}) = \varepsilon_{cp} + \sqrt{\varepsilon_{cp}^2 + \frac{2 * f_{ctd} * \varepsilon_{ctd} - f_{ctd} * \varepsilon_{ct}}{E_{cm}} + 2 * \varepsilon_{cp} * \varepsilon_{ctd}} \qquad \text{Equation (34)}$$

Where ε_c is the compressive strain in most compressed fibre if no external compressive force is present. Using this strain value and the stress and strain relationships of Figure 69 the height of the compressive and tensile zones can be determined:

$$x_u = \frac{f_{ctd} * t_{ft} + \varepsilon_{cp} * E_{cm} * t_{ft}}{\frac{1}{2} * (\varepsilon_c + \varepsilon_{cp}) * E_{cm} + \frac{1}{2} * f_{ctd} * \frac{\varepsilon_{ct}}{\varepsilon_c + \varepsilon_{cp}} + f_{ctd}} \qquad \text{Equation (35)}$$

$$x_1 = \frac{\varepsilon_{ct}}{\varepsilon_c + \varepsilon_{cp}} * x_u \qquad \text{Equation (36)}$$

$$x_2 = t_{ft} - x_u - \frac{\varepsilon_{ct}}{\varepsilon_c + \varepsilon_{cp}} * x_u \qquad \text{Equation (37)}$$

For the derivation of these equations reference is made to annex VII. Using equations (35) to (37) the concrete compressive and tensile forces can be determined after which the bending moment capacity at the section under consideration follows from:

$$M_{Rd} = -N_c * \frac{1}{3} * x_u + N_{t1} * \left(x_u + \frac{2}{3} * x_1\right) + N_{t2} * \left(x_u + x_1 + \frac{1}{2} * x_2\right) + P_{m,\infty} * \frac{1}{2} * t_{ft} \quad \text{Equation (38)}$$

This procedure is carried out for all interval points and the results have been plotted in the following graph:

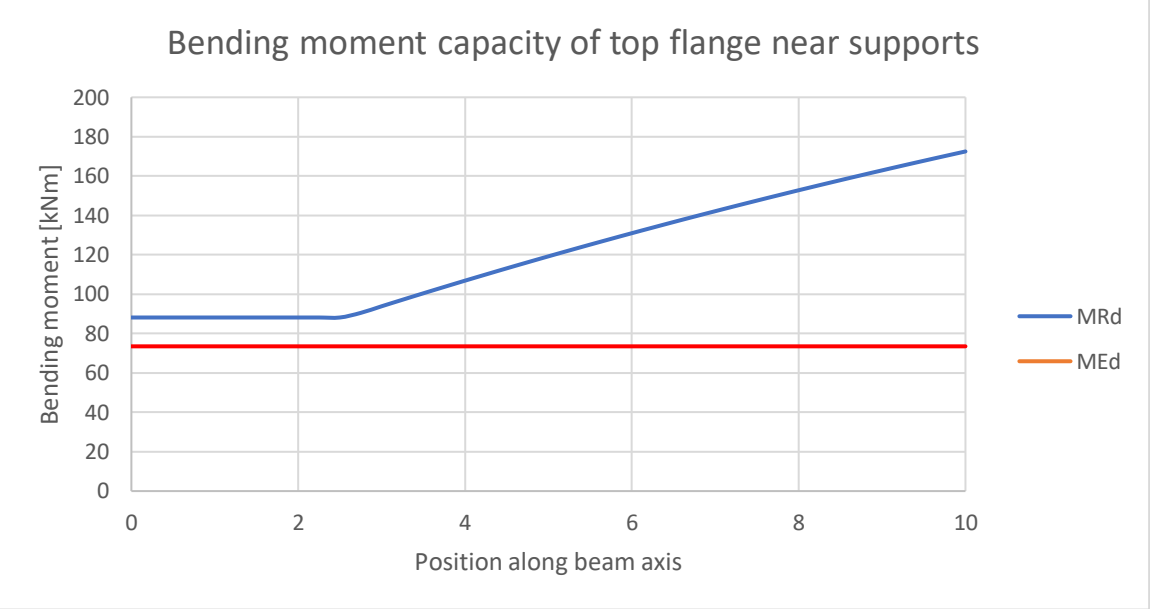


Figure 70 Bending moment capacity top flange in longitudinal direction near the support

The capacity of the top flange in longitudinal direction depends on the position along the beam axis and the section near the supports is governing because the expected compressive force in the top flange is the smallest in this region. From the graph it can be seen that also over the full length of this region the bending moment capacity is sufficient, at the most unfavourable position the unity check is $73{,}5/88{,}2 = 0{,}83$. Reference is made to annexes III and IV for the full elaboration of this verification.

7.4 Bibliography chapter seven

Braam, C. (2012). *Cement en beton 3 Constructieleer Voorgespannen Beton* (Vijfde herziene druk 2012 ed.). Aeneas.

Groupe de travail BFUP. (2013, June). Ultra High Performance Fibre-Reinforced Concretes. *Recommendations*. Association Francaise de Génie Civil.

NEN. (2011, november). NEN-EN 1992-1-1+C2. *Eurocode 2: Ontwerp en berekening van betonconstructies - Deel 1-1: Algemene regels en regels voor gebouwen*.

NEN. (2011, december). NEN-EN 1992-2+C1. *Eurocode 2: Ontwerp en berekening van betonconstructies - Betonnen bruggen - Regels voor ontwerp, berekening en detaillering*.

NEN. (2019, november). NEN-EN 1991-2+C1/NB. *Nationale bijlage bij NEN-EN 1991-2+C1: Eurocode 1: Belastingen op constructies – Deel 2: Verkeersbelasting op bruggen*.

NEN. (2020, februari). NEN-EN 1992-1-1+C2/NB+A1. *Nationale bijlage bij NEN-EN 1992-1-1+C2 Eurocode 2: Ontwerp en berekening van betonconstructies - Deel 1-1: Algemene regels en regels voor gebouwen*.

Walraven, J., & Braam, C. (2019, February). Prestressed Concrete.

8

DESIGN OF MAIN BEAMS – FATIGUE VERIFICATION

8.1 Fatigue verification

8.1.1 Importance of fatigue verification and approach

Importance of fatigue verification

In case of a typical concrete structure of conventional concrete fatigue failure is typically not expected to be the governing failure mode. The reason for this is that the stress cycles are relatively small because the loads due to the self-weight of the structure are relatively large compared to the cyclic variable loads.

During the thesis project it is strived for to design a UHPC deck that is as light as possible to achieve the goal of the project. By reducing the self-weight, the relative contribution of the variable loads to the total loads acting on the structure increases. For this reason, in this chapter specific attention is paid to fatigue failure.

Approach

The fatigue capacity of the concrete and prestressing steel of the main beams are verified for the governing cross section, which is for the middle beam at mid span. The first steps of the verification are the same for the steel and concrete:

- **Selecting suitable load model**: First a load model has to be selected which is appropriate for the verification. As discussed in 4.2.3 fatigue load model 1 (FLM1) from Eurocode 1-2 is selected, which can be used to determine the maximum and minimum stresses in the structure;

- **Formulating load combinations**: Because fatigue (FAT) is a different ultimate limit state than the static strength of the structure (STR) which was verified in the previous sections, different load combinations have to be formulated. Reference is made to 4.5.2 for details;

- **Determining force distributions (RFEM)**: Using the fatigue load model and load combinations the force distributions are determined using RFEM, the results are the input for the individual verifications of the steel and concrete.

The fatigue verification of the capacity of the material is material specific and will be covered in the final two sections of this chapter.

8.1.2 Load model & force distribution

The selection of the appropriate load model (FLM1) and the formulation of the load combinations is covered in chapter 4. The load combinations for fatigue are given in 8.3 of Eurocode 2-1-1. These provisions boil down to the formulation of two load combinations. One consists only of non-cyclic loads while the other also includes the cyclic load. By applying these two load combinations a stress range can be calculated.

The cross section under consideration is mid span. The stress range is deduced form the difference between the effects of the non-cyclic and cyclic loads. Because the cyclic loads have their maximum bending moment at mid span the largest stress range is expected to occur at this point. If the fatigue verification is satisfied for this point it also covers the verification of all other points along the length of the deck.

The application of the loads is covered in more detail in chapter 5. The configuration of FLM1 is the same as that of load model 1, the difference is the magnitude of the loads. Because for the ULS limit state configuration 2 as depicted in Figure 22 resulted in the governing bending moment (at the middle beam), this configuration has also been applied for fatigue load model 1. Note that the axle loads are positioned at midspan. This results in the following load configuration.

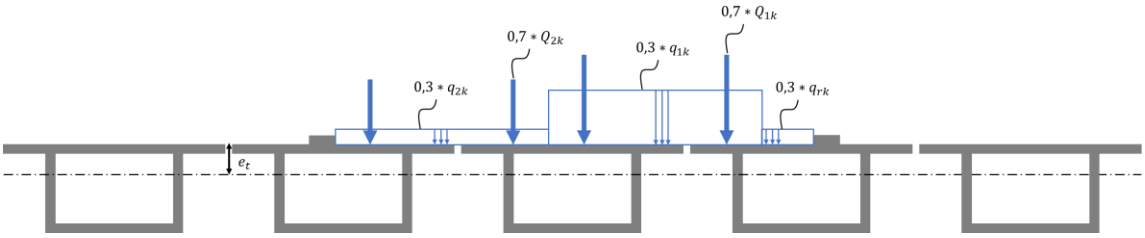


Figure 71 Configuration FLM1

The force distribution was subsequently determined using RFEM. The maximum value of the bending moment (combination including the cyclic load) is denoted as $M_{fat,\max}$ while the minimum value (combination without cyclic loads) is denoted as $M_{fat,min}$. The values can be found in 5.4.3.

8.1.3 Verification prestressing steel

Provisions from the codes

Before elaborating on the calculation, the relevant provisions from the codes are summarised. Fatigue verifications of prestressing steel are covered in section 6.8 of Eurocode 2-1-1, Eurocode 2-2 and their national annexes.

Single stress amplitude: For a single stress amplitude the fatigue damage may be calculated using the following S-N curve as given in the code:

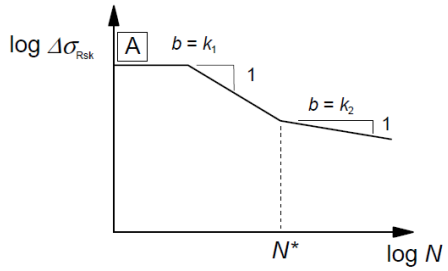


Figure 72 S-N diagram of reinforcing and prestressing steel – Eurocode 2, p.122

It subsequently has to be verified that:

$$\Delta\sigma * \gamma_{F,fat} \leq \frac{\Delta\sigma_{Rsk}}{\gamma_{S,fat}} \qquad \text{Equation (39)}$$

Note that according to 2.4.2.3 and 2.4.2.4 of the national annex to Eurocode 2-1-1 the factors $\gamma_{F,fat}$ and $\gamma_{S,fat}$ are 1,0 and 1,1 respectively.

Multiple stress amplitudes: In case multiple stress cycles occur with different amplitudes, the Palmgren-Miner rule is prescribed to determine the total damage:

$$D_{Ed} = \frac{\sum n(\Delta\sigma_i)}{N(\Delta\sigma_i)} < 1$$

Parameters S-N curve: For the parameters belonging to the S-N curve of prestressing steel the national annex refers to the following table, which is from Eurocode 2-1-1.

Tabel 6.4N — Parameters voor S-N-curven van voorspanstaal

S-N-curve van voorspanstaal gebruikt voor	N^*	Spanningsexponent		$\Delta\sigma_{Rsk}$ (MPa)
		k_1	k_2	bij N^* wisselingen
voorgerekt staal	10^6	5	9	185
nagerekt staal				
— enkelvoudige strengen in kunststofkanalen	10^6	5	9	185
— rechte of gebogen spanelementen in kunststofkanalen	10^6	5	10	150
— gebogen spanelementen in stalen kanalen	10^6	5	7	120
— koppelingen	10^6	5	5	80

Figure 73 Parameters S-N curve for prestressing steel – Eurocode 2-1-1, p.123

Note that when verifying the fatigue capacity of the prestressing steel the stresses should not exceed the yield strength of the material.

Fatigue verification prestressing steel

For the fatigue varication only the eccentric prestressing strands are assumed as this strand group will be governing above the centric prestressing. The calculation is summarized in this report. For the full elaboration reference is made to annexes III and IV.

Maximum and minimum stresses: Using the bending moments obtained from RFEM the maximum and minimum stresses in the prestressing steel are calculated. In order to this first the stress in the concrete adjacent to the centre lines of the tendons in the bottom flange is calculated:

$$\sigma_{c,min} = \frac{M_{fat,min} * e_p}{I_c} - \frac{P_{m,\infty,c}}{A_c} - \frac{P_{m,\infty,fb}}{A_c} - \frac{P_{m,\infty,fb} * e_P}{I_c}$$

$$\sigma_{c,max} = \frac{M_{fat,max} * e_p}{I_c} - \frac{P_{m,\infty,c}}{A_c} - \frac{P_{m,\infty,fb}}{A_c} - \frac{P_{m,\infty,fb} * e_P}{I_c}$$

The calculation is performed under the assumption of the cross section remaining plane and of strain compatibility between the steel and concrete. Under this assumption the steel stresses can be calculated from the concrete stresses by multiplying with the ratio in moduli of elasticity:

$$\sigma_{p,min} = \frac{E_p}{E_c} * \sigma_{c,min}$$

$$\sigma_{p,max} = \frac{E_p}{E_c} * \sigma_{c,max}$$

Stress range: The stress range found in the prestressing steel is the difference between the maximum and minimum value:

$$\Delta\sigma_p = \sigma_{p,max} - \sigma_{p,min}$$

The minimum stress value (largest compressive or lowest tensile stress) in the steel is -19,4 N/mm^2 while the maximum value (smallest compressive or largest tensile stress) is -5,2 N/mm^2. The difference $\Delta\sigma_p$ therefore is 14,1 N/mm^2.

Number of cycles: Only a single stress amplitude is considered, which means that the fatigue resistance is calculated following equation (39). The allowable stress depends on the number of cycles:

$$n = N_{obs} * n_{years}$$

Where:
N_{obs}: Number of heavy vehicles per year
n_{years}: Design service life

In section 3.1.2 the design service life was determined to be 100 years while in 4.2.3 the number of heavy vehicles per year was taken equal to $0{,}5 * 10^6$.

The table in Figure 73 gives the parameters for the S-N curve. For pretensioned steel the exponents k_1 and k_2 are 5 and 9 respectively. The stress $\Delta\sigma_{Rsk}$ is 185 N/mm^2 and corresponds to of N^* cycles ($1 * 10^6$) cycles. Using these parameters, the stress corresponding to the actual number of cycles is to be calculated. Because the actual number of cycles $n = 100 * 0{,}5 * 10^6 > N^* = 1 * 10^6$, this is done as follows, note that the partial factor is already included to directly obtain the design value:

$$\Delta\sigma_{Rsd} = \frac{\Delta\sigma_{Rsk}}{\gamma_{S,fat}} * \left(\frac{N^*}{n}\right)^{\frac{1}{k_2}} \rightarrow \frac{185}{1{,}1} * \left(\frac{1 * 10^6}{100 * 0{,}5 * 10^6}\right)^{\frac{1}{9}} = 108{,}9\ [MPa]$$

Using this result the verification of the fatigue capacity can be performed:

$$\Delta\sigma_p * \gamma_{F,fat} \leq \Delta\sigma_{Rsd} \rightarrow 14{,}1 * 1{,}0 < 108{,}9$$

The fatigue capacity of the prestressing steel is therefore sufficient.

8.1.4 Verification concrete

Provisions from the codes

Before elaborating on the calculation, the relevant provisions from the codes are summarised. Fatigue verifications of concrete are covered in section 6.8 of Eurocode 2-1-1, Eurocode 2-2 and their national annexes. Most information in this section is taken from Eurocode 2-2 as this focusses specifically on concrete bridges.

Verification of concrete: The Eurocode 2-2 prescribes that for the verification of concrete the miner rule has to be applied. For concrete under compression sufficient fatigue capacity may be assumed if:

$$\sum_{i=1}^{m} \frac{n_i}{N_i} \leq 1 \qquad \text{Equation (40)}$$

Where:
m: Maximum number of intervals with constant amplitude
n_i: Actual number of cycles with constant amplitude in interval 'i'
N_i: Maximum number of cycles with constant amplitude in interval 'i' that can be taken before failure

Number of cycles to failure: According to Eurocode 2-2 the number of cycles to failure at constant amplitude 'i', N_i, is calculated as follows:

$$N_i = 10^{14 * \frac{1 - E_{cd,max,i}}{\sqrt{1 - R_i}}} \qquad \text{Equation (41)}$$

In this equation:

$$R_i = \frac{E_{cd,min,i}}{E_{cd,max,i}}$$

$$E_{cd,min,i} = \frac{\sigma_{cd,min,i}}{f_{cd,fat}}$$

$$E_{cd,max,i} = \frac{\sigma_{cd,max,i}}{f_{cd,fat}}$$

The different symbols denote the following:
R_i: Stress ratio
$E_{cd,min,i}$: Minimum compressive stress level
$E_{cd,max,i}$: Maximum compressive stress level
$f_{cd,fat}$: Design value of fatigue strength of concrete
$\sigma_{cd,max,i}$: Highest stress in a cycle
$\sigma_{cd,min,i}$: Lowest stress in a cycle

Fatigue strength of concrete: The national annex to Eurocode 2-2 modifies the equation for the fatigue compressive strength of concrete compared to the main text of this code. One may use the following equation:

$$f_{cd,fat} = k_1 * \beta_{cc}(t_0) * f_{cd} * \left(1 - \frac{f_{ck}}{400}\right)$$

Where:
$\beta_{cc}(t_0)$: Factor for the strength of the concrete at the first load
t_0: Time in days from the start of the application of stress cycles onto the concrete
k_1: Factor, to be taken 1,0 except for parts loaded under water, in which case $k_1 = 0{,}85$.

The difference with the main text of Eurocode 2-2 is that the latter prescribes $f_{ck}/250$ instead of $f_{ck}/400$ in the final term of the equation. In (Fehling, Schmidt, Walraven, Leutbecher, & Fröhlich, 2014) the equation for the fatigue compressive strength is written as:

$$f_{cd,fat} = 0{,}85 * \beta_{cc}(t) * f_{ck} * \left(1 - \frac{f_{ck}}{40 * f_{ck0}}\right) * \frac{1}{\gamma_c} \qquad \text{Equation (42)}$$

Where:
f_{ct0}: 10 N/mm^2
$\beta_{cc}(t)$: Factor to allow for the increase of strength as the hydration progresses

In this source the difference between the equation given in Eurocode 2-2 and the corresponding national annex is also clarified further. By taking the term in the denominator equal to 40 instead of 25 it is prevented that the fatigue strength of the concrete is reduced within the range of very-high and ultra-high strength.

The difference between the given equation and the equation in the Eurocode is that the denominator has the term 40 instead of 25, this prevents a reduction of fatigue strength for concrete within the very high and ultra-high strength range.

Concrete strength at first load: The factor for the concrete strength at the moment of the first load, the value $\beta_{cc}(t)$, can be determined in accordance with 3.1.2 (6) of Eurocode 2-1-1:

$$\beta_{cc}(t) = \exp\left\{s\left[1 - \left(\frac{28}{t}\right)^{\frac{1}{2}}\right]\right\}$$

In this equation 't' denotes the age of the concrete in days and 's' is a coefficient depending on the type of cement. For an age of 28 days the factor β_{cc} 1,0.

AFGC-SETRA 2013: The guideline gives an additional requirement for elements in tension that are subjected to fatigue and that will be loaded in tension under service conditions. In persistent design situations the stresses under the frequent load combinations must be limited to:

$$\min\left(f_{ctm,el}; f_{ctfm}\right) \qquad \text{Equation (43)}$$

According to information from annex 12 of the guideline bending tests with cyclic loading leading to compressive and tensile stresses indicated that no irreversible damage occurs if the tensile stress remains smaller than the elastic limit strength $f_{ctm,el}$, which justifies this requirement.

Fatigue verification concrete

For the fatigue varication the top and bottom fibre of the cross section at midspan is analysed. The calculation is summarized in this report while for the full elaboration reference is made to annexes III and IV.

Fatigue strength: The fatigue strength is calculated in accordance with equation (42), taking $\beta_{cc}(t) = 1{,}0$ and $f_{ck0} = 10$ this results in 56,7 N/mm^2.

Calculating stress amplitude: The maximum and minimum compressive stress in the outer fibres of the concrete are subsequently calculated, $\sigma_{cd,max}$ is the largest compressive value while $\sigma_{cd,min}$ is the smallest compressive value (i.e. closest to zero). If $\sigma_{cd,min}$ is a tensile stress, then it is taken equal to zero and an additional verification is required.

- Top fibre:

$$\sigma_{cd,max} = -\frac{M_{fat,max}}{W_t} - \frac{P_{m,\infty,c}}{A_c} - \frac{P_{m,\infty,fb}}{A_c} + \frac{P_{m,\infty,fb} * e_P}{W_t} = -23{,}2\ [MPa]$$

$$\sigma_{cd,min} = -\frac{M_{fat,min} * e_p}{W_t} - \frac{P_{m,\infty,c}}{A_c} - \frac{P_{m,\infty,fb}}{A_c} + \frac{P_{m,\infty,fb} * e_P}{W_t} = -19{,}5\ [MPa]$$

- Bottom fibre:

$$\sigma_{cd,max} = \frac{M_{fat,min}}{W_b} - \frac{P_{m,\infty,c}}{A_c} - \frac{P_{m,\infty,fb}}{A_c} - \frac{P_{m,\infty,fb} * e_P}{W_b} = -4{,}1\ [MPa]$$

$$\sigma_{cd,min} = \frac{M_{fat,max} * e_p}{W_b} - \frac{P_{m,\infty,c}}{A_c} - \frac{P_{m,\infty,fb}}{A_c} - \frac{P_{m,\infty,fb} * e_P}{W_b} = 0{,}0\ [MPa]$$

Note that compressive stresses are taken positive for the remainder of the fatigue verification. The minimum stress in the bottom fibre gave a tensile stress of $5{,}8 * 10^{-3}$ N/mm^2, which is by approximation zero.

Maximum number of cycles at calculated stress amplitude: Using equation (41) the maximum number of cycles at the calculated stress range until failure can be calculated, both for the top and bottom fibre. This results in $4{,}41 * 10^{20}$ cycles for the top fibre and $9{,}85 * 10^{12}$ for the bottom fibre.

Fatigue verification: The number of cycles for which has to be designed has already been determined in the fatigue calculation of the prestressing steel. Because only one stress amplitude is found Miner's rule in equation (40) is simplified to:

$$\frac{n}{N} \leq 1{,}0$$

This has to hold for both the top and bottom fibres. For both of these verifications a value found which is by approximation equal to zero, this criterion has therefore been satisfied.

Additional verification: The AFGC-SETRA 2013 guideline gives an additional verification for elements in tension under service conditions, which prescribes that in the persistent design situations the tensile stresses under the frequent load combination should satisfy equation (43). The prestressing of the beam has been designed as such that the tensile stresses under the characteristic combination are smaller than 6,7 N/mm^2, see equation (17) in section 6.2.4. Because this condition is more stringent than the condition in equation (43), the latter is automatically satisfied and not covered separately.

8.2 Bibliography chapter nine

Fehling, E., Schmidt, M., Walraven, J., Leutbecher, T., & Fröhlich, S. (2014). *Ultra-High Performance Concrete UHPC*. Berlin: Wilhelm Ernst & Sohn.

Groupe de travail BFUP. (2013, June). Ultra High Performance Fibre-Reinforced Concretes. *Recommendations*. Association Francaise de Génie Civil.

NEN. (2011, november). NEN-EN 1992-1-1+C2. *Eurocode 2: Ontwerp en berekening van betonconstructies - Deel 1-1: Algemene regels en regels voor gebouwen*.

NEN. (2011, december). NEN-EN 1992-2+C1. *Eurocode 2: Ontwerp en berekening van betonconstructies - Betonnen bruggen - Regels voor ontwerp, berekening en detaillering*.

NEN. (2016, november). NEN-EN 1992-2+C1/NB. *Nationale bijlage bij NEN-EN 1992-2+C1 Eurocode 2: Ontwerp en berekening van betonconstructies - Betonnen bruggen - Regels voor ontwerp, berekening en detaillering*.

NEN. (2020, februari). NEN-EN 1992-1-1+C2/NB+A1. *Nationale bijlage bij NEN-EN 1992-1-1+C2 Eurocode 2: Ontwerp en berekening van betonconstructies - Deel 1-1: Algemene regels en regels voor gebouwen*.

9

DESIGN OF MAIN BEAMS – SERVICEABILITY LIMIT STATE

9.1 Serviceability limit state

9.1.1 Deflections

Calculating deflections

In this section the deflection of the bridge is calculated. Section 7.4 of the Eurocode 2 covers deflections, the main principle is that deflections should be limited as such that the functionality (or aesthetics) of the structure are influenced negatively.

The deflections are calculated using the frequent load combination in the SLS, see 4.5.4. The deflections are calculated in two ways. The first approach gives an upper bound of the deflection by performing a hand calculation using standard engineering formulas and which is based on more conservative assumptions. These calculations are performed to validate the results of the second approach, which is the use of RFEM.

Assumptions

Both the hand calculation and the calculation using RFEM makes use of the following two assumptions.

Effective modulus of elasticity: Conforming the AFGC-SETRA 2013 guideline the modulus of elasticity E_{cm} of the concrete is replaced by an effective modulus of elasticity $E_{c,eff}$ to account for the increase of deformation due to long term effects. This value is calculated as follows:

$$E_{c,eff} = \frac{E_{cm}}{1+\varphi}$$

This reduction is applied to all loads to cover all potential increases of deflection that my occur during the service life of the structure, e.g. due to creep, shrinkage, reduction of stiffness due to cracking by unexpected causes, etc.

Maximum deflection: A maximum value of the deflection has to be defined, the following value has been chosen:

$$\delta_{max} \leq \frac{l}{300} \rightarrow \frac{68.000}{300} = 226{,}7\ [mm]$$

Upper limit – Hand calculation

First a simple calculation is performed using standard engineering formulas to obtain a first impression of the deflections. Conservative assumptions are used, this way an upper limit of the deflections is calculated.

Loads: The following loads are taken into consideration:

- The self-weight and permanent loads of the beam are $G_{k,total} = G_{k,beam} + b_{eff,i} * G_{k,surf}$;
- For the prestressing the working prestressing in the bottom flange, $P_{m,\infty,fb}$, is used;
- Variable load.

It is assumed that no interaction between the beams takes place. By following this approach and by applying load configuration 3 with the axle loads at mid span, see Figure 23, the maximum value (upper limit) of the deflection is found. This occurs at mid span of the middle beam. Note that for the variable traffic load the factor $\psi_1 = 0{,}8$ is applied because the frequent load combination in the SLS is used, see 4.5.4.

Deflection due to each load: The contribution of each action to the total deflection is calculated using standard engineering formulas is subsequently calculated.

- Self-Weight and permanent loads ($G_{k,total}$):

$$\delta_G = \frac{5 * G_{k,total} * l^4}{384 * E_{c,eff} * I_y} = 255{,}3\ [mm]$$

- Upward bending due to the prestressing ($P = P_{m,\infty} * e_p$):

$$\delta_P = \frac{P_{m,\infty} * e_p * l^2}{8 * E_{c,eff} * I_y} = 232{,}4\ [mm]$$

- Uniformly distributed component of variable load ($\psi_{1,1} Q_{k,1} = 0{,}8 * Q_{k,UDL}$):

$$\delta_{Q,UDL} = \frac{5 * (0{,}8 * Q_{k,UDL}) * l^4}{384 * E_{c,eff} * I_y} = 129{,}5\ [mm]$$

- Concentrated load due to axles ($\psi_{1,1} Q_{k,1} = 0{,}8 * 2 * Q_{k,axle}$):

$$\delta_{Q,axle} = \frac{0{,}8 * 2 * Q_{k,axle} * l^3}{48 * E_{c,eff} * I_y} = 66\ [mm]$$

Total deflection: The total deflection at mid span of the middle beam is calculated by adding up the individual components. Note that upward bending is taken as a negative value:

$$\delta_{tot} = \delta_G - \delta_P + \delta_{Q,UDL} + \delta_{Q,axle}$$

$$w_{tot} = 255{,}3 - 232{,}4 + 129{,}5 + 66 = 218{,}4\ [mm]$$

The total resulting deflection is 218,4 mm (downwards), which is smaller than the maximum value of 226,7 mm, this criterion is therefore satisfied.

RFEM calculation

After determining this upper bound value, a more elaborate verification is performed using RFEM.

Modelling: In addition, the deflections have been calculated using RFEM. In 5.4.5 the load combinations used for this calculation have been determined. After calculating the deflection for these individual load combinations, the governing value was determined.

Using this way of modelling different load configurations can be analysed while the interaction between the beams is also taken into consideration. Because of the latter a smaller deflection should be found than the value calculated using the standard engineering formulas.

Also note that the RFEM model is more 'complete', more load cases are included. Loads such as the railing, variable loads on the pedestrian lanes, kerbs, etc., were not included in the hand calculation. In the load combinations used to determine the deflections the modulus of elasticity of the UHPC was reduced by a factor of:

$$\frac{1}{1+\varphi} \rightarrow \frac{1}{1{,}3} = 0{,}77$$

This way the effective modulus of elasticity is also included in the RFEM calculation.

Results: The total deflection found using RFEM is 344,4 mm. This does not include the upward bending due to the prestressing, which was calculated to be 232,4 mm. The resulting deflection is:

$$344{,}4 - 232{,}4 = 112{,}0 < 226{,}7\ [mm]$$

The deflection is indeed smaller than the value found in the hand calculation, thus verifying the RFEM result. For both calculations the results are smaller than the maximum value, the deflection criterion has therefore been satisfied.

9.1.2 Crack width

Crack width verifications are covered in sections 7.3 of Eurocode 2-1 and the AFGC-SETRA 2013 guideline. The main reason of performing crack width calculations is that excessive cracking negatively influences the functionality and durability of the structure. At the same time the aesthetics of the structure should remain acceptable as well.

According to (10) of 7.3.1 of the AFGC-SETRA 2013 guideline it is not required to verify the crack widths of elements made of UHPC with average and characteristic strain hardening constitutive laws. Because this is assumed to hold true for the material used for the main beams the verification can therefore be omitted. However, the section on crack width of the guideline contains useful information to determine the maximum allowable tensile strength in the beams, which is determined next.

In the guideline a certain maximum allowable crack width w_{max} is given, by limiting the crack width to this value the durability of the steel fibres and reinforcement is ensured:

Classe d'exposition *Exposure class*	Eléments en BFUP armé et éléments en BFUP précontraint à armatures non adhérentes *Reinforced UHPFRC members and prestressed UHPFRC members with unbonded tendons*	Eléments en BFUP précontraint à armatures adhérentes *Prestressed UHPFRC members with bonded tendons*	Eléments en BFUP non armé et non précontraint *Non-reinforced and non prestressed UHPFRC members*
AN de l'EC2 NA of EC2	Combinaison quasi-permanente des charges *Quasi-permanent load combination*	Combinaison fréquente des charges *Frequent load combination*	Combinaison caractéristique des charges *Characteristic load combination*
X0, XC1	0,3	0,2	0,3 combinaison caractéristique et 0,3 combinaison fréquente *0.3 characteristic load combination and 0.3 frequent load combination*
XC2, XC3, XC4	0,2 (*) (**)	0,1 (*)	0,2 (*) combinaison caractéristique et 0,05 combinaison fréquente *0.2 (*) characteristic load combination 0.05 frequent load combination*
XD1, XD2, XS1, XS2, XS3	0,1 (*) (**)	Limitation traction à 2/3.min($f_{ctm,el}$, f_{ctfm}/K) *Limitation of tensile stress to 2/3.min($f_{ctm,el}$, f_{ctfm}/K)*	0,1 (*) combinaison caractéristique et 0,05 combinaison fréquente *0.1 (*) characteristic load combination 0.05 frequent load combination*

Figure 74 Recommended values wmax - AFGC-SETRA 2013, p.119

Given the exposure classes as determined in 3.2.3 (XC4 and XD3) and the type of structure (prestressed UHPC with bonded tendons) the decision is made to apply the requirement that under the frequent load combination the tensile stresses should be limited to a value of:

$$\sigma_{t,max} = \frac{2}{3} * \min\left\{f_{ctm,el}; \frac{f_{ctfm}}{K}\right\}$$

In this equation '$f_{ctm,el}$' represents the mean limit of elasticity under tension (i.e. the mean value elastic tensile strength) and 'f_{ctfm}' represents the mean maximum post-cracking stress (peak value).

None of these stress values have been defined as parameters, they are not listed in the overview of 2.3.1. However, according to (Fehling, Schmidt, Walraven, Leutbecher, & Fröhlich, 2014) the use of the following equation is also justified for UHPC, despite the fact that its properties are different from conventional strength concrete for which this equation is given in Eurocode 2:

$$f_{ctm} = 0{,}3 * f_{ck}^{\frac{2}{3}} \rightarrow 0{,}3 * 200^{\frac{2}{3}} \approx 10\ [N/mm^2]$$ Equation (44)

For f_{ctfm} no equation is given, the parameter depends on the mixture composition. Given the range of values found in literature and the fact that a strain hardening material is assumed it is realistic and justifiable to assume that the value of f_{ctfm}/K will be at least equal to that of $f_{ctm,el}$. Hence the stress limit is taken as:

$$\sigma_{max} = \frac{2}{3} * 10 = 6{,}7\ [N/mm^2]$$

This stress value will be applied for the design of the prestressing of the main beams, as is shown in equation (17) in section 6.2.4. Instead of applying the frequent combination in the SLS, the characteristic combination was used in this calculation, which is more stringent.

9.1.3 Cracking bending moment

As discussed in 6.2.1 the non-brittleness of the cross section has to be verified as well. This means that the elastic bending moment in the uncracked section should be smaller than the ultimate bending moment capacity. The cracking bending moment of the cross section is calculated as follows:

$$M_{cr} = \left(f_{ctm} + \frac{P_{m,\infty,c} + P_{m,\infty,fb}}{A_c}\right) * W_{min}$$

In this equation $W_{min} = \min\{W_t; W_b\}$ and f_{ctm} follows from equation (44). This results in a cracking bending moment of 23.917 kNm, which is smaller than the ultimate bending moment of 38.756 kNm. The non-brittleness condition is therefore satisfied.

9.1.4 Vibrations

Vibrations also play a role in the design of bridges and this aspect is of particular importance to very slender or light bridges. The importance of this aspect has to be acknowledged, but it is not expected that this criterion would be governing for the detailed design as presented in this report. The slenderness of the concrete deck is relatively low and its weight is relatively high compared to structures for which vibrations do play a predominant role, such as slender steel decks or pedestrian bridges. Therefore, the aspect of vibrations is not further considered in the design.

9.2 Bibliography chapter nine

Fehling, E., Schmidt, M., Walraven, J., Leutbecher, T., & Fröhlich, S. (2014). *Ultra-High Performance Concrete UHPC*. Berlin: Wilhelm Ernst & Sohn.

Groupe de travail BFUP. (2013, June). Ultra High Performance Fibre-Reinforced Concretes. *Recommendations*. Association Francaise de Génie Civil.

NEN. (2011, november). NEN-EN 1992-1-1+C2. *Eurocode 2: Ontwerp en berekening van betonconstructies - Deel 1-1: Algemene regels en regels voor gebouwen*.

NEN. (2020, februari). NEN-EN 1992-1-1+C2/NB+A1. *Nationale bijlage bij NEN-EN 1992-1-1+C2 Eurocode 2: Ontwerp en berekening van betonconstructies - Deel 1-1: Algemene regels en regels voor gebouwen*.

Walraven, J., & Braam, C. (2019, February). Prestressed Concrete.

10

DESIGN OF END CROSS BEAM

10.1 Design of the end cross beam

10.1.1 Goal and assumptions

In this chapter the design of the post-tensioned end cross beam is discussed. The function of the beam is to restrain the ends of the prefab beams. In combination with the transverse post tensioning in the top flange this results in a solid deck structure.

The main goal of this chapter is to determine the required prestressing and to demonstrate that the cross section of the beam in combination with the prestressing results in sufficient bending moment and shear capacity. No other verifications are included in the chapter, given the large cross section deflections are not expected to exceed the limit while it also provides the possibility to accommodate measures such as reinforcement should this turn out to be required if more detailed calculations are carried out (e.g. splitting reinforcement, etc.).

In the analysis of the beam the following assumptions are made:

- The beam has a rectangular cross section and it is analysed as if the beam is solid over the full width of the deck (the presence of the beam ends of the prefab beams is neglected);
- The height and width of the beam are equal to the height of the prefab beams, see 2.2.2;
- An equal number of prestressing tendons is positioned at both sides of the beam, the resultant prestressing is therefore acting centrically onto the beam, see Figure 9;
- For the design of the prestressing the requirement is that no tensile stresses are allowed to occur over the cross section under service conditions (full prestressing).

The latter requirement is formulated to prevent cracking of the beam. The normal strength concrete applied for the end cross beam has a less optimal durability performance compared to the UHPC applied for the main beams. By imposing a more stringent criterion and thus preventing tensile stresses using a sufficiently large prestressing force, the durability of the end cross beams is ensured.

10.1.2 Input parameters

The input parameters for the calculation are summarized in 2.2.2 (dimensions), 2.3.2 (concrete properties) and 2.3.4 (prestressing). Two parameters require additional clarification, being the creep factor and the shrinkage of the concrete.

Shrinkage

Shrinkage and creep are covered in section 3.14 of Eurocode 2-1-1. The total shortening due to shrinkage is calculated as follows:

$$\varepsilon_{cs} = \varepsilon_{cd} + \varepsilon_{ca}$$

Where:
ε_{cs}: Total shortening due to shrinkage
ε_{cd}: Contribution to shortening due to drying shrinkage
ε_{ca}: Contribution to shortening due to autogenous shrinkage

Different components: In the Eurocode approach two contributions can be distinguished: autogenous shrinkage and drying shrinkage. Drying shrinkage is caused by the drying of the concrete element, it is dependent on outside influences and can continue for long periods of time. This is expected to be the case given the large dimensions of the end cross beam. Autogenous shrinkage is related to the hydration process, therefore most of the autogenous shrinkage occurs within the first few days after casting the concrete.

The shrinkage is calculated to determine the time dependent prestress losses. Because the prestressing is not applied within the first few days after casting, this value will not be taken into consideration. Most of the autogenous shrinkage will have occurred before the prestressing is applied, thus hardly influencing the end result. In the calculation of the prestress losses the total shrinkage is thus taken equal to the drying shrinkage.

Drying shrinkage: The end value for drying shrinkage $\varepsilon_{cd,\infty}$ is determined as follows:

$$\varepsilon_{cd,\infty} = k_h * \varepsilon_{cd,0}$$

Where:
k_h: Coefficient that depends on the fictitious thickness h_0
$\varepsilon_{cd,0}$: Nominal unrestrained drying shrinkage

Values for the unrestrained drying shrinkage can be deduced from a table given in the code, but it can also be calculated by using equations from annex B of Eurocode 2-1-1. Because the equations are performed using Excel the latter approach has been chosen. The nominal unrestrained drying shrinkage is calculated as follows:

$$\varepsilon_{cd,0} = 0{,}85 * \left[(220 + 110 * \alpha_{ds1}) * \exp\left(-\alpha_{ds2} * \frac{f_{cm}}{f_{cmo}}\right)\right] * 10^{-6} * \beta_{RH}$$

Where:
f_{cm}: Average compressive strength
f_{cmo}: 10 MPa
α_{ds1}: Coefficient depending on the cement type (3 for S, 4 for N and 6 for R)
α_{ds2}: Coefficient depending on the cement type (0,13 for S, 0,12 for N and 0,11 for R)

Cement type N is applied in the calculations. If it is subsequently assumed that for outside conditions the relative humidity is 80%, then the factor β_{RH} is calculated as follows:

$$\beta_{RH} = 1{,}55 * \left[1 - \left(\frac{RH}{RH_0}\right)^3\right] \rightarrow 1{,}55 * \left[1 - \left(\frac{80}{100}\right)^3\right] = 0{,}76$$

The second term that is to be determined is the factor k_h, which depends on the fictitious thickness h_0:

$$h_0 = \frac{2 * A_c}{u}$$

Where:
A_c: cross sectional area
u: Circumference of the cross section exposed to drying (i.e. in contact with the atmosphere)

The largest circumference where the concrete is in contact with the atmosphere is found underneath the outstand flanges. At these parts, once casted and hardened, three sides of the beam are in contact with the

atmosphere. Only the top side is covered by the top flange of the prefab beams. Under the assumption that the height and width of the beam are equal, this results in:

$$h_0 = \frac{2 * A_c}{u} \rightarrow \frac{2 * h_{cb} * w_{cb}}{h_{cb} + w_{cb} + h_{cb}} \rightarrow \frac{2 * h_{cb}^2}{3h_{cb}} = \frac{2}{3} * h_{cb}$$

This results in $h_0 = 1433$ mm. From the following table the factor k_h is subsequently determined: the result is $k_h = 0{,}70$. A low value was to be expected, the large fictitious thickness indicates that the full value of the nominal unrestrained drying shrinkage will not be achieved given the large cross section.

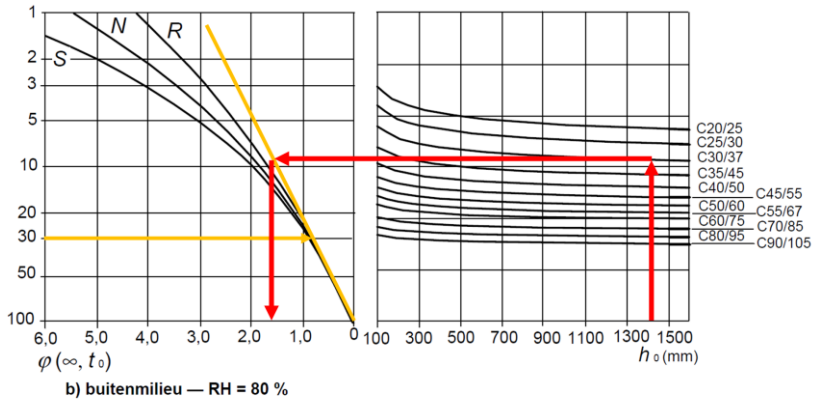
Tabel 3.3 — Waarden voor k_h in vergelijking (3.9)

h_0	k_h
100	1,0
200	0,85
300	0,75
≥ 500	0,70

Figure 75 Factor kh – Eurocode 2-1-1, p.34

Creep

The creep coefficient can be determined using the provisions as given in 3.1.4. For the calculation of the prestressing the creep factor for $t \rightarrow \infty$, i.e. $\varphi(\infty, t_0)$, is required. This value can be determined using the following graph:



b) buitenmilieu — RH = 80 %

Figuur 3.1 — Methode voor de bepaling van de kruipcoëfficiënt $\varphi(\infty, t_0)$ voor beton onder normale milieu-omstandigheden

Figure 76 Determining the creep factor – Eurocode 2-1-1, p.32

Where:
t_0: Age of concrete in days at moment of loading
h_0: Fictitious thickness

It is assumed that the prestressing is applied at $t = 28$ days, the graph of 30 days is applied for simplicity. The fictitious thickness is determined in the previous section on shrinkage. Curve 'N' (normal rate of hydration) is assumed. The curve for outside conditions (RH=80%) is chosen. The value of the creep factor is rounded off to $\varphi(\infty, t_0) = 1{,}75$.

10.2 Design of the prestressing

10.2.1 Calculating prestress losses

Using the assumptions for the prestressing as described in 2.3.4 the prestress losses are calculated. The approach is similar to that of the transverse prestressing as given in 7.2.2, which is also post tensioned. One difference is the calculation of the elastic losses because in case of the end beams multiple tendons are applied whereas in the case of the top flange only a single tendon was present at each section of the deck.

The elastic losses are calculated using the following equation. Because the four tendons might not be stressed simultaneously, the elastic losses are calculated using the total value of the losses:

$$\Delta P_{el} = n_{ducts} * \frac{(n_{ducts} - 1)}{2} * \frac{P_{max}}{n_{ducts}} * \frac{E_p A_p}{n_{ducts} E_{cm} A_c}$$

Where:

$$A_p = n_{ducts} * n_{strands} * A_{p_{strand}}$$

$$P_{max} = A_p * \sigma_{p,max}$$

Note that n_{ducts} appears in the denominator twice because P_{max} is calculated in Excel considering all tendons simultaneously (the total maximum prestressing force) while the elastic loss is calculated using the maximum force and cross section A_p of the individual tendons. By dividing by the number of tendons this is corrected for in the calculations.

As done for the top flange the initial prestressing force $P_{m0}(x)$ and direct losses are calculated at a large number of points along the width of the deck. Subsequently the mean value of the initial prestressing force $P_{m0}(x)$ over the width of the deck is calculated by applying equation (33). This results in a mean value for the initial prestressing force, P_{m0}, which is applied for the remainder of the calculation, a simplification which is deemed to be sufficiently accurate for this design stage. As a result of this simplification also one value for the time dependent losses is found, instead of a value dependent on the coordinate 'x' along the width of the deck.

The following graph summarizes the results by giving the maximum prestressing force P_{max}, the initial prestressing force $P_{m0}(x)$ (as a function of the coordinate 'x'), the mean value of the initial prestressing force P_{m0} and the working prestressing force $P_{m,\infty}$ (calculated using the mean value of the initial prestressing force) along the width of the deck.

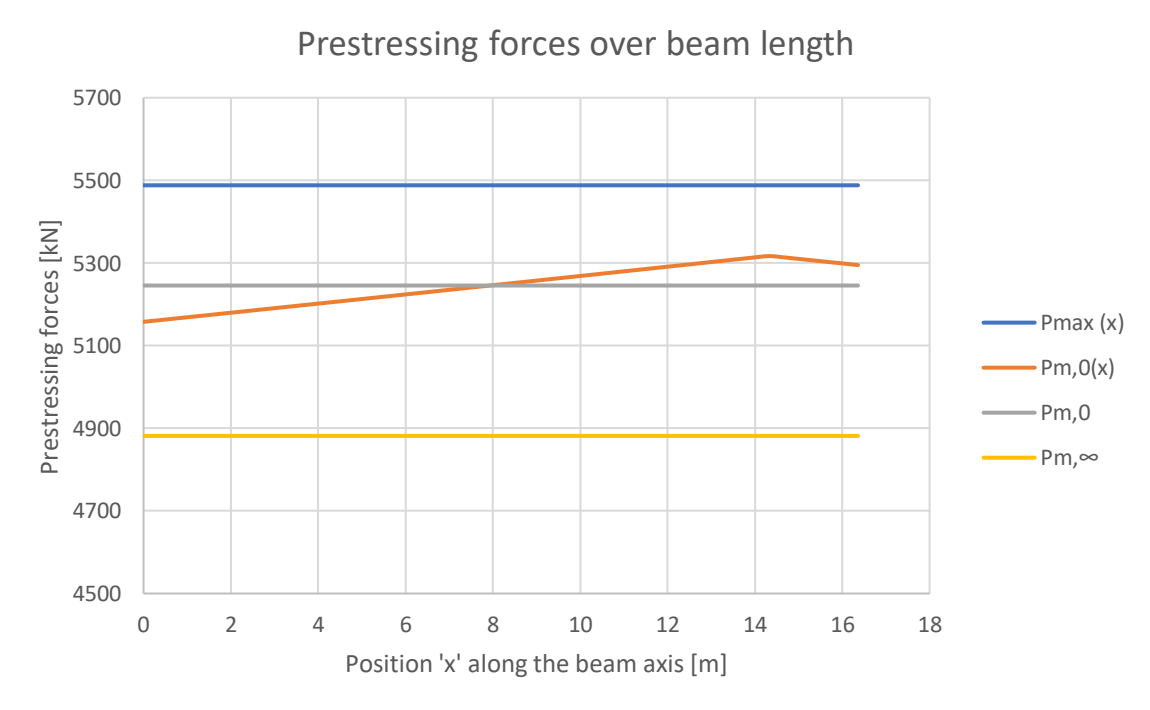


Figure 77 Prestressing forces along the length of the end cross beam

The working prestressing force equals 4881 kN, which implies a working prestress of 1245 N/mm^2 in the steel and a loss of approximately 11 %.

10.2.2 Determining stresses over beam height

Using the working prestressing values and the bending moments calculated using RFEM it has to be verified if the cross section is kept under compression. This analysis is performed for the governing value of the hogging and sagging bending moment (these values are determined using RFEM) and the stresses are for both cases calculated in the top and bottom fibres.

- Hogging bending moment:

$$\sigma_{t,hog} = \frac{M_{E,hog}}{W_{cb}} - \frac{P_{m,\infty}}{A_{cb}} \leq 0$$

$$\sigma_{b,hog} = -\frac{M_{E,hog}}{W_{cb}} - \frac{P_{m,\infty}}{A_{cb}} \leq 0$$

- Sagging bending moment:

$$\sigma_{t,sag} = -\frac{M_{E,sag}}{W_{cb}} - \frac{P_{m,\infty}}{A_{cb}} \leq 0$$

$$\sigma_{b,sag} = \frac{M_{E,sag}}{W_{cb}} - \frac{P_{m,\infty}}{A_{cb}} \leq 0$$

The results are given in the following graphs, which show the stresses over the height of the beam for the hogging and sagging bending moment.

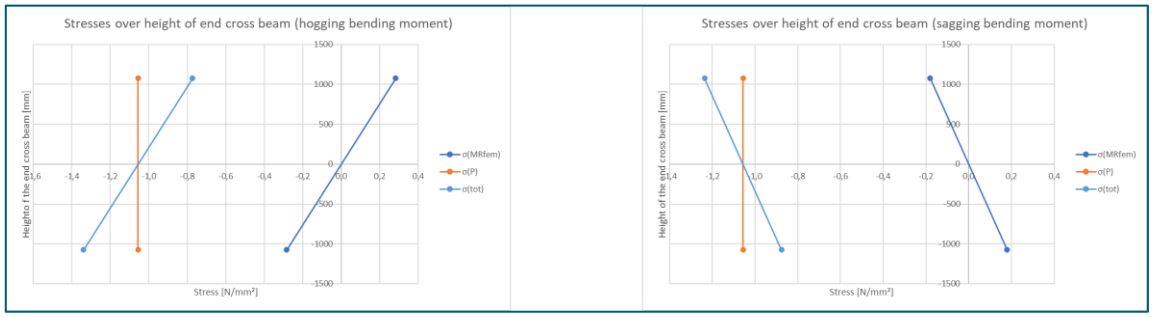


Figure 78 Stresses end cross beam over height of the cross section

It can be seen that for both the hogging and sagging bending moment the cross section is kept under compressive stress, the prestressing is thus sufficient for this requirement. For the full calculation procedure of the prestressing reference is made to annexes III and IV.

Note that the compressive stress is relatively large. The amount of prestressing applied to the beam is larger than required for this criterion. The reason for applying this large amount of prestressing is to obtain a larger height for the concrete compressive zone in the ULS verification. This way the maximum tensile strain of the prestressing steel, which is governing over the compressive strain of the concrete, is not exceeded before the strain value ε_{cu3} in the concrete is reached.

10.3 Ultimate limit state verifications

10.3.1 Verification bending moment capacity

The bending moment capacity in the ultimate limit state is calculated following largely the same procedure as applied for the main beam. In the ULS the following (simplified) strain and stress distributions are assumed to occur over the height of the end cross beam:

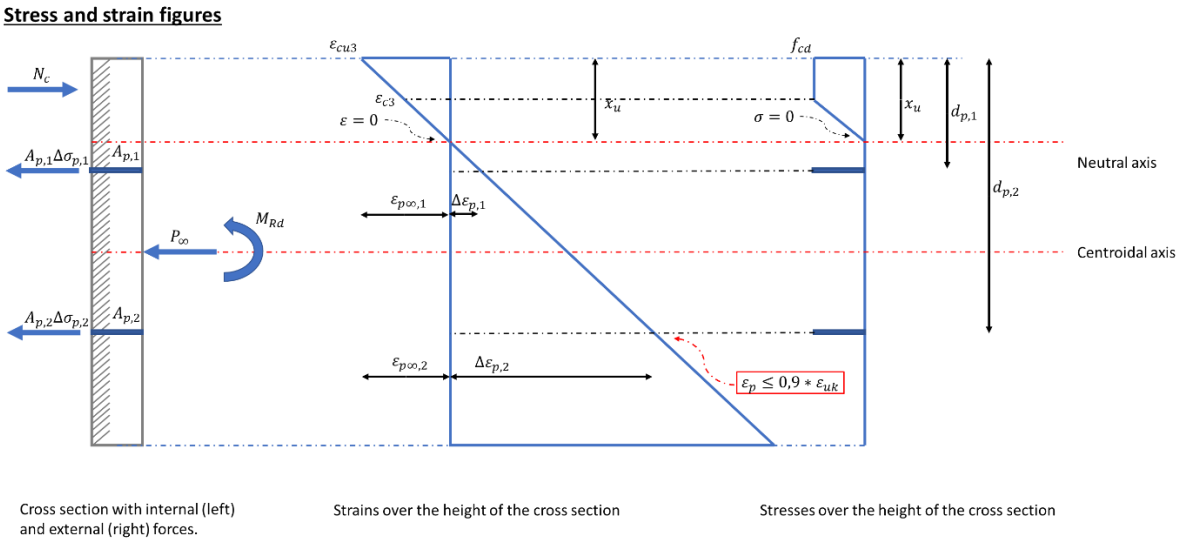


Figure 79 Assumed stress and strain distributions over the beam height in the ULS

The design value of the bending moment is the maximum of the hogging and sagging bending moment in the ULS, which have been calculated using RFEM: $M_{Ed} = M_{Ed,RFEM} = \max\{M_{Ed,hog}; M_{Ed,sag}\}$. Subsequently the following criterion has to be satisfied:

$$UC = \frac{M_{Ed}}{M_{Rd}} \leq 1{,}0 \rightarrow \frac{1212}{6416} = 0{,}19$$

The bending moment capacity is sufficient. In addition, the rotation capacity has to be verified, which is done as follows:

$$\frac{x_u}{d_{p_{ave}}} \leq \frac{500}{500 + f}$$

In this equation the effective height is taken as the average value of the upper and lower prestressing strands. This results in:

$$0{,}18 \leq 0{,}53$$

This criterion is therefore satisfied. For the full calculation procedure of the bending moment capacity and rotation capacity reference is made to annexes III and IV.

10.3.2 Verification shear force capacity

The shear force capacity is verified by applying the equations from Eurocode 2-1-1 for elements without shear reinforcement. It is assumed that no longitudinal reinforcement is present either, which is why the capacity of the cross section may be calculated using the equation for the minimum value:

$$V_{Rd,c} = \left(v_{min} + k_1 * \sigma_{cp}\right) * b_{cb,nom} * d_{p,2} \qquad \text{Equation (45)}$$

In this equation the effective height is taken equal to the effective height of the lower prestressing strand. Because tendons are present it should be verified if a reduction of the width is required. Because $\emptyset_{Duct} < w_{cb}/8$ the nominal width may be taken equal to the full width of the beam. The other symbols from equation (45) are:

$$k = 1 + \sqrt{\frac{200}{d_{p,2}}} \leq 2{,}0$$

$$v_{min} = 0{,}035 * k^{1{,}5} * \sqrt{f_{ck}}$$

$$\sigma_{cp} = \frac{P_{m,\infty}}{A_{cb}} \leq 0{,}2 * f_{cd}$$

This results in a minimum value of the concrete capacity of $V_{Rd,c} = 1562$ kN.

In addition, it has to be verified that the upper limit of the capacity is not exceeded, which is dictated by the failure of the concrete compressive strut:

$$V_{Rd,max} = \alpha_{cw} * b_{cb,nom} * z * v_1 * f_{cd} * \frac{1}{\cot(\theta) + \tan(\theta)} \quad \text{Equation (46)}$$

In this equation the factor $z \approx 0{,}9 * d_{p,2}$, the factor α_{cw} is a factor accounting for the stress state in the compressive strut and v_1 is a reduction factor for concrete cracked due to shear. This results in capacity $V_{Rd,max}$ of 11.683 kN.

The shear resistance of the cross section is taken equal to:

$$V_{Rd} = \min\{V_{Rd,c}; V_{Rd,max}\} = 1562\ kN$$

The following verification has subsequently to be verified:

$$UC = \frac{V_{Ed}}{V_{Rd}} \leq 1{,}0 \rightarrow \frac{837}{1562} = 0{,}54$$

The shear force capacity is sufficient. For the full calculation procedure of the shear force capacity reference is made to annexes III and IV.

10.3.3 Force introduction

A point not considered in detail but worth mentioning is the connection or transition between the solid beam end beam and the slenderer cross section of the prefab beam. At both ends of the deck solid end beams are present, these beams are formed by the solid ends of the prefab beams and the solid infill in between the beams. These components are subsequently post-tensioned.

The solid end beams are directly connected to the slenderer cross section of the prefab beams. This direct connection between a stiff and solid element and a slenderer element may cause local failure. Verifying these details involve more detailed calculations which are not included in the project, however, the importance of detailing has to be acknowledged.

If more detailed verifications would be made of this section, and measures would have to be applied, then this could be done by locally increasing the thickness of the element of the prefab beam cross section. This way a more gradual transition is formed from the solid end beam to the slender cross section of the box beam.

Although such elaborate verifications of these details are not included in the project it is expected that the results of the project would be hardly influenced if these would have been. From an executional point of view these measures can be realised by adjustments of the formwork while at the same time the effect on the total weight of the structure is expected to be negligible: Even if detailed verifications indicate that measures are required these measures be applied only over a limited length and therefore the increase of the total weight of the bridge would be minimal.

10.4 Bibliography chapter ten

Braam, C. (2012). *Cement en beton 3 Constructieleer Voorgespannen Beton* (Vijfde herziene druk 2012 ed.). Aeneas.

NEN. (2011, november). NEN-EN 1992-1-1+C2. *Eurocode 2: Ontwerp en berekening van betonconstructies - Deel 1-1: Algemene regels en regels voor gebouwen*.

NEN. (2020, februari). NEN-EN 1992-1-1+C2/NB+A1. *Nationale bijlage bij NEN-EN 1992-1-1+C2 Eurocode 2: Ontwerp en berekening van betonconstructies - Deel 1-1: Algemene regels en regels voor gebouwen*.

Walraven, J., & Braam, C. (2019, February). Prestressed Concrete.

11

WEIGHT CALCULATION

11.1 Weight calculation

11.1.1 Setup of the calculation

The final part of the detailed design calculations is a calculation of an estimation of the weight of the structure. The goal of this calculation is twofold:

- To make a comparison with the results of the preliminary design to determine the effects of the improvements as mentioned in chapter 1 that have been included in the design;

- To determine the reference point for the work that will be performed in the optimization phase.

The approach is largely the same as done for the weight calculation in the preliminary design:

- The main structural components of both bridges are listed after which the dimensions and self-weight of these elements are calculated. Subsequently the total weight is obtained by adding up the separate values;

- For the capping beam no design calculations have been performed and the same estimated dimensions are used as in the preliminary design are applied, see 2.2.4;

- As done for the preliminary design a number of simplifications are made by not considering elements such as bearings, railings, joints, etc. in the weight calculation. It is not expected that these elements will be the decisive factor for the weight calculation.

- For completeness the weight of the existing bridge is also estimated, for this the same calculation is used as was performed in the preliminary design report.

For the full elaboration of the weight calculation reference is made to annexes III and IV. A drawing of the design can be found in annex VIII.

11.1.2 Results and comparison with the preliminary design

According to the performed calculation the bridge as designed in this report has a total weight of 19.190 kN compared to the 22.785 kN of the existing bridge (reduction of 16%) and the 28.753 kN of the preliminary design (reduction of 33%).

The conclusion of the weight calculation performed in the preliminary design was that the potential to reduce the weight of the new bridge was large enough to obtain a design with a weight equal to or lower than the weight of the existing bridge. With this result of the detailed design this impression has indeed been confirmed and further optimisations in the next design stage will indicate to what extent the self-weight can be reduced even further.

A remaining question is what the different contributing factors were to the reduction of the weight. The following table gives an overview of the weight per element as calculated in the preliminary design and the detailed design and the difference between the two calculations.

Table 20 Different contributions to weight reduction

	Preliminary design	**Detailed design**	**Difference**
Element	[kN]	[kN]	[kN]
Prefab UHPC beams	19.214	14.703	-4511
In-situ UHPC joints	178	119	-59
Cross beams	4422	2887*	-1535
Asphalt layer	3724	266	-3458
Kerbs	601	601	0
Capping beam	614	614	0
Total	28.753	19.190	-9563

Note: The given value for the weight of the cross beam of the detailed design already includes the correction for the overlap of the cross beams and the prefab beam ends. This value is calculated as follows: 3781 kN (weight as if the end cross beam is solid) minus 894 kN (overlap with prefab beams) results in 2887 kN.

From the values in the table the following observations can be made:

- It is clear that an explanation for the weight reduction should not be sought for in the kerbs or capping beam because these are calculated while following the same assumptions in both designs;

- In the preliminary design report, it was expected that a large weight reduction could already be realised by reducing the thickness of the asphalt layer and to a lesser extent by correcting for the overlap of the end cross beam. This is indeed a large contributor and accounts for approximately 45% of the weight reduction: $(894 + 3458)/9563 * 100\% \approx 45\%$;

- However, even a larger contribution is contributable to the main beams, which contribute approximately half of the total weight reduction, making the prefab beams the largest contributor of all elements considered. This is the combined result of different improvements of the design (see chapter 1) and the changes to the dimensions that had to be made to satisfy the verifications as covered in the previous chapters;

- Because the dimensions of the beam were changed multiple times during the detailed design process the dimensions of the joints and end cross beam also changed, which explains the remaining contribution to the decrease in weight: the joints contribute for 59 kN while the cross beams contribute $1535 - 894 = 641$ kN.

11.1.3 Conclusion

In the preliminary design report, it was already concluded that there was a sufficiently large potential to reduce the weight of the new bridge down to or even below that of the existing bridge. The results of the preliminary design confirm this, the total weight of the result of the detailed design is approximately 16% lower than that of the existing bridge.

As expected, based on the preliminary design the reduction of the asphalt layer was a large contributor, but the largest contribution turns out to be the weight reduction of the prefab beams. This reduction is a combined result of improvements of the design and changes to the dimensions that had to be made to satisfy the verifications that were performed.

12

EXECUTIONAL ASPECTS

12.1 Considering executional aspects

In the first chapter of this report four factors were given that were implemented to obtain a more detailed design. One of these factors, which has hardly been discussed in the previous chapters, is a discussion on what is denoted as 'boundary conditions from practice' or in other words: boundary conditions related to the execution of the project.

In this chapter this will be discussed in more detail by giving a phased description of the main beams of the bridge deck from the production to the use phase. This is a more elaborate description than the brief description given in 2.1.2. The goal of this description is to cover all stages of the beam to identify how the deck would be constructed and to identify possible limitations (boundary conditions for the project).

12.2 Phased description of the main beams

All phases of the main beams from the production phase to the use phase are described in chronological order in the next sub sections.

12.2.1 Production of the beams

Production of the prestressed beams
The beams are produced in the prefab factory using pretensioned steel. Prestressing using pretensioned steel is typically applied in three steps as can be seen in the following figure: the strands, casting and hardening of the concrete and releasing the strands to prestress the hardened concrete.

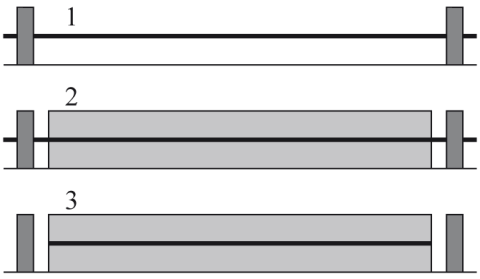


Figure 80 Prestressing using pretensioned steel – (Braam C. , 2012), p.18

Because the project revolves around the application of UHPC and the application of heat treatment, this approach has to be changed slightly. The production of the beams could take place in the following steps:

- **Phase 1**. The first elements of the formwork (the frames required for the prestressing) are placed, the strands are guided through. These are fixated on one end using a fixed supporting structure and stressed on the other using jacks. The strands are stressed after which the remaining elements of the formwork are placed to close the mould.

- **Phase 2**. The concrete is subsequently placed, the prestressing elements are fully encased. The concrete hardens inside the mould and bonds with the concrete over the full length of the tendons within the formwork.

- **Phase 3**. After a certain period of time, while the concrete is still in the mould, heat treatment is applied to improve its characteristics. After applying the heat treatment, the material is allowed to cool down slowly.

- **Phase 4**. After parts of the formwork that may restrain the deformation are removed, the prestressing strands are gradually released. As a result of this the strands have the tendency to shorten but this is prevented by the hardened concrete. Due to the bond between the steel and concrete shortening is only possible if the concrete shortens as well, this way the initially tensile force on the strands turns into a compressive force acting on the concrete.

When the prestressing force is applied onto the concrete the self-weight of the concrete is also activated and the elements bends upwards. At these outer points where the beam is supported the self-weight has no effect and the stresses are determined by the prestressing only. The remaining parts of the formwork are subsequently removed and the element is finished, for example by treatment of the beam ends to protect the prestressing steel. Note that the prestressing capacity might be a possible limiting factor in the production of the beams.

Application of heat treatment

One of the assumptions made and on which the material parameters in 2.3.1 are based, is that heat treatment is applied. Although mechanical properties are also improved by the application of heat treatment, the main reasons for the application are to increase the durability and reduce and/or control creep and shrinkage (time dependent deformations).

This corresponds to what is described in the AFGC-SETRA 2013 guideline as ''type 2 heat treatment'', which achieves the following affects:

- The components have reached their final maturity (the 28-day strength), no further hydration takes place afterwards;
- An improvement of the mechanical properties;
- Improvement of the durability due to a reduction of the porosity;
- The shrinkage after treatment equals zero and the creep is reduced.

This type of heat treatment is applied when the concrete has already hardened and it leads to the formation of new hydrates and the aforementioned effects. To achieve this the element is heated to a temperate of about 90 ^{o}C under a high moisture content, this is applied for 48 hours after which the elements cool down slowly to prevent cracking.

Prestressing capacity

Because the forces are transferred from steel to concrete via bond only relatively small prestressing elements are used, namely wires or strands. In addition, sufficient intermediate distance is to be kept. By taking these two measures the transmission length and tensile stresses in the concrete around the prestressing elements are kept low.

Although a single wire or strand can only be loaded by a small prestressing force, it is possible to apply a large number of wires or strands to apply large prestressing forces onto larger elements, provided that sufficient spacing and cover is kept in between and onto the strands. However, there is a certain upper limit in terms of the prestressing force that can be applied, this is a boundary condition for the design of prefab beams.

The value of the upper limit has been established by contacting a firm that produces prefab concrete elements. According to the received information the limit for prestressing using pretensioned steel is approximately 2500 tons (i.e. about 25.000 kN). This corresponds to 120 strands with diameter Ø15,7, each stressed with a force of approximately 21 tons (i.e. about 210 kN).

12.2.2 Storing the beams

After the beams are finished these are typically stored. Therefore, the element should be able to carry at least their own weight after prestressing, this way the beams can be hoisted and transported to the storage site. The support conditions during hoisting, transportation and storage are therefore important parameters for design. During the design calculations it was assumed that the beams are supported and lifted at the same point along their length (i.e. the same span as in the final situation.

At the moment the steel was released and the concrete prestressed, the direct losses already took place. But after this phase the time dependent effects and losses also start to develop. Due to creep of the concrete deformations due to prestressing and self-weight can increase while the element is in storage. In practice if multiple beams are applied for the same project, it should be noted that every element has its own time dependent deformation at the moment of placing the beams.

This makes time an important parameter, although this effect is expected to be reduced in the case of UHPC beams: the heat treatment reduces creep and the shrinkage after treatment equals zero. These deformations are not considered in more detail in the project.

12.2.3 Transport to and placement on site

At a certain moment in time the beams are moved from the storage location at the prefab factory to the construction site, to be subsequently hoisted into place. Because transportation and hoisting can be limiting factors, information is collected on the limits in terms of transportation and hoisting capacity by discussing two relevant reference projects. These projects are examples of structures containing larger prefab elements and were selected because these can be interpreted as an indication of the upper limit of what is possible for prefab beams in terms of transportation and hoisting. One project serves as an example on transportation of prefab beams via land and the other via water.

Transportation over road – Vervoersknooppunt Bleizo (August 2017)

The first example covers 'Vervoersknooppunt Bleizo', the interchange at Bleizo connects train, tram and bus routes between Den Haag, Rotterdam and Zoetermeer. It was constructed to give commuters the possibility of transferring between the trains stopping at station Lansingerland and these different modes of transport.



Figure 81 Placement of beams at Bleizo – Spanbeton

The interchange is formed by four fields, spanned using prefabricated concrete beams. The main span crosses the A12 highway. A requirement was that no intermediate support would be constructed. To enable this, prefabricated box beams with a length of 61 m and a height of 2,20 m would be required, with an approximate weight of 200 Tons each. Such dimensions and weight are challenging in terms of logistics: special equipment would be needed and the loads acting on the road surface would be very large.

Spanbeton produced 31 box beams (type SKK) for the main span. To deal with the logistical challenges the beam was optimised in order to reduce the weight. The beam was kept 2,20 m high at mid span, but towards the beam ends this was reduced to 1,60 m. This resulted in a weight reduction from 200 tons to 172 tons. Once placed on site, in situ concrete would be used to bring the beams up to the required height of 2,20 m over their full length and to create one solid deck structure.

The prefab beams had to be placed during a single weekend in which the highway was closed for other traffic. To minimise risks and to prevent delays the beams were temporarily stored at a storage site nearby the actual construction site. The transportation of the beams took place via road, using special transport, which required special provisions. At the weekend of placement, the beams were taken (one at the time) to the construction site using trucks and then hoisted into position using two cranes (one at each end). This way the beams were placed into their final position within the allocated time.

Transportation via water – Lienebrug (June 2020)

As an example of transport via water the Lienebrug in Wanssum is discussed. The current record of longest prefabricated beams (box beams) is claimed by Haitsma for their box beams used for this bridge. The bridge is part of the new alignment of the provincial road which was reconstructed around the town centre, instead of the current alignment directly through it. The new provincial road crosses the harbour, therefore a bridge was required. Long beams were beneficial, because spanning the water without intermediate support and with minimizing the cantilevers of the abutments gives maximum free space underneath the bridge.

The bridge consists of eight box beams (type HKP) that were post tensioned in transverse direction on site. Each beam is 1,48 m in width, 2,25 m high and 69,0 m long. The weight of a single beam is 256 tons. As is common for prefab bridges, the bridge is designed as a statically determinate structure. At the ends the beams have a solid cross section over a length of 2,25 m. Use was made of 112 prestressing strands, each one stressed by a force of 210 kN. Because of the dimensions, which had to be kept limited as much as possible, a higher concrete strength class (C90/105) was used. The following figure gives the cross section of the bridge as well as a picture in the factory.

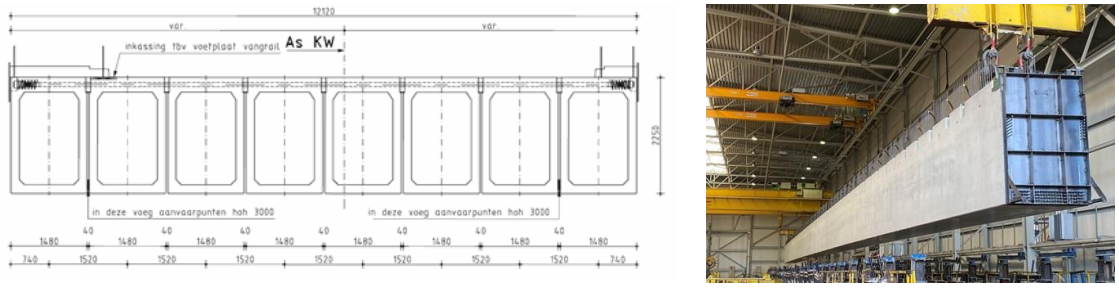


Figure 82 Cross section and production of the beams – Haitsma Beton

Due to the dimensions and weight transport via road was not possible. Therefore, the beams were transported from the prefab factory to the construction site via water, using three pontoons and pusher boats. Once on site, the beams were hoisted into their final position using two floating sheerlegs (of 160 and 250 ton), because there was insufficient room for the use of cranes from the shore. Transport and placement can be seen from the following pictures.

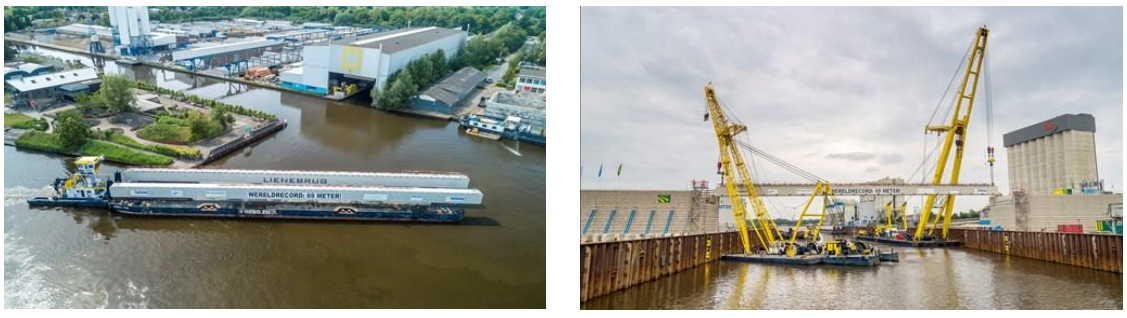


Figure 83 Transportation and placement of beams Lienebrug – Haitsma Beton

After placing the beams, the joints were filled with mortar after which prestressing strands were guided through the ducts and the beams were post tensioned in transverse direction, the typical approach for box beams. No in situ layer was required, the project was finished by applying the asphalt layer directly after stressing.

12.2.4 On site construction work

Once the prefab box beams are placed on their bearings the remaining work is carried out. This can be divided into two categories: work on the main load bearing structure and non-structural work.

Structural work
Two different actions have to be taken to finalize the load bearing structure. The first one in the construction of the cross beams and the beam ends and the second is the prestressing in transverse direction.

- End cross beams: The end cross beams are constructed by casing concrete in between the solid ends of the box beams with in situ concrete. After hardening, prestressing tendons are guided through the ducts and these are subsequently post tensioned, this way solid end beams are constructed.

- Joints and transverse prestressing: The joints are filled with UHPC after which prestressing elements are guided through the ducts in the top flanges of the beams. After sufficient hardening of the joints the deck is prestressed in transverse direction.

Non-structural
After the load bearing structure is finished the remaining work (focussed on the use of the bridge and/or aesthetics) is carried out, e.g. placing railings, barriers, etc.

12.2.5 Use phase

After constructing and finishing the structure the bridge is ready for use, this is the start of the use phase. During this phase the bridge should be able to function without requiring excessive repairs or maintenance under the anticipated use.

12.3 Implications for design

In the previous paragraph a phased description of the beam was given with the focus on execution. During the discussion two aspects were identified that may prove to be a limiting factor the bridge design:

- Prestressing capacity
- Transportation and placement

The implications of these two factors for the design are briefly discussed in the next two sections.

12.3.1 Prestressing capacity

The maximum prestressing capacity is approximately 120 strands Ø15,7, resulting in a total force of approximately 2500 tons. In the detailed design a total of 130 strands Ø15,2 is applied, the maximum prestressing force is approximately 26.300 kN (2630 tons).

That means that the maximum capacity is exceeded. However, if one calculated the total area of the prestressing (given the difference in cross section between Ø15,2 and Ø15,7 strands) and the total maximum force, the difference is relatively small. Therefore, it is expected that after the optimisation phase the required prestressing force and number of strands can be reduced to or below this maximum value. Therefore, the maximum value of 120 strands Ø15,7 (or equivalent) will be imposed onto the optimisation phase as a boundary condition.

12.3.2 Transportation and placement

The weight of an individual prefab beam as designed in this report is as follows:

$$W_{beam} = A_c * l_{tot} * \rho \rightarrow 1{,}66 * 70{,}7 * 25 \approx 2940 \text{ kN}$$

$W_{end} = 2 * h_b * w_b * w_{cb} * \rho \rightarrow 2 * 1{,}71 * 1{,}9 * 2{,}15 * 25 \approx 350$ kN

This is approximately equal to a total of 329 tons. In 12.2.3 two reference projects were given to give an impression of possibilities from the construction practice. The viaduct at Bleizo consists of prefab beams with a total weight of 172 tons and a length of 61,0 m. These beams already imposed challenges in terms of transportation. Because the beams designed in this report are longer and heavier it is deemed very unlikely that transportation via road is possible.

The example of the Lienebrug is more promising: By transportation via water and the use of floating sheerlegs it was possible to transport and place 69,0 m long beams with a weight of 256 tons each. The beams required for the Eefdesebrug are only slightly longer (70,7 m versus 69,0 m) while the difference in weight is 73 tons.

The position of the bridge at a main waterway, the Twentekanaal near the IJssel river, makes that the transportation of bigger elements via water is a plausible solution. The reference project has demonstrated that beams of approximately the same size could be transported and hoisted into place using pontoons and floating sheerlegs. Therefore, it is deemed plausible that this could be achieved for the Eefdesebrug as well. Further reduction of the weight of the beams during the optimisation phase would be an additional benefit.

12.4 Bibliography chapter twelve

Braam, C. (2012). *Cement en beton 3 Constructieleer Voorgespannen Beton* (Vijfde herziene druk 2012 ed.). Aeneas.

Fehling, E., Schmidt, M., Walraven, J., Leutbecher, T., & Fröhlich, S. (2014). *Ultra-High Performance Concrete UHPC*. Berlin: Wilhelm Ernst & Sohn.

Groupe de travail BFUP. (2013, June). Ultra High Performance Fibre-Reinforced Concretes. *Recommendations*. Association Francaise de Génie Civil.

Haitsma Beton. (2020, 05 25). *'s Wereld langste prefab voorgespannen liggers*. Opgeroepen op 06 12, 2020, van Haitsma Beton: https://www.haitsma.nl/nieuws/brugliggers-wanssum/

Haitsma Beton. (sd). *Lang langer langst - Langste prefab voorgespannen liggers ter wereld*. Opgeroepen op 09 17, 2020, van Haitsma Beton: https://www.haitsma.nl/landingspagina/langste-prefab-voorgespannen-liggers-ter-wereld/

Haitsma Beton. (sd). *Nieuw record prefab voorgespannen liggers*. Opgeroepen op 09 17, 2020, van Haitsma Beton: https://www.haitsma.nl/nieuws/nieuw-lengterecord-prefab-voorgespannen-liggers/

Spanbeton. (sd). *Bleizo - Vervoersknoop Lansingerland/Zoetermeer*. Opgeroepen op 09 17, 2020, van Spanbeton: https://www.spanbeton.nl/nl/references/item/bleizo-vervoersknoop-lansingerland-zoetermeer/

Walraven, J., & Braam, C. (2019, February). Prestressed Concrete.

Yang, Y. (2020). Lecture Notes Concrete Bridges CIE5127.

Figures

Figure 81 From: *https://www.spanbeton.nl/nl/references/item/bleizo-vervoersknoop-lansingerland-zoetermeer/*, on 17-09-2020

Figure 82 (left) From: *https://www.haitsma.nl/landingspagina/langste-prefab-voorgespannen-liggers-ter-wereld/*, on 17-09-2020

Figure 82 (right) From: *https://www.haitsma.nl/nieuws/brugliggers-wanssum/*, on 17-09-2020

Figure 83 (left) From: *https://www.haitsma.nl/nieuws/brugliggers-wanssum/*, on 17-09-2020

Figure 83 (right) From: *https://www.haitsma.nl/landingspagina/langste-prefab-voorgespannen-liggers-ter-wereld/*, on 17-09-2020

Sources of all other figures have been mentioned in the text.

13

CONCLUSIONS AND PROSPECTS

Conclusions

This report covered the elaboration of the detailed design. The goal of this design was to perform a more complete and accurate analysis to obtain more insight into the behaviour of the structure and to identify the best options for optimization. By achieving this goal, the answers can be formulated to the research questions as given in the preface of this report, the answers to these questions can be found in the corresponding chapters.

After the outline of the design (chapter 1), a description of the geometry and dimensions (chapter 2), various principles from the relevant codes and guidelines that were not covered before (chapter 3) and the loads and load combinations (chapter 4) were covered, a finite element model was set up to determine the force distribution in the structure (chapter 5).

Using this model and the various verifications insight was gained into the behaviour of the structure under different loads and load combinations. In the chapters 6 to 8 various ultimate limit state verifications were performed using the governing internal force values as calculated using RFEM. The set of verifications was more elaborate compared to the preliminary design and included global and local strength verifications as well as a fatigue verification. In addition, the deflections of the bridge were verified (chapter 9) and a brief analysis of the end cross beam was performed (chapter 10).

Because of this elaborate set of verifications more insight was gained regarding possible optimisations, the various unity checks that have been performed can be interpreted as one of the indications for this. If margins are very large, a certain verification may hint towards options for optimisation. The following summarizing table gives an overview of various verifications.

Table 21 Summarizing table unity checks

Verification	Element	Value unity check
Bending moment capacity	Main beams (global)	0,77
Shear force capacity	Main beams (global)	0,56
Torsional moment capacity	Main beams (global)	0,17
Combination shear and torsion	Main beams (global)	0,61
Combination shear and torsion – Compressive strut	Main beams (global)	0,42
Ship collision – Static equilibrium	Whole deck (global)	0,14
Bending moment capacity joint	Longitudinal joints (local)	0,45
Bending moment capacity transverse direction	Top flange (local)	0,78 and 0,79
Bending moment capacity longitudinal direction	Top flange (local)	0,83
Fatigue verification – Prestressing steel	Main beams (global)	0,13
Fatigue verification – Concrete	Main beams (global)	≈0
Deflection	Main beams (global)	0,50
Bending moment capacity	End cross beams (global)	0,19
Shear force capacity	End cross beams (global)	0,54

From this table it can be seen that in terms of resistance (strength) the main beams have sufficient capacity although due to the combination of shear and torsion the room for optimisation in the webs is limited. In addition, the results give the impression that the room for optimisation at the top flanges is also limited.

However, the verification of the beams does not depend on verifications in the ultimate limit state (strength), serviceability limit state criteria such as deflection have to be considered as well. When calculated with RFEM the result is 0,5. During optimization sufficient bending stiffness should be provided to the deck.

Apart from the structural verifications a weight calculation has also been performed (chapter 11). In the preliminary design it was concluded that there would be a sufficiently large potential to reduce the weight of the new bridge down to or even below that of the existing bridge. With the results of the detailed design this has been confirmed: the total weight of the detailed design is approximately 33% lower than that of the preliminary design and 16% lower than that of the existing bridge.

In the preliminary design it was already expected that a large weight reduction would be achieved by taking measures such as reducing the asphalt layer, but eventually the largest contributor turned out to be the weight reduction of the prefab beams, accounting for approximately 50% of the total weight reduction. This reduction is a combined result of improvements of the design and changes to the dimensions that had to be made to satisfy the verifications that were performed.

In addition, executional aspects were discussed in chapter 12. A phased description of the beam was given from the fabrication to the use phase, to identify possible limitation from practice. Two limiting factors were identified: prestressing capacity and transportation & placement. The current design exceeds the maximum possible prestressing capacity although this exceedance is only limited. Therefore, this remains a point of attention for the next design phase. Reference projects for transportation & placements of larger prefab beam bridges were discussed, from which it was concluded that transportation and placement of the beams as designed in this report is already feasible via waterways. Further optimizations resulting in further decrease of the weight would only be beneficial with respect to the transportation and placement.

Prospects

This report covered the elaboration of a design which satisfied all verifications that have been performed and which resulted in a 16% weight reduction compared to the existing bridge. That means that another step has been taken towards achieving the goal of the project.

However, still a number of remarks can be made, to which an answer will have to be found in the next design phase: the optimisation phase. One stringent point of attention is the maximum prestressing force. Either the design has to be optimized as such that only a smaller number of strands per beam is required, or an alternative approach to prestress the beams has to be sought for.

In addition, the question remains to what extent the weight of the deck can be reduced even further while still satisfying the relevant requirements. This will be the main objective of the optimization phase and it is expected that if further weight reduction turns out to be possible the number of strands per beam will also be reduced towards or below the maximum possible force.

The optimisation will be carried out by varying different parameters such as the number and dimensions of the beams while other factors such as material parameters will be kept (largely) the same. This way the influence of varying different parameters can be identified and the most optimal design can be determined.

Annex(es)

ANNEX: DETERMINING MATERIAL PARAMETERS – DUCTAL FM

DETERMINING MATERIAL PARAMETERS – DUCTAL FM

1. Goal and approach

One of the key points of the detailed design phase is the use of material parameters that correspond to a specific UHPC mixture. Determining such parameters is not as straightforward as it is for conventional concrete. Although there are certain commercial products for example, these mixtures are often adjusted to optimally meet the requirements of specific a project after which tests are to be performed to further characterise the material and its performance.

As a result of this one will usually find a range of characteristic values when going through literature or information provided by manufacturers. This document covers the process of selecting a certain type of UHPC and quantifying the required material parameters for the detailed design phase.

The AFGC-SETRA 2013 guideline used in the design covers only a number of commercial products: Ductal, BSI/CERACEM and BCV. Although this does not mean that the guideline cannot be used under any circumstance with any other type of UHPC, discussion is avoided by choosing for one of these commercial products.

Throughout the literature study and elaboration of the preliminary design it was found that of these three mentioned products information on Ductal is most easily available. Therefore it has been decided to base the material parameters on Ductal products. In the remainder of this document the following topics are covered:

- General description of different ranges of Ductal products currently available on the construction market;
- Selection of the most appropriate range of Ductal products after which the performance of these materials are described into more detail;
- Formulation of conditions and requirements under which the material would be applied after which the parameters are formulated, quantified and substantiated by taking account of these conditions and requirements.

1.1 General description of Ductal products

1.1.1 Development of Ductal

In the 90's Reactive Powder Concrete (RPC) was developed, a milestone in concrete development. This eventually resulted into the development of the commercial product Ductal, which is a type of UHPC, more specifically a type of RPC. Ductal is known for a very dense structure and a very high compressive strength. Fibres are added to enhance its performance (tensile strength, ductility and/or resistance in case of fire). Compressive strengths above 200 N/mm^2 are possible and flexural strength above 40 N/mm^2 are reported as well.

This results in a material that combines high mechanical properties (high compressive strength and flexural strength) with durability and ductility. The combination of excellent mechanical properties on one hand and ductility on the other sets it apart from conventional concrete and HPC, because these materials remain brittle and require additional passive reinforcement. In addition it offers many possibilities for aesthetics as well due to large freedom in design.

1.1.2 Main principles

In the literature study the main concepts of UHPC were already covered and discussed extensively. As is to be expected Ductal, being a fibre-reinforced UHPC, is also based on these main concepts.

The main concept is minimisation of the number of defects in the structure of the material (e.g. micro-cracking and pores). This can be achieved by optimizing the mixture for homogeneity and packing of the particles, resulting in higher load carrying capacity and better performance related to durability.

This concept is put into practice by combining particles from a whole ranges of sizes, the largest being 600 µm (0,6 mm) and going down the smallest of 0,1 µm, which explains the origin of the notion 'Reactive Powder Concrete'. Using small particles through this range of sizes results in a very dense material (very dense packing), the volume of voids in the structure is minimized.

Ductal is the result of extensive research, which was performed aiming at the following five main principles:

1. Increasing the homogeneity by eliminating coarse aggregate;
2. Increasing the density by optimizing the particle sizing of the mixture;
3. Post-set heat treatment to increase the microstructure properties;
4. Increase of ductility by adding fibres of the appropriate size;
5. Mixing and casting procedures are to be kept as close to current practice as possible.

The first three points result in high compressive strength, but also in a very brittle material. Heat treatment is optional and can be applied to improve the properties of the material. Especially the mechanical properties are strongly influenced this way. The fourth point, addition of fibres, provides ductility and an increase of the tensile strength. The fifth point resulted in a material that has properties in its fresh state that are beneficial for the execution of the work (e.g. with respect to flowability and placement through the formwork). In addition it is reported that most of the standard concrete plants would be able to mix the material without large adjustments that have to be carried out.

1.2 Types of Ductal products

1.2.1 Selecting type of Ductal product

Given the performance of the material, the application of Ductal (and UHPC in general) in a project can be beneficial if it is required to achieve at least one of the following three aspects. The addition benefits of the other aspects only work beneficial.

- **Mechanical performance (strength)**: The mechanical properties create new possibilities for design, the use of conventional reinforcement is in most cases not required. Optimizing as such that the UHPC is used to its full potential can result in thinner and innovative cross sections of shapes that were not possible in conventional concrete. This results in more slender and lighter structures.

- **Durability performance**: Due to the dense microstructure the material performs well in demanding or even aggressive environments. Even if durability is not the main reason of applying the material, the high durability means a reduction of maintenance during the service life. As illustrated in the first part of the literature study, UHPC (and therefore also Ductal) can contribute to more sustainable solutions.

- **Performance related to aesthetics**: The application of the material gives large freedom of shape and addition of colours and the ability to create textures gives many options with respect to architectural designs.

For the thesis project the first aspect is of most importance, after all a slender and lighter structure contributes to the project goal. In addition the second aspect is definitely beneficial as it opens new possibilities for design. The third point is not taken into consideration.

It is important to note that Ductal is not a single mixture, different ''ranges'' of Ductal materials can be distinguished based on the applied type of fibres. These different ranges of materials each have a certain field of application for which they are especially suitable:

- **Steel fibres – Ductal FM**: For structural applications Ductal FM is developed. By adding steel fibres mechanical properties superior to conventional concrete can be achieved. Especially in combination with prestressing this paves the way for the design of very slender structures. Due to the mechanical performance, passive reinforcement is not needed in most cases.

- **Organic fibres – Ductal FO**: This product range aims more towards architectural applications. Ductal can be used to produce elements of complicated shapes and with different textures due to the fine particles, dense structure and flowability in fresh state. In addition there is the option to add pigments to the mixture. This gives many possibilities for architectural applications, but in these cases the mechanical properties are often not the governing factor. In these cases organic instead of steel fibres can therefore be used.

- **Steel and organic fibres – Ductal AF**: The dense structure of UHPC gives the risk of spalling in case of fire. To counter this, Ductal AF was developed which makes use of both steel fibres and organic fibres. The latter melt in case of fibre thus creating free space for the water vapour and enable it to escape. This reduces the built up of pressure, and there with the risk of spalling. Despite the addition of organic fibres the mechanical properties of Ductal AF are similar to that of Ductal FM thanks to the steel fibres and optimization of the mix.

Within these three ranges the mixture composition can be optimized for each specific project, e.g. based on technical and economical requirements. This way the most optimal mixture is obtained to meet the requirements for the specific application. All points considered the use of a product of the Ductal FM range is most appropriate, therefore the focus will be on this range of product.

1.2.2 Ductal FM and its main features

The general characteristics of Ductal have been discussed and three different ranges of Ductal products have been introduced. In addition it was decided that the focus would be on the range of Ductal FM products for the detailed design. In this paragraph the characteristics of Ductal and Ductal FM in particular will be discussed in more detail because this will aid in formulating requirements and parameters in the next section of the annex. The reader might notice that the values mentioned in this paragraph are very similar to values found in the first part of the literature study and the AFGC-SETRA 2013 guideline.

Mix design

As mentioned before, Ductal FM was developed for structural applications. For these applications high mechanical properties (compression and tension/bending) are generally required. This is achieved by the use of steel fibres. Based on research it was concluded that an optimum was found for 2% of fibres by volume, the fibres being 13 – 15 mm in length and a diameter of approximately 0,2 mm.

Mechanical properties – Compression

The following graph shows the behaviour of Ductal loaded in compression. The material behaves linearly until the maximum stress is reached, at this point the plastic stage starts which means that the strain increases while the stress remains approximately equal. Post-peak behaviour can be seen as well, which means that the strain increases while stress (the capacity of the material) reduces.

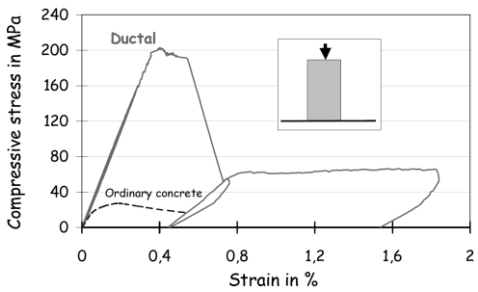


Figure 1 Behaviour of Ductal in compression – [2], p.13

Mechanical properties – Tension & bending

The following load-deflection graph shows the behaviour typical of Ductal in bending (three point bending test).

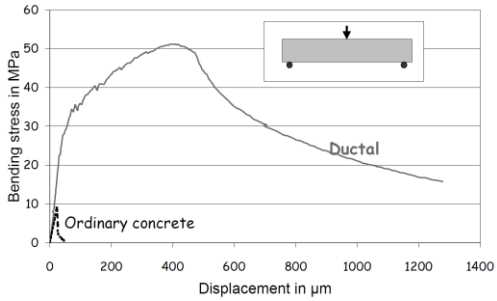


Figure 2 Behaviour of Ductal in bending – [2], p.13

Three different stages can clearly be distinguished:

- **Linear phase**: The material behaves (approximately) linear until the tensile strength of the matrix is reached and the first crack occurs;

- **Hardening phase**: After the first crack (the post cracking stage) hardening occurs. More cracks are formed and the stress increases until the ultimate load is reached;

- **Softening phase**: After the maximum load is reached softening occurs.

In addition it can be observed that the ultimate stress is significantly higher than the stress at which the matrix cracks and the first crack is formed, in other words: strain hardening is very predominant in this case. This is typical behaviour of Ductal FM, which is known to show strain hardening behaviour.

From experiments it is known that the ductile behaviour in the hardening phase is characterised by the formation of a large number of very fine cracks. During the hardening phase no localisation takes place yet, new small cracks are formed. Only once the peak load is reached localisation occurs. One crack becomes wider and softening occurs as the fibres are pulled out of the matrix.

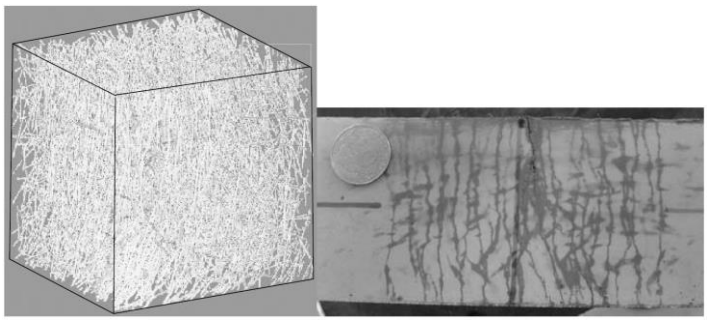


Figure 3 3D image (left part) and multiple cracking of Ductal (right part) – [4], p.1284

The left shows the X-ray of a concrete cube taken from a beam (made of Ductal) can be seen, it reveals the distribution of the fibres. The right picture shows the cracking of Ductal in the tensile zone after failure, indeed most of the cracks are very small and these were wetted to make them visible. One crack can be seen clearly from the middle though. Once the peak load is reached localisation of the crack opening takes place at one crack, which starts to open up further.

Creep

Creep of UHPC in general is lower than that of conventional or high strength concrete. For Ductal the creep coefficient without heat treatment is less than 0,8. In case of applying heat treatment the coefficient can be reduced to 0,2. Given the smaller creep coefficient the prestress losses are reduced when applying prestressing.

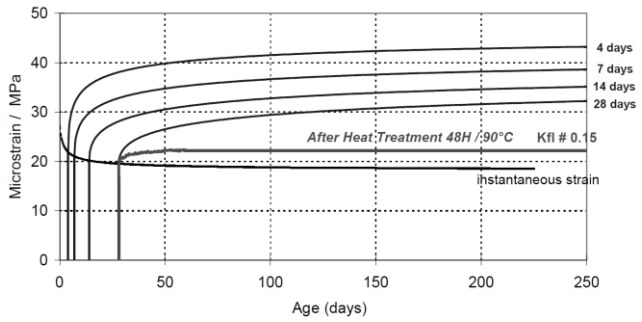


Figure 4 Basic Ductal creep – [2], p.15

Shrinkage

Due to the low water cement ratio typical for Ductal (and UHPC in general) there is no drying shrinkage. Autogenous shrinkage is a factor of importance though. High autogenous shrinkage can be observed, but by applying heat treatment this can be controlled. The autogenous shrinkage process will take place completely during the treatment after which no residual autogenous shrinkage occurs afterwards.

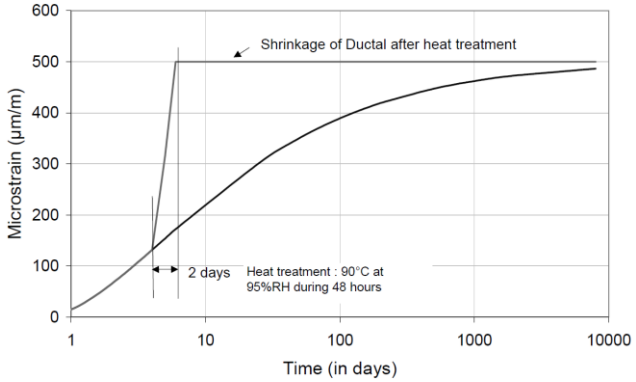


Figure 5 Autogenous shrinkage of Ductal with and without heat treatment– [2], p.16

Durability

Because of its closed microstructure, Ductal is practically impermeable to water and harmful substances. As a result Ductal has excellent performance related to durability. In literature mention is made of good resistance to corrosion, freeze-thaw cycles, chemical attacks and resistance against various gasses. In addition, good resistance to abrasion and the ability to self-healing was also demonstrated, which is of relevance for the long term durability.

1.3 Specifying material performance and parameters

1.3.1 Approach of specifying the material

In the previous paragraphs the reasoning behind focussing on Ductal FM was substantiated after which the properties of the material were discussed in more detail. The next step, which is required as input for the elaboration of the detailed design, is to quantify the required parameters.

It is highlighted once more that Ductal FM is not a specific mixture, but rather a range of mixtures. In practice requirements for the concrete are formulated after which the composition is adjusted within this material range to optimally meet the requirements for the given project: the material is tailor made to meet the project specific demands. This means that no specific numerical values can be found for this material in literature, generally a range of values is given.

Working with a range of values is not a practical solution and for obvious reasons no specific mixture is designed for the project. However, this process is still followed by first formulating a number of requirements the material should fulfil along with a number of relevant points on how the material will be applied.

In practice a mix would be designed in accordance with these points, but in this report a list of parameters will be formulated after which numerical values will be assigned. Each of these parameters is based on values for products within the Ductal FM range and/or general information on UHPC to obtain a realistic and optimistic overview of parameters. The values are deduced from the different sources listed in the bibliography. The reasoning behind each numerical value is given as well. The parameters of this assumed ''fictitious mix'' will be applied for further design in the thesis project.

1.3.2 Requirements and material application

The following points describe requirements that would have to be met by the material or describe the way in which the material will be applied for the new Eefdesebrug:

- **Mechanical performance**: A concrete mixture is required with properties at least equal to the recommended values used in the preliminary design phase, this allows for a more refined and optimized design:
    - Characteristic 28-day compressive strength of at least 150 N/mm^2;
    - Characteristic elastic tensile strength of at least 9 N/mm^2, a characteristic maximum post-cracking stress of at least 9 N/mm^2;
    - Modulus of elasticity of 50.000 N/mm^2 is required;

- **Strain-hardening behaviour**: The material has to show strain hardening behaviour (denoted as type 3 material in the AFGC-SETRA 2013 guideline), this is on the more favourable side compared to the preliminary design where prescribed parameters corresponding to a low strain-hardening material (type 2 material) were assumed;

- **Application**: A flowable, self-compacting concrete is required because of the possible local presence of a large amount of prestressing reinforcement at the beam ends;

- **Heat treatment**: Heat treatment will be applied to the material, this way the mechanical properties are enhanced (higher values are possible) and creep and shrinkage are reduced and/or controlled;

- **Prefabrication**: The beams will be prefabricated and later on transported to site. This allows for more controlled conditions than in-situ and for the application of heat treatment.

1.3.3 Assigning parameters to the ''fictitious mix''

The requirements that have to be met by the material or provisions on how the material will be applied have been formulated. The next and final step is to quantify these parameters by assigning specific numerical values. These values are used as input for the design calculations.

The numerical values assigned to the parameters will be based on values of the Ductal FM range of materials as found in the sources considered. Although there remains some uncertainty because no specific mix is designed and tested, it is strived for to formulate realistic values. The assumed values for the parameters are on the more favourable but yet realistic side of the range of values found in the literature considered. The decision to assume such values is justified by the following two arguments:

1. **Technological advancement**: The ranges of values found in the literature are sometimes dated at the moment of writing this report. Upper values reached with difficulty a number of years ago may have become more common due to technological advancements in the construction industry;

2. **Formulating challenges**: Formulating requirements that may provide a challenge to manufacturers and contractors may function as an incentive to innovate and shifting boundaries of what is possible. This contributes to further technological advancements in the construction industry.

The following table gives all assumed numerical values for the required parameters. For each parameter the definition, adopted symbol and unit is given. If relevant the symbol according to the AFGC-SETRA 2013 guideline is also included.

Tabel 1 Assumed parameters Ductal FM

Parameters mixture composition				
Definition	**Symbol**		**Value**	**Unit**
Density	ρ		2500	[Kg/m^3]
Fibre length	l_f		13	[mm]
Parameters concrete compression				
Definition	**AFGC**	**Symbol**	**Value**	**Unit**
Characteristic value compressive strength	f_{ck}	f_{ck}	200	[N/mm^2]
Design value compressive strength	f_{cd}	f_{cd}	113	[N/mm^2]
Strain at reaching concrete compressive strength	ε_{c0d}	ε_{c3}	2,3	[‰]
Maximum compressive strain at ULS	ε_{cud}	ε_{cu3}	2,6	[‰]
Parameters concrete tension				
Definition	**AFGC**	**Symbol**	**Value**	**Unit**
Characteristic elastic (5% percentile value) tensile strength	$f_{ctk,el}$	$f_{ctk,el}$	9	[N/mm^2]
Design value of tensile strength (tensile strength 1st crack)	-	f_{ctd}	6,0	[N/mm^2]
Characteristic value maximal post cracking stress (at $w = 0{,}30$)	f_{ctfk}	-	10,0	[N/mm^2]
Design value maximal post cracking stress (at $w = 0{,}30$)	f_{ctfk}/(Y *K)	$f_{ctd;2}$	6,15	[N/mm^2]
Fibre orientation factor (global)	K_{global}	K_{global}	1,25	[-]
Fibre orientation factor (local)	K_{local}	K_{local}	1,75	[-]
Parameters stiffness and deformations (temperature, creep and shrinkage)				
Definition	**Symbol**		**Value**	**Unit**
Modulus of elasticity	E_{cm}		50.000	[N/mm^2]
Shear modulus	G		20.833	[N/mm^2]
Poisson ratio	v		0,2	[-]
Coefficient of thermal expansion	α		12*10^{-6}	[K^{-1}]
Creep	φ		0,3	[-]
Autogenous shrinkage (during HT)	ε_{shr}		0,8	[‰]
Parameters concrete other				
Definition	**Symbol**		**Value**	**Unit**
Factor for shape of concrete compressive zone	α		0,56	[-]
Factor position centre of gravity of concrete compressive zone	β		0,34	[-]
Long term effects and unfavourable loading (compression)	α_{cc}		0,85	[-]
Long term effects and unfavourable loading (tension)	α_{ct}		1,0	[-]

1.3.4 Quantification of the parameters

Parameters mixture composition

Density ρ: In various sources the density of UHPC is close to that of reinforced concrete, because of the presence of steel fibres, although the exact value varies between different commercial products. Based on [3], [6] and [8] the value of 2500 kg/m^3 has been selected.

Fibre length l_f: The fibre length is taken equal to 13 mm, this is a common value for Ductal FM.

Parameters concrete in compression

Characteristic compressive strength f_{ck}: The different sources that were considered mention ranges for the characteristic 28-day compressive strength of 150–180 or 150–200 N/mm^2 for UHPC and Ductal in particular, a value of 200 N/mm^2, being the upper limit of these ranges of values.

This value is justified because of the assumption that heat treatment will be used to enhance mechanical properties and because of the fact that experiments (e.g. [7]) have already shown that this value can be approached without requiring special provisions, raw materials or treatment.

Design value compressive strength f_{cd}: From the characteristic compressive strength the design value of the compressive strength can be calculated through the following relationship:

$$f_{cd} = \alpha_{cc} * \frac{f_{ck}}{\gamma_C} \rightarrow 0{,}85 * \frac{200}{1{,}5} = 113\ [N/mm^2]$$

Strains under compression ε_{c3} and ε_{cu3}: Information on equations or values for the strains in compression can be found in [6] and [8]. A complete overview of experimental results is difficult to be found, therefore the approach as described in [8] is applied, as was done in the preliminary design. This provides the best substantiated assumption found in the literature that was considered.

In the article reference was made to experiments performed on Ductal FM in compression, from the results it was concluded that there is only a small difference between the strains from the experiments and those given in Eurocode 2 for the higher strength classes. In Eurocode 2 the strain at failure decreases as the concrete compressive strength increases, but remains constant for C80/95 and higher. Therefore it was chosen to apply the compressive strain values for the highest strength class C90/105 from Eurocode 2 to the UHPC as well.

Parameters concrete in tension

Characteristic elastic tensile strength $f_{ctk,el}$: For the characteristic elastic tensile strength (at 28 days) values can be found generally in the range of 6-10 N/mm^2, for example take [3], annex 9 in [6] or [5]. A value at the higher end of this range is chosen: 9 N/mm^2.

Design value of tensile strength f_{ctd}: From the characteristic tensile strength the design value can be calculated using the following equation:

$$f_{ctd} = \alpha_{ct} * \frac{f_{ctk,el}}{\gamma_C} \rightarrow 1{,}0 * \frac{9}{1{,}5} = 6{,}0\ [N/mm^2]$$

Characteristic value maximal post cracking strength f_{ctfk}: This value corresponds to the stress at which a crack width $w = 0{,}30$ mm is reached. Ductal FM is known to be strain hardening, which implies that this value would be higher than (or at least equal to) the elastic tensile strength. [3] gives 7,5 N/mm^2 at w=0,3 versus an elastic tensile strength of 8,0 N/mm^2 (both characteristic values). Annex 9 of [6] gives a range of 7-10 N/mm^2 (mean values) versus 9-10 N/mm^2 for the elastic tensile strength. [8] gives a tensile strength of 12 N/mm^2 versus an elastic tensile strength of 8,0 N/mm^2 (both characteristic values).

A value at the higher end of the aforementioned ranges and above the elastic tensile strength (this implies strain hardening behaviour) is chosen. The value f_{ctfk} is taken equal to 10 N/mm^2.

Design value maximal post cracking strength $f_{ctd;2}$: The design value for the maximum post cracking strength (design value of the tensile strength at a crack width of $w = 0{,}30$ mm) is calculated as follows:

$$f_{ctd;2} = \frac{f_{ctfk}}{\gamma_{cf} * K_{global}} \rightarrow \frac{10}{1{,}3 * 1{,}25} = 6{,}15\ [N/mm^2]$$

NOTE: The AFGC-SETRA 2013 guideline prescribes f_{ctd} to be calculated by dividing $f_{ctk,el}$ over γ_{cf} (equal to 1,3) instead of γ_c (equal to 1,5). Nonetheless γ_c is used because this is consistent with concrete tensile strength calculations according to Eurocode 2. For the $f_{ctd;2}$, it has been decided to use γ_{cf} instead of γ_c as prescribed by the AFGC-SETRA 2013 guideline. The reason for this is that $f_{ctd;2}$ is a quantity that does not exist in Eurocode 2. Therefore, dividing it by the product of γ_c and the fibre orientation factor would yield too conservative results.

Fibre orientation factors K_{global} and K_{local}: From the review of [6] as part of the preliminary design report, it is known that the fibre orientation factors can be determined by following procedures and information given in the AFGC-SETRA 2013 guideline (see for example paragraph 1.4 and annex 6). Determining the K-factor requires specimen, for obvious reasons these are not available during this thesis. Therefore, appropriate values have to be deduced from reference projects.

As long as no 'real' mock-ups are produced using the actual mixture to determine these factors, there will be uncertainty in the values of these factors. At the same time, from the examples in annex 6 it is concluded that the recommended values (1,25 for K_{global} and 1,75 for K_{local}) as given in the AFGC-SETRA 2013 guideline are in the same order of magnitude as those from the mentioned reference projects. Therefore, because nothing else is known, the recommended values will be kept (these values were also applied during the preliminary design phase). Given the lack of more specific information this is deemed to be sufficiently accurate.

Parameters stiffness and deformations (temperature, creep and shrinkage)

Modulus of elasticity E_{cm}: Values given for the modulus of elasticity are often in the range of 45 GPa to 55 GPa, see [5] for example, although examples can be found where higher values were achieved. The value of 50 GPa is applied as an intermediate value. This is consistent with the assumed values for the compressive strains and stress and in addition it is a value which is typically recommended for use in UHPC design.

Shear modulus G: A value of 24 GPa is given in annex 9 of [6], this value being specifically for Ductal. However, following theory this value can also be calculated. The values for the modulus of elasticity and Poisson ratio are well established for the material, therefore the value for G is calculated as follows:

$$G = \frac{E}{2(1+v)} \rightarrow \frac{50}{2(1+0{,}2)} \approx 20{,}8\ GPa$$

Poisson ratio v: According to [5] the typical value for the Poisson ratio for both conventional concrete and UHPC equals 0,2. This value has therefore been chosen. This corresponds with the indicative value from annex 9 of [6].

Coefficient of thermal expansion α: A value of $12 * 10^{-6}\ K^{-1}$ has been chosen, which is in accordance with annex 9 of [6]. This is a typical value for Ductal and is in the same order of magnitude as other (conventional) concrete types.

Creep φ: Values for the creep factor of UHPC without heat treatment are often around 0,8. For UHPC and Ductal FM in particular it is known that by using heat treatment this value can be reduced to 0,2 – 0,4. For the calculations the average of these values (i.e. 0,3) has therefore been chosen.

Shrinkage ε_{shr}: From the previous discussions in this document it is known that there is no drying shrinkage for Ductal due to the low water cement ratio. However, the autogenous shrinkage is significant and according to annex 9 of [6] the value can be 600-800 µm/m. The higher value of 800 µm/m is assumed, which equals to 0,8 ‰. Note that heat treatment is assumed to be applied, that means that the total autogenous shrinkage takes place during this process. Afterwards no remaining shrinkage occurs.

Parameters concrete other

Shape factors α and β: By adopting strain values ε_{c3} and ε_{cu3} that correspond with C90/105 of Eurocode 2, the values of 0,56 and 0,34 are adopted for α (factor for the shape of the concrete compressive zone) and β (factor for the position of the centre of gravity of the concrete compressive zone), respectively.

Factors α_{cc} and α_{ct}: In accordance with the AFGC-SETRA 2013 guideline these values are taken equal to 0,85 and 1,0, respectively.

Remarks

The parameters as defined in this report will be applied in the further elaboration of the project, this will be done in combination with assumptions (e.g. the stress-strain diagrams) as reported on in the preliminary design report.

A large number of parameters have been quantified. However, if during the further elaboration of the project it turns out that certain parameters are missing, addition substantiated assumptions will be made.

1.3.5 Summary

In this document a range of materials has been selected on which the UHPC design will be based: Ductal FM. In practice the UHPC mixtures are tailor made to meet the project specifications. To simulate this for the thesis project, requirements have been formulated which the material would have to satisfy as well as a number of assumptions on how the material would be applied.

Important requirements and assumptions are that the material is strain hardening (type 3 material), that heat treatment is applied and that the mechanical properties have to be at least equal to the values applied in the preliminary design. By consulting various sources the required parameters have subsequently been quantified in a substantiated way, these values will be used for the detailed design.

The assumed numerical values are on the optimistic yet realistic side. This is justified by technological advancements made in the construction industry and by formulating challenges that may contribute as an incentive to further technological advancements in the construction industry. In addition it is known that heat treatment can be applied to Ductal FM to enhance its performance even further, and that it shows strain-hardening behaviour, this is also reflected in the numerical values that have been assumed.

1.4 Bibliography

[1]. Betoniek. (2017). Da's sterk! *Betoniek Standaard*, 1-12.

[2]. Behloul, M., & Acker, P. (2004). Ductal Technology: A large spectrum of properties, a wide range of applications. In M. Schmidt, E. Fehling, & C. Geisenhanslüke (Red.), *Ultra High Performance Concrete* (pp. 11-23). Kassel: Kassel University Press.

[3]. Behloul, M., & Batoz, J.-F. (2008). Ductal applications over the last Olympiad. In E. Fehling, M. Schmidt, & S. Stürwald (Red.), *Ultra High Performance Concrete (UHPC)* (pp. 855-902). Kassel: Kassel University Press.

[4]. Behloul, M., Durukal, A., Batoz, J.-F., & Chanvillard, G. (2004). Ductal: Ultra High-Performance Concrete technology with ductility. In M. Di Prisco, & G. A. Plizzari (Red.), *6th International RILEM Symposium on Fibre-Reinforced Concretes (FRC)* (pp. 1281-1290). Varenna: RILEM.

[5]. Fehling, E., Schmidt, M., Walraven, J., Leutbecher, T., & Fröhlich, S. (2014). *Ultra-High Performance Concrete UHPC*. Berlin: Wilhelm Ernst & Sohn.

[6]. Groupe de travail BFUP. (2013, June). Ultra High Performance Fibre-Reinforced Concretes. *Recommendations*. Association Francaise de Génie Civil.

[7]. Hunger, M., & Spiesz, P. (2016). Praktijkproef bewijst potentie UHSB. *Betoniek Vakblad*, 12-16.

[8]. Ketel, H., Willemse, R., Van Rijen, P., & Koolen, E. (2011). Rekenmodel VVUHSB (1). *Cement*, 50-57.

ANNEX: PRODUCT SHEET DUCTAL JS1000

PRODUCT DATA SHEET

JS1000

Ductal®

LAFARGE
Building better cities™

JS1000







Field-cast UHPC closure pour solutions for prefabricated bridge element connections

DESCRIPTION:

Ductal® JS1000 is an ultra-high performance concrete (UHPC) that offers superior strength, durability, ductility, and bond capacity compared to conventional and high performance concretes and grouts. Composed of an optimized gradation of fine granular particles and a water-to-cementitious ratio less than 0.25, Ductal® is denser than conventional concrete giving it a discontinuous pore structure that attributes to remarkable imperviousness and durability against liquid ingress, chloride penetration, freeze-thaw, abrasion, scaling, chemical attack, alkali reactivity, and carbonation.

Internally reinforced with millions of discrete steel fibers (2% by volume, typ.), Ductal® JS1000 is extremely strong in compression and flexible in bending. Cracking is controlled and maintained at microscopic levels, ensuring impermeability and long-term durability against adverse conditions, aggressive agents and environments.

APPLICATIONS:

Ductal® JS1000 is primarily used as a closure pour material to connect prefabricated structural elements on-site. Its fluidity, strength, and enhanced bond properties make it ideal for this application; enabling engineers and contractors to create optimized, durable designs using precast systems. Typical applications include: beam haunch connections and connections between Precast Deck Panels, Deck Bulb-Tees, Next D Beams, and Adjacent Box Beams for bridge structures. Other applications include: link slabs, expansion joint headers, and pier jackets.

TYPICAL MATERIAL PROPERTIES
In accordance with ASTM C1856 / C1856M.
Material and curing conditions at 73ºF (23ºC) and 50% R.H.(1)

Density	150 - 160 lb/ft³ (2,400 – 2,565 kg/m³)	
Flow	7 to 10 in. (175 to 250 mm) diameter without visible sign of fiber segregation	
Working Time / Set Time	approx. 120 min. / 15 to 18 hrs	
Compressive Strength(2)	> 14 ksi (100 MPa)(3)	at 4 days (4,5)
Compressive Strength(2)	> 21 ksi (150 MPa)	at 28 days
Tensile Strength(6)	> 725 psi (5 MPa)	at 28 days
Modulus of Elasticity	> 6,500 ksi (45 GPa)	at 28 days
Long-term Shrinkage	< 800 microstrain	at 28 days
Chloride Ion Penetrability	< 250 coulombs (very low)	at 56 days
Freeze -Thaw Resistance	> 96% RDM	at 300 cycles

(1) Field results may differ depending on mixing/test methods, equipment used, temperature, and site/curing conditions.
(2) Compression tests are performed on 3 in. x 6 in. (75 mm x 150 mm) cylinders with ends ground flush prior to testing.
(3) 14 ksi (100 MPa) is the typical minimum compressive strength required before application of design live load for most closure pour applications; consult the Engineer or Project Specifications to verify.
(4) 4 days or less is typical when the ambient curing temperature is greater than 60ºF (16ºC). For colder temperatures, an accelerating admixture may be required to obtain 14 ksi (100 MPa) in 4 days.
(5) For 14 ksi (100 MPa) compressive strength in 12-36 hours, consider using rapid-set Ductal® JS1212.
(6) This test measures the sustainable, post-cracking, direct tension strength of a mix with 2% (by volume) steel fibers.



JS1000

COMPONENTS, PACKAGING & YIELD:



1. **Premix** (dark-grey): pre-blended cement, sand, ground quartz, silica fume
   - 50 lb (23 kg) bags; 48 bags per pallet. 1 pallet yields approx. 0.65 yd³ (0.50 m³)
   - 750 lb (340 kg) mini-bulk bags; 3 bags per pallet. 1 pallet yields approx. 0.60 yd³ (0.46 m³)
   - 2,460 lb (1,115 kg) bulk bags; 1 bag per pallet. 1 pallet yields approx. 0.65 yd³ (0.50 m³)
2. **Liquid Admixture:** high range water reducer, accelerator*
   - 5 gal (19 L) pails or 264 gal (1,000 L) totes
     *An accelerator is required for curing temperatures below 50ºF (10ºC)
3. **Steel Fibers:** 0.008 in (0.20 mm) dia. x 0.5 in (13 mm) long; Tensile Strength >290 ksi (2,000 MPa).
   - 44 lb (20 kg) bags
   - 33 lb (15 kg) bags
4. **Water and/or Ice*:** to be provided by the Contractor
   *Ice may be required when batching in warm/hot weather

STORAGE:

All materials should be stored in a dry environment and/or be thoroughly covered to prevent moisture ingress, seepage, corrosion, and UV exposure. Materials should be stored between 40-95ºF (4-35ºC) and conditioned to 65-75ºF (18-24ºC) prior to use for optimum performance. Premix may be stored for up to one year in the original, unopened packaging.

PREPARATION:

Concrete surfaces to be in contact with Ductal® should be sound, have a roughened or exposed aggregate finish with 0.25 in. (6 mm) average amplitude, and be pre-wetted to a saturated surface-dry (SSD) condition prior to placing Ductal® to ensure a watertight bond. All dirt, oil, grease, and other bond-inhibiting materials should be removed prior to placement. Forms should be installed watertight to prevent leaking. Forms should be lined or coated to prevent absorption of water from the fresh material.

BATCHING:

Ductal® JS1000 should be batched on-site in accordance with Lafarge's *Ductal® Batching Procedure.* A Lafarge field representative shall be on-site during all Ductal® operations (service fee applies), unless directed otherwise. The components should be proportioned, weighed, and sequenced in accordance with the representative's recommendations based on field conditions. Ice and/or chilled water is required when the mix temperature is expected to exceed 85ºF (29ºC). An accelerating admixture is required when the curing temperature is below 50ºF (10ºC). Record the mix temperature and perform a flow test on each batch of Ductal® prior to placing.

High-shear mixers are recommended to properly and efficiently mix Ductal®. At least two mixers are recommended for most projects. Note that advertised batch capacities of most mixers are not appropriate for Ductal®. Consult a Lafarge representative to evaluate the proposed mixing equipment. High-shear mixers may be rented from Lafarge (subject to availability) with Ductal® mixing capacities of 0.20, 0.65, or 1.30 yd³ (0.15, 0.50, or 1.00 m³) per batch. Typical output is 2 to 3 batches per hour, per mixer.

Disclaimer: The values indicated above depend on the product characteristics, experimentation method, raw materials, formulae, manufacturing procedures and equipment used; all of which may vary. This data sheet provides no guarantee or commitment that the values set forth above will be achieved in any particular application of Ductal®. Ductal® is a registered trademark and may not be used without permission. The ultra-high performance material that is Ductal® and its various components are protected by various patents and may not be used except pursuant to the terms of a license agreement with the patent holder.

PLACING:

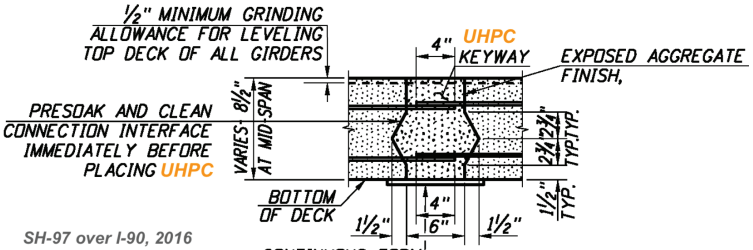
Ductal® JS1000 should be poured in-place using a bucket, wheelbarrow, or buggy and placed within 120 minutes of batching. Ductal® is self-leveling and self-consolidating and should not be vibrated as fiber segregation may occur. Exposed surfaces should be covered with poly or vapor barriers immediately after placement to prevent surface dehydration. Top forms are required when casting JS1000 on a sloping grade; properly secure top forms to restrain the hydrostatic pressure of the material. Cold weather placement procedures should be implemented when ambient temperatures drop below 50ºF (10ºC). Refer to Lafarge's *Ductal® Jointing Procedure* for additional guidance on placements in closure pour applications.

FINISHING:

The top surface of Ductal® JS1000 should be poured 0.375 in. (10 mm) higher than the finish grade and ground flush to remove all surface air voids. Top forms may be removed and grinding may commence using lightweight equipment <2,500 lb (1,135 kg) once the material has obtained 10 ksi (70 MPa) compressive strength, or as directed by a Lafarge representative.

CLOSURE POUR DESIGN & DETAILING:

UHPC's high strength and fiber confinement allow for substantially reduced closure pour widths for structural connections. Detailing of the connection is drastically simplified through the use of short, straight reinforcing bars with development lengths as short as 6 in. (150 mm) for #6 (#19) epoxy-coated rebars. Fabrication and installation of prefabricated elements is also simplified due to the use of non-obstructive, non-contact lap splice detailing. One example of a closure pour connection with a UHPC keyway is provided below. Refer to FHWA Publication No: FHWA-HRT-14-084 for guidance on the design and construction of field-cast UHPC connections. For design assistance with Ductal®, please contact a Lafarge engineering representative.



SH-97 over I-90, 2016
Deck Bulb-T Connection
Idaho Transp. Dept.

CLOSURE POUR DETAIL



Contact one of our representatives to discover more ways to use Ductal®!

Lafarge North America Inc.
8700 W Bryn Mawr Ave., Suite 300
Chicago, Illinois, USA 60631
ductal-na@lafargeholcim.com
www.ductal.com

A technology of LafargeHolcim

LAFARGE

III

ANNEX: CALCULATIONS DETAILED DESIGN

Detailed Design Calculations - Calculation parameters

Project: MSc thesis "Redesign of bridges Twentekanaal in UHPC"
Name: M. Dorland
Date: 11-11-2020
Version: D1.0

Legend: Input / Output

Geometry of the structure

Main dimensions of the deck

l	68,00	[m]	*Span of the main beams*
w_{tot}	16,36	[m]	*Total width of the deck*
l_{tot}	70,70	[m]	*Total length of the main beams*
n_{beams}	5	[-]	*Number of prefab UHPC beams*

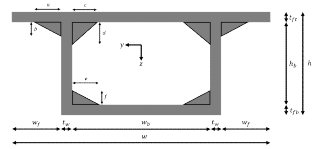
Cross sectional properties main beams

Main properties

w	3200	[mm]	*Total width*
h	2150	[mm]	*Total height*
t_{fb}	250	[mm]	*Thickness bottom flange*
t_w	150	[mm]	*Thickness of web*
w_f	500	[mm]	*Width of the flanges*
w_b	1900	[mm]	*Internal width of the box*

Chamfer of flanges

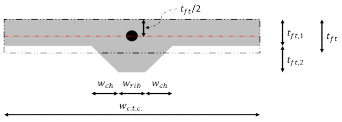
a	0	[mm]	*Width outer chamfer top flange*
b	0	[mm]	*Height outer chamfer top flange*
c	0	[mm]	*Width inner chamfer top flange*
d	0	[mm]	*Height inner chamfer top flange*
e	0	[mm]	*Width inner chamfer bottom flange*
f	0	[mm]	*Height inner chamfer bottom flange*



Top flange - transverse direction

Remark: For top flange with continuous thickness: only enter values tft1 and wc.t.c.!

$w_{c.t.c.}$	1000	[mm]	*Centre to centre distance of the transverse prestressing ribs/ducts*
$t_{ft,1}$	125	[mm]	*Continuous thickness of the top flange*
$t_{ft,2}$	125	[mm]	*Local increase thickness top flange at transverse rib*
w_{rib}	250	[mm]	*Width of the transverse prestressing rib*
w_{ch}	250	[mm]	*Width of chamfer next to the transverse prestressing rib*



Calculated parameters

t_{ft}	187,5	[mm]	*Mean value thickness top flange*
h_b	1712,5	[mm]	*Internal height of the box*

Determining cross sectional properties

Part i	Description	w_i	h_i	A_i	e_i	S_i	I_i	a_i	$I_{i,y,Steiner}$	$I_{i,y}$
[-]	[-]	[mm]	[mm]	[mm²]	[mm]	[mm³]	[mm⁴]	[mm]	[mm⁴]	[mm⁴]
1	Top flange	3200	187,5	600000,0	93,8	5,625E+07	1,758E+09	932	5,209E+11	5,227E+11
2	Web	300	1712,5	513750,0	1043,8	5,362E+08	1,256E+11	18	1,705E+08	1,257E+11
3	Bottom flange	2200	250,0	550000,0	2025,0	1,114E+09	2,865E+09	999	5,494E+11	5,523E+11
4	Chamfer top flange out	0	0,0	0,0	187,5	0,000E+00	0,000E+00	838	0,000E+00	0,000E+00
5	Chamfer top flange in	0	0,0	0,0	187,5	0,000E+00	0,000E+00	838	0,000E+00	0,000E+00
6	Chamfer bottom flange in	0	0,0	0,0	1900,0	0,000E+00	0,000E+00	874	0,000E+00	0,000E+00
Total				1663750,0		1,706E+09				1,201E+12

Symbols:

w_i	*Width of part 'i'*
h_i	*Height of part 'i'*
A_i	*Area of part 'i'*
e_i	*Distance from centre of gravity of part 'i' to the top fibre*
S_i	*First moment of area of part 'i' with respect to top fibre*
I_i	*Second moment of area of individual part 'i'*
a_i	*Distance from the centre of gravity of part 'i' to centre of gravity of the cross section*
$I_{i,y,Steiner}$	*Steiner part of part 'i'to the second moment of area of the cross section*
$I_{i,y}$	*Contribution part 'i' to second moment of area of cross section*

Main parameters

A_c	1663750,0	[mm²]	*Cross sectional area of total cross section*
z	1025,5	[mm]	*Position centre of gravity from the top flange*
I_y	1,201E+12	[mm⁴]	*Second moment of area of the combined cross section*
z_t	1025,5	[mm]	*Distance from centre of gravity to top fibre*
z_b	1124,5	[mm]	*Distance from centre of gravity to bottom fibre*
$W_{y,t}$	1,171E+09	[mm³]	*Section modulus with respect to top fibre*
$W_{y,b}$	1,068E+09	[mm³]	*Section modulus with respect to bottom fibre*

Cross sectional properties end cross beams

Main dimensions

h_{cb}	2150	[mm]	*Total height of the end cross beam*
w_{cb}	2150	[mm]	*Total width of the end cross beam*

Determining cross sectional properties

A_{cb}	4622500	[mm²]	*Cross sectional area of the cross beam*
$W_{y,cb}$	1,656E+09	[mm³]	*Section modulus of the cross section*
$I_{y,cb}$	1,781E+12	[mm⁴]	*Second moment of area of the cross section*

Cross sectional properties longitudinal joints

Main dimensions

t_j	162,5	[mm]	*Height of the longitudinal joint*
w_j	90	[mm]	*Transverse width of the longitudinal joint*

Determining cross sectional properties

A_j	162500	[mm²]	*Cross sectional area of the longitudinal joint*
W_j	4,401E+06	[mm³]	*Section modulus of the longitudinal joint*
I_j	3,576E+08	[mm⁴]	*Second moment of the cross section of the longitudinal joint*

Material and calculation parameters

Concrete

Material properties concrete main beams (Ductal FM)

Parameters mixture composition

ρ	25	[kN/m³]	*Density*
l_f	13	[mm]	*Fibre length*

Parameters concrete in compression

f_{ck}	200	[N/mm²]	*Characteristic value compressive strength*
ε_{c3}	2,3	[‰]	*Strain at reaching concrete compressive strength*
ε_{cu3}	2,6	[‰]	*Maximum compressive strain at ULS*

Parameters concrete in tension

$f_{ctk,el}$	9	[N/mm²]	*Characteristic elastic (5% percentile value) tensile strength*
f_{ctfk}	10	[N/mm²]	*Characteristic value maximal post cracking stress (w=0,30)*
K_{global}	1,25	[-]	*Fibre orientation factor (global)*
K_{local}	1,75	[-]	*Fibre orientation factor (local)*

Parameters stiffness and deformations (temperature, creep and shrinkage)

E_{cm}	50000	[N/mm²]	*Modulus of elasticity*
G	20833	[N/mm²]	*Shear modulus*
ν	0,2	[-]	*Poisson ratio*
α	0,000012	[K-1]	*Coefficient of thermal expansion*
φ	0,3	[-]	*Creep*
ε_{shr}	0,8	[‰]	*Autogenous shrinkage (during HT)*

Parameters concrete other

α	0,56	[-]	*Factor for shape of concrete compressive zone*
β	0,34	[-]	*Factor position centre of gravity concrete compressive zone*
α_{cc}	0,85	[-]	*Long term effects and unfavourable loading (compression)*
α_{ct}	1,0	[-]	*Long term effects and unfavourable loading (tension)*

Parameters fatigue

$\beta_{cc}(t)$	1,0	[-]	*Factor for increase of strength due to progressive hydration*
f_{ck0}	10	[N/mm²]	*Standard value (10 Mpa)*

Calculated values

f_{cd}	113	[N/mm²]	*Design value concrete compressive strength*
f_{ctd}	6,0	[N/mm²]	*Design value of tensile strength (tensile strength 1st crack)*
$f_{ctd;2}$	6,15	[N/mm²]	*Design value maximal post cracking stress (at w=0,30)*

Concrete longitudinal joints

Parameters mixture composition

ρ	25	[kN/m³]	*Density*

Parameters concrete in compression

f_{ck}	100	[N/mm²]	*Characteristic value compressive strength*
ε_{cu3}	2,6	[‰]	*Maximum compressive strain at ULS*

Parameters stiffness and deformations (temperature, creep and shrinkage)

E_{cm}	45000	[N/mm²]	*Modulus of elasticity*
φ	0,8	[-]	*Creep factor*
ε_{cs}	0,8	[‰]	*Shrinkage (long term)*

Parameters concrete other

α	0,56	[-]	*Factor for shape of concrete compressive zone*
β	0,34	[-]	*Factor position centre of gravity concrete compressive zone*
α_{cc}	0,85	[-]	*Long term effects and unfavourable loading (compression)*

Calculated values

f_{cd}	57	[N/mm²]	*Design value concrete compressive strength*

Material properties concrete end cross beams

Parameters mixture composition

ρ	25	[kN/m³]	*Density*

Parameters concrete in compression

f_{ck}	30	[N/mm²]	*Characteristic cylinder compressive strength at 28 days*
$f_{ck,cube}$	37	[N/mm²]	*Characteristic cube compressive strength*
f_{cm}	38	[N/mm²]	*Mean value cylinder compressive strength*
ε_{c3}	1,75	[‰]	*Strain at reaching concrete compressive strength*
ε_{cu3}	3,5	[‰]	*Maximum compressive strain at ULS*

Parameters concrete in tension

f_{ctm}	2,9	[N/mm²]	*Mean value axial tensile strength*
$f_{ctk;0,05}$	2,0	[N/mm²]	*5%-fractile of the axial tensile strength*

Parameters stiffness and deformations (temperature, creep and shrinkage)

E_{cm}	33000	[N/mm²]	*Secant modulus of elasticity*
φ	1,75	[-]	*Creep*
Hydration	Normal (N)	[-]	*Rate of hydration: Rapid (R), Normal (N) or slow (S)*
RH	80,0	[%]	*Relative humidity*

Parameters concrete other

α	0,75	[-]	*Factor for shape of concrete compressive zone*
β	0,39	[-]	*Factor position centre of gravity concrete compressive zone*
α_{cc}	1,0	[-]	*Long term effects and unfavourable loading (compression)*

Calculated values

f_{cd}	20	[N/mm²]	*Design value concrete compressive strength*

Prestressing steel & parameters strands and tendons

Parameters prestressing main beams

Material properties prestressing steel

f_{pk}	1860	[N/mm²]	*Characteristic value tensile strength*
f_{pd}	1522	[N/mm²]	*Design value steel stress*
σ_{pm0}	1395	[N/mm²]	*Maximum allowed stress directly after tensioning*
$\sigma_{p,max}$	1488	[N/mm²]	*Maximum prestressing stress during tensioning*
E_p	195000	[N/mm²]	*Modulus of elasticity*
ε_{uk}	35	[‰]	*Characteristic value strain at failure*

Properties prestressing strands

Parameters transverse prestressing

Material properties prestressing steel

f_{pk}	1860	[N/mm²]	*Characteristic value tensile strength*
f_{pd}	1522	[N/mm²]	*Design value steel stress*
σ_{pm0}	1395	[N/mm²]	*Maximum allowed stress directly after tensioning*
$\sigma_{p,max}$	1488	[N/mm²]	*Maximum prestressing stress during tensioning*
E_p	195000	[N/mm²]	*Modulus of elasticity*
ε_{uk}	35	[‰]	*Characteristic value strain at failure*

Properties prestressing tendons

Parameters prestressing end cross beams

Material properties prestressing steel

f_{pk}	1860	[N/mm²]	*Characteristic value tensile strength*
f_{pd}	1522	[N/mm²]	*Design value steel stress*
σ_{pm0}	1395	[N/mm²]	*Maximum allowed stress directly after tensioning*
$\sigma_{p,max}$	1488	[N/mm²]	*Maximum prestressing stress during tensioning*
E_p	195000	[N/mm²]	*Modulus of elasticity*
ε_{uk}	35	[‰]	*Characteristic value strain at failure*

Properties prestressing tendons

n_c	10	[pcs]	Assumed number of strands positioned centrically in the cross section	n	5,00	[pcs]	Assumed number of strands per tendon	n_{ducts}	4	[pcs]	Number of ducts in total
$D_{strand,c}$	15,2	[mm]	Diameter of strands positioned centrically	D_{strand}	15,2	[mm]	Diameter of single strand	a_{vert}	500	[mm]	Vertical position centre of duct from centre of beam
$A_{p,strand,c}$	140	[N/mm²]	Cross sectional area per strand	$A_{p,strand}$	140,00	[mm²]	Cross sectional area per strand	a_{hor}	750	[mm]	Horizontal position centre of duct from centre of beam
$\sigma_{p,max,prov,c}$	1390	[mm²]	Assumed maximum stress applied to centrically positioned strands	$\sigma_{p,max,prov}$	1400,00	[N/mm²]	Assumed maximum stress applied to prestressing element				
								n_{strand}	7	[pcs]	Assumed number of strands per tendon
n_{fb}	120	[pcs]	Assumed number of strands positioned in bottom flange	μ	0,23	[-]	Friction coefficient	D_{strand}	15,2	[mm]	Diameter of single strand
$D_{strand,fb}$	15,2	[mm]	Diameter of strands positioned in bottom flange	k	0,009	[rad]	Unintentional angular rotation due to the Wobble-effect	$A_{p,strand}$	140	[mm²]	Cross sectional area per strand
$A_{p,strand,fb}$	140	[N/mm²]	Cross sectional area per strand	w_{set}	3	[mm]	Estimated wedge set	$\sigma_{p,max,prov}$	1400	[N/mm²]	Assumed maximum stress applied to prestressing element
$\sigma_{p,max,prov,fb}$	1450	[mm²]	Assumed maximum stress applied to strands in bottom flange								
				Relaxation	Class 2	[-]	Select relaxation class: normal (1), low (2) or bars (3)	ϕ_{Duct}	65	[mm]	Outer diameter of prestressing ducts
Relaxation	Class 2	[-]	Select relaxation class: normal (1), low (2) or bars (3)	t	500000	[h]	The value of the relaxation loss (in %) at 1000 h				
t	500000	[h]	The value of the relaxation loss (in %) at 1000 h	ρ	2,5	[%]	Time after stressing (for final value of the relaxation loss)	μ	0,23	[-]	Friction coefficient
ρ	2,5	[%]	Time after stressing (for final value of the relaxation loss)					k	0,009	[rad]	Unintentional angular rotation due to the Wobble-effect
t_{eq}	461935	[h]	Equivalant time (optional), NOTE: Calculated manually!					w_{set}	3	[mm]	Estimated wedge set
								Relaxation	Class 2	[-]	Select relaxation class: normal (1), low (2) or bars (3)
								t	500000	[h]	The value of the relaxation loss (in %) at 1000 h
								ρ	2,5	[%]	Time after stressing (for final value of the relaxation loss)

Parameters detailing beam ends

η	1,35	[-]	Bond factor conforming table 7.2 of AFGC-SETRA 2013
η_1	1,0	[-]	Factor accounting for bond conditions, cf EC2-1-1
κ	1,5	[-]	Factor for bond strength improvement due to the presence of fibres
α_1	1,0	[-]	Factor depending on way of releasing the strands
α_2	0,19	[-]	Factor depending on the type of tendon
$n_{fb,1}$	120	[pcs]	Selected number of strands introduced in first set
$n_{fb,2}$	0	[pcs]	Selected number of strands introduced in second set (optional)
$x_{debond,1}$	0	[m]	Length over which first set of strands is debonded (optional)
$x_{debond,2}$	0,0	[m]	Length over which second set of strands is debonded (optional)

Parameters fatigue verification

$\Delta\sigma_{Rsk}$	185	[N/mm²]	Stress range at N* cycles
N^*	1000000	[-]	Number of cycles with single stress range
k_1	5	[-]	Stress exponent first branch
k_2	9	[-]	Stress exponent second branch

Partial factors material resistance

γ_C	1,5	[-]	Partial factor concrete (cf EC2)	$\gamma_{F,fat}$	1,0	[-]	See 2.4.2.3 of NA to NEN-EN 1992-1-1	γ_{spl}	1,2	[-]	Partial factor splitting forces
γ_{cf}	1,3	[-]	Partial factor for fibre reinforced concrete in tension (cf AFGC)	$\gamma_{S,fat}$	1,1	[-]	See 2.4.2.4 of NA to NEN-EN 1992-1-1				
$\gamma_E * \gamma_{cf}$	1,5	[-]	Product of partial factor for uncertainty in extrapolation * factor Ycf								
γ_S	1,1	[-]	Partial factor prestressing steel (cf EC2)								

Calculation parameters

Calculation parameters main beams

σ_{max}	6,7	[N/mm²]	Maximum allowed stress at outer concrete fibres
θ	30	[°]	Angle of the concrete compressive strut of the main beams
Cover	35	[mm]	Assumed minimum cover bottom flange(all sides)
$\emptyset_{spl,f1}$	10	[mm]	Assumed diameter splitting reinforcement bottom flange
μ	0,5	[-]	Friction coefficient concrete and supports
$1/\delta$	300	[-]	Maximum deflection in SLS

Calculation parameters longitudinal joints and top flange

$\emptyset_{spl,ft}$	10	[mm]	Assumed diameter splitting reinforcement top flange
h_1	100	[mm]	Anchor plate (height and width)

Calculation parameters end cross beams

k_1	0,15	[-]	Factor from 6.2.2 of the NA to NEN-EN 1992-1-1
θ	21,8	[°]	Angle concrete compressive strut of end cross beam

Design of bridge and main carriageway - Actions

Design main carriageway

Kerbs

h_{kerb}	340	[mm]	Assumed height of the kerb
w_{kerb}	500	[mm]	Assumed width of the kerb
ρ_C	25	[kN/m³]	Density of the concrete used

Road surface

t_{surf}	10	[mm]	Assumed thickness of the surface layer
$\rho_{asphalt}$	23	[kN/m³]	Density of the material used

Effective width of the beams

$b_{eff,0}$	3,245	[m]	Effective width of the outer beams to determine loads
$b_{eff,i}$	3,29	[m]	Effective width of the inner beams to determine loads

Permanent actions (G)

Self-weight prefab beams

$G_{k,beam}$	41,59	[kN/m]	Line load representing the self-weight of the prefab beams

Self-weight end cross beams

$G_{k,cb}$	115,56	[kN/m]	Line load representing the self-weight of the end cross beams

Self-weight longitudinal joints

A_j''	0,016875	[m²]	Area of the total joint using tft and wj
$G_{k,j}$	0,421875	[kN/m]	Line load representing the self-weight of the joints

Permanent load road surface

$G_{k,surf}$	0,23	[kN/m²]	Area load representing the surface layer

Permanent load kerbs

A_{kerb}	0,17	[m²]	Cross sectional area of the kerb
$G_{k,kerb}$	8,5	[kN/m²]	Area load representing the kerb

Variable actions (Q)

Load model 1

Lane	Q_{ik} [kN]	q_{ik} [kN/m²]
1	291	8,73
2	194	2,425
rk	0	2,25

Load model 2

$\beta_Q Q_{ak}$	388	[kN/axle]	Axle load according to LM2

Accidental actions (A)

F_{equi}	1000	[kN]	Equivalent static force, see: (4) of 4.6.2. EC1-1-7

Fatigue

n_y	100	[-]	Design service life
N_{obs}	500000	[-]	Number of heavy vehicles per year

Combinations of actions

γ_G	1,4	[-]	See tabel NB.16 – A2.4(B) of NA to NEN-EN 1990
$\zeta * \gamma_G$	1,25	[-]	See tabel NB.16 – A2.4(B) of NA to NEN-EN 1990
γ_P	1,0	[-]	See 2.4.2.2 of NA to NEN-EN 1992-1-1
γ_Q	1,5	[-]	See tabel NB.16 – A2.4(B) of NA to NEN-EN 1990
ψ_0	0,8	[-]	See tabel NB.12 – A2.1 of NA to NEN-EN 1990
ψ_1	0,8	[-]	See tabel NB.12 – A2.1 of NA to NEN-EN 1990

Determining force distribution (RFEM input)

Design of main prestressing and verification capacity of the main beams

Ultimate limit state verifications main beams

M_{Ed}	48426	[kNm]	Governing bending moment value (mid span)
V_{Ed}	4090	[kN]	Governing shear force value (near supports)
T_{Ed}	1222	[kNm]	Governing torsional moment

Serviceability limit state - Design of prestressing (characteristic combination)

$M_{E,G,perm}$	1727	[kNm]	Bending moment imposed permanent loads in SLS at midspan
$M_{E,Q}$	9694	[kNm]	Bending moment variable loads in SLS at midspan

Serviceability limit state - Deflections (frequent combination)

δ_{max}	344,4	[mm]	Max. deflection at midspan in SLS (frequent combination)

Fatigue analysis main beams

$M_{fat,max}$	31539	[kNm]	Maximum bending moment at midspan (found using RFEM)
$M_{fat,min}$	27183	[kNm]	Minimum bending moment at midspan (found using RFEM)

Design of prestressing and verification capacity of the end cross beams

Ultimate limit state verifications end beams

$M_{Ed,hog}$	1212	[kNm]	Maximum hogging bending moment (all loads considered)
$M_{Ed,sag}$	436	[kNm]	Maximum sagging bending moment (all loads considered)
V_{Ed}	837	[kN]	Maximum shear force (all loads considered)

Serviceability limit state - Design of prestressing

$M_{E,hog}$	469	[kNm]	Maximum hogging bending moment SLS
$M_{E,sag}$	298	[kNm]	Maximum sagging bending moment SLS

Detailed Design Calculations - Design of main beams - Main prestressing and ULS (STR)

Project: MSc thesis "Redesign of bridges Twentekanaal in UHPC"
Name: M. Dorland
Date: 11-11-2020
Version: D1.0

Input parameters

Input parameters - Cross sectional properties and calculation parameters

Cross sectional properties

A_c	1663750	[mm²]	*Cross sectional area of total cross section*
z_t	1025,5	[mm]	*Distance from centre of gravity to top fibre*
e_p	999,47	[mm]	*Eccentricity of tendons in bottom flange*
I_y	1,20069E+12	[mm⁴]	*Second moment of area of the combined cross section*
$W_{y,t}$	1170801541	[mm³]	*Section modulus with respect to top fibre*
$W_{y,b}$	1067786143	[mm³]	*Section modulus with respect to bottom fibre*

Calculation parameters

θ	30	[°]	*Angle of the concrete compressive strut of the main beams*

Input parameters - Material properties & main prestressing

Concrete

Parameters mixture composition

ρ	25	[kN/m³]	*Density*
l_f	13	[mm]	*Fibre length*

Parameters concrete in compression

f_{ck}	200	[N/mm²]	*Characteristic value compressive strength*
ε_{c3}	2,3	[‰]	*Strain at reaching concrete compressive strength*
ε_{cu3}	2,6	[‰]	*Maximum compressive strain at ULS*

Parameters concrete in tension

$f_{ctk,el}$	9	[N/mm²]	*Characteristic elastic (5% percentile value) tensile strength*
f_{ctfk}	10	[N/mm²]	*Characteristic value maximal post cracking stress (w=0,30)*
K_{global}	1,25	[-]	*Fibre orientation factor (global)*
K_{local}	1,75	[-]	*Fibre orientation factor (local)*

Parameters stiffness and deformations (temperature, creep and shrinkage)

E_{cm}	50000	[N/mm²]	*Modulus of elasticity*
G	20833	[N/mm²]	*Shear modulus*
ν	0,2	[-]	*Poisson ratio*
α	0,000012	[K-1]	*Coefficient of thermal expansion*
φ	0,3	[-]	*Creep*
ε_{shr}	0,8	[‰]	*Autogenous shrinkage (during HT)*

Parameters concrete other

α	0,56	[-]	*Factor for shape of concrete compressive zone*
β	0,34	[-]	*Factor position centre of gravity concrete compressive zone*
α_{cc}	0,85	[-]	*Long term effects and unfavourable loading (compression)*
α_{ct}	1	[-]	*Long term effects and unfavourable loading (tension)*

Calculated design values

f_{cd}	113	[N/mm²]	*Design value concrete compressive strength*
f_{ctd}	6,0	[N/mm²]	*Design value of tensile strength (tensile strength 1st crack)*
$f_{ctd;2}$	6,15	[N/mm²]	*Design value maximal post cracking stress (at w=0,30)*

Parameters main prestressing

Material properties prestressing steel

f_{pk}	1860	[N/mm²]	*Characteristic value tensile strength*
f_{pd}	1522	[N/mm²]	*Design value steel stress*
σ_{pm0}	1395	[N/mm²]	*Maximum allowed stress directly after tensioning*
$\sigma_{p,max}$	1488	[N/mm²]	*Maximum prestressing stress during tensioning*
E_p	195000	[N/mm²]	*Modulus of elasticity*
ε_{uk}	35	[‰]	*Characteristic value strain at failure*

Parameters prestressing strands

n_c	10	[-]	*Assumed number of strands positioned centrically in the cross section*
$D_{strand,c}$	15,2	[mm]	*Diameter of strands positioned centrically*
$A_{p,strand,c}$	140	[N/mm²]	*Cross sectional area per strand*
$\sigma_{p,max,prov,c}$	1390	[mm²]	*Assumed maximum stress applied to centrically positioned strands*
n_{fb}	120	[-]	*Assumed number of strands positioned in bottom flange*
$D_{strand,fb}$	15,2	[mm]	*Diameter of strands positioned in bottom flange*
$A_{p,strand,fb}$	140	[N/mm²]	*Cross sectional area per strand*
$\sigma_{p,max,prov,fb}$	1450	[mm²]	*Assumed maximum stress applied to strands positioned in bottom flange*
Relaxation	Class 2	[-]	*Select relaxation class: normal (1), low (2) or bars (3)*
t	500000	[h]	*The value of the relaxation loss (in %) at 1000 h*
ρ	2,5	[%]	*Time after stressing (to determine the final value of the relaxation loss)*
t_{eq}	461935	[h]	*Equivalant time, NOTE: Calculated manually!*

Parameters detailing beam ends

η	1,35	[-]	*Bond factor conforming table 7.2 of AFGC-SETRA 2013*
η_1	1,0	[-]	*Factor accounting for bond conditions, cf EC2-1-1*
κ	1,5	[-]	*Factor for bond strength improvement due to the presence of fibres*
α_1	1,0	[-]	*Factor depending on way of releasing the strands*
α_2	0,19	[-]	*Facor depending on the type of tendon*
$n_{fb,1}$	120	[pcs]	*Selected number of strands introduced in first set*
$n_{fb,2}$	0	[pcs]	*Selected number of strands introduced in second set*
$x_{debond,1}$	0	[m]	*Length over which first set of strands is debonded*
$x_{debond,2}$	0	[m]	*Length over which second set of strands is debonded*

Other parameters

γ_C	1,5	[-]	*Partial factor concrete (cf EC2)*
γ_{cf}	1,3	[-]	*Partial factor for fibre reinforced concrete in tension*
$\gamma_E * \gamma_{cf}$	1,5	[-]	*Product of partial factors (AFGC-SETRA 2013)*
γ_S	1,1	[-]	*Partial factor prestressing steel (cf EC2)*
γ_{spl}	1,2	[-]	*Partial factor splitting forces*

Input parameters - Loads

$M_{E,G,sw}$	24041	[kNm]	*Bending moment midspan due to self-weight of the beams in SLS*
$M_{E,G,perm}$	1727	[kNm]	*Bending moment mid span due to imposed permanent loads in SLS (RFEM)*
$M_{E,Q}$	9694	[kNm]	*Bending moment due to variable loads in SLS (RFEM)*

Design of the main prestressing

Calculating prestress losses

Applied maximum force onto prestressing element & stress verification

$\sigma_{p,max,prov,c}$	1390	[mm²]	*Assumed maximum stress applied to centrically positioned strands*
$P_{max,prov,c}$	1946	[kN]	*Assumed maximum force applied to centrically positioned strands*
$\sigma_{p,max,prov,fb}$	1450	[mm²]	*Assumed maximum stress applied to strands positioned in bottom flange*
$P_{max,prov,fb}$	24360	[kN]	*Assumed maximum force applied to strands positioned in bottom flange*

Verification maximum stress prestressing steel

$\sigma_{p,max,prov,c}$	1390,00	[N/mm²]	*Assumed maximum stress applied to centric prestressing*
Verification	Satisfied	[-]	*Verification*
$\sigma_{p,max,prov,fb}$	1450	[N/mm²]	*Assumed maximum stress applied to strands positioned in bottom flange*
Verification	Satisfied	[-]	*Verification*

Verifications maximum concrete compressive stress

$\sigma_{c,prov,c+fb}$	38,61	[N/mm²]	*Maximum compressive stress in concrete due to prestressing*
$\sigma_{c,limit}$	140,00	[N/mm²]	*Maximum value concrete compressive stress*
Verification	Satisfied	[-]	*Verification*

Applied value maxinum force applied onto prestressing strands

$\sigma_{p,max,c}$	1390,00	[N/mm²]	*Applied value maximum stress centric prestressing*
$A_{p,c}$	1400,00	[mm²]	*Applied cross section centric prestressing*
$P_{max,c}$	1946,00	[kN]	*Applied value maximum force centric prestressing*
$\sigma_{p,max,fb}$	1450,00	[N/mm²]	*Applied value maximum stress eccentric prestressing*
$A_{p,fb}$	16800,00	[mm²]	*Applied cross section eccentric prestressing*
$P_{max,fb}$	24360,00	[kN]	*Applied value maximum force eccentric prestressing*

Direct prestressing losses

Elastic losses centric prestressing

α_e	3,90	[-]	*Ratio moduli of elasticity*
$\rho_{p,c}$	0,0008	[-]	*Ratio of cross section steel and concrete*
I_c	NA	[-]	*Factor for eccentricity*
$\Delta P_{el,c}$	6,37	[KN]	*Elastic loss centric prestressing*

Elastic losses eccentric prestressing flange

α_e	3,90	[-]	*Ratio moduli of elasticity*
$\rho_{p,fb}$	0,0101	[-]	*Ratio of cross section steel and concrete*
I_{fb}	2,38	[-]	*Factor for eccentricity*
$\Delta P_{el,fb}$	2090,88	[KN]	*Elastic loss eccentric prestressing*

Determining initial prestressing force & stress verification

Applied force and stress values

$P_{m0,c}$	1940	[kN]	*Initial prestressing force centric prestressing*
$\sigma_{pm0,c}$	1385	[N/mm²]	*Initial prestressing stress centric prestressing*
$P_{m0,fb}$	22269	[kN]	*Initial prestressing force eccentric prestressing*
$\sigma_{pm0,fb}$	1326	[N/mm²]	*Initial prestressing stress eccentric prestressing*

Stress limit and verification

Verification	Satisfied	[-]	*Verification initial prestressing stress (centric prestressing)*
Verification	Satisfied	[-]	*Verification initial prestressing stress (eccentric prestressing)*

Verified values initial prestressing force

$P_{m0,c}$	1940	[kN]	*Applied value initial prestressing force centric prestressing*
$\sigma_{pm0,c}$	1385	[N/mm²]	*Applied value initial stress centric prestressing*
$P_{m0,fb}$	22269	[kN]	*Applied value initial prestressing force eccentric prestressing*
$\sigma_{pm0,fb}$	1326	[N/mm²]	*Applied value initial stresseccentric prestressing*

Time dependent losses

Centric prestressing - Relaxation

Class	Class 2	[-]	*Relaxation class (normal relaxation, low relaxation and bars)*
ρ_{1000}	2,5	[%]	*The value of the relaxation loss (in %) at 1000 h*
μ_c	0,74	[-]	*Factor depending on steel stresses*
t	961935	[h]	*Time after stressing (for final value of the relaxation loss)*
$\Delta\sigma_{pr,c}/\sigma_{pi,c}$	0,054	[-]	*Relaxation coefficient*
$\sigma_{pi,c}$	1385,5	[N/mm²]	*Absolute value of the initial prestressing (σ_pm0)*
$\Delta\sigma_{pr,c}$	74,8	[N/mm²]	*Prestress loss due to relaxation*

Centric prestressing - Accounting for heat treatment (if applicable)

t_{eq}	461935	[h]	*Equivalant time, NOTE: Calculated manually!*

Centric prestressing - Relaxation classes

Class 1	Wires and strands normal relaxation
Class 2	Wires and strands low relaxation
Class 3	Bars

Centric prestressing - Creep & shrinkage

φ	0,3	[-]	*Creep factor*
$\sigma_{c,QP,c}$	14,55071573	[N/mm²]	*Stress in concrete adjacent to centric prestressing strands*
ε_{cs}	0,0008	[-]	*Shrinkage of the concrete*

Centric prestressing - Total time dependent losses

$\Delta\sigma_{p,c+s+r,c}$	231,9	[N/mm²]	*Time dependent prestressing losses (stress, centric)*
$\Delta P_{p,c+s+r,c}$	324,6	[kN]	*Time dependent prestressing losses (force, centric)*

Eccentric prestressing flange - Relaxation

Class	Class 2	[-]	*Relaxation class (normal relaxation, low relaxation and bars)*
ρ_{1000}	2,5	[%]	*The value of the relaxation loss (in %) at 1000 h*
μ_{fb}	0,71	[-]	*Factor depending on steel stresses*
t	961935	[h]	*Time after stressing (for final value of the relaxation loss)*
$\Delta\sigma_{pr,fb}/\sigma_{pi,fb}$	0,047517272	[-]	*Relaxation coefficient*
$\sigma_{pi,fb}$	1325,5	[N/mm²]	*Absolute value of the initial prestressing (σ_pm0)*
$\Delta\sigma_{pr,fb}$	63,0	[N/mm²]	*Prestress loss due to relaxation*

Eccentric prestressing flange - Accounting for heat treatment (if applicable)

t_{eq}	461935	[h]	*Equivalant time, NOTE: Calculated manually!*

Eccentric prestressing flange - Relaxation classes

Class 1	Wires and strands normal relaxation
Class 2	Wires and strands low relaxation
Class 3	Bars

Eccentric prestressing flange - Creep & shrinkage

φ	0,3	[-]	*Creep factor*
$\sigma_{c,QP,fb}$	33,07792915	[N/mm²]	*Stress in concrete adjacent to eccentric prestressing strands*
ε_{cs}	0,0008	[-]	*Shrinkage of the concrete*

Eccentric prestressing flange - Total time dependent losses

$\Delta\sigma_{p,c+s+r,fb}$	219,5	[N/mm²]	*Time dependent prestressing losses (stress, eccentric)*
$\Delta P_{p,c+s+r,fb}$	3688,1	[kN]	*Time dependent prestressing losses (force, eccentric)*

Working prestress force and total prestress losses

$P_{m,\infty,c}$	1615	[kN]	*Working prestressing force centric prestressing*
$\sigma_{pm,\infty,c}$	1154	[N/mm²]	*Working prestressing stress centric prestressing*
$P_{m,\infty,fb}$	18581	[kN]	*Working prestressing force eccentric prestressing*
$\sigma_{pm,\infty,fb}$	1106	[N/mm²]	*Working prestressing stress eccentric prestressing*

Summary of results (middle cross section)

	Prestressing forces			Prestress losses forces			
	P_{max}	P_{m0}	$P_{m,\infty}$	ΔP_i	$\Delta P_{p,c+s+r}$	ΔP_{tot}	$\Delta P_{\%}$
Prestressing:	[kN]	[kN]	[kN]	[kN]	[kN]	[kN]	[%]
Centric	1946	1940	1615	6	325	331	17,0
Eccentric	24360	22269	18581	2091	3688	5779	23,7

	Prestressing stresses			Prestress losses forces			
	σ_{max}	σ_{pm0}	$\sigma_{pm,\infty}$	$\Delta\sigma_i$	$\Delta\sigma_{p,c+s+r}$	$\Delta\sigma_{tot}$	$\Delta\sigma_{\%}$
Prestressing:	[N/mm²]	[N/mm²]	[N/mm²]	[N/mm²]	[N/mm²]	[N/mm²]	[%]
Centric	1390	1385	1154	5	232	236	17,0
Eccentric	1450	1326	1106	124	220	344	23,7

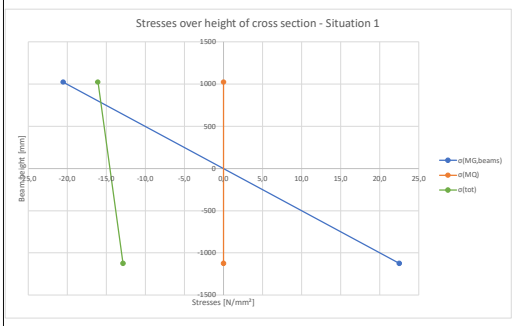
Determining stresses at midspan

σ_{max}	6,7	[N/mm²]	*Maximum tensile stress allowed at outer fibres*

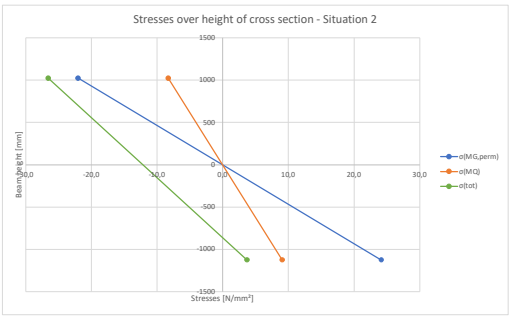
Stresses situation 1

Stresses situation 2

	Height [mm]	σ(MG,beams) [N/mm²]	σ(MQ) [N/mm²]	σ(Pt) [N/mm²]	σ(Pfb) [N/mm²]	σ(Mr,fb) [N/mm²]	σ(tot) [N/mm²]
Top fibre	1026	-20,5	0,0	-1,2	-13,4	19,0	-16,1
Bottom fibre	-1124	22,5	0,0	-1,2	-13,4	-20,8	-12,9
Maximum	2150						-12,9



	Height [mm]	σ(MG,perm) [N/mm²]	σ(MQ) [N/mm²]	σ(Pt) [N/mm²]	σ(Pfb) [N/mm²]	σ(Mr,fb) [N/mm²]	σ(tot) [N/mm²]
Top fibre	1026	-22,0	-8,3	-1,0	-11,2	15,9	-26,6
Bottom fibre	-1124	24,1	9,1	-1,0	-11,2	-17,4	3,7
Maximum	2150						3,7



Detailing beam ends

Bond stresses and transmission length

Determining bond stress

η	1,35	[-]	*Bond factor conforming table 7.2 of AFGC-SETRA 2013*
η_1	1,0	[-]	*Factor accounting for bond conditions, cf EC2-1-1*
κ	1,5	[-]	*Factor for bond strength improvement due to the presence of fibres*
f_{ctd}	6,0	[N/mm²]	*Design value tensile strength*
f_{bpt}	12,15	[N/mm²]	*Bond strength*

Transmission length centric prestressing

α_1	1,0	[-]	*Factor depending on way of releasing the strands*
α_2	0,19	[-]	*Facor depending on the type of tendon*
Ø	15,2	[-]	*Diameter of the prestressing element*
σ_{pm0}	1385,5	[N/mm²]	*Stress in tendon just after release (i.e. initial stress)*
$l_{pt,c}$	329,3	[mm]	*Transfer length*
$l_{pt1,c}$	0,132	[m]	*Design value transmission length centric prestressing*

Transmission length eccentric prestressing

α_1	1,0	[-]	*Factor depending on way of releasing the strands*
α_2	0,19	[-]	*Facor depending on the type of tendon*
Ø	15,2	[-]	*Diameter of the prestressing element*
σ_{pm0}	1325,5	[N/mm²]	*Stress in tendon just after release (i.e. initial stress)*
$l_{pt,fb}$	315,1	[mm]	*Transfer length*
$l_{pt1,fb}$	0,126	[m]	*Design value transmission length eccentric prestressing*

Tensile stresses at top fibre

Centric prestressing

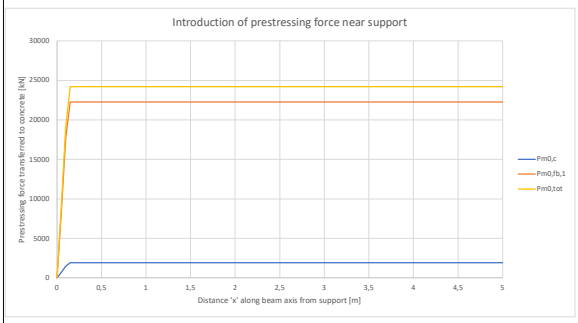
P_{m0}	1940	[kN]	*Initial prestressing force centric prestresssing*
$l_{pt1,c}$	0,132	[m]	*Design value transmission length centric prestressing*

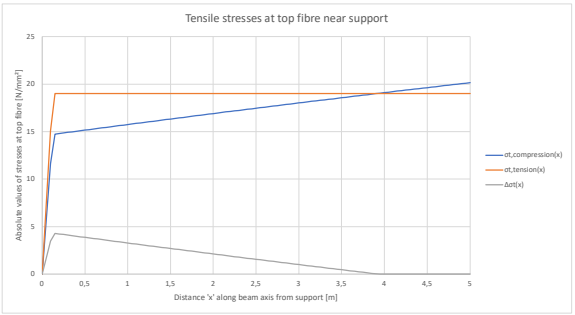
Eccentric prestressing

n_{fb}	120	[pcs]	*Total number of strands in bottom flange*
$n_{fb,1}$	120	[pcs]	*Selected number of strands introduced in first set*
$n_{fb,2}$	0	[pcs]	*Selected number of strands introduced in second set*
$x_{debond,1}$	0	[m]	*Length over which first set of strands is debonded*
$x_{debond,2}$	0	[m]	*Length over which second set of strands is debonded*

Parameters sets of strands eccentric prestressing

$P_{m0,fb}$	22269	[kN]	*Total initial prestressing force eccentric prestressing*
$P_{m0,fb,1}$	22269	[kN]	*Initial prestressing force first set of strands*
$P_{m0,fb,2}$	0	[kN]	*Initial prestressing force second set of strands*
$l_{pt1,fb}$	0,126	[m]	*Design value transmission length eccentric prestressing*





Verification remaining tensile stress

$\Delta\sigma_t$	4,3	[N/mm²]	*Highest value remaining tensile stress*
σ_{max}	6,7	[N/mm²]	*Maximum allowable tensile stress*
Verification	Satisfied	[-]	*Verification*

Positioning of strands in the bottom flange

Auxiliary parameters (dimensions)

h	2150	[mm]	*Total height*
w_b	1900	[mm]	*Internal width of the box*
b	2200	[mm]	*Width lower end of beam (webs and internal width)*
w_{cb}	2150	[mm]	*Total width end cross beam (solid part)*
t_{fb}	250	[mm]	*Thickness bottom flange*
t_w	150	[mm]	*Thickness of web*

Positioning of the strands - Parameters

$D_{strand,fb}$	15,2	[mm]	*Assumed strand diameter*
Cover min	35	[mm]	*Assumed minimum cover (all sides)*
Spacing	30,4	[mm]	*Assumed minimum spacing (horizontal and vertical)*
d_{min}	45,6	[mm]	*Minimum c.t.c. distance in horizontal and vertical direction*
$h_{available}$	180	[mm]	*Available height bottom flange for positioning of the strands*
$w_{available}$	2130	[mm]	*Available width bottom flange for positioning of the strands*
$n_{max,rows}$	3	[pcs]	*Maximum number of rows in bottom flange*
$n_{max,strands}$	46	[pcs]	*Maximum number of strands per row in bottom flange*
$n_{max,fb}$	138	[pcs]	*Maximum allowable number of strands in bottm flange*

Positioning of the strands - Applied values

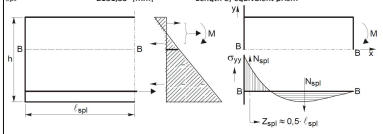
n_{fb}	120	[pcs]	*Total number of strands in bottom flange*
n_{rows}	3	[pcs]	*Required number of rows*
$n_{strands}$	40	[pcs]	*Number of strands per row*
d_{vert}	82,40	[mm]	*Applied vertical c.t.c. distance between the applied strands*
d_{hor}	54,23	[mm]	*Applied horizontal c.t.c. distance between the applied strands*

Splitting reinforcement - Vertical distribution

Spalling stresses

Equivalent prism spalling (See: Textbook CIE4160 - Section 10.2.2):

l_{pt}	126	[mm]	*Transfer length*
ζ_{spl}	1,00	[-]	*Factor for splitting*
l_{spl}	2151,33	[mm]	*Length of equivalent prism*



First set of strands:

σ_{top}	4,5	[N/mm²]	*Stress due to prestressing in top fibre at end of prism*
σ_{bottom}	-35,4	[N/mm²]	*Stress due to prestressing in bottom fibre at end of prism*
h_{prism}	481,2	[mm]	*Height of equivalent prism*
b	2200	[mm]	*Width of cs at height where spalling occurs (at start of the prism)*
M	378561783	[Nm]	*Bending moment (elastic stress distribution) due to prestressing*
N_{spl}	351933	[N]	*Spalling tensile force*
σ_{spl}	0,59	[N/mm²]	*Spalling tensile stress*
γ_{spl}	1,2	[-]	*Partial factor splitting*
$\sigma_{Rd,d}$	0,71	[N/mm²]	*Design value splitting stress*
$\sigma_{Rd,f}$	4,40	[N/mm²]	*Residual tensile strength, calculated with Klocal*
Verification	Satisfied	[-]	*If verification is satisfied no spalling reinforcement needed*

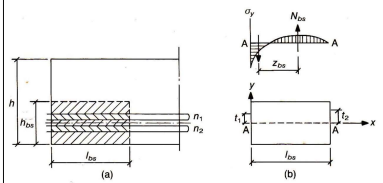
Second set of strands (if applicable):

σ_{top}	4,5	[N/mm²]	*Stress due to prestressing in top fibre at end of prism*
σ_{bottom}	-35,4	[N/mm²]	*Stress due to prestressing in bottom fibre at end of prism*
h_{prism}	481,2	[mm]	*Height of equivalent prism*
b	2200	[mm]	*Width of cs at height where spalling occurs*
M	378561783	[Nm]	*Bending moment due (elastic stress distribution prestressing)*
N_{spl}	351933	[N]	*Spalligh tensile force*
σ_{spl}	0,59	[N/mm²]	*Spalling tensile stress*
γ_{spl}	1,2	[-]	*Partial factor splitting*
$\sigma_{Rd,d}$	0,71	[N/mm²]	*Design value splitting stress*
$\sigma_{Rd,f}$	4,40	[N/mm²]	*Residual tensile strength, calculated with Klocal*
Verification	Satisfied	[-]	*If verification is satisfied no spalling reinforcement needed*

Bursting stresses

Symmetric prism analogy (See: fib Model Code 2010 - Section 7.13.6.5.2):

h_{bs}	250	[mm]	*Height of the virtual prismatic element*
l_{pt}	126	[mm]	*Transfer length of the strands*
ζ_{bs}	1,04	[-]	*Factor for bursting*
l_{bs}	261,19	[mm]	*Length of equivalent prism*



First set of strands:

n_1	40	[pcs]	*Set 1: Number of tendons above the centroid of the prism*
n_2	40	[pcs]	*Set 1: Number of tendons below the centroid of the prism*
t_1	82,4	[mm]	*Set 1: Distance centroid tendons above section to centroid of prism*
t_2	62,5	[mm]	*Set 1: Distance centroid of stress block to centroid of prism*
$P_{m0,fb}$	185,6	[kN]	*Initial prestressing force for a single tendon*
z_{bs}	130,6	[mm]	*Internal lever arm of bursting forces*
N_{bs}	-1131	[kN]	*Set 1: Bursting force*
b_{bs}	2200	[mm]	*Width of prism at the position of strands*
σ_{bs}	-1,97	[N/mm²]	*Set 1: Maximum bursting stresses*
γ_{spl}	1,2	[-]	*Partial factor splitting*
$\sigma_{Rd,d}$	-2,36	[N/mm²]	*Set 1: Design value maximum bursting stresses*
$\sigma_{Rd,f}$	4,40	[N/mm²]	*Residual tensile strength, calculated with Klocal*
Verification	Satisfied	[-]	*Set 1: Verification of bursting stresses and material strength*

Second set of strands (if applicable):

n_1	0	[pcs]	*Set 2: Number of tendons above the centroid of the prism*
n_2	0	[pcs]	*Set 2: Number of tendons below the centroid of the prism*
t_1	82,4	[mm]	*Set 2: Distance centroid tendons to centroid of prism*
t_2	62,5	[mm]	*Set 2: Distance centroid of stress block to centroid of prism*
$P_{m0,fb,1}$	185,6	[kN]	*Initial prestressing force for a single tendon*
z_{bs}	130,6	[mm]	*Internal lever arm of bursting forces*
N_{bs}	0	[kN]	*Set 2: Bursting force*
b_{bs}	2200	[mm]	*Width of prism at the position of strands*
σ_{bs}	0,00	[N/mm²]	*Set 2: Maximum bursting stresses*
γ_{spl}	1,2	[-]	*Partial factor splitting*
$\sigma_{Rd,d}$	0,00	[N/mm²]	*Set 2: Design value maximum bursting stresses*
$\sigma_{Rd,f}$	4,40	[N/mm²]	*Residual tensile strength, calculated with Klocal*
Verification	Satisfied	[-]	*Set 2: Verification of bursting stresses and material strength*

Splitting stresses

- Splitting is accounted for by selecting appropriate values for cover and centre to centre distance.
- By appling these minimum values this requirement is automatically satisfied.

Splitting reinforcement - Horizontal distribution

Distribution of single strand

d_{hor}	54,2	[mm]	*Applied horizontal c.t.c. distance between the applied strands*
s	2200	[mm]	*Length of disturbed region (length of St. Venant)*
γ_{spl}	1,2	[-]	*Partial factor for splitting*
$P_{m0,fb,i}$	185,6	[kN]	*Initial prestressing force single strand in bottom flange*
$N_{spl,hor,i}$	1,4	[kN]	*Splitting force due to single strand*

Splitting force first set of strands

$n_{fb,1}$	120	[pcs]	*Number of strands applied in first set*
$N_{spl,hor,1}$	164,7	[kN]	*Horizontal splitting force first set*
$\emptyset_{spl,f1}$	10	[mm]	*Assumed diameter splitting reinforcement*
f_s	300	[N/mm²]	*Maximum allowable stress in reinforcement*
$A_{s,min}$	549	[mm²]	*Minimum required cross section of the reinforcement*
$n_{s,req,1}$	7	[pcs]	*Required number of rebars*

Splitting force second set of strands (if applicable)

$n_{fb,2}$	0	[pcs]	*Number of strands applied in second set*
$N_{spl,hor,2}$	0,0	[kN]	*Horizontal splitting force second set*
$\emptyset_{spl}$	10	[mm]	*Assumed diameter splitting reinforcement*
f_s	300	[N/mm²]	*Maximum allowable stress in reinforcement*
$A_{s,min}$	0	[mm²]	*Minimum required cross section of the reinforcement*
$n_{s,req,2}$	0	[pcs]	*Required number of rebars*

Verification bending moment capacity

Identifying all horizontal forces

Concrete

w	3200	[mm]	*Width of the beam*
f_{cd}	113	[N/mm²]	*Design value concrete compressive strength*
x_u	167,58792	[mm]	*Height concrete compressive zone (iteration)*

Active contribution prestressing

$A_{p,c}$	1400,00	[mm²]	*Applied cross section centric prestressing*
$\sigma_{p,m,c}$	1153,56	[N/mm²]	*Working prestressing stress centric prestressing*
$A_{p,fb}$	16800,00	[mm²]	*Applied cross section eccentric prestressing*
$\sigma_{p,m,fb}$	1106,01	[N/mm²]	*Working prestressing stress eccentric prestressing*

Contribution concrete under tension

f_{ctd}	6,0	[N/mm²]	*Design value of tensile strength (tensile strength 1st crack)*
$f_{ctd,2}$	6,15	[N/mm²]	*Design value maximal post cracking stress (at w=0,30)*
b_{web}	300	[mm]	*Width of tensile zone (width of the webs)*

Auxiliary parameters

l_c	1433,3	[mm]	*Characteristic length*

Height of concrete compressive and tensile zone

Parameters compressive zone

ε_{c3}	0,0023	[-]	*Strain at reaching concrete compressive strength*
f_{cd}	113	[N/mm²]	*Design value concrete compressive strength*
b	3200	[mm]	*Width of the beam*
t_{ft}	187,5	[mm]	*Mean value thickness top flange*
b_{red}	300	[mm]	*Reduced width of the cross section (width of the webs)*
$\varepsilon_{c,f1}$	-0,000273	[-]	*Strains at lower side top flange*
$\sigma_{c,f1}$	-13,47	[N/mm²]	*Stresses at lower side top flange*
N_c	30389276	[N]	*Compressive force in the concrete*
e_c	55,9	[mm]	*Eccentricity compressive force with respect to top fibre*

Case	Concrete compressive forces		Lever arm (from top fibre)		Eccentricity with respect to top fibre	
Case 1	Nc1	30389276 [N]	S1	N.A. [Nmm]		
	Nc2	0 [N]	S2	N.A. [Nmm]	ec	55,9 [mm]
	Nc3	0 [N]	S3	N.A. [Nmm]		
Case 2	Nc1	0 [N]	S1	0 [Nmm]		
	Nc2	0 [N]	S2	0 [Nmm]	ec	0,0 [mm]
	Nc3	0 [N]	S3	0 [Nmm]		

Parameters tensile zone

ε_{ct}	0,00012	[-]	*Strain corresponding to cracking of the beam*
$\varepsilon_{ct,0,3}$	0,00033	[-]	*Strain corresponding to maximum post cracking stress*
ε_{ctd}	0,00038	[-]	*Strain corresponding to declining branch stress-strain curve*
ε_{ctu}	0,00227	[-]	*Strain corresponding ultimate capacity (pull-out of fibre)*
x_1	8,7	[mm]	*Height first concrete tensile zone*
x_2	18,8	[mm]	*Height second concrete tensile zone*
x_3	137,7	[mm]	*Height third concrete tensile zone*
N_t	165597	[N]	*Total concrete tensile force*
e_t	226,5	[mm]	*Eccentricity concrete tensile force with respect to top fibre*

	Concrete tensile forces		Lever arm (from top fibre)		Eccentricity with respect to top fibre
Zones	Nt1	7869 [N]	S1	1364679 [Nmm]	
	Nt2	33806 [N]	S2	6278556 [Nmm]	
	Nt3	123922 [N]	S3	29866313 [Nmm]	

Determining the strains

Centrical prestressing

$d_{p,c}$	1026	[mm]	*Effective height centric prestressing*
$\Delta\varepsilon_{p,c}$	0,0118	[-]	*Strain increase centric prestressing steel (passive contribution)*
$\varepsilon_{p,m,c}$	0,0059	[-]	*Strain in centric prestressing steel due to working prestressing*
$\varepsilon_{p,c}$	0,0177	[-]	*Total strain in centric prestressing steel*

Eccentric prestressing

$d_{p,fb}$	2025	[mm]	*Effective height eccentric prestressing*
$\Delta\varepsilon_{p,fb}$	0,0255	[-]	*Strain increase eccentric prestressing steel (passive contribution)*
$\varepsilon_{p,m,fb}$	0,0057	[-]	*Strain in eccentric prestressing steel due to working prestressing*
$\varepsilon_{p,fb}$	0,0312	[-]	*Total strain in eccentric prestressing steel*

Steel stresses

Main parameters

f_{pk}/γ_s	1691	[N/mm²]	*Design value stress at failure*
f_{pd}	1522	[N/mm²]	*Design value steel stress*
ε_{uk}	0,035	[-]	*Characteristic value strain at failure*
f_{pd}/E_p	0,0078	[-]	*Strain at design value of the steel stress*

Centric prestressing

$\sigma_{pu,c}$	1583	[N/mm²]	*Actual stress centric prestressing steel at calculated strain*
$\sigma_{p,m,c}$	1154	[N/mm²]	*Working prestressing stress centric prestressing*
$A_{p,c}$	1400	[mm²]	*Applied cross section centric prestressing*
$P_{m,m,c}$	1614989	[N]	*Working prestressing force centric prestressing*
$\Delta N_{p,c}$	601766	[N]	*Passive contribution centric prestressing*

Eccentric prestressing

$\sigma_{pu,fb}$	1667	[N/mm²]	*Actual stress eccentric prestressing steel at calculated strain*
$\sigma_{p,m,fb}$	1106	[N/mm²]	*Working prestressing stress eccentric prestressing*
$A_{p,fb}$	16800	[mm²]	*Applied cross section eccentric prestressing*
$P_{m,m,fb}$	18580996	[N]	*Working prestressing force eccentric prestressing*
$\Delta N_{p,fb}$	9425926	[N]	*Passive contribution eccentric prestressing*

Check equilibrium

N_c	-30389	[kN]	*Compressive force in the concrete*
N_t	166	[kN]	*Total concrete tensile force*
$P_{m,m}$	20196	[kN]	*Total working prestressing force (centric and eccentric)*
ΔN_p	10028	[kN]	*Total passive contribution of the prestressing (centric and eccentric)*
$\sum H$	0	[kN]	*Verification of horizontal equilibrium*

Determine bending moment capacity

- Bending moment is calculated using the top fibre as point of reference

Determining bending moment capacity

	Force [kN]	Lever arm [m]	Moment [kNm]
N_c	-30389	0,056	-1698
N_t	166	0,227	38
$P_{m,m,c}$	1615	1,026	1656
$P_{m,m,fb}$	18581	1,026	19055
$\Delta N_{p,c}$	602	1,026	617
$\Delta N_{p,fb}$	9426	2,025	19088

Determining design value bending moment

$M_{Ed,RFEM}$	48426	[kNm]	*Bending moment due to loads calculated using RFEM*
$M_{Ed,P}$	18571	[kNm]	*Upward bending moment due to the prestressing*
M_{Ed}	29855	[kNm]	*Design value bending moment*

Verification

M_{Ed}	29855	[kNm]	*Design value bending moment*
M_{Rd}	38756	[kNm]	*Bending moment capacity*
UC	0,77	[-]	*Unity check*

Verifying the rotational capacity

ε_{cu}	0,00230	[-]	*Strain at failure of the concrete*
$d_{p,ave}$	1948,1	[mm]	*Weighted average effective height centric and eccentric prestressing*
$\sigma_{p,m,ave}$	1109,7	[mm]	*Weighted average centric and eccentric working prestressing stress*
$A_{p,ave}$	15615,4	[mm]	*Weighted average cross section centric and eccentric prestressing*
f	581	[N/mm²]	*Factor for weighed contribution of reinforcing and prestressing steel*
$x_{u,prov}/d_{p,ave}$	0,09	[-]	*Ratio height compressive zone and effective height*

Limit value	0,36	[-]	*Limit value ratio height compressive zone and effective height*
UC	0,24	[-]	*Verification of rotational capacity (expressed as UC)*
Verification	Satisfied	[-]	*Verification of rotational capacity*

Verification shear force capacity

Resistance of prestressed concrete cross section without shear reinforcement

Contribution of the concrete

N_{Ed}	20196	[kN]	*Working prestressing force (centric and eccentric)*
A_c	1663750	[mm²]	*Cross sectional area of total cross section*
f_{ck}	200	[N/mm²]	*Characteristic value compressive strength*
b_w	300	[mm]	*Total width of both webs*
h	2150	[mm]	*Total height*
σ_{cp}	12,1	[N/mm²]	*Compressive stress due to working prestressing force*
k	1,2	[-]	*Factor depending on compressive stress and fck*
z	1822,5	[mm]	*Lever arm, taken as 0,9 * d*
$V_{Rd,c}$	1462	[kN]	*Concrete contribution to shear capacity*

Contribution of the steel fibres

A_{fv}	546750	[mm²]	*Area of the fibre effect, taken as bw * z*
$f_{ctd,2}$	6,15	[N/mm²]	*Design value maximal post cracking stress (at w=0,30)*
θ	30	[°]	*Angle of the concrete compressive strut of the main beams*
$V_{Rd,f}$	5828	[kN]	*Steel fibre contribution to shear capacity*

Total concrete capacity

$V_{Rd,tot}$	7290	[kN]	*Summation of concrete and steel fibre contribution.*

Concrete compressive strut

α_{cc}	0,85	[-]	*Long term effects and unfavourable loading (compression)*
γ_c	1,5	[-]	*Partial factor concrete (cf EC2)*
b_w	300	[mm]	*Total width of both webs*
z	1822,5	[mm]	*Lever arm, taken as 0,9 * d*
$f_{ck}\text{^}(2/3)$	34,2	[N/mm²]	*Value depending on characteristic value compressive strength*
$V_{Rd,max}$	10461	[kN]	*Capacity of concrete compressive strut*
$\tan(\theta)$	0,577	[-]	*Auxiliary value*
$\cot(\theta)$	1,732	[-]	*Auxiliary value*

Shear capacity and verification

V_{tot}	7290	[kN]	*Summation of concrete and steel fibre contribution.*
$V_{Rd,max}$	10461	[kN]	*Capacity of concrete compressive strut*
V_{Ed}	4090	[kN]	*Design value shear force*
V_{Rd}	7290	[kN]	*Shear force capacity*
UC	0,56	[kN]	*Unity check*

Verification torsional resistance

Torsional capacity

Dimensions

t_{ft}	187,5	[mm]	*Mean value thickness top flange*
t_w	150	[mm]	*Thickness of web*
t_{fb}	250	[mm]	*Thickness bottom flange*
h_b	1712,5	[mm]	*Internal height of the box*
w_b	1900	[mm]	*Internal width of the box*

Parameters torsional capacity

A	4730000	[mm²]	*Total area of the cross section within the outer circumference*
u	8700	[mm]	*Outer circumference of the cross section*
t_{ef}	150	[mm]	*Effective wall thickness (limited by the smallest actual thickness)*
A_k	3959063	[mm2]	*Area enclosed by centre lines of the connected walls*
f_{ctd}	6,0	[N/mm²]	*Design value of tensile strength (tensile strength 1st crack)*

Torsional capacity verification

T_{Ed}	1222	[kNm]	*Design value torsional moment*
$T_{Rd,c}$	7126,3125	[kNm]	*Torsional moment capacity (torsional cracking moment)*
UC	0,17	[-]	*Unity check*

Combination of shear and torsion

A_k	3959063	[mm2]	*Area enclosed by centre lines of the connected walls*
z_1	1931,3	[mm]	*Length of element 1 (left web)*
z_2	2050,0	[mm]	*Length of element 2 (bottom flange)*
z_3	1931,3	[mm]	*Length of element 3 (right web)*
z_4	2050,0	[mm]	*Length of element 4 (top flange)*

Shear forces in the elements of the cross section

$V_{Ed,V,1}$	2045,0	[kN]	*Shear force to be carried by element 1 (left web)*
$V_{Ed,V,2}$	0,0	[kN]	*Shear force to be carried by element 2 (bottom flange)*
$V_{Ed,V,3}$	2045,0	[kN]	*Shear force to be carried by element 3 (right web)*
$V_{Ed,V,4}$	0,0	[kN]	*Shear force to be carried by element 4 (top flange)*

$V_{Ed,T,1}$	298,0	[kN]	*Shear force in element 1 due to torsion (left web)*
$V_{Ed,T,2}$	316,4	[kN]	*Shear force in element 2 due to torsion (bottom flange)*
$V_{Ed,T,3}$	298,0	[kN]	*Shear force in element 3 due to torsion (right web)*
$V_{Ed,T,4}$	316,4	[kN]	*Shear force in element 4 due to torsion (top flange)*

$V_{Ed,V+T,1}$	2343,0	[kN]	*Total shear force in element 1 due to shear and torsion*
$V_{Ed,V+T,2}$	316,4	[kN]	*Total shear force in element 2 due to shear and torsion*
$V_{Ed,V+T,3}$	1747,0	[kN]	*Total shear force in element 3 due to shear and torsion*
$V_{Ed,V+T,4}$	316,4	[kN]	*Total shear force in element 4 due to shear and torsion*

Verifying shear force capacity per element

k	1,182082515	[-]	*Factor depending on compressive stress and fck*
f_{ck}	200	[N/mm²]	*Characteristic value compressive strength*
$\gamma_E * \gamma_{cf}$	1,5	[-]	*Product of partial factors (AFGC-SETRA 2013)*
$f_{ctd;2}$	6,1538	[N/mm²]	*Design value of tensile strength (tensile strength 1st crack)*
ϑ	30	[°]	*Angle of the concrete compressive strut of the main beams*

Element [-]	$h_{w,i}$ [mm]	z_i [mm]	$V_{Rd,c,i}$ [kN]	A_{Fv} [mm²]	$V_{Rd,f,i}$ [kN]	$V_{Rd,i}$ [kN]	UC [-]
1	150,0	1931,3	774,8	289687,5	3087,7	3862,6	0,61
2	250,0	2050,0	1370,8	512500	5462,6	6833,4	0,05
3	150,0	1931,3	774,8	289687,5	3087,7	3862,6	0,45
4	187,5	2050,0	1028,1	384375	4097,0	5125,1	0,06

Verifying concrete compressive strut per element

α_{cc}	0,85	[-]	*Long term effects and unfavourable loading (compression)*
γ_c	1,5	[-]	*Partial factor concrete (cf EC2)*
f_{ck}^(2/3)	34,2	[N/mm²]	*Value depending on characteristic value compressive strength*
A_k	3959063	[mm²]	*Area enclosed by centre lines of the connected walls*
$\sin(\vartheta)$	0,500	[-]	*Auxiliary value*
$\cos(\vartheta)$	0,866	[-]	*Auxiliary value*
$\tan(\vartheta)$	0,577	[-]	*Auxiliary value*
$\cot(\vartheta)$	1,732	[-]	*Auxiliary value*

Element [-]	$t_{ef,i}$ [mm]	z_i [mm]	$V_{Ed,V+T,i}$ [kN]	$V_{Rd,max}$ [kN]	UC [-]
1	150,0	1931,3	2343,0	5542,6	0,42
2	250,0	2050,0	316,4	9805,7	0,03
3	150,0	1931,3	1747,0	5542,6	0,32
4	187,5	2050,0	316,4	7354,2	0,04

Global verification ship collision (stability)

Collision force and friction coefficient

F_{equi}	1000	[kN]	*Equivalent static force, see: (4) of 4.6.2. EC1-1-7*
μ	0,5	[-]	*Friction coefficient*

Self-weight of the deck

n_{beams}	5	[-]	*Number of prefab UHPC beams*
L_{tot}	70,70	[m]	*Total length of the main beams*
A_C	1,66	[m²]	*Cross sectional area of total cross section*
ρ	25	[kN/m³]	*Density*
F_{sw}	14703	[kN]	*Self-weight of the UHPC beams*

Verification

Action	1000	[kN]	*Action - Equivalent static force*
Resistance	7352	[kN]	*Self weight multiplied with friction coefficient*
UC	0,14	[-]	*Verification expressed as unity check*
Verification	Satisfied	[-]	*Verification*

Detailed Design Calculations - Design of main beams - Top flange and transverse prestressing

Project: MSc thesis "Redesign of bridges Twentekanaal in UHPC"
Name: M. Dorland
Date: 11-11-2020
Version: D1.0

Input parameters

Input parameters - Material properties & transverse prestressing

Concrete of longitudinal joint

Parameters concrete in compression

f_{ck}	100	[N/mm²]	Characteristic value compressive strength
ε_{cu3}	2,6	[‰]	Maximum compressive strain at ULS

Parameters stiffness and deformations (temperature, creep and shrinkage)

E_{cm}	45000	[N/mm²]	Modulus of elasticity
φ	0,8	[-]	Creep factor

Parameters concrete other

α	0,56	[-]	Factor for shape of concrete compressive zone
β	0,34	[-]	Factor position centre of gravity concrete compressive zone
α_{cc}	0,85	[-]	Long term effects and unfavourable loading (compression)

Calculated values

f_{cd}	57	[N/mm²]	Design value concrete compressive strength

Parameters transverse prestressing

Material properties prestressing steel

f_{pk}	1860	[N/mm²]	Characteristic value tensile strength
f_{pd}	1522	[N/mm²]	Design value steel stress
σ_{pm0}	1395	[N/mm²]	Maximum allowed stress directly after tensioning
$\sigma_{p,max}$	1488	[N/mm²]	Maximum prestressing stress during tensioning
E_p	195000	[N/mm²]	Modulus of elasticity
ε_{uk}	35	[‰]	Characteristic value strain at failure

Calculation parameters tendons (input values)

n	5,00	[pcs]	Assumed number of strands per tendon
D_{strand}	15,2	[mm]	Diameter of single strand
$A_{p,strand}$	140	[mm²]	Cross sectional area per strand
$\sigma_{p,max,prov}$	1400	[N/mm²]	Assumed maximum stress applied to prestressing element
μ	0,23	[-]	Friction coefficient
k	0,01	[rad]	Unintensional angular rotation due to the Wobble-effect
w_{set}	3,00	[mm]	Estimated wedge set
Relaxation	Class 2	[-]	Select relaxation class: normal (1), low (2) or bars (3)
t	500000,00	[h]	The value of the relaxation loss (in %) at 1000 h
ρ	2,50	[%]	Time after stressing (for final value of the relaxation loss)

Other parameters

γ_C	1,5	[-]	Partial factor concrete (cf EC2)
γ_S	1,1	[-]	Partial factor prestressing steel (cf EC2)
γ_{spl}	1,2	[-]	Partial factor splitting forces

Design of transverse prestressing

Calculating prestress losses

Dimensions top flange

$w_{c.t.c.}$	1000	[mm]	Centre to centre distance of the transverse prestressing ribs/ducts
t_{ft}	187,5	[mm]	Mean value thickness top flange
y	93,75	[mm]	Positioning of prestressing ducts with respect to top fibre, assumption: tft/2

Applied maximum force onto prestressing element & stress verification

Applied stress values

$\sigma_{p,max,prov}$	1400,0	[N/mm²]	Assumed maximum stress applied to prestressing element
$\sigma_{c,prov}$	5,2	[N/mm²]	Maximum compressive stress in concrete due to prestressing

Stress limit and verification

$\sigma_{p,max}$	1488	[N/mm²]	Maximum prestressing stress during tensioning
$\sigma_{c,limit}$	60	[N/mm²]	Maximum value concrete compressive stress
Verification	Satisfied	[-]	Verification maximum stress values

Applied value maxinum force applied onto prestressing element

P_{max}	980	[kN]	Applied value maximum prestressing force
$\sigma_{p,max}$	1400	[N/mm²]	Applied value maximum prestressing stress
A_p	700	[mm²]	Applied cross section prestressing tendon

Direct prestressing losses

Elastic losses

w_{tot}	16,36	[m]	Total width of the deck
ΔP_{el}	15,9	[KN]	Elastic loss prestressing

Friction losses

μ	0,23	[-]	Friction coefficient
k	0,009	[1/m]	Coefficient Wobble-effect
$\Delta P_\mu(x=0)$	0,00	[kN]	Prestress loss due to friction at x=0 m
$\Delta P_\mu(x=w_{tot})$	32,6	[kN]	Prestress loss (force) due to friction at x=width deck
$\Delta\sigma_{Pp}(x=w_{tot})$	46,6	[N/mm²]	Prestress loss (stress) due to friction at x=width deck

Wedge set

w_{set}	3,00	[mm]	Assumed value wedge set
$\Delta\sigma_{Pset}/w_{tot}$	0,0028	[N/mm²/mm]	Stress reduction due to friction per unit of length
l_w	14328,3	[mm]	Influence length of the wedge set
ΔP_{set}	57,2	[kN]	Prestress losses due to wedge set (at active side)

Determining initial prestressing force & stress verification

Applied force and stress values

$\max\{P_{m,0}(x)\}$	935	[kN]	Initial prestressing force - maximum value over beam length
$\max\{\sigma_{pm0}(x)\}$	1336	[N/mm²]	Initial prestressing stress - maximum value over beam length
$P_{m,0}$	923	[kN]	Initial prestressing force - mean value over beam length

Stress limit and verification

σ_{pm0}	1395	[N/mm²]	Maximum allowed stress directly after tensioning
Verification	Satisfied	[-]	Verification initial prestressing stress

Applied value initial prestressing force and losses

$P_{m,0}$	923	[kN]	Inital prestressing force - Mean value over beam length
ΔP_i	57	[kN]	Initial losses - Mean value over beam length: Pmax-Pm,0

Time dependent losses

Relaxation

Class	Class 2	[-]	Relaxation class (normal relaxation, low relaxation and bars)
ρ_{1000}	2,5	[%]	The value of the relaxation loss (in %) at 1000 h
μ	0,71	[-]	Factor depending on steel stresses
t	500000	[h]	Time after stressing (for final value of the relaxation loss)
$\Delta\sigma_{pr}/\sigma_{pi}$	0,0405	[-]	Relaxation coefficient
σ_{pi}	1318,1	[N/mm²]	Absolute value of the initial prestressing (σ_pm0)
$\Delta\sigma_{pr}$	53,4	[N/mm²]	Prestress loss due to relaxation

Class 1	Wires and strands normal relaxation
Class 2	Wires and strands low relaxation
Class 3	Bars

Creep & shrinkage

φ	0,8	[-]	Creep factor
$\sigma_{c,QP}$	4,92	[N/mm²]	Stress in concrete adjacent to prestressing tendon
ε_{cs}	0,0008	[-]	Shrinkage of the concrete

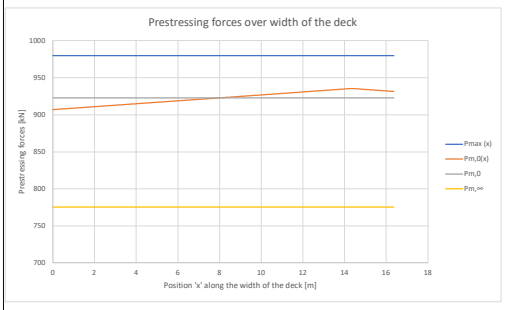
Total time dependent losses

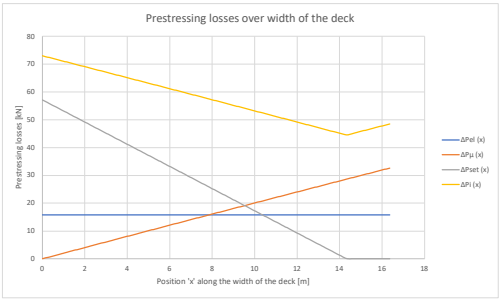
$\Delta\sigma_{p,c+s+r}$	210	[N/mm²]	Time dependent prestressing losses (stress)
$\Delta P_{p,c+s+r}$	147	[kN]	Time dependent prestressing losses (force)

Working prestress force and total prestress losses

$P_{m,\infty}$	776	[kN]	Working prestressing force in tendon
$\sigma_{pm,\infty}$	1108	[N/mm²]	Working prestressing stress in tendon
ΔP	-20,9	[%]	Total prestressing loss (percentage)

Plotting prestressing forces and losses over beam length





Detailing of the prestressing - Horizontal and vertical distribution

Parameters

$\emptyset_{spl,ft}$	10	[mm]	Assumed diameter splitting reinforcement top flange
γ_{spl}	1,2	[-]	Partial factor splitting forces
$w_{c.t.c.}$	1000,0	[mm]	Centre to centre distance of the transverse prestressing ribs/ducts
t_{ft}	187,5	[mm]	Mean value thickness top flange
h_1	100,0	[mm]	Anchor plate (height and width)

Converting width from wc.t.c. to standard width

$w_{c.t.c.}$	1,00	[m]	Centre to centre distance of the transverse prestressing ribs/ducts

Width:	wc.t.c	1,0	[m]
$P_{m,0}$	775,5	775,5	[kN]
A_p	700,0	700,0	[mm²]
$\sigma_{pm,\infty}$	1107,9	1107,9	[N/mm²]

Horizontal force distribution

P_{m0}	922,7	[kN]	Inital prestressing force - Mean value over beam length
$N_{spl,w}$	249,1	[kN]	Horizontal tensile force
f_s	300	[N/mm²]	Maximum stress in reinforcement
$A_{s,req}$	830	[mm²]	Minimum required cross section of the reinforcement
$n_{s,req}$	11	[pcs]	Minimum number of rebars requried

Vertical force distribution

P_{m0}	922,7	[kN]	Inital prestressing force - Mean value over beam length
$N_{spl,v}$	129,2	[kN]	Vertical tensile force
f_s	300	[N/mm²]	Maximum stress in reinforcement
$A_{s,req}$	431	[mm²]	Minimum required cross section of the reinforcement
$n_{s,req}$	6	[pcs]	Minimum number of rebars requried

Forces acting on top flange and joint

Parameters longitudinal joint

t_{ft}	187,5	[mm]	Height of the top flange
t_j	162,5	[mm]	Height of the longitudinal joint
$w_{j,t}$	90	[mm]	Width of joint along longitudinal direction

Cross sectional properties & parameters of the joint

A_j	162500	[mm²]	Cross sectional area of the longitudinal joint
W_j	4,4010E+06	[mm³]	Section modulus of the longitudinal joint
I_j	3,5758E+08	[mm⁴]	Second moment of the cross section of the longitudinal joint
e_j	12,5	[mm]	Eccentricity prestressing tendon with centre of joint: 0,5*tft - 0,5*tj
l	1240	[mm]	Span of the mechanical model
d_p	93,75	[mm]	Effective height longitudinal joint

Actions on the joint

$G_{k,sf}$	4,6875	[kN/m]	Self-weigth UHPC top flange
$G_{k,asfalt}$	0,23	[kN/m]	Permanent load due to asphalt/protection layer
G_k	4,92	[kN/m]	Self-weight + permanent load
$Q_{k,LM2}$	194	[kN]	Single wheel load model 2

Factors

Bending moments joint (SLS)

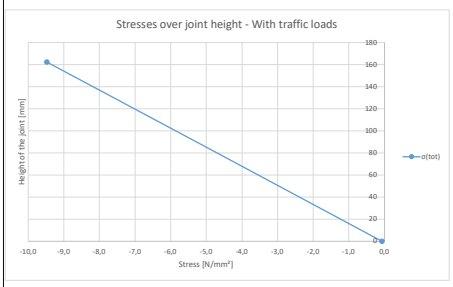
Bending moments (ULS)

γ_G	1,4	[-]	*See tabel NB.16 – A2.4(B) of NA to NEN-EN 1990*	M_C	0,32	[kNm]	*Bending moment due to self-weigth and asphalt layer*	$M_{Ed,a}$	26,8	[kNm]	*Design value bending moment equation 6.10a*
$\xi * \gamma_G$	1,25	[-]	*See tabel NB.16 – A2.4(B) of NA to NEN-EN 1990*	M_P	9,69	[kNm]	*Bending moment due to eccentricity of tendons*	$M_{Ed,b}$	35,8	[kNm]	*Design value bending moment equation 6.10b*
γ_P	1,0	[-]	*See 2.4.2.2 of NA to NEN-EN 1992-1-1*	M_Q	30,07	[kNm]	*Bending moment due to varaible load (LM2)*	M_{Ed}	35,8	[kNm]	*Design value bending moment*
γ_Q	1,5	[-]	*See tabel NB.16 – A2.4(B) of NA to NEN-EN 1990*								
ψ_0	0,8	[-]	*See tabel NB.13 – A2.1 of NA to NEN-EN 1990*								

Verifying stresses over joint height

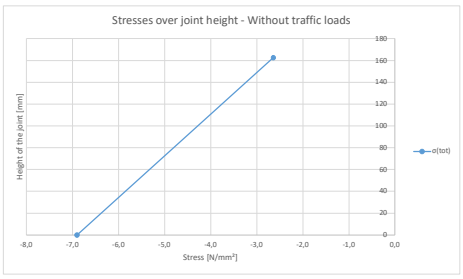
Stress distribution over the height of the joint with traffic loads:

	Height [mm]	σ(M_B) [N/mm²]	σ(M_{Cb}) [N/mm²]	σ(P) [N/mm²]	σ(M_P) [N/mm²]	σ(tot) [N/mm²]
Top fibre	163	-0,1	-6,8	-4,8	2,2	-9,5
Bottom fibre	0	0,1	6,8	-4,8	-2,2	-0,1



Stress distribution over the height of the joint without traffic loads:

	Height [mm]	σ(M_B) [N/mm²]	σ(M_{Cb}) [N/mm²]	σ(P) [N/mm²]	σ(M_P) [N/mm²]	σ(tot) [N/mm²]
Top fibre	163	-0,1	0,0	-4,8	2,2	-2,6
Bottom fibre	0	0,1	0,0	-4,8	-2,2	-6,9



Local verification (transverse direction) - Verification bending moment capacity longitudinal joint

Parameters concrete

α	0,56	[-]	*Factor for shape of concrete compressive zone*
β	0,34	[-]	*Factor position centre of gravity concrete compressive zone*
f_{cd}	56,7	[N/mm²]	*Design value concrete compressive strength*
x_u	33,91114178	[mm]	*Height concrete compressive zone (iteration)*

Horizontal equilibrium

N_c	-1076114	[N]	*Compressive force in the concrete*
$P_{m,\infty}$	775510	[N]	*Working prestressing force*
ΔN_p	300604	[N]	*Passive contribution of the prestressing*
$\sum H$	0	[N]	*Verification of horizontal equilibrium*

Parameters steel

A_p	700,00	[mm²]	*Applied cross section of the prestressing*
$\sigma_{pm,\infty}$	1107,87	[N/mm²]	*Working prestressing stress*

Bending moment capacity

	Force [N]	Lever arm [mm]	Moment [kNm]
N_c	-1076114	11,5	-12,4
$P_{m,\infty}$	775510	81,3	63,0
ΔN_p	300604	93,8	28,2
M_{Rd}			78,8

Determining strains and stresses

$\epsilon_{p,\infty}$	0,0057	[-]	*Strain in prestressing steel due to working prestressing*
$\Delta\epsilon_p$	0,0046	[-]	*Strain increase prestressing steel (passive contribution)*
ϵ_p	0,0103	[-]	*Total strain in prestressing steel*
σ_{pu}	1537	[N/mm²]	*Actual stress in prestressing steel at calculated strain*

Verification

M_{Ed}	35,8	[kNm]	*Design value bending moment*
M_{Rd}	78,8	[kNm]	*Bending moment capacity*
UC	0,45	[-]	*Unity check*

Local verification (transverse direction) - Bending moment capacity top flange between the webs

Calculation model and design value bending moment

Parameters longitudinal joint

t_{f1}	187,5	[mm]	*Mean value thickness top flange*

Factors

γ_G	1,4	[-]	*See tabel NB.16 – A2.4(B) of NA to NEN-EN 1990*
$\xi * \gamma_G$	1,25	[-]	*See tabel NB.16 – A2.4(B) of NA to NEN-EN 1990*
γ_P	1,0	[-]	*See 2.4.2.2 of NA to NEN-EN 1992-1-1*
γ_Q	1,5	[-]	*See tabel NB.16 – A2.4(B) of NA to NEN-EN 1990*
ψ_0	0,8	[-]	*See tabel NB.13 – A2.1 of NA to NEN-EN 1990*

Cross sectional properties & parameters of the flange

l	2,05	[m]	*Span, i.e. distance inside the box + 2*0,5*tweb*
d_p	93,75	[mm]	*Effective height prestressing tendon*

Bending moments top flange (SLS)

$M_{E,sag}$	50,6	[kNm]	*Sagging moment, SLS*
$M_{E,hog}$	51,4	[kNm]	*Hogging moment, SLS*

Actions on the top flange

G_k	4,9175	[kN/m]	*Self-weight + permanent load*
$Q_{k,LM2}$	194	[kN]	*Single wheel load model 2*

Bending moments (ULS)

$M_{Ed,a,sag}$	60,9	[kNm]	*Design value sagging bending moment equation 6.10a*
$M_{Ed,b,sag}$	75,6	[kNm]	*Design value sagging bending moment equation 6.10b*
$M_{Ed,a,hog}$	62,1	[kNm]	*Design value hogging bending moment equation 6.10a*
$M_{Ed,b,hog}$	76,7	[kNm]	*Design value hogging bending moment equation 6.10b*

Verification of bending moment capacity

Parameters concrete

α	0,56	[-]	*Factor for shape of concrete compressive zone*
β	0,34	[-]	*Factor position centre of gravity concrete compressive zone*
f_{cd}	113,3	[N/mm²]	*Design value concrete compressive strength*
x_u	17,42162856	[mm]	*Height concrete compressive zone (iteration)*

Horizontal equilibrium

N_c	-1105693	[N]	*Compressive force in the concrete*
$P_{m,\infty}$	775510	[N]	*Working prestressing force*
ΔN_p	330183	[N]	*Passive contribution of the prestressing*
$\sum H$	0	[N]	*Verification of horizontal equilibrium*

Parameters steel

A_p	700,00	[mm²]	*Applied cross section of the prestressing*
$\sigma_{pm,\infty}$	1107,87	[N/mm²]	*Working prestressing stress*

Bending moment capacity

	Force [kN]	Lever arm [m]	Moment [kNm]
N_c	-1106	0,0059	-6,5
$P_{m,\infty}$	776	0,0938	72,7
ΔN_p	330	0,0938	31,0
M_{Rd}			97,1

Determining strains and stresses

$\epsilon_{p,\infty}$	0,0057	[-]	*Strain in prestressing steel due to working prestressing*
$\Delta\epsilon_p$	0,0114	[-]	*Strain increase prestressing steel (passive contribution)*
ϵ_p	0,0171	[-]	*Total strain in prestressing steel*
σ_p	1580	[N/mm²]	*Actual stress in prestressing steel at calculated strain*

Bending moment verification - Sagging bending moment

$M_{Ed,sag}$	75,6	[kNm]	*Design value sagging bending moment*
M_{Rd}	97,1	[kNm]	*Bending moment capacity*
UC	0,78	[-]	*Unity check sagging bending moment*

Bending moment verification - Hogging bending moment

$M_{Ed,hog}$	76,7	[kNm]	*Design value hogging bending moment*
M_{Rd}	97,1	[kNm]	*Bending moment capacity*
UC	0,79	[-]	*Unity check hogging bending moment*

Local verification (longitudinal direction) - Bending moment capcity top flange between prestressing ribs

Calculation model and design value bending moment

Parameters longitudinal joint

t_{f1}	187,5	[mm]	*Mean value thickness top flange*

Factors

γ_G	1,4	[-]	*See tabel NB.16 – A2.4(B) of NA to NEN-EN 1990*
$\xi * \gamma_G$	1,25	[-]	*See tabel NB.16 – A2.4(B) of NA to NEN-EN 1990*
γ_P	1,0	[-]	*See 2.4.2.2 of NA to NEN-EN 1992-1-1*
γ_Q	1,5	[-]	*See tabel NB.16 – A2.4(B) of NA to NEN-EN 1990*
ψ_0	0,8	[-]	*See tabel NB.13 – A2.1 of NA to NEN-EN 1990*

Cross sectional properties & parameters of the flange

l	1,00	[m]	*Span, i.e. centre to centre distance prestressing ribs*

Bending moments top flange (SLS)

M_E	49,1	[kNm]	*Sagging moment, SLS*

Actions on the top flange

G_k	4,9175	[kN/m]	*Self-weight + permanent load*
$Q_{k,LM2}$	194	[kN]	*Single wheel load model 2*

Bending moments (ULS)

$M_{Ed,a}$	59,1	[kNm]	*Design value bending moment equation 6.10a*
$M_{Ed,b}$	73,5	[kNm]	*Design value bending moment equation 6.10b*

Verification of bending moment capacity

Parameters concrete

f_{ctd}	6	[N/mm²]	*Design value of tensile strength (tensile strength 1st crack)*
$f_{ctd;2}$	6,15	[N/mm²]	*Design value maximal post cracking stress (at w=0,30)*
E_{cm}	50000	[N/mm²]	*Modulus of elasticity*
l_f	13	[mm]	*Fibre length*

Bending moment verification

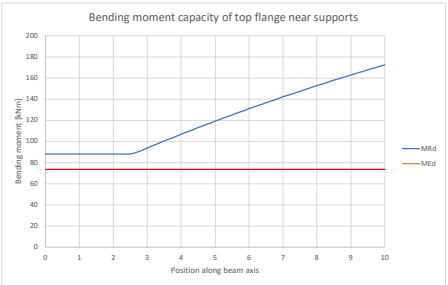
M_{Ed}	73,5	[kNm]	*Design value bending moment*
M_{Rd}	88,2	[kNm]	*Bending moment capacity at intersection*
UC	0,83	[-]	*Unity check at intersection*
Coordinate 'x'	0,0	[m]	*Location of intersection (sufficient capacity)*

External axial force (self-weight beams and prestressing)

$G_{k,beam}$	41,59	[kN/m]	*Line load representing the self-weight of the prefab beams*
l	68,00	[m]	*Span of the main beams*
$P_{m0,c}$	1940	[kN]	*Applied value initial prestressing force centric prestressing*
$P_{m0,fb}$	22269	[kN]	*Applied value initial prestressing force eccentric prestressing*

Verifying strains

ϵ_{cc}	0,00200	[-]	*Compressive strain top fibre at midspan*
ϵ_{c3}	0,00230	[-]	*Strain at reaching concrete compressive strength*
Verify strains:	Satisfied	[-]	*Verify if it holds that $\epsilon_c \leq \epsilon_{c3}$*



Detailed Design Calculations - Design of main beams - Fatigue verification

Project: MSc thesis "Redesign of bridges Twentekanaal in UHPC"
Name: M. Dorland
Date: 11-11-2020
Version: D1.0

Fatigue

Parameters - Loads, cross sectional properties and materials

Forces & loads

$M_{fat,max}$	31539	kNm	*Maximum bending moment at midspan (found using RFEM)*
$M_{fat,min}$	27183	kNm	*Minimum bending moment at midspan (found using RFEM)*
$P_{m,0,c}$	1615	[kN]	*Working prestress force - Centric strands*
$P_{m,0,fb}$	18581	[kN]	*Working prestress force - Eccentric strands*
$\gamma_{F,fat}$	1,00	[-]	*See 2.4.2.3 of NA to NEN-EN 1992-1-1*

Cross sectional properties

A_c	1663750	[mm²]	*Cross sectional area of total cross section*
e_p	999,5	[mm]	*Eccentricity of tendons in bottom flange*
I_y	1,2007E+12	[mm⁴]	*Second moment of area of the combined cross section*
$W_{y,t}$	1,170BE+09	[mm³]	*Section modulus with respect to top fibre*
$W_{y,b}$	1,067BE+09	[mm³]	*Section modulus with respect to bottom fibre*

Material properties concrete & steel

E_{cm}	50000	[N/mm²]	*Modulus of elasticity*
$\beta_{cc}(t)$	1,0	[-]	*Factor for increase of strength due to progressive hydration*
f_{ck}	200	[N/mm²]	*Characteristic value compressive strength*
f_{cko}	10	[N/mm²]	*Standard value (10 Mpa)*
E_p	195000	[N/mm²]	*Modulus of elasticity*
$\gamma_{S,fat}$	1,1	[-]	*See 2.4.2.4 of NA to NEN-EN 1992-1-1*
γ_C	1,5	[-]	*Partial factor concrete (cf EC2)*

Fatigue verification - Prestressing steel at midspan

Occuring stress range

α_e	3,90	[-]	*Ratio of moduli of elasticity*
$\sigma_{c,max}$	-1,3	[N/mm²]	*Maximum stress in concrete at tendon height (i.e. highest stress)*
$\sigma_{p,max}$	-5,2	[N/mm²]	*Maximum stress in prestressing steel (i.e. highest stress)*
$\sigma_{c,min}$	-5,0	[N/mm²]	*Minimum stress in concrete at tendon height (i.e. lowest stress)*
$\sigma_{p,min}$	-19,4	[N/mm²]	*Minimum stress in prestressing steel (i.e. lowest stress)*
$\Delta\sigma_p$	14,1	[N/mm2]	*Stress range in prestressing steel*

S-N curve and number of cycles

$\Delta\sigma_{Rsk}$	185	[N/mm²]	*Stress range at N* cycles*
N^*	1000000	[-]	*Number of cycles with single stress range*
k_1	5	[-]	*Stress exponent first branch*
k_2	9	[-]	*Stress exponent second branch*
n_y	100	[-]	*Design service life*
N_{obs}	500000	[-]	*Number of heavy vehicles per year*
n	50000000	[-]	*Number of cycles to be designed for*

Fatigue verification

$\Delta\sigma_{pd}$	14,1	[N/mm²]	*Stress range in prestressing steel*
$\Delta\sigma_{Rsd}$	108,9	[N/mm²]	*Allowable stress range (design value)*
Verification	Satisfied	[-]	*Fatigue verificaiton prestressing steel*

Fatigue verification - Concrete at midspan

Highest and lowest stress values top fibre

$\sigma_{cd,max}$	23,2	[N/mm²]	*Highest compressive stress in a cycle (i.e. most negative value)*
$\sigma_{cd,min}$	19,5	[N/mm²]	*Lowest compressive stress in a cycle (i.e. value closest to zero or positive)*

Verification stresses top fibre

$E_{cd,max}$	0,41	[-]	*Maximum compressive stress level (top fibre)*
$E_{cd,min}$	0,34	[-]	*Minimum compressive stress level (top fibre)*
R	0,84	[-]	*Ratio minimum and maximum stress level (top fibre)*
n	50000000	[-]	*Number of cycles to be designed for*
N	4,41E+20	[-]	*Number of cycles until failure at given stress range*
UC	0,00	[-]	*Fatigue verificaton concrete at top fibre (as UC)*
Verification	Satisfied	[-]	*Fatigue verificaton concrete at top fibre*

Highest and lowest stress values bottom fibre

$\sigma_{cd,max}$	4,1	[N/mm²]	*Highest compressive stress in a cycle (i.e. most negative value)*
$\sigma_{cd,min}$	0,0	[N/mm²]	*Lowest compressive stress in a cycle (i.e. value closest to zero or positive)*

Verification stresses bottom fibre

$E_{cd,max}$	0,07	[-]	*Maximum compressive stress level (bottom fibre)*
$E_{cd,min}$	0,00	[-]	*Minimum compressive stress level (bottom fibre)*
R	0,00	[-]	*Ratio minimum and maximum stress level (bottom fibre)*
n	50000000	[-]	*Number of cycles to be designed for*
N	9,85E+12	[-]	*Number of cycles until failure at given stress range*
UC	0,00	[-]	*Fatigue verificaton concrete at bottom fibre (as UC)*
Verification	Satisfied	[-]	*Fatigue verificaton concrete at bottom fibre*

Concrete fatigue strength

$f_{ck,fat}$	85	[N/mm²]	*Characteristic value fatigue strength*
$f_{cd,fat}$	56,67	[N/mm²]	*Design value fatigue strength*

Detailed Design Calculations - Design of main beams - Serviceability Limit State

Project: MSc thesis "Redesign of bridges Twentekanaal in UHPC"
Name: M. Dorland
Date: 11-11-2020
Version: D1.0

Serviceability limit state - Deflection at midspan

Input parameters loads

$G_{k,total}$	42,35	[kN/m]	*Line load composed of self-weight beam and road surfacing*
$P_{m,0,fb}$	18581	[kN]	*Working prestressing force centric prestressing*
$Q_{k,UDL}$	26,8425	[kN/m]	*Line load acting on the beam (due to UDL of LM1)*
$Q_{k,axle}$	291	[kN/axle]	*Axle load acting on the beam (LM1)*
ψ_1	0,8	[-]	*See tabel NB.13 – A2.1 of NA to NEN-EN 1990*
e_p	1,00	[m]	*Eccentricity of tendons in bottom flange*

Maximum deflection

$1/\delta$	300	[-]	*Maximum deflection in SLS*
δ_{max}	226,7	[mm]	*Calculated value maximum delfection*

Input parameters structure and material

l	68	[m]	*Span of the main beams*
E_{cm}	50000	[N/mm²]	*Modulus of elasticity*
I_y	1,2007E+12	[mm⁴]	*Second moment of area of the combined cross section*
φ	0,3	[-]	*Creep factor*
$E_{c,eff}$	38462	[N/mm²]	*Effective modulus of elasticity to account for time dependent effects*

Deflections

δ_G	255,3	[mm]	*Deflection (downwards) due to self weight & permanent loads*
δ_P	-232,4	[mm]	*Deflection (upwards) due to prestressing*
$\delta_{Q,UDL}$	129,5	[mm]	*Deflection (downwards) due to UDL component variable loads*
$\delta_{Q,axle}$	66,0	[mm]	*Deflection (downwards) due to axle loads*
δ_{tot}	218,4	[mm]	*Summation of all individual components*
$\delta_{tot,FEM}$	112,0	[mm]	*Total deflection determined using RFEM*

Verifications

$\delta_{tot} < \delta_{max}$?	Satisfied	[-]	*Verification maximum deflection*
$\delta_{tot,RFEM} < \delta_{max}$	Satisfied	[-]	*Verification maximum deflection using RFEM results*

Serviceability limit state - Crack width verification

Calculating cracking bending moment (SLS)

f_{ctk}	200	[N/mm²]	*Characteristic value compressive strength*
$f_{ctm,el}$	10,3	[N/mm²]	*Mean value of the axial tensile strength*
$P_{m,\infty}$	20196	[kN]	*Axial working prestressing force (centric and eccentric)*
A_c	1663750	[mm²]	*Cross sectional area of total cross section*
σ_c	12,1	[N/mm²]	*Compressive stress due to axial prestressing force*
W_{min}	1,0678E+09	[mm³]	*Minimum value of section moduli with respect to top and bottom fibre*
M_{cr}	23917	[kNm]	*Cracking bending moment*

Verification non-brittleness criterion

M_{cr}	23917	[kNm]	*Cracking bending moment*
M_{Rd}	38756	[kNm]	*Bending moment capacity*
Verification	Satisfied	[-]	*Verification*

Detailed Design Calculations - Design of end cross beam

Project: MSc thesis "Redesign of bridges Twentekanaal in UHPC"
Name: M. Dorland
Date: 11-11-2020
Version: D1.0

Input parameters

Input parameters - Cross sectional properties and calculation parameters

Cross sectional properties

h_{cb}	2150	[mm]	*Total height of the end cross beam*
w_{cb}	2150	[mm]	*Total width of the end cross beam*
A_{cb}	4622500	[mm²]	*Cross sectional area of the cross beam*
$W_{y,cb}$	1,6564E+09	[mm³]	*Section modulus of the cross section*
$I_{y,cb}$	1,7806E+12	[mm⁴]	*Second moment of area of the cross section*

Calculation parameters

k_1	0,15	[-]	*Factor from 6.2.2 of the NA to NEN-EN 1992-1-1*
θ	21,8	[°]	*Angle concrete compressive strut of end cross beam*

Input parameters - Material properties & prestressing

Concrete

Parameters concrete in compression

f_{ck}	30	[N/mm²]	*Characteristic cylinder compressive strength at 28 days*
$f_{ck,cube}$	37	[N/mm²]	*Characteristic cube compressive strength*
f_{cm}	38	[N/mm²]	*Mean value cylinder compressive strength*
ε_{c3}	1,75	[‰]	*Strain at reaching concrete compressive strength*
ε_{cu3}	3,5	[‰]	*Maximum compressive strain at ULS*

Parameters concrete in tension

f_{ctm}	2,9	[N/mm²]	*Mean value axial tensile strength*
$f_{ctk,0,05}$	2,0	[N/mm²]	*5%-fractile of the axial tensile strength*

Parameters stiffness and deformations (temperature, creep and shrinkage)

E_{cm}	33000	[N/mm²]	*Secant modulus of elasticity*
φ	1,75	[-]	*Creep*
Hydration	Normal (N)	[-]	*Rate of hydration: Rapid (R), Normal (N) or slow (S)*
RH	80,0	[%]	*Relative humidity*

Parameters concrete other

α	0,75	[-]	*Factor for shape of concrete compressive zone*
β	0,39	[-]	*Factor position centre of gravity concrete compressive zone*
α_{cc}	1,0	[-]	*Long term effects and unfavourable loading (compression)*
α_{ct}	0,0	[-]	*Long term effects and unfavourable loading (tension)*

Parameters prestressing End cross beams

Material properties prestressing steel

f_{pk}	1860	[N/mm²]	*Characteristic value tensile strength*
f_{pd}	1522	[N/mm²]	*Design value steel stress*
σ_{pm0}	1395	[N/mm²]	*Maximum allowed stress directly after tensioning*
$\sigma_{p,max}$	1488	[N/mm²]	*Maximum prestressing stress during tensioning*
E_p	195000	[N/mm²]	*Modulus of elasticity*
ε_{uk}	35	[‰]	*Characteristic value strain at failure*

Properties prestressing tendons

n_{ducts}	4	[pcs]	*Number of ducts in total*
a_{vert}	500	[mm]	*Vertical position centre of duct from centre of beam*
a_{hor}	750	[mm]	*Horizontal position centre of duct from centre of beam*
n_{strand}	7	[pcs]	*Assumed number of strands per tendon*
D_{strand}	15,2	[mm]	*Diameter of single strand*
$A_{p,strand}$	140	[mm²]	*Cross sectional area per strand*
$\sigma_{p,max,prov}$	1400	[N/mm²]	*Assumed maximum stress applied to prestressing element*
ϕ_{Duct}	65	[mm]	*Outer diameter of prestressing ducts*
μ	0,23	[-]	*Friction coefficient*
k	0,009	[rad]	*Unintensional angular rotation due to the Wobble-effect*
w_{set}	3	[mm]	*Estimated wedge set*
Relaxation	Class 2	[-]	*Select relaxation class: normal (1), low (2) or bars (3)*
t	500000	[h]	*The value of the relaxation loss (in %) at 1000 h*
ρ	2,5	[%]	*Time after stressing (for final value of the relaxation loss)*

Other parameters

γ_C	1,5	[-]	*Partial factor concrete (cf EC2)*
γ_S	1,1	[-]	*Partial factor prestressing steel (cf EC2)*

Input parameters - Determining creep and shrinkage

Shrinkage

h_0	1433	[mm]	*Fictitious thickness, assumed to be (2/3)*hcb (3 sides exposed)*
k_h	0,7	[-]	*Coefficient depending on fictitious thickness*
RH	80,0	[%]	*Relative humidity*
β_{RH}	0,7564	[-]	*Factor for relative humidity*
Hydration	Normal (N)	[-]	*Rate of hydration: Rapid (R), Normal (N) or slow (S)*
α_{ds1}	4	[-]	*Coefficient depending on cement type*
α_{ds2}	0,12	[-]	*Coefficient depending on cement type*
f_{cm}	38	[N/mm²]	*Mean value cylinder compressive strength*
$\varepsilon_{cd,0}$	0,000269	[-]	*Nominal unrestrained drying shrinkage*
$\varepsilon_{cd,\infty}$	0,000188	[-]	*End value drying shrinkage*

h0	k_h
100	1
200	0,85
300	0,75
500	0,7

	α_{ds1}	α_{ds2}
Slow (S)	3	0,13
Normal (N)	4	0,12
Rapid (R)	6	0,11

Creep

φ	1,75	[-]	*Creep factor*

Input parameters - Loads

Ultimate Limit State (ULS)

$M_{Ed,hog}$	1212	[kNm]	*Maximum hogging bending moment (all loads considered)*
$M_{Ed,sag}$	436	[kNm]	*Maximum sagging bending moment (all loads considered)*
V_{Ed}	837	[kN]	*Maximum shear force (all loads considered)*

Serviceability Limit State (SLS)

$M_{E,hog}$	469	[kNm]	*Maximum hogging bending moment (all loads considered) SLS*
$M_{E,sag}$	298	[kNm]	*Maximum sagging bending moment (all loads considered) SLS*

Design of the prestressing

Calculating prestress losses

Applied maximum force onto prestressing elements & stress verification

Applied stress values

$\sigma_{p,max,prov}$	1400	[N/mm²]	*Assumed maximum stress applied to prestressing element*
$\sigma_{c,prov}$	1,19	[N/mm²]	*Concrete stress due to assumed initial applied force*

Stress limit and verification

$\sigma_{p,max,limit}$	1488	[N/mm²]	*Maximum prestressing stress during tensioning*
$\sigma_{c,limit}$	18	[N/mm²]	*Maximum value concrete compressive stress*
Verification	Satisfied	[-]	*Verification maximum stress values*

Applied value maxinum force applied onto prestressing

P_{max}	5488	[kN]	*Applied value maximum prestressing force*
$\sigma_{p,max}$	1400	[N/mm²]	*Applied value maximum prestressing stress*
A_p	3920	[mm²]	*Applied cross section prestressing tendon*

Direct prestressing losses

Elastic losses

ΔP_{el}	10,3	[kN]	*Total elastic loss all prestressing tendons*

Friction losses

μ	0,23	[-]	*Friction coefficient*
k	0,009	[1/m]	*Coefficient Wobble-effect*
$\Delta P_\mu(x=0)$	0,00	[kN]	*Prestress loss due to friction at x=0 m*
$\Delta P_\mu(x=w)$	182,7	[kN]	*Prestress loss (force) due to friction at x=width deck*
$\Delta\sigma_{P\mu}(x=w)$	46,6	[N/mm²]	*Prestress loss (stress) due to friction at x=width deck*

Wedge set

w_{set}	3,00	[mm]	*Assumed value wedge set*
k	0,0028	[N/mm²/mm]	*Stress reduction due to friction per unit of length*
l_w	14328,3	[mm]	*Influence length of the wedge set*
ΔP_{set}	320,1	[kN]	*Prestress losses due to wedge set (at active side)*

Determining initial prestressing force & stress verification

Applied force and stress values

$\max\{P_{m,0}(x)\}$	5317	[kN]	*Initial prestressing force - maximum value over beam length*
$\max\{\sigma_{pm0}(x)\}$	1356	[N/mm²]	*Initial prestressing stress - maximum value over beam length*
$P_{m,0}$	5245	[kN]	*Initial prestressing force - mean value over beam length*

Stress limit and verification

σ_{pm0}	1395	[N/mm²]	*Maximum allowed stress directly after tensioning*
Verification	Satisfied	[-]	*Verification initial prestressing stress*

Applied value initial prestressing force and losses

$P_{m,0}$	5245	[kN]	*Inital prestressing force - Mean value over beam length*
ΔP_i	243	[kN]	*Initial losses - Mean value over beam length: Pmax-Pm,0*

Time dependent losses

Relaxation

Class	Class 2	[-]	*Relaxation class (normal relaxation, low relaxation and bars)*
ρ_{1000}	2,5	[%]	*The value of the relaxation loss (in %) at 1000 h*
μ	0,72	[-]	*Factor depending on steel stresses*
t	500000	[h]	*Time after stressing (for final value of the relaxation loss)*
$\Delta\sigma_{pr}/\sigma_{pi}$	0,0425	[-]	*Relaxation coefficient*
σ_{pi}	1338,1	[N/mm²]	*Absolute value of the initial prestressing (σ_pm0)*
$\Delta\sigma_{pr}$	56,9	[N/mm²]	*Prestress loss due to relaxation*

Class 1	Wires and strands normal relaxation
Class 2	Wires and strands low relaxation
Class 3	Bars

Creep & shrinkage

φ	1,75	[-]	*Creep factor*
$\sigma_{c,QP}$	1,1	[N/mm²]	*Stress in concrete adjacent to tendons (middle cross section)*
ε_{cs}	0,000188	[-]	*Shrinkage of the concrete*

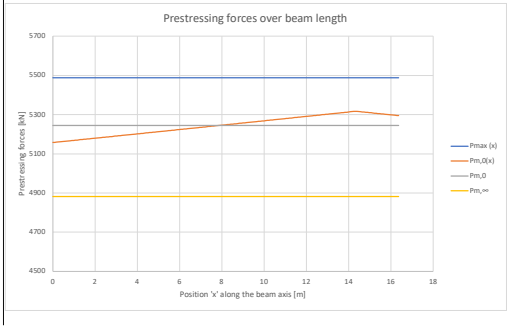
Total time dependent losses

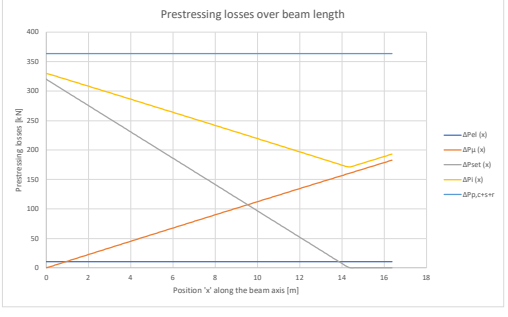
$\Delta\sigma_{p,c+s+r}$	93	[N/mm²]	*Time dependent prestressing losses (stress)*
$\Delta P_{p,c+s+r}$	364	[kN]	*Time dependent prestressing losses (force)*

Working prestress force and total prestress losses

$P_{m,\infty}$	4881	[kN]	*Total working prestressing force*
$\sigma_{pm,\infty}$	1245	[N/mm²]	*Working prestressing stress in the tendons*
ΔP	-11,1	[%]	*Total prestressing loss (percentage)*

Plotting prestressing forces and losses over beam length

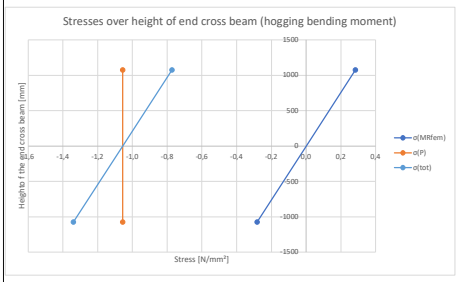




Determining stresses over beam height

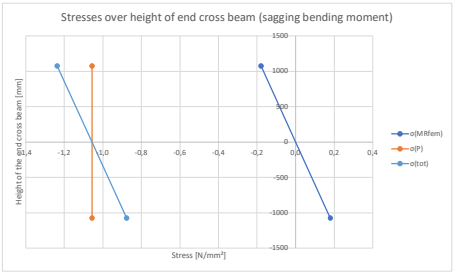
Stress distribution governing hogging bending moment in SLS:

	Height [mm]	σ(MRfem) [N/mm²]	σ(P) [N/mm²]	σ(tot) [N/mm²]
Top fibre	1075	0,3	-1,1	-0,8
Bottom fibre	-1075	-0,3	-1,1	-1,3



Stress distribution governing sagging bending moment in SLS:

	Height [mm]	σ(MRfem) [N/mm²]	σ(P) [N/mm²]	σ(tot) [N/mm²]
Top fibre	1075	-0,2	-1,1	-1,2
Bottom fibre	-1075	0,2	-1,1	-0,9



Verification bending moment capacity

Identifying all horizontal forces

Concrete

α	0,75	[-]	*Factor for shape of concrete compressive zone*
w_{cb}	2150	[mm]	*Factor position centre of gravity concrete compressive zone*
f_{cd}	20	[N/mm²]	*Design value concrete compressive strength*
N_c	6314	[kN]	*Compressive force in the concrete*

Active contribution of prestressing

A_p	3920	[mm²]	*Applied cross section of the prestressing*
$P_{m,\infty}$	4881	[kN]	*Working prestressing stress*
$\sigma_{p,\infty}$	1245	[N/mm²]	*Working prestressing stress in the tendons*

Height of concrete compressive zone

x_u	195,7937034	[mm]	*Height concrete compressive zone (iteration)*

x_1	575	[mm]	*Distance from outermost compressed fibre to centre of first row of tendons*
x_2	1575	[mm]	*Distance from outermost compressed fibre to centre of second row of tendons*

Determining the strains

First row of tendons

$d_{p,1}$	575	[mm]	*Effective height prestressing - row 1*
$\Delta\varepsilon_{p,1}$	0,0068	[-]	*Strain increase prestressing steel (passive contribution) - row 1*
$\varepsilon_{p,\infty,1}$	0,0064	[-]	*Strain in prestressing steel due to working prestressing - row 1*
$\varepsilon_{p,1}$	0,0132	[-]	*Total strain in prestressing steel - row 1*

Second row of tendons

$d_{p,2}$	1575	[mm]	*Effective height prestressing - row 2*
$\Delta\varepsilon_{p,2}$	0,0247	[-]	*Strain increase prestressing steel (passive contribution) - row 2*
$\varepsilon_{p,\infty,2}$	0,0064	[-]	*Strain in prestressing steel due to working prestressing - row 2*
$\varepsilon_{p,2}$	0,0310	[-]	*Total strain in prestressing steel - row 2*

Steel stresses

Parameters

f_{pk}/γ_s	1691	[N/mm²]	*Design value stress at failure*
f_{pd}	1522	[N/mm²]	*Design value steel stress*
ε_{uk}	0,035	[-]	*Characteristic value strain at failure*
f_{pd}/E_p	0,0078	[-]	*Strain at design value of the steel stress*

First row of tendons

$\sigma_{pu,1}$	1555	[N/mm²]	*Actual stress in prestressing steel at calculated strain - row 1*
$\sigma_{p,\infty}$	1245	[N/mm²]	*Working prestressing stress - row 1*
$0,5 * A_p$	1960	[mm²]	*Applied cross section prestressing - row 1*
$P_{m,\infty,1}$	2441	[kN]	*Working prestressing force - row 1*
$\Delta N_{p,1}$	608	[kN]	*Passive contribution prestressing - row 1*

Second row of tendons

$\sigma_{pu,2}$	1666	[N/mm²]	*Actual stress in prestressing steel at calculated strain - row 2*
$\sigma_{p,\infty}$	1245	[N/mm²]	*Working prestressing stress - row 2*
$0,5 * A_p$	1960	[mm²]	*Applied cross section prestressing - row 2*
$P_{m,\infty,2}$	2441	[kN]	*Working prestressing force - row 2*
$\Delta N_{p,2}$	825	[kN]	*Passive contribution prestressing - row 2*

Check equilibrium

N_c	-6314	[kN]	*Compressive force in the concrete*
$P_{m,\infty,1}$	2441	[kN]	*Working prestressing force - row 1*
$\Delta N_{p,1}$	608	[kN]	*Passive contribution of the prestressing - row 1*
$P_{m,\infty,2}$	2441	[kN]	*Working prestressing force - row 2*
$\Delta N_{p,2}$	825	[kN]	*Passive contribution of the prestressing - row 2*

$\sum H$	0	[kN]	*Verification of horizontal equilibrium*

Determine bending moment capacity

- Bending moment is calculated using the most compressed fibre as reference

Determining bending moment capacity

	Force [kN]	Lever arm [m]	Moment [kNm]
N_c	-6314	0,076	-481
$P_{m,\infty,1}$	2441	1,075	2624
$\Delta N_{p,1}$	608	0,575	349
$P_{m,\infty,2}$	2441	1,075	2624
$\Delta N_{p,2}$	825	1,575	1300

Determining design value bending moment

$M_{Ed,RFEM}$	1212	[kNm]	*Bending moment due to loads calculated using RFEM*

Verification

M_{Ed}	1212	[kNm]	*Design value bending moment*
M_{Rd}	6416	[kNm]	*Bending moment capacity*
UC	0,19	[-]	*Unity check*

Verifying the rotational capacity

d_{ave}	1075	[mm]	*Average effective height of both rows of tendons*
f	446	[N/mm²]	*Factor for weighed contribution of reinforcing and prestressing steel*
x_u/d_{ave}	0,18	[mm]	*Ratio height compressive zone and effective height*
Limit value	0,53	[mm]	*Limit value ratio height compressive zone and effective height*
UC	0,34	[-]	*Verification of rotational capacity (expressed as UC)*
Verification	Satisfied	[-]	*Verification of rotational capacity*

Verification shear force capacity

Parameters

Effective height

$d_{p,2}$	1575	[mm]	*Effective height prestressing - row 2*

Effective width of the cross beam

n_{row}	2	[pcs]	*Assumed number of ducts per row*
ϕ_{Duct}	65	[mm]	*Outer diameter of prestressing ducts*
w_{cb}	2150	[mm]	*Total width of the end cross beam*
$b_{cb,nom}$	2150	[mm]	*Effective width of the cross beam*

Capacity of concrete elements without shear reinforcement

k	1,36	[-]	*Scale factor*
f_{ck}	30	[N/mm²]	*Characteristic value concrete compressive strength*
v_{min}	0,30	[N/mm²]	*Reduction value for concrete cracked due to shear*
k_1	0,15	[-]	*Factor, value is deduced from the NA of EC2-1-1*
σ_{cp}	1,06	[N/mm²]	*Factor for presence of normal forces (compression positive)*

$V_{Rd,c,min}$	1562	[kN]	*Minimum value shear capacity of elements without shear reinforcement*

Upper limit - Failure of the concrete compressive strut

α_{cw}	1,05	[-]	*Factor accounting for the stress state in the compression strut*
z	1417,5	[mm]	*Internal lever arm*
v_1	0,53	[-]	*Reduction factor of concrete cracked due to shear*
(θ)	21,8	[°]	*Angle of compressive strut with beam axis*
$\tan(\theta)$	0,400	[-]	*Auxiliary value*
$\cot(\theta)$	2,500	[-]	*Auxiliary value*

$V_{Rd,max}$	11683	[kN]	*Shear force limit due to failure of concrete compressive strut*

Verification

V_{Ed}	837	[kN]	*Design value shear force*
V_{Rd}	1562	[kN]	*Shear force capacity*
UC	0,54	[-]	*Unity check*

Detailed Design Calculations - Weight calculation

Project: MSc thesis ''Redesign of bridges Twentekanaal in UHPC''
Name: M. Dorland
Date: 12-11-2020
Version: D1.0

Description	Length [m]	Height/depth [m]	Width [m]	Cross-section [m²]	Number [-]	Weight [kN/m³]	Result [-]	Units [-]	Remarks/notes
Detailed design prefab UHPC deck									
Prefab UHPC beams	70,70			1,66	5	25	14703	[kN]	
In-situ UHPC joints	70,70	0,19	0,09		4	25	119	[kN]	
Cross beams	16,36	2,15	2,15		2	25	3781	[kN]	
Subtraction overlap main beams			2,150	1,66	10	25	-894	[kN]	
Asphalt layer	70,70	0,01	16,36			23	266	[kN]	
Kerbs	70,70	0,34	0,50		2	25	601	[kN]	
Capping beam	16,36	1,00	0,75		2	25	614	[kN]	*See CH8. preliminary design report*
Total							**19190**	[kN]	
Existing concrete arch bridge - Eefdesebrug									
Arches	75,00	1,80	0,90		2	25,0	6075	[kN]	*Arch length is measured using AutoCAD.*
Supporting elements arches (''windverband'')	8,00	0,36	1,60		4	25,0	461	[kN]	*See drawing B.3622*
Main girders	70,70	1,30	1,90		2	25,0	8731	[kN]	
Cross beams	7,00	0,80	0,80		12	25,0	1344	[kN]	
end cross beams	7,00	1,20	1,30		2	25,0	546	[kN]	*Average height, see ''detail B-B'' of B.7125*
Deck between main girders	70,70	0,25	7,00			25,0	3093	[kN]	
Deck pedestrian lanes	70,70	0,20	2,78		2	25,0	1965	[kN]	*An verage height of 0,20 m is assumed.*
Asphalt layer	70,70	0,05	7,00			23,0	569	[kN]	*Assumption: layer of 50 mm acc to B.5109.*
Total							**22785**	[kN]	
Comparison									
Percentual change of weight	-16	[%]							

IV

ANNEX: OVERVIEW DESIGN CALCULATIONS

OVERVIEW DESIGN CALCULATIONS

This document gives an overview of all the calculations that have been performed as part of the detailed design phase, as well as the corresponding assumptions that have been made. This document has been prepared to provide additional clarifications to the Excelsheet, it provides all the equations of the calculations that have been performed. For easy reference a table of content has been added, the order in which all calculations are discussed in this annex follows the setup of the calculation sheet in Excel.

Table of content:

1 CALCULATION PARAMETERS 4

1.1 Geometry of the structure 4
- 1.1.1 Main dimensions of the deck 4
- 1.1.2 Cross sectional properties main beams 4
- 1.1.3 Cross sectional properties end cross beams 7
- 1.1.4 Cross sectional properties longitudinal joints 8

1.2 Material and calculation parameters 8
- 1.2.1 Concrete 8
- 1.2.2 Prestressing steel & parameters strands and tendons 11
- 1.2.3 Partial factors material resistance 13
- 1.2.4 Calculation parameters 13

1.3 Design of bridge and main carriageway – Actions 13
- 1.3.1 Design main carriageway 13
- 1.3.2 Effective width of the beams 14
- 1.3.3 Permanent actions (G) 14
- 1.3.4 Variable actions (Q) 14
- 1.3.5 Accidental actions (A) 15
- 1.3.6 Fatigue 15
- 1.3.7 Combinations of actions 15

1.4 Determining force distribution (RFEM input) 15
- 1.4.1 Design of main prestressing and verification capacity of the main beams 15
- 1.4.2 Fatigue analysis main beams 16
- 1.4.3 Design of prestressing and verification capacity of the end cross beams 16

2 ULS – STR 17

2.1 Input parameters 17

2.2 Design of the main prestressing 17
- 2.2.1 Calculating prestress losses 17
- 2.2.2 Determining stresses at midspan 19

2.3 Detailing beam ends 20
- 2.3.1 Bond stresses and transmission length 20
- 2.3.2 Tensile stresses at top fibre 20

2.3.3 Positioning of strands in the bottom flange 21
2.3.4 Splitting reinforcement – Vertical distribution 22
2.3.5 Splitting reinforcement – Horizontal distribution 24
2.4 Verification bending moment capacity 25
2.4.1 Assumptions 25
2.4.2 Calculating the capacity and verifications 25
2.5 Verification shear force capacity 29
2.5.1 Assumptions and limitations 29
2.5.2 Calculating the resistance and unity check 29
2.6 Verification torsional resistance 30
2.6.1 Assumptions & approach 30
2.6.2 Torsional capacity 30
2.6.3 Combination of shear and torsion 31
2.7 Global verification ship collision 33
3 DESIGN OF MAIN BEAMS – TOP FLANGE AND TRANSVERSE PRESTRESSING 34
3.1 Design of transverse prestressing 34
3.1.1 Calculating prestress losses 34
3.1.2 Forces acting on top flange and joint 36
3.1.3 Verifying stresses over joint height 37
3.1.4 Detailing 38
3.2 Local verification – Verification bending moment capacity longitudinal joint 39
3.3 Local verification – Bending moment capacity top flange between the webs 40
3.3.1 Calculation model and design value bending moments 40
3.3.2 Verification of bending moment capacity 41
3.4 Local verification – Bending moment capacity top flange between prestressing ribs 42
3.4.1 Calculation model and design value bending moments 42
3.4.2 Verification of bending moment capacity 43
4 DESIGN OF MAIN BEAMS – FATIGUE VERIFICATION 47
4.1 Fatigue verification 47
4.1.1 Assumptions and approach 47
4.1.2 Fatigue verification – Prestressing steel at midspan 47
4.1.3 Fatigue verification – Concrete at midspan 48
5 MAIN BEAMS – SERVICEABILITY LIMIT STATE 50
5.1 Deflections 50
5.1.1 Assumptions and approach 50
5.1.2 Upper limit of deflections 50
5.1.3 Comparison with RFEM 51

5.2 Crack width verification 51

6 END CROSS BEAM 52

6.1 Assumptions and parameters 52
6.1.1 Assumptions 52
6.1.2 Input parameters 52
6.2 Design of the prestressing 53
6.2.1 Calculating prestress losses 53
6.2.2 Determining stresses over beam height 55
6.3 Verification bending moment capacity 56
6.3.1 Assumptions 56
6.3.2 Calculating the capacity and verifications 56
6.4 Verification shear force capacity 58
6.5 Assumptions and parameters 58
6.5.1 Calculating the capacity and verifications 58

7 WEIGHT CALCULATION 60

7.1 Weight calculation 60

1

CALCULATION PARAMETERS

The overview in this chapter describes all the calculation parameters and input required for the calculation.

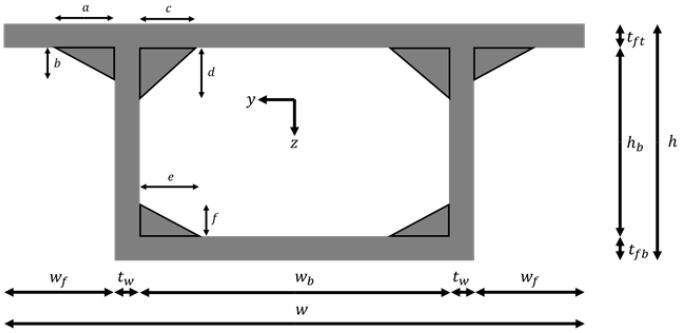
1.1 Geometry of the structure

1.1.1 Main dimensions of the deck

Symbol	Value	Units	Definition
l	68,0	[m]	Span of the main beams
w_{tot}	16,36	[m]	Total width of the deck
l_{tot}	70,70	[m]	Total length of the main beams
n_{beams}	5	[pcs]	Number of prefab UHPC beams

1.1.2 Cross sectional properties main beams

Main properties



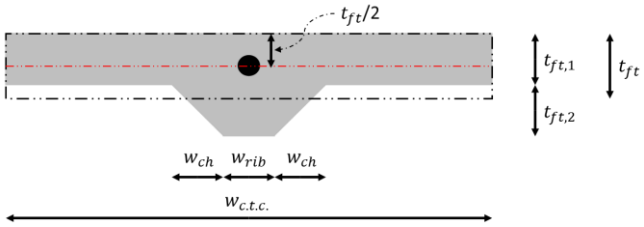
Symbol	Value	Units	Definition
w	3200	[mm]	Total width
h	2150	[mm]	Total height
t_{fb}	250	[mm]	Thickness bottom flange
t_w	150	[mm]	Thickness of web
w_f	500	[mm]	Width of the flanges
w_b	1900	[mm]	Internal width of the box

Chamfer of flanges

Symbol	Value	Units	Definition
a	0	[mm]	Width outer chamfer top flange
b	0	[mm]	Height outer chamfer top flange
c	0	[mm]	Width inner chamfer top flange
d	0	[mm]	Height inner chamfer top flange
e	0	[mm]	Width inner chamfer bottom flange
f	0	[mm]	Height inner chamfer bottom flange

Top flange – transverse direction

Values can be entered to apply a variable height of the top flange. If a top flange with continuous thickness is to be applied only the values t_{ft1} and $w_{c.t.c.}$ should be applied.



Input parameters: The following parameters can be defined:

Symbol	Value	Units	Definition
$w_{c.t.c.}$	1000	[mm]	Centre to centre distance of the transverse prestressing ribs/ducts
$t_{ft,1}$	125	[mm]	Continuous thickness of the top flange
$t_{ft,2}$	125	[mm]	Local increase thickness top flange at transverse rib
w_{rib}	250	[mm]	Width of the transverse prestressing rib
w_{ch}	250	[mm]	Width of chamfer next to the transverse prestressing rib

Calculated parameters: Using the aforementioned values the remaining dimensions required to determine the cross sectional properties are calculated.

- Mean value thickness top flange t_{ft}: If the option of defining a variable height for the top flange in transverse direction is used, a mean value of the thickness of the top flange is calculated:

$$t_{ft} = \frac{w_{c.t.c.} * t_{ft,1} + w_{rib} * t_{ft,2} + 2 * 0{,}5 * w_{ch} * t_{ft,2}}{w_{c.t.c.}} \rightarrow \frac{1000 * 125 + 250 * 125 + 2 * 0{,}5 * 250 * 125}{1000} = 187{,}5\ [mm]$$

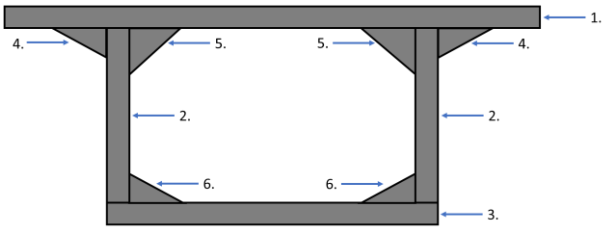
  Using this mean value all other cross sectional properties are calculated and all verifications are performed. In the case an equal thickness of the top flange is used $t_{ft} = t_{ft,1}$.

- Internal height of the box h_b: Using the mean height of the top flange the internal height of the box is calculated:

$$h_b = h - t_{fb} - t_{ft} \rightarrow 2150 - 250 - 187{,}5 = 1712{,}5\ [mm]$$

Determining cross sectional properties and main parameters

Using all previously defined or calculated main dimensions the cross sectional properties of the main beams can be determined. To approach this in a structured manner the cross section is divided into a number of standard shapes, this is depicted in the following figure.



Cross sectional area: The cross sectional area of the concrete cross section is as follows:

$$A_c = \sum_{i=1}^{n} A_i$$

Where:
A_i: Cross sectional area of individual segment 'i'

Centre of gravity: The position of the centre of gravity with respect to the top fibre is defined as follows. It is calculated using the summation of the first moments of area of all individual segments with respect to the top fibre and the cross sectional area of the cross section.

$$z = \frac{\sum_{i=1}^{n} A_i * e_i}{\sum_{i=1}^{n} A_i}$$

Where:
e_i: Distance from centre of an individual element 'i' to the top fibre of the cross section

Second moment of area: The second moment of area of the total cross section along the horizontal axis (y-axis) is calculated using Steiner's rule. First the second moment of the individual elements has to be calculated, for rectangles or triangles this is respectively:

$$I_i = \frac{1}{12} * b_i * h_i^3$$

$$I_i = 36 * b_i * h_i^3$$

Where:
b_i: Width of individual element'i'
h_i: height of individual element 'i'

Subsequently the Steiner part of the contribution of each individual element to the total second moment of area has to be calculated. In order to do so the distance between the centre of gravity of the individual element and the centre of gravity of the whole cross section, a_i, has to be calculated. Using the top fibre as a reference point this is done as follows:

$$a_i = |e_i - z|$$

The second moment of area of the total cross section now becomes:

$$I_y = \sum_{i=1}^{n} (I_i + A_i * a_i^2)$$

Distances to the outer fibres: The distances from the centre of gravity of the cross section to the outer fibres at the top and bottom are defined as:

$$e_t = z$$

$$e_b = h - z$$

Section moduli: Using the second moment of area of the total cross section and the distances to the outer fibres the section moduli of the cross section with respect to the outer fibres can be calculated:

$$W_{y,t} = \frac{I_y}{e_t}$$
$$W_{y,b} = \frac{I_y}{e_b}$$

The results are:

Symbol	Value	Units	Definition
A_c	1663750,0	[mm²]	Cross sectional area of total cross section
z	1025,5	[mm]	Position centre of gravity from the top flange
I_y	1,201E+12	[mm⁴]	Second moment of area of the combined cross section
e_t	1025,5	[mm]	Distance from centre of gravity to top fibre
e_b	1124,5	[mm]	Distance from centre of gravity to bottom fibre
$W_{y,t}$	1,171E+09	[mm³]	Section modulus with respect to top fibre
$W_{y,b}$	1,068E+09	[mm³]	Section modulus with respect to bottom fibre

The results are verified by comparing the cross sectional area and second moment of area with the values calculated by RFEM using the same dimensions.

Excel: $A_c = 1663750$ mm², $e_t = 1025{,}5$ mm and $I_y = 1{,}201 * 10^{12}$ mm⁴. RFEM: $A_c = 1663750$ mm², $e_t = 1025{,}5$ mm and $I_y = 1{,}201 * 10^{12}$ mm⁴. The results are in exact agreement.

1.1.3 Cross sectional properties end cross beams

Main dimensions

It is assumed that the end cross beams have a solid rectangular cross section. The height and width can be defined in Excel:

Symbol	Value	Units	Definition
h_{cb}	2150	[mm]	Total height of the end cross beam
w_{cb}	2150	[mm]	Total width of the end cross beam

Determining cross sectional properties

The following cross sectional properties are defined:

- Cross sectional area:

$$A_{cb} = h_{cb} * w_{cb}$$

- Section modulus of the cross section:

$$W_{y,cb} = \frac{1}{6} * w_{cb} * h_{cb}^2$$

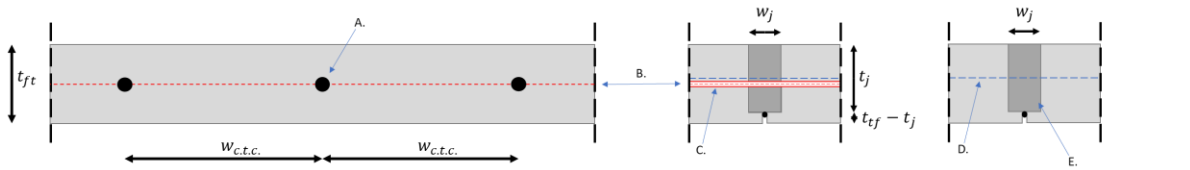
- Second moment of area of the cross section:

$$I_{y,cb} = \frac{1}{12} * w_{cb} * h_{cb}^3$$

1.1.4 Cross sectional properties longitudinal joints

Main dimensions

The longitudinal joints are analysed while making use of the mean value t_{ft} for the thickness of the top flange, the following sketch shows all relevant dimensions.



Side view part of the deck | Cross section joint with tendon | Cross section joint without tendon

Symbols:
A. Position prestressing tendon
B. Centre of gravity of prestressing tendon
C. Prestressing tendon
D. Centre of gravity of the joint
E. In-situ concrete (joint)

In the analysis of the longitudinal joint two main assumptions are made:

- The thickness of the top flange is the mean value t_{ft};
- Transverse prestressing is present with its centre at half the thickness of the top flange.

The following additional dimensions have to be defined:

Symbol	Value	Units	Definition
t_j	162,5	[mm]	Height of the longitudinal joint
w_j	90	[mm]	Transverse width of the longitudinal joint

The thickness of the joint is chosen while the width of the joint is calculated automatically:

$$w_j = \frac{w_{tot} - n_{beams} * w}{n_{beams} - 1} \rightarrow \frac{16.360 - 5 * 3200}{5 - 1} = 90\ [mm]$$

Determining cross sectional properties

For the analysis of the joint it is assumed that a strip with a transverse width of 1000 mm is analysed. The cross sectional area, section modulus and second moment of area of the joint are as follows:

$$A_j = 1000 * t_j\ [mm^2]$$

$$W_j = \frac{1}{6} * 1000 * t_j^2\ [mm^3]$$

$$I_j = \frac{1}{12} * 1000 * t_j^3\ [mm^4]$$

1.2 Material and calculation parameters

1.2.1 Concrete

Material properties concrete main beams (Ductal FM)

For the main beams the following material properties have to be defined:

Parameters mixture composition			
Symbol	**Value**	**Units**	**Definition**
ρ	25	[kN/m^3]	Density

l_f	13	[mm]	Fibre length

Parameters concrete in compression

f_{ck}	200	[N/mm^2]	Characteristic value compressive strength
ε_{c3}	2,3	[‰]	Strain at reaching concrete compressive strength
ε_{cu3}	2,6	[‰]	Maximum compressive strain at ULS

Parameters concrete in tension

$f_{ctk,el}$	9	[N/mm^2]	Characteristic elastic (5% percentile value) tensile strength
f_{ctfk}	10	[N/mm^2]	Characteristic value maximal post cracking stress (w=0,30)
K_{global}	1,25	[-]	Fibre orientation factor (global)
K_{local}	1,75	[-]	Fibre orientation factor (local)

Parameters stiffness and deformations (temperature, creep and shrinkage)

E_{cm}	50000	[N/mm^2]	Modulus of elasticity
G	20833	[N/mm^2]	Shear modulus
v	0,2	[-]	Poisson ratio
α	0,000012	[K-1]	Coefficient of thermal expansion
φ	0,3	[-]	Creep
ε_{shr}	0,8	[‰]	Autogenous shrinkage (during HT)

Parameters concrete other

α	0,56	[-]	Factor for shape of concrete compressive zone
β	0,34	[-]	Factor position centre of gravity concrete compressive zone
α_{cc}	0,85	[-]	Long term effects and unfavourable loading (compression)
α_{ct}	1,0	[-]	Long term effects and unfavourable loading (tension)

Parameters fatigue

$\beta_{cc}(t)$	1,0	[-]	Factor for increase of strength due to progressive hydration
f_{ck0}	10,0	[N/mm^2]	Standard value (10 Mpa)

Calculated values: The following values are calculated using the aforementioned values:

- Design value concrete compressive strength:

$$f_{cd} = \frac{\alpha_{cc} * f_{ck}}{\gamma_C} \rightarrow \frac{0{,}85 * 200}{1{,}5} \approx 113\ [MPa]$$

- Design value of tensile strength (elastic limit, formation of first crack):

$$f_{ctd} = \frac{\alpha_{ct} * f_{ctk,el}}{\gamma_C} \rightarrow \frac{1{,}0 * 9{,}0}{1{,}5} = 6{,}0\ [MPa]$$

- Design value maximum post cracking stress (at $w = 0{,}3$ mm):

$$f_{ctd;2} = \frac{f_{ctfk}}{K_{global} * \gamma_{cf}} \rightarrow \frac{10}{1{,}25 * 1{,}3} \approx 6{,}15\ [MPa]$$

Material properties concrete longitudinal joints

For the longitudinal joints the following material properties have to be defined:

Parameters mixture composition

Symbol	Value	Units	Definition
ρ	25	[kN/m^3]	Density

Parameters concrete in compression

f_{ck}	100	[N/mm^2]	Characteristic value compressive strength

ε_{cu3}	2,6	[‰]	Maximum compressive strain at ULS

Parameters stiffness and deformations (temperature, creep and shrinkage)

E_{cm}	45000	[N/mm^2]	Modulus of elasticity
φ	0,8	[-]	Creep factor

Parameters concrete other

α	0,56	[-]	Factor for shape of concrete compressive zone
β	0,34	[-]	Factor position centre of gravity concrete compressive zone
α_{cc}	0,85	[-]	Long term effects and unfavourable loading (compression)

Calculated values: The design value of the concrete compressive strength is calculated using the aforementioned values:

$$f_{cd} = \frac{\alpha_{cc} * f_{ck}}{\gamma_C} \rightarrow \frac{0{,}85 * 100}{1{,}5} \approx 57\ [MPa]$$

Material properties concrete end cross beams

For the main beams the following material properties have to be defined:

Parameters mixture composition

Symbol	Value	Units	Definition
ρ	25	[kN/m^3]	Density

Parameters concrete in compression

f_{ck}	30	[N/mm^2]	Characteristic cylinder compressive strength at 28 days
$f_{ck,cube}$	37	[N/mm^2]	Characteristic cube compressive strength
f_{cm}	38	[N/mm^2]	Mean value cylinder compressive strength
ε_{c3}	1,75	[‰]	Strain at reaching concrete compressive strength
ε_{cu3}	3,5	[‰]	Maximum compressive strain at ULS

Parameters concrete in tension

f_{ctm}	2,9	[N/mm^2]	Mean value axial tensile strength
$f_{ctk;0,05}$	2,0	[N/mm^2]	5%-fractile of the axial tensile strength

Parameters stiffness and deformations (temperature, creep and shrinkage)

E_{cm}	33000	[N/mm^2]	Secant modulus of elasticity
φ	1,75	[-]	Creep
Hydration	Normal (N)	[-]	Rate of hydration: Rapid (R), Normal (N) or slow (S)
RH	80,0	[%]	Relative humidity

Parameters concrete other

α	0,75	[-]	Factor for shape of concrete compressive zone
β	0,39	[-]	Factor position centre of gravity concrete compressive zone
α_{cc}	1,0	[-]	Long term effects and unfavourable loading (compression)

Calculated values: The design value of the concrete compressive strength is calculated using the aforementioned values:

$$f_{cd} = \frac{\alpha_{cc} * f_{ck}}{\gamma_C} \rightarrow \frac{1{,}0 * 30}{1{,}5} = 20\ [MPa]$$

1.2.2 Prestressing steel & parameters strands and tendons

Parameters prestressing main beams

For the prestressing of the main beams using pretensioned steel the following parameters have to be defined:

Material properties prestressing steel

Symbol	Value	Units	Definition
f_{pk}	1860	[N/mm^2]	Characteristic value tensile strength
f_{pd}	1522	[N/mm^2]	Design value steel stress
σ_{pm0}	1395	[N/mm^2]	Maximum allowed stress directly after tensioning
$\sigma_{p,max}$	1488	[N/mm^2]	Maximum prestressing stress during tensioning
E_p	195000	[N/mm^2]	Modulus of elasticity
ε_{uk}	35	[‰]	Characteristic value strain at failure

Properties prestressing strands

n_c	10	[pcs]	Assumed number of strands positioned centrically in the cross section
$D_{strand,c}$	15,2	[mm]	Diameter of strands positioned centrically
$A_{p,strand,c}$	140	[N/mm^2]	Cross sectional area per strand
$\sigma_{p,max,prov,c}$	1390	[mm^2]	Assumed maximum stress applied to centrically positioned strands
n_{fb}	120	[pcs]	Assumed number of strands positioned in bottom flange
$D_{strand,fb}$	15,2	[mm]	Diameter of strands positioned in bottom flange
$A_{p,strand,fb}$	140	[N/mm^2]	Cross sectional area per strand
$\sigma_{p,max,prov,fb}$	1450	[mm^2]	Assumed maximum stress applied to strands in bottom flange
Relaxation	Class 2	[-]	Select relaxation class: normal (1), low (2) or bars (3)
t	500000	[h]	The value of the relaxation loss (in %) at 1000 h
ρ	2,5	[%]	Time after stressing (to determine final value of the relaxation loss)
t_{eq}	461935	[h]	Equivalant time (optional), NOTE: Calculated manually!

Parameters detailing beam ends

η	1,35	[-]	Bond factor conforming table 7.2 of AFGC-SETRA 2013
η_1	1,0	[-]	Factor accounting for bond conditions, cf EC2-1-1
κ	1,5	[-]	Factor for bond strength improvement due to the presence of fibres
α_1	1,0	[-]	Factor depending on way of releasing the strands
α_2	0,19	[-]	Factor depending on the type of tendon
$n_{fb,1}$	120	[pcs]	Selected number of strands introduced in first set
$n_{fb,2}$	0	[pcs]	Selected number of strands introduced in second set (optional)
$x_{debond,1}$	0	[m]	Length over which first set of strands is debonded (optional)
$x_{debond,2}$	0,0	[m]	Length over which second set of strands is debonded (optional)

Parameters fatigue verification

$\Delta\sigma_{Rsk}$	185	[N/mm^2]	Stress range at N* cycles
N*	1000000	[-]	Number of cycles with single stress range
k_1	5	[-]	Stress exponent first branch
k_2	9	[-]	Stress exponent second branch

Parameters transverse prestressing

For the transverse prestressing of the deck (post tensioned steel) the following parameters have to be defined:

Material properties prestressing steel

Symbol	Value	Units	Definition
f_{pk}	1860	[N/mm^2]	Characteristic value tensile strength
f_{pd}	1522	[N/mm^2]	Design value steel stress
σ_{pm0}	1395	[N/mm^2]	Maximum allowed stress directly after tensioning
$\sigma_{p,max}$	1488	[N/mm^2]	Maximum prestressing stress during tensioning
E_p	195000	[N/mm^2]	Modulus of elasticity

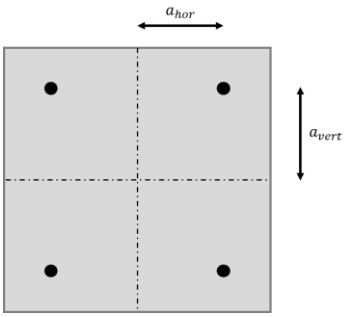
ε_{uk}	35	[‰]	Characteristic value strain at failure

Properties prestressing tendons

n	5	[pcs]	Assumed number of strands per tendon
D_{strand}	15,2	[mm]	Diameter of single strand
$A_{p,strand}$	140	[mm^2]	Cross sectional area per strand
$\sigma_{p,max,prov}$	1400	[N/mm2]	Assumed maximum stress applied to prestressing element
μ	0,23	[-]	Friction coefficient
k	0,009	[rad]	Unintentional angular rotation due to the Wobble-effect
w_{set}	3	[mm]	Estimated wedge set
Relaxation	Class 2	[-]	Select relaxation class: normal (1), low (2) or bars (3)
t	500000	[h]	The value of the relaxation loss (in %) at 1000 h
ρ	2,5	[%]	Time after stressing (for final value of the relaxation loss)

Parameters prestressing end cross beams

The position of the tendons is defined with respect to the centre of the beam, the prestressing is position symmetrically:



For the prestressing of the cross beams using pretensioned steel the following parameters have to be defined:

Material properties prestressing steel

Symbol	Value	Units	Definition
f_{pk}	1860	[N/mm^2]	Characteristic value tensile strength
f_{pd}	1522	[N/mm^2]	Design value steel stress
σ_{pm0}	1395	[N/mm^2]	Maximum allowed stress directly after tensioning
$\sigma_{p,max}$	1488	[N/mm^2]	Maximum prestressing stress during tensioning
E_p	195000	[N/mm^2]	Modulus of elasticity
ε_{uk}	35	[‰]	Characteristic value strain at failure

Properties prestressing tendons

n_{ducts}	4	[pcs]	Number of ducts in total
a_{vert}	500	[mm]	Vertical position centre of duct from centre of beam
a_{hor}	750	[mm]	Horizontal position centre of duct from centre of beam
n_{strand}	7	[pcs]	Assumed number of strands per tendon
D_{strand}	15,2	[mm]	Diameter of single strand
$A_{p,strand}$	140	[mm^2]	Cross sectional area per strand
$\sigma_{p,max,prov}$	1400	[N/mm2]	Assumed maximum stress applied to prestressing element
$\emptyset_{Duct}$	65	[mm]	Outer diameter of prestressing ducts
μ	0,23	[-]	Friction coefficient
k	0,009	[rad]	Unintentional angular rotation due to the Wobble-effect
w_{set}	3	[mm]	Estimated wedge set
Relaxation	Class 2	[-]	Select relaxation class: normal (1), low (2) or bars (3)
t	500000	[h]	The value of the relaxation loss (in %) at 1000 h
ρ	2,5	[%]	Time after stressing (for final value of the relaxation loss)

1.2.3 Partial factors material resistance

The following partial factors for the material resistance are distinguished in the calculation:

Symbol	Value	Clarification
γ_C	1,5	Partial factor concrete (cf EC2)
γ_{cf}	1,3	Partial factor for fibre reinforced concrete in tension (cf AFGC)
$\gamma_E * \gamma_{cf}$	1,5	Product of partial factor for uncertainty in extrapolation * factor Ycf
γ_S	1,1	Partial factor prestressing steel (cf EC2)
$\gamma_{F,fat}$	1,0	See 2.4.2.3 of NA to NEN-EN 1992-1-1
$\gamma_{S,fat}$	1,1	See 2.4.2.4 of NA to NEN-EN 1992-1-1
γ_{spl}	1,2	Partial factor splitting forces

1.2.4 Calculation parameters

Calculation parameters main beams

A number of additional parameters are defined for the main beams:

Symbol	Value	Units	Definition
σ_{max}	6,7	[N/mm^2]	Maximum allowed stress at outer concrete fibres
θ	30	[^{0}]	Angle of the concrete compressive strut of the main beams
Cover	35	[mm]	Assumed minimum cover bottom flange(all sides)
$\emptyset_{spl,fl}$	10	[mm]	Assumed diameter splitting reinforcement bottom flange
μ	0,5	[-]	Friction coefficient concrete and supports
δ	300	[-]	Maximum deflection in SLS

Calculation parameters longitudinal joints and top flange

A number of additional parameters are defined for the longitudinal joints and top flanges:

Symbol	Value	Units	Definition
$\emptyset_{spl,ft}$	10	[mm]	Assumed diameter splitting reinforcement top flange
h_1	100	[mm]	Anchor plate (height and width)

Calculation parameters end cross beams

A number of additional parameters are defined for the end cross beams:

Symbol	Value	Units	Definition
k_1	0,15	[-]	Factor from 6.2.2 of the NA to NEN-EN 1992-1-1
θ	21,8	[^{0}]	Angle concrete compressive strut of end cross beam

1.3 Design of bridge and main carriageway – Actions

1.3.1 Design main carriageway

Parameters regarding the design of the main carriageway that have to be defined are:

Symbol	Value	Units	Clarification
h_{kerb}	340	[mm]	Assumed height of the kerb
w_{kerb}	500	[mm]	Assumed width of the kerb
ρ_C	25	[kN/m3]	Density of the concrete used
t_{surf}	1,1	10	[mm]
$\rho_{asphalt}$	1,0	23	[kN/m^3]

1.3.2 Effective width of the beams

To determine distributed loads acting on the different beams the ''effective widths'' of the outer and inner beams are determined:

- The effective width of the outer beams (beams 1 and 5):

$$b_{eff,o} = w + \frac{w_{joint}}{2} \rightarrow 3{,}2 + \frac{0{,}09}{2} = 3{,}245\ [m]$$

- The effective width of the inner beams (beams 2 – 4):

$$b_{eff,i} = w + 2 * \frac{w_{joint}}{2} \rightarrow 3{,}2 + 2 * \frac{0{,}09}{2} = 3{,}29\ [m]$$

1.3.3 Permanent actions (G)

Using the defined parameters the Excelsheet calculates the values of the different permanent actions that have to be plugged into the RFEM model.

- Self-weight prefab beams:

$$G_{k,beam} = A_c * \rho \rightarrow 1663750 * 10^{-6} * 25 = 41{,}59\ [kN/m]$$

- Self-weight end cross beams:

$$G_{k,cb} = A_{cb} * \rho \rightarrow 4622500 * 10^{-6} * 25 = 115{,}56\ [kN/m]$$

- Self-weight of the joints: First the area of the total joint is calculated including both the joint height and the part of the prefab beam on top of which the joint material is casted:

$$A_j'' = w_j * t_{ft} \rightarrow 80 * 187{,}5 * 10^{-6} = 0{,}0169\ [m^2]$$

The line load representing the self-weight of the joints then is:

$$G_{k,j} = A_j'' * \rho \rightarrow 0{,}0169 * 25 = 0{,}42\ [kN/m]$$

- Permanent load road surface:

$$G_{k,surf} = t_{surf} * \rho_{asphalt} \rightarrow 10 * 10^{-3} * 23 = 0{,}23\ [kN/m^2]$$

- Permanent load kerbs:

$$G_{k,kerb} = h_{kerb} * \rho \rightarrow 0{,}34 * 25 = 8{,}75\ [kN/m^2]$$

1.3.4 Variable actions (Q)

The following values of variable loads have to be entered into the Excelsheet:

- Load model 1:
    - Lane 1: $Q_{1k} = 291$ kN and $q_{1k} = 8{,}73$ kN/m^2
    - Lane 2: $Q_{2k} = 194$ kN and $q_{2k} = 2{,}425$ kN/m^2
    - Remaining area: $q_{rk} = 2{,}25$ kN/m^2
- Load model 2: $\beta_Q Q_{ak} = 388$ kN per axle

1.3.5 Accidental actions (A)

The following values of variable loads have to be entered into the Excelsheet:

Symbol	Value	Units	Clarification
F_{equi}	1000	[kN]	Equivalent static force, see: (4) of 4.6.2. EC1-1-7

1.3.6 Fatigue

The following values of variable loads have to be entered into the Excelsheet:

Symbol	Value	Units	Clarification
n_y	100	[-]	Design service life
N_{obs}	500000	[-]	Number of heavy vehicles per year

1.3.7 Combinations of actions

To formulate combinations of actions the following factors have to be defined:

Symbol	Value	Units	Clarification
γ_G	1,4	[-]	See tabel NB.16 – A2.4(B) of NA to NEN-EN 1990
$\zeta * \gamma_G$	1,25	[-]	See tabel NB.16 – A2.4(B) of NA to NEN-EN 1990
γ_P	1,0	[-]	See 2.4.2.2 of NA to NEN-EN 1992-1-1
γ_Q	1,5	[-]	See tabel NB.16 – A2.4(B) of NA to NEN-EN 1990
ψ_0	0,8	[-]	See tabel NB.13 – A2.1 of NA to NEN-EN 1990
ψ_1	0,8	[-]	See tabel NB.13 – A2.1 of NA to NEN-EN 1990

1.4 Determining force distribution (RFEM input)

To complete the input various values of internal forces have to be determined (using RFEM) and plugged into the Excelsheet.

1.4.1 Design of main prestressing and verification capacity of the main beams

For the ultimate limit state verifications of the main beams the following values are required:

Symbol	Value	Units	Clarification
M_{Ed}	48426	[kNm]	Governing bending moment value (mid span)
V_{Ed}	4090	[kN]	Governing shear force value (near supports)
T_{Ed}	1222	[kNm]	Governing torsional moment

To determine the required prestressing, values corresponding to the characteristic combination of the serviceability limit state are required:

Symbol	Value	Units	Clarification
$M_{E,G,perm}$	1727	[kNm]	Bending moment imposed permanent loads in SLS at midspan
$M_{E,Q}$	9694	[kNm]	Bending moment variable loads in SLS at midspan

To check the calculation of the deflections using the Excelsheet, the deflection can also be determined directly using RFEM:

Symbol	Value	Units	Clarification
δ_{max}	344,4	[mm]	Maximum deflection at midspan in the SLS (frequent combination)

1.4.2 Fatigue analysis main beams

For the fatigue analysis two values are to be determined using RFEM (one using the fatigue load combination with fatigue load, the other without fatigue load).

Symbol	Value	Units	Clarification
$M_{fat,max}$	31539	kNm	Maximum bending moment at midspan (found using RFEM)
$M_{fat,min}$	27183	kNm	Minimum bending moment at midspan (found using RFEM)

1.4.3 Design of prestressing and verification capacity of the end cross beams

For the ultimate limit state verifications of the end cross beams the following values are required:

Symbol	Value	Units	Clarification
$M_{Ed,hog}$	1212	[kNm]	Maximum hogging bending moment (all loads considered)
$M_{Ed,sag}$	436	[kNm]	Maximum sagging bending moment (all loads considered)
V_{Ed}	837	[kN]	Maximum shear force (all loads considered)

To determine the required prestressing, values corresponding to the characteristic combination of the serviceability limit state are required:

Symbol	Value	Units	Clarification
$M_{E,hog}$	469	[kNm]	Maximum hogging bending moment SLS
$M_{E,sag}$	298	[kNm]	Maximum sagging bending moment SLS

2

ULS – STR

2.1 Input parameters

The required parameters are taken from the overview (see the first chapter). To determine the eccentricity of the tendons in the bottom flange it is assumed that the centre of gravity of the tendons is positioned at the centre of the bottom flange:

$$e_p = e_b - 0{,}5 * t_{fb}$$

Additionally, the bending moment at mid span due to the self-weight of the beams only is calculated:

$$M_{E,G,sw} = \frac{1}{8} * G_{k,beam} * l^2 \rightarrow \frac{1}{8} * 41{,}59 * 68{,}0^2 = 24.039\ [kNm] \approx 24.041\ [Excel]$$

2.2 Design of the main prestressing

2.2.1 Calculating prestress losses

Applied maximum force onto prestressing element and stress verification

The provided maximum prestressing forces by the centric and eccentric group of strands are respectively:

$$P_{max,prov,c} = n_c * A_{p,c} * \sigma_{p,max,prov,c}$$

$$P_{max,prov,c} = n_c * A_{p,c} * \sigma_{p,max,prov,c}$$

It has to be verified that the maximum stress applied to the prestressing strands does not exceed the maximum value, hence the following verification has to be performed.

$$\sigma_{p,max,prov,c} \leq \sigma_{p,max} \wedge \sigma_{p,max,prov,fb} \leq \sigma_{p,max}$$

The compressive stresses are to be verified as well, the governing point is the bottom fibre at the support:

$$\sigma_c = \frac{P_{max,c}}{A_c} + \frac{P_{max,fb}}{A_c} + \frac{P_{max,fb} * e_p}{W_b} \leq 0{,}7 * f_{ck}$$

Direct losses

Centric prestressing: By definition the eccentricity of the tendons with respect to the centre of gravity of the cross section equals zero. That means that $e_{p,c} = 0$ and $f_c = 1$. Hence:

$$\Delta P_{el,c} = \frac{\alpha_e \rho_p}{1 + \alpha_e \rho_p} * P_{max,c}$$

Where:

$$\alpha_e = \frac{E_p}{E_c}$$

$$\rho_{p,c} = \frac{A_{p,c}}{A_c}$$

Eccentric prestressing: The elastic loss of the eccentric prestressing is:

$$\Delta P_{el,fb} = \frac{\alpha_e \rho_p f_{fb}}{1 + \alpha_e \rho_p f_{fb}} * P_{max,fb}$$

Where:

$$\rho_{p,fb} = \frac{A_{p,fb}}{A_c}$$

$$f_{fb} = 1 + A_c * \frac{e_p^2}{I_y}$$

Determining initial prestressing force and stress verification

The initial prestressing force for the centric and eccentric prestressing is:

$$P_{m0,c} = P_{max,c} - \Delta P_{el,c}$$

$$P_{m0,fb} = P_{max,fb} - \Delta P_{el,fb}$$

It has to be verified that the stresses in the strands are not larger than the maximum allowable value:

$$\frac{P_{m0,c}}{A_{p,c}} \leq \sigma_{pm0} \wedge \frac{P_{m0,fb}}{A_{p,fb}} \leq \sigma_{pm0}$$

Time dependent losses

Centric prestressing: For the centric prestressing the time dependent losses are calculated as follows:

$$\Delta P_{c+s+r,c} = A_{p,c} * \Delta\sigma_{p,c+s+r,c} = A_{p,c} * \frac{\varepsilon_{cs} E_p + 0{,}8\Delta\sigma_{pr,c} + \frac{E_p}{E_{cm}} \varphi(\infty, t_0) \sigma_{c,QP,c}}{1 + \frac{E_p}{E_{cm}} \frac{A_{p,c}}{A_c} [1 + 0{,}8 * \varphi(\infty, t_0)]}$$

Where (for relaxation class 2):

$$\frac{\Delta\sigma_{pr,c}}{\sigma_{pi,c}} = 0{,}66 * \rho_{1000} * e^{9{,}1\mu_c} * \left(\frac{t}{1000}\right)^{0{,}75(1-\mu_c)} * 10^{-5}$$

$$\sigma_{pi,c} = \sigma_{pm,0,c}$$

$$\mu_c = \sigma_{pm,0,c} / f_{pk}$$

$$t = 500.000 + t_{eq}$$

$$\sigma_{c,QP,c} = \frac{P_{m0,c}}{A_c} + \frac{P_{m0,fb}}{A_c}$$

Eccentric prestressing: For the eccentric prestressing the time dependent losses are calculated as follows:

$$\Delta P_{c+s+r,fb} = A_{p,fb} * \Delta\sigma_{p,c+s+r,fb} = A_{p,fb} * \frac{\varepsilon_{cs} E_p + 0{,}8\Delta\sigma_{pr,fb} + \frac{E_p}{E_{cm}} \varphi(\infty, t_0) \sigma_{c,QP,fb}}{1 + \frac{E_p}{E_{cm}} \frac{A_{p,fb}}{A_c} \left(1 + \frac{A_c}{I_c} z_{cp}^2\right) [1 + 0{,}8 * \varphi(\infty, t_0)]}$$

Where (for relaxation class 2):

$$\frac{\Delta\sigma_{pr,fb}}{\sigma_{pi,fb}} = 0{,}66 * \rho_{1000} * e^{9{,}1\mu_{fb}} * \left(\frac{t}{1000}\right)^{0{,}75(1-\mu_{fb})} * 10^{-5}$$

$$\sigma_{pi,fb} = \sigma_{pm,0,fb}$$

$$\mu_{fb} = \frac{\sigma_{pm,0,fb}}{f_{pk}}$$

$$t = 500.000 + t_{eq}$$

$$z_{cp} = e_b - \frac{t_{fb}}{2} = e_p$$

$$\sigma_{c,QP,fb} = \frac{P_{m0,c}}{A_c} + \frac{P_{m0,fb}}{A_c} + \frac{P_{m0,fb} * e_p * z_{cp}}{I_c} - \frac{M_{G,sw} * z_{cp}}{I_c} - \frac{M_{G,perm} * z_{cp}}{I_c}$$

Working prestress force

The working prestressing force for the centric and eccentric prestressing is:

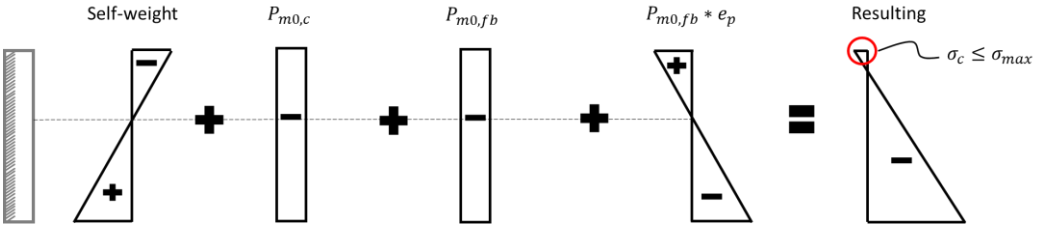
$$P_{m,\infty,c} = P_{m0,c} - \Delta P_{c+s+r,c}$$

$$P_{m,\infty,fb} = P_{m0,fb} - \Delta P_{c+s+r,fb}$$

2.2.2 Determining stresses at midspan

Two situations are considered, for both situations the concrete stress has to be smaller than the maximum value, both at the top and bottom fibre.

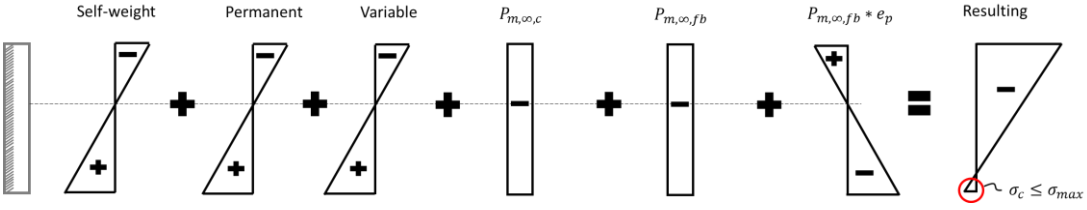
- **Self-weight and prestressing only ($t = 0$)**:



$$\sigma_{c,t} = -\frac{M_{G,sw}}{W_t} - \frac{P_{m0,c}}{A_c} - \frac{P_{m0,fb}}{A_c} + \frac{P_{m0,fb} * e_p}{W_t} \leq \sigma_{max}$$

$$\sigma_{c,b} = +\frac{M_{G,sw}}{W_b} - \frac{P_{m0,c}}{A_c} - \frac{P_{m0,fb}}{A_c} - \frac{P_{m0} * e_p}{W_b} \leq \sigma_{max}$$

- **Use phase ($t \to \infty$)**:



$$\sigma_{c,t} = -\frac{(M_{G,sw} + M_{G,perm})}{W_t} - \frac{M_Q}{W_t} - \frac{P_{m,\infty,c}}{A_c} - \frac{P_{m,\infty,fb}}{A_c} + \frac{P_{m,\infty,fb} * e_p}{W_t} \leq \sigma_{max}$$

$$\sigma_{c,b} = +\frac{(M_{G,sw} + M_{G,perm})}{W_t} + \frac{M_Q}{W_b} - \frac{P_{m,\infty,c}}{A_c} - \frac{P_{m,\infty,fb}}{A_c} - \frac{P_{m,\infty,fb} * e_p}{W_b} \leq \sigma_{max}$$

2.3 Detailing beam ends

2.3.1 Bond stresses and transmission length

The bond stresses are calculated as follows:

$$f_{bpt} = \eta * \eta_1 * \kappa * \frac{f_{ctk,el}(t)}{\gamma_c}$$

The transfer length of the centric and eccentric prestressing is:

$$l_{pt,c} = 1{,}0 * 0{,}19 * 15{,}2 * \frac{\sigma_{pm0,c}}{f_{bpt}}$$

$$l_{pt,fb} = \alpha_1 * \alpha_2 * \emptyset * \frac{\sigma_{pm0,fb}}{f_{bpt}}$$

The design values used in the analysis are:

$$l_{pt1,c} = 0{,}4 * l_{pt,c}$$

$$l_{pt1,fb} = 0{,}4 * l_{pt,fb}$$

2.3.2 Tensile stresses at top fibre

For the calculations it is assumed that the centric prestressing is transferred onto the concrete from the support while for the eccentric prestressing the option is given to de-bond the strands over a certain length and introduce the total number of eccentric strands over two 'sets'.

The development of stresses at the top fibre is calculated by determining the stresses due to self-weight and prestressing at a number of points along the beam.

Centric prestressing: The compressive stresses due to the centric prestressing for $x < l_{pt,c}$ and $x > l_{pt,c}$ are:

$$\sigma_{t,c}(x) = -\frac{P_{m0,c}}{l_{pt,c}} * x * \frac{1}{A_c}, x \leq l_{pt,c}$$

$$\sigma_{t,c}(x) = -\frac{P_{m0,c}}{A_c}, x > l_{pt,c}$$

Eccentric prestressing – Axial component: The compressive stresses due to the axial component of the eccentric prestressing for $x < l_{pt,fb}$ and $x > l_{pt,fb}$ are:

$$\sigma_{t,fb,P}(x) = -\frac{P_{m0,fb}}{l_{pt,fb}} * x * \frac{1}{A_c}, x \leq l_{pt,fb}$$

$$\sigma_{t,fb,P}(x) = -\frac{P_{m0,fb}}{A_c}, x > l_{pt,fb}$$

Eccentric prestressing – Bending: The tensile stresses due to upward bending caused by the eccentric prestressing for $x < l_{pt,fb}$ and $x > l_{pt,fb}$ are:

$$\sigma_{t,fb,M}(x) = -\frac{P_{m0,fb}}{l_{pt,fb}} * x * \frac{e_p}{W_t}, x \leq l_{pt,fb}$$

$$\sigma_{t,fb,M}(x) = --\frac{P_{m0,fb} * e_p}{W_t}, x > l_{pt,fb}$$

Self-weight beams: The bending moment due to the self-weight along the beam axis can be determined as:

$$M_{sw}(x) = \frac{1}{2} * G_{k,beam} * x * (l - x), 0 \leq x \leq l$$

The compressive stresses at the top fibre along the beam axis due to the self-weight are therefore:

$$\sigma_{t,sw}(x) = -\frac{M(x)}{W_t}$$

Total stresses: By adding up the absolute values of the compressive stresses the total stress in the top fibre is determined:

$$\sigma_{t,compression}(x) = |\sigma_{t,sw}(x)| + |\sigma_{t,c}(x)| + |\sigma_{t,fb,P}(x)|$$

Verification: It has to be verified that the highest remaining tensile stress (if present) is smaller than the maximum value along the beam segment under consideration:

$$\Delta\sigma_t \leq \sigma_{max}$$

If this requirement is met no de-bonding of strands is required.

2.3.3 Positioning of strands in the bottom flange

Maximum number of strands

The total area of the bottom flange is:

$$t_{fb} * (t_w + w_b + t_w)$$

The concrete cover is subtracted to determine the ''available area'':

$$h_{available} * w_{available} = \left(t_{fb} - 2 * c_{nom}\right) * (t_w + w_b + t_w - 2 * c_{nom})$$

The minimum centre to centre distance is calculated using the minimum spacing:

$$d_{min} = s_{min} + D_{strand}$$

The maximum number of rows that can be applied is (rounded off to the nearest lower integer):

$$n_{max,rows} = Int\left(\frac{h_{available}}{d_{min}}\right)$$

The maximum number of strands per row (also rounded off to the nearest lower integer):

$$n_{max,strands} = Int\left(\frac{w_{available}}{d_{min}}\right)$$

The maximum number of strands is $n_{max,rows} * n_{max,strands}$.

Positioning the strands

The number of rows required with the assumed number of strands in the bottom flange is as follows. Note that the result is rounded off to the nearest highest integer.

$$n_{rows} = Int\left(\frac{n_{fb}}{n_{max,strands}}\right)$$

The number of strands per row is:

$$n_{strands} = \frac{n_{fb}}{n_{rows}}$$

The vertical and horizontal centre to centre distance of the strands then is:

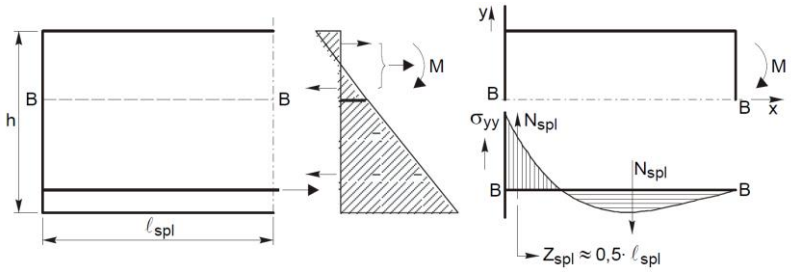
$$d_{vert} = \frac{h_{available} - D_{strand}}{n_{rows} - 1}$$

$$d_{hor} = \frac{w_{available} - D_{strand}}{n_{strands} - 1}$$

2.3.4 Splitting reinforcement – Vertical distribution

Spalling

Note: If the option is used to apply the strands in the bottom flange in two sets at various points along the beam axis then the following calculations are performed separately for both sets. It is verified if the point under consideration is within the cross section of the end cross beam or outside this section, because this affects the width of the cross section where spalling occurs.



The length of the equivalent prism is:

$$l_{spl} = C_{spl} * h \rightarrow \sqrt{1 + \left(0{,}6 * \frac{l_{pt,fb}}{h}\right)^2} * h$$

The bending moment is calculated as follows:

$$\sigma_{top} = -\frac{P_{m0,c}}{A_c} - \frac{P_{m0,fb}}{A_c} + \frac{P_{m0,fb} * e_p}{W_t}$$

$$\sigma_{bottom} = -\frac{P_{m0,c}}{A_c} - \frac{P_{m0,fb}}{A_c} - \frac{P_{m0,fb} * e_p}{W_t}$$

$$h_{prism} = 2 * \frac{h * \sigma_{top}}{\sigma_{top} + |\sigma_{bottom}|}$$

$$M = \frac{1}{6} * b * h_{prism}^2 * \sigma_{top}$$

The spalling force is:

$$N_{spl} * 0{,}5 * l_{spl} - M = 0 \rightarrow N_{spl} = \frac{2 * M}{l_{spl}}$$

The spalling stresses are calculated as follows:

$$\sigma_{spl} = \frac{16 * M}{l_{spl}^2 * b}$$

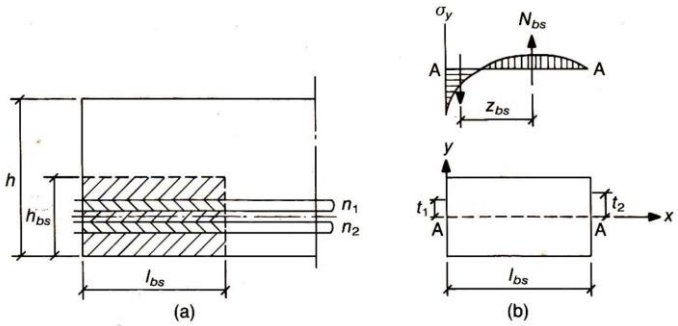
The stress verification is subsequently performed:

$$\sigma_{Rd,f} \approx \frac{f_{ctfk}}{K_{local} * \gamma_{cf}}$$

$$\gamma_{spl} * \sigma_{spl} \leq \sigma_{Rd,f}$$

Bursting

Note that the equations for bursting have been formulated for 3 or 4 rows of strands in the bottom flange only. In case the number of tendons changes, the lever arms t_1 and t_2 have to be recalculated.



The height and length of the prism are respectively:

$$h_{bs} = t_{fb}$$

$$l_{bt} = C_{bs} * h_{bs} \rightarrow h_{bs} * \sqrt{1 + \left(0{,}6 * \frac{l_{pt,fb}}{h_{bs}}\right)^2}$$

The bursting force follows from:

$$N_{bs} = \frac{(n_1 * t_2 - n_1 * t_1)}{0{,}5 * l_{bt}} * P_{m0,fb}$$

The maximum bursting stresses are:

$$\sigma_{bs} = \frac{N_{bs}}{b_{bs} * l_{bs}}$$

In this equation the width of the prism is taken equal to the width of the section at the height of the tendons:

$$b_{bs} = t_w + b_w + t_w$$

The final step is the verification of the stresses:

$$\sigma_{Rd,f} \approx \frac{f_{ctfk}}{K_{local} * \gamma_{cf}}$$

$$\gamma_{spl} * \sigma_{spl} \leq \sigma_{Rd,f}$$

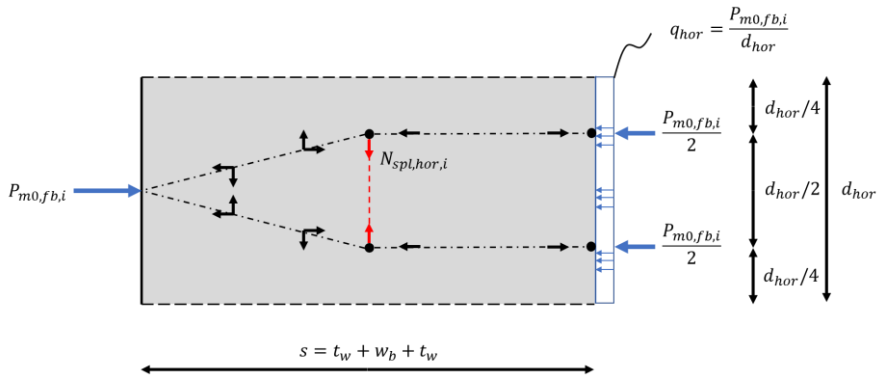
Splitting

Splitting is dealt with implicitly by applying sufficient spacing and cover between and onto the prestressing strands.

2.3.5 Splitting reinforcement – Horizontal distribution

For determining the splitting reinforcement it is assumed that the forces themselves over the full width of the beam. The splitting force caused by a single strand is calculated as follows:

$$N_{spl,hor,i} = \frac{1}{4} * \gamma_{spl} * P_{m0,fb,i} * \frac{b_{hor}}{2 * t_w + w_b}$$



This value is multiplied with the number of strands to determine the total splitting force:

$$N_{spl,hor} = n_{fb} * N_{spl,hor,i}$$

The maximum allowable stresses in the rebars are:

$$f_s = \frac{3000}{\emptyset_k} \leq 360\ [MPa]$$

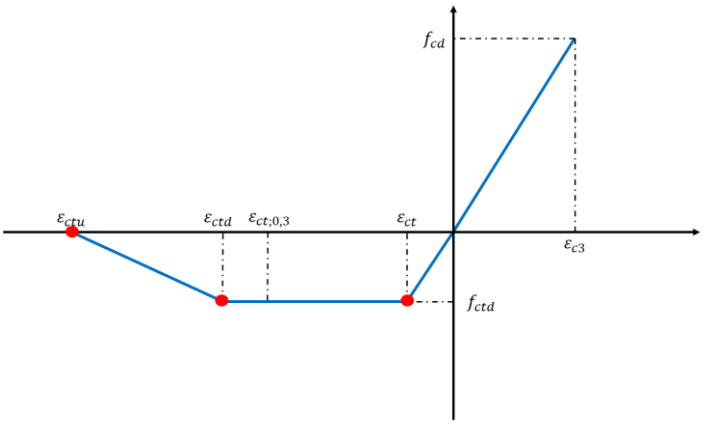
The minimum required diameter of the reinforcement follows from:

$$A_{s,min} = \frac{N_{spl,hor}}{f_s}$$

2.4 Verification bending moment capacity

2.4.1 Assumptions

The following stress-strain relation for concrete in compression and tension has been adopted for the ultimate limit state verification of the main beams:



Calculating stresses:

$$f_{cd} = \frac{\alpha_{cc} * f_{ck}}{\gamma_C}$$

$$f_{ctd} = \frac{\alpha_{ct} * f_{ctk,el}}{\gamma_C}$$

Calculating strains:

$$\varepsilon_{ct} = \frac{f_{ctd}}{E_{cm}} = \frac{f_{ctk,el}}{\gamma_c * E_{cm}}$$

$$\varepsilon_{ct;0,3} = \frac{w_{0,3}}{l_c} + \varepsilon_{ct}$$

$$\varepsilon_{ctd} = \varepsilon_{ctu} - \frac{f_{ctd}}{f_{ctd;2}} * (\varepsilon_{ctu} - \varepsilon_{ct;0,3})$$

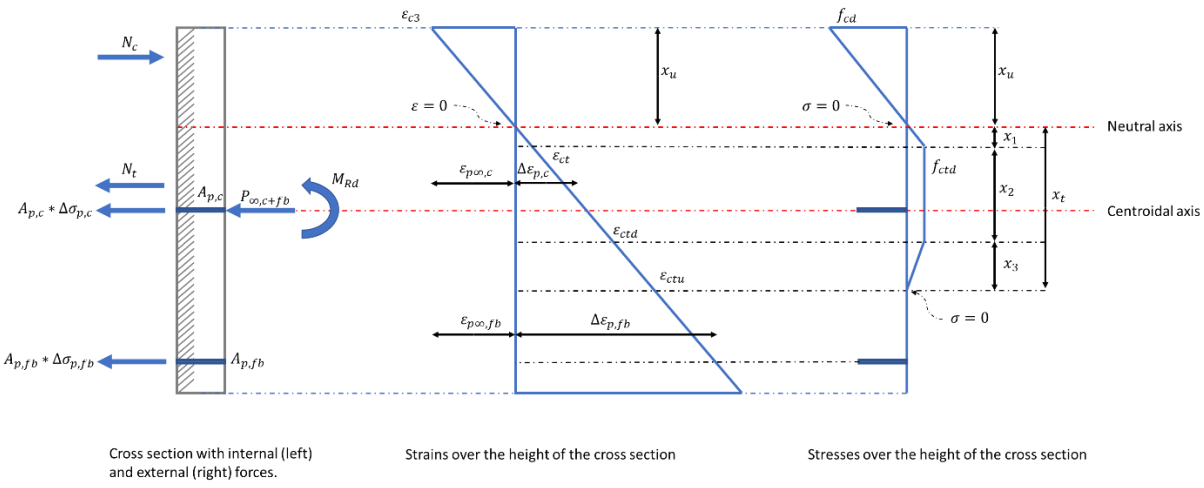
$$\varepsilon_{ctu} = \frac{l_f}{4 * l_c}$$

Furthermore it is assumed that for the verification of the rotational capacity the redistribution is zero.

2.4.2 Calculating the capacity and verifications

In the ULS the following strain and stress distributions are assumed to occur over the height of the beam:

Stress and strain figures



Cross section with internal (left) and external (right) forces.

Strains over the height of the cross section

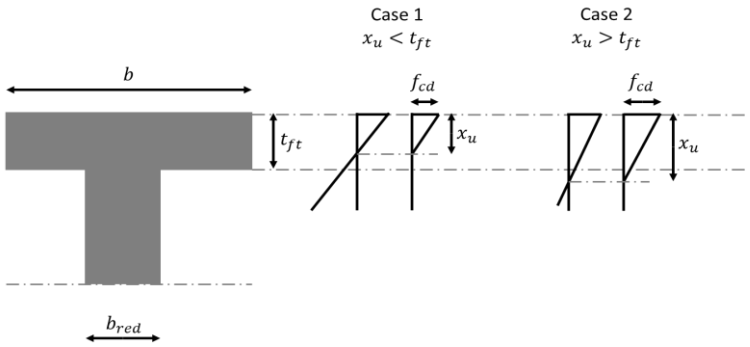
Stresses over the height of the cross section

Identifying all horizontal forces

The calculation has been made iterative, the Excelsheet assumes a value for the height of the concrete compressive zone and verifies whether horizontal equilibrium has been reached. If so, then this value will be taken for x_u. The full calculation procedure is as follows:

Height of concrete compressive and tensile zone

Concrete compressive zone: The concrete compressive force is calculated using the assumed value for x_u. Two cases can be distinguished.



Case 1: $x_u \leq t_{ft}$ and standard equations can be used for a rectangular cross section:

$$N_c = \frac{1}{2} * w * f_{cd} * x_u$$

$$e_c = \frac{1}{3} * x_u$$

Case 2: $x_u > t_{ft}$ and thus the width varies over the height of the compressive zone. The stresses and strains at the bottom of the top flange are:

$$\varepsilon_{c,fl} = \varepsilon_{c3} * \left(1 - \frac{t_{ft}}{x_u}\right)$$

$$\sigma_{c,fl} = f_{cd} * \left(1 - \frac{t_{ft}}{x_u}\right)$$

The total concrete compressive force is:

$$N_c = N_{c,1} + N_{c,2} + N_{c,3} \rightarrow \frac{1}{2} * t_{ft} * \left(f_{cd} - \sigma_{c,fl}\right) * b + t_{ft} * \sigma_{c,fl} * b + \frac{1}{2} * \left(x_u - t_{ft}\right) * \sigma_{c,fl} * b_{red}$$

$$b_{red} = 2 * t_w$$

The centre of gravity with respect to the top fibre is:

$$e_c = \frac{S_1 + S_2 + S_3}{N_{c,1} + N_{c,2} + N_{c,3}} \rightarrow \frac{N_{c,1} * \frac{1}{3} * t_{ft} + N_{c,2} * \frac{1}{2} * t_{ft} + N_{c,3} * \left(t_{ft} + \frac{1}{3} * \left(x_u - t_{ft}\right)\right)}{N_{c,1} + N_{c,2} + N_{c,3}}$$

Concrete tensile zone: First the required strain values are calculated as follows:

$$\varepsilon_{ct} = \frac{f_{ctd}}{E_{cm}} = \frac{f_{ctk,el}}{\gamma_c * E_{cm}}$$

$$\varepsilon_{ct;0,3} = \frac{w_{0,3}}{l_c} + \varepsilon_{ct}$$

$$\varepsilon_{ctu} = \frac{l_f}{4 * l_c} \leq 2{,}5\ ‰$$

$$\varepsilon_{ctd} = \varepsilon_{ctu} - \frac{f_{ctd}}{f_{ctd;2}} * \left(\varepsilon_{ctu} - \varepsilon_{ct;0,3}\right)$$

The height of the tensile zones are calculated by considering the assumed strain diagram:

$$x_1 = \frac{\varepsilon_{ct}}{\varepsilon_{cu3}} * x_u$$

$$x_2 = \frac{\varepsilon_{ctd} - \varepsilon_{ct}}{\varepsilon_{cu3}} * x_u$$

$$x_3 = \frac{\varepsilon_{ctu} - \varepsilon_{ctd}}{\varepsilon_{cu3}} * x_u$$

The total concrete tensile force is:

$$N_t = N_{t1} + N_{t2} + N_{t3} \rightarrow \frac{1}{2} * x_1 * b * f_{ctd} + x_2 * b * f_{ctd} + \frac{1}{2} * x_3 * b * f_{ctd}$$

In this equation the width is always taken equal to twice the web thickness, if the concrete compressive zone is smaller than the height of the top flange the contribution in tension is still limited to the width equal to $2 * t_w$.

The resulting force of the individual tensile forces is determined by taking the top fibre of the cross section as reference point.

$$e_t = \frac{N_{t1} * (x_u + \frac{2}{3} * x_1) + N_{t2} * \left(x_u + x_1 + \frac{1}{2} * x_2\right) + N_{t3} * \left(x_u + x_1 + x_2 + \frac{1}{3} * x_3\right)}{N_{t1} + N_{t2} + N_{t3}}$$

Determining the strains

The strains are calculated for both the centric and eccentric prestressing. Both procedures are given below.

- Centric prestressing:

$$d_{p,c} = e_t$$

$$\Delta\varepsilon_{p,c} = \varepsilon_{c3} * \left(\frac{d_{p,c}}{x_u} - 1\right)$$

$$\varepsilon_{p,\infty,c} = \frac{\sigma_{p,\infty,c}}{E_p}$$

$$\varepsilon_{p,c} = \varepsilon_{p,\infty,c} + \Delta\varepsilon_{p,c} \leq 0{,}9 * \varepsilon_{uk}$$

- Eccentric prestressing:

$$d_{p,fb} = h - 0{,}5 * t_{fb}$$

$$\Delta\varepsilon_{p,fb} = \varepsilon_{c3} * \left(\frac{d_{p,fb}}{x_u} - 1\right)$$

$$\varepsilon_{p,\infty,fb} = \frac{\sigma_{p,\infty,fb}}{E_p}$$

$$\varepsilon_{p,fb} = \varepsilon_{p,\infty,fb} + \Delta\varepsilon_{p,fb} \leq 0{,}9 * \varepsilon_{uk}$$

Steel stresses

Using the calculated strain values the stresses in the prestressing steel are calculated.

- Centric prestressing:

$$\sigma_{pu,c} = f_{pd} + \frac{\varepsilon_{p,c} - \frac{f_{pd}}{E_p}}{\varepsilon_{uk} - \frac{f_{pd}}{E_p}} * \left(\frac{f_{pk}}{\gamma_s} - f_{pd}\right)$$

- Eccentric prestressing:

$$\sigma_{pu,fb} = f_{pd} + \frac{\varepsilon_{p,fb} - \frac{f_{pd}}{E_p}}{\varepsilon_{uk} - \frac{f_{pd}}{E_p}} * \left(\frac{f_{pk}}{\gamma_s} - f_{pd}\right)$$

The increase of the force in the prestressing steel (the passive contribution) is for the centric and eccentric prestressing respectively:

$$\Delta N_{p,c} = A_{p,c} * (\sigma_{pu,c} - \sigma_{p,\infty,c})$$

$$\Delta N_{p,fb} = A_{p,fb} * (\sigma_{pu,fb} - \sigma_{p,\infty,fb})$$

Check equilibrium

Equilibrium is checked by considering all horizontal forces:

$$-N_c + N_t + P_{m,\infty,c} + P_{m,\infty,fb} + \Delta N_{p,c} + \Delta N_{p,fb} = 0$$

Determining bending moment capacity

If equilibrium is achieved the bending moment capacity is calculated using the top fibre as the reference point:

$$M_{Rd} = -N_c * e_c + N_t * e_t + P_{m,\infty,c} * d_{p,c} + P_{m,\infty,fb} * d_{p,c} + \Delta N_{p,c} * d_{p,c} + \Delta N_{p,fb} * d_{p,fb}$$

The design value of the bending moment is as follows:

$$M_{Ed} = M_{Ed,RFEM} - P_{m,\infty,fb} * e_p$$

The following criterion is to be satisfied:

$$\frac{M_{Ed}}{M_{Rd}} \leq 1{,}0$$

Verifying rotational capacity

To verify the rotational capacity the following basic equation is applied:

$$\frac{x_u}{d_p} \leq \frac{\varepsilon_{c3} * 10^6}{\varepsilon_{c3} * 10^6 + 7f}$$

$$f = \frac{\left(\frac{f_{pk}}{\gamma_s} - \sigma_{pm,\infty}\right) A_p + f_{yd} A_s}{A_p + A_s}$$

Because prestressing is applied at two different heights, the weighted average values are used for d_p, A_p and $\sigma_{pm,\infty}$. These are calculated as follows:

$$d_{p,ave} = \frac{n_c * d_{p,c} + n_{fb} * d_{p,fb}}{n_c + n_{fb}}$$

$$A_{p,ave} = \frac{n_c * A_{p,c} + n_{fb} * A_{p,fb}}{n_c + n_{fb}}$$

$$\sigma_{p,\infty,ave} = \frac{n_c * \sigma_{p,\infty,c} + n_{fb} * \sigma_{p,\infty,fb}}{n_c + n_{fb}}$$

2.5 Verification shear force capacity

2.5.1 Assumptions and limitations

The calculation is based on the following assumptions:

- It is assumed the concrete is loaded in compression due to the prestressing;

$$\sigma_{cp} = \frac{N_{Ed}}{A_c} \rightarrow \frac{P_{m,\infty,c} + P_{m,\infty,fb}}{A_c}$$

- It is assumed that no conventional shear reinforcement is present;
- No reduction is taken into consideration to account for ducts etc. as these are not present;
- For the effective height the value for the prestressing with respect to the bottom flange is applied:

$$d_p = h - 0{,}5 * t_{fb}$$

2.5.2 Calculating the resistance and unity check

Tensile resistance of the concrete ties

First the contributions of the two components (concrete and steel fibres) taken into consideration are calculated after which these are added up.

Concrete component: The concrete contribution to the shear capacity:

$$V_{Rd,c} = \frac{0{,}24}{\gamma_{cf}\gamma_E} k f_{ck}^{\frac{1}{2}} b_w z$$

Factor accounting for compressive stress due to the prestressing:

$$k = 1 + 3 * \frac{\sigma_{cp}}{f_{ck}}$$

Where $z = 0{,}9 * d_p$

Steel fibre component: The contribution of the steel fibres to the shear force capacity:

$$V_{Rd,f} = \frac{A_{fv}\sigma_{Rd,f}}{\gamma_{cf} * tan\theta} \approx \frac{A_{fv} * f_{ctd;2}}{\gamma_{cf} * K_{global} * tan\theta}$$

Where:

$$A_{fv} \approx b_w * z$$

$$f_{ctd;2} = \frac{f_{ctfk}}{\gamma_{cf} * K_{global}}$$

Total resistance: The total resistance is the summation of the contribution of concrete and steel fibres:

$$V_{Rd} = V_{Rd,c} + V_{Rd,f}$$

Resistance of the concrete compressive strut

The upper limit of the shear force capacity is the capacity of the concrete compressive strut:

$$V_{Rd,max} = 2 * 1{,}14 * \frac{\alpha_{cc}}{\gamma_c} b_w z f_{ck}^{\frac{2}{3}} * \frac{1}{cot\theta + tan\theta}$$

Shear force capacity

The shear force capacity of the cross section is taken as the lesser value of the tensile resistance of the ties and the resistance of the compressive strut:

$$V_{Rd} = \min\left(V_{Rd,c} + V_{Rd,f}; V_{Rd,max}\right)$$

Verification

The following criterion is to be satisfied:

$$\frac{V_{Ed}}{V_{Rd}} \leq 1{,}0$$

2.6 Verification torsional resistance

2.6.1 Assumptions & approach

The calculation is based on the following assumptions:

- The shear force is only taken by web (direction shear force parallel to centreline of the webs);
- The same angle is applied for the shear and torsion when calculating the capacity of the concrete compressive strut;
- For the combination of shear and torsion and failure of the concrete compressive strut each wall segment is analysed separately.

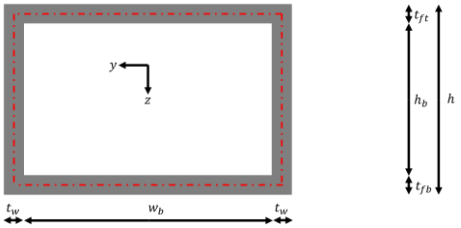
2.6.2 Torsional capacity

The first analysis comprises the verification of the torsional capacity of the cross section as a whole, by comparing the torsional cracking moment (resistance) and torsional moment determined using the RFEM model. The torsional cracking moment is:

$$T_{Rd,c} = f_{ctd} * t_{ef} * 2 * A_k$$

Where:
A_k: Area enclosed by the centre lines of the connected walls, including enclosed hollow parts
t_{ef}: Effective wall thickness
A: Total area of the cross section within the outer circumference, including enclosed hollow parts
u: Outer circumference of the cross section

The simplified cross section is as follows, its properties are calculated below.



$$A = (t_w + w_b + t_w) * \left(t_{ft} + h_b + t_{fb}\right)$$

$$u = 2 * (t_w + w_b + t_w) + 2 * \left(t_{ft} + h_b + t_{fb}\right)$$

$$t_{ef} = \frac{A}{u} \leq \min\{t_w; t_{ft}; t_{fb}\}$$

$$A_k = \left(\frac{1}{2} * t_w + w_b + \frac{1}{2} * t_w\right) * \left(\frac{1}{2} * t_{ft} + h_b + \frac{1}{2} * t_{fb}\right)$$

Note that the real wall thickness of the thinnest element is the limiting factor for the effective wall thickness. It has subsequently to be verified that:

$$\frac{T_{Ed}}{T_{Rd,c}} \leq 1{,}0$$

2.6.3 Combination of shear and torsion

Decomposing the cross section

The cross section is decomposed into four segments that are analysed separately:

- Left web – Part 1
- Bottom flange – Part 2
- Right web – Part 3
- Top flange – Part 4

Forces acting on each segment

The equivalent shear forces due to shear and torsion acting on each part are determined.

Shear forces: It is assumed that only the web contributes to the shear capacity and that the contributions of both webs are equal in magnitude:

$$V_{Ed,V,1} = V_{Ed,V,3} = \frac{V_{Ed}}{2}$$

$$V_{Ed,V,2} = V_{Ed,V,4} = 0$$

Torsion: The shear force in segment 'i' due to torsion is calculated as:

$$V_{Ed,T,i} = \tau_{t,i} * t_{ef,i} * z_i = \frac{T_{Ed}}{2 * A_k} * z_i$$

Where 'z_i' is the length of segment 'i':

$$z_1 = \frac{1}{2} * t_{ft} + h_b + \frac{1}{2} * t_{fb}$$

$$z_2 = \frac{1}{2} * t_w + w_b + \frac{1}{2} * t_w$$

$$z_3 = \frac{1}{2} * t_{ft} + h_b + \frac{1}{2} * t_{fb}$$

$$z_4 = \frac{1}{2} * t_w + w_b + \frac{1}{2} * t_w$$

Combined effect: The combined effect (equivalent shear force) of shear and torsion per segment is:

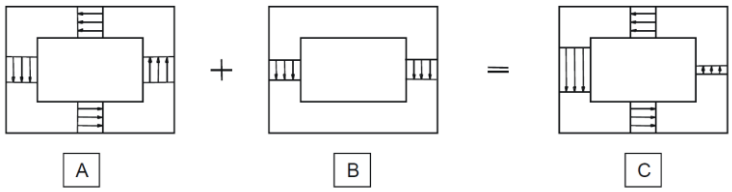
$$V_{Ed,T+V,1} = V_{Ed,V,1} + V_{Ed,T,1}$$

$$V_{Ed,T+V,2} = V_{Ed,T,2}$$

$$V_{Ed,T+V,3} = V_{Ed,V,3} - V_{Ed,T,3}$$

$$V_{Ed,T+V,4} = V_{Ed,T,4}$$

This is based on the following principle:



Legenda

A wringing
B afschuiving
C combinatie

Eurocode 2-2, p.32

Capacity of each segment

For each segment it has to be verified whether the capacity is sufficient. As there is no shear or torsional reinforcement present, the capacity of each segment is:

$$V_{Rd,i} = V_{Rd,c,i} + V_{Rd,f,i}$$

Where:
b_w: Width of the segment (depending on the segment under consideration this equals t_w, t_{fb} or t_{ft});
z: Lever arm (in these calculations 'z' is taken equal to the length 'z_i' of each segment)

The equations for the capacity are the same as used for the shear capacity but different dimensions are applied, the width and length are dependent on the segment under consideration. For each segment it subsequently has to be verified that:

$$\frac{V_{Ed,T+V,i}}{V_{Rd,i}} \leq 1{,}0$$

Failure of the concrete compressive strut

The resistance of the sections to the combined effect of shear and torsion are limited by the capacity of the concrete compressive strut. Because the beams have a box type cross section, each segment is verified separately by applying the following verification:

$$V_{Ed,i} + \frac{T_{Ed}}{2 * A_k} * z_i \leq V_{Rd,max,i}$$

Where:

$$V_{Rd,max,i} = 2 * 1{,}14 * \frac{\alpha_{cc}}{\gamma_C} * b_{w,i} * z_i * f_{ck}^{\frac{2}{3}} * \frac{1}{cot\theta + tan\theta}$$

The values of the (effective) thickness depend on the segment under consideration:

$$b_{w,i} = t_{ef,i}$$

$$t_{ef,i} = \frac{A}{u} \leq t_i$$

2.7 Global verification ship collision

The global verification is performed by considering the static equilibrium of the structure. In order to do so the self-weight of the bridge deck is, as a simplification, calculated by determining the weight of the prefab beams:

$$F_{sw} = n_{beams} * l_{tot} * A_c * \rho$$

It subsequently has to be verified that:

$$F_{eq} \leq \mu * F_{sw}$$

F_{eq}: Equivalent static force caused by ship collision
μ: Friction coefficient for friction between the concrete beams and its supports

3

DESIGN OF MAIN BEAMS – TOP FLANGE AND TRANSVERSE PRESTRESSING

3.1 Design of transverse prestressing

3.1.1 Calculating prestress losses

The calculation the transverse prestressing is based on the following points:

- To design the transverse prestressing a strip of the top flange is analysed with width $w_{c.t.c.}$ and the average thickness t_{ft}, the centre of the strip in horizontal direction coincides with the centre of the prestressing rib. The prestressing tendon is positioned at the centre of the prestressing rib at a height of $0{,}5 * t_{ft}$.

- At each rib a prestressing tendon is applied consisting of n strands, each with an area of $A_{p,strand}$ and an assumed maximum stress of $\sigma_{p,max,prov}$.

- The longitudinal joint has a thickness t_j, which is smaller than the thickness t_{ft}. That means that there is always an eccentricity between the centre of the tendon and top flange on one hand and the centre of the joint on the other of:

$$e_j = 0{,}5 * t_{ft} - 0{,}5 * t_j$$

Applied maximum force onto prestressing element and stress verification

It has to be verified that the maximum stress applied to the tendon does not exceed the maximum value:

$$\sigma_{p,max,prov} \leq \sigma_{p,max}$$

Additionally it is verified that the maximum allowed concrete compressive stress is not exceeded:

$$\sigma_c = \frac{P_{max}}{A_{tf}} = \frac{\sigma_{p,max} * n * A_{p_{strand}}}{w_{c.t.c.} * t_{ft}} \leq 0{,}6 * f_{ck}$$

Direct losses

Elastic shortening: The elastic loss of the single tendon within the strip is:

$$\Delta P_{el} = P_{max} * \frac{E_p A_p}{E_{cm} A_c} = P_{max} * \frac{E_p * A_p}{E_{cm} * w_{c.t.c.} * t_{ft}}$$

Friction: The friction losses for the straight tendon only depend on the Wobble-effect as the angular rotation equals zero:

$$\Delta P_\mu(x) = (1 - e^{-\mu * k * x}) * P_{max}$$

At the far end of the deck ($x = w_{tot}$) the friction loss is:

$$\Delta P_\mu(x = w_{tot}) = (1 - e^{-\mu * k * w_{tot}}) * P_{max}$$

The friction loss converted into a stress value is:

$$\Delta\sigma_{P\mu}(x = w_{tot}) = \frac{\Delta P_{\mu}(x = w_{tot})}{A_p}$$

Wedge set: It is assumed that the friction develops linearly over the full width of the deck, the stress reduction per unit of length is:

$$k = \frac{\Delta\sigma_{P\mu}(x = w_{tot})}{w_{tot}}$$

The influence length over which the wedge set influences the prestressing force then is:

$$l_w = \sqrt{\frac{w_{set} * E_p}{k}}$$

The prestress loss follows from:

$$\Delta P_{set} = 2 * A_p * \frac{\Delta\sigma_{p\mu,m}}{\Delta x} * l_w$$

Determining initial prestressing force and stress verification

The initial prestressing force is:

$$P_{m0}(x) = P_{max} - \Delta P_{el} - \Delta P_{\mu}(x) - \Delta P_{set}(x)$$

It has to be verified that the stresses in the strands are not larger than the maximum allowable value. The deck is divided into a number of intervals and the prestressing forces and losses are subsequently calculated at a total of '*j*' points along the width of the deck. The maximum value of the initial prestressing force is used to perform the verification:

$$\frac{\max\{P_{m0}(x)\}}{A_p} \leq \sigma_{pm0}$$

Time dependent losses

The remainder of the analysis is performed using the mean value of the initial prestressing force calculated at the different points over the length of the beam, which is determined using:

$$P_{m0} = \frac{1}{j} * \sum_{i=1}^{i=j} P_{m0,i}$$

For the centric prestressing in the top flange the time dependent losses can be calculated as follows:

$$\Delta P_{c+s+r} = A_p * \Delta\sigma_{p,c+s+r} = A_p * \frac{\varepsilon_{cs}E_p + 0{,}8\Delta\sigma_{pr} + \frac{E_p}{E_{cm}}\varphi(\infty, t_0)\sigma_{c,QP}}{1 + \frac{E_p}{E_{cm}}\frac{A_p}{A_c}[1 + 0{,}8 * \varphi(\infty, t_0)]}$$

Where (for relaxation class 2):

$$\frac{\Delta\sigma_{pr}}{\sigma_{pi}} = 0{,}66 * \rho_{1000} * e^{9{,}1\mu} * \left(\frac{t}{1000}\right)^{0{,}75(1-\mu)} * 10^{-5}$$

$$\sigma_{pi} = \sigma_{pm,0} = \frac{P_{m0}}{A_p}$$

$$\mu = \frac{\sigma_{pm,0}}{f_{pk}}$$

$$t = 500.000$$

$$\sigma_{c,QP} = \frac{P_{m0}}{w_{c.t.c.} * t_{ft}}$$

Working prestressing force

The mean value of the working prestressing force over the width of the deck is found by subtracting the value for time dependent losses from the mean value of the initial prestressing force over the width of the beam:

$$P_{m,\infty} = P_{m0} - \Delta P_{c+s+r}$$

3.1.2 Forces acting on top flange and joint

To determine the stresses over the joint height first the loads acting on the top flange and joint have to be determined. A strip of the deck in transverse direction with a width of 1,0 m is analysed. Relevant loads are:

- Self-weight and permanent load:

$$G_k = t_{tf} * \rho_{UHPC} + t_{asphalt} * \rho_{asphalt} \text{ [kN/m]}$$

- Variable load (follows from LM2 and only half an axle force is considered given the span):

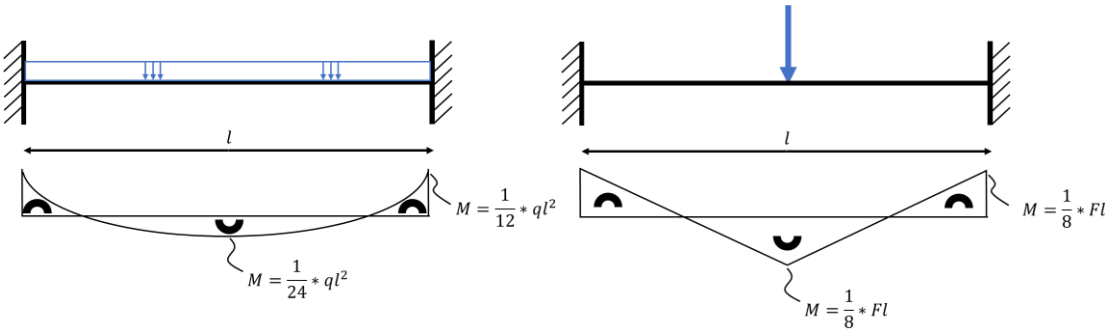
$$Q_k = \frac{1}{2} * \beta_Q Q_{ak} \ [kN]$$

- Upward bending moment prestressing:

$$M_P = \frac{P_{m,\infty} * e_j}{w_{c.t.c.}}$$

Note: The axial prestressing force $P_{m,\infty}$ is calculated for a width $w_{c.t.c.}$, in case this is not equal to 1,0 m the prestressing force is converted to a force corresponding to this unity width.

The top flange is schematized using simple models with uniformly distributed or point loads, as given below. The joint is positioned at mid span.



The bending moments (due to permanent load, prestressing and variable load) acting on the joint without partial load factors are:

$$M_G = \frac{1}{24} * G_k * l^2$$

$$M_P = \frac{P_{m,\infty} * e_j}{w_{c.t.c.}}$$

$$M_Q = \frac{1}{8} * Q_k * l$$

To verify the bending moment capacity later on the design value of the bending moment is also determined. The bending moment is calculated both using equations 6.10a and 6.10b and the maximum value is subsequently applied.

$$M_{Ed} = \max\{\gamma_G * M_G - \gamma_P * M_P + \psi_0 * \gamma_Q * M_Q; \zeta * \gamma_G * M_G - \gamma_P * M_P + \gamma_Q * M_Q\}$$

3.1.3 Verifying stresses over joint height

Using the aforementioned loads and model the stresses are calculated over the joint height using the prestressing force acting on a strip of 1,0 m width and for $t \to \infty$. The stresses are calculated at the top and bottom fibre and this is done for the situation with and without traffic.

- With traffic:

$$\sigma_{j,t} = -\frac{M_G}{W_j} - \frac{M_Q}{W_j} - \frac{P_{m,\infty}}{w_{c.t.c.} * A_j} + \frac{M_P}{W_j} \leq 0$$

$$\sigma_{j,b} = +\frac{M_G}{W_j} + \frac{M_Q}{W_j} - \frac{P_{m,\infty}}{w_{c.t.c.} * A_j} - \frac{M_P}{W_j} \leq 0$$

- Without traffic:

$$\sigma_{j,t} = -\frac{M_G}{W_j} - \frac{P_{m,\infty}}{w_{c.t.c.} * A_j} + \frac{M_P}{W_j} \leq 0$$

$$\sigma_{j,b} = +\frac{M_G}{W_j} - \frac{P_{m,\infty}}{w_{c.t.c.} * A_j} - \frac{M_P}{W_j} \leq 0$$

The properties of the joint are:

$$A_j = 1000 * t_j \; [mm^2]$$

$$W_j = \frac{1}{6} * 1000 * t_j^2 \; [mm^3]$$

$$I_j = \frac{1}{12} * 1000 * t_j^3 \; [mm^4]$$

$$e_j = \frac{1}{2} * t_{tf} - \frac{1}{2} * t_j \; [mm]$$

$$l = 2 * w_f + w_j + t_w$$

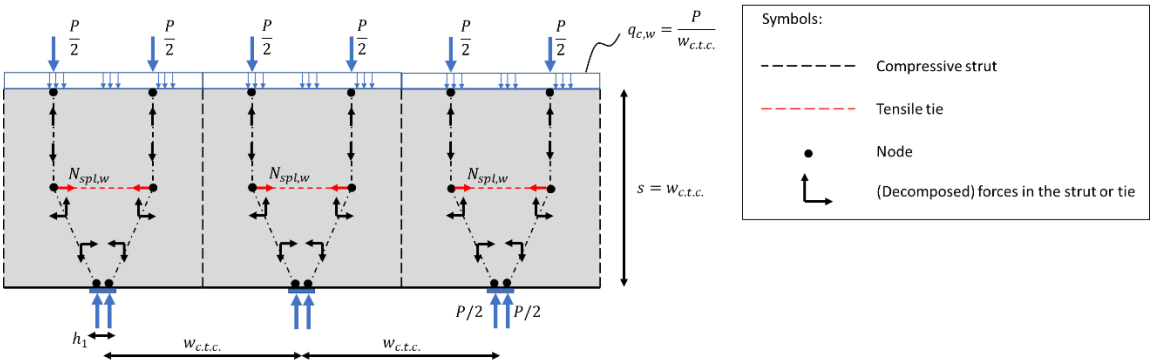
$$d_p = 0{,}5 * t_j + e_j$$

If the joint is in compression over its full height in both cases the working prestressing force is sufficiently large.

3.1.4 Detailing

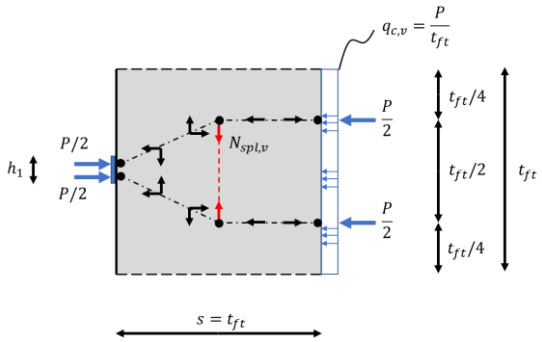
The force distribution is analysed at the anchors, both in horizontal and vertical direction. In horizontal direction the force is given by:

$$N_{spl,w} = \frac{1}{4} * \gamma_{spl} * P_{m0} * \left(1 - \frac{w_{c.t.c.}}{h_1}\right)$$



In vertical direction the force equals:

$$N_{spl,w} = \frac{1}{4} * \gamma_{spl} * P_{m0} * \left(1 - \frac{t_{ft}}{h_1}\right)$$



The maximum stress in the reinforcement, required minimum reinforcement diameter and minimum required reinforcement bars for that given diameter are respectively:

$$f_s = \frac{3000}{\emptyset_{spl,ft}}$$

$$A_{s,req} = \frac{N_{spl}}{f_s}$$

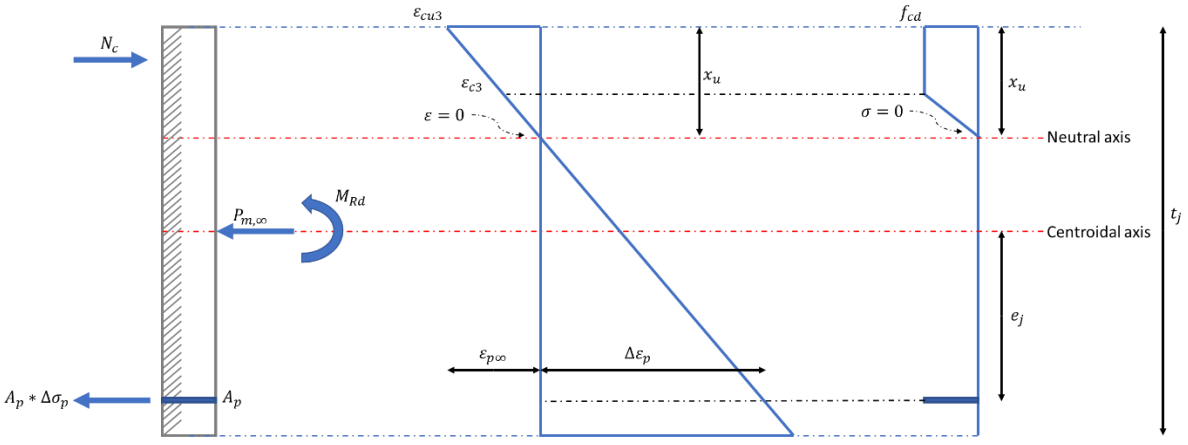
$$n_{s,req} = Int\left(\frac{A_{s,req}}{\pi * \left(\frac{\emptyset}{2}\right)^2}\right)$$

The maximum stress and required reinforcement are calculated for the horizontal and vertical direction separately, to obtain the most conservative result in terms of amount of reinforcement the tensile capacity of the UHPC is not taken into consideration.

3.2 Local verification – Verification bending moment capacity longitudinal joint

To verify the capacity of the longitudinal joint the aforementioned design values of the bending moment are applied. The same strip of 1,0 m width is analysed. The material parameters of the joint material are used. The following strain and stress relations over the joint height are assumed:

Stress and strain figures



Cross section with internal (left) and external (right) forces.

Strains over the height of the cross section

Stresses over the height of the cross section

The calculation is made iteratively, different values for x_u are assumed until horizontal equilibrium is found. The capacity is calculated as follows:

Parameters concrete: Using the assumed value for x_u the compressive force is:

$$N_c = \alpha * f_{cd} * x_u * 1000\ [N]$$

Parameters steel: The cross section of the tendon per strip of 1,0 is denoted as A_p and the working prestressing stress as $\sigma_{pm,\infty}$.

Determining strains and stresses: The strains and stresses in the prestressing are calculated as follows:

$$\varepsilon_{p,\infty} = \frac{\sigma_{p,\infty}}{E_p}$$

$$\Delta\varepsilon_p = \varepsilon_{cu3} * \left(\frac{d_p}{x_u} - 1\right)$$

$$\varepsilon_p = \varepsilon_{p,\infty} + \Delta\varepsilon_p \leq 0{,}9 * \varepsilon_{uk}$$

$$\sigma_{pu} = f_{pd} + \frac{\varepsilon_p - \frac{f_{pd}}{E_p}}{\varepsilon_{uk} - \frac{f_{pd}}{E_p}} * \left(\frac{f_{pk}}{\gamma_s} - f_{pd}\right)$$

Horizontal equilibrium: The remaining horizontal forces are:

$$P_{m,\infty} = A_p * \sigma_{pm,\infty}$$

$$\Delta N_p = A_p * (\sigma_{pu} - \sigma_{p,\infty})$$

It subsequently has to be verified that:

$$-N_c + P_{m,\infty} + \Delta N_p = 0$$

Bending moment capacity: If the horizontal equilibrium is satisfied the bending moment capacity is calculated:

$$M_{Rd} = -N_c * \beta * x_u + P_{m,\infty} * \frac{1}{2} * t_j + \Delta N_p * d_p$$

Verification: It subsequently has to be verified that:

$$\frac{M_{Ed}}{M_{Rd}} \leq 1{,}0$$

3.3 Local verification – Bending moment capacity top flange between the webs

3.3.1 Calculation model and design value bending moments

The capacity of the top flange is verified by comparing the bending moment capacity with the sagging bending moment at mid span and the hogging bending moment at the webs. The analysis is based on a strip of the top flange with a width of 1,0 m. The same type of model is used as applied for the verification of the longitudinal joint and the same permanent and variable loads are applied.

Differences are different cross sectional properties (those belonging to the top flange instead of the joint), the span and the material properties (the properties of the main beams are used instead of those of the longitudinal joints).

$$l = 2 * t_w + w_b$$

$$d_p = \frac{1}{2} * t_{ft}$$

The design value of the bending moments is calculated by assessing both equations 6.10a and 6.10b of the Eurocode, after which the maximum value is selected.

- For the sagging bending moment this results in:

$$M_{Ed} = max\{\gamma_G * M_G + \psi_0 * \gamma_Q * M_Q; \zeta * \gamma_G * M_G + \gamma_Q * M_Q\}\}$$

Where:

$$M_G = \frac{1}{24} * G_k * l^2$$

$$M_Q = \frac{1}{8} * Q_k * l$$

- For the hogging bending moment this results in:

$$M_{Ed} = max\{\gamma_G * M_G + \psi_0 * \gamma_Q * M_Q; \zeta * \gamma_G * M_G + \gamma_Q * M_Q\}\}$$

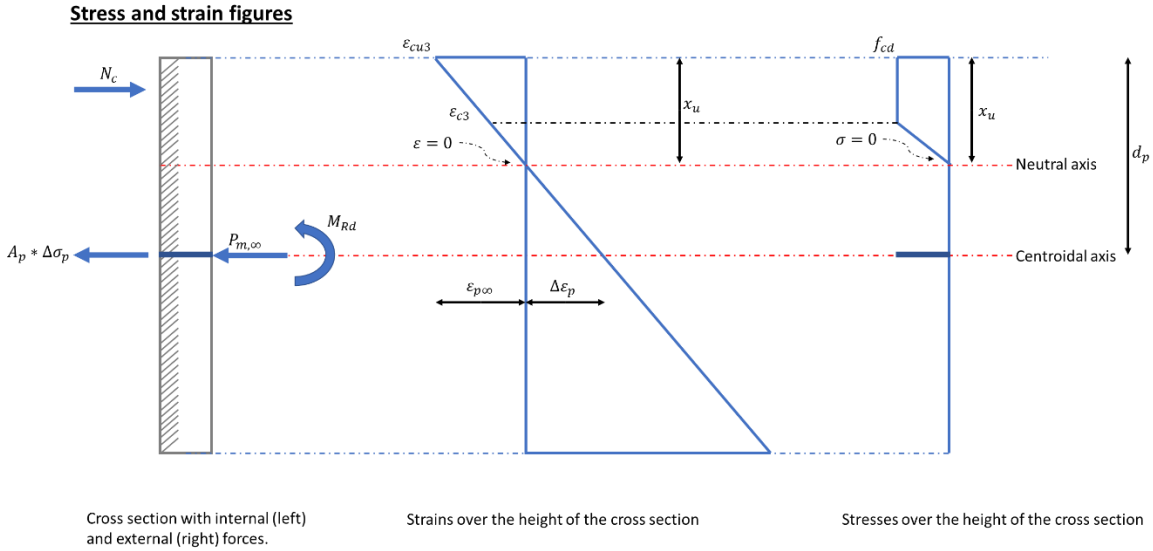
Where:

$$M_G = \frac{1}{12} * G_k * l^2$$

$$M_Q = \frac{1}{8} * Q_k * l$$

3.3.2 Verification of bending moment capacity

The bending moment is calculated once, because the prestressing is centrically the resistance for the sagging and hogging bending moment is equal. The following strain and stress relations over the height of the top flange in the ULS are assumed:



The calculation is made iteratively, different values for x_u are assumed after which it is checked if horizontal equilibrium is found. The capacity is calculated as:

Parameters concrete: The compressive force is:

$$N_c = \alpha * f_{cd} * x_u * 1000\ [N]$$

Parameters steel: The cross section of the tendon per strip of 1,0 is denoted as A_p and the working prestressing stress is $\sigma_{pm,\infty}$.

Determining strains and stresses: The strains and stresses in the prestressing are as follows.

$$\varepsilon_{p,\infty} = \frac{\sigma_{p,\infty}}{E_p}$$

$$\Delta\varepsilon_p = \varepsilon_{cu3} * \left(\frac{d_p}{x_u} - 1\right)$$

$$\varepsilon_p = \varepsilon_{p,\infty} + \Delta\varepsilon_p \leq 0{,}9 * \varepsilon_{uk}$$

$$\sigma_{pu} = f_{pd} + \frac{\varepsilon_p - \frac{f_{pd}}{E_p}}{\varepsilon_{uk} - \frac{f_{pd}}{E_p}} * \left(\frac{f_{pk}}{\gamma_s} - f_{pd}\right)$$

Horizontal equilibrium: The remaining horizontal forces are calculated.

$$P_{m,\infty} = A_p * \sigma_{pm,\infty}$$

$$\Delta N_p = A_p * (\sigma_{pu} - \sigma_{p,\infty})$$

Horizontal equilibrium is subsequently verified, the following requirement has to be satisfied:

$$-N_c + P_{m,\infty} + \Delta N_p = 0$$

Bending moment capacity: If horizontal equilibrium is found the bending moment capacity is calculated:

$$M_{Rd} = -N_c * \beta * x_u + P_{m,\infty} * \frac{1}{2} * t_{ft} + \Delta N_p * \frac{1}{2} * t_{ft}$$

Verification: It subsequently has to be verified that:

$$\frac{M_{Ed,sag}}{M_{Rd}} \leq 1{,}0$$

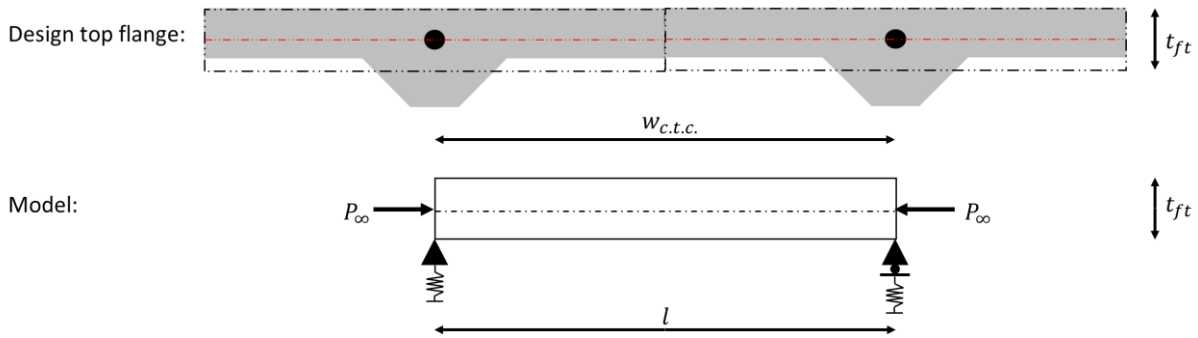
And:

$$\frac{M_{Ed,hog}}{M_{Rd}} \leq 1{,}0$$

3.4 Local verification – Bending moment capacity top flange between prestressing ribs

3.4.1 Calculation model and design value bending moments

The top flange between the prestressing ribs is analysed to verify its bending moment capacity. It is modelled as a 1,0 m wide beam spanning between two adjacent prestressing ribs and prestressed by an external axial force. The model is as follows:



Properties of the beam are:

- The height of the beam is t_{ft};
- The width of the beam is 1,0 m;
- The span is equal to the centre to centre distance between the ribs: $l = w_{c.t.c.}$;
- The beam is prestressed by external prestressing force P_∞, which is assumed to act centrically.

The external prestressing force depends on the bending moment due to the self-weight of the beams, the axial force due to the prestressing and the upward bending moment due to the prestressing. For this reason the compressive force is not constant over the beam length. It is at its maximum at mid span and at its minimum near the supports. If there is a tensile force present, which may occur at the supports, P_∞ is taken equal to zero.

The beam is supported as a simply supported beam, loaded by permanent load G_k and Q_k as given in the aforementioned verifications of the joint and top flange. The bending moment is at its maximum at mid span:

$$M_G = \frac{1}{8} * G_k * l^2$$

$$M_Q = \frac{1}{4} * Q_k * l$$

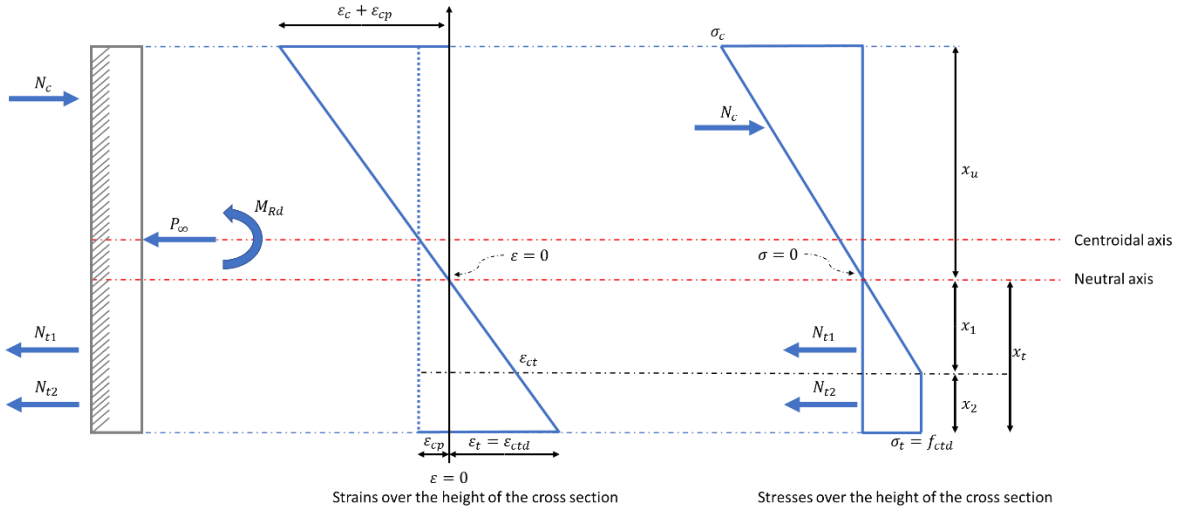
The design value of the bending moments is calculated by assessing both equations 6.10a and 6.10b of the Eurocode, after which the maximum value is selected:

$$M_{Ed} = max\{\gamma_G * M_G + \psi_0 * \gamma_Q * M_Q; \zeta * \gamma_G * M_G + \gamma_Q * M_Q\}\}$$

3.4.2 Verification of bending moment capacity

Assumptions

The following strain and stress distributions are assumed over the height of the beam in the ULS. The material properties of the main beam are applied.



Because the external axial force depends on the position along the beam the capacity does depend on it as well. For this reason a part of the beams is analysed directly next to the support (the governing part as this will be the governing beam part) and the capacity is calculated on a large number of intervals (0,25 m apart). The influence of the transfer length is neglected in these calculations: As a simplification it is assumed that the full prestressing forces $P_{m0,c}$ and $P_{m0,fb}$ are applied directly from the support, this also results in the most conservative situation.

Capacity at each point under consideration

At each of the points where the capacity is calculated the following set of calculations is carried out:

Calculating external force: The external force depends on the self-weight of the beams and the prestressing and the stresses in the middle fibre due to each of these loads is calculated.

- Self-weight of the beams:

$$\sigma_{t,sw}(x) = -\frac{M_{sw} * (e_t - 0{,}5 * t_{ft})}{I_y} \rightarrow -\frac{\frac{1}{2} * G_{k,beam} * x * (l - x) * (e_t - 0{,}5 * t_{ft})}{I_y}$$

- Centric prestressing:

$$\sigma_{t,c} = -\frac{P_{m0,c}}{A_c}$$

- Eccentric prestressing:

$$\sigma_{t,fb} = -\frac{P_{m0,fb}}{A_c} + \frac{P_{m0,fb} * e_p * \left(e_t - 0{,}5 * t_{ft}\right)}{I_y}$$

- Total stresses:

$$\sigma_{t,tot}(x) = \sigma_{t,sw}(x) + \sigma_{t,c} + \sigma_{t,fb}$$

- External axial force:

$$P_\infty = \sigma_{t,tot}(x) * t_{ft} * 1000 * 10^{-3}\ [kN]$$

Compressive strain: If $P_\infty > 0$ a tensile force is present and the effect of the tensile force is neglected in the calculation of the capacity, hence P_∞ is taken equal to zero in this situation. If $P_\infty < 0$ a compressive force is present which compresses the cross section.

In case a compressive force is present its absolute value is taken and the compressive strain in the cross section is calculated as follows:

$$\varepsilon_{cp} = \frac{|\sigma_{t,tot}(x)|}{E_{cm}}$$

Strain values fibre reinforced concrete: To calculate the capacity of the cross section on the different intervals the different strain values on the stress-strain diagram have to be calculated:

$$\varepsilon_{ct} = \frac{f_{ctd}}{E_{cm}} = \frac{f_{ctk,el}}{\gamma_c * E_{cm}}$$

$$\varepsilon_{ct;0,3} = \frac{0{,}3}{l_c} + \varepsilon_{ct}$$

$$\varepsilon_{ctd} = \varepsilon_{ctu} - \frac{f_{ctd}}{f_{ctd;2}} * \left(\varepsilon_{ctu} - \varepsilon_{ct;0,3}\right)$$

$$\varepsilon_{ctu} = \frac{l_f}{4 * l_c}$$

Where:

$$l_c = \frac{2}{3} * t_{ft}$$

Total compressive strain: The total compressive strain in the cross section at the moment its maximum capacity is reached (tensile strain at the lowest fibre equals f_{ctd}) is as follows.

$$(\varepsilon_c + \varepsilon_{cp}) = \varepsilon_{cp} + \sqrt{\varepsilon_{cp}^2 + \frac{2 * f_{ctd} * \varepsilon_{ctd} - f_{ctd} * \varepsilon_{ct}}{E_{cm}} + 2 * \varepsilon_{cp} * \varepsilon_{ctd}}$$

Where:
ε_c: Compressive strain in most compressed fibre if no external compressive force is present

Height of concrete compressive and tensile zones: Using the total strain value at the top of the cross section and the diagram of the strain relationship over the beam height the height of the compressive and tensile zones can be determined:

$$x_u = \frac{f_{ctd} * t_{ft} + \varepsilon_{cp} * E_{cm} * t_{ft}}{\left(\frac{1}{2} * (\varepsilon_c + \varepsilon_{cp}) * E_{cm} + \frac{1}{2} * f_{ctd} * \frac{\varepsilon_{ct}}{\varepsilon_c + \varepsilon_{cp}} + f_{ctd}\right)}$$

$$x_1 = \frac{\varepsilon_{ct}}{\varepsilon_c + \varepsilon_{cp}} * x_u$$

$$x_2 = t_{ft} - x_u - \frac{\varepsilon_{ct}}{\varepsilon_c + \varepsilon_{cp}} * x_u$$

Normal forces: The horizontal forces are determined as follows, note that in these expressions the width 'b' represents a strip of the top flange with a width of 1,0 m.

$$N_c = \frac{1}{2} * \sigma_c * x_u * b = \frac{1}{2} * (\varepsilon_c + \varepsilon_{cp}) * E_{cm} * x_u * b$$

$$N_{t1} = \frac{1}{2} * f_{ctd} * x_1 * b$$

$$N_{t2} = f_{ctd} * x_2 * b$$

Bending moment capacity: The bending moment capacity is subsequently calculated as follows.

$$M_{Rd} = -N_c * \frac{1}{3} * x_u + N_{t1} * \left(x_u + \frac{2}{3} * x_1\right) + N_{t2} * \left(x_u + x_1 + \frac{1}{2} * x_2\right) + P_{m,\infty} * \frac{1}{2} * t_{ft}$$

NOTE: Reference is made to the main report and other annexes for the derivations of the capacity of an unreinforced UHPC cross section with and without external compressive force.

Bending moment verification

Subsequently two graphs are plotted. One is a horizontal line denoting the required capacity (M_{Ed}) and one graph is the actual capacity calculated at the different points along the beam axis near the support. It is subsequently determined from which coordinate 'x' the capacity is (approximately) larger than the design value of the bending moments.

In the graph this is visualized as the intersection between two curves. If the capacity line is above the line of the design bending moment over the full length, the capacity is sufficient over the full length. Depending on the design it might occur that over a certain length the capacity might not be sufficient because there is no external prestressing force. In such a region additional measures might be required.

Verifying strains

The equations used for determining the capacity are based on the assumption that the compressive strain in the concrete does not exceed the value ε_{c3}. It has to be verified that this requirement is met, otherwise the assumed strain and stress distributions are no longer valid and new derivations of the equations have to be performed.

The verification is performed for midspan ($x = l/2$) because the compressive stresses are the largest at this zone, the total compressive strain in the most compressed fibre is:

$$\varepsilon_{cc} = (\varepsilon_c + \varepsilon_{cp}) = \varepsilon_{cp} + \sqrt{\varepsilon_{cp}^2 + \frac{2 * f_{ctd} * \varepsilon_{ctd} - f_{ctd} * \varepsilon_{ct}}{E_{cm}} + 2 * \varepsilon_{cp} * \varepsilon_{ctd}}$$

Where:

$$\varepsilon_{cp} = \frac{\sigma_{t,tot}\left(x = \frac{l}{2}\right)}{E_{cm}}$$

$$\sigma_{t,tot}\left(x=\frac{l}{2}\right)=-\frac{\frac{1}{8}*G_{k,beam}*l^2*\left(e_t-0{,}5*t_{ft}\right)}{I_y}-\frac{P_{m0,c}}{A_c}-\frac{P_{m0,fb}}{A_c}+\frac{P_{m0,fb}*e_p*\left(e_t-0{,}5*t_{ft}\right)}{I_y}$$

It has to be verified that:

$\varepsilon_{cc} \leq \varepsilon_{c3}$

4

DESIGN OF MAIN BEAMS – FATIGUE VERIFICATION

4.1 Fatigue verification

4.1.1 Assumptions and approach

The fatigue verification is based on the following points:

- The point under consideration is midspan because the bending moments due to the cyclic loads reach their maximum value at this point;
- The maximum and minimum bending moments at this point caused by the load combinations for fatigue as covered by Eurocode 2 are determined using RFEM;
- The prestressing tendons in the bottom flange are verified (these are governing over the centric prestressing) as well as the concrete at the top and bottom fibres of the cross section.

4.1.2 Fatigue verification – Prestressing steel at midspan

Stresses at tendon height: The stresses in the concrete adjacent to the centre line of the tendons (eccentricity e_p) in the bottom flange are:

$$\sigma_{c,max} = \frac{M_{fat,max} * e_p}{I_c} - \frac{P_{m,\infty,c}}{A_c} - \frac{P_{m,\infty,fb}}{A_c} - \frac{P_{m,\infty,fb} * e_P^2}{I_c}$$

$$\sigma_{c,min} = \frac{M_{fat,min} * e_p}{I_c} - \frac{P_{m,\infty,c}}{A_c} - \frac{P_{m,\infty,fb}}{A_c} - \frac{P_{m,\infty,fb} * e_P^2}{I_c}$$

Stresses in the steel: The steel stresses are calculated from the concrete stresses using the ratio of the moduli of elasticity:

$$\alpha_e = \frac{E_p}{E_c}$$

Stress range: The maximum and minimum stresses in the prestressing steel are respectively:

$$\sigma_{p,min} = \alpha_e * \sigma_{c,min}$$

$$\sigma_{p,max} = \alpha_e * \sigma_{c,max}$$

The stress range then is:

$$\Delta\sigma_p = \sigma_{p,max} - \sigma_{p,min}$$

Number of cycles: The number of cycles that has to be designed for is as follows.

$$n = N_{obs} * n_{years}$$

Where:
N_{obs}: Number of heavy vehicles per year
n_{years}: Design service life

Allowable stress range: The allowable stress range corresponding to the aforementioned number of cycles is determined as follows.

- If $N < N^*$:

$$\Delta\sigma_{Rsd} = \frac{\Delta\sigma_{Rsk}}{\gamma_{S,fat}} * \left(\frac{N^*}{N}\right)^{\frac{1}{k_1}}$$

- If $N = N_{obs}$:

$$\Delta\sigma_{Rsd} = \frac{\Delta\sigma_{Rsk}}{\gamma_{S,fat}}$$

- If $N > N^*$:

$$\Delta\sigma_{Rsd} = \frac{\Delta\sigma_{Rsk}}{\gamma_{S,fat}} * \left(\frac{N^*}{N}\right)^{\frac{1}{k_2}}$$

Fatigue verification: Subsequently the fatigue verification is performed. It has to be verified that:

$$\Delta\sigma_p * \gamma_{F,fat} \leq \Delta\sigma_{Rsd}$$

4.1.3 Fatigue verification – Concrete at midspan

Concrete fatigue strength: The fatigue strength of concrete is determined as follows:

$$f_{cd,fat} = 0{,}85 * \beta_{cc}(t) * f_{ck} * \left(1 - \frac{f_{ck}}{40 * f_{ck0}}\right) * \frac{1}{\gamma_c}$$

Determine stress range: The maximum and minimum compressive stress in the concrete outer fibres are as follows (note that the compressive stresses are taken as a positive value and $\sigma_{cd,max}$ is the largest compressive value while $\sigma_{cd,min}$ is the smallest compressive value (i.e. closest to zero). If $\sigma_{cd,min}$ is a tensile stress, then it is taken equal to zero):

- Top fibre:

$$\sigma_{cd,max} = -\frac{M_{fat,max}}{W_t} - \frac{P_{m,\infty,c}}{A_c} - \frac{P_{m,\infty,fb}}{A_c} + \frac{P_{m,\infty,fb} * e_P}{W_t}$$

$$\sigma_{cd,min} = -\frac{M_{fat,min} * e_p}{W_t} - \frac{P_{m,\infty,c}}{A_c} - \frac{P_{m,\infty,fb}}{A_c} + \frac{P_{m,\infty,fb} * e_P}{W_t}$$

- Bottom fibre:

$$\sigma_{cd,max} = \frac{M_{fat,min}}{W_b} - \frac{P_{m,\infty,c}}{A_c} - \frac{P_{m,\infty,fb}}{A_c} - \frac{P_{m,\infty,fb} * e_P}{W_b}$$

$$\sigma_{cd,min} = \frac{M_{fat,max} * e_p}{W_b} - \frac{P_{m,\infty,c}}{A_c} - \frac{P_{m,\infty,fb}}{A_c} - \frac{P_{m,\infty,fb} * e_P}{W_b}$$

Using Excel the absolute values are subsequently calculated, or, the value is set to zero if the stress turns out to be negative.

Determine maximum number of cycles at stress range: For both the top and bottom fibre of the cross section the following calculations are performed:

$$N_i = 10^{14*\frac{1-E_{cd,max,i}}{\sqrt{1-R_i}}}$$

$$R_i = \frac{E_{cd,min,i}}{E_{cd,max,i}}$$

$$E_{cd,min,i} = \frac{\sigma_{cd,min,i}}{f_{cd,fat}}$$

$$E_{cd,max,i} = \frac{\sigma_{cd,max,i}}{f_{cd,fat}}$$

Number of cycles: The number of cycles in the stress range that will occur are:

$$n = N_{obs} * n_{years}$$

Miner's rule: To perform the fatigue verification Miner's rule is applied, however, given the fact that there is only one stress amplitude this is written as:

$$\frac{n}{N} \leq 1{,}0$$

This is performed both for the top and bottom fibre.

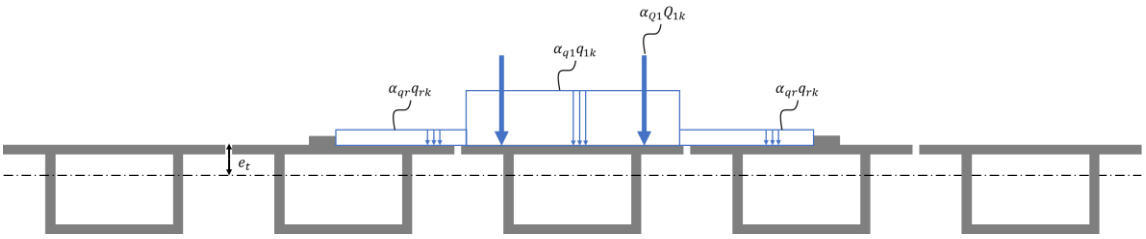
5

MAIN BEAMS – SERVICEABILITY LIMIT STATE

5.1 Deflections

5.1.1 Assumptions and approach

The deflections are calculated using the frequent load combination in the serviceability limit state. The middle beam is considered with lane 1 centred on it (configuration 3) as given in the following figure.



The calculation is performed under the conservative assumption that there is no interaction with other beams. In combination with the aforementioned positioning of the variable load this results in an upper limit of the deflection. This calculation serves as comparison with the results from RFEM.

The deflection is calculated assuming the middle beam with a permanent load (a line load) of:

$$G_{k,total} = G_{k,beam} + b_{eff,i} * G_{k,surf} \; [kN/m]$$

For the prestressing force the working prestress in the bottom flange, $P_{m,\infty,fb}$, is applied. Furthermore the stiffness of the concrete is reduced by introducing an effective modulus of elasticity:

$$E_{c,eff} = \frac{E_{cm}}{1+\varphi}$$

5.1.2 Upper limit of deflections

Deflection at midspan

The contribution of each action to the total deflection is calculated using standard engineering formulas:

- Self-Weight and permanent loads ($G_{k,total}$):

$$\delta_G = \frac{5 * G_{k,total} * l^4}{384 * E_{c,eff} * I_y}$$

- Upward bending due to the prestressing ($P = P_{m,\infty} * e_p$):

$$\delta_P = \frac{P_{m,\infty} * e_p * l^2}{8 * E_{c,eff} * I_y}$$

- Uniformly distributed component of variable load ($\psi_1 Q_{k,1} = 0{,}8 * Q_{k,UDL}$):

$$\delta_{Q,UDL} = \frac{5 * (\psi_1 * Q_{k,UDL}) * l^4}{384 * E_{c,eff} * I_y}$$

- Concentrated load due to axles ($\psi_1 Q_{k,1} = 0{,}8 * 2 * Q_{k,axle}$):

$$\delta_{Q,axle} = \frac{\psi_1 * 2 * Q_{k,axle} * l^3}{48 * E_{c,eff} * I_y}$$

Upward deflection is denoted as negative while downward deflection is denoted as positive. The total deflection is:

$$\delta_{tot} = \delta_G - \delta_P + \delta_{Q,UDL} + \delta_{Q,axle}$$

Maximum deflection

It has to be verified that the total deflection is smaller than or equal to the maximum deflection:

$$\frac{\delta_{tot}}{\delta_{max}} \leq 1{,}0$$

5.1.3 Comparison with RFEM

A comparison is also made with the total deflection value for the frequent combination as determined using RFEM (denoted as 'δ^*_{max}' in the following equation). The total deflection and requirement then is:

$$\delta_{tot,RFEM} = \delta^*_{max} - \delta_P \leq \delta_{max}$$

5.2 Crack width verification

Conforming the AFGC-SETRA 2013 guideline crack width does not have to be verified, however, the cracking bending moment is calculated and compared to the ultimate bending moment capacity (non-brittleness requirement). In order to do so the mean value of the axial tensile strength has to be determined:

$$f_{ctm} = 0{,}30 * f_{ck}^{\frac{2}{3}}$$

Using this value the cracking bending moment can be calculated:

$$M_{cr} = \left(f_{ctm} + \frac{P_{m,\infty,c} + P_{m,\infty,fb}}{A_c}\right) * W_{min}$$

Where $W_{min} = \min\{W_t; W_b\}$. It subsequently has to be verified that:

$$M_{cr} < M_{Rd}$$

6

END CROSS BEAM

6.1 Assumptions and parameters

6.1.1 Assumptions

In the analysis of the beam the following assumptions are made:

- The beam has a rectangular cross section and it is analysed as if it is a solid cross section over its full width (presence of the prefab beams is neglected);
- It is assumed that the height is equal to the width, and that the height of the end cross beam is equal to that of the prefab beams;
- An equal number of prestressing tendons is positioned at both sides of the beam, thus the resultant of the prestressing force is assumed to act centrically on the beam;
- No tensile stresses are allowed to occur in the cross section, that means that full prestressing has to be achieved.

6.1.2 Input parameters

Using the parameters plugged into the Excel sheet the shrinkage of the beam has to be determined to calculate the prestress losses. Only the drying shrinkage is considered.

Fictitious thickness: The fictitious thickness of the cross section is as follows. It is assumed that the beam is in contact with the atmosphere on three sides while the fourth is covered by the top flange of the prefab beams.

$$h_0 = \frac{2 * A_c}{u} \rightarrow \frac{2 * h_{cb} * w_{cb}}{h_{cb} + w_{cb} + h_{cb}} \rightarrow \frac{2 * h_{cb}^2}{3h_{cb}} = \frac{2}{3} * h_{cb}$$

Where:
A_c: cross sectional area
u: Circumference of the cross section exposed to drying (i.e. in contact with the atmosphere)

Parameter k_h: The parameter is selected from the following table as a function of h_0. In case the value of h_0 falls within two predefined values from the table, the most unfavourable (i.e. highest) value of k_h is taken.

h_0	k_h
100	1
200	0,85
300	0,75
500	0,7

Factor for relative humidity: Relative humidity is accounted for by applying the following factor.

$$\beta_{RH} = 1{,}55 * \left[1 - \left(\frac{RH}{RH_0}\right)^3\right]$$

Nominal unrestrained drying shrinkage: The value of the nominal unrestrained drying shrinkage is as follows.

$$\varepsilon_{cd,0} = 0{,}85 * \left[(220 + 110 * \alpha_{ds1}) * \exp\left(-\alpha_{ds2} * \frac{f_{cm}}{f_{cmo}}\right)\right] * 10^{-6} * \beta_{RH}$$

End value drying shrinkage: The end value of drying shrinkage can be calculated using the nominal unrestrained value and the parameter k_h.

$$\varepsilon_{cd,\infty} = k_h * \varepsilon_{cd,0}$$

6.2 Design of the prestressing

6.2.1 Calculating prestress losses

Although tendons are applied at both halves of the beam the prestressing losses are calculated assuming a resulting prestressing force acting at midspan.

Applied maximum force onto prestressing element and stress verification

It is verified that the maximum stress applied to the prestressing strands does not exceed the maximum value:

$$\sigma_{p,max,prov} \leq \sigma_{p,max}$$

The compressive stresses are to be verified as well:

$$\sigma_c = \frac{P_{max}}{A_{cb}} = \frac{n_{ducts} * n_{strands} * A_{p_{strand}} * \sigma_{p,max}}{A_{cb}} \leq 0{,}6 * f_{ck}$$

Direct prestressing losses

Elastic shortening: Because the four tendons might not be stressed simultaneously, the elastic loss is calculated by using the total value:

$$\Delta P_{el} = n_{ducts} * \frac{(n_{ducts} - 1)}{2} * \frac{P_{max}}{n_{ducts}} * \frac{E_p A_p}{n_{ducts} E_{cm} A_c}$$

Where:

$$A_p = n_{ducts} * n_{strands} * A_{p_{strand}}$$

$$P_{max} = A_p * \sigma_{p,max}$$

Note n_{ducts} appears in the denominator twice because P_{max} is calculated in Excel considering all tendons simultaneously while the elastic loss is calculated using the maximum force and cross section A_p of the individual tendons.

Friction: Because the tendons are straight the friction loss depends on the Wobble-effect only:

$$\Delta P_\mu(x) = (1 - e^{-\mu * k * x}) * P_{max}$$

At the other end from the active end of the deck ($x = w_{tot}$) the friction loss is:

$$\Delta P_\mu(x = w_{tot}) = (1 - e^{-\mu * k * w_{tot}}) * P_{max}$$

The friction loss expressed at stress then is:

$$\Delta\sigma_{P\mu}(x = w_{tot}) = \frac{\Delta P_{\mu}(x = w_{tot})}{A_p}$$

Wedge set: The stress reduction due to friction per unit of length is:

$$k = \frac{\Delta\sigma_{P\mu}(x = w_{tot})}{w_{tot}}$$

The influence length over which the wedge set influences the prestressing force then is:

$$l_w = \sqrt{\frac{w_{set} * E_p}{k}}$$

The prestress loss follows from:

$$\Delta P_{set} = 2 * A_p * \frac{\sigma_{P\mu}(x = w_{tot})}{w_{tot}} * l_w$$

Determining initial prestressing force and stress verification

The initial prestressing force is:

$$P_{m0}(x) = P_{max} - \Delta P_{el} - \Delta P_{\mu}(x) - \Delta P_{set}(x)$$

It has to be verified that the stresses in the strands are not larger than the maximum allowable value. The beam is divided into a number of intervals and the prestressing forces and losses are calculated at a total of 'j' points along the width of the deck. The maximum value along the beam length is used to perform the verification.

$$\frac{\max\{P_{m0}(x)\}}{A_p} \leq \sigma_{pm0}$$

Time dependent losses

The remainder of the analysis is performed using the mean value of the initial prestressing force over the length of the beam, which is determined using:

$$P_{m0} = \frac{1}{j} * \sum_{i=1}^{i=j} P_{m0,j}$$

For centric prestressing the time dependent losses are calculated as follows:

$$\Delta P_{c+s+r} = A_p * \Delta\sigma_{p,c+s+r} = A_p * \frac{\varepsilon_{cs}E_p + 0{,}8\Delta\sigma_{pr} + \frac{E_p}{E_{cm}}\varphi(\infty, t_0)\sigma_{c,QP}}{1 + \frac{E_p}{E_{cm}}\frac{A_p}{A_c}[1 + 0{,}8 * \varphi(\infty, t_0)]}$$

Where (for relaxation class 2):

$$\frac{\Delta\sigma_{pr}}{\sigma_{pi}} = 0{,}66 * \rho_{1000} * e^{9{,}1\mu} * \left(\frac{t}{1000}\right)^{0{,}75(1-\mu)} * 10^{-5}$$

$$\sigma_{pi} = \sigma_{pm,0} = \frac{P_{m0}}{A_p}$$

$$\mu = \frac{\sigma_{pm,0}}{f_{pk}}$$

$t = 500.000$

$$\sigma_{pm,0} = \frac{P_{m0}}{A_p}$$

$$\sigma_{c,QP} = \frac{P_{m0}}{A_c}$$

Working prestressing force

The mean value of the working prestressing force over the width of the deck is found by subtracting the value for time dependent losses from the mean value of the initial prestressing force over the width of the beam:

$$P_{m,\infty} = P_{m0} - \Delta P_{c+s+r}$$

6.2.2 Determining stresses over beam height

Using the bending moments calculated using RFEM the stress distribution over the beam height is determined in order to verify the requirement is met that the stresses in the cross section should be compressive. This analysis is performed for the governing value of the hogging and sagging bending moment and the stresses are for both cases calculated in the top and bottom fibres.

- Hogging bending moment:

$$\sigma_{t,hog} = \frac{M_{E,hog}}{W_{cb}} - \frac{P_{m,\infty}}{A_{cb}} \leq 0$$

$$\sigma_{b,hog} = -\frac{M_{E,hog}}{W_{cb}} - \frac{P_{m,\infty}}{A_{cb}} \leq 0$$

- Sagging bending moment:

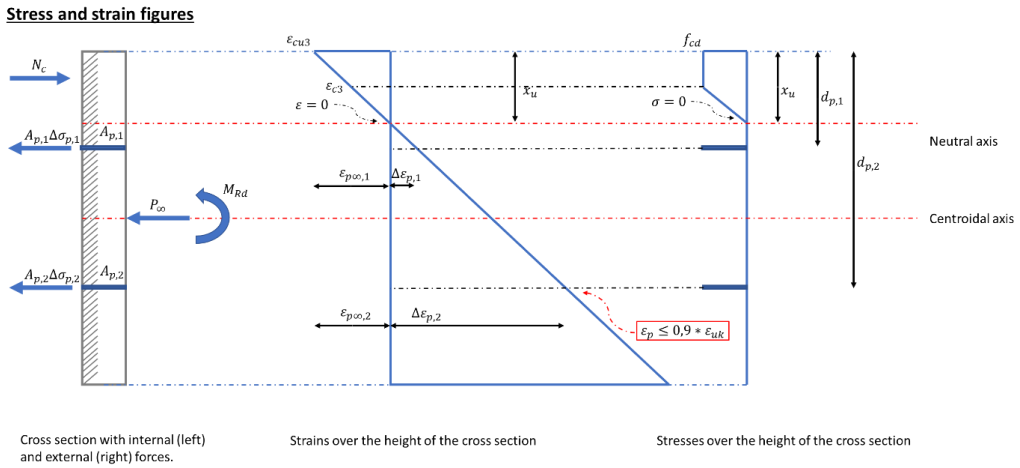
$$\sigma_{t,sag} = -\frac{M_{E,sag}}{W_{cb}} - \frac{P_{m,\infty}}{A_{cb}} \leq 0$$

$$\sigma_{b,sag} = \frac{M_{E,sag}}{W_{cb}} - \frac{P_{m,\infty}}{A_{cb}} \leq 0$$

6.3 Verification bending moment capacity

6.3.1 Assumptions

In the ULS the following strain and stress distributions are assumed to occur over the height of the end cross beam:



Furthermore it is assumed that for the verification of the rotational capacity the redistribution is zero.

6.3.2 Calculating the capacity and verifications

Identifying all horizontal forces

The calculation has been made iterative, the Excelsheet assumes a value for the height of the concrete compressive zone and verifies whether horizontal equilibrium has been reached. If so, then this value will be taken for x_u. Given the rectangular cross section the compressive force is:

$$N_c = \alpha * x_u * f_{cd} * w_{cb}$$

The active contribution of the prestressing is:

$$P_{m,\infty} = A_p * \sigma_{p,\infty}$$

Height of concrete compressive and tensile zone

The height of the concrete compressive zone is determined iteratively. However, it determines if all tendons are taken into consideration when calculating the bending moment capacity. The distance from the outermost compressed fibre (top fibre) to the first row of tendons is denoted as x_1 while the distance to the centre of the second row is denoted as x_2.

$$x_1 = 0{,}5 * h_{cb} - a_{vert}$$

$$x_2 = x_1 + 2 * a_{vert}$$

If it holds that:

$$x_1 < x_u$$

Then the first row is within the compressive zone and it is not taken into consideration while calculating the passive contribution. The second row is always considered.

Determining the strains

The strains are calculated for both rows of tendons:

- Top row (only if $x_1 > x_u$, otherwise zero):

$$d_{p,1} = x_1$$

$$\Delta\varepsilon_{p,1} = \varepsilon_{cu3} * \left(\frac{d_{p,1}}{x_u} - 1\right)$$

$$\varepsilon_{p,\infty,1} = \frac{\sigma_{p,\infty,1}}{E_p}$$

$$\varepsilon_{p,1} = \varepsilon_{p,\infty,1} + \Delta\varepsilon_{p,1} \leq 0{,}9 * \varepsilon_{uk}$$

- Bottom row prestressing:

$$d_{p,2} = x_2$$

$$\Delta\varepsilon_{p,2} = \varepsilon_{cu3} * \left(\frac{d_{p,2}}{x_u} - 1\right)$$

$$\varepsilon_{p,\infty,2} = \frac{\sigma_{p,\infty,2}}{E_p}$$

$$\varepsilon_{p,2} = \varepsilon_{p,\infty,2} + \Delta\varepsilon_{p,2} \leq 0{,}9 * \varepsilon_{uk}$$

Steel stresses

Using the calculated strain values the stresses in the prestressing steel are calculated.

- Top row (only if $x_1 > x_u$, otherwise zero):

$$\sigma_{pu,1} = f_{pd} + \frac{\varepsilon_{p,1} - \frac{f_{pd}}{E_p}}{\varepsilon_{uk} - \frac{f_{pd}}{E_p}} * \left(\frac{f_{pk}}{\gamma_s} - f_{pd}\right)$$

- Bottom row prestressing:

$$\sigma_{pu,2} = f_{pd} + \frac{\varepsilon_{p,2} - \frac{f_{pd}}{E_p}}{\varepsilon_{uk} - \frac{f_{pd}}{E_p}} * \left(\frac{f_{pk}}{\gamma_s} - f_{pd}\right)$$

The increase of the force in the prestressing steel (the passive contribution) is for both rows of tendons respectively:

$$\Delta N_{p,1} = \frac{1}{2} * A_p * (\sigma_{pu,1} - \sigma_{p,\infty})$$

$$\Delta N_{p,2} = \frac{1}{2} * A_p * (\sigma_{pu,2} - \sigma_{p,\infty})$$

Check equilibrium

Equilibrium is checked by considering all horizontal forces:

$$-N_c + P_{m,\infty,1} + P_{m,\infty,2} + \Delta N_{p,1} + \Delta N_{p,2} = 0$$

Determining bending moment capacity

If equilibrium is achieved the bending moment capacity is calculated using the top fibre as the reference point:

$$M_{Rd} = -N_c * \beta * x_u + P_{m,\infty,1} * \frac{1}{2} * h_{cb} + \Delta N_{p,1} * d_{p,1} + P_{m,\infty,2} * \frac{1}{2} * h_{cb} + \Delta N_{p,2} * d_{p,2}$$

The design value of the bending moment is as follows:

$$M_{Ed} = M_{Ed,RFEM} = \max\{M_{Ed,hog}; M_{Ed,sag}\}$$

The following criterion is to be satisfied:

$$\frac{M_{Ed}}{M_{Rd}} \leq 1{,}0$$

Verifying rotational capacity

To verify the rotational capacity the following basic equation is applied:

$$\frac{x_u}{d_p} \leq \frac{500}{500 + f}$$

$$f = \frac{\left(\frac{f_{pk}}{\gamma_s} - \sigma_{pm,\infty}\right) A_p + f_{yd} A_s}{A_p + A_s}$$

In case $x_1 < x_u$, then $d_p = d_{p,2}$ because the passive contribution of the top row of tendons is neglected. In case $x_1 > x_u$, then the average value of both is used:

$$d_{p,ave} = 0{,}5 * \left(d_{p,1} + d_{p,2}\right)$$

6.4 Verification shear force capacity

6.5 Assumptions and parameters

To determine the shear force capacity the equations from Eurocode 2 for elements without shear reinforcement are applied. It is assumed that no longitudinal reinforcement is present either, which is why the capacity is equal to the minimum value of $V_{Rd,c}$ that may be used.

In calculating the capacity the effective width is assumed to be equal to the effective width of the lower set of tendons, i.e. $d_{p,2}$. Given the presence of two rows of ducts, a width reduction might be appropriate. In accordance with the code this is verified as follows:

- If $\emptyset_{Duct} < w_{cb}/8$, then $b_{cb,nom} = w_{cb}$;
- If $\emptyset_{Duct} > w_{cb}/8$, then

$$b_{cb,nom} = w_{cb} - 0{,}5 * \sum \emptyset_{Duct} \rightarrow w_{cb} - \emptyset_{Duct}$$

6.5.1 Calculating the capacity and verifications

Capacity of concrete elements without shear reinforcement

The shear capacity is taken equal to the minimum value of the concrete capacity of an element under compression:

$$V_{Rd,c} = \left(v_{min} + k_1 * \sigma_{cp}\right) * b_{cb,nom} * d_{p,2}$$

Where:

$$k = 1 + \sqrt{\frac{200}{d_{p,2}}} \leq 2{,}0$$

$$v_{min} = 0{,}035 * k^{1{,}5} * \sqrt{f_{ck}}$$

$$\sigma_{cp} = \frac{P_{m,\infty}}{A_{cb}} \leq 0{,}2 * f_{cd}$$

Upper limit – Failure of the concrete compressive strut

The upper limit follows from the capacity of the concrete compressive strut, which is calculated as follows:

$$V_{Rd,max} = \alpha_{cw} * b_{cb,nom} * z * v_1 * f_{cd} * \frac{1}{\cot(\theta) + \tan(\theta)}$$

Where:

$z \approx 0{,}9 * d_{p,2}$

$v_1 = v = 0{,}6 * \left[1 - \frac{f_{ck}}{250}\right]$

Value α_{cw}:	Situation:
$\alpha_{cw} = 1$	$\sigma_{cp} = 0$
$\alpha_{cw} = \left(1 + \frac{\sigma_{cp}}{f_{cd}}\right)$	For $0 < \sigma_{cp} \leq 0{,}25 * f_{cd}$
$\alpha_{cw} = 1{,}25$	For $0{,}25 < \sigma_{cp} \leq 0{,}5 * f_{cd}$
$\alpha_{cw} = 2{,}5 * \left(1 - \frac{\sigma_{cp}}{f_{cd}}\right)$	For $0{,}5 * f_{cd} < \sigma_{cp} < 1{,}0 * f_{cd}$

Verification

The shear resistance of the cross section is taken equal to:

$V_{Rd} = \min\{V_{Rd,c}; V_{Rd,max}\}$

It has to be verified that:

$\frac{V_{Ed}}{V_{Rd}} \leq 1{,}0$

7

WEIGHT CALCULATION

7.1 Weight calculation

The weight of the detailed design is calculated as the final step in the calculation process. Each component of relevance is calculated separately.

Prefab UHPC beams – The weight of the prefab beams is:

$l_{tot} * A_c * n_{beams} * \rho$

In-situ UHPC joints – The weight of the joints is calculated using the mean value of the top flange:

$l_{tot} * t_{ft} * w_j * (n_{beams} - 1) * \rho$

Cross beams – To calculate the weight of the cross beams first it is assumed that the beams are solid:

$w_{tot} * h_{cb} * w_{cb} * 2 * \rho$

Subtraction overlap main beams – The overlap of the prefab beams and cross beams have to be subtracted:

$-2 * n_{beams} * w_{cb} * A_c * \rho$

Asphalt layer – An asphalt layer is assumed over the total surface of the deck:

$l_{tot} * w_{tot} * t_{asphalt} * \rho_{asphalt}$

Kerbs – The weight of the kerbs is calculated as follows:

$2 * l_{tot} * w_{kerb} * h_{kerb} * \rho_C$

Total weight – The total weight is determined by adding up all previously mentioned contributions.

Increase/decrease in weight – The difference in weight between the existing bridge and the new design is calculated as follows:

$$\Delta\% = \frac{W_n - W_e}{W_e} * 100\%$$

Where $\Delta\%$ is the percentual change, W_n is the weight of the new bridge and W_e is the weight of the existing bridge.

Remarks:

- The capping beam and weight of the existing structure are deduced from the preliminary design;
- Note that the 'ρ' of the prefab beams, joints and cross beams can be entered separately in the Excelsheet, the same symbol does not have to denote the same value.

V

ANNEX: INPUT RFEM MODEL

INPUT RFEM MODEL

In this document all main input parameters of the RFEM model have been listed and are complemented with additional information on the modelling of the load cases.

1.1 Modelling the structure

1.1.1 Geometry of the structure

A 3D RFEM model is set up where the x-axis in the programme coincides with the longitudinal axis of the bridge and the y-axis coincides with the transverse direction of the bridge.

Nodal coordinates

The following nodes have been defined:

Node No.	Node Type	Reference Node	Coordinate System	X [m]	Y [m]	Z [m]
1	Standard	0	Cartesian	0	-8,18	0
2	Standard	0	Cartesian	0	-6,58	0
3	Standard	0	Cartesian	0	-3,29	0
4	Standard	0	Cartesian	0	0	0
5	Standard	0	Cartesian	0	3,29	0
6	Standard	0	Cartesian	0	6,58	0
7	Standard	0	Cartesian	0	8,18	0
8	Standard	0	Cartesian	34,0	-8,18	0
9	Standard	0	Cartesian	34,0	-6,58	0
10	Standard	0	Cartesian	34,0	-3,29	0
11	Standard	0	Cartesian	34,0	0	0
12	Standard	0	Cartesian	34,0	3,29	0
13	Standard	0	Cartesian	34,0	6,58	0
14	Standard	0	Cartesian	34,0	8,18	0
15	Standard	0	Cartesian	68,0	-8,18	0
16	Standard	0	Cartesian	68,0	-6,58	0
17	Standard	0	Cartesian	68,0	-3,29	0
18	Standard	0	Cartesian	68,0	0	0
19	Standard	0	Cartesian	68,0	3,29	0
20	Standard	0	Cartesian	68,0	6,58	0
21	Standard	0	Cartesian	68,0	8,18	0

Lines main beams

For the main beams the following lines have been defined:

Line No.	Line Type	Nodes No.	Line Length L [m]
1	Polyline	2,9	34,0
2	Polyline	9,16	34,0
3	Polyline	3,10	34,0
4	Polyline	10,17	34,0
5	Polyline	4,11	34,0
6	Polyline	11,18	34,0
7	Polyline	5,12	34,0
8	Polyline	12,19	34,0
9	Polyline	6,13	34,0
10	Polyline	13,20	34,0

Lines end beams and boundary surface element

The following lines have been defined to model the end cross beams and/or to serve as boundary lines for the surface elements:

Line No.	Line Type	Nodes No.	Line Length L [m]
11	Polyline	1,2	1,6
12	Polyline	2,3	3,29
13	Polyline	3,4	3,29
14	Polyline	4,5	3,29
15	Polyline	5,6	3,29
16	Polyline	6,7	1,6
17	Polyline	7,14	34,0
18	Polyline	14,21	34,0
19	Polyline	21,20	1,6
20	Polyline	20,19	3,29
21	Polyline	19,18	3,29
22	Polyline	18,17	3,29
23	Polyline	17,16	3,29
24	Polyline	16,15	1,6
25	Polyline	15,8	34,0
26	Polyline	8,1	34,0

Supports

The beams are supported by hinges on one side and sliding supports (in x-direction) on the other:

Support No.	On Nodes No.	Axis system	Column in Z	Support			Rotational restraint		
				u_x	u_y	u_z	φ_x	φ_y	φ_z
1	2-6	Global X,Y,Z	-	+	+	+	-	-	+
2	16-20	Global X,Y,Z	-	-	+	+	-	-	+

1.1.2 Cross sections and materials

By assigning member types, cross sections and material parameters to the line segments, the beams and distribution element (surface) are modelled

Main beams

Cross section: Description (in mm): BOX(A) 3200/187.5/150/1900/2150/2200/250/0/0

Member type: The member type and cross section are assigned to the lines to model the beams:

Member No.	Line No.	Member Type	Cross-Section No.	
			Start	End
1	1	Beam	1	1
2	2	Beam	1	1
3	3	Beam	1	1
4	4	Beam	1	1
5	5	Beam	1	1
6	6	Beam	1	1
7	7	Beam	1	1
8	8	Beam	1	1
9	9	Beam	1	1
10	10	Beam	1	1

Material parameters: The UHPC is defined in the model as follows:

- The following material constants are entered into RFEM:

Modulus of elasticity (E)	50000	[N/mm^2]
Shear modulus (G)	20833	[N/mm^2]
Poisson ratio (v)	0,2	[-]
Specific weight (γ)	25	[kN/m^3]
Coefficient of thermal expansion (α)	1,2*10^{-5}	[K^{-1}]
Partial safety factor (γ_M)	1,0	[-]

- The additional properties are set equal to zero;

- The selected material model is 'isotropic linear elastic'.

NOTE: In the model this material is referred to as 'Material 1'.

End cross beams

Cross section: Cross-section Description (in mm): **Rectangle 2150/2150**

Member type: The member type and cross section are assigned to the lines to model the beams:

- Defining members side 1

Member No.	Line No.	Member Type	Cross-Section No.	
			Start	End
11	**12**	**Beam**	**2**	**2**
12	**13**	**Beam**	**2**	**2**
13	**14**	**Beam**	**2**	**2**
14	**15**	**Beam**	**2**	**2**

- Defining members side 2

Member No.	Line No.	Member Type	Cross-Section No.	
			Start	End
15	**20**	**Beam**	**2**	**2**
16	**21**	**Beam**	**2**	**2**
17	**22**	**Beam**	**2**	**2**
18	**23**	**Beam**	**2**	**2**

To aid in retrieving results from the programme, the separate elements are combined into so-called ''sets of members'' as well:

Set of Member No.	Set of Members Description	Type	Members No.
1	**End Beam left**	**Continuous**	**11-14**
2	**End beam right**	**Continuous**	**15-18**

Material parameters: Concrete type C30/37 is selected. The material model is 'isotropic linear elastic'. In the model this material is referred to as 'Material 2'.

Assigning the materials

The materials are assigned to the cross sections as follows:

Section No.	Cross-Section Description	Material No.
1	BOX(A) 3200/187.5/150/1900/2150/2200/250/0/0	1
2	Rectangle 2150/2150	2

Surface element

The input properties of the surface element are as follows:

Geometry	Stiffness	Boundary Lines No.	Material No.	Thickness		Eccentricity
				Type	e [mm]	ez [mm]
Plane	Standard	11-26	1	Constant	187.5	0.0

1.2 Load cases and load combinations

1.2.1 Permanent actions (G)

Load case 1 – Self-weight prefab beams: The self-weight of the beams are modelled as member loads over the full span of the main beams.

$G_{k,beams} = 41{,}59$ kN/m

RFEM input:

Reference to	On Members No.	Load Type	Load Distribution	Load Direction	P [kN/m]
Members	1-10	Force	Uniform	ZL	41,59

Load case 2 – Self-weight end cross beams: The self-weight of the end cross beams are modelled as member loads over the full span of the end cross beams.

$G_{k,cb} = 115{,}56$ kN/m

RFEM input:

Reference to	On Members No.	Load Type	Load Distribution	Load Direction	P [kN/m]
Members	11-18	Force	Uniform	ZL	115,56

Load case 3 – Self weight longitudinal joints: The joints are taken into consideration by placing free line loads on top of the surface, positioned on locations corresponding with the centre line of the joints.

$G_{k,j} = 0{,}42$ kN/m

The width of the beams is $w = 3200$ mm and width of the joints is $w_j = 90$ mm. That means that the position of these free line loads with respect to the longitudinal axis of the deck should be:

- Inner joints: $\pm\, 0{,}5 * (3200 + 90) = \pm\, 1645$ mm
- Outer joints: $\pm\big(\, 1645 + (3200 + 90)\big) = \pm\, 4935$ mm

RFEM input:

No.	On Surface No.	Projection	Load Distribution	Load Direction	Load Position				Magnitude [kN/m]
					X1 [m]	Y1 [m]	X2 [m]	Y2 [m]	P1
1	1	XY	Uniform	ZL	0.000	-4,935	68.000	-4.935	0,42
2	1	XY	Uniform	ZL	0.000	-1,645	68.000	-1.645	0,42
3	1	XY	Uniform	ZL	0.000	1,645	68.000	1.645	0,42
4	1	XY	Uniform	ZL	0.000	4,935	68.000	4.935	0,42

Load case 4 – Road surface: The road surface is modelled as a surface load acting over the entire surface of the deck.

$G_{k,surf} = 0{,}23$ kN/m^2

RFEM input:

No.	On Surfaces No.	Load Type	Load Distribution	Load Direction	P1
1	1	Force	Uniform	ZL	0,23

Load case 5 – Kerbs: The kerbs are modelled as two free rectangular loads acting on the surface of the deck.

$G_{k,kerb} = 8{,}5$ kN/m^2

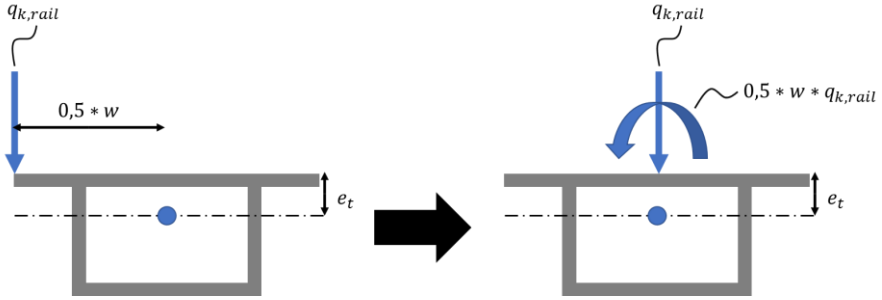
The width of the kerb is 340 mm while the width of the carriageway is 7000 mm. That means that the edges of the kerbs are positioned (with respect to the longitudinal axis of the deck) at:

- $y = \pm(0{,}5 * 7000) = \pm 3500$ mm
- $y = \pm(0{,}5 * 7000 + 500) = \pm 4000$ mm

RFEM input:

No.	On Surface No.	Projection	Load Distribution	Load Direction	Load Position				Magnitude [kN/m^2]
					X1 [m]	Y1 [m]	X2 [m]	Y2 [m]	P1
1	1	XY	Uniform	ZL	0,000	-4,000	68,000	-3,500	8,50
2	1	XY	Uniform	ZL	0,000	3,500	68,000	4,000	8,50

Load case 6 – Railing: To represent the railing a value for a line load was determined and when modelling this load it should be noted that in reality it acts eccentrically with respect to the beam axis. In the FEA model the railing can be modelled by replacing the eccentric line load by a centric line load and bending moment, both acting over the full beam length. This is depicted in the figure below.



The vertical component is modelled as member load acting over the full length of the beam, applied onto the outer beams (beams 1 and 5):

$G_{k,rail,V} = 0{,}5$ kN/m

The bending moment is calculated as the multiplication of the vertical force and half the beam width. It is applied over the full length of the outer beams (beams 1 and 5):

$G_{k,rail,M} = 1{,}6 * 0{,}5 = 0{,}8$ kNm/m

RFEM input:

Reference to	On Members No.	Load Type	Load Distribution	Load Direction	P [kN/m] or [kNm/m]
Members	1,2,9,10	Force	Uniform	ZL	0,50
Members	1,2	Moment	Uniform	XL	-0,80
Members	9,10	Moment	Uniform	XL	0,80

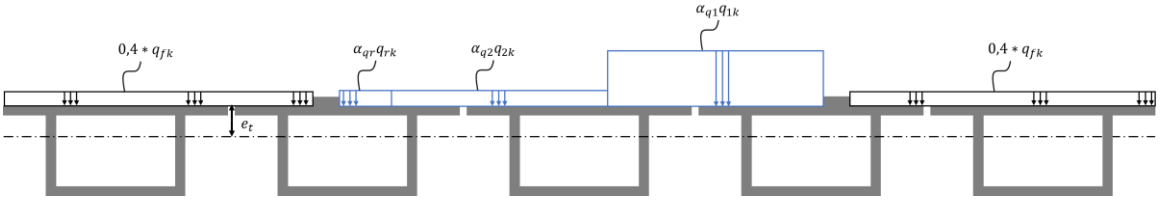
Load case 7 – Permanent loads: For practical reasons all aforementioned loads have been combined into a single load case.

1.2.2 Variable loads (Q)

First the uniformly distributed variable loads are modelled. To determine the positioning of the uniformly distributed loads use has made of the following dimensions:

- Main carriageway: $-3{,}5 \leq y \leq 3{,}5$ [m]
- Pedestrian lanes: $-8{,}18 \leq y \leq -4{,}18$ and $4{,}18 \leq y \leq 8{,}18$ [m]
- Width of theoretical traffic lane: 3,0 [m]

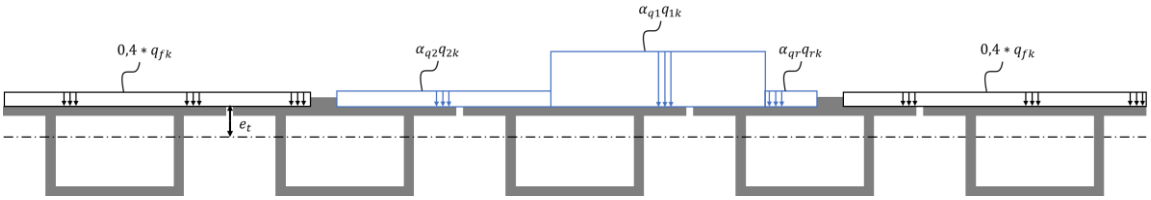
Load Case 8 – gr1a configuration 1 – UDL: The positioning of the uniformly distributed load corresponds to configuration 1 of load model 1. Note: The load on the pedestrian lane is included with a combination value of 0,4 for load group gr1a. The forces are modelled as free rectangular loads acting on the surface.



RFEM input:

No.	On Surface No.	Projection	Load Distribution	Load Direction	Load Position				Magnitude [kN/m^2]
					X1 [m]	Y1 [m]	X2 [m]	Y2 [m]	P1
1	1	XY	Uniform	ZL	0,000	-3,500	68,000	-2,500	2,25
2	1	XY	Uniform	ZL	0,000	-2,500	68,000	0,500	2,425
3	1	XY	Uniform	ZL	0,000	0,500	68,000	3,500	8,73
4	1	XY	Uniform	ZL	0,000	-8,18	68,000	-4,000	1,29
5	1	XY	Uniform	ZL	0,000	4,000	68,000	8,180	1,29

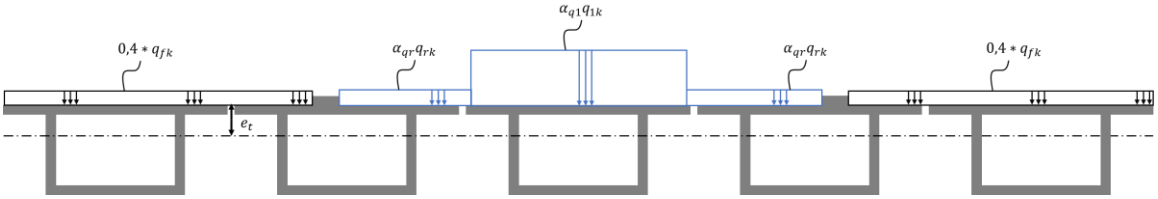
Load Case 9 – gr1a configuration 2 – UDL: The positioning of the uniformly distributed load corresponds to configuration 2 of load model 1. Note: The load on the pedestrian lane is included with a combination value of 0,4 for load group gr1a. The forces are modelled as free rectangular loads acting on the surface.



RFEM input:

No.	On Surface No.	Projection	Load Distribution	Load Direction	Load Position				Magnitude [kN/m²]
					X1 [m]	Y1 [m]	X2 [m]	Y2 [m]	P1
1	1	XY	Uniform	ZL	0,000	-3,500	68,000	-0,500	2,425
2	1	XY	Uniform	ZL	0,000	-0,500	68,000	2,500	8,73
3	1	XY	Uniform	ZL	0,000	2,500	68,000	3,500	2,25
4	1	XY	Uniform	ZL	0,000	-8,18	68,000	-4,000	1,29
5	1	XY	Uniform	ZL	0,000	4,000	68,000	8,180	1,29

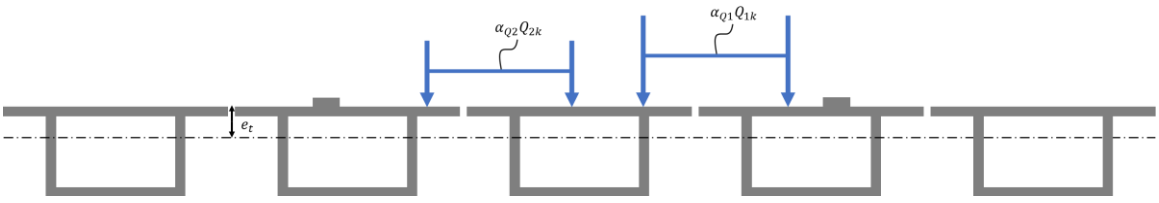
Load Case 10 – gr1a configuration 3 – UDL: The positioning of the uniformly distributed load corresponds to configuration 3 of load model 1. Note: The load on the pedestrian lane is included with a combination value of 0,4 for load group gr1a. The forces are modelled as free rectangular loads acting on the surface.



RFEM input:

No.	On Surface No.	Projection	Load Distribution	Load Direction	Load Position				Magnitude [kN/m²]
					X1 [m]	Y1 [m]	X2 [m]	Y2 [m]	P1
1	1	XY	Uniform	ZL	0,000	-3,500	68,000	-1,500	2,25
2	1	XY	Uniform	ZL	0,000	-1,500	68,000	1,500	8,73
3	1	XY	Uniform	ZL	0,000	1,500	68,000	3,500	2,25
4	1	XY	Uniform	ZL	0,000	-8,18	68,000	-4,000	1,29
5	1	XY	Uniform	ZL	0,000	4,000	68,000	8,180	1,29

Load case 11 – gr1a configuration 1 – Axle – Moment: In transverse direction the positioning of the concentrated loads corresponds to configuration 1 of load model 1, while in longitudinal direction the forces have been centred around mid-span to achieve the maximum bending moment. The forces are modelled as free concentrated loads acting on the surface.



Determining the centre lines of the theoretical lanes to position the free concentrated loads:

- Centre line lane 1: $(3{,}5 + 0{,}5) * 0{,}5 = 2{,}0$ m
- Centre line lane 2: $(-2{,}5 + 0{,}5) * 0{,}5 = -1{,}0$ m

RFEM input:

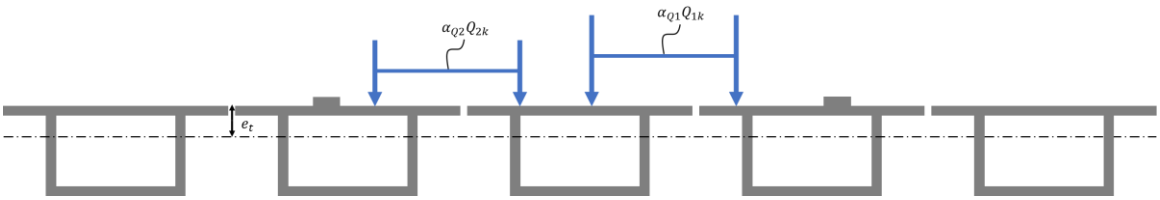
No.	On Surfaces No.	Projection	Load Type	Load Direction	Load Position		Magnitude
					X [m]	Y [m]	P [kN]
1	1	XY	Force	Z	33,400	1,000	145,500
2	1	XY	Force	Z	33,400	3,000	145,500
3	1	XY	Force	Z	34,600	1,000	145,500
4	1	XY	Force	Z	34,600	3,000	145,500
5	1	XY	Force	Z	33,400	-2,000	97,000
6	1	XY	Force	Z	33,400	0,000	97,000
7	1	XY	Force	Z	34,600	-2,000	97,000
8	1	XY	Force	Z	34,600	0,000	97,000

Load case 12 – gr1a configuration 1 – Axle – Shear: In transverse direction the positioning of the concentrated loads corresponds to configuration 1 of load model 1, while in longitudinal direction the forces have been placed near the supports with one axle directly above the end cross beam to achieve the maximum shear force. The forces are modelled as free concentrated loads acting on the surface.

RFEM input:

No.	On Surfaces No.	Projection	Load Type	Load Direction	Load Position		Magnitude
					X [m]	Y [m]	P [kN]
1	1	XY	Force	Z	0,00	1,000	145,500
2	1	XY	Force	Z	0,00	3,000	145,500
3	1	XY	Force	Z	1,2	1,000	145,500
4	1	XY	Force	Z	1,2	3,000	145,500
5	1	XY	Force	Z	0,00	-2,000	97,000
6	1	XY	Force	Z	0,00	0,000	97,000
7	1	XY	Force	Z	1,2	-2,000	97,000
8	1	XY	Force	Z	1,2	0,000	97,000

Load case 13 – gr1a configuration 2 – Axle – Moment: In transverse direction the positioning of the concentrated loads corresponds to configuration 2 of load model 1, while in longitudinal direction the forces have been centred around mid-span to achieve the maximum bending moment. The forces are modelled as free concentrated loads acting on the surface.



Determining the centre lines of the theoretical lanes to position the free concentrated loads:

- Centre line lane 1: $(2{,}5 + -0{,}5) * 0{,}5 = 1{,}0$ m
- Centre line lane 2: $(-3{,}5 - 0{,}5) * 0{,}5 = -2{,}0$ m

RFEM input:

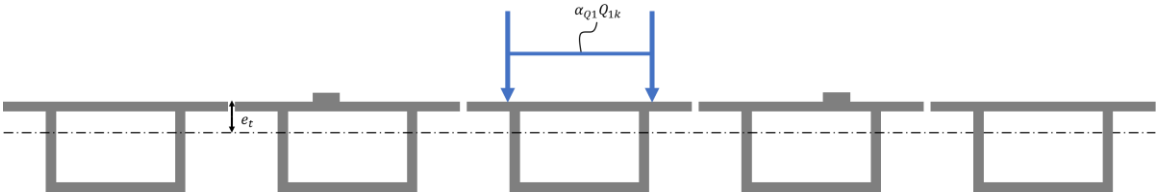
No.	On Surfaces No.	Projection	Load Type	Load Direction	Load Position		Magnitude
					X [m]	Y [m]	P [kN]
1	1	XY	Force	Z	33,400	0,000	145,500
2	1	XY	Force	Z	33,400	2,000	145,500
3	1	XY	Force	Z	34,600	0,000	145,500
4	1	XY	Force	Z	34,600	2,000	145,500
5	1	XY	Force	Z	33,400	-3,000	97,000
6	1	XY	Force	Z	33,400	-1,000	97,000
7	1	XY	Force	Z	34,600	-3,000	97,000
8	1	XY	Force	Z	34,600	-1,000	97,000

Load case 14 – gr1a configuration 2 – Axle – Shear: In transverse direction the positioning of the concentrated loads corresponds to configuration 2 of load model 1, while in longitudinal direction the forces have been placed near the supports with one axle directly above the end cross beam to achieve the maximum shear force. The forces are modelled as free concentrated loads acting on the surface.

RFEM input:

No.	On Surfaces No.	Projection	Load Type	Load Direction	Load Position		Magnitude
					X [m]	Y [m]	P [kN]
1	1	XY	Force	Z	0,00	0,000	145,500
2	1	XY	Force	Z	0,00	2,000	145,500
3	1	XY	Force	Z	1,2	0,000	145,500
4	1	XY	Force	Z	1,2	2,000	145,500
5	1	XY	Force	Z	0,00	-3,000	97,000
6	1	XY	Force	Z	0,00	-1,000	97,000
7	1	XY	Force	Z	1,2	-3,000	97,000
8	1	XY	Force	Z	1,2	-1,000	97,000

Load case 15 – gr1a configuration 3 – Axle – Moment: In transverse direction the positioning of the concentrated loads corresponds to configuration 3 of load model 1, while in longitudinal direction the forces have been centred around mid-span to achieve the maximum bending moment. The forces are modelled as free concentrated loads acting on the surface.



Determining the centre lines of the theoretical lane to position the free concentrated loads:

- Centre line lane 1: $(1{,}5 + -1{,}5) * 0{,}5 = 0$ m

RFEM input:

No.	On Surfaces No.	Projection	Load Type	Load Direction	Load Position		Magnitude
					X [m]	Y [m]	P [kN]
1	1	XY	Force	Z	33,400	-1,000	145,500
2	1	XY	Force	Z	33,400	1,000	145,500
3	1	XY	Force	Z	34,600	-1,000	145,500
4	1	XY	Force	Z	34,600	1,000	145,500

Load case 16 – gr1a configuration 3 – Axle – Shear: In transverse direction the positioning of the concentrated loads corresponds to configuration 3 of load model 1, while in longitudinal direction the forces have been placed near the supports with one axle directly above the end cross beam to achieve the maximum shear force. The forces are modelled as free concentrated loads acting on the surface.

RFEM input:

No.	On Surfaces No.	Projection	Load Type	Load Direction	Load Position		Magnitude
					X [m]	Y [m]	P [kN]
1	1	XY	Force	Z	0,00	-1,000	145,500
2	1	XY	Force	Z	0,00	1,000	145,500
3	1	XY	Force	Z	1,2	-1,000	145,500
4	1	XY	Force	Z	1,2	1,000	145,500

Load case 17 – Variable load Railing:
To model the variable load acting on the railing the same approach is used as done for the self-weight of the railing. The vertical and horizontal component have to be considered separately, but given the lever arm and combination with other loads only the vertical component is considered because this gives the most unfavourable result.

$Q_{k,rail,v} = 3$ kN/m

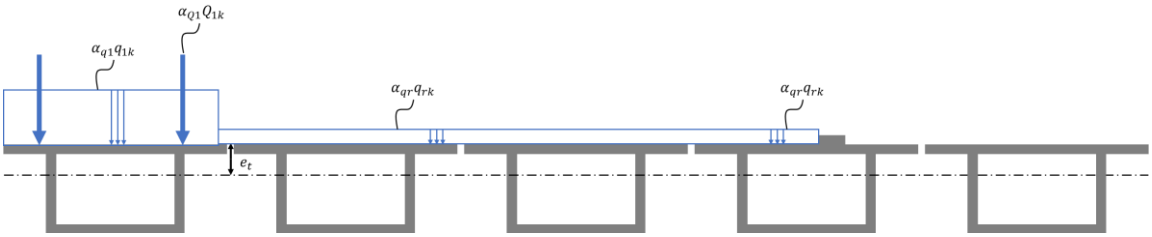
$Q_{k,rail,M} = 1{,}6 * 3 = 4{,}8$ kNm/m

RFEM input:

Reference to	On Members No.	Load Type	Load Distribution	Load Direction	P [kN/m] or [kNm/m]
Members	1,2,9,10	Force	Uniform	ZL	3,0
Members	1,2	Moment	Uniform	XL	-4,80
Members	9,10	Moment	Uniform	XL	4,80

1.2.3 Accidental loads (A)

Load case 18 – Traffic accident – Moment: In this load case a traffic accident is simulated that caused a heavy vehicle to be positioned directly at the edge of the bridge. The load values corresponding to lane 1 and the remaining area of load model 1 were used and the axle loads were positioned centred around mid-span to give the largest possible bending moment for the outer beam.



The load case is modelled using rectangular surface loads to represent the uniformly distributed loads and free concentrated loads to represent the concentrated loads.

RFEM input UDL (Rectangular surface load):

No.	On Surface No.	Projection	Load Distribution	Load Direction	Load Position				Magnitude [kN/m^2]
					X1 [m]	Y1 [m]	X2 [m]	Y2 [m]	P1
1	1	XY	Uniform	ZL	0,000	-8,18	68,000	-5,18	8,73
2	1	XY	Uniform	ZL	0,000	-5,18	68,000	3,500	2,25

RFEM input axle loads:

No.	On Surfaces No.	Projection	Load Type	Load Direction	Load Position		Magnitude
					X [m]	Y [m]	P [kN]
1	1	XY	Force	Z	33,400	-7,67	145,500
2	1	XY	Force	Z	33,400	-5,67	145,500
3	1	XY	Force	Z	34,600	-7,67	145,500
4	1	XY	Force	Z	34,600	-5,67	145,500

Load case 19 – Traffic accident – Shear: For this load case the same input has been used as for load case 18, the only difference being the positioning of the concentrated loads. These have been placed close to the supports to obtain the maximum shear force, with one axle placed directly at the centre of the edge beam.

RFEM input UDL (Rectangular surface load):

No.	On Surface No.	Projection	Load Distribution	Load Direction	Load Position				Magnitude [kN/m^2]
					X1 [m]	Y1 [m]	X2 [m]	Y2 [m]	P1
1	1	XY	Uniform	ZL	0,000	-8,18	68,000	-5,18	8,73
2	1	XY	Uniform	ZL	0,000	-5,18	68,000	3,500	2,25

RFEM input axle loads:

No.	On Surfaces No.	Projection	Load Type	Load Direction	Load Position		Magnitude
					X [m]	Y [m]	P [kN]
1	1	XY	Force	Z	0,00	-7,67	145,500
2	1	XY	Force	Z	0,00	-5,67	145,500
3	1	XY	Force	Z	1,2	-7,67	145,500
4	1	XY	Force	Z	1,2	-5,67	145,500

1.2.4 Fatigue loads

Load case 20 – Fatigue – Non-cyclic: The non-cyclic variable fatigue loads refer to the variable loads acting on the railing of the bridge (modelled as member loads, i.e. line loads and bending moments along the length of the outer main beams) and the load on the pedestrian lanes (modelled as a free rectangular load).

RFEM input member loads:

Reference to	On Members No.	Load Type	Load Distribution	Load Direction	P [kN/m] or [kNm/m]
Members	1,2,9,10	Force	Uniform	ZL	1,20
Members	1,2	Moment	Uniform	XL	-1,920
Members	9,10	Moment	Uniform	XL	1,920

RFEM input free rectangular load:

No.	On Surface No.	Projection	Load Distribution	Load Direction	Load Position				Magnitude [kN/m^2]
					X1 [m]	Y1 [m]	X2 [m]	Y2 [m]	P1
1	1	XY	Uniform	ZL	0,000	-8,18	68,000	-4,000	1,29
2	1	XY	Uniform	ZL	0,000	4,000	68,000	8,180	1,29

Load case 21 – Fatigue – Cyclic: The load case for cyclic fatigue loads is composed of uniformly distributed loads (modelled as free rectangular loads) and axle loads (modelled as free concentrated loads) in accordance with fatigue load model 1. The positioning of the loads is the same as configuration 2 of load model 1, with the axle loads at midspan.

RFEM input free rectangular load:

No.	On Surface No.	Projection	Load Distribution	Load Direction	Load Position				Magnitude [kN/m^2]
					X1 [m]	Y1 [m]	X2 [m]	Y2 [m]	P1
1	1	XY	Uniform	ZL	0,000	-3,500	68,000	-0,500	0,75
2	1	XY	Uniform	ZL	0,000	-0,500	68,000	2,500	2,70
3	1	XY	Uniform	ZL	0,000	2,500	68,000	3,500	0,75

RFEM input free concentrated loads:

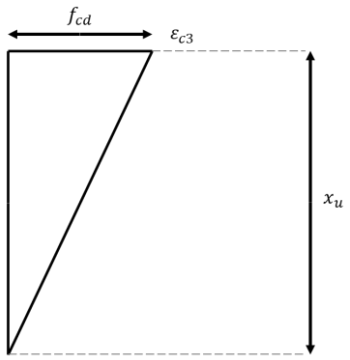
No.	On Surfaces No.	Projection	Load Type	Load Direction	Load Position		Magnitude
					X [m]	Y [m]	P [kN]
1	1	XY	Force	Z	33,400	0,000	105,00
2	1	XY	Force	Z	33,400	2,000	105,00
3	1	XY	Force	Z	34,600	0,000	105,00
4	1	XY	Force	Z	34,600	2,000	105,00
5	1	XY	Force	Z	33,400	-3,000	70,00
6	1	XY	Force	Z	33,400	-1,000	70,00
7	1	XY	Force	Z	34,600	-3,000	70,00
8	1	XY	Force	Z	34,600	-1,000	70,00

VI

ANNEX: DERIVATIONS CONCRETE COMPRESSIVE ZONE OVER VARIABLE WIDTH

Derivations concrete compressive zone over variable width

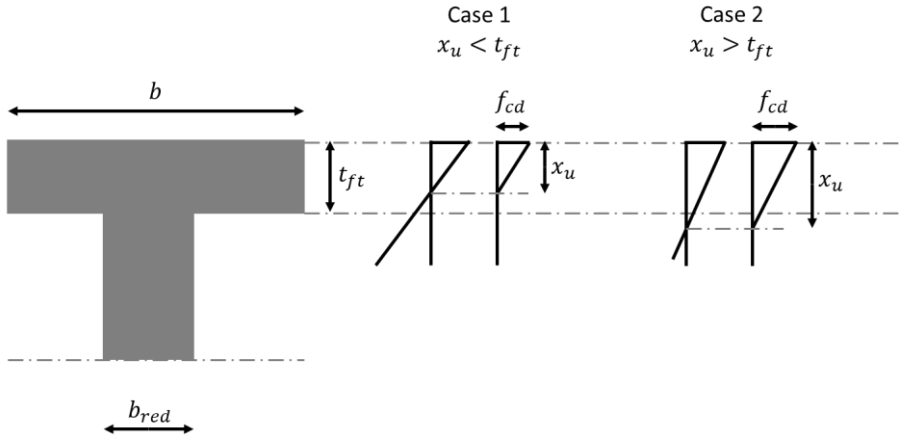
In this annex derivations are given to determine the normal force of the concrete compressive zone in the case a cross section with variable width is analysed (e.g. cross beam). For these derivations it is assumed that the plastic stage of the concrete will not be reached, the stress-strain figure (schematically) for concrete under compression is therefore as follows:



Definitions used in the following derivations are:

- Thickness top flange: t_{ft}
- Width top flange: b
- Reduced width: b_{red}

For a T-section two different ''scenarios'' can be distinguished:



- Scenario 1: $x_u < t_{ft}$ – Because the height of the compressive zone is smaller than the height of the top flange, standard equations for rectangular cross sections can be applied with a shape factor α of 0,5;

- Scenario 2: $x_u > t_{ft}$ – Equations are to be modified to account for a reduced effective width over the web of the section.

The equations will now be formulated/derived for each of these two cases.

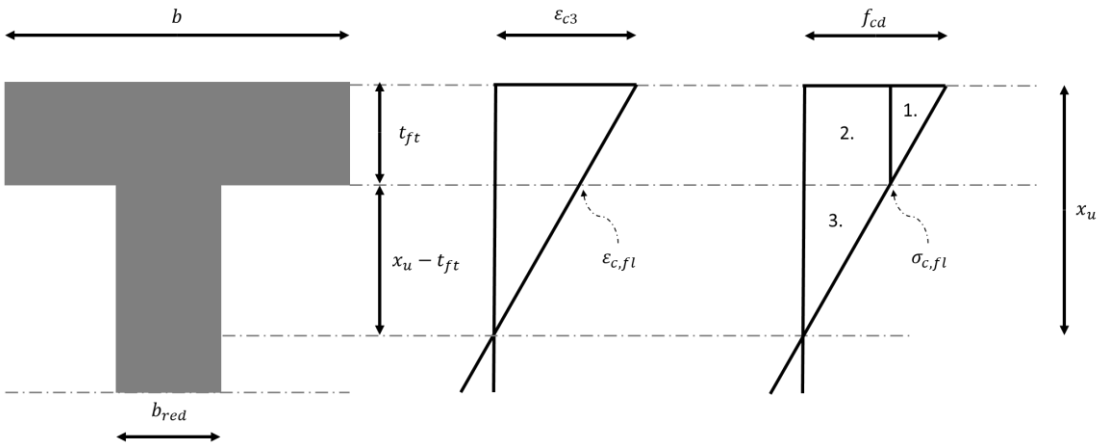
Scenario 1: The height of the compressive zone is smaller than the height of the top flange. Therefore the ''basic equations'' for rectangular cross sections can be applied:

$$N_c = \frac{1}{2} * b * f_{cd} * x_u$$

The position of the resulting force of the concrete compressive zone with respect to the top fibre (most compressed fibre) is:

$$e_c = \frac{1}{3} * x_u$$

Scenario 2: The height of the compressive zone is larger than the thickness of the top flange, a part of the ascending part is positioned at the part of het cross section with reduced width. Therefore the equations have to be modified. The stress diagram and cross section are divided into multiple parts to calculate the compressive force.



First expressions have to be formulated for the strains and stresses at the lower end of the top flange:

$$\frac{\varepsilon_{c,fl}}{x_u - t_{ft}} = \frac{\varepsilon_{c3}}{x_u} \rightarrow \varepsilon_{c,fl} = \varepsilon_{c3} * \left(1 - \frac{t_{ft}}{x_u}\right)$$

$$\frac{\sigma_{c,fl}}{x_u - t_{ft}} = \frac{f_{cd}}{x_u} \rightarrow \sigma_{c,fl} = f_{cd} * \left(1 - \frac{t_{ft}}{x_u}\right)$$

The stress and strain diagrams have now been fully defined and expressions can be formulated for the compressive forces. Distinction is made between three contributions, the numbers indicating these can be found in the previous figure.

- Contribution 1:

$$N_{c,1} = \frac{1}{2} * t_{ft} * (f_{cd} - \sigma_{c,fl}) * b$$

- Contribution 2:

$$N_{c,2} = t_{ft} * \sigma_{c,fl} * b$$

- Contribution 3:

$$N_{c,3} = \frac{1}{2} * (x_u - t_{ft}) * \sigma_{c,fl} * b_{red}$$

If the position of the resulting force (with respect to the top fibre) is to be determined, then first the moment of each individual force with respect to the top fibre of the cross section should be calculated (analogous to calculating the centre of gravity of a cross section).

$$S_1 = N_{c,1} * \frac{1}{3} * t_{ft}$$

$$S_2 = N_{c,2} * \frac{1}{2} * t_{ft}$$

$$S_3 = N_{c,3} * \left(t_{ft} + \frac{1}{3} * (x_u - t_{ft}) \right)$$

The position of the resulting force of the compressive zone is positioned at a distance e_c with respect to the top fibre, which subsequently follows from:

$$e_c = \frac{S_1 + S_2 + S_3}{N_{c,1} + N_{c,2} + N_{c,3}}$$

VII

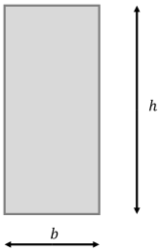
ANNEX: UNREINFORCED UHPC BEAMS WITH AND WITHOUT PRESTRESSING

Unreinforced UHPC beams without prestressing

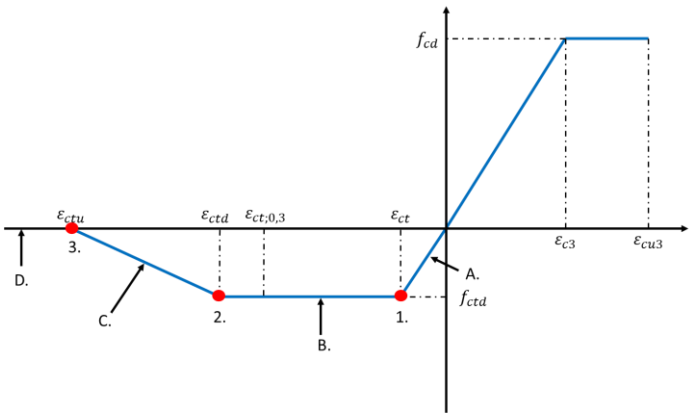
This document covers a description of UHPC beams in bending without reinforcement and with or without prestressing. The goal is to analyse the behaviour of these beams, derive equations to describe this and to derive equations that can be used for the bridge design. First the beams without prestressing are covered while the second part covers beams with prestressing in the form of external compressive forces.

Assumptions

Given is the following beam with height h and width b:



The top fibre (most compressed fibre) has strain ε_c and stress σ_c while the bottom fibre (fibre with largest tensile strain) has strain ε_t and stress σ_t. In accordance with what has been covered in the preliminary design, the following simplified constitutive law is adopted. In the tensile zone three characteristic points can be distinguished as well as four branches. To fully describe the behaviour of the unreinforced beam in bending, equations will be formulated for all these points and branches.



Branches:
- A. Linear elastic branch
- B. Post cracking and fibre activation
- C. Pull-out phase outer fibre
- D. Reduction effective height

Points:
1. Cracking of the beam
2. Start pull-out phase outer fibre
3. Pull-out of the fibre

It is assumed that the concrete compressive strain will remain well below ε_{c3} (i.e. in the elastic branch of concrete in compression) because the tensile strength is much smaller than the concrete compressive strength, when calculating it has to be confirmed that his is indeed the case for the given calculation. The different strain values on the diagram are:

$$\varepsilon_{ct} = \frac{f_{ctd}}{E_{cm}} = \frac{f_{ctk,el}}{\gamma_c * E_{cm}}$$

$$\varepsilon_{ct;0,3} = \frac{w_{0,3}}{l_c} + \varepsilon_{ct}$$

$$\varepsilon_{ctd} = \varepsilon_{ctu} - \frac{f_{ctd}}{f_{ctd;2}} * \left(\varepsilon_{ctu} - \varepsilon_{ct;0,3}\right)$$

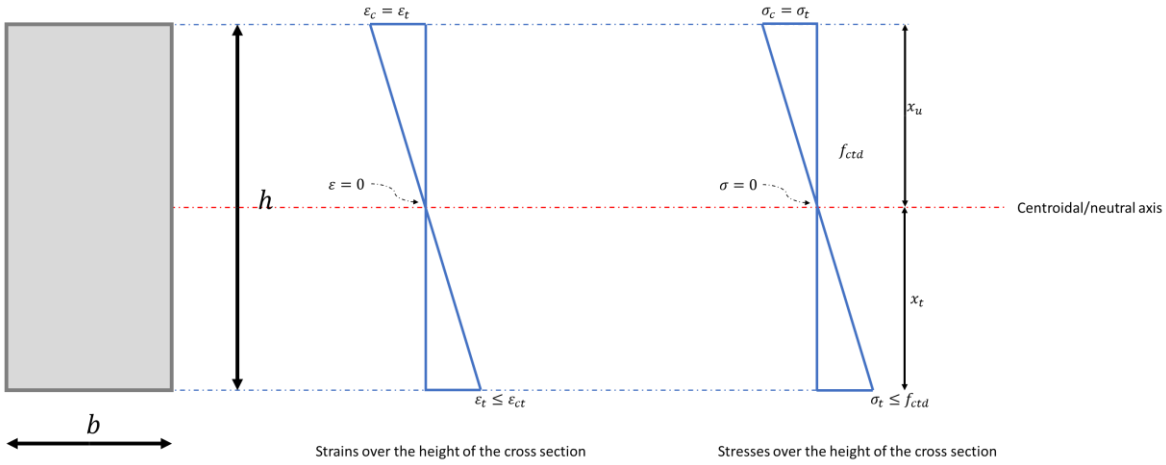
$$\varepsilon_{ctu} = \frac{l_f}{4 * l_c} \leq 2{,}5\ ‰$$

$$l_c = \frac{2}{3} * h$$

The concrete compressive strains will be predefined as numerical values (the independent variable). In the following subsections equations will be formulated to describe the three characteristic points and branches of the diagram.

Branch A – Linear elastic stage and characteristic point 1 – cracking of the beam

The following figure gives an overview of the strains and stresses over the height of the cross section during the linear elastic stage.



Range of validity: The equations belonging to this branch of the stress-strain curve are valid if:

$\varepsilon_t \leq \varepsilon_{ct}$

With: $\varepsilon_c = \varepsilon_t$

Equilibrium & bending moment: The requirement of horizontal equilibrium is automatically satisfied because $\varepsilon_t = \varepsilon_c$ and $\sigma_t = \sigma_c$. The horizontal forces are: $N_c = N_t = 0{,}5 * \sigma_c * b * h$. The occurring bending moment is:

$M = \sigma_c * W$

Where:

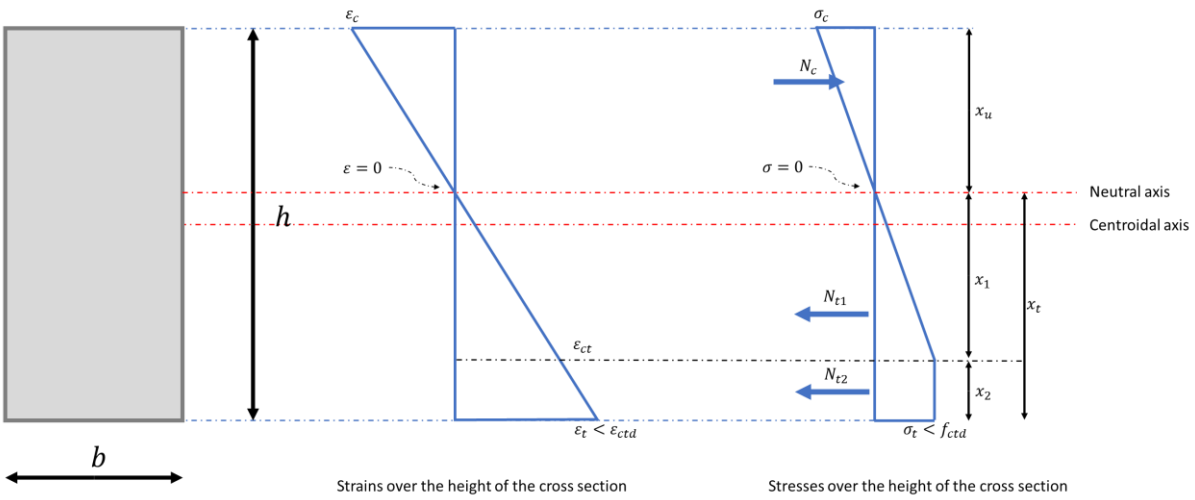
$W = \frac{1}{6} * b * h^2$

For the first characteristic point (cracking of the beam) the same stress and strain diagrams and equations hold. However, $\varepsilon_t = \varepsilon_c$ and $\sigma_t = \sigma_c$. The cracking bending moment is as follows:

$M_{cr} = f_{ctd} * W$

Branch B – Post cracking and activation of the fibres

As the strain increases the concrete cracks and the steel fibres are activated. The more strain increases, the larger the height becomes over which the concrete cracks and the fibres are activated. Over a certain height x_2 the tensile contribution of the concrete is assumed to be constant (see the adopted stress-strain diagram).



Range of validity: The equations belonging to this branch of the stress-strain curve are valid if:

$$\varepsilon_{ct} < \varepsilon_t < \varepsilon_{ctd}$$

With:

$$\varepsilon_t = \frac{x_1 + x_2}{x_u} * \varepsilon_c$$

Horizontal forces: There are three horizontal forces, namely the horizontal compressive force and two tensile forces.

$$N_c = \frac{1}{2} * \sigma_c * x_u * b$$

$$N_{t1} = \frac{1}{2} * f_{ctd} * x_1 * b$$

$$N_{t2} = f_{ctd} * x_2 * b$$

Height of compressive and tensile zone: There are three unknowns in these equations: x_u, x_1 and x_2. The equations for the height of the tensile zones are as follows:

$$\frac{x_u}{\varepsilon_c} = \frac{x_1}{\varepsilon_{ct}} \rightarrow x_1 = \frac{\varepsilon_{ct}}{\varepsilon_c} * x_u$$

$$x_2 = h - x_u - x_1 \rightarrow x_2 = h - x_u - \frac{\varepsilon_{ct}}{\varepsilon_c} * x_u$$

Horizontal equilibrium: Making use of these aforementioned equations it has to be verified that horizontal equilibrium has been achieved. This gives the required third equation to determine x_u:

$$N_c = N_{t1} + N_{t2}$$

Substitute:

$$\frac{1}{2} * \sigma_c * x_u * b = \frac{1}{2} * f_{ctd} * x_1 * b + f_{ctd} * x_2 * b$$

$$\frac{1}{2} * \sigma_c * x_u * b = \frac{1}{2} * f_{ctd} * b * \frac{\varepsilon_{ct}}{\varepsilon_c} * x_u + f_{ctd} * b * \left(h - x_u - \frac{\varepsilon_{ct}}{\varepsilon_c} * x_u\right)$$

$$\frac{1}{2} * \sigma_c * x_u * b = \frac{1}{2} * f_{ctd} * b * \frac{\varepsilon_{ct}}{\varepsilon_c} * x_u + f_{ctd} * b * h - f_{ctd} * b * x_u - f_{ctd} * b * \frac{\varepsilon_{ct}}{\varepsilon_c} * x_u$$

$$\frac{1}{2} * \sigma_c * x_u * b + \frac{1}{2} * f_{ctd} * b * \frac{\varepsilon_{ct}}{\varepsilon_c} * x_u + f_{ctd} * b * x_u = f_{ctd} * b * h$$

Rewrite:

$$x_u * b * (\frac{1}{2} * \sigma_c + \frac{1}{2} * f_{ctd} * \frac{\varepsilon_{ct}}{\varepsilon_c} + f_{ctd}) = f_{ctd} * b * h$$

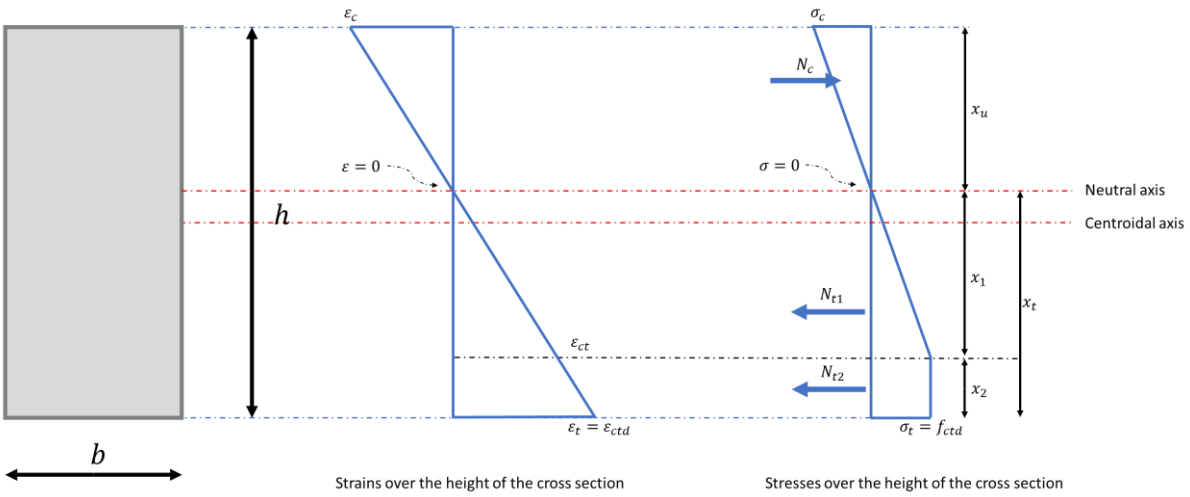
$$x_u = \frac{f_{ctd} * h}{\frac{1}{2} * \sigma_c + \frac{1}{2} * f_{ctd} * \frac{\varepsilon_{ct}}{\varepsilon_c} + f_{ctd}}$$

Bending moment: The other unknowns can now be determined as well and the bending moment is subsequently calculated (with respect to the top fibre):

$$M = -N_c * \frac{1}{3} * x_u + N_{t1} * \left(x_u + \frac{2}{3} * x_1\right) + N_{t2} * \left(x_u + x_1 + \frac{1}{2} * x_2\right)$$

Characteristic point 2 – Start of pull-out phase

As the strain increases further, at some point the strain in the outermost tensile fibre becomes equal to $\varepsilon_t = \varepsilon_{ctd}$. The corresponding strain and stress diagrams are:



Compared with the approach used to describe the cross section at branch B some adjustments have to be made. In this case it is the tensile strain that is defined ($\varepsilon_t = \varepsilon_{ctd}$) and the corresponding compressive strain has to be determined instead of the other way round. The unknowns are x_1, x_2 and ε_c. The relations for the first two unknowns are:

$$\frac{x_u}{\varepsilon_c} = \frac{x_1}{\varepsilon_{ct}} \rightarrow x_1 = \frac{\varepsilon_{ct}}{\varepsilon_c} * x_u$$

$$\frac{x_1 + x_2}{\varepsilon_{ctd}} = \frac{x_u}{\varepsilon_c} \rightarrow x_2 = \varepsilon_{ctd} * \left(\frac{x_u}{\varepsilon_c} - \frac{x_1}{\varepsilon_{ctd}}\right) \rightarrow x_2 = \frac{\varepsilon_{ctd} - \varepsilon_{ct}}{\varepsilon_c} * x_u$$

The horizontal forces are:

$$N_c = \frac{1}{2} * \sigma_c * x_u * b = \frac{1}{2} * \varepsilon_c * E_{cm} * x_u * b$$

$$N_{t1} = \frac{1}{2} * f_{ctd} * x_1 * b$$

$$N_{t2} = f_{ctd} * x_2 * b$$

Horizontal equilibrium gives the third equation to determine ε_c:

$$N_c = N_{t1} + N_{t2}$$

$$\frac{1}{2} * \varepsilon_c * E_{cm} * x_u * b = \frac{1}{2} * f_{ctd} * x_1 * b + f_{ctd} * x_2 * b$$

Substitute x_1 and x_2:

$$\frac{1}{2} * \varepsilon_c * E_{cm} * x_u * b = \frac{1}{2} * f_{ctd} * \frac{\varepsilon_{ct}}{\varepsilon_c} * x_u * b + f_{ctd} * \frac{\varepsilon_{ctd} - \varepsilon_{ct}}{\varepsilon_c} * x_u * b$$

$$\frac{1}{2} * \varepsilon_c * E_{cm} * x_u * b = \frac{1}{2} * f_{ctd} * \frac{\varepsilon_{ct}}{\varepsilon_c} * x_u * b + f_{ctd} * \frac{\varepsilon_{ctd}}{\varepsilon_c} * x_u * b - f_{ctd} * \frac{\varepsilon_{ct}}{\varepsilon_c} * x_u * b$$

Simplify:

$$\frac{1}{2} * \varepsilon_c * E_{cm} = \frac{1}{2} * f_{ctd} * \frac{\varepsilon_{ct}}{\varepsilon_c} + f_{ctd} * \frac{\varepsilon_{ctd}}{\varepsilon_c} - f_{ctd} * \frac{\varepsilon_{ct}}{\varepsilon_c}$$

$$\frac{1}{2} * \varepsilon_c * E_{cm} = f_{ctd} * \frac{\varepsilon_{ctd}}{\varepsilon_c} - \frac{1}{2} * f_{ctd} * \frac{\varepsilon_{ct}}{\varepsilon_c}$$

Determine concrete compressive strains:

$$\frac{1}{2} * \varepsilon_c^2 * E_{cm} = f_{ctd} * \varepsilon_{ctd} - \frac{1}{2} * f_{ctd} * \varepsilon_{ct}$$

$$\varepsilon_c = \pm \sqrt{\frac{2 * f_{ctd} * \varepsilon_{ctd} - f_{ctd} * \varepsilon_{ct}}{E_{cm}}}$$

Only the positive solution is used for further elaboration. The concrete compressive strains have now been determined the other parameters can subsequently be determined as well, starting with the height of the compressive and tensile zones. The same equations as defined for branch B are used:

$$x_u = \frac{f_{ctd} * h}{\frac{1}{2} * \sigma_c + \frac{1}{2} * f_{ctd} * \frac{\varepsilon_{ct}}{\varepsilon_c} + f_{ctd}}$$

$$x_1 = \frac{\varepsilon_{ct}}{\varepsilon_c} * x_u$$

$$x_2 = h - x_u - x_1$$

Forces:

$$N_c = \frac{1}{2} * \varepsilon_c * E_{cm} * x_u * b$$

$$N_{t1} = \frac{1}{2} * f_{ctd} * x_1 * b$$

$$N_{t2} = f_{ctd} * x_2 * b$$

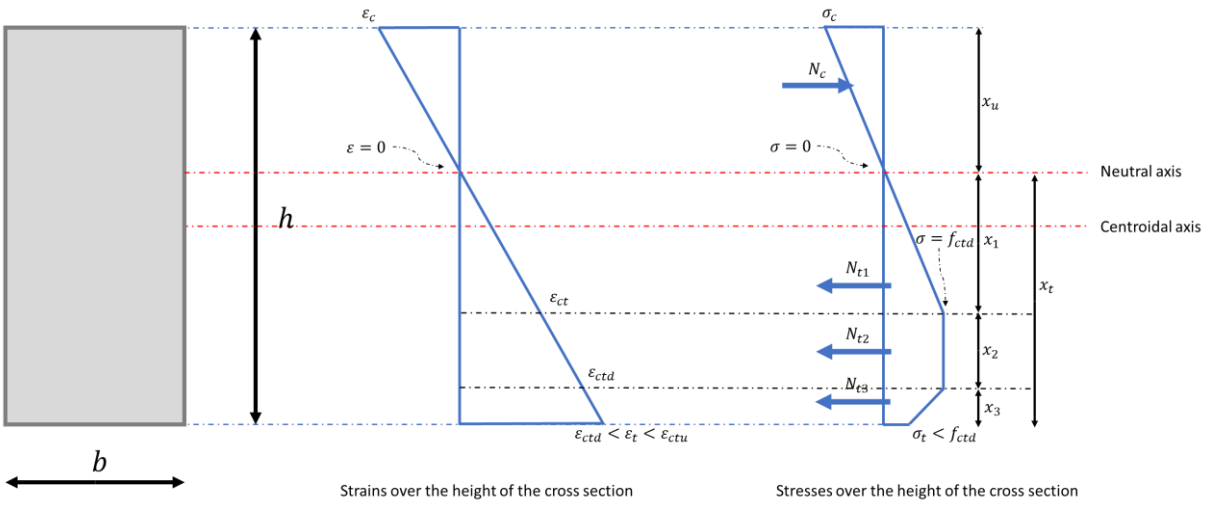
Bending moment:

$$M_{ctd} = -N_c * \frac{1}{3} * x_u + N_{t1} * \left(x_u + \frac{2}{3} * x_1\right) + N_{t2} * \left(x_u + x_1 + \frac{1}{2} * x_2\right)$$

NOTE: Strictly speaking the pull-out phase already starts when $\varepsilon_{ct;0,3}$ is achieved, depending on the values for f_{ctd} and $f_{ctd;2}$ this strain value does not have to be the same as ε_{ctd}, it can also be smaller but it cannot be greater ($\varepsilon_{ct;0,3} \leq \varepsilon_{ctd}$). However, in the simplified stress-strain figure that is adopted the pull-out phase is assumed to start once $\varepsilon_t = \varepsilon_{ctd}$.

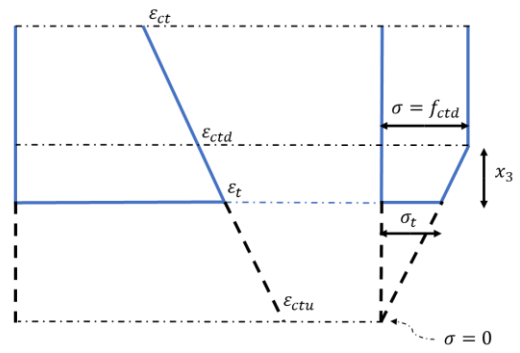
Branch C – Pull-out phase

If the strains increase further the pull out phase starts and at the end of the phase no contribution of the outermost tensile fibre remains (see characteristic point 3). The situation during this phase is as follows:

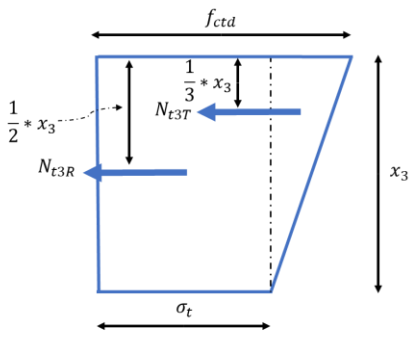


Additional definitions: To simplify the calculation the force N_{t3} is subdivided into two terms: $N_{t3} = N_{t3R} + N_{t3T}$. For the derivations the lower part of the strain and stress diagram are studied more closely.

Lower part of strain and stress diagrams



Lower part of tensile zone



An equation is formulated to determine the stress σ_t at the bottom of the cross section. In order to do so the strain figure is used, a different approach compared to earlier because stresses and strains are no longer directly proportional through E_{cm} at this stage.

$$\sigma_t = f_{ctd} - \frac{\varepsilon_t - \varepsilon_{ctd}}{\varepsilon_{ctu} - \varepsilon_{ctd}} * f_{ctd} = f_{ctd} * \left(1 - \frac{\varepsilon_t - \varepsilon_{ctd}}{\varepsilon_{ctu} - \varepsilon_{ctd}}\right)$$

Where:

$$\varepsilon_t = \frac{x_1 + x_2 + x_3}{x_u} * \varepsilon_c$$

Horizontal forces: Because the lower tensile zone is divided into two forces, there is a total of five horizontal forces:

$$N_c = \frac{1}{2} * \sigma_c * x_u * b$$

$$N_{t1} = \frac{1}{2} * f_{ctd} * x_1 * b$$

$$N_{t2} = f_{ctd} * x_2 * b$$

$$N_{t3R} = \sigma_t * x_3 * b = f_{ctd} * \left(1 - \frac{\varepsilon_t - \varepsilon_{ctd}}{\varepsilon_{ctu} - \varepsilon_{ctd}}\right) * x_3 * b$$

$$N_{t3T} = \frac{1}{2} * (f_{ctd} - \sigma_t) * b * x_3 = \frac{1}{2} * \left(f_{ctd} - f_{ctd} * \left(1 - \frac{\varepsilon_t - \varepsilon_{ctd}}{\varepsilon_{ctu} - \varepsilon_{ctd}}\right)\right) * b * x_3 = \frac{1}{2} * f_{ctd} * \left(\frac{\varepsilon_t - \varepsilon_{ctd}}{\varepsilon_{ctu} - \varepsilon_{ctd}}\right) * x_3 * b$$

Height of compressive and tensile zone: There are four unknowns (x_1, x_2, x_3 and x_u). Using the strain distribution over the height of the cross section the dimensions three equations can be found:

$$\frac{x_u}{\varepsilon_c} = \frac{x_1}{\varepsilon_{ct}} \rightarrow x_1 = \frac{\varepsilon_{ct}}{\varepsilon_c} * x_u$$

$$\frac{x_u}{\varepsilon_c} = \frac{x_1 + x_2}{\varepsilon_{ctd}} \rightarrow x_2 = \varepsilon_{ctd} * \left(\frac{x_u}{\varepsilon_c} - \frac{x_1}{\varepsilon_{ctd}}\right) \rightarrow x_2 = \frac{\varepsilon_{ctd} - \varepsilon_{ct}}{\varepsilon_c} * x_u$$

$$x_3 = h - x_u - x_1 - x_2 \rightarrow x_3 = h - x_u - \frac{\varepsilon_{ct}}{\varepsilon_c} * x_u - \frac{\varepsilon_{ctd} - \varepsilon_{ct}}{\varepsilon_c} * x_u = h - x_u - \frac{\varepsilon_{ctd}}{\varepsilon_c} * x_u$$

Horizontal equilibrium: Making use of these aforementioned equations it has to be verified that horizontal equilibrium has been achieved, this results in the fourth equation to determine x_u:

$$N_c = N_{t1} + N_{t2} + N_{t3R} + N_{t3T}$$

Substitute expressions for horizontal forces:

$$\frac{1}{2} * \sigma_c * x_u * b = \frac{1}{2} * f_{ctd} * x_1 * b + f_{ctd} * x_2 * b + f_{ctd} * \left(1 - \frac{\varepsilon_t - \varepsilon_{ctd}}{\varepsilon_{ctu} - \varepsilon_{ctd}}\right) * x_3 * b + \frac{1}{2} * f_{ctd} * \left(\frac{\varepsilon_t - \varepsilon_{ctd}}{\varepsilon_{ctu} - \varepsilon_{ctd}}\right) * x_3 * b$$

Substitute expressions for x_1, x_2 and x_3:

$$\frac{1}{2} * \sigma_c * x_u * b = \frac{1}{2} * f_{ctd} * \frac{\varepsilon_{ct}}{\varepsilon_c} * x_u * b + f_{ctd} * \frac{\varepsilon_{ctd} - \varepsilon_{ct}}{\varepsilon_c} * x_u * b + f_{ctd} * \left(1 - \frac{\varepsilon_t - \varepsilon_{ctd}}{\varepsilon_{ctu} - \varepsilon_{ctd}}\right) * (h - x_u - \frac{\varepsilon_{ctd}}{\varepsilon_c} * x_u) * b + \frac{1}{2} * f_{ctd} * \left(\frac{\varepsilon_t - \varepsilon_{ctd}}{\varepsilon_{ctu} - \varepsilon_{ctd}}\right) * (h - x_u - \frac{\varepsilon_{ctd}}{\varepsilon_c} * x_u) * b$$

Solve for x_u (this step is performed using Maple to avoid errors):

$$x_{u1} = \frac{\left(\sqrt{f_{ctd} * (-\varepsilon_{ctu} + \varepsilon_{ctd}) * \left((-\varepsilon_{ctd} + \varepsilon_{ct} - \varepsilon_{ctu}) * f_{ctd} + \sigma_c * \varepsilon_c\right)} + f_{ctd} * (\varepsilon_c + \varepsilon_{ctu})\right) * \varepsilon_c * h}{\left(\varepsilon_c^2 + 2 * \varepsilon_c * \varepsilon_{ctu} + \varepsilon_{ct} * \varepsilon_{ctu} - \varepsilon_{ctd} * (-\varepsilon_{ctd} + \varepsilon_{ct})\right) * f_{ctd} - \sigma_c * \varepsilon_c * (-\varepsilon_{ctu} + \varepsilon_{ctd})}$$

$$x_{u2} = \frac{\left(-\sqrt{f_{ctd} * (-\varepsilon_{ctu} + \varepsilon_{ctd}) * \left((-\varepsilon_{ctd} + \varepsilon_{ct} - \varepsilon_{ctu}) * f_{ctd} + \sigma_c * \varepsilon_c\right)} + f_{ctd} * (\varepsilon_c + \varepsilon_{ctu})\right) * \varepsilon_c * h}{\left(\varepsilon_c^2 + 2 * \varepsilon_c * \varepsilon_{ctu} + \varepsilon_{ct} * \varepsilon_{ctu} - \varepsilon_{ctd} * (-\varepsilon_{ctd} + \varepsilon_{ct})\right) * f_{ctd} - \sigma_c * \varepsilon_c * (-\varepsilon_{ctu} + \varepsilon_{ctd})}$$

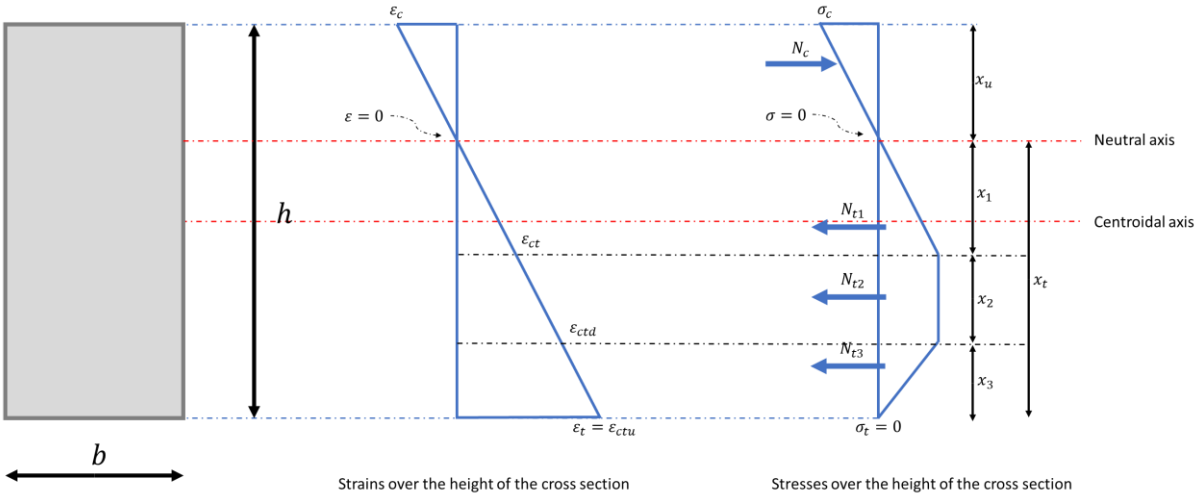
Because a second order equation was found for x_u, there are two solutions. The first solution is used for further elaborations.

Bending moment: All unknowns have now been defined and the bending moment can subsequently be calculated. With respect to the top fibre this is done as follows:

$$M = -N_c * \frac{1}{3} * x_u + N_{t1}\left(x_u + \frac{2 * x_1}{3}\right) + N_{t2}\left(x_u + x_1 + \frac{x_2}{2}\right) + N_{t3R}\left(x_u + x_1 + x_2 + \frac{x_3}{2}\right) + N_{t3T}\left(x_u + x_1 + x_2 + \frac{x_3}{3}\right)$$

Characteristic point 3 – Pull-out of the outermost fibre

If the strains increase further the stage is reached where no contribution of the outer most tensile fibre remains. The following figure gives the stresses and strains over the height of the cross section at this stage.



For this specific situation it is the tensile strains that are defined ($\varepsilon_t = \varepsilon_{ctu}$) instead of the compressive strains. Therefore, first the corresponding compressive strain has to be determined. The unknowns are x_1, x_2, x_3 and ε_c:

$$\frac{x_u}{\varepsilon_c} = \frac{x_1}{\varepsilon_{ct}} \rightarrow x_1 = \frac{\varepsilon_{ct}}{\varepsilon_c} * x_u$$

$$\frac{x_u}{\varepsilon_c} = \frac{x_1 + x_2}{\varepsilon_{ctd}} \rightarrow x_2 = \frac{\varepsilon_{ctd} - \varepsilon_{ct}}{\varepsilon_c} * x_u$$

$$\frac{x_u}{\varepsilon_c} = \frac{x_1 + x_2 + x_3}{\varepsilon_{ctu}} \rightarrow x_3 = \frac{\varepsilon_{ctu} - \varepsilon_{ctd}}{\varepsilon_c} * x_u$$

The horizontal forces over the cross section are:

$$N_c = \frac{1}{2} * \sigma_c * x_u * b = \frac{1}{2} * \varepsilon_c * E_{cm} * x_u * b$$

$$N_{t1} = \frac{1}{2} * f_{ctd} * x_1 * b$$

$$N_{t2} = f_{ctd} * x_2 * b$$

$$N_{t3} = \frac{1}{2} * f_{ctd} * x_3 * b$$

By assessing the horizontal force equilibrium a fourth equation is found for ε_c:

$$N_c = N_{t1} + N_{t2} + N_{t3}$$

$$\frac{1}{2} * \varepsilon_c * E_{cm} * x_u * b = \frac{1}{2} * f_{ctd} * x_1 * b + f_{ctd} * x_2 * b + \frac{1}{2} * f_{ctd} * x_3 * b$$

Substitute x_1, x_2 and x_3:

$$\frac{1}{2} * \varepsilon_c * E_{cm} * x_u * b = \frac{1}{2} * f_{ctd} * \frac{\varepsilon_{ct}}{\varepsilon_c} * x_u * b + f_{ctd} * \frac{\varepsilon_{ctd} - \varepsilon_{ct}}{\varepsilon_c} * x_u * b + \frac{1}{2} * f_{ctd} * \frac{\varepsilon_{ctu} - \varepsilon_{ctd}}{\varepsilon_c} * x_u * b$$

$$\frac{1}{2} * \varepsilon_c * E_{cm} * x_u * b = -\frac{1}{2} * f_{ctd} * \frac{\varepsilon_{ct}}{\varepsilon_c} * x_u * b + \frac{1}{2} * f_{ctd} * \frac{\varepsilon_{ctd}}{\varepsilon_c} * x_u * b + \frac{1}{2} * f_{ctd} * \frac{\varepsilon_{ctu}}{\varepsilon_c} * x_u * b$$

Simplify:

$$\frac{1}{2} * \varepsilon_c * E_{cm} = -\frac{1}{2} * f_{ctd} * \frac{\varepsilon_{ct}}{\varepsilon_c} + \frac{1}{2} * f_{ctd} * \frac{\varepsilon_{ctd}}{\varepsilon_c} + \frac{1}{2} * f_{ctd} * \frac{\varepsilon_{ctu}}{\varepsilon_c}$$

$$\frac{1}{2} * \varepsilon_c * E_{cm} = \frac{1}{2} * f_{ctd} * \frac{\varepsilon_{ctu}}{\varepsilon_c} + \frac{1}{2} * f_{ctd} * \frac{\varepsilon_{ctd}}{\varepsilon_c} - \frac{1}{2} * f_{ctd} * \frac{\varepsilon_{ct}}{\varepsilon_c}$$

Determine the concrete compressive strains:

$$\frac{1}{2} * \varepsilon_c^2 * E_{cm} = \frac{1}{2} * f_{ctd} * \varepsilon_{ctu} + \frac{1}{2} * f_{ctd} * \varepsilon_{ctd} - \frac{1}{2} * f_{ctd} * \varepsilon_{ct}$$

$$\varepsilon_c = \pm \sqrt{\frac{f_{ctd} * \varepsilon_{ctu} + f_{ctd} * \varepsilon_{ctd} - f_{ctd} * \varepsilon_{ct}}{E_{cm}}}$$

The positive solution is used for further elaboration and because the concrete compressive strains have now been defined, the other parameters can also be determined, starting with the height of the compressive and tensile zones. The equation for x_3 is formulated as:

$$x_3 = h - x_u - x_1 - x_2$$

The equilibrium equation is again formulated:

$$\frac{1}{2} * \varepsilon_c * E_{cm} * x_u * b = \frac{1}{2} * f_{ctd} * \frac{\varepsilon_{ct}}{\varepsilon_c} * x_u * b + f_{ctd} * \frac{\varepsilon_{ctd} - \varepsilon_{ct}}{\varepsilon_c} * x_u * b + \frac{1}{2} * f_{ctd} * (h - x_u - x_1 - x_2) * b$$

Hence:

$$\frac{1}{2} * \varepsilon_c * E_{cm} * x_u * b = \frac{1}{2} * f_{ctd} * \frac{\varepsilon_{ct}}{\varepsilon_c} x_u * b + f_{ctd} * \frac{\varepsilon_{ctd} - \varepsilon_{ct}}{\varepsilon_c} x_u * b + \frac{1}{2} * f_{ctd} * (h - x_u - \frac{\varepsilon_{ct}}{\varepsilon_c} x_u - (\frac{\varepsilon_{ctd} - \varepsilon_{ct}}{\varepsilon_c}) x_u) b$$

Elaborate:

$$\frac{1}{2} * \varepsilon_c * E_{cm} * x_u * b = -\frac{1}{2} * f_{ctd} * \frac{\varepsilon_{ct}}{\varepsilon_c} * x_u * b + \frac{1}{2} * f_{ctd} * \frac{\varepsilon_{ctd}}{\varepsilon_c} * x_u * b + \frac{1}{2} * f_{ctd} * h * b - \frac{1}{2} * f_{ctd} * x_u * b$$

$$x_u * b * \left(\frac{1}{2} * \varepsilon_c * E_{cm} + \frac{1}{2} * f_{ctd} * \frac{\varepsilon_{ct}}{\varepsilon_c} - \frac{1}{2} * f_{ctd} * \frac{\varepsilon_{ctd}}{\varepsilon_c} + \frac{1}{2} * f_{ctd}\right) = \frac{1}{2} * f_{ctd} * h * b$$

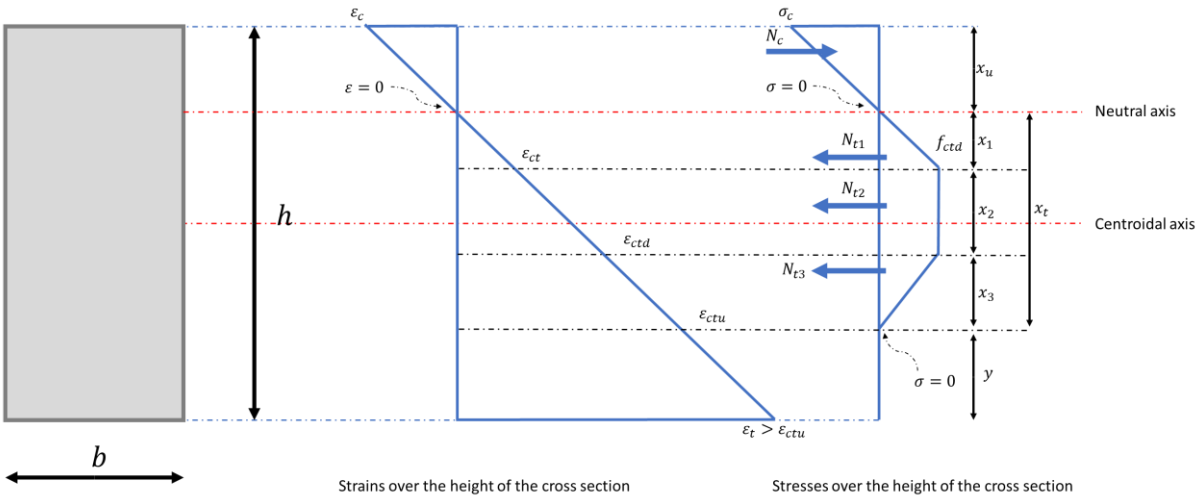
$$x_u = \frac{f_{ctd} * h}{\varepsilon_c * E_{cm} + f_{ctd} * \frac{\varepsilon_{ct}}{\varepsilon_c} - f_{ctd} * \frac{\varepsilon_{ctd}}{\varepsilon_c} + f_{ctd}}$$

Subsequently x_1, x_2 and x_3 can be calculated followed by the normal forces, these calculations are performed using the aforementioned equations. The final step is to determine the bending moment capacity (done with respect to the top fibre):

$$M_{ctu} = -N_c * \frac{1}{3} * x_u + N_{t1} * \left(x_u + \frac{2}{3} * x_1\right) + N_{t2} * \left(x_u + x_1 + \frac{1}{2} * x_2\right) + N_{t3} * \left(x_u + x_1 + x_2 + \frac{1}{3} * x_u\right)$$

Branch D – Reduction effective height

If the deflection increases further, at some point the bottom fibre reaches strains greater than ε_{ctu}. This implies that the bottom fibres no longer contribute to the capacity of the cross section and the effective height starts to decrease. At a arbitrary moment during this phase the stress and strain figures are as follows:



This situation is not considered further because it implies that failure of the cross section in bending occurs.

Case study

The aforementioned equations are applied in a case study. In this case study parameters are applied that are close to the parameters applied in the detailed design:

Parameters mixture composition				
Definition	**AFGC**	**Symbol**	**Value**	**Unit**
Fibre length	l_f	l_f	13	[mm]
Design value compressive strength	f_{cd}	f_{cd}	113	[N/mm^2]
Strain at reaching concrete compressive strength	ε_{c0d}	ε_{c3}	2,3	[‰]
Design value of tensile strength (tensile strength 1st crack)	-	f_{ctd}	6,0	[N/mm^2]
Design value maximal post cracking stress (at $w = 0{,}30$)	f_{ctfk}/(Y *K)	$f_{ctd;2}$	6,15	[N/mm^2]
Modulus of elasticity	E_{cm}		55.000	[N/mm^2]

A beam is assumed with height h of 600 mm and width b of 250 mm, these are arbitrary values. Using the aforementioned parameters first the strain values ε_{ct}, $\varepsilon_{ct;0,3}$, ε_{ctd} and ε_{ctu} are calculated. The goal is to plot a M- κ diagram to study the behaviour of the beam in bending. Note that the curvature at any stage is determined as:

$$\kappa = \frac{\varepsilon_c}{x_u}$$

An Excelsheet is prepared to carry out the analysis using the aforementioned values. The setup of this case study is as follows:

- First the three characteristic points on the curve are determined: the bending moment and curvature at the moment of cracking, the bending moment and curvature at the moment ε_{ctd} is reached at the lowest fibre and the bending moment and curvature when ε_{ctu} is reached at this point;

- The next step is that a table is prepared in which values for the concrete compressive strain ε_c are assumed (the independent variable). Values from $\varepsilon_c = 0$ to $\varepsilon_c = \varepsilon_{c3}$ are given with increments of 0,05‰;

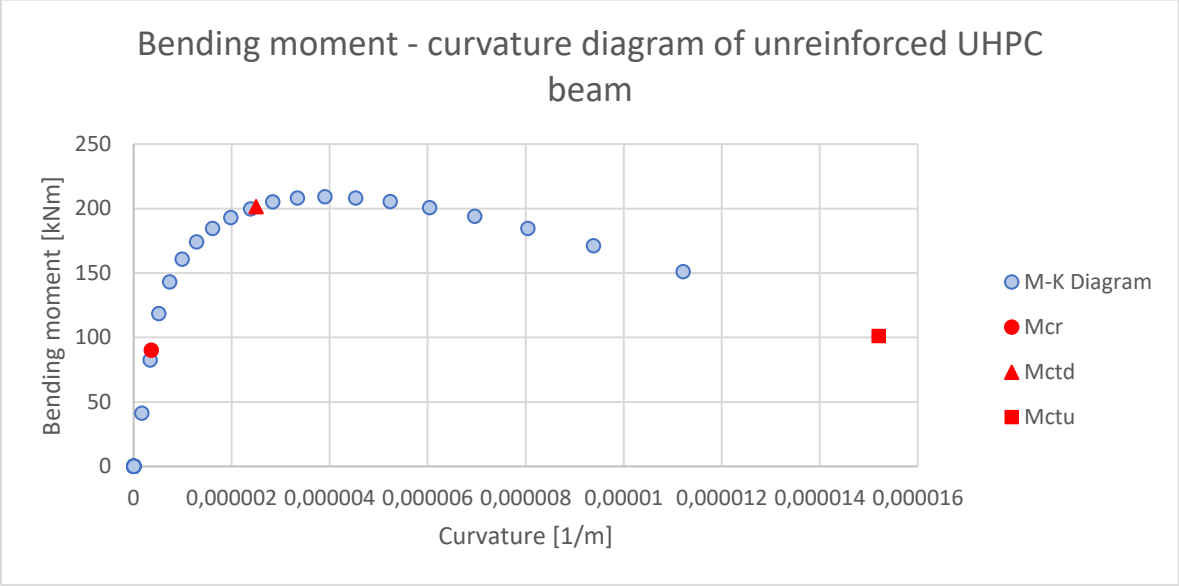
- Three sets of calculations are subsequently carried out using these assumed values for the concrete compressive strain. The first set follows the equations corresponding to branch A, the second to branch B and the third to branch C;

- For each incremental value of the concrete compressive strain the height of the compressive and tensile zone is calculated after which the bending moment and curvature are also determined. This is done following these three approaches. In addition the tensile strain value ε_t is calculated as well;

- Finally, using the tensile strain value, the appropriate values of the bending moment and curvature are selected from the calculation sets corresponding to branches A, B and C. This way a table is obtained with values for the bending moment and curvature and using these the M- κ diagram is plotted.

Results of the case study

The following graph is the M- κ diagram which was plotted using all aforementioned equations and parameters.



Interpretation of the results

From the graph it can be seen that there are three branches. The maximum value for the bending moment is (by approximation) found at the characteristic point 2 (for which $\varepsilon_t = \varepsilon_{ctd}$). However, after reaching the strains corresponding to this point the cross section does not fail immediately. Instead, if the deflection is increased the bending moment capacity decreases towards the value M_{ctu} (for which $\varepsilon_t = \varepsilon_{ctu}$) after which failure starts.

In the case of unreinforced UHPC without prestressing the bending moment capacity depends on the force equilibrium between the compressive and tensile zones of the concrete (instead of the compressive zone of the concrete and the reinforcement as done for the conventional approach). The governing value is de tensile strength of the material and because this is relatively low compared to the compressive strength, failure occurs well before $\varepsilon_c = \varepsilon_{c3}$ is reached at the most compressed fibres. By introducing a compressive force the capacity can

therefore be increased and a larger part of the potential compressive strength is used. The first crack forms at a later stage and the ultimate bending moment is thus increased.

Calculation procedure

Based on the analysis as described in this report it is concluded that the maximum bending moment capacity can be calculated using the equations corresponding to the situation where the outermost tensile fibre has a strain of $\varepsilon_t = \varepsilon_{ctd}$. This gives (by approximation) the maximum bending moment capacity. Assume a rectangular beam with height h and width b, then the capacity can be calculated as follows:

- Compressive strain if tensile strain $\varepsilon_t = \varepsilon_{ctd}$:

$$\varepsilon_c = \sqrt{\frac{2 * f_{ctd} * \varepsilon_{ctd} - f_{ctd} * \varepsilon_{ct}}{E_{cm}}}$$

- Height of compressive and tensile zones:

$$x_u = \frac{f_{ctd} * h}{\frac{1}{2} * \sigma_c + \frac{1}{2} * f_{ctd} * \frac{\varepsilon_{ct}}{\varepsilon_c} + f_{ctd}}$$

$$x_1 = \frac{\varepsilon_{ct}}{\varepsilon_c} * x_u$$

$$x_2 = h - x_u - x_1$$

- Internal compressive and tensile forces:

$$N_c = \frac{1}{2} * \varepsilon_c * E_{cm} * x_u * b$$

$$N_{t1} = \frac{1}{2} * f_{ctd} * x_1 * b$$

$$N_{t2} = f_{ctd} * x_2 * b$$

- Bending moment capacity:

$$M_{ctd} = -N_c * \frac{1}{3} * x_u + N_{t1} * \left(x_u + \frac{2}{3} * x_1\right) + N_{t2} * \left(x_u + x_1 + \frac{1}{2} * x_2\right)$$

Unreinforced UHPC beams with prestressing (External compressive force)

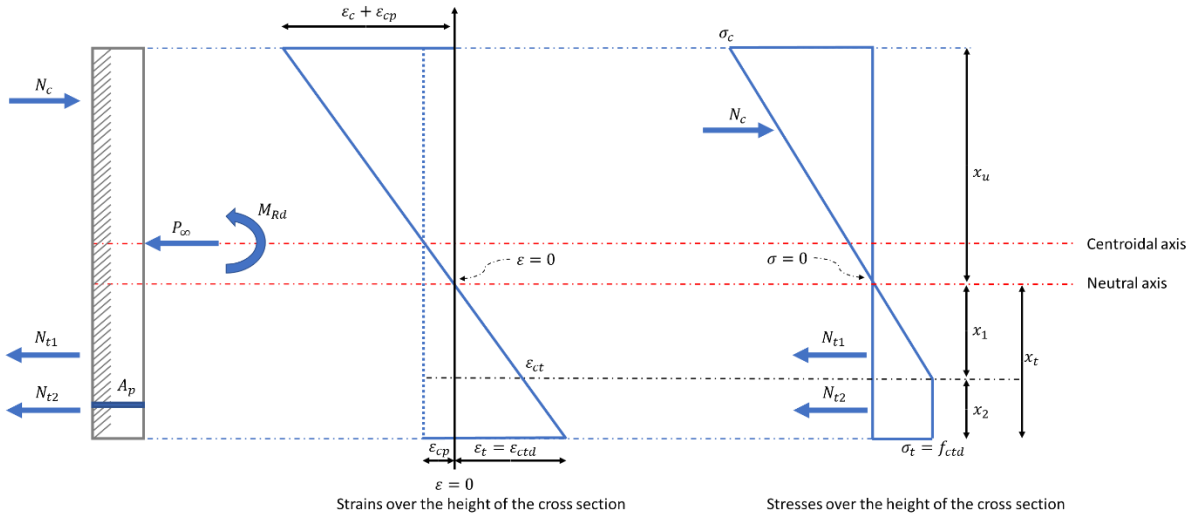
In practice prestressing forces are often present. The effect of the presence of a compressive force is that the cross section is the delay of the occurrence of the first crack and subsequently the delay of the other characteristic points. A larger compressive zone is expected, because equilibrium has to be found with the external prestressing force and the tensile force.

In this paragraph the equations to determine M_{ctd} are reconsidered to include the presence of an external prestressing force. In essence the equilibrium has to be reconsidered including this external force. It is assumed that the prestressing force acts centrically (i.e. at $1/2 * h$) and this results in a uniform concrete compressive strain over the full height of the cross section equal to:

$$\varepsilon_{cp} = \frac{P_\infty}{A_c * E_{cm}}$$

Derivations unreinforced UHPC beams with external compressive force

Consider the following modified figure. It can be seen that if no other forces are present the full cross section would be under compression. If the cross section deflects, the strain and stress state as given in the figure develops. For this situation the bending moment capacity will be derived, note the similarities with the aforementioned procedures related to M_{ctd}.



The governing situation is the situation where the tensile strains in the outermost tensile fibre become equal to $\varepsilon_t = \varepsilon_{ctd}$. However, because the strain figure starts with compression ε_{cp} the total admissible strain at the outermost tensile fibre becomes $\varepsilon_{cp} + \varepsilon_t$. To determine the capacity first the compressive strain is to be determined. The unknowns are x_1, x_2, x_u and ε_c. That means that a total of four equations is required. The first three are:

$$\frac{x_u}{\varepsilon_c + \varepsilon_{cp}} = \frac{x_1}{\varepsilon_{ct}} \rightarrow x_1 = \frac{\varepsilon_{ct}}{\varepsilon_c + \varepsilon_{cp}} * x_u$$

$$\frac{x_u}{\varepsilon_c + \varepsilon_{cp}} = \frac{x_1 + x_2}{\varepsilon_{ctd}} \rightarrow x_2 = \varepsilon_{ctd} * \left(\frac{x_u}{\varepsilon_c + \varepsilon_{cp}} - \frac{x_1}{\varepsilon_{ctd}} \right) \rightarrow x_2 = \frac{\varepsilon_{ctd} - \varepsilon_{ct}}{\varepsilon_c + \varepsilon_{cp}} * x_u$$

$$h = x_u + x_1 + x_2 = x_u + \frac{\varepsilon_{ct}}{\varepsilon_c + \varepsilon_{cp}} * x_u + \frac{\varepsilon_{ctd} - \varepsilon_{ct}}{\varepsilon_c + \varepsilon_{cp}} * x_u = x_u + \frac{\varepsilon_{ctd}}{\varepsilon_c + \varepsilon_{cp}} * x_u$$

The fourth relation is found by considering the horizontal equilibrium. That means that first equations for the horizontal forces have to be formulated, these are:

$$N_c = \frac{1}{2} * \sigma_c * x_u * b = \frac{1}{2} * (\varepsilon_c + \varepsilon_{cp}) * E_{cm} * x_u * b$$

$$N_{t1} = \frac{1}{2} * f_{ctd} * x_1 * b$$

$$N_{t2} = f_{ctd} * x_2 * b$$

Horizontal equilibrium is assessed to obtain the fourth equation to determine $(\varepsilon_c + \varepsilon_{cp})$:

$$N_c = N_{t1} + N_{t2} + P_\infty$$

$$\frac{1}{2} * (\varepsilon_c + \varepsilon_{cp}) * E_{cm} * x_u * b = \frac{1}{2} * f_{ctd} * x_1 * b + f_{ctd} * x_2 * b + P_\infty$$

Substitute x_1 and x_2:

$$\frac{1}{2} * (\varepsilon_c + \varepsilon_{cp}) * E_{cm} * x_u * b = \frac{1}{2} * f_{ctd} * \frac{\varepsilon_{ct}}{\varepsilon_c + \varepsilon_{cp}} * x_u * b + f_{ctd} * \frac{\varepsilon_{ctd} - \varepsilon_{ct}}{\varepsilon_c + \varepsilon_{cp}} * x_u * b + P_\infty$$

$$\frac{1}{2} * (\varepsilon_c + \varepsilon_{cp}) * E_{cm} * x_u * b = \frac{1}{2} * f_{ctd} * \frac{\varepsilon_{ct}}{\varepsilon_c + \varepsilon_{cp}} * x_u * b + f_{ctd} * \frac{\varepsilon_{ctd}}{\varepsilon_c + \varepsilon_{cp}} * x_u * b - f_{ctd} * \frac{\varepsilon_{ct}}{\varepsilon_c + \varepsilon_{cp}} * x_u * b + P_\infty$$

Simplify:

$$\frac{1}{2} * (\varepsilon_c + \varepsilon_{cp}) * E_{cm} * x_u * b = \frac{1}{2} * f_{ctd} * \frac{\varepsilon_{ct}}{\varepsilon_c + \varepsilon_{cp}} * x_u * b + f_{ctd} * \frac{\varepsilon_{ctd}}{\varepsilon_c + \varepsilon_{cp}} * x_u * b - f_{ctd} * \frac{\varepsilon_{ct}}{\varepsilon_c + \varepsilon_{cp}} * x_u * b + P_\infty$$

$$\frac{1}{2} * (\varepsilon_c + \varepsilon_{cp}) * E_{cm} * x_u * b = f_{ctd} * \frac{\varepsilon_{ctd}}{\varepsilon_c + \varepsilon_{cp}} * x_u * b - \frac{1}{2} * f_{ctd} * \frac{\varepsilon_{ct}}{\varepsilon_c + \varepsilon_{cp}} * x_u * b + P_\infty$$

Note that:

$$P_\infty = \sigma_{p,\infty} * A_p = \sigma_{cp} * A_c = \varepsilon_{cp} * E_{cm} * h * b$$

Introducing the expression for 'h':

$$P_\infty = \varepsilon_{cp} * E_{cm} * b * \left(x_u + \frac{\varepsilon_{ctd}}{\varepsilon_c + \varepsilon_{cp}} * x_u \right) = \varepsilon_{cp} * E_{cm} * b * x_u + \varepsilon_{cp} * E_{cm} * b * \frac{\varepsilon_{ctd}}{\varepsilon_c + \varepsilon_{cp}} * x_u$$

Substitute back into the main expression for the horizontal equilibrium and cancel out the width 'b' of the beam:

$$\frac{1}{2} * (\varepsilon_c + \varepsilon_{cp}) * E_{cm} * x_u = f_{ctd} * \frac{\varepsilon_{ctd}}{\varepsilon_c + \varepsilon_{cp}} * x_u - \frac{1}{2} * f_{ctd} * \frac{\varepsilon_{ct}}{\varepsilon_c + \varepsilon_{cp}} * x_u + \varepsilon_{cp} * E_{cm} * x_u + \varepsilon_{cp} * E_{cm} * \frac{\varepsilon_{ctd}}{\varepsilon_c + \varepsilon_{cp}} * x_u$$

It can be seen that also the term 'x_u' is present in all terms, which means this term also drops out of the equation after which an expression for the compressive strains can be formulated.

$$\frac{1}{2} * (\varepsilon_c + \varepsilon_{cp}) * E_{cm} = f_{ctd} * \frac{\varepsilon_{ctd}}{\varepsilon_c + \varepsilon_{cp}} - \frac{1}{2} * f_{ctd} * \frac{\varepsilon_{ct}}{\varepsilon_c + \varepsilon_{cp}} + \varepsilon_{cp} * E_{cm} + \varepsilon_{cp} * E_{cm} * \frac{\varepsilon_{ctd}}{\varepsilon_c + \varepsilon_{cp}}$$

Multiply left and right by $2/E_{cm}$:

$$(\varepsilon_c + \varepsilon_{cp}) = \frac{2 * f_{ctd}}{E_{cm}} * \frac{\varepsilon_{ctd}}{\varepsilon_c + \varepsilon_{cp}} - \frac{f_{ctd}}{E_{cm}} * \frac{\varepsilon_{ct}}{\varepsilon_c + \varepsilon_{cp}} + 2 * \varepsilon_{cp} + 2 * \varepsilon_{cp} * \frac{\varepsilon_{ctd}}{\varepsilon_c + \varepsilon_{cp}}$$

Multiply left and right by $(\varepsilon_c + \varepsilon_{cp})$, and move all terms to the left hand side:

$$(\varepsilon_c + \varepsilon_{cp})^2 = \frac{2 * f_{ctd}}{E_{cm}} * \varepsilon_{ctd} - \frac{f_{ctd}}{E_{cm}} * \varepsilon_{ct} + 2 * \varepsilon_{cp} * (\varepsilon_c + \varepsilon_{cp}) + 2 * \varepsilon_{cp} * \varepsilon_{ctd}$$

$$(\varepsilon_c + \varepsilon_{cp})^2 - 2 * \varepsilon_{cp} * (\varepsilon_c + \varepsilon_{cp}) + \frac{f_{ctd}}{E_{cm}} * \varepsilon_{ct} - 2 * \varepsilon_{cp} * \varepsilon_{ctd} - \frac{2 * f_{ctd}}{E_{cm}} * \varepsilon_{ctd} = 0$$

A quadratic equation of the form $ax^2 + bx + c = 0$ has now been obtained, where:

$$x = (\varepsilon_c + \varepsilon_{cp})$$

$$a = 1$$

$$b = -2 * \varepsilon_{cp}$$

$$c = \frac{f_{ctd}}{E_{cm}} * \varepsilon_{ct} - 2 * \varepsilon_{cp} * \varepsilon_{ctd} - \frac{2 * f_{ctd}}{E_{cm}} * \varepsilon_{ctd}$$

This equation can be solved using the quadratic formula. The solutions are of the form:

$$x_{1,2} = \frac{-b \pm \sqrt{D}}{2 * a}$$

First the discriminant 'D' has to be determined:

$$D = b^2 - 4 * a * c$$

$$D = (-2 * \varepsilon_{cp})^2 - 4 * 1 * \left(\frac{f_{ctd}}{E_{cm}} * \varepsilon_{ct} - 2 * \varepsilon_{cp} * \varepsilon_{ctd} - \frac{2 * f_{ctd}}{E_{cm}} * \varepsilon_{ctd}\right)$$

$$D = 4 * \varepsilon_{cp}^2 - 4 * \frac{f_{ctd}}{E_{cm}} * \varepsilon_{ct} + 8 * \varepsilon_{cp} * \varepsilon_{ctd} + \frac{8 * f_{ctd}}{E_{cm}} * \varepsilon_{ctd}$$

Substitute the terms a, b, c and D into the quadratic formula, the two solutions for $(\varepsilon_c + \varepsilon_{cp})$ are:

$$(\varepsilon_c + \varepsilon_{cp})_{1,2} = \frac{- - 2 * \varepsilon_{cp} \pm \sqrt{4 * \varepsilon_{cp}^2 - 4 * \frac{f_{ctd}}{E_{cm}} * \varepsilon_{ct} + 8 * \varepsilon_{cp} * \varepsilon_{ctd} + \frac{8 * f_{ctd}}{E_{cm}} * \varepsilon_{ctd}}}{2 * 1}$$

$$(\varepsilon_c + \varepsilon_{cp})_{1,2} = \varepsilon_{cp} \pm \sqrt{\varepsilon_{cp}^2 - \frac{f_{ctd}}{E_{cm}} * \varepsilon_{ct} + 2 * \varepsilon_{cp} * \varepsilon_{ctd} + \frac{2 * f_{ctd}}{E_{cm}} * \varepsilon_{ctd}}$$

Only one of these solutions has a physical meaning, and after rewriting the end result of the derivations is:

$$(\varepsilon_c + \varepsilon_{cp}) = \varepsilon_{cp} + \sqrt{\varepsilon_{cp}^2 + \frac{2 * f_{ctd} * \varepsilon_{ctd} - f_{ctd} * \varepsilon_{ct}}{E_{cm}} + 2 * \varepsilon_{cp} * \varepsilon_{ctd}}$$

Calculation procedure

The concrete compressive strains have now been determined, that means that the other parameters followed by the bending moment capacity can also be calculated. The full calculation procedure to determine the bending moment capacity is covered in this section.

First the total strains at the top fibre are calculated with the equation derived in the previous section, aft er which the height of the compressive and tensile zones are calculated, the unknowns are: x_u, x_1 and x_2. From the strain figure the following two equations are deduced:

$$\frac{x_u}{\varepsilon_c + \varepsilon_{cp}} = \frac{x_1}{\varepsilon_{ct}} \rightarrow x_1 = \frac{\varepsilon_{ct}}{\varepsilon_c + \varepsilon_{cp}} * x_u$$

$$x_2 = h - x_u - x_1 \rightarrow x_2 = h - x_u - \frac{\varepsilon_{ct}}{\varepsilon_c + \varepsilon_{cp}} * x_u$$

Formulate the equation for horizontal equilibrium:

$$N_c = N_{t1} + N_{t2} + P_{m,\infty}$$

$$\frac{1}{2} * (\varepsilon_c + \varepsilon_{cp}) * E_{cm} * x_u * b = \frac{1}{2} * f_{ctd} * x_1 * b + f_{ctd} * x_2 * b + \varepsilon_{cp} * E_{cm} * h * b$$

Substitute for x_1 and x_2:

$$\frac{1}{2} * (\varepsilon_c + \varepsilon_{cp}) * E_{cm} * x_u * b = \frac{1}{2} * f_{ctd} * \frac{\varepsilon_{ct}}{\varepsilon_c + \varepsilon_{cp}} * x_u * b + f_{ctd} * (h - x_u - \frac{\varepsilon_{ct}}{\varepsilon_c + \varepsilon_{cp}} * x_u) * b + \varepsilon_{cp} * E_{cm} * h * b$$

Take the symbol 'b' out of the equation and elaborate:

$$\frac{1}{2} * (\varepsilon_c + \varepsilon_{cp}) * E_{cm} * x_u = \frac{1}{2} * f_{ctd} * \frac{\varepsilon_{ct}}{\varepsilon_c + \varepsilon_{cp}} * x_u + f_{ctd} * (h - x_u - \frac{\varepsilon_{ct}}{\varepsilon_c + \varepsilon_{cp}} * x_u) + \varepsilon_{cp} * E_{cm} * h$$

$$\frac{1}{2} * (\varepsilon_c + \varepsilon_{cp}) * E_{cm} * x_u = -\frac{1}{2} * f_{ctd} * \frac{\varepsilon_{ct}}{\varepsilon_c + \varepsilon_{cp}} * x_u + f_{ctd} * h - f_{ctd} * x_u + \varepsilon_{cp} * E_{cm} * h$$

Rewrite:

$$\frac{1}{2} * (\varepsilon_c + \varepsilon_{cp}) * E_{cm} * x_u + \frac{1}{2} * f_{ctd} * \frac{\varepsilon_{ct}}{\varepsilon_c + \varepsilon_{cp}} * x_u + f_{ctd} * x_u = f_{ctd} * h + \varepsilon_{cp} * E_{cm} * h$$

$$x_u * \left(\frac{1}{2} * (\varepsilon_c + \varepsilon_{cp}) * E_{cm} + \frac{1}{2} * f_{ctd} * \frac{\varepsilon_{ct}}{\varepsilon_c + \varepsilon_{cp}} + f_{ctd}\right) = f_{ctd} * h + \varepsilon_{cp} * E_{cm} * h$$

$$x_u = \frac{f_{ctd} * h + \varepsilon_{cp} * E_{cm} * h}{\left(\frac{1}{2} * (\varepsilon_c + \varepsilon_{cp}) * E_{cm} + \frac{1}{2} * f_{ctd} * \frac{\varepsilon_{ct}}{\varepsilon_c + \varepsilon_{cp}} + f_{ctd}\right)}$$

The height of the compressive zone is now known. The height of the tensile zones x_1 and x_2 can now be calculated as well. This is done using the two aforementioned equations:

$$x_1 = \frac{\varepsilon_{ct}}{\varepsilon_c + \varepsilon_{cp}} * x_u \; AND \; x_2 = h - x_u - \frac{\varepsilon_{ct}}{\varepsilon_c + \varepsilon_{cp}} * x_u$$

The horizontal forces and the bending moment can now be determined. Note that he prestressing is assumed to be applied centrically.

$$M = -N_c * \frac{1}{3} * x_u + N_{t1} * \left(x_u + \frac{2}{3} * x_1\right) + N_{t2} * \left(x_u + x_1 + \frac{1}{2} * x_2\right) + P_\infty * \frac{1}{2} * h$$

Note that as a final step it has to be verified that $\varepsilon_c \leq \varepsilon_{c3}$. If this does not hold, then the derivations should be reformulated with a different assumption for the concrete compressive zone.

Validation and conclusion

Equations have been derived to determine the cross-sectional capacity in the case an external compressive force (centrically applied) is present. The expectation was that the addition would result in an increase of the height of the compressive zone and to an increase of the bending moment capacity.

As a final check the results are compared with the case where no prestressing is present. If P_∞ is set to zero, and as a result ε_{cp} is equal to zero as well, then the same equations should be obtained as derived in the first part of this report for the case without prestressing.

- Equation for concrete compressive stress at most compressed fibre:

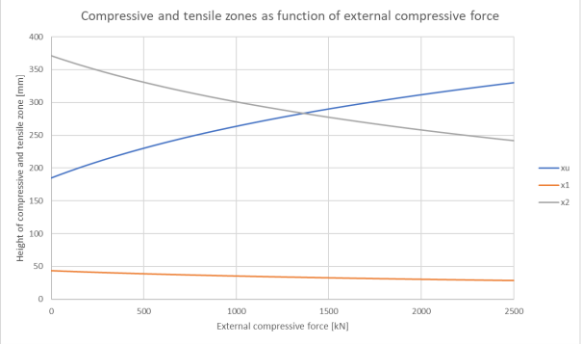
$$(\varepsilon_c + 0) = 0 + \sqrt{0^2 + \frac{2 * f_{ctd} * \varepsilon_{ctd} - f_{ctd} * \varepsilon_{ct}}{E_{cm}} + 2 * 0 * \varepsilon_{ctd}} \rightarrow \varepsilon_c = \sqrt{\frac{2 * f_{ctd} * \varepsilon_{ctd} - f_{ctd} * \varepsilon_{ct}}{E_{cm}}}$$

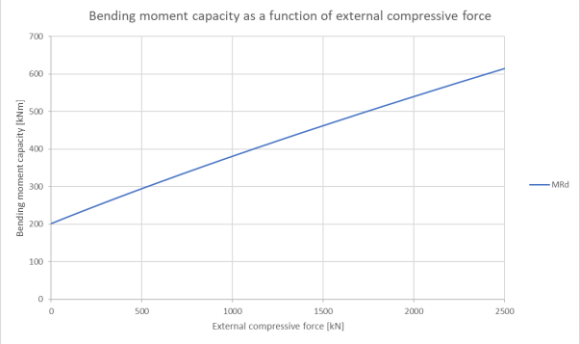
- Equation for height of compressive zone:

$$x_u = \frac{f_{ctd} * h + 0 * E_{cm} * h}{\left(\frac{1}{2} * (\varepsilon_c + 0) * E_{cm} + \frac{1}{2} * f_{ctd} * \frac{\varepsilon_{ct}}{\varepsilon_c + 0} + f_{ctd}\right)} \rightarrow x_u = \frac{f_{ctd} * h}{\frac{1}{2} * \sigma_c + \frac{1}{2} * f_{ctd} * \frac{\varepsilon_{ct}}{\varepsilon_c} + f_{ctd}}$$

The results are in agreement with what would be expected if the external prestressing force is set equal to zero.

The Excelsheet that was prepared for the case study in the first report is modified to include external compressive forces. An external prestressing force was applied with a magnitude that was increased with 25 kN intervals from 0 kN (no prestressing) to a maximum of 2500 kN. The following graphs show the height of the concrete compressive and tensile zones (left) and the bending moment capacity (right).





These graphs confirm the expectations that the height of the compressive zone and the bending moment capacity would increase if the external compressive force increases as well. This concludes the discussion on unreinforced UHPC beams with and without an external compressive force.

Bibliography

Gowripalan, N., & Gilbert, I. (2000, May). *Design Duidelines for Ductal Prestressed Concrete Beams.* University of New South Wales, School of Civil and Environmental Engineering.

Groupe de travail BFUP. (2013, June). Ultra High Performance Fibre-Reinforced Concretes. *Recommendations*. Association Francaise de Génie Civil.

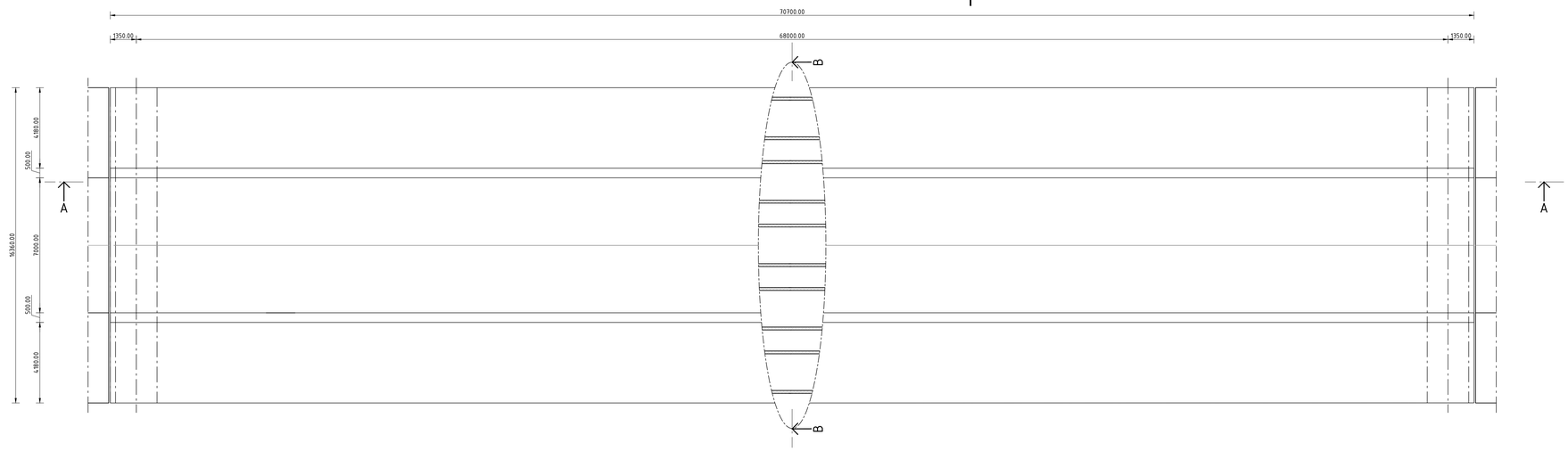
Lagendijk, P., & Braam, C. (2011). *Cement en beton 2 Constructieleer Gewapend Beton* (Zevende gewijzigde druk 2011 ed.). Aeneas.

Oostra, A. (2015, 08 18). A study on the application of UHPFRC in the superstructure of an incrementally launched box girder bridge in The Netherlands. *Master's Thesis – Main Study*.

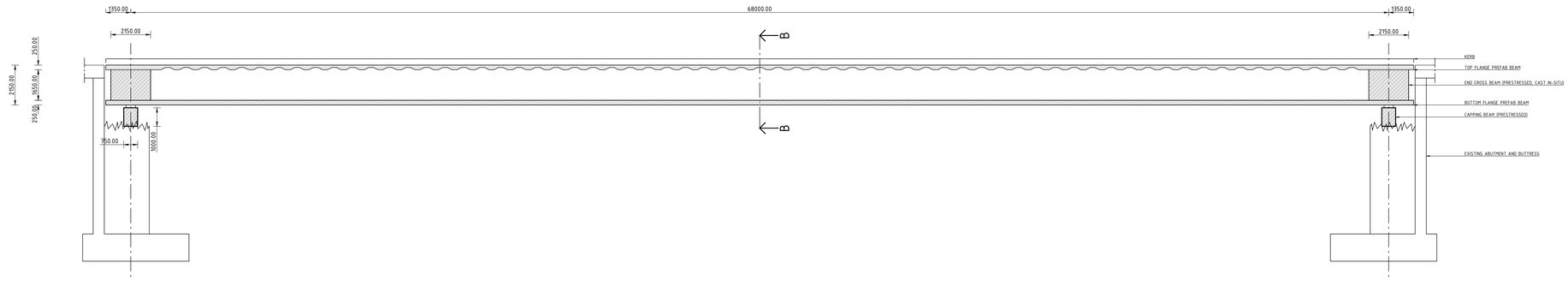
Oostra, A. (2015, 08 18). Ultra-high performance fiber-reinforced concrete in incremental bridge launching. *Master's Thesis – Appendices*.

VIII

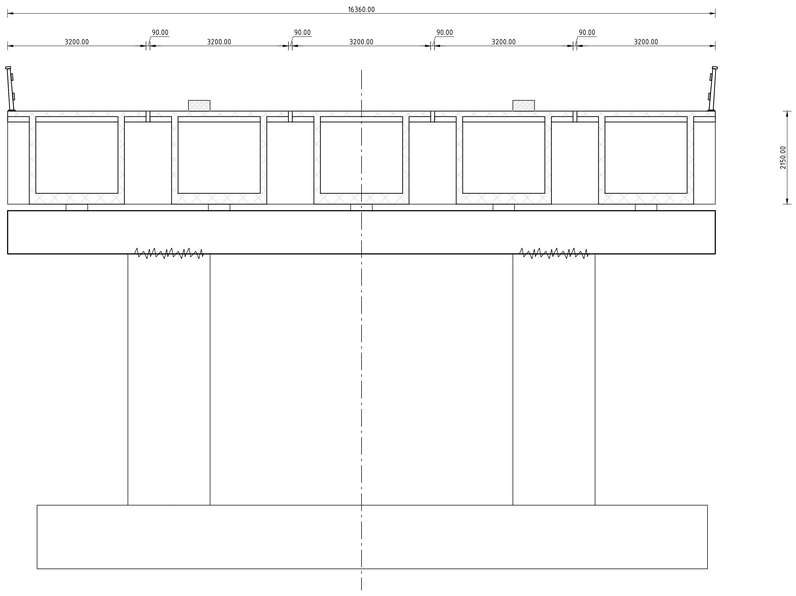
ANNEX: DRAWING DETAILED DESIGN



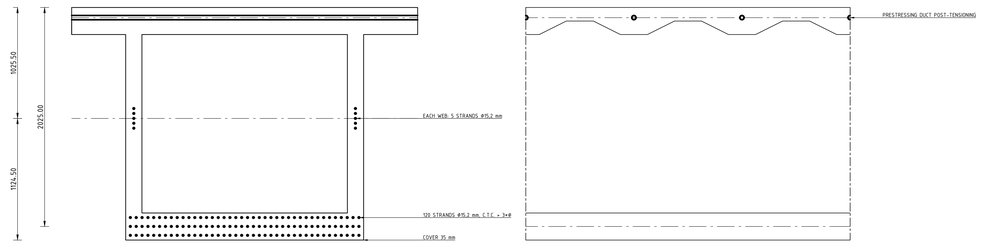
TOP VIEW
SCALE 1 : 50



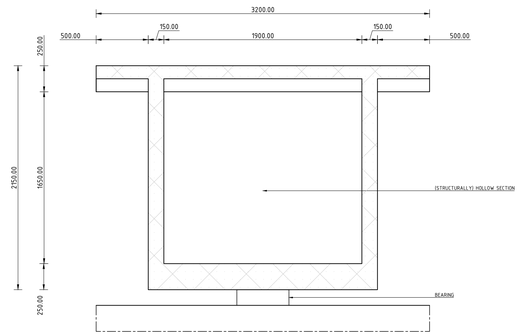
SECTION A-A: LONGITUDINAL SECTION
SCALE 1 : 50



SECTION B-B: CROSS SECTION AND POSITIONING OF TRAFFIC LANES
SCALE 1 : 50



POSITIONING PRESTRESSING STRANDS AND DUCTS
SCALE 1 : 10



DIMENSIONS OF PREFAB BEAM
SCALE 1 : 10

REMARKS:

- ALL UNITS IN mm
- ABUTMENTS, RAILINGS AND BEARINGS ONLY FOR INDICATION
- FOR OVERVIEW PRESTRESSING DUCTS & STRANDS ARE NOT DRAWN UNLESS SPECIFICALLY STATED
- SEE REPORT FOR DETAILED DESIGN AND ASSUMPTIONS, BOUNDARY CONDITIONS & REQUIREMENTS

OPDRACHTGEVER
–

PROJECTOMSCHRIJVING
MSC THESIS
REDESIGN OF BRIDGES TWENTEKANAAL IN UHPC

TEKENINGOMSCHRIJVING
DETAILED DESIGN
DRAWING DETAILED DESIGN

DOCUMENTSOORT
DRAWING

STATUS
FINAL VERSION

TEKENAAR
SCHAAL
SEE DRAWINGS
PROJECTLEIDER
FORMAAT
A0
BLAD IN BLADEN
1 IN 1
TEKENINGNUMMER
WIJZ NR

Plaats hier uw logo

VII

OPTIMIZATION & FINAL DESIGN



Optimization & Final Design

Redesign of bridges Twentekanaal in Ultra-High Performance Concrete

MSc Thesis

28 January 2021

Company	Witteveen+Bos
MSc thesis project	Redesign of bridges Twentekanaal in Ultra-High Performance Concrete
Document	Optimization & Final Design
Status	Final version
Version	D1.0
Date	28 January 2021

Author	ing. M. Dorland
Student id	4719980
Degree programme	MSc Civil Engineering
Track	Structural Engineering – Concrete Structures

Company Supervisors	ing. T. Petersen RC ir. A. ten Voorde
Supervisors TU Delft	Dr. ir. Y. Yang Dr. ir. M.A.N. Hendriks Dr. ir. S. Grünewald

TABLE OF CONTENT

PREFACE 1

1 APPROACH TO THE OPTIMAZATION PHASE 3

1.1 Approach to the optimization phase 3
1.1.1 Results detailed design 3
1.1.2 Analysis of the results 3
1.1.3 Options for optimization 5
1.1.4 Approach to the optimization phase 5

2 CONSTRAINTS OPTIMISATION 7

2.1 Cover and spacing 7
2.1.1 Top flange 7
2.1.2 Webs 10
2.1.3 Bottom flange 11
2.2 Capacity as function of beam height 12
2.2.1 Estimating capacity 12
2.2.2 Capacity as function of beam height 13

3 OPTIMIZATION PHASE 16

3.1 Approach to calculations of the optimization phase 16
3.2 Determining dimensions 16
3.2.1 Determining dimensions 16
3.2.2 Beam height 17
3.2.3 Web thickness 17
3.2.4 Bottom flange 17
3.2.5 Top flange 18
3.2.6 Summary 18
3.3 Cross sectional properties and loads 19
3.3.1 Cross sectional properties 19
3.3.2 Loads 19
3.4 Determining force distribution 19
3.4.1 Modifying RFEM model 19
3.4.2 Governing forces 20
3.5 Design verification 22

3.5.1 Approach 22
3.5.2 Results of calculation 22
3.5.3 Further modifications to the design 23
3.6 Final result 25
3.6.1 Results optimized design 25
3.6.2 Options for further analysis 25

4 FINAL DESIGN 26

4.1 Final design 26
4.1.1 Global geometry 26
4.1.2 Main beams 26
4.1.3 End cross beams 28
4.1.4 Capping beam 28
4.1.5 Self-weight of the deck 28

5 APPROACH TO GLOBAL ANALYSIS OF THE FOUNDATION 29

5.1 Approach to global analysis of the foundation 29
5.1.1 Relation to the project goal 29
5.1.2 Verification criteria 29
5.2 Codes and guidelines existing structure 30
5.2.1 Former design codes 30
5.2.2 Gewapend Beton Voorschriften 1950 (GBV 1950) 31
5.2.3 Voorschriften voor het Ontwerpen van Stalen Bruggen 1938 (VOSB 1938) 31

6 COMPARISON OF THE DESIGNS – DETERMINING LOADS AND FACTORS 32

6.1 Self-weight of the structures 32
6.1.1 Self-weight optimized design 32
6.1.2 Self-weight existing arch bridge 34
6.2 Vertical variable loads 41
6.2.1 Vertical variable loads optimized design 41
6.2.2 Variable vertical loads existing bridge 42
6.3 Safety philosophies and load factors 44
6.3.1 Safety philosophy Eurocode 44
6.3.2 Safety philosophy GBV 1950 and VOSB 1938 45
6.3.3 Comparison of approaches and implications 47

7 ASSESSMENT OF FOUNDATION & ANALYSIS OF RESULTS 50

7.1 Outline global analysis of the foundation 50
7.1.1 Outline global analysis of the foundation 50

7.2 Global analysis foundation – Total vertical force 50
7.2.1 Verification criterion 50
7.2.2 Comparison total vertical forces 51
7.3 Global analysis of foundation – Forces in foundation piles 52
7.3.1 Approach to determine forces in foundation piles 52
7.3.2 Design existing foundation 53
7.3.3 Derivation of model 55
7.3.4 Determining loads 61
7.3.5 Determining forces in foundation piles 64
7.3.6 Comparison and analysis of results 64

8 CONCLUSIONS AND PROSPECTS 66

9 BIBLIOGRAPHY 68

Final page 68

Annex(es)

		Number of pages
I	Overview calculations optimization phase	63
II	Calculations Optimization phase – Part I	15
III	Calculations Optimization phase – Part II	15
IV	Drawing final design	1
V	Weight comparison	3
VI	Estimating forces foundation piles	8

PREFACE

This report comprises the finalization of the design stage via optimization of the detailed design and the subsequent analysis of the results as part of the thesis 'Redesign of bridges Twentekanaal in Ultra-High Performance Concrete'. The goal is to optimize the detailed design and to perform a global analysis of the foundation by means of a weight comparison between the existing situation and the new design. By achieving these goals an answer can be formulated to the following research questions:

- What should the dimensions of the beams (and/or superstructure in general) be in order to obtain the most optimal (i.e. the least amount of material) redesign which complies with the relevant codes and standards?

- What are the vertical loads on the foundation in the new situation after finalizing the redesign and the old situation?

The relation between the activities (partially) covered in this report and the total project is given in the following figure. With finalizing these activities all required information is obtained that is needed for the formulation of conclusions, recommendations and the generalisation in the main report.

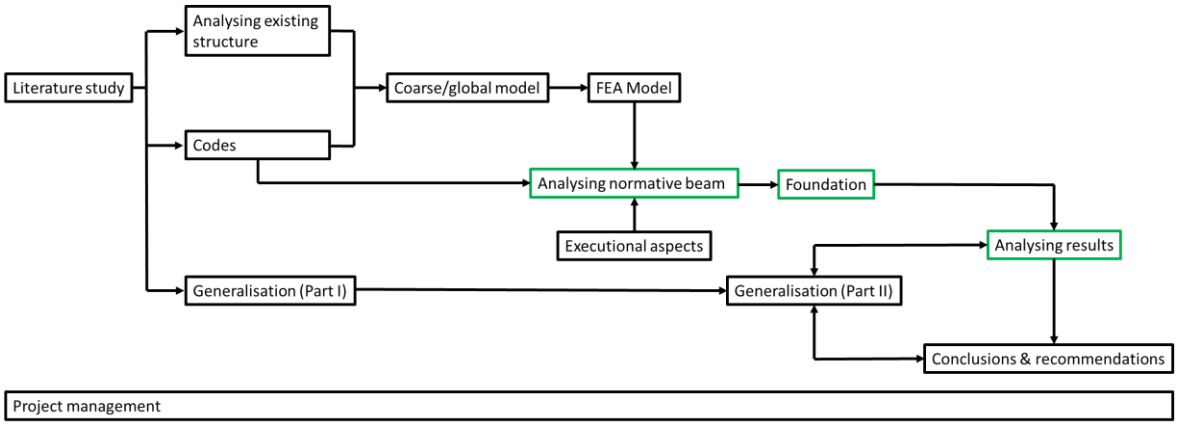


Figure 1 Optimization & final design in relation to the project

Reading guide

This report consists of two parts, the first part comprises chapters 1 to 4 and covers the optimization phase and final design of the project:

- Chapter 1: The report starts with an overview and analysis of the results of the detailed design, after which the approach to the optimization is formulated;

- Chapter 2: In the second chapter a number of constraints of the optimization are formulated and discussed. Based on these aspects such as concrete cover, spacing between prestressing strands and capacity of the beams as a function of their height, it will be possible to estimate the minimum required dimensions of the main beams in the subsequent chapter;

- Chapter 3: In the third chapter new dimensions are established based on the findings of the second chapter, after which a new design is verified resulting in the optimized design;

- Chapter 4: In the fourth chapter the properties and parameters of this optimized design, the final design of the project, are summarized.

The second part of the project comprises chapters 5 to 7 and covers the global analysis of the foundation, using the final design from the optimization phase and properties of the existing bridge. The results are subsequently compared and analysed:

- Chapter 5: The fifth chapter gives the intended approach to the global analysis of the foundation. In addition, the codes that were most probably used for the design of the existing structure are identified and briefly discussed;

- Chapter 6: In the sixth chapter all information is collected that is required to perform the global analysis of the foundation. For example: the permanent and vertical variable loads are calculated for both the existing structure and the new design, and the codes used for the design of the existing structure are briefly compared with the Eurocode to determine if the intended approach of the global analysis is feasible;

- Chapter 7: The seventh chapter covers the actual global analysis of the foundation and the analysis and interpretation of its results.

The report is finalized with the eighth chapter, which gives a summary of the previous chapters as well as the prospects of formulating a conclusion and recommendations in the main report.

1

APPROACH TO THE OPTIMAZATION PHASE

1.1 Approach to the optimization phase

1.1.1 Results detailed design

As a starting point for the optimisation the results from the detailed design phase are summarized. The following table summarizes the unity checks:

Table 1 Results verifications detailed design

Verification	Element	Value unity check
Bending moment capacity	Main beams (global)	0,77
Shear force capacity	Main beams (global)	0,56
Torsional moment capacity	Main beams (global)	0,17
Combination shear and torsion	Main beams (global)	0,61
Combination shear and torsion – Compressive strut	Main beams (global)	0,42
Ship collision – Static equilibrium	Whole deck (global)	0,14
Bending moment capacity joint	Longitudinal joints (local)	0,45
Bending moment capacity transverse direction	Top flange (local)	0,78 and 0,79
Bending moment capacity longitudinal direction	Top flange (local)	0,83
Fatigue verification – Prestressing steel	Main beams (global)	0,13
Fatigue verification – Concrete	Main beams (global)	≈0
Deflection	Main beams (global)	0,50
Bending moment capacity	End cross beams (global)	0,19
Shear force capacity	End cross beams (global)	0,54

In the next section these values will be interpreted along with other aspects to determine the potential to further optimization of the design.

1.1.2 Analysis of the results

The overview of the unity checks already gives a first indication of where optimization of the design is possible and where the options are limited. A high value for a unity check implies that most of the capacity is required to satisfy the respective design criterion, while a lower value indicates that the capacity is sufficiently high to allow for optimization. Based on the aforementioned table the following observations are made regarding the results of the detailed design.

Top flange: The unity checks related to the local verifications of the top flange, which are around 0,8, indicate that there is little room to reduce the dimensions or increase the distance between the prestressing ribs. In addition, the top flange accommodates the ducts of the post-tensioned prestressing onto which sufficient cover should be applied, which is also a limiting factor;

Webs: The webs provide and contribute to the capacity of shear and torsion. The results of the verifications indicate that there is room for optimization of the dimensions. However, this is not the only criterion; Sufficient thickness should remain to accommodate the pretensioned strands with the required cover. In

addition, the webs have an important role in the overall stability of the box beams and the resistance to ship collision.

Bottom flange: For the bottom flanges the stringent criterion determining the thickness is accommodating the required number of pretensioned prestressing strands. Sufficient cover has to be provided onto the strands, as well as sufficient spacing in between. During the elaboration of the detailed design, it turned out that the applied number of strands is smaller than the theoretical maximum number of strands, optimisation of the dimensions of the bottom flange is therewith possible.

End cross beam: The results of the verifications indicate that the cross-sectional dimensions are sufficiently large to provide the required shear and bending moment capacity. However, the end cross beams are not separately discussed in the optimization process. Given the assumption that the height and width of these beams are equal to the height of the prefab beams, the beams are implicitly included through the optimisation of the main prefab beams.

The end results in the aforementioned table are not the only indicator of opportunities to further optimization. Other observations can be made based on the actual elaboration of the calculations, two specific examples are given:

Bending moment capacity: The results of the calculations indicate that the bending moment capacity of the main beams (global verification) is sufficient. However, during the elaboration of the calculation it was noticed that the tensile strains of the prestressing steel are governing over the compressive strains in the concrete.

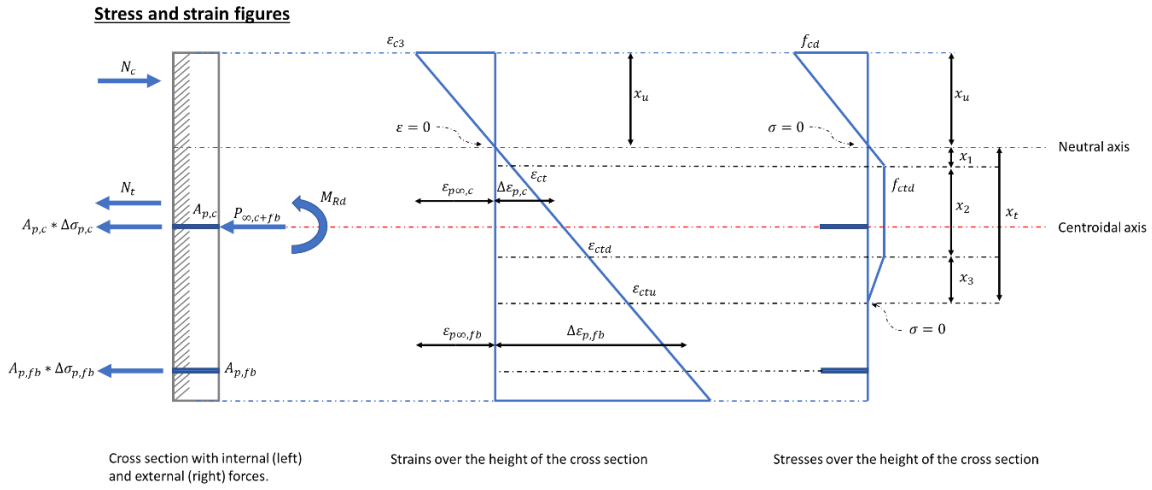


Figure 2 Adopted stress and strain relation of the main beams in the ULS

The previous figure gives the assumed stress-strain diagram over the height of the main beams. It can be seen that the bi-linear diagram for concrete in compression is replaced by a linear diagram. Achieving the plastic branch of concrete in compression implies a tensile strain in the pretensioned steel larger than the maximum value, which cannot occur in reality. The conclusion is that a larger compressive stress in the concrete can be allowed, in the current design the capacity of the material is not exploited to its full potential.

Stresses at mid span: Prestressed beams are generally designed first based on the stresses corresponding to the serviceability limit state. The largest stress found in the detailed design is a tensile stress of 3,7 N/mm^2, which is found at mid span for $t \rightarrow \infty$ and including variable loads. This stress value is governed by various parameters such as prestressing force and global dimensions, but indicates that a higher tensile stress value can be allowed at the bottom fibre.

1.1.3 Options for optimization

Various options are possible in order to reduce the self-weight of the deck by reducing the cross-sectional dimensions. Based on the discussions in this chapter, three possibilities have been formulated. These can be applied separately or combined.

- Option 1: Variation in dimensions of current cross section
- Option 2: Variation in beam type and number of beams
- Option 3: Application of different design approach

Variation in dimensions of current cross section

The first option involves the variation of the dimensions of the cross section designed in the detailed design phase. The discussion in the previous sections indicates that a further reduction of the self-weight is possible via this strategy.

Variation in beam type and number of beams

The current design involves a type of box beams called 'top hat' beams. This option involves the variation with the type of box beam (e.g. leaving out the outstand flanges) and corresponding variation in the number of beams.

Application of different design approach

The third approach is specifically aimed at exploiting the high compressive strength of UHPC to a higher extent. By combining post-tensioned and pretensioned prestressing elements, larger prestressing forces beyond the limit of pretensioning in prestressing factories can be applied. By introducing this higher compressive force onto the cross section, the compressive strength of the material is exploited to a higher degree, which enables the design of more slender structures.

1.1.4 Approach to the optimization phase

Selecting suitable option

From the identified possible approaches to the optimization the focus will be put on the first option, i.e. the variation in dimensions of the current cross section. The second and third option are not included due to the reasons stated below.

The second option is not expected to yield reductions in the self-weight of the deck unless the heigh of the beams significantly change, because additional webs and bottom flanges are added to the cross section when replacing the outstand flanges by additional beams. Variations within the current design are not expected to result in such a large change of structural height that this option becomes viable yet.

Although the third option aims at exploiting the potential of the material to a higher degree which may result in significant savings in the amounts of material, it comprises a different approach to the setup of the design. This might not be required to achieve the goal of the project and is therefore not considered at this stage.

Approach to the optimization

The intended approach to the optimization is as follows:

- **Step 1. Establish new dimensions** – The first part of the optimization is to establish the new dimensions of the cross section, see chapter 2 and paragraph 3.2 for the elaboration of this step. The starting point is the cross section obtained in the detailed design phase, the dimensions of which will be adjusted by implementing the remarks in the previous parts of this chapter;

- **Step 2. Verifications –** After the new dimensions have been determined in a substantiated way a full verification is carried out to verify whether all requirements included in the verification are met. If this is not the case, then modifications are made within the given design. See paragraphs 3.2 to 3.6 for the elaboration of this step;

- **Step 3. Analysis of results –** The results of the verifications are analysed. If the verifications are satisfied and the reduction of the self-weight is deemed to be satisfactorily, then the optimization is concluded by summarizing the parameters of the final design. If not, then the aforementioned steps are repeated to obtain a more optimized cross section.

These three steps will be elaborated in the following chapters. The optimization is concluded by the formulation of this final design in chapter 4, which will be used as one of the starting points for the global analysis of the foundation.

2

CONSTRAINTS OPTIMISATION

2.1 Cover and spacing

The most obvious constraint for the dimensions of all structural elements is those related to the capacity of the elements in ULS and SLS verifications. However, other constraints are of relevance as well, examples are given in the following figure:



Figure 3 Constraints of the design other than ULS capacity

In the next sub sections approximate minimum dimensions for the top flange, webs and bottom flange will be determined based on these criteria. These results will give a first indication of the minimum dimensions in the optimisation phase.

2.1.1 Top flange

Requirement top flange

The minimum dimensions of the top flange are determined by accommodating the prestressing ducts for the transverse post-tensioning, which requires a sufficiently large cross section with sufficient cover onto the tendons.

Provided cover onto tendon

The following figure gives the positioning of the prestressing tendon. If no additional eccentricity is applied, then it is assumed that its position coincides with the centre of gravity of the top flange.

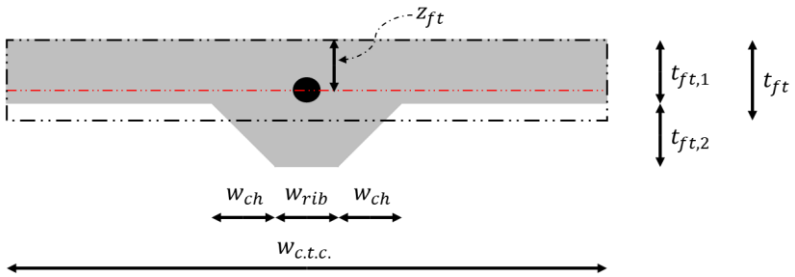


Figure 4 Section of the top flange

If the diameter of the duct is denoted as ∅, then the cover onto the duct at the top side with respect to the top of the prestressing rib is:

$$c_{top} = \frac{1}{2} * z_{ft} - \frac{1}{2} * \emptyset$$

The cover from the lower side is:

$$c_{bottom} = t_{ft,1} + t_{ft,2} - \left(z_{ft} + \frac{\emptyset}{2}\right)$$

Estimating duct diameter

In the detailed design calculations tendons with five strands with a diameter of 15,2 mm were assumed, with a cross section of 140 mm^2 per strand. Although the number of strands might change as a result of the optimisation, it is assumed that a duct with a diameter of 40 to 45 mm will be sufficient.

Determining minimum cover

The minimum cover onto the tendon is calculated following the AFGC-SETRA 2013 guideline. Assumptions or results from the detailed design:

- Exposure classes XC4 and XD3;
- Duct of $\emptyset = 45$ mm is assumed.

The cover is determined as follows:

Determining $c_{min,b}$: The minimum cover for bond, $c_{min,b}$, for circular post-tensioning ducts is as follows:

$c_{min,b} = \emptyset \leq 80$ [mm] $\rightarrow$ 45 mm

Determining $c_{min,dur}$: The minimum cover for durability is determined using the following tables, using service class S6 because the design service life is 100 years.

Tableau 4.4NF* : Valeurs de l'enrobage minimal $c_{min,dur}$ requis vis-à-vis de la durabilité dans le cas des armatures de béton armé conformes à l'EN 10080

Table 4.4NF : Values of minimum cover, $c_{min,dur}$, requirements with regard to durability for reinforcing steel in accordance with EN 10080.*

Exigence environnementale pour $c_{min,dur}$ (mm)/ *Environmental requirement for $c_{min,dur}$ (mm)*							
Classe structurale / *Structural class*	*Classe d'exposition suivant le tableau 4.1/ Exposure class according to Table 4.1*						
	X0	XC1	XC2/XC3	XC4	XD1/XS1	XD2/XS2	XD3/XS3
S1	5	5	5	10	10	15	15
S2	5	5	10	10	15	15	20
S3	5	5	10	15	15	20	20
S4	5	10	15	15	20	20	20
S5	10	10	15	20	20	20	25
S6	10	15	20	20	20	25	25

Tableau 4.5NF* : Valeurs de l'enrobage minimal $c_{min,dur}$ requis vis-à-vis de la durabilité dans le cas des armatures de précontrainte

Tableau 4.5NF: Values of minimum cover, $c_{min,dur}$, requirements with regard to durability for prestressing steel.*

Exigence environnementale pour $c_{min,dur}$ (mm)/ *Environmental requirement for $c_{min,dur}$ (mm)*							
Classe structurale / *Structural class*	*Classe d'exposition suivant le tableau 4.1/ Exposure class according to Table 4.1*						
	X0	XC1	XC2/XC3	XC4	XD1/XS1	XD2/XS2	XD3/XS3
S1	irrelevant	5	10	15	15	20	20
S2		10	15	15	20	20	20
S3		10	15	20	20	20	25
S4		15	20	20	20	25	25
S5		15	20	20	25	25	30
S6		20	20	25	25	30	30

Figure 5 Minimum cover for durability for reinforcing steel (left) and prestressing steel (right) – AFGC-SETRA 2013, p.95-96

Exposure class XD3 gives the governing result, which is $c_{min,dur} = 30$ mm.

Determining $c_{min,p}$: The minimum cover for placement conditions, $c_{min,p}$, is determined as follows. In this expression l_f represents the fibre length, D_{max} represents the maximum aggregate size and $\emptyset$ represents the diameter of the duct, strand or rebar (in this case the diameter of the duct).

$$c_{min,p} = \max\{1{,}5 * l_f; 1{,}5 * D_{max}; \emptyset\}$$

For reactive powder concrete (RPC) $D_{max} \approx 0$ mm and with a fibre length of 13 mm the expression results in $c_{min,p} = \max\{19{,}5; 0; 45\} = 45$ mm.

Determining c_{min}: The minimum cover c_{min} is determined as follows:

$$c_{min} = \max\{c_{min,b}; c_{min,dur}; c_{min,p}; 10\ mm\}$$

With all aforementioned results this gives $c_{min} = \max\{40; 30; 45; 10\ mm\} = 45$ mm

Determining Δc_{dev}: The tolerance for execution, Δc_{dev}, is taken equal to 5 mm. All values required to determine the nominal cover have now been determined.

Determining c_{nom}: The nominal cover onto the prestressing ducts is determined as follows:

$$c_{nom} = c_{min} + \Delta c_{dev} \rightarrow 45 + 5 = 50 \text{ mm}$$

Anchors and ducts

For illustration purposes examples of prestressing products are added to this report, these are taken from brochures of manufacturers to give an impression of the order of magnitude of the dimensions of post-tensioning ducts and anchors.

Post-tensioning ducts: As an example of actual products the following figures from the Dywidag brochure are added to the report. The table and figure correspond to corrugated ducts made of thin-walled sheet metal.

Dimensions of Corrugated Duct (Standard Sizes)

Tendon Type		Sheating	
0.5"	0.6"/0.62"	I.D. [mm]	O.D. [mm]
5901	6801	25	30
5902	6802	40	45
5904	6803	45	50
5905	6804	50	55
5907	6805	55	60
5909	6807	60	65
5912	6809	70	75
5915	6812	80	85
5920	6815	85	90
5927	6819	95	100
5932	6822	100	105
5937	6827	110	117
–	6831	120	127
–	6837	130	137
–	6843	140	147
–	6849	150	157
–	6855	160	167

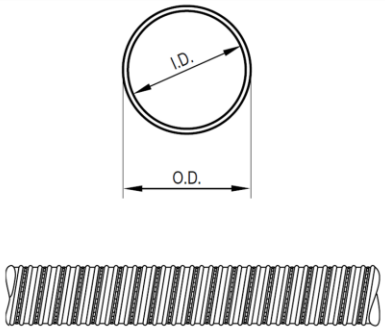


Figure 6 Example of prestressing ducts for post-tensioned transverse prestressing – DYWIDAG , p.7

The duct provides bond between the post-tensioned prestressing tendons and adjacent concrete and additional protection of the tendon against corrosion. After stressing the duct is grouted, together with the concrete this provides the most important protection of the tendon against corrosion.

Anchorage elements: An anchor of the transverse prestressing in the top flange should satisfy two requirements:

- Transfer of the force: Based on the detailed design phase, an anchor should be able to provide a prestressing force with a maximum value of 980 kN (force P_{max} during stressing);
- Dimensions: The anchor is positioned in the prestressing rib, which in the detailed design is assumed to have a total height of 250 mm, while the prestressing tendon is assumed to be applied at a height of about 94 mm. Although in the optimisation attention will be paid to the positioning of the tendon to increase the distance with respect to the top fibre and create more space for anchorage, the dimensions of the top flange remain limited.

Different types of anchorage systems are available in practice and these are devised for a wide range of applications. Some are more suitable for transverse prestressing than others, given their dimensions and/or capacity. One specific example of a prestressing anchor that might be suitable is the plate anchorage type 'SD' of Dywidag, a figure from the brochure is added below.

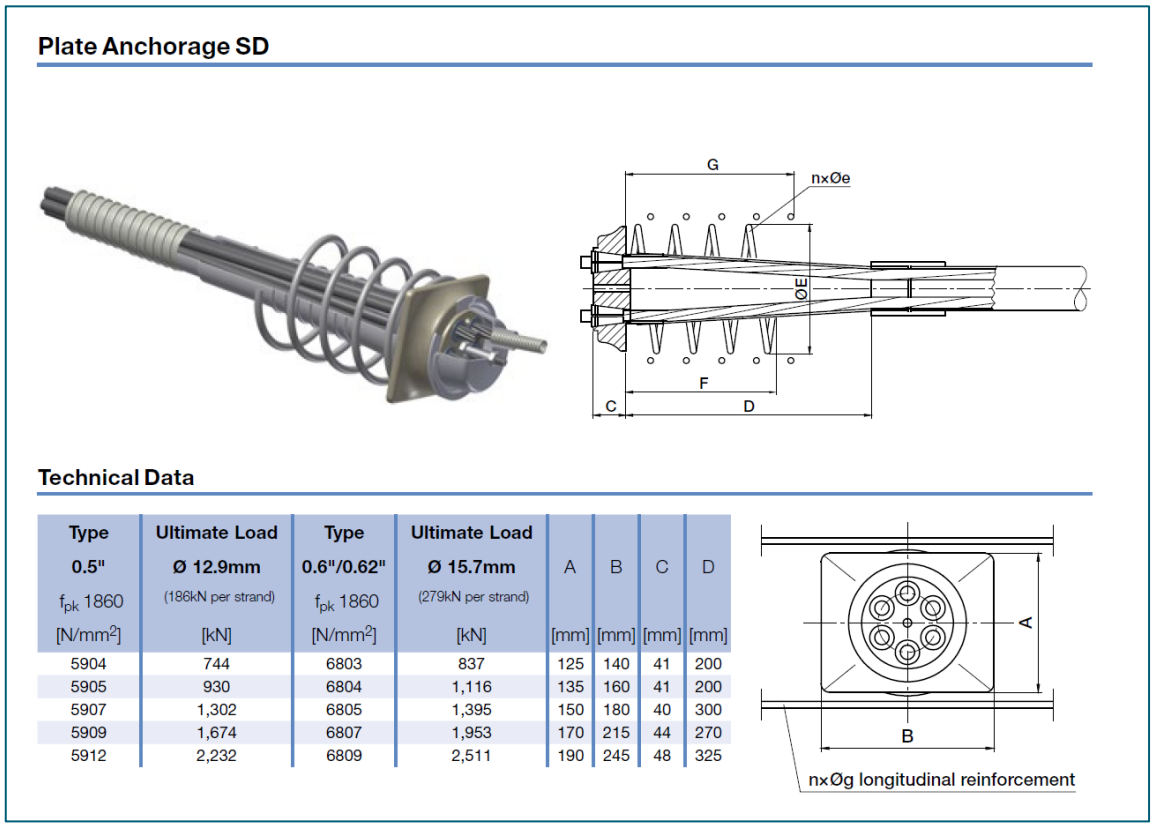


Figure 7 Example of anchorage system for post-tensioned transverse prestressing – DYWIDAG, p.24

Although this is just one example of a possible anchorage system for the transverse prestressing, it gives an indication of the order of magnitude of dimensions that is to be expected. This also illustrates that the dimensions required to be able to apply anchorage systems for the prestressing will be more stringent than the dimensions required to provide sufficient cover on the prestressing ducts.

2.1.2 Webs

Requirement webs

The minimum dimensions of the webs are determined by two aspects. First the pretensioned strands of the main prestressing have to be able to be accommodated with sufficient cover. Second the dimensions of the web have to be sufficient with respect to the accidental load case of ship collision.

Determining minimum cover

The cover onto the prestressing strands is calculated following the AFGC-SETRA 2013 guideline. In accordance with the detailed design exposure classes XC4 and XD3 are assumed, as well as a strand diameter Ø of 15,2 mm.

Determining $c_{min,b}$: The minimum cover for bond, $c_{min,b}$, for pretensioned strands is calculated as follows:

$$c_{min,b} = \max\{2 * \emptyset; 2 * D_{max}\}$$

For RPC $D_{max} \approx 0$, thus $c_{min,b} \approx 30$ mm.

Determining $c_{min,dur}$: The minimum cover for durability is determined using the tables in Figure 5, using service class S6 because the design service life is 100 years. Again, XD3 gives the governing result, which is $c_{min,dur} = 30$ mm.

Determining $c_{min,p}$: The minimum cover for placement conditions, $c_{min,p}$, is determined as follows:
$c_{min,p} = \max\{1{,}5 * 13; 1{,}5 * 0; 15{,}2\} \approx 20$ mm

Determining c_{min}: The minimum cover c_{min} is determined: $c_{min} = \max\{30; 30; 20; 10\ mm\}$, resulting in $c_{min} = 30$ mm.

Determining Δc_{dev}: The tolerance for execution, Δc_{dev}, is taken equal to 5 mm.

Determining c_{nom}: The nominal cover onto the prestressing strand is determined as follows:

$c_{nom} = c_{min} + \Delta c_{dev} \rightarrow 30 + 5 = 35$ mm

Following this criterion, the thickness of the web has to be at least:

$t_{min} = 2 * c_{nom} + \emptyset$

This results in $t_{min} = 2 * 35 + 15{,}2 \approx 85$ mm

Stability & ship collision

Although the local verifications of the capacity to withstand the forces due to the accidental load case of ship collision are not part of the design as presented in the project, this criterion should not be neglected completely. In addition, the webs contribute to the overall stability of the box beams.

Sufficient thickness of the webs is required to provide stability and withstand a collision force, also if slender diaphragm elements are applied to reinforce the beams. A minimum thickness of 100 mm is deemed to be sufficient to meet both requirements.

2.1.3 Bottom flange

For the bottom flange the most stringent criterion is the accommodation of all prestressing strands: sufficient cover onto and spacing in between the strands has to be assured. In addition, tensile reinforcement might be present, onto which sufficient cover has to be provided as well.

Cover onto strands

The calculation of the nominal cover onto the strands is identical to the calculation for the cover onto the pretensioned strands in the web, hence $c_{nom} = 35$ mm.

Cover onto the reinforcement

The cover onto the reinforcement is calculated assuming ∅10 rebars and environmental classes XC4 and XD3, as applied for the previous calculations.

Determining $c_{min,b}$: For reinforcing steel (single rebars) the minimum cover for bond, $c_{min,b}$, equals the diameter ∅ of the rebar. In case ∅10mm, this results in $c_{min,b} = 10$.

Determining $c_{min,dur}$: The minimum cover for durability is determined using the tables in Figure 5. Because of the service life of 100 years, service class S6 is used. For exposure class XD3 the cover $c_{min,dur} = 25$ mm for passive reinforcement.

Determining $c_{min,p}$: The minimum cover for placement conditions, $c_{min,p}$, is determined as follows:

$c_{min,p} = \max\{1{,}5 * 13; 1{,}5 * 0; 10\} \approx 20$ mm

Determining c_{min}: The minimum cover c_{min} is determined as follows:

$c_{min} = \max\{10; 25; 20; 10\ mm\} = 25$ mm

Determining Δc_{dev}: The tolerance for execution, Δc_{dev}, is taken equal to 5 mm.

Determining c_{nom}: The nominal cover on the reinforcement bars is: $c_{nom} = c_{min} + \Delta c_{dev} \rightarrow 25 + 5 = 30$ mm.

Applied cover

To provide sufficient cover onto the rebars, the cover onto the strands also has to be increased as such that both requirements are met. If $c_{nom,s}$ denotes the cover onto the prestressing strands, $c_{nom,r}$ denotes the cover onto the rebars and $\emptyset_r$ the diameter of the rebars, then the expression for the actual cover applied onto the strands can be written as:

$$c_{nom,s} = c_{nom,r} + \emptyset_r$$

Spacing of the prestressing strands

The AFGC-SETRA 2013 guideline prescribes the provisions from the Eurocode 2 to be satisfied, these are given in the following figure. In addition, the AFGC-SETRA 2013 prescribes that the spacing between the strands should be at least $1{,}5 * l_f$ to enable the flow of the fibre reinforced UHPC, which is influenced by the presence of the fibres.

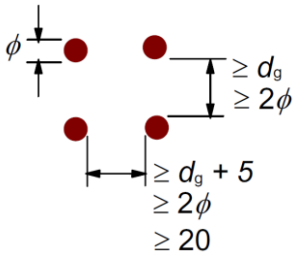


Figure 8 Minimum spacing between prestressing elements - Eurocode 2-1-1, p.156

One could summarize the requirements in the following way:

$$s_{min,hor} = \max\{2 * \emptyset; d_g + 5; 1{,}5 * l_f; 20\}$$

$$s_{min,vert} = \max\{2 * \emptyset; d_g; 1{,}5 * l_f\}$$

If the dimensions are as such that $\emptyset > l_f$ and that $d_g \approx 0$ (reactive powder concrete), then these criteria can be rewritten into:

$$s_{min} = s_{min,hor} = s_{min,vert} = 2 * \emptyset$$

2.2 Capacity as function of beam height

2.2.1 Estimating capacity

In the next section graphs will be presented in which certain properties of the beam are given as a function of the total beam height: the stresses at mid span at the outer fibres, the bending moment capacity, the shear force capacity, the torsional capacity and the capacity to the combined effect of shear and torsion. The graphs will be prepared by following the same procedures as those carried out in the detailed design. The only difference is that the height of the beams is made variable and that the capacity is calculated for a thickness of the web of 150 mm (current thickness) and 100 mm (minimum thickness). All other parameters are identical to those applied in the detailed design.

Although the graphs do not give all relevant information, such as strains in the prestressing steel, local verifications, etc., the value of these graphs is in the fact that they give a first indication of the dimensions required to satisfy the most important or stringent global verifications. In addition, these give an indication of the correlation between alterations of different values. In combination with the points discussed in 2.1, these graphs can be used to make a quick and substantiated estimation of the required minimum dimensions of the main beams. In 2.2.2 the graphs are given for various properties of the beam.

2.2.2 Capacity as function of beam height

Stresses in outer fibres at midspan

Prestressed beams are generally designed starting with the serviceability limit state: the stresses occurring in the beam are taken as a design criterion, which is why this is also the first aspect considered. Figure 9 gives the stresses in the bottom fibres at midspan of the main beams, for a web thickness of 150 mm and 100 mm. Graphs are plotted for $t \rightarrow \infty$ and full loading (permanent + variable) as this turned out to be the governing situation in the detailed design. The stresses in the bottom fibre are tensile, and thus governing over those in the top flange, because these are compressive.

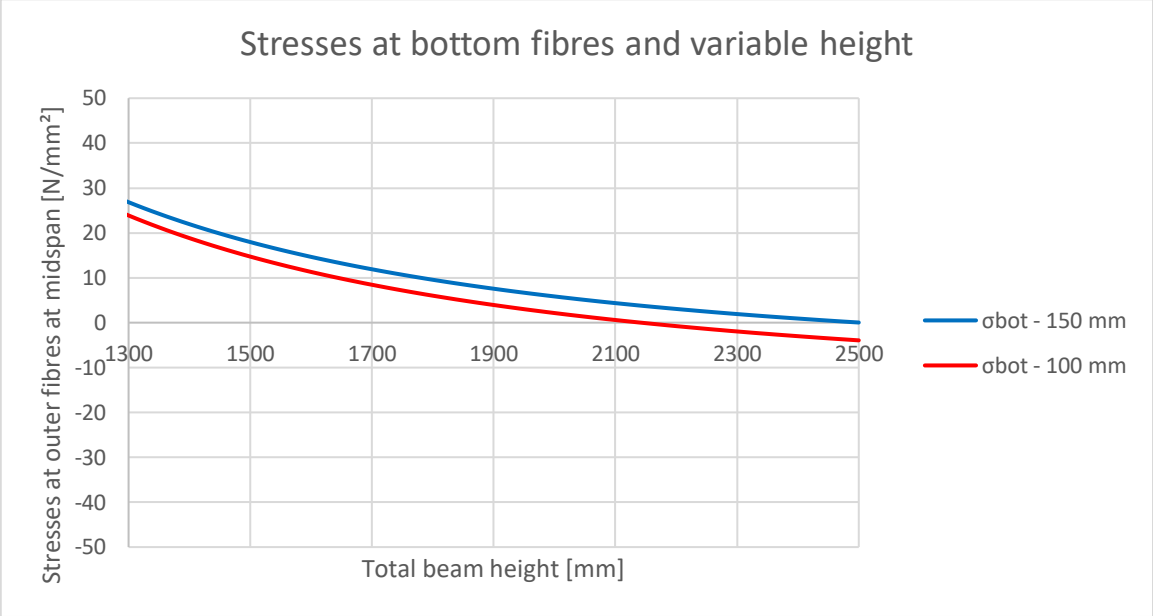


Figure 9 Stresses in top and bottom fibres at midspan as a function of the beam height

Bending moment capacity

Figure 10 gives a plot of the bending moment capacity of the main beams as a function of their height. The graphs are approximately linear and in addition it can be seen that a variation of the thickness of the webs has a negligible effect on the bending moment capacity. That was to be expected because the only contribution of the webs themselves is through the tensile zone of the concrete, which is only of a limited height compared to the total height of the beam. As a result, the influence of this effect is limited compared to other contributions (the compressive force in the concrete and the tensile forces in the prestressing steel).

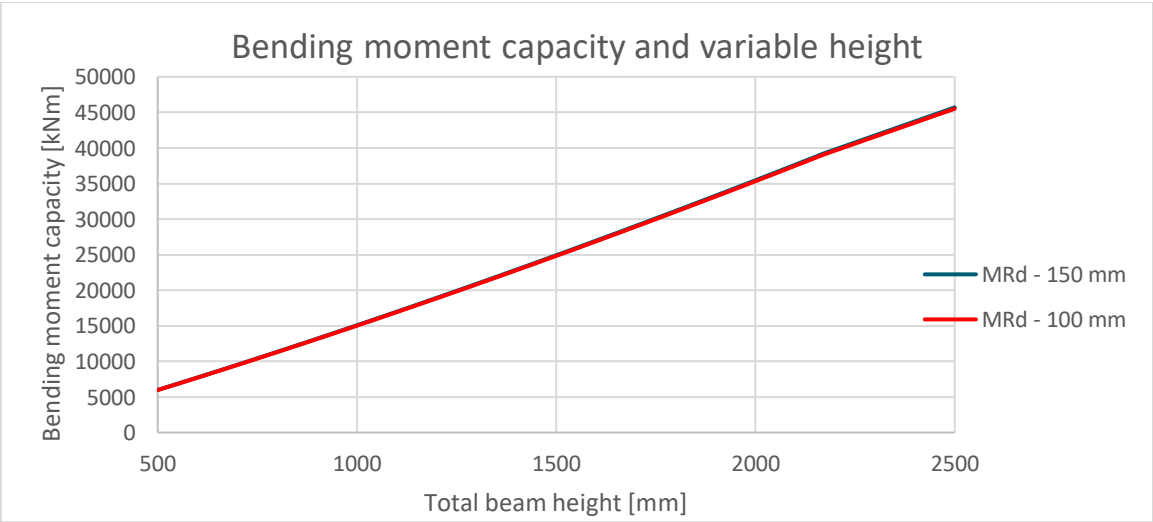


Figure 10 Bending moment capacity as a function of the beam height

Shear force capacity

Figure 11 gives the graphs of the shear capacity of the main beams as a function of the beam height. A reduction of the web thickness has a large effect on the beam capacity, this is explained by the fact that most of the shear capacity is provided by the webs of the beam.

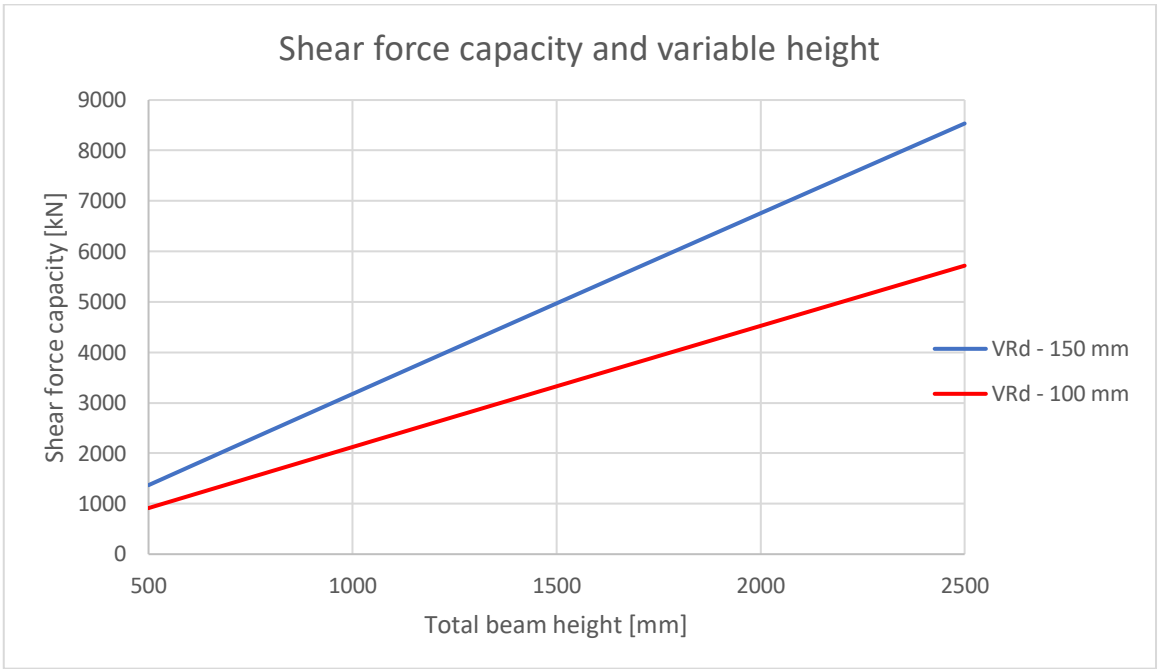


Figure 11 Shear force capacity as a function of the beam height

Torsional moment capacity

Figure 12 gives the torsional moment capacity of the beams as a function of the beam height. The graphs give a similar impression as those of the shear force. This was to be expected because an important factor in the calculation of the torsional moment capacity is the capacity of the webs.

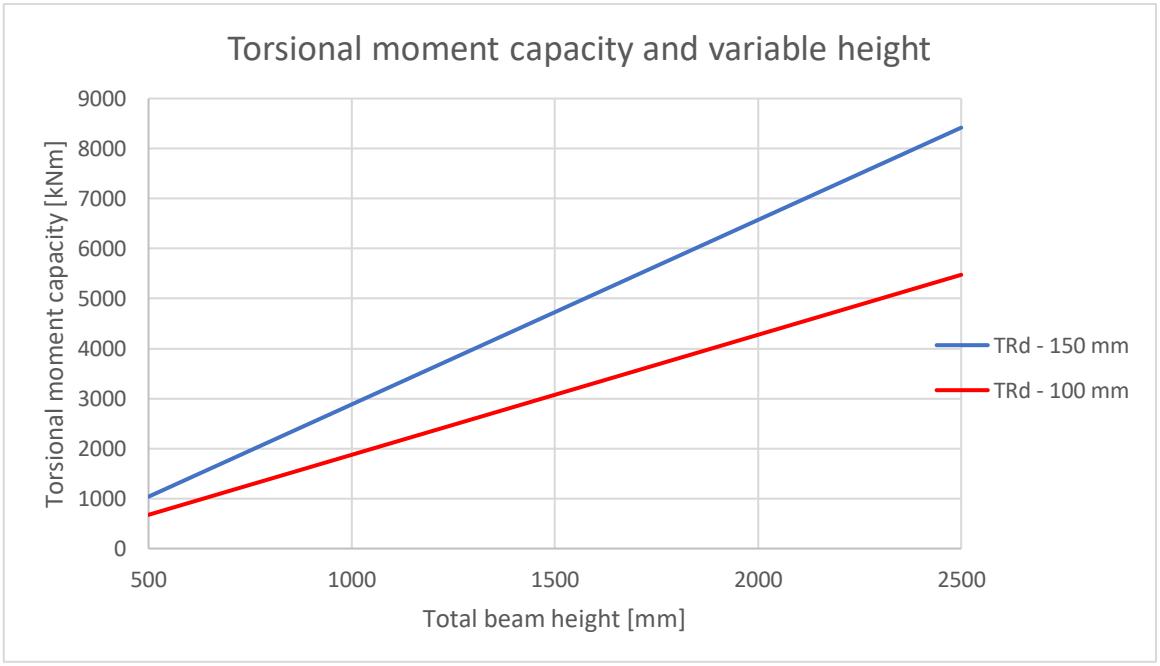


Figure 12 Torsional moment capacity as a function of the beam height

Resistance to combined effect of shear and torsion

Figure 13 gives the capacity to the combined effect of shear and torsion. Again, the same pattern as for shear and torsion can be observed. For the verification the cross section is divided into individual segments, in which case the webs are commonly the governing segments, which explains the large influence of the variation in web thickness.



Figure 13 Capacity under combined effect of shear and torsion as a function of the beam height

3

OPTIMIZATION PHASE

3.1 Approach to calculations of the optimization phase

The optimization of a design is often an iterative process. The following figure gives an overview of the approach to the verifications of the optimization phase. The steps are denoted in black while denoted in green are examples of the required input parameters or the methods used to perform each step.

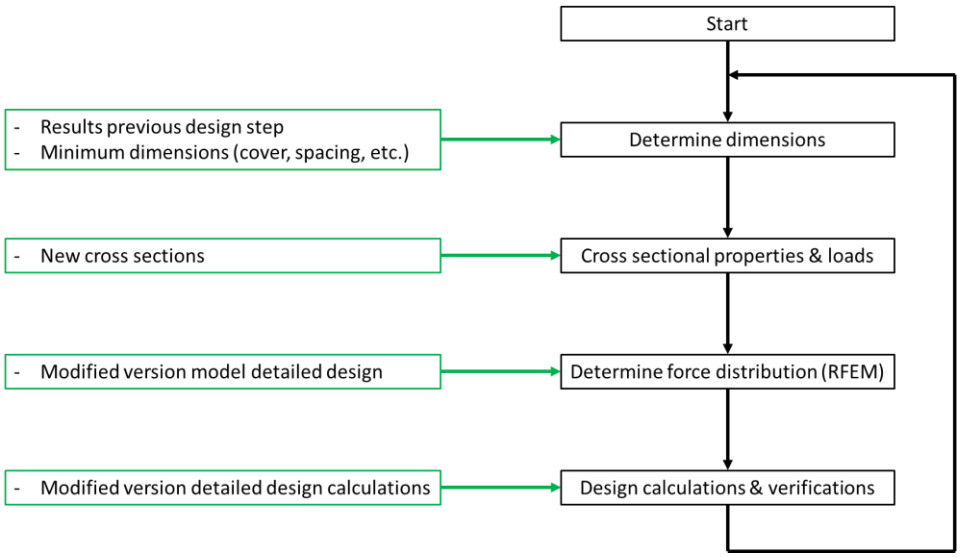


Figure 14 Steps of the verifications in the optimization phase

3.2 Determining dimensions

3.2.1 Determining dimensions

The results of the detailed design have indicated that there is room for optimisation of the design, for example in the form of a reduction of the beam height or thickness of the webs and bottom flanges. In this section new dimensions will be determined to obtain a more optimised design. These dimensions will be based on the following points:

- Results of the detailed design, as discussed in section 1.1.1;
- Minimum dimensions that have been determined in section 2.1;
- Graphs of beam capacity as function of beam height, as given in section 2.2.

Although optimization is up to some point an iterative process, the combination of these different aspects enables a new assumption to be made of the required cross-sectional dimensions in a substantiated way. By subsequently going through the full design procedure, a complete overview of the capacity of the new design with corresponding loads is obtained.

To use the graphs the internal forces obtained from the detailed design are used. The design values of the bending moment, shear force, torsional moment and combined effect of shear and torsion were 29.855 kNm, 4090 kN, 1222 kNm and 2343 kN (occurring in one of the webs), respectively.

3.2.2 Beam height

The first dimension that will be established is the required beam height. When designing prestressed concrete beams, the design is usually first based on the stresses in the serviceability limit state over the cross section. Subsequently the ultimate limit state (ultimate capacity, i.e. capacity at failure) is considered. This approach will be followed here as well.

Stresses in outer fibres: Figure 9 gives the stresses in the outer fibres of the beams for a variable beam height. The permanent loads are made dependent on the beam height, while for the imposed permanent and variable loads the same values are taken as were used in the detailed design. This is reasonable because these loads remain the same in magnitude and also the force distribution is expected to remain more or less the same, because no relative difference between the beams is introduced (different cross sections). It is expected that at most the contribution of redistribution of variable loads will increase slightly, because the stiffness of the single beams will be reduced while the stiffness of the distribution element remains the same as in the detailed design. The bottom fibre is governing. With a maximum tensile strength of 6,7 N/mm^2 the minimum required beam height is approximately 1900 mm.

Bending moment capacity: Figure 10 gives the bending moment capacity. Indeed, it can be seen that the stresses in the cross section are governing over its ultimate capacity. The estimated capacity at 1900 mm height is sufficient for the expected loads and the internal forces caused by these.

3.2.3 Web thickness

The thickness of the web has little effect on the bending moment capacity. However, it is an important parameter for the shear and torsion capacity.

Shear and torsion capacity: Figure 11, Figure 12 and Figure 13 indicate a similar trend although the shear capacity and capacity to the combined effect of shear and torsion are most important, as these are more stringent criteria than the torsional capacity.

The graphs indicate that a height of 1900 mm is sufficient when compared to the internal forces from the detailed design, and the capacity allows for a reduction of the web thickness. Because the loads will be lower than those in the detailed design, it is deemed to be reasonable to reduce the thickness from 150 mm to the minimum value of 100 mm.

3.2.4 Bottom flange

Because the bottom flange has to accommodate a large number of pretensioned strands, a different criterion than the capacity is most stringent: the cover onto and the spacing in between the prestressing strands. Under the assumption that three horizontal rows of strands will be used the minimum required height of the bottom flange can be determined, Figure 15 gives a vertical section of the bottom flange.

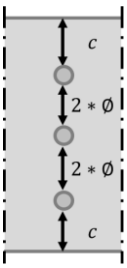


Figure 15 Segment of bottom flange

Note that the possible application of horizontal reinforcement bars because of splitting forces is incorporated in the applied concrete cover 'c'. If conventional cover because of splitting forces with a diameter $\emptyset_r = 10$ mm is applied, then this results in a cover of 40 mm onto the strands. An assumed diameter of the strands of $\emptyset_s = 15{,}2$ mm results in a minimum spacing of $2 * \emptyset_s = 30{,}4$ mm. Based on these assumptions a minimum thickness of the bottom flange is found of:

$$t_{fb,min} = 2 * c + 3 * \emptyset_s + 2 * 2 * \emptyset_s \rightarrow 2 * 40 + 3 * 15{,}2 + 2 * 2 * 15{,}2 = 186{,}4 \text{ mm}$$

This value is rounded off to 200 mm. This is not only a practical value, but it also gives some room to vary with the diameter of the strands or passive reinforcement.

3.2.5 Top flange

The dimensions of the top flange are not changed compared to the detailed design, the reason for this is that based on the results from the detailed design it is expected that no substantial further optimization can be made. The only difference is that an additional eccentricity is given to the transverse prestressing of:

$$\Delta e_{ft} = 0{,}5 * (t_{ft,1} + t_{ft,2}) - 0{,}5 * t_{ft} \rightarrow 125 - 93{,}75 = 31{,}25 \text{ [mm]}$$

This way the centre of the tendon will be positioned at half the height of the actual prestressing rib, instead of the fictitious top flange with height t_{ft}. The reason of positioning the tendon in such a way is to accommodate the anchor of the prestressing tendon, which generally has larger dimensions than the actual tendon. Therefore, additional room has to be created for the positioning of the anchor.

It is expected that keeping the current dimensions of the top flange will have implications for the results from the finite element analysis that will be performed using RFEM. The parameters of the distribution element are based on the top flange, hence its parameters do not change. This is compared to the main beams, of which the stiffness will be reduced. Because of this reason a (limited) increase of distribution of variable loads over the beams is expected to occur.

3.2.6 Summary

The new adopted dimensions are summarized in the following table.

Table 2 New dimensions for optimization phase

Symbol	Value	Units	Definition
w	3200	[mm]	Total width
h	1900	[mm]	Total height
t_{fb}	200	[mm]	Thickness of the bottom flange
t_w	100	[mm]	Thickness of the web
w_f	500	[mm]	Width of the outstand flanges
w_b	2000	[mm]	Internal width of the box

The parameters of the transverse prestressing ribs are as follows.

Table 3 New dimensions for optimization phase – Prestressing ribs

Symbol	Value	Units	Definition
$w_{c.t.c.}$	1000	[mm]	Centre to centre distance of the transverse prestressing ribs/ducts
$t_{ft,1}$	125	[mm]	Continuous thickness of the top flange
$t_{ft,2}$	125	[mm]	Local increase thickness top flange at transverse rib
w_{rib}	250	[mm]	Width of the transverse prestressing rib
w_{ch}	250	[mm]	Width of chamfer next to the transverse prestressing rib

This results in $t_{ft} = 187{,}5$ mm and $h_b = 1512{,}5$ mm.

3.3 Cross sectional properties and loads

With the dimensions established the calculation procedure is carried out. The first step is to determine the cross-sectional properties and loads on the structure after which the force distribution can be calculated using RFEM.

3.3.1 Cross sectional properties

All calculations other than those involving RFEM are carried out using an Excelsheet. The starting point is the Excelsheet of the detailed design, to which a number of changes have been made to make it more suitable for the optimisation (see 3.5.1 for the modifications). The results from the calculation are:

Table 4 Cross sectional properties optimized cross section

Symbol	Value	Units	Definition
A_c	1342500	[mm^2]	Cross sectional area of total cross section
z	844,5	[mm]	Position centre of gravity from the top flange
I_y	8,038E+11	[mm^4]	Second moment of area of the combined cross section
e_t	844,5	[mm]	Distance from centre of gravity to top fibre
e_b	1055,5	[mm]	Distance from centre of gravity to bottom fibre
$W_{y,t}$	9,518E+08	[mm^3]	Section modulus with respect to top fibre
$W_{y,b}$	7,615E+08	[mm^3]	Section modulus with respect to bottom fibre

These values will be used to validate the input of the cross sections in RFEM later on. In addition, the cross section of the cross beams is changed, it is again assumed that these have a rectangular cross section with the height and width equal to the height of the main beams. The results are as follows.

Table 5 Cross sectional properties optimized cross section – End cross beams

Symbol	Value	Units	Definition
A_{cb}	3610000	[mm^2]	Cross sectional area of the cross beam
$W_{y,cb}$	1,143E+09	[mm^3]	Section modulus of the cross section
$I_{y,cb}$	1,086E+12	[mm^4]	Second moment of area of the cross section

3.3.2 Loads

Because of the adjustments made to the dimensions, two load values are changed: the self-weight of the main beams and the self-weight of the end cross beams. The adjusted value for the self-weight of the main beams is:

$$G_{k,beams} = A_c * \gamma_{UHPC} \rightarrow 1{,}34 * 25 = 33{,}56 \text{ kN/m}$$

The adjusted value for the self-weight of the end cross beams is:

$$G_{k,cb} = A_{cb} * \gamma_C \rightarrow 3{,}61 * 25 = 90{,}25 \text{ kN/m}$$

These loads are calculated in the Excelsheet and will be plugged into the RFEM model.

3.4 Determining force distribution

3.4.1 Modifying RFEM model

As a starting point the RFEM model of the detailed design is used. However, various modifications will have to be made in accordance with the changes discussed in the previous sections. The changes made are summarized and listed in this subsection.

- Cross sections and materials:
    - Main beams: The cross section of the main beams (denoted as 'cross section number 1' in the model) is adjusted by replacing the dimensions by those given in 3.2;
    - End cross beams: The cross section of the end cross beams (denoted as 'cross section number 2' in the model) is adjusted by replacing the dimensions by those given in 3.2;
- Load cases and load combinations:
    - Load case 1: Load case 1 resembles the self-weight of the prefab beams, given the modified cross section its value has to be adjusted as well, see 3.3.2;
    - Load case 2: Load case 2 resembles the self-weight of the end cross beams, because of the modified cross section its value has to be adjusted as well, see 3.3.2;
    - Load case 7: Load case 7 includes all permanent loads, and the loads resembling the self-weight of the main beams and end cross beams therefore have to be adjusted.

All other input parameters, loads, load cases and load combinations are kept identical to those used in the model of the detailed design.

3.4.2 Governing forces

The following table gives an overview of the governing cross-sectional forces in the main load bearing elements of the deck. In addition, the values and descriptions belonging to the detailed design are given in grey, this way a comparison can be made as well.

Table 6 Results from RFEM model

ULS verifications of main beams				
Definition	**Symbol**	**Value**	**Units**	**Description**
Governing bending moment value (mid span)	M_{Ed}	41.753 (48.426)	[kNm]	Beam 3, CO3, config. 2, eq. 6.10a and axles at mid-span (Beam 3, CO3, config. 2, eq. 6.10a and axles at mid-span).
Governing shear force value (near supports)	V_{Ed}	3632 (4090)	[kN]	Beam 3, CO10, config 2, eq. 6.10b and axles at support (Beam 3, CO10, config. 2, eq. 6.10b and axles at supports).
Governing torsional moment	T_{Ed}	1268 (1222)	[kNm]	Beam 3, CO13, accidental situation with axles at mid-span (Beam 3 for combination CO13).
Prestressing main beams – Characteristic combination of the SLS				
Definition	**Symbol**	**Value**	**Units**	**Description**
Bending moment imposed permanent loads in SLS at midspan	$M_{E,G,perm}$	1725 (1727)	[kNm]	Value of beam 3 is applied (approximately equal values for all beams, value of beam 3 was applied).
Bending moment variable loads in SLS at midspan	$M_{E,Q}$	9553 (9694)	[kNm]	Governing value is beam 3, which is found for config 2 (Maximum found at beam 3 for configuration 2).
Deflections main beams – Frequent combination of the SLS				
Definition	**Symbol**	**Value**	**Units**	**Description**
Maximum deflection at midspan in the SLS (frequent combination)	δ_{max}	440,9 (344,4)	[mm]	Value of beam 3 is applied, which is found for config 2 (Maximum found at mid span of beam 3 for configuration 2).
Fatigue analysis main beams				

Definition	Symbol	Value	Units	Description
Maximum bending moment at midspan (found using RFEM)	$M_{fat,max}$	26.812 (31.539)	kNm	Value for beam 3 is applied (Value for beam 3 is applied).
Minimum bending moment at midspan (found using RFEM)	$M_{fat,min}$	22.543 (27.183)	kNm	Value for beam 3 is applied (Value for beam 3 is applied).
ULS verification end cross beams				
Definition	**Symbol**	**Value**	**Units**	**Description**
Maximum hogging bending moment (all loads considered)	$M_{Ed,hog}$	1271 (1212)	[kNm]	Support of beam 1, found for CO13 with axle loads at mid-span (Support of beam 1 for CO13).
Maximum sagging bending moment (all loads considered)	$M_{Ed,sag}$	396 (436)	[kNm]	Span between supports of beams 3 and 4, for CO8 (span between supports of beams 3 and 4, for CO8).
Maximum shear force (all loads considered)	V_{Ed}	846 (837)	[kN]	Support of beam 1, found for CO14 with axle loads near supports (At support of beam 1 for CO14).
Prestressing end cross beams – Characteristic combination of the SLS				
Definition	**Symbol**	**Value**	**Units**	**Description**
Maximum hogging bending moment SLS	$M_{E,hog}$	453 (469)	[kNm]	Support of beam 3, found for CO27 (Found at support of beam 3 for CO24).
Maximum sagging bending moment SLS	$M_{E,sag}$	270 (298)	[kNm]	Span between supports of beams 3 and 4, for CO27 (Found at span between supports of beams 3 and 4 for CO27).

The expectation was that compared to the detailed design most of the internal forces would be reduced because of the reduction of the self-weight. In addition, an increase of the deflection was expected because the modification of the cross section also resulted in a reduction of the second moment of area, and thus of the bending stiffness if the modulus of elasticity stays constant. Some of the main features of the results are:

- **ULS main beams**: The design values of the bending moment, shear force and torsional moment occur at the same locations as for the detailed design. It should be noted that for the torsion beam number 2 has a larger value of 1531 kNm, however this is combined with a lower shear force of 2782 kN (instead of 3632 kN for beam 3), which makes that beam 3 still governing over beam 2;

- **Prestressing design**: The characteristic values to be used for the design of the main prestressing also follow the same pattern. As expected, (permanent loads are not changed) the bending moment due to imposed permanent loads is approximately equal to the detailed design. Note that these values are almost equal for all beams, but the value for beam 3 has been selected. For the bending moment due to the variable loads the difference is more predominant;

- **Deflection**: The maximum value of the deflection is found at beam 3 for load configuration 2, as was the case for the detailed design. The deflection has increased though, due to the reduction in bending stiffness;

- **Fatigue**: The largest difference between both load cases was found for beam 3. It can be observed that the bending moments for the load combinations for fatigue are smaller compared to those of the detailed design, this is explained by the reduction of the self-weight.

Another expectation was that because the self-weight of the structure reduced, the effect of the variable loads to the force distribution relative to the effect of the self-weight would increase, which perhaps would cause other load combinations to become governing over those that were governing in the detailed design.

- **ULS end beams**: The design values of the bending moments and shear force are found at the same locations, although a different load combination was found to be governing for the hogging bending moment; CO27 became governing over CO24, although the magnitude of the results of both combinations at this location are close. The hogging bending moment increased while the sagging bending moment and shear force decreased. These effects are attributable to the modifications made to the design.

- **Prestressing design**: Both bending moment values are reduced compared to the detailed design, which was to be expected. A different load combination became governing for the hogging bending moment. Further inspection of the results indicated that for the detailed design the hogging bending moment was at the same point and the values for CO24 and CO27 were already close. For the optimized design the differences are more predominant due to the reduction of the self-weight, but still relatively small.

3.5 Design verification

3.5.1 Approach

Design verifications Excel

With the internal forces obtained using RFEM, the design verifications can be performed using Excel. The setup of the calculation is identical to that of the detailed design, except for the following modifications that have been made:

- It is made possible to exclude centric prestressing;

- The position of the tendons of the transverse prestressing is made variable instead of being fixed at $0{,}5 * t_{ft}$;

- The concrete cover onto the passive (splitting) reinforcement at the anchorage zone is included;

- For the top flange the option is added to provide an additional eccentricity to the transverse prestressing, and the verification of the bending moment capacity of the top flange has been modified accordingly;

- The top flange is no longer modelled as a beam with equivalent rectangular cross section, but using the actual dimensions of the top flange with variable width.

These modifications allow for the investigation of different options for optimization and/or for a more accurate analysis. An overview of all verifications that are performed using the Excelsheet can be found in annex I.

3.5.2 Results of calculation

Overview of the results

The calculations are performed using Excel. For the full elaboration of these calculations reference is made to annex II. The results of the main verifications (unity checks) are summarized in the following table.

Table 7 Results calculations optimization phase – Set I

Verification	Element	Unity check
Bending moment capacity	Main beams (global)	0,75
Shear force capacity	Main beams (global)	0,84
Torsional moment capacity	Main beams (global)	0,29
Combination shear and torsion	Main beams (global)	0,93
Combination shear and torsion – Compressive strut	Main beams (global)	0,65

Ship collision – Static equilibrium	Whole deck (global)	0,17
Bending moment capacity joint	Longitudinal joints (local)	0,04
Top flange transverse - Sagging moment	Top flange (local)	0,45
Top flange transverse - Hogging moment	Top flange (local)	0,82
Bending moment capacity longitudinal direction	Top flange (local)	0,83
Fatigue verification – Prestressing steel	Main beams (global)	0,18
Fatigue verification – Concrete at top fibre	Main beams (global)	≈0
Fatigue verification – Concrete at bottom fibre	Main beams (global)	≈0
Deflection	Main beams (global)	0,52
Bending moment capacity	End cross beams (global)	0,23
Shear force capacity	End cross beams (global)	0,60

Important are also the stresses over the height of the cross section at mid span. As it turns out the maximum tensile stress at the bottom fibre for $t \rightarrow \infty$ is 3,0 N/mm^2.

Another result of importance but not given in the table is the stress criterion of the longitudinal joint. This is the only verification that is not satisfied, making it the governing criterion at this point. The maximum tensile stress of 0 N/mm^2 in the longitudinal joint is exceeded, the maximum occurring value is 4,16 N/mm^2.

Study of the results

The first condition is the stress verification of the main beams at mid span. The tensile stress in the most unfavourable situation (full loading and $t \rightarrow \infty$) is 3,0 N/mm^2, which is below the maximum allowable tensile strength and leaves some margin to reduce the prestressing force. The performed global ULS and SLS verifications confirm that the ultimate capacity and fatigue capacity of the beam are also sufficient.

The governing criterion turns out to be related to the top flange, which includes various local verifications and it turns out that the stress criterion of the longitudinal joint is not satisfied. This indicates that measures are to be taken. The prestressing force with its eccentric positioning does not result in a longitudinal joint under compression.

The other verifications are all satisfied. The deflection is within limits and the capacity of the end cross beams also suffices, indicating that the cross-sectional dimensions of the main beams are sufficient to restrain the forces.

3.5.3 Further modifications to the design

Adjustments have to be made to satisfy all included verifications. In addition, modifications can or have to be made to satisfy requirements that are not part of the verification sheet, such as the maximum number of pretensioned strands because this is a boundary condition from practice. In addition, reduction of transverse prestressing results in a more economical solution. These points are considered in the second set of verifications, which can be found in annex III.

Prestressing strands

One of the conclusions of the detailed design was that the number of prestressing strands would have to be reduced. Although the number of strands influence various criteria, the dominant criterion is the stress at mid span of the beam in use phase for $t \rightarrow \infty$. The starting point is that the number of centric strands is kept equal while the eccentric strands will be reduced in number. This is to keep the tensile stresses at the top fibres near the beam ends limited.

The initial number of strands is 120, which results in a tensile stress of 3,0 N/mm^2 in the bottom fibre. The maximum stress at stressing $\sigma_{max,fb} = 1450$ N/mm^2;

- A reduction of the number of strands to 108 results in a tensile stress of 6,2 N/mm^2 and gives the practical number of 36 strands per row. This is the minimum number of strands if all other parameters are kept equal;

- The stresses in the eccentric strands are increased, it turns out to be possible to increase the stresses to the maximum value of $\sigma_{max,fb} = 1488$ N/mm^2. With 108 strands this results in a stress of 5,4 N/mm^2. This indicates that the number of strands can be decreased further;

- A number of 105 strands with this maximum stress results in a stress at the bottom fibre of 6,2 N/mm^2, this is deemed to be a satisfactory result. This results in the practical number of 35 strands per row.

The number of strands in the webs are not changed. However, it turns out that the maximum stress in the strands can be increased slightly up to $\sigma_{max,c} = 1400$ N/mm^2.

Top flange

The results of the calculations indicate that with the initial input parameters one of the verifications is not satisfied: the stress criterion of the longitudinal joint. Tensile stresses occur at the top fibre of the joint in the case no variable loads are present. The cause for this is that the additional eccentricity of the prestressing force causes an upward bending moment, not compensated for by the downward bending moment of the traffic loads.

The initial value of the additional eccentricity is $\Delta e_{ft} = 32{,}5$ mm, this way the tendon is positioned at half the height of the prestressing rib. It turns out that it is the eccentricity that results in the tensile stresses. To accommodate prestressing anchors, it is positive if a certain eccentricity can be kept though, because this was the sole reason of introducing the eccentricity.

Trial and error results in a value $\Delta e_{ft} = 8{,}0$ mm. In this case the joint is kept just under compression (stress of -0,01 N/mm^2 at top fibre) and even allows the number of strands in the tendon to be reduced from 5 to 4 strands. The latter is profitable, as it reduces splitting forces and anchor forces as well. With these modifications the ULS verifications of the top flange in transverse direction are still satisfied with all other parameters kept constant.

Note that the reason to introduce an additional eccentricity Δe_{ft} was to create room to position prestressing anchors, this means that the eccentricity can be reduced provided that sufficient room is provided to position such anchors. The example of the anchor in section 2.1.1 suggest that the current positioning is likely to be sufficient. In addition, all calculations of the joint are based on two assumptions: one is the use of the mean value t_{ft} of the thickness and the second is an outstand part of the prefab beam of 25 mm. In practice changes can be made to this, thus leaving room for further detailing of the joint design.

Fatigue of concrete

A final additional check is the fatigue of concrete, because only concrete in compression is included while AFGC-SETRA 2013 makes extra remarks on concrete in tension. At the bottom fibre the highest stress (the lowest compressive stress) turns out to be tensile with a value of 1,1 N/mm^2. This occurs in case both permanent and variable loads are considered.

The AFGC-SETRA 2013 guideline prescribes that for elements subjected to fatigue and that are loaded in tension under service conditions in persistent design situations, the tensile stress should be limited to $\sigma_{max} = \min\{f_{ctm,el}; f_{ctfm}\}$. Given the tensile stress limit for the design of the prestressing, which is more stringent than the tensile stress limit for fatigue, this criterion has implicitly already been satisfied and results in a unity check of 0,16.

End cross beam

Although not further discussed in this report, calculation results indicate that smaller prestressing tendons are sufficient. The number of strands per tendon are reduced from 7 to 4.

Buckling of webs

The optimization results in a significant reduction of the thickness of the webs, resulting in very slender elements. As a result of this reduction of the dimensions the risk increases that instability phenomena occur that are generally not expected to be governing for more conventional structures: local buckling or plate buckling of the webs.

Verifications for these phenomena have not been included because these are generally not expected to be governing for concrete structures. However, given the significant slenderness of the webs these are worth being mentioned and in practice these verifications should be included as part of the design if the bridge would be constructed.

If it turns out that measures are required, then this will involve extensive detailing, for example by providing stiffeners, but such detailing aspects can be solved well in practice. This could also be combined with the function of the reinforcing elements for ship collision. At the same time, it is expected that such a solution would have a negligible effect on the results of the project, because stiffeners would result only in a limited increase of the self-weight of the structure, especially if this function is combined with that of the reinforcing diaphragm elements for ship collision.

3.6 Final result

3.6.1 Results optimized design

With the current design a significant difference in self-weight has been achieved compared to the existing bridge. Given the results of the calculations it is expected that with the current type of design and design approach no further significant reduction of weight will be achieved. This is exemplified by the tensile stress under service conditions, which is 6,2 N/mm^2. Table 8 gives an overview of all unity checks.

Table 8 Results calculations optimization phase – Set II (final design)

Verification	**Element**	**Unity check**
Bending moment capacity	Main beams (global)	0,90
Shear force capacity	Main beams (global)	0,84
Torsional moment capacity	Main beams (global)	0,29
Combination shear and torsion	Main beams (global)	0,93
Combination shear and torsion – Compressive strut	Main beams (global)	0,65
Ship collision – Static equilibrium	Whole deck (global)	0,17
Bending moment capacity joint	Longitudinal joints (local)	0,38
Top flange transverse - Sagging moment	Top flange (local)	0,81
Top flange transverse - Hogging moment	Top flange (local)	0,76
Bending moment capacity longitudinal direction	Top flange (local)	0,83
Fatigue verification – Prestressing steel	Main beams (global)	0,18
Fatigue verification – Concrete at top fibre	Main beams (global)	≈0
Fatigue verification – Concrete at bottom fibre	Main beams (global)	0,16
Deflection	Main beams (global)	0,65
Bending moment capacity	End cross beams (global)	0,38
Shear force capacity	End cross beams (global)	0,72

3.6.2 Options for further analysis

These results indicate that there is very limited room for further weight reduction if the current design approach is used. If a substantial further weight reduction is to be achieved, then a different approach should be applied, such as the second and third option from 1.1.3.

4

FINAL DESIGN

4.1 Final design

This chapter summarizes the properties of the 'final design', i.e. the design that resulted from the optimization phase. Reference is also made to annex IV, which is the drawing of the final design, and to annex III, which contains all verifications and input parameters.

4.1.1 Global geometry

The deck comprises five beams, each with a span l of 68,0 and a length l_{tot} of 70,70 m. The total width w_{tot} of the deck is 16,36 m. These dimensions are based on the existing bridge deck. The following figure gives a part of the cross section of the deck.

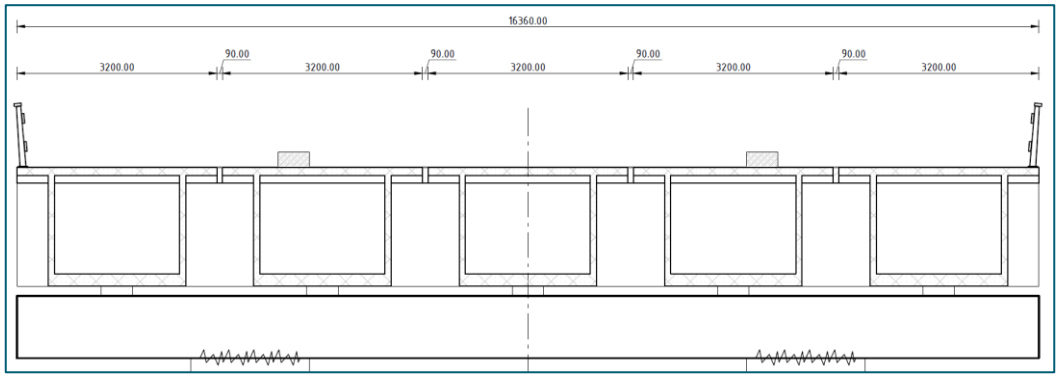


Figure 16 Optimized cross section of the deck

4.1.2 Main beams

Dimensions of the main beams

The following figure gives a cross section of the main beams:

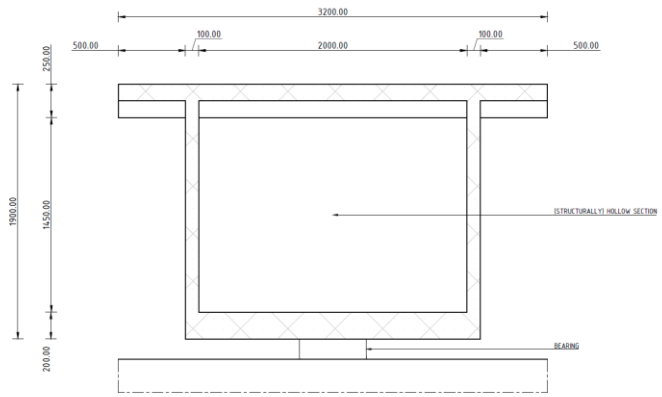


Figure 17 Optimized cross section main beams

The dimensions of the main beams are summarized in the following table.

Table 9 Properties of optimized main beams

Symbol	Value	Units	Definition
w	3200	[mm]	Total width
h	1900	[mm]	Total height
t_{fb}	200	[mm]	Thickness bottom flange
t_w	100	[mm]	Thickness of web
w_f	500	[mm]	Width of the flanges
w_b	2000	[mm]	Internal width of the box
$w_{c.t.c.}$	1000	[mm]	Centre to centre distance of the transverse prestressing ribs/ducts
$t_{ft,1}$	125	[mm]	Continuous thickness of the top flange
$t_{ft,2}$	125	[mm]	Local increase thickness top flange at transverse rib
w_{rib}	250	[mm]	Width of the transverse prestressing rib
w_{ch}	250	[mm]	Width of chamfer next to the transverse prestressing rib
Δe_{ft}	8,0	[mm]	Additional eccentricity transverse prestressing

This results in $t_{ft} = 187{,}5$ mm and $h_b = 1512{,}5$ mm. The beams have solid end sections at the location where the in-situ concrete will be casted to create the end cross beams.

Details of the prestressing

Pretensioned strands: The main beams are prestressed in longitudinal direction using both centric and eccentric pretensioned strands with a diameter of 15,2 mm. The following table gives the main features of the main prestressing.

Table 10 Parameters pretensioned prestressing

n_c	10	[pcs]	Assumed number of strands positioned centrically in cross section
$\sigma_{p,max,prov,c}$	1400	[mm^2]	Assumed maximum stress applied to centrically positioned strands
n_{fb}	105	[pcs]	Assumed number of strands positioned in bottom flange
$\sigma_{p,max,prov,fb}$	1488	[mm^2]	Assumed maximum stress applied to strands in bottom flange

Transverse prestressing: The top flange is post-tensioned in transverse direction using tendons positioned in the prestressing ribs, these tendons are made up of several 7-wire strands Ø15,2. The main features of these tendons are given in the following table.

Table 11 Parameters tendons prestressing top flange

n	4	[pcs]	Assumed number of strands per tendon
$\sigma_{p,max,prov}$	1400	[N/mm^2]	Assumed maximum stress applied to prestressing element
μ	0,23	[-]	Friction coefficient
k	0,009	[rad]	Unintentional angular rotation due to the Wobble-effect
w_{set}	3	[mm]	Estimated wedge set

For a complete overview of properties reference is made to annex III.

Key figures prefab UHPC beams

From the calculation the following key results are obtained:

- Total number of pretensioned strands: 115 [pcs]
- Total volume of UHPC: 106,4 [m^3]
- Weight of a single prefab beam (including solid beam ends): 2660 [kN]

4.1.3 End cross beams

The end cross beams are beams with a rectangular cross section of 1900 mm high and 1900 mm wide, these are constructed by casting in situ concrete segments in between the solid end sections of the prefab UHPC beams. The beams are post-tensioned after sufficient hardening to create solid end beams, the position of the prestressing elements is as follows:

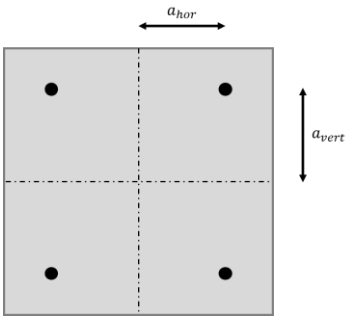


Figure 18 Position of the prestressing ducts in the end cross beams

A total of four tendons is used with their centre of gravity coinciding with that of the end cross beam. The tendons are made up of several 7-wire strands Ø15,2. The main parameters are given in the following table.

Table 12 Parameters tendons prestressing end cross beams

n_{ducts}	4	[pcs]	Number of ducts in total
a_{vert}	500	[mm]	Vertical position centre of duct from centre of beam
a_{hor}	750	[mm]	Horizontal position centre of duct from centre of beam
n_{strand}	4	[pcs]	Assumed number of strands per tendon
$\sigma_{p,max,prov}$	1400	[N/mm^2]	Assumed maximum stress applied to prestressing element

For all details and parameters reference is made to annex III.

4.1.4 Capping beam

For the capping beam the same assumed dimensions are used as those in the preliminary design and detailed design. The length is set to 16,36 m, the height is set to 1,0 m and the width is taken equal to 0,75 m. The beam is assumed to be made of prestressed concrete, with a volumetric weight of 25 kN/m^3.

4.1.5 Self-weight of the deck

Table 13 summarizes the results of the weight calculation for the optimized deck. Reference is made to 6.1 and annex V for the elaboration of the calculation.

Table 13 Results weight calculation optimized design

	Final design
Element	[kN]
Prefab UHPC beams	11.864
Solid ends prefab UHPC beams	1437
In-situ cross beams	878
In-situ UHPC joints	119
Surface layer	266
Kerbs	601
Capping beams	614
Total	15.779

5

APPROACH TO GLOBAL ANALYSIS OF THE FOUNDATION

5.1 Approach to global analysis of the foundation

5.1.1 Relation to the project goal

The previous chapters of this report covered the optimization phase and final design, which concludes the design stage of the project. With the different design stages finished, it has to be judged whether the weight reduction which has been achieved with the optimized design is sufficient to meet the project goal, which is:

''To design an ultra-high performance concrete bridge deck for the existing bridges across the Twentekanaal, in such a way that the existing foundations can be reused with only limited modifications.''

The most accurate way of determining whether the existing foundation can be reused is to set up a full analysis of the existing foundation. However, as written in the work plan of the project the focus was placed on the superstructure and a full analysis of the foundation is outside the project scope, only a global analysis of the foundation is carried out. This analysis will comprise a comparison of the vertical loads on the foundation between the new situation (final design) and existing situation (the current bridge). In the remainder of this chapter a clear verification criterion will be defined, after which this will be elaborated on in the remaining chapters of the report. This way all information required to draw conclusions in the main report will be collected.

5.1.2 Verification criteria

Initial verification criterion

Because a full analysis of the foundation is excluded from the project scope, it has to be resorted to a more global analysis which will have to be sufficient to be able to draw a conclusion. The initial criterion as presented in the workplan of the project the global assessment of the existing foundation makes use of a comparison of the vertical loads on the foundation in both the new situation and existing situation. Note that in reality both the vertical and horizontal variable loads are higher according to current codes than according to older codes. However, these horizontal forces are excluded from the scope of the project because strengthening measures for increased horizontal variable loads can be taken in more practically applicable ways compared to those to strengthen for increased vertical variable loads.

The forces in the new situation due to the permanent and vertical variable actions should be smaller than or equal to the permanent and vertical variable actions from the design of the existing bridge. Under the assumption that the codes used for the design of the existing structure followed a similar approach with regard to structural reliability as the Eurocode does, and including load factors in the comparison, this criterion may be written as follows:

$$\gamma_{G,N} * G_N + \gamma_{Q,N} * Q_N \leq \gamma_{G,E} * G_E + \gamma_{Q,E} * Q_E \qquad \text{Equation (1)}$$

Where:
$\gamma_{G,N}$: Load factor permanent actions new bridge design
$\gamma_{Q,N}$: Load factor variable actions new bridge design
$\gamma_{G,E}$: Load factor permanent actions existing bridge
$\gamma_{Q,E}$: Load factor variable actions existing bridge

The symbols G_N and G_E represent the vertical actions due to permanent loads in the new design and existing situation, respectively. These values will be based on the final design as discussed in chapter 4 and the design drawings of the existing bridge as provided by Rijkswaterstaat. The symbols Q_N and Q_E represent the vertical variable actions in the new design and the existing situation, respectively. The value Q_N is determined in accordance with the Eurocode, while the value of Q_E will have to be determined in accordance with the codes used for the design of the existing bridge.

Finally, the load factors have to be determined as well to account for the different 'safety margins' that have been used in the designs. The values of the new design are those determined in accordance with the Eurocode, while those of the existing structure will have to be taken from the code used for the design of the existing structure. In 5.2 the codes used for the design of the existing bridge will be identified and briefly discussed.

By using this approach, the right-hand side of equation (1) represents the design value of the vertical forces the foundation of the existing bridge should theoretically be designed for. If the design value of these forces will be smaller in the new situation, then theoretically the capacity of the foundation should be sufficient for reuse under the actions considered in the comparison.

5.2 Codes and guidelines existing structure

5.2.1 Former design codes

Importance of former codes for the project

To be able to follow the strategy as outlined in 5.1 it has to be known which codes were used for the design of the existing bridge. This way the vertical variable loads and load factors can be established. The remainder of this chapter is dedicated to the search for and a brief discussion of these formerly used codes.

TGB 1949

Given the year of construction of the bridge it is estimated that the design work for the Eefdesebrug must have taken place in the period 1950 – 1955. During this period the basis of the structural design of most structures was outlined in N 1055, which was also referred to as TGB 1949 (Technische Grondslagen voor Bouwvoorschriften). This code was published in 1949 and a second reviewed version was published in 1955.

The TGB 1949 covered general aspects such as loads and stress limits for various materials such as steel, timber and stone and deflections. However, provisions for concrete were not given. Already in the preface it is mentioned that the committee responsible for the TGB 1949 did not include the design of reinforced concrete structures, because this was part of the task of the reinforced-concrete committee.

Former codes on reinforced concrete

Because the TGB 1949 does not give the required information the discussion of the former codes continues with a search for codes on reinforced concrete. The first Dutch code on reinforced concrete was published in 1912, with a new code being published almost every decade until the introduction of Eurocode 2. The following table, based on information given in (Gijsbers, 2012), gives an overview of all codes on reinforced (or: structural) concrete since the introduction of the first code in 1912.

Table 14 Overview of codes on reinforced/structural concrete in The Netherlands

Year	Title of the code	Denoted as:
1912	Gewapend Beton Voorschriften	GBV 1912
1918	Gewapend Beton Voorschriften	GBV 1918
1930	Gewapend Beton Voorschriften	GBV 1930
1940	Gewapend Beton Voorschriften	GBV 1940
1950	Gewapend Beton Voorschriften	GBV 1950
1962	Gewapend Beton Voorschriften	GBV 1962
1974	Voorschriften Beton	VB 1974
1984	NEN 3880 – Voorschriften Beton	VB 1974/1984

1990	NEN 6720 – Voorschriften Beton	VBC 1990
1995	NEN 6720 – Voorschriften Beton	VBC 1995
2012	Eurocode 2: Ontwerp en berekening van betonconstructies	NEN-EN 1992

Based on the estimated year of design, it is most likely that the GBV 1950 was used for the design of the Eefdesebrug. This code will therefore briefly be described in 5.2.2.

5.2.2 Gewapend Beton Voorschriften 1950 (GBV 1950)

Content of the code

The GBV 1950 was adopted in 1950, it was published by the predecessor of NEN (Hoofdcommissie voor de Normalisatie in Nederland) while writing the actual content of the document was the task of the committee for structural concrete (gewapende-betoncommissie), which was part of KIVI (Koninklijk Instituut van Ingenieurs). The code was a revision and extension of the previous code, the GBV 1940, and contained the addition of a new topic (flat slabs). The code consists of the following eight sections:

- Section 1: General provisions
- Section 2: Materials
- Section 3: Execution and construction
- Section 4: Design calculations
- Section 5: Allowable stresses
- Section 6: Control of the construction
- Section 7: Deviations from the code
- Section 8: Flat slabs

Relation to other codes

The GBV 1950 contains various references to other codes and as such it cannot be used as a standalone document. With regard to this project the codes required to determine the actions due to variable loads on bridges are most important.

In article 28-d of section 4 of the GBV 1950 provisions are given to determine actions on concrete structures, in essence the provisions for steel structures are used because the GBV 1950 prescribes that the actions on the structure should be determined in accordance with the first chapter of N 1055 (TGB 1949). In addition the GBV 1950 adds a small number of provisions specifically for actions on concrete structures. Traffic loads are determined in accordance with the 'Voorschriften voor het Ontwerpen van Stalen Bruggen', see 5.2.3, a reference which was also found on the design drawings of the existing bridge.

5.2.3 Voorschriften voor het Ontwerpen van Stalen Bruggen 1938 (VOSB 1938)

On one of the design drawings of the existing bridge provided by Rijkswaterstaat it is mentioned that the variable loads used in the design were in accordance with 'class A' of the VOSB (Voorschriften voor het Ontwerpen van Stalen Bruggen). This was a former Dutch code on the design of steel bridges. It was revised multiple times and different versions have been used:

- N 1008 – V.O.S.B. 1933
- N 1008 – V.O.S.B. 1938
- N 1008 – V.O.S.B. 1963

Given the year of construction of the Eefdesebrug the version of 1938 was most probably used. Because no original design calculations have been found, the relevant articles of the VOSB 1938 will have to be interpreted and applied to determine the vertical loads in accordance with this code, see section 6.2.2.

6

COMPARISON OF THE DESIGNS – DETERMINING LOADS AND FACTORS

6.1 Self-weight of the structures

6.1.1 Self-weight optimized design

The self-weight of the optimized design is calculated by decomposing the deck into various components after which the individual results are added up. Symbols and notations as used in the verifications of the new design are kept as much as possible, and clarified if otherwise.

Component 1 – Prefab UHPC beams
The weight of the prefab beams is calculated by multiplying the total length of the deck l_{tot} with the cross section A_c of the main beams, the number of beams n_{beams} and weight of the UHPC γ_{UHPC}.

$$W_1 = l_{tot} * A_c * n_{beams} * \gamma_{UHPC}$$

Note that this calculation is based on a cross section calculated using the mean value of the thickness of the top flange, t_{ft}, and that the calculation is based on a hollow beam. The solid beam end is a separate component in the calculation.

Component 2 – Solid ends prefab UHPC beams
The solid beam ends are calculated using the internal width w_b and height h_b of the box, the width w_{cb} of the end cross beam and the weight γ_{UHPC} of the UHPC. The weight is calculated as follows:

$$W_2 = w_{cb} * h_b * w_b * 2 * n_{beams} * \gamma_{UHPC}$$

Together with the dimensions of the prefab UHPC beams under the first component a solid beam end is obtained with total dimensions h_{cb} by w_{cb}.

Component 3 – In-situ cross beams
In-situ concrete is applied in between the solid sections of the prefab beams to create solid end beams that can subsequently be prestressed. The weight of the in-situ concrete is calculated as follows: first the volume is calculated assuming solid beams with cross-sectional dimensions w_{cb} by h_{cb} over the full width of the deck after which the volume of the cross section of the prefab beams and the solid ends of these beams are subtracted. The remaining volume is multiplied by a factor '2' (because two end cross beams are constructed) and by the weight of concrete.

$$W_3 = [w_{cb} * h_{cb} * w_{tot} - A_c * w_{cb} * n_{beams} - w_{cb} * h_b * w_b * n_{beams}] * 2 * \gamma_c$$

Component 4 – In-situ UHPC joints
The weight of the joints is calculated by considering the mean value t_{ft} for the thickness of the top flange, the width w_j of the joints, the total length l_{tot} of the deck, the number of joints $(n_{beams} - 1)$ and the weight γ_{UHPC} of UHPC:

$$W_4 = l_{tot} * t_{ft} * w_j * (n_{beams} - 1) * \gamma_{UHPC}$$

Note that the weight of the joints is calculated by assuming that these are solid and have total height of t_{ft}, this way the notches on which the in-situ concrete is casted are included in the calculation as well.

Component 5 – Surface layer

A thin asphalt (surfacing) layer is assumed to be present on the deck. Its contribution is calculated by assuming that the total area of the deck is covered by a thin layer with thickness $t_{asphalt}$ and a specific weight $\gamma_{asphalt}$ of asphalt:

$$W_5 = l_{tot} * w_{tot} * t_{asphalt} * \gamma_{asphalt}$$

Component 6 – Kerbs

The kerbs are accounted for by multiplying the full length l_{tot} of the deck with the cross section and specific weight of the kerbs. Note the factor '2' because two kerbs are present:

$$W_6 = l_{tot} * w_{kerb} * h_{kerb} * 2 * \gamma_c$$

Component 7 – Capping beams

Following the assumed dimensions from the preliminary and detailed design, the weight of the two capping beams is calculated as follows:

$$W_7 = w_{tot} * w_{cap} * h_{cap} * 2 * \gamma_c$$

Total weight

The total weight is determined by adding up all previously mentioned components:

$$W_n = \sum_{i=1}^{7} W_i$$

Weight of single beam

Using the aforementioned equations, the weight of a single prefab beam can be calculated as follows:

$$W_{beam} = \frac{W_1 + W_2}{n_{beams}}$$

6.1.2 Self-weight existing arch bridge

In this section the self-weight of the existing bridge is calculated. Although this calculation has already been performed for the weight comparisons part of the preliminary and detailed design, these estimations were quite rough. Therefore, this calculation is repeated in a more accurate way, this might result in additional or different values compared to those in the previous calculations. Figure 19 gives an overview of the different components that will be considered.

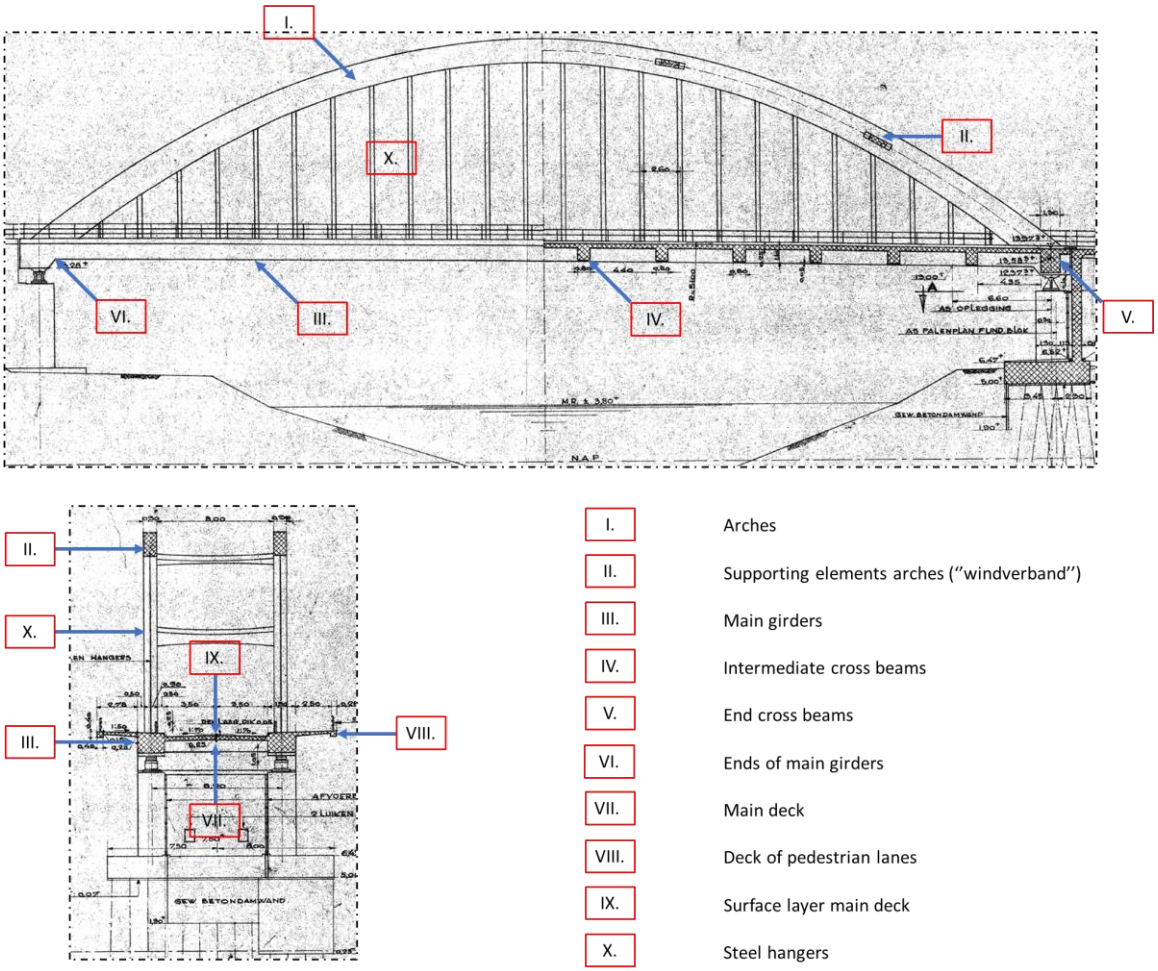


Figure 19 Components considered for weight calculation existing bridge – Part of drawing B.3806 (from Rijkswaterstaat archives)

As a part of the calculation values have to be assumed for the specific weight of the different materials that were applied. The following assumptions are made:

- Reinforced concrete: $\gamma_c = 25$ kN/m^3
- Asphalt: $\gamma_a = 23$ kN/m^3
- Steel: $\gamma_s = 78{,}5$ kN/m^3

In the following sections all aforementioned components will be covered. First the reference documents are mentioned based on which the dimensions are estimated. Subsequently the dimensions are established based on these sources, after which equations are given to calculate the contribution of the component under consideration to the total self-weight of the structure.

Component I – Arches

The first component of the calculation are the two concrete arches of the bridge.

References component I: Dimensions are established based on the AutoCAD drawing of the existing structure and drawings B.5109 (overview of the structure), B.7167 (supporting structure arches), B.7126 & B.7127 (extension pieces of the arch) and B.3622.

Dimensions component I: Based on B.3622 and B.5109 it can be seen that the width of the arches is 0,9 m and is constant over the span. The height however varies from 1,60 at the crest of the arch (midspan) towards approximately 2,0 m near the supports. Based on the drawing of the arches the average height along the arch length is approximated to be 1,7 m.

The arch length is determined based on drawings of the supporting structure and extension pieces from where the arches were built (B.7126 and B.7127). The arch is estimated to be 72,5 m along its centre line. By measuring the centreline of the arch in the AutoCAD drawing (75 m starting from the intersection of the arch and the centre of the main girders) and drawing B.3622 this is deemed to be a sufficiently accurate value. The estimated dimensions used for the calculation are:

- $l_I = 72{,}5$ m
- $h_I = 1{,}7$ m
- $w_I = 0{,}9$ m
- $n_I = 2$ pcs

Weight calculation component I: The weight contribution of the arches is calculated as follows:

$$W_I = l_I * h_I * w_I * n_I * \gamma_c$$

Component II – Supporting elements arches (''windverband'')

The second component of the calculation comprises the four reinforced concrete support elements between the arches.

References component II: References used are the drawings B.3622 and B.7166.

Dimensions component II: Figure 20 presents the top view of one of the elements, note that in the drawing the dimensions are given in cm.

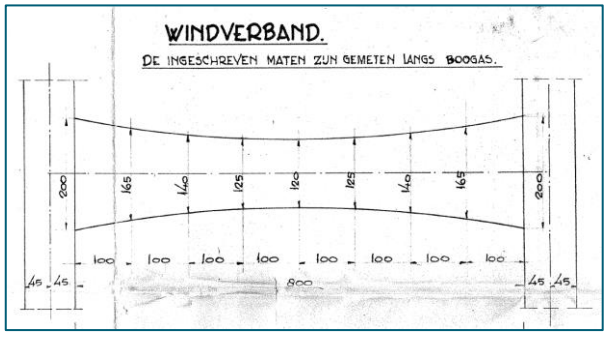


Figure 20 Detail ''windverband'' – Part of drawing B.3622 (from Rijkswaterstaat archives)

The length of the elements is 8,0 m, which is the distance measured in between the arches. The thickness of the elements is constant and is 0,36 m. The width varies from 2,0 at the arches to 1,2 m in the middle and therefore the average is used of 1,6 m. This results in:

- $l_{II} = 8{,}0$ m
- $h_{II} = 0{,}36$ m
- $w_{II} = 1{,}6$ m
- $n_{II} = 4$ pcs

Weight calculation component II: The weight of the elements is approximated as follows:

$$W_{II} = l_{II} * h_{II} * w_{II} * n_{II} * \gamma_c$$

Component III – Main girders

The third component are the two main girders, which form the arch girders together with the concrete arches and steel hangers.

References component III: Dimensions of the main girders are determined using drawings B.3622, B.5109 and B.7125.

Dimensions component III: Based on the three aforementioned drawings, the total length of the main girders is determined to be 70,7 m. Figure 21 gives a part of a cross section of the deck (part of drawing B.7125) and is used to determine the dimensions of the cross section.

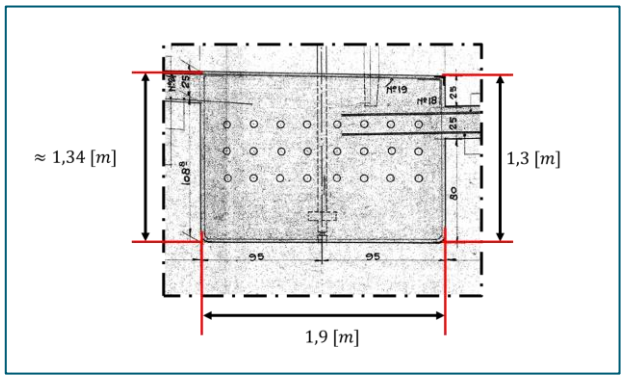


Figure 21 Dimensions of main girders – Part of drawing B.7125 (from Rijkswaterstaat archives)

It can be seen that the width of the girder is 1,9 m while the height is variable due to the 1:50 slope given to the top of the girder and adjacent outstand deck of the pedestrian lane. However, this is not accounted for and the lower value of the height of 1,3 m is used in the calculation:

- $l_{III} = 70{,}7$ m
- $h_{III} = 1{,}3$ m
- $w_{III} = 1{,}9$ m
- $n_{III} = 2$ pcs

Weight calculation component III: The weight of the main girders is approximated as follows:

$$W_{III} = l_{III} * h_{III} * w_{III} * n_{III} * \gamma_c$$

Component IV – Intermediate cross beams

A total of fourteen cross beams are constructed spanning the two main girders in transverse direction. Two of these cross beams are positioned at the supports, these are denoted as the end cross beams, while there are twelve intermediate cross beams, positioned 5,2 m apart (measured centre to centre).

References component IV: The dimensions of the intermediate cross beams are determined based on drawings B.3622, B.5109 and B.7125.

Dimensions component IV: The cross beams support the concrete deck of the main carriageway, and their length is thus equal to the distance between the main girders, which is 7,0 m (see B.7125 for example). From the top view of B.7125 and sections of B.3622 it can be determined that the width and height of these beams are 0,8 m. To summarize, the dimensions are:

- $l_{IV} = 7{,}0$ m
- $h_{IV} = 0{,}8$ m
- $w_{IV} = 0{,}8$ m
- $n_{IV} = 12$ pcs

Weight calculation component IV: The contribution of the intermediate cross beams to the total self-weight of the structure is:

$$W_{IV} = l_{Iv} * h_{IV} * w_{IV} * n_{IV} * \gamma_c$$

Component V – End cross beams

In addition to the intermediate cross beams, two end cross beams are applied. These are positioned at the supports and because the end cross beams have different dimensions than the intermediate sections, these are covered separately.

References component V: The dimensions are established using B.3622 and B.7125.

Dimensions component V: Because the beams span the distance between the main girders, the length is 7,0 m (for example, see B.7125). Figure 22 gives a cross section of the end beams at both sides of the deck, these are part of drawing B.7125.

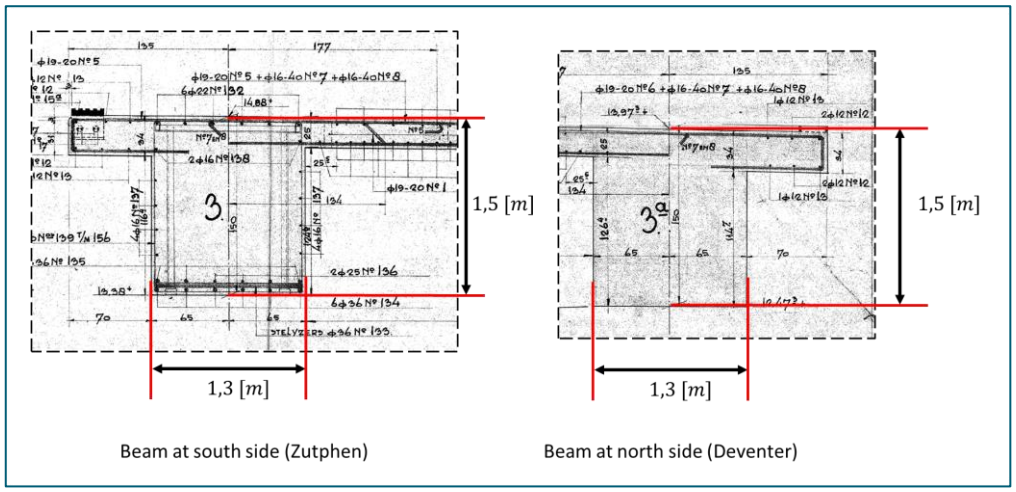


Figure 22 Dimensions of end cross beams – Part of drawing B.7125 (from Rijkswaterstaat archives)

When subtracting the thickness of the deck (this is 0,25 m and will be covered separately), the height of the beams is 1,25 m while the width for both beams is 1,30 m. To summarize, the dimensions are:

- $l_V = 7{,}0$ m
- $h_V = 1{,}25$ m
- $w_V = 1{,}3$ m
- $n_V = 2$ pcs

Note: Note that from the drawings it can be seen that in between the end beam and the abutments a cantilevering part of the deck is present with a larger thickness (0,34 m instead of 0,25). This local increase in thickness is not considered in further calculations.

Weight calculation component V: The contribution of the end cross beams to the total weight of the structure is calculated as follows:

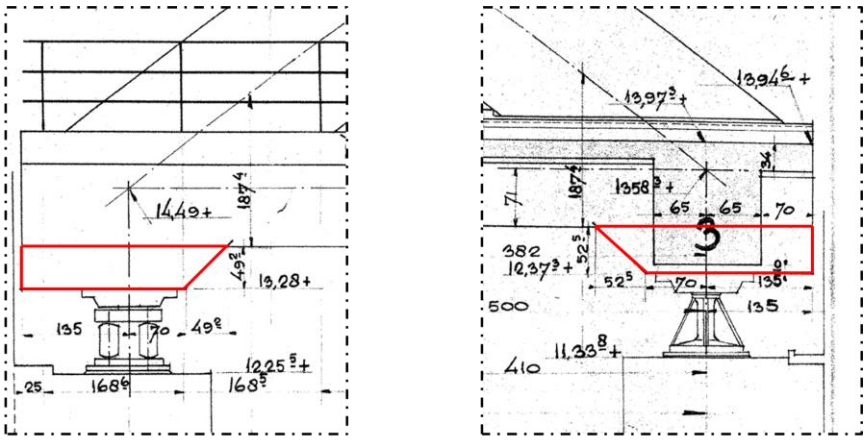
$$W_V = l_V * h_V * w_V * n_V * \gamma_c$$

Component VI – Ends main girders

From the design drawings of the existing bridge, it can be seen that the height of the main girders is increased at the location of the supports. Given the width of the main girders this increase in height is included in the calculation because it will result in a considerable contribution to the self-weight.

References component VI: The increase in height of the main girders at the supports is taken from drawing B.3622 while the width of the main girders follows from B.7125.

Dimensions component VI: Figure 23 gives parts of drawing B.3622, in which the areas under consideration are denoted with red.



Beam end at south side (Zutphen) Beam end at north side (Deventer)

Figure 23 Dimensions ends of main girders – Part of drawing B.3622 (from Rijkswaterstaat archives)

Because the dimensions differ between the abutments at the north and south side, the smaller value is applied in the calculation to obtain a more conservative result. The dimensions in the drawings are in cm. Based on the smaller values the area of the parts denoted in red is calculated as follows:

$$A_{VI} = \frac{1}{2} * 0{,}492 * 0{,}492 + (1{,}35 + 0{,}7) * 0{,}492 = 1{,}13\ [m^2]$$

The width is equal to the width of the main girders, which is 1,9 m. This results in:

- $A_{VI} = 1{,}13\ \text{m}^2$
- $w_{VI} = 1{,}9\ \text{m}$
- $n_{VI} = 4\ \text{pcs}$

Weight calculation component VI: The contribution of these four elements of the main girders to the total weight of the structure is calculated as:

$$W_{VI} = A_{VI} * w_{VI} * n_{VI} * \gamma_c$$

Component VII – Main deck

The seventh contribution is the concrete deck in between the main girders, which functions as the rolling surface for the main traffic.

References component VII: The dimensions are determined using drawings B.5109 and B.7125.

Dimensions component VII: The full length of the bridge deck is covered, which results in a length of 70,7 m and because the distance in between the main girders is spanned, the width is 7,0 m. Figure 24 gives a cross section of the deck as part of drawing B.5109.

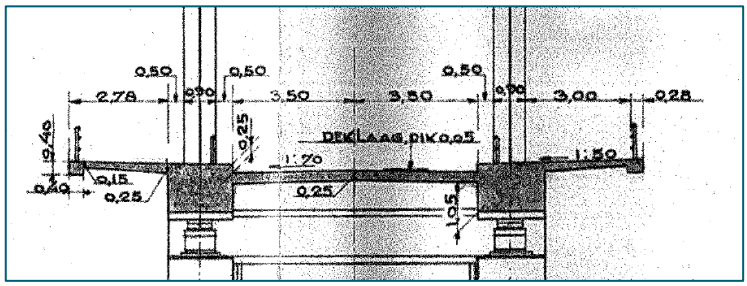


Figure 24 Dimensions of bridge deck – Part of drawing B.5109 (from Rijkswaterstaat archives)

From the drawings mentioned it can be seen that the thickness of the deck is 0,25. The local increase of the parts cantilevering outwards from the end cross beams towards the abutments is neglected. The dimensions therefore are:

- $l_{VII} = 70{,}7$ m
- $h_{VII} = 0{,}25$ m
- $w_{VII} = 7{,}0$ m
- $n_{VII} = 1$ pcs

Weight calculation component VII: The contribution of the concrete deck to the self-weight of the structure is calculated as follows:

$$W_{VII} = l_{VII} * h_{VII} * w_{VII} * n_{VII} * \gamma_c$$

Component VIII – Deck pedestrian lanes

The eighth component accounts for the parts of the deck that are cantilevering outwards from the main girders, these form the deck of the two separate pedestrian lanes.

References component VIII: The dimensions of these segments of the deck are established based on drawings B.3622, B.5109 and B.7125.

Dimensions component VIII: Figure 25 gives a part of the cross section of the deck. This is part of drawing B.3622 and clearly gives the dimensions of the outstand parts of the deck.

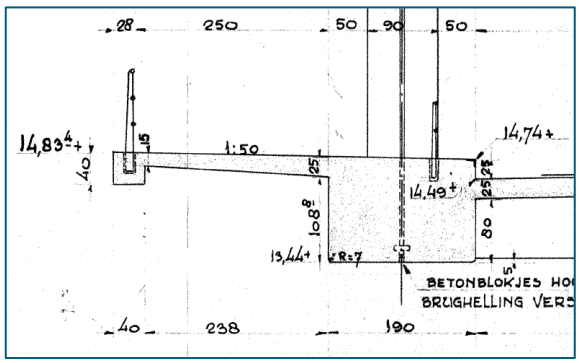


Figure 25 Dimensions deck pedestrian lanes – Part of drawing B.3622 (from Rijkswaterstaat archives)

The total width of the cantilevering section is 2,78 m with a variable thickness and 1:50 slope. Two parts can be distinguished in this cross section. To support the railing an approximately rectangular edge element with dimensions 0,40 by 0,40 m is constructed. Cantilevering outwards is a 2,38 m wide section with a thickness that varies from 0,25 m at the main girder to 0,15 m at the edge for the railing. For the calculation an average thickness of 0,20 m is applied, with which the area of the cross section of the outstand part of the deck is calculated as follows:

$$A_{VIII} = 0{,}40 * 0{,}40 + 0{,}20 * 2{,}38 = 0{,}636 \text{ m}^2$$

The length of the pedestrian lanes is 70,7 m (length of the deck). To summarize the dimensions are:

- $l_{VIII} = 70{,}7$ m
- $A_{VIII} = 0{,}636$ m^2
- $n_{VIII} = 2$ pcs

Weight calculation component VIII: The contribution of the pedestrian lanes to the total self-weight of the structure is calculated as follows:

$$W_{VIII} = l_{VIII} * A_{VIII} * n_{VIII} * \gamma_c$$

Component IX – Surface layer main deck

Various drawings make reference of a surface layer applied onto the deck of the main carriageway, the original dimensions will be applied in the calculation.

References component IX: Information is obtained from drawings B.3622 and B.5109.

Dimensions component IX: The aforementioned two drawings mention a surfacing layer with a thickness of 0,05 m which is applied on the main carriageway. The latter has a length of 70,7 m and width of 7,0 m. This results in the following dimensions:

- $l_{IX} = 70{,}7$ m
- $h_{IX} = 0{,}05$ m
- $w_{IX} = 7{,}0$ m
- $n_{IX} = 1$ pcs

Weight calculation component IX: The weight of the surface layer, which is assumed to be made of asphalt concrete or another bituminous material, is calculated as follows:

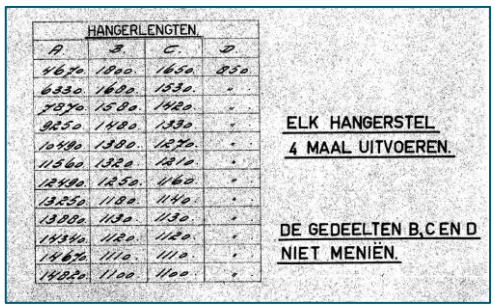
$$W_{IX} = l_{IX} * h_{IX} * w_{IX} * n_{IX} * \gamma_a$$

Component X – Steel hangers

The main girders and arches are connected with steel hangers, these will also be included in the weight calculation as the final component.

References component X: More detailed information on the hangers can be found in the following drawings: B.3622 (longitudinal section and detail in section A-A), drawing B.7125 (section C-C, application of hangers in main girders), drawings B.7164 and B.7165 (details of hangers in arches) and B.7144 (details of the hangers).

Dimensions component X: The steel hangers are applied in sets of two, with each set consisting of two identical hangers. Twelve different types of hangers are applied Figure 26 presents a table taken from drawing B.7144, in which the lengths of these twelve different hanger types are given, see column A. Note that these dimensions are in mm.


HANGERLENGTEN.

A	B	C	D
4670	1800	1650	850
6330	1690	1330	"
7830	1580	1420	"
9250	1480	1330	"
10480	1390	1270	"
11560	1320	1210	"
12490	1250	1160	"
13250	1180	1140	"
13880	1130	1130	"
14340	1120	1120	"
14670	1110	1110	"
14820	1100	1100	"

ELK HANGERSTEL 4 MAAL UITVOEREN.

DE GEDEELTEN B,C EN D NIET MENIËN.

Figure 26 Length of hangers – Part of drawing B.7144 (from Rijkswaterstaat archives)

Because each hanger set is applied four times (two times per single arch girder) and each hanger set comprises two identical hangers, each hanger length in the table is applied eight times. Each steel hanger has a solid circular cross section with a diameter of 65 mm. The dimensions for the twelve different types of hangers are:

- $A_h = \pi * 0{,}25 * 65^2 * 10^{-6}$ m^2
- $l_{X,i}$ = see column 'A' in table
- $n_{X,i} = 8$ pcs

Weight calculation component X: The total contribution of all hangers to the total self-weight of the structure is calculated by adding up the twelve different components:

$$W_X = \sum_{i=1}^{12} A_h * l_{X,i} * n_{X,i} * \gamma_s$$

Note that the steel hangers are anchored in the concrete arches and concrete main girders using anchor plates, but these are not included in the calculation.

Total self-weight

The total self-weight of the existing structure follows from the summation of all aforementioned components:

$$W_e = \sum_{i=I}^{X} W_i$$

6.2 Vertical variable loads

To compare the two bridges the maximum vertical variable loads are also determined. For the new design the loads are based on those applied in the detailed and optimized design. For the existing structure the loads will be determined in accordance with the VOSB 1938.

6.2.1 Vertical variable loads optimized design

In terms of the vertical loads the largest total value, and thus the most unfavourable situation, is obtained if the following actions are considered simultaneously:

- Load on main carriageway: Load model 1
- Load on pedestrian lanes: Load model 4
- Vertical actions on railing

The actions discussed in this section are without any additional load or combination factor ψ.

Load on main carriageway – Load model 1

The largest total vertical load is obtained if load model 1 is applied over the full length of the deck using the first or second configuration as presented in the detailed design.

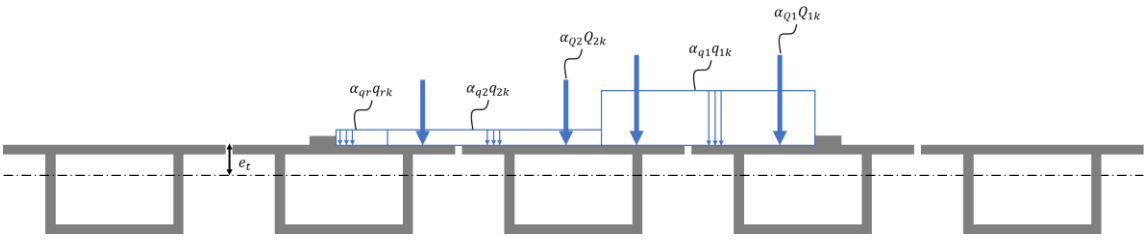


Figure 27 LM1 applied using configuration 1

Figure 27 gives the first configuration of LM1, the values for the actions of the load model are:

- Theoretical lane 1: $\alpha_{Q1} * Q_{1k} = 0{,}97 * 300 = 291$ kN per axle, $\alpha_{q1} * q_{1k} = 0{,}97 * 9{,}0 = 8{,}73$ kN/m^2
- Theoretical lane 2: $\alpha_{Q2} * Q_{2k} = 0{,}97 * 200 = 194$ kN per axle, $\alpha_{q2} * q_{2k} = 0{,}97 * 2{,}5 = 2{,}425$ kN/m^2
- Remaining area: $\alpha_{qr} * q_{rk} = 0{,}9 * 2{,}5 = 2{,}25$ kN/m^2

With a length of 70,7 m and two axles for the tandems to be considered the maximum value is obtained.

Load on pedestrian lanes – Load model 4

The largest total vertical load is obtained if the pedestrian lanes are loaded over their full length and width using the load as calculated for the detailed design:

$$q_{fk} = 2{,}0 + \frac{120}{68 + 30} = 3{,}22\ [kN/m^2]$$

The pedestrian lanes have a width of 4,18 m and the length of the deck is 70,70 m.

Loads on railing

To obtain the largest total vertical load, the vertical loads on the railing are applied as well. The vertical load on the railing has a magnitude of:

$$Q_{k,rail,v} = 3 \text{ kN/m}$$

Overview of variable loads in vertical direction – Eurocode

Figure 28 gives an overview of the different vertical variable loads to obtain the maximum vertical variable load on the bridge deck.

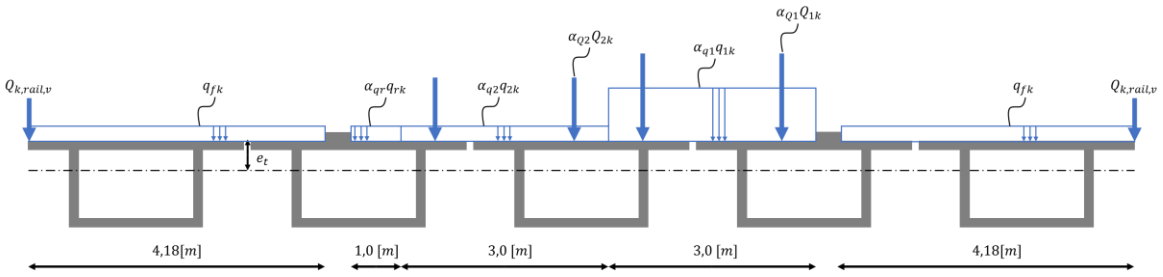


Figure 28 Total variable vertical load on the deck

6.2.2 Variable vertical loads existing bridge

Vertical loads on main carriageway

The loads are determined in accordance with the VOSB 1938. Loads on traffic bridges for road traffic are given in articles 28 and 29. In article 28 four different traffic classes are defined. The Eefdesebrug is classified as a bridge of ''class A'', which are bridges for main traffic roads, where diverting the traffic is not possible.

Article 29 defines the actual loads based on the classification. The loads comprise a uniformly distributed load over the deck surface and a set of concentrated loads.

- For a carriageway with a width smaller than 5,0 m class A comprises a uniformly distributed load of 400 kg/m^2, which is combined with one vehicle that results in three axles of 20 t. Figure 29 gives an overview of this load model.

- In case the deck is wider than 5,0 m multiple heavy vehicles have to be placed adjacent to each other (provided this gives the most unfavourable effect). The number of heavy vehicles is determined by dividing the width of the deck by the width of the lanes (2,5 m) and rounding off to the nearest lower integer.

- Depending on the number of heavy vehicles that are positioned adjacent to each other reductions are prescribed. For two vehicles the concentrated and uniformly distributed loads are multiplied by a factor of 0,9 while for three or four or more vehicles the prescribed factors are 0,7 and 0,6, respectively.

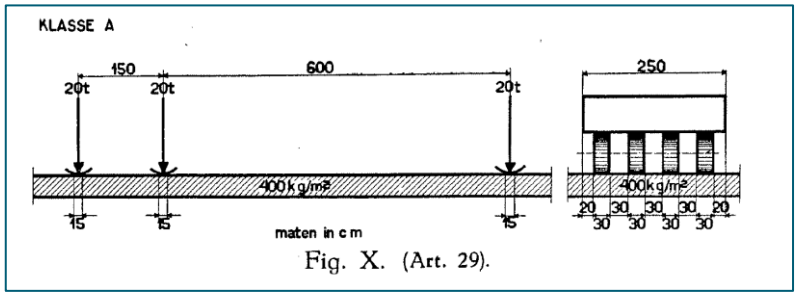


Figure 29 Variable load model ''Klasse A'' from the VOSB 1938 – VOSB 1938, p.55

For the Eefdesebrug the number of heavy vehicles is $Int(7{,}0/2{,}5) = 2$ and a reduction of 10% is thus applied, the values for the loads on the main carriageway are:

- Uniformly distributed load of $0{,}9 * 400 = 360$ kg/m^2, applied over the full surface;

- Two heavy vehicles, each comprising three axles of $0{,}9 * 20 = 18$ tons and thus a total of 108 tons.

Vertical loads on pedestrian lanes

Values for the vertical loads on bicycle/pedestrian lanes is found in article 30. For bridges of class A the prescribed value is a uniformly distributed load of 400 kg/m^2. This load represents crowd loading and is to be applied over the full area of the pedestrian lanes provided this gives the most unfavourable result.

Actions on railing

In article 38 loads on railings are defined. Only horizontal loads are prescribed, because these are not included in the comparison, the loads on the railing are not taken into consideration.

Dynamic amplification factor

Although the loads from the Eurocode already include dynamic amplification factors, this is not the case for the VOSB: a separate factor is prescribed, which is discussed in article 34.

Variable loads on the main deck and the loads for pedestrian/bicycle lanes have to be multiplied with a dynamic amplification factor 'S'. For bridges for road traffic this factor is calculated as follows:

$$S = 1 + \frac{40}{100 + L}$$

In this equation the term 'L' represents the span of the beams under consideration (in metres). For the Eefdesebrug this would result in a value of:

$$S = 1 + \frac{40}{100 + 68} = 1{,}24$$

According to the code, for the design of abutments made of concrete the variable load does not have to be multiplied with a dynamic amplification factor.

The reason for applying the factor 'S' to the loads representing pedestrians (in case of crowd load this load would only move slowly, which does not require an additional factor to account for dynamic effects) is clarified in the additional remarks that have been added to the code. The reason is that the authors assumed that for a bridge with larger length a crowd would not be as dense as in the case a bridge with a smaller length. The application of the dynamic amplification factor is applied to 'scale' the crowd loading to the

length of the bridge, thus including this expected reduction of the uniformly distributed load if the length of the bridge increases.

Article 54 covers the verification of allowable stresses in concrete and reinforced concrete. It is prescribed that provisions from N 1009 – (G.B.V. 1930) are to be applied (this was the code on structure concrete at the time of publication of the VOSB 1938, but at the time of the design of the Eefdesebrug it had already been superseded by the GBV 1940 and GBV 1950). In addition, it is specifically stated that the dynamic amplification factor for steel bridges in article 34 should be applied for the design of concrete decks.

Overview of variable loads in vertical direction – VOSB 1938

The following figure gives an overview of the values of the loads that have been applied conforming the VOSB 1938. Note that the dynamic factor is not included in these values and that the uniformly distributed loads are applied over the full length of the deck.

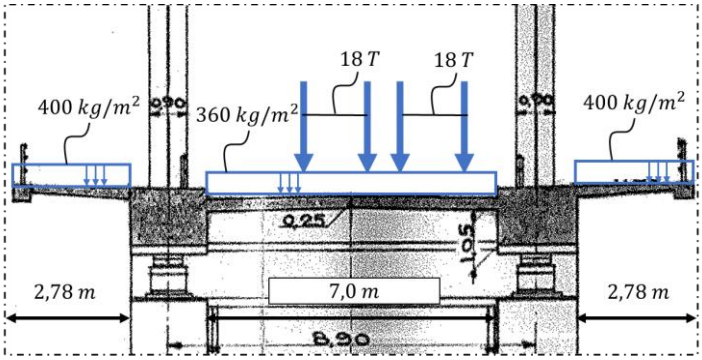


Figure 30 Traffic loads on the existing structure following the VOSB 1938 – Part of drawing B.5109 (from RWS archives)

6.3 Safety philosophies and load factors

Equation (1) as mentioned in 5.1 was written down under the implicit assumption that the codes used in the past followed a safety philosophy similar to that used in the Eurocode (method of partial factors, thus a load factor at the load side and a material factor at the resistance side of the equation). However, this assumption has to be substantiated to determine whether the approach given by equation (1) is actually applicable.

For this reason, the safety philosophy of the Eurocode and the former codes used for the design of the existing bridge will be briefly discussed after which a comparison will be made to determine whether the proposed approach from 5.1 is valid or not. Note that the full background of the codes will not be given, but that only the aspects required for the structural engineer on a daily basis for the design work will be covered, because these are the aspects that are required for the comparison.

6.3.1 Safety philosophy Eurocode

The starting point for the design using the Eurocode is given in part 0, in which it is prescribed that the structure should be verified in two limit states: the ultimate limit state (failure of the structure) and the serviceability limit state (deflection and use of the structure).

Characteristic values

Verifying the structural reliability using the ultimate limit state revolves around characteristic values for the effects of the actions and the resistance of the structure. These characteristic values are defined as such that the probability of the occurrence of an action larger or a resistance value smaller than the characteristic value is a certain percentage. A common value is 5%, which means that the characteristic value corresponds with the 5%-fractile, the value an observation falls below or exceeds in only 5% of the cases.

Determining design values

Using the characteristic values, the design values are determined. The design value of the effect of actions is obtained by multiplying the characteristic value of the effect of actions with the partial factor for actions:

$$E_d = \gamma_F * E_k$$

The design value of the resistance is obtained by dividing the characteristic value of the resistance by a partial factor associated to the resistance:

$$R_d = \frac{R_k}{\gamma_M}$$

Partial factors

Each of these two partial factors account for certain effects or uncertainties. For example, the factor for actions accounts for effects such as the possibility unfavourable deviations of the values of the actual loads with respect to the characteristic values or uncertainty in the models used to determine actions. The factor associated to the resistance incorporates effects such as the possibility of an unfavourable deviation of a material property compared to the characteristic value or uncertainty in the mechanical model used to represent the actual structure.

Demonstrating structural reliability

Using the two aforementioned design values, the requirement that has to be satisfied to demonstrate sufficient structural reliability can be formulated:

$$\frac{E_d}{R_d} \leq 1{,}0 \leftrightarrow E_d \leq R_d$$

Fully written out this equation becomes:

$$E_k * \gamma_F \leq \frac{R_k}{\gamma_M}$$

Satisfying this requirement demonstrates that the probability of failure of the design is sufficiently small. The effect of the actions, resistance values and partial factors are subsequently determined in accordance with the relevant parts of the Eurocode, in order to provide the required level of structural reliability for the given structure. This is related to notions such as reliability and consequence classes and design service life, which are used to classify the structure and to determine the required level of structural reliability for a structure of the given classification.

6.3.2 Safety philosophy GBV 1950 and VOSB 1938

Global safety factor

A study of the content of the GBV 1950 and the VOSB 1938 indicate that the safety philosophy in the period 1950 – 1955 was different compared to the approach that is used nowadays in the Eurocode.

Variable loads were determined in accordance with the VOSB 1938. Although this code mentions an additional factor '*S*' which has to be applied for certain verifications to account for dynamic effects, load factors were not used in the design. That means that without using load factors, the values of the actions represent the actions under use conditions.

Using these values for the actions the force distribution was determined after which the verification of the capacity of reinforcement concrete components took place, which is covered in section 5 of the GBV 1950. The verifications are based on maximum stresses, i.e. the stresses in the components were calculated and subsequently compared with the maximum allowable stresses. These maximum values included a safety margin. Although the option to deviate from such verification procedures was already given in the GBV 1950, the option to verify the actual ultimate capacity (the ULS verification in the Eurocode) was only added in the GBV 1962.

Example of maximum allowable stresses

A safety margin was incorporated in the calculation by reducing the maximum allowable stress in the concrete and steel. As an example, one can look at article 34 – B, which prescribes the maximum stresses in the reinforcement in case if supervision during construction is present. For structural elements loaded in bending or a combination of bending and axle force, the maximum allowable tensile stresses in the reinforcement are as follows:

Staalsoort		Toelaatbare trekspanning in kg/cm²
a) Betonstaal QR 22		1300
b) „ QR 24		1400
c) „ QR 30	volgens V 1035	1600
„ QR 36 en QRn36		1800
„ QR 42 en QRn42		2000
„ QRn48		2200
„ QRn54		2400

Figure 31 Allowable stresses in reinforcement – GBV 1950, p.83

For steel classified as steel of grade QR22, the minimum yield stress is 2200 kg/cm^2, which is approximately 220 N/mm^2, while the maximum allowable tensile stress is 1300 kg/cm^2, which is approximately 130 N/mm^2. This means that there is a safety margin incorporated in the admissible steel stress of:

$$\gamma = \frac{2200}{1300} \approx 1{,}7$$

This safety margin increases if higher steel grades are applied, because the increase of the admissible stress is not proportional to the actual yield stress of the material. For example, for grade QR54:

$$\gamma = \frac{5400}{2400} \approx 2{,}25$$

Different safety margins can be found for concrete of different strength classes and for different verifications (e.g. centric compressive force, elements in bending, etc.).

Meaning of the global safety factor

In the comments added to the GBV 1950 under article 26 it is mentioned what the safety margin, which is obtained by a reduction of the stresses, actually represents. The safety coefficient compensates for a range of different effects and uncertainties, such as:

- Values of loads that turn out to be higher than the values designed for
- Local deviations of material quality
- Inaccuracies in the execution of the work, such as positioning of the rebars
- Inaccuracies in the elaboration of the design calculation

This demonstrates that the safety factor in the verifications following the GBV 1950 is a global safety factor. In these comments it was also mentioned that these safety factors are 'theoretical values'. For example, when using QR22 steel the theoretical safety of elements in bending is 1,7 because beams are designed as such that failure in bending is the result of the yielding of the steel. However, based on literature the author concluded that when using standard design procedures an average global safety margin of 2,5 was found compared to the theoretical factor of 1,7. This was contributed to the fact that calculations do not fully represent reality because of the assumptions included in the calculations.

Design of the existing foundation

The GBV 1950 gives specific safety factors for a range of verifications, such as the aforementioned stresses in reinforcement in bending or concrete under an axial compressive force. Because the analysis that is to be performed focusses on the foundation, the safety factor used for the design of the foundation is required if

any sensible comparison is to be made with the Eurocode. However, no such information has been obtained from the GBV 1950 nor the VOSB 1938.

6.3.3 Comparison of approaches and implications

Comparison codes existing structure and new design

In sections 6.3.1 and 6.3.2 a brief description was given of the safety philosophy of the Eurocode and the older GBV 1950 and VOSB 1938. The reason of describing this is to determine whether the proposed approach from 5.1 is valid or not.

First it has to be noted that it was already expected that there would be differences between the code related to developments in the field. The design practice changes over time due to technological developments. Because codes always represent common practice at the moment of their publication, the content of codes also changes over time. New approaches may be added or may replace older calculation methods. In addition, certain aspects may become obsolete as time progresses.

However, differences were sought for on a more fundamental level, by comparing the safety philosophy that both sets of codes employ. As it turns out, there is also a difference on this more fundamental level: the Eurocode applies the method of partial factors while the GBV 1950 applies a global safety factor. This makes that the requirement as presented in equation (1) cannot be applied as such, and this is especially because of the following two aspects:

- Meaning of the factors
- Design margin of the existing foundation

What is meant with these two aspects will be clarified in the following sections.

Meaning of the factors

The Eurocode is transparent in the sense that it clearly distinguishes factors on the load and material side and between different actions, ULS verifications and materials. This makes it clear that the partial factors account for different effects, for example the factors for actions include, among other others, effects of possible uncertainty in the magnitude of the load which may vary from the value of the characteristic load.

This is contrary to the GBV 1950, which is less transparent in this way because it uses a global factor which has to account for all possible uncertainties. Although a distinction is made between reinforcing steel and concrete, as well as a distinction between different verifications, it does not have the same kind of transparency the Eurocode has.

Design margin existing foundation

Next to the different safety philosophy, a further complicating factor is the safety margin included in the design of the existing foundation. The GBV 1950 distinguishes different safety factors for different materials and verifications. Because it is the foundation that is being considered, it is required to know what safety margins were included in the design of the foundation if any sensible comparison with the Eurocode is to be made.

Because the GBV 1950 follows vastly different design approaches than those in the Eurocode, this suggests that the approach to the design of the pile foundations will also have been different in the period 1950 – 1955 compared to the approach used nowadays. However, no further information has been obtained regarding the design of the foundation, neither the GBV 1950 nor the VOSB 1938 give more detailed information on the design of foundations.

Different sources had therefore to be consulted, information on how investigation of the soil took place and how pile foundations were designed in the Netherlands in the past can for example be found in (Van Tol, 1994), according to which roughly three periods can be distinguished regarding investigation of soil and design of pile foundations:

- **Period 1 (until 1940)**: Initially the investigation of the soil conditions was very limited and took place in the form of bore holes. Although this provided information on the different layers in the soil it did not give the information required to determine the capacity bearing capacity of the soil. In addition, these methods were often costly, which is why often only a few bore holes were drilled at the construction site, and did not always give accurate results if many thin layers were present.

  The required length of foundation piles was therefore determined in a very practical way: using a test pile the depth of the stiffer sand layers was determined. However, this only gave an indication of the actual bearing capacity of the pile. Using so-called 'heiformules' a prediction could be made of the bearing capacity, but this method shows a large scatter between different relationships used.

- **Period 2 (1945 – 1992)**: One important development was the introduction of the cone penetration test, it gives direct information regarding the capacity of the soil layers because it can be interpreted as a sort of testing pile. Another development was the introduction of new types of foundation piles. While the traditional approach was the use of wooden piles, different pile types became available such as prefabricated concrete piles (with different pile tips), cast in-situ piles, etc.

  During this period the design gradually became more based on the cone penetration tests. Initially these were used to determine where the deeper and stiffer layers were. The older design approach is that allowable values were prescribed for stresses at the tip of the piles by, for example, the local construction authorities. Generally, such values were based on extensive local experience and were on the conservative side.

  During the first start of this period cone penetration tests started to be interpreted more as test piles and attempts were made to derive empirical methods to determine the capacity directly from the results on a cone penetration test. Over the course of time the different approaches made place for more consensus. The 'methode Koppejan', which is widely used in the Netherlands, became the method of choice.

- **Period 3 (after 1992)**: In 1992 the new building regulations were adopted, which meant that from October 1992 all new designs had to meet the requirements of the TGB 1990-series. This included the first code on geotechnical design, the NEN 6743. The calculation methods over which consensus had already been reached were therefore also formally standardized.

  With the TGB 1990 series, statistics were first introduced in geotechnical design by means of the method of partial factors. This is in correspondence with the codes for all other materials that were also part of this series, such as concrete as covered in the VBC 1990, in which this method was also applied. A required level of reliability was defined, expressed in the probability of failure. To prevent that probabilistic analyses would have to be made for each design, the method of partial factors was adopted: through probabilistic analyses the value of the partial factors was determined that was required to be within the required level of reliability.

Given the fact that the design and construction of the Eefdesebrug is at the beginning of the second period, there will probably have been some form of design methodology (for example, the ''Methode Koppejan'' dates from this period). However, it is still not known what the exact approach was and thus it remains unclear what the safety margin was that was included in the design.

Though the study has provided some additional insights. First it has shed light on the fact that the introduction of design using the method of partial factors took place later than the Eefdesebrug was designed and constructed. In addition, it has become clear that methods for soil investigation and the design of pile foundations were still in their earlier stages of development compared to nowadays practice, the first code on geotechnical design was only to be introduced in 1992. It is therefore self-explanatory that no specific information or specific safety factor for the design of pile foundations was found in the older codes that were considered.

Implications for the global analysis of the foundation

In this paragraph a brief description was given of the safety philosophy used in the GBV 1950 and VOSB 1938 on one hand and the Eurocode on the other. From these descriptions and subsequent comparison, it was found that there are two complicating factors which make that the proposed approach from 5.1 is not valid.

The first aspect is that the way in which the structural reliability is provided is different: the Eurocode uses the method of partial factors while the older codes work with a global safety factor. The second aspect is that it is not clear what the safety margin was which was included in the design of the existing foundation. The implication of these differences is that the proposed approach as given in equation (1) cannot be used and will have to be adjusted. An alternative approach will be introduced and elaborated on in the next chapter.

7

ASSESSMENT OF FOUNDATION & ANALYSIS OF RESULTS

7.1 Outline global analysis of the foundation

7.1.1 Outline global analysis of the foundation

In 5.1 an approach was presented for the global analysis of the foundation. Based on insights from chapter 6 that followed from a further discussion of the content and safety philosophies of the Eurocode on one hand and the older codes used for the design of the existing bridge on the other, it was concluded that this approach actually is not valid. Therefore, a different approach will have to be devised. A global analysis of the foundation will be performed by comparing the new situation and the existing situation in two ways:

- **Comparison based on total vertical force**: The first part of the analysis will be based on the total vertical forces due to permanent and vertical variable loads as determined in 6.1 and 6.2, these loads will be compared without any additional factors and thus represent the loads under use conditions. In addition, it will be included what the effects are if the axle loads are positioned directly at one of the abutments;

- **Comparison based on forces in foundation piles**: As an addition to the project the force distribution between the foundation piles will be analysed by reducing the foundation to a simple model, after which the difference in compressive forces in the heaviest loaded pile group will be calculated. Although this model will be formulated using various simplifications and neglecting certain load cases, it has nonetheless been added to the analysis because it is expected that this will provide useful insights that cannot be obtained by only comparing the vertical forces.

These two different comparisons will be elaborated on and provided with more details in sections 7.2 and 7.3, respectively.

7.2 Global analysis foundation – Total vertical force

7.2.1 Verification criterion

The first part of the analysis of the foundation is a comparison of the summation of total vertical forces due to the permanent loads and variable loads in the case of the new design and the existing bridge. No further multiplication factors are used, which implies that these representative values of the loads that are used in this comparison resemble the loads under use conditions. This way equation (1) can be rewritten into:

$$G_N + Q_N \leq G_E + Q_E \qquad \text{Equation (2)}$$

Although contrarily to equation (1) no additional factors are included, the principle behind the equation remains the same. Note that the representative values of the actions used in this equation, which are the values without any further load or combination factors, represent the loads under use conditions. The requirement therefore is that these representative values of the forces in the new situation due to the permanent and vertical variable actions should be smaller than or equal to the permanent and vertical variable actions from the design of the existing bridge.

7.2.2 Comparison total vertical forces

Summation of all vertical forces

Table 15 summarizes the results from the weight calculation as presented in 6.1 and 6.2 of this report. Note that conforming the VOSB 1938 no dynamic amplification factor '*S*' is included in the values for the variable loads. For a more detailed calculation reference is made to annex VI.

Table 15 Vertical loads existing structure and optimized new design

Action	Existing structure	New design	Percentage change
[-]	[kN]	[kN]	[%]
Permanent loads	23.055	15.779	-32
Variable loads	4434	5822	31
Total vertical load	27.489	21.602	-21

Figure 32 visualises the values from the table.

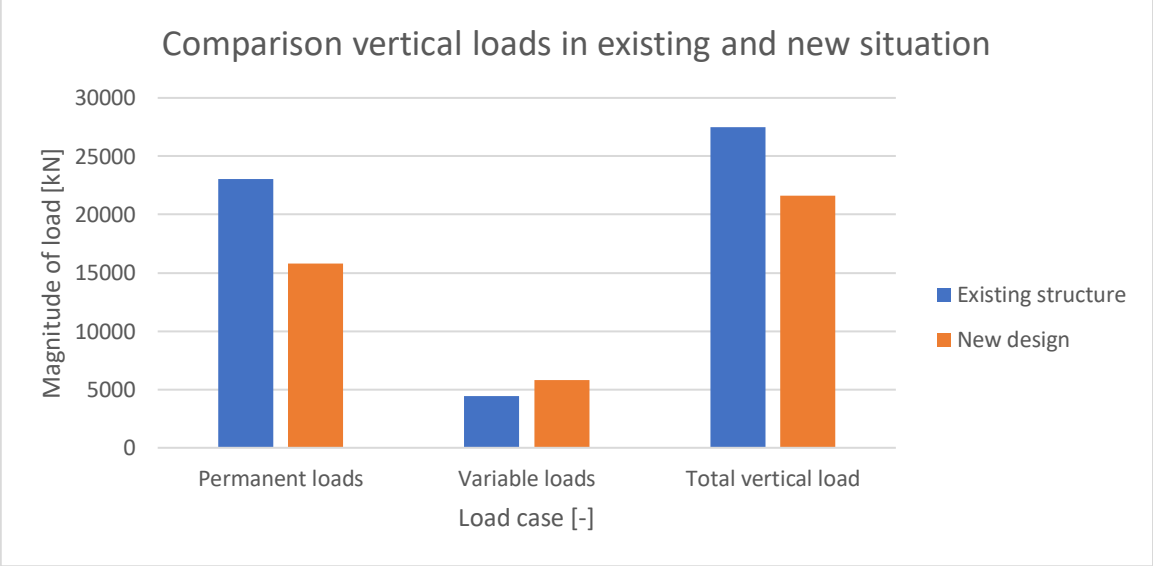


Figure 32 Comparison of vertical loads of existing structure and optimized new design

First it has to be noted that in both cases the result makes an impression which is typical for concrete bridges: for longer spans it is usually the self-weight that is the largest load. It can also be concluded that in terms of the total vertical load the new design results in a significantly lower value. The result of this comparison is an overall decrease of 21% of the vertical loads between the existing and new situations.

This decrease is despite the fact that the Eurocode results in a higher variable load compared to the VOSB. In absolute terms the increase of 31% is a significant difference, but in relative terms it is less significant when compared to the reduction of the permanent load of the structure due to the large reduction of the self-weight. These results give a positive impression with regard to achieving the project goal.

Summation of forces with axles near support

Figure 32 does not include any load effects, it is assumed that the loads are as such that both abutments carry half the total load. However, in reality such situations will usually not be the case and therefore an additional situation will be included in this section. It will be examined what the effect will be if one abutment carries the full variable load caused by the concentrated loads.

Table 16 summarizes the actions of the heaviest loaded abutment. It is assumed that the permanent actions and uniformly distributed variable loads can be distributed equally over both abutments. These loads are combined with the full axle loads to represent the situation where these are positioned directly above one of the supports.

Table 16 Vertical loads existing structure and optimized new design – Single abutment

Action	Existing structure	New design	Percentage change
[-]	[kN]	[kN]	[%]
Permanent loads	11.527	7890	-32
Variable loads	2757	3396	23
Total vertical load	14.284	11.286	-21

The permanent loads are half the values of those presented in Table 15 and will be visualised in a graph. The percentual increase of the variable loads is lower than in the previous case, this is contributable to the fact that it is the uniformly distributed variable loads where the Eurocode is more unfavourable compared to the VOSB 1938 while in this calculation the effect of the axle loads increased relatively to that of the uniformly distributed loads.

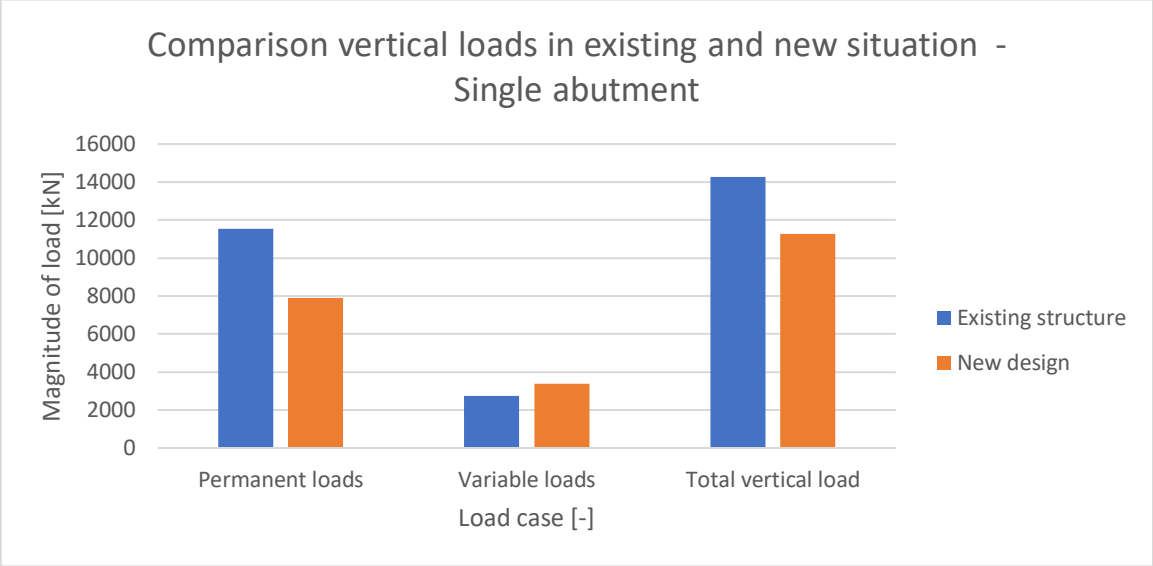


Figure 33 Comparison of vertical loads of existing structure and optimized new design – Single abutment

Figure 33 visualises the results. It can be seen that in total there is no difference in percentage change, which indicates that although this situation is more unfavourable for a single abutment, the permanent loads are still the largest contributor to the total loads. The effect of changing the position of the axle loads is only marginal when compared to the effects of the permanent loads. Just like the previous case, these results give a positive impression with regard to achieving the goal of the project.

7.3 Global analysis of foundation – Forces in foundation piles

7.3.1 Approach to determine forces in foundation piles

A full analysis of the foundation has been excluded from the scope of the project and a global verification by comparing the vertical forces is carried out instead. However, as an additional part to the project a closer look is taken to some of the aspects of the pile foundation: by using various simplifications and assumptions an approximating calculation of the forces in the foundation piles will be performed. This additional calculation has been added because it is expected that it will provide useful additional insights that cannot be obtained by only comparing the vertical forces, insights such as:

- Obtaining a rough estimate of the forces in the different pile groups and determine to what extent the percentual change of total vertical forces relates to a change of the forces in the foundation piles;

- Including the effects of the eccentricity of the bearings with respect to the centre of the pile group and that of horizontal forces acting on the bridge deck;

- Determine the heaviest loaded pile group of the foundation as well as the percentual change in the compressive forces in this pile group.

This additional calculation is, despite simplifications, expected to provide insight into effects that cannot be captured by only comparing the total vertical loads. The calculation will be carried out using various simplifications and assumptions:

- The situation will be reduced to a 2D problem and all included forces are assumed to act in the direction of the longitudinal axis of the bridge deck;

- The calculation only includes actions on the pile foundation due to the permanent and variable loads of and acting upon the superstructure, these are: self-weight of the deck, imposed permanent load on the deck, vertical variable loads acting on the deck and horizontal variable loads acting on the deck;

- The actions are taken into consideration without load factors. Actions that are thus explicitly not included in the calculation are:

    - Actions in transverse direction (e.g. ship collision);
    - Rotational effects due to, for example, eccentric horizontal traffic loads;
    - Elongation or shortening due to temperature effects;
    - Actions related to the soil pressure acting upon the substructure;
    - Self-weight of the substructure.

Figure 34 gives the approach to the calculation.

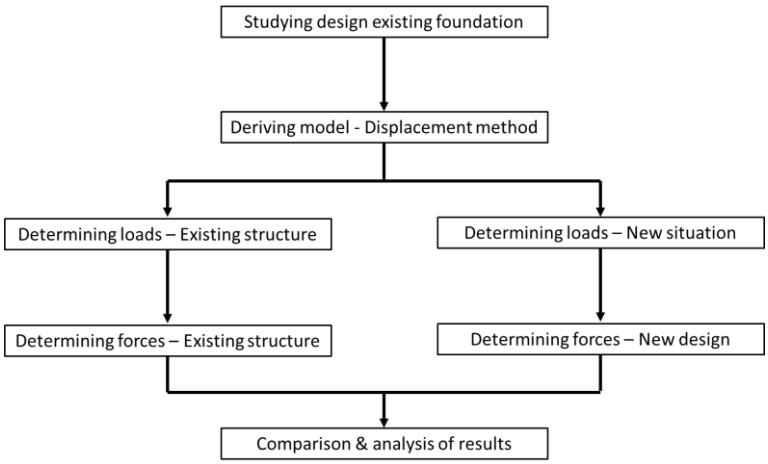


Figure 34 Approach to approximate forces in the foundation piles

7.3.2 Design existing foundation

Reference documents

The first step of the calculation is to analyse the design of the existing foundation to obtain the information required for the remainder of the calculation. The following table gives an overview of the reference documents (drawings from Rijkswaterstaat archives) in which the required information has been found.

Table 17 Reference documents existing foundation

Number	Description
B.3806	Herstelling Eefdesebrug 1954-'56 – Blad 1 brief 19-07-1954
B.3807	Herstelling Eefdesebrug 1954-'56 – Bestaande toestand – Blad 2 bij brief 19-07-1954
B.3797	Herstel Eefdesebrug 1954-'56 – Heiplan
B.5109	Herstelling Eefdesebrug 1954-'56 – Overzichtstekening met toekomstige kanaalverbreding

For the analysis of the foundation only the piles under the foundation block supporting the main span are included. Piles supporting the abutment are expected to hardly contribute to the foundation of the main span, and mainly support the abutment instead.

Brief description of north and south foundation blocks

Using the reference documents the design of the foundations have been studied. Although the foundation blocks at both abutments are largely similar, small differences have been observed. The main characteristics of both pile groups are as follows.

North side: On the north side five rows of piles can be distinguished with 13 piles in each row, resulting in 65 piles in total. The piles are positioned following a grid: the rows are positioned centre to centre 1,0 m while the piles within each row are positioned 1,2 m apart. According to the original design drawings the piles have a length of 13,6 m and are positioned under an 8:1 inclination, which can be in both directions.

South side: Although the pile foundation on the south side has many similarities in terms of design, there is more variation in the positioning of the piles. The same grid is followed but there is more variance in inclination and the fact that one pile less is applied. A reason for this could be found in the presence of the remains of an existing foundation of an older bridge at this position.

Eccentricity and results: At both abutments the eccentricity between the axis of the supports and the axis of the pile group is 0,3 m. As a result, a moment is introduced onto the foundation block.

More details on the construction of the pile foundation have been found on the drawing B.3797. These were added after the construction of the bridge and include: the height of the block of the pile driver and the number of times the weight had to hit the pile to drive it for the last 25 cm into the soil. The depth of the pile tip is also given on the drawings, which is approximately 8,0 m NAP on average over all piles.

Analysis of foundation north side

Given the regular grid the foundation of the north side will be analysed. It is expected that, although this calculation is easier than that of the south side, will also be sufficiently representative for the south side given the large similarities in the design. The length along the vertical side is $12 * 1{,}2 = 14{,}4$ m while the length along the horizontal side is $4 * 1{,}0 = 4{,}0$ m.

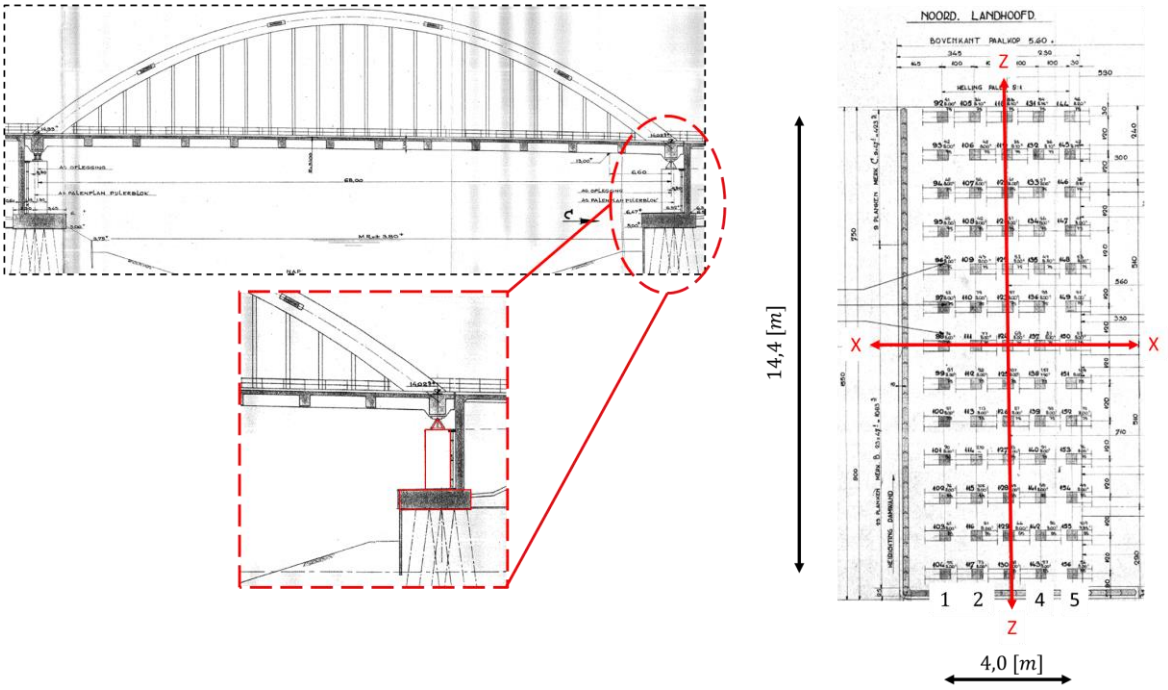


Figure 35 Abutment (left) and top view of the pile group (right) – Parts of drawings B.5109 & B.3797 (from Rijkswaterstaat archives)

The piles have been divided into five groups along the horizontal axis that has been added in Figure 35. All piles are inclined, either towards the left or right. Table 18 gives an overview of the number of piles per row as well as their inclination.

Table 18 Number of piles and inclination

Number of piles	Row 1	Row 2	Row 3	Row 4	Row 5
Inclined left	13	8	8	8	-
Inclined right	-	5	5	5	13
Total number	13	13	13	13	13

7.3.3 Derivation of model

Main principles

Figure 36 gives a side view of the foundation block from Figure 36 and presents the main principles of the model that will be derived. The foundation block is reduced to a 2D model with three degrees of freedom, the positive directions are indicated. The model will include three loads, being a vertical load, horizontal load and moment.

Suppose that a force R_v acts upon the buttress due to the superstructure and the loads upon it (A). Via the buttress this load acts onto the foundation block and the resulting force has an eccentricity 'e' with respect to the centre of the pile group (B). The eccentric force can be replaced by a force acting centrically onto the centre of the pile group and a bending moment M_v (C).

As a first approximation the foundation slab and buttress are assumed to be rigid and are supported by the foundation piles, which will be modelled as groups of translational springs (D). That means that these are only assumed to give reaction forces to displacements in the direction of their longitudinal axis. In addition, it is assumed that all individual piles have the same stiffness 'k'. There are eight pile groups (group a to h).

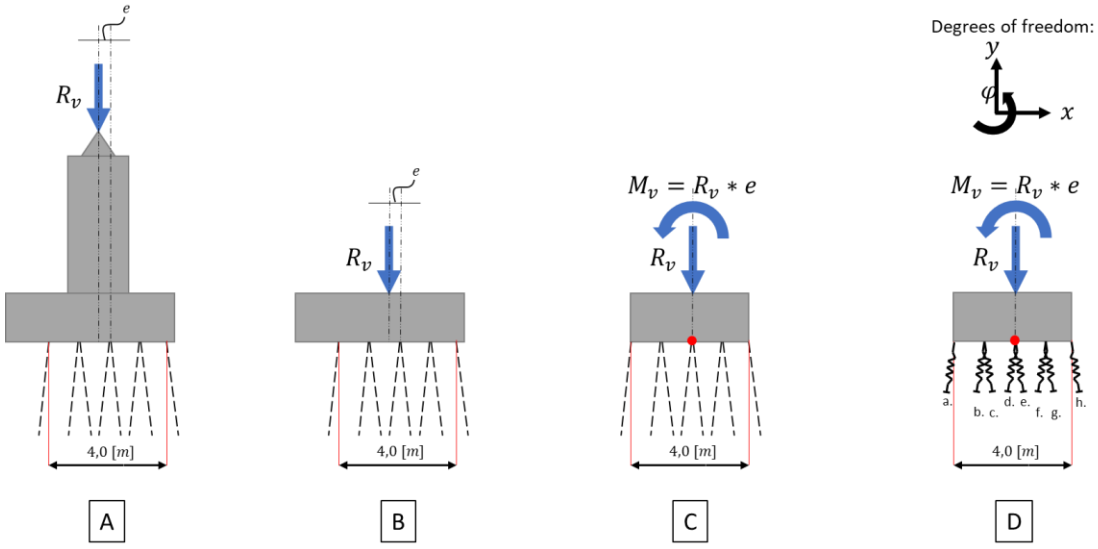


Figure 36 Model for the analysis

If a single translational spring deforms over a distance 'u' along its longitudinal axis, then the reaction force is calculated as follows:

$$N = k * u$$

Depending on the direction of their inclination, the piles (springs) will be grouped, creating groups of parallel springs with the same deformation 'u_i'. The resulting reaction force N_i of a pile group consisting of 'n_i' springs with the same stiffness k_i is the summation of individual capacities:

$$N_i = n_i * k_i * u_i$$

Displacement method

To derive equations in order to determine the forces in the foundation piles the displacement method will be used. To apply this method, first the following three steps have to be taken:

- Determine the degrees of freedom – Subsequently displace the system in the positive direction of the degrees of freedom and determine the forces N_i in each pile row;
- Internal forces – The internal forces of the pile rows can subsequently be expressed in the displacements in the directions of the degrees of freedom;
- Equilibrium equations – The third step is to formulate the equilibrium equations of the system.

With these three steps taken the problem can be solved and a model is obtained to determine the pile forces for different loads. All equations will be derived in this report while solving the equations will be done using a Maple sheet. Reference is made to annex VI for the latter.

Degrees of freedom

There are three degrees of freedom, these are the horizontal displacement 'x', the vertical displacement'y' and the rotation 'φ'. The following figure gives their positive directions, as well as the origin. In preparation of the following steps a triangle has been added which gives the inclination of the foundation piles.

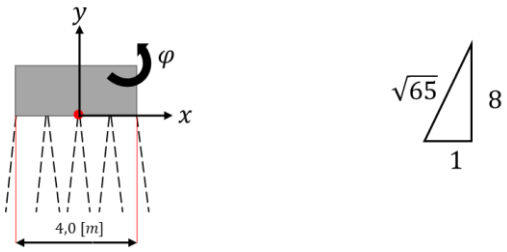


Figure 37 Degrees of freedom and inclination of the piles

Horizontal displacement: First the foundation block is moved horizontally over Δx and the forces N_i in the pile rows are calculated. Figure 38 give the required relations to determine the piles forces. Table 19 summarizes the results. The reaction forces for pile group 'i' consisting of 'n_i' piles can be written as follows.

$$N_i = \pm n_i * k * \frac{1}{\sqrt{65}} * \Delta x$$

Table 19 Results for each pile group in case of positive horizontal displacement Δx

Pile row	No. piles	Forces	Sign
a	13	$N_a = +13 * k * \frac{1}{\sqrt{65}} * \Delta x$	Tensile
b	8	$N_b = +8 * k * \frac{1}{\sqrt{65}} * \Delta x$	Tensile
c	5	$N_c = -5 * k * \frac{1}{\sqrt{65}} * \Delta x$	Compressive
d	8	$N_d = +8 * k * \frac{1}{\sqrt{65}} * \Delta x$	Tensile
e	5	$N_e = -5 * k * \frac{1}{\sqrt{65}} * \Delta x$	Compressive
f	8	$N_f = +8 * k * \frac{1}{\sqrt{65}} * \Delta x$	Tensile
g	5	$N_g = -5 * k * \frac{1}{\sqrt{65}} * \Delta x$	Compressive
h	13	$N_h = -13 * k * \frac{1}{\sqrt{65}} * \Delta x$	Compressive

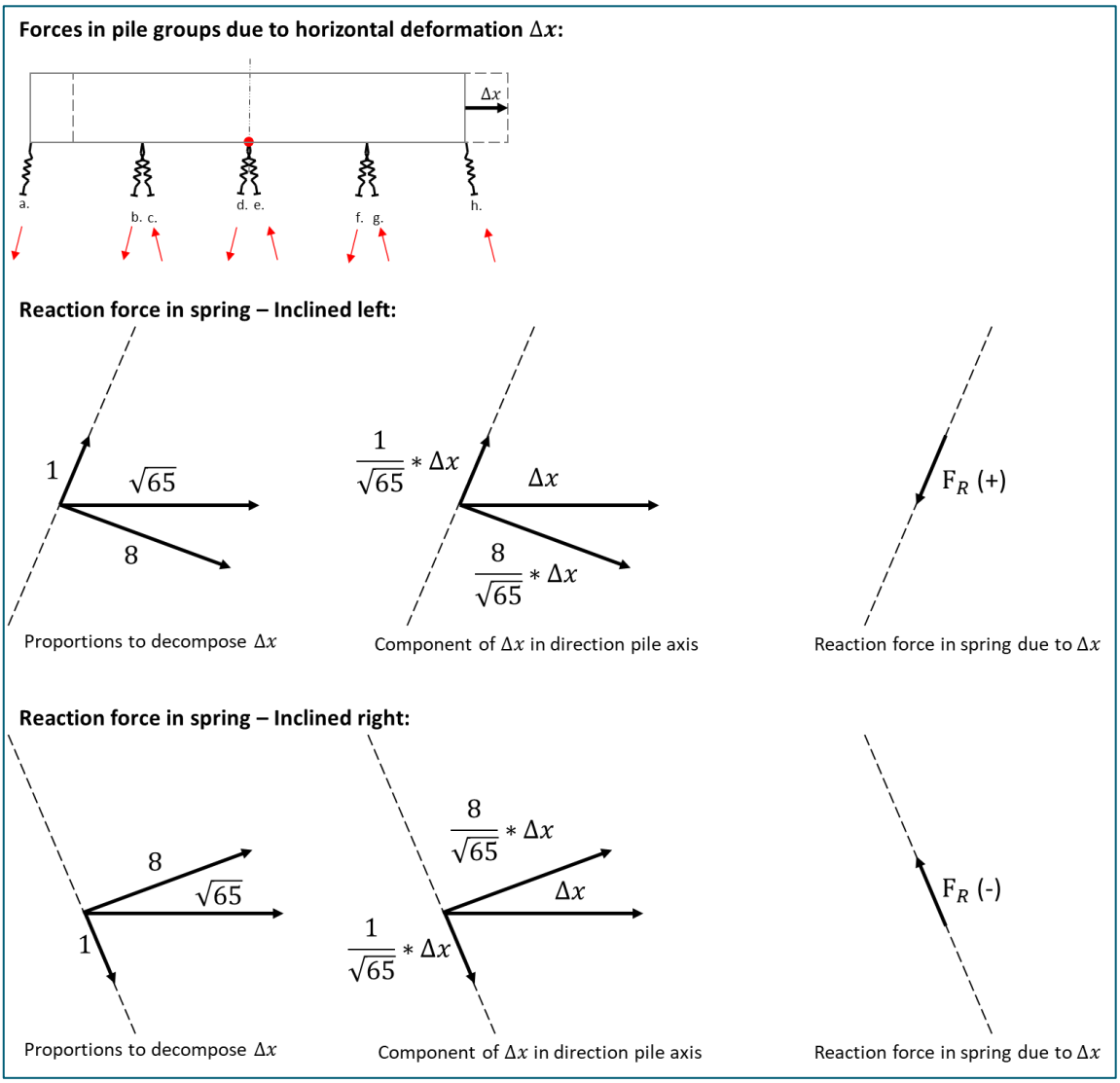


Figure 38 Determining reaction forces in case of positive horizontal displacement Δx

Vertical displacement: Subsequently the foundation block is moved vertically over Δy in positive direction, for each pile group 'i' the pile force N_i is:

$$N_i = +n_i * k * \frac{8}{\sqrt{65}} * \Delta y$$

Table 20 summarizes the results. Tensile forces in the piles are denoted as positive.

Table 20 Results for each pile group in case of positive vertical displacement Δy

Pile row	No. piles	Forces	Sign
a	13	$N_a = +13 * k * \frac{8}{\sqrt{65}} * \Delta y$	Tensile
b	8	$N_b = +8 * k * \frac{8}{\sqrt{65}} * \Delta y$	Tensile
c	5	$N_c = +5 * k * \frac{8}{\sqrt{65}} * \Delta y$	Tensile
d	8	$N_d = +8 * k * \frac{8}{\sqrt{65}} * \Delta y$	Tensile
e	5	$N_e = +5 * k * \frac{8}{\sqrt{65}} * \Delta y$	Tensile

f	8	$N_f = +8 * k * \frac{8}{\sqrt{65}} * \Delta y$	Tensile
g	5	$N_g = +5 * k * \frac{8}{\sqrt{65}} * \Delta y$	Tensile
h	13	$N_h = +13 * k * \frac{8}{\sqrt{65}} * \Delta y$	Tensile

Figure 39 gives the relevant derivations.

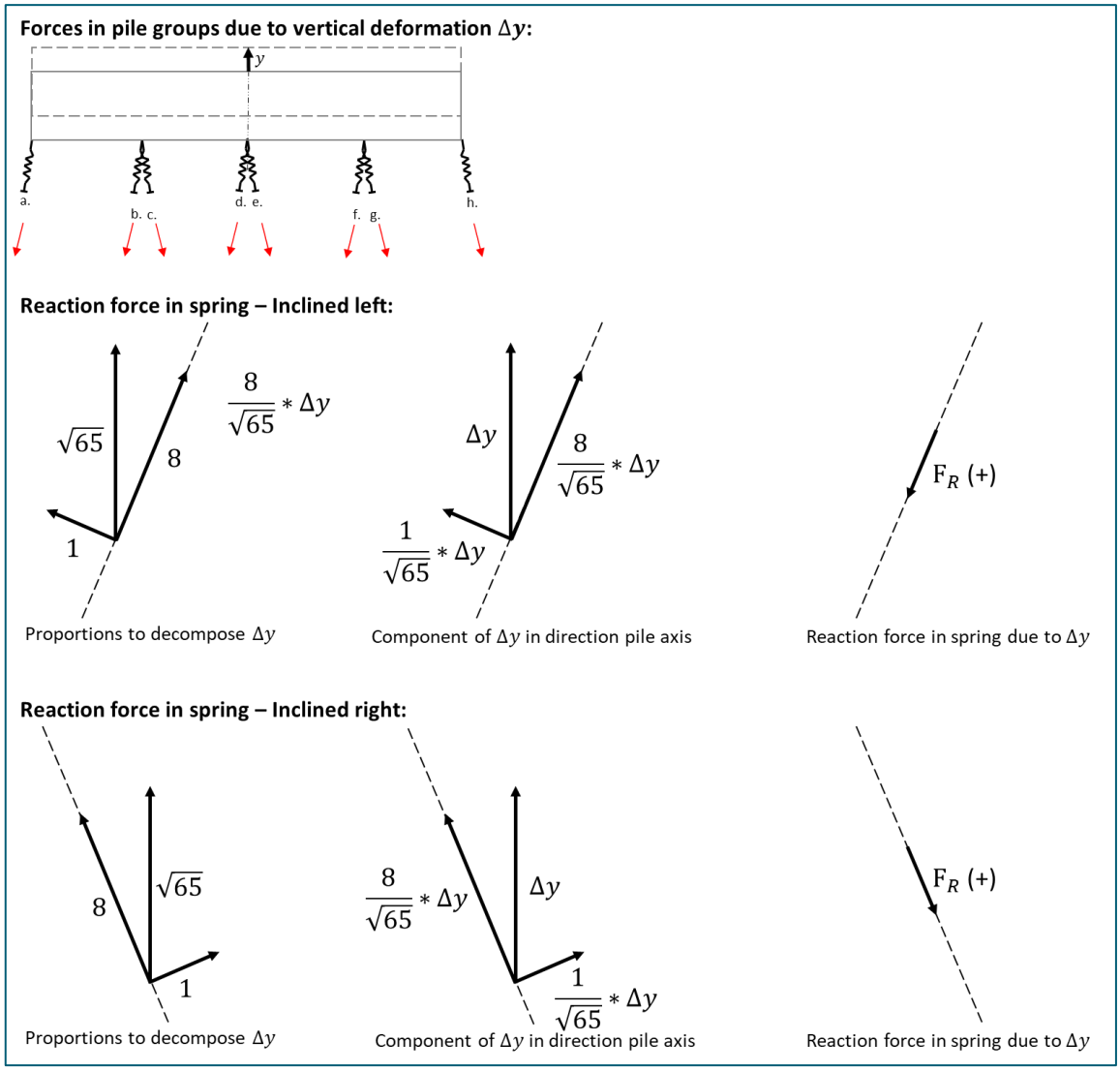


Figure 39 Determining reaction forces in case of positive vertical displacement Δy

Rotation: The final displacement occurs due to the rotation φ. It is assumed that the foundation block rotates over the centre of the pile groups. Figure 40 gives the required relations while Table 21 summarizes the results.

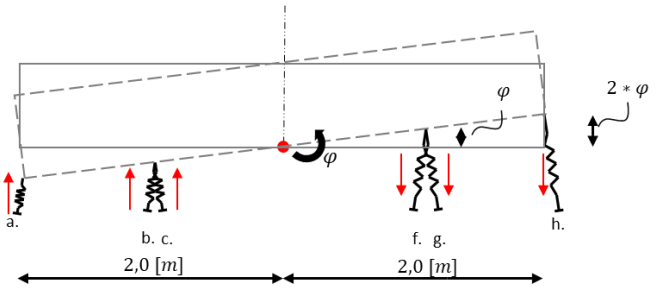


Figure 40 Determining reaction forces in case of positive rotation φ

The outermost groups of springs have a vertical displacement of $2 * \varphi$ while the inner groups of springs have a vertical displacement of φ. Displacements at the middle group are equal to zero. The compressive or tensile force can subsequently be determined following the approach of the vertical displacements.

Table 21 Results for each pile group in case of positive rotation φ

Pile row	No. piles	Forces	Sign
a	13	$N_a = -13 * k * \frac{8}{\sqrt{65}} * 2 * \varphi$	Compressive
b	8	$N_b = -8 * k * \frac{8}{\sqrt{65}} * \varphi$	Compressive
c	5	$N_c = -5 * k * \frac{8}{\sqrt{65}} * \varphi$	Compressive
f	8	$N_f = +8 * k * \frac{8}{\sqrt{65}} * \varphi$	Tensile
g	5	$N_g = +5 * k * \frac{8}{\sqrt{65}} * \varphi$	Tensile
h	13	$N_h = +13 * k * \frac{8}{\sqrt{65}} * 2 * \varphi$	Tensile

Internal forces

The system has been displaced in the positive directions of the degrees of freedom and the corresponding forces in the piles have been determined. Based on these results equations are formulated for the pile forces as a function of the displacements in the positive directions of the degrees of freedom:

$$N_a = +13 * k * \frac{1}{\sqrt{65}} * \Delta x + 13 * k * \frac{8}{\sqrt{65}} * \Delta y - 13 * k * \frac{8}{\sqrt{65}} * 2 * \varphi$$

$$N_b = +8 * k * \frac{1}{\sqrt{65}} * \Delta x + 8 * k * \frac{8}{\sqrt{65}} * \Delta y - 8 * k * \frac{8}{\sqrt{65}} * \varphi$$

$$N_c = -5 * k * \frac{1}{\sqrt{65}} * \Delta x + 5 * k * \frac{8}{\sqrt{65}} * \Delta y - 5 * k * \frac{8}{\sqrt{65}} * \varphi$$

$$N_d = +8 * k * \frac{1}{\sqrt{65}} * \Delta x + 8 * k * \frac{8}{\sqrt{65}} * \Delta y$$

$$N_e = -5 * k * \frac{1}{\sqrt{65}} * \Delta x + 5 * k * \frac{8}{\sqrt{65}} * \Delta y$$

$$N_f = +8 * k * \frac{1}{\sqrt{65}} * \Delta x + 8 * k * \frac{8}{\sqrt{65}} * \Delta y + 8 * k * \frac{8}{\sqrt{65}} * \varphi$$

$$N_g = -5 * k * \frac{1}{\sqrt{65}} * \Delta x + 5 * k * \frac{8}{\sqrt{65}} * \Delta y + 5 * k * \frac{8}{\sqrt{65}} * \varphi$$

$$N_h = -13 * k * \frac{1}{\sqrt{65}} * \Delta x + 13 * k * \frac{8}{\sqrt{65}} * \Delta y + 13 * k * \frac{8}{\sqrt{65}} * 2 * \varphi$$

These equations can also be written in matrix-vector form:

$$\underline{n} = \boldsymbol{K}\underline{u} \qquad \text{Equation (3)}$$

In this equation $\underline{n}$ is a vector containing the forces in the piles, $\underline{n} = (N_a \dots N_h)^T$, $\boldsymbol{K}$ is a matrix with eight rows and three columns relating pile forces to displacements and $\underline{u}$ is a vector containing the three degrees of freedom, each multiplied with the stiffness 'k' of a single pile.

$$\begin{pmatrix} N_a \\ N_b \\ N_c \\ N_d \\ N_e \\ N_f \\ N_g \\ N_h \end{pmatrix} = \begin{bmatrix} 13 * \frac{1}{\sqrt{65}} & 13 * \frac{8}{\sqrt{65}} & -13 * \frac{8}{\sqrt{65}} * 2 \\ 8 * \frac{1}{\sqrt{65}} & 8 * \frac{8}{\sqrt{65}} & -8 * \frac{8}{\sqrt{65}} \\ -5 * \frac{1}{\sqrt{65}} & 5 * \frac{8}{\sqrt{65}} & -5 * \frac{8}{\sqrt{65}} \\ 8 * \frac{1}{\sqrt{65}} & 8 * \frac{8}{\sqrt{65}} & 0 \\ -5 * \frac{1}{\sqrt{65}} & 5 * \frac{8}{\sqrt{65}} & 0 \\ 8 * \frac{1}{\sqrt{65}} & 8 * \frac{8}{\sqrt{65}} & 8 * \frac{8}{\sqrt{65}} \\ -5 * \frac{1}{\sqrt{65}} & 5 * \frac{8}{\sqrt{65}} & 5 * \frac{8}{\sqrt{65}} \\ -13 * \frac{1}{\sqrt{65}} & 13 * \frac{8}{\sqrt{65}} & 13 * \frac{8}{\sqrt{65}} * 2 \end{bmatrix} \begin{pmatrix} k * \Delta x \\ k * \Delta y \\ k * \varphi \end{pmatrix}$$

Equilibrium equations

The next step is to formulate the equilibrium equations. Figure 41 shows the forces in positive directions as well as the assumed forces in the foundation piles. In addition, the decomposition of the forces in the piles into horizontal and vertical components is presented.

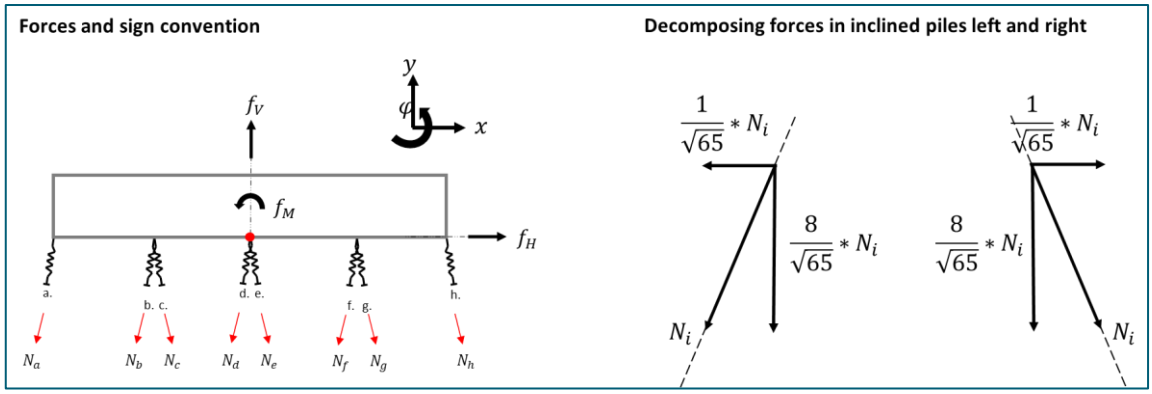


Figure 41 Formulating the equilibrium equations

The equations for horizontal equilibrium, vertical equilibrium and moment equilibrium are formulated around the assumed point of rotation (the origin). In order to do so the assumed forces in the foundation piles are first decomposed in horizontal and vertical components. Horizontal equilibrium yields the following equation:

$$-13\frac{1}{\sqrt{65}}N_a - 8\frac{1}{\sqrt{65}}N_b + 5\frac{1}{\sqrt{65}}N_c - 8\frac{1}{\sqrt{65}}N_d + 5\frac{1}{\sqrt{65}}N_e - 8\frac{1}{\sqrt{65}}N_f + 5\frac{1}{\sqrt{65}}N_g + 13\frac{1}{\sqrt{65}}N_h + f_H = 0$$

Vertical equilibrium yields:

$$-13\frac{8}{\sqrt{65}}N_a - 8\frac{8}{\sqrt{65}}N_b - 5\frac{8}{\sqrt{65}}N_c - 8\frac{8}{\sqrt{65}}N_d - 5\frac{8}{\sqrt{65}}N_e - 8\frac{8}{\sqrt{65}}N_f - 5\frac{8}{\sqrt{65}}N_g - 13\frac{8}{\sqrt{65}}N_h + f_V = 0$$

Moment equilibrium yields:

$$+13\frac{8}{\sqrt{65}}N_a * 2 + 8\frac{8}{\sqrt{65}}N_b + 5\frac{8}{\sqrt{65}}N_c - 8\frac{8}{\sqrt{65}}N_f - 5\frac{8}{\sqrt{65}}N_g - 13\frac{8}{\sqrt{65}}N_h * 2 + f_M = 0$$

The known terms (the forces and moment) are moved to the right-hand side and both sides of the equation are multiplied with minus one. This way the signs of the forces and moment in the equation correspond to the sign conventions as given in Figure 41. The equations can also be rewritten in matrix-vector form:

$$\boldsymbol{C}\underline{n} = \underline{f} \qquad \text{Equation (4)}$$

In this equation $\boldsymbol{C}$ is a matrix with three rows and eight columns, representing the factors to multiply the forces in the piles. $\underline{n}$ denotes the vector containing all pile forces: $\underline{n} = (N_a \dots N_h)^T$. Finally, $\underline{f}$ is the vector containing the external forces acting on the foundation block: $\underline{f} = (f_H, f_V, f_M)^T$. Fully written out this equation becomes:

$$\begin{bmatrix} 13\frac{1}{\sqrt{65}} & 8\frac{1}{\sqrt{65}} & -5\frac{1}{\sqrt{65}} & 8\frac{1}{\sqrt{65}} & -5\frac{1}{\sqrt{65}} & 8\frac{1}{\sqrt{65}} & -5\frac{1}{\sqrt{65}} & -13\frac{1}{\sqrt{65}} \\ 13\frac{8}{\sqrt{65}} & 8\frac{8}{\sqrt{65}} & 5\frac{8}{\sqrt{65}} & 8\frac{8}{\sqrt{65}} & 5\frac{8}{\sqrt{65}} & 8\frac{8}{\sqrt{65}} & 5\frac{8}{\sqrt{65}} & 13\frac{8}{\sqrt{65}} \\ -13\frac{8}{\sqrt{65}}2 & -8\frac{8}{\sqrt{65}} & -5\frac{8}{\sqrt{65}} & 0 & 0 & 8\frac{8}{\sqrt{65}} & 5\frac{8}{\sqrt{65}} & 13\frac{8}{\sqrt{65}}2 \end{bmatrix} \begin{pmatrix} N_a \\ N_b \\ N_c \\ N_d \\ N_e \\ N_f \\ N_g \\ N_h \end{pmatrix} = \begin{pmatrix} f_H \\ f_V \\ f_M \end{pmatrix}$$

One can see that the $\boldsymbol{C}$-matrix is actually the transpose of the $\boldsymbol{K}$-matrix defined in equation (3). Also note that the force vector is at the right-hand side is positive. After solving the equations, the actions can directly be plugged into the Maple sheet as long as their signs are in accordance with the conventions in figure 35.

Solving the equations

The necessary equations have been derived and the equations can now be solved to complete the derivations. The remainder of the work is carried out using Maple, but the approach is discussed in the report. First equation (3) is substituted into equation (4):

$$\boldsymbol{CK}\underline{u} = \underline{f} \qquad \text{Equation (5)}$$

By means of this equation the equilibrium of the system is expressed in the displacements of the spring, in other words: the displacements of the springs required to obtain equilibrium with the given external forces is obtained. If the multiplication of matrices $\boldsymbol{C}$ and $\boldsymbol{K}$, which is a 3 by 3 matrix, is denoted as $\boldsymbol{H}$, then the expression for the displacement vector is:

$$\underline{u} = \boldsymbol{H^{-1}}\underline{f} \qquad \text{Equation (6)}$$

The next step is to substitute the obtained values for the displacements, which are stored in the vector $\underline{u}$, back into equation (3). This way the forces in the piles are obtained that correspond to the displacements that have been calculated. Reference is made to annex VI for the full elaboration of these steps.

This concludes the derivations, a model has been obtained that can be used to determine the forces in the pile foundation if the external forces are known. The next step therefore is to determine the external forces.

7.3.4 Determining loads

Actions existing structures

The actions to be considered in the calculation will be determined for the existing structure first. Because horizontal forces due to braking and acceleration of traffic can also result in significant forces in foundation piles, the horizontal forces due to variable loads will also be included.

Note that, in order to obtain the most unfavourable situation, it is assumed that the full horizontal load is restrained by the support at the abutment under consideration. This is in accordance with the mechanical scheme of a simply supported beam, one of the supports being a hinge.

Vertical loads – Permanent actions: It is assumed that half of the permanent load is supported by each of the foundation blocks. The vertical load due to the permanent actions is determined using the results from the calculations of section 7.2:

$F_{V,G} = 0{,}5 * 23.055 = 11.528$ [kN]

Vertical loads – Variable actions: It is assumed that half of the uniformly distributed variable loads are supported by each of the foundation blocks. To obtain a more unfavourable situation, the axle loads are assumed to be positioned at the abutment under consideration and is by approximation therefore fully supported by this pile group.

$F_{V,Q} = 0{,}5 * F_{V,Q,UDL} + F_{V,Q,axle} = 0{,}5 * (1782 + 1572) + 1080 = 2757$ [kN]

Horizontal loads: The horizontal loads are determined in accordance with the VOSB 1938, the horizontal actions due to braking are covered in article 40. According to the relevant sections of this article, the braking forces are taken equal to 1/7 of the concentrated variable loads. The dynamic amplification factor does not have to be accounted for while reduction of the variable load with two or more lanes may be included. The horizontal forces therefore are:

$F_{H,Q} = \frac{1}{7} * 1080 = 154\ [kN]$

Moments: Moments are introduced in two different ways. Figure 36 already indicates that an eccentricity (which is 0,3 m) is present between the centre of the support and the centre of the pile group. This results in a moment of:

$M_I = (F_{V,G} + F_{V,Q}) * e = (11.528 + 2757) * 0{,}3 = 4286$ [kNm]

A second moment is introduced due to the eccentricity between the horizontal forces, which act at the top side of the deck, and the top of the foundation piles. The eccentricity is determined based on the original design drawings provided by Rijkswaterstaat. Taking the value corresponding to the top of the surfacing layer and the centre of the deck, the difference in height is at both banks of the canal:

- Zuidzijde (Zutphen): 14,93 [m + NAP] - 5,0 [m + NAP] = 9,93 [m]
- Noordzijde (Deventer): 14,02 [m + NAP] - 5,0 [m + NAP] = 9,02 [m]

To obtain the most unfavourable result the largest eccentricity is taken into consideration, hence:

$M_{II} = F_{H,Q} * e_{II} = 154 * 9{,}93 = 1529$ [kNm]

The direction of both bending moments determines whether a favourable or unfavourable effect occurs. The horizontal force can act in both directions (acceleration or braking). If its direction is chosen as such that the moment has the same sigh as the moment M_I, then the most unfavourable situation is obtained.

Defining force vector: The final step is to determine the values of the forces with the appropriate signs to plug into the Maple sheet. Figure 42 gives an overview of the model and the direction in which the forces will be applied.

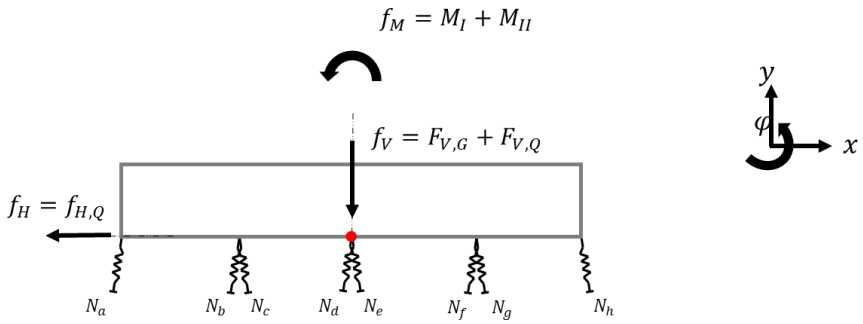


Figure 42 Forces acting on the foundation block

When accounting for the sign conventions, the terms become:

- $f_H = -154$ [kN]
- $f_V = -14.285$ [kN]
- $f_M = +5815$ [kNm]

Actions new design

The actions corresponding to the new design are defined in a similar way as done for the existing structure.

Vertical loads – Permanent actions: Under the assumption of half the permanent load being supported by the foundation block under consideration:

$F_{V,G} = 0{,}5 * 15.779 = 7890$ [kN]

Vertical loads – Variable actions: Under the assumption that half the uniformly distributed variable load and the total value of the concentrated loads are supported by the foundation:

$F_{V,Q} = 0{,}5 * F_{V,Q,UDL} + F_{V,Q,axle} = 0{,}5 * (1852 + 514 + 159 + 1903 + 424) + 582 + 388 = 3396$ [kN]

Horizontal loads: The horizontal actions due to braking and acceleration are covered in section 4.4.1 of Eurocode 1-2. The relevant provisions are as follows:

- A braking force Q_{lk} has to be determined acting in the longitudinal direction of the deck and acts at the top of the deck;

- The characteristic value of Q_{lk} is calculated using the following equation as a percentage of the total maximum vertical loads acting on lane 1 following LM1. The national annex limits the force for the total width of the deck to 800 kN:

$Q_{lk} = 0{,}6 * \alpha_{Q1} * (2 * Q_{1k}) + 0{,}10 * \alpha_{q1} * q_{1k} * w_1 * L \leq 800\ [kN]$

- The action due to acceleration have the same magnitude as the braking force, but acts in the opposite direction and has to be accounted for as well.

According to 4.5.1 of the national annex, these horizontal actions are combined with the vertical actions of LM1 and those on the pedestrian lanes into load group gr1a. In order to do so the characteristic value of the horizontal force is multiplied with a factor 0,8. The final value to be included in the calculation therefore is:

$Q_{hor} = 0{,}8 * \{0{,}6 * 0{,}97 * (2 * 300) + 0{,}10 * 0{,}97 * 9{,}0 * 3{,}0 * 70{,}7\} \leq 0{,}8 * 800\ [kN] \rightarrow F_{H,Q} = 428$ [kN]

Moments: As for the existing structure the total bending moment comprises two components. The first is the result of the eccentricity between the centres of the support and pile group:

$M_I = (F_{V,G} + F_{V,Q}) * e = (7890 + 3396) * 0{,}3 = 3386$ [kNm]

The second moment is due to the eccentricity between the top side of the deck and the top of the foundation piles. The prefab UHPC beams are 0,6 m higher than the main girders of the existing structure, the eccentricity is therefore increased with the same value to 10,53 m:

$M_{II} = F_{H,Q} * e_{II} = 428 * 10{,}53 = 4507$ [kNm]

Defining force vector: Figure 42 gives an overview of how the forces are applied onto the foundation block. When accounting for the sign conventions the loads to be plugged into the Maple sheet are:

- $f_H = -428$ [kN]
- $f_V = -11.286$ [kN]
- $f_M = +7893$ [kNm]

7.3.5 Determining forces in foundation piles

The values of the horizontal forces, vertical forces and moments for the existing structure and new design are plugged into the Maple file, after which the calculations are performed as outlined in section 7.3.3.

7.3.6 Comparison and analysis of results

Overview of results

Table 22 summarizes the results from the calculations performed in the Maple file. Note that the calculation has been performed in the serviceability limit state, i.e. without load factors, and that the forces in the table represent the forces in a single pile, not those of the pile group.

Table 22 Forces in foundation piles in SLS

Pile force	Existing situation [kN]	New design [kN]	Absolute difference [kN]
N_a	-423,5	-387,6	35,9
N_b	-178,5	-168,7	9,8
N_c	-257,2	-185,2	72,0
N_d	-96,4	-98,9	2,5
N_e	-205,9	-141,6	64,3
N_f	-14,3	-29,1	14,8
N_g	-154,6	-98,0	56,6
N_h	-268,4	-141,3	127,1

Analysis of the results

With regards to the results summarized in the table various observations can be made. Given the direction of the actions, it was already expected that pile group 'a' would be loaded with the largest compressive load, which indeed turns out to be the case. In addition, it can be observed that, with the expectation of two cases, the pile forces in the new situation are lower than those in the existing situation, within the scope of the actions that have been taken into consideration. Furthermore, it can be seen that there is a large scatter in the percentual change of the forces in the piles, especially the pile groups e – f show large differences between the new design and existing foundation. Within the context of the limitations of and simplifications incorporated in the model and the actions considered, the following conclusions can be drawn:

1. The reduction of the vertical force as calculated in section 7.2 indeed results in a reduction of the forces in the foundation piles in the serviceability limit state, the reduction of the governing piles, from -423,5 kN to -387,6 kN, being 8,5%. This is with the exception of two pile groups, but in those situations the pile forces remain relatively low compared to the governing foundation piles;

2. The second conclusion is that the reduction of the total vertical load expressed as a certain percentual change does not result in a reduction of the forces in the foundation piles with a percentual change of equal magnitude, confirming the expectation that a comparison of just the total vertical loads does not fully capture the distribution of the loads over the foundation piles.

Thus, although the reduction of total vertical forces is an indicator that the forces in the piles will reduce as well, it does not give information specifically enough to determine the actual reduction of the forces on the level of a pile group or single pile. This raises the question what the causes are of this difference, multiple contributing factors can be given:

- **Design of the foundation**: The design of the foundation with the inclined piles and different numbers of piles per rows already causes an uneven distribution of the forces over the pile groups, this can be demonstrated using the Maple file. If for example the horizontal force and moment are taken equal to zero and only a single vertical load is applied, one can see that the force distribution is uneven and that the outer rows a and h carry the largest loads.

- **Introduction of moments**: The eccentricity of the support with respect to the centre of the pile group also contributes. Again, this can be investigated using the Maple file. Suppose that one case is considered with a downward vertical force and one case with a downward vertical force and a positive bending moment. As to be expected, the first case results in approximately equal compressive forces in rows a and h while the second case results in larger forces in pile row a and smaller forces in row h.

- **Including horizontal forces**: Another contributing factor is including horizontal forces and the moments caused by these forces while these were not included in the comparison in section 7.2. Again, using Maple, the influence of including these actions can be demonstrated, which causes tensile actions in the piles that are inclined as such that the horizontal component of their reaction force is in the direction opposite of the line of action of the external horizontal force acting on the foundation block.

Validation of the results

The final step of the comparison and analysis of the results is a brief validation to determine whether the obtained results of the pile forces are realistic. A simple calculation is performed to estimate the stresses at the tip of the foundation pile, after which this value will be used to judge the result and determine whether the order of magnitude is realistic.

Determine cross section of pile: Although the drawings indicate that the piles are prefabricated concrete foundation piles with rectangular cross sections, no specific dimensions are given. By means of measuring and scaling the drawings, it is estimated that the piles have a rectangular 320 by 320 mm cross section.

Stresses: Next the stresses at the pile tip are calculated. The heaviest loaded pile group is considered, with a compressive force of approximately 388 kN per pile.

$$\sigma_s = \frac{N_{max}}{A_p}$$

In this equation σ_s denotes the stress at the tip of the foundation pile, N_{max} denotes the force in the governing pile and A_p denotes the cross-sectional dimension of the foundation pile.

With a force of $N_{max} = 388$ kN and a cross section of 320 by 320 mm^2, this results in a stress of 6,2 N/mm^2. Note that this value does not include any load factors. In addition, it is based on the actions due to the self-weight of the superstructure and the vertical and horizontal loads acting upon it. Other loads such as the self-weight of the abutments will result in a limited increase of this value.

Conclusion: The stress value of 6,2 N/mm^2 is deemed to be plausible given the fact that older foundation piles used lower concrete classes and were not prestressed, compared to nowadays practice. In addition, older sources such as (Dwars, 1946) make mention of a guiding value of 40 t for piles of reinforced concrete as an upper limit, which is about 400 kN, after which cone penetration tests were used to determine the required pile dimensions and depth to which it should be driven into the subsoil. The governing pile force is around (existing structure) or below (new situation) this guiding value, which may have been used during the design of the bridge, and is an additional confirmation that the result is plausible.

8

CONCLUSIONS AND PROSPECTS

Conclusions

This report comprised two different topics. The first four chapters were dedicated to the optimization of the detailed design. The goal of this part was to determine the dimensions of the beams in order to obtain the most optimal design which complies with the relevant codes and standards. The elaboration of this design took place in a stepwise fashion and included all loads, boundary conditions & requirements and executional aspects that are part of the project.

The first chapter started with a discussion on the results of the detailed design. Different options for the optimization were given, after which one of these options was chosen. It was decided to base the optimization on the variation of dimensions within the detailed design. The intended approach to the optimization was also defined.

A cross section has certain minimum values, these were denoted as 'constraints of the optimization' and were covered in the second chapter. The first set of limitations that were discussed was based on criteria such as concrete cover and spacing between prestressing strands. The second set of minimum dimensions was based on the capacity of the beam, by properties or results such as the stresses at mid span or the bending moment capacity to the dimensions of the beam (height and web thickness).

The third chapter started with dimensioning a more optimized beam by making use of the information in the previous two chapters, after which this design was fully verified in two series of calculations, resulting in an optimized design that satisfied all included requirements. This design is denoted as the 'final design' of the project. The results of the verifications indicated that there was only very limited room for further weight reduction if the same approach would be used. If a substantial further weight reduction is desired, then a different approach should be applied. In the fourth chapter the properties and dimensions of the 'final design' were subsequently summarized.

The second part of the report covered the global analysis of the existing foundation, using the results of the final design and the properties of the existing structure. The fifth chapter gave the outline of the initially intended approach to the global analysis of the foundation and the analysis of the results. In addition, the codes on which the design of the existing bridge was most likely based were identified: the GBV 1950 and the VOSB 1938.

In the sixth chapter, the self-weight of the existing structure and the new design were determined. Based on the Eurocode 1-2 and the VOSB 1938 the vertical variable actions on the newly designed deck and the existing structure were determined as well. Furthermore, a brief comparison was made to determine if the intended approach to the global analysis of the foundation would be feasible based on the safety philosophies of the Eurocode and the GBV 1950 and VOSB 1938. It turned out that this is not the case because of two reasons. The first reason is that the Eurocode uses the method of partial factors while the older codes work with a global safety factor. The second reason is that it remains unclear what safety margin was included in the original design of the existing foundation, this further complicates a comparison by means of the intended approach. An alternative approach therefore had to be devised.

In the seventh chapter this alternative approach was presented and the actual global verification of the foundation was carried out. It comprises two parts. The first part is a comparison based on the total vertical

forces between the new design and existing structure without load factors. The second part is a comparison based on the forces in the foundation piles and also included horizontal forces, to obtain a more complete impression. The latter part of the calculation was included because it was expected, despite simplifications and assumptions, to provide insight into effects that cannot be captured by only comparing the total vertical loads.

It turned out that in terms of vertical forces the final design results in a reduction of 21% compared to the existing structure. Although the variable loads in the new situation according to Eurocode 1-2 were 31% higher than those of the existing bridge according to VOSB 1938, the total forces still resulted in this significant reduction because the permanent loads were reduced by 32%. It was noted that for this span the permanent load is significantly larger than the variable load, an impression which is typical for concrete structures of larger spans.

The additional calculation of the forces in the foundation piles resulted in two conclusions. The first conclusion was that there was a reduction of forces in the governing foundation piles. The second conclusion was that the reduction of the total vertical load expressed as a certain percentual change does not result in a percentual decrease of the forces in the foundation piles of equal magnitude. This was contributed to the design of the foundation, the introduction of moments acting on the foundation block and to including horizontal forces in the verification.

Prospects

In this report the remaining information has been collected that is required to conclude the project. With the finalization of the detailed design, the design stage of the project has been concluded. In addition, by performing the global verification of the foundation, the most important parts of the analysis of the results of the design stage and of the comparison with the existing structure have also been finalized.

Using this information, the remaining project activities can be finished in the main report. Using the results and the analyses outlined in this report, conclusions can be drawn, the generalisation of results will be elaborated on and recommendations will be formulated. This will be done while paying attention to any questions or uncertainties that may remain after finalizing the design stage and while accounting for implications and consequences of the decisions and assumptions that have been made during the elaboration of the project up to and including the project activities as described in this report.

9

BIBLIOGRAPHY

Commissie F1 voor de normalisatie van technische grondslagen voor bouwvoorschriften. (1949). N 1055. *TGB 1949 - Technische Grondslagen voor Bouwvoorschriften*.

Dwars, A. (1946). *Waterbouwkunde* (Vierde, herziene druk ed., Deel 1 - Algemene inleiding - ontwerpen - bodemonderzoek en draagkracht van de bodem - funderingen - beschoeiingen en keermuren). (A. D. Colijn, Red.) Amsterdam: LJ. Veen's Uitgeversmaatschapppij N.V.

DYWIDAG. (2017, juni 01). DYWIDAG Bonded Post-Tensioning Systems using Strands.

Gijsbers, J. (2012). 100 jaar betonvoorschriften. *Cement*, 68 - 77.

Groupe de travail BFUP. (2013, June). Ultra High Performance Fibre-Reinforced Concretes. *Recommendations*. Association Francaise de Génie Civil.

Koninklijk Instituut van Ingenieurs (KIVI) - Afdeling voor Bouw- en Waterbouwkunde. (1938). N 1008. *VOSB 1938 - Voorschriften voor het Ontwerpen van Stalen Bruggen*.

Koninklijk Instituut van Ingenieurs (KIVI) - Afdeling voor Bouw- en Waterbouwkunde. (1950). N 1009. *GBV 1950 - Gewapend-Betonvoorschriften 1950*.

NEN. (2011, november). NEN-EN 1992-1-1+C2. *Eurocode 2: Ontwerp en berekening van betonconstructies - Deel 1-1: Algemene regels en regels voor gebouwen*.

NEN. (2015, oktober). NEN-EN 1991-2+C1. *Eurocode 1: Belastingen op constructies – Deel 2: Verkeersbelasting op bruggen*.

NEN. (2019, november). NEN-EN 1990+A1+A1/C2. *Eurocode: Grondslagen voor het constructief ontwerp*.

NEN. (2019, november). NEN-EN 1990+A1+A1/C2/NB. *Nationale bijlage bij NEN-EN 1990+A1:2006+A1:2006/C2:2019 Eurocode: Grondslagen van het constructief ontwerp*.

NEN. (2019, november). NEN-EN 1991-2+C1/NB. *Nationale bijlage bij NEN-EN 1991-2+C1: Eurocode 1: Belastingen op constructies – Deel 2: Verkeersbelasting op bruggen*.

NEN. (2020, februari). NEN-EN 1992-1-1+C2/NB+A1. *Nationale bijlage bij NEN-EN 1992-1-1+C2 Eurocode 2: Ontwerp en berekening van betonconstructies - Deel 1-1: Algemene regels en regels voor gebouwen*.

Snijder, H., & Steenbergen, H. (2011). *Krachtswerking.* Zoetermeer: Bouwen met Staal.

Van Tol, F. (1994, juni 3). Hoe betrouwbaar is de paalfundering? *Intreerede*. Technische Universiteit Delft.

Verruijt, A. (2001). *Grondmechanica.* Delft: Technische Universiteit Delft.

Annex(es)

ANNEX: OVERVIEW CALCULATIONS OPTIMIZATION PHASE

OVERVIEW CALCULATIONS OPTIMIZATION PHASE

This document gives an overview of all the calculations that have been performed as part of the optimization phase, as well as the corresponding assumptions that have been made. This document has been prepared to provide additional clarifications to the Excelsheet, it provides all the equations of the calculations that have been performed. For easy reference a table of content has been added, the order in which all calculations are discussed in this annex follows the setup of the calculation sheet in Excel.

Table of content:

1 CALCULATION PARAMETERS 4

1.1 Geometry of the structure 4
1.1.1 Main dimensions of the deck 4
1.1.2 Cross sectional properties main beams 4
1.1.3 Cross sectional properties end cross beams 8
1.1.4 Cross sectional properties longitudinal joints 9

1.2 Material and calculation parameters 10
1.2.1 Concrete 10
1.2.2 Prestressing steel & parameters strands and tendons 12
1.2.3 Partial factors material resistance 14
1.2.4 Calculation parameters 14

1.3 Design of bridge and main carriageway – Actions 15
1.3.1 Design main carriageway 15
1.3.2 Effective width of the beams 15
1.3.3 Permanent actions (G) 15
1.3.4 Variable actions (Q) 16
1.3.5 Accidental actions (A) 16
1.3.6 Fatigue 16
1.3.7 Combinations of actions 16

1.4 Determining force distribution (RFEM input) 16
1.4.1 Design of main prestressing and verification capacity of the main beams 16
1.4.2 Fatigue analysis main beams 17
1.4.3 Design of prestressing and verification capacity of the end cross beams 17

2 ULS – STR 18

2.1 Input parameters 18

2.2 Design of the main prestressing 18
2.2.1 Calculating prestress losses 18
2.2.2 Determining stresses at midspan 20

2.3 Detailing beam ends 21
2.3.1 Bond stresses and transmission length 21
2.3.2 Tensile stresses at top fibre 21

2.3.3 Positioning of strands in the bottom flange 22
2.3.4 Splitting reinforcement – Vertical distribution 23
2.3.5 Splitting reinforcement – Horizontal distribution 25
2.4 Verification bending moment capacity 26
2.4.1 Assumptions 26
2.4.2 Calculating the capacity and verifications 26
2.5 Verification shear force capacity 30
2.5.1 Assumptions and limitations 30
2.5.2 Calculating the resistance and unity check 30
2.6 Verification torsional resistance 31
2.6.1 Assumptions & approach 31
2.6.2 Torsional capacity 31
2.6.3 Combination of shear and torsion 32
2.7 Global verification ship collision 34
3 DESIGN OF MAIN BEAMS – TOP FLANGE AND TRANSVERSE PRESTRESSING 35
3.1 Design of transverse prestressing 35
3.1.1 Calculating prestress losses 35
3.1.2 Forces acting on top flange and joint 37
3.1.3 Verifying stresses over joint height 38
3.1.4 Detailing 39
3.2 Local verification – Verification bending moment capacity longitudinal joint 40
3.3 Local verification – Bending moment capacity top flange between the webs 41
3.3.1 Calculation model and design value bending moments 41
3.3.2 Verification of bending moment capacity 42
3.4 Local verification – Bending moment capacity top flange between prestressing ribs 46
3.4.1 Calculation model and design value bending moments 46
3.4.2 Verification of bending moment capacity 46
4 DESIGN OF MAIN BEAMS – FATIGUE VERIFICATION 50
4.1 Fatigue verification 50
4.1.1 Assumptions and approach 50
4.1.2 Fatigue verification – Prestressing steel at midspan 50
4.1.3 Fatigue verification – Concrete at midspan 51
5 MAIN BEAMS – SERVICEABILITY LIMIT STATE 53
5.1 Deflections 53
5.1.1 Assumptions and approach 53
5.1.2 Upper limit of deflections 53
5.1.3 Comparison with RFEM 54

5.2 Crack width verification 54

6 END CROSS BEAM 55

6.1 Assumptions and parameters 55
6.1.1 Assumptions 55
6.1.2 Input parameters 55
6.2 Design of the prestressing 56
6.2.1 Calculating prestress losses 56
6.2.2 Determining stresses over beam height 58
6.3 Verification bending moment capacity 59
6.3.1 Assumptions 59
6.3.2 Calculating the capacity and verifications 59
6.4 Verification shear force capacity 61
6.5 Assumptions and parameters 61
6.5.1 Calculating the capacity and verifications 61

7 WEIGHT CALCULATION 63

7.1 Weight calculation 63

1

CALCULATION PARAMETERS

The overview in this chapter describes all the calculation parameters and input required for the calculation. For completeness all values used for the final design are added and marked in grey.

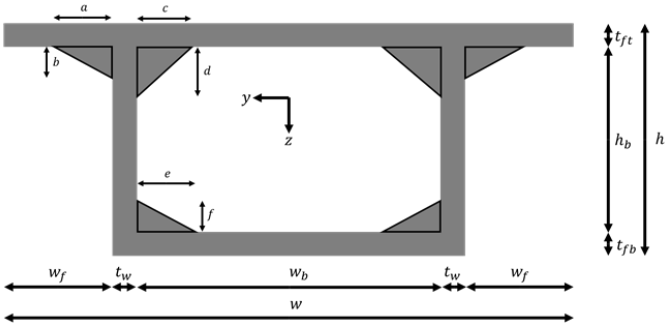
1.1 Geometry of the structure

1.1.1 Main dimensions of the deck

Symbol	Value	Units	Definition
l	68,00	[m]	Span of the main beams
w_{tot}	16,36	[m]	Total width of the deck
l_{tot}	70,70	[m]	Total length of the main beams
n_{beams}	5	[pcs]	Number of prefab UHPC beams

1.1.2 Cross sectional properties main beams

Main properties



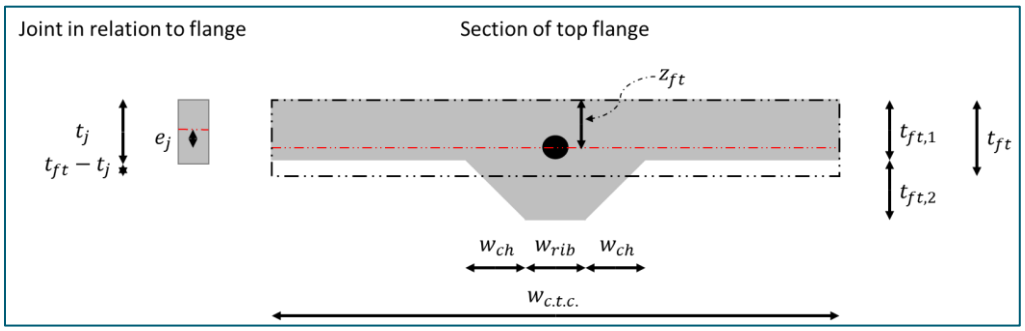
Symbol	Value	Units	Definition
w	3200	[mm]	Total width
h	1900	[mm]	Total height
t_{fb}	200	[mm]	Thickness bottom flange
t_w	100	[mm]	Thickness of web
w_f	500	[mm]	Width of the flanges
w_b	2000	[mm]	Internal width of the box

Chamfer of flanges

Symbol	Value	Units	Definition
a	0	[mm]	Width outer chamfer top flange
b	0	[mm]	Height outer chamfer top flange
c	0	[mm]	Width inner chamfer top flange
d	0	[mm]	Height inner chamfer top flange
e	0	[mm]	Width inner chamfer bottom flange
f	0	[mm]	Height inner chamfer bottom flange

Top flange – transverse direction

Values can be entered to apply a variable height of the top flange. If a top flange with continuous thickness is to be applied, then only the values t_{ft1} and $w_{c.t.c.}$ should be entered. A section of the top flange with one rib is given in the following figure, as well as a section of the longitudinal joint.



Input parameters: The following parameters can be defined:

Symbol	Value	Units	Definition
$w_{c.t.c.}$	1000	[mm]	Centre to centre distance of the transverse prestressing ribs/ducts
$t_{ft,1}$	125	[mm]	Continuous thickness of the top flange
$t_{ft,2}$	125	[mm]	Local increase thickness top flange at transverse rib
w_{rib}	250	[mm]	Width of the transverse prestressing rib
w_{ch}	250	[mm]	Width of chamfer next to the transverse prestressing rib

Using the aforementioned values various properties and dimensions are calculated that are required to perform various calculations and verifications.

Mean value thickness top flange t_{ft}: If the option of defining a variable height for the top flange in transverse direction is used, a mean value of the thickness of the top flange is calculated:

$$t_{ft} = \frac{w_{c.t.c.} * t_{ft,1} + w_{rib} * t_{ft,2} + 2 * 0{,}5 * w_{ch} * t_{ft,2}}{w_{c.t.c.}} \rightarrow \frac{1000 * 125 + 250 * 125 + 2 * 0{,}5 * 250 * 125}{1000} = 187{,}5\ [mm]$$

This mean value (or: equivalent thickness) is used to perform the following calculations or verifications:

- Calculation of the cross sectional properties of the main beam as a whole (e.g. internal height of the box, cross-sectional area, centre of gravity, second moment of area, etc.);
- Local verification of the longitudinal joints between the prefab beams;
- Local verification of the top flange in longitudinal direction;

Note that in the case an equal thickness of the top flange is used $t_{ft} = t_{ft,1}$.

Internal height of the box h_b: Using the mean height of the top flange the internal height of the box is calculated:

$$h_b = h - t_{fb} - t_{ft} \rightarrow 1900 - 200 - 187{,}5 = 1512{,}5\ [mm]$$

Centre of gravity z_{ft} of top flange: The position of the centre of gravity of the top flange with respect to the top fibre in transverse direction is calculated as follows:

$$z_{ft} = \frac{w_{c.t.c.} * t_{ft,1} * \frac{t_{ft,1}}{2} + 2 * \frac{1}{2} * w_{ch} * t_{ft,2} * \left(t_{ft,1} + \frac{t_{ft,2}}{3}\right) + w_{rib} * t_{ft,2} * \left(t_{ft,1} + \frac{t_{ft,2}}{2}\right)}{w_{c.t.c.} * t_{ft,1} + 2 * \frac{1}{2} * w_{ch} * t_{ft,2} + w_{rib} * t_{ft,2}}$$

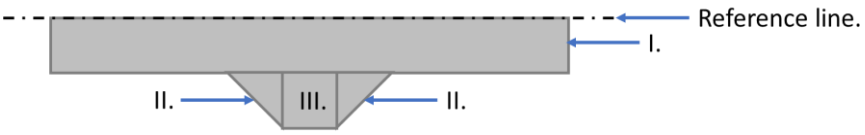
$$z_{ft} = \frac{1000 * 125 * \frac{125}{2} + 2 * \frac{1}{2} * 250 * 125 * \left(125 + \frac{125}{3}\right) + 250 * 125 * (125 + \frac{125}{2})}{1000 * 125 + 2 * \frac{1}{2} * 250 * 125 + 250 * 125} = \frac{18.880.208}{187.500} = 100{,}7\ [mm]$$

This value is applied for:

- The design of the transverse prestressing;
- The local verifications of the top flange in transverse direction;
- The calculation of all cross sectional properties of the top flange required for the design of the transverse prestressing and local verifications of the top flange in transverse direction.

Second moment of area I_{ft} of top flange: The second moment of area of a section of the top flange with one prestressing rib is calculated as follows:

$$I_{ft} = \sum_{i=1}^{n} (I_{ft,i} + A_{,fti} * a_{ft,i}^2)$$



The value of the second moment of area is required for the calculation of the prestress losses in case an additional eccentricity Δe_{ft} is applied. The individual contributions are calculated as follows:

Section	$\boldsymbol{I_{ft,i}\ [mm^4]}$	$\boldsymbol{A_{ft,i}\ [mm^2]}$	$\boldsymbol{a_{ft,i}^2\ [mm]}$
I.	$\frac{1}{12} * w_{c.t.c.} * t_{ft,1}^3$	$w_{c.t.c.} * t_{ft,1}$	$\left(z_{ft} - \frac{t_{ft,1}}{2}\right)^2$
II.	$\frac{1}{36} * 2 * w_{ch} * t_{ft,2}^3$	$2 * \frac{1}{2} * w_{ch} * t_{ft,2}$	$\left(z_{ft} - \left(t_{ft,1} + \frac{t_{ft,2}}{3}\right)\right)^2$
III.	$\frac{1}{12} * w_{rib} * t_{ft,2}^3$	$w_{rib} * t_{ft,2}$	$\left(z_{ft} - \left(t_{ft,1} + \frac{t_{ft,2}}{2}\right)\right)^2$

Section	$\boldsymbol{I_{ft,i}\ [mm^4]}$	$\boldsymbol{A_{ft,i}\ [mm^2]}$	$\boldsymbol{a_{ft,i}^2\ [mm]}$
I.	$\frac{1}{12} * 1000 * 125^3 = 162.760.417$	$1000 * 125 = 125.000$	$\left(100{,}7 - \frac{125}{2}\right)^2 = 1459$
II.	$\frac{1}{36} * 2 * 250 * 125^3 = 27.126.736$	$2 * \frac{1}{2} * 250 * 125 = 31.250$	$\left(100{,}7 - \left(125 + \frac{125}{3}\right)\right)^2 = 4352$
III.	$\frac{1}{12} * 250 * 125^3 = 40.690.104$	$250 * 125 = 31.250$	$\left(100{,}7 - \left(125 + \frac{125}{2}\right)\right)^2 = 7534$

$$I_{ft} = 162760417 + 125000 * 1459 + 27126736 + 31250 * 4352 + 40690104 + 31250 * 7534 = 7{,}844 * 10^8\ [mm^4]$$

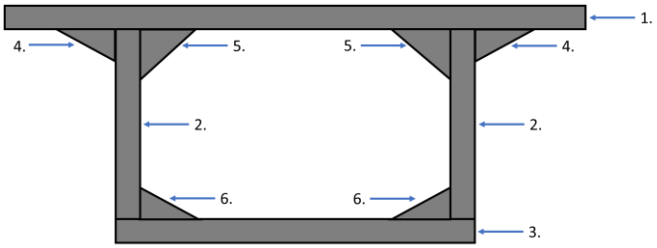
Additional eccentricity Δe_{ft}: It is also possible to apply an additional eccentricity Δe_{ft} to move the centre of the tendons of the transverse prestressing further downwards compared to the centre of gravity z_{ft} of a section of the top flange.

If no additional eccentricity is applied, then the transverse prestressing is assumed to be applied centrically onto the top flange. If an additional eccentricity is applied, then the transverse prestressing is assumed to be applied eccentrically onto the top flange, causing upward bending.

Applied value: $\Delta e_{ft} = 8{,}0$ mm

Determining cross sectional properties and main parameters

Using all previously defined or calculated main dimensions the cross sectional properties of the main beams can be determined. To approach this in a structured manner the cross section is divided into a number of standard shapes, this is depicted in the following figure.



Cross sectional area: The cross sectional area of the concrete cross section is as follows:

$$A_c = \sum_{i=1}^{n} A_i$$

Where:
A_i: Cross sectional area of individual segment 'i'

Centre of gravity: The position of the centre of gravity with respect to the top fibre is defined as follows. It is calculated using the summation of the first moments of area of all individual segments with respect to the top fibre and the cross sectional area of the cross section.

$$z = \frac{\sum_{i=1}^{n} A_i * e_i}{\sum_{i=1}^{n} A_i}$$

Where:
e_i: Distance from centre of an individual element 'i' to the top fibre of the cross section

Second moment of area: The second moment of area of the total cross section along the horizontal axis (y-axis) is calculated using Steiner's rule. First the second moment of the individual elements has to be calculated, for rectangles or triangles this is respectively:

$$I_i = \frac{1}{12} * b_i * h_i^3$$

$$I_i = 36 * b_i * h_i^3$$

Where:
b_i: Width of individual element'i'
h_i: height of individual element 'i'

Subsequently the Steiner part of the contribution of each individual element to the total second moment of area has to be calculated. In order to do so the distance between the centre of gravity of the individual element and the centre of gravity of the whole cross section, a_i, has to be calculated. Using the top fibre as a reference point this is done as follows:

$$a_i = |e_i - z|$$

The second moment of area of the total cross section now becomes:

$$I_y = \sum_{i=1}^{n} (I_i + A_i * a_i^2)$$

Distances to the outer fibres: The distances from the centre of gravity of the cross section to the outer fibres at the top and bottom are defined as:

$$e_t = z$$

$$e_b = h - z$$

Section moduli: Using the second moment of area of the total cross section and the distances to the outer fibres the section moduli of the cross section with respect to the outer fibres can be calculated:

$$W_{y,t} = \frac{I_y}{e_t}$$
$$W_{y,b} = \frac{I_y}{e_b}$$

The results are:

Symbol	Value	Units	Definition
A_c	1342500,0	[mm²]	Cross sectional area of total cross section
z	844,5	[mm]	Position centre of gravity from the top flange
I_y	8,038E+11	[mm⁴]	Second moment of area of the combined cross section
e_t	844,5	[mm]	Distance from centre of gravity to top fibre
e_b	1055,5	[mm]	Distance from centre of gravity to bottom fibre
$W_{y,t}$	9,518E+08	[mm³]	Section modulus with respect to top fibre
$W_{y,b}$	7,615E+08	[mm³]	Section modulus with respect to bottom fibre

The results are verified by comparing the cross sectional area and second moment of area with the values calculated by RFEM using the same dimensions.

1.1.3 Cross sectional properties end cross beams

Main dimensions

It is assumed that the end cross beams have a solid rectangular cross section. The height and width can be defined in Excel:

Symbol	Value	Units	Definition
h_{cb}	1900	[mm]	Total height of the end cross beam
w_{cb}	1900	[mm]	Total width of the end cross beam

Determining cross sectional properties

The following cross sectional properties are defined:

- Cross sectional area:

$$A_{cb} = h_{cb} * w_{cb}$$

- Section modulus of the cross section:

$$W_{y,cb} = \frac{1}{6} * w_{cb} * h_{cb}^2$$

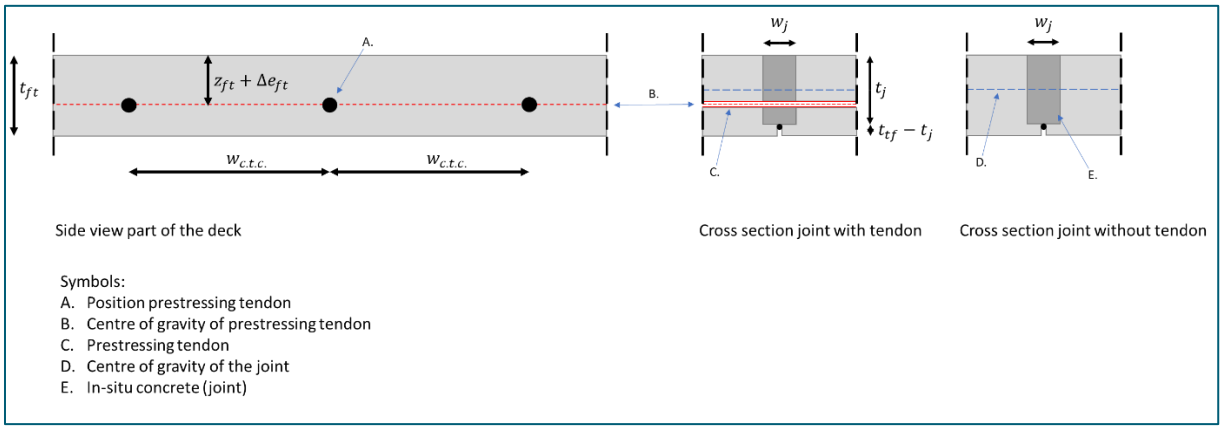
- Second moment of area of the cross section:

$$I_{y,cb} = \frac{1}{12} * w_{cb} * h_{cb}^3$$

1.1.4 Cross sectional properties longitudinal joints

Main dimensions

The longitudinal joints are analysed while making use of the mean value t_{ft} for the thickness of the top flange, the following sketch shows all relevant dimensions.



In the analysis of the longitudinal joint two main assumptions are made:

- The thickness of the top flange is the mean value t_{ft};
- Transverse prestressing is present with its centre of gravity at a distance of z_{ft} from the top fibre (if no additional eccentricity is provided), or at distance $z_{ft} + \Delta e_{ft}$ (if additional eccentricity is provided).

The following additional dimensions have to be defined:

Symbol	Value	Units	Definition
t_j	162,5	[mm]	Height of the longitudinal joint
w_j	90	[mm]	Transverse width of the longitudinal joint

The thickness of the joint is chosen while the width of the joint is calculated automatically:

$$w_j = \frac{w_{tot} - n_{beams} * w}{n_{beams} - 1} \rightarrow \frac{16.360 - 5 * 3200}{5 - 1} = 90\ [mm]$$

Determining cross sectional properties

For the analysis of the joint it is assumed that a strip with a transverse width of 1000 mm is analysed. The cross sectional area, section modulus and second moment of area of the joint are as follows:

$$A_j = 1000 * t_j \ [mm^2]$$

$$W_j = \frac{1}{6} * 1000 * t_j^2 \ [mm^3]$$

$$I_j = \frac{1}{12} * 1000 * t_j^3 \ [mm^4]$$

1.2 Material and calculation parameters

1.2.1 Concrete

Material properties concrete main beams (Ductal FM)

For the main beams the following material properties have to be defined:

Parameters mixture composition			
Symbol	**Value**	**Units**	**Definition**
ρ	25	[kN/m^3]	Density
l_f	13	[mm]	Fibre length
Parameters concrete in compression			
f_{ck}	200	[N/mm^2]	Characteristic value compressive strength
ε_{c3}	2,3	[‰]	Strain at reaching concrete compressive strength
ε_{cu3}	2,6	[‰]	Maximum compressive strain at ULS
Parameters concrete in tension			
$f_{ctk,el}$	9	[N/mm^2]	Characteristic elastic (5% percentile value) tensile strength
f_{ctfk}	10	[N/mm^2]	Characteristic value maximal post cracking stress (w=0,30)
K_{global}	1,25	[-]	Fibre orientation factor (global)
K_{local}	1,75	[-]	Fibre orientation factor (local)
Parameters stiffness and deformations (temperature, creep and shrinkage)			
E_{cm}	50000	[N/mm^2]	Modulus of elasticity
G	20833	[N/mm^2]	Shear modulus
v	0,2	[-]	Poisson ratio
α	0,000012	[K-1]	Coefficient of thermal expansion
φ	0,3	[-]	Creep
ε_{shr}	0,8	[‰]	Autogenous shrinkage (during HT)
Parameters concrete other			
α	0,56	[-]	Factor for shape of concrete compressive zone
β	0,34	[-]	Factor position centre of gravity concrete compressive zone
α_{cc}	0,85	[-]	Long term effects and unfavourable loading (compression)
α_{ct}	1,0	[-]	Long term effects and unfavourable loading (tension)
Parameters fatigue			
$\beta_{cc}(t)$	1,0	[-]	Factor for increase of strength due to progressive hydration
f_{ck0}	10,0	[N/mm^2]	Standard value (10 Mpa)

Calculated values: The following values are calculated using the aforementioned values:

- Design value concrete compressive strength:

$$f_{cd} = \frac{\alpha_{cc} * f_{ck}}{\gamma_C} \rightarrow \frac{0{,}85 * 200}{1{,}5} \approx 113\ [MPa]$$

- Design value of tensile strength (elastic limit, formation of first crack):

$$f_{ctd} = \frac{\alpha_{ct} * f_{ctk,el}}{\gamma_C} \rightarrow \frac{1{,}0 * 9{,}0}{1{,}5} = 6{,}0\ [MPa]$$

- Design value maximum post cracking stress (at $w = 0{,}3$ mm):

$$f_{ctd;2} = \frac{f_{ctfk}}{K_{global} * \gamma_{cf}} \rightarrow \frac{10}{1{,}25 * 1{,}3} \approx 6{,}15\ [MPa]$$

Material properties concrete longitudinal joints

For the longitudinal joints the following material properties have to be defined:

Parameters mixture composition			
Symbol	**Value**	**Units**	**Definition**
ρ	25	[kN/m^3]	Density
Parameters concrete in compression			
f_{ck}	100	[N/mm^2]	Characteristic value compressive strength
ε_{cu3}	2,6	[‰]	Maximum compressive strain at ULS
Parameters stiffness and deformations (temperature, creep and shrinkage)			
E_{cm}	45000	[N/mm^2]	Modulus of elasticity
φ	0,8	[-]	Creep factor
Parameters concrete other			
α	0,56	[-]	Factor for shape of concrete compressive zone
β	0,34	[-]	Factor position centre of gravity concrete compressive zone
α_{cc}	0,85	[-]	Long term effects and unfavourable loading (compression)

Calculated values: The design value of the concrete compressive strength is calculated using the aforementioned values:

$$f_{cd} = \frac{\alpha_{cc} * f_{ck}}{\gamma_C} \rightarrow \frac{0{,}85 * 100}{1{,}5} \approx 57\ [MPa]$$

Material properties concrete end cross beams

For the main beams the following material properties have to be defined:

Parameters mixture composition			
Symbol	**Value**	**Units**	**Definition**
ρ	25	[kN/m^3]	Density
Parameters concrete in compression			
f_{ck}	30	[N/mm^2]	Characteristic cylinder compressive strength at 28 days
$f_{ck,cube}$	37	[N/mm^2]	Characteristic cube compressive strength
f_{cm}	38	[N/mm^2]	Mean value cylinder compressive strength
ε_{c3}	1,75	[‰]	Strain at reaching concrete compressive strength
ε_{cu3}	3,5	[‰]	Maximum compressive strain at ULS
Parameters concrete in tension			
f_{ctm}	2,9	[N/mm^2]	Mean value axial tensile strength
$f_{ctk;0,05}$	2,0	[N/mm^2]	5%-fractile of the axial tensile strength

Parameters stiffness and deformations (temperature, creep and shrinkage)

E_{cm}	33000	[N/mm^2]	Secant modulus of elasticity
φ	1,75	[-]	Creep
Hydration	Normal (N)	[-]	Rate of hydration: Rapid (R), Normal (N) or slow (S)
RH	80,0	[%]	Relative humidity

Parameters concrete other

α	0,75	[-]	Factor for shape of concrete compressive zone
β	0,39	[-]	Factor position centre of gravity concrete compressive zone
α_{cc}	1,0	[-]	Long term effects and unfavourable loading (compression)

Calculated values: The design value of the concrete compressive strength is calculated using the aforementioned values:

$$f_{cd} = \frac{\alpha_{cc} * f_{ck}}{\gamma_C} \rightarrow \frac{1{,}0 * 30}{1{,}5} = 20\ [MPa]$$

1.2.2 Prestressing steel & parameters strands and tendons

Parameters prestressing main beams

For the prestressing of the main beams using pretensioned steel the following parameters have to be defined:

Material properties prestressing steel

Symbol	Value	Units	Definition
f_{pk}	1860	[N/mm^2]	Characteristic value tensile strength
f_{pd}	1522	[N/mm^2]	Design value steel stress
σ_{pm0}	1395	[N/mm^2]	Maximum allowed stress directly after tensioning
$\sigma_{p,max}$	1488	[N/mm^2]	Maximum prestressing stress during tensioning
E_p	195000	[N/mm^2]	Modulus of elasticity
ε_{uk}	35	[‰]	Characteristic value strain at failure

Properties prestressing strands

n_c	10	[pcs]	Assumed number of strands positioned centrically in the cross section
$D_{strand,c}$	15,2	[mm]	Diameter of strands positioned centrically
$A_{p,strand,c}$	140	[N/mm^2]	Cross sectional area per strand
$\sigma_{p,max,prov,c}$	1400	[mm^2]	Assumed maximum stress applied to centrically positioned strands
n_{fb}	105	[pcs]	Assumed number of strands positioned in bottom flange
$D_{strand,fb}$	15,2	[mm]	Diameter of strands positioned in bottom flange
$A_{p,strand,fb}$	140	[N/mm^2]	Cross sectional area per strand
$\sigma_{p,max,prov,fb}$	1488	[mm^2]	Assumed maximum stress applied to strands in bottom flange
Relaxation	Class 2	[-]	Select relaxation class: normal (1), low (2) or bars (3)
t	500000	[h]	The value of the relaxation loss (in %) at 1000 h
ρ	2,5	[%]	Time after stressing (to determine final value of the relaxation loss)
t_{eq}	461935	[h]	Equivalant time (optional), NOTE: Calculated manually!

Parameters detailing beam ends

η	1,35	[-]	Bond factor conforming table 7.2 of AFGC-SETRA 2013
η_1	1,0	[-]	Factor accounting for bond conditions, cf EC2-1-1
κ	1,5	[-]	Factor for bond strength improvement due to the presence of fibres
α_1	1,0	[-]	Factor depending on way of releasing the strands
α_2	0,19	[-]	Factor depending on the type of tendon
$n_{fb,1}$	105	[pcs]	Selected number of strands introduced in first set
$n_{fb,2}$	0	[pcs]	Selected number of strands introduced in second set (optional)
$x_{debond,1}$	0	[m]	Length over which first set of strands is debonded (optional)

$x_{debond,2}$	0,0	[m]	Length over which second set of strands is debonded (optional)

Parameters fatigue verification

$\Delta\sigma_{Rsk}$	185	[N/mm^2]	Stress range at N* cycles
N*	1000000	[-]	Number of cycles with single stress range
k_1	5	[-]	Stress exponent first branch
k_2	9	[-]	Stress exponent second branch

Parameters transverse prestressing

For the transverse prestressing of the deck (post tensioned steel) the following parameters have to be defined:

Material properties prestressing steel

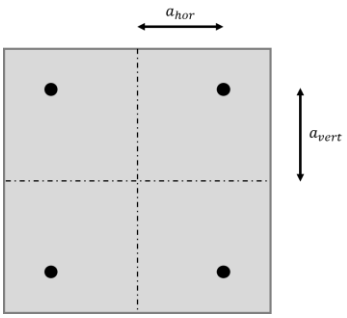
Symbol	Value	Units	Definition
f_{pk}	1860	[N/mm^2]	Characteristic value tensile strength
f_{pd}	1522	[N/mm^2]	Design value steel stress
σ_{pm0}	1395	[N/mm^2]	Maximum allowed stress directly after tensioning
$\sigma_{p,max}$	1488	[N/mm^2]	Maximum prestressing stress during tensioning
E_p	195000	[N/mm^2]	Modulus of elasticity
ε_{uk}	35	[‰]	Characteristic value strain at failure

Properties prestressing tendons

n	4	[pcs]	Assumed number of strands per tendon
D_{strand}	15,2	[mm]	Diameter of single strand
$A_{p,strand}$	140	[mm^2]	Cross sectional area per strand
$\sigma_{p,max,prov}$	1400	[N/mm2]	Assumed maximum stress applied to prestressing element
μ	0,23	[-]	Friction coefficient
k	0,009	[rad]	Unintentional angular rotation due to the Wobble-effect
w_{set}	3	[mm]	Estimated wedge set
Relaxation	Class 2	[-]	Select relaxation class: normal (1), low (2) or bars (3)
t	500000	[h]	The value of the relaxation loss (in %) at 1000 h
ρ	2,5	[%]	Time after stressing (for final value of the relaxation loss)

Parameters prestressing end cross beams

The position of the tendons is defined with respect to the centre of the beam, the prestressing is position symmetrically:



For the prestressing of the cross beams using pretensioned steel the following parameters have to be defined:

Material properties prestressing steel

Symbol	Value	Units	Definition
f_{pk}	1860	[N/mm^2]	Characteristic value tensile strength
f_{pd}	1522	[N/mm^2]	Design value steel stress
σ_{pm0}	1395	[N/mm^2]	Maximum allowed stress directly after tensioning
$\sigma_{p,max}$	1488	[N/mm^2]	Maximum prestressing stress during tensioning
E_p	195000	[N/mm^2]	Modulus of elasticity

ε_{uk}	35	[‰]	Characteristic value strain at failure

Properties prestressing tendons

n_{ducts}	4	[pcs]	Number of ducts in total
a_{vert}	500	[mm]	Vertical position centre of duct from centre of beam
a_{hor}	750	[mm]	Horizontal position centre of duct from centre of beam
n_{strand}	4	[pcs]	Assumed number of strands per tendon
D_{strand}	15,2	[mm]	Diameter of single strand
$A_{p,strand}$	140	[mm^2]	Cross sectional area per strand
$\sigma_{p,max,prov}$	1400	[N/mm2]	Assumed maximum stress applied to prestressing element
$\emptyset_{Duct}$	65	[mm]	Outer diameter of prestressing ducts
μ	0,23	[-]	Friction coefficient
k	0,009	[rad]	Unintentional angular rotation due to the Wobble-effect
w_{set}	3	[mm]	Estimated wedge set
Relaxation	Class 2	[-]	Select relaxation class: normal (1), low (2) or bars (3)
t	500000	[h]	The value of the relaxation loss (in %) at 1000 h
ρ	2,5	[%]	Time after stressing (for final value of the relaxation loss)

1.2.3 Partial factors material resistance

The following partial factors for the material resistance are distinguished in the calculation:

Symbol	Value	Clarification
γ_C	1,5	Partial factor concrete (cf EC2)
γ_{cf}	1,3	Partial factor for fibre reinforced concrete in tension (cf AFGC)
$\gamma_E * \gamma_{cf}$	1,5	Product of partial factor for uncertainty in extrapolation * factor Ycf
γ_S	1,1	Partial factor prestressing steel (cf EC2)
$\gamma_{F,fat}$	1,0	See 2.4.2.3 of NA to NEN-EN 1992-1-1
$\gamma_{S,fat}$	1,1	See 2.4.2.4 of NA to NEN-EN 1992-1-1
γ_{spl}	1,2	Partial factor splitting forces

1.2.4 Calculation parameters

Calculation parameters main beams

A number of additional parameters are defined for the main beams:

Symbol	Value	Units	Definition
σ_{max}	6,7	[N/mm^2]	Maximum allowed stress at outer concrete fibres
θ	30	[^{0}]	Angle of the concrete compressive strut of the main beams
$c_{nom,s}$	35	[mm]	Minimum applied cover onto strands bottom flange (all sides)
$c_{nom,r}$	30	[mm]	Minimum applied cover onto rebars bottom flange (all sides)
$\emptyset_{spl,fl}$	10	[mm]	Assumed diameter splitting reinforcement bottom flange
μ	0,5	[-]	Friction coefficient concrete and supports
δ	300	[-]	Maximum deflection in SLS

Calculation parameters longitudinal joints and top flange

A number of additional parameters are defined for the longitudinal joints and top flanges:

Symbol	Value	Units	Definition
$\emptyset_{spl,ft}$	10	[mm]	Assumed diameter splitting reinforcement top flange
h_1	100	[mm]	Anchor plate (height and width)

Calculation parameters end cross beams

A number of additional parameters are defined for the end cross beams:

Symbol	Value	Units	Definition
k_1	0,15	[-]	Factor from 6.2.2 of the NA to NEN-EN 1992-1-1
θ	21,8	[^{0}]	Angle concrete compressive strut of end cross beam

1.3 Design of bridge and main carriageway – Actions

1.3.1 Design main carriageway

Parameters regarding the design of the main carriageway that have to be defined are:

Symbol	Value	Units	Clarification
h_{kerb}	340	[mm]	Assumed height of the kerb
w_{kerb}	500	[mm]	Assumed width of the kerb
ρ_c	25	[kN/m^3]	Density of the concrete used
t_{surf}	10	[mm]	Assumed thickness of the surface layer
$\rho_{asphalt}$	23	[kN/m^3]	Density of the material used

1.3.2 Effective width of the beams

To determine distributed loads acting on the different beams the ''effective widths'' of the outer and inner beams are determined:

- The effective width of the outer beams (beams 1 and 5):

$$b_{eff,o} = w + \frac{w_{joint}}{2} \rightarrow 3{,}2 + \frac{0{,}09}{2} = 3{,}245\ [m]$$

- The effective width of the inner beams (beams 2 – 4):

$$b_{eff,i} = w + 2 * \frac{w_{joint}}{2} \rightarrow 3{,}2 + 2 * \frac{0{,}09}{2} = 3{,}29\ [m]$$

1.3.3 Permanent actions (G)

Using the defined parameters the Excelsheet calculates the values of the different permanent actions that have to be plugged into the RFEM model.

- Self-weight prefab beams:

$$G_{k,beam} = A_c * \rho \rightarrow 1342500 * 10^{-6} * 1{,}0 * 25 = 33{,}56\ \text{[kN/m]}$$

- Self-weight end cross beams:

$$G_{k,cb} = A_{cb} * \rho \rightarrow 1900 * 1900 * 10^{-6} * 1{,}0 * 25 = 90{,}25\ \text{[kN/m]}$$

- Self-weight of the joints: First the area of the total joint is calculated including both the joint height and the part of the prefab beam on top of which the joint material is casted:

$$A_j'' = w_j * t_{ft} \rightarrow 80 * 187{,}5 * 10^{-6} = 0{,}0169\ [m^2]$$

The line load representing the self-weight of the joints then is:

$$G_{k,j} = A_j'' * \rho \rightarrow 0{,}0169 * 25 = 0{,}42\ [kN/m]$$

- Permanent load road surface:

$G_{k,surf} = t_{surf} * \rho_{asphalt} \rightarrow 10 * 10^{-3} * 23 = 0{,}23\ [kN/m^2]$

- Permanent load kerbs:

$G_{k,kerb} = h_{kerb} * \rho \rightarrow 0{,}34 * 25 = 8{,}5\ [kN/m^2]$

1.3.4 Variable actions (Q)

The following values of variable loads have to be entered into the Excelsheet:

- Load model 1:
    - Lane 1: $Q_{1k} = 291$ kN and $q_{1k} = 8{,}73$ kN/m^2
    - Lane 2: $Q_{2k} = 194$ kN and $q_{2k} = 2{,}425$ kN/m^2
    - Remaining area: $q_{rk} = 2{,}25$ kN/m^2
- Load model 2: $\beta_Q Q_{ak} = 388$ kN per axle

1.3.5 Accidental actions (A)

The following values of variable loads have to be entered into the Excelsheet:

Symbol	Value	Units	Clarification
F_{equi}	1000	[kN]	Equivalent static force, see: (4) of 4.6.2. EC1-1-7

1.3.6 Fatigue

The following values of variable loads have to be entered into the Excelsheet:

Symbol	Value	Units	Clarification
n_y	100	[-]	Design service life
N_{obs}	500000	[-]	Number of heavy vehicles per year

1.3.7 Combinations of actions

To formulate combinations of actions the following factors have to be defined:

Symbol	Value	Units	Clarification
γ_G	1,4	[-]	See tabel NB.16 – A2.4(B) of NA to NEN-EN 1990
$\zeta * \gamma_G$	1,25	[-]	See tabel NB.16 – A2.4(B) of NA to NEN-EN 1990
γ_P	1,0	[-]	See 2.4.2.2 of NA to NEN-EN 1992-1-1
γ_Q	1,5	[-]	See tabel NB.16 – A2.4(B) of NA to NEN-EN 1990
ψ_0	0,8	[-]	See tabel NB.13 – A2.1 of NA to NEN-EN 1990
ψ_1	0,8	[-]	See tabel NB.13 – A2.1 of NA to NEN-EN 1990

1.4 Determining force distribution (RFEM input)

To complete the input various values of internal forces have to be determined (using RFEM) and plugged into the Excelsheet.

1.4.1 Design of main prestressing and verification capacity of the main beams

For the ultimate limit state verifications of the main beams the following values are required:

Symbol	Value	Units	Clarification
M_{Ed}	41753	[kNm]	Governing bending moment value (mid span)
V_{Ed}	3632	[kN]	Governing shear force value (near supports)
T_{Ed}	1268	[kNm]	Governing torsional moment

To determine the required prestressing, values corresponding to the characteristic combination of the serviceability limit state are required:

Symbol	Value	Units	Clarification
$M_{E,G,perm}$	1725	[kNm]	Bending moment imposed permanent loads in SLS at midspan
$M_{E,Q}$	9553	[kNm]	Bending moment variable loads in SLS at midspan

For the most accurate result the deflection can also be determined directly using RFEM:

Symbol	Value	Units	Clarification
δ_{max}	440,9	[mm]	Maximum deflection at midspan in the SLS (frequent combination)

1.4.2 Fatigue analysis main beams

For the fatigue analysis two values are to be determined using RFEM (one using the fatigue load combination with fatigue load, the other without fatigue load).

Symbol	Value	Units	Clarification
$M_{fat,max}$	26812	kNm	Maximum bending moment at midspan (found using RFEM)
$M_{fat,min}$	22543	kNm	Minimum bending moment at midspan (found using RFEM)

1.4.3 Design of prestressing and verification capacity of the end cross beams

For the ultimate limit state verifications of the end cross beams the following values are required:

Symbol	Value	Units	Clarification
$M_{Ed,hog}$	1271	[kNm]	Maximum hogging bending moment (all loads considered)
$M_{Ed,sag}$	396	[kNm]	Maximum sagging bending moment (all loads considered)
V_{Ed}	846	[kN]	Maximum shear force (all loads considered)

To determine the required prestressing, values corresponding to the characteristic combination of the serviceability limit state are required:

Symbol	Value	Units	Clarification
$M_{E,hog}$	453	[kNm]	Maximum hogging bending moment SLS
$M_{E,sag}$	270	[kNm]	Maximum sagging bending moment SLS

2

ULS – STR

2.1 Input parameters

The required parameters are taken from the overview (see the first chapter). To determine the eccentricity of the tendons in the bottom flange it is assumed that the centre of gravity of the tendons is positioned at the centre of the bottom flange:

$$e_p = e_b - 0{,}5 * t_{fb}$$

Additionally, the bending moment at mid span due to the self-weight of the beams only is calculated:

$$M_{E,G,sw} = \frac{1}{8} * G_{k,beam} * l^2$$

2.2 Design of the main prestressing

2.2.1 Calculating prestress losses

Applied maximum force onto prestressing element and stress verification

The provided maximum prestressing forces by the centric and eccentric group of strands are respectively:

$$P_{max,prov,c} = n_c * A_{p,c} * \sigma_{p,max,prov,c}$$

$$P_{max,prov,c} = n_c * A_{p,c} * \sigma_{p,max,prov,c}$$

It has to be verified that the maximum stress applied to the prestressing strands does not exceed the maximum value, hence the following verification has to be performed.

$$\sigma_{p,max,prov,c} \leq \sigma_{p,max} \wedge \sigma_{p,max,prov,fb} \leq \sigma_{p,max}$$

The compressive stresses are to be verified as well, the governing point is the bottom fibre at the support:

$$\sigma_c = \frac{P_{max,c}}{A_c} + \frac{P_{max,fb}}{A_c} + \frac{P_{max,fb} * e_p}{W_b} \leq 0{,}7 * f_{ck}$$

Direct losses

Centric prestressing: By definition the eccentricity of the tendons with respect to the centre of gravity of the cross section equals zero. That means that $e_{p,c} = 0$ and $f_c = 1$. Hence:

$$\Delta P_{el,c} = \frac{\alpha_e \rho_p}{1 + \alpha_e \rho_p} * P_{max,c}$$

Where:

$$\alpha_e = \frac{E_p}{E_c}$$

$$\rho_{p,c} = \frac{A_{p,c}}{A_c}$$

Eccentric prestressing: The elastic loss of the eccentric prestressing is:

$$\Delta P_{el,fb} = \frac{\alpha_e \rho_p f_{fb}}{1 + \alpha_e \rho_p f_{fb}} * P_{max,fb}$$

Where:

$$\rho_{p,fb} = \frac{A_{p,fb}}{A_c}$$

$$f_{fb} = 1 + A_c * \frac{e_p^2}{I_y}$$

Determining initial prestressing force and stress verification

The initial prestressing force for the centric and eccentric prestressing is:

$$P_{m0,c} = P_{max,c} - \Delta P_{el,c}$$

$$P_{m0,fb} = P_{max,fb} - \Delta P_{el,fb}$$

It has to be verified that the stresses in the strands are not larger than the maximum allowable value:

$$\frac{P_{m0,c}}{A_{p,c}} \leq \sigma_{pm0} \wedge \frac{P_{m0,fb}}{A_{p,fb}} \leq \sigma_{pm0}$$

Time dependent losses

Centric prestressing: For the centric prestressing the time dependent losses are calculated as follows:

$$\Delta P_{c+s+r,c} = A_{p,c} * \Delta\sigma_{p,c+s+r,c} = A_{p,c} * \frac{\varepsilon_{cs} E_p + 0{,}8\Delta\sigma_{pr,c} + \frac{E_p}{E_{cm}} \varphi(\infty, t_0) \sigma_{c,QP,c}}{1 + \frac{E_p}{E_{cm}} \frac{A_{p,c}}{A_c} [1 + 0{,}8 * \varphi(\infty, t_0)]}$$

Where (for relaxation class 2):

$$\frac{\Delta\sigma_{pr,c}}{\sigma_{pi,c}} = 0{,}66 * \rho_{1000} * e^{9{,}1\mu_c} * \left(\frac{t}{1000}\right)^{0{,}75(1-\mu_c)} * 10^{-5}$$

$$\sigma_{pi,c} = \sigma_{pm,0,c}$$

$$\mu_c = \sigma_{pm,0,c} / f_{pk}$$

$$t = 500.000 + t_{eq}$$

$$\sigma_{c,QP,c} = \frac{P_{m0,c}}{A_c} + \frac{P_{m0,fb}}{A_c}$$

Eccentric prestressing: For the eccentric prestressing the time dependent losses are calculated as follows:

$$\Delta P_{c+s+r,fb} = A_{p,fb} * \Delta\sigma_{p,c+s+r,fb} = A_{p,fb} * \frac{\varepsilon_{cs} E_p + 0{,}8\Delta\sigma_{pr,fb} + \frac{E_p}{E_{cm}} \varphi(\infty, t_0) \sigma_{c,QP,fb}}{1 + \frac{E_p}{E_{cm}} \frac{A_{p,fb}}{A_c} \left(1 + \frac{A_c}{I_c} z_{cp}^2\right) [1 + 0{,}8 * \varphi(\infty, t_0)]}$$

Where (for relaxation class 2):

$$\frac{\Delta\sigma_{pr,fb}}{\sigma_{pi,fb}} = 0{,}66 * \rho_{1000} * e^{9{,}1\mu_{fb}} * \left(\frac{t}{1000}\right)^{0{,}75(1-\mu_{fb})} * 10^{-5}$$

$$\sigma_{pi,fb} = \sigma_{pm,0,fb}$$

$$\mu_{fb} = \frac{\sigma_{pm,0,fb}}{f_{pk}}$$

$$t = 500.000 + t_{eq}$$

$$z_{cp} = e_b - \frac{t_{fb}}{2} = e_p$$

$$\sigma_{c,QP,fb} = \frac{P_{m0,c}}{A_c} + \frac{P_{m0,fb}}{A_c} + \frac{P_{m0,fb} * e_p * z_{cp}}{I_c} - \frac{M_{G,sw} * z_{cp}}{I_c} - \frac{M_{G,perm} * z_{cp}}{I_c}$$

Working prestress force

The working prestressing force for the centric and eccentric prestressing is:

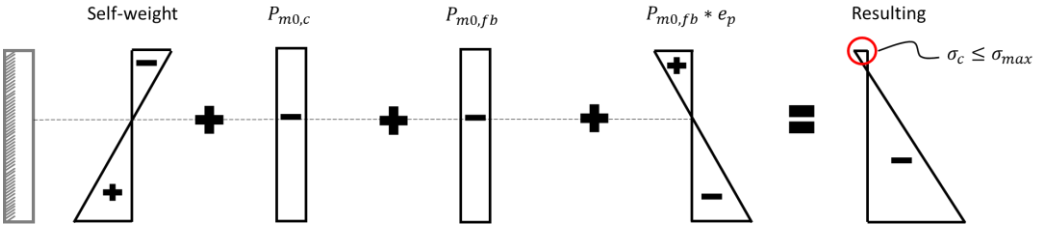
$$P_{m,\infty,c} = P_{m0,c} - \Delta P_{c+s+r,c}$$

$$P_{m,\infty,fb} = P_{m0,fb} - \Delta P_{c+s+r,fb}$$

2.2.2 Determining stresses at midspan

Two situations are considered, for both situations the concrete stress has to be smaller than the maximum value, both at the top and bottom fibre.

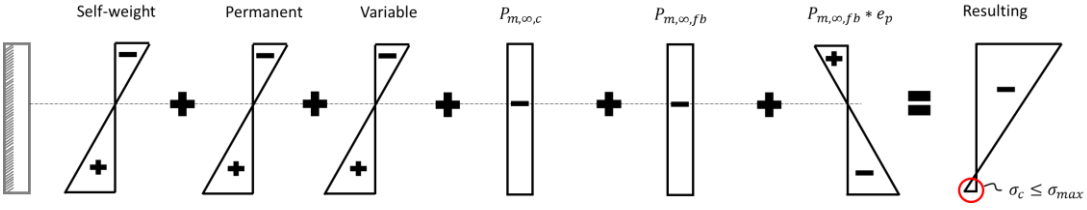
- **Self-weight and prestressing only ($t = 0$)**:



$$\sigma_{c,t} = -\frac{M_{G,sw}}{W_t} - \frac{P_{m0,c}}{A_c} - \frac{P_{m0,fb}}{A_c} + \frac{P_{m0,fb} * e_p}{W_t} \leq \sigma_{max}$$

$$\sigma_{c,b} = +\frac{M_{G,sw}}{W_b} - \frac{P_{m0,c}}{A_c} - \frac{P_{m0,fb}}{A_c} - \frac{P_{m0} * e_p}{W_b} \leq \sigma_{max}$$

- **Use phase ($t \to \infty$)**:



$$\sigma_{c,t} = -\frac{(M_{G,sw} + M_{G,perm})}{W_t} - \frac{M_Q}{W_t} - \frac{P_{m,\infty,c}}{A_c} - \frac{P_{m,\infty,fb}}{A_c} + \frac{P_{m,\infty,fb} * e_p}{W_t} \leq \sigma_{max}$$

$$\sigma_{c,b} = +\frac{(M_{G,sw} + M_{G,perm})}{W_t} + \frac{M_Q}{W_b} - \frac{P_{m,\infty,c}}{A_c} - \frac{P_{m,\infty,fb}}{A_c} - \frac{P_{m,\infty,fb} * e_p}{W_b} \leq \sigma_{max}$$

2.3 Detailing beam ends

2.3.1 Bond stresses and transmission length

The bond stresses are calculated as follows:

$$f_{bpt} = \eta * \eta_1 * \kappa * \frac{f_{ctk,el}(t)}{\gamma_c}$$

The transfer length of the centric and eccentric prestressing is:

$$l_{pt,c} = 1{,}0 * 0{,}19 * 15{,}2 * \frac{\sigma_{pm0,c}}{f_{bpt}}$$

$$l_{pt,fb} = \alpha_1 * \alpha_2 * \emptyset * \frac{\sigma_{pm0,fb}}{f_{bpt}}$$

The design values used in the analysis are:

$$l_{pt1,c} = 0{,}4 * l_{pt,c}$$

$$l_{pt1,fb} = 0{,}4 * l_{pt,fb}$$

2.3.2 Tensile stresses at top fibre

For the calculations it is assumed that the centric prestressing is transferred onto the concrete from the support while for the eccentric prestressing the option is given to de-bond the strands over a certain length and introduce the total number of eccentric strands over two 'sets'.

The development of stresses at the top fibre is calculated by determining the stresses due to self-weight and prestressing at a number of points along the beam.

Centric prestressing: The compressive stresses due to the centric prestressing for $x < l_{pt,c}$ and $x > l_{pt,c}$ are:

$$\sigma_{t,c}(x) = -\frac{P_{m0,c}}{l_{pt,c}} * x * \frac{1}{A_c}, x \leq l_{pt,c}$$

$$\sigma_{t,c}(x) = -\frac{P_{m0,c}}{A_c}, x > l_{pt,c}$$

Eccentric prestressing – Axial component: The compressive stresses due to the axial component of the eccentric prestressing for $x < l_{pt,fb}$ and $x > l_{pt,fb}$ are:

$$\sigma_{t,fb,P}(x) = -\frac{P_{m0,fb}}{l_{pt,fb}} * x * \frac{1}{A_c}, x \leq l_{pt,fb}$$

$$\sigma_{t,fb,P}(x) = -\frac{P_{m0,fb}}{A_c}, x > l_{pt,fb}$$

Eccentric prestressing – Bending: The tensile stresses due to upward bending caused by the eccentric prestressing for $x < l_{pt,fb}$ and $x > l_{pt,fb}$ are:

$$\sigma_{t,fb,M}(x) = -\frac{P_{m0,fb}}{l_{pt,fb}} * x * \frac{e_p}{W_t}, x \leq l_{pt,fb}$$

$$\sigma_{t,fb,M}(x) = --\frac{P_{m0,fb} * e_p}{W_t}, x > l_{pt,fb}$$

Self-weight beams: The bending moment due to the self-weight along the beam axis can be determined as:

$$M_{sw}(x) = \frac{1}{2} * G_{k,beam} * x * (l - x), 0 \leq x \leq l$$

The compressive stresses at the top fibre along the beam axis due to the self-weight are therefore:

$$\sigma_{t,sw}(x) = -\frac{M(x)}{W_t}$$

Total stresses: By adding up the absolute values of the compressive stresses the total stress in the top fibre is determined:

$$\sigma_{t,compression}(x) = |\sigma_{t,sw}(x)| + |\sigma_{t,c}(x)| + |\sigma_{t,fb,P}(x)|$$

Verification: It has to be verified that the highest remaining tensile stress (if present) is smaller than the maximum value along the beam segment under consideration:

$$\Delta\sigma_t \leq \sigma_{max}$$

If this requirement is met no de-bonding of strands is required.

2.3.3 Positioning of strands in the bottom flange

Maximum number of strands

The total area of the bottom flange is:

$$t_{fb} * (t_w + w_b + t_w)$$

Using the values of the minimum applied cover onto the strands in the bottom flange ($c_{nom,s}$), the minimum applied cover onto the rebars in the bottom flange ($c_{nom,r}$) and the diameter of the rebars ($\emptyset_r$), the value of the applied cover onto the strands is calculated.

For this calculation it is assumed that (provided that reinforcement is applied) the rebars are positioned around the strands. Under this assumption the applied cover onto the strands, $c_{prov,s}$, is calculated. The calculation is performed as such that both separate cover requirements of the strands and rebars are satisfied simultaneously:

- If $c_{nom,s} \geq c_{nom,r} + \emptyset_r$, then: $c_{prov,s} = c_{nom,s}$
- If $c_{nom,s} < c_{nom,r} + \emptyset_r$, then: $c_{nom,r} + \emptyset_r$

In addition it is assumed that the minimum horizontal and vertical spacing between the bars, s_{min}, is as follows:

$$s_{min} = 2 * D_{strand,fb}$$

Using the applied concrete cover the ''available area'' can be calculated, which is the area which can be used to accommodate prestressing strands. The concrete cover is subtracted to determine the ''available area'':

$$h_{available} * w_{available} = (t_{fb} - 2 * c_{nom}) * (t_w + w_b + t_w - 2 * c_{nom})$$

The minimum centre to centre distance in horizontal and vertical direction is calculated using the minimum spacing:

$$d_{min} = s_{min} + D_{strand}$$

The maximum number of rows that can be applied is (rounded off to the nearest lower integer):

$$n_{max,rows} = 1 + Int\left(\frac{h_{available} - D_{strand,fb}}{d_{min}}\right)$$

The maximum number of strands per row (also rounded off to the nearest lower integer):

$$n_{max,strands} = 1 + Int\left(\frac{w_{available} - D_{strand,fb}}{d_{min}}\right)$$

The maximum number of strands is $n_{max,rows} * n_{max,strands}$.

Positioning the strands

The number of rows required with the assumed number of strands in the bottom flange is as follows. Note that the result is rounded off to the nearest highest integer.

$$n_{rows} = Int\left(\frac{n_{fb}}{n_{max,strands}}\right)$$

The number of strands per row is:

$$n_{strands} = \frac{n_{fb}}{n_{rows}}$$

The vertical and horizontal centre to centre distance of the strands then is:

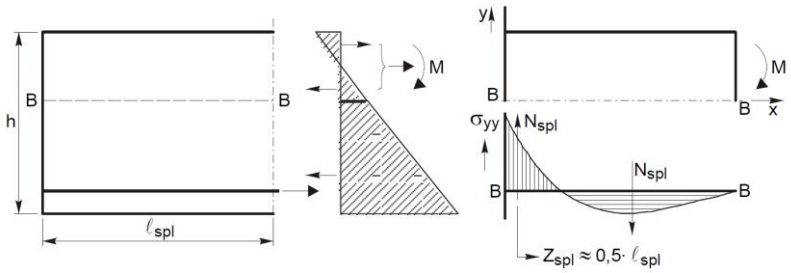
$$d_{vert} = \frac{h_{available} - D_{strand}}{n_{rows} - 1}$$

$$d_{hor} = \frac{w_{available} - D_{strand}}{n_{strands} - 1}$$

2.3.4 Splitting reinforcement – Vertical distribution

Spalling

Note: If the option is used to apply the strands in the bottom flange in two sets at various points along the beam axis then the following calculations are performed separately for both sets. It is verified if the point under consideration is within the cross section of the end cross beam or outside this section, because this affects the width of the cross section where spalling occurs.



The length of the equivalent prism is:

$$l_{spl} = C_{spl} * h \rightarrow \sqrt{1 + \left(0{,}6 * \frac{l_{pt,fb}}{h}\right)^2} * h$$

The bending moment is calculated as follows:

$$\sigma_{top} = -\frac{P_{m0,c}}{A_c} - \frac{P_{m0,fb}}{A_c} + \frac{P_{m0,fb} * e_p}{W_t}$$

$$\sigma_{bottom} = -\frac{P_{m0,c}}{A_c} - \frac{P_{m0,fb}}{A_c} - \frac{P_{m0,fb} * e_p}{W_t}$$

$$h_{prism} = 2 * \frac{h * \sigma_{top}}{\sigma_{top} + |\sigma_{bottom}|}$$

$$M = \frac{1}{6} * b * h_{prism}^2 * \sigma_{top}$$

The spalling force is:

$$N_{spl} * 0{,}5 * l_{spl} - M = 0 \rightarrow N_{spl} = \frac{2 * M}{l_{spl}}$$

The spalling stresses are calculated as follows:

$$\sigma_{spl} = \frac{16 * M}{l_{spl}^2 * b}$$

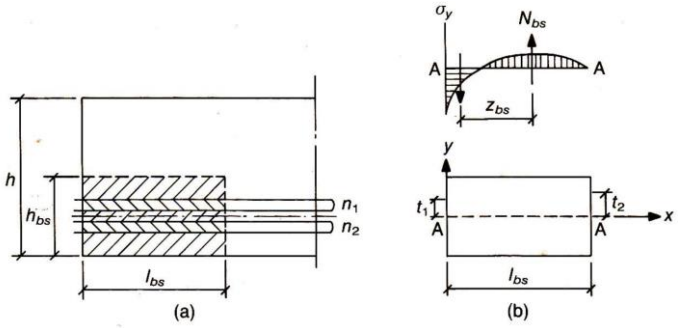
The stress verification is subsequently performed:

$$\sigma_{Rd,f} \approx \frac{f_{ctfk}}{K_{local} * \gamma_{cf}}$$

$$\gamma_{spl} * \sigma_{spl} \leq \sigma_{Rd,f}$$

Bursting

Note that the equations for bursting have been formulated for 3 or 4 rows of strands in the bottom flange only. In case the number of tendons changes, the lever arms t_1 and t_2 have to be recalculated.



The height and length of the prism are respectively:

$$h_{bs} = t_{fb}$$

$$l_{bt} = C_{bs} * h_{bs} \rightarrow h_{bs} * \sqrt{1 + \left(0{,}6 * \frac{l_{pt,fb}}{h_{bs}}\right)^2}$$

The bursting force follows from:

$$N_{bs} = \frac{(n_1 * t_2 - n_1 * t_1)}{0{,}5 * l_{bt}} * P_{m0,fb}$$

The maximum bursting stresses are:

$$\sigma_{bs} = \frac{N_{bs}}{b_{bs} * l_{bs}}$$

In this equation the width of the prism is taken equal to the width of the section at the height of the tendons:

$$b_{bs} = t_w + b_w + t_w$$

The final step is the verification of the stresses:

$$\sigma_{Rd,f} \approx \frac{f_{ctfk}}{K_{local} * \gamma_{cf}}$$

$$\gamma_{spl} * \sigma_{spl} \leq \sigma_{Rd,f}$$

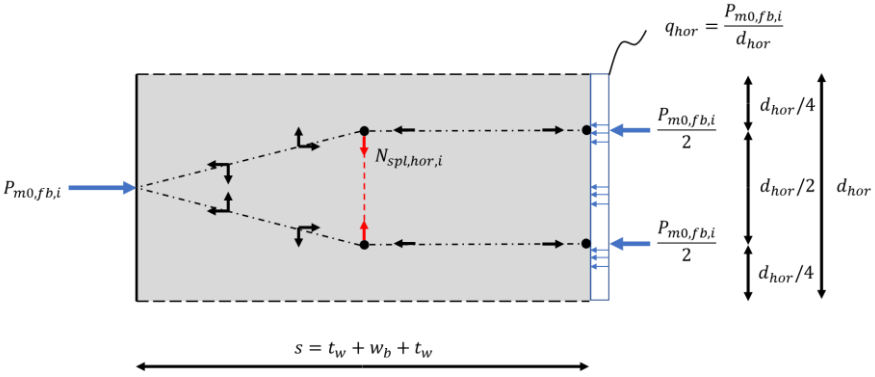
Splitting

Splitting is dealt with implicitly by applying sufficient spacing and cover between and onto the prestressing strands.

2.3.5 Splitting reinforcement – Horizontal distribution

For determining the splitting reinforcement it is assumed that the forces themselves over the full width of the beam. The splitting force caused by a single strand is calculated as follows:

$$N_{spl,hor,i} = \frac{1}{4} * \gamma_{spl} * P_{m0,fb,i} * \frac{b_{hor}}{2 * t_w + w_b}$$



This value is multiplied with the number of strands to determine the total splitting force:

$$N_{spl,hor} = n_{fb} * N_{spl,hor,i}$$

The maximum allowable stresses in the rebars are:

$$f_s = \frac{3000}{\emptyset_k} \leq 360\ [MPa]$$

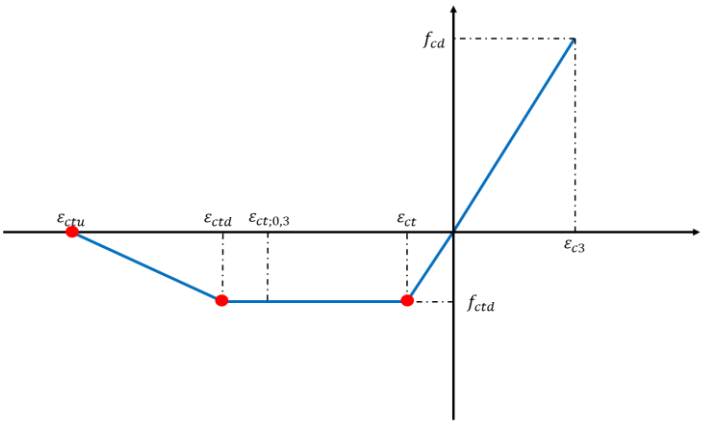
The minimum required diameter of the reinforcement follows from:

$$A_{s,min} = \frac{N_{spl,hor}}{f_s}$$

2.4 Verification bending moment capacity

2.4.1 Assumptions

The following stress-strain relation for concrete in compression and tension has been adopted for the ultimate limit state verification of the main beams:



Calculating stresses:

$$f_{cd} = \frac{\alpha_{cc} * f_{ck}}{\gamma_C}$$

$$f_{ctd} = \frac{\alpha_{ct} * f_{ctk,el}}{\gamma_C}$$

Calculating strains:

$$\varepsilon_{ct} = \frac{f_{ctd}}{E_{cm}} = \frac{f_{ctk,el}}{\gamma_c * E_{cm}}$$

$$\varepsilon_{ct;0,3} = \frac{w_{0,3}}{l_c} + \varepsilon_{ct}$$

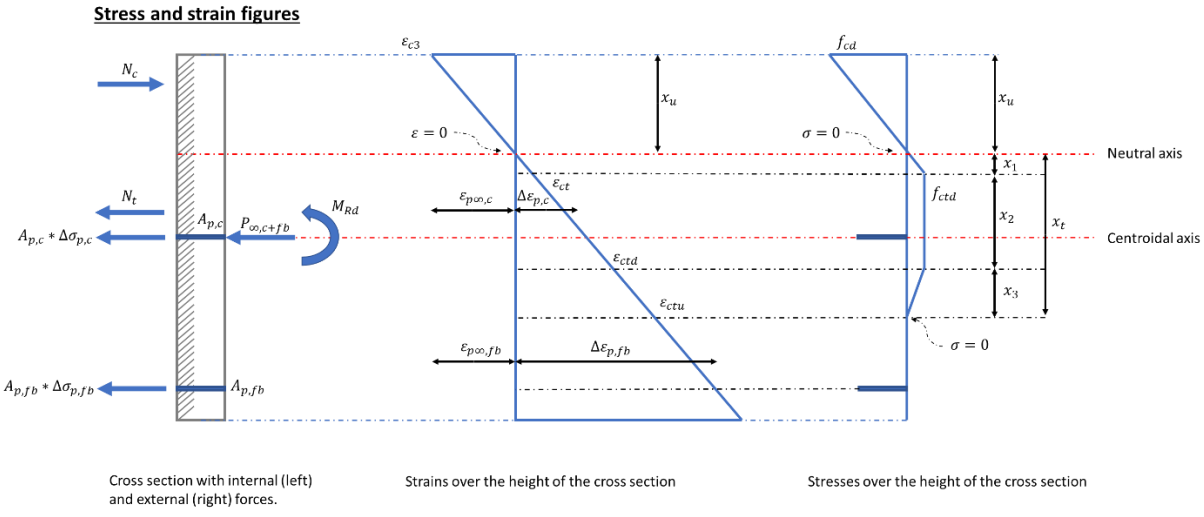
$$\varepsilon_{ctd} = \varepsilon_{ctu} - \frac{f_{ctd}}{f_{ctd;2}} * (\varepsilon_{ctu} - \varepsilon_{ct;0,3})$$

$$\varepsilon_{ctu} = \frac{l_f}{4 * l_c}$$

Furthermore it is assumed that for the verification of the rotational capacity the redistribution is zero.

2.4.2 Calculating the capacity and verifications

In the ULS the following strain and stress distributions are assumed to occur over the height of the beam:

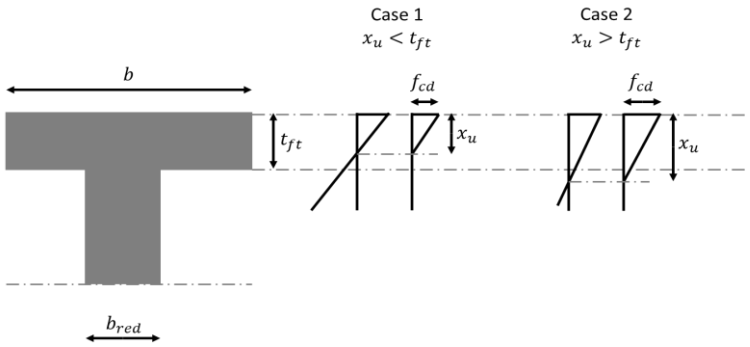


Identifying all horizontal forces

The calculation has been made iterative, the Excelsheet assumes a value for the height of the concrete compressive zone and verifies whether horizontal equilibrium has been reached. If so, then this value will be taken for x_u. The full calculation procedure is as follows:

Height of concrete compressive and tensile zone

Concrete compressive zone: The concrete compressive force is calculated using the assumed value for x_u. Two cases can be distinguished.



Case 1: $x_u \leq t_{ft}$ and standard equations can be used for a rectangular cross section:

$$N_c = \frac{1}{2} * w * f_{cd} * x_u$$

$$e_c = \frac{1}{3} * x_u$$

Case 2: $x_u > t_{ft}$ and thus the width varies over the height of the compressive zone. The stresses and strains at the bottom of the top flange are:

$$\varepsilon_{c,fl} = \varepsilon_{c3} * \left(1 - \frac{t_{ft}}{x_u}\right)$$

$$\sigma_{c,fl} = f_{cd} * \left(1 - \frac{t_{ft}}{x_u}\right)$$

The total concrete compressive force is:

$$N_c = N_{c,1} + N_{c,2} + N_{c,3} \rightarrow \frac{1}{2} * t_{ft} * \left(f_{cd} - \sigma_{c,fl}\right) * b + t_{ft} * \sigma_{c,fl} * b + \frac{1}{2} * \left(x_u - t_{ft}\right) * \sigma_{c,fl} * b_{red}$$

$$b_{red} = 2 * t_w$$

The centre of gravity with respect to the top fibre is:

$$e_c = \frac{S_1 + S_2 + S_3}{N_{c,1} + N_{c,2} + N_{c,3}} \rightarrow \frac{N_{c,1} * \frac{1}{3} * t_{ft} + N_{c,2} * \frac{1}{2} * t_{ft} + N_{c,3} * \left(t_{ft} + \frac{1}{3} * \left(x_u - t_{ft}\right)\right)}{N_{c,1} + N_{c,2} + N_{c,3}}$$

Concrete tensile zone: First the required strain values are calculated as follows:

$$\varepsilon_{ct} = \frac{f_{ctd}}{E_{cm}} = \frac{f_{ctk,el}}{\gamma_c * E_{cm}}$$

$$\varepsilon_{ct;0,3} = \frac{w_{0,3}}{l_c} + \varepsilon_{ct}$$

$$\varepsilon_{ctu} = \frac{l_f}{4 * l_c} \leq 2{,}5\ ‰$$

$$\varepsilon_{ctd} = \varepsilon_{ctu} - \frac{f_{ctd}}{f_{ctd;2}} * \left(\varepsilon_{ctu} - \varepsilon_{ct;0,3}\right)$$

The height of the tensile zones are calculated by considering the assumed strain diagram:

$$x_1 = \frac{\varepsilon_{ct}}{\varepsilon_{cu3}} * x_u$$

$$x_2 = \frac{\varepsilon_{ctd} - \varepsilon_{ct}}{\varepsilon_{cu3}} * x_u$$

$$x_3 = \frac{\varepsilon_{ctu} - \varepsilon_{ctd}}{\varepsilon_{cu3}} * x_u$$

The total concrete tensile force is:

$$N_t = N_{t1} + N_{t2} + N_{t3} \rightarrow \frac{1}{2} * x_1 * b * f_{ctd} + x_2 * b * f_{ctd} + \frac{1}{2} * x_3 * b * f_{ctd}$$

In this equation the width is always taken equal to twice the web thickness, if the concrete compressive zone is smaller than the height of the top flange the contribution in tension is still limited to the width equal to $2 * t_w$.

The resulting force of the individual tensile forces is determined by taking the top fibre of the cross section as reference point.

$$e_t = \frac{N_{t1} * (x_u + \frac{2}{3} * x_1) + N_{t2} * \left(x_u + x_1 + \frac{1}{2} * x_2\right) + N_{t3} * \left(x_u + x_1 + x_2 + \frac{1}{3} * x_3\right)}{N_{t1} + N_{t2} + N_{t3}}$$

Determining the strains

The strains are calculated for both the centric and eccentric prestressing. Both procedures are given below.

- Centric prestressing:

$$d_{p,c} = e_t$$

$$\Delta\varepsilon_{p,c} = \varepsilon_{c3} * \left(\frac{d_{p,c}}{x_u} - 1\right)$$

$$\varepsilon_{p,\infty,c} = \frac{\sigma_{p,\infty,c}}{E_p}$$

$$\varepsilon_{p,c} = \varepsilon_{p,\infty,c} + \Delta\varepsilon_{p,c} \leq 0{,}9 * \varepsilon_{uk}$$

- Eccentric prestressing:

$$d_{p,fb} = h - 0{,}5 * t_{fb}$$

$$\Delta\varepsilon_{p,fb} = \varepsilon_{c3} * \left(\frac{d_{p,fb}}{x_u} - 1\right)$$

$$\varepsilon_{p,\infty,fb} = \frac{\sigma_{p,\infty,fb}}{E_p}$$

$$\varepsilon_{p,fb} = \varepsilon_{p,\infty,fb} + \Delta\varepsilon_{p,fb} \leq 0{,}9 * \varepsilon_{uk}$$

Steel stresses

Using the calculated strain values the stresses in the prestressing steel are calculated.

- Centric prestressing:

$$\sigma_{pu,c} = f_{pd} + \frac{\varepsilon_{p,c} - \frac{f_{pd}}{E_p}}{\varepsilon_{uk} - \frac{f_{pd}}{E_p}} * \left(\frac{f_{pk}}{\gamma_s} - f_{pd}\right)$$

- Eccentric prestressing:

$$\sigma_{pu,fb} = f_{pd} + \frac{\varepsilon_{p,fb} - \frac{f_{pd}}{E_p}}{\varepsilon_{uk} - \frac{f_{pd}}{E_p}} * \left(\frac{f_{pk}}{\gamma_s} - f_{pd}\right)$$

The increase of the force in the prestressing steel (the passive contribution) is for the centric and eccentric prestressing respectively:

$$\Delta N_{p,c} = A_{p,c} * (\sigma_{pu,c} - \sigma_{p,\infty,c})$$

$$\Delta N_{p,fb} = A_{p,fb} * (\sigma_{pu,fb} - \sigma_{p,\infty,fb})$$

Check equilibrium

Equilibrium is checked by considering all horizontal forces:

$$-N_c + N_t + P_{m,\infty,c} + P_{m,\infty,fb} + \Delta N_{p,c} + \Delta N_{p,fb} = 0$$

Determining bending moment capacity

If equilibrium is achieved the bending moment capacity is calculated using the top fibre as the reference point:

$$M_{Rd} = -N_c * e_c + N_t * e_t + P_{m,\infty,c} * d_{p,c} + P_{m,\infty,fb} * d_{p,c} + \Delta N_{p,c} * d_{p,c} + \Delta N_{p,fb} * d_{p,fb}$$

The design value of the bending moment is as follows:

$$M_{Ed} = M_{Ed,RFEM} - P_{m,\infty,fb} * e_p$$

The following criterion is to be satisfied:

$$\frac{M_{Ed}}{M_{Rd}} \leq 1{,}0$$

Verifying rotational capacity

To verify the rotational capacity the following basic equation is applied:

$$\frac{x_u}{d_p} \leq \frac{\varepsilon_{c3} * 10^6}{\varepsilon_{c3} * 10^6 + 7f}$$

$$f = \frac{\left(\frac{f_{pk}}{\gamma_s} - \sigma_{pm,\infty}\right) A_p + f_{yd} A_s}{A_p + A_s}$$

Because prestressing is applied at two different heights, the weighted average values are used for d_p, A_p and $\sigma_{pm,\infty}$. These are calculated as follows:

$$d_{p,ave} = \frac{n_c * d_{p,c} + n_{fb} * d_{p,fb}}{n_c + n_{fb}}$$

$$A_{p,ave} = \frac{n_c * A_{p,c} + n_{fb} * A_{p,fb}}{n_c + n_{fb}}$$

$$\sigma_{p,\infty,ave} = \frac{n_c * \sigma_{p,\infty,c} + n_{fb} * \sigma_{p,\infty,fb}}{n_c + n_{fb}}$$

2.5 Verification shear force capacity

2.5.1 Assumptions and limitations

The calculation is based on the following assumptions:

- It is assumed the concrete is loaded in compression due to the prestressing;

$$\sigma_{cp} = \frac{N_{Ed}}{A_c} \rightarrow \frac{P_{m,\infty,c} + P_{m,\infty,fb}}{A_c}$$

- It is assumed that no conventional shear reinforcement is present;
- No reduction is taken into consideration to account for ducts etc. as these are not present;
- For the effective height the value for the prestressing with respect to the bottom flange is applied:

$$d_p = h - 0{,}5 * t_{fb}$$

2.5.2 Calculating the resistance and unity check

Tensile resistance of the concrete ties

First the contributions of the two components (concrete and steel fibres) taken into consideration are calculated after which these are added up.

Concrete component: The concrete contribution to the shear capacity:

$$V_{Rd,c} = \frac{0{,}24}{\gamma_{cf}\gamma_E} k f_{ck}^{\frac{1}{2}} b_w z$$

Factor accounting for compressive stress due to the prestressing:

$$k = 1 + 3 * \frac{\sigma_{cp}}{f_{ck}}$$

Where $z = 0{,}9 * d_p$

Steel fibre component: The contribution of the steel fibres to the shear force capacity:

$$V_{Rd,f} = \frac{A_{fv}\sigma_{Rd,f}}{\gamma_{cf} * tan\theta} \approx \frac{A_{fv} * f_{ctd;2}}{\gamma_{cf} * K_{global} * tan\theta}$$

Where:

$$A_{fv} \approx b_w * z$$

$$f_{ctd;2} = \frac{f_{ctfk}}{\gamma_{cf} * K_{global}}$$

Total resistance: The total resistance is the summation of the contribution of concrete and steel fibres:

$$V_{Rd} = V_{Rd,c} + V_{Rd,f}$$

Resistance of the concrete compressive strut

The upper limit of the shear force capacity is the capacity of the concrete compressive strut:

$$V_{Rd,max} = 2 * 1{,}14 * \frac{\alpha_{cc}}{\gamma_c} b_w z f_{ck}^{\frac{2}{3}} * \frac{1}{cot\theta + tan\theta}$$

Shear force capacity

The shear force capacity of the cross section is taken as the lesser value of the tensile resistance of the ties and the resistance of the compressive strut:

$$V_{Rd} = \min\left(V_{Rd,c} + V_{Rd,f}; V_{Rd,max}\right)$$

Verification

The following criterion is to be satisfied:

$$\frac{V_{Ed}}{V_{Rd}} \leq 1{,}0$$

2.6 Verification torsional resistance

2.6.1 Assumptions & approach

The calculation is based on the following assumptions:

- The shear force is only taken by web (direction shear force parallel to centreline of the webs);
- The same angle is applied for the shear and torsion when calculating the capacity of the concrete compressive strut;
- For the combination of shear and torsion and failure of the concrete compressive strut each wall segment is analysed separately.

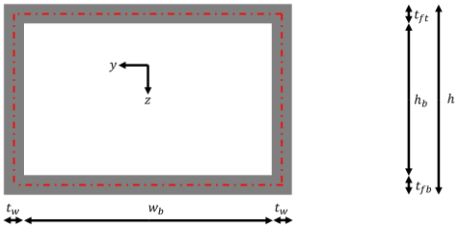
2.6.2 Torsional capacity

The first analysis comprises the verification of the torsional capacity of the cross section as a whole, by comparing the torsional cracking moment (resistance) and torsional moment determined using the RFEM model. The torsional cracking moment is:

$$T_{Rd,c} = f_{ctd} * t_{ef} * 2 * A_k$$

Where:
A_k: Area enclosed by the centre lines of the connected walls, including enclosed hollow parts
t_{ef}: Effective wall thickness
A: Total area of the cross section within the outer circumference, including enclosed hollow parts
u: Outer circumference of the cross section

The simplified cross section is as follows, its properties are calculated below.



$$A = (t_w + w_b + t_w) * \left(t_{ft} + h_b + t_{fb}\right)$$

$$u = 2 * (t_w + w_b + t_w) + 2 * \left(t_{ft} + h_b + t_{fb}\right)$$

$$t_{ef} = \frac{A}{u} \leq \min\{t_w; t_{ft}; t_{fb}\}$$

$$A_k = \left(\frac{1}{2} * t_w + w_b + \frac{1}{2} * t_w\right) * \left(\frac{1}{2} * t_{ft} + h_b + \frac{1}{2} * t_{fb}\right)$$

Note that the real wall thickness of the thinnest element is the limiting factor for the effective wall thickness. It has subsequently to be verified that:

$$\frac{T_{Ed}}{T_{Rd,c}} \leq 1{,}0$$

2.6.3 Combination of shear and torsion

Decomposing the cross section

The cross section is decomposed into four segments that are analysed separately:

- Left web – Part 1
- Bottom flange – Part 2
- Right web – Part 3
- Top flange – Part 4

Forces acting on each segment

The equivalent shear forces due to shear and torsion acting on each part are determined.

Shear forces: It is assumed that only the web contributes to the shear capacity and that the contributions of both webs are equal in magnitude:

$$V_{Ed,V,1} = V_{Ed,V,3} = \frac{V_{Ed}}{2}$$

$$V_{Ed,V,2} = V_{Ed,V,4} = 0$$

Torsion: The shear force in segment 'i' due to torsion is calculated as:

$$V_{Ed,T,i} = \tau_{t,i} * t_{ef,i} * z_i = \frac{T_{Ed}}{2 * A_k} * z_i$$

Where 'z_i' is the length of segment 'i':

$$z_1 = \frac{1}{2} * t_{ft} + h_b + \frac{1}{2} * t_{fb}$$

$$z_2 = \frac{1}{2} * t_w + w_b + \frac{1}{2} * t_w$$

$$z_3 = \frac{1}{2} * t_{ft} + h_b + \frac{1}{2} * t_{fb}$$

$$z_4 = \frac{1}{2} * t_w + w_b + \frac{1}{2} * t_w$$

Combined effect: The combined effect (equivalent shear force) of shear and torsion per segment is:

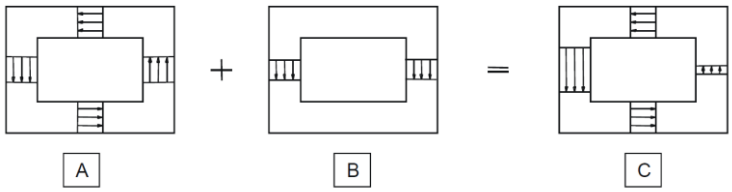
$$V_{Ed,T+V,1} = V_{Ed,V,1} + V_{Ed,T,1}$$

$$V_{Ed,T+V,2} = V_{Ed,T,2}$$

$$V_{Ed,T+V,3} = V_{Ed,V,3} - V_{Ed,T,3}$$

$$V_{Ed,T+V,4} = V_{Ed,T,4}$$

This is based on the following principle:



Legenda

A wringing
B afschuiving
C combinatie

Eurocode 2-2, p.32

Capacity of each segment

For each segment it has to be verified whether the capacity is sufficient. As there is no shear or torsional reinforcement present, the capacity of each segment is:

$$V_{Rd,i} = V_{Rd,c,i} + V_{Rd,f,i}$$

Where:
b_w: Width of the segment (depending on the segment under consideration this equals t_w, t_{fb} or t_{ft});
z: Lever arm (in these calculations 'z' is taken equal to the length 'z_i' of each segment)

The equations for the capacity are the same as used for the shear capacity but different dimensions are applied, the width and length are dependent on the segment under consideration. For each segment it subsequently has to be verified that:

$$\frac{V_{Ed,T+V,i}}{V_{Rd,i}} \leq 1{,}0$$

Failure of the concrete compressive strut

The resistance of the sections to the combined effect of shear and torsion are limited by the capacity of the concrete compressive strut. Because the beams have a box type cross section, each segment is verified separately by applying the following verification:

$$V_{Ed,i} + \frac{T_{Ed}}{2 * A_k} * z_i \leq V_{Rd,max,i}$$

Where:

$$V_{Rd,max,i} = 2 * 1{,}14 * \frac{\alpha_{cc}}{\gamma_C} * b_{w,i} * z_i * f_{ck}^{\frac{2}{3}} * \frac{1}{cot\theta + tan\theta}$$

The values of the (effective) thickness depend on the segment under consideration:

$$b_{w,i} = t_{ef,i}$$

$$t_{ef,i} = \frac{A}{u} \leq t_i$$

2.7 Global verification ship collision

The global verification is performed by considering the static equilibrium of the structure. In order to do so the self-weight of the bridge deck is, as a simplification, calculated by determining the weight of the prefab beams:

$$F_{sw} = n_{beams} * l_{tot} * A_c * \rho$$

It subsequently has to be verified that:

$$F_{eq} \leq \mu * F_{sw}$$

F_{eq}: Equivalent static force caused by ship collision
μ: Friction coefficient for friction between the concrete beams and its supports

3

DESIGN OF MAIN BEAMS – TOP FLANGE AND TRANSVERSE PRESTRESSING

3.1 Design of transverse prestressing

3.1.1 Calculating prestress losses

The calculation of the transverse prestressing is based on the following points:

- To design the transverse prestressing, a strip of the top flange is analysed with width $w_{c.t.c.}$ and properties as defined in 1.1.2;
- At each rib a prestressing tendon is applied consisting of n strands, each with an area of $A_{p,strand}$ and an assumed maximum stress of $\sigma_{p,max,prov}$;
- If no additional eccentricity Δe_{ft} is applied, then the centre of the section of the flange coincides with the centre of the prestressing tendon. The top flange is then prestressed centrically, with the tendon positioned at a height of z_{ft} with respect to the top fibres;
- If an additional eccentricity Δe_{ft} is applied, then the top flange is prestressed using an eccentric force with eccentricity Δe_{ft}. This force causes an upward bending moment in the top flange;
- The longitudinal joint has a thickness t_j, which is smaller than the thickness t_{ft}. That means that there is always an eccentricity e_j between the centre of the tendon and top flange on one hand and the centre of the joint on the other. If no additional eccentricity Δe_{ft} is applied, then $e_j = z_{ft} - 0{,}5 * t_j$;
- If an additional eccentricity Δe_{ft} is applied, then the value of e_j increases: $e_j = z_{ft} + \Delta e_{ft} - 0{,}5 * t_j$.

Applied maximum force onto prestressing element and stress verification

It has to be verified that the maximum stress applied to the tendon does not exceed the maximum value:

$$\sigma_{p,max,prov} \leq \sigma_{p,max}$$

Additionally it is verified that the maximum allowed concrete compressive stress is not exceeded. If no additional eccentricity Δe_{ft} is applied, then:

$$\sigma_c = \frac{P_{max}}{A_{ft}} = \frac{\sigma_{p,max} * n * A_{p_{strand}}}{A_{ft}} \leq 0{,}6 * f_{ck}$$

If an additional eccentricity Δe_{ft} is applied, then the previous equation is replaced by (note that the term between brackets in the denominator indicates the section modulus with respect to the bottom fibre of the rib):

$$\sigma_c = \frac{P_{max}}{A_{ft}} + \frac{P_{max} * \Delta e_{ft}}{W_{tf}} = \frac{\sigma_{p,max} * n * A_{p_{strand}}}{A_{ft}} + \frac{\sigma_{p,max} * n * A_{p_{strand}} * \Delta e_{ft}}{\left(\frac{I_{ft}}{t_{ft,1} + t_{ft,2} - z_{ft}}\right)} \leq 0{,}6 * f_{ck}$$

Direct losses

Elastic shortening: The elastic loss of the single tendon within the section of the top flange is calculated as:

$$\Delta P_{el} = P_{max} * \frac{E_p A_p}{E_{cm} A_{ft}}$$

Friction: The friction losses for the straight tendon only depend on the Wobble-effect as the angular rotation equals zero:

$$\Delta P_{\mu}(x) = (1 - e^{-\mu * k * x}) * P_{max}$$

At the far end of the deck ($x = w_{tot}$) the friction loss is:

$$\Delta P_{\mu}(x = w_{tot}) = (1 - e^{-\mu * k * w_{tot}}) * P_{max}$$

The friction loss converted into a stress value is:

$$\Delta \sigma_{P\mu}(x = w_{tot}) = \frac{\Delta P_{\mu}(x = w_{tot})}{A_p}$$

Wedge set: It is assumed that the friction develops linearly over the full width of the deck, the stress reduction per unit of length is:

$$k = \frac{\Delta \sigma_{P\mu}(x = w_{tot})}{w_{tot}}$$

The influence length over which the wedge set influences the prestressing force then is:

$$l_w = \sqrt{\frac{w_{set} * E_p}{k}}$$

The prestress loss follows from:

$$\Delta P_{set} = 2 * A_p * \frac{\Delta \sigma_{p\mu,m}}{\Delta x} * l_w$$

Determining initial prestressing force and stress verification

The initial prestressing force is:

$$P_{m0}(x) = P_{max} - \Delta P_{el} - \Delta P_{\mu}(x) - \Delta P_{set}(x)$$

It has to be verified that the stresses in the strands are not larger than the maximum allowable value. The deck is divided into a number of intervals and the prestressing forces and losses are subsequently calculated at a total of 'j' points along the width of the deck. The maximum value of the initial prestressing force is used to perform the verification:

$$\frac{\max\{P_{m0}(x)\}}{A_p} \leq \sigma_{pm0}$$

Time dependent losses

The remainder of the analysis is performed using the mean value of the initial prestressing force values calculated at the different points over the width of the deck, which is determined using:

$$P_{m0} = \frac{1}{j} * \sum_{i=1}^{i=j} P_{m0,i}$$

If no additional eccentricity Δe_{ft} is applied, then the top flange is centrically prestressed, for the centric prestressing in the top flange the time dependent losses can be calculated as follows:

$$\Delta P_{c+s+r} = A_p * \Delta\sigma_{p,c+s+r} = A_p * \frac{\varepsilon_{cs}E_p + 0{,}8\Delta\sigma_{pr} + \frac{E_p}{E_{cm}}\varphi(\infty,t_0)\sigma_{c,QP}}{1 + \frac{E_p}{E_{cm}}\frac{A_p}{A_{ft}}[1 + 0{,}8 * \varphi(\infty,t_0)]}$$

If an additional eccentricity Δe_{ft} is applied, then the aforementioned equation is replaced by the following expression:

$$\Delta P_{c+s+r} = A_p * \Delta\sigma_{p,c+s+r} = A_p * \frac{\varepsilon_{cs}E_p + 0{,}8\Delta\sigma_{pr} + \frac{E_p}{E_{cm}}\varphi(\infty,t_0)\sigma_{c,QP}}{1 + \frac{E_p}{E_{cm}}\frac{A_p}{A_{ft}}\left(1 + \frac{A_{ft}}{I_{ft}}z_{cp}^2\right)[1 + 0{,}8 * \varphi(\infty,t_0)]}$$

Where (for relaxation class 2 and while only accounting for permanent loads to calculate $\sigma_{c,QP}$):

Case: $\Delta e_{ft} = 0$	**Case:** $\Delta e_{ft} > 0$
$\frac{\Delta\sigma_{pr}}{\sigma_{pi}} = 0{,}66 * \rho_{1000} * e^{9{,}1\mu} * \left(\frac{t}{1000}\right)^{0{,}75(1-\mu)} * 10^{-5}$	
$\sigma_{pi} = \sigma_{pm,0} = \frac{P_{m0}}{A_p}$	
$\mu = \frac{\sigma_{pm,0}}{f_{pk}}$	
$t = 500.000$	
$\sigma_{c,QP} = \frac{P_{m0}}{A_{ft}}$	$\sigma_{c,QP} = \frac{P_{m0}}{A_{ft}} + \frac{P_{m0} * \Delta e_{ft}^2}{I_{ft}} + \frac{\frac{1}{12} * G_k * w_{c.t.c.} * l^2 * \Delta e_{ft}}{I_{ft}}$
	$z_{cp} = \Delta e_{ft}$

Note: See 3.1.2 for the calculation of the permanent load G_k and the hogging bending moment caused by this action. By combining the values of the hogging (i.e. upward) bending moments due to the prestressing and the self-weight, the largest compressive stress value in the concrete adjacent to the tendon is found. The value of 'l' is determined as follows: $l = \max\{2 * w_f + w_j + t_w; 2 * 0{,}5 * t_w + w_b\}$.

Working prestressing force

The mean value of the working prestressing force over the width of the deck is found by subtracting the value for time dependent losses from the mean value of the initial prestressing force over the width of the beam:

$$P_{m,\infty} = P_{m0} - \Delta P_{c+s+r}$$

3.1.2 Forces acting on top flange and joint

To determine the stresses over the joint height first the loads acting on the top flange and joint have to be determined. A strip of the deck in transverse direction with a width of 1,0 m is analysed. Relevant loads are:

- Self-weight and permanent load:

$G_k = t_{tf} * \rho_{UHPC} + t_{asphalt} * \rho_{asphalt}$ [kN/m]

- Variable load (follows from LM2 and only half an axle force is considered given the span):

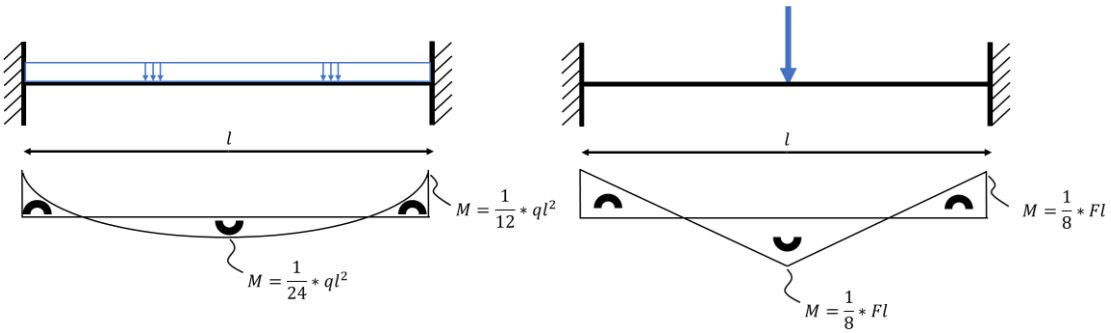
$$Q_k = \frac{1}{2} * \beta_Q Q_{ak} \; [kN]$$

- Upward bending moment due to prestressing:

$$M_P = \frac{P_{m,\infty} * e_j}{w_{c.t.c.}}$$

Note: The prestressing force $P_{m,\infty}$ was calculated for a width $w_{c.t.c.}$, in case this is not equal to 1,0 m the prestressing force is converted to a force corresponding to this unity width for use in the remainder of the calculations.

The top flange is schematized using simple models with uniformly distributed or point loads, as given below. The joint is positioned at mid span.



The bending moments (due to permanent load, prestressing and variable load) acting on the joint without partial load factors are:

$$M_G = \frac{1}{24} * G_k * l^2$$

$$M_P = \frac{P_{m,\infty} * e_j}{w_{c.t.c.}}$$

$$M_Q = \frac{1}{8} * Q_k * l$$

To verify the bending moment capacity later on, the design value of the bending moment is also determined. The design value of the bending moment is calculated both using equations 6.10a and 6.10b of the Eurocode 0 and the larger value is subsequently applied:

$$M_{Ed} = \max\{\gamma_G * M_G - \gamma_P * M_P + \psi_0 * \gamma_Q * M_Q; \zeta * \gamma_G * M_G - \gamma_P * M_P + \gamma_Q * M_Q\}$$

3.1.3 Verifying stresses over joint height

Using the aforementioned loads and models, the stresses are calculated over the joint height using the prestressing force acting on a strip of 1,0 m width for $t \to \infty$. The stresses are calculated at the top and bottom fibre and this is done for the situation with and without traffic.

- With traffic:

$$\sigma_{j,t} = -\frac{M_G}{W_j} - \frac{M_Q}{W_j} - \frac{P_{m,\infty}}{w_{c.t.c.} * A_j} + \frac{M_P}{W_j} \leq 0$$

$$\sigma_{j,b} = +\frac{M_G}{W_j} + \frac{M_Q}{W_j} - \frac{P_{m,\infty}}{w_{c.t.c.} * A_j} - \frac{M_P}{W_j} \leq 0$$

- Without traffic:

$$\sigma_{j,t} = -\frac{M_G}{W_j} - \frac{P_{m,\infty}}{w_{c.t.c.} * A_j} + \frac{M_P}{W_j} \leq 0$$

$$\sigma_{j,b} = +\frac{M_G}{W_j} - \frac{P_{m,\infty}}{w_{c.t.c.} * A_j} - \frac{M_P}{W_j} \leq 0$$

The properties of the joint are:

$$A_j = 1000 * t_j \; [mm^2]$$

$$W_j = \frac{1}{6} * 1000 * t_j^2 \; [mm^3]$$

$$I_j = \frac{1}{12} * 1000 * t_j^3 \; [mm^4]$$

$$l = 2 * w_f + w_j + t_w$$

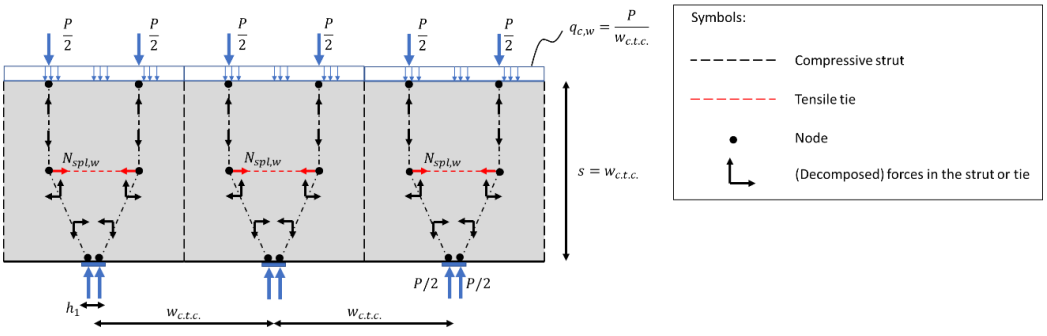
$$d_p = 0{,}5 * t_j + e_j$$

If the joint is in compression over its full height in both cases, then it is concluded that the working prestressing force is sufficiently large. Note that the calculation of e_j is given in 3.1.1.

3.1.4 Detailing

The force distribution is analysed at the anchors, both in horizontal and vertical direction. In horizontal direction the force is given by:

$$N_{spl,w} = \frac{1}{4} * \gamma_{spl} * P_{m0} * \left(1 - \frac{h_1}{w_{c.t.c.}}\right)$$

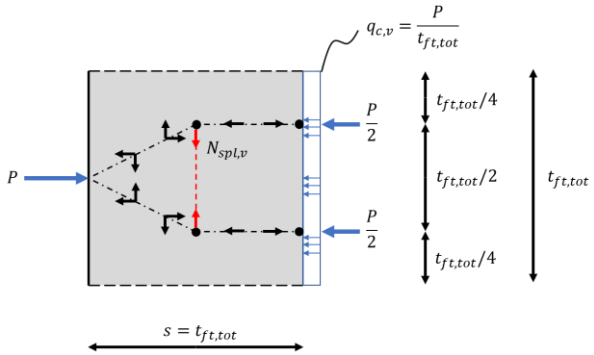


In vertical direction the force equals:

$$N_{spl,w} = \frac{1}{4} * \gamma_{spl} * P_{m0} * \left(1 - \frac{h_1}{t_{ft,tot}}\right)$$

In this equation $t_{ft,tot} = t_{ft,1} + t_{ft,2}$, note that it is therefore assumed that the prestressing is applied at half the height of the rib (not necessarily the centre of gravity) and that a compressive stress results which is constant over

the height of the rib. Depending on the positioning of the tendons and the dimensions of the top flange, this does not have to be the case in reality. Therefore the calculation should be interpreted only as a first indication, depending on the situation it should be verified whether the assumed distribution is sufficiently accurate to analyse the force distribution.



The maximum stress in the reinforcement, required minimum reinforcement diameter and minimum required reinforcement bars for that given diameter are respectively:

$$f_s = \frac{3000}{\emptyset_{spl,ft}}$$

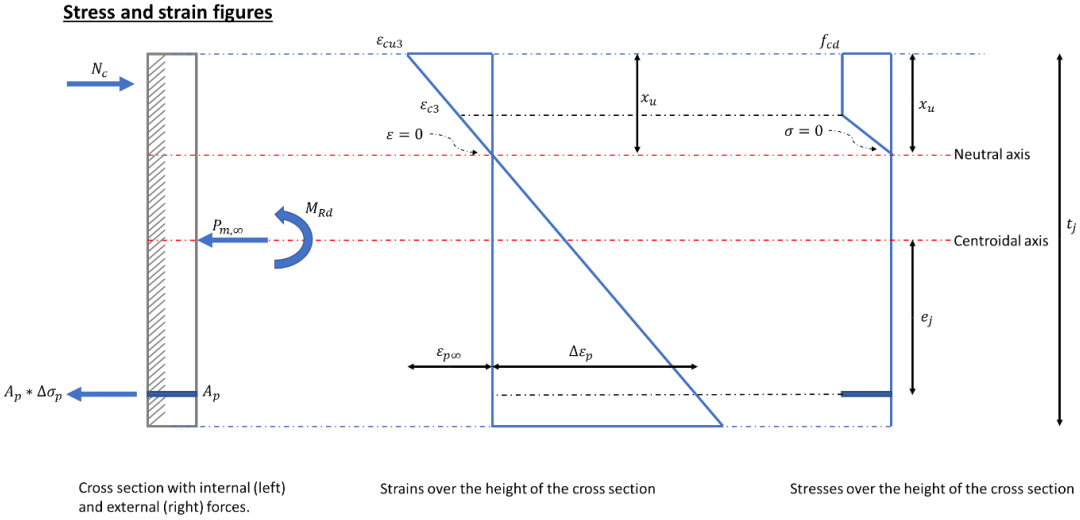
$$A_{s,req} = \frac{N_{spl}}{f_s}$$

$$n_{s,req} = Int\left(\frac{A_{s,req}}{\pi * \left(\frac{\emptyset}{2}\right)^2}\right)$$

The maximum stress and required reinforcement are calculated for the horizontal and vertical direction separately, to obtain the most conservative result in terms of amount of reinforcement the tensile capacity of the UHPC is not taken into consideration.

3.2 Local verification – Verification bending moment capacity longitudinal joint

To verify the capacity of the longitudinal joint the aforementioned design values of the bending moment are applied. The same strip of 1,0 m width is analysed. The material parameters of the joint material are used. The following strain and stress relations over the joint height are assumed in the ultimate limit state:



The calculation is made iteratively, different values for x_u are assumed until horizontal equilibrium is found. The capacity is calculated as follows:

Parameters concrete: Using the assumed value for x_u the compressive force is:

$$N_c = \alpha * f_{cd} * x_u * 1000\ [N]$$

Parameters steel: The cross section of the tendon per strip of 1,0 m is denoted as A_p and the working prestressing stress as $\sigma_{pm,\infty}$.

Determining strains and stresses: The strains and stresses in the prestressing are calculated as follows:

$$\varepsilon_{p,\infty} = \frac{\sigma_{p,\infty}}{E_p}$$

$$\Delta\varepsilon_p = \varepsilon_{cu3} * \left(\frac{d_p}{x_u} - 1\right)$$

$$\varepsilon_p = \varepsilon_{p,\infty} + \Delta\varepsilon_p \leq 0{,}9 * \varepsilon_{uk}$$

$$\sigma_{pu} = f_{pd} + \frac{\varepsilon_p - \frac{f_{pd}}{E_p}}{\varepsilon_{uk} - \frac{f_{pd}}{E_p}} * \left(\frac{f_{pk}}{\gamma_s} - f_{pd}\right)$$

Horizontal equilibrium: The remaining horizontal forces are:

$$P_{m,\infty} = A_p * \sigma_{pm,\infty}$$

$$\Delta N_p = A_p * (\sigma_{pu} - \sigma_{p,\infty})$$

It subsequently has to be verified that:

$$-N_c + P_{m,\infty} + \Delta N_p = 0$$

Bending moment capacity: If the horizontal equilibrium is satisfied the bending moment capacity is calculated:

$$M_{Rd} = -N_c * \beta * x_u + P_{m,\infty} * \frac{1}{2} * t_j + \Delta N_p * d_p$$

Verification: It subsequently has to be verified that:

$$\frac{M_{Ed}}{M_{Rd}} \leq 1{,}0$$

3.3 Local verification – Bending moment capacity top flange between the webs

3.3.1 Calculation model and design value bending moments

The capacity of the top flange is verified by comparing the bending moment capacity with the design value of the sagging bending moment at mid span between the webs of a prefab beam and the hogging bending moment at the webs. The analysis is based on a strip of the top flange with a width of 1,0 m. The same type of model is used as applied for the verification of the longitudinal joint and the same permanent and variable loads are applied.

Differences are different cross sectional properties (those belonging to the top flange instead of the joint), the span and the material properties (the properties of the main beams are used instead of those of the longitudinal joints):

$l = 2 * 0{,}5 * t_w + w_b$

$d_p = z_{ft} + \Delta e_{ft}$

The design value of the bending moments is calculated by assessing both equations 6.10a and 6.10b of Eurocode 0, after which the maximum value is selected.

- For the sagging bending moment this results in:

$M_{Ed} = max\{\gamma_G * M_G - \gamma_P * M_{P,ft} + \psi_0 * \gamma_Q * M_Q; \zeta * \gamma_G * M_G - \gamma_P * M_{P,ft} + \gamma_Q * M_Q\}$

Where:

$M_G = \frac{1}{24} * G_k * l^2$

$M_Q = \frac{1}{8} * Q_k * l$

$M_{P,ft} = P_{m,\infty} * \Delta e_{tf}$

- For the hogging bending moment this results in:

$M_{Ed} = max\{\gamma_G * M_G + \gamma_P * M_{P,ft} + \psi_0 * \gamma_Q * M_Q; \zeta * \gamma_G * M_G + \gamma_P * M_{P,ft} + \gamma_Q * M_Q\}\}$

Where:

$M_G = \frac{1}{12} * G_k * l^2$

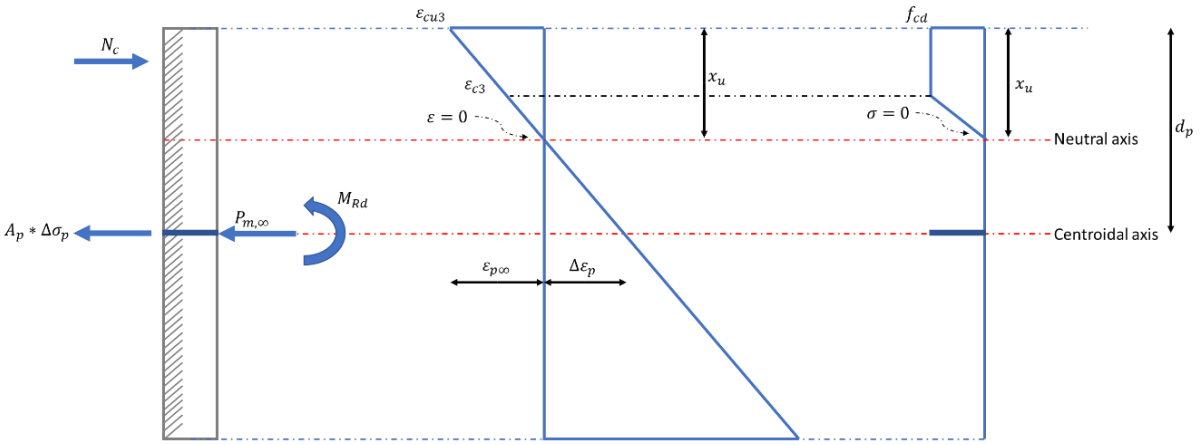
$M_Q = \frac{1}{8} * Q_k * l$

$M_{P,ft} = P_{m,\infty} * \Delta e_{tf}$

3.3.2 Verification of bending moment capacity

The bending moment capacity is calculated to verify the design values of the sagging and hogging bending moments. The following strain and stress relations over the height of the top flange in the ULS are assumed. These diagrams hold for the verification of the sagging bending moment:

Stress and strain figures



Cross section with internal (left) and external (right) forces.

Strains over the height of the cross section

Stresses over the height of the cross section

Note that for the hogging bending moment a different diagram is to be applied. Therefore, both cases will be covered separately.

Sagging bending moment capacity

The calculation is made iteratively, different values for x_u are assumed after which it is checked if horizontal equilibrium is found. The capacity is calculated as follows:

Parameters concrete: The compressive force is:

$$N_c = \alpha * f_{cd} * x_u * 1000\ [N]$$

Parameters steel: The cross section of the tendon per strip of 1,0 m is denoted as A_p and the working prestressing stress is $\sigma_{pm,\infty}$.

Determining strains and stresses: The strains and stresses in the prestressing are as follows.

$$\varepsilon_{p,\infty} = \frac{\sigma_{p,\infty}}{E_p}$$

$$\Delta\varepsilon_p = \varepsilon_{cu3} * \left(\frac{d_p}{x_u} - 1\right)$$

$$\varepsilon_p = \varepsilon_{p,\infty} + \Delta\varepsilon_p \leq 0{,}9 * \varepsilon_{uk}$$

$$\sigma_{pu} = f_{pd} + \frac{\varepsilon_p - \frac{f_{pd}}{E_p}}{\varepsilon_{uk} - \frac{f_{pd}}{E_p}} * \left(\frac{f_{pk}}{\gamma_s} - f_{pd}\right)$$

Horizontal equilibrium: The remaining horizontal forces are calculated:

$$P_{m,\infty} = A_p * \sigma_{pm,\infty}$$

$$\Delta N_p = A_p * (\sigma_{pu} - \sigma_{p,\infty})$$

Horizontal equilibrium is subsequently verified, the following requirement has to be satisfied:

$$-N_c + P_{m,\infty} + \Delta N_p = 0$$

Bending moment capacity: If horizontal equilibrium is found the bending moment capacity is calculated:

$$M_{Rd} = -N_c * \beta * x_u + P_{m,\infty} * z_{ft} + \Delta N_p * d_p$$

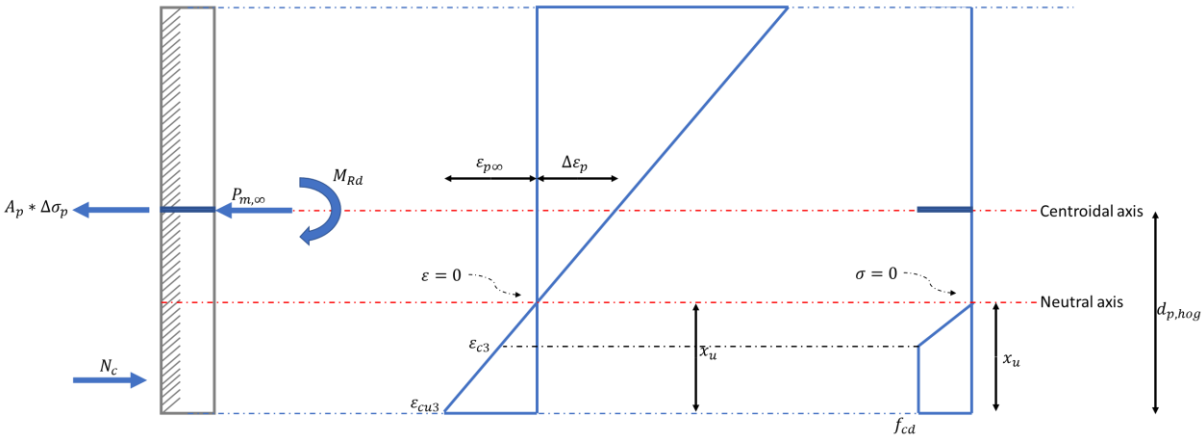
Verification: It subsequently has to be verified that:

$$\frac{M_{Ed,sag}}{M_{Rd}} \leq 1{,}0$$

Hogging bending moment capacity

For the hogging bending moment the following stress and strain relations over the height of the top flange are assumed in the ultimate limit state.

Stress and strain figures



Cross section with internal (left) and external (right) forces.

Strains over the height of the cross section

Stresses over the height of the cross section

Note that the effective height for the hogging bending moment, $d_{p,hog}$, is calculated as follows using the effective height of the sagging bending moment:

$$d_{p,hog} = t_{ft,tot} - d_p = t_{ft,1} + t_{ft,2} - z_{ft} - \Delta e_{ft}$$

The calculation is made iteratively, different values for x_u are assumed after which it is checked if horizontal equilibrium is found. The capacity is calculated as follows:

Parameters concrete: The concrete compressive force is:

$$N_c = \alpha * f_{cd} * x_u * b_{eff}\ [N]$$

In this equation the term b_{eff} is calculated as follows:

- If $t_{ft,2} = 0$:

In this case no variable height is applied and thus the width is taken equal to the unity width of 1000 mm.

- If $t_{ft,2} > 0$:

In this case a variable height is applied and the lower end of the prestressing ribs with width w_{rib} form the compressive force. To account for the fact that these ribs might not be applied with a spacing of 1000 mm, the effective width is calculated as follows:

$$b_{eff} = w_{rib} * \frac{1000}{c.t.c.}$$

In reality the chamfers with width w_{ch} may also contribute to the total width of the compressive zone, increasing the width beyond the value of w_{rib}. However, this is not included in the calculation because it is expected that the height of the compressive zone is limited given the high compressive strength of UHPC. Including the chamfers would result in a value for the bending moment capacity which is larger than the calculated value, although this increase is expected to be minimal.

Parameters steel: The cross section of the tendon per strip of 1,0 m is denoted as A_p and the working prestressing stress is $\sigma_{pm,\infty}$.

Determining strains and stresses: The strains and stresses in the prestressing are:

$$\varepsilon_{p,\infty} = \frac{\sigma_{p,\infty}}{E_p}$$

$$\Delta\varepsilon_p = \varepsilon_{cu3} * \left(\frac{d_{p,hog}}{x_u} - 1\right)$$

$$\varepsilon_p = \varepsilon_{p,\infty} + \Delta\varepsilon_p \leq 0{,}9 * \varepsilon_{uk}$$

$$\sigma_{pu} = f_{pd} + \frac{\varepsilon_p - \frac{f_{pd}}{E_p}}{\varepsilon_{uk} - \frac{f_{pd}}{E_p}} * \left(\frac{f_{pk}}{\gamma_s} - f_{pd}\right)$$

Horizontal equilibrium: The remaining horizontal forces are calculated.

$$P_{m,\infty} = A_p * \sigma_{pm,\infty}$$

$$\Delta N_p = A_p * (\sigma_{pu} - \sigma_{p,\infty})$$

Horizontal equilibrium is subsequently verified, for equilibrium it has to hold that:

$$-N_c + P_{m,\infty} + \Delta N_p = 0$$

Bending moment capacity: If horizontal equilibrium is found the bending moment capacity is calculated using the following equation. Note that the bottom fibre is used as the point of reference.

$$M_{Rd} = -N_c * \beta * x_u + P_{m,\infty} * (t_{ft,tot} - z_{ft}) + \Delta N_p * d_{p,hog}$$

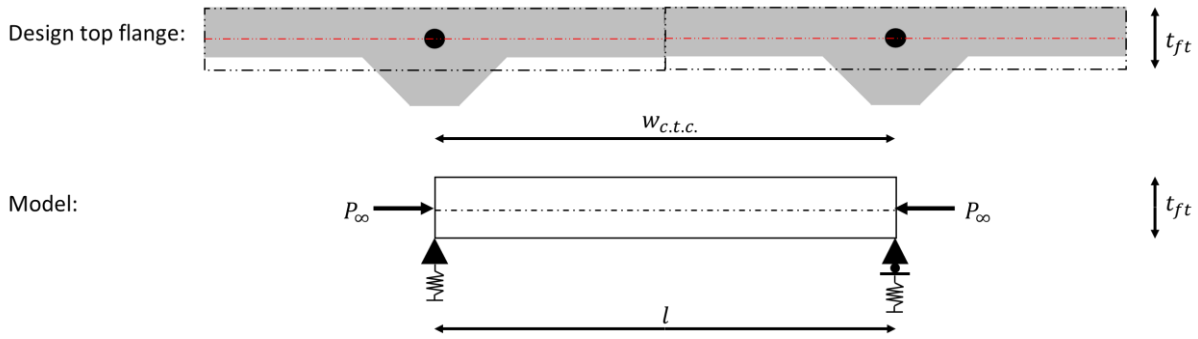
Verification: It subsequently has to be verified that:

$$\frac{M_{Ed,hog}}{M_{Rd}} \leq 1{,}0$$

3.4 Local verification – Bending moment capacity top flange between prestressing ribs

3.4.1 Calculation model and design value bending moments

The top flange between the prestressing ribs is analysed to verify its bending moment capacity. It is modelled as a 1,0 m wide beam spanning between two adjacent prestressing ribs and prestressed by an external axial force. The model is as follows:



Properties of the beam are:

- The height of the beam is t_{ft};
- The width of the beam is 1,0 m;
- The span is equal to the centre to centre distance between the ribs: $l = w_{c.t.c.}$;
- The beam is prestressed by external prestressing force P_∞, which is assumed to act centrically.

The external prestressing force depends on the bending moment due to the self-weight of the beams, the axial force due to the prestressing and the upward bending moment due to the prestressing. For this reason the compressive force is not constant over the beam length. It is at its maximum at mid span and at its minimum near the supports. If there is a tensile force present, which may occur at the supports, P_∞ is taken equal to zero.

The beam is supported as a simply supported beam, loaded by permanent load G_k and Q_k as given in the aforementioned verifications of the joint and top flange. The bending moment is at its maximum at mid span:

$$M_G = \frac{1}{8} * G_k * l^2$$

$$M_Q = \frac{1}{4} * Q_k * l$$

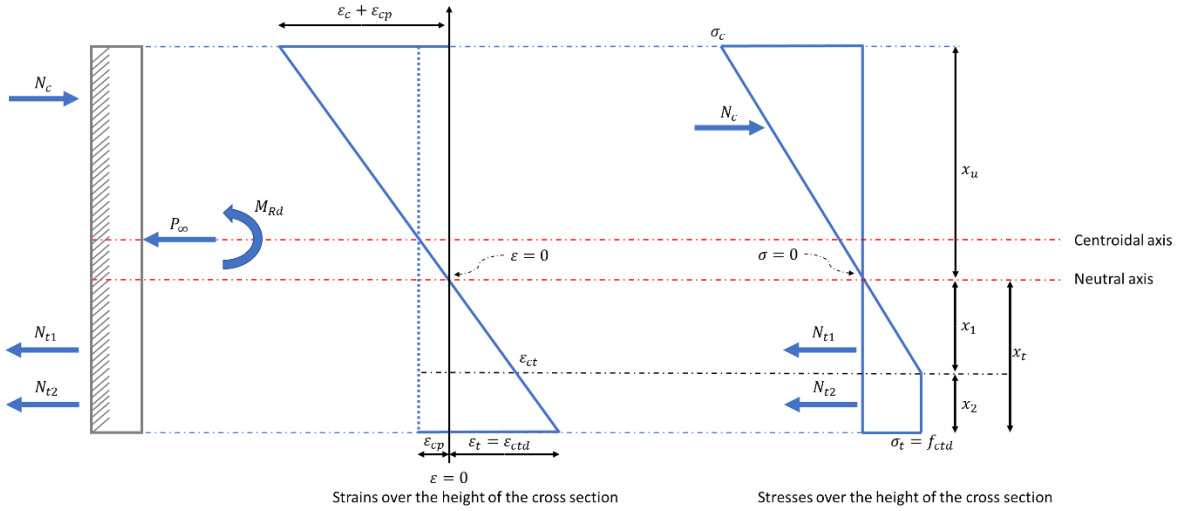
The design value of the bending moments is calculated by assessing both equations 6.10a and 6.10b of the Eurocode, after which the maximum value is selected:

$$M_{Ed} = max\{\gamma_G * M_G + \psi_0 * \gamma_Q * M_Q; \zeta * \gamma_G * M_G + \gamma_Q * M_Q\}$$

3.4.2 Verification of bending moment capacity

Assumptions

The following strain and stress distributions are assumed over the height of the beam in the ULS. The material properties of the main beam are applied.



Because the external axial force depends on the position along the beam the capacity does depend on it as well. For this reason a part of the beams is analysed directly next to the support (the governing part as this will be the governing beam part) and the capacity is calculated on a large number of intervals (0,25 m apart). The influence of the transfer length is neglected in these calculations: As a simplification it is assumed that the full prestressing forces $P_{m0,c}$ and $P_{m0,fb}$ are applied directly from the support, this also results in the most conservative situation.

Capacity at each point under consideration

At each of the points where the capacity is calculated the following set of calculations is carried out:

Calculating external force: The external force depends on the self-weight of the beams and the prestressing and the stresses in the middle fibre due to each of these loads is calculated.

- Self-weight of the beams:

$$\sigma_{t,sw}(x) = -\frac{M_{sw} * (e_t - 0{,}5 * t_{ft})}{I_y} \rightarrow -\frac{\frac{1}{2} * G_{k,beam} * x * (l - x) * (e_t - 0{,}5 * t_{ft})}{I_y}$$

- Centric prestressing:

$$\sigma_{t,c} = -\frac{P_{m0,c}}{A_c}$$

- Eccentric prestressing:

$$\sigma_{t,fb} = -\frac{P_{m0,fb}}{A_c} + \frac{P_{m0,fb} * e_p * (e_t - 0{,}5 * t_{ft})}{I_y}$$

- Total stresses:

$$\sigma_{t,tot}(x) = \sigma_{t,sw}(x) + \sigma_{t,c} + \sigma_{t,fb}$$

- External axial force:

$$P_\infty = \sigma_{t,tot}(x) * t_{ft} * 1000 * 10^{-3}\ [kN]$$

Compressive strain: If $P_\infty > 0$ a tensile force is present and the effect of the tensile force is neglected in the calculation of the capacity, hence P_∞ is taken equal to zero in this situation. If $P_\infty < 0$ a compressive force is present which compresses the cross section.

In case a compressive force is present its absolute value is taken and the compressive strain in the cross section is calculated as follows:

$$\varepsilon_{cp} = \frac{|\sigma_{t,tot}(x)|}{E_{cm}}$$

Strain values fibre reinforced concrete: To calculate the capacity of the cross section on the different intervals the different strain values on the stress-strain diagram have to be calculated:

$$\varepsilon_{ct} = \frac{f_{ctd}}{E_{cm}} = \frac{f_{ctk,el}}{\gamma_c * E_{cm}}$$

$$\varepsilon_{ct;0,3} = \frac{0,3}{l_c} + \varepsilon_{ct}$$

$$\varepsilon_{ctd} = \varepsilon_{ctu} - \frac{f_{ctd}}{f_{ctd;2}} * \left(\varepsilon_{ctu} - \varepsilon_{ct;0,3}\right)$$

$$\varepsilon_{ctu} = \frac{l_f}{4 * l_c}$$

Where:

$$l_c = \frac{2}{3} * t_{ft}$$

Total compressive strain: The total compressive strain in the cross section at the moment its maximum capacity is reached (tensile strain at the lowest fibre equals f_{ctd}) is as follows.

$$(\varepsilon_c + \varepsilon_{cp}) = \varepsilon_{cp} + \sqrt{\varepsilon_{cp}^2 + \frac{2 * f_{ctd} * \varepsilon_{ctd} - f_{ctd} * \varepsilon_{ct}}{E_{cm}} + 2 * \varepsilon_{cp} * \varepsilon_{ctd}}$$

Where:
ε_c: Compressive strain in most compressed fibre if no external compressive force is present

Height of concrete compressive and tensile zones: Using the total strain value at the top of the cross section and the diagram of the strain relationship over the beam height the height of the compressive and tensile zones can be determined:

$$x_u = \frac{f_{ctd} * t_{ft} + \varepsilon_{cp} * E_{cm} * t_{ft}}{\left(\frac{1}{2} * \left(\varepsilon_c + \varepsilon_{cp}\right) * E_{cm} + \frac{1}{2} * f_{ctd} * \frac{\varepsilon_{ct}}{\varepsilon_c + \varepsilon_{cp}} + f_{ctd}\right)}$$

$$x_1 = \frac{\varepsilon_{ct}}{\varepsilon_c + \varepsilon_{cp}} * x_u$$

$$x_2 = t_{ft} - x_u - \frac{\varepsilon_{ct}}{\varepsilon_c + \varepsilon_{cp}} * x_u$$

Normal forces: The horizontal forces are determined as follows, note that in these expressions the width 'b' represents a strip of the top flange with a width of 1,0 m.

$$N_c = \frac{1}{2} * \sigma_c * x_u * b = \frac{1}{2} * (\varepsilon_c + \varepsilon_{cp}) * E_{cm} * x_u * b$$

$$N_{t1} = \frac{1}{2} * f_{ctd} * x_1 * b$$

$$N_{t2} = f_{ctd} * x_2 * b$$

Bending moment capacity: The bending moment capacity is subsequently calculated as follows.

$$M_{Rd} = -N_c * \frac{1}{3} * x_u + N_{t1} * \left(x_u + \frac{2}{3} * x_1\right) + N_{t2} * \left(x_u + x_1 + \frac{1}{2} * x_2\right) + P_{m,\infty} * \frac{1}{2} * t_{ft}$$

NOTE: Reference is made to the report and annexes of the detailed design for the derivations of the capacity of an unreinforced UHPC cross section with and without external compressive force.

Bending moment verification

Subsequently two graphs are plotted. One is a horizontal line denoting the required capacity (M_{Ed}) and one graph is the actual capacity calculated at the different points along the beam axis near the support. It is subsequently determined from which coordinate 'x' the capacity is (approximately) larger than the design value of the bending moments.

In the graph this is visualized as the intersection between two curves. If the capacity line is above the line of the design bending moment over the full length, the capacity is sufficient over the full length. Depending on the design it might occur that over a certain length the capacity might not be sufficient because there is no external prestressing force. In such a region additional measures might be required.

Verifying strains

The equations used for determining the capacity are based on the assumption that the compressive strain in the concrete does not exceed the value ε_{c3}. It has to be verified that this requirement is met, otherwise the assumed strain and stress distributions are no longer valid and new derivations of the equations have to be performed.

The verification is performed for midspan ($x = l/2$) because the compressive stresses are the largest at this zone, the total compressive strain in the most compressed fibre is:

$$\varepsilon_{cc} = (\varepsilon_c + \varepsilon_{cp}) = \varepsilon_{cp} + \sqrt{\varepsilon_{cp}^2 + \frac{2 * f_{ctd} * \varepsilon_{ctd} - f_{ctd} * \varepsilon_{ct}}{E_{cm}} + 2 * \varepsilon_{cp} * \varepsilon_{ctd}}$$

Where:

$$\varepsilon_{cp} = \frac{\sigma_{t,tot}\left(x = \frac{l}{2}\right)}{E_{cm}}$$

$$\sigma_{t,tot}\left(x = \frac{l}{2}\right) = -\frac{\frac{1}{8} * G_{k,beam} * l^2 * \left(e_t - 0{,}5 * t_{ft}\right)}{I_y} - \frac{P_{m0,c}}{A_c} - \frac{P_{m0,fb}}{A_c} + \frac{P_{m0,fb} * e_p * \left(e_t - 0{,}5 * t_{ft}\right)}{I_y}$$

It has to be verified that:

$$\varepsilon_{cc} \leq \varepsilon_{c3}$$

4

DESIGN OF MAIN BEAMS – FATIGUE VERIFICATION

4.1 Fatigue verification

4.1.1 Assumptions and approach

The fatigue verification is based on the following points:

- The point under consideration is midspan because the bending moments due to the cyclic loads reach their maximum value at this point;
- The maximum and minimum bending moments at this point caused by the load combinations for fatigue as covered by Eurocode 2 are determined using RFEM;
- The prestressing tendons in the bottom flange are verified (these are governing over the centric prestressing) as well as the concrete at the top and bottom fibres of the cross section.

4.1.2 Fatigue verification – Prestressing steel at midspan

Stresses at tendon height: The stresses in the concrete adjacent to the centre line of the tendons (eccentricity e_p) in the bottom flange are:

$$\sigma_{c,max} = \frac{M_{fat,max} * e_p}{I_c} - \frac{P_{m,\infty,c}}{A_c} - \frac{P_{m,\infty,fb}}{A_c} - \frac{P_{m,\infty,fb} * e_P^2}{I_c}$$

$$\sigma_{c,min} = \frac{M_{fat,min} * e_p}{I_c} - \frac{P_{m,\infty,c}}{A_c} - \frac{P_{m,\infty,fb}}{A_c} - \frac{P_{m,\infty,fb} * e_P^2}{I_c}$$

Stresses in the steel: The steel stresses are calculated from the concrete stresses using the ratio of the moduli of elasticity:

$$\alpha_e = \frac{E_p}{E_c}$$

Stress range: The maximum and minimum stresses in the prestressing steel are respectively:

$$\sigma_{p,min} = \alpha_e * \sigma_{c,min}$$

$$\sigma_{p,max} = \alpha_e * \sigma_{c,max}$$

The stress range then is:

$$\Delta\sigma_p = \sigma_{p,max} - \sigma_{p,min}$$

Number of cycles: The number of cycles that has to be designed for is as follows.

$$n = N_{obs} * n_{years}$$

Where:
N_{obs}: Number of heavy vehicles per year
n_{years}: Design service life

Allowable stress range: The allowable stress range corresponding to the aforementioned number of cycles is determined as follows.

- If $N < N^*$:

$$\Delta\sigma_{Rsd} = \frac{\Delta\sigma_{Rsk}}{\gamma_{S,fat}} * \left(\frac{N^*}{N}\right)^{\frac{1}{k_1}}$$

- If $N = N_{obs}$:

$$\Delta\sigma_{Rsd} = \frac{\Delta\sigma_{Rsk}}{\gamma_{S,fat}}$$

- If $N > N^*$:

$$\Delta\sigma_{Rsd} = \frac{\Delta\sigma_{Rsk}}{\gamma_{S,fat}} * \left(\frac{N^*}{N}\right)^{\frac{1}{k_2}}$$

Fatigue verification: Subsequently the fatigue verification is performed. It has to be verified that:

$$\Delta\sigma_p * \gamma_{F,fat} \leq \Delta\sigma_{Rsd}$$

4.1.3 Fatigue verification – Concrete at midspan

Concrete fatigue strength: The fatigue strength of concrete is determined as follows:

$$f_{cd,fat} = 0{,}85 * \beta_{cc}(t) * f_{ck} * \left(1 - \frac{f_{ck}}{40 * f_{ck0}}\right) * \frac{1}{\gamma_c}$$

Determine stress range: The maximum and minimum compressive stress in the concrete outer fibres are as follows (note that the compressive stresses are taken as a positive value and $\sigma_{cd,max}$ is the largest compressive value while $\sigma_{cd,min}$ is the smallest compressive value (i.e. closest to zero). If $\sigma_{cd,min}$ is a tensile stress, then it is taken equal to zero):

- Top fibre:

$$\sigma_{cd,max} = -\frac{M_{fat,max}}{W_t} - \frac{P_{m,\infty,c}}{A_c} - \frac{P_{m,\infty,fb}}{A_c} + \frac{P_{m,\infty,fb} * e_P}{W_t}$$

$$\sigma_{cd,min} = -\frac{M_{fat,min} * e_p}{W_t} - \frac{P_{m,\infty,c}}{A_c} - \frac{P_{m,\infty,fb}}{A_c} + \frac{P_{m,\infty,fb} * e_P}{W_t}$$

- Bottom fibre:

$$\sigma_{cd,max} = \frac{M_{fat,min}}{W_b} - \frac{P_{m,\infty,c}}{A_c} - \frac{P_{m,\infty,fb}}{A_c} - \frac{P_{m,\infty,fb} * e_P}{W_b}$$

$$\sigma_{cd,min} = \frac{M_{fat,max} * e_p}{W_b} - \frac{P_{m,\infty,c}}{A_c} - \frac{P_{m,\infty,fb}}{A_c} - \frac{P_{m,\infty,fb} * e_P}{W_b}$$

Using Excel the absolute values are subsequently calculated, or, the value is set to zero if the stress turns out to be negative.

Determine maximum number of cycles at stress range: For both the top and bottom fibre of the cross section the following calculations are performed:

$$N_i = 10^{14*\frac{1-E_{cd,max,i}}{\sqrt{1-R_i}}}$$

$$R_i = \frac{E_{cd,min,i}}{E_{cd,max,i}}$$

$$E_{cd,min,i} = \frac{\sigma_{cd,min,i}}{f_{cd,fat}}$$

$$E_{cd,max,i} = \frac{\sigma_{cd,max,i}}{f_{cd,fat}}$$

Number of cycles: The number of cycles in the stress range that will occur are:

$$n = N_{obs} * n_{years}$$

Miner's rule: To perform the fatigue verification Miner's rule is applied, however, given the fact that there is only one stress amplitude this is written as:

$$\frac{n}{N} \leq 1{,}0$$

This is performed both for the top and bottom fibre.

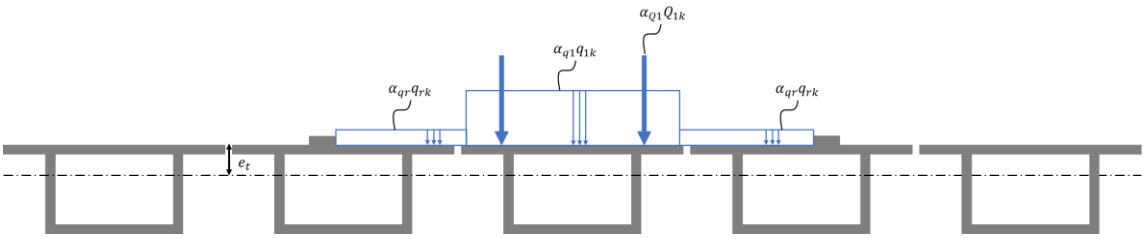
5

MAIN BEAMS – SERVICEABILITY LIMIT STATE

5.1 Deflections

5.1.1 Assumptions and approach

The deflections are calculated using the frequent load combination in the serviceability limit state. The middle beam is considered with lane 1 centred on it (configuration 3) as given in the following figure.



The calculation is performed under the conservative assumption that there is no interaction with other beams. In combination with the aforementioned positioning of the variable load this results in an upper limit of the deflection. This calculation serves as comparison with the results from RFEM.

The deflection is calculated assuming the middle beam with a permanent load (a line load) of:

$$G_{k,total} = G_{k,beam} + b_{eff,i} * G_{k,surf} \; [kN/m]$$

For the prestressing force the working prestress in the bottom flange, $P_{m,\infty,fb}$, is applied. Furthermore the stiffness of the concrete is reduced by introducing an effective modulus of elasticity:

$$E_{c,eff} = \frac{E_{cm}}{1+\varphi}$$

5.1.2 Upper limit of deflections

Deflection at midspan

The contribution of each action to the total deflection is calculated using standard engineering formulas:

- Self-Weight and permanent loads ($G_{k,total}$):

$$\delta_G = \frac{5 * G_{k,total} * l^4}{384 * E_{c,eff} * I_y}$$

- Upward bending due to the prestressing ($P = P_{m,\infty} * e_p$):

$$\delta_P = \frac{P_{m,\infty} * e_p * l^2}{8 * E_{c,eff} * I_y}$$

- Uniformly distributed component of variable load ($\psi_1 Q_{k,1} = 0{,}8 * Q_{k,UDL}$):

$$\delta_{Q,UDL} = \frac{5 * (\psi_1 * Q_{k,UDL}) * l^4}{384 * E_{c,eff} * I_y}$$

- Concentrated load due to axles ($\psi_1 Q_{k,1} = 0{,}8 * 2 * Q_{k,axle}$):

$$\delta_{Q,axle} = \frac{\psi_1 * 2 * Q_{k,axle} * l^3}{48 * E_{c,eff} * I_y}$$

Upward deflection is denoted as negative while downward deflection is denoted as positive. The total deflection is:

$$\delta_{tot} = \delta_G - \delta_P + \delta_{Q,UDL} + \delta_{Q,axle}$$

Maximum deflection

It has to be verified that the total deflection is smaller than or equal to the maximum deflection:

$$\frac{\delta_{tot}}{\delta_{max}} \leq 1{,}0$$

5.1.3 Comparison with RFEM

A comparison is also made with the total deflection value for the frequent combination as determined using RFEM (denoted as 'δ^*_{max}' in the following equation). The total deflection and requirement then is:

$$\delta_{tot,RFEM} = \delta^*_{max} - \delta_P \leq \delta_{max}$$

5.2 Crack width verification

Conforming the AFGC-SETRA 2013 guideline crack width does not have to be verified, however, the cracking bending moment is calculated and compared to the ultimate bending moment capacity (non-brittleness requirement). In order to do so the mean value of the axial tensile strength has to be determined:

$$f_{ctm} = 0{,}30 * f_{ck}^{\frac{2}{3}}$$

Using this value the cracking bending moment can be calculated:

$$M_{cr} = \left(f_{ctm} + \frac{P_{m,\infty,c} + P_{m,\infty,fb}}{A_c}\right) * W_{min}$$

Where $W_{min} = \min\{W_t; W_b\}$. It subsequently has to be verified that:

$$M_{cr} < M_{Rd}$$

6

END CROSS BEAM

6.1 Assumptions and parameters

6.1.1 Assumptions

In the analysis of the beam the following assumptions are made:

- The beam has a rectangular cross section and it is analysed as if it is a solid cross section over its full width (presence of the prefab beams is neglected);
- It is assumed that the height is equal to the width, and that the height of the end cross beam is equal to that of the prefab beams;
- An equal number of prestressing tendons is positioned at both sides of the beam, thus the resultant of the prestressing force is assumed to act centrically on the beam;
- No tensile stresses are allowed to occur in the cross section, that means that full prestressing has to be achieved.

6.1.2 Input parameters

Using the parameters plugged into the Excel sheet the shrinkage of the beam has to be determined to calculate the prestress losses. Only the drying shrinkage is considered.

Fictitious thickness: The fictitious thickness of the cross section is as follows. It is assumed that the beam is in contact with the atmosphere on three sides while the fourth is covered by the top flange of the prefab beams.

$$h_0 = \frac{2 * A_c}{u} \rightarrow \frac{2 * h_{cb} * w_{cb}}{h_{cb} + w_{cb} + h_{cb}} \rightarrow \frac{2 * h_{cb}^2}{3h_{cb}} = \frac{2}{3} * h_{cb}$$

Where:
A_c: cross sectional area
u: Circumference of the cross section exposed to drying (i.e. in contact with the atmosphere)

Parameter k_h: The parameter is selected from the following table as a function of h_0. In case the value of h_0 falls within two predefined values from the table, the most unfavourable (i.e. highest) value of k_h is taken.

h_0	k_h
100	1
200	0,85
300	0,75
500	0,7

Factor for relative humidity: Relative humidity is accounted for by applying the following factor.

$$\beta_{RH} = 1{,}55 * \left[1 - \left(\frac{RH}{RH_0}\right)^3\right]$$

Nominal unrestrained drying shrinkage: The value of the nominal unrestrained drying shrinkage is as follows.

$$\varepsilon_{cd,0} = 0{,}85 * \left[(220 + 110 * \alpha_{ds1}) * \exp\left(-\alpha_{ds2} * \frac{f_{cm}}{f_{cmo}}\right)\right] * 10^{-6} * \beta_{RH}$$

End value drying shrinkage: The end value of drying shrinkage can be calculated using the nominal unrestrained value and the parameter k_h.

$$\varepsilon_{cd,\infty} = k_h * \varepsilon_{cd,0}$$

6.2 Design of the prestressing

6.2.1 Calculating prestress losses

Although tendons are applied at both halves of the beam the prestressing losses are calculated assuming a resulting prestressing force acting at midspan.

Applied maximum force onto prestressing element and stress verification

It is verified that the maximum stress applied to the prestressing strands does not exceed the maximum value:

$$\sigma_{p,max,prov} \leq \sigma_{p,max}$$

The compressive stresses are to be verified as well:

$$\sigma_c = \frac{P_{max}}{A_{cb}} = \frac{n_{ducts} * n_{strands} * A_{p_{strand}} * \sigma_{p,max}}{A_{cb}} \leq 0{,}6 * f_{ck}$$

Direct prestressing losses

Elastic shortening: Because the four tendons might not be stressed simultaneously, the elastic loss is calculated by using the total value:

$$\Delta P_{el} = n_{ducts} * \frac{(n_{ducts} - 1)}{2} * \frac{P_{max}}{n_{ducts}} * \frac{E_p A_p}{n_{ducts} E_{cm} A_c}$$

Where:

$$A_p = n_{ducts} * n_{strands} * A_{p_{strand}}$$

$$P_{max} = A_p * \sigma_{p,max}$$

Note n_{ducts} appears in the denominator twice because P_{max} is calculated in Excel considering all tendons simultaneously while the elastic loss is calculated using the maximum force and cross section A_p of the individual tendons.

Friction: Because the tendons are straight the friction loss depends on the Wobble-effect only:

$$\Delta P_\mu(x) = (1 - e^{-\mu * k * x}) * P_{max}$$

At the other end from the active end of the deck ($x = w_{tot}$) the friction loss is:

$$\Delta P_\mu(x = w_{tot}) = (1 - e^{-\mu * k * w_{tot}}) * P_{max}$$

The friction loss expressed at stress then is:

$$\Delta\sigma_{P\mu}(x = w_{tot}) = \frac{\Delta P_{\mu}(x = w_{tot})}{A_p}$$

Wedge set: The stress reduction due to friction per unit of length is:

$$k = \frac{\Delta\sigma_{P\mu}(x = w_{tot})}{w_{tot}}$$

The influence length over which the wedge set influences the prestressing force then is:

$$l_w = \sqrt{\frac{w_{set} * E_p}{k}}$$

The prestress loss follows from:

$$\Delta P_{set} = 2 * A_p * \frac{\sigma_{P\mu}(x = w_{tot})}{w_{tot}} * l_w$$

Determining initial prestressing force and stress verification

The initial prestressing force is:

$$P_{m0}(x) = P_{max} - \Delta P_{el} - \Delta P_{\mu}(x) - \Delta P_{set}(x)$$

It has to be verified that the stresses in the strands are not larger than the maximum allowable value. The beam is divided into a number of intervals and the prestressing forces and losses are calculated at a total of 'j' points along the width of the deck. The maximum value along the beam length is used to perform the verification.

$$\frac{\max\{P_{m0}(x)\}}{A_p} \leq \sigma_{pm0}$$

Time dependent losses

The remainder of the analysis is performed using the mean value of the initial prestressing force over the length of the beam, which is determined using:

$$P_{m0} = \frac{1}{j} * \sum_{i=1}^{i=j} P_{m0,j}$$

For centric prestressing the time dependent losses are calculated as follows:

$$\Delta P_{c+s+r} = A_p * \Delta\sigma_{p,c+s+r} = A_p * \frac{\varepsilon_{cs}E_p + 0{,}8\Delta\sigma_{pr} + \frac{E_p}{E_{cm}}\varphi(\infty, t_0)\sigma_{c,QP}}{1 + \frac{E_p}{E_{cm}}\frac{A_p}{A_c}[1 + 0{,}8 * \varphi(\infty, t_0)]}$$

Where (for relaxation class 2):

$$\frac{\Delta\sigma_{pr}}{\sigma_{pi}} = 0{,}66 * \rho_{1000} * e^{9{,}1\mu} * \left(\frac{t}{1000}\right)^{0{,}75(1-\mu)} * 10^{-5}$$

$$\sigma_{pi} = \sigma_{pm,0} = \frac{P_{m0}}{A_p}$$

$$\mu = \frac{\sigma_{pm,0}}{f_{pk}}$$

$t = 500.000$

$$\sigma_{pm,0} = \frac{P_{m0}}{A_p}$$

$$\sigma_{c,QP} = \frac{P_{m0}}{A_c}$$

Working prestressing force

The mean value of the working prestressing force over the width of the deck is found by subtracting the value for time dependent losses from the mean value of the initial prestressing force over the width of the beam:

$$P_{m,\infty} = P_{m0} - \Delta P_{c+s+r}$$

6.2.2 Determining stresses over beam height

Using the bending moments calculated using RFEM the stress distribution over the beam height is determined in order to verify the requirement is met that the stresses in the cross section should be compressive. This analysis is performed for the governing value of the hogging and sagging bending moment and the stresses are for both cases calculated in the top and bottom fibres.

- Hogging bending moment:

$$\sigma_{t,hog} = \frac{M_{E,hog}}{W_{cb}} - \frac{P_{m,\infty}}{A_{cb}} \leq 0$$

$$\sigma_{b,hog} = -\frac{M_{E,hog}}{W_{cb}} - \frac{P_{m,\infty}}{A_{cb}} \leq 0$$

- Sagging bending moment:

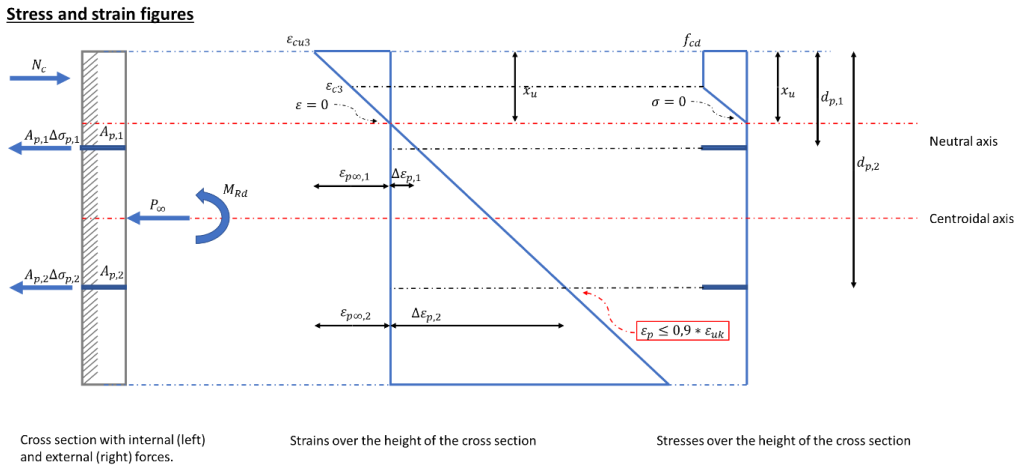
$$\sigma_{t,sag} = -\frac{M_{E,sag}}{W_{cb}} - \frac{P_{m,\infty}}{A_{cb}} \leq 0$$

$$\sigma_{b,sag} = \frac{M_{E,sag}}{W_{cb}} - \frac{P_{m,\infty}}{A_{cb}} \leq 0$$

6.3 Verification bending moment capacity

6.3.1 Assumptions

In the ULS the following strain and stress distributions are assumed to occur over the height of the end cross beam:



Furthermore it is assumed that for the verification of the rotational capacity the redistribution is zero.

6.3.2 Calculating the capacity and verifications

Identifying all horizontal forces

The calculation has been made iterative, the Excelsheet assumes a value for the height of the concrete compressive zone and verifies whether horizontal equilibrium has been reached. If so, then this value will be taken for x_u. Given the rectangular cross section the compressive force is:

$$N_c = \alpha * x_u * f_{cd} * w_{cb}$$

The active contribution of the prestressing is:

$$P_{m,\infty} = A_p * \sigma_{p,\infty}$$

Height of concrete compressive and tensile zone

The height of the concrete compressive zone is determined iteratively. However, it determines if all tendons are taken into consideration when calculating the bending moment capacity. The distance from the outermost compressed fibre (top fibre) to the first row of tendons is denoted as x_1 while the distance to the centre of the second row is denoted as x_2.

$$x_1 = 0{,}5 * h_{cb} - a_{vert}$$

$$x_2 = x_1 + 2 * a_{vert}$$

If it holds that:

$$x_1 < x_u$$

Then the first row is within the compressive zone and it is not taken into consideration while calculating the passive contribution. The second row is always considered.

Determining the strains

The strains are calculated for both rows of tendons:

- Top row (only if $x_1 > x_u$, otherwise zero):

$$d_{p,1} = x_1$$

$$\Delta\varepsilon_{p,1} = \varepsilon_{cu3} * \left(\frac{d_{p,1}}{x_u} - 1\right)$$

$$\varepsilon_{p,\infty,1} = \frac{\sigma_{p,\infty,1}}{E_p}$$

$$\varepsilon_{p,1} = \varepsilon_{p,\infty,1} + \Delta\varepsilon_{p,1} \leq 0{,}9 * \varepsilon_{uk}$$

- Bottom row prestressing:

$$d_{p,2} = x_2$$

$$\Delta\varepsilon_{p,2} = \varepsilon_{cu3} * \left(\frac{d_{p,2}}{x_u} - 1\right)$$

$$\varepsilon_{p,\infty,2} = \frac{\sigma_{p,\infty,2}}{E_p}$$

$$\varepsilon_{p,2} = \varepsilon_{p,\infty,2} + \Delta\varepsilon_{p,2} \leq 0{,}9 * \varepsilon_{uk}$$

Steel stresses

Using the calculated strain values the stresses in the prestressing steel are calculated.

- Top row (only if $x_1 > x_u$, otherwise zero):

$$\sigma_{pu,1} = f_{pd} + \frac{\varepsilon_{p,1} - \frac{f_{pd}}{E_p}}{\varepsilon_{uk} - \frac{f_{pd}}{E_p}} * \left(\frac{f_{pk}}{\gamma_s} - f_{pd}\right)$$

- Bottom row prestressing:

$$\sigma_{pu,2} = f_{pd} + \frac{\varepsilon_{p,2} - \frac{f_{pd}}{E_p}}{\varepsilon_{uk} - \frac{f_{pd}}{E_p}} * \left(\frac{f_{pk}}{\gamma_s} - f_{pd}\right)$$

The increase of the force in the prestressing steel (the passive contribution) is for both rows of tendons respectively:

$$\Delta N_{p,1} = \frac{1}{2} * A_p * (\sigma_{pu,1} - \sigma_{p,\infty})$$

$$\Delta N_{p,2} = \frac{1}{2} * A_p * (\sigma_{pu,2} - \sigma_{p,\infty})$$

Check equilibrium

Equilibrium is checked by considering all horizontal forces:

$$-N_c + P_{m,\infty,1} + P_{m,\infty,2} + \Delta N_{p,1} + \Delta N_{p,2} = 0$$

Determining bending moment capacity

If equilibrium is achieved the bending moment capacity is calculated using the top fibre as the reference point:

$$M_{Rd} = -N_c * \beta * x_u + P_{m,\infty,1} * \frac{1}{2} * h_{cb} + \Delta N_{p,1} * d_{p,1} + P_{m,\infty,2} * \frac{1}{2} * h_{cb} + \Delta N_{p,2} * d_{p,2}$$

The design value of the bending moment is as follows:

$$M_{Ed} = M_{Ed,RFEM} = \max\{M_{Ed,hog}; M_{Ed,sag}\}$$

The following criterion is to be satisfied:

$$\frac{M_{Ed}}{M_{Rd}} \leq 1{,}0$$

Verifying rotational capacity

To verify the rotational capacity the following basic equation is applied:

$$\frac{x_u}{d_p} \leq \frac{500}{500 + f}$$

$$f = \frac{\left(\frac{f_{pk}}{\gamma_s} - \sigma_{pm,\infty}\right) A_p + f_{yd} A_s}{A_p + A_s}$$

In case $x_1 < x_u$, then $d_p = d_{p,2}$ because the passive contribution of the top row of tendons is neglected. In case $x_1 > x_u$, then the average value of both is used:

$$d_{p,ave} = 0{,}5 * \left(d_{p,1} + d_{p,2}\right)$$

6.4 Verification shear force capacity

6.5 Assumptions and parameters

To determine the shear force capacity the equations from Eurocode 2 for elements without shear reinforcement are applied. It is assumed that no longitudinal reinforcement is present either, which is why the capacity is equal to the minimum value of $V_{Rd,c}$ that may be used.

In calculating the capacity the effective width is assumed to be equal to the effective width of the lower set of tendons, i.e. $d_{p,2}$. Given the presence of two rows of ducts, a width reduction might be appropriate. In accordance with the code this is verified as follows:

- If $\emptyset_{Duct} < w_{cb}/8$, then $b_{cb,nom} = w_{cb}$;
- If $\emptyset_{Duct} > w_{cb}/8$, then

$$b_{cb,nom} = w_{cb} - 0{,}5 * \sum \emptyset_{Duct} \rightarrow w_{cb} - \emptyset_{Duct}$$

6.5.1 Calculating the capacity and verifications

Capacity of concrete elements without shear reinforcement

The shear capacity is taken equal to the minimum value of the concrete capacity of an element under compression:

$$V_{Rd,c} = \left(v_{min} + k_1 * \sigma_{cp}\right) * b_{cb,nom} * d_{p,2}$$

Where:

$$k = 1 + \sqrt{\frac{200}{d_{p,2}}} \leq 2{,}0$$

$$v_{min} = 0{,}035 * k^{1{,}5} * \sqrt{f_{ck}}$$

$$\sigma_{cp} = \frac{P_{m,\infty}}{A_{cb}} \leq 0{,}2 * f_{cd}$$

Upper limit – Failure of the concrete compressive strut

The upper limit follows from the capacity of the concrete compressive strut, which is calculated as follows:

$$V_{Rd,max} = \alpha_{cw} * b_{cb,nom} * z * v_1 * f_{cd} * \frac{1}{\cot(\theta) + \tan(\theta)}$$

Where:

$z \approx 0{,}9 * d_{p,2}$

$v_1 = v = 0{,}6 * \left[1 - \frac{f_{ck}}{250}\right]$

Value α_{cw}:	Situation:
$\alpha_{cw} = 1$	$\sigma_{cp} = 0$
$\alpha_{cw} = \left(1 + \frac{\sigma_{cp}}{f_{cd}}\right)$	For $0 < \sigma_{cp} \leq 0{,}25 * f_{cd}$
$\alpha_{cw} = 1{,}25$	For $0{,}25 < \sigma_{cp} \leq 0{,}5 * f_{cd}$
$\alpha_{cw} = 2{,}5 * \left(1 - \frac{\sigma_{cp}}{f_{cd}}\right)$	For $0{,}5 * f_{cd} < \sigma_{cp} < 1{,}0 * f_{cd}$

Verification

The shear resistance of the cross section is taken equal to:

$V_{Rd} = \min\{V_{Rd,c}; V_{Rd,max}\}$

It has to be verified that:

$\frac{V_{Ed}}{V_{Rd}} \leq 1{,}0$

7

WEIGHT CALCULATION

7.1 Weight calculation

The weight of the design is calculated as the final step in the calculation process. Each component of relevance is calculated separately.

Prefab UHPC beams – The weight of the prefab beams is:

$$l_{tot} * A_c * n_{beams} * \rho$$

In-situ UHPC joints – The weight of the joints is calculated using the mean value of the top flange:

$$l_{tot} * t_{ft} * w_j * (n_{beams} - 1) * \rho$$

Cross beams – To calculate the weight of the cross beams first it is assumed that the beams are solid:

$$w_{tot} * h_{cb} * w_{cb} * 2 * \rho$$

Subtraction overlap main beams – The overlap of the prefab beams and cross beams have to be subtracted:

$$-2 * n_{beams} * w_{cb} * A_c * \rho$$

Asphalt layer – An asphalt layer is assumed over the total surface of the deck:

$$l_{tot} * w_{tot} * t_{asphalt} * \rho_{asphalt}$$

Kerbs – The weight of the kerbs is calculated as follows:

$$2 * l_{tot} * w_{kerb} * h_{kerb} * \rho_C$$

Total weight – The total weight is determined by adding up all previously mentioned contributions.

Increase/decrease in weight – The difference in weight between the existing bridge and the new design is calculated as follows:

$$\Delta\% = \frac{W_n - W_e}{W_e} * 100\%$$

Where $\Delta\%$ is the percentual change, W_n is the weight of the new bridge and W_e is the weight of the existing bridge.

Remarks:

- The capping beam and weight of the existing structure are deduced from the preliminary design;
- Note that the 'ρ' of the prefab beams, joints and cross beams can be entered separately in the Excelsheet, the same symbol does not have to denote the same value.

ANNEX: CALCULATIONS OPTIMIZATION PHASE – PART I

Design Calculations Optimization - Calculation parameters

Project: MSc thesis "Redesign of bridges Twentekanaal in UHPC"
Name: M. Dorland
Date: 21-12-2020
Version: D1.0

Legend: Input / Output

Geometry of the structure

Main dimensions of the deck

l	68,00	[m]	*Span of the main beams*
w_{tot}	16,36	[m]	*Total width of the deck*
l_{tot}	70,70	[m]	*Total length of the main beams*
n_{beams}	5	[-]	*Number of prefab UHPC beams*

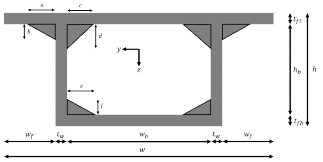
Cross sectional properties main beams

Main properties

w	3200	[mm]	*Total width*
h	1900	[mm]	*Total height*
t_{fb}	200	[mm]	*Thickness bottom flange*
t_w	100	[mm]	*Thickness of web*
w_f	500	[mm]	*Width of the flanges*
w_b	2000	[mm]	*Internal width of the box*

Chamfer of flanges

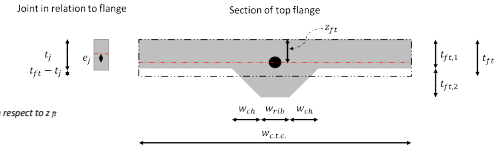
a	0	[mm]	*Width outer chamfer top flange*
b	0	[mm]	*Height outer chamfer top flange*
c	0	[mm]	*Width inner chamfer top flange*
d	0	[mm]	*Height inner chamfer top flange*
e	0	[mm]	*Width inner chamfer bottom flange*
f	0	[mm]	*Height inner chamfer bottom flange*



Top flange - transverse direction

Remark: For top flange with continuous thickness: only enter values tft1 and wc.t.c.!

$w_{c.t.c.}$	1000	[mm]	*Centre to centre distance of the transverse prestressing ribs/ducts*
$t_{ft,1}$	125	[mm]	*Continuous thickness of the top flange*
$t_{ft,2}$	125	[mm]	*Local increase thickness top flange at transverse rib*
w_{rib}	250	[mm]	*Width of the transverse prestressing rib*
w_{ch}	250	[mm]	*Width of chamfer next to the transverse prestressing rib*



Calculated top flange parameters

t_{ft}	187,5	[mm]	*Mean value thickness top flange*
h_b	1512,5	[mm]	*Internal height of the box*
z_{ft}	100,7	[mm]	*Centre of gravity top flange with respect to top fibre*

Δe_{ft} 31,25 [mm] *Downward eccentricity transverse prestressing with respect to z ft*

Part i	Description	$I_{ft,i}$	$A_{ft,i}$	a_{fti}	$I_{ft,i,y}$
[-]	[-]	[mm⁴]	[mm²]	[mm]	[mm⁴]
I	Continuous part top flange	162760417	125000	38,19	3,451E+08
II	Chamfer top flange	27126736	31250	65,97	1,631E+08
III	Rib top flange	40690104	31250	86,81	2,762E+08
Total			187500		7,844E+08

Symbols:

$I_{ft,i}$	*Second moment of area of individual part 'i' of the top flange*
$A_{ft,i}$	*Area of part 'i' of the top flange*
a_{fti}	*Distance from the centre of gravity of part 'i' to centre of gravity of the top flange section*
$I_{ft,i,y}$	*Contribution part 'i' to second moment of area of section of the top flange*

A_{ft}	187500	[mm²]	*Cross sectional area of top flange section*
I_{ft}	7,844E+08	[mm⁴]	*Second moment of area of top flange section*

Determining global cross sectional properties

Part i	Description	w_i	h_i	A_i	e_i	S_i	I_i	a_i	$I_{i,y,Steiner}$	$I_{i,y}$
[-]	[-]	[mm]	[mm]	[mm²]	[mm]	[mm³]	[mm⁴]	[mm]	[mm⁴]	[mm⁴]
1	Top flange	3200	187,5	600000,0	93,8	5,625E+07	1,758E+09	751	3,382E+11	3,399E+11
2	Web	200	1512,5	302500,0	943,8	2,855E+08	5,767E+10	99	2,980E+09	6,065E+10
3	Bottom flange	2200	200,0	440000,0	1800,0	7,920E+08	1,467E+09	956	4,017E+11	4,032E+11
4	Chamfer top flange out	0	0,0	0,0	187,5	0,000E+00	0,000E+00	657	0,000E+00	0,000E+00
5	Chamfer top flange in	0	0,0	0,0	187,5	0,000E+00	0,000E+00	657	0,000E+00	0,000E+00
6	Chamfer bottom flange in	0	0,0	0,0	1700,0	0,000E+00	0,000E+00	856	0,000E+00	0,000E+00
Total				1342500,0		1,134E+09				8,038E+11

Symbols:

w_i	*Width of part 'i'*
h_i	*Height of part 'i'*
A_i	*Area of part 'i'*
e_i	*Distance from centre of gravity of part 'i' to the top fibre*
S_i	*First moment of area of part 'i' with respect to top fibre*
I_i	*Second moment of area of individual part 'i'*
a_i	*Distance from the centre of gravity of part 'i' to centre of gravity of the cross section*
$I_{i,y,Steiner}$	*Steiner part of part 'i'to the second moment of area of the cross section*
$I_{i,y}$	*Contribution part 'i' to second moment of area of cross section*

Main parameters

A_c	1342500,0	[mm²]	*Cross sectional area of total cross section*
z	844,5	[mm]	*Position centre of gravity from the top flange*
I_y	8,038E+11	[mm⁴]	*Second moment of area of the combined cross section*
z_t	844,5	[mm]	*Distance from centre of gravity to top fibre*
z_b	1055,5	[mm]	*Distance from centre of gravity to bottom fibre*
$W_{y,t}$	9,518E+08	[mm³]	*Section modulus with respect to top fibre*
$W_{y,b}$	7,615E+08	[mm³]	*Section modulus with respect to bottom fibre*

Cross sectional properties end cross beams

Main dimensions

h_{cb}	1900	[mm]	*Total height of the end cross beam*
w_{cb}	1900	[mm]	*Total width of the end cross beam*

Determining cross sectional properties

A_{cb}	3610000	[mm²]	*Cross sectional area of the cross beam*
$W_{y,cb}$	1,143E+09	[mm³]	*Section modulus of the cross section*
$I_{y,cb}$	1,086E+12	[mm⁴]	*Second moment of area of the cross section*

Cross sectional properties longitudinal joints

Main dimensions

t_j	162,5	[mm]	*Height of the longitudinal joint*
w_j	90	[mm]	*Transverse width of the longitudinal joint*

Determining cross sectional properties

A_j	162500	[mm²]	*Cross sectional area of the longitudinal joint*
W_j	4,401E+06	[mm³]	*Section modulus of the longitudinal joint*
I_j	3,576E+08	[mm⁴]	*Second moment of the cross section of the longitudinal joint*

Material and calculation parameters

Concrete

Material properties concrete main beams (Ductal FM)

Parameters mixture composition

ρ	25	[kN/m³]	*Density*
l_f	13	[mm]	*Fibre length*

Parameters concrete in compression

f_{ck}	200	[N/mm²]	*Characteristic value compressive strength*
ε_{c3}	2,3	[‰]	*Strain at reaching concrete compressive strength*
ε_{cu3}	2,6	[‰]	*Maximum compressive strain at ULS*

Parameters concrete in tension

$f_{ctk,el}$	9	[N/mm²]	*Characteristic elastic (5% percentile value) tensile strength*
f_{ctfk}	10	[N/mm²]	*Characteristic value maximal post cracking stress (w=0,30)*
α_{global}	1,25	[-]	*Fibre orientation factor (global)*
K_{local}	1,75	[-]	*Fibre orientation factor (local)*

Parameters stiffness and deformations (temperature, creep and shrinkage)

E_{cm}	50000	[N/mm²]	*Modulus of elasticity*
G	20833	[N/mm²]	*Shear modulus*
ν	0,2	[-]	*Poisson ratio*
α	0,000012	[K-1]	*Coefficient of thermal expansion*
φ	0,3	[-]	*Creep*
ε_{shr}	0,8	[‰]	*Autogenous shrinkage (during HT)*

Parameters concrete other

α	0,56	[-]	*Factor for shape of concrete compressive zone*
β	0,34	[-]	*Factor position centre of gravity concrete compressive zone*
α_{cc}	0,85	[-]	*Long term effects and unfavourable loading (compression)*
α_{ct}	1,0	[-]	*Long term effects and unfavourable loading (tension)*

Parameters fatigue

$\beta_{cc}(t)$	1,0	[-]	*Factor for increase of strength due to progressive hydration*
f_{cko}	10	[N/mm²]	*Standard value (10 Mpa)*

Calculated values

f_{cd}	113	[N/mm²]	*Design value concrete compressive strength*
f_{ctd}	6,0	[N/mm²]	*Design value of tensile strength (tensile strength 1st crack)*
$f_{ctd,2}$	6,15	[N/mm²]	*Design value maximal post cracking stress (at w=0,30)*

Concrete longitudinal joints

Parameters mixture composition

ρ	25	[kN/m³]	*Density*

Parameters concrete in compression

f_{ck}	100	[N/mm²]	*Characteristic value compressive strength*
ε_{cu3}	2,6	[‰]	*Maximum compressive strain at ULS*

Parameters stiffness and deformations (temperature, creep and shrinkage)

E_{cm}	45000	[N/mm²]	*Modulus of elasticity*
φ	0,8	[-]	*Creep factor*
ε_{cs}	0,8	[‰]	*Shrinkage (long term)*

Parameters concrete other

α	0,56	[-]	*Factor for shape of concrete compressive zone*
β	0,34	[-]	*Factor position centre of gravity concrete compressive zone*
α_{cc}	0,85	[-]	*Long term effects and unfavourable loading (compression)*

Calculated values

f_{cd}	57	[N/mm²]	*Design value concrete compressive strength*

Material properties concrete end cross beams

Parameters mixture composition

ρ	25	[kN/m³]	*Density*

Parameters concrete in compression

f_{ck}	30	[N/mm²]	*Characteristic cylinder compressive strength at 28 days*
$f_{ck,cube}$	37	[N/mm²]	*Characteristic cube compressive strength*
f_{cm}	38	[N/mm²]	*Mean value cylinder compressive strength*
ε_{c3}	1,75	[‰]	*Strain at reaching concrete compressive strength*
ε_{cu3}	3,5	[‰]	*Maximum compressive strain at ULS*

Parameters concrete in tension

f_{ctm}	2,9	[N/mm²]	*Mean value axial tensile strength*
$f_{ctk,0,05}$	2,0	[N/mm²]	*5%-fractile of the axial tensile strength*

Parameters stiffness and deformations (temperature, creep and shrinkage)

E_{cm}	33000	[N/mm²]	*Secant modulus of elasticity*
φ	1,75	[-]	*Creep*
Hydration	Normal (N)	[-]	*Rate of hydration: Rapid (R), Normal (N) or slow (S)*
RH	80,0	[%]	*Relative humidity*

Parameters concrete other

α	0,75	[-]	*Factor for shape of concrete compressive zone*
β	0,39	[-]	*Factor position centre of gravity concrete compressive zone*
α_{cc}	1,0	[-]	*Long term effects and unfavourable loading (compression)*

Calculated values

f_{cd}	20	[N/mm²]	*Design value concrete compressive strength*

Prestressing steel & parameters strands and tendons

Parameters prestressing main beams

Parameters transverse prestressing

Parameters prestressing end cross beams

Material properties prestressing steel

f_{pk}	1860	[N/mm²]	Characteristic value tensile strength
f_{pd}	1522	[N/mm²]	Design value steel stress
σ_{pm0}	1395	[N/mm²]	Maximum allowed stress directly after tensioning
$\sigma_{p,max}$	1488	[N/mm²]	Maximum prestressing stress during tensioning
E_p	195000	[N/mm²]	Modulus of elasticity
ε_{uk}	35	[‰]	Characteristic value strain at failure

Properties prestressing strands

n_c	10	[pcs]	Assumed number of strands positioned centrically in the cross section
$D_{strand,c}$	15,2	[mm]	Diameter of strands positioned centrically
$A_{p,strand,c}$	140	[N/mm²]	Cross sectional area per strand
$\sigma_{p,max,prov,c}$	1390	[mm²]	Assumed maximum stress applied to centrically positioned strands
n_{fb}	120	[pcs]	Assumed number of strands positioned in bottom flange
$D_{strand,fb}$	15,2	[mm]	Diameter of strands positioned in bottom flange
$A_{p,strand,fb}$	140	[N/mm²]	Cross sectional area per strand
$\sigma_{p,max,prov,fb}$	1450	[mm²]	Assumed maximum stress applied to strands in bottom flange
Relaxation	Class 2	[-]	Select relaxation class: normal (1), low (2) or bars (3)
t	500000	[h]	The value of the relaxation loss (in %) at 1000 h
ρ	2,5	[%]	Time after stressing (to determine final value of the relaxation loss)
t_{eq}	461935	[h]	Equivalent time (optional), NOTE: Calculated manually!

Parameters detailing beam ends

η	1,35	[-]	Bond factor conforming table 7.2 of AFGC-SETRA 2013
η_1	1,0	[-]	Factor accounting for bond conditions, cf EC2-1-1
κ	1,5	[-]	Factor for bond strength improvement due to the presence of fibres
α_1	1,0	[-]	Factor depending on way of releasing the strands
α_2	0,19	[-]	Factor depending on the type of tendon
$n_{fb,1}$	120	[pcs]	Selected number of strands introduced in first set
$n_{fb,2}$	0	[pcs]	Selected number of strands introduced in second set (optional)
$x_{debond,1}$	0	[m]	Length over which first set of strands is debonded (optional)
$x_{debond,2}$	0,0	[m]	Length over which second set of strands is debonded (optional)

Parameters fatigue verification

$\Delta\sigma_{Rsk}$	185	[N/mm²]	Stress range at N* cycles
N^*	1000000	[-]	Number of cycles with single stress range
k_1	5	[-]	Stress exponent first branch
k_2	9	[-]	Stress exponent second branch

Material properties prestressing steel

f_{pk}	1860	[N/mm²]	Characteristic value tensile strength
f_{pd}	1522	[N/mm²]	Design value steel stress
σ_{pm0}	1395	[N/mm²]	Maximum allowed stress directly after tensioning
$\sigma_{p,max}$	1488	[N/mm²]	Maximum prestressing stress during tensioning
E_p	195000	[N/mm²]	Modulus of elasticity
ε_{uk}	35	[‰]	Characteristic value strain at failure

Properties prestressing tendons

n	5	[pcs]	Assumed number of strands per tendon
D_{strand}	15,2	[mm]	Diameter of single strand
$A_{p,strand}$	140	[mm²]	Cross sectional area per strand
$\sigma_{p,max,prov}$	1400	[N/mm²]	Assumed maximum stress applied to prestressing element
μ	0,23	[-]	Friction coefficient
k	0,009	[rad]	Unintentional angular rotation due to the Wobble-effect
w_{set}	3	[mm]	Estimated wedge set
Relaxation	Class 2	[-]	Select relaxation class: normal (1), low (2) or bars (3)
t	500000	[h]	The value of the relaxation loss (in %) at 1000 h
ρ	2,5	[%]	Time after stressing (for final value of the relaxation loss)

Material properties prestressing steel

f_{pk}	1860	[N/mm²]	Characteristic value tensile strength
f_{pd}	1522	[N/mm²]	Design value steel stress
σ_{pm0}	1395	[N/mm²]	Maximum allowed stress directly after tensioning
$\sigma_{p,max}$	1488	[N/mm²]	Maximum prestressing stress during tensioning
E_p	195000	[N/mm²]	Modulus of elasticity
ε_{uk}	35	[‰]	Characteristic value strain at failure

Properties prestressing tendons

n_{ducts}	4	[pcs]	Number of ducts in total
α_{vert}	500	[mm]	Vertical position centre of duct from centre of beam
α_{hor}	750	[mm]	Horizontal position centre of duct from centre of beam
n_{strand}	7	[pcs]	Assumed number of strands per tendon
D_{strand}	15,2	[mm]	Diameter of single strand
$A_{p,strand}$	140	[mm²]	Cross sectional area per strand
$\sigma_{p,max,prov}$	1400	[N/mm²]	Assumed maximum stress applied to prestressing element
$\emptyset_{Duct}$	65	[mm]	Outer diameter of prestressing ducts
μ	0,23	[-]	Friction coefficient
k	0,009	[rad]	Unintentional angular rotation due to the Wobble-effect
w_{set}	3	[mm]	Estimated wedge set
Relaxation	Class 2	[-]	Select relaxation class: normal (1), low (2) or bars (3)
t	500000	[h]	The value of the relaxation loss (in %) at 1000 h
ρ	2,5	[%]	Time after stressing (for final value of the relaxation loss)

Partial factors material resistance

γ_C	1,5	[-]	Partial factor concrete (cf EC2)	$\gamma_{F,fat}$	1,0	[-]	See 2.4.2.3 of NA to NEN-EN 1992-1-1	γ_{spl}	1,2	[-]	Partial factor splitting forces
γ_{cf}	1,3	[-]	Partial factor for fibre reinforced concrete in tension (cf AFGC)	$\gamma_{S,fat}$	1,1	[-]	See 2.4.2.4 of NA to NEN-EN 1992-1-1				
$\gamma_E * \gamma_{cf}$	1,5	[-]	Product of partial factor for uncertainty in extrapolation * factor Ycf								
γ_S	1,1	[-]	Partial factor prestressing steel (cf EC2)								

Calculation parameters

Calculation parameters main beams

σ_{max}	6,7	[N/mm²]	Maximum allowed stress at outer concrete fibres
θ	30	[°]	Angle of the concrete compressive strut of the main beams
$c_{nom,s}$	35	[mm]	Minimum applied cover onto strands bottom flange (all sides)
$c_{nom,r}$	30	[mm]	Minimum applied cover onto rebars bottom flange (all sides)
$\emptyset_{spl,f1}$	10	[mm]	Assumed diameter splitting reinforcement bottom flange
μ	0,5	[-]	Friction coefficient concrete and supports
$1/\delta$	300	[-]	Maximum deflection in SLS

Calculation parameters longitudinal joints and top flange

$\emptyset_{spl,ft}$	10	[mm]	Assumed diameter splitting reinforcement top flange
h_1	100	[mm]	Anchor plate (height and width)

Calculation parameters end cross beams

k_1	0,15	[-]	Factor from 6.2.2 of the NA to NEN-EN 1992-1-1
θ	21,8	[°]	Angle concrete compressive strut of end cross beam

Design of bridge and main carriageway - Actions

Design main carriageway

Kerbs

h_{kerb}	340	[mm]	Assumed height of the kerb
w_{kerb}	500	[mm]	Assumed width of the kerb
ρ_C	25	[kN/m³]	Density of the concrete used

Road surface

t_{surf}	10	[mm]	Assumed thickness of the surface layer
$\rho_{asphalt}$	23	[kN/m³]	Density of the material used

Effective width of the beams

$b_{eff,0}$	3,245	[m]	Effective width of the outer beams to determine loads
$b_{eff,i}$	3,29	[m]	Effective width of the inner beams to determine loads

Permanent actions (G)

Self-weight prefab beams

$G_{k,beam}$	33,56	[kN/m]	Line load representing the self-weight of the prefab beams

Permanent load road surface

$G_{k,surf}$	0,23	[kN/m²]	Area load representing the surface layer

Self-weight end cross beams

$G_{k,cb}$	90,25	[kN/m]	Line load representing the self-weight of the end cross beams

Permanent load kerbs

A_{kerb}	0,17	[m²]	Cross sectional area of the kerb
$G_{k,kerb}$	8,5	[kN/m²]	Area load representing the kerb

Self-weight longitudinal joints

A_j''	0,016875	[m²]	Area of the total joint using tft and wj
$G_{k,j}$	0,421875	[kN/m]	Line load representing the self-weight of the joints

Variable actions (Q)

Load model 1

Lane	Q_{ik} [kN]	q_{ik} [kN/m²]
1	291	8,73
2	194	2,425
rk	0	2,25

Load model 2

$\beta_Q Q_{ak}$	388	[kN/axle]	Axle load according to LM2

Accidental actions (A)

F_{equi}	1000	[kN]	Equivalent static force, see: (4) of 4.6.2. EC1-1-7

Fatigue

n_y	100	[-]	Design service life
N_{obs}	500000	[-]	Number of heavy vehicles per year

Combinations of actions

γ_G	1,4	[-]	See tabel NB.16 – A2.4(B) of NA to NEN-EN 1990
$\zeta * \gamma_G$	1,25	[-]	See tabel NB.16 – A2.4(B) of NA to NEN-EN 1990
γ_P	1,0	[-]	See 2.4.2.2 of NA to NEN-EN 1992-1-1
γ_Q	1,5	[-]	See tabel NB.16 – A2.4(B) of NA to NEN-EN 1990
ψ_0	0,8	[-]	See tabel NB.12 – A2.1 of NA to NEN-EN 1990
ψ_1	0,8	[-]	See tabel NB.12 – A2.1 of NA to NEN-EN 1990

Determining force distribution (RFEM input)

Design of main prestressing and verification capacity of the main beams

Ultimate limit state verifications main beams

M_{Ed}	41753	[kNm]	Governing bending moment value (mid span)
V_{Ed}	3632	[kN]	Governing shear force value (near supports)
T_{Ed}	1268	[kNm]	Governing torsional moment

Serviceability limit state - Design of prestressing (characteristic combination)

$M_{E,G,perm}$	1725	[kNm]	Bending moment imposed permanent loads in SLS at midspan
$M_{E,Q}$	9553	[kNm]	Bending moment variable loads in SLS at midspan

Serviceability limit state - Deflections (frequent combination)

δ_{max}	440,9	[mm]	Max. deflection at midspan in SLS (frequent combination)

Fatigue analysis main beams

$M_{fat,max}$	26812	[kNm]	Maximum bending moment at midspan (found using RFEM)
$M_{fat,min}$	22543	[kNm]	Minimum bending moment at midspan (found using RFEM)

Design of prestressing and verification capacity of the end cross beams

Ultimate limit state verifications end beams

$M_{Ed,hog}$	1271	[kNm]	Maximum hogging bending moment (all loads considered)
$M_{Ed,sag}$	396	[kNm]	Maximum sagging bending moment (all loads considered)
V_{Ed}	846	[kN]	Maximum shear force (all loads considered)

Serviceability limit state - Design of prestressing

$M_{E,hog}$	453	[kNm]	Maximum hogging bending moment SLS
$M_{E,sag}$	270	[kNm]	Maximum sagging bending moment SLS

Design Calculations Optimization - Design of main beams - Main prestressing and ULS (STR)

Project: MSc thesis "Redesign of bridges Twentekanaal in UHPC"
Name: M. Dorland
Date: 21-12-2020
Version: D1.0

Input parameters

Input parameters - Cross sectional properties and calculation parameters

Cross sectional properties

A_c	1342500	[mm²]	*Cross sectional area of total cross section*
z_t	844,5	[mm]	*Distance from centre of gravity to top fibre*
e_p	955,51	[mm]	*Eccentricity of tendons in bottom flange*
I_y	8,038E+11	[mm⁴]	*Second moment of area of the combined cross section*
$W_{y,t}$	9,518E+08	[mm³]	*Section modulus with respect to top fibre*
$W_{y,b}$	7,615E+08	[mm³]	*Section modulus with respect to bottom fibre*

Calculation parameters

θ	30	[°]	*Angle of the concrete compressive strut of the main beams*

Input parameters - Material properties & main prestressing

Concrete

Parameters mixture composition

ρ	25	[kN/m³]	*Density*
l_f	13	[mm]	*Fibre length*

Parameters concrete in compression

f_{ck}	200	[N/mm²]	*Characteristic value compressive strength*
ε_{c3}	2,3	[‰]	*Strain at reaching concrete compressive strength*
ε_{cu3}	2,6	[‰]	*Maximum compressive strain at ULS*

Parameters concrete in tension

$f_{ctk,el}$	9	[N/mm²]	*Characteristic elastic (5% percentile value) tensile strength*
f_{ctfk}	10	[N/mm²]	*Characteristic value maximal post cracking stress (w=0,30)*
K_{global}	1,25	[-]	*Fibre orientation factor (global)*
K_{local}	1,75	[-]	*Fibre orientation factor (local)*

Parameters stiffness and deformations (temperature, creep and shrinkage)

E_{cm}	50000	[N/mm²]	*Modulus of elasticity*
G	20833	[N/mm²]	*Shear modulus*
ν	0,2	[-]	*Poisson ratio*
α	0,000012	[K-1]	*Coefficient of thermal expansion*
φ	0,3	[-]	*Creep*
ε_{shr}	0,8	[‰]	*Autogenous shrinkage (during HT)*

Parameters concrete other

α	0,56	[-]	*Factor for shape of concrete compressive zone*
β	0,34	[-]	*Factor position centre of gravity concrete compressive zone*
α_{cc}	0,85	[-]	*Long term effects and unfavourable loading (compression)*
α_{ct}	1	[-]	*Long term effects and unfavourable loading (tension)*

Calculated design values

f_{cd}	113	[N/mm²]	*Design value concrete compressive strength*
f_{ctd}	6,0	[N/mm²]	*Design value of tensile strength (tensile strength 1st crack)*
$f_{ctd;2}$	6,15	[N/mm²]	*Design value maximal post cracking stress (at w=0,30)*

Parameters main prestressing

Material properties prestressing steel

f_{pk}	1860	[N/mm²]	*Characteristic value tensile strength*
f_{pd}	1522	[N/mm²]	*Design value steel stress*
σ_{pm0}	1395	[N/mm²]	*Maximum allowed stress directly after tensioning*
$\sigma_{p,max}$	1488	[N/mm²]	*Maximum prestressing stress during tensioning*
E_p	195000	[N/mm²]	*Modulus of elasticity*
ε_{uk}	35	[‰]	*Characteristic value strain at failure*

Parameters prestressing strands

n_c	10	[-]	*Assumed number of strands positioned centrically in the cross section*
$D_{strand,c}$	15,2	[mm]	*Diameter of strands positioned centrically*
$A_{p,strand,c}$	140	[N/mm²]	*Cross sectional area per strand*
$\sigma_{p,max,prov,c}$	1390	[mm²]	*Assumed maximum stress applied to centrically positioned strands*
n_{fb}	120	[-]	*Assumed number of strands positioned in bottom flange*
$D_{strand,fb}$	15,2	[mm]	*Diameter of strands positioned in bottom flange*
$A_{p,strand,fb}$	140	[N/mm²]	*Cross sectional area per strand*
$\sigma_{p,max,prov,fb}$	1450	[mm²]	*Assumed maximum stress applied to strands positioned in bottom flange*
Relaxation	Class 2	[-]	*Select relaxation class: normal (1), low (2) or bars (3)*
t	500000	[h]	*The value of the relaxation loss (in %) at 1000 h*
ρ	2,5	[%]	*Time after stressing (to determine the final value of the relaxation loss)*
t_{eq}	461935	[h]	*Equivalant time, NOTE: Calculated manually!*

Parameters detailing beam ends

η	1,35	[-]	*Bond factor conforming table 7.2 of AFGC-SETRA 2013*
η_1	1,0	[-]	*Factor accounting for bond conditions, cf EC2-1-1*
κ	1,5	[-]	*Factor for bond strength improvement due to the presence of fibres*
α_1	1,0	[-]	*Factor depending on way of releasing the strands*
α_2	0,19	[-]	*Facor depending on the type of tendon*
$n_{fb,1}$	120	[pcs]	*Selected number of strands introduced in first set*
$n_{fb,2}$	0	[pcs]	*Selected number of strands introduced in second set*
$x_{debond,1}$	0	[m]	*Length over which first set of strands is debonded*
$x_{debond,2}$	0	[m]	*Length over which second set of strands is debonded*

Other parameters

γ_C	1,5	[-]	*Partial factor concrete (cf EC2)*
γ_{cf}	1,3	[-]	*Partial factor for fibre reinforced concrete in tension*
$\gamma_E * \gamma_{cf}$	1,5	[-]	*Product of partial factors (AFGC-SETRA 2013)*
γ_S	1,1	[-]	*Partial factor prestressing steel (cf EC2)*
γ_{spl}	1,2	[-]	*Partial factor splitting forces*

Input parameters - Loads

$M_{E,G,sw}$	19399	[kNm]	*Bending moment midspan due to self-weight of the beams in SLS*
$M_{E,G,perm}$	1725	[kNm]	*Bending moment mid span due to imposed permanent loads in SLS (RFEM)*
$M_{E,Q}$	9553	[kNm]	*Bending moment due to variable loads in SLS (RFEM)*

Design of the main prestressing

Calculating prestress losses

Applied maximum force onto prestressing element & stress verification

$\sigma_{p,max,prov,c}$	1390	[mm²]	*Assumed maximum stress applied to centrically positioned strands*
$P_{max,prov,c}$	1946	[kN]	*Assumed maximum force applied to centrically positioned strands*
$\sigma_{p,max,prov,fb}$	1450	[mm²]	*Assumed maximum stress applied to strands positioned in bottom flange*
$P_{max,prov,fb}$	24360	[kN]	*Assumed maximum force applied to strands positioned in bottom flange*

Verification maximum stress prestressing steel

$\sigma_{p,max,prov,c}$	1390,00	[N/mm²]	*Assumed maximum stress applied to centric prestressing*
Verification	Satisfied	[-]	*Verification*
$\sigma_{p,max,prov,fb}$	1450	[N/mm²]	*Assumed maximum stress applied to strands positioned in bottom flange*
Verification	Satisfied	[-]	*Verification*

Verifications maximum concrete compressive stress

$\sigma_{c,prov,c+fb}$	50,16	[N/mm²]	*Maximum compressive stress in concrete due to prestressing*
$\sigma_{c,limit}$	140,00	[N/mm²]	*Maximum value concrete compressive stress*
Verification	Satisfied	[-]	*Verification*

Applied value maxinum force applied onto prestressing strands

$\sigma_{p,max,c}$	1390,00	[N/mm²]	*Applied value maximum stress centric prestressing*
$A_{p,c}$	1400	[mm²]	*Applied cross section centric prestressing*
$P_{max,c}$	1946,00	[kN]	*Applied value maximum force centric prestressing*
$\sigma_{p,max,fb}$	1450,00	[N/mm²]	*Applied value maximum stress eccentric prestressing*
$A_{p,fb}$	16800	[mm²]	*Applied cross section eccentric prestressing*
$P_{max,fb}$	24360,00	[kN]	*Applied value maximum force eccentric prestressing*

Direct prestressing losses

Elastic losses centric prestressing

α_e	3,90	[-]	*Ratio moduli of elasticity*
$\rho_{p,c}$	0,0010	[-]	*Ratio of cross section steel and concrete*
I_c	NA	[-]	*Factor for eccentricity*
$\Delta P_{el,c}$	7,88	[kN]	*Elastic loss centric prestressing*

Elastic losses eccentric prestressing flange

α_e	3,90	[-]	*Ratio moduli of elasticity*
$\rho_{p,fb}$	0,0125	[-]	*Ratio of cross section steel and concrete*
I_{fb}	2,52	[-]	*Factor for eccentricity*
$\Delta P_{el,fb}$	2672,52	[kN]	*Elastic loss eccentric prestressing*

Determining initial prestressing force & stress verification

Applied force and stress values

$P_{m0,c}$	1938	[kN]	*Initial prestressing force centric prestressing*
$\sigma_{pm0,c}$	1384	[N/mm²]	*Initial prestressing stress centric prestressing*
$P_{m0,fb}$	21687	[kN]	*Initial prestressing force eccentric prestressing*
$\sigma_{pm0,fb}$	1291	[N/mm²]	*Initial prestressing stress eccentric prestressing*

Stress limit and verification

Verification	Satisfied	[-]	*Verification initial prestressing stress (centric prestressing)*
Verification	Satisfied	[-]	*Verification initial prestressing stress (eccentric prestressing)*

Verified values initial prestressing force

$P_{m0,c}$	1938	[kN]	*Applied value initial prestressing force centric prestressing*
$\sigma_{pm0,c}$	1384	[N/mm²]	*Applied value initial stress centric prestressing*
$P_{m0,fb}$	21687	[kN]	*Applied value initial prestressing force eccentric prestressing*
$\sigma_{pm0,fb}$	1291	[N/mm²]	*Applied value initial stresseccentric prestressing*

Time dependent losses

Centric prestressing - Relaxation

Class	Class 2	[-]	*Relaxation class (normal relaxation, low relaxation and bars)*
ρ_{1000}	2,5	[%]	*The value of the relaxation loss (in %) at 1000 h*
μ_c	0,74	[-]	*Factor depending on steel stresses*
t	961935	[h]	*Time after stressing (for final value of the relaxation loss)*
$\Delta\sigma_{pr,c}/\sigma_{pi,c}$	0,054	[-]	*Relaxation coefficient*
$\sigma_{pi,c}$	1384,4	[N/mm²]	*Absolute value of the initial prestressing (σ_pm0)*
$\Delta\sigma_{pr,c}$	74,5	[N/mm²]	*Prestress loss due to relaxation*

Centric prestressing - Accounting for heat treatment (if applicable)

t_{eq}	461935	[h]	*Equivalant time, NOTE: Calculated manually!*

Centric prestressing - Relaxation classes

Class 1	Wires and strands normal relaxation
Class 2	Wires and strands low relaxation
Class 3	Bars

Centric prestressing - Creep & shrinkage

φ	0,3	[-]	*Creep factor*
$\sigma_{c,QP,c}$	17,6	[N/mm²]	*Stress in concrete adjacent to centric prestressing strands*
ε_{cs}	0,0008	[-]	*Shrinkage of the concrete*

Centric prestressing - Total time dependent losses

$\Delta\sigma_{p,c+s+r,c}$	235,0	[N/mm²]	*Time dependent prestressing losses (stress, centric)*
$\Delta P_{p,c+s+r,c}$	329,0	[kN]	*Time dependent prestressing losses (force, centric)*

Eccentric prestressing flange - Relaxation

Class	Class 2	[-]	*Relaxation class (normal relaxation, low relaxation and bars)*
ρ_{1000}	2,5	[%]	*The value of the relaxation loss (in %) at 1000 h*
μ_{fb}	0,69	[-]	*Factor depending on steel stresses*
t	961935	[h]	*Time after stressing (for final value of the relaxation loss)*
$\Delta\sigma_{pr,fb}/\sigma_{pi,fb}$	0,044	[-]	*Relaxation coefficient*
$\sigma_{pi,fb}$	1290,9	[N/mm²]	*Absolute value of the initial prestressing (σ_pm0)*
$\Delta\sigma_{pr,fb}$	57,0	[N/mm²]	*Prestress loss due to relaxation*

Eccentric prestressing flange - Accounting for heat treatment (if applicable)

t_{eq}	461935	[h]	*Equivalant time, NOTE: Calculated manually!*

Eccentric prestressing flange - Relaxation classes

Class 1	Wires and strands normal relaxation
Class 2	Wires and strands low relaxation
Class 3	Bars

Eccentric prestressing flange - Creep & shrinkage

φ	0,3	[-]	*Creep factor*
$\sigma_{c,QP,fb}$	42,2	[N/mm²]	*Stress in concrete adjacent to eccentric prestressing strands*
ε_{cs}	0,0008	[-]	*Shrinkage of the concrete*

Eccentric prestressing flange - Total time dependent losses

$\Delta\sigma_{p,c+s+r,fb}$	217,7	[N/mm²]	*Time dependent prestressing losses (stress, eccentric)*
$\Delta P_{p,c+s+r,fb}$	3658,0	[kN]	*Time dependent prestressing losses (force, eccentric)*

Working prestress force and total prestress losses

$P_{m,\infty,c}$	1609	[kN]	*Working prestressing force centric prestressing*
$\sigma_{pm,\infty,c}$	1149	[N/mm²]	*Working prestressing stress centric prestressing*
$P_{m,\infty,fb}$	18029	[kN]	*Working prestressing force eccentric prestressing*
$\sigma_{pm,\infty,fb}$	1073	[N/mm²]	*Working prestressing stress eccentric prestressing*

Summary of results (middle cross section)

	Prestressing forces			Prestress losses forces			
	P_{max}	P_{m0}	$P_{m,\infty}$	ΔP_i	$\Delta P_{p,c+s+r}$	ΔP_{tot}	$\Delta P_{\%}$
Prestressing:	[kN]	[kN]	[kN]	[kN]	[kN]	[kN]	[%]
Centric	1946	1938	1609	8	329	337	17,3
Eccentric	24360	21687	18029	2673	3658	6331	26,0

	Prestressing stresses			Prestress losses forces			
	σ_{max}	σ_{pm0}	$\sigma_{pm,\infty}$	$\Delta\sigma_i$	$\Delta\sigma_{p,c+s+r}$	$\Delta\sigma_{tot}$	$\Delta\sigma_{\%}$
Prestressing:	[N/mm²]	[N/mm²]	[N/mm²]	[N/mm²]	[N/mm²]	[N/mm²]	[%]
Centric	1390	1384	1149	6	235	241	17,3
Eccentric	1450	1291	1073	159	218	377	26,0

Determining stresses at midspan

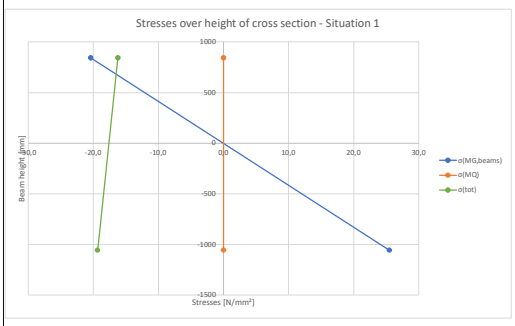
σ_{max}	6,7	[N/mm²]	*Maximum tensile stress allowed at outer fibres*

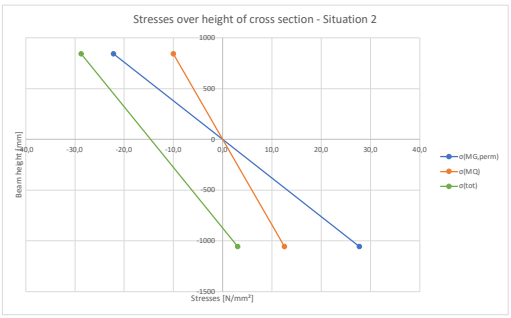
Stresses situation 1

Stresses situation 2

	Height [mm]	σ(MG,beams) [N/mm²]	σ(MQ) [N/mm²]	σ(P∞) [N/mm²]	σ(Pfb) [N/mm²]	σ(Mr,fb) [N/mm²]	σ(tot) [N/mm²]
Top fibre	844	-20,4	0,0	-1,4	-16,2	21,8	-16,2
Bottom fibre	-1056	25,5	0,0	-1,4	-16,2	-27,2	-19,3
Maximum	1900						-16,2

	Height [mm]	σ(MG,perm) [N/mm²]	σ(MQ) [N/mm²]	σ(P∞) [N/mm²]	σ(Pfb) [N/mm²]	σ(Mr,fb) [N/mm²]	σ(tot) [N/mm²]
Top fibre	844	-22,2	-10,0	-1,2	-13,4	18,1	-28,8
Bottom fibre	-1056	27,7	12,5	-1,2	-13,4	-22,6	3,0
Maximum	1900						3,0





Detailing beam ends

Bond stresses and transmission length

Determining bond stress

η	1,35	[-]	*Bond factor conforming table 7.2 of AFGC-SETRA 2013*
η_1	1,0	[-]	*Factor accounting for bond conditions, cf EC2-1-1*
κ	1,5	[-]	*Factor for bond strength improvement due to the presence of fibres*
f_{ctd}	6,0	[N/mm²]	*Design value tensile strength*
f_{bpt}	12,15	[N/mm²]	*Bond strength*

Transmission length centric prestressing

α_1	1,0	[-]	*Factor depending on way of releasing the strands*
α_2	0,19	[-]	*Facor depending on the type of tendon*
Ø	15,2	[-]	*Diameter of the prestressing element*
σ_{pm0}	1384,4	[N/mm²]	*Stress in tendon just after release (i.e. initial stress)*
$l_{pt,c}$	329,1	[mm]	*Transfer length*
$l_{pt1,c}$	0,132	[m]	*Design value transmission length centric prestressing*

Transmission length eccentric prestressing

α_1	1,0	[-]	*Factor depending on way of releasing the strands*
α_2	0,19	[-]	*Facor depending on the type of tendon*
Ø	15,2	[-]	*Diameter of the prestressing element*
σ_{pm0}	1290,9	[N/mm²]	*Stress in tendon just after release (i.e. initial stress)*
$l_{pt,fb}$	306,8	[mm]	*Transfer length*
$l_{pt1,fb}$	0,123	[m]	*Design value transmission length eccentric prestressing*

Tensile stresses at top fibre

Centric prestressing

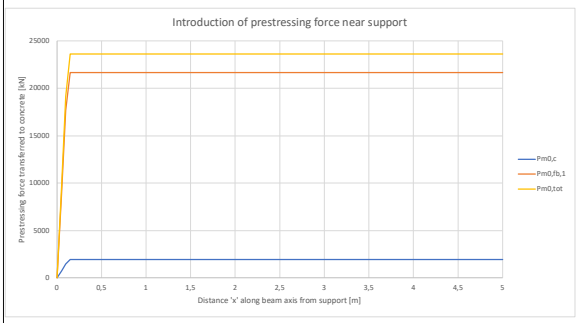
P_{m0}	1938	[kN]	*Initial prestressing force centric prestresssing*
$l_{pt1,c}$	0,132	[m]	*Design value transmission length centric prestressing*

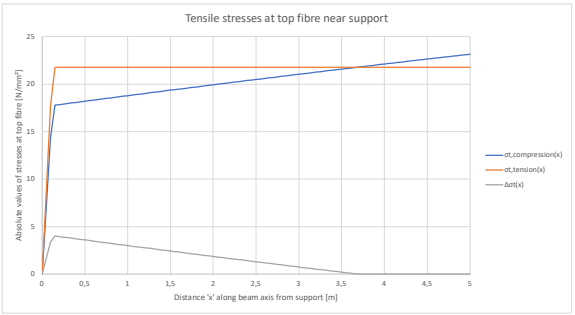
Eccentric prestressing

n_{fb}	120	[pcs]	*Total number of strands in bottom flange*
$n_{fb,1}$	120	[pcs]	*Selected number of strands introduced in first set*
$n_{fb,2}$	0	[pcs]	*Selected number of strands introduced in second set*
$x_{debond,1}$	0	[m]	*Length over which first set of strands is debonded*
$x_{debond,2}$	0	[m]	*Length over which second set of strands is debonded*

Parameters sets of strands eccentric prestressing

$P_{m0,fb}$	21687	[kN]	*Total initial prestressing force eccentric prestressing*
$P_{m0,fb,1}$	21687	[kN]	*Initial prestressing force first set of strands*
$P_{m0,fb,2}$	0	[kN]	*Initial prestressing force second set of strands*
$l_{pt1,fb}$	0,123	[m]	*Design value transmission length eccentric prestressing*





Verification remaining tensile stress

$\Delta\sigma_t$	4,0	[N/mm²]	*Highest value remaining tensile stress*
σ_{max}	6,7	[N/mm²]	*Maximum allowable tensile stress*
Verification	Satisfied	[-]	*Verification*

Positioning of strands in the bottom flange

Auxiliary parameters (dimensions and cover)

h	1900	[mm]	*Total height*
w_b	2000	[mm]	*Internal width of the box*
b	2200	[mm]	*Width lower end of beam (webs and internal width)*
w_{cb}	1900	[mm]	*Total width end cross beam (solid part)*
t_{fb}	200	[mm]	*Thickness bottom flange*
t_w	100	[mm]	*Thickness of web*
$c_{nom,s}$	35	[mm]	*Minimum applied cover onto strands bottom flange (all sides)*
$c_{nom,r}$	30	[mm]	*Minimum applied cover onto rebars bottom flange (all sides)*
$\emptyset_r$	10	[mm]	*Assumed diameter splitting reinforcement bottom flange*

Positioning of the strands - Parameters

$D_{strand,fb}$	15,2	[mm]	*Assumed strand diameter*
$c_{prov,s}$	40	[mm]	*Applied cover onto the strands (all sides)*
s_{min}	30,4	[mm]	*Assumed minimum spacing (horizontal and vertical)*
d_{min}	45,6	[mm]	*Minimum c.t.c. distance in horizontal and vertical direction*
$h_{available}$	120	[mm]	*Available height bottom flange for positioning of the strands*
$w_{available}$	2120	[mm]	*Available width bottom flange for positioning of the strands*
$n_{max,rows}$	3	[pcs]	*Maximum number of rows in bottom flange*
$n_{max,strands}$	47	[pcs]	*Maximum number of strands per row in bottom flange*
$n_{max,fb}$	141	[pcs]	*Maximum allowable number of strands in bottm flange*

Positioning of the strands - Applied values

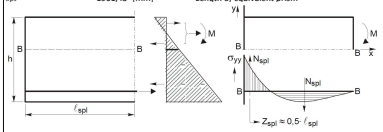
n_{fb}	120	[pcs]	*Total number of strands in bottom flange*
n_{rows}	3	[pcs]	*Required number of rows*
$n_{strands}$	40	[pcs]	*Number of strands per row*
d_{vert}	52,40	[mm]	*Applied vertical c.t.c. distance between the applied strands*
d_{hor}	53,97	[mm]	*Applied horizontal c.t.c. distance between the applied strands*

Splitting reinforcement - Vertical distribution

Spalling stresses

Equivalent prism spalling (See: Textbook CIE4160 - Section 10.2.2):

l_{pt}	123	[mm]	*Transfer length*
ζ_{spl}	1,00	[-]	*Factor for splitting*
l_{spl}	1901,43	[mm]	*Length of equivalent prism*



First set of strands:

σ_{top}	4,2	[N/mm²]	*Stress due to prestressing in top fibre at end of prism*
σ_{bottom}	-44,8	[N/mm²]	*Stress due to prestressing in bottom fibre at end of prism*
h_{prism}	323,8	[mm]	*Height of equivalent prism*
b	2200	[mm]	*Width of cs at height where spalling occurs (at start of the prism)*
M	160518525	[Nm]	*Bending moment (elastic stress distribution) due to prestressing*
N_{spl}	168840	[N]	*Spalling tensile force*
σ_{spl}	0,32	[N/mm²]	*Spalling tensile stress*
γ_{spl}	1,2	[-]	*Partial factor splitting*
$\sigma_{bs,d}$	0,39	[N/mm²]	*Design value splitting stress*
$\sigma_{Rd,f}$	4,40	[N/mm²]	*Residual tensile strength, calculated with Klocal*
Verification	Satisfied	[-]	*If verification is satisfied no spalling reinforcement needed*

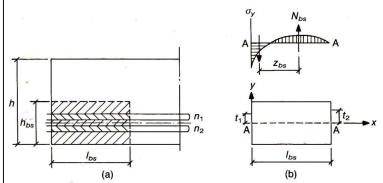
Second set of strands (if applicable):

σ_{top}	4,2	[N/mm²]	*Stress due to prestressing in top fibre at end of prism*
σ_{bottom}	-44,8	[N/mm²]	*Stress due to prestressing in bottom fibre at end of prism*
h_{prism}	323,8	[mm]	*Height of equivalent prism*
b	2200	[mm]	*Width of cs at height where spalling occurs*
M	160518525	[Nm]	*Bending moment due (elastic stress distribution prestressing)*
N_{spl}	168840	[N]	*Spalligh tensile force*
σ_{spl}	0,32	[N/mm²]	*Spalling tensile stress*
γ_{spl}	1,2	[-]	*Partial factor splitting*
$\sigma_{bs,d}$	0,39	[N/mm²]	*Design value splitting stress*
$\sigma_{Rd,f}$	4,40	[N/mm²]	*Residual tensile strength, calculated with Klocal*
Verification	Satisfied	[-]	*If verification is satisfied no spalling reinforcement needed*

Bursting stresses

Symmetric prism analogy (See: fib Model Code 2010 - Section 7.13.6.5.2):

h_{bs}	200	[mm]	*Height of the virtual prismatic element*
l_{pt}	123	[mm]	*Transfer length of the strands*
ζ_{bs}	1,07	[-]	*Factor for bursting*
l_{bs}	213,13	[mm]	*Length of equivalent prism*



First set of strands:

n_1	40	[pcs]	*Set 1: Number of tendons above the centroid of the prism*
n_2	40	[pcs]	*Set 1: Number of tendons below the centroid of the prism*
t_1	52,4	[mm]	*Set 1: Distance centroid tendons above section to centroid of prism*
t_2	50	[mm]	*Set 1: Distance centroid of stress block to centroid of prism*
$P_{m0,fb}$	180,7	[kN]	*Initial prestressing force for a single tendon*
z_{bs}	106,6	[mm]	*Internal lever arm of bursting forces*
N_{bs}	-163	[kN]	*Set 1: Bursting force*
b_{bs}	2200	[mm]	*Width of prism at the position of strands*
σ_{bs}	-0,35	[N/mm²]	*Set 1: Maximum bursting stresses*
γ_{spl}	1,2	[-]	*Partial factor splitting*
$\sigma_{bs,d}$	-0,42	[N/mm²]	*Set 1: Design value maximum bursting stresses*
$\sigma_{Rd,f}$	4,40	[N/mm²]	*Residual tensile strength, calculated with Klocal*
Verification	Satisfied	[-]	*Set 1: Verification of bursting stresses and material strength*

Second set of strands (if applicable):

n_1	0	[pcs]	*Set 2: Number of tendons above the centroid of the prism*
n_2	0	[pcs]	*Set 2: Number of tendons below the centroid of the prism*
t_1	52,4	[mm]	*Set 2: Distance centroid tendons to centroid of prism*
t_2	50	[mm]	*Set 2: Distance centroid of stress block to centroid of prism*
$P_{m0,fb,1}$	180,7	[kN]	*Initial prestressing force for a single tendon*
z_{bs}	106,6	[mm]	*Internal lever arm of bursting forces*
N_{bs}	0	[kN]	*Set 2: Bursting force*
b_{bs}	2200	[mm]	*Width of prism at the position of strands*
σ_{bs}	0,00	[N/mm²]	*Set 2: Maximum bursting stresses*
γ_{spl}	1,2	[-]	*Partial factor splitting*
$\sigma_{bs,d}$	0,00	[N/mm²]	*Set 2: Design value maximum bursting stresses*
$\sigma_{Rd,f}$	4,40	[N/mm²]	*Residual tensile strength, calculated with Klocal*
Verification	Satisfied	[-]	*Set 2: Verification of bursting stresses and material strength*

Splitting stresses

- Splitting is accounted for by selecting appropriate values for cover and centre to centre distance.
- By appling these minimum values this requirement is automatically satisfied.

Splitting reinforcement - Horizontal distribution

Distribution of single strand

d_{hor}	54,0	[mm]	*Applied horizontal c.t.c. distance between the applied strands*
s	2200	[mm]	*Length of disturbed region (length of St. Venant)*
γ_{spl}	1,2	[-]	*Partial factor for splitting*
$P_{m0,fb,i}$	180,7	[kN]	*Initial prestressing force single strand in bottom flange*
$N_{spl,hor,i}$	1,3	[kN]	*Splitting force due to single strand*

Splitting force first set of strands

$n_{fb,1}$	120	[pcs]	*Number of strands applied in first set*
$N_{spl,hor,1}$	159,6	[kN]	*Horizontal splitting force first set*
$\emptyset_{spl,f1}$	10	[mm]	*Assumed diameter splitting reinforcement*
f_s	300	[N/mm²]	*Maximum allowable stress in reinforcement*
$A_{s,min}$	532	[mm²]	*Minimum required cross section of the reinforcement*
$n_{s,req,1}$	7	[pcs]	*Required number of rebars*

Splitting force second set of strands (if applicable)

$n_{fb,2}$	0	[pcs]	*Number of strands applied in second set*
$N_{spl,hor,2}$	0,0	[kN]	*Horizontal splitting force second set*
$\emptyset_{spl}$	10	[mm]	*Assumed diameter splitting reinforcement*
f_s	300	[N/mm²]	*Maximum allowable stress in reinforcement*
$A_{s,min}$	0	[mm²]	*Minimum required cross section of the reinforcement*
$n_{s,req,2}$	0	[pcs]	*Required number of rebars*

Verification bending moment capacity

Identifying all horizontal forces

Concrete

w	3200	[mm]	*Width of the beam*
f_{cd}	113	[N/mm²]	*Design value concrete compressive strength*
x_u	165,5289573	[mm]	*Height concrete compressive zone (iteration)*

Active contribution prestressing

$A_{p,c}$	1400	[mm²]	*Applied cross section centric prestressing*
$\sigma_{p,m,c}$	1149,34	[N/mm²]	*Working prestressing stress centric prestressing*
$A_{p,fb}$	16800	[mm²]	*Applied cross section eccentric prestressing*
$\sigma_{p,m,fb}$	1073,18	[N/mm²]	*Working prestressing stress eccentric prestressing*

Contribution concrete under tension

f_{ctd}	6,0	[N/mm²]	*Design value of tensile strength (tensile strength 1st crack)*
$f_{ctd,2}$	6,15	[N/mm²]	*Design value maximal post cracking stress (at w=0,30)*
b_{web}	200	[mm]	*Width of tensile zone (width of the webs)*

Auxiliary parameters

l_c	1266,7	[mm]	*Characteristic length*

Height of concrete compressive and tensile zone

Parameters compressive zone

ε_{c3}	0,0023	[-]	*Strain at reaching concrete compressive strength*
f_{cd}	113	[N/mm²]	*Design value concrete compressive strength*
b	3200	[mm]	*Width of the beam*
h_f	187,5	[mm]	*Mean value thickness top flange*
b_{red}	200	[mm]	*Reduced width of the cross section (width of the webs)*
$\varepsilon_{c,f1}$	-0,000305	[-]	*Strains at lower side top flange*
$\sigma_{c,f1}$	-15,04	[N/mm²]	*Stresses at lower side top flange*
N_c	30015918	[N]	*Compressive force in the concrete*
e_c	55,2	[mm]	*Eccentricity compressive force with respect to top fibre*

Case	Concrete compressive forces		Lever arm (from top fibre)		Eccentricity with respect to top fibre	
Case 1	Nc1	30015918 [N]	S1	N.A. [Nmm]		
	Nc2	0 [N]	S2	N.A. [Nmm]	ec	55,2 [mm]
	Nc3	0 [N]	S3	N.A. [Nmm]		
Case 2	Nc1	0 [N]	S1	0 [Nmm]		
	Nc2	0 [N]	S2	0 [Nmm]	ec	0,0 [mm]
	Nc3	0 [N]	S3	0 [Nmm]		

Parameters tensile zone

ε_{ct}	0,00012	[-]	*Strain corresponding to cracking of the beam*
$\varepsilon_{ct;0,3}$	0,00036	[-]	*Strain corresponding to maximum post cracking stress*
ε_{ctd}	0,00041	[-]	*Strain corresponding to declining branch stress-strain curve*
ε_{ctu}	0,00250	[-]	*Strain corresponding ultimate capacity (pull-out of fibre)*
x_1	8,6	[mm]	*Height first concrete tensile zone*
x_2	20,9	[mm]	*Height second concrete tensile zone*
x_3	150,4	[mm]	*Height third concrete tensile zone*
N_t	120494	[N]	*Total concrete tensile force*
e_t	229,4	[mm]	*Eccentricity concrete tensile force with respect to top fibre*

	Concrete tensile forces		Lever arm (from top fibre)		Eccentricity with respect to top fibre
Zones	Nt1	5182 [N]	S1	887568 [Nmm]	
	Nt2	25082 [N]	S2	4630465 [Nmm]	
	Nt3	90231 [N]	S3	22124209 [Nmm]	

Determining the strains

Centrical prestressing

$d_{p,c}$	844	[mm]	*Effective height centric prestressing*
$\Delta\varepsilon_{p,c}$	0,0094	[-]	*Strain increase centric prestressing steel (passive contribution)*
$\varepsilon_{p,m,c}$	0,0059	[-]	*Strain in centric prestressing steel due to working prestressing*
$\varepsilon_{p,c}$	0,0153	[-]	*Total strain in centric prestressing steel*

Eccentric prestressing

$d_{p,fb}$	1800	[mm]	*Effective height eccentric prestressing*
$\Delta\varepsilon_{p,fb}$	0,0227	[-]	*Strain increase eccentric prestressing steel (passive contribution)*
$\varepsilon_{p,m,fb}$	0,0055	[-]	*Strain in eccentric prestressing steel due to working prestressing*
$\varepsilon_{p,fb}$	0,0282	[-]	*Total strain in eccentric prestressing steel*

Steel stresses

Main parameters

f_{pk}/γ_s	1691	[N/mm²]	*Design value stress at failure*
f_{pd}	1522	[N/mm²]	*Design value steel stress*
ε_{uk}	0,035	[-]	*Characteristic value strain at failure*
f_{pd}/E_p	0,0078	[-]	*Strain at design value of the steel stress*

Centric prestressing

$\sigma_{pu,c}$	1569	[N/mm²]	*Actual stress centric prestressing steel at calculated strain*
$\sigma_{p,m,c}$	1149	[N/mm²]	*Working prestressing stress centric prestressing*
$A_{p,c}$	1400	[mm²]	*Applied cross section centric prestressing*
$P_{m,m,c}$	1609077	[N]	*Working prestressing force centric prestressing*
$\Delta N_{p,c}$	587140	[N]	*Passive contribution centric prestressing*

Eccentric prestressing

$\sigma_{pu,fb}$	1649	[N/mm²]	*Actual stress eccentric prestressing steel at calculated strain*
$\sigma_{p,m,fb}$	1073	[N/mm²]	*Working prestressing stress eccentric prestressing*
$A_{p,fb}$	16800	[mm²]	*Applied cross section eccentric prestressing*
$P_{m,m,fb}$	18029494	[N]	*Working prestressing force eccentric prestressing*
$\Delta N_{p,fb}$	9669713	[N]	*Passive contribution eccentric prestressing*

Check equilibrium

N_c	-30016	[kN]	*Compressive force in the concrete*
N_t	120	[kN]	*Total concrete tensile force*
$P_{m,m}$	19639	[kN]	*Total working prestressing force (centric and eccentric)*
ΔN_p	10257	[kN]	*Total passive contribution of the prestressing (centric and eccentric)*
ΣH	0	[kN]	*Verification of horizontal equilibrium*

Determine bending moment capacity

- Bending moment is calculated using the top fibre as point of reference

Determining bending moment capacity

	Force [kN]	Lever arm [m]	Moment [kNm]
N_c	-30016	0,055	-1656
N_t	120	0,229	28
$P_{m,m,c}$	1609	0,844	1359
$P_{m,m,fb}$	18029	0,844	15226
$\Delta N_{p,c}$	587	0,844	496
$\Delta N_{p,fb}$	9670	1,800	17405

Determining design value bending moment

$M_{Ed,RFEM}$	41753	[kNm]	*Bending moment due to loads calculated using RFEM*
$M_{Ed,P}$	17227	[kNm]	*Upward bending moment due to the prestressing*
M_{Ed}	24526	[kNm]	*Design value bending moment*

Verification

M_{Ed}	24526	[kNm]	*Design value bending moment*
M_{Rd}	32857	[kNm]	*Bending moment capacity*
UC	0,75	[-]	*Unity check*

Verifying the rotational capacity

ε_{cu}	0,00230	[-]	*Strain at failure of the concrete*
$d_{p,ave}$	1726,5	[mm]	*Weighted average effective height centric and eccentric prestressing*
$\sigma_{p,m,ave}$	1079,0	[mm]	*Weighted average centric and eccentric working prestressing stress*
$A_{p,ave}$	15615,4	[mm]	*Weighted average cross section centric and eccentric prestressing*
f	612	[N/mm²]	*Factor for weighed contribution of reinforcing and prestressing steel*
$x_{u,prov}/d_{p,ave}$	0,10	[-]	*Ratio height compressive zone and effective height*

Limit value	0,35	[-]	*Limit value ratio height compressive zone and effective height*
UC	0,27	[-]	*Verification of rotational capacity (expressed as UC)*
Verification	Satisfied	[-]	*Verification of rotational capacity*

Verification shear force capacity

Resistance of prestressed concrete cross section without shear reinforcement

Contribution of the concrete

N_{Ed}	19639	[kN]	*Working prestressing force (centric and eccentric)*
A_c	1342500	[mm²]	*Cross sectional area of total cross section*
f_{ck}	200	[N/mm²]	*Characteristic value compressive strength*
b_w	200	[mm]	*Total width of both webs*
h	1900	[mm]	*Total height*
σ_{cp}	14,6	[N/mm²]	*Compressive stress due to working prestressing force*
k	1,2	[-]	*Factor depending on compressive stress and fck*
z	1620,0	[mm]	*Lever arm, taken as 0,9 * d*
$V_{Rd,c}$	894	[kN]	*Concrete contribution to shear capacity*

Contribution of the steel fibres

A_{fv}	324000	[mm²]	*Area of the fibre effect, taken as bw * z*
$f_{ctd,2}$	6,15	[N/mm²]	*Design value maximal post cracking stress (at w=0,30)*
θ	30	[°]	*Angle of the concrete compressive strut of the main beams*
$V_{Rd,f}$	3453	[kN]	*Steel fibre contribution to shear capacity*

Total concrete capacity

$V_{Rd,tot}$	4347	[kN]	*Summation of concrete and steel fibre contribution.*

Concrete compressive strut

α_{cc}	0,85	[-]	*Long term effects and unfavourable loading (compression)*
γ_c	1,5	[-]	*Partial factor concrete (cf EC2)*
b_w	200	[mm]	*Total width of both webs*
z	1620,0	[mm]	*Lever arm, taken as 0,9 * d*
$f_{ck}\text{^}(2/3)$	34,2	[N/mm²]	*Value depending on characteristic value compressive strength*
$V_{Rd,max}$	6199	[kN]	*Capacity of concrete compressive strut*
$\tan(\theta)$	0,577	[-]	*Auxiliary value*
$\cot(\theta)$	1,732	[-]	*Auxiliary value*

Shear capacity and verification

V_{tot}	4347	[kN]	*Summation of concrete and steel fibre contribution.*
$V_{Rd,max}$	6199	[kN]	*Capacity of concrete compressive strut*
V_{Ed}	3632	[kN]	*Design value shear force*
V_{Rd}	4347	[kN]	*Shear force capacity*
UC	0,84	[kN]	*Unity check*

Verification torsional resistance

Torsional capacity

Dimensions

t_{ft}	187,5	[mm]	*Mean value thickness top flange*
t_w	100	[mm]	*Thickness of web*
t_{fb}	200	[mm]	*Thickness bottom flange*
h_b	1512,5	[mm]	*Internal height of the box*
w_b	2000	[mm]	*Internal width of the box*

Parameters torsional capacity

A	4180000	[mm²]	*Total area of the cross section within the outer circumference*
u	8200	[mm]	*Outer circumference of the cross section*
t_{ef}	100	[mm]	*Effective wall thickness (limited by the smallest actual thickness)*
A_k	3583125	[mm2]	*Area enclosed by centre lines of the connected walls*
f_{ctd}	6,0	[N/mm²]	*Design value of tensile strength (tensile strength 1st crack)*

Torsional capacity verification

T_{Ed}	1268	[kNm]	*Design value torsional moment*
$T_{Rd,c}$	4300	[kNm]	*Torsional moment capacity (torsional cracking moment)*
UC	0,29	[-]	*Unity check*

Combination of shear and torsion

A_k	3583125	[mm2]	*Area enclosed by centre lines of the connected walls*
z_1	1706,3	[mm]	*Length of element 1 (left web)*
z_2	2100,0	[mm]	*Length of element 2 (bottom flange)*
z_3	1706,3	[mm]	*Length of element 3 (right web)*
z_4	2100,0	[mm]	*Length of element 4 (top flange)*

Shear forces in the elements of the cross section

$V_{Ed,V,1}$	1816,0	[kN]	*Shear force to be carried by element 1 (left web)*
$V_{Ed,V,2}$	0,0	[kN]	*Shear force to be carried by element 2 (bottom flange)*
$V_{Ed,V,3}$	1816,0	[kN]	*Shear force to be carried by element 3 (right web)*
$V_{Ed,V,4}$	0,0	[kN]	*Shear force to be carried by element 4 (top flange)*

$V_{Ed,T,1}$	301,9	[kN]	*Shear force in element 1 due to torsion (left web)*
$V_{Ed,T,2}$	371,6	[kN]	*Shear force in element 2 due to torsion (bottom flange)*
$V_{Ed,T,3}$	301,9	[kN]	*Shear force in element 3 due to torsion (right web)*
$V_{Ed,T,4}$	371,6	[kN]	*Shear force in element 4 due to torsion (top flange)*

$V_{Ed,V+T,1}$	2117,9	[kN]	*Total shear force in element 1 due to shear and torsion*
$V_{Ed,V+T,2}$	371,6	[kN]	*Total shear force in element 2 due to shear and torsion*
$V_{Ed,V+T,3}$	1514,1	[kN]	*Total shear force in element 3 due to shear and torsion*
$V_{Ed,V+T,4}$	371,6	[kN]	*Total shear force in element 4 due to shear and torsion*

Verifying shear force capacity per element

k	1,22	[-]	*Factor depending on compressive stress and fck*
f_{ck}	200	[N/mm²]	*Characteristic value compressive strength*
$\gamma_E * \gamma_{cf}$	1,5	[-]	*Product of partial factors (AFGC-SETRA 2013)*
$f_{ctd;2}$	6,15	[N/mm²]	*Design value of tensile strength (tensile strength 1st crack)*
ϑ	30	[°]	*Angle of the concrete compressive strut of the main beams*

Element [-]	$b_{w,i}$ [mm]	z_i [mm]	$V_{Rd,c,i}$ [kN]	A_{fv} [mm²]	$V_{Rd,f,i}$ [kN]	$V_{Rd,i}$ [kN]	UC [-]
1	100,0	1706,3	470,8	170625	1818,7	2289,4	0,93
2	200,0	2100,0	1158,9	420000	4476,7	5635,6	0,07
3	100,0	1706,3	470,8	170625	1818,7	2289,4	0,66
4	187,5	2100,0	1086,5	393750	4196,9	5283,3	0,07

Verifying concrete compressive strut per element

α_{cc}	0,85	[-]	*Long term effects and unfavourable loading (compression)*
γ_c	1,5	[-]	*Partial factor concrete (cf EC2)*
f_{ck}^(2/3)	34,2	[N/mm²]	*Value depending on characteristic value compressive strength*
A_k	3583125	[mm²]	*Area enclosed by centre lines of the connected walls*
$\sin(\vartheta)$	0,500	[-]	*Auxiliary value*
$\cos(\vartheta)$	0,866	[-]	*Auxiliary value*
$\tan(\vartheta)$	0,577	[-]	*Auxiliary value*
$\cot(\vartheta)$	1,732	[-]	*Auxiliary value*

Element [-]	$b_{ef,i}$ [mm]	z_i [mm]	$V_{Ed,V+T,i}$ [kN]	$V_{Rd,max}$ [kN]	UC [-]
1	100,0	1706,3	2117,9	3264,6	0,65
2	200,0	2100,0	371,6	8035,9	0,05
3	100,0	1706,3	1514,1	3264,6	0,46
4	187,5	2100,0	371,6	7533,6	0,05

Global verification ship collision (stability)

Collision force and friction coefficient

F_{equi}	1000	[kN]	*Equivalent static force, see: (4) of 4.6.2. EC1-1-7*
μ	0,5	[-]	*Friction coefficient*

Self-weight of the deck

n_{beams}	5	[-]	*Number of prefab UHPC beams*
L_{tot}	70,70	[m]	*Total length of the main beams*
A_C	1,34	[m²]	*Cross sectional area of total cross section*
ρ	25	[kN/m³]	*Density*
F_{sw}	11864	[kN]	*Self-weight of the UHPC beams*

Verification

Action	1000	[kN]	*Action - Equivalent static force*
Resistance	5932	[kN]	*Self weight multiplied with friction coefficient*
UC	0,17	[-]	*Verification expressed as unity check*
Verification	Satisfied	[-]	*Verification*

Design Calculations Optimization - Design of main beams - Top flange and transverse prestressing

Project: MSc thesis "Redesign of bridges Twentekanaal in UHPC"
Name: M. Dorland
Date: 21-12-2020
Version: D1.0

Input parameters

Input parameters - Material properties & transverse prestressing

Concrete of longitudinal joint

Parameters concrete in compression

f_{ck}	100	[N/mm²]	Characteristic value compressive strength
ε_{cu3}	2,6	[‰]	Maximum compressive strain at ULS

Parameters stiffness and deformations (temperature, creep and shrinkage)

E_{cm}	45000	[N/mm²]	Modulus of elasticity
φ	0,8	[-]	Creep factor

Parameters concrete other

α	0,56	[-]	Factor for shape of concrete compressive zone
β	0,34	[-]	Factor position centre of gravity concrete compressive zone
α_{cc}	0,85	[-]	Long term effects and unfavourable loading (compression)

Calculated values

f_{cd}	57	[N/mm²]	Design value concrete compressive strength

Parameters transverse prestressing

Material properties prestressing steel

f_{pk}	1860	[N/mm²]	Characteristic value tensile strength
f_{pd}	1522	[N/mm²]	Design value steel stress
σ_{pm0}	1395	[N/mm²]	Maximum allowed stress directly after tensioning
$\sigma_{p,max}$	1488	[N/mm²]	Maximum prestressing stress during tensioning
E_p	195000	[N/mm²]	Modulus of elasticity
ε_{uk}	35	[‰]	Characteristic value strain at failure

Calculation parameters tendons (input values)

n	5,00	[pcs]	Assumed number of strands per tendon
D_{strand}	15,2	[mm]	Diameter of single strand
$A_{p,strand}$	140	[mm²]	Cross sectional area per strand
$\sigma_{p,max,prov}$	1400	[N/mm²]	Assumed maximum stress applied to prestressing element
μ	0,23	[-]	Friction coefficient
k	0,01	[rad]	Unintensional angular rotation due to the Wobble-effect
w_{set}	3,00	[mm]	Estimated wedge set
Relaxation	Class 2	[-]	Select relaxation class: normal (1), low (2) or bars (3)
t	500000,00	[h]	The value of the relaxation loss (in %) at 1000 h
ρ	2,50	[%]	Time after stressing (for final value of the relaxation loss)

Other parameters

γ_C	1,5	[-]	Partial factor concrete (cf EC2)
γ_S	1,1	[-]	Partial factor prestressing steel (cf EC2)
γ_{spl}	1,2	[-]	Partial factor splitting forces

Design of transverse prestressing

Calculating prestress losses

Dimensions top flange

$w_{c.t.c.}$	1000	[mm]	Centre to centre distance of the transverse prestressing ribs/ducts
t_{ft}	187,5	[mm]	Mean value thickness top flange
Δe_{ft}	31,25	[mm]	Downward eccentricity transverse prestressing with respect to z_{ft}

Properties top flange

z_{ft}	100,7	[mm]	Centre of gravity top flange with respect to top fibre
A_{ft}	187500	[mm²]	Cross sectional area of top flange section
I_{ft}	7,844E+08	[mm⁴]	Second moment of area of top flange section

Applied maximum force onto prestressing element & stress verification

Applied stress values

$\sigma_{p,max,prov}$	1400,0	[N/mm²]	Assumed maximum stress applied to prestressing element
$\sigma_{c,prov}$	11,1	[N/mm²]	Maximum compressive stress in concrete due to prestressing

Stress limit and verification

$\sigma_{p,max}$	1488	[N/mm²]	Maximum prestressing stress during tensioning
$\sigma_{c,limit}$	60	[N/mm²]	Maximum value concrete compressive stress
Verification	Satisfied	[-]	Verification maximum stress values

Applied value maxinum force applied onto prestressing element

P_{max}	980	[kN]	Applied value maximum prestressing force
$\sigma_{p,max}$	1400	[N/mm²]	Applied value maximum prestressing stress
A_p	700	[mm²]	Applied cross section prestressing tendon

Direct prestressing losses

Elastic losses

w_{tot}	16,36	[m]	Total width of the deck
ΔP_{el}	15,9	[KN]	Elastic loss prestressing

Friction losses

μ	0,23	[-]	Friction coefficient
k	0,009	[1/m]	Coefficient Wobble-effect
$\Delta P_\mu(x=0)$	0,00	[kN]	Prestress loss due to friction at x=0 m
$\Delta P_\mu(x=w_{tot})$	32,6	[kN]	Prestress loss (force) due to friction at x=width deck
$\Delta\sigma_{Pp}(x=w_{tot})$	46,6	[N/mm²]	Prestress loss (stress) due to friction at x=width deck

Wedge set

w_{set}	3,00	[mm]	Assumed value wedge set
$\Delta\sigma_{Pset}/w_{tot}$	0,0028	[N/mm²/mm]	Stress reduction due to friction per unit of length
l_w	14328,3	[mm]	Influence length of the wedge set
ΔP_{set}	57,2	[kN]	Prestress losses due to wedge set (at active side)

Determining initial prestressing force & stress verification

Applied force and stress values

$\max\{P_{m,0}(x)\}$	935	[kN]	Initial prestressing force - maximum value over beam length
$\max\{\sigma_{pm0}(x)\}$	1336	[N/mm²]	Initial prestressing stress - maximum value over beam length
$P_{m,0}$	923	[kN]	Initial prestressing force - mean value over beam length

Stress limit and verification

σ_{pm0}	1395	[N/mm²]	Maximum allowed stress directly after tensioning
Verification	Satisfied	[-]	Verification initial prestressing stress

Applied value initial prestressing force and losses

$P_{m,0}$	923	[kN]	Inital prestressing force - Mean value over beam length
ΔP_i	57	[kN]	Initial losses - Mean value over beam length: Pmax-Pm,0

Time dependent losses

Relaxation

Class	Class 2	[-]	Relaxation class (normal relaxation, low relaxation and bars)
ρ_{1000}	2,5	[%]	The value of the relaxation loss (in %) at 1000 h
μ	0,71	[-]	Factor depending on steel stresses
t	500000	[h]	Time after stressing (for final value of the relaxation loss)
$\Delta\sigma_{pr}/\sigma_{pi}$	0,0405	[-]	Relaxation coefficient
σ_{pi}	1318,1	[N/mm²]	Absolute value of the initial prestressing (σ_pm0)
$\Delta\sigma_{pr}$	53,4	[N/mm²]	Prestress loss due to relaxation

Class 1	Wires and strands normal relaxation
Class 2	Wires and strands low relaxation
Class 3	Bars

Creep & shrinkage

φ	0,8	[-]	Creep factor
$\sigma_{c,QP}$	6,14	[N/mm²]	Stress in concrete adjacent to prestressing tendon
ε_{cs}	0,0008	[-]	Shrinkage of the concrete

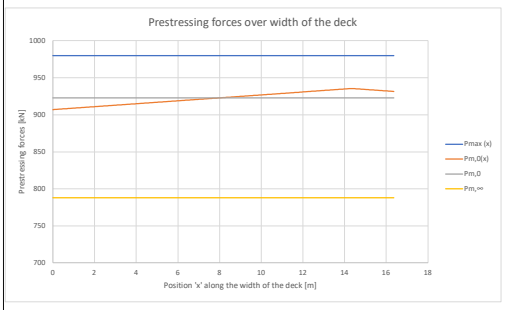
Total time dependent losses

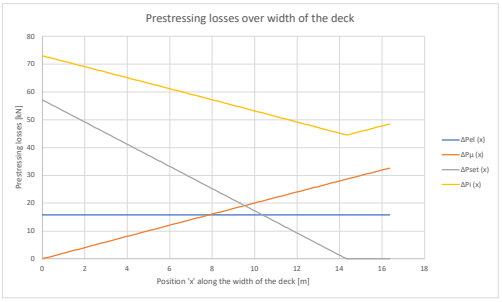
$\Delta\sigma_{p,cswr}$	192	[N/mm²]	Time dependent prestressing losses (stress)
$\Delta P_{p,cswr}$	135	[kN]	Time dependent prestressing losses (force)

Working prestress force and total prestress losses

$P_{m,\infty}$	788	[kN]	Working prestressing force in tendon
$\sigma_{pm,\infty}$	1126	[N/mm²]	Working prestressing stress in tendon
ΔP	-19,6	[%]	Total prestressing loss (percentage)

Plotting prestressing forces and losses over beam length





Detailing of the prestressing - Horizontal and vertical distribution

Parameters

$\emptyset_{spl,ft}$	10	[mm]	Assumed diameter splitting reinforcement top flange
γ_{spl}	1,2	[-]	Partial factor splitting forces
$w_{c.t.c.}$	1000	[mm]	Centre to centre distance of the transverse prestressing ribs/ducts
$t_{ft,tot}$	250	[mm]	Total height top flange at location of prestressing rib
h_1	100	[mm]	Anchor plate (height and width)

Converting width from wc.t.c. to standard width

$w_{c.t.c.}$	1,00	[m]	Centre to centre distance of the transverse prestressing ribs/ducts

Width:	wc.t.c	1,0	[m]
$P_{m,\infty}$	788,0	788,0	[kN]
A_p	700,0	700,0	[mm²]
$\sigma_{pm,\infty}$	1125,7	1125,7	[N/mm²]

Horizontal force distribution

P_{m0}	922,7	[kN]	Inital prestressing force - Mean value over beam length
$N_{spl,w}$	249,1	[kN]	Horizontal tensile force
f_s	300	[N/mm²]	Maximum stress in reinforcement
$A_{s,req}$	830	[mm²]	Minimum required cross section of the reinforcement
$n_{s,req}$	11	[pcs]	Minimum number of rebars requried

Vertical force distribution

P_{m0}	922,7	[kN]	Inital prestressing force - Mean value over beam length
$N_{spl,v}$	166,1	[kN]	Vertical tensile force
f_s	300	[N/mm²]	Maximum stress in reinforcement
$A_{s,req}$	554	[mm²]	Minimum required cross section of the reinforcement
$n_{s,req}$	8	[pcs]	Minimum number of rebars requried

Forces acting on top flange and joint

Parameters longitudinal joint

t_{ft}	187,5	[mm]	Height of the top flange
t_j	162,5	[mm]	Height of the longitudinal joint
$w_{j,t}$	90	[mm]	Width of joint along longitudinal direction

Additional tendon eccentricity

Δe_{ft}	31,25	[mm]	Downward eccentricity transverse prestressing with respect to z_{ft}

Cross sectional properties & parameters of the joint

A_j	162500	[mm²]	Cross sectional area of the longitudinal joint
W_j	4,401OE+06	[mm³]	Section modulus of the longitudinal joint
I_j	3,575BE+08	[mm⁴]	Second moment of the cross section of the longitudinal joint
e_j	50,7	[mm]	Eccentricity prestressing tendon with centre of joint
l	1190	[mm]	Span of the mechanical model
d_p	131,9	[mm]	Effective height longitudinal joint

Actions on the joint

$G_{k,sf}$	4,6875	[kN/m]	Self-weigth UHPC top flange
$G_{k,asfalt}$	0,23	[kN/m]	Permanent load due to asphalt/protection layer
G_k	4,92	[kN/m]	Self-weight + permanent load
$Q_{k,LM2}$	194	[kN]	Single wheel load model 2

Factors

Bending moments joint (SLS)

Bending moments (ULS)

γ_G	1,4 [-]	*See tabel NB.16 – A2.4(B) of NA to NEN-EN 1990*	
$\xi * \gamma_G$	1,25 [-]	*See tabel NB.16 – A2.4(B) of NA to NEN-EN 1990*	
γ_P	1,0 [-]	*See 2.4.2.2 of NA to NEN-EN 1992-1-1*	
γ_Q	1,5 [-]	*See tabel NB.16 – A2.4(B) of NA to NEN-EN 1990*	
ψ_0	0,8 [-]	*See tabel NB.13 – A2.1 of NA to NEN-EN 1990*	

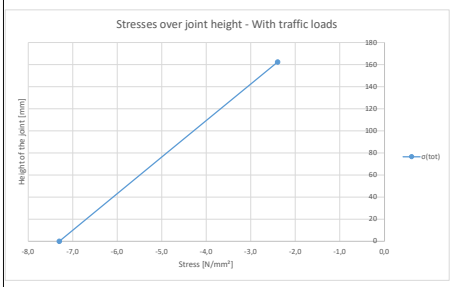
M_G	0,29 [kNm]	*Bending moment due to self-weigth and asphalt layer*
M_P	39,94 [kNm]	*Bending moment due to eccentricity of tendons*
M_Q	28,86 [kNm]	*Bending moment due to varaible load (LM2)*

$M_{Ed,a}$	-4,9 [kNm]	*Design value bending moment equation 6.10a*
$M_{Ed,b}$	3,7 [kNm]	*Design value bending moment equation 6.10b*
M_{Ed}	3,7 [kNm]	*Design value bending moment*

Verifying stresses over joint height

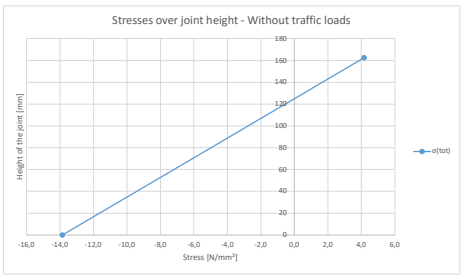
Stress distribution over the height of the joint with traffic loads:

	Height [mm]	σ(M$_G$) [N/mm²]	σ(M$_G$) [N/mm²]	σ(P) [N/mm²]	σ(M$_P$) [N/mm²]	σ(tot) [N/mm²]
Top fibre	163	-0,1	-6,6	-4,8	9,1	-2,4
Bottom fibre	0	0,1	6,6	-4,8	-9,1	-7,3



Stress distribution over the height of the joint without traffic loads:

	Height [mm]	σ(M$_G$) [N/mm²]	σ(M$_G$) [N/mm²]	σ(P) [N/mm²]	σ(M$_P$) [N/mm²]	σ(tot) [N/mm²]
Top fibre	163	-0,1	0,0	-4,8	9,1	4,2
Bottom fibre	0	0,1	0,0	-4,8	-9,1	-13,9



Local verification (transverse direction) - Verification bending moment capacity longitudinal joint

Parameters concrete

α	0,56 [-]	*Factor for shape of concrete compressive zone*
β	0,34 [-]	*Factor position centre of gravity concrete compressive zone*
f_{cd}	56,7 [N/mm²]	*Design value concrete compressive strength*
x_u	34,30878663 [mm]	*Height concrete compressive zone (iteration)*

Parameters steel

A_p	700,00 [mm²]	*Applied cross section of the prestressing*
$\sigma_{pm,\infty}$	1125,65 [N/mm²]	*Working prestressing stress*

Determining strains and stresses

$\varepsilon_{p,\infty}$	0,0058 [-]	*Strain in prestressing steel due to working prestressing*
$\Delta\varepsilon_p$	0,0074 [-]	*Strain increase prestressing steel (passive contribution)*
ε_p	0,0132 [-]	*Total strain in prestressing steel*
σ_{pu}	1555 [N/mm²]	*Actual stress in prestressing steel at calculated strain*

Horizontal equilibrium

N_c	-1088732 [N]	*Compressive force in the concrete*
$P_{m,\infty}$	787955 [N]	*Working prestressing force*
ΔN_p	300777 [N]	*Passive contribution of the prestressing*
$\sum H$	0 [N]	*Verification of horizontal equilibrium*

Bending moment capacity

	Force [N]	Lever arm [mm]	Moment [kNm]
N_c	-1088732	11,7	-12,7
$P_{m,\infty}$	787955	81,3	64,0
ΔN_p	300777	131,9	39,7
M_{Rd}			91,0

Verification

M_{Ed}	3,7 [kNm]	*Design value bending moment*
M_{Rd}	91,0 [kNm]	*Bending moment capacity*
UC	0,04 [-]	*Unity check*

Local verification (transverse direction) - Bending moment capacity top flange between the webs

Calculation model and design value bending moment

Parameters longitudinal joint

z_{ft}	100,7 [mm]	*Centre of gravity top flange with respect to top fibre*
Δe_{ft}	31,3 [mm]	*Downward eccentricity transverse prestressing with respect to z ft*
$t_{ft,tot}$	250 [mm]	*Total height top flange at location of prestressing rib*

Cross sectional properties & parameters of the flange

l	2,1 [m]	*Span, i.e. distance inside the box + 2*0,5*tweb*
d_p	131,9 [mm]	*Effective height prestressing tendon with respect to top fibre*
$d_{p,hog}$	118,1 [mm]	*Effective height prestressing tendon with respect to bottom fibre*

Actions on the top flange

G_k	4,9175 [kN/m]	*Self-weight + permanent load*
$Q_{k,LM2}$	194 [kN]	*Single wheel load model 2*
$M_{P,ft}$	24,62 [kNm]	*Upward bending moment in case of eccentric prestressing*

Factors

γ_G	1,4 [-]	*See tabel NB.16 – A2.4(B) of NA to NEN-EN 1990*
$\xi * \gamma_G$	1,25 [-]	*See tabel NB.16 – A2.4(B) of NA to NEN-EN 1990*
γ_P	1,0 [-]	*See 2.4.2.2 of NA to NEN-EN 1992-1-1*
γ_Q	1,5 [-]	*See tabel NB.16 – A2.4(B) of NA to NEN-EN 1990*
ψ_0	0,8 [-]	*See tabel NB.13 – A2.1 of NA to NEN-EN 1990*

Bending moments top flange (SLS)

$M_{E,sag}$	27,2 [kNm]	*Sagging moment, SLS*
$M_{E,hog}$	77,4 [kNm]	*Hogging moment, SLS*

Bending moments (ULS)

$M_{Ed,a,sag}$	37,8 [kNm]	*Design value sagging bending moment equation 6.10a*
$M_{Ed,b,sag}$	52,9 [kNm]	*Design value sagging bending moment equation 6.10b*
$M_{Ed,a,hog}$	88,3 [kNm]	*Design value hogging bending moment equation 6.10a*
$M_{Ed,b,hog}$	103,3 [kNm]	*Design value hogging bending moment equation 6.10b*

Verification of bending moment capacity - Sagging bending moment

Parameters concrete

α	0,56 [-]	*Factor for shape of concrete compressive zone*
β	0,34 [-]	*Factor position centre of gravity concrete compressive zone*
f_{cd}	113,3 [N/mm²]	*Design value concrete compressive strength*
x_u	17,79039685 [mm]	*Height concrete compressive zone (iteration)*

Parameters steel

A_p	700,00 [mm²]	*Applied cross section of the prestressing*
$\sigma_{pm,\infty}$	1125,65 [N/mm²]	*Working prestressing stress*

Determining strains and stresses

$\varepsilon_{p,\infty}$	0,0058 [-]	*Strain in prestressing steel due to working prestressing*
$\Delta\varepsilon_p$	0,0167 [-]	*Strain increase prestressing steel (passive contribution)*
ε_p	0,0225 [-]	*Total strain in prestressing steel*
σ_p	1613 [N/mm²]	*Actual stress in prestressing steel at calculated strain*

Horizontal equilibrium

N_c	-1129097 [N]	*Compressive force in the concrete*
$P_{m,\infty}$	787955 [N]	*Working prestressing force*
ΔN_p	341142 [N]	*Passive contribution of the prestressing*
$\sum H$	0 [N]	*Verification of horizontal equilibrium*

Bending moment capacity

	Force [kN]	Lever arm [m]	Moment [kNm]
N_c	-1129	0,0060	-6,8
$P_{m,\infty}$	788	0,1007	79,3
ΔN_p	341	0,1319	45,0
M_{Rd}			117,5

Bending moment verification - Sagging bending moment

$M_{Ed,sag}$	52,9 [kNm]	*Design value sagging bending moment*
M_{Rd}	117,5 [kNm]	*Bending moment capacity*
UC	0,45 [-]	*Unity check sagging bending moment*

Verification of bending moment capacity - Hogging bending moment

Parameters concrete

α	0,56 [-]	*Factor for shape of concrete compressive zone*
β	0,34 [-]	*Factor position centre of gravity concrete compressive zone*
f_{cd}	113,3 [N/mm²]	*Design value concrete compressive strength*
x_u	67,13056017 [mm]	*Height concrete compressive zone (iteration)*

Parameters steel

A_p	700,00 [mm²]	*Applied cross section of the prestressing*
$\sigma_{pm,\infty}$	1125,65 [N/mm²]	*Working prestressing stress*

Determining strains and stresses

$\varepsilon_{p,\infty}$	0,0058 [-]	*Strain in prestressing steel due to working prestressing*
$\Delta\varepsilon_p$	0,0020 [-]	*Strain increase prestressing steel (passive contribution)*
ε_p	0,0077 [-]	*Total strain in prestressing steel*
σ_p	1522 [N/mm²]	*Actual stress in prestressing steel at calculated strain*

Horizontal equilibrium

N_c	-1065138 [N]	*Compressive force in the concrete*
$P_{m,\infty}$	787955 [N]	*Working prestressing force*
ΔN_p	277183 [N]	*Passive contribution of the prestressing*
$\sum H$	0 [N]	*Verification of horizontal equilibrium*

Bending moment capacity

	Force [kN]	Lever arm [m]	Moment [kNm]
N_c	-1065	0,0228	-24,3
$P_{m,\infty}$	788	0,1493	117,6
ΔN_p	277	0,1181	32,7
M_{Rd}			126,1

Bending moment verification - Hogging bending moment

$M_{Ed,hog}$	103,3 [kNm]	*Design value hogging bending moment*
M_{Rd}	126,1 [kNm]	*Bending moment capacity*
UC	0,82 [-]	*Unity check hogging bending moment*

Local verification (longitudinal direction) - Bending moment capcity top flange between prestressing ribs

Calculation model and design value bending moment

Parameters longitudinal joint

t_{ft}	187,5 [mm]	*Mean value thickness top flange*

Cross sectional properties & parameters of the flange

l	1,00 [m]	*Span, i.e. centre to centre distance prestressing ribs*

Actions on the top flange

G_k	4,9175 [kN/m]	*Self-weight + permanent load*
$Q_{k,LM2}$	194 [kN]	*Single wheel load model 2*

Factors

γ_G	1,4 [-]	*See tabel NB.16 – A2.4(B) of NA to NEN-EN 1990*
$\xi * \gamma_G$	1,25 [-]	*See tabel NB.16 – A2.4(B) of NA to NEN-EN 1990*
γ_P	1,0 [-]	*See 2.4.2.2 of NA to NEN-EN 1992-1-1*
γ_Q	1,5 [-]	*See tabel NB.16 – A2.4(B) of NA to NEN-EN 1990*
ψ_0	0,8 [-]	*See tabel NB.13 – A2.1 of NA to NEN-EN 1990*

Bending moments top flange (SLS)

M_E	49,1 [kNm]	*Sagging moment, SLS*

Bending moments (ULS)

$M_{Ed,a}$	59,1 [kNm]	*Design value bending moment equation 6.10a*
$M_{Ed,b}$	73,5 [kNm]	*Design value bending moment equation 6.10b*

Verification of bending moment capacity

Parameters concrete

f_{ctd}	6 [N/mm²]	*Design value of tensile strength (tensile strength 1st crack)*
$f_{ctd;2}$	6,15 [N/mm²]	*Design value maximal post cracking stress (at w=0,30)*
E_{cm}	50000 [N/mm²]	*Modulus of elasticity*
l_f	13 [mm]	*Fibre length*

External axial force (self-weight beams and prestressing)

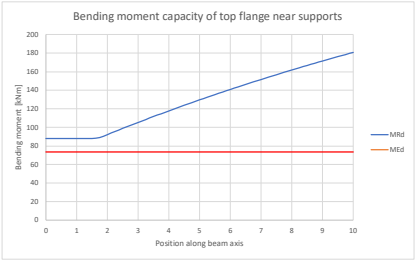
$G_{k,beam}$	33,56 [kN/m]	*Line load representing the self-weight of the prefab beams*
l	68,00 [m]	*Span of the main beams*
$P_{m0,c}$	1938 [kN]	*Applied value initial prestressing force centric prestressing*
$P_{m0,fb}$	21687 [kN]	*Applied value initial prestressing force eccentric prestressing*

Bending moment verification

M_{Ed}	73,5 [kNm]	*Design value bending moment*
M_{Rd}	88,2 [kNm]	*Bending moment capacity at intersection*
UC	0,83 [-]	*Unity check at intersection*
Coordinate 'x'	0,0 [m]	*Location of intersection (sufficient capacity)*

Verifying strains

ε_{cc}	0,00202 [-]	*Compressive strain top fibre at midspan*
ε_{c3}	0,00230 [-]	*Strain at reaching concrete compressive strength*
Verify strains:	Satisfied [-]	*Verify if it holds that $\varepsilon_c \leq \varepsilon_{c3}$*



Design Calculations Optimization - Design of main beams - Fatigue verification

Project: MSc thesis "Redesign of bridges Twentekanaal in UHPC"
Name: M. Dorland
Date: 21-12-2020
Version: D1.0

Fatigue

Parameters - Loads, cross sectional properties and materials

Forces & loads

$M_{fat,max}$	26812	kNm	*Maximum bending moment at midspan (found using RFEM)*
$M_{fat,min}$	22543	kNm	*Minimum bending moment at midspan (found using RFEM)*
$P_{m,0,c}$	1609	[kN]	*Working prestress force - Centric strands*
$P_{m,0,fb}$	18029	[kN]	*Working prestress force - Eccentric strands*
$\gamma_{F,fat}$	1,00	[-]	*See 2.4.2.3 of NA to NEN-EN 1992-1-1*

Cross sectional properties

A_c	1342500	[mm²]	*Cross sectional area of total cross section*
e_p	955,5	[mm]	*Eccentricity of tendons in bottom flange*
I_y	8,038E+11	[mm⁴]	*Second moment of area of the combined cross section*
$W_{y,t}$	9,518E+08	[mm³]	*Section modulus with respect to top fibre*
$W_{y,b}$	7,615E+08	[mm³]	*Section modulus with respect to bottom fibre*

Material properties concrete & steel

E_{cm}	50000	[N/mm²]	*Modulus of elasticity*
$\beta_{cc}(t)$	1,0	[-]	*Factor for increase of strength due to progressive hydration*
f_{ck}	200	[N/mm²]	*Characteristic value compressive strength*
f_{cko}	10	[N/mm²]	*Standard value (10 Mpa)*
E_p	195000	[N/mm²]	*Modulus of elasticity*
$\gamma_{S,fat}$	1,1	[-]	*See 2.4.2.4 of NA to NEN-EN 1992-1-1*
γ_C	1,5	[-]	*Partial factor concrete (cf EC2)*

Fatigue verification - Prestressing steel at midspan

Occuring stress range

α_e	3,90	[-]	*Ratio of moduli of elasticity*
$\sigma_{c,max}$	-3,2	[N/mm²]	*Maximum stress in concrete at tendon height (i.e. highest stress)*
$\sigma_{p,max}$	-12,6	[N/mm²]	*Maximum stress in prestressing steel (i.e. highest stress)*
$\sigma_{c,min}$	-8,3	[N/mm²]	*Minimum stress in concrete at tendon height (i.e. lowest stress)*
$\sigma_{p,min}$	-32,4	[N/mm²]	*Minimum stress in prestressing steel (i.e. lowest stress)*
$\Delta\sigma_p$	19,8	[N/mm2]	*Stress range in prestressing steel*

S-N curve and number of cycles

$\Delta\sigma_{Rsk}$	185	[N/mm²]	*Stress range at N* cycles*
N^*	1000000	[-]	*Number of cycles with single stress range*
k_1	5	[-]	*Stress exponent first branch*
k_2	9	[-]	*Stress exponent second branch*
n_y	100	[-]	*Design service life*
N_{obs}	500000	[-]	*Number of heavy vehicles per year*
n	50000000	[-]	*Number of cycles to be designed for*

Fatigue verification

$\Delta\sigma_{pd}$	19,8	[N/mm²]	*Stress range in prestressing steel*
$\Delta\sigma_{Rsd}$	108,9	[N/mm²]	*Allowable stress range (design value)*
Verification	Satisfied	[-]	*Fatigue verificaiton prestressing steel*

Fatigue verification - Concrete at midspan

Highest and lowest stress values top fibre

$\sigma_{cd,max}$	24,7	[N/mm²]	*Highest compressive stress in a cycle (i.e. most negative value)*
$\sigma_{cd,min}$	20,2	[N/mm²]	*Lowest compressive stress in a cycle (i.e. value closest to zero or positive)*

Verification stresses top fibre

$E_{cd,max}$	0,44	[-]	*Maximum compressive stress level (top fibre)*
$E_{cd,min}$	0,36	[-]	*Minimum compressive stress level (top fibre)*
R	0,82	[-]	*Ratio minimum and maximum stress level (top fibre)*
n	50000000	[-]	*Number of cycles to be designed for*
N	3,41E+18	[-]	*Number of cycles until failure at given stress range*
UC	0,00	[-]	*Fatigue verificaton concrete at top fibre (as UC)*
Verification	Satisfied	[-]	*Fatigue verificaton concrete at top fibre*

Highest and lowest stress values bottom fibre

$\sigma_{cd,max}$	7,6	[N/mm²]	*Highest compressive stress in a cycle (i.e. most negative value)*
$\sigma_{cd,min}$	2,0	[N/mm²]	*Lowest compressive stress in a cycle (i.e. value closest to zero or positive)*

Verification stresses bottom fibre

$E_{cd,max}$	0,13	[-]	*Maximum compressive stress level (bottom fibre)*
$E_{cd,min}$	0,04	[-]	*Minimum compressive stress level (bottom fibre)*
R	0,27	[-]	*Ratio minimum and maximum stress level (bottom fibre)*
n	50000000	[-]	*Number of cycles to be designed for*
N	1,40E+14	[-]	*Number of cycles until failure at given stress range*
UC	0,00	[-]	*Fatigue verificaton concrete at bottom fibre (as UC)*
Verification	Satisfied	[-]	*Fatigue verificaton concrete at bottom fibre*

Concrete fatigue strength

$f_{ck,fat}$	85	[N/mm²]	*Characteristic value fatigue strength*
$f_{cd,fat}$	56,67	[N/mm²]	*Design value fatigue strength*

Design Calculations Optimization - Design of main beams - Serviceability Limit State

Project: MSc thesis "Redesign of bridges Twentekanaal in UHPC"
Name: M. Dorland
Date: 21-12-2020
Version: D1.0

Serviceability limit state - Deflection at midspan

Input parameters loads

$G_{k,total}$	34,32	[kN/m]	*Line load composed of self-weight beam and road surfacing*
$P_{m,o,fb}$	18029	[kN]	*Working prestressing force centric prestressing*
$Q_{k,UDL}$	26,8425	[kN/m]	*Line load acting on the beam (due to UDL of LM1)*
$Q_{k,axle}$	291	[kN/axle]	*Axle load acting on the beam (LM1)*
ψ_1	0,8	[-]	*See tabel NB.13 – A2.1 of NA to NEN-EN 1990*
e_p	0,96	[m]	*Eccentricity of tendons in bottom flange*

Maximum deflection

$1/\delta$	300	[-]	*Maximum deflection in SLS*
δ_{max}	226,7	[mm]	*Calculated value maximum delfection*

Input parameters structure and material

l	68	[m]	*Span of the main beams*
E_{cm}	50000	[N/mm²]	*Modulus of elasticity*
I_y	8,038E+11	[mm⁴]	*Second moment of area of the combined cross section*
φ	0,3	[-]	*Creep factor*
$E_{c,eff}$	38462	[N/mm²]	*Effective modulus of elasticity to account for time dependent effects*

Deflections

δ_G	309,1	[mm]	*Deflection (downwards) due to self weight & permanent loads*
δ_P	-322,1	[mm]	*Deflection (upwards) due to prestressing*
$\delta_{Q,UDL}$	193,4	[mm]	*Deflection (downwards) due to UDL component variable loads*
$\delta_{Q,axle}$	98,7	[mm]	*Deflection (downwards) due to axle loads*
δ_{tot}	279,0	[mm]	*Summation of all individual components*
$\delta_{tot,FEM}$	118,8	[mm]	*Total deflection determined using RFEM*

Verifications

$\delta_{tot} < \delta_{max}$?	Not satisfied	[-]	*Verification maximum deflection*
$\delta_{tot,RFEM} < \delta_{max}$	Satisfied	[-]	*Verification maximum deflection using RFEM results*

Serviceability limit state - Crack width verification

Calculating cracking bending moment (SLS)

f_{ctk}	200	[N/mm²]	*Characteristic value compressive strength*
$f_{ctm,el}$	10,3	[N/mm²]	*Mean value of the axial tensile strength*
$P_{m,o}$	19639	[kN]	*Axial working prestressing force (centric and eccentric)*
A_c	1342500	[mm²]	*Cross sectional area of total cross section*
σ_c	14,6	[N/mm²]	*Compressive stress due to axial prestressing force*
W_{min}	7,615E+08	[mm³]	*Minimum value of section moduli with respect to top and bottom fibre*
M_{cr}	18952	[kNm]	*Cracking bending moment*

Verification non-brittleness criterion

M_{cr}	18952	[kNm]	*Cracking bending moment*
M_{Rd}	32857	[kNm]	*Bending moment capacity*
Verification	Satisfied	[-]	*Verification*

Design Calculations Optimization - Design of end cross beam

Project: MSc thesis "Redesign of bridges Twentekanaal in UHPC"
Name: M. Dorland
Date: 21-12-2020
Version: D1.0

Input parameters

Input parameters - Cross sectional properties and calculation parameters

Cross sectional properties

h_{cb}	1900	[mm]	Total height of the end cross beam
w_{cb}	1900	[mm]	Total width of the end cross beam
A_{cb}	3610000	[mm²]	Cross sectional area of the cross beam
$W_{y,cb}$	1,143E+09	[mm³]	Section modulus of the cross section
$I_{y,cb}$	1,086E+12	[mm⁴]	Second moment of area of the cross section

Calculation parameters

k_1	0,15	[-]	Factor from 6.2.2 of the NA to NEN-EN 1992-1-1
θ	21,8	[°]	Angle concrete compressive strut of end cross beam

Input parameters - Material properties & prestressing

Concrete

Parameters concrete in compression

f_{ck}	30	[N/mm²]	Characteristic cylinder compressive strength at 28 days
$f_{ck,cube}$	37	[N/mm²]	Characteristic cube compressive strength
f_{cm}	38	[N/mm²]	Mean value cylinder compressive strength
ε_{c3}	1,75	[‰]	Strain at reaching concrete compressive strength
ε_{cu3}	3,5	[‰]	Maximum compressive strain at ULS

Parameters concrete in tension

f_{ctm}	2,9	[N/mm²]	Mean value axial tensile strength
$f_{ctk,0,05}$	2,0	[N/mm²]	5%-fractile of the axial tensile strength

Parameters stiffness and deformations (temperature, creep and shrinkage)

E_{cm}	33000	[N/mm²]	Secant modulus of elasticity
φ	1,75	[-]	Creep
Hydration	Normal (N)	[-]	Rate of hydration: Rapid (R), Normal (N) or slow (S)
RH	80,0	[%]	Relative humidity

Parameters concrete other

α	0,75	[-]	Factor for shape of concrete compressive zone
β	0,39	[-]	Factor position centre of gravity concrete compressive zone
α_{cc}	1,0	[-]	Long term effects and unfavourable loading (compression)
α_{ct}	0,0	[-]	Long term effects and unfavourable loading (tension)

Parameters prestressing End cross beams

Material properties prestressing steel

f_{pk}	1860	[N/mm²]	Characteristic value tensile strength
f_{pd}	1522	[N/mm²]	Design value steel stress
σ_{pm0}	1395	[N/mm²]	Maximum allowed stress directly after tensioning
$\sigma_{p,max}$	1488	[N/mm²]	Maximum prestressing stress during tensioning
E_p	195000	[N/mm²]	Modulus of elasticity
ε_{uk}	35	[‰]	Characteristic value strain at failure

Properties prestressing tendons

n_{ducts}	4	[pcs]	Number of ducts in total
a_{vert}	500	[mm]	Vertical position centre of duct from centre of beam
a_{hor}	750	[mm]	Horizontal position centre of duct from centre of beam
n_{strand}	7	[pcs]	Assumed number of strands per tendon
D_{strand}	15,2	[mm]	Diameter of single strand
$A_{p,strand}$	140	[mm²]	Cross sectional area per strand
$\sigma_{p,max,prov}$	1400	[N/mm²]	Assumed maximum stress applied to prestressing element
ϕ_{Duct}	65	[mm]	Outer diameter of prestressing ducts
μ	0,23	[-]	Friction coefficient
k	0,009	[rad]	Unintensional angular rotation due to the Wobble-effect
w_{set}	3	[mm]	Estimated wedge set
Relaxation	Class 2	[-]	Select relaxation class: normal (1), low (2) or bars (3)
t	500000	[h]	The value of the relaxation loss (in %) at 1000 h
ρ	2,5	[%]	Time after stressing (for final value of the relaxation loss)

Other parameters

γ_C	1,5	[-]	Partial factor concrete (cf EC2)
γ_S	1,1	[-]	Partial factor prestressing steel (cf EC2)

Input parameters - Determining creep and shrinkage

Shrinkage

h_0	1267	[mm]	Fictitious thickness, assumed to be (2/3)*hcb (3 sides exposed)
k_h	0,7	[-]	Coefficient depending on fictitious thickness
RH	80,0	[%]	Relative humidity
β_{RH}	0,7564	[-]	Factor for relative humidity
Hydration	Normal (N)	[-]	Rate of hydration: Rapid (R), Normal (N) or slow (S)
α_{ds1}	4	[-]	Coefficient depending on cement type
α_{ds2}	0,12	[-]	Coefficient depending on cement type
f_{cm}	38	[N/mm²]	Mean value cylinder compressive strength
$\varepsilon_{cd,0}$	0,000269	[-]	Nominal unrestrained drying shrinkage
$\varepsilon_{cd,\infty}$	0,000188	[-]	End value drying shrinkage

h0	kh
100	1
200	0,85
300	0,75
500	0,7

	α_{ds1}	α_{ds2}
Slow (S)	3	0,13
Normal (N)	4	0,12
Rapid (R)	6	0,11

Creep

φ	1,75	[-]	Creep factor

Input parameters - Loads

Ultimate Limit State (ULS)

$M_{Ed,hog}$	1271	[kNm]	Maximum hogging bending moment (all loads considered)
$M_{Ed,sag}$	396	[kNm]	Maximum sagging bending moment (all loads considered)
V_{Ed}	846	[kN]	Maximum shear force (all loads considered)

Serviceability Limit State (SLS)

$M_{E,hog}$	453	[kNm]	Maximum hogging bending moment (all loads considered) SLS
$M_{E,sag}$	270	[kNm]	Maximum sagging bending moment (all loads considered) SLS

Design of the prestressing

Calculating prestress losses

Applied maximum force onto prestressing elements & stress verification

Applied stress values

$\sigma_{p,max,prov}$	1400	[N/mm²]	Assumed maximum stress applied to prestressing element
$\sigma_{c,prov}$	1,52	[N/mm²]	Concrete stress due to assumed initial applied force

Stress limit and verification

$\sigma_{p,max,limit}$	1488	[N/mm²]	Maximum prestressing stress during tensioning
$\sigma_{c,limit}$	18	[N/mm²]	Maximum value concrete compressive stress
Verification	Satisfied	[-]	Verification maximum stress values

Applied value maxinum force applied onto prestressing

P_{max}	5488	[kN]	Applied value maximum prestressing force
$\sigma_{p,max}$	1400	[N/mm²]	Applied value maximum prestressing stress
A_p	3920	[mm²]	Applied cross section prestressing tendon

Direct prestressing losses

Elastic losses

ΔP_{el}	13,2	[kN]	Total elastic loss all prestressing tendons

Friction losses

μ	0,23	[-]	Friction coefficient
k	0,009	[1/m]	Coefficient Wobble-effect
$\Delta P_\mu(x=0)$	0,00	[kN]	Prestress loss due to friction at x=0 m
$\Delta P_\mu(x=w)$	182,7	[kN]	Prestress loss (force) due to friction at x=width deck
$\Delta\sigma_{p\mu}(x=w)$	46,6	[N/mm²]	Prestress loss (stress) due to friction at x=width deck

Wedge set

w_{set}	3,00	[mm]	Assumed value wedge set
k	0,0028	[N/mm²/mm]	Stress reduction due to friction per unit of length
l_w	14328,3	[mm]	Influence length of the wedge set
ΔP_{set}	320,1	[kN]	Prestress losses due to wedge set (at active side)

Determining initial prestressing force & stress verification

Applied force and stress values

$\max\{P_{m,0}(x)\}$	5314	[kN]	Initial prestressing force - maximum value over beam length
$\max\{\sigma_{pm0}(x)\}$	1356	[N/mm²]	Initial prestressing stress - maximum value over beam length
$P_{m,0}$	5243	[kN]	Initial prestressing force - mean value over beam length

Stress limit and verification

σ_{pm0}	1395	[N/mm²]	Maximum allowed stress directly after tensioning
Verification	Satisfied	[-]	Verification initial prestressing stress

Applied value initial prestressing force and losses

$P_{m,0}$	5243	[kN]	Inital prestressing force - Mean value over beam length
ΔP_i	245	[kN]	Initial losses - Mean value over beam length: Pmax-Pm,0

Time dependent losses

Relaxation

Class	Class 2	[-]	Relaxation class (normal relaxation, low relaxation and bars)
ρ_{1000}	2,5	[%]	The value of the relaxation loss (in %) at 1000 h
μ	0,72	[-]	Factor depending on steel stresses
t	500000	[h]	Time after stressing (for final value of the relaxation loss)
$\Delta\sigma_{pr}/\sigma_{pi}$	0,0425	[-]	Relaxation coefficient
σ_{pi}	1337,4	[N/mm²]	Absolute value of the initial prestressing (σ_pm0)
$\Delta\sigma_{pr}$	56,8	[N/mm²]	Prestress loss due to relaxation

Class 1	Wires and strands normal relaxation
Class 2	Wires and strands low relaxation
Class 3	Bars

Creep & shrinkage

φ	1,75	[-]	Creep factor
$\sigma_{c,QP}$	1,5	[N/mm²]	Stress in concrete adjacent to tendons (middle cross section)
ε_{cs}	0,000188	[-]	Shrinkage of the concrete

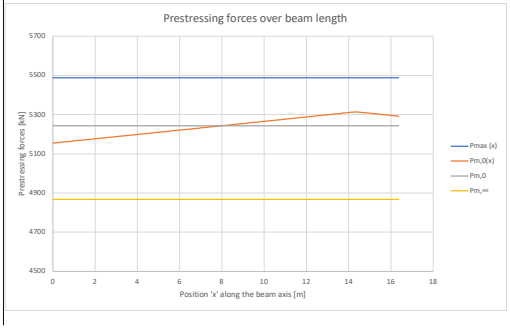
Total time dependent losses

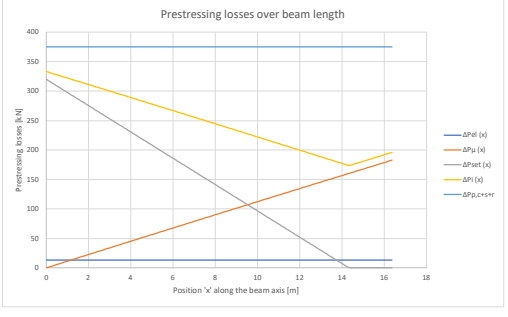
$\Delta\sigma_{p,c+s+r}$	96	[N/mm²]	Time dependent prestressing losses (stress)
$\Delta P_{p,c+s+r}$	375	[kN]	Time dependent prestressing losses (force)

Working prestress force and total prestress losses

$P_{m,\infty}$	4867	[kN]	Total working prestressing force
$\sigma_{pm,\infty}$	1242	[N/mm²]	Working prestressing stress in the tendons
ΔP	-11,3	[%]	Total prestressing loss (percentage)

Plotting prestressing forces and losses over beam length

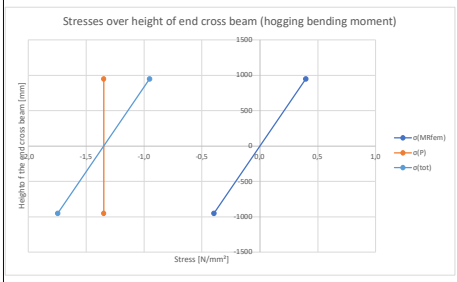




Determining stresses over beam height

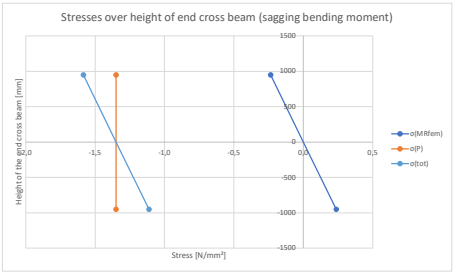
Stress distribution governing hogging bending moment in SLS:

	Height [mm]	σ(MRfem) [N/mm²]	σ(P) [N/mm²]	σ(tot) [N/mm²]
Top fibre	950	0,4	-1,3	-1,0
Bottom fibre	-950	-0,4	-1,3	-1,7



Stress distribution governing sagging bending moment in SLS:

	Height [mm]	σ(MRfem) [N/mm²]	σ(P) [N/mm²]	σ(tot) [N/mm²]
Top fibre	950	-0,2	-1,3	-1,6
Bottom fibre	-950	0,2	-1,3	-1,1



Verification bending moment capacity

Identifying all horizontal forces

Concrete

α	0,75	[-]	*Factor for shape of concrete compressive zone*
w_{cb}	1900	[mm]	*Factor position centre of gravity concrete compressive zone*
f_{cd}	20	[N/mm²]	*Design value concrete compressive strength*
N_c	6217	[kN]	*Compressive force in the concrete*

Active contribution of prestressing

A_p	3920	[mm²]	*Applied cross section of the prestressing*
$P_{m,\infty}$	4867	[kN]	*Working prestressing stress*
$\sigma_{p,\infty}$	1242	[N/mm²]	*Working prestressing stress in the tendons*

Height of concrete compressive zone

x_u	218,1450474	[mm]	*Height concrete compressive zone (iteration)*

x_1	450	[mm]	*Distance from outermost compressed fibre to centre of first row of tendons*
x_2	1450	[mm]	*Distance from outermost compressed fibre to centre of second row of tendons*

Determining the strains

First row of tendons

$d_{p,1}$	450	[mm]	*Effective height prestressing - row 1*
$\Delta\varepsilon_{p,1}$	0,0037	[-]	*Strain increase prestressing steel (passive contribution) - row 1*
$\varepsilon_{p,\infty,1}$	0,0064	[-]	*Strain in prestressing steel due to working prestressing - row 1*
$\varepsilon_{p,1}$	0,0101	[-]	*Total strain in prestressing steel - row 1*

Second row of tendons

$d_{p,2}$	1450	[mm]	*Effective height prestressing - row 2*
$\Delta\varepsilon_{p,2}$	0,0198	[-]	*Strain increase prestressing steel (passive contribution) - row 2*
$\varepsilon_{p,\infty,2}$	0,0064	[-]	*Strain in prestressing steel due to working prestressing - row 2*
$\varepsilon_{p,2}$	0,0261	[-]	*Total strain in prestressing steel - row 2*

Steel stresses

Parameters

f_{pk}/γ_s	1691	[N/mm²]	*Design value stress at failure*
f_{pd}	1522	[N/mm²]	*Design value steel stress*
ε_{uk}	0,035	[-]	*Characteristic value strain at failure*
f_{pd}/E_p	0,0078	[-]	*Strain at design value of the steel stress*

First row of tendons

$\sigma_{pu,1}$	1536	[N/mm²]	*Actual stress in prestressing steel at calculated strain - row 1*
$\sigma_{p,\infty}$	1242	[N/mm²]	*Working prestressing stress - row 1*
$0,5 * A_p$	1960	[mm²]	*Applied cross section prestressing - row 1*
$P_{m,\infty,1}$	2434	[kN]	*Working prestressing force - row 1*
$\Delta N_{p,1}$	577	[kN]	*Passive contribution prestressing - row 1*

Second row of tendons

$\sigma_{pu,2}$	1636	[N/mm²]	*Actual stress in prestressing steel at calculated strain - row 2*
$\sigma_{p,\infty}$	1242	[N/mm²]	*Working prestressing stress - row 2*
$0,5 * A_p$	1960	[mm²]	*Applied cross section prestressing - row 2*
$P_{m,\infty,2}$	2434	[kN]	*Working prestressing force - row 2*
$\Delta N_{p,2}$	772	[kN]	*Passive contribution prestressing - row 2*

Check equilibrium

N_c	-6217	[kN]	*Compressive force in the concrete*
$P_{m,\infty,1}$	2434	[kN]	*Working prestressing force - row 1*
$\Delta N_{p,1}$	577	[kN]	*Passive contribution of the prestressing - row 1*
$P_{m,\infty,2}$	2434	[kN]	*Working prestressing force - row 2*
$\Delta N_{p,2}$	772	[kN]	*Passive contribution of the prestressing - row 2*

ΣH	0	[kN]	*Verification of horizontal equilibrium*

Determine bending moment capacity

- Bending moment is calculated using the most compressed fibre as reference

Determining bending moment capacity

	Force [kN]	Lever arm [m]	Moment [kNm]
N_c	-6217	0,085	-527
$P_{m,\infty,1}$	2434	0,950	2312
$\Delta N_{p,1}$	577	0,450	260
$P_{m,\infty,2}$	2434	0,950	2312
$\Delta N_{p,2}$	772	1,450	1120

Determining design value bending moment

$M_{Ed,RFEM}$	1271	[kNm]	*Bending moment due to loads calculated using RFEM*

Verification

M_{Ed}	1271	[kNm]	*Design value bending moment*
M_{Rd}	5477	[kNm]	*Bending moment capacity*
UC	0,23	[-]	*Unity check*

Verifying the rotational capacity

d_{ave}	950	[mm]	*Average effective height of both rows of tendons*
f	449	[N/mm²]	*Factor for weighed contribution of reinforcing and prestressing steel*
x_u/d_{ave}	0,23	[mm]	*Ratio height compressive zone and effective height*
Limit value	0,53	[mm]	*Limit value ratio height compressive zone and effective height*
UC	0,44	[-]	*Verification of rotational capacity (expressed as UC)*
Verification	Satisfied	[-]	*Verification of rotational capacity*

Verification shear force capacity

Parameters

Effective height

$d_{p,2}$	1450	[mm]	*Effective height prestressing - row 2*

Effective width of the cross beam

n_{row}	2	[pcs]	*Assumed number of ducts per row*
ϕ_{Duct}	65	[mm]	*Outer diameter of prestressing ducts*
w_{cb}	1900	[mm]	*Total width of the end cross beam*
$b_{cb,nom}$	1900	[mm]	*Effective width of the cross beam*

Capacity of concrete elements without shear reinforcement

k	1,37	[-]	*Scale factor*
f_{ck}	30	[N/mm²]	*Characteristic value concrete compressive strength*
v_{min}	0,31	[N/mm²]	*Reduction value for concrete cracked due to shear*
k_1	0,15	[-]	*Factor, value is deduced from the NA of EC2-1-1*
σ_{cp}	1,35	[N/mm²]	*Factor for presence of normal forces (compression positive)*

$V_{Rd,c,min}$	1405	[kN]	*Minimum value shear capacity of elements without shear reinforcement*

Upper limit - Failure of the concrete compressive strut

α_{cw}	1,07	[-]	*Factor accounting for the stress state in the compression strut*
z	1305	[mm]	*Internal lever arm*
v_1	0,53	[-]	*Reduction factor of concrete cracked due to shear*
(θ)	21,8	[°]	*Angle of compressive strut with beam axis*
$\tan(\theta)$	0,400	[-]	*Auxiliary value*
$\cot(\theta)$	2,500	[-]	*Auxiliary value*

$V_{Rd,max}$	9637	[kN]	*Shear force limit due to failure of concrete compressive strut*

Verification

V_{Ed}	846	[kN]	*Design value shear force*
V_{Rd}	1405	[kN]	*Shear force capacity*
UC	0,60	[-]	*Unity check*

Design Calculations Optimization - Weight calculation

Project: MSc thesis ''Redesign of bridges Twentekanaal in UHPC''
Name: M. Dorland
Date: 21-12-2020
Version: D1.0

Description	Length [m]	Height/depth [m]	Width [m]	Cross-section [m²]	Number [-]	Weight [kN/m³]	Result [-]	Units [-]	Remarks/notes
New design prefab UHPC deck									
Prefab UHPC beams	70,70			1,34	5	25	11864	[kN]	
In-situ UHPC joints	70,70	0,19	0,09		4	25	119	[kN]	
Cross beams	16,36	1,9	1,9		2	25	2953	[kN]	
Subtraction overlap main beams			1,900	1,34	10	25	-638	[kN]	
Asphalt layer	70,70	0,01	16,36			23	266	[kN]	
Kerbs	70,70	0,34	0,50		2	25	601	[kN]	
Capping beam	16,36	1,00	0,75		2	25	614	[kN]	*See CH8. preliminary design report*
Total							**15779**	[kN]	
Existing concrete arch bridge - Eefdesebrug									
Arches	75,00	1,80	0,90		2	25,0	6075	[kN]	*Arch length is measured using AutoCAD.*
Supporting elements arches (''windverband'')	8,00	0,36	1,60		4	25,0	461	[kN]	*See drawing B.3622*
Main girders	70,70	1,30	1,90		2	25,0	8731	[kN]	
Cross beams	7,00	0,80	0,80		12	25,0	1344	[kN]	
end cross beams	7,00	1,20	1,30		2	25,0	546	[kN]	*Average height, see ''detail B-B'' of B.7125*
Deck between main girders	70,70	0,25	7,00			25,0	3093	[kN]	
Deck pedestrian lanes	70,70	0,20	2,78		2	25,0	1965	[kN]	*An verage height of 0,20 m is assumed.*
Asphalt layer	70,70	0,05	7,00			23,0	569	[kN]	*Assumption: layer of 50 mm acc to B.5109.*
Total							**22785**	[kN]	
Comparison									
Percentual change of weight	-31	[%]							

Design Calculations Optimization - Calculation output

Project: MSc thesis "Redesign of bridges Twentekanaal in UHPC"
Name: M. Dorland
Date: 21-12-2020
Version: D1.0

Summary calculation results

Conclusion: Verifications are NOT satisfied.

Overview of unity checks:

Verification	Element	Unity check
Bending moment capacity:	*Main beams (global)*	0,75
Shear force capacity:	*Main beams (global)*	0,84
Torsional moment capacity:	*Main beams (global)*	0,29
Combination shear and torsion:	*Main beams (global)*	0,93
Combination shear and torsion – Compressive strut:	*Main beams (global)*	0,65
Ship collision – Static equilibrium:	*Whole deck (global)*	0,17
Bending moment capacity joint:	*Longitudinal joints (local)*	0,04
Top flange transverse - Sagging moment:	*Top flange (local)*	0,45
Top flange transverse - Hogging moment:	*Top flange (local)*	0,82
Bending moment capacity longitudinal direction:	*Top flange (local)*	0,83
Fatigue verification – Prestressing steel:	*Main beams (global)*	0,18
Fatigue verification – Concrete at top fibre:	*Main beams (global)*	0,00
Fatigue verification – Concrete at bottom fibre:	*Main beams (global)*	0,00
Deflection:	*Main beams (global)*	0,52
Bending moment capacity:	*End cross beams (global)*	0,23
Shear force capacity:	*End cross beams (global)*	0,60

Calculation results - Cross section

A_c	1342500,0	[mm²]	*Cross sectional area of total cross section*
z	844,5	[mm]	*Position centre of gravity from the top flange*
I_y	8,038E+11	[mm⁴]	*Second moment of area of the combined cross section*
e_t	844,5	[mm]	*Distance from centre of gravity to top fibre*
e_b	1055,5	[mm]	*Distance from centre of gravity to bottom fibre*
$W_{y,t}$	9,518E+08	[mm³]	*Section modulus with respect to top fibre*
$W_{y,b}$	7,615E+08	[mm³]	*Section modulus with respect to bottom fibre*

Calculation results - Design of main beams - Mean prestressing and global ULS verifications (STR)

Number of prestressing strands:

n_c	10	[pcs]	*Assumed number of strands positioned centrically in the cross section*
n_{fb}	120	[pcs]	*Assumed number of strands positioned in bottom flange*

Verification maximum stresses prestressing steel and concrete: Satisfied

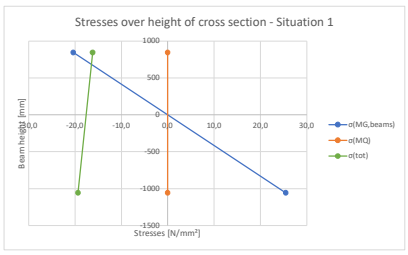
Symbol [-]	Value [N/mm²]	Limit [N/mm²]	Conclusion [-]
$\sigma_{p,max,c}$	1390,00	1488	Satisfied
$\sigma_{p,max,fb}$	1450	1488	Satisfied
$\sigma_{c,c+fb}$	50,16	140,00	Satisfied
$\sigma_{pm,0,c}$	1384	1395	Satisfied
$\sigma_{pm,0,fb}$	1291	1395	Satisfied

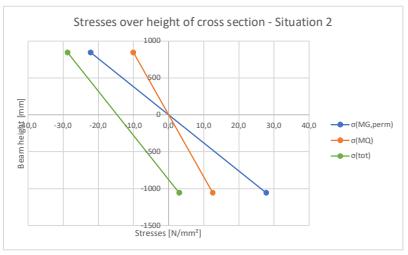
Prestressing forces and prestress losses:

Symbol	Unit	Centric	Eccentric
P_{max}	[kN]	1946	24360
P_{m0}	[kN]	1938	21687
$P_{m,\infty}$	[kN]	1609	18029
ΔP_i	[kN]	8	2673
$\Delta P_{p,c+s+r}$	[kN]	329	3658
ΔP_{tot}	[kN]	337	6331
$\Delta P_{\%}$	[%]	17	26

Stress criterion - Stresses over beam height at midspan: Satisfied

$\sigma_{tot,1}$	-16,2	[N/mm²]	*Largest stress situation 1*
$\sigma_{tot,2}$	3,0	[N/mm²]	*Largest stress situation 2*
σ_{max}	6,7	[N/mm²]	*Maximum allowed tensile stress*





Calculation results - Detailing of the beam ends

Verifications vertical force distribution and positioning of strands: Satisfied

Tensile stress top fibre near support:	Satisfied
Number of strands smaller than maximum:	Satisfied
Vertical force distribution - Splitting stresses:	Satisfied
Vertical force distribution - Bursting stresses:	Satisfied

Horizontal force distribution:

$n_{fb,1}$	120	[pcs]	*Number of strands applied in first set*
$A_{s,min}$	532	[mm²]	*Minimum required cross section of the reinforcement*
$n_{s,req,1}$	7	[pcs]	*Required number of rebars*
$n_{fb,2}$	0	[pcs]	*Number of strands applied in second set*
$A_{s,min}$	0	[mm²]	*Minimum required cross section of the reinforcement*
$n_{s,req,2}$	0	[pcs]	*Required number of rebars*

Calculation results - ULS verifications - Global verifications main beams

Global ultimate limit state verifications of the main beams: All performed global verifications of the main beam are satisfied.

Verification	Units	Design value	Capacity	Unity check	Conclusion
Bending moment capacity:	[kNm]	24526	32857	0,75	Satisfied
Rotational capacity:	[-]	0,10	0,35	0,27	Satisfied
Shear force capacity:	[kN]	3632	4347	0,84	Satisfied
Torsional capacity:	[kNm]	1268	4300	0,29	Satisfied
Combination shear and torsion:	[kN]	2118	2289	0,93	Satisfied
Combination shear and torsion – Compressive strut:	[kN]	2118	3265	0,65	Satisfied
Global verification ship collision (stability):	[kN]	1000	5932	0,17	Satisfied

Calculation results - Design of main beams - Top flange and transverse prestressing

Strands per tendon and centre to centre of prestressing ribs:

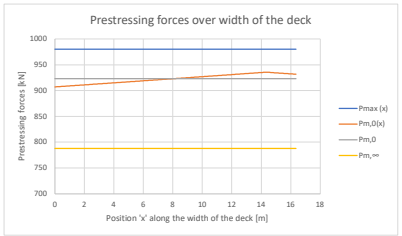
n	5	[pcs]	*Assumed number of strands per tendon*
$w_{c.t.c.}$	1000	[mm]	*Centre to centre distance of the transverse prestressing ribs/ducts*

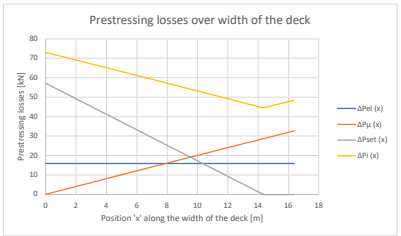
Verification maximum stresses prestressing steel and concrete: Satisfied

Symbol [-]	Value [N/mm²]	Limit [N/mm²]	Conclusion [-]
$\sigma_{p,max}$	1400	1488	Satisfied
$\sigma_{c,prov}$	11,1	60	Satisfied
σ_{pm0}	1336	1395	Satisfied

Prestressing forces and prestress losses:

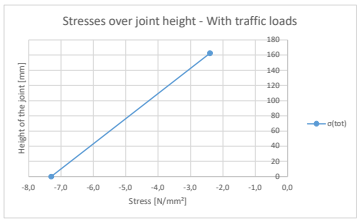
Symbol	Unit	Value
P_{max}	[kN]	980
P_{m0}	[kN]	923
$P_{m,\infty}$	[kN]	788
ΔP_i	[kN]	57
$\Delta P_{p,c+s+r}$	[kN]	135
ΔP_{tot}	[kN]	192
$\Delta P_{\%}$	[%]	-20

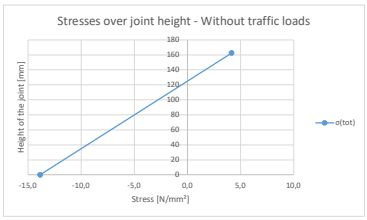




Stress criterion - Stresses at longitudinal joint: NOT satisfied

$\sigma_{tot,1}$	-2,40	[N/mm²]	*Largest stress situation with traffic*
$\sigma_{tot,2}$	4,16	[N/mm²]	*Largest stress situation without traffic*





ULS verifications - Local verifications top flange - Transverse direction: Satisfied

Verification	Units	Design value	Capacity	Unity check	Conclusion
Longitudinal joint:	[kNm]	3,7	91,0	0,04	Satisfied
Sagging bending moment top flange:	[kNm]	52,9	117,5	0,45	Satisfied
Hogging bending moment top flange:	[kNm]	103,3	126,1	0,82	Satisfied

ULS verifications - Local verifications top flange - Longitudinal direction: Satisfied

Verification	Units	Design value	Capacity	Unity check	Conclusion
Longitudinal direction - Capacity:	[kNm]	73,5	88,2	0,83	Satisfied
Compressive strain limit:	[-]	0,0020	0,0023	0,88	Satisfied

The corresponding location of the intersection is: 0 [m]

Calculation results - Fatigue

Fatigue verifications: The performed fatigue verifications of the main beams are satisfied

Prestressing steel at mid span:	0,18	Satisfied
Concrete at midspan - top fibre:	0,00	Satisfied
Concrete at midspan - bottom fibre:	0,00	Satisfied

Calculation results - SLS Deflection

Verification of the deflections in the SLS: Satisfied

δ_{tot}	118,8	[mm]	*Total deflection determined using RFEM*
δ_{max}	226,7	[mm]	*Calculated value maximum deflection*

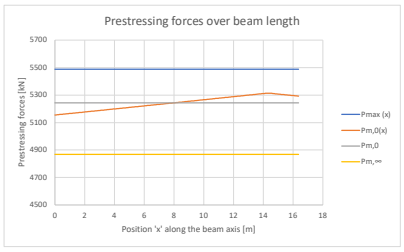
Calculation results - Design of the end cross beam

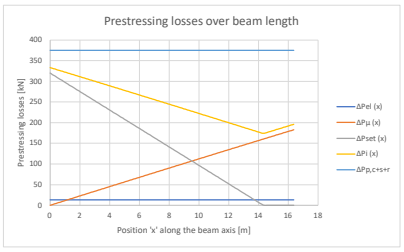
Number of prestressing tendons and strands per tendon:

n_{ducts}	4	[pcs]	*Number of ducts in total*
n_{strand}	7	[pcs]	*Assumed number of strands per tendon*

Verification maximum stresses prestressing steel and concrete: Satisfied

Symbol [-]	Value [N/mm²]	Limit [N/mm²]	Conclusion [-]
$\sigma_{p,max}$	1400	1488	Satisfied
σ_c	1,52	18	Satisfied
σ_{pm0}	1356	1395	Satisfied



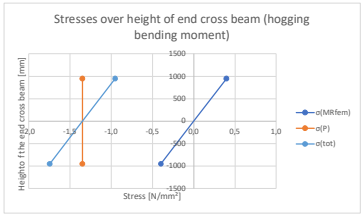


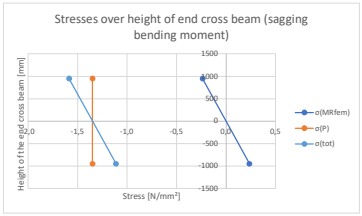
Prestressing forces and prestress losses:

Symbol	Unit	Value
P_{max}	[kN]	5488
P_{m0}	[kN]	5243
$P_{m,\infty}$	[kN]	4867
ΔP_l	[kN]	245
$\Delta P_{p,c+s+r}$	[kN]	375
ΔP_{tot}	[kN]	621
$\Delta P_{\%}$	[%]	-11

Stress criterion - Stresses over beam height: Satisfied

$\sigma_{tot,hog}$	-0,95	[N/mm²]	*Stress distribution hogging moment*
$\sigma_{tot,sag}$	-1,11	[N/mm²]	*Stress distribution sagging moment*





ULS verifications end cross beam: Satisfied

Verification	Units	Design value	Capacity	Unity check	Conclusion
Bending moment capacity:	[kNm]	1271	5477	0,23	Satisfied
Rotation capacity:	[-]	0,23	0,53	0,44	Satisfied
Shear force capacity:	[kN]	846	1405	0,60	Satisfied

Calculation results - Weight calculation and beam properties

Concrete volume and weight of single beam:

Single beam excl. solid ends:	94,9	[m³]
Solid ends single beam:	11,5	[m³]
Total volume single beam:	106,4	[m³]
Self-weight per beam	2660	[kN]

Comparison new design and existing bridge:

Optimized design deck:	15779	[kN]
Existing concrete arch bridge:	22785	[kN]
Difference in total weight:	-31	[%]

ANNEX: CALCULATIONS OPTIMIZATION PHASE – PART II

Design Calculations Optimization - Calculation parameters

Project: MSc thesis "Redesign of bridges Twentekanaal in UHPC"
Name: M. Dorland
Date: 22-12-2020
Version: D1.0

Legend: Input / Output

Geometry of the structure

Main dimensions of the deck

l	68,00	[m]	*Span of the main beams*
w_{tot}	16,36	[m]	*Total width of the deck*
l_{tot}	70,70	[m]	*Total length of the main beams*
n_{beams}	5	[-]	*Number of prefab UHPC beams*

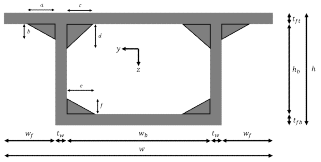
Cross sectional properties main beams

Main properties

w	3200	[mm]	*Total width*
h	1900	[mm]	*Total height*
t_{fb}	200	[mm]	*Thickness bottom flange*
t_w	100	[mm]	*Thickness of web*
w_f	500	[mm]	*Width of the flanges*
w_b	2000	[mm]	*Internal width of the box*

Chamfer of flanges

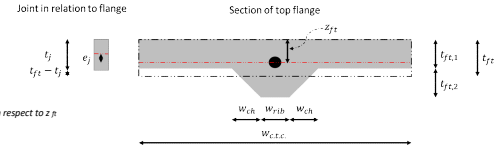
a	0	[mm]	*Width outer chamfer top flange*
b	0	[mm]	*Height outer chamfer top flange*
c	0	[mm]	*Width inner chamfer top flange*
d	0	[mm]	*Height inner chamfer top flange*
e	0	[mm]	*Width inner chamfer bottom flange*
f	0	[mm]	*Height inner chamfer bottom flange*



Top flange - transverse direction

Remark: For top flange with continuous thickness: only enter values tft1 and wc.t.c.!

$w_{c.t.c.}$	1000	[mm]	*Centre to centre distance of the transverse prestressing ribs/ducts*
$t_{ft,1}$	125	[mm]	*Continuous thickness of the top flange*
$t_{ft,2}$	125	[mm]	*Local increase thickness top flange at transverse rib*
w_{rib}	250	[mm]	*Width of the transverse prestressing rib*
w_{ch}	250	[mm]	*Width of chamfer next to the transverse prestressing rib*



Calculated top flange parameters

t_{ft}	187,5	[mm]	*Mean value thickness top flange*
h_b	1512,5	[mm]	*Internal height of the box*
z_{ft}	100,7	[mm]	*Centre of gravity top flange with respect to top fibre*
Δe_{ft}	8,0	[mm]	*Downward eccentricity transverse prestressing with respect to z ft*

Part i [-]	Description [-]	$I_{ft,i}$ [mm⁴]	$A_{ft,i}$ [mm²]	$a_{ft,i}$ [mm]	$I_{ft,i,y}$ [mm⁴]
I	Continuous part top flange	162760417	125000	38,19	3,451E+08
II	Chamfer top flange	27126736	31250	65,97	1,631E+08
III	Rib top flange	40690104	31250	86,81	2,762E+08
Total			187500		7,844E+08

Symbols:

$I_{ft,i}$	*Second moment of area of individual part 'i' of the top flange*
$A_{ft,i}$	*Area of part 'i' of the top flange*
$a_{ft,i}$	*Distance from the centre of gravity of part 'i' to centre of gravity of the top flange section*
$I_{ft,i,y}$	*Contribution part 'i' to second moment of area of section of the top flange*

A_{ft}	187500	[mm²]	*Cross sectional area of top flange section*
I_{ft}	7,844E+08	[mm⁴]	*Second moment of area of top flange section*

Determining global cross sectional properties

Part i [-]	Description [-]	w_i [mm]	h_i [mm]	A_i [mm²]	e_i [mm]	S_i [mm³]	I_i [mm⁴]	a_i [mm]	$I_{i,y,Steiner}$ [mm⁴]	$I_{i,y}$ [mm⁴]
1	Top flange	3200	187,5	600000,0	93,8	5,625E+07	1,758E+09	751	3,382E+11	3,399E+11
2	Web	200	1512,5	302500,0	943,8	2,855E+08	5,767E+10	99	2,980E+09	6,065E+10
3	Bottom flange	2200	200,0	440000,0	1800,0	7,920E+08	1,467E+09	956	4,017E+11	4,032E+11
4	Chamfer top flange out	0	0,0	0,0	187,5	0,000E+00	0,000E+00	657	0,000E+00	0,000E+00
5	Chamfer top flange in	0	0,0	0,0	187,5	0,000E+00	0,000E+00	657	0,000E+00	0,000E+00
6	Chamfer bottom flange in	0	0,0	0,0	1700,0	0,000E+00	0,000E+00	856	0,000E+00	0,000E+00
Total				1342500,0		1,134E+09				8,038E+11

Symbols:

w_i	*Width of part 'i'*
h_i	*Height of part 'i'*
A_i	*Area of part 'i'*
e_i	*Distance from centre of gravity of part 'i' to the top fibre*
S_i	*First moment of area of part 'i' with respect to top fibre*
I_i	*Second moment of area of individual part 'i'*
a_i	*Distance from the centre of gravity of part 'i' to centre of gravity of the cross section*
$I_{i,y,Steiner}$	*Steiner part of part 'i'to the second moment of area of the cross section*
$I_{i,y}$	*Contribution part 'i' to second moment of area of cross section*

Main parameters

A_c	1342500,0	[mm²]	*Cross sectional area of total cross section*
z	844,5	[mm]	*Position centre of gravity from the top flange*
I_y	8,038E+11	[mm⁴]	*Second moment of area of the combined cross section*
z_t	844,5	[mm]	*Distance from centre of gravity to top fibre*
z_b	1055,5	[mm]	*Distance from centre of gravity to bottom fibre*
$W_{y,t}$	9,518E+08	[mm³]	*Section modulus with respect to top fibre*
$W_{y,b}$	7,615E+08	[mm³]	*Section modulus with respect to bottom fibre*

Cross sectional properties end cross beams

Main dimensions

h_{cb}	1900	[mm]	*Total height of the end cross beam*
w_{cb}	1900	[mm]	*Total width of the end cross beam*

Determining cross sectional properties

A_{cb}	3610000	[mm²]	*Cross sectional area of the cross beam*
$W_{y,cb}$	1,143E+09	[mm³]	*Section modulus of the cross section*
$I_{y,cb}$	1,086E+12	[mm⁴]	*Second moment of area of the cross section*

Cross sectional properties longitudinal joints

Main dimensions

t_j	162,5	[mm]	*Height of the longitudinal joint*
w_j	90	[mm]	*Transverse width of the longitudinal joint*

Determining cross sectional properties

A_j	162500	[mm²]	*Cross sectional area of the longitudinal joint*
W_j	4,401E+06	[mm³]	*Section modulus of the longitudinal joint*
I_j	3,576E+08	[mm⁴]	*Second moment of the cross section of the longitudinal joint*

Material and calculation parameters

Concrete

Material properties concrete main beams (Ductal FM)

Parameters mixture composition

ρ	25	[kN/m³]	*Density*
l_f	13	[mm]	*Fibre length*

Parameters concrete in compression

f_{ck}	200	[N/mm²]	*Characteristic value compressive strength*
ε_{c3}	2,3	[‰]	*Strain at reaching concrete compressive strength*
ε_{cu3}	2,6	[‰]	*Maximum compressive strain at ULS*

Parameters concrete in tension

$f_{ctk,el}$	9	[N/mm²]	*Characteristic elastic (5% percentile value) tensile strength*
f_{ctfk}	10	[N/mm²]	*Characteristic value maximal post cracking stress (w=0,30)*
α_{global}	1,25	[-]	*Fibre orientation factor (global)*
K_{local}	1,75	[-]	*Fibre orientation factor (local)*

Parameters stiffness and deformations (temperature, creep and shrinkage)

E_{cm}	50000	[N/mm²]	*Modulus of elasticity*
G	20833	[N/mm²]	*Shear modulus*
ν	0,2	[-]	*Poisson ratio*
α	0,000012	[K-1]	*Coefficient of thermal expansion*
φ	0,3	[-]	*Creep*
ε_{shr}	0,8	[‰]	*Autogenous shrinkage (during HT)*

Parameters concrete other

α	0,56	[-]	*Factor for shape of concrete compressive zone*
β	0,34	[-]	*Factor position centre of gravity concrete compressive zone*
α_{cc}	0,85	[-]	*Long term effects and unfavourable loading (compression)*
α_{ct}	1,0	[-]	*Long term effects and unfavourable loading (tension)*

Parameters fatigue

$\beta_{cc}(t)$	1,0	[-]	*Factor for increase of strength due to progressive hydration*
f_{ck0}	10	[N/mm²]	*Standard value (10 Mpa)*

Calculated values

f_{cd}	113	[N/mm²]	*Design value concrete compressive strength*
f_{ctd}	6,0	[N/mm²]	*Design value of tensile strength (tensile strength 1st crack)*
$f_{ctd,2}$	6,15	[N/mm²]	*Design value maximal post cracking stress (at w=0,30)*

Concrete longitudinal joints

Parameters mixture composition

ρ	25	[kN/m³]	*Density*

Parameters concrete in compression

f_{ck}	100	[N/mm²]	*Characteristic value compressive strength*
ε_{cu3}	2,6	[‰]	*Maximum compressive strain at ULS*

Parameters stiffness and deformations (temperature, creep and shrinkage)

E_{cm}	45000	[N/mm²]	*Modulus of elasticity*
φ	0,8	[-]	*Creep factor*
ε_{cs}	0,8	[‰]	*Shrinkage (long term)*

Parameters concrete other

α	0,56	[-]	*Factor for shape of concrete compressive zone*
β	0,34	[-]	*Factor position centre of gravity concrete compressive zone*
α_{cc}	0,85	[-]	*Long term effects and unfavourable loading (compression)*

Calculated values

f_{cd}	57	[N/mm²]	*Design value concrete compressive strength*

Material properties concrete end cross beams

Parameters mixture composition

ρ	25	[kN/m³]	*Density*

Parameters concrete in compression

f_{ck}	30	[N/mm²]	*Characteristic cylinder compressive strength at 28 days*
$f_{ck,cube}$	37	[N/mm²]	*Characteristic cube compressive strength*
f_{cm}	38	[N/mm²]	*Mean value cylinder compressive strength*
ε_{c3}	1,75	[‰]	*Strain at reaching concrete compressive strength*
ε_{cu3}	3,5	[‰]	*Maximum compressive strain at ULS*

Parameters concrete in tension

f_{ctm}	2,9	[N/mm²]	*Mean value axial tensile strength*
$f_{ctk,0,05}$	2,0	[N/mm²]	*5%-fractile of the axial tensile strength*

Parameters stiffness and deformations (temperature, creep and shrinkage)

E_{cm}	33000	[N/mm²]	*Secant modulus of elasticity*
φ	1,75	[-]	*Creep*
Hydration	Normal (N)	[-]	*Rate of hydration: Rapid (R), Normal (N) or slow (S)*
RH	80,0	[%]	*Relative humidity*

Parameters concrete other

α	0,75	[-]	*Factor for shape of concrete compressive zone*
β	0,39	[-]	*Factor position centre of gravity concrete compressive zone*
α_{cc}	1,0	[-]	*Long term effects and unfavourable loading (compression)*

Calculated values

f_{cd}	20	[N/mm²]	*Design value concrete compressive strength*

Prestressing steel & parameters strands and tendons

Parameters prestressing main beams

Parameters transverse prestressing

Parameters prestressing end cross beams

Material properties prestressing steel

f_{pk}	1860	[N/mm²]	Characteristic value tensile strength
f_{pd}	1522	[N/mm²]	Design value steel stress
σ_{pm0}	1395	[N/mm²]	Maximum allowed stress directly after tensioning
$\sigma_{p,max}$	1488	[N/mm²]	Maximum prestressing stress during tensioning
E_p	195000	[N/mm²]	Modulus of elasticity
ε_{uk}	35	[‰]	Characteristic value strain at failure

Properties prestressing strands

n_c	10	[pcs]	Assumed number of strands positioned centrically in the cross section
$D_{strand,c}$	15,2	[mm]	Diameter of strands positioned centrically
$A_{p,strand,c}$	140	[N/mm²]	Cross sectional area per strand
$\sigma_{p,max,prov,c}$	1400	[mm²]	Assumed maximum stress applied to centrically positioned strands
n_{fb}	105	[pcs]	Assumed number of strands positioned in bottom flange
$D_{strand,fb}$	15,2	[mm]	Diameter of strands positioned in bottom flange
$A_{p,strand,fb}$	140	[N/mm²]	Cross sectional area per strand
$\sigma_{p,max,prov,fb}$	1488	[mm²]	Assumed maximum stress applied to strands in bottom flange
Relaxation	Class 2	[-]	Select relaxation class: normal (1), low (2) or bars (3)
t	500000	[h]	The value of the relaxation loss (in %) at 1000 h
ρ	2,5	[%]	Time after stressing (to determine final value of the relaxation loss)
t_{eq}	461935	[h]	Equivalent time (optional), NOTE: Calculated manually!

Parameters detailing beam ends

η	1,35	[-]	Bond factor conforming table 7.2 of AFGC-SETRA 2013
η_1	1,0	[-]	Factor accounting for bond conditions, cf EC2-1-1
κ	1,5	[-]	Factor for bond strength improvement due to the presence of fibres
α_1	1,0	[-]	Factor depending on way of releasing the strands
α_2	0,19	[-]	Factor depending on the type of tendon
$n_{fb,1}$	105	[pcs]	Selected number of strands introduced in first set
$n_{fb,2}$	0	[pcs]	Selected number of strands introduced in second set (optional)
$x_{debond,1}$	0	[m]	Length over which first set of strands is debonded (optional)
$x_{debond,2}$	0,0	[m]	Length over which second set of strands is debonded (optional)

Parameters fatigue verification

$\Delta\sigma_{Rsk}$	185	[N/mm²]	Stress range at N* cycles
N^*	1000000	[-]	Number of cycles with single stress range
k_1	5	[-]	Stress exponent first branch
k_2	9	[-]	Stress exponent second branch

Material properties prestressing steel

f_{pk}	1860	[N/mm²]	Characteristic value tensile strength
f_{pd}	1522	[N/mm²]	Design value steel stress
σ_{pm0}	1395	[N/mm²]	Maximum allowed stress directly after tensioning
$\sigma_{p,max}$	1488	[N/mm²]	Maximum prestressing stress during tensioning
E_p	195000	[N/mm²]	Modulus of elasticity
ε_{uk}	35	[‰]	Characteristic value strain at failure

Properties prestressing tendons

n	4	[pcs]	Assumed number of strands per tendon
D_{strand}	15,2	[mm]	Diameter of single strand
$A_{p,strand}$	140	[mm²]	Cross sectional area per strand
$\sigma_{p,max,prov}$	1400	[N/mm²]	Assumed maximum stress applied to prestressing element
μ	0,23	[-]	Friction coefficient
k	0,009	[rad]	Unintentional angular rotation due to the Wobble-effect
w_{set}	3	[mm]	Estimated wedge set
Relaxation	Class 2	[-]	Select relaxation class: normal (1), low (2) or bars (3)
t	500000	[h]	The value of the relaxation loss (in %) at 1000 h
ρ	2,5	[%]	Time after stressing (for final value of the relaxation loss)

Material properties prestressing steel

f_{pk}	1860	[N/mm²]	Characteristic value tensile strength
f_{pd}	1522	[N/mm²]	Design value steel stress
σ_{pm0}	1395	[N/mm²]	Maximum allowed stress directly after tensioning
$\sigma_{p,max}$	1488	[N/mm²]	Maximum prestressing stress during tensioning
E_p	195000	[N/mm²]	Modulus of elasticity
ε_{uk}	35	[‰]	Characteristic value strain at failure

Properties prestressing tendons

n_{ducts}	4	[pcs]	Number of ducts in total
α_{vert}	500	[mm]	Vertical position centre of duct from centre of beam
α_{hor}	750	[mm]	Horizontal position centre of duct from centre of beam
n_{strand}	4	[pcs]	Assumed number of strands per tendon
D_{strand}	15,2	[mm]	Diameter of single strand
$A_{p,strand}$	140	[mm²]	Cross sectional area per strand
$\sigma_{p,max,prov}$	1400	[N/mm²]	Assumed maximum stress applied to prestressing element
$\emptyset_{Duct}$	65	[mm]	Outer diameter of prestressing ducts
μ	0,23	[-]	Friction coefficient
k	0,009	[rad]	Unintentional angular rotation due to the Wobble-effect
w_{set}	3	[mm]	Estimated wedge set
Relaxation	Class 2	[-]	Select relaxation class: normal (1), low (2) or bars (3)
t	500000	[h]	The value of the relaxation loss (in %) at 1000 h
ρ	2,5	[%]	Time after stressing (for final value of the relaxation loss)

Partial factors material resistance

γ_C	1,5	[-]	Partial factor concrete (cf EC2)
γ_{cf}	1,3	[-]	Partial factor for fibre reinforced concrete in tension (cf AFGC)
$\gamma_E * \gamma_{cf}$	1,5	[-]	Product of partial factor for uncertainty in extrapolation * factor Ycf
γ_S	1,1	[-]	Partial factor prestressing steel (cf EC2)
$\gamma_{F,fat}$	1,0	[-]	See 2.4.2.3 of NA to NEN-EN 1992-1-1
$\gamma_{S,fat}$	1,1	[-]	See 2.4.2.4 of NA to NEN-EN 1992-1-1
γ_{spl}	1,2	[-]	Partial factor splitting forces

Calculation parameters

Calculation parameters main beams

σ_{max}	6,7	[N/mm²]	Maximum allowed stress at outer concrete fibres
θ	30	[°]	Angle of the concrete compressive strut of the main beams
$c_{nom,s}$	35	[mm]	Minimum applied cover onto strands bottom flange (all sides)
$c_{nom,r}$	30	[mm]	Minimum applied cover onto rebars bottom flange (all sides)
$\emptyset_{spl,f1}$	10	[mm]	Assumed diameter splitting reinforcement bottom flange
μ	0,5	[-]	Friction coefficient concrete and supports
$1/\delta$	300	[-]	Maximum deflection in SLS

Calculation parameters longitudinal joints and top flange

$\emptyset_{spl,ft}$	10	[mm]	Assumed diameter splitting reinforcement top flange
h_1	100	[mm]	Anchor plate (height and width)

Calculation parameters end cross beams

k_1	0,15	[-]	Factor from 6.2.2 of the NA to NEN-EN 1992-1-1
θ	21,8	[°]	Angle concrete compressive strut of end cross beam

Design of bridge and main carriageway - Actions

Design main carriageway

Kerbs

h_{kerb}	340	[mm]	Assumed height of the kerb
w_{kerb}	500	[mm]	Assumed width of the kerb
ρ_C	25	[kN/m³]	Density of the concrete used

Road surface

t_{surf}	10	[mm]	Assumed thickness of the surface layer
$\rho_{asphalt}$	23	[kN/m³]	Density of the material used

Effective width of the beams

$b_{eff,0}$	3,245	[m]	Effective width of the outer beams to determine loads
$b_{eff,i}$	3,29	[m]	Effective width of the inner beams to determine loads

Permanent actions (G)

Self-weight prefab beams

$G_{k,beam}$	33,56	[kN/m]	Line load representing the self-weight of the prefab beams

Permanent load road surface

$G_{k,surf}$	0,23	[kN/m²]	Area load representing the surface layer

Self-weight end cross beams

$G_{k,cb}$	90,25	[kN/m]	Line load representing the self-weight of the end cross beams

Permanent load kerbs

A_{kerb}	0,17	[m²]	Cross sectional area of the kerb
$G_{k,kerb}$	8,5	[kN/m²]	Area load representing the kerb

Self-weight longitudinal joints

A_j''	0,016875	[m²]	Area of the total joint using tft and wj
$G_{k,j}$	0,421875	[kN/m]	Line load representing the self-weight of the joints

Variable actions (Q)

Load model 1

Lane	Q_{ik} [kN]	q_{ik} [kN/m²]
1	291	8,73
2	194	2,425
rk	0	2,25

Load model 2

$\beta_Q Q_{ak}$	388	[kN/axle]	Axle load according to LM2

Accidental actions (A)

F_{equi}	1000	[kN]	Equivalent static force, see: (4) of 4.6.2. EC1-1-7

Fatigue

n_y	100	[-]	Design service life
N_{obs}	500000	[-]	Number of heavy vehicles per year

Combinations of actions

γ_G	1,4	[-]	See tabel NB.16 – A2.4(B) of NA to NEN-EN 1990
$\zeta * \gamma_G$	1,25	[-]	See tabel NB.16 – A2.4(B) of NA to NEN-EN 1990
γ_P	1,0	[-]	See 2.4.2.2 of NA to NEN-EN 1992-1-1
γ_Q	1,5	[-]	See tabel NB.16 – A2.4(B) of NA to NEN-EN 1990
ψ_0	0,8	[-]	See tabel NB.12 – A2.1 of NA to NEN-EN 1990
ψ_1	0,8	[-]	See tabel NB.12 – A2.1 of NA to NEN-EN 1990

Determining force distribution (RFEM input)

Design of main prestressing and verification capacity of the main beams

Ultimate limit state verifications main beams

M_{Ed}	41753	[kNm]	Governing bending moment value (mid span)
V_{Ed}	3632	[kN]	Governing shear force value (near supports)
T_{Ed}	1268	[kNm]	Governing torsional moment

Serviceability limit state - Design of prestressing (characteristic combination)

$M_{E,G,perm}$	1725	[kNm]	Bending moment imposed permanent loads in SLS at midspan
$M_{E,Q}$	9553	[kNm]	Bending moment variable loads in SLS at midspan

Serviceability limit state - Deflections (frequent combination)

δ_{max}	440,9	[mm]	Max. deflection at midspan in SLS (frequent combination)

Fatigue analysis main beams

$M_{fat,max}$	26812	[kNm]	Maximum bending moment at midspan (found using RFEM)
$M_{fat,min}$	22543	[kNm]	Minimum bending moment at midspan (found using RFEM)

Design of prestressing and verification capacity of the end cross beams

Ultimate limit state verifications end beams

$M_{Ed,hog}$	1271	[kNm]	Maximum hogging bending moment (all loads considered)
$M_{Ed,sag}$	396	[kNm]	Maximum sagging bending moment (all loads considered)
V_{Ed}	846	[kN]	Maximum shear force (all loads considered)

Serviceability limit state - Design of prestressing

$M_{E,hog}$	453	[kNm]	Maximum hogging bending moment SLS
$M_{E,sag}$	270	[kNm]	Maximum sagging bending moment SLS

Design Calculations Optimization - Design of main beams - Main prestressing and ULS (STR)

Project: MSc thesis "Redesign of bridges Twentekanaal in UHPC"
Name: M. Dorland
Date: 22-12-2020
Version: D1.0

Input parameters

Input parameters - Cross sectional properties and calculation parameters

Cross sectional properties

A_c	1342500	[mm²]	*Cross sectional area of total cross section*
z_c	844,5	[mm]	*Distance from centre of gravity to top fibre*
e_p	955,51	[mm]	*Eccentricity of tendons in bottom flange*
I_y	8,038E+11	[mm⁴]	*Second moment of area of the combined cross section*
$W_{y,t}$	9,518E+08	[mm³]	*Section modulus with respect to top fibre*
$W_{y,b}$	7,615E+08	[mm³]	*Section modulus with respect to bottom fibre*

Calculation parameters

θ	30	[°]	*Angle of the concrete compressive strut of the main beams*

Input parameters - Material properties & main prestressing

Concrete

Parameters mixture composition

ρ	25	[kN/m³]	*Density*
l_f	13	[mm]	*Fibre length*

Parameters concrete in compression

f_{ck}	200	[N/mm²]	*Characteristic value compressive strength*
ε_{c3}	2,3	[‰]	*Strain at reaching concrete compressive strength*
ε_{cu3}	2,6	[‰]	*Maximum compressive strain at ULS*

Parameters concrete in tension

$f_{ctk,el}$	9	[N/mm²]	*Characteristic elastic (5% percentile value) tensile strength*
f_{ctfk}	10	[N/mm²]	*Characteristic value maximal post cracking stress (w=0,30)*
K_{global}	1,25	[-]	*Fibre orientation factor (global)*
K_{local}	1,75	[-]	*Fibre orientation factor (local)*

Parameters stiffness and deformations (temperature, creep and shrinkage)

E_{cm}	50000	[N/mm²]	*Modulus of elasticity*
G	20833	[N/mm²]	*Shear modulus*
ν	0,2	[-]	*Poisson ratio*
α	0,000012	[K-1]	*Coefficient of thermal expansion*
φ	0,3	[-]	*Creep*
ε_{shr}	0,8	[‰]	*Autogenous shrinkage (during HT)*

Parameters concrete other

α	0,56	[-]	*Factor for shape of concrete compressive zone*
β	0,34	[-]	*Factor position centre of gravity concrete compressive zone*
α_{cc}	0,85	[-]	*Long term effects and unfavouurable loading (compression)*
α_{ct}	1	[-]	*Long term effects and unfavouurable loading (tension)*

Calculated design values

f_{cd}	113	[N/mm²]	*Design value concrete compressive strength*
f_{ctd}	6,0	[N/mm²]	*Design value of tensile strength (tensile strength 1st crack)*
$f_{ctd;2}$	6,15	[N/mm²]	*Design value maximal post cracking stress (at w=0,30)*

Parameters main prestressing

Material properties prestressing steel

f_{pk}	1860	[N/mm²]	*Characteristic value tensile strength*
f_{pd}	1522	[N/mm²]	*Design value steel stress*
σ_{pm0}	1395	[N/mm²]	*Maximum allowed stress directly after tensioning*
$\sigma_{p,max}$	1488	[N/mm²]	*Maximum prestressing stress during tensioning*
E_p	195000	[N/mm²]	*Modulus of elasticity*
ε_{uk}	35	[‰]	*Characteristic value strain at failure*

Parameters prestressing strands

n_c	10	[-]	*Assumed number of strands positioned centrically in the cross section*
$D_{strand,c}$	15,2	[mm]	*Diameter of strands positioned centrically*
$A_{p,strand,c}$	140	[N/mm²]	*Cross sectional area per strand*
$\sigma_{p,max,prov,c}$	1400	[mm²]	*Assumed maximum stress applied to centrically positioned strands*
n_{fb}	105	[-]	*Assumed number of strands positioned in bottom flange*
$D_{strand,fb}$	15,2	[mm]	*Diameter of strands positioned in bottom flange*
$A_{p,strand,fb}$	140	[N/mm²]	*Cross sectional area per strand*
$\sigma_{p,max,prov,fb}$	1488	[mm²]	*Assumed maximum stress applied to strands positioned in bottom flange*
Relaxation	Class 2	[-]	*Select relaxation class: normal (1), low (2) or bars (3)*
t	500000	[h]	*The value of the relaxation loss (in %) at 1000 h*
ρ	2,5	[%]	*Time after stressing (to determine the final value of the relaxation loss)*
t_{eq}	461935	[h]	*Equivalant time, NOTE: Calculated manually!*

Parameters detailing beam ends

η	1,35	[-]	*Bond factor conforming table 7.2 of AFGC-SETRA 2013*
η_1	1,0	[-]	*Factor accounting for bond conditions, cf EC2-1-1*
κ	1,5	[-]	*Factor for bond strength improvement due to the presence of fibres*
α_1	1,0	[-]	*Factor depending on way of releasing the strands*
α_2	0,19	[-]	*Facor depending on the type of tendon*
$n_{fb,1}$	105	[pcs]	*Selected number of strands introduced in first set*
$n_{fb,2}$	0	[pcs]	*Selected number of strands introduced in second set*
$x_{debond,1}$	0	[m]	*Length over which first set of strands is debonded*
$x_{debond,2}$	0	[m]	*Length over which second set of strands is debonded*

Other parameters

γ_C	1,5	[-]	*Partial factor concrete (cf EC2)*
γ_{cf}	1,3	[-]	*Partial factor for fibre reinforced concrete in tension*
$\gamma_E * \gamma_{cf}$	1,5	[-]	*Product of partial factors (AFGC-SETRA 2013)*
γ_S	1,1	[-]	*Partial factor prestressing steel (cf EC2)*
γ_{spl}	1,2	[-]	*Partial factor splitting forces*

Input parameters - Loads

$M_{E,G,sw}$	19399	[kNm]	*Bending moment midspan due to self-weight of the beams in SLS*
$M_{E,G,perm}$	1725	[kNm]	*Bending moment mid span due to imposed permanent loads in SLS (RFEM)*
$M_{E,Q}$	9553	[kNm]	*Bending moment due to variable loads in SLS (RFEM)*

Design of the main prestressing

Calculating prestress losses

Applied maximum force onto prestressing element & stress verification

$\sigma_{p,max,prov,c}$	1400	[mm²]	*Assumed maximum stress applied to centrically positioned strands*
$P_{max,prov,c}$	1960	[kN]	*Assumed maximum force applied to centrically positioned strands*
$\sigma_{p,max,prov,fb}$	1488	[mm²]	*Assumed maximum stress applied to strands positioned in bottom flange*
$P_{max,prov,fb}$	21873,6	[kN]	*Assumed maximum force applied to strands positioned in bottom flange*

Verification maximum stress prestressing steel

$\sigma_{p,max,prov,c}$	1400,00	[N/mm²]	*Assumed maximum stress applied to centric prestressing*
Verification	Satisfied	[-]	*Verification*
$\sigma_{p,max,prov,fb}$	1488	[N/mm²]	*Assumed maximum stress applied to strands positioned in bottom flange*
Verification	Satisfied	[-]	*Verification*

Verifications maximum concrete compressive stress

$\sigma_{c,prov,c+fb}$	45,20	[N/mm²]	*Maximum compressive stress in concrete due to prestressing*
$\sigma_{c,limit}$	140,00	[N/mm²]	*Maximum value concrete compressive stress*
Verification	Satisfied	[-]	*Verification*

Applied value maxinum force applied onto prestressing strands

$\sigma_{p,max,c}$	1400,00	[N/mm²]	*Applied value maximum stress centric prestressing*
$A_{p,c}$	1400	[mm²]	*Applied cross section centric prestressing*
$P_{max,c}$	1960,00	[kN]	*Applied value maximum force centric prestressing*
$\sigma_{p,max,fb}$	1488,00	[N/mm²]	*Applied value maximum stress eccentric prestressing*
$A_{p,fb}$	14700	[mm²]	*Applied cross section eccentric prestressing*
$P_{max,fb}$	21873,60	[kN]	*Applied value maximum force eccentric prestressing*

Direct prestressing losses

Elastic losses centric prestressing

α_e	3,90	[-]	*Ratio moduli of elasticity*
$\rho_{p,c}$	0,0010	[-]	*Ratio of cross section steel and concrete*
I_c	NA	[-]	*Factor for eccentricity*
$\Delta P_{el,c}$	7,94	[kN]	*Elastic loss centric prestressing*

Elastic losses eccentric prestressing flange

α_e	3,90	[-]	*Ratio moduli of elasticity*
$\rho_{p,fb}$	0,0109	[-]	*Ratio of cross section steel and concrete*
I_{fb}	2,52	[-]	*Factor for eccentricity*
$\Delta P_{el,fb}$	2128,97	[kN]	*Elastic loss eccentric prestressing*

Determining initial prestressing force & stress verification

Applied force and stress values

$P_{m0,c}$	1952	[kN]	*Initial prestressing force centric prestressing*
$\sigma_{pm0,c}$	1394	[N/mm²]	*Initial prestressing stress centric prestressing*
$P_{m0,fb}$	19745	[kN]	*Initial prestressing force eccentric prestressing*
$\sigma_{pm0,fb}$	1343	[N/mm²]	*Initial prestressing stress eccentric prestressing*

Stress limit and verification

Verification	Satisfied	[-]	*Verification initial prestressing stress (centric prestressing)*
Verification	Satisfied	[-]	*Verification initial prestressing stress (eccentric prestressing)*

Verified values initial prestressing force

$P_{m0,c}$	1952	[kN]	*Applied value initial prestressing force centric prestressing*
$\sigma_{pm0,c}$	1394	[N/mm²]	*Applied value initial stress centric prestressing*
$P_{m0,fb}$	19745	[kN]	*Applied value initial prestressing force eccentric prestressing*
$\sigma_{pm0,fb}$	1343	[N/mm²]	*Applied value initial stresseccentric prestressing*

Time dependent losses

Centric prestressing - Relaxation

Class	Class 2	[-]	*Relaxation class (normal relaxation, low relaxation and bars)*
ρ_{1000}	2,5	[%]	*The value of the relaxation loss (in %) at 1000 h*
μ_c	0,75	[-]	*Factor depending on steel stresses*
t	961935	[h]	*Time after stressing (for final value of the relaxation loss)*
$\Delta\sigma_{pr,c}/\sigma_{pi,c}$	0,055	[-]	*Relaxation coefficient*
$\sigma_{pi,c}$	1394,3	[N/mm²]	*Absolute value of the initial prestressing (σ_pm0)*
$\Delta\sigma_{pr,c}$	76,7	[N/mm²]	*Prestress loss due to relaxation*

Centric prestressing - Accounting for heat treatment (if applicable)

t_{eq}	461935	[h]	*Equivalant time, NOTE: Calculated manually!*

Centric prestressing - Relaxation classes

Class 1	Wires and strands normal relaxation
Class 2	Wires and strands low relaxation
Class 3	Bars

Centric prestressing - Creep & shrinkage

φ	0,3	[-]	*Creep factor*
$\sigma_{c,QP,c}$	16,2	[N/mm²]	*Stress in concrete adjacent to centric prestressing strands*
ε_{cs}	0,0008	[-]	*Shrinkage of the concrete*

Centric prestressing - Total time dependent losses

$\Delta\sigma_{p,c+s+r,c}$	235,1	[N/mm²]	*Time dependent prestressing losses (stress, centric)*
$\Delta P_{p,c+s+r,c}$	329,1	[kN]	*Time dependent prestressing losses (force, centric)*

Eccentric prestressing flange - Relaxation

Class	Class 2	[-]	*Relaxation class (normal relaxation, low relaxation and bars)*
ρ_{1000}	2,5	[%]	*The value of the relaxation loss (in %) at 1000 h*
μ_{fb}	0,72	[-]	*Factor depending on steel stresses*
t	961935	[h]	*Time after stressing (for final value of the relaxation loss)*
$\Delta\sigma_{pr,fb}/\sigma_{pi,fb}$	0,049	[-]	*Relaxation coefficient*
$\sigma_{pi,fb}$	1343,2	[N/mm²]	*Absolute value of the initial prestressing (σ_pm0)*
$\Delta\sigma_{pr,fb}$	66,3	[N/mm²]	*Prestress loss due to relaxation*

Eccentric prestressing flange - Accounting for heat treatment (if applicable)

t_{eq}	461935	[h]	*Equivalant time, NOTE: Calculated manually!*

Eccentric prestressing flange - Relaxation classes

Class 1	Wires and strands normal relaxation
Class 2	Wires and strands low relaxation
Class 3	Bars

Eccentric prestressing flange - Creep & shrinkage

φ	0,3	[-]	*Creep factor*
$\sigma_{c,QP,fb}$	38,6	[N/mm²]	*Stress in concrete adjacent to eccentric prestressing strands*
ε_{cs}	0,0008	[-]	*Shrinkage of the concrete*

Eccentric prestressing flange - Total time dependent losses

$\Delta\sigma_{p,c+s+r,fb}$	224,2	[N/mm²]	*Time dependent prestressing losses (stress, eccentric)*
$\Delta P_{p,c+s+r,fb}$	3295,5	[kN]	*Time dependent prestressing losses (force, eccentric)*

Working prestress force and total prestress losses

$P_{m,\infty,c}$	1623	[kN]	*Working prestressing force centric prestressing*
$\sigma_{pm,\infty,c}$	1159	[N/mm²]	*Working prestressing stress centric prestressing*
$P_{m,\infty,fb}$	16449	[kN]	*Working prestressing force eccentric prestressing*
$\sigma_{pm,\infty,fb}$	1119	[N/mm²]	*Working prestressing stress eccentric prestressing*

Summary of results (middle cross section)

	Prestressing forces			Prestress losses forces			
	P_{max}	P_{m0}	$P_{m,\infty}$	ΔP_i	$\Delta P_{p,c+s+r}$	ΔP_{tot}	$\Delta P_{\%}$
Prestressing:	[kN]	[kN]	[kN]	[kN]	[kN]	[kN]	[%]
Centric	1960	1952	1623	8	329	337	17,2
Eccentric	21874	19745	16449	2129	3295	5424	24,8

	Prestressing stresses			Prestress losses forces			
	σ_{max}	σ_{pm0}	$\sigma_{pm,\infty}$	$\Delta\sigma_i$	$\Delta\sigma_{p,c+s+r}$	$\Delta\sigma_{tot}$	$\Delta\sigma_{\%}$
Prestressing:	[N/mm²]	[N/mm²]	[N/mm²]	[N/mm²]	[N/mm²]	[N/mm²]	[%]
Centric	1400	1394	1159	6	235	241	17,2
Eccentric	1488	1343	1119	145	224	369	24,8

Determining stresses at midspan

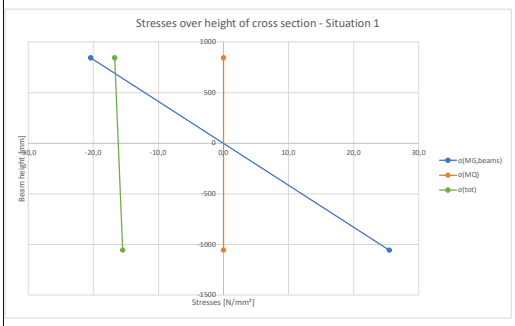
σ_{max}	6,7	[N/mm²]	*Maximum tensile stress allowed at outer fibres*

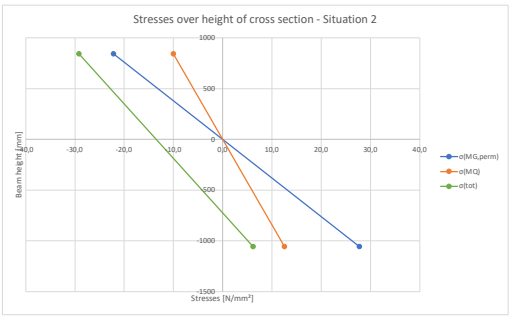
Stresses situation 1

Stresses situation 2

	Height [mm]	σ(MG,beams) [N/mm²]	σ(MQ) [N/mm²]	σ(Pt) [N/mm²]	σ(Pfb) [N/mm²]	σ(Mr,fb) [N/mm²]	σ(tot) [N/mm²]
Top fibre	844	-20,4	0,0	-1,5	-14,7	19,8	-16,7
Bottom fibre	-1056	25,5	0,0	-1,5	-14,7	-24,8	-15,5
Maximum	1900						-15,5

	Height [mm]	σ(MG,perm) [N/mm²]	σ(MQ) [N/mm²]	σ(Pt) [N/mm²]	σ(Pfb) [N/mm²]	σ(Mr,fb) [N/mm²]	σ(tot) [N/mm²]
Top fibre	844	-22,2	-10,0	-1,2	-12,3	16,5	-29,2
Bottom fibre	-1056	27,7	12,5	-1,2	-12,3	-20,6	6,2
Maximum	1900						6,2





Detailing beam ends

Bond stresses and transmission length

Determining bond stress

η	1,35	[-]	*Bond factor conforming table 7.2 of AFGC-SETRA 2013*
η_1	1,0	[-]	*Factor accounting for bond conditions, cf EC2-1-1*
κ	1,5	[-]	*Factor for bond strength improvement due to the presence of fibres*
f_{ctd}	6,0	[N/mm²]	*Design value tensile strength*
f_{bpt}	12,15	[N/mm²]	*Bond strength*

Transmission length centric prestressing

α_1	1,0	[-]	*Factor depending on way of releasing the strands*
α_2	0,19	[-]	*Facor depending on the type of tendon*
Ø	15,2	[-]	*Diameter of the prestressing element*
σ_{pm0}	1394,3	[N/mm²]	*Stress in tendon just after release (i.e. initial stress)*
$l_{pt,c}$	331,4	[mm]	*Transfer length*
$l_{pt1,c}$	0,133	[m]	*Design value transmission length centric prestressing*

Transmission length eccentric prestressing

α_1	1,0	[-]	*Factor depending on way of releasing the strands*
α_2	0,19	[-]	*Facor depending on the type of tendon*
Ø	15,2	[-]	*Diameter of the prestressing element*
σ_{pm0}	1343,2	[N/mm²]	*Stress in tendon just after release (i.e. initial stress)*
$l_{pt,fb}$	319,3	[mm]	*Transfer length*
$l_{pt1,fb}$	0,128	[m]	*Design value transmission length eccentric prestressing*

Tensile stresses at top fibre

Centric prestressing

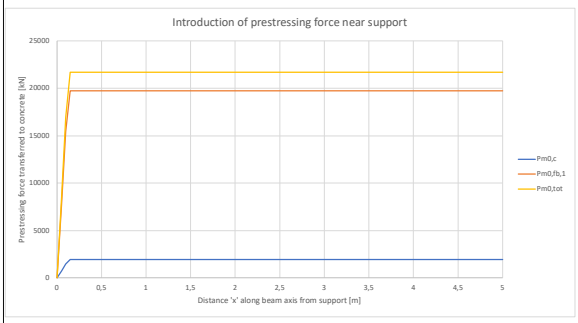
P_{m0}	1952	[kN]	*Initial prestressing force centric prestresssing*
$l_{pt1,c}$	0,133	[m]	*Design value transmission length centric prestressing*

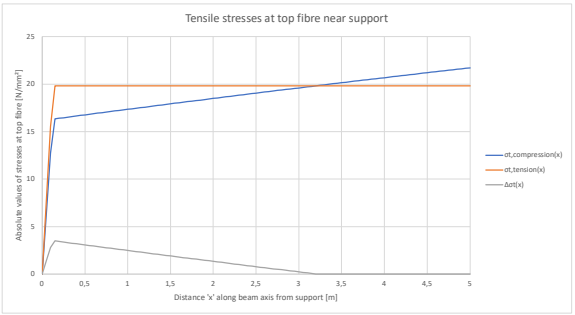
Eccentric prestressing

n_{fb}	105	[pcs]	*Total number of strands in bottom flange*
$n_{fb,1}$	105	[pcs]	*Selected number of strands introduced in first set*
$n_{fb,2}$	0	[pcs]	*Selected number of strands introduced in second set*
$x_{debond,1}$	0	[m]	*Length over which first set of strands is debonded*
$x_{debond,2}$	0	[m]	*Length over which second set of strands is debonded*

Parameters sets of strands eccentric prestressing

$P_{m0,fb}$	19745	[kN]	*Total initial prestressing force eccentric prestressing*
$P_{m0,fb,1}$	19745	[kN]	*Initial prestressing force first set of strands*
$P_{m0,fb,2}$	0	[kN]	*Initial prestressing force second set of strands*
$l_{pt1,fb}$	0,128	[m]	*Design value transmission length eccentric prestressing*





Verification remaining tensile stress

$\Delta\sigma_t$	3,5	[N/mm²]	*Highest value remaining tensile stress*
σ_{max}	6,7	[N/mm²]	*Maximum allowable tensile stress*
Verification	Satisfied	[-]	*Verification*

Positioning of strands in the bottom flange

Auxiliary parameters (dimensions and cover)

h	1900	[mm]	*Total height*
w_b	2000	[mm]	*Internal width of the box*
b	2200	[mm]	*Width lower end of beam (webs and internal width)*
w_{cb}	1900	[mm]	*Total width end cross beam (solid part)*
t_{fb}	200	[mm]	*Thickness bottom flange*
t_w	100	[mm]	*Thickness of web*
$c_{nom,s}$	35	[mm]	*Minimum applied cover onto strands bottom flange (all sides)*
$c_{nom,r}$	30	[mm]	*Minimum applied cover onto rebars bottom flange (all sides)*
$Ø_r$	10	[mm]	*Assumed diameter splitting reinforcement bottom flange*

Positioning of the strands - Parameters

$D_{strand,fb}$	15,2	[mm]	*Assumed strand diameter*
$c_{prov,s}$	40	[mm]	*Applied cover onto the strands (all sides)*
s_{min}	30,4	[mm]	*Assumed minimum spacing (horizontal and vertical)*
d_{min}	45,6	[mm]	*Minimum c.t.c. distance in horizontal and vertical direction*
$h_{available}$	120	[mm]	*Available height bottom flange for positioning of the strands*
$w_{available}$	2120	[mm]	*Available width bottom flange for positioning of the strands*
$n_{max,rows}$	3	[pcs]	*Maximum number of rows in bottom flange*
$n_{max,strands}$	47	[pcs]	*Maximum number of strands per row in bottom flange*
$n_{max,fb}$	141	[pcs]	*Maximum allowable number of strands in bottm flange*

Positioning of the strands - Applied values

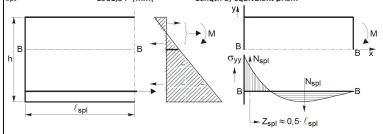
n_{fb}	105	[pcs]	*Total number of strands in bottom flange*
n_{rows}	3	[pcs]	*Required number of rows*
$n_{strands}$	35	[pcs]	*Number of strands per row*
d_{vert}	52,40	[mm]	*Applied vertical c.t.c. distance between the applied strands*
d_{hor}	61,91	[mm]	*Applied horizontal c.t.c. distance between the applied strands*

Splitting reinforcement - Vertical distribution

Spalling stresses

Equivalent prism spalling (See: Textbook CIE4160 - Section 10.2.2):

l_{pt}	128	[mm]	*Transfer length*
ζ_{spl}	1,00	[-]	*Factor for splitting*
l_{spl}	1901,54	[mm]	*Length of equivalent prism*



First set of strands:

σ_{top}	3,7	[N/mm²]	*Stress due to prestressing in top fibre at end of prism*
σ_{bottom}	-40,9	[N/mm²]	*Stress due to prestressing in bottom fibre at end of prism*
h_{prism}	311,9	[mm]	*Height of equivalent prism*
b	2200	[mm]	*Width of cs at height where spalling occurs (at start of the prism)*
M	130607024	[Nm]	*Bending moment (elastic stress distribution) due to prestressing*
N_{spl}	137369	[N]	*Spalling tensile force*
σ_{spl}	0,26	[N/mm²]	*Spalling tensile stress*
γ_{spl}	1,2	[-]	*Partial factor splitting*
$\sigma_{bs,d}$	0,32	[N/mm²]	*Design value splitting stress*
$\sigma_{Rd,f}$	4,40	[N/mm²]	*Residual tensile strength, calculated with Klocal*
Verification	Satisfied	[-]	*If verification is satisfied no spalling reinforcement needed*

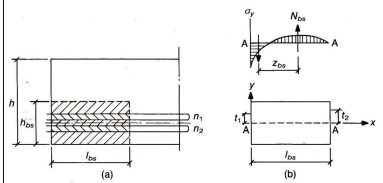
Second set of strands (if applicable):

σ_{top}	3,7	[N/mm²]	*Stress due to prestressing in top fibre at end of prism*
σ_{bottom}	-40,9	[N/mm²]	*Stress due to prestressing in bottom fibre at end of prism*
h_{prism}	311,9	[mm]	*Height of equivalent prism*
b	2200	[mm]	*Width of cs at height where spalling occurs*
M	130607024	[Nm]	*Bending moment due (elastic stress distribution prestressing)*
N_{spl}	137369	[N]	*Spalligh tensile force*
σ_{spl}	0,26	[N/mm²]	*Spalling tensile stress*
γ_{spl}	1,2	[-]	*Partial factor splitting*
$\sigma_{bs,d}$	0,32	[N/mm²]	*Design value splitting stress*
$\sigma_{Rd,f}$	4,40	[N/mm²]	*Residual tensile strength, calculated with Klocal*
Verification	Satisfied	[-]	*If verification is satisfied no spalling reinforcement needed*

Bursting stresses

Symmetric prism analogy (See: fib Model Code 2010 - Section 7.13.6.5.2):

h_{bs}	200	[mm]	*Height of the virtual prismatic element*
l_{pt}	128	[mm]	*Transfer length of the strands*
ζ_{bs}	1,07	[-]	*Factor for bursting*
l_{bs}	214,18	[mm]	*Length of equivalent prism*



First set of strands:

n_1	35	[pcs]	*Set 1: Number of tendons above the centroid of the prism*
n_2	35	[pcs]	*Set 1: Number of tendons below the centroid of the prism*
t_1	52,4	[mm]	*Set 1: Distance centroid tendons above section to centroid of prism*
t_2	50	[mm]	*Set 1: Distance centroid of stress block to centroid of prism*
$P_{m0,fb}$	188,0	[kN]	*Initial prestressing force for a single tendon*
z_{bs}	107,1	[mm]	*Internal lever arm of bursting forces*
N_{bs}	-148	[kN]	*Set 1: Bursting force*
b_{bs}	2200	[mm]	*Width of prism at the position of strands*
σ_{bs}	-0,31	[N/mm²]	*Set 1: Maximum bursting stresses*
γ_{spl}	1,2	[-]	*Partial factor splitting*
$\sigma_{bs,d}$	-0,38	[N/mm²]	*Set 1: Design value maximum bursting stresses*
$\sigma_{Rd,f}$	4,40	[N/mm²]	*Residual tensile strength, calculated with Klocal*
Verification	Satisfied	[-]	*Set 1: Verification of bursting stresses and material strength*

Second set of strands (if applicable):

n_1	0	[pcs]	*Set 2: Number of tendons above the centroid of the prism*
n_2	0	[pcs]	*Set 2: Number of tendons below the centroid of the prism*
t_1	52,4	[mm]	*Set 2: Distance centroid tendons to centroid of prism*
t_2	50	[mm]	*Set 2: Distance centroid of stress block to centroid of prism*
$P_{m0,fb,1}$	188,0	[kN]	*Initial prestressing force for a single tendon*
z_{bs}	107,1	[mm]	*Internal lever arm of bursting forces*
N_{bs}	0	[kN]	*Set 2: Bursting force*
b_{bs}	2200	[mm]	*Width of prism at the position of strands*
σ_{bs}	0,00	[N/mm²]	*Set 2: Maximum bursting stresses*
γ_{spl}	1,2	[-]	*Partial factor splitting*
$\sigma_{bs,d}$	0,00	[N/mm²]	*Set 2: Design value maximum bursting stresses*
$\sigma_{Rd,f}$	4,40	[N/mm²]	*Residual tensile strength, calculated with Klocal*
Verification	Satisfied	[-]	*Set 2: Verification of bursting stresses and material strength*

Splitting stresses

- Splitting is accounted for by selecting appropriate values for cover and centre to centre distance.
- By appling these minimum values this requirement is automatically satisfied.

Splitting reinforcement - Horizontal distribution

Distribution of single strand

d_{hor}	61,9	[mm]	*Applied horizontal c.t.c. distance between the applied strands*
s	2200	[mm]	*Length of disturbed region (length of St. Venant)*
γ_{spl}	1,2	[-]	*Partial factor for splitting*
$P_{m0,fb,i}$	188,0	[kN]	*Initial prestressing force single strand in bottom flange*
$N_{spl,hor,i}$	1,6	[kN]	*Splitting force due to single strand*

Splitting force first set of strands

$n_{fb,1}$	105	[pcs]	*Number of strands applied in first set*
$N_{spl,hor,1}$	166,7	[kN]	*Horizontal splitting force first set*
$\emptyset_{spl,f1}$	10	[mm]	*Assumed diameter splitting reinforcement*
f_s	300	[N/mm²]	*Maximum allowable stress in reinforcement*
$A_{s,min}$	556	[mm²]	*Minimum required cross section of the reinforcement*
$n_{s,req,1}$	8	[pcs]	*Required number of rebars*

Splitting force second set of strands (if applicable)

$n_{fb,2}$	0	[pcs]	*Number of strands applied in second set*
$N_{spl,hor,2}$	0,0	[kN]	*Horizontal splitting force second set*
$\emptyset_{spl}$	10	[mm]	*Assumed diameter splitting reinforcement*
f_s	300	[N/mm²]	*Maximum allowable stress in reinforcement*
$A_{s,min}$	0	[mm²]	*Minimum required cross section of the reinforcement*
$n_{s,req,2}$	0	[pcs]	*Required number of rebars*

Verification bending moment capacity

Identifying all horizontal forces

Concrete

w	3200	[mm]	*Width of the beam*
f_{cd}	113	[N/mm²]	*Design value concrete compressive strength*
x_u	148,0395667	[mm]	*Height concrete compressive zone (iteration)*

Active contribution prestressing

$A_{p,c}$	1400	[mm²]	*Applied cross section centric prestressing*
$\sigma_{p,m,c}$	1159,27	[N/mm²]	*Working prestressing stress centric prestressing*
$A_{p,fb}$	14700	[mm²]	*Applied cross section eccentric prestressing*
$\sigma_{p,m,fb}$	1118,99	[N/mm²]	*Working prestressing stress eccentric prestressing*

Contribution concrete under tension

f_{ctd}	6,0	[N/mm²]	*Design value of tensile strength (tensile strength 1st crack)*
$f_{ctd,2}$	6,15	[N/mm²]	*Design value maximal post cracking stress (at w=0,30)*
b_{web}	200	[mm]	*Width of tensile zone (width of the webs)*

Auxiliary parameters

l_c	1266,7	[mm]	*Characteristic length*

Height of concrete compressive and tensile zone

Parameters compressive zone

ε_{c3}	0,0023	[-]	*Strain at reaching concrete compressive strength*
f_{cd}	113	[N/mm²]	*Design value concrete compressive strength*
b	3200	[mm]	*Width of the beam*
h_f	187,5	[mm]	*Mean value thickness top flange*
b_{red}	200	[mm]	*Reduced width of the cross section (width of the webs)*
$\varepsilon_{c,f1}$	-0,000613	[-]	*Strains at lower side top flange*
$\sigma_{c,f1}$	-30,21	[N/mm²]	*Stresses at lower side top flange*
N_c	26844508	[N]	*Compressive force in the concrete*
e_c	49,3	[mm]	*Eccentricity compressive force with respect to top fibre*

Case	Concrete compressive forces		Lever arm (from top fibre)		Eccentricity with respect to top fibre	
Case 1	Nc1	26844508 [N]	S1	N.A. [Nmm]		
	Nc2	0 [N]	S2	N.A. [Nmm]	ec	49,3 [mm]
	Nc3	0 [N]	S3	N.A. [Nmm]		
Case 2	Nc1	0 [N]	S1	0 [Nmm]		
	Nc2	0 [N]	S2	0 [Nmm]	ec	0,0 [mm]
	Nc3	0 [N]	S3	0 [Nmm]		

Parameters tensile zone

ε_{ct}	0,00012	[-]	*Strain corresponding to cracking of the beam*
$\varepsilon_{ct;0,3}$	0,00036	[-]	*Strain corresponding to maximum post cracking stress*
ε_{ctd}	0,00041	[-]	*Strain corresponding to declining branch stress-strain curve*
ε_{ctu}	0,00250	[-]	*Strain corresponding ultimate capacity (pull-out of fibre)*
x_1	7,7	[mm]	*Height first concrete tensile zone*
x_2	18,7	[mm]	*Height second concrete tensile zone*
x_3	134,5	[mm]	*Height third concrete tensile zone*
N_t	107763	[N]	*Total concrete tensile force*
e_t	205,2	[mm]	*Eccentricity concrete tensile force with respect to top fibre*

	Concrete tensile forces		Lever arm (from top fibre)		Eccentricity with respect to top fibre
Zones	Nt1	4634 [N]	S1	709920 [Nmm]	
	Nt2	22432 [N]	S2	3703670 [Nmm]	
	Nt3	80697 [N]	S3	17696012 [Nmm]	

Determining the strains

Centrical prestressing

$d_{p,c}$	844	[mm]	*Effective height centric prestressing*
$\Delta\varepsilon_{p,c}$	0,0108	[-]	*Strain increase centric prestressing steel (passive contribution)*
$\varepsilon_{p,m,c}$	0,0059	[-]	*Strain in centric prestressing steel due to working prestressing*
$\varepsilon_{p,c}$	0,0168	[-]	*Total strain in centric prestressing steel*

Eccentric prestressing

$d_{p,fb}$	1800	[mm]	*Effective height eccentric prestressing*
$\Delta\varepsilon_{p,fb}$	0,0257	[-]	*Strain increase eccentric prestressing steel (passive contribution)*
$\varepsilon_{p,m,fb}$	0,0057	[-]	*Strain in eccentric prestressing steel due to working prestressing*
$\varepsilon_{p,fb}$	0,0314	[-]	*Total strain in eccentric prestressing steel*

Steel stresses

Main parameters

f_{pk}/γ_s	1691	[N/mm²]	*Design value stress at failure*
f_{pd}	1522	[N/mm²]	*Design value steel stress*
ε_{uk}	0,035	[-]	*Characteristic value strain at failure*
f_{pd}/E_p	0,0078	[-]	*Strain at design value of the steel stress*

Centric prestressing

$\sigma_{pu,c}$	1578	[N/mm²]	*Actual stress centric prestressing steel at calculated strain*
$\sigma_{p,m,c}$	1159	[N/mm²]	*Working prestressing stress centric prestressing*
$A_{p,c}$	1400	[mm²]	*Applied cross section centric prestressing*
$P_{m,m,c}$	1622977	[N]	*Working prestressing force centric prestressing*
$\Delta N_{p,c}$	585737	[N]	*Passive contribution centric prestressing*

Eccentric prestressing

$\sigma_{pu,fb}$	1669	[N/mm²]	*Actual stress eccentric prestressing steel at calculated strain*
$\sigma_{p,m,fb}$	1119	[N/mm²]	*Working prestressing stress eccentric prestressing*
$A_{p,fb}$	14700	[mm²]	*Applied cross section eccentric prestressing*
$P_{m,m,fb}$	16449161	[N]	*Working prestressing force eccentric prestressing*
$\Delta N_{p,fb}$	8078871	[N]	*Passive contribution eccentric prestressing*

Check equilibrium

N_c	-26845	[kN]	*Compressive force in the concrete*
N_t	108	[kN]	*Total concrete tensile force*
$P_{m,m}$	18072	[kN]	*Total working prestressing force (centric and eccentric)*
ΔN_p	8665	[kN]	*Total passive contribution of the prestressing (centric and eccentric)*
$\sum H$	0	[kN]	*Verification of horizontal equilibrium*

Determine bending moment capacity

- Bending moment is calculated using the top fibre as point of reference

Determining bending moment capacity

	Force [kN]	Lever arm [m]	Moment [kNm]
N_c	-26845	0,049	-1325
N_t	108	0,205	22
$P_{m,m,c}$	1623	0,844	1371
$P_{m,m,fb}$	16449	0,844	13891
$\Delta N_{p,c}$	586	0,844	495
$\Delta N_{p,fb}$	8079	1,800	14542

Determining design value bending moment

$M_{Ed,RFEM}$	41753	[kNm]	*Bending moment due to loads calculated using RFEM*
$M_{Ed,P}$	15717	[kNm]	*Upward bending moment due to the prestressing*
M_{Ed}	26036	[kNm]	*Design value bending moment*

Verification

M_{Ed}	26036	[kNm]	*Design value bending moment*
M_{Rd}	28996	[kNm]	*Bending moment capacity*
UC	0,90	[-]	*Unity check*

Verifying the rotational capacity

ε_{cu}	0,00230	[-]	*Strain at failure of the concrete*
$d_{p,ave}$	1716,9	[mm]	*Weighted average effective height centric and eccentric prestressing*
$\sigma_{p,m,ave}$	1122,5	[mm]	*Weighted average centric and eccentric working prestressing stress*
$A_{p,ave}$	13543,5	[mm]	*Weighted average cross section centric and eccentric prestressing*
f	568	[N/mm²]	*Factor for weighed contribution of reinforcing and prestressing steel*
$x_{u,prov}/d_{p,ave}$	0,09	[-]	*Ratio height compressive zone and effective height*

Limit value	0,37	[-]	*Limit value ratio height compressive zone and effective height*
UC	0,24	[-]	*Verification of rotational capacity (expressed as UC)*
Verification	Satisfied	[-]	*Verification of rotational capacity*

Verification shear force capacity

Resistance of prestressed concrete cross section without shear reinforcement

Contribution of the concrete

N_{Ed}	18072	[kN]	*Working prestressing force (centric and eccentric)*
A_c	1342500	[mm²]	*Cross sectional area of total cross section*
f_{ck}	200	[N/mm²]	*Characteristic value compressive strength*
b_w	200	[mm]	*Total width of both webs*
h	1900	[mm]	*Total height*
σ_{cp}	13,5	[N/mm²]	*Compressive stress due to working prestressing force*
k	1,2	[-]	*Factor depending on compressive stress and fck*
z	1620,0	[mm]	*Lever arm, taken as 0,9 * d*
$V_{Rd,c}$	881	[kN]	*Concrete contribution to shear capacity*

Contribution of the steel fibres

A_{fv}	324000	[mm²]	*Area of the fibre effect, taken as bw * z*
$f_{ctd,2}$	6,15	[N/mm²]	*Design value maximal post cracking stress (at w=0,30)*
θ	30	[°]	*Angle of the concrete compressive strut of the main beams*
$V_{Rd,f}$	3453	[kN]	*Steel fibre contribution to shear capacity*

Total concrete capacity

$V_{Rd,tot}$	4335	[kN]	*Summation of concrete and steel fibre contribution.*

Concrete compressive strut

α_{cc}	0,85	[-]	*Long term effects and unfavourable loading (compression)*
γ_c	1,5	[-]	*Partial factor concrete (cf EC2)*
b_w	200	[mm]	*Total width of both webs*
z	1620,0	[mm]	*Lever arm, taken as 0,9 * d*
$f_{ck}\text{^}(2/3)$	34,2	[N/mm²]	*Value depending on characteristic value compressive strength*
$V_{Rd,max}$	6199	[kN]	*Capacity of concrete compressive strut*
$\tan(\theta)$	0,577	[-]	*Auxiliary value*
$\cot(\theta)$	1,732	[-]	*Auxiliary value*

Shear capacity and verification

V_{tot}	4335	[kN]	*Summation of concrete and steel fibre contribution.*
$V_{Rd,max}$	6199	[kN]	*Capacity of concrete compressive strut*
V_{Ed}	3632	[kN]	*Design value shear force*
V_{Rd}	4335	[kN]	*Shear force capacity*
UC	0,84	[kN]	*Unity check*

Verification torsional resistance

Torsional capacity

Dimensions

h_f	187,5	[mm]	*Mean value thickness top flange*
t_w	100	[mm]	*Thickness of web*
t_{fb}	200	[mm]	*Thickness bottom flange*
h_b	1512,5	[mm]	*Internal height of the box*
w_b	2000	[mm]	*Internal width of the box*

Parameters torsional capacity

A	4180000	[mm²]	*Total area of the cross section within the outer circumference*
u	8200	[mm]	*Outer circumference of the cross section*
t_{ef}	100	[mm]	*Effective wall thickness (limited by the smallest actual thickness)*
A_k	3583125	[mm2]	*Area enclosed by centre lines of the connected walls*
f_{ctd}	6,0	[N/mm²]	*Design value of tensile strength (tensile strength 1st crack)*

Torsional capacity verification

T_{Ed}	1268	[kNm]	*Design value torsional moment*
$T_{Rd,c}$	4300	[kNm]	*Torsional moment capacity (torsional cracking moment)*
UC	0,29	[-]	*Unity check*

Combination of shear and torsion

A_k	3583125	[mm2]	*Area enclosed by centre lines of the connected walls*
z_1	1706,3	[mm]	*Length of element 1 (left web)*
z_2	2100,0	[mm]	*Length of element 2 (bottom flange)*
z_3	1706,3	[mm]	*Length of element 3 (right web)*
z_4	2100,0	[mm]	*Length of element 4 (top flange)*

Shear forces in the elements of the cross section

$V_{Ed,V,1}$	1816,0	[kN]	*Shear force to be carried by element 1 (left web)*	$V_{Ed,T,1}$	301,9	[kN]	*Shear force in element 1 due to torsion (left web)*	$V_{Ed,V+T,1}$	2117,9	[kN]	*Total shear force in element 1 due to shear and torsion*
$V_{Ed,V,2}$	0,0	[kN]	*Shear force to be carried by element 2 (bottom flange)*	$V_{Ed,T,2}$	371,6	[kN]	*Shear force in element 2 due to torsion (bottom flange)*	$V_{Ed,V+T,2}$	371,6	[kN]	*Total shear force in element 2 due to shear and torsion*
$V_{Ed,V,3}$	1816,0	[kN]	*Shear force to be carried by element 3 (right web)*	$V_{Ed,T,3}$	301,9	[kN]	*Shear force in element 3 due to torsion (right web)*	$V_{Ed,V+T,3}$	1514,1	[kN]	*Total shear force in element 3 due to shear and torsion*
$V_{Ed,V,4}$	0,0	[kN]	*Shear force to be carried by element 4 (top flange)*	$V_{Ed,T,4}$	371,6	[kN]	*Shear force in element 4 due to torsion (top flange)*	$V_{Ed,V+T,4}$	371,6	[kN]	*Total shear force in element 4 due to shear and torsion*

Verifying shear force capacity per element

k	1,20	[-]	*Factor depending on compressive stress and fck*
f_{ck}	200	[N/mm²]	*Characteristic value compressive strength*
$\gamma_E * \gamma_{cf}$	1,5	[-]	*Product of partial factors (AFGC-SETRA 2013)*
$f_{ctd;2}$	6,15	[N/mm²]	*Design value of tensile strength (tensile strength 1st crack)*
ϑ	30	[°]	*Angle of the concrete compressive strut of the main beams*

Element	$b_{w,i}$	z_i	$V_{Rd,c,i}$	A_{fv}	$V_{Rd,f,i}$	$V_{Rd,i}$	UC
[-]	[mm]	[mm]	[kN]	[mm²]	[kN]	[kN]	[-]
1	100,0	1706,3	464,0	170625	1818,7	2282,7	0,93
2	200,0	2100,0	1142,2	420000	4476,7	5618,9	0,07
3	100,0	1706,3	464,0	170625	1818,7	2282,7	0,66
4	187,5	2100,0	1070,9	393750	4196,9	5267,8	0,07

Verifying concrete compressive strut per element

α_{cc}	0,85	[-]	*Long term effects and unfavourable loading (compression)*
γ_c	1,5	[-]	*Partial factor concrete (cf EC2)*
f_{ck}^(2/3)	34,2	[N/mm²]	*Value depending on characteristic value compressive strength*
A_k	3583125	[mm²]	*Area enclosed by centre lines of the connected walls*
$\sin(\theta)$	0,500	[-]	*Auxiliary value*
$\cos(\theta)$	0,866	[-]	*Auxiliary value*
$\tan(\theta)$	0,577	[-]	*Auxiliary value*
$\cot(\theta)$	1,732	[-]	*Auxiliary value*

Element	$b_{ef,i}$	z_i	$V_{Ed,V+T,i}$	$V_{Rd,max}$	UC
[-]	[mm]	[mm]	[kN]	[kN]	[-]
1	100,0	1706,3	2117,9	3264,6	0,65
2	200,0	2100,0	371,6	8035,9	0,05
3	100,0	1706,3	1514,1	3264,6	0,46
4	187,5	2100,0	371,6	7533,6	0,05

Global verification ship collision (stability)

Collision force and friction coefficient

F_{equi}	1000	[kN]	*Equivalent static force, see: (4) of 4.6.2. EC1-1-7*
μ	0,5	[-]	*Friction coefficient*

Self-weight of the deck

n_{beams}	5	[-]	*Number of prefab UHPC beams*
L_{tot}	70,70	[m]	*Total length of the main beams*
A_c	1,34	[m²]	*Cross sectional area of total cross section*
ρ	25	[kN/m³]	*Density*
F_{sw}	11864	[kN]	*Self-weight of the UHPC beams*

Verification

Action	1000	[kN]	*Action - Equivalent static force*
Resistance	5932	[kN]	*Self weight multiplied with friction coefficient*
UC	0,17	[-]	*Verification expressed as unity check*
Verification	Satisfied	[-]	*Verification*

Design Calculations Optimization - Design of main beams - Top flange and transverse prestressing

Project: MSc thesis "Redesign of bridges Twentekanaal in UHPC"
Name: M. Dorland
Date: 22-12-2020
Version: D1.0

Input parameters

Input parameters - Material properties & transverse prestressing

Concrete of longitudinal joint

Parameters concrete in compression

f_{ck}	100	[N/mm²]	Characteristic value compressive strength
ε_{cu3}	2,6	[‰]	Maximum compressive strain at ULS

Parameters stiffness and deformations (temperature, creep and shrinkage)

E_{cm}	45000	[N/mm²]	Modulus of elasticity
φ	0,8	[-]	Creep factor

Parameters concrete other

α	0,56	[-]	Factor for shape of concrete compressive zone
β	0,34	[-]	Factor position centre of gravity concrete compressive zone
α_{cc}	0,85	[-]	Long term effects and unfavourable loading (compression)

Calculated values

f_{cd}	57	[N/mm²]	Design value concrete compressive strength

Parameters transverse prestressing

Material properties prestressing steel

f_{pk}	1860	[N/mm²]	Characteristic value tensile strength
f_{pd}	1522	[N/mm²]	Design value steel stress
σ_{pm0}	1395	[N/mm²]	Maximum allowed stress directly after tensioning
$\sigma_{p,max}$	1488	[N/mm²]	Maximum prestressing stress during tensioning
E_p	195000	[N/mm²]	Modulus of elasticity
ε_{uk}	35	[‰]	Characteristic value strain at failure

Calculation parameters tendons (input values)

n	4,00	[pcs]	Assumed number of strands per tendon
D_{strand}	15,2	[mm]	Diameter of single strand
$A_{p,strand}$	140	[mm²]	Cross sectional area per strand
$\sigma_{p,max,prov}$	1400	[N/mm²]	Assumed maximum stress applied to prestressing element
μ	0,23	[-]	Friction coefficient
k	0,01	[rad]	Unintensional angular rotation due to the Wobble-effect
w_{set}	3,00	[mm]	Estimated wedge set
Relaxation	Class 2	[-]	Select relaxation class: normal (1), low (2) or bars (3)
t	500000,00	[h]	The value of the relaxation loss (in %) at 1000 h
ρ	2,50	[%]	Time after stressing (for final value of the relaxation loss)

Other parameters

γ_C	1,5	[-]	Partial factor concrete (cf EC2)
γ_S	1,1	[-]	Partial factor prestressing steel (cf EC2)
γ_{spl}	1,2	[-]	Partial factor splitting forces

Design of transverse prestressing

Calculating prestress losses

Dimensions top flange

$w_{c.t.c.}$	1000	[mm]	Centre to centre distance of the transverse prestressing ribs/ducts
t_{ft}	187,5	[mm]	Mean value thickness top flange
Δe_{ft}	8	[mm]	Downward eccentricity transverse prestressing with respect to z_{ft}

Properties top flange

z_{ft}	100,7	[mm]	Centre of gravity top flange with respect to top fibre
A_{ft}	187500	[mm²]	Cross sectional area of top flange section
I_{ft}	7,844E+08	[mm⁴]	Second moment of area of top flange section

Applied maximum force onto prestressing element & stress verification

Applied stress values

$\sigma_{p,max,prov}$	1400,0	[N/mm²]	Assumed maximum stress applied to prestressing element
$\sigma_{c,prov}$	5,4	[N/mm²]	Maximum compressive stress in concrete due to prestressing

Stress limit and verification

$\sigma_{p,max}$	1488	[N/mm²]	Maximum prestressing stress during tensioning
$\sigma_{c,limit}$	60	[N/mm²]	Maximum value concrete compressive stress
Verification	Satisfied	[-]	Verification maximum stress values

Applied value maxinum force applied onto prestressing element

P_{max}	784	[kN]	Applied value maximum prestressing force
$\sigma_{p,max}$	1400	[N/mm²]	Applied value maximum prestressing stress
A_p	560	[mm²]	Applied cross section prestressing tendon

Direct prestressing losses

Elastic losses

w_{tot}	16,36	[m]	Total width of the deck
ΔP_{el}	10,1	[KN]	Elastic loss prestressing

Friction losses

μ	0,23	[-]	Friction coefficient
k	0,009	[1/m]	Coefficient Wobble-effect
$\Delta P_\mu(x=0)$	0,00	[kN]	Prestress loss due to friction at x=0 m
$\Delta P_\mu(x=w_{tot})$	26,1	[kN]	Prestress loss (force) due to friction at x=width deck
$\Delta\sigma_{Pp}(x=w_{tot})$	46,6	[N/mm²]	Prestress loss (stress) due to friction at x=width deck

Wedge set

w_{set}	3,00	[mm]	Assumed value wedge set
$\Delta\sigma_{Pset}/w_{tot}$	0,0028	[N/mm²/mm]	Stress reduction due to friction per unit of length
l_w	14328,3	[mm]	Influence length of the wedge set
ΔP_{set}	45,7	[kN]	Prestress losses due to wedge set (at active side)

Determining initial prestressing force & stress verification

Applied force and stress values

$\max\{P_{m,0}(x)\}$	751	[kN]	Initial prestressing force - maximum value over beam length
$\max\{\sigma_{pm0}(x)\}$	1341	[N/mm²]	Initial prestressing stress - maximum value over beam length
$P_{m,0}$	741	[kN]	Initial prestressing force - mean value over beam length

Stress limit and verification

σ_{pm0}	1395	[N/mm²]	Maximum allowed stress directly after tensioning
Verification	Satisfied	[-]	Verification initial prestressing stress

Applied value initial prestressing force and losses

$P_{m,0}$	741	[kN]	Inital prestressing force - Mean value over beam length
ΔP_i	43	[kN]	Initial losses - Mean value over beam length: Pmax-Pm,0

Time dependent losses

Relaxation

Class	Class 2	[-]	Relaxation class (normal relaxation, low relaxation and bars)
ρ_{1000}	2,5	[%]	The value of the relaxation loss (in %) at 1000 h
μ	0,71	[-]	Factor depending on steel stresses
t	500000	[h]	Time after stressing (for final value of the relaxation loss)
$\Delta\sigma_{pr}/\sigma_{pi}$	0,0410	[-]	Relaxation coefficient
σ_{pi}	1322,6	[N/mm²]	Absolute value of the initial prestressing (σ_{pm0})
$\Delta\sigma_{pr}$	54,2	[N/mm²]	Prestress loss due to relaxation

Class 1	Wires and strands normal relaxation
Class 2	Wires and strands low relaxation
Class 3	Bars

Creep & shrinkage

φ	0,8	[-]	Creep factor
$\sigma_{c,QP}$	4,03	[N/mm²]	Stress in concrete adjacent to prestressing tendon
ε_{cs}	0,0008	[-]	Shrinkage of the concrete

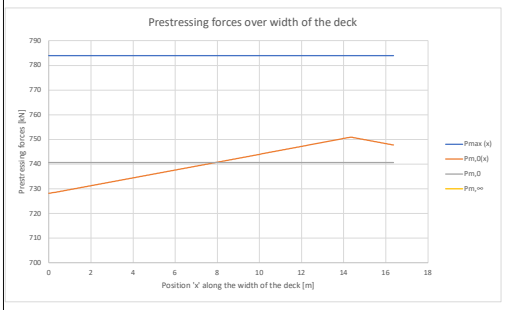
Total time dependent losses

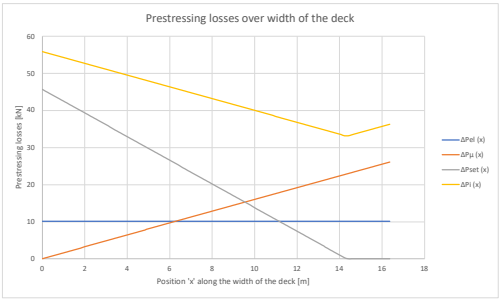
$\Delta\sigma_{p,cswr}$	195	[N/mm²]	Time dependent prestressing losses (stress)
$\Delta P_{p,cswr}$	109	[kN]	Time dependent prestressing losses (force)

Working prestress force and total prestress losses

$P_{m,\infty}$	631	[kN]	Working prestressing force in tendon
$\sigma_{pm,\infty}$	1127	[N/mm²]	Working prestressing stress in tendon
ΔP	-19,5	[%]	Total prestressing loss (percentage)

Plotting prestressing forces and losses over beam length





Detailing of the prestressing - Horizontal and vertical distribution

Parameters

$\emptyset_{spl,ft}$	10	[mm]	Assumed diameter splitting reinforcement top flange
γ_{spl}	1,2	[-]	Partial factor splitting forces
$w_{c.t.c.}$	1000	[mm]	Centre to centre distance of the transverse prestressing ribs/ducts
$t_{ft,tot}$	250	[mm]	Total height top flange at location of prestressing rib
h_1	100	[mm]	Anchor plate (height and width)

Converting width from wc.t.c. to standard width

$w_{c.t.c.}$	1,00	[m]	Centre to centre distance of the transverse prestressing ribs/ducts

Width:	wc.t.c	1,0	[m]
$P_{m,\infty}$	631,4	631,4	[kN]
A_p	560,0	560,0	[mm²]
$\sigma_{pm,\infty}$	1127,5	1127,5	[N/mm²]

Horizontal force distribution

P_{m0}	740,7	[kN]	Inital prestressing force - Mean value over beam length
$N_{spl,w}$	200,0	[kN]	Horizontal tensile force
f_s	300	[N/mm²]	Maximum stress in reinforcement
$A_{s,req}$	667	[mm²]	Minimum required cross section of the reinforcement
$n_{s,req}$	9	[pcs]	Minimum number of rebars requried

Vertical force distribution

P_{m0}	740,7	[kN]	Inital prestressing force - Mean value over beam length
$N_{spl,v}$	133,3	[kN]	Vertical tensile force
f_s	300	[N/mm²]	Maximum stress in reinforcement
$A_{s,req}$	444	[mm²]	Minimum required cross section of the reinforcement
$n_{s,req}$	6	[pcs]	Minimum number of rebars requried

Forces acting on top flange and joint

Parameters longitudinal joint

t_{ft}	187,5	[mm]	Height of the top flange
t_j	162,5	[mm]	Height of the longitudinal joint
$w_{j,t}$	90	[mm]	Width of joint along longitudinal direction

Additional tendon eccentricity

Δe_{ft}	8	[mm]	Downward eccentricity transverse prestressing with respect to z_{ft}

Cross sectional properties & parameters of the joint

A_j	162500	[mm²]	Cross sectional area of the longitudinal joint
W_j	4,401OE+06	[mm³]	Section modulus of the longitudinal joint
I_j	3,575BE+08	[mm⁴]	Second moment of the cross section of the longitudinal joint
e_j	27,4	[mm]	Eccentricity prestressing tendon with centre of joint
l	1190	[mm]	Span of the mechanical model
d_p	108,7	[mm]	Effective height longitudinal joint

Actions on the joint

$G_{k,sf}$	4,6875	[kN/m]	Self-weigth UHPC top flange
$G_{k,asfalt}$	0,23	[kN/m]	Permanent load due to asphalt/protection layer
G_k	4,92	[kN/m]	Self-weight + permanent load
$Q_{k,LM2}$	194	[kN]	Single wheel load model 2

Factors

Bending moments joint (SLS)

Bending moments (ULS)

γ_G	1,4 [-]	*See tabel NB.16 – A2.4(B) of NA to NEN-EN 1990*	
$\xi * \gamma_G$	1,25 [-]	*See tabel NB.16 – A2.4(B) of NA to NEN-EN 1990*	
γ_P	1,0 [-]	*See 2.4.2.2 of NA to NEN-EN 1992-1-1*	
γ_Q	1,5 [-]	*See tabel NB.16 – A2.4(B) of NA to NEN-EN 1990*	
ψ_0	0,8 [-]	*See tabel NB.13 – A2.1 of NA to NEN-EN 1990*	

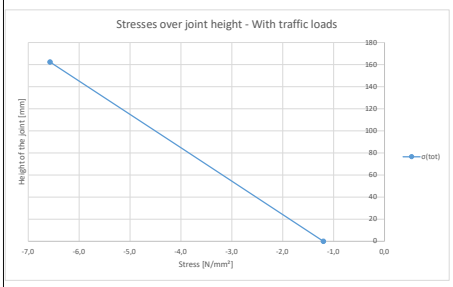
M_G	0,29 [kNm]	*Bending moment due to self-weigth and asphalt layer*
M_P	17,33 [kNm]	*Bending moment due to eccentricity of tendons*
M_Q	28,86 [kNm]	*Bending moment due to varaible load (LM2)*

$M_{Ed,a}$	17,7 [kNm]	*Design value bending moment equation 6.10a*
$M_{Ed,b}$	26,3 [kNm]	*Design value bending moment equation 6.10b*
M_{Ed}	26,3 [kNm]	*Design value bending moment*

Verifying stresses over joint height

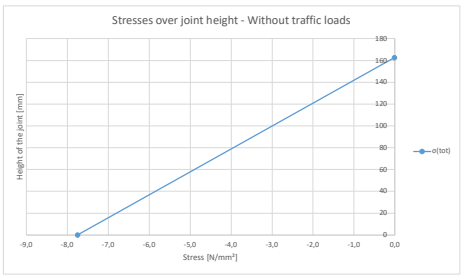
Stress distribution over the height of the joint with traffic loads:

	Height [mm]	σ(M$_G$) [N/mm²]	σ(M$_{Q1}$) [N/mm²]	σ(P) [N/mm²]	σ(M$_P$) [N/mm²]	σ(tot) [N/mm²]
Top fibre	163	-0,1	-6,6	-3,9	3,9	-6,6
Bottom fibre	0	0,1	6,6	-3,9	-3,9	-1,2



Stress distribution over the height of the joint without traffic loads:

	Height [mm]	σ(M$_G$) [N/mm²]	σ(M$_{Q1}$) [N/mm²]	σ(P) [N/mm²]	σ(M$_P$) [N/mm²]	σ(tot) [N/mm²]
Top fibre	163	-0,1	0,0	-3,9	3,9	0,0
Bottom fibre	0	0,1	0,0	-3,9	-3,9	-7,8



Local verification (transverse direction) - Verification bending moment capacity longitudinal joint

Parameters concrete

α	0,56 [-]	*Factor for shape of concrete compressive zone*
β	0,34 [-]	*Factor position centre of gravity concrete compressive zone*
f_{cd}	56,7 [N/mm²]	*Design value concrete compressive strength*
x_u	27,47931918 [mm]	*Height concrete compressive zone (iteration)*

Horizontal equilibrium

N_c	-872010 [N]	*Compressive force in the concrete*
$P_{m,\infty}$	631386 [N]	*Working prestressing force*
ΔN_p	240624 [N]	*Passive contribution of the prestressing*
$\sum H$	0 [N]	*Verification of horizontal equilibrium*

Parameters steel

A_p	560,00 [mm²]	*Applied cross section of the prestressing*
$\sigma_{pm,\infty}$	1127,47 [N/mm²]	*Working prestressing stress*

Bending moment capacity

	Force [N]	Lever arm [mm]	Moment [kNm]
N_c	-872010	9,3	-8,1
$P_{m,\infty}$	631386	81,3	51,3
ΔN_p	240624	108,7	26,2
M_{Rd}			69,3

Determining strains and stresses

$\varepsilon_{p,\infty}$	0,0058 [-]	*Strain in prestressing steel due to working prestressing*
$\Delta\varepsilon_p$	0,0077 [-]	*Strain increase prestressing steel (passive contribution)*
ε_p	0,0135 [-]	*Total strain in prestressing steel*
σ_{pu}	1557 [N/mm²]	*Actual stress in prestressing steel at calculated strain*

Verification

M_{Ed}	26,3 [kNm]	*Design value bending moment*
M_{Rd}	69,3 [kNm]	*Bending moment capacity*
UC	0,38 [-]	*Unity check*

Local verification (transverse direction) - Bending moment capacity top flange between the webs

Calculation model and design value bending moment

Parameters longitudinal joint

z_{ft}	100,7 [mm]	*Centre of gravity top flange with respect to top fibre*
Δe_{ft}	8,0 [mm]	*Downward eccentricity transverse prestressing with respect to z_{ft}*
$t_{ft,tot}$	250 [mm]	*Total height top flange at location of prestressing rib*

Factors

γ_G	1,4 [-]	*See tabel NB.16 – A2.4(B) of NA to NEN-EN 1990*
$\xi * \gamma_G$	1,25 [-]	*See tabel NB.16 – A2.4(B) of NA to NEN-EN 1990*
γ_P	1,0 [-]	*See 2.4.2.2 of NA to NEN-EN 1992-1-1*
γ_Q	1,5 [-]	*See tabel NB.16 – A2.4(B) of NA to NEN-EN 1990*
ψ_0	0,8 [-]	*See tabel NB.13 – A2.1 of NA to NEN-EN 1990*

Cross sectional properties & parameters of the flange

l	2,1 [m]	*Span, i.e. distance inside the box + 2*0,5*tweb*
d_p	108,7 [mm]	*Effective height prestressing tendon with respect to top fibre*
$d_{p,hog}$	141,3 [mm]	*Effective height prestressing tendon with respect to bottom fibre*

Bending moments top flange (SLS)

$M_{E,sag}$	46,8 [kNm]	*Sagging moment, SLS*
$M_{E,hog}$	57,8 [kNm]	*Hogging moment, SLS*

Actions on the top flange

G_k	4,9175 [kN/m]	*Self-weight + permanent load*
$Q_{k,LM2}$	194 [kN]	*Single wheel load model 2*
$M_{P,ft}$	5,05 [kNm]	*Upward bending moment in case of eccentric prestressing*

Bending moments (ULS)

$M_{Ed,a,sag}$	57,3 [kNm]	*Design value sagging bending moment equation 6.10a*
$M_{Ed,b,sag}$	72,5 [kNm]	*Design value sagging bending moment equation 6.10b*
$M_{Ed,a,hog}$	68,7 [kNm]	*Design value hogging bending moment equation 6.10a*
$M_{Ed,b,hog}$	83,7 [kNm]	*Design value hogging bending moment equation 6.10b*

Verification of bending moment capacity - Sagging bending moment

Parameters concrete

α	0,56 [-]	*Factor for shape of concrete compressive zone*
β	0,34 [-]	*Factor position centre of gravity concrete compressive zone*
f_{cd}	113,3 [N/mm²]	*Design value concrete compressive strength*
x_u	14,26199151 [mm]	*Height concrete compressive zone (iteration)*

Horizontal equilibrium

N_c	-905161 [N]	*Compressive force in the concrete*
$P_{m,\infty}$	631386 [N]	*Working prestressing force*
ΔN_p	273775 [N]	*Passive contribution of the prestressing*
$\sum H$	0 [N]	*Verification of horizontal equilibrium*

Parameters steel

A_p	560,00 [mm²]	*Applied cross section of the prestressing*
$\sigma_{pm,\infty}$	1127,47 [N/mm²]	*Working prestressing stress*

Bending moment capacity

	Force [kN]	Lever arm [m]	Moment [kNm]
N_c	-905	0,0048	-4,4
$P_{m,\infty}$	631	0,1007	63,6
ΔN_p	274	0,1087	29,8
M_{Rd}			88,9

Determining strains and stresses

$\varepsilon_{p,\infty}$	0,0058 [-]	*Strain in prestressing steel due to working prestressing*
$\Delta\varepsilon_p$	0,0172 [-]	*Strain increase prestressing steel (passive contribution)*
ε_p	0,0230 [-]	*Total strain in prestressing steel*
σ_p	1616 [N/mm²]	*Actual stress in prestressing steel at calculated strain*

Bending moment verification - Sagging bending moment

$M_{Ed,sag}$	72,5 [kNm]	*Design value sagging bending moment*
M_{Rd}	88,9 [kNm]	*Bending moment capacity*
UC	0,81 [-]	*Unity check sagging bending moment*

Verification of bending moment capacity - Hogging bending moment

Parameters concrete

α	0,56 [-]	*Factor for shape of concrete compressive zone*
β	0,34 [-]	*Factor position centre of gravity concrete compressive zone*
f_{cd}	113,3 [N/mm²]	*Design value concrete compressive strength*
x_u	54,19038061 [mm]	*Height concrete compressive zone (iteration)*

Horizontal equilibrium

N_c	-859821 [N]	*Compressive force in the concrete*
$P_{m,\infty}$	631386 [N]	*Working prestressing force*
ΔN_p	228435 [N]	*Passive contribution of the prestressing*
$\sum H$	0 [N]	*Verification of horizontal equilibrium*

Parameters steel

A_p	560,00 [mm²]	*Applied cross section of the prestressing*
$\sigma_{pm,\infty}$	1127,47 [N/mm²]	*Working prestressing stress*

Bending moment capacity

	Force [kN]	Lever arm [m]	Moment [kNm]
N_c	-860	0,0184	-15,8
$P_{m,\infty}$	631	0,1493	94,3
ΔN_p	228	0,1413	32,3
M_{Rd}			110,7

Determining strains and stresses

$\varepsilon_{p,\infty}$	0,0058 [-]	*Strain in prestressing steel due to working prestressing*
$\Delta\varepsilon_p$	0,0042 [-]	*Strain increase prestressing steel (passive contribution)*
ε_p	0,0100 [-]	*Total strain in prestressing steel*
σ_p	1535 [N/mm²]	*Actual stress in prestressing steel at calculated strain*

Bending moment verification - Hogging bending moment

$M_{Ed,hog}$	83,7 [kNm]	*Design value hogging bending moment*
M_{Rd}	110,7 [kNm]	*Bending moment capacity*
UC	0,76 [-]	*Unity check hogging bending moment*

Local verification (longitudinal direction) - Bending moment capcity top flange between prestressing ribs

Calculation model and design value bending moment

Parameters longitudinal joint

t_{ft}	187,5 [mm]	*Mean value thickness top flange*

Factors

γ_G	1,4 [-]	*See tabel NB.16 – A2.4(B) of NA to NEN-EN 1990*
$\xi * \gamma_G$	1,25 [-]	*See tabel NB.16 – A2.4(B) of NA to NEN-EN 1990*
γ_P	1,0 [-]	*See 2.4.2.2 of NA to NEN-EN 1992-1-1*
γ_Q	1,5 [-]	*See tabel NB.16 – A2.4(B) of NA to NEN-EN 1990*
ψ_0	0,8 [-]	*See tabel NB.13 – A2.1 of NA to NEN-EN 1990*

Cross sectional properties & parameters of the flange

l	1,00 [m]	*Span, i.e. centre to centre distance prestressing ribs*

Bending moments top flange (SLS)

M_E	49,1 [kNm]	*Sagging moment, SLS*

Actions on the top flange

G_k	4,9175 [kN/m]	*Self-weight + permanent load*
$Q_{k,LM2}$	194 [kN]	*Single wheel load model 2*

Bending moments (ULS)

$M_{Ed,a}$	59,1 [kNm]	*Design value bending moment equation 6.10a*
$M_{Ed,b}$	73,5 [kNm]	*Design value bending moment equation 6.10b*

Verification of bending moment capacity

Parameters concrete

f_{ctd}	6 [N/mm²]	*Design value of tensile strength (tensile strength 1st crack)*
$f_{ctd;2}$	6,15 [N/mm²]	*Design value maximal post cracking stress (at w=0,30)*
E_{cm}	50000 [N/mm²]	*Modulus of elasticity*
l_f	13 [mm]	*Fibre length*

Bending moment verification

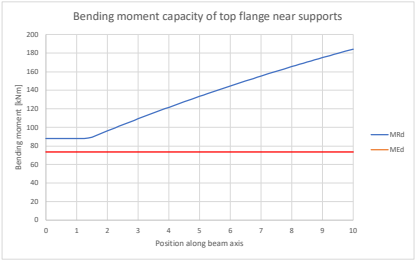
M_{Ed}	73,5 [kNm]	*Design value bending moment*
M_{Rd}	88,2 [kNm]	*Bending moment capacity at intersection*
UC	0,83 [-]	*Unity check at intersection*
Coordinate 'x'	0,0 [m]	*Location of intersection (sufficient capacity)*

External axial force (self-weight beams and prestressing)

$G_{k,beam}$	33,56 [kN/m]	*Line load representing the self-weight of the prefab beams*
l	68,00 [m]	*Span of the main beams*
$P_{m0,c}$	1952 [kN]	*Applied value initial prestressing force centric prestressing*
$P_{m0,fb}$	19745 [kN]	*Applied value initial prestressing force eccentric prestressing*

Verifying strains

ε_{cc}	0,00204 [-]	*Compressive strain top fibre at midspan*
ε_{c3}	0,00230 [-]	*Strain at reaching concrete compressive strength*
Verify strains:	Satisfied [-]	*Verify if it holds that $\varepsilon_c \leq \varepsilon_{c3}$*



Design Calculations Optimization - Design of main beams - Fatigue verification

Project: MSc thesis "Redesign of bridges Twentekanaal in UHPC"
Name: M. Dorland
Date: 22-12-2020
Version: D1.0

Fatigue

Parameters - Loads, cross sectional properties and materials

Forces & loads

$M_{fat,max}$	26812	kNm	*Maximum bending moment at midspan (found using RFEM)*
$M_{fat,min}$	22543	kNm	*Minimum bending moment at midspan (found using RFEM)*
$P_{m,0,c}$	1623	[kN]	*Working prestress force - Centric strands*
$P_{m,0,fb}$	16449	[kN]	*Working prestress force - Eccentric strands*
$\gamma_{F,fat}$	1,00	[-]	*See 2.4.2.3 of NA to NEN-EN 1992-1-1*

Cross sectional properties

A_c	1342500	[mm²]	*Cross sectional area of total cross section*
e_p	955,5	[mm]	*Eccentricity of tendons in bottom flange*
I_y	8,038E+11	[mm⁴]	*Second moment of area of the combined cross section*
$W_{y,t}$	9,518E+08	[mm³]	*Section modulus with respect to top fibre*
$W_{y,b}$	7,615E+08	[mm³]	*Section modulus with respect to bottom fibre*

Material properties concrete & steel

E_{cm}	50000	[N/mm²]	*Modulus of elasticity*
$\beta_{cc}(t)$	1,0	[-]	*Factor for increase of strength due to progressive hydration*
f_{ck}	200	[N/mm²]	*Characteristic value compressive strength*
f_{ck0}	10	[N/mm²]	*Standard value (10 Mpa)*
E_p	195000	[N/mm²]	*Modulus of elasticity*
$\gamma_{S,fat}$	1,1	[-]	*See 2.4.2.4 of NA to NEN-EN 1992-1-1*
γ_C	1,5	[-]	*Partial factor concrete (cf EC2)*

Fatigue verification - Prestressing steel at midspan

Occuring stress range

α_e	3,90	[-]	*Ratio of moduli of elasticity*
$\sigma_{c,max}$	-0,3	[N/mm²]	*Maximum stress in concrete at tendon height (i.e. highest stress)*
$\sigma_{p,max}$	-1,1	[N/mm²]	*Maximum stress in prestressing steel (i.e. highest stress)*
$\sigma_{c,min}$	-5,3	[N/mm²]	*Minimum stress in concrete at tendon height (i.e. lowest stress)*
$\sigma_{p,min}$	-20,9	[N/mm²]	*Minimum stress in prestressing steel (i.e. lowest stress)*
$\Delta\sigma_p$	19,8	[N/mm2]	*Stress range in prestressing steel*

S-N curve and number of cycles

$\Delta\sigma_{Rsk}$	185	[N/mm²]	*Stress range at N* cycles*
N^*	1000000	[-]	*Number of cycles with single stress range*
k_1	5	[-]	*Stress exponent first branch*
k_2	9	[-]	*Stress exponent second branch*
n_y	100	[-]	*Design service life*
N_{obs}	500000	[-]	*Number of heavy vehicles per year*
n	50000000	[-]	*Number of cycles to be designed for*

Fatigue verification

$\Delta\sigma_{pd}$	19,8	[N/mm²]	*Stress range in prestressing steel*
$\Delta\sigma_{Rsd}$	108,9	[N/mm²]	*Allowable stress range (design value)*
Verification	Satisfied	[-]	*Fatigue verificaiton prestressing steel*

Fatigue verification - Concrete at midspan

Highest and lowest stress values top fibre

$\sigma_{cd,max}$	25,1	[N/mm²]	*Highest compressive stress in a cycle (i.e. most negative value)*
$\sigma_{cd,min}$	20,6	[N/mm²]	*Lowest compressive stress in a cycle (i.e. value closest to zero or positive)*

Verification stresses top fibre

$E_{cd,max}$	0,44	[-]	*Maximum compressive stress level (top fibre)*
$E_{cd,min}$	0,36	[-]	*Minimum compressive stress level (top fibre)*
R	0,82	[-]	*Ratio minimum and maximum stress level (top fibre)*
n	50000000	[-]	*Number of cycles to be designed for*
N	2,78E+18	[-]	*Number of cycles until failure at given stress range*
UC	0,00	[-]	*Fatigue verificaton concrete at top fibre (as UC)*
Verification	Satisfied	[-]	*Fatigue verificaton concrete at top fibre*

Highest and lowest stress values bottom fibre

$\sigma_{cd,max}$	4,5	[N/mm²]	*Highest compressive stress in a cycle (i.e. most negative value)*
$\sigma_{cd,min}$	0,0	[N/mm²]	*Lowest compressive stress in a cycle (i.e. value closest to zero or positive)*

Verification stresses bottom fibre

$E_{cd,max}$	0,08	[-]	*Maximum compressive stress level (bottom fibre)*
$E_{cd,min}$	0,00	[-]	*Minimum compressive stress level (bottom fibre)*
R	0,00	[-]	*Ratio minimum and maximum stress level (bottom fibre)*
n	50000000	[-]	*Number of cycles to be designed for*
N	7,74E+12	[-]	*Number of cycles until failure at given stress range*
UC	0,00	[-]	*Fatigue verificaton concrete at bottom fibre (as UC)*
Verification	Satisfied	[-]	*Fatigue verificaton concrete at bottom fibre*

Concrete fatigue strength

$f_{ck,fat}$	85	[N/mm²]	*Characteristic value fatigue strength*
$f_{cd,fat}$	56,67	[N/mm²]	*Design value fatigue strength*

Design Calculations Optimization - Design of main beams - Serviceability Limit State

Project: MSc thesis "Redesign of bridges Twentekanaal in UHPC"
Name: M. Dorland
Date: 22-12-2020
Version: D1.0

Serviceability limit state - Deflection at midspan

Input parameters loads

$G_{k,total}$	34,32	[kN/m]	*Line load composed of self-weight beam and road surfacing*
$P_{m,o,fb}$	16449	[kN]	*Working prestressing force centric prestressing*
$Q_{k,UDL}$	26,8425	[kN/m]	*Line load acting on the beam (due to UDL of LM1)*
$Q_{k,axle}$	291	[kN/axle]	*Axle load acting on the beam (LM1)*
ψ_1	0,8	[-]	*See tabel NB.13 – A2.1 of NA to NEN-EN 1990*
e_p	0,96	[m]	*Eccentricity of tendons in bottom flange*

Maximum deflection

$1/\delta$	300	[-]	*Maximum deflection in SLS*
δ_{max}	226,7	[mm]	*Calculated value maximum delfection*

Input parameters structure and material

l	68	[m]	*Span of the main beams*
E_{cm}	50000	[N/mm²]	*Modulus of elasticity*
I_y	8,038E+11	[mm⁴]	*Second moment of area of the combined cross section*
φ	0,3	[-]	*Creep factor*
$E_{c,eff}$	38462	[N/mm²]	*Effective modulus of elasticity to account for time dependent effects*

Deflections

δ_G	309,1	[mm]	*Deflection (downwards) due to self weight & permanent loads*
δ_P	-293,9	[mm]	*Deflection (upwards) due to prestressing*
$\delta_{Q,UDL}$	193,4	[mm]	*Deflection (downwards) due to UDL component variable loads*
$\delta_{Q,axle}$	98,7	[mm]	*Deflection (downwards) due to axle loads*
δ_{tot}	307,3	[mm]	*Summation of all individual components*
$\delta_{tot,FEM}$	147,0	[mm]	*Total deflection determined using RFEM*

Verifications

$\delta_{tot} < \delta_{max}$?	Not satisfied	[-]	*Verification maximum deflection*
$\delta_{tot,RFEM} < \delta_{max}$	Satisfied	[-]	*Verification maximum deflection using RFEM results*

Serviceability limit state - Crack width verification

Calculating cracking bending moment (SLS)

f_{ctk}	200	[N/mm²]	*Characteristic value compressive strength*
$f_{ctm,el}$	10,3	[N/mm²]	*Mean value of the axial tensile strength*
$P_{m,o}$	18072	[kN]	*Axial working prestressing force (centric and eccentric)*
A_c	1342500	[mm²]	*Cross sectional area of total cross section*
σ_c	13,5	[N/mm²]	*Compressive stress due to axial prestressing force*
W_{min}	7,615E+08	[mm³]	*Minimum value of section moduli with respect to top and bottom fibre*
M_{cr}	18064	[kNm]	*Cracking bending moment*

Verification non-brittleness criterion

M_{cr}	18064	[kNm]	*Cracking bending moment*
M_{Rd}	28996	[kNm]	*Bending moment capacity*
Verification	Satisfied	[-]	*Verification*

Design Calculations Optimization - Design of end cross beam

Project: MSc thesis "Redesign of bridges Twentekanaal in UHPC"
Name: M. Dorland
Date: 22-12-2020
Version: D1.0

Input parameters

Input parameters - Cross sectional properties and calculation parameters

Cross sectional properties

h_{cb}	1900	[mm]	*Total height of the end cross beam*
w_{cb}	1900	[mm]	*Total width of the end cross beam*
A_{cb}	3610000	[mm²]	*Cross sectional area of the cross beam*
$W_{y,cb}$	1,143E+09	[mm³]	*Section modulus of the cross section*
$I_{y,cb}$	1,086E+12	[mm⁴]	*Second moment of area of the cross section*

Calculation parameters

k_1	0,15	[-]	*Factor from 6.2.2 of the NA to NEN-EN 1992-1-1*
θ	21,8	[°]	*Angle concrete compressive strut of end cross beam*

Input parameters - Material properties & prestressing

Concrete

Parameters concrete in compression

f_{ck}	30	[N/mm²]	*Characteristic cylinder compressive strength at 28 days*
$f_{ck,cube}$	37	[N/mm²]	*Characteristic cube compressive strength*
f_{cm}	38	[N/mm²]	*Mean value cylinder compressive strength*
ε_{c3}	1,75	[‰]	*Strain at reaching concrete compressive strength*
ε_{cu3}	3,5	[‰]	*Maximum compressive strain at ULS*

Parameters concrete in tension

f_{ctm}	2,9	[N/mm²]	*Mean value axial tensile strength*
$f_{ctk,0,05}$	2,0	[N/mm²]	*5%-fractile of the axial tensile strength*

Parameters stiffness and deformations (temperature, creep and shrinkage)

E_{cm}	33000	[N/mm²]	*Secant modulus of elasticity*
φ	1,75	[-]	*Creep*
Hydration	Normal (N)	[-]	*Rate of hydration: Rapid (R), Normal (N) or slow (S)*
RH	80,0	[%]	*Relative humidity*

Parameters concrete other

α	0,75	[-]	*Factor for shape of concrete compressive zone*
β	0,39	[-]	*Factor position centre of gravity concrete compressive zone*
α_{cc}	1,0	[-]	*Long term effects and unfavourable loading (compression)*
α_{ct}	0,0	[-]	*Long term effects and unfavourable loading (tension)*

Parameters prestressing End cross beams

Material properties prestressing steel

f_{pk}	1860	[N/mm²]	*Characteristic value tensile strength*
f_{pd}	1522	[N/mm²]	*Design value steel stress*
σ_{pm0}	1395	[N/mm²]	*Maximum allowed stress directly after tensioning*
$\sigma_{p,max}$	1488	[N/mm²]	*Maximum prestressing stress during tensioning*
E_p	195000	[N/mm²]	*Modulus of elasticity*
ε_{uk}	35	[‰]	*Characteristic value strain at failure*

Properties prestressing tendons

n_{ducts}	4	[pcs]	*Number of ducts in total*
a_{vert}	500	[mm]	*Vertical position centre of duct from centre of beam*
a_{hor}	750	[mm]	*Horizontal position centre of duct from centre of beam*
n_{strand}	4	[pcs]	*Assumed number of strands per tendon*
D_{strand}	15,2	[mm]	*Diameter of single strand*
$A_{p,strand}$	140	[mm²]	*Cross sectional area per strand*
$\sigma_{p,max,prov}$	1400	[N/mm²]	*Assumed maximum stress applied to prestressing element*
$\emptyset_{Duct}$	65	[mm]	*Outer diameter of prestressing ducts*
μ	0,23	[-]	*Friction coefficient*
k	0,009	[rad]	*Unintensional angular rotation due to the Wobble-effect*
w_{set}	3	[mm]	*Estimated wedge set*
Relaxation	Class 2	[-]	*Select relaxation class: normal (1), low (2) or bars (3)*
t	500000	[h]	*The value of the relaxation loss (in %) at 1000 h*
ρ	2,5	[%]	*Time after stressing (for final value of the relaxation loss)*

Other parameters

γ_C	1,5	[-]	*Partial factor concrete (cf EC2)*
γ_S	1,1	[-]	*Partial factor prestressing steel (cf EC2)*

Input parameters - Determining creep and shrinkage

Shrinkage

h_0	1267	[mm]	*Fictitious thickness, assumed to be (2/3)*hcb (3 sides exposed)*
k_h	0,7	[-]	*Coefficient depending on fictitious thickness*
RH	80,0	[%]	*Relative humidity*
β_{RH}	0,7564	[-]	*Factor for relative humidity*
Hydration	Normal (N)	[-]	*Rate of hydration: Rapid (R), Normal (N) or slow (S)*
α_{ds1}	4	[-]	*Coefficient depending on cement type*
α_{ds2}	0,12	[-]	*Coefficient depending on cement type*
f_{cm}	38	[N/mm²]	*Mean value cylinder compressive strength*
$\varepsilon_{cd,0}$	0,000269	[-]	*Nominal unrestrained drying shrinkage*
$\varepsilon_{cd,\infty}$	0,000188	[-]	*End value drying shrinkage*

h0	k_h
100	1
200	0,85
300	0,75
500	0,7

	α_{ds1}	α_{ds2}
Slow (S)	3	0,13
Normal (N)	4	0,12
Rapid (R)	6	0,11

Creep

φ	1,75	[-]	*Creep factor*

Input parameters - Loads

Ultimate Limit State (ULS)

$M_{Ed,hog}$	1271	[kNm]	*Maximum hogging bending moment (all loads considered)*
$M_{Ed,sag}$	396	[kNm]	*Maximum sagging bending moment (all loads considered)*
V_{Ed}	846	[kN]	*Maximum shear force (all loads considered)*

Serviceability Limit State (SLS)

$M_{E,hog}$	453	[kNm]	*Maximum hogging bending moment (all loads considered) SLS*
$M_{E,sag}$	270	[kNm]	*Maximum sagging bending moment (all loads considered) SLS*

Design of the prestressing

Calculating prestress losses

Applied maximum force onto prestressing elements & stress verification

Applied stress values

$\sigma_{p,max,prov}$	1400	[N/mm²]	*Assumed maximum stress applied to prestressing element*
$\sigma_{c,prov}$	0,87	[N/mm²]	*Concrete stress due to assumed initial applied force*

Stress limit and verification

$\sigma_{p,max,limit}$	1488	[N/mm²]	*Maximum prestressing stress during tensioning*
$\sigma_{c,limit}$	18	[N/mm²]	*Maximum value concrete compressive stress*
Verification	Satisfied	[-]	*Verification maximum stress values*

Applied value maxinum force applied onto prestressing

P_{max}	3136	[kN]	*Applied value maximum prestressing force*
$\sigma_{p,max}$	1400	[N/mm²]	*Applied value maximum prestressing stress*
A_p	2240	[mm²]	*Applied cross section prestressing tendon*

Direct prestressing losses

Elastic losses

ΔP_{el}	4,3	[kN]	*Total elastic loss all prestressing tendons*

Friction losses

μ	0,23	[-]	*Friction coefficient*
k	0,009	[1/m]	*Coefficient Wobble-effect*
$\Delta P_\mu(x=0)$	0,00	[kN]	*Prestress loss due to friction at x=0 m*
$\Delta P_\mu(x=w)$	104,4	[kN]	*Prestress loss (force) due to friction at x=width deck*
$\Delta\sigma_{P\mu}(x=w)$	46,6	[N/mm²]	*Prestress loss (stress) due to friction at x=width deck*

Wedge set

w_{set}	3,00	[mm]	*Assumed value wedge set*
k	0,0028	[N/mm²/mm]	*Stress reduction due to friction per unit of length*
l_w	14328,3	[mm]	*Influence length of the wedge set*
ΔP_{set}	182,9	[kN]	*Prestress losses due to wedge set (at active side)*

Determining initial prestressing force & stress verification

Applied force and stress values

$\max\{P_{m,0}(x)\}$	3040	[kN]	*Initial prestressing force - maximum value over beam length*
$\max\{\sigma_{pm0}(x)\}$	1357	[N/mm²]	*Initial prestressing stress - maximum value over beam length*
$P_{m,0}$	2999	[kN]	*Initial prestressing force - mean value over beam length*

Stress limit and verification

σ_{pm0}	1395	[N/mm²]	*Maximum allowed stress directly after tensioning*
Verification	Satisfied	[-]	*Verification initial prestressing stress*

Applied value initial prestressing force and losses

$P_{m,0}$	2999	[kN]	*Inital prestressing force - Mean value over beam length*
ΔP_i	137	[kN]	*Initial losses - Mean value over beam length: Pmax-Pm,0*

Time dependent losses

Relaxation

Class	Class 2	[-]	*Relaxation class (normal relaxation, low relaxation and bars)*
ρ_{1000}	2,5	[%]	*The value of the relaxation loss (in %) at 1000 h*
μ	0,72	[-]	*Factor depending on steel stresses*
t	500000	[h]	*Time after stressing (for final value of the relaxation loss)*
$\Delta\sigma_{pr}/\sigma_{pi}$	0,0426	[-]	*Relaxation coefficient*
σ_{pi}	1338,8	[N/mm²]	*Absolute value of the initial prestressing (σ_pm0)*
$\Delta\sigma_{pr}$	57,0	[N/mm²]	*Prestress loss due to relaxation*

Class 1	Wires and strands normal relaxation
Class 2	Wires and strands low relaxation
Class 3	Bars

Creep & shrinkage

φ	1,75	[-]	*Creep factor*
$\sigma_{c,QP}$	0,8	[N/mm²]	*Stress in concrete adjacent to tendons (middle cross section)*
ε_{cs}	0,000188	[-]	*Shrinkage of the concrete*

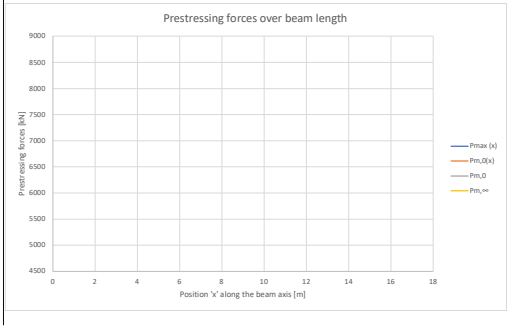
Total time dependent losses

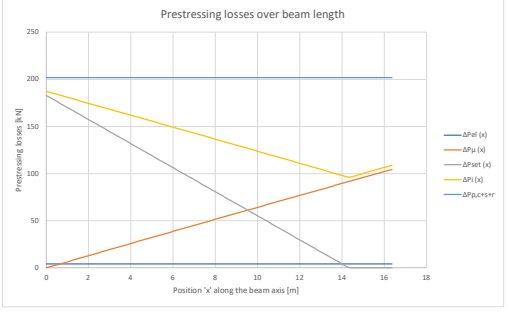
$\Delta\sigma_{p,c+s+r}$	90	[N/mm²]	*Time dependent prestressing losses (stress)*
$\Delta P_{p,c+s+r}$	202	[kN]	*Time dependent prestressing losses (force)*

Working prestress force and total prestress losses

$P_{m,\infty}$	2797	[kN]	*Total working prestressing force*
$\sigma_{pm,\infty}$	1249	[N/mm²]	*Working prestressing stress in the tendons*
ΔP	-10,8	[%]	*Total prestressing loss (percentage)*

Plotting prestressing forces and losses over beam length

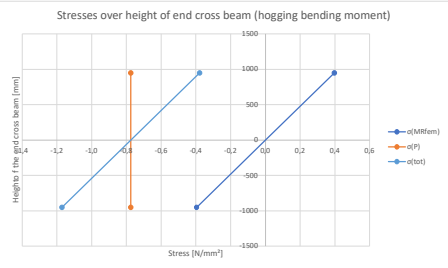




Determining stresses over beam height

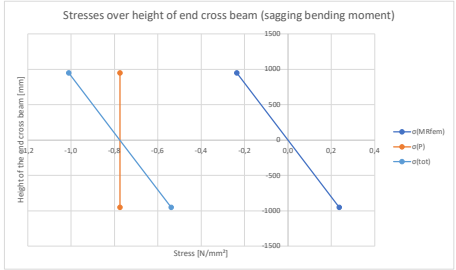
Stress distribution governing hogging bending moment in SLS:

	Height [mm]	σ(MRfem) [N/mm²]	σ(P) [N/mm²]	σ(tot) [N/mm²]
Top fibre	950	0,4	-0,8	-0,4
Bottom fibre	-950	-0,4	-0,8	-1,2



Stress distribution governing sagging bending moment in SLS:

	Height [mm]	σ(MRfem) [N/mm²]	σ(P) [N/mm²]	σ(tot) [N/mm²]
Top fibre	950	-0,2	-0,8	-1,0
Bottom fibre	-950	0,2	-0,8	-0,5



Verification bending moment capacity

Identifying all horizontal forces

Concrete

α	0,75	[-]	*Factor for shape of concrete compressive zone*
w_{cb}	1900	[mm]	*Factor position centre of gravity concrete compressive zone*
f_{cd}	20	[N/mm²]	*Design value concrete compressive strength*
N_c	3626	[kN]	*Compressive force in the concrete*

Active contribution of prestressing

A_p	2240	[mm²]	*Applied cross section of the prestressing*
$P_{m,\infty}$	2797	[kN]	*Working prestressing stress*
$\sigma_{p,\infty}$	1249	[N/mm²]	*Working prestressing stress in the tendons*

Height of concrete compressive zone

x_u	127,2324955	[mm]	*Height concrete compressive zone (iteration)*

x_1	450	[mm]	*Distance from outermost compressed fibre to centre of first row of tendons*
x_2	1450	[mm]	*Distance from outermost compressed fibre to centre of second row of tendons*

Determining the strains

First row of tendons

$d_{p,1}$	450	[mm]	*Effective height prestressing - row 1*
$\Delta\varepsilon_{p,1}$	0,0089	[-]	*Strain increase prestressing steel (passive contribution) - row 1*
$\varepsilon_{p,\infty,1}$	0,0064	[-]	*Strain in prestressing steel due to working prestressing - row 1*
$\varepsilon_{p,1}$	0,0153	[-]	*Total strain in prestressing steel - row 1*

Second row of tendons

$d_{p,2}$	1450	[mm]	*Effective height prestressing - row 2*
$\Delta\varepsilon_{p,2}$	0,0364	[-]	*Strain increase prestressing steel (passive contribution) - row 2*
$\varepsilon_{p,\infty,2}$	0,0064	[-]	*Strain in prestressing steel due to working prestressing - row 2*
$\varepsilon_{p,2}$	0,0315	[-]	*Total strain in prestressing steel - row 2*

Steel stresses

Parameters

f_{pk}/γ_s	1691	[N/mm²]	*Design value stress at failure*
f_{pd}	1522	[N/mm²]	*Design value steel stress*
ε_{uk}	0,035	[-]	*Characteristic value strain at failure*
f_{pd}/E_p	0,0078	[-]	*Strain at design value of the steel stress*

First row of tendons

$\sigma_{pu,1}$	1568	[N/mm²]	*Actual stress in prestressing steel at calculated strain - row 1*
$\sigma_{p,\infty}$	1249	[N/mm²]	*Working prestressing stress - row 1*
$0,5 * A_p$	1120	[mm²]	*Applied cross section prestressing - row 1*
$P_{m,\infty,1}$	1399	[kN]	*Working prestressing force - row 1*
$\Delta N_{p,1}$	358	[kN]	*Passive contribution prestressing - row 1*

Second row of tendons

$\sigma_{pu,2}$	1669	[N/mm²]	*Actual stress in prestressing steel at calculated strain - row 2*
$\sigma_{p,\infty}$	1249	[N/mm²]	*Working prestressing stress - row 2*
$0,5 * A_p$	1120	[mm²]	*Applied cross section prestressing - row 2*
$P_{m,\infty,2}$	1399	[kN]	*Working prestressing force - row 2*
$\Delta N_{p,2}$	471	[kN]	*Passive contribution prestressing - row 2*

Check equilibrium

N_c	-3626	[kN]	*Compressive force in the concrete*
$P_{m,\infty,1}$	1399	[kN]	*Working prestressing force - row 1*
$\Delta N_{p,1}$	358	[kN]	*Passive contribution of the prestressing - row 1*
$P_{m,\infty,2}$	1399	[kN]	*Working prestressing force - row 2*
$\Delta N_{p,2}$	471	[kN]	*Passive contribution of the prestressing - row 2*

ΣH	0	[kN]	*Verification of horizontal equilibrium*

Determine bending moment capacity

- Bending moment is calculated using the most compressed fibre as reference

Determining bending moment capacity

	Force [kN]	Lever arm [m]	Moment [kNm]
N_c	-3626	0,049	-179
$P_{m,\infty,1}$	1399	0,950	1329
$\Delta N_{p,1}$	358	0,450	161
$P_{m,\infty,2}$	1399	0,950	1329
$\Delta N_{p,2}$	471	1,450	683

Determining design value bending moment

$M_{Ed,RFEM}$	1271	[kNm]	*Bending moment due to loads calculated using RFEM*

Verification

M_{Ed}	1271	[kNm]	*Design value bending moment*
M_{Rd}	3322	[kNm]	*Bending moment capacity*
UC	0,38	[-]	*Unity check*

Verifying the rotational capacity

d_{ave}	950	[mm]	*Average effective height of both rows of tendons*
f	442	[N/mm²]	*Factor for weighed contribution of reinforcing and prestressing steel*
x_u/d_{ave}	0,13	[mm]	*Ratio height compressive zone and effective height*
Limit value	0,53	[mm]	*Limit value ratio height compressive zone and effective height*
UC	0,25	[-]	*Verification of rotational capacity (expressed as UC)*
Verification	Satisfied	[-]	*Verification of rotational capacity*

Verification shear force capacity

Parameters

Effective height

$d_{p,2}$	1450	[mm]	*Effective height prestressing - row 2*

Effective width of the cross beam

n_{row}	2	[pcs]	*Assumed number of ducts per row*
ϕ_{Duct}	65	[mm]	*Outer diameter of prestressing ducts*
w_{cb}	1900	[mm]	*Total width of the end cross beam*
$b_{cb,nom}$	1900	[mm]	*Effective width of the cross beam*

Capacity of concrete elements without shear reinforcement

k	1,37	[-]	*Scale factor*
f_{ck}	30	[N/mm²]	*Characteristic value concrete compressive strength*
v_{min}	0,31	[N/mm²]	*Reduction value for concrete cracked due to shear*
k_1	0,15	[-]	*Factor, value is deduced from the NA of EC2-1-1*
σ_{cp}	0,77	[N/mm²]	*Factor for presence of normal forces (compression positive)*

$V_{Rd,c,min}$	1168	[kN]	*Minimum value shear capacity of elements without shear reinforcement*

Upper limit - Failure of the concrete compressive strut

α_{cw}	1,04	[-]	*Factor accounting for the stress state in the compression strut*
z	1305	[mm]	*Internal lever arm*
v_1	0,53	[-]	*Reduction factor of concrete cracked due to shear*
$\cot(\theta)$	21,8	[°]	*Angle of compressive strut with beam axis*
$\tan(\theta)$	0,400	[-]	*Auxiliary value*
$\cot(\theta)$	2,500	[-]	*Auxiliary value*

$V_{Rd,max}$	9378	[kN]	*Shear force limit due to failure of concrete compressive strut*

Verification

V_{Ed}	846	[kN]	*Design value shear force*
V_{Rd}	1168	[kN]	*Shear force capacity*
UC	0,72	[-]	*Unity check*

Design Calculations Optimization - Weight calculation

Project: MSc thesis ''Redesign of bridges Twentekanaal in UHPC''
Name: M. Dorland
Date: 22-12-2020
Version: D1.0

Description	Length [m]	Height/depth [m]	Width [m]	Cross-section [m²]	Number [-]	Weight [kN/m³]	Result [-]	Units [-]	Remarks/notes
New design prefab UHPC deck									
Prefab UHPC beams	70,70			1,34	5	25	11864	[kN]	
In-situ UHPC joints	70,70	0,19	0,09		4	25	119	[kN]	
Cross beams	16,36	1,9	1,9		2	25	2953	[kN]	
Subtraction overlap main beams			1,900	1,34	10	25	-638	[kN]	
Asphalt layer	70,70	0,01	16,36			23	266	[kN]	
Kerbs	70,70	0,34	0,50		2	25	601	[kN]	
Capping beam	16,36	1,00	0,75		2	25	614	[kN]	*See CH8. preliminary design report*
Total							**15779**	[kN]	
Existing concrete arch bridge - Eefdesebrug									
Arches	75,00	1,80	0,90		2	25,0	6075	[kN]	*Arch length is measured using AutoCAD.*
Supporting elements arches (''windverband'')	8,00	0,36	1,60		4	25,0	461	[kN]	*See drawing B.3622*
Main girders	70,70	1,30	1,90		2	25,0	8731	[kN]	
Cross beams	7,00	0,80	0,80		12	25,0	1344	[kN]	
end cross beams	7,00	1,20	1,30		2	25,0	546	[kN]	*Average height, see ''detail B-B'' of B.7125*
Deck between main girders	70,70	0,25	7,00			25,0	3093	[kN]	
Deck pedestrian lanes	70,70	0,20	2,78		2	25,0	1965	[kN]	*An verage height of 0,20 m is assumed.*
Asphalt layer	70,70	0,05	7,00			23,0	569	[kN]	*Assumption: layer of 50 mm acc to B.5109.*
Total							**22785**	[kN]	
Comparison									
Percentual change of weight	-31	[%]							

Design Calculations Optimization - Calculation output

Project: MSc thesis "Redesign of bridges Twentekanaal in UHPC"
Name: M. Dorland
Date: 22-12-2020
Version: D1.0

Summary calculation results

Conclusion: All included verifications are satisfied.

Overview of unity checks:

Verification	Element	Unity check
Bending moment capacity:	*Main beams (global)*	0,90
Shear force capacity:	*Main beams (global)*	0,84
Torsional moment capacity:	*Main beams (global)*	0,29
Combination shear and torsion:	*Main beams (global)*	0,93
Combination shear and torsion – Compressive strut:	*Main beams (global)*	0,65
Ship collision – Static equilibrium:	*Whole deck (global)*	0,17
Bending moment capacity joint:	*Longitudinal joints (local)*	0,38
Top flange transverse - Sagging moment:	*Top flange (local)*	0,81
Top flange transverse - Hogging moment:	*Top flange (local)*	0,76
Bending moment capacity longitudinal direction:	*Top flange (local)*	0,83
Fatigue verification – Prestressing steel:	*Main beams (global)*	0,18
Fatigue verification – Concrete at top fibre:	*Main beams (global)*	0,00
Fatigue verification – Concrete at bottom fibre:	*Main beams (global)*	0,00
Deflection:	*Main beams (global)*	0,65
Bending moment capacity:	*End cross beams (global)*	0,38
Shear force capacity:	*End cross beams (global)*	0,72

Calculation results - Cross section

A_c	1342500,0	[mm²]	*Cross sectional area of total cross section*
z	844,5	[mm]	*Position centre of gravity from the top flange*
I_y	8,038E+11	[mm⁴]	*Second moment of area of the combined cross section*
e_t	844,5	[mm]	*Distance from centre of gravity to top fibre*
e_b	1055,5	[mm]	*Distance from centre of gravity to bottom fibre*
$W_{y,t}$	9,518E+08	[mm³]	*Section modulus with respect to top fibre*
$W_{y,b}$	7,615E+08	[mm³]	*Section modulus with respect to bottom fibre*

Calculation results - Design of main beams - Mean prestressing and global ULS verifications (STR)

Number of prestressing strands:

n_c	10	[pcs]	*Assumed number of strands positioned centrically in the cross section*
n_{fb}	105	[pcs]	*Assumed number of strands positioned in bottom flange*

Verification maximum stresses prestressing steel and concrete: Satisfied

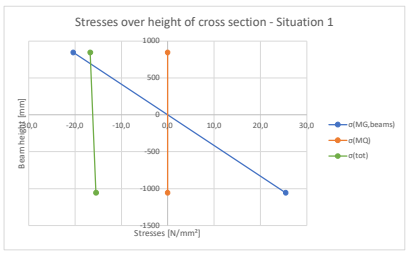
Symbol [-]	Value [N/mm²]	Limit [N/mm²]	Conclusion [-]
$\sigma_{p,max,c}$	1400,00	1488	Satisfied
$\sigma_{p,max,fb}$	1488	1488	Satisfied
$\sigma_{c,c+fb}$	45,20	140,00	Satisfied
$\sigma_{pm,0,c}$	1394	1395	Satisfied
$\sigma_{pm,0,fb}$	1343	1395	Satisfied

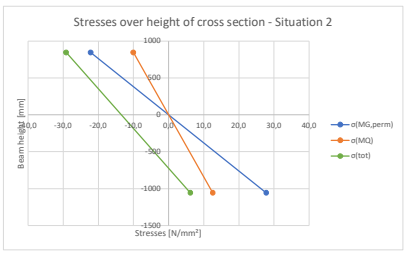
Prestressing forces and prestress losses:

Symbol	Unit	Centric	Eccentric
P_{max}	[kN]	1960	21874
P_{m0}	[kN]	1952	19745
$P_{m,\infty}$	[kN]	1623	16449
ΔP_i	[kN]	8	2129
$\Delta P_{p,c+s+r}$	[kN]	329	3295
ΔP_{tot}	[kN]	337	5424
$\Delta P_{\%}$	[%]	17	25

Stress criterion - Stresses over beam height at midspan: Satisfied

$\sigma_{tot,1}$	-15,5	[N/mm²]	*Largest stress situation 1*
$\sigma_{tot,2}$	6,2	[N/mm²]	*Largest stress situation 2*
σ_{max}	6,7	[N/mm²]	*Maximum allowed tensile stress*





Calculation results - Detailing of the beam ends

Verifications vertical force distribution and positioning of strands: Satisfied

Tensile stress top fibre near support:	Satisfied
Number of strands smaller than maximum:	Satisfied
Vertical force distribution - Splitting stresses:	Satisfied
Vertical force distribution - Bursting stresses:	Satisfied

Horizontal force distribution:

$n_{fb,1}$	105	[pcs]	*Number of strands applied in first set*
$A_{s,min}$	556	[mm²]	*Minimum required cross section of the reinforcement*
$n_{s,req,1}$	8	[pcs]	*Required number of rebars*
$n_{fb,2}$	0	[pcs]	*Number of strands applied in second set*
$A_{s,min}$	0	[mm²]	*Minimum required cross section of the reinforcement*
$n_{s,req,2}$	0	[pcs]	*Required number of rebars*

Calculation results - ULS verifications - Global verifications main beams

Global ultimate limit state verifications of the main beams: All performed global verifications of the main beam are satisfied.

Verification	Units	Design value	Capacity	Unity check	Conclusion
Bending moment capacity:	[kNm]	26036	28996	0,90	Satisfied
Rotational capacity:	[-]	0,09	0,37	0,24	Satisfied
Shear force capacity:	[kN]	3632	4335	0,84	Satisfied
Torsional capacity:	[kNm]	1268	4300	0,29	Satisfied
Combination shear and torsion:	[kN]	2118	2283	0,93	Satisfied
Combination shear and torsion – Compressive strut:	[kN]	2118	3265	0,65	Satisfied
Global verification ship collision (stability):	[kN]	1000	5932	0,17	Satisfied

Calculation results - Design of main beams - Top flange and transverse prestressing

Strands per tendon and centre to centre of prestressing ribs:

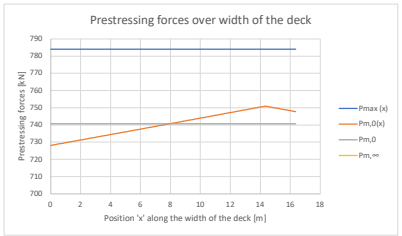
n	4	[pcs]	*Assumed number of strands per tendon*
$w_{c.t.c.}$	1000	[mm]	*Centre to centre distance of the transverse prestressing ribs/ducts*

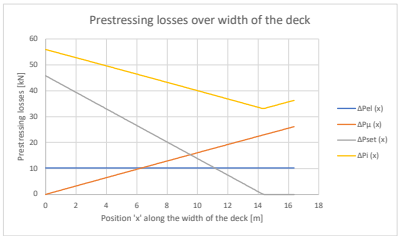
Verification maximum stresses prestressing steel and concrete: Satisfied

Symbol [-]	Value [N/mm²]	Limit [N/mm²]	Conclusion [-]
$\sigma_{p,max}$	1400	1488	Satisfied
$\sigma_{c,prov}$	5,4	60	Satisfied
σ_{pm0}	1341	1395	Satisfied

Prestressing forces and prestress losses:

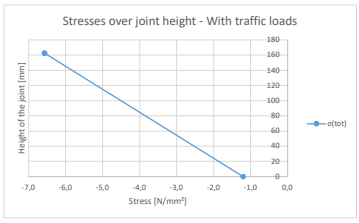
Symbol	Unit	Value
P_{max}	[kN]	784
P_{m0}	[kN]	741
$P_{m,\infty}$	[kN]	631
ΔP_i	[kN]	43
$\Delta P_{p,c+s+r}$	[kN]	109
ΔP_{tot}	[kN]	153
$\Delta P_{\%}$	[%]	-19

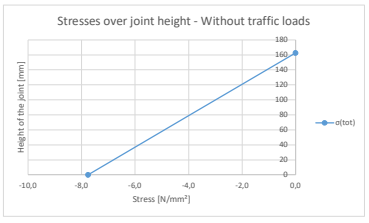




Stress criterion - Stresses at longitudinal joint: Satisfied

$\sigma_{tot,1}$	-1,20	[N/mm²]	*Largest stress situation with traffic*
$\sigma_{tot,2}$	-0,01	[N/mm²]	*Largest stress situation without traffic*





ULS verifications - Local verifications top flange - Transverse direction: Satisfied

Verification	Units	Design value	Capacity	Unity check	Conclusion
Longitudinal joint:	[kNm]	26,3	69,3	0,38	Satisfied
Sagging bending moment top flange:	[kNm]	72,5	88,9	0,81	Satisfied
Hogging bending moment top flange:	[kNm]	83,7	110,7	0,76	Satisfied

ULS verifications - Local verifications top flange - Longitudinal direction: Satisfied

Verification	Units	Design value	Capacity	Unity check	Conclusion
Longitudinal direction - Capacity:	[kNm]	73,5	88,2	0,83	Satisfied
Compressive strain limit:	[-]	0,0020	0,0023	0,89	Satisfied

The corresponding location of the intersection is: 0 [m]

Calculation results - Fatigue

Fatigue verifications: The performed fatigue verifications of the main beams are satisfied

Prestressing steel at mid span:	0,18	Satisfied
Concrete at midspan - top fibre:	0,00	Satisfied
Concrete at midspan - bottom fibre:	0,00	Satisfied

Calculation results - SLS Deflection

Verification of the deflections in the SLS: Satisfied

δ_{tot}	147,0	[mm]	*Total deflection determined using RFEM*
δ_{max}	226,7	[mm]	*Calculated value maximum deflection*

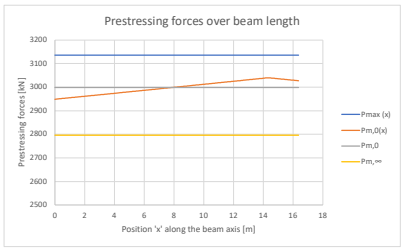
Calculation results - Design of the end cross beam

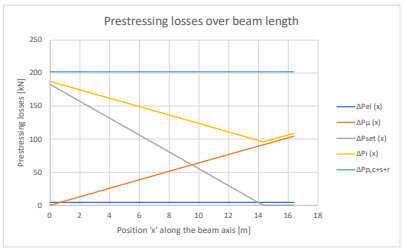
Number of prestressing tendons and strands per tendon:

n_{ducts}	4	[pcs]	*Number of ducts in total*
n_{strand}	4	[pcs]	*Assumed number of strands per tendon*

Verification maximum stresses prestressing steel and concrete: Satisfied

Symbol [-]	Value [N/mm²]	Limit [N/mm²]	Conclusion [-]
$\sigma_{p,max}$	1400	1488	Satisfied
σ_c	0,87	18	Satisfied
σ_{pm0}	1357	1395	Satisfied



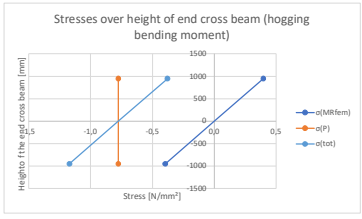


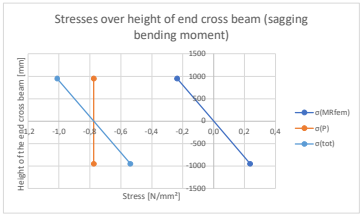
Prestressing forces and prestress losses:

Symbol	Unit	Value
P_{max}	[kN]	3136
P_{m0}	[kN]	2999
$P_{m,\infty}$	[kN]	2797
ΔP_l	[kN]	137
$\Delta P_{p,c+s+r}$	[kN]	202
ΔP_{tot}	[kN]	339
$\Delta P_{\%}$	[%]	-11

Stress criterion - Stresses over beam height: Satisfied

$\sigma_{tot,hog}$	-0,38	[N/mm²]	*Stress distribution hogging moment*
$\sigma_{tot,sag}$	-0,54	[N/mm²]	*Stress distribution sagging moment*





ULS verifications end cross beam: Satisfied

Verification	Units	Design value	Capacity	Unity check	Conclusion
Bending moment capacity:	[kNm]	1271	3322	0,38	Satisfied
Rotation capacity:	[-]	0,13	0,53	0,25	Satisfied
Shear force capacity:	[kN]	846	1168	0,72	Satisfied

Calculation results - Weight calculation and beam properties

Concrete volume and weight of single beam:

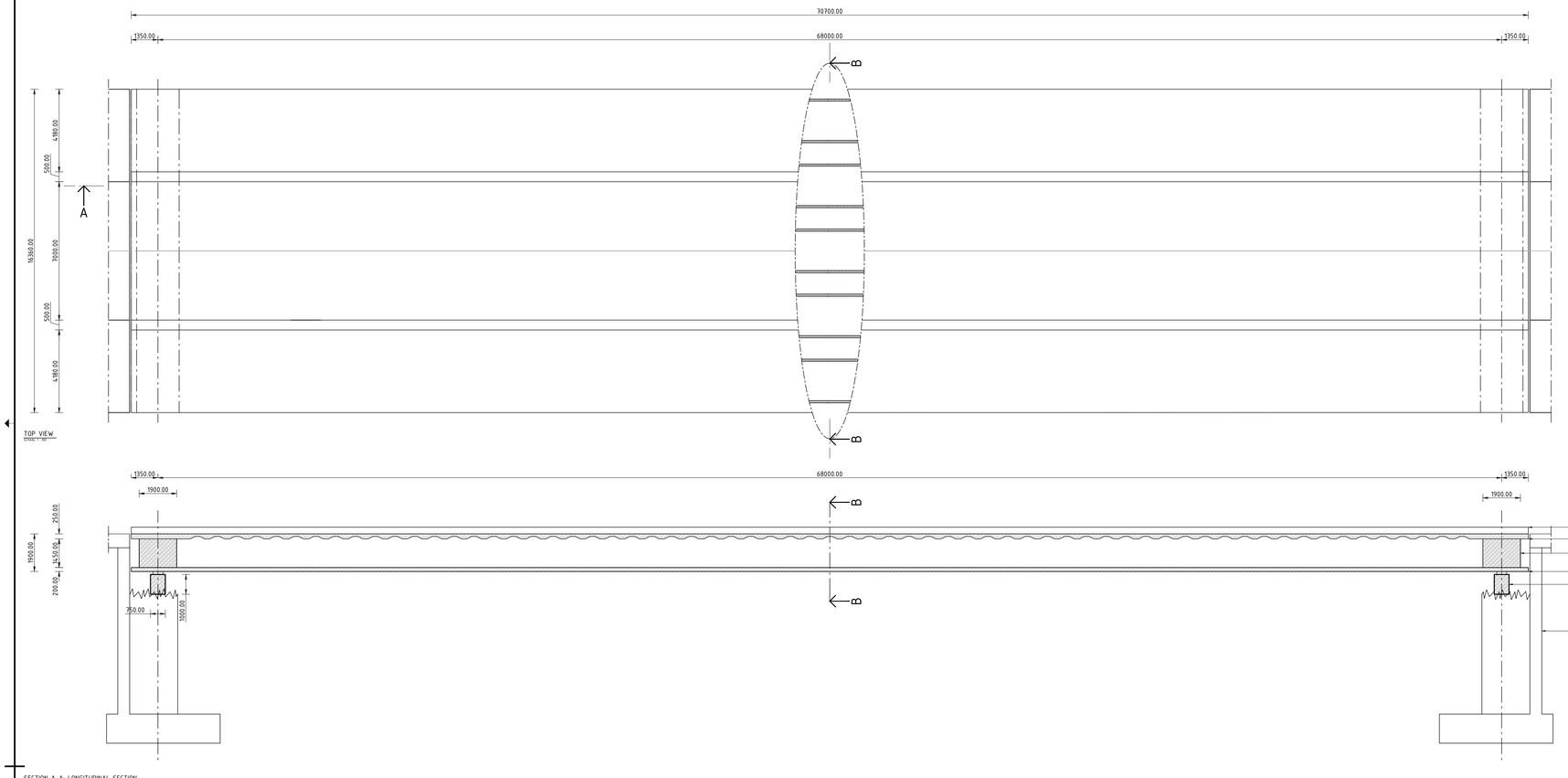
Single beam excl. solid ends:	94,9	[m³]
Solid ends single beam:	11,5	[m³]
Total volume single beam:	106,4	[m³]
Self-weight per beam	2660	[kN]

Comparison new design and existing bridge:

Optimized design deck:	15779	[kN]
Existing concrete arch bridge:	22785	[kN]
Difference in total weight:	-31	[%]

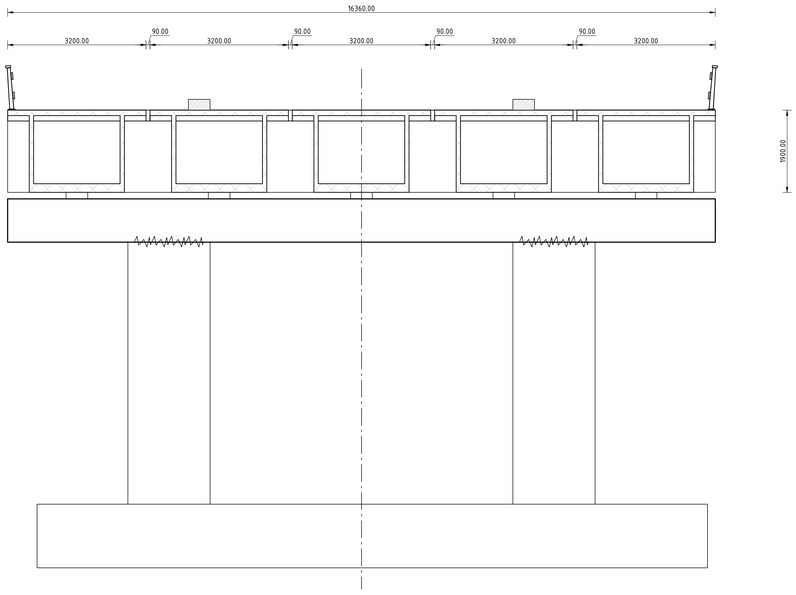
IV

ANNEX: DRAWING FINAL DESIGN

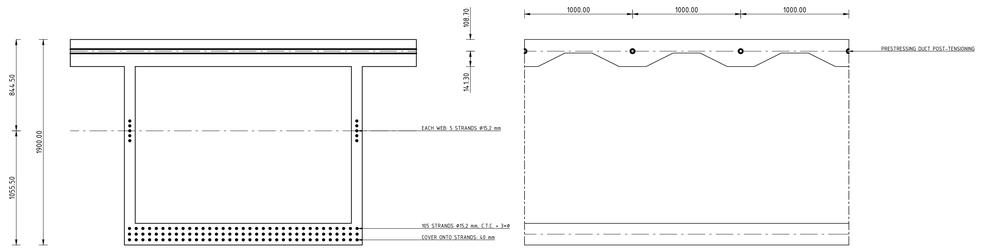


TOP VIEW
SCALE 1 : 50

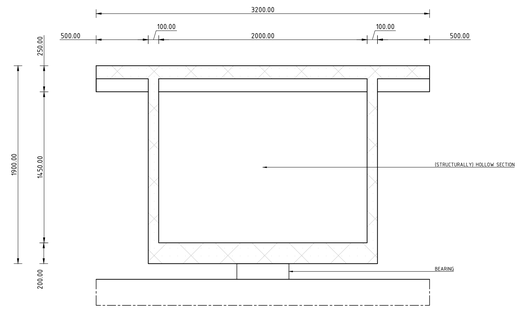
SECTION A-A: LONGITUDINAL SECTION
SCALE 1 : 50



SECTION B-B: CROSS SECTION AND POSITIONING OF TRAFFIC LANES
SCALE 1 : 10



POSITIONING PRESTRESSING STRANDS AND DUCTS
SCALE 1 : 10



DIMENSIONS OF PREFAB BEAM
SCALE 1 : 10

REMARKS:

- ALL UNITS IN mm
- ABUTMENTS, RAILINGS AND BEARINGS ONLY FOR INDICATION
- FOR OVERVIEW PRESTRESSING DUCTS & STRANDS ARE NOT DRAWN UNLESS SPECIFICALLY STATED
- SEE REPORT FOR DETAILS

OPDRACHTGEVER
–

PROJECTOMSCHRIJVING
MSC THESIS
REDESIGN OF BRIDGES TWENTEKANAAL IN UHPC

TEKENINGOMSCHRIJVING
FINAL DESIGN
DRAWING FINAL DESIGN

DOCUMENTSOORT
DRAWING

STATUS
FINAL VERSION

TEKENAAR
SEE DRAWINGS

PROJECTLEIDER

SCHAAL

FORMAAT
A0

BLAD IN BLADEN
1 IN 1

TEKENINGNUMMER

WIJZ NR

Plaats hier uw logo

V

ANNEX: WEIGHT COMPARISON

Weight Comparison - Permanent loads

Project: MSc thesis "Redesign of bridges Twentekanaal in UHPC"
Name: M. Dorland
Date: 5-1-2021
Version: D1.0

Description	Length [m]	Height/depth [m]	Width [m]	Cross-section [m²]	Number [-]	Volume [m³]	Weight [kN/m³]	Result [-]	Units [kN]	Remarks/notes
New design prefab UHPC deck										
Component 1 - Prefab UHPC beams	70,70			1,3425	5		25	11864	[kN]	
Component 2 - Solid ends prefab UHPC beams	1,90	1,51	2,00		10		25	1437	[kN]	
Component 3 - In-situ cross beams					2	17,57	25	878	[kN]	
Total volume solid end beams	16,36	1,90	1,90		1	59,06	25			
Subtraction cross section component 1			1,90	1,3425	5	-12,75	25			*Overlap with cross section prefab beam*
Subtraction cross section component 2	1,90	1,51	2,00		5	-28,74	25			*Overlap with solid end prefab beam*
Component 4 - In-situ UHPC joints	70,70	0,1875	0,090		4		25	119	[kN]	
Component 5 - Surface layer	70,70	0,010	16,36		1		23	266	[kN]	
Component 6 - Kerbs	70,70	0,34	0,50		2		25	601	[kN]	
Component 7 - Capping beams	16,36	1,0	0,75		2		25	614	[kN]	*See preliminary & detailed design report*
Total								**15779**	[kN]	
Single prefab UHPC beam						**106,4**		**2660**	[kN]	
Existing concrete arch bridge - Eefdesebrug										
Component I - Arches	72,50	1,70	0,90		2		25	5546	[kN]	
Component II - Supporting elements arches	8,00	0,36	1,60		4		25	461	[kN]	
Component III - Main girders	70,70	1,30	1,90		2		25	8731	[kN]	
Component IV - Intermediate cross beams	7,00	0,80	0,80		12		25	1344	[kN]	
Component V - End cross beams	7,00	1,25	1,30		2		25	569	[kN]	
Component VI - Ends main girders			1,90	1,13	4		25	215	[kN]	
Component VII - Main deck	70,70	0,25	7,00		1		25	3093	[kN]	
Component VIII - Deck pedestrian lanes	70,70			0,636	2		25	2248	[kN]	
Component IX - Surface layer main deck	70,70	0,05	7,00		1		23	569	[kN]	
Component X - Steel hangers	133,62			3,32E-03	8		78,5	278	[kN]	
Hanger set 1	4,67			3,32E-03	8		78,5	10	[kN]	
Hanger set 2	6,33			3,32E-03	8		78,5	13	[kN]	
Hanger set 3	7,87			3,32E-03	8		78,5	16	[kN]	
Hanger set 4	9,25			3,32E-03	8		78,5	19	[kN]	
Hanger set 5	10,49			3,32E-03	8		78,5	22	[kN]	
Hanger set 6	11,56			3,32E-03	8		78,5	24	[kN]	
Hanger set 7	12,49			3,32E-03	8		78,5	26	[kN]	
Hanger set 8	13,25			3,32E-03	8		78,5	28	[kN]	
Hanger set 9	13,88			3,32E-03	8		78,5	29	[kN]	
Hanger set 10	14,34			3,32E-03	8		78,5	30	[kN]	
Hanger set 11	14,67			3,32E-03	8		78,5	31	[kN]	
Hanger set 12	14,82			3,32E-03	8		78,5	31	[kN]	
Total								**23055**	[kN]	
Comparison										
Percentual change of weight (no factors)	-32	[%]								

Weight Comparison - Variable loads (vertical)

Project: MSc thesis "Redesign of bridges Twentekanaal in UHPC"
Name: M. Dorland
Date: 6-1-2021
Version: D1.0

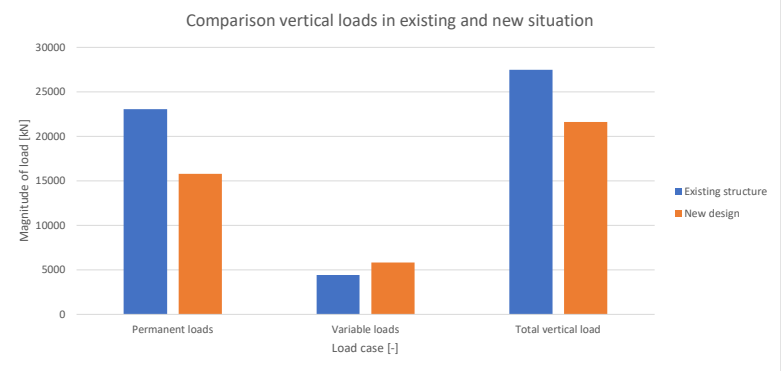
Description	Length [m]	Width [m]	Load (concentrated) [kN]	Load (line load) [kN/m]	Load (UDL) [kN/m²]	Number [-]	Factor [-]	Result [-]	Units [-]	Remarks/notes
New design prefab UHPC deck										
Main carriageway - UDL - Lane 1	70,70	3,0			8,73	1	1,0	1852	[kN]	
Main carriageway - UDL - Lane 2	70,70	3,0			2,425	1	1,0	514	[kN]	
Main carriageway - UDL - Remaining area	70,70	1,0			2,25	1	1,0	159	[kN]	
Main carriageway - Axle load - Lane 1			291			2	1,0	582	[kN]	
Main carriageway - Axle load - Lane 2			194			2	1,0	388	[kN]	
Pedestrian/bicycle lanes - UDL	70,70	4,18			3,22	2	1,0	1903	[kN]	
Railings - Vertical load	70,70			3,0		2	1,0	424	[kN]	
Total								**5822**	[kN]	
Existing concrete arch bridge - Eefdesebrug										
Main carriageway - UDL	70,70	7,0			3,6	1	1,0	1782	[kN]	
Main carriageway - Axle load - both vehicles			180			6	1,0	1080	[kN]	
Pedestrian/bicycle lanes - UDL	70,70	2,78			4,0	2	1,0	1572	[kN]	*Width: Distance outermost part of railing edge to main girder*
Total								**4434**	[kN]	
Comparison										
Percentual change of weight	31	[%]								

Weight Comparison - Comparison & analysis of results

Project: MSc thesis ''Redesign of bridges Twentekanaal in UHPC''
Name: M. Dorland
Date: 13-1-2021
Version: D1.0

Comparison vertical loads in existing and new situation - Comparison without additional factors

Action [-]	Existing structure [kN]	New design [kN]	Percentage change [%]
Permanent loads	23055	15779	-32
Variable loads	4434	5822	31
Total vertical load	27489	21602	-21



Comparison vertical loads in existing and new situation - Comparison with additional factors

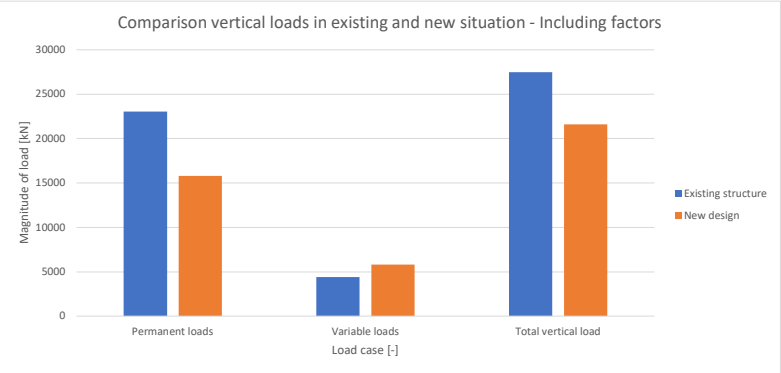
Safety factor GBV 1950/VOSB 1938:

Factor 1,00 [-]

Partial factors actions Eurocode:

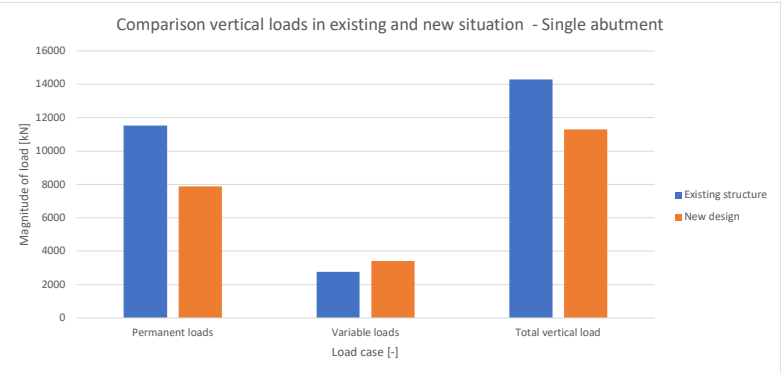
Actions	Equation 6.10a	Equation 6.10b
Permanent [-]	1,00	1,00
Variable [-]	1,00	1,00

Action [-]	Existing structure [kN]	New design [kN]	Percentage change [%]
Permanent loads	23055	15779	-32
Variable loads	4434	5822	31
Total vertical load	27489	21602	-21



Comparison vertical loads in existing and new situation - Concentrated loads at single abutment

Action [-]	Existing structure [kN]	New design [kN]	Percentage change [%]
Permanent loads	11527	7890	-32
Variable loads	2757	3396	23
Total vertical load	14284	11286	-21



VI

ANNEX: ESTIMATING FORCES FOUNDATION PILES

Estimating forces foundation piles

Name: M. Dorland

Date: 21-01-2021

Version: D1.0

```
> restart :
> with(LinearAlgebra) :
```

External forces acting on foundation block:

```
> f_{H,E} := '-154': f_{V,E} := '-14285': f_{M,E} := '5815':
> f_{H,N} := '-428': f_{V,N} := '-11286': f_{M,N} := '7893':
```

Defining first equation - Expressing internal forces in displacements

Force vector (vector containing forces in the individual foundation piles):

```
> n := Matrix([[N_a], [N_b], [N_c], [N_d], [N_e], [N_f], [N_g], [N_h]]);
```

$$n := \begin{bmatrix} N_a \\ N_b \\ N_c \\ N_d \\ N_e \\ N_f \\ N_g \\ N_h \end{bmatrix} \tag{1}$$

Matrix (stiffness matrix) relating forces and displacements:

```
> K := Matrix([[13·1/sqrt(65), 13·8/sqrt(65), -13·8/sqrt(65)·2], [8·1/sqrt(65), 8·8/sqrt(65), -8·8/sqrt(65)], [-5·1/sqrt(65), 5·8/sqrt(65), -5·8/sqrt(65)], [8·1/sqrt(65), 8·8/sqrt(65), 0], [-5·1/sqrt(65), 5·8/sqrt(65), 0], [8·1/sqrt(65), 8·8/sqrt(65), 8·8/sqrt(65)], [-5·1/sqrt(65), 5·8/sqrt(65), 5·8/sqrt(65)], [-13·1/sqrt(65), 13·8/sqrt(65), 13·8/sqrt(65)·2]])
```

$$K := \begin{bmatrix} \frac{\sqrt{65}}{5} & \frac{8\sqrt{65}}{5} & -\frac{16\sqrt{65}}{5} \\ \frac{8\sqrt{65}}{65} & \frac{64\sqrt{65}}{65} & -\frac{64\sqrt{65}}{65} \\ -\frac{\sqrt{65}}{13} & \frac{8\sqrt{65}}{13} & -\frac{8\sqrt{65}}{13} \\ \frac{8\sqrt{65}}{65} & \frac{64\sqrt{65}}{65} & 0 \\ -\frac{\sqrt{65}}{13} & \frac{8\sqrt{65}}{13} & 0 \\ \frac{8\sqrt{65}}{65} & \frac{64\sqrt{65}}{65} & \frac{64\sqrt{65}}{65} \\ -\frac{\sqrt{65}}{13} & \frac{8\sqrt{65}}{13} & \frac{8\sqrt{65}}{13} \\ -\frac{\sqrt{65}}{5} & \frac{8\sqrt{65}}{5} & \frac{16\sqrt{65}}{5} \end{bmatrix} \quad (2)$$

Displacement vector (containing displacements multiplied with stiffness of the piles):

> $u := Matrix([[k \cdot x], [k \cdot y], [k \cdot \mathrm{phi}]])$;

$$u := \begin{bmatrix} k\,x \\ k\,y \\ k\,\phi \end{bmatrix} \quad (3)$$

Matrix-vector equation:

> $n = K \cdot u$;

(4)

$$\begin{bmatrix} N_a \\ N_b \\ N_c \\ N_d \\ N_e \\ N_f \\ N_g \\ N_h \end{bmatrix} = \begin{bmatrix} \frac{\sqrt{65}\,k\,x}{5} + \frac{8\sqrt{65}\,k\,y}{5} - \frac{16\sqrt{65}\,k\,\phi}{5} \\ \frac{8\sqrt{65}\,k\,x}{65} + \frac{64\sqrt{65}\,k\,y}{65} - \frac{64\sqrt{65}\,k\,\phi}{65} \\ -\frac{\sqrt{65}\,k\,x}{13} + \frac{8\sqrt{65}\,k\,y}{13} - \frac{8\sqrt{65}\,k\,\phi}{13} \\ \frac{8\sqrt{65}\,k\,x}{65} + \frac{64\sqrt{65}\,k\,y}{65} \\ -\frac{\sqrt{65}\,k\,x}{13} + \frac{8\sqrt{65}\,k\,y}{13} \\ \frac{8\sqrt{65}\,k\,x}{65} + \frac{64\sqrt{65}\,k\,y}{65} + \frac{64\sqrt{65}\,k\,\phi}{65} \\ -\frac{\sqrt{65}\,k\,x}{13} + \frac{8\sqrt{65}\,k\,y}{13} + \frac{8\sqrt{65}\,k\,\phi}{13} \\ -\frac{\sqrt{65}\,k\,x}{5} + \frac{8\sqrt{65}\,k\,y}{5} + \frac{16\sqrt{65}\,k\,\phi}{5} \end{bmatrix} \quad (4)$$

Defining second equation - Equilibrium

Matrix relating internal and external forces (transpose of stiffness matrix):

```
> C := Matrix([[[13·1/sqrt(65), 8·1/sqrt(65), -5·1/sqrt(65), 8·1/sqrt(65), -5·1/sqrt(65), 8·1/sqrt(65),
      -5·1/sqrt(65), -13·1/sqrt(65)], [13·8/sqrt(65), 8·8/sqrt(65), 5·8/sqrt(65), 8·8/sqrt(65), 5·8/sqrt(65),
      8·8/sqrt(65), 5·8/sqrt(65), 13·8/sqrt(65)], [-13·8/sqrt(65)·2, -8·8/sqrt(65), -5·8/sqrt(65), 0, 0,
      8·8/sqrt(65), 5·8/sqrt(65), 13·8/sqrt(65)·2]]):
```

$$C := \begin{bmatrix} \frac{\sqrt{65}}{5}, \frac{8\sqrt{65}}{65}, -\frac{\sqrt{65}}{13}, \frac{8\sqrt{65}}{65}, -\frac{\sqrt{65}}{13}, \frac{8\sqrt{65}}{65}, -\frac{\sqrt{65}}{13}, -\frac{\sqrt{65}}{5} \\ \frac{8\sqrt{65}}{5}, \frac{64\sqrt{65}}{65}, \frac{8\sqrt{65}}{13}, \frac{64\sqrt{65}}{65}, \frac{8\sqrt{65}}{13}, \frac{64\sqrt{65}}{65}, \frac{8\sqrt{65}}{13}, \frac{8\sqrt{65}}{5} \\ -\frac{16\sqrt{65}}{5}, -\frac{64\sqrt{65}}{65}, -\frac{8\sqrt{65}}{13}, 0, 0, \frac{64\sqrt{65}}{65}, \frac{8\sqrt{65}}{13}, \frac{16\sqrt{65}}{5} \end{bmatrix} \quad (5)$$

Vector containing external forces:

```
> f := Matrix([[f_H], [f_V], [f_M]]);
```

(6)

$$f := \begin{bmatrix} f_H \\ f_V \\ f_M \end{bmatrix} \tag{6}$$

Matrix-vector equation:

> $C \cdot n = f;$

$$\left[\left[\frac{\sqrt{65}\, N_a}{5} + \frac{8\sqrt{65}\, N_b}{65} - \frac{\sqrt{65}\, N_c}{13} + \frac{8\sqrt{65}\, N_d}{65} - \frac{\sqrt{65}\, N_e}{13} + \frac{8\sqrt{65}\, N_f}{65} - \frac{\sqrt{65}\, N_g}{13} - \frac{\sqrt{65}\, N_h}{5} \right], \left[\frac{8\sqrt{65}\, N_a}{5} + \frac{64\sqrt{65}\, N_b}{65} + \frac{8\sqrt{65}\, N_c}{13} + \frac{64\sqrt{65}\, N_d}{65} + \frac{8\sqrt{65}\, N_e}{13} + \frac{64\sqrt{65}\, N_f}{65} + \frac{8\sqrt{65}\, N_g}{13} + \frac{8\sqrt{65}\, N_h}{5} \right], \left[-\frac{16\sqrt{65}\, N_a}{5} - \frac{64\sqrt{65}\, N_b}{65} - \frac{8\sqrt{65}\, N_c}{13} + \frac{64\sqrt{65}\, N_f}{65} + \frac{8\sqrt{65}\, N_g}{13} + \frac{16\sqrt{65}\, N_h}{5} \right] \right] = \begin{bmatrix} f_H \\ f_V \\ f_M \end{bmatrix} \tag{7}$$

Solving the problem

Matrix multiplication (expressing equilibrium in terms of displacement):

> $H := C \cdot K;$

$$H := \begin{bmatrix} \frac{121}{13} & \frac{72}{5} & -\frac{416}{5} \\ \frac{72}{5} & \frac{7744}{13} & 0 \\ -\frac{416}{5} & 0 & \frac{19584}{13} \end{bmatrix} \tag{8}$$

Newly obtained equation of equilibrium expressed in the displacements:

> $H \cdot u = f;$

$$\begin{bmatrix} \frac{121}{13} k x + \frac{72}{5} k y - \frac{416}{5} k \phi \\ \frac{72}{5} k x + \frac{7744}{13} k y \\ -\frac{416}{5} k x + \frac{19584}{13} k \phi \end{bmatrix} = \begin{bmatrix} f_H \\ f_V \\ f_M \end{bmatrix} \tag{9}$$

Determining the unknowns (internal forces):

```
> u := evalf(MatrixInverse(H) . f);
```

$$u := \begin{bmatrix} 0.2291181461\, f_H - 0.005538599814\, f_V + 0.01265391069\, f_M \\ -0.005538599814\, f_H + 0.001812606648\, f_V - 0.0003058899897\, f_M \\ 0.01265391069\, f_H - 0.0003058899897\, f_V + 0.001362666963\, f_M \end{bmatrix} \quad \textbf{(10)}$$

Determining the forces in the foundation piles:

```
> n := evalf(K . u);
```

$$n := \begin{bmatrix} -0.02846496742\, f_H + 0.02234292393\, f_V - 0.01869779570\, f_M \\ 0.08293266210\, f_H + 0.01132126870\, f_V - 0.000689181565\, f_M \\ -0.2323531707\, f_H + 0.01394558052\, f_V - 0.01612598302\, f_M \\ 0.1833822271\, f_H + 0.008893045746\, f_V + 0.01012797268\, f_M \\ -0.1695721925\, f_H + 0.01242794117\, f_V - 0.009365261616\, f_M \\ 0.2838317921\, f_H + 0.006464822791\, f_V + 0.02094512692\, f_M \\ -0.1067912144\, f_H + 0.01091030182\, f_V - 0.002604540213\, f_M \\ -0.1144266142\, f_H + 0.02442092243\, f_V + 0.01080607110\, f_M \end{bmatrix} \quad \textbf{(11)}$$

Existing structure

```
> f := Matrix([[f_{H,E}], [f_{V,E}], [f_{M,E}]]);
```

$$f := \begin{bmatrix} -154 \\ -14285 \\ 5815 \end{bmatrix} \quad \textbf{(12)}$$

```
> K : C : H :
> u := evalf(MatrixInverse(H) . f) :
> n := evalf(K . u);
```

$$n := \begin{bmatrix} -423.5127456 \\ -178.5035441 \\ -257.2028207 \\ -96.38386029 \\ -205.8780183 \\ -14.26417645 \\ -154.5532159 \\ -268.3938749 \end{bmatrix} \quad \textbf{(13)}$$

Forces in the individual foundation piles of each pile group:

```
> N_{a,E} := n(1) :
> N_{b,E} := n(2) :
```

> $N_{c,E} := n(3)$:

> $N_{d,E} := n(4)$:

> $N_{e,E} := n(5)$:

> $N_{f,E} := n(6)$:

> $N_{g,E} := n(7)$:

> $N_{h,E} := n(8)$:

Verifying results: Summation should be approximately zero.

> $S_{H,E} := evalf\left(\frac{13 \cdot 1}{\mathrm{sqrt}(65)} \cdot N_{a,E} + \frac{8 \cdot 1}{\mathrm{sqrt}(65)} \cdot N_{b,E} - \frac{5 \cdot 1}{\mathrm{sqrt}(65)} \cdot N_{c,E} + \frac{8 \cdot 1}{\mathrm{sqrt}(65)} \cdot N_{d,E} - \frac{5 \cdot 1}{\mathrm{sqrt}(65)} \cdot N_{e,E} + \frac{8 \cdot 1}{\mathrm{sqrt}(65)} \cdot N_{f,E} - \frac{5 \cdot 1}{\mathrm{sqrt}(65)} \cdot N_{g,E} - \frac{13 \cdot 1}{\mathrm{sqrt}(65)} \cdot N_{h,E} \right);$

$$S_{H,E} := -153.9999999 \quad (14)$$

> $S_{V,E} := evalf\left(\frac{13 \cdot 8}{\mathrm{sqrt}(65)} \cdot N_{a,E} + \frac{8 \cdot 8}{\mathrm{sqrt}(65)} \cdot N_{b,E} + \frac{5 \cdot 8}{\mathrm{sqrt}(65)} \cdot N_{c,E} + \frac{8 \cdot 8}{\mathrm{sqrt}(65)} \cdot N_{d,E} + \frac{5 \cdot 8}{\mathrm{sqrt}(65)} \cdot N_{e,E} + \frac{8 \cdot 8}{\mathrm{sqrt}(65)} \cdot N_{f,E} + \frac{5 \cdot 8}{\mathrm{sqrt}(65)} \cdot N_{g,E} + \frac{13 \cdot 8}{\mathrm{sqrt}(65)} \cdot N_{h,E} \right);$

$$S_{V,E} := -14285.00000 \quad (15)$$

> $S_{M,E} := evalf\left(-\frac{13 \cdot 8}{\mathrm{sqrt}(65)} \cdot 2 \cdot N_{a,E} - \frac{8 \cdot 8}{\mathrm{sqrt}(65)} \cdot N_{b,E} - \frac{5 \cdot 8}{\mathrm{sqrt}(65)} \cdot N_{c,E} + 0 \cdot N_{d,E} + 0 \cdot N_{e,E} + \frac{8 \cdot 8}{\mathrm{sqrt}(65)} \cdot N_{f,E} + \frac{5 \cdot 8}{\mathrm{sqrt}(65)} \cdot N_{g,E} + \frac{13 \cdot 8}{\mathrm{sqrt}(65)} \cdot 2 \cdot N_{h,E} \right);$

$$S_{M,E} := 5815.000003 \quad (16)$$

> $S_{H,E} - f_{H,E}; S_{V,E} - f_{V,E}; S_{M,E} - f_{M,E};$

$$1.\ 10^{-7}$$
$$0.$$
$$3.\ 10^{-6} \quad (17)$$

New design

> $f := Matrix([[f_{H,N}], [f_{V,N}], [f_{M,N}]]);$

$$f := \begin{bmatrix} -428 \\ -11286 \\ 7893 \end{bmatrix} \quad (18)$$

> $K : C : H :$

> $u := evalf(MatrixInverse(H) \cdot f) :$

> $n := evalf(K \cdot u);$

(19)

$$n := \begin{bmatrix} -387.5609351 \\ -168.7067281 \\ -185.2250486 \\ -98.91441918 \\ -141.6048555 \\ -29.12211028 \\ -97.98466244 \\ -141.3476205 \end{bmatrix} \quad (19)$$

Forces in the individual foundation piles of each pile group:

> $N_{a,N} := n(1)$:

> $N_{b,N} := n(2)$:

> $N_{c,N} := n(3)$:

> $N_{d,N} := n(4)$:

> $N_{e,N} := n(5)$:

> $N_{f,N} := n(6)$:

> $N_{g,N} := n(7)$:

> $N_{h,N} := n(8)$:

Verifying results: Summation should be approximately zero.

> $S_{H,N} := evalf\left(\frac{13 \cdot 1}{\mathrm{sqrt}(65)} \cdot N_{a,N} + \frac{8 \cdot 1}{\mathrm{sqrt}(65)} \cdot N_{b,N} - \frac{5 \cdot 1}{\mathrm{sqrt}(65)} \cdot N_{c,N} + \frac{8 \cdot 1}{\mathrm{sqrt}(65)} \cdot N_{d,N} - \frac{5 \cdot 1}{\mathrm{sqrt}(65)} \cdot N_{e,N} + \frac{8 \cdot 1}{\mathrm{sqrt}(65)} \cdot N_{f,N} - \frac{5 \cdot 1}{\mathrm{sqrt}(65)} \cdot N_{g,N} - \frac{13 \cdot 1}{\mathrm{sqrt}(65)} \cdot N_{h,N} \right);$

$$S_{H,N} := -428.0000003 \quad (20)$$

> $S_{V,N} := evalf\left(\frac{13 \cdot 8}{\mathrm{sqrt}(65)} \cdot N_{a,N} + \frac{8 \cdot 8}{\mathrm{sqrt}(65)} \cdot N_{b,N} + \frac{5 \cdot 8}{\mathrm{sqrt}(65)} \cdot N_{c,N} + \frac{8 \cdot 8}{\mathrm{sqrt}(65)} \cdot N_{d,N} + \frac{5 \cdot 8}{\mathrm{sqrt}(65)} \cdot N_{e,N} + \frac{8 \cdot 8}{\mathrm{sqrt}(65)} \cdot N_{f,N} + \frac{5 \cdot 8}{\mathrm{sqrt}(65)} \cdot N_{g,N} + \frac{13 \cdot 8}{\mathrm{sqrt}(65)} \cdot N_{h,N} \right);$

$$S_{V,N} := -11285.99999 \quad (21)$$

> $S_{M,N} := evalf\left(-\frac{13 \cdot 8}{\mathrm{sqrt}(65)} \cdot 2 \cdot N_{a,N} - \frac{8 \cdot 8}{\mathrm{sqrt}(65)} \cdot N_{b,N} - \frac{5 \cdot 8}{\mathrm{sqrt}(65)} \cdot N_{c,N} + 0 \cdot N_{d,N} + 0 \cdot N_{e,N} + \frac{8 \cdot 8}{\mathrm{sqrt}(65)} \cdot N_{f,N} + \frac{5 \cdot 8}{\mathrm{sqrt}(65)} \cdot N_{g,N} + \frac{13 \cdot 8}{\mathrm{sqrt}(65)} \cdot 2 \cdot N_{h,N} \right);$

$$S_{M,N} := 7893.000000 \quad (22)$$

> $S_{H,N} - f_{H,N}; S_{V,N} - f_{V,N}; S_{M,N} - f_{M,N};$

$$\begin{bmatrix} -3. \cdot 10^{-7} \\ 0.00001 \\ 0. \end{bmatrix} \quad (23)$$

Comparison pile forces existing structure and new design

> $N_{a,E}; N_{a,N}; \mathrm{abs}\left(N_{a,N} - N_{a,E}\right);$

$$-423.5127456$$
$$-387.5609351$$
$$35.9518105 \quad \textbf{(24)}$$

> $N_{b,E}; N_{b,N}; \mathrm{abs}\left(N_{b,N} - N_{b,E}\right);$

$$-178.5035441$$
$$-168.7067281$$
$$9.7968160 \quad \textbf{(25)}$$

> $N_{c,E}; N_{c,N}; \mathrm{abs}\left(N_{c,N} - N_{c,E}\right);$

$$-257.2028207$$
$$-185.2250486$$
$$71.9777721 \quad \textbf{(26)}$$

> $N_{d,E}; N_{d,N}; \mathrm{abs}\left(N_{d,N} - N_{d,E}\right);$

$$-96.38386029$$
$$-98.91441918$$
$$2.53055889 \quad \textbf{(27)}$$

> $N_{e,E}; N_{e,N}; \mathrm{abs}\left(N_{e,N} - N_{e,E}\right);$

$$-205.8780183$$
$$-141.6048555$$
$$64.2731628 \quad \textbf{(28)}$$

> $N_{f,E}; N_{f,N}; \mathrm{abs}\left(N_{f,N} - N_{f,E}\right);$

$$-14.26417645$$
$$-29.12211028$$
$$14.85793383 \quad \textbf{(29)}$$

> $N_{g,E}; N_{g,N}; \mathrm{abs}\left(N_{g,N} - N_{g,E}\right);$

$$-154.5532159$$
$$-97.98466244$$
$$56.56855346 \quad \textbf{(30)}$$

> $N_{h,E}; N_{h,N}; \mathrm{abs}\left(N_{h,N} - N_{h,E}\right);$

$$-268.3938749$$
$$-141.3476205$$
$$127.0462544 \quad \textbf{(31)}$$

>